

Insights in atherosclerosis and vascular medicine 2022

Edited by
Masanori Aikawa

Published in
Frontiers in Cardiovascular Medicine



FRONTIERS EBOOK COPYRIGHT STATEMENT

The copyright in the text of individual articles in this ebook is the property of their respective authors or their respective institutions or funders. The copyright in graphics and images within each article may be subject to copyright of other parties. In both cases this is subject to a license granted to Frontiers.

The compilation of articles constituting this ebook is the property of Frontiers.

Each article within this ebook, and the ebook itself, are published under the most recent version of the Creative Commons CC-BY licence. The version current at the date of publication of this ebook is CC-BY 4.0. If the CC-BY licence is updated, the licence granted by Frontiers is automatically updated to the new version.

When exercising any right under the CC-BY licence, Frontiers must be attributed as the original publisher of the article or ebook, as applicable.

Authors have the responsibility of ensuring that any graphics or other materials which are the property of others may be included in the CC-BY licence, but this should be checked before relying on the CC-BY licence to reproduce those materials. Any copyright notices relating to those materials must be complied with.

Copyright and source acknowledgement notices may not be removed and must be displayed in any copy, derivative work or partial copy which includes the elements in question.

All copyright, and all rights therein, are protected by national and international copyright laws. The above represents a summary only. For further information please read Frontiers' Conditions for Website Use and Copyright Statement, and the applicable CC-BY licence.

ISSN 1664-8714
ISBN 978-2-8325-4611-6
DOI 10.3389/978-2-8325-4611-6

About Frontiers

Frontiers is more than just an open access publisher of scholarly articles: it is a pioneering approach to the world of academia, radically improving the way scholarly research is managed. The grand vision of Frontiers is a world where all people have an equal opportunity to seek, share and generate knowledge. Frontiers provides immediate and permanent online open access to all its publications, but this alone is not enough to realize our grand goals.

Frontiers journal series

The Frontiers journal series is a multi-tier and interdisciplinary set of open-access, online journals, promising a paradigm shift from the current review, selection and dissemination processes in academic publishing. All Frontiers journals are driven by researchers for researchers; therefore, they constitute a service to the scholarly community. At the same time, the *Frontiers journal series* operates on a revolutionary invention, the tiered publishing system, initially addressing specific communities of scholars, and gradually climbing up to broader public understanding, thus serving the interests of the lay society, too.

Dedication to quality

Each Frontiers article is a landmark of the highest quality, thanks to genuinely collaborative interactions between authors and review editors, who include some of the world's best academicians. Research must be certified by peers before entering a stream of knowledge that may eventually reach the public - and shape society; therefore, Frontiers only applies the most rigorous and unbiased reviews. Frontiers revolutionizes research publishing by freely delivering the most outstanding research, evaluated with no bias from both the academic and social point of view. By applying the most advanced information technologies, Frontiers is catapulting scholarly publishing into a new generation.

What are Frontiers Research Topics?

Frontiers Research Topics are very popular trademarks of the *Frontiers journals series*: they are collections of at least ten articles, all centered on a particular subject. With their unique mix of varied contributions from Original Research to Review Articles, Frontiers Research Topics unify the most influential researchers, the latest key findings and historical advances in a hot research area.

Find out more on how to host your own Frontiers Research Topic or contribute to one as an author by contacting the Frontiers editorial office: frontiersin.org/about/contact

Insights in atherosclerosis and vascular medicine: 2022

Topic editor

Masanori Aikawa — Brigham and Women's Hospital, Harvard Medical School, United States

Citation

Aikawa, M., ed. (2024). *Insights in atherosclerosis and vascular medicine: 2022*. Lausanne: Frontiers Media SA. doi: 10.3389/978-2-8325-4611-6

Table of contents

- 06 **Deciphering Cell-Cell Communication in Abdominal Aortic Aneurysm From Single-Cell RNA Transcriptomic Data**
Huan Yang, Elise DeRoo, Ting Zhou and Bo Liu
- 18 **Low Molecular Weight Apolipoprotein(a) Phenotype Rather Than Lipoprotein(a) Is Associated With Coronary Atherosclerosis and Myocardial Infarction**
Olga I. Afanasieva, Marat V. Ezhov, Narek A. Tmoyan, Oksana A. Razova, Marina I. Afanasieva, Yuri G. Matchin and Sergei N. Pokrovsky
- 25 **CagA⁺ *Helicobacter pylori*, Not CagA⁻ *Helicobacter pylori*, Infection Impairs Endothelial Function Through Exosomes-Mediated ROS Formation**
Xiujuan Xia, Linfang Zhang, Hao Wu, Feng Chen, Xuanyou Liu, Huifang Xu, Yuqi Cui, Qiang Zhu, Meifang Wang, Hong Hao, De-Pei Li, William P. Fay, Luis A. Martinez-Lemus, Michael A. Hill, Canxia Xu and Zhenguo Liu
- 39 **Abdominal Aortic Endothelial Dysfunction Occurs in Female Mice With Dextran Sodium Sulfate-Induced Chronic Colitis Independently of Reactive Oxygen Species Formation**
Hao Wu, Tingzi Hu, Linfang Zhang, Xiujuan Xia, Xuanyou Liu, Qiang Zhu, Meifang Wang, Zhe Sun, Hong Hao, Yuqi Cui, Alan R. Parrish, De-Pei Li, Michael A. Hill, Canxia Xu and Zhenguo Liu
- 51 **Embracing Diversity, Equity, and Inclusion in the Scientific Community—Viewpoints of the Diversity, Equity, and Inclusion Committee of the North American Vascular Biology Organization**
Mahdi Garelnabi, Mitzy Cowdin, Yun Fang, Bandana Shrestha, Masuko Ushio-Fukai, Elena Aikawa, Garth Graham, Grietje Molema, Hiromi Yanagisawa and Masanori Aikawa
- 60 **Long-Term Effect of Febuxostat on Endothelial Function in Patients With Asymptomatic Hyperuricemia: A Sub-Analysis of the PRIZE Study**
Tatsuya Maruhashi, Yukihiro Higashi, Hisako Yoshida, Atsushi Tanaka, Kazuo Eguchi, Hirofumi Tomiyama, Kazuomi Kario, Toru Kato, Nozomu Oda, Nobuhiro Tahara, Mitsutoshi Oguri, Hirotaka Watada and Koichi Node for the PRIZE Study Investigators
- 70 **Prognostic Impact of Multiple Lymphocyte-Based Inflammatory Indices in Acute Coronary Syndrome Patients**
Qiuxuan Li, Xiaoteng Ma, Qiaoyu Shao, Zhiqiang Yang, Yufei Wang, Fei Gao, Yujie Zhou, Lixia Yang and Zhijian Wang
- 79 **Mechanical Strain Induces Transcriptomic Reprogramming of Saphenous Vein Progenitors**
Davide Maselli, Gloria Garoffolo, Giada Andrea Cassanmagnago, Rosa Vono, Matthijs S. Ruiters, Anita C. Thomas, Paolo Madeddu, Maurizio Pesce and Gaia Spinetti

- 97 **The effect of percutaneous vs. cutdown access in patients after Endovascular aortic repair (SWEET): Study protocol for a single-blind, single-center, randomized controlled trial**
Yuhang Zhou, Jiarong Wang, Jichun Zhao, Ding Yuan, Chengxin Weng, Tiehao Wang and Bin Huang
- 106 **MAG11 inhibits interferon signaling to promote influenza A infection**
Yin Wang, Jun-ichi Abe, Khanh M. Chau, Yongxing Wang, Hang Thi Vu, Loka Reddy Velatooru, Fahad Gulraiz, Masaki Imanishi, Venkata S. K. Samanthapudi, Minh T. H. Nguyen, Kyung Ae Ko, Ling-Ling Lee, Tamlyn N. Thomas, Elizabeth A. Olmsted-Davis, Sivareddy Kotla, Keigi Fujiwara, John P. Cooke, Di Zhao, Scott E. Evans and Nhat-Tu Le
- 124 **Simplification of ankle-brachial-index measurement using Doppler-waveform classification in symptomatic patients suspected of lower extremity artery disease**
Antoine Métairie, Quentin Tollenaere, Damien Lanéelle, Alexis Le Faucheur, Estelle Le Pabic, Loukman Omarjee and Guillaume Mahé
- 134 **Expanding role of deoxyribonucleic acid-sensing mechanism in the development of lifestyle-related diseases**
Sachiko Nishimoto, Masataka Sata and Daiju Fukuda
- 148 **Distinct role of mitochondrial function and protein kinase C in intimal and medial calcification *in vitro***
Marina A. Heuschkel, Anne Babler, Jonas Heyn, Emiel P. C. van der Vorst, Marja Steenman, Maren Gesper, Ben A. Kappel, David Magne, Yann Gouëffic, Rafael Kramann, Willi Jahnen-Dechent, Nikolaus Marx, Thibaut Quillard and Claudia Goettsch
- 166 **Sox13 is a novel flow-sensitive transcription factor that prevents inflammation by repressing chemokine expression in endothelial cells**
Catherine Demos, Janie Johnson, Aitor Andueza, Christian Park, Yerin Kim, Nicolas Villa-Roel, Dong-Won Kang, Sandeep Kumar and Hanjoong Jo
- 185 **Dual pathway inhibition as compared to acetylsalicylic acid monotherapy in relation to endothelial function in peripheral artery disease, a phase IV clinical trial**
Loes H. Willems, Dick H. J. Thijssen, Laszlo A. Groh, Nina I. Kooijman, Hugo Ten Cate, Henri M. H. Spronk, A. Rogier T. Donders, Rozemarijn J. van der Vijver-Coppen, Frank van Hoek, Magdolna Nagy, Michel M. P. J. Reijnen and Michiel C. Warlé
- 195 **DANCER: Study protocol of a prospective, non-randomized controlled trial for crossed limb versus standard limb configuration in endovascular abdominal aortic aneurysm repair**
Yinzhi Shen, Jiarong Wang, Jichun Zhao, Ding Yuan, Tiehao Wang and Bin Huang

- 204 **The ethanol extract of *Edgeworthia gardneri* (Wall.) Meisn attenuates macrophage foam cell formation and atherogenesis in ApoE^{-/-} mice**
Le Tang, Cuifang Kuang, Dan Shan, Min Shi, Jiangsheng Li, Liang Qiu and Jun Yu
- 218 **Arterial dissections: Common features and new perspectives**
Monique Bax, Valentin Romanov, Keerat Junday, Eleni Giannoulatou, Boris Martinac, Jason C. Kovacic, Renjing Liu, Siiri E. Iismaa and Robert M. Graham
- 246 **Endothelial ADAM10 controls cellular response to oxLDL and its deficiency exacerbates atherosclerosis with intraplaque hemorrhage and neovascularization in mice**
Emiel P. C. van der Vorst, Sanne L. Maas, Kosta Theodorou, Linsey J. F. Peters, Han Jin, Timo Rademakers, Marion J. Gijbels, Mat Rousch, Yvonne Jansen, Christian Weber, Michael Lehrke, Corinna Lebherz, Daniela Yildiz, Andreas Ludwig, Jacob F. Bentzon, Erik A. L. Biessen and Marjo M. P. C. Donners
- 259 **Genetic deficiency of protein inhibitor of activated STAT3 suppresses experimental abdominal aortic aneurysms**
Weilai Fu, Haole Liu, Panpan Wei, Congcong Xia, Qingqing Yu, Kangli Tian, Yankui Li, Enqi Liu, Baohui Xu, Masaaki Miyata, Rong Wang and Sihai Zhao
- 266 **Role of plaque imaging for identification of vulnerable patients beyond the stage of myocardial ischemia**
Ryoko Kitada, Kenichiro Otsuka and Daiju Fukuda
- 280 **Use of the Walking Impairment Questionnaire and Walking Estimated-Limitation Calculated by History questionnaire to detect maximal walking distance equal to or lower than 250 m in patients with lower extremity arterial disease**
Quentin Tollenaere, Antoine Métairie, Estelle Le Pabic, Alexis Le Faucheur and Guillaume Mahé
- 292 **The interplay between nonalcoholic fatty liver disease and atherosclerotic cardiovascular disease**
Alexandra C. Finney, Sandeep Das, Dhananjay Kumar, M. Peyton McKinney, Bishuang Cai, Arif Yurdagul Jr and Oren Rom



Deciphering Cell-Cell Communication in Abdominal Aortic Aneurysm From Single-Cell RNA Transcriptomic Data

Huan Yang¹, Elise DeRoo¹, Ting Zhou^{1*} and Bo Liu^{1,2*}

¹ Department of Surgery, School of Medicine and Public Health, University of Wisconsin-Madison, Madison, WI, United States, ² Department of Cellular and Regenerative Biology, School of Medicine and Public Health, University of Wisconsin-Madison, Madison, WI, United States

OPEN ACCESS

Edited by:

Ha Won Kim,
Augusta University, United States

Reviewed by:

Yang Shi,
Augusta University, United States
Yanbo Fan,
University of Cincinnati Medical
Center, United States

*Correspondence:

Ting Zhou
zhou@surgey.wisc.edu
Bo Liu
liub@surgey.wisc.edu

Specialty section:

This article was submitted to
Atherosclerosis and Vascular
Medicine,
a section of the journal
Frontiers in Cardiovascular Medicine

Received: 08 December 2021

Accepted: 03 January 2022

Published: 04 February 2022

Citation:

Yang H, DeRoo E, Zhou T and Liu B
(2022) Deciphering Cell-Cell
Communication in Abdominal Aortic
Aneurysm From Single-Cell RNA
Transcriptomic Data.
Front. Cardiovasc. Med. 9:831789.
doi: 10.3389/fcvm.2022.831789

Cell-cell communication coordinates cellular differentiation, tissue homeostasis, and immune responses in states of health and disease. In abdominal aortic aneurysm (AAA), a relatively common and potentially life-threatening vascular disease, intercellular communications between multiple cell types are not fully understood. In this study, we analyzed published single-cell RNA sequencing (scRNA-seq) datasets generated from the murine CaCl₂ model, perivascular elastase model, Angiotensin II model, and human AAA using bioinformatic approaches. We inferred the intercellular communication network in each experimental AAA model and human AAA and predicted commonly altered signaling pathways, paying particular attention to thrombospondin (THBS) signaling between different cell populations. Together, our analysis inferred intercellular signaling in AAA based on single-cell transcriptomics. This work provides important insight into cell-cell communications in AAA and has laid the groundwork for future experimental investigations that can elucidate the cell signaling pathways driving AAA.

Keywords: abdominal aortic aneurysm, cell-cell communication, single-cell RNA sequencing, thrombospondin, animal models

INTRODUCTION

Abdominal aortic aneurysm (AAA), defined as a focal dilation of the abdominal aorta beyond 50% of its normal diameter, is a common and potentially lethal aortic disease (1). Decades of basic and clinical research have revealed multiple molecular processes that underlie the development and growth of AAAs, including infiltration of immune cells, degeneration of extracellular matrix (ECM), and depletion of medial smooth muscle cells (SMCs) (2). Experimental data also implicate the importance of intercellular communication between inflammatory cells and SMCs during aneurysm development (3). Various anti-inflammatory strategies that were found to prevent aneurysm formation in mice were shown to reduce SMC death and preserve the contractile phenotype in the aortic wall (4, 5). Reciprocally, inhibiting cell death in aneurysm models has been shown to reduce intra-aortic accumulation of inflammatory cells (6, 7). Despite these early insights, a comprehensive understanding of communication patterns between different cell populations in healthy and aneurysmal aorta remains elusive.

Single-cell RNA sequencing (scRNA-seq) is a powerful research tool that has been recently employed by multiple groups to investigate transcriptomic profiles of human and experimental aortic aneurysm tissue at single-cell resolution (3, 8–11). The large data sets produced by published scRNA-seq studies confirmed the involvement of multiple cell types and subtypes in aneurysm pathophysiology. In addition, the published scRNA-seq data contained information on gene expression of ligands, receptors, and cofactors that could be used to analyze cell-cell communication status in the tissues (12, 13). CellChat is an analytic tool developed by Jin and colleagues that quantitatively deduces intercellular communication networks from scRNA-seq data (14). In this study, we applied CellChat to our scRNA-seq dataset as well as other published datasets generated from analyzing murine and human AAA tissues. Our data inferred the intercellular communication status of healthy and diseased aortas, and predicted potential signaling pathways altered by AAA in each model.

MATERIALS AND METHODS

CaCl₂-, elastase-, or Angiotensin II (Ang II) induced mouse experimental AAA as well as human AAA scRNA-seq datasets were downloaded from the NCBI GEO data repository (GSE164678, GSE152583, GSE118237, and GSE166676). Data preprocessing, normalization, scaling, and cell clustering were performed with Seurat package (version 4.0.3) in R (version 4.1.1) environment (15). Cell populations were determined using the marker genes in the original studies (3, 9–11). Red blood cells were excluded for cell-cell interaction analysis. Seurat preprocessed data was then subjected to CellChat package (version 1.1.3) to infer, analyze, and visualize cell-cell communication (14). The ligand-receptor interaction database was included in the package. Conserved and context-specific signaling pathways identified by CellChat were subjected to EVenN to generate Venn diagrams or Venn networks for the visualization for set relationships (16).

Statistics

Statistical analysis was performed within the CellChat package. Interaction strength represents ligand-receptor mediated intercellular communication probability, quantified by the law of mass action. Incoming (or outgoing) interaction strength is the communication probabilities of the incoming (or outgoing) signaling to (or from) a cell population. The overall information flow for a given signaling pathway is the sum of communication probability among all pairs of cell groups in the inferred network (14).

RESULTS

Cell-Cell Communication in Murine CaCl₂ Model

CellChat is an R toolkit that includes a database comprising 2,021 validated mouse molecular interactions or 1,939 human molecular interactions between signaling ligands, receptors, and their cofactors (14). The communication probability of a specific

signaling pathway (such as COLLAGEN signaling) was the sum of the communication probability of each ligand-receptor pair of that specific signaling pathway. We evaluated cell-cell communication patterns in the murine CaCl₂ model by applying CellChat to the scRNA-seq dataset published by our lab (GSE164678). In that study, we perivascularly treated the infrarenal abdominal aortas of C57BL/6J mice with 0.5 M CaCl₂ (AAA group) or NaCl (sham group). Aortas were collected 4 days after AAA induction (10) to capture acute transcriptional responses within the aortic wall. This CaCl₂ scRNA-seq dataset contains 3,896 cells in total, including 2,537 cells from the sham group and 1,359 cells from the AAA group. Cells were clustered into 12 populations, including two fibroblast (Fib), two smooth muscle cell (SMC), and three macrophage (Maph) populations, as well as several other cell types such as endothelial cell (EC), neutrophil (Neutro), dendritic cell (DC), T and natural killer cell (T/NK), and B cell (**Supplementary Figure 1A**).

CellChat analysis of the CaCl₂ dataset revealed 8,799 total ligand-receptor interactions in the sham group and 8,601 interactions in the AAA group (**Supplementary Figure 1B**). The strength of a given ligand-receptor interaction is quantified by a probability value. This probability value is modeled by the law of mass action based on the average expression value of a ligand by one cell group and the expression value of a corresponding receptor in another cell group, as well as the cofactors of the ligand or receptor (14). On post-surgery day 4, the total interaction strength of the AAA group was moderately lower than that of the sham group (**Figure 1A**). When comparing the outgoing and incoming signals of each cell population in sham and AAA tissues, we found that SMCs and Fib-1 were the major signaling sources, and that SMCs also functioned as the major signaling target in both tissues (**Figure 1B**). Compared to the sham group, AAA induction increased signals sent from Maph-2 to SMC-1 and from DC to SMC-2, and decreased signals from fibroblasts (Fib-1 and Fib-2) and SMCs (SMC-1 and SMC-2) to SMC-2 (**Figure 1C**).

To identify the conserved and context-specific signaling pathways induced by AAA, we compared the overall information flow for each signaling pathway, which was defined by the sum of communication probability among all cell populations in each condition (14). As shown in **Figure 1D**, the majority of signaling pathways were found in both sham and AAA groups. There were seven signaling pathways (PTN, ANNEXIN, GDF, VISTA, CD6, ALCAM, SN) unique to sham, and three pathways (TNF, FASLG, LIFR) unique to AAA.

We next investigated the signaling changes in each population. Since SMC-1 and SMC-2 are enriched in transcripts related to the contractile and synthetic phenotypes, respectively (10), we examined signaling activities of these two cell populations more closely. AAA induction increased incoming SPP1 signaling and decreased incoming LAMININ signaling in both SMC-1 and SMC-2. In contrast, SMC-1 of the AAA group showed more outputs related to THBS signaling and less COLLAGEN signaling, whereas SMC-2 sent less THBS signaling and more COLLAGEN signaling upon AAA stimulation. Of note, SPP1 signaling in SMC-1 was AAA specific, which means in the sham group SPP1 signaling was undetectable (**Figures 1E,F**). All

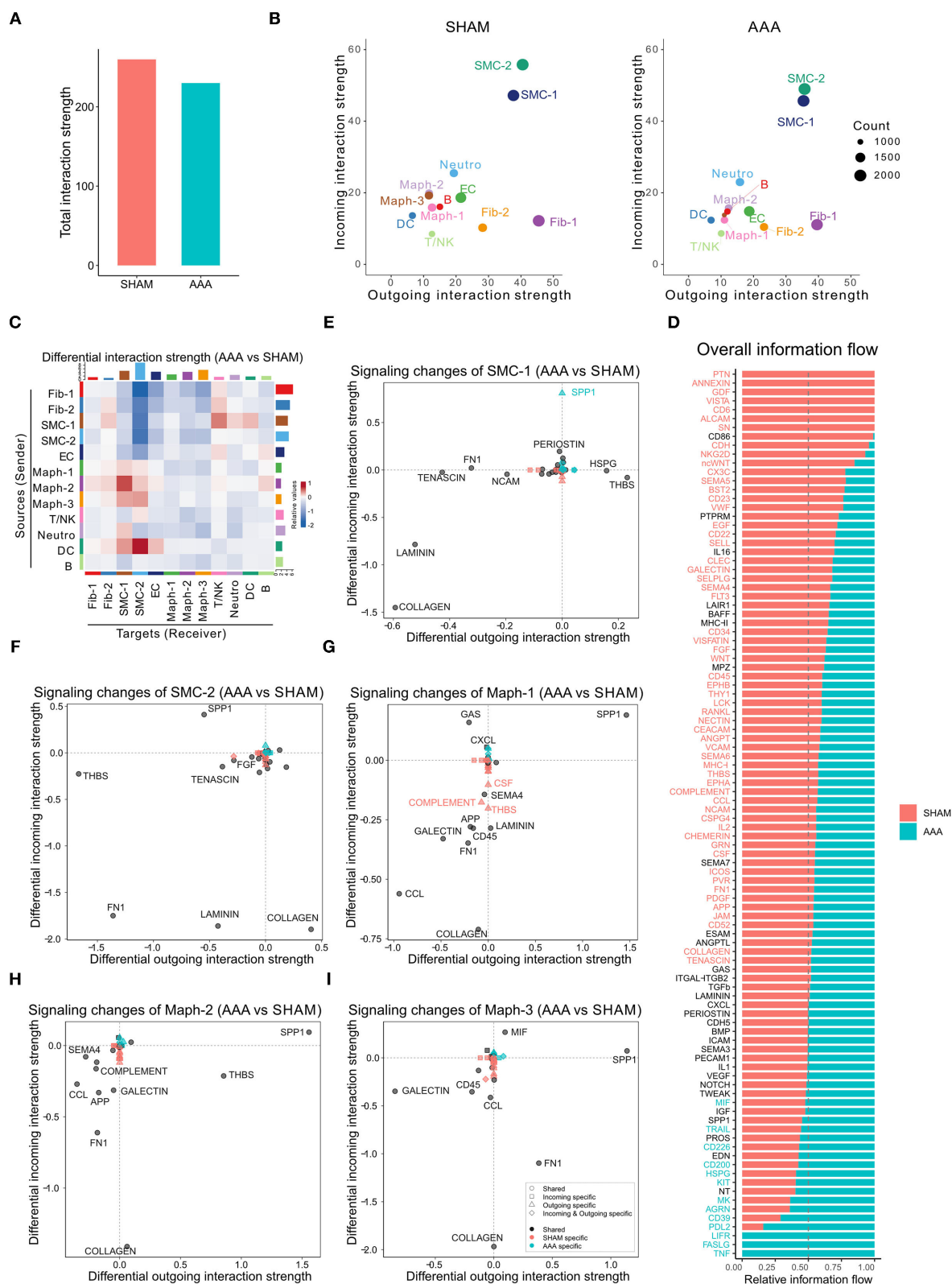


FIGURE 1 | Inferred intercellular communication network in the murine CaCl_2 model. **(A)** Total interaction strength in sham (NaCl treated) and AAA (CaCl_2 treated) groups. **(B)** Scatter plot of incoming and outgoing interaction strength of each cell population in sham and AAA groups. **(C)** Heatmap of differential interaction strength in AAA group compared to sham group. The top colored bar plot represents the sum of column of values displayed in the heatmap (incoming signaling). (Continued)

FIGURE 1 | The right colored bar plot represents the sum of row of values (outgoing signaling). In the heatmap, red (or blue) represents increased (or decreased) signaling in AAA compared to sham group. Relative value = the interaction strength from source to target in AAA group – the interaction strength from source to target in sham group. **(D)** Overall information flow of each signaling pathway in sham and AAA groups. Relative information flow is the ratio of the communication probability of a certain group (sham or AAA group) relative to sham and AAA combined. **(E–I)** Signaling changes of SMC-1 **(E)**, SMC-2 **(F)**, Maph-1 **(G)**, Maph-2 **(H)**, Maph-3 **(I)** in AAA compared to sham group.

three macrophage populations sent out more SPP1 signaling and received less COLLAGEN signaling in AAA group compared to sham. Maph-2 also sent out more THBS signaling in the AAA group (**Figures 1G–I**). Fibroblasts showed elevated incoming COLLAGEN signals and reduced outgoing COLLAGEN signals (**Supplementary Figure 1C**).

Cell-Cell Communication in Murine Peri-Adventitial Elastase Model

We next analyzed the scRNA-seq dataset published by Zhao et al. using the peri-adventitial elastase model (GSE152583) (11). In this model, infrarenal abdominal aortas from C57BL/6J mice were treated with 30 μ l elastase or heat-inactivated elastase (control). Aortas were collected 7 or 14 days after elastase exposure or 14 days after heat-inactivated elastase exposure (control group) (11). After filtering out the red blood cells, we identified 16 cell populations using the markers from Zhao et al.'s study, including two fibroblast, two EC, three SMC, three macrophage, and two DC populations, as well as T cells, B cells, NK cells, and neural cells (**Supplementary Figure 2A**). Among the three macrophage populations, Maph-1 highly expressed the inflammatory gene *Il1b*, Maph-2 was enriched for the M2 macrophage marker *Cd163*, and Maph-3 expressed high levels of the proliferation marker *Mki67* (**Supplementary Figures 2D–G**). SMC-1 expressed high level of contractile genes such as *Acta2* (**Supplementary Figure 2H**). SMC-2 highly expressed inflammatory genes such as *Neat1* and *Cebpb* (**Supplementary Figures 2I,J**).

Application of CellChat to this dataset identified 7,233 total interactions in the control group, 10,453 interactions in Day 7 group, and 9,343 interactions in Day 14 group (**Supplementary Figure 2B**). We also calculated the interaction strength of all cell populations in each group. The AAA induction by elastase treatment increased communication probability over the control group, with higher interaction strength at Day 7 than Day 14 (**Figure 2A**). Additionally, the AAA induction altered the communication patterns (**Figures 2B–D**). In both AAA groups, SMCs and fibroblasts served as the major signal source and target. Macrophage populations, especially Maph-3 and Maph-1, showed increased incoming signaling in elastase treatment groups compared to the control group (**Figures 2B–D**).

A more detailed dissection of the communication probability between each population highlights Fib-2 as an important node in aneurysmal tissues. Fib-2 received intensive signals from SMCs and fibroblasts and also sent abundant signals to SMCs and macrophages. Interestingly, SMC-3 became idle in response to elastase, sending fewer signals to the SMC populations compared to control (**Figures 2E,F**). Comparing Day 14 with Day 7, signals sent from Fib-2 to B cells and NK

cells, as well as Fib-2 autocrine signaling were further elevated (**Supplementary Figure 2C**).

We next examined the overall changes in each signaling pathway in both conditions. As shown in **Figure 2G** and **Supplementary Figures 2K,L**, five signaling pathways were exclusively expressed in the control group (ncWNT, IL16, CEACAM, OCLN, and NEGR) and 21 pathways were only expressed by elastase treated groups. Among these 21 pathways, 5 of them were only expressed by Day 7 group (SN, CD23, BAFF, CD137, and TRAIL), and 4 out of 21 pathways were expressed only by Day 14 group (CALCR, SEMA7, VISTA, and CX3C).

We further evaluated the specific signaling pathways that were altered during the early aneurysmal response. In macrophages, particularly Maph-1 (the pro-inflammatory type), THBS signaling was prominent in the elastase treated group however absent in the control. All macrophage populations also showed elevated incoming COLLAGEN signaling and increased outgoing SPP1, MIF, and GALECTIN signaling. Outgoing COLLAGEN signaling was also upregulated, but only in Maph-2 and Maph-3. Similarly, COLLAGEN signaling was also the most increased incoming signaling pathway in all SMC populations and the most enhanced outgoing signaling pathway in SMC-1 and SMC-2 (**Figure 2H**). All fibroblast populations showed elevated incoming and outgoing COLLAGEN as well as FN1 signaling (**Supplementary Figure 2M**).

Cell-Cell Communication in Murine Ang II Model

We next examined the scRNA-seq dataset published by Hadi et al. (GSE118237) (3). In this model, *Apoe*^{-/-} mice were infused with 1,000 ng/kg/min Ang II *via* osmotic pumps for 28 days. No control group was included in this data set. Our analysis identified nine cell populations, including two SMC, two fibroblast, two EC populations, and macrophage, T/NK, and B cell populations (**Supplementary Figure 3A**). Specifically, SMC-1, the cell population characterized by enrichment of contractile marker *Myh11* (**Supplementary Figure 3B**), was the major signal sender and receiver (**Figure 3A**). As shown in **Figure 3B**, fibroblast and SMC populations were the major signal source, and SMC-1 was the major signal receiver. COLLAGEN, FN1, LAMININ, THBS, APP, and TENASCIN were overall highly expressed signaling pathways.

Cell-Cell Communication in Human Aneurysm Tissue

Davis et al. conducted scRNA-seq on infrarenal abdominal aortas of patients undergoing open aortic aneurysm repair (AAA group) or open aortobifemoral bypass (control group) (GSE166676) (9). We identified 14 populations in this dataset,

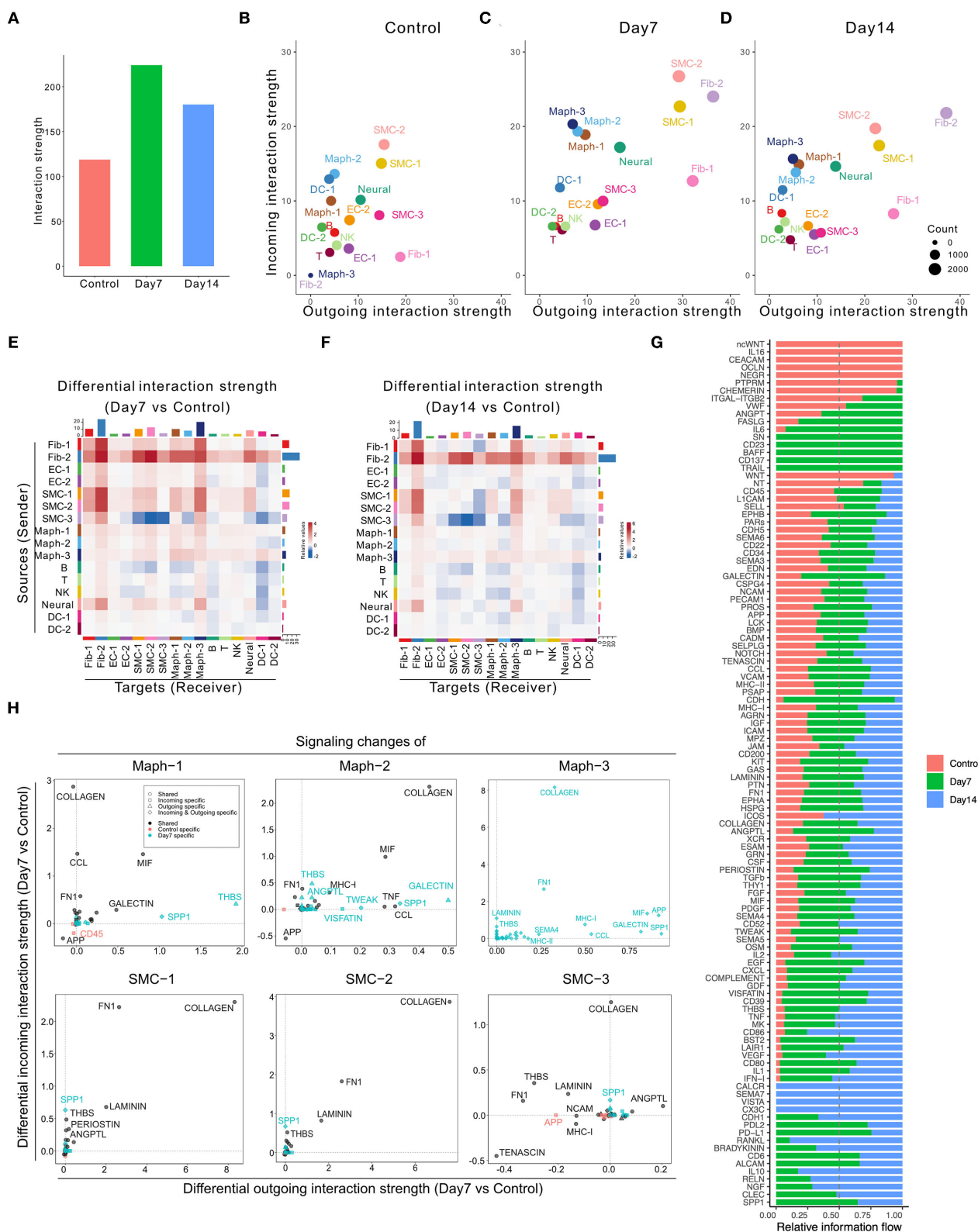
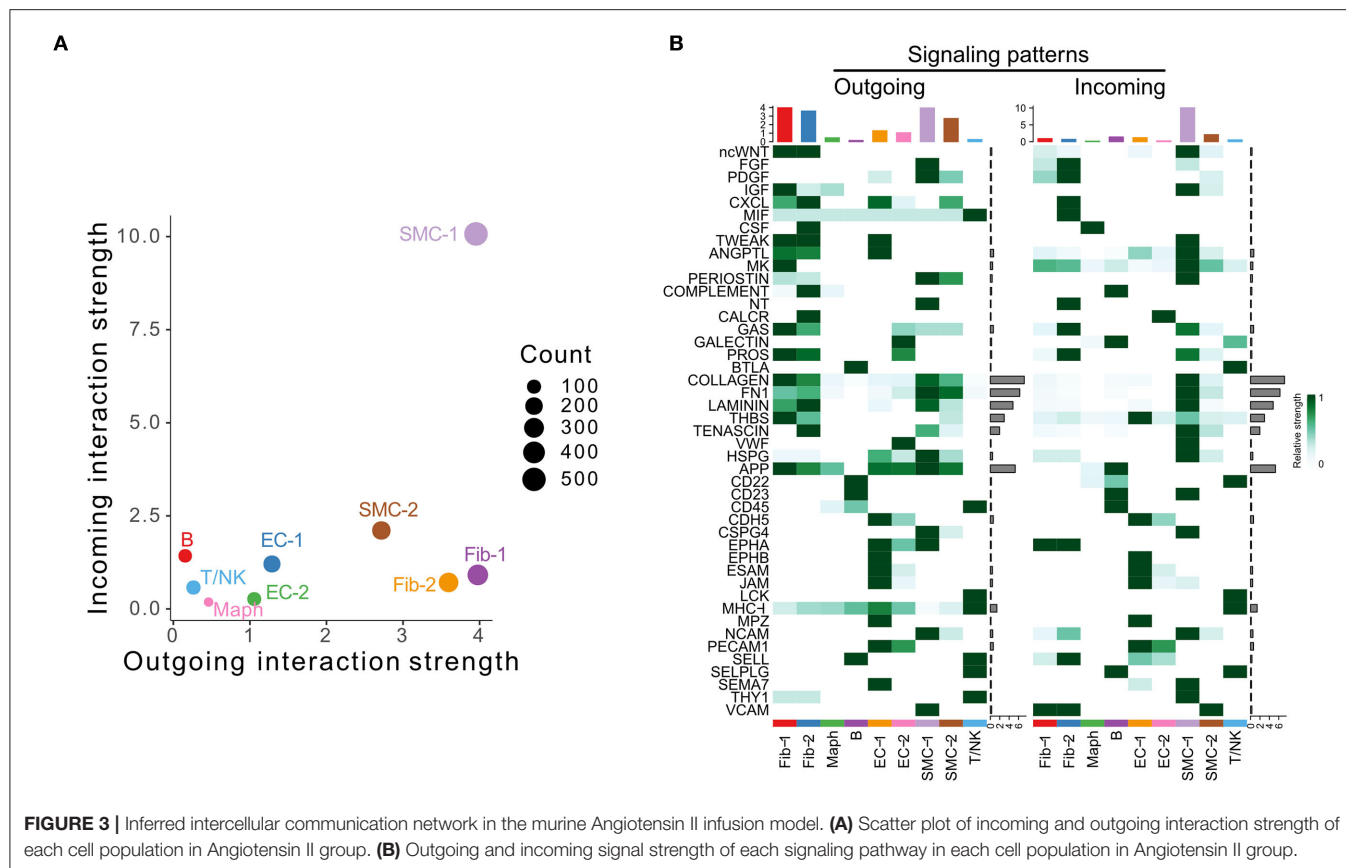


FIGURE 2 | Inferred intercellular communication network in the murine perivascular elastase model. **(A)** Total interaction strength in control, Day 7, and 14 groups. **(B–D)** Scatter plot of incoming and outgoing interaction strength of each cell population in control **(B)**, Day 7 **(C)**, and Day 14 **(D)** groups. **(E,F)** Heatmap of differential interaction strength in Day 7 compared to control group **(E)**, and Day 14 compared to control group **(F)**. The top colored bar plot represents the sum of column of *(Continued)*

FIGURE 2 | values displayed in the heatmap (incoming signaling). The right colored bar plot represents the sum of row of values (outgoing signaling). In the heatmap, red (or blue) represents increased (or decreased) signaling in Day 7 (E) or Day 14 (F) compared to control group. Relative value = the interaction strength from source to target in Day 7 (E) or Day 14 (F) group—the interaction strength from source to target in control group. (G) Overall information flow of each signaling pathway in control, Day 7, and 14 groups. Relative information flow is the ratio of the communication probability of a certain group (control, Day 7, or Day 14) relative to all groups combined. (H) Signaling changes of SMC and macrophage populations in Day 7 compared to control group.



including two monocyte and two macrophage populations, SMC, fibroblast, EC, CD4⁺ T cell, CD8⁺ T cell, NK, B, plasma, and mast cell populations, as well as one unknown population (Supplementary Figure 4A). We ran CellChat analysis on this dataset and identified 52 total interactions in the control group, and 972 total interactions in AAA group (Supplementary Figure 4B). The AAA group showed higher communication probability than the control group, as the interaction strength of control group was almost undetectable (Figures 4A,B). In the AAA group, SMC and fibroblast populations were the major signal senders, and the NK cell population was the major signal receiver (Figure 4C). Compared to the control group, the AAA group showed more signals sent from SMCs and fibroblasts to monocytes and macrophages, especially Mono-2 and Maph-1, as well as to B cells and mast cells. Signaling from Mono-2 to EC was the only decreased interaction in AAA compared to the control group (Figure 4D). Most signaling pathways were exclusively expressed in the AAA group, with only MK signaling being expressed primarily in the control group (Figure 4E). COLLAGEN signaling was

enhanced at both the incoming and outgoing level in SMC and fibroblast populations, and was also elevated among incoming signals in monocytes, macrophages, CD4⁺ T cells, B cells, and mast cells, especially in Mono-2 and Maph-1. There were more incoming MHC-II signals in Mono-1 and Maph-2 populations, and increased outgoing MHC-II signals from Maph-1 and B cells (Figure 4F and Supplementary Figure 4C).

Commonly Altered Signaling Pathways Among Different AAA Models

As demonstrated in Figures 1–4, numerous signaling pathways were significantly altered in aneurysm tissues. Among the altered pathways (including both upregulated and downregulated pathways), eight were common to all murine models and time points as well as human AAA tissue. These include the MK, MIF, COLLAGEN, PDGF, FN1, COMPLEMENT, THBS, and CLEC signaling pathways (Figure 5A). MIF signaling was upregulated in all AAA groups compared to their respective controls, and eight signaling pathways were upregulated in all murine AAA groups (MIF, KIT, MK, CD39, HSPG, TNE, CD200, and PDL2)

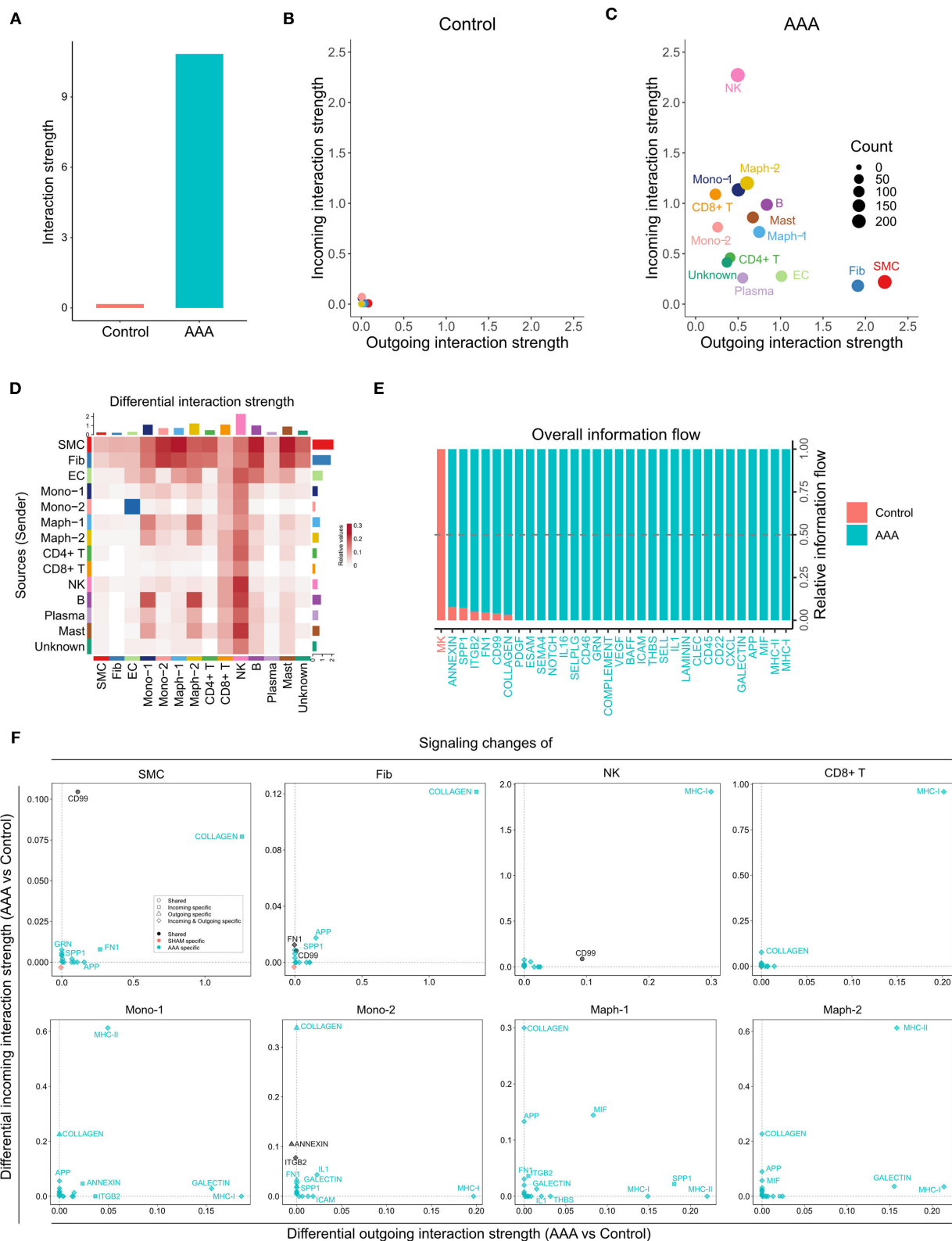


FIGURE 4 | Inferred intercellular communication network in human AAA tissues. **(A)** Total interaction strength in control and AAA samples. **(B,C)** Scatter plot of incoming and outgoing interaction strength of each cell population in control **(B)** and AAA **(C)** groups. **(D)** Heatmap of differential interaction strength in AAA compared to control group. The top colored bar plot represents the sum of column of values displayed in the heatmap (incoming signaling). The right colored bar plot represents (Continued)

FIGURE 4 | the sum of row of values (outgoing signaling). In the heatmap, red (or blue) represents increased (or decreased) signaling in AAA compared to control group. Relative value = the interaction strength from source to target in AAA group – the interaction strength from source to target in control group. **(E)** Overall information flow of each signaling pathway in control and AAA groups. Relative information flow is the ratio of the communication probability of a certain group (control or AAA group) relative to control and AAA combined. **(F)** Signaling changes of different cell populations in AAA compared to control group.

(Figure 5B). Regarding downregulated signaling pathways, three pathways were decreased in all murine AAA groups (ncWNT, CEACAM, CHEMERIN), while MK signaling was the only downregulated signaling pathway in human AAA (Figure 5C and Supplementary Figure 5).

THBS Signaling in AAA

Since we have previously reported the importance of thrombospondin-1 (TSP1)—the matricellular protein encoded by *THBS1*—in two murine AAA models, we examined THBS signaling in a greater detail. Consistent with our previous reports (17, 18), THBS signaling was found to be common to the three murine scRNA-seq data sets analyzed in the current study as well as to human AAA (3, 9–11). However, in each murine model and human AAA, THBS signaling appeared to be produced by different cell populations, received by different cell populations, and the contribution of each ligand-receptor pair was different.

In the sham group of the CaCl₂ model, SMC-2 and Fib-1 were the major cell types sending out THBS signaling. Upon AAA induction, THBS signaling sent from SMC-2 and Fib-1 populations was diminished, while signaling generated by Maph-2 was elevated. Specifically, THBS signaling sent from Maph-2 to SMC-1 or SMC-2 was most abundant in AAA (Figure 6A). Among the ligand-receptor pairs of THBS signaling, the Thbs1-Sdc4 ligand-receptor pair showed the highest communication probability, especially in Maph-2 to SMC-2 communication (Figure 6B). In contrast, the SMCs to macrophage communication that was prominent in sham tissue utilized the Thbs1-Cd47 ligand-receptor pair (Supplementary Figure 6A). As the communication probabilities were calculated based on the expression of ligands, receptors, and co-factors, we further plotted the gene expression of each ligand and receptor of THBS signaling. As shown in Supplementary Figure 6B, ligand Thbs1 was highly expressed by SMC-2 in the sham group, and reduced in AAA group. Thbs1 was also expressed by Maph-2, and its expression was elevated in AAA. Expression of receptor Sdc4 was also increased by AAA treatment in SMC-2, but Cd47 expression was comparable between sham and AAA in all populations.

In the peri-adventitia elastase model, THBS signaling was not highly expressed by the control group, but was elevated after elastase treatment. Signals from Fib-2 to SMCs and macrophages, and from Maph-1 to SMCs were increased the most by AAA induction (Figure 6C). Examination of each ligand-receptor pair in THBS signaling revealed that Thbs1-Sdc4 signaling was the dominant pathway from macrophages to SMCs, especially from Maph-1 to SMC-2 (Figure 6D). Thbs1-Sdc4 and Thbs1-Cd47 were responsible for communication from SMCs to macrophages, and from Fib-2 to fibroblasts, SMCs, and macrophages (Supplementary Figures 6C,D). Gene expression

of each ligand and receptor of THBS signaling also showed that Thbs1 was strongly induced by AAA in Fib-2 and Maph-1, and that receptors Sdc4 and Cd47 were increased by AAA in Fib-2 and Maph-3 (Supplementary Figure 6E).

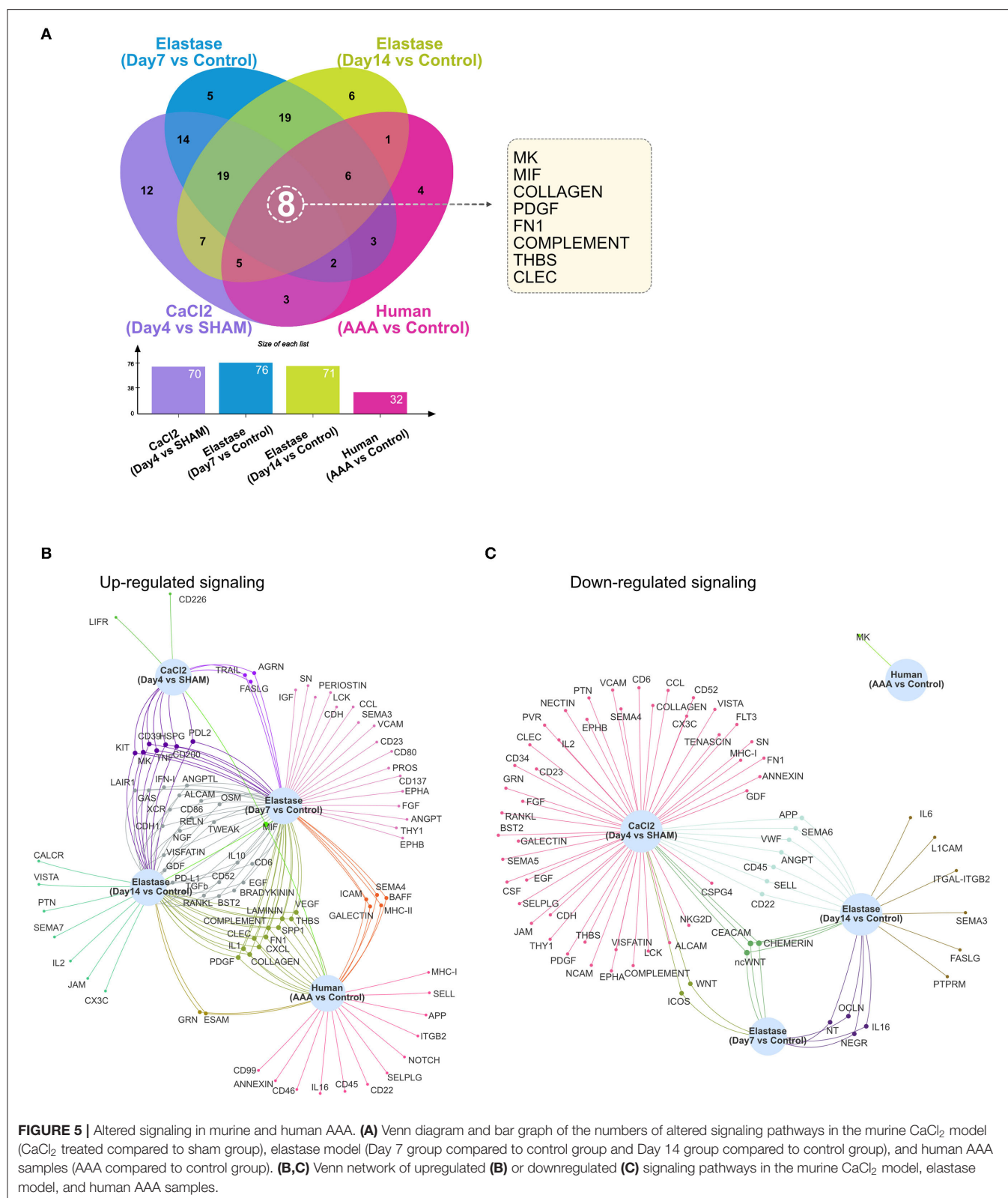
Similar to the elastase model, THBS signaling was not detected in control human aorta. In the human AAA group, THBS signaling originated from Maph-1 and was received by SMCs and other cell populations such as Mono-1, Maph-2, CD4+ T cells, B cells, NK cells, and Mast cells (Figure 6E). THBS1-CD47 was the main contributor of THBS signaling in the human AAA group (Figure 6F).

Since the murine Ang II model data set does not contain a control/sham group, we could only examine THBS signaling in the Ang II group. As shown in Supplementary Figures 6G,H, THBS signaling in this model was generated from Fib-1 and received by EC-1 (mediated by Comp-Cd36) and from Fib-2 to EC-1 (mediated by Thbs3-Cd36). Examination of ligand and receptor expression also confirmed that Comp and Thbs3 were highly expressed by Fib-1 and Fib-2 respectively, and that Cd36 was enriched in EC-1 (Supplementary Figure 6I).

DISCUSSION

Within a multicellular environment, cell-cell communication plays a fundamental role in governing tissue function, regulating individual cell processes, and intercellular relationships, thus driving tissue homeostasis and pathophysiology in states of health and disease (12, 13). Historically, studies investigating cell-cell communication could only be performed in the *in vitro* setting, examining one or two cell types and a limited number of genes at a time. This investigative approach fails to capture the rich network of cell-cell communications that occur in a diverse multicellular environment. In recent years, single-cell transcriptomics, which allows gene expression to be studied at the single-cell level, has generated an opportunity to examine complex networks of cell-cell communication in a multicellular community. Studies of single-cell transcriptomics in mouse models and human tissues have revealed cell clusters present in healthy and aneurysmal aortas. In this study, we inferred intercellular relationships between cell populations in AAA, in particular focusing on communications between SMCs and macrophages.

In an early-stage of the mouse CaCl₂ model (Day 4 after AAA induction), we predicted that SMCs were actively sending and receiving signals in both sham and AAA groups. CaCl₂ treatment increased signal sending from Maph-2 (pro-inflammatory macrophages) to SMC-1 (contractile SMCs). Among all the signaling pathways altered by AAA, SPP1 signaling was the most up-regulated outgoing signal in Maph-2, and the most



elevated incoming signal in SMC-1. Similarly, in an early-stage of the elastase model (Day 7), macrophages also sent out more SPP1 signals compared to control, and increased incoming SPP1

signaling was detected in SMCs. Spp1 encodes osteopontin, which participates in vascular calcification and is associated with the synthetic SMC phenotype (19, 20). Our analysis suggests that

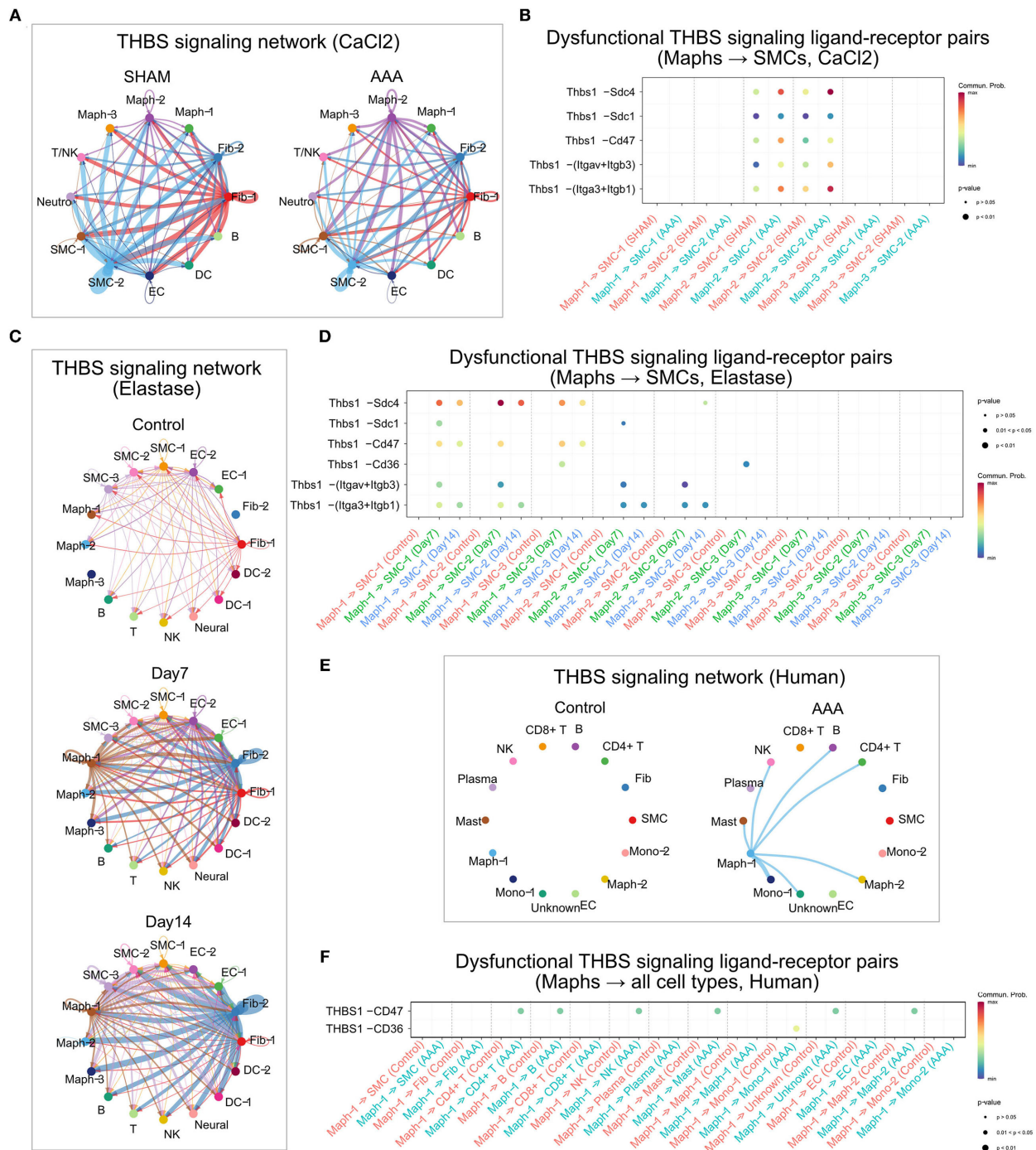


FIGURE 6 | THBS signaling in murine and human AAA. **(A,C,E)** Circle plot of THBS signaling network in the murine CaCl₂ model **(A)**, elastase model **(C)**, or human AAA **(E)**. The edge colors are consistent with the signal sender, and edge weights are proportional to the interaction strength. Thicker edge line indicates a stronger signal. **(B,D,F)** Bubble plot of the communication probability of all the significant ligand-receptor pairs that contributed to THBS signaling sent from macrophages to SMCs in the murine CaCl₂ model **(B)** or elastase model **(D)**, and from Maph-1 to each cell population in human AAA **(F)**. The dot color and size represent the communication probability and *p*-values, respectively. *p*-values were computed from one-sided permutation test.

pro-inflammatory macrophages may regulate SMC phenotypic changes through SPP1 signaling at an early-stage in murine AAA models.

In the perivascular elastase model, we inferred that fibroblasts became the primary signal source after elastase incubation. Signaling changes of each cell population also confirmed that

COLLAGEN signaling was the most increased outgoing signaling in fibroblasts, and the most elevated incoming signaling in SMCs, macrophages, and endothelial cells in the Day 7 group compared to the control group. In contrast, SMCs, macrophages, and endothelial cells in the CaCl_2 model received fewer COLLAGEN signals compared to the sham group; fibroblasts received more incoming COLLAGEN signals, but likely from synthetic SMCs. These results indicate that vascular remodeling and fibrosis may contribute to early progression of AAA in elastase model, but not CaCl_2 model.

Our analysis revealed that THBS signaling was one of the eight signaling pathways that were altered in all AAA groups compared to their respective controls. Thrombospondins are a family of secreted glycoproteins that regulate multiple biological processes such as angiogenesis, apoptosis, and migration (21). Among the five family members, TSP1 is most studied in the context of AAA. How TSP1 contributes to AAA pathogenesis is still not entirely clear. Our group found that TSP1 level was upregulated in human AAA as well as in murine models including CaCl_2 , Ang II, and intraluminal elastase perfusion model (17). In contrast, Krishna et al. reported reduced TSP1 expression in aneurysm tissues from AAA patients (22). Similarly, opposing outcomes were observed when globally deleting *Thbs1* in mouse models for AAA (17, 22). These controversial findings may highlight the cell type specificity of TSP1 functions in aneurysmal disease. TSP1 binds to a wide range of receptors including syndecans, CD36, integrins, and CD47 (23, 24), but the role of these ligand-receptor pairs in AAA has not been investigated.

In this study, we inferred that synthetic SMCs (SMC-2) were the main source of THBS signaling in the sham group of CaCl_2 model. AAA treatment decreased THBS signals sent from SMC-2, and enhanced THBS signals sent from pro-inflammatory macrophages (Maph-2) to other cell types, especially SMCs. This finding is consistent with our previous publication in which we showed that macrophages are the major source of TSP1 in murine CaCl_2 , Ang II models, and human AAA tissues (18). By analyzing each ligand-receptor pair of THBS signaling between macrophages and SMCs, we identified that *Thbs1-Sdc4* was the most elevated pathway sent from Maph-2 to SMCs (especially synthetic SMC-2), and that *Thbs1-Cd47* signaling sent from SMC-2 to macrophages (especially pro-inflammatory Maph-2) was decreased by AAA. Expression of each THBS signaling gene further showed that ligand *Thbs1* expression was increased in Maph-2 and decreased in SMC-2. Receptor *Sdc4* expression was elevated in SMC-2, explaining the signaling changes between macrophages and SMCs.

In the elastase model, THBS signaling was relatively quiescent in the control group, but was induced by elastase stimulation. Similar to the CaCl_2 model, the *Thbs1-Sdc4* pathway was also the most increased pathway sent from pro-inflammatory macrophages (Maph-1) to SMCs (especially synthetic SMC-2). Of note, *Thbs1-Sdc4* signaling was increased the most at Day 7, and slightly decreased at Day 14. Expression of each THBS signaling gene also showed that, in Maph-1, *Thbs1* was robustly increased at Day 7 and slightly decreased at Day 14 compared to control. *Thbs1-Sdc4* and *Thbs1-Cd47* were the major signaling pathways sent from SMCs (SMC-3) to

macrophages. In contrast to observations in macrophages, these two signaling pathways were most elevated at Day 14, consistent with the up-regulated expression of *Thbs1* in SMC-3 at Day 14. These results suggested that THBS signaling from pro-inflammatory macrophages to SMCs was activated at early stage, and from SMCs to macrophages at a later stage.

This study has several limitations. First, our analysis infers cell-cell communication based on gene expression of ligands and their receptors and cofactors, while cell signaling ultimately occurs at the protein level. In the setting of post-transcriptional and post-translational modifications, as well as multi-subunit protein complex assembly, gene expression may not always accurately reflect protein level. Second, the proximity of cells, ligands, cofactors, and receptors to one another is critically important to cell signaling. Many ligands activate signaling cascades either by diffusing through the extracellular environment from a sender cell to a nearby receiver cell, or through gap-junctions between directly adjacent cells. Unfortunately, this spatial information is not captured in scRNA-seq data (12). In addition, the ligand-receptor database used in this study is CellChatDB, which is included in the CellChat package. It is a manually curated database of literature-supported ligand-receptor interactions in both human and mouse. CellChatDB in mouse contains 2,021 validated molecular interactions, and is composed of 60% secreted autocrine/paracrine signaling interactions, 21% extracellular matrix (ECM)-receptor interactions, and 19% cell-cell contact interactions. CellChatDB in human contains 1,939 validated molecular interactions, and is composed of 61.8% paracrine/autocrine signaling interactions, 21.7% extracellular matrix (ECM)-receptor interactions, and 16.5% cell-cell contact interactions (14). The inference of cell-cell communication relies highly upon the quality of the ligand-receptor database, and different ligand-receptor databases used in different computational tools could lead to various predicted results. Finally, currently there is no single animal model that mimics the full clinical characteristics of human AAA, and human AAA tissue can only be obtained at an advanced stage during surgical repair. In this study, we predicted cell-cell communication in human AAA and different animal models at different disease stages. Validation of these intercellular signaling networks would be informative.

In conclusion, we inferred intercellular communication networks in the murine CaCl_2 model, elastase model, and Ang II model, as well as in human AAA. Our analysis also predicted commonly altered signaling pathways in AAA, paying particular attention to THBS signaling between different cell populations. Our data provide a guide for future experimental investigations to elucidate the cell-cell communications driving AAA.

DATA AVAILABILITY STATEMENT

The datasets presented in this study can be found in online repositories. The names of the repository/repositories and accession number(s) can be found in the article/Supplementary Material.

AUTHOR CONTRIBUTIONS

HY, TZ, and BL designed research studies. HY analyzed data. TZ, ED, and BL wrote the manuscript. All authors contributed to the article and approved the submitted version.

FUNDING

This study was supported by the National Institute of Health (R01HL149404 and R01HL158073-01 to

BL, and F32HL158171-01 to ED) and the American Heart Association (17POST33680095 and 20CDA3535 0009 to TZ).

SUPPLEMENTARY MATERIAL

The Supplementary Material for this article can be found online at: <https://www.frontiersin.org/articles/10.3389/fcvm.2022.831789/full#supplementary-material>

REFERENCES

- Chaikof EL, Dalman RL, Eskandari MK, Jackson BM, Lee WA, Mansour MA, et al. The Society for Vascular Surgery practice guidelines on the care of patients with an abdominal aortic aneurysm. *J Vasc Surg.* (2018) 67:2–77.e72. doi: 10.1016/j.jvs.2017.10.044
- Quintana RA, Taylor WR. Cellular mechanisms of aortic aneurysm formation. *Circ Res.* (2019) 124:607–18. doi: 10.1161/CIRCRESAHA.118.313187
- Hadi T, Boytard L, Silvestro M, Alebrahim D, Jacob S, Feinstein J, et al. Macrophage-derived netrin-1 promotes abdominal aortic aneurysm formation by activating MMP3 in vascular smooth muscle cells. *Nat Commun.* (2018) 9:5022. doi: 10.1038/s41467-018-07495-1
- Salmon M, Johnston WF, Woo A, Pope NH, Su G, Upchurch GR Jr, et al. KLF4 regulates abdominal aortic aneurysm morphology and deletion attenuates aneurysm formation. *Circulation.* (2013) 128:S163–174. doi: 10.1161/CIRCULATIONAHA.112.000238
- Li G, Qin L, Wang L, Li X, Caulk AW, Zhang J, et al. Inhibition of the mTOR pathway in abdominal aortic aneurysm: implications of smooth muscle cell contractile phenotype, inflammation, and aneurysm expansion. *Am J Physiol Heart Circ Physiol.* (2017) 312:H1110–9. doi: 10.1152/ajpheart.00677.2016
- Yamanouchi D, Morgan S, Kato K, Lengfeld J, Zhang F, Liu B. Effects of caspase inhibitor on angiotensin II-induced abdominal aortic aneurysm in apolipoprotein E-deficient mice. *Arterioscler Thromb Vasc Biol.* (2010) 30:702–7. doi: 10.1161/ATVBAHA.109.200527
- Zhou T, Wang Q, Phan N, Ren J, Yang H, Feldman CC, et al. Identification of a novel class of RIP1/RIP3 dual inhibitors that impede cell death and inflammation in mouse abdominal aortic aneurysm models. *Cell Death Dis.* (2019) 10:226. doi: 10.1038/s41419-019-1468-6
- Boytard L, Hadi T, Silvestro M, Qu H, Kumpfbek A, Sleiman R, et al. Lung-derived HMGB1 is detrimental for vascular remodeling of metabolically imbalanced arterial macrophages. *Nat Commun.* (2020) 11:4311. doi: 10.1038/s41467-020-18088-2
- Davis FM, Tsoi LC, Melvin WJ, Dendekker A, Wasikowski R, Joshi AD, et al. Inhibition of macrophage histone demethylase JMJD3 protects against abdominal aortic aneurysms. *J Exp Med.* (2021) 218:e20201839. doi: 10.1084/jem.20201839
- Yang H, Zhou T, Stranz A, Deroo E, Liu B. Single-cell RNA sequencing reveals heterogeneity of vascular cells in early stage murine abdominal aortic aneurysm—brief report. *Arterioscler Thromb Vasc Biol.* (2021) 41:1158–66. doi: 10.1161/ATVBAHA.120.315607
- Zhao G, Lu H, Chang Z, Zhao Y, Zhu T, Chang L, et al. Single-cell RNA sequencing reveals the cellular heterogeneity of aneurysmal infrarenal abdominal aorta. *Cardiovasc Res.* (2021) 117:1402–16. doi: 10.1093/cvr/cvab214
- Almet AA, Cang Z, Jin S, Nie Q. The landscape of cell-cell communication through single-cell transcriptomics. *Curr Opin Syst Biol.* (2021) 26:12–23. doi: 10.1016/j.coisb.2021.03.007
- Armingol E, Officer A, Harismendy O, Lewis NE. Deciphering cell-cell interactions and communication from gene expression. *Nat Rev Genet.* (2021) 22:71–88. doi: 10.1038/s41576-020-00292-x
- Jin S, Guerrero-Juarez CF, Zhang L, Chang I, Ramos R, Kuan CH, et al. Inference and analysis of cell-cell communication using CellChat. *Nat Commun.* (2021) 12:1088. doi: 10.1038/s41467-021-21246-9
- Hao Y, Hao S, Andersen-Nissen E, Mauck WM 3rd, Zheng S, Butler A, et al. Integrated analysis of multimodal single-cell data. *Cell.* (2021) 184:3573–87.e3529. doi: 10.1016/j.cell.2021.04.048
- Chen T, Zhang H, Liu Y, Liu YX, Huang L. EYenn: Easy to create repeatable and editable Venn diagrams and Venn networks online. *J Genet Genomics.* (2021) 48:863–6. doi: 10.1016/j.jgg.2021.07.007
- Liu Z, Morgan S, Ren J, Wang Q, Annis DS, Mosher DF, et al. Thrombospondin-1 (TSP1) contributes to the development of vascular inflammation by regulating monocytic cell motility in mouse models of abdominal aortic aneurysm. *Circ Res.* (2015) 117:129–41. doi: 10.1161/CIRCRESAHA.117.305262
- Yang H, Zhou T, Sorenson CM, Sheibani N, Liu B. Myeloid-derived TSP1 (Thrombospondin-1) contributes to abdominal aortic aneurysm through suppressing tissue inhibitor of metalloproteinases-1. *Arterioscler Thromb Vasc Biol.* (2020) 40:e350–66. doi: 10.1161/ATVBAHA.120.314913
- Speer MY, Chien YC, Quan M, Yang HY, Vali H, McKee MD, et al. Smooth muscle cells deficient in osteopontin have enhanced susceptibility to calcification *in vitro*. *Cardiovasc Res.* (2005) 66:324–33. doi: 10.1016/j.cardiores.2005.01.023
- Rensen SS, Doevedans PA, Van Eys GJ. Regulation and characteristics of vascular smooth muscle cell phenotypic diversity. *Neth Heart J.* (2007) 15:100–8. doi: 10.1007/BF03085963
- Adams JC, Lawler J. The thrombospondins. *Cold Spring Harb Perspect Biol.* (2011) 3:a009712. doi: 10.1101/cshperspect.a009712
- Krishna SM, Seto SW, Jose R, Li J, Moxon J, Clancy P, et al. High serum thrombospondin-1 concentration is associated with slower abdominal aortic aneurysm growth and deficiency of thrombospondin-1 promotes angiotensin II induced aortic aneurysm in mice. *Clin Sci.* (2017) 131:1261–81. doi: 10.1042/CS20160970
- Isenberg JS, Roberts DD. THBS1 (thrombospondin-1). *Atlas Genet Cytogenet Oncol Haematol.* (2020) 24:291–9. doi: 10.4267/2042/70774
- Morandi V, Petrik J, Lawler J. Endothelial cell behavior is determined by receptor clustering induced by thrombospondin-1. *Front Cell Dev Biol.* (2021) 9:664696. doi: 10.3389/fcell.2021.664696

Conflict of Interest: The authors declare that the research was conducted in the absence of any commercial or financial relationships that could be construed as a potential conflict of interest.

Publisher's Note: All claims expressed in this article are solely those of the authors and do not necessarily represent those of their affiliated organizations, or those of the publisher, the editors and the reviewers. Any product that may be evaluated in this article, or claim that may be made by its manufacturer, is not guaranteed or endorsed by the publisher.

Copyright © 2022 Yang, DeRoo, Zhou and Liu. This is an open-access article distributed under the terms of the Creative Commons Attribution License (CC BY). The use, distribution or reproduction in other forums is permitted, provided the original author(s) and the copyright owner(s) are credited and that the original publication in this journal is cited, in accordance with accepted academic practice. No use, distribution or reproduction is permitted which does not comply with these terms.



Low Molecular Weight Apolipoprotein(a) Phenotype Rather Than Lipoprotein(a) Is Associated With Coronary Atherosclerosis and Myocardial Infarction

Olga I. Afanasieva¹, Marat V. Ezhov^{2*}, Narek A. Tmoyan², Oksana A. Razova¹, Marina I. Afanasieva¹, Yuri G. Matchin² and Sergei N. Pokrovsky¹

OPEN ACCESS

Edited by:

Dmitri Sviridov,
Baker Heart and Diabetes
Institute, Australia

Reviewed by:

Nigora Mukhamedova,
Baker Heart and Diabetes
Institute, Australia
Dick C. Chan,
University of Western
Australia, Australia

*Correspondence:

Marat V. Ezhov
marat_ezhov@mail.ru

Specialty section:

This article was submitted to
Atherosclerosis and Vascular
Medicine,
a section of the journal
Frontiers in Cardiovascular Medicine

Received: 26 December 2021

Accepted: 15 February 2022

Published: 11 March 2022

Citation:

Afanasieva OI, Ezhov MV, Tmoyan NA,
Razova OA, Afanasieva MI,
Matchin YG and Pokrovsky SN (2022)
Low Molecular Weight
Apolipoprotein(a) Phenotype Rather
Than Lipoprotein(a) Is Associated With
Coronary Atherosclerosis and
Myocardial Infarction.
Front. Cardiovasc. Med. 9:843602.
doi: 10.3389/fcvm.2022.843602

¹ National Medical Research Center of Cardiology, Institute of Experimental Cardiology, Ministry of Health of the Russian Federation, Moscow, Russia, ² National Medical Research Center of Cardiology, A. L. Myasnikov Institute of Clinical Cardiology, Ministry of Health of the Russian Federation, Moscow, Russia

Background and Aims: Current evidence suggests that lipoprotein(a) [Lp(a)] level above 50 mg/dL is associated with increased cardiovascular risk. Our study aim was to determine the relationship of apolipoprotein(a) [apo(a)] phenotypes and Lp(a) concentration below and above 50 mg/dL with coronary atherosclerosis severity and myocardial infarction (MI).

Material and Methods: The study population consisted of 540 patients (mean age 54.0 ± 8.8 years, 82% men) who passed through coronary angiography. The number of diseased major coronary arteries assessed atherosclerosis severity. Lipids, glucose, Lp(a) levels and apo(a) phenotypes were determined in all patients. All patients were divided into four groups: with Lp(a) <50 mg/dL [“normal” Lp(a)] or ≥ 50 mg/dL [hyperLp(a)], and with low-molecular (LMW) or high-molecular weight (HMW) apo(a) phenotypes.

Results: Baseline clinical and biochemical characteristics were similar between the groups. In groups with LMW apo(a) phenotypes, the odds ratio (OR; 95% confidence interval) of multivessel disease was higher [10.1; 3.1–33.5, $p < 0.005$ for hyperLp(a) and 2.2; 1.0–4.9, $p = 0.056$ for normal Lp(a)], but not in the group with HMW apo(a) and hyperLp(a) [1.1; 0.3–3.3, $p = 0.92$] compared with the reference group with HMW apo(a) and normal Lp(a). Similarly, MI was observed more often in patients with LMW apo(a) phenotype and hyperLp(a) and normal Lp(a) than in groups with HMW apo(a) phenotype.

Conclusion: The LMW apo(a) phenotype is associated with the severity of coronary atherosclerosis and MI even when Lp(a) level is below 50 mg/dL. The combination of Lp(a) level above 50 mg/dL and LMW apo(a) phenotype increases the risk of severe coronary atherosclerosis, regardless of other risk factors.

Keywords: lipoprotein(a), coronary atherosclerosis, apolipoprotein(a) [apo(a)], myocardial infarction, phenotypes

INTRODUCTION

Lipoprotein(a) [Lp(a)] is the supramolecular complex consisting of low-density lipoprotein (LDL)-like particle and highly-glycosylated protein—apolipoprotein(a) [apo(a)]. Apo(a) is a unique one among the apolipoproteins family. First, the structure and primary sequence of apo(a) has high homology with the plasminogen and consists of the kringle domains that are specific for such blood coagulation factors as plasminogen, prothrombin, urokinase, and tissue-type plasminogen activator. Second, apo(a) is one of the most polymorphic proteins in blood plasma, having more than 40 isoforms, and third, apo(a) plasma level is controlled by the *LPA* gene (1).

The relationship between Lp(a) level and polymorphism of apo(a) with cardiovascular diseases (CVD) have been studied for several decades. The association of the low molecule weight (LMW) apo(a) isoforms with a higher risk of CHD in various populations was shown in 1992 (2). It was shown that Lp(a) level with LMW apo(a) phenotype is associated with CVD to a greater extent than with high molecular weight (HMW) apo(a) phenotypes (3–5). However, there are conflicting results from some studies regarding the role of apo(a) phenotype in CVD (6, 7). The European Atherosclerosis Society considers desirable Lp(a) level below the 80th percentile or <50 mg/dL (8). Given the high prevalence of LMW apo(a) isoforms in the population (9), the question of the significance of apo(a) phenotypes in the evaluation of CVD risk remains to be actual. Our study was aimed to determine the relationship of apo(a) phenotypes and Lp(a) concentration with coronary atherosclerosis severity and myocardial infarction (MI).

MATERIALS AND METHODS

In the single-center study, we included 540 consecutive patients (mean age 54.0 ± 8.8 years, 82% men) who passed through coronary angiography with subsequent angiogram analysis. The Institutional Review Board approved the study. All patients provided their informed consent for participation in the study. Main exclusion criteria were acute, inflammatory, or autoimmune diseases, significant thyroid, liver or kidney dysfunction, alcohol abuse, treatment with any hormones, PCSK9 inhibitors, and apheresis. In accordance with clinical indications, patients received different doses of statins and ezetimibe. However, some of them ($n = 257$) admitted for initial examination and/or without CHD were statin naïve.

The quantitative analysis of coronary artery lesions was conducted with an integrated computer system (Philips Medical Systems, Germany). Stenosis of more than 50% in a magistral artery or its major branches was considered significant. Patients were classified in accordance with the number of affected main coronary arteries: 0—no lesions ($n = 57$), 1—one vessel ($n = 127$), two- and three-vessel disease ($n = 356$). Coronary heart disease (CHD) was diagnosed in those with diseased coronary arteries ($n = 483$). CHD manifestation should be confirmed by history of MI, and/or typical angina pectoris with subsequent angiography confirmation. Discharge summaries had to be provided by subjects.

Laboratory Tests

Lipids, glucose, Lp(a) level, and apo(a) phenotypes were determined in all patients. Total cholesterol (TC), triglycerides (TG), and high-density lipoprotein cholesterol (HDL-C) were measured in blood serum. LDL-cholesterol (LDL-C) was estimated by the Friedewald equation for patients with TG levels <4.5 mmol/L: $LDL-C = TC - HDL-C - TG/2.2$ (mmol/L). The level of LDL-C corrected (LDL-Ccorr) for Lp(a)-cholesterol was estimated with the modified Friedewald formula: $LDL-Ccorr$ (mmol/L) = $LDL-C - 0.3 \times Lp(a)$ mass (mg/dL)/38.7 (10). Lp(a) concentration was determined by enzyme-linked immunosorbent assay (ELISA) with monospecific polyclonal sheep anti-human-apo(a) antibodies as previously reported (11). Apo(a) phenotyping was performed by sodium dodecyl sulfate-polyacrylamide gel electrophoresis of plasma under reducing conditions followed by immunoblotting (12) with the same antibodies. All isoforms were divided into two major types according to the original G. Uttermann nomenclature (13). High-molecular weight (HMW) phenotype included S3, S3S4, S4 isoforms (more than 22 KIV2 repeats), and “null” alleles; low-molecular weight (LMW) phenotype had at least one of the B, S1, or S2 isoforms (up to 22 KIV2 repeats). In the presence of two bands and the major band was as follows—S2, S1, B, or F, the subject was considered as the one with LMW apo(a) phenotype. Serum samples were kept at 70°C until use.

Statistical Analysis

For continuous variables with an approximately normal distribution, data were presented as means \pm standard deviation (SD). For parameters with non-Gaussian distribution, data were expressed as median and interquartile intervals. In univariate analysis, variables were compared by *t*-tests and Mann–Whitney test. To compare the frequency data in the groups, the Chi-squared criterion or Fisher's exact test was used. Spearman's correlation analysis and the multiple logistic regression method were used to assess the association of risk factors with the severity of coronary atherosclerosis. The odds ratio (OR) with 95% confidential interval (CI) in different patients' groups was calculated to assess the relationship of Lp(a) concentration and apo(a) phenotype with coronary atherosclerosis severity or MI. *P*-values for all tests were two-tailed, and differences were significant at the *p* level below 0.05. An independent investigator double-checked all measurement calculations and database entries. All statistical analyses were performed with MedCalc 20.022 software (MedCalc Software Ltd, Ostend, Belgium).

RESULTS

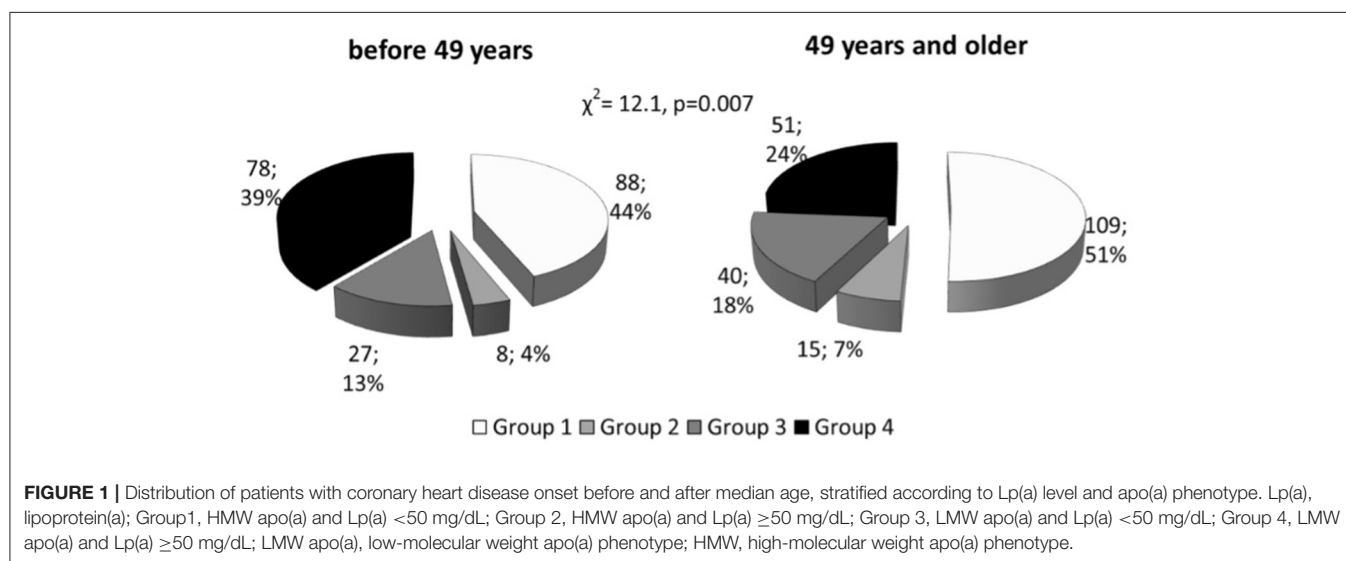
We included 540 patients (mean age 54.0 ± 8.8 years, 82% men) subjected to coronary angiography in the Institute of Clinical Cardiology. We observed a wide distribution of Lp(a) concentrations, most pronounced for LMW apo(a) (Supplementary Figure 1).

All patients were divided into four groups: in accordance with Lp(a) concentration (<50 mg/dL [“normal” Lp(a)] or ≥ 50 mg/dL [hyperLp(a)]), and apolipoprotein(a) phenotypes: low-molecular weight (LMW) or high-molecular weight (HMW)

TABLE 1 | The clinical and biochemical characteristics of patients with different lipoprotein(a) levels and apolipoprotein(a) phenotype.

Parameter	Group 1 HMW apo(a) and Lp(a) <50 mg/dL	Group 2 HMW apo(a) and Lp(a) ≥50 mg/dL	Group 3 LMW apo(a) and Lp(a) <50 mg/dL	Group 4 LMW apo(a) and Lp(a) ≥50 mg/dL
Number	266	29	94	151
Sex, male (%)	218 (82%)	23 (79%)	82 (87%)	119 (79%)
Age	54.5 ± 8.5	55.0 ± 9.4	54.0 ± 9.4	52.9 ± 8.7
BMI	27.1 ± 3.6	27.0 ± 4.8	27.1 ± 3.2	26.9 ± 3.5
Smoking	145 (54%)	13 (45%)	60 (64%)	77 (51%)
Hyperlipidemia	222 (83%)	23 (79%)	80 (85%)	131 (88%)
Obesity	175 (44%)	5 (23%)	18 (19%)	23 (15%)
Hypertension	172 (68%)	14 (49%)	60 (64%)	87 (58%)
CHD family history	105 (40%)	8 (28%)	47 (50%)	55 (36%)
Diabetes mellitus	32 (12%)	2 (7%)	6 (6%)	5 (3%)
TC, mmol/L	6.4 ± 1.2	6.8 ± 1.6	6.4 ± 1.3	6.7 ± 1.3*
TG, mmol/L	2.3 ± 0.9	2.1 ± 1.0	2.1 ± 1.0	2.1 ± 0.9*
HDL-C, mmol/L	1.2 ± 0.3	1.2 ± 0.3	1.2 ± 0.2	1.2 ± 0.3
LDL-C, mmol/L	4.4 ± 1.2	5.0 ± 1.4	4.3 ± 1.2	4.7 ± 1.1*
LDL-Ccorr, mmol/L	4.3 ± 1.2	4.5 ± 1.4	4.1 ± 1.2	3.9 ± 1.1
Glucose, mmol/L	5.8 ± 1.1	5.3 ± 0.9**	5.5 ± 0.7	5.7 ± 2.2*
Lp(a), mg/dL	11.0 [4.3; 21.1]	64.0 [56.3; 81.5]**	24.3 [13.0; 39.1]*	83.0 [65.2; 108.3]**
Lp(a) ≥30 mg/dL	11%	100%**	41%**	100%**

* $p < 0.05$, ** $p < 0.005$ vs. Group 1. BMI, body mass index; CHD, coronary heart disease; TC, total cholesterol; TG, triglycerides; HDL-C, high density cholesterol; LDL-C, low density cholesterol; LDL-Ccorr, LDL-C corrected for Lp(a)-cholesterol; Lp(a), lipoprotein(a); Group 1, HMW apo(a) and Lp(a) <50 mg/dL; Group 2, HMW apo(a) and Lp(a) ≥50 mg/dL; Group 3, LMW apo(a) and Lp(a) <50 mg/dL; Group 4, LMW apo(a) and Lp(a) ≥50 mg/dL; LMW apo(a), low-molecular weight apo(a) phenotype; HMW, high-molecular weight apo(a) phenotype.



(Table 1 and Supplementary Figure 2). There no differences in medications between the groups. CHD in patients with hyperLp(a) and LMW apo(a) phenotype (Group 4) was manifested by 5 years earlier than in patients with HMW apo(a) type (Group 1): median [95% CI] 45 [45;47] vs. 50 [48;50] years ($p < 0.01$). CHD manifestation before the age of 49 years was observed in patients with LMW apo(a) phenotype more frequently, than HMW apo(a) phenotype (Figure 1). The

presence of LMW apo(a) phenotype (group 4) was associated with earlier CHD debut in comparison with group with HMW apo(a) phenotype (group 2) for patients with Lp(a) concentration more than 50 mg/dL (OR = 2.9; 95% CI 1.1–7.3, $p = 0.026$).

According to multiple regression analysis adjusted for sex, age, hypertension, and hyperlipidemia, Lp(a) concentration ($r = 0.14$, $p = 0.0006$) was an independent predictor of severity of coronary atherosclerosis, as well as sex ($r = 0.15$, $p = 0.0001$),

and hyperlipidemia ($r = 0.22$, $p < 0.0001$). The level of Lp(a) ≥ 50 mg/dL as a categorical binary variable or the presence of the LMW apo(a) phenotype were associated with the number of affected coronary arteries (Table 2). When the apo(a) phenotype and Lp(a) concentrations above 50 mg/dL were simultaneously introduced into the regression model, the LMW apo(a) phenotype remained an independent predictor of the severity of coronary atherosclerosis (Table 2). LMW apo(a) phenotype was associated with CHD and MI independent of age, sex, hypertension, hyperlipidemia and Lp(a) ≥ 50 mg/dL according to logistic regression analysis (Supplementary Table 1).

The proportion of patients with more severe atherosclerosis increased steadily in groups stratified by apo(a) phenotype and Lp(a) concentration and reached 98% in group 4. There was a trend to association between the presence of LMW apo(a) and coronary atherosclerosis in patients with Lp(a) level below 50 mg/dL. For patients with LMW apo(a) and Lp(a) ≥ 50 mg/dL (group 4) the CHD probability increased by nine-fold (OR = 9.3, $p < 0.0005$; Table 3). There were no differences between groups 1 and 2. Coronary atherosclerosis was more severe in the presence of LMW phenotype regardless of Lp(a) concentration (Figure 2).

TABLE 2 | Multiple regression analysis of the relationship of lipoprotein(a) with the number of affected coronary arteries.

Parameter	Model 1	Model 2	Model 3
Male sex	0.18***	0.17***	0.18***
Age	0.11*	0.12*	0.12*
Hypertension	0.04	0.03	0.03
Hyperlipidemia	0.23**	0.23**	0.23**
Lp(a) ≥ 50 mg/dL	0.16**	–	0.06
LMW apo(a)	–	0.21**	0.14**

* $p < 0.01$, ** $p < 0.001$, *** $p < 0.0001$. LMW apo(a), low-molecular weight apo(a) phenotype; Lp(a), lipoprotein(a). Data are presented as r_{partial} —partial correlation coefficient—the correlation of the independent variable with the dependent variable, adjusted for the effect of the other variables in the model (partial correlation is the correlation between an independent variable and the dependent variable after the linear effects of the other variables have been removed from both the independent variable and the dependent variable). Regression models include sex, age, hypertension, hyperlipidemia and Lp(a) level (Model 1), LMW apo(a) (Model 2), or both (Model 3).

The patients with hyperLp(a) and LMW apo(a) phenotype had stenotic lesions in three coronary vessels more frequently than patients with Lp(a) < 50 mg/dL and HMW apo(a) (OR = 2.4; 1.01–5.4, $p = 0.046$).

Of all cohort, 338 (62.6%) patients had MI, the proportion of patients with MI were comparable in groups of patients with HMW apo(a) phenotype and different Lp(a) levels (56 and 55% for Lp(a) < 50 mg/dL and Lp(a) ≥ 50 mg/dL, correspondingly). In group 3 [LMW apo(a) and normal Lp(a)] MI was registered in 72%, that was more frequent than in group 1 (OR = 2.1; 1.2–3.4, $p = 0.006$). The probability of MI in patients from group 3 was comparable with those from group 4 (OR = 1.8; 1.2–2.7, $p = 0.007$; Table 3). Thus, the presence of LMW apo(a) phenotype doubled the likelihood of MI regardless the Lp(a) level.

We have analyzed the relationship between apo(a) phenotypes and atherosclerosis severity in the subgroup of 74 patients with Lp(a) level between 30 and 49 mg/dL. Multivessel disease was detected in 31 out of 42 patients (74%) with the LMW apo(a) phenotype and in 17 out of 32 (53%) patients with the HMW apo(a) phenotype, $p = 0.08$. Of 42 patients with the LMW apo(a) phenotype and Lp(a) concentration in the range from 30 to 49 mg/dL, 36 (86%) had MI, and this accounted for 11% of all patients with MI. LMW apo(a) phenotype was associated with MI in 360 patients with Lp(a) < 50 mg/dL (OR = 2.2; 1.3–3.6, $p = 0.003$).

DISCUSSION

Lp(a) concentration varies widely between individuals from < 0.1 mg/dL to more than 300 mg/dL, while there is a minimum number of people who have not detectable levels of Lp(a) in plasma [reviewed in (1)]. In 1990, the Lp(a) level of 30 mg/dL was selected as a cut-off level and was associated with the presence and severity of coronary atherosclerosis (10, 14). According to epidemiological data from the Copenhagen General Population Study, about 20% of the population have a concentration of Lp(a) > 50 mg/dL (8). This level is associated with the increased risk of atherosclerosis and cardiovascular events and hyperLp(a) is one of the most common lipid metabolism disorders (8).

Lp(a) plasma concentration is under strong genetic control and a major part of this variability is explained by KIV2 repeat

TABLE 3 | The odds ratios for coronary atherosclerosis and myocardial infarction depending on lipoprotein(a) levels and apolipoprotein(a) phenotype.

Condition	Group 1 HMW apo(a) and Lp(a) < 50 mg/dL	Group 2 HMW apo(a) and Lp(a) ≥ 50 mg/dL	Group 3 LMW apo(a) and Lp(a) < 50 mg/dL	Group 4 LMW apo(a) and Lp(a) ≥ 50 mg/dL
Coronary heart disease	1	1.2 (0.4–3.5) $p = 0.29$	2.0 (0.9–4.5) $p = 0.08$	9.3 (2.8–30.4) $p < 0.0005$
Multivessel disease*	1	1.1 (0.3–3.3) $p = 0.92$	2.2 (1.0–4.9) $p = 0.056$	10.1 (3.1–33.5) $p = 0.0001$
Myocardial infarction	1	1.0 (0.5–2.1) $p = 0.94$	2.1 (1.2–3.4) $p = 0.006$	1.8 (1.2–2.7) $p = 0.007$

Data are presented as Odds ratio (95% confidential interval) [OR (95% CI)]. OR for coronary atherosclerosis, multivessel disease, and MI was calculated for groups 2–4 vs. Group 1. LMW apo(a), low-molecular weight apo(a) phenotype; HMW, high-molecular weight apo(a) phenotype; Lp(a), lipoprotein(a). *Two and three diseased coronary arteries.

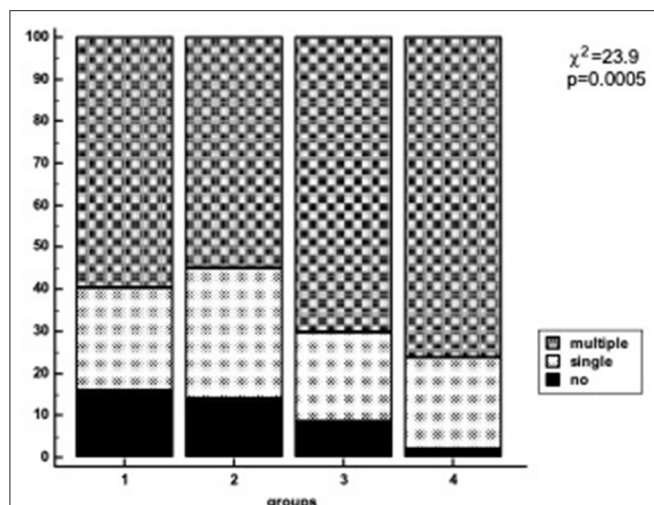


FIGURE 2 | Number of diseased coronary vessels in different groups of patients regarding Lp(a) levels and apo(a) phenotype. Lp(a), lipoprotein(a); Group 1, HMW apo(a) and Lp(a) <50 mg/dL; Group 2, HMW apo(a) and Lp(a) ≥50 mg/dL; Group 3, LMW apo(a) and Lp(a) <50 mg/dL; Group 4, LMW apo(a) and Lp(a) ≥50 mg/dL; LMW apo(a), low-molecular weight apo(a) phenotype; HMW, high-molecular weight apo(a) phenotype.

size polymorphism (15). As a rule, individuals expressing LMW apo(a) isoforms (up to 22 KIV2 repeats or electrophoretic mobility S2 and faster) have higher Lp(a) concentrations than individuals carrying only HMW apo(a) isoforms (more than 22 KIV2 repeats or electrophoretic mobility S3 and slower) (1). In accordance with population studies an inverse correlation between the Lp(a) concentration and apo(a) phenotype is not strictly linear, and ethnic differences contribute significantly to the variability of allele-specific Lp(a) concentrations (15). It was demonstrated the widest variation in Lp(a) level for LMW apo(a) phenotype (16). A highly frequent SNP in the KIV2 region was identified recently and possibly explains the strikingly wide range of Lp(a) levels observed in LMW carriers (17). In addition, several genetic mutations have been described in KIV2 and KIV8 that lead to the synthesis of a truncated protein that is degraded within the cell and is associated with low Lp(a) concentration (18). The same wide variation of Lp(a) concentration for LMW apo(a) phenotype was seen in our study.

There is an assumption, that at the same elevated Lp(a) level, a person with LMW apo(a) isoform will have a higher risk of CVD and coronary events. Determination of apo(a) isoforms would have been able to serve as an additional tool for assessing CVD risk. However, the methodological complexity of immunoblotting for the serum apo(a) phenotyping or DNA genotyping and the limitations of the quantitative polymerase chain reaction (qPCR) method, which takes into account the sum of KIV2 repeats in the two alleles, complicates the assessment of the significance of apo(a) isoforms as a cardiovascular risk discriminator.

Our study was conducted in the single center, this excluded the variability of results due to different methods, as it occurs

in meta-analyses (19). We showed the significant association of Lp(a) level with coronary atherosclerosis and MI in patients with the presence of LMW apo(a) phenotype independently of classic risk factors. It seems that elevated Lp(a) concentration (≥50 mg/dL) in the presence of HMW apo(a) phenotype is a less pronounced risk factor for CHD. The presence of LMW apo(a) phenotype, even at Lp(a) concentration lower than 50 mg/dL increases the probability of CHD and multivessel atherosclerosis by almost two-fold (Table 2).

It was shown that LMW apo(a) phenotype especially in combination with high concentrations of Lp(a) increased the risk of CHD, acute coronary syndrome, atherosclerosis of different vascular beds (5, 20, 21). However, one large-scale study (995 CHD patients and 998 controls) showed that Lp(a) concentration could be a more significant risk factor than LMW apo(a) phenotype (7). The authors concluded that the effect of KIV2 repeats on CHD risk is mediated through their impact on Lp(a) levels, suggesting that absolute level of Lp(a), rather than apo(a) isoform size, is the main determinant of CHD risk. The concentration of Lp(a), but not the size of apo(a) isoform, was independently associated with the severity of atherosclerosis in coronary or carotid arteries according to the study included 263 patients with early CHD development (6). The differences between this study and ours were the inclusion of patients with premature CHD and another method of assessment of severity of coronary atherosclerosis. LMW apo(a) phenotypes were associated with severe carotid atherosclerosis in patients with Lp(a) concentrations ≤32 mg/dL (4). Similar results were obtained in patients with symptomatic peripheral arterial disease (22). Our study demonstrates that the combination of elevated Lp(a) level and LMW apo(a) phenotype increases the probability of multivessel coronary disease. But the presence of the LMW apo(a) phenotype even at concentrations <50 mg/dL is associated with myocardial infarction in the past confirming the role of apo(a) in atherothrombosis. The reason of the same risk of MI in the groups with LMW apo(a) phenotype could be explained the difference in mechanisms of atherosclerosis and thrombosis. The severity of atherosclerosis depends on time-cumulative effects of lipoproteins and apo(a) whereas MI depends on plaque instability and associated with it inflammation and thrombosis. Thus, we found the significant relationship of LMW apo(a) phenotype with multivessel disease only if Lp(a) level >50 mg/dL and the same and statistically significant probability of MI in subjects with LMW apo(a) phenotype regardless Lp(a) concentration (Table 3).

The Mendelian randomization Pakistan Risk of the Myocardial Infarction Study (PROMIS) consisted of 9,015 patients with acute MI and 8,629 controls demonstrated that both apo(a) size and Lp(a) concentration are independent risk factors for MI. OR for MI was 0.93 (95% CI 0.90–0.97, $p < 0.0001$) per 1 SD increase in the number of LPA KIV2 repeats after adjustment for Lp(a) and lipids plasma levels. OR for MI was 1.10 (1.05–1.14, $p < 0.0001$) per 1 SD increase of Lp(a) concentration after adjustment for LPA KIV2 repeats and lipids levels (5).

In the Copenhagen City Heart Study ($n = 10,855$) and the Copenhagen General Population Study ($n = 87,242$), the risk

of heart failure due to MI and aortic stenosis increased in the subgroups of participants with Lp(a) concentration more than 20 mg/dL (23). The association of the LMW apo(a) phenotype with the risk of all-cause mortality has been described for patients with T2D younger than 66 years old (24).

It has been shown that Lp(a) with LMW apo(a) isoforms can circulate longer in blood plasma (25). It has also been suggested that different receptors may be involved in Lp(a) catabolism depending on the isoform expressed (26, 27). Lp(a) is the carrier of a larger part of the total pool of oxidized phospholipids (28). The oxidized phospholipids concentration is associated with the allele-specific Lp(a) level and predominantly with LMW apo(a) isoforms, and this fact can explain differences in the atherogenicity of Lp(a) due to apo(a) phenotype (29, 30).

The incubation of the serum samples from patients with LMW apo(a) phenotype causes a significantly greater accumulation of cholesterol by macrophage cells of THP-1, compared with serum samples from patients with HMW apo(a) phenotype, regardless of Lp(a) concentration (31) and this observation may be related to the difference in Lp(a) particles atherogenicity.

Our data, obtained in a single-center study of 540 subjects, provide a new information on LMW apo(a) phenotype significance for coronary atherosclerosis severity and MI development. Unlike all the studies described above, we have shown that LMW apo(a) phenotype with Lp(a) below 50 mg/dL is associated with a significant increase of probability of CHD, MI, and multivessel coronary lesions compared to HMW apo(a) phenotype.

Thus, the results of our study on the association of LMW apo(a) phenotype with coronary atherosclerosis and MI requires additional studies for a possible revision of the cut-off Lp(a) level.

STUDY LIMITATIONS

Lp(a) concentration was determined by an in-house ELISA utilizing monospecific polyclonal sheep anti-human-apo(a) antibodies. The method was validated with concern to two known kits “TintElize Lp(a)” (Biopool AB Sweden) and “Immunozymp Lp(a)” (Progen Biotechnik GmbH, Germany). Control samples approved by the International Federation of Clinical Chemistry (“Technoclone” Austria), were used to standardize the ELISA. The ELISA method was sensitive to apo(a) isoforms toward a slight increase in Lp(a) concentration in samples with HMW apo(a) isoforms and low Lp(a) concentration. The absolute bias (median [25%; 75%]) was ~1.5 [−0.4 to 5.7] mg/dL.

Considering the results of a meta-analysis of the relationship between the Lp(a) level and development of CHD did not show

significant differences in the relative risk in studies using methods sensitive and insensitive to the size of apo(a) isoforms (32) and high variability in the Lp(a) measurement, regardless of isoforms (33, 34), allows us to assume that sensitivity of ELISA to apo(a) isoforms did not affect the results of our study.

We did not determine the number of KIV-2 kringles, but used a classification based on mobility of apo(a) isoforms in polyacrylamide gel electrophoresis and dichotomized all patients into those with LMW or HMW apo(a) phenotypes.

CONCLUSIONS

The low-molecular phenotypes of apo(a) are associated with the severity of coronary atherosclerosis and myocardial infarction even when Lp(a) level is <50 mg/dL. The combination of elevated concentrations of Lp(a) and low molecular weight apo(a) phenotype potentiate the risk of atherosclerosis and MI, regardless of other risk factors.

DATA AVAILABILITY STATEMENT

The raw data supporting the conclusions of this article will be made available by the authors, without undue reservation.

ETHICS STATEMENT

The studies involving human participants were reviewed and approved by the Ethics Committee of Russian Cardiology Research and Production Center of Ministry of Healthcare of Russian Federation. The patients/participants provided their written informed consent to participate in this study.

AUTHOR CONTRIBUTIONS

OA and ME: conceptualization and writing—original draft preparation. OR, NT, MA, and YM: methodology. SP and ME: validation. OA: formal analysis. OR, ME, and NT: investigation. SP: resources. ME and NT: data curation. OA, ME, and SP: writing—review and editing. YM: visualization. All authors have read and agreed to the published version of the manuscript.

SUPPLEMENTARY MATERIAL

The Supplementary Material for this article can be found online at: <https://www.frontiersin.org/articles/10.3389/fcvm.2022.843602/full#supplementary-material>

REFERENCES

- Kronenberg F. Prediction of cardiovascular risk by Lp(a) concentrations or genetic variants within the LPA gene region. *Clin Res Cardiol Suppl.* (2019) 14(Suppl. 1):5–12. doi: 10.1007/s11789-019-00093-5
- Sandholzer C, Saha N, Kark JD, Rees A, Jaross W, Dieplinger H, et al. Apo(a) isoforms predict risk for coronary heart disease. A study in six populations. *Arterioscler Thromb.* (1992) 12:1214–26. doi: 10.1161/01.ATV.12.10.1214
- Paultre F, Pearson TA, Weil HF, Tuck CH, Myerson M, Rubin J, et al. High levels of Lp(a) with a small apo(a) isoform are associated with coronary artery disease in African American and white men. *Arterioscler Thromb Vasc Biol.* (2000) 20:2619–24. doi: 10.1161/01.ATV.20.12.2619

4. Paultre F, Tuck CH, Boden-Albala B, Kargman DE, Todd E, Jones J, et al. Relation of Apo(a) size to carotid atherosclerosis in an elderly multiethnic population. *Arterioscler Thromb Vasc Biol.* (2002) 22:141–6. doi: 10.1161/hq0102.101097
5. Saleheen D, Haycock PC, Zhao W, Rasheed A, Taleb A, Imran A, et al. Apolipoprotein(a) isoform size, lipoprotein(a) concentration, and coronary artery disease: a mendelian randomisation analysis. *Lancet Diabetes Endocrinol.* (2017) 5:524–33. doi: 10.1016/S2213-8587(17)30088-8
6. Ooi EM, Ellis KL, Barrett PHR, Watts GF, Hung J, Beilby JP, et al. Lipoprotein(a) and apolipoprotein(a) isoform size: associations with angiographic extent and severity of coronary artery disease, and carotid artery plaque. *Atherosclerosis.* (2018) 275:232–8. doi: 10.1016/j.atherosclerosis.2018.06.863
7. Hopewell JC, Seedorf U, Farrall M, Parish S, Kyriakou T, Goel A et al. Impact of lipoprotein(a) levels and apolipoprotein(a) isoform size on risk of coronary heart disease. *J Intern Med.* (2014) 276:260–8. doi: 10.1111/joim.12187
8. Nordestgaard BG, Chapman MJ, Ray K, Borén J, Andreotti F, Watts GF, et al. Lipoprotein(a) as a cardiovascular risk factor: current status. *Eur Heart J.* (2010) 31:2844–53. doi: 10.1093/eurheartj/ehq386
9. Kronenberg F. Human genetics and the causal role of Lipoprotein(a) for various diseases. *Cardiovasc Drugs Ther.* (2016) 30:87–100. doi: 10.1007/s10557-016-6648-3
10. Dahlen GH. Incidence of Lp(a) lipoprotein among populations. In: Scanu AM, editor. *"Lipoprotein(a)".* San Diego, CA: Academic Press, Inc (1990). p. 151–75. doi: 10.1016/B978-0-12-620990-7.50014-0
11. Ezhov MV, Safarova MS, Afanasieva OI, Kukharchuk VV, Pokrovsky SN. Lipoprotein(a) level and apolipoprotein(a) phenotype as predictors of long-term cardiovascular outcomes after coronary artery bypass grafting. *Atherosclerosis.* (2014) 235:477–82. doi: 10.1016/j.atherosclerosis.2014.05.944
12. Kraft HG, Dieplinger H, Hoyer E, Utermann G. Lp(a) phenotyping by immunoblotting with polyclonal and monoclonal antibodies. *Arteriosclerosis.* (1988) 8:212–6. doi: 10.1161/01.ATV.8.3.212
13. Utermann G, Menzel H, Kraft H, Duba H, Kemmler H, Seitz C. Lp(a) glycoprotein phenotypes: inheritance and relation to Lp(a)-lipoprotein concentrations in plasma. *J Clin Invest.* (1987) 80:458–65. doi: 10.1172/JCI113093
14. Kostner KM, Kostner GM. Lipoprotein (a): a historical appraisal. *J Lipid Res.* (2017) 58:1–14. doi: 10.1194/jlr.R071571
15. Kronenberg F, Utermann G. Lipoprotein(a) - resurrected by genetics. *J Intern Med.* (2013) 273:6–30. doi: 10.1111/j.1365-2796.2012.02592.x
16. Nordestgaard BG, Langsted A. Lipoprotein(a) as a cause of cardiovascular disease: insights from epidemiology, genetics, and biology. *J Lipid Res.* (2016) 57:1953–75. doi: 10.1194/jlr.R071233
17. Coassin S, Erhart G, Weissensteiner H, Eca Guimarães de Araújo M, Lamina C, Schönherr S, et al. A novel but frequent variant in LPA KIV-2 is associated with a pronounced Lp(a) and cardiovascular risk reduction. *Eur Heart J.* (2017) 38:1823–31. doi: 10.1093/eurheartj/ehx174
18. Morgan BM, Brown AN, Deo N, Harrop TW, Taiaroa G, Mace PD, et al. Nonsynonymous SNPs in LPA homologous to plasminogen deficiency mutants represent novel null apo(a) alleles. *J Lipid Res.* (2020) 61:432–44. doi: 10.1194/jlr.M094540
19. Erqou S, Thompson A, Di Angelantonio E, Saleheen D, Kaptoge S, Marcovina S, et al. Apolipoprotein(a) isoforms and the risk of vascular disease: systematic review of 40 studies involving 58,000 participants. *J Am Coll Cardiol.* (2010) 55:2160–67. doi: 10.1016/j.jacc.2009.10.080
20. Emanuele E, Peros E, Minorette P, D'Angelo A, Montagna L, Falcone C, et al. Significance of apolipoprotein(a) phenotypes in acute coronary syndromes: relation with clinical presentation. *Clin Chim Acta.* (2004) 350:159–65. doi: 10.1016/j.cccn.2004.07.023
21. Suzuki T, Futami-Suda S, Igari Y, Watanabe K, Ouchi M, Suzuki K, et al. Low-molecular-weight lipoprotein(a) and low relative lymphocyte concentration are significant and independent risk factors for coronary heart disease in patients with type 2 diabetes mellitus: Lp(a) phenotype, lymphocyte, and coronary heart disease. *Lipids Health Dis.* (2013) 12:31. doi: 10.1186/1476-511X-12-31
22. Dieplinger B, Lingenhel B, Baumgartner N, Poelz W, Dieplinger H, Haltmayer M, et al. Increased serum lipoprotein(a) concentrations and low molecular weight phenotypes of apolipoprotein(a) are associated with symptomatic peripheral arterial disease. *Clin Chem.* (2007) 53:1298–305. doi: 10.1373/clinchem.2007.088013
23. Kamstrup PR, Nordestgaard BJ. Elevated Lipoprotein(a) levels, LPA risk genotypes, and increased risk of heart failure in the general population. *JACC Heart Failure.* (2016) 4:78–87. doi: 10.1016/j.jchf.2015.08.006
24. Kollerits B, Drechsler C, Krane V, Lamina C, März W, Dieplinger H, et al. Lipoprotein(a) concentrations, apolipoprotein(a) isoforms and clinical endpoints in haemodialysis patients with type 2 diabetes mellitus: results from the 4D Study. *Nephrol Dial Transplant.* (2016) 31:1901–8. doi: 10.1093/ndt/gfv428
25. Frischmann ME, Ikewaki K, Trenkwalder E, Lamina C, Dieplinger B, Soufi M, et al. *In vivo* stable-isotope kinetic study suggests intracellular assembly of lipoprotein(a). *Atherosclerosis.* (2012) 225:322–7. doi: 10.1016/j.atherosclerosis.2012.09.031
26. März W, Beckmann A, Scharnagl H, Siekmeier R, Mondorf U, Held I, et al. Heterogeneous lipoprotein (a) size isoforms differ by their interaction with the low density lipoprotein receptor and the low density lipoprotein receptor-related protein/alpha 2-macroglobulin receptor. *FEBS Lett.* (1993) 325:271–5. doi: 10.1016/0014-5793(93)81087-G
27. McCormick SPA, Schneider WJ. Lipoprotein(a) catabolism: a case of multiple receptors. *Pathology.* (2019) 51:155–64. doi: 10.1016/j.pathol.2018.11.003
28. Bergmark C, Dewan A, Orsoni A, Merki E, Miller ER, Shin MJ, et al. A novel function of lipoprotein [a] as a preferential carrier of oxidized phospholipids in human plasma. *J Lipid Res.* (2008) 49:2230–9. doi: 10.1194/jlr.M800174-JLR200
29. Tsimikas S, Clopton P, Brilakis ES, Marcovina SM, Khera A, Miller ER, et al. Relationship of oxidized phospholipids on apolipoprotein B-100 particles to race/ethnicity, apolipoprotein(a) isoform size, and cardiovascular risk factors: results from the Dallas Heart Study. *Circulation.* (2009) 119:1711–9. doi: 10.1161/CIRCULATIONAHA.108.836940
30. Berglund L, Kim K, Zhang W, Prakash N, Truax K, Anuurad E, et al. Lp(a)-associated oxidized phospholipids in healthy black and white participants in relation to apo(a) size, age, and family structure. *J Am Heart Assoc.* (2021) 10:e020158. doi: 10.1161/JAHA.120.020158
31. Afanas'eva OI, Vikhrova EB, Razova OA, Utkina EA, Afanas'eva MI, Klesareva EA, et al. A low-molecular-weight phenotype of apolipoprotein(a) as a factor provoking accumulation of cholesterol by THP-1 monocyte-like cells. *Bull Exp Biol Med.* (2019) 167:24–9. doi: 10.1007/s10517-019-04452-w
32. Emerging Risk Factors Collaboration, Erqou S, Kaptoge S, Perry PL, Di Angelantonio E, Thompson A, et al. Lipoprotein(a) concentration and the risk of coronary heart disease, stroke, and nonvascular mortality. *JAMA.* (2009) 302:412–23. doi: 10.1001/jama.2009.1063
33. Kronenberg F, Tsimikas S. The challenges of measuring Lp(a): a fight against Hydra? *Atherosclerosis.* (2019) 289:181–3. doi: 10.1016/j.atherosclerosis.2019.08.019
34. Scharnagl H, Stojakovic T, Dieplinger B, Dieplinger H, Erhart G, Kostner GM, et al. Comparison of lipoprotein(a) serum concentrations measured by six commercially available immunoassays. *Atherosclerosis.* (2019) 289:206–13. doi: 10.1016/j.atherosclerosis.2019.08.015

Conflict of Interest: The authors declare that the research was conducted in the absence of any commercial or financial relationships that could be construed as a potential conflict of interest.

Publisher's Note: All claims expressed in this article are solely those of the authors and do not necessarily represent those of their affiliated organizations, or those of the publisher, the editors and the reviewers. Any product that may be evaluated in this article, or claim that may be made by its manufacturer, is not guaranteed or endorsed by the publisher.

Copyright © 2022 Afanasieva, Ezhov, Tmoyan, Razova, Afanasieva, Matchin and Pokrovsky. This is an open-access article distributed under the terms of the Creative Commons Attribution License (CC BY). The use, distribution or reproduction in other forums is permitted, provided the original author(s) and the copyright owner(s) are credited and that the original publication in this journal is cited, in accordance with accepted academic practice. No use, distribution or reproduction is permitted which does not comply with these terms.



CagA⁺ *Helicobacter pylori*, Not CagA⁻ *Helicobacter pylori*, Infection Impairs Endothelial Function Through Exosomes-Mediated ROS Formation

OPEN ACCESS

Edited by:

Hong Chen,
Boston Children's Hospital
and Harvard Medical School,
United States

Reviewed by:

Kalpna Gupta,
University of California, Irvine,
United States
Liya Yin,
Northeast Ohio Medical University,
United States

*Correspondence:

Zhenguo Liu
liuzheng@health.missouri.edu

[†]These authors have contributed
equally to this work and share first
authorship

Specialty section:

This article was submitted to
Atherosclerosis and Vascular
Medicine,
a section of the journal
Frontiers in Cardiovascular Medicine

Received: 22 February 2022

Accepted: 08 March 2022

Published: 31 March 2022

Citation:

Xia X, Zhang L, Wu H, Chen F,
Liu X, Xu H, Cui Y, Zhu Q, Wang M,
Hao H, Li D-P, Fay WP,
Martinez-Lemus LA, Hill MA, Xu C
and Liu Z (2022) CagA⁺ *Helicobacter*
pylori, Not CagA⁻ *Helicobacter pylori*,
Infection Impairs Endothelial Function
Through Exosomes-Mediated ROS
Formation.
Front. Cardiovasc. Med. 9:881372.
doi: 10.3389/fcvm.2022.881372

Xiujuan Xia^{1,2†}, Linfang Zhang^{1,2†}, Hao Wu¹, Feng Chen¹, Xuanyou Liu¹, Huifang Xu¹,
Yuqi Cui¹, Qiang Zhu¹, Meifang Wang¹, Hong Hao¹, De-Pei Li¹, William P. Fay¹,
Luis A. Martinez-Lemus^{1,3,4}, Michael A. Hill^{3,4}, Canxia Xu² and Zhenguo Liu^{1*}

¹ Center for Precision Medicine and Division of Cardiovascular Medicine, Department of Medicine, University of Missouri
School of Medicine, Columbia, MO, United States, ² Department of Gastroenterology, The Third Xiangya Hospital, Central
South University, Changsha, China, ³ Dalton Cardiovascular Research Center, University of Missouri, Columbia, MO,
United States, ⁴ Department of Medical Pharmacology and Physiology, Columbia, MO, United States

Background: *Helicobacter pylori* (*H. pylori*) infection increases the risk for atherosclerosis, and ROS are critical to endothelial dysfunction and atherosclerosis. CagA is a major *H. pylori* virulence factor associated with atherosclerosis. The present study aimed to test the hypothesis that CagA⁺ *H. pylori* effectively colonizes gastric mucosa, and CagA⁺ *H. pylori*, but not CagA⁻ *H. pylori*, infection impairs endothelial function through exosomes-mediated ROS formation.

Methods: C57BL/6 were used to determine the colonization ability of CagA⁺ *H. pylori* and CagA⁻ *H. pylori*. ROS production, endothelial function of thoracic aorta and atherosclerosis were measured in CagA⁺ *H. pylori* and CagA⁻ *H. pylori* infected mice. Exosomes from CagA⁺ *H. pylori* and CagA⁻ *H. pylori* or without *H. pylori* infected mouse serum or GES-1 were isolated and co-cultured with bEND.3 and HUVECs to determine how CagA⁺ *H. pylori* infection impairs endothelial function. Further, GW4869 was used to determine if CagA⁺ *H. pylori* infection could lead to endothelial dysfunction and atherosclerosis through an exosomes-mediated mechanism.

Results: CagA⁺ *H. pylori* colonized gastric mucosa more effectively than CagA⁻ *H. pylori* in mice. CagA⁺ *H. pylori*, not CagA⁻ *H. pylori*, infection significantly increased aortic ROS production, decreased ACh-induced aortic relaxation, and enhanced early atherosclerosis formation, which were prevented with N-acetylcysteine treatment. Treatment with CagA-containing exosomes significantly increased intracellular ROS production in endothelial cells and impaired their function. Inhibition of exosomes

secretion with GW4869 effectively prevented excessive aortic ROS production, endothelial dysfunction, and atherosclerosis in mice with CagA⁺ *H. pylori* infection.

Conclusion: These data suggest that CagA⁺ *H. pylori* effectively colonizes gastric mucosa, impairs endothelial function, and enhances atherosclerosis *via* exosome-mediated ROS formation in mice.

Keywords: CagA, *Helicobacter pylori*, endothelial dysfunction, atherosclerosis, exosomes, reactive oxygen species

INTRODUCTION

Helicobacter pylori (*H. pylori*) colonizes the human gastric epithelium in a significant portion of the general population, ranging from 30 to 50% in developed countries and to approximately 80% in developing countries especially in Asia (1, 2). *H. pylori* has multiple strains, and based on the presence of cytotoxin-associated gene antigen (CagA), *H. pylori* is divided into two major categories: CagA-positive and CagA-negative (3, 4). The majority of patients in East Asian countries with *H. pylori* infection (>90%) are infected with CagA-positive *H. pylori* (5). CagA is a major virulence factor in *H. pylori*, which encodes the CagA protein and can be translocated into host cells through the type IV secretion system (T4SS) (5). Epidemiological data and meta-analysis reveal a much stronger correlation between infection with CagA⁺ *H. pylori* strains and atherosclerosis in patients compared to that of CagA⁻ *H. pylori* strains (6). However, it is not clear why CagA⁺ *H. pylori* is the dominant strain in patient infections, and how it is associated with extra gastrointestinal conditions including atherosclerosis.

Endothelial dysfunction contributes to the development and progression of atherosclerosis (7). *H. pylori* infection significantly increases the risk for cardiovascular diseases including atherosclerosis and hypertension (8, 9). Recent studies with both human subjects and animal models have demonstrated that *H. pylori* infection significantly impairs endothelial function through a pathway involving exosomes (10). Exosomes are known to be critically involved in cell-to-cell communication and cell functions through various mechanisms including regulation of extra- and intracellular redox states *via* direct and/or indirect modification (either increase or decrease) of reactive oxygen species (ROS) content (11–13). The present study was to test the hypotheses that: (1) CagA⁺ *H. pylori* colonizes gastric mucosa more effectively than CagA⁻ *H. pylori*; and (2) CagA⁺ *H. pylori* infection, but not CagA⁻ *H. pylori* infection, impairs endothelial function through CagA-containing exosome-mediated ROS formation. The objectives were to determine: (1) if there was a significant difference in gastric colonization between CagA⁺ *H. pylori* and CagA⁻ *H. pylori*; (2) if there were significant differences in endothelial function and atherosclerosis between mice infected with CagA⁺ *H. pylori* and CagA⁻ *H. pylori* infection; (3) if a significant difference in exosome production was evident in human gastric epithelial cells (GES-1) co-cultured with either CagA⁺ *H. pylori* or CagA⁻ *H. pylori*; and 4) if CagA-containing exosomes impair endothelial function and enhance development of atherosclerosis *via* increased ROS formation.

MATERIALS AND METHODS

Helicobacter pylori Culture

CagA⁺ *H. pylori* in the present study was isolated from the gastric specimens of a gastric ulcer patient during gastroscopy at the Third Xiangya Hospital of Central South University (Changsha, Hunan, China), and its identity confirmed using the complete sequence data of *H. pylori* 16S rRNA gene from GenBank data and positive biochemical tests as described (10). CagA⁻ *H. pylori* (ATCC 51932) were purchased from American Type Culture Collection (ATCC, Manassas, VA, United States). Both strains were cultured for 3–4 days on Columbia blood agar plates supplemented with antibiotics and 10% sheep blood (Fisher Scientific 50863755, Waltham, MA, United States) under a microaerophilic milieu (5% O₂, 10% CO₂, and 85% N₂) at 37°C. The concentration of *H. pylori* was determined by measuring the optical density at OD 600 nm, where 1 unit of OD 600 nm corresponds to about 2 × 10⁸ colony-forming unit (CFU)/ml (10).

Cell Culture and Cell-Bacteria Co-culture

Human gastric epithelial cell line (GES-1) was obtained from Professor Canxia Xu in Department of Gastroenterology, the Third Xiangya Hospital, Central South University; Changsha, Hunan, China. Human umbilical vein endothelial cells (HUVECs) and mouse brain microvascular endothelial cells (bEnd.3) were purchased from ATCC and cultured in RPMI-1640 (Gibco, Grand Island, NY, United States), endothelial cell medium (Sciencell Research Laboratories, Carlsbad, CA, United States), and DMEM (Gibco, Grand Island, NY, United States), respectively, supplemented with 10% fetal bovine serum (FBS) (Gibco, Grand Island, NY, United States), 100 U/ml penicillin, and 100 mg/ml streptomycin in a controlled humidified incubator with 5% CO₂ and 95% room air. To evaluate the effect of exosomes on endothelial cells, exosomes (100 ug/ml) from conditioned media of GES-1 co-cultured with CagA⁺ *H. pylori*, CagA⁻ *H. pylori* or PBS without *H. pylori*, or exosomes from the serum of mice with CagA⁺ *H. pylori*, CagA⁻ *H. pylori* infection or without *H. pylori* infection were cultured with HUVECs or bEND.3. After being cultured for 4 h, HUVECs or bEND.3 were tested for ROS production using the fluorescent dye 2',7'-dichlorodihydrofluorescein diacetate (H2DCFDA, Invitrogen D399, Waltham, MA, United States) as described (14). GES-1 was cultured with *H. pylori* at a MOI (multiplicity of infection) of 100 for 12 h as described (10).

Animal Models

All animal experiments were performed in accordance with the “Guide for the Care and Use of Laboratory Animals of the US National Institutes of Health.” The experimental protocols were reviewed and approved by the Institutional Animal Care and Use Committee of the University of Missouri School of Medicine, Columbia, MO, United States. Specific-pathogen-free 4–6 week-old male C57BL/6 wild-type mice (WT) and LDLR knockout mice (LDLR^{-/-}) were from Jackson Lab (ME, United States), and were fed rodent diet and water *ad libitum*.

After fasting overnight, mice were given 0.2 ml of PBS, CagA⁻ *H. pylori* or CagA⁺ *H. pylori* inoculums (approximate 4×10^9 CFU/ml) by intragastric gavage as described (10). The presence of *H. pylori* infection was assessed at 1-week post-infection or at the time when mice were sacrificed, using Rapid Urease Test (RUT) and Giemsa staining of gastric mucosa. To evaluate the effect of *H. pylori* infection on the development of early atherosclerosis, LDLR^{-/-} mice were fed a high fat diet (HFD) (Envigo TD.88137, Indianapolis, IN, United States) beginning 1 week after *H. pylori* gavage. WT mice were sacrificed 1 week after the last gavage to collect thoracic aorta to determine endothelium-dependent and -independent vascular relaxation responses and ROS production (see details below). LDLR^{-/-} mice were sacrificed after week 3, 5, and 12 of HFD feeding to collect whole aorta and aortic root for atherosclerotic lesion analysis (see details below).

Evaluation of Vascular Endothelium Relaxation in Mice

Thoracic aorta was isolated from mice to evaluate endothelium-dependent and -independent vascular relaxation responses as described (10). The thoracic aorta was cut into 2–3 mm segments and mounted onto a four-channel Wire Myograph System (610M; DMT, Aarhus, Denmark). Aortic segments were equilibrated with a resting tension of 4.9 mN for 45–60 min in a temperature-controlled tissue bath filled with 5 ml of Krebs' solution and bubbled continuously with 95% O₂ and 5% CO₂, at 37°C. The aortic preparations were then tested for maximal contraction with 50 mM KCl, and concentration-dependent vasocontractile responses to phenylephrine (PE). After adequate washout with Krebs solution and equilibration, the aortic tissues were examined for endothelium-dependent relaxation to cumulative doses of acetylcholine (ACh, 10⁻⁹–10⁻⁵M) and endothelium-independent relaxation to cumulative doses of nitroglycerin (NTG, 10⁻⁹–10⁻⁵M) after submaximal contraction with PE.

Administration of N-Acetylcysteine

To further confirmed the role of oxidative stress on endothelial dysfunction caused by *H. pylori* infection, the antioxidant NAC was used to treat the mice *in vivo* and endothelial cells *in vitro*. NAC is an FDA-approved drug and has been traditionally considered an antioxidant that effectively attenuates ROS production (15).

Mice in the NAC treatment group received NAC (Sigma-Aldrich, MO, United States, 1 mg/ml in drinking water) 3 days

before the first gavage until the end of the experiment (16). NAC was changed every other day and covered with aluminum foil to avoid exposure to direct light. For the *in vitro* study, endothelial cells were incubated with 10 mM NAC as described (17).

Quantification of Atherosclerotic Lesions

Atherosclerotic burden in thoracic aorta and cross sections of aortic root was quantified with Oil Red O staining as described (18). Briefly, the thoracic aorta was collected immediately from euthanized mice and carefully prepared with the removal of periadventitial fat after perfusion with sterile phosphate-buffered saline (PBS). Thoracic aorta was cut open longitudinally after being washed twice with 60% isopropanol and images taken with a digital camera after being stained with Oil Red O dye for 30 min at room temperature. Aortic roots were frozen with optimum cutting temperature O.C.T. Compound (Fisher, Waltham, MA, United States) and serial sections (10-μm thick) were cut through the aortic valve as described (18). The sections were stained with Oil Red O for plaque quantification in the cross-section areas. The total lesion area and lesion area percentage were analyzed and quantified using Image J software.

Determination of Reactive Oxygen Species Formation in Cryostat Sections of Aorta

Dihydroethidium (DHE, Invitrogen D23107, Waltham, MA, United States) was used to assess ROS formation in cryostat sections of aorta using fluorescence microscopy (19). Cryostat sections (5 μm) of mouse aortic rings were incubated with 5 μM DHE in normal physiological saline solution (NPSS, composition in mmol L⁻¹: NaCl 140, KCl 5, CaCl₂ 1, MgCl₂ 1, glucose 10, and HEPES 5) for 7 min as described (19). Aortic rings were washed three times to remove DHE after incubation, and then examined with a fluorescence microscope. The fluorescence intensity was evaluated with 518 nm excitation and 606 nm emission, and the images were analyzed using Image J software.

Measurement of Intracellular Reactive Oxygen Species Production

The level of intracellular ROS in HUVECs or bEND.3 was evaluated using the fluorescent dye 2',7'-dichlorodihydrofluorescein diacetate (H2DCFDA; Invitrogen D399) (14) after treatment with exosomes from conditioned media or mouse serum as describe (14). H2DCFDA is a non-polar compound that is converted by cellular esterase to the polar and membrane impermeable derivative H2DCF. H2DCF is non-fluorescent but becomes highly fluorescent 2',7'-dichlorofluorescein (DCF) when oxidized in the presence of intracellular ROS. After treatment with exosomes for 4 h, endothelial cells were washed twice with pre-warmed PBS, and then incubated with 15 μM H2DCFDA for 30 min at 37°C in the dark. Cells were washed twice with pre-warmed PBS after removing the dye. The fluorimetric signal in the cells was examined and analyzed using a fluorescence microscope. The fluorescence intensity was evaluated using ImageJ software.

Exosome Isolation and Characterization

To prepare exosomes from conditioned media, human gastric epithelium cells (GES-1) were cultured with PBS, CagA[−] *H. pylori* or CagA⁺ *H. pylori* at MOI of 100 for 12 h. The conditioned media and mice serum were collected to isolate the exosomes as described (20). Briefly, the conditioned media were successive centrifuged at 4°C (300 × *g* for 10 min, 2,000 × *g* for 20 min, and 10,000 × *g* for 30 min) to eliminate the cells and cell debris. The supernatant was then ultracentrifuged at 100,000 × *g* at 4°C for 70 min for two times (Beckman Coulter, Indianapolis, IN, United States). Exosome pellets were re-suspended in PBS for further analysis. Serum from mice with CagA[−] *H. pylori* or CagA⁺ *H. pylori* infection and control mice was collected for exosome isolation similar to conditioned media as described above (20). Exosomes identification of morphologies, size distribution, and biomarkers were assessed using a transmission electron microscopy (TECNAI G2 Spirit; FEI, Hillsboro, OR, United States), dynamic light scattering with a particle and molecular size analyzer (Zetasizer Nano ZS) and Western blotting as described (10).

Statistical Analysis

Data were expressed as mean ± standard error of the mean (SEM) and analyzed with SPSS statistical software (22.0 for Windows; SPSS, Chicago, IL, United States). A two-tailed unpaired *t*-test was used for the analysis of two groups of data with normal distribution and equal variance, and a two-tailed unpaired *t*-test with Welch's correction for analyzing two groups of data with normal distribution and unequal variance. Mann–Whitney U test was used for comparisons between two groups of data with abnormal distributions. One-way analysis of variance (ANOVA) was used for three or more groups of data analysis with normal distributions and equal variance, and the Kruskal–Wallis test with Dunn *post-hoc* multiple comparison tests was used for three or more groups of data analysis with normal distributions and unequal variance or abnormal distributions. *P* < 0.05 was considered significant.

RESULTS

CagA⁺ *Helicobacter pylori* Colonized Gastric Mucosa More Effectively Than CagA[−] *Helicobacter pylori* in Mice

As over 90% of Asian *H. pylori* patients are infected with CagA⁺ *H. pylori*, we hypothesized that CagA⁺ *H. pylori* would exhibit greater gastric colonization than CagA[−] *H. pylori*. A total of 110 male C57BL/6 mice were divided into 11 groups (10 mice in each group) and infected with either CagA⁺ *H. pylori* or CagA[−] *H. pylori* using 4 different infection protocols (Table 1). Phospho-buffered saline (PBS) treatment served as negative control. Animals were considered infected when both RUT and Giemsa staining were positive. A 100% infection rate was achieved in mice receiving three daily doses of CagA⁺ *H. pylori*, whereas six doses of CagA[−] *H. pylori* were required to achieve a 100% infection rate (Table 1). CagA⁺ *H. pylori* exhibited a

TABLE 1 | Infection rate of CagA⁺ *Helicobacter pylori* and CagA[−] *H. pylori* 1 week after last intragastric gavage.

Group	N	Rapid urease tests positive (N)	Geimsa staining positive (N)	Infection rate (%)
Method 1^a				
Control	10	0	0	0
CagA ⁺ <i>H. pylori</i>	10	2	2	20
CagA [−] <i>H. pylori</i>	10	1	1	10
Method 2^b				
Control	10	0	0	0
CagA ⁺ <i>H. pylori</i>	10	6	6	60
CagA [−] <i>H. pylori</i>	10	4	4	40
Method 3^c				
Control	10	0	0	0
CagA ⁺ <i>H. pylori</i>	10	10	10	100
CagA [−] <i>H. pylori</i>	10	8	8	80
Method 4^d				
Control	10	0	0	0
CagA [−] <i>H. pylori</i>	10	10	10	100

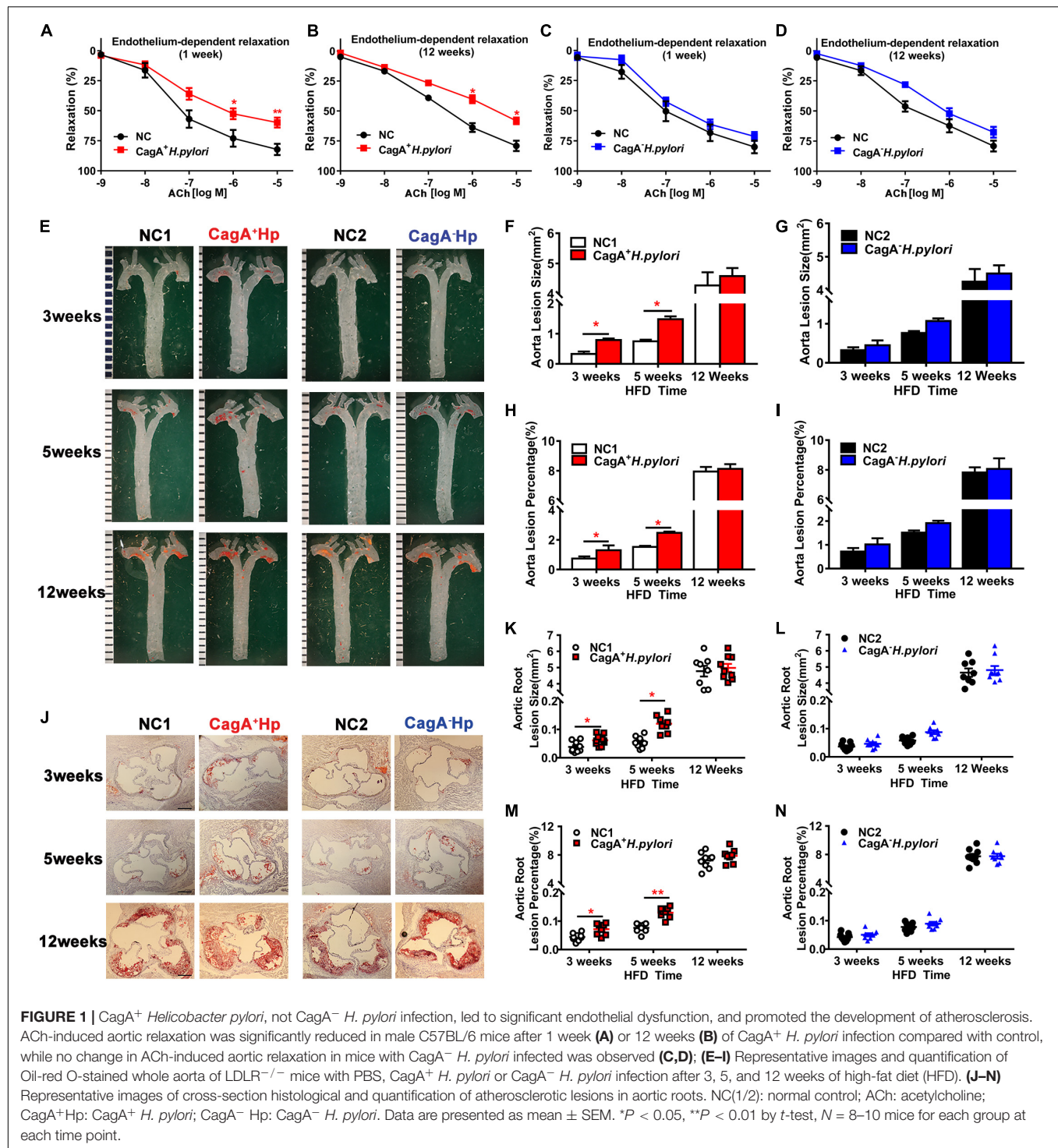
^aMethod 1: Intragastric gavage once a day for 1 day; ^bMethod 2: Intragastric gavage once a day for 2 days; ^cMethod 3: Intragastric gavage once a day for 3 days; ^dMethod 4: Intragastric gavage once a day for 3 days, take 1 day break, then gavage once a day for 3 days again.

higher gastric colonization rate than CagA[−] *H. pylori* under all infection conditions. All control mice were negative for *H. pylori* infection, confirming that no *H. pylori* contamination existed in the animal facility.

CagA⁺ *Helicobacter pylori*, Not CagA[−] *Helicobacter pylori* Infection, Induced Endothelial Dysfunction, and Promoted Atherosclerosis

To determine if a significant difference in endothelial dysfunction existed between mice infected with CagA⁺ *H. pylori* and CagA[−] *H. pylori*, both acute (1 week) and chronic (12 weeks) infection models were established using C57BL/6 mice with PBS as control. *Ex vivo* acetylcholine (ACh)-induced endothelium-dependent relaxation of aortic rings was significantly decreased in mice with CagA⁺ *H. pylori* infection at both 1 week and 12 weeks post-infection compared with control (Figures 1A,B). Endothelium-independent relaxation to nitroglycerin (NTG) was unchanged between the groups (Supplementary Figures 1A,B). In contrast, no significant changes in ACh-induced relaxation (Figures 1C,D) or NTG-induced relaxation (Supplementary Figures 1C,D) were observed in mice with CagA[−] *H. pylori* infection compared with control.

To determine if CagA⁺ *H. pylori* infection promotes the development of atherosclerosis, LDLR^{−/−} mice were infected with CagA⁺ *H. pylori* or CagA[−] *H. pylori* with PBS as control. Infection with CagA⁺ *H. pylori* significantly increased aortic atherosclerotic lesion areas in mice compared with PBS-treated controls after 3 and 5 weeks of HFD. However, no significant differences in aortic atherosclerotic lesion areas were present



between LDLR^{-/-} mice with CagA⁻ *H. pylori* infection and PBS-treated controls. After 12 weeks of HFD, all LDLR^{-/-} mice developed extensive atherosclerotic lesions with or without CagA⁺ *H. pylori* or CagA⁻ *H. pylori* infection (Figures 1E–N). These data suggest that CagA⁺ *H. pylori*, but not CagA⁻ *H. pylori* infection, accelerates early atherosclerotic development in LDLR^{-/-} mice on an HFD.

CagA⁺ *Helicobacter pylori* Infection Impaired Endothelial Function via Reactive Oxygen Species Production in Aorta

To test the hypothesis that CagA⁺ *H. pylori* infection impairs endothelial function through increased ROS production, aortic

vasodilation and ROS levels were assessed in C57BL/6 mice infected with CagA⁺ *H. pylori* or CagA⁻ *H. pylori* and controls receiving PBS. CagA⁺ *H. pylori* infection significantly decreased ACh-induced aortic relaxation in association with significantly increased aortic ROS production compared with their controls (Figure 2A). In contrast, CagA⁻ *H. pylori* infection had no significant effect on either aortic ACh-induced relaxation or ROS levels compared with controls (Figure 2A). There was no change in NTG-induced aortic relaxation in mice infected with CagA⁺ *H. pylori* or CagA⁻ *H. pylori* (Supplementary Figure 1). N-acetylcysteine (NAC) treatment effectively blocked excessive ROS production in aortic segments (Figure 2B) and preserved ACh-induced relaxation in mice after 1 or 12 weeks of CagA⁺ *H. pylori* infection (Figures 2C,D), without differences in NTG-induced relaxation (Figures 2E,F).

CagA⁺ *H. pylori*, not CagA⁻ *H. pylori* infection also significantly increased aortic ROS production in LDLR^{-/-} mice with 3 or 5 weeks of HFD feeding compared with their controls (Supplementary Figures 2A,B). After 12 weeks of HFD feeding, all LDLR^{-/-} mice exhibited increased ROS production with or without CagA⁺ *H. pylori* or CagA⁻ *H. pylori* infection (Supplementary Figure 2C).

CagA-Containing Exosomes Impaired Endothelial Function

To test the hypothesis that CagA⁺ *H. pylori*, but not CagA⁻ *H. pylori*, infection promotes exosomes production, leading to endothelial dysfunction, serum exosomes were prepared from mice with CagA⁺ *H. pylori* and CagA⁻ *H. pylori* infection as

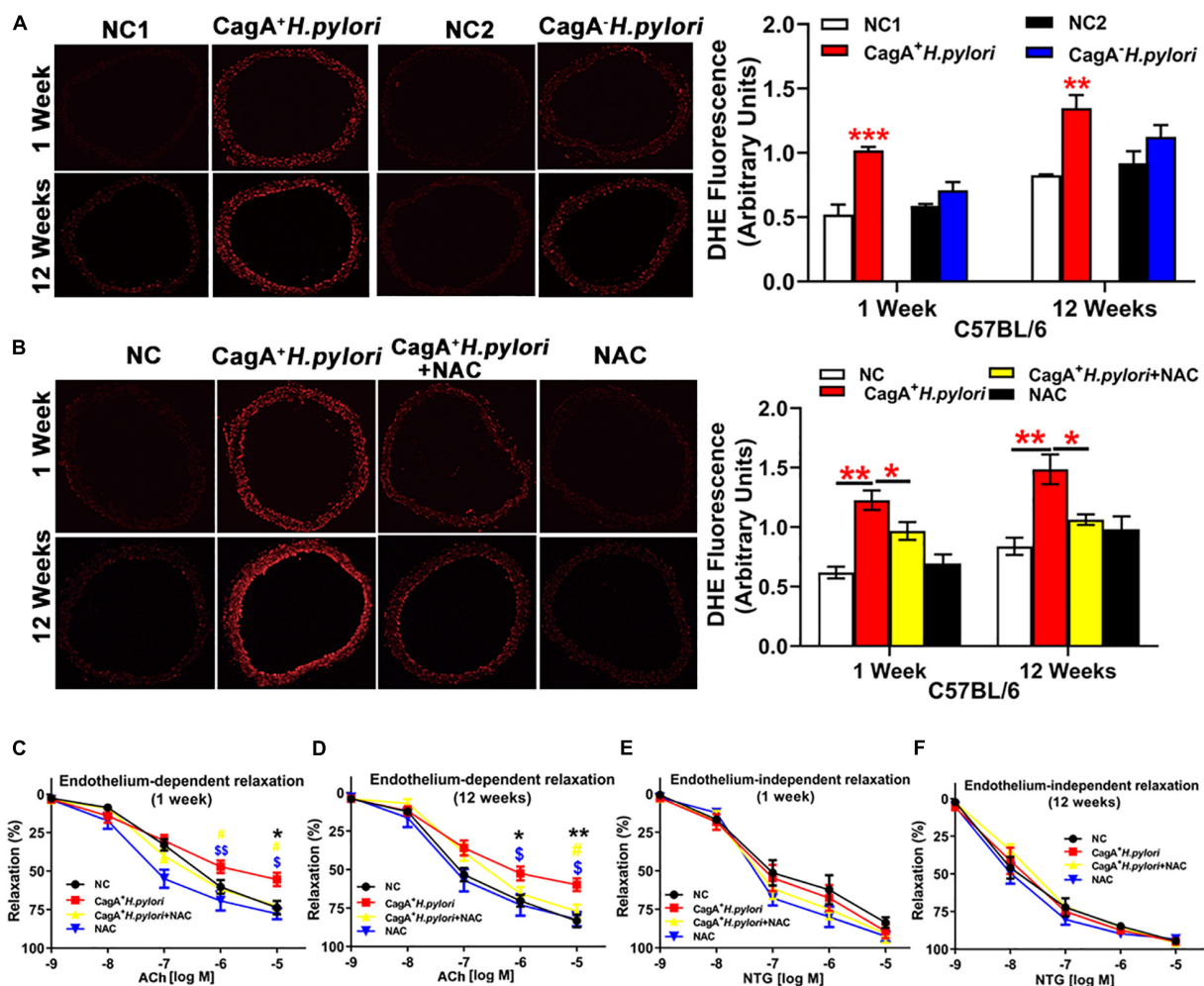


FIGURE 2 | CagA⁺ *H. pylori*, not CagA⁻ *H. pylori* infection, impaired endothelial function through increased ROS production in mice. Representative fluorescent images and quantification of ROS formation in the aorta of male C57BL/6 mice (A) (***P* < 0.01, ****P* < 0.001 by *t*-test) with CagA⁺ *H. pylori*, CagA⁻ *H. pylori* or PBS gavage. Aortic ROS production was significantly increased in mice with CagA⁺ *H. pylori* infection, not with CagA⁻ *H. pylori* infection. Treatment with NAC prevented aortic ROS production (B) (**P* < 0.05, ***P* < 0.01 by one-way ANOVA) and preserved ACh-induced aortic relaxation (C,D) in mice with 1 or 12 weeks of CagA⁺ *H. pylori* infection, without change in NTG-induced aortic relaxation (E,F). **P* < 0.05, ***P* < 0.01 (compared with NC), #*P* < 0.05 (compared with CagA⁺ *H. pylori* + NAC); \$*P* < 0.05, \$\$*P* < 0.01 (compared with NAC) by one-way ANOVA. NC(1/2): normal control. NAC: N-acetylcysteine; ACh: acetylcholine; NTG: nitroglycerin. Data are presented as mean ± SEM; *N* = 8–10 mice for each group at each time point.

well as non-infected control mice. Exosomes were characterized using transmission electron microscopy (TEM), nanoparticle tracking analysis (NTA), and western blotting (Figures 3A–C). Although there was no significant difference in serum exosomes level from mice infected with either *H. pylori* strain or controls (Figure 3D), treatment with serum exosomes from mice infected with CagA⁺ *H. pylori* significantly inhibited the function of

mouse bEND.3 cells *in vitro* with decreases in migration, tube formation and proliferation compared with control exosomes (Figures 3E–G). Culture with serum exosomes from mice with CagA[−] *H. pylori* infection had no significant effect on endothelial function (Figures 3E–G).

Exosomes from conditioned medium of human gastric epithelial cells (GES-1) cultured with CagA⁺ *H. pylori* or with

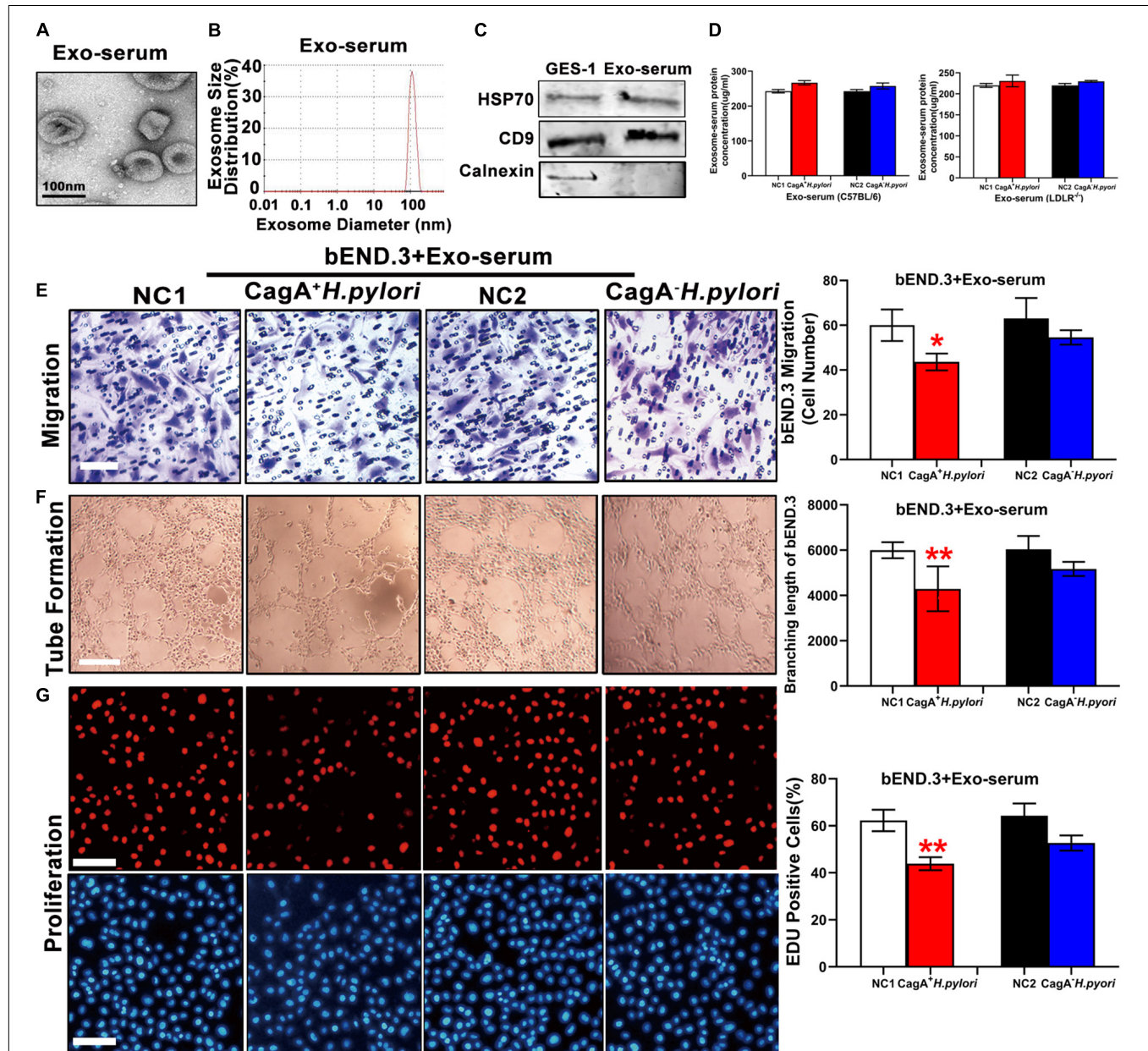


FIGURE 3 | Serum exosomes from CagA⁺ *H. pylori* infected mice impaired endothelial function. Mouse serum exosomes displayed typical features for exosomes including morphology on transmission electron microscopy (A) and size distribution (B). Western blotting analysis showed that the exosomes markers HSP70 and CD9 were present in the exosomes without the presence of calnexin (C). Although there was no significant difference in serum exosomes levels from mice infected with *H. pylori* compared to the controls (D), treatment with serum exosomes from mice with CagA⁺ *H. pylori* infection significantly inhibited the function of mouse bEND.3 cells *in vitro* with decreased migration (E, scale bars = 25 μ m), tube formation (F, scale bars = 25 μ m), and proliferation (G, scale bars = 100 μ m). Exo, Exosomes; Exo-serum: exosomes isolated from mouse serum; NC(1/2): normal control. Data are resented as mean \pm SEM; **P* < 0.05; ***P* < 0.01 by *t*-test, *N* = 8–10 mice for each group. Experiment was repeated 3 times for every measurement.

CagA⁻ *H. pylori* were prepared and similarly characterized by TEM, NTA and western blotting (Figures 4A–C). Co-culture of GES-1 with CagA⁺ *H. pylori*, not CagA⁻ *H. pylori*, significantly increased the exosomes level in conditioned media (Figure 4D). When using the same amount of exosomes (by protein level), exosomes from GES-1 co-cultured with CagA⁺ *H. pylori* significantly inhibited the functional properties of HUVECs *in vitro* with decreased proliferation, migration, and tube formation compared with non-infected control, while

exosomes from GES-1 co-cultured with CagA⁻ *H. pylori* did not significantly impact endothelial cell function (Figures 4E–G).

CagA-Containing Exosomes Impaired Endothelial Function *via* Reactive Oxygen Species Production

To test the hypothesis that CagA-containing exosomes impair endothelial function *via* ROS-mediated mechanisms, mouse

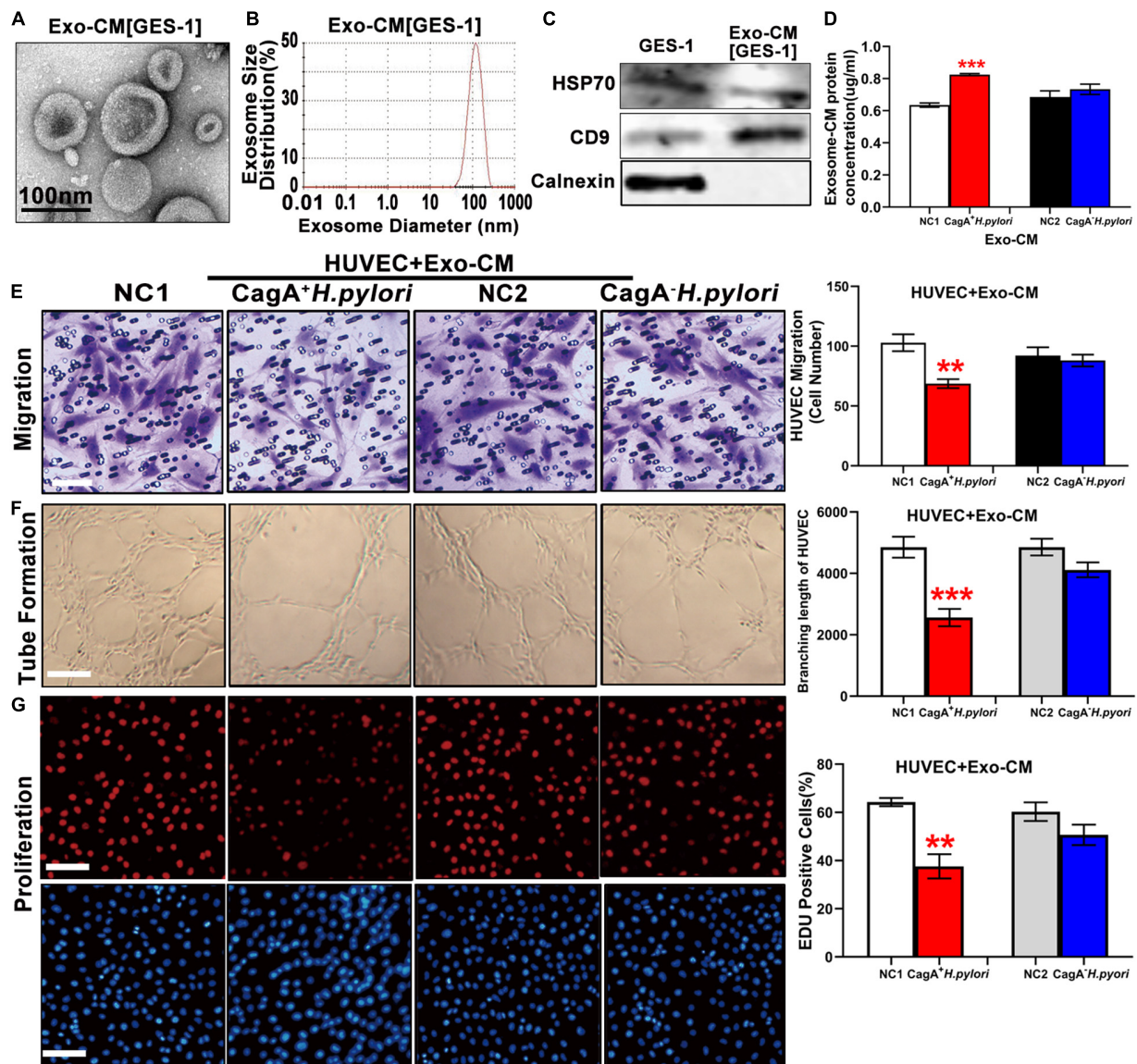


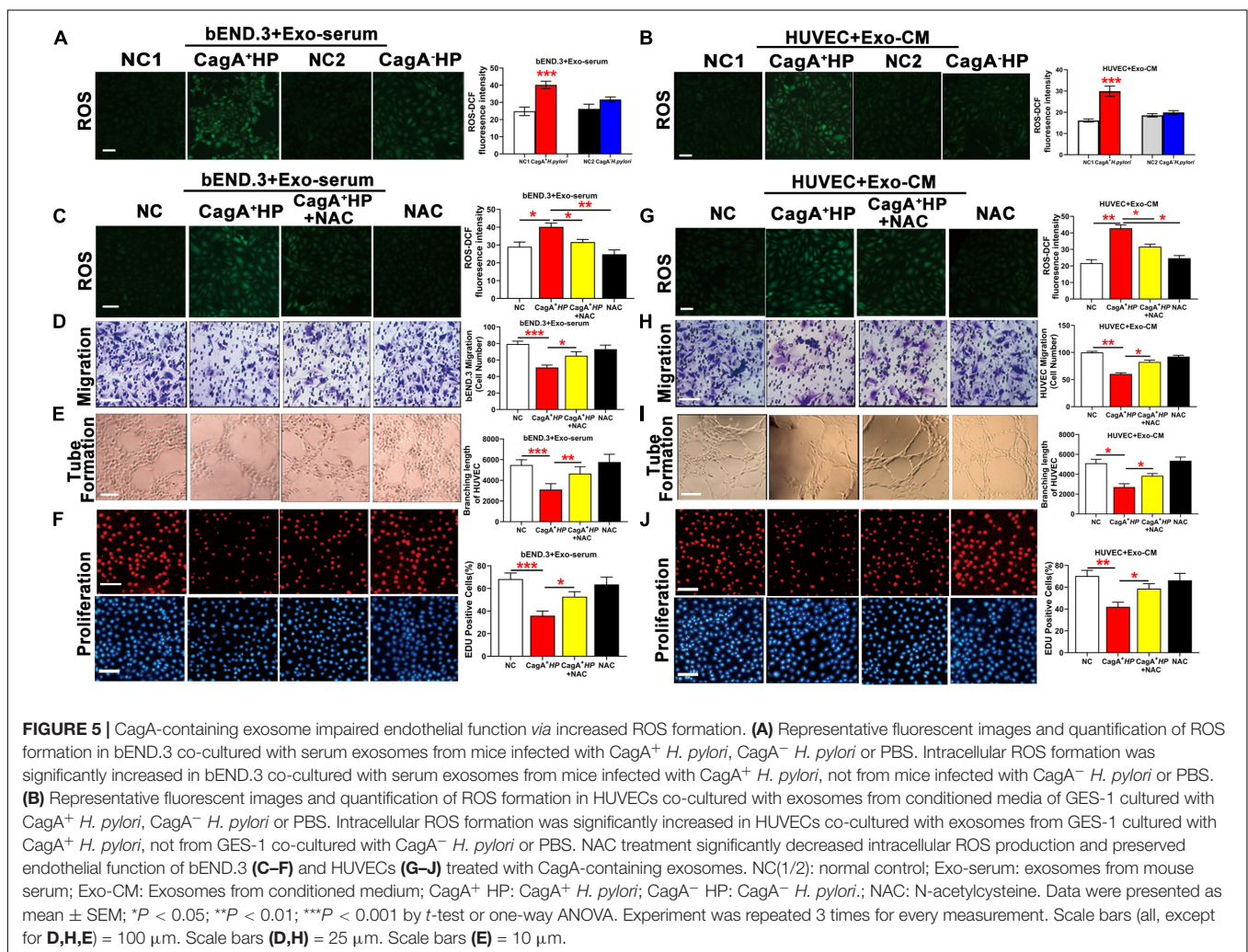
FIGURE 4 | Exosomes from conditioned medium of human gastric epithelial cells (GES-1) cultured with CagA⁺ *H. pylori*, not with CagA⁻ *H. pylori*, impaired endothelial function *in vitro*. Exosomes from conditioned medium of GES-1 cultured with CagA⁺ *H. pylori* exhibited typical exosome morphology (A) and size distribution (B). Western blotting analysis confirmed the presence of exosomes markers (HSP70, CD9) and absence of calnexin in exosomes (C). Exosome protein concentration was significantly higher in the conditioned medium of GES-1 cultured with CagA⁺ *H. pylori* than that cultured with CagA⁻ *H. pylori* (D). Treatment of HUVECs with exosomes-CM (100 ug/ml) from CagA⁺ *H. pylori*, not from CagA⁻ *H. pylori*, infected GES-1 significantly inhibited the function of HUVECs with decreased migration (E, scale bars = 25 μ m), tube formation (F, scale bars = 100 μ m), and proliferation (G, scale bars = 100 μ m). NC(1/2): normal control; GES-1: human gastric epithelial cells; HUVEC: human umbilical vein endothelial cell; Exo-CM: Exosomes from conditioned medium. Data are presented as mean \pm SEM; ** P < 0.01; *** P < 0.001 by *t*-test. Experiment was repeated 3 times for every measurement.

bEND.3 cells were treated with serum exosomes from mice infected with CagA⁺ *H. pylori*, or CagA⁻ *H. pylori* or from non-infected control mice. HUVECs were treated with exosomes from conditioned medium of GES-1 co-cultured with CagA⁺ *H. pylori*, CagA⁻ *H. pylori* or PBS. H2DCFDA assay showed that serum exosomes from mice with CagA⁺ *H. pylori*, not CagA⁻ *H. pylori* infection, significantly increased intracellular ROS formation in mouse bEND.3 cells compared to exosomes from non-infected controls (**Figure 5A**). Similarly, exosomes from conditioned media of GES-1 co-cultured with CagA⁺ *H. pylori*, not CagA⁻ *H. pylori*, significantly increased intracellular ROS levels in HUVECs (**Figure 5B**). CagA-containing exosomes-induced increase in intracellular ROS formation was associated with decreased endothelial function with reduced proliferation, migration, and tube formation in both bEND.3 (**Figures 5C–F**) and HUVECs (**Figures 5G–J**). NAC treatment decreased intracellular ROS production, and preserved function of bEND.3 (**Figure 5C**) and HUVECs (**Figure 5G**) in the presence of CagA-containing exosomes (**Figures 5D–F,H–J**). These data suggest that the effect of CagA-containing exosomes on endothelial function was indeed mediated *via* ROS formation.

Treatment With GW4869 Prevented CagA⁺ *Helicobacter pylori* Infection-Induced Reactive Oxygen Species Production, Endothelial Dysfunction, and Atherosclerosis

To further test the hypothesis that CagA⁺ *H. pylori* infection impairs endothelial function through CagA-containing exosomes-mediated ROS formation, C57BL/6 mice were pre-treated with GW4869 to block exosomes release *in vivo*. As detailed earlier, CagA⁺ *H. pylori* infection significantly increased aortic ROS level (**Figure 2A**) in mice in association with impaired ACh-induced relaxation (**Figures 1A,C**). Treatment with GW4869 significantly reduced serum exosomes levels (**Figure 6A**), prevented excessive aortic ROS production (**Figures 6B,C**) and preserved ACh-induced relaxation in mice with CagA⁺ *H. pylori* infection (**Figures 6D,E**).

Treatment with GW4869 significantly decreased serum exosomes level in LDLR^{-/-} mice with *H. pylori* infection (**Figure 6F**), and effectively prevented excessive aortic ROS formation (**Figures 6G,H**). Blocking exosomes release with



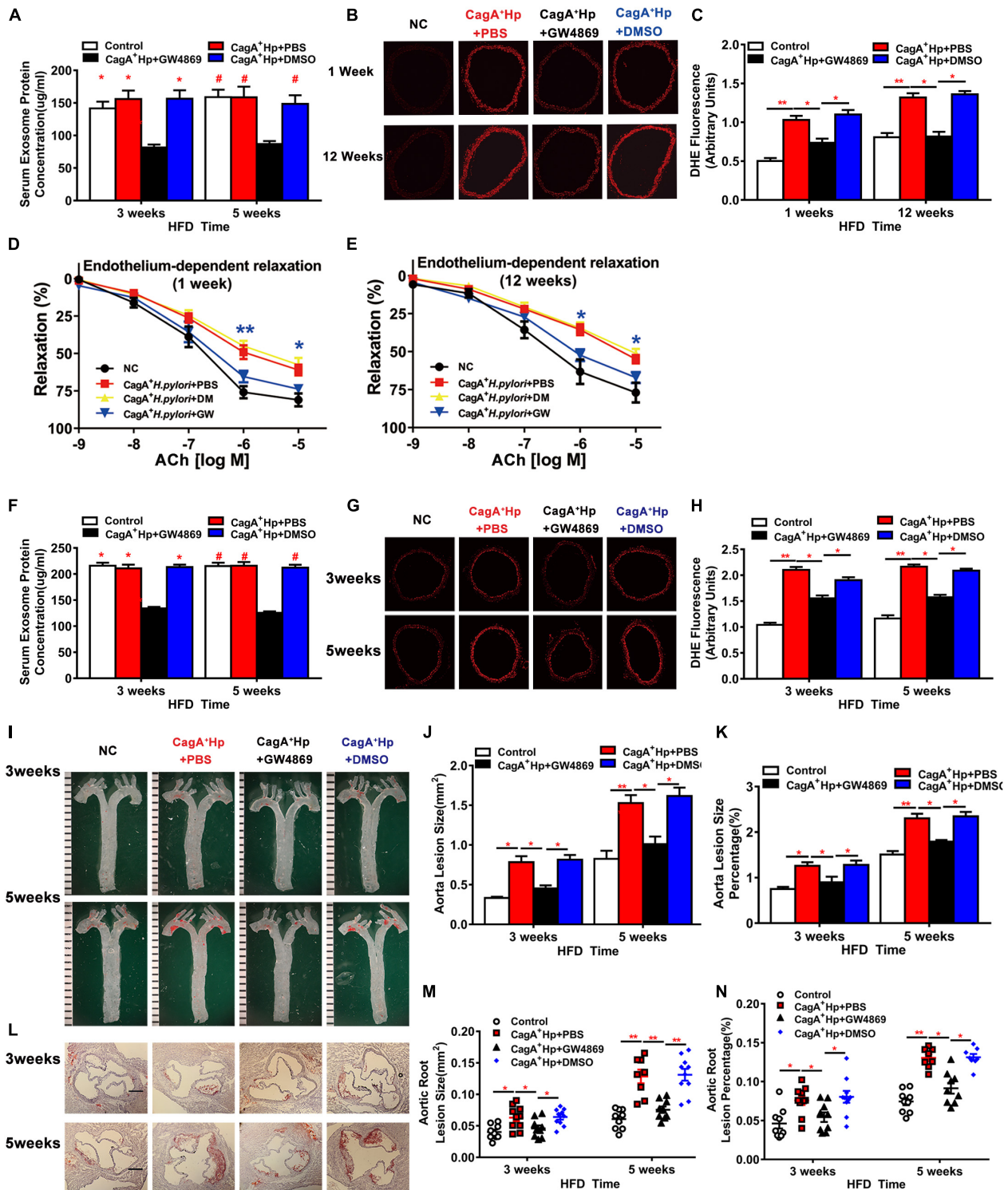


FIGURE 6 | Blocking exosomes release with GW4869 prevented endothelial dysfunction and atherosclerosis in mice with CagA⁺ *H. pylori* infection. Treatment with GW4869 significantly decreased the serum exosome level (A) and ROS formation in thoracic aorta (B–C) with improved ACh-induced aortic relaxation (D,E) (**P* < 0.05, ***P* < 0.01, CagA⁺ *H. pylori* vs. CagA⁺ *H. pylori* + NAC by one-way ANOVA) in C57BL/6 mice with CagA⁺ *H. pylori* infection. GW4869 treatment also significantly decreased serum exosomes level in LDLR^{-/-} mice with CagA⁺ *H. pylori* infection (F). After 3 or 5 weeks of high-fat diet (HFD), ROS formation (G,H) and atherosclerotic plaque formation in aorta and aortic root (I–N) were significantly increased in LDLR^{-/-} mice with CagA⁺ *H. pylori* infection that were prevented with GW4869 treatment. NC: normal control; ACh: acetylcholine; CagA⁺ Hp: CagA⁺ *H. pylori*; DMSO: dimethylsulfoxide (solvent for GW4869). Data are presented as mean ± SEM. **P* < 0.05, ***P* < 0.01 by one-way ANOVA, *N* = 8–10 mice for each group at each time point.

GW4869 also prevented CagA⁺ *H. pylori* infection-induced increases in aortic atherosclerotic burden. At three and 5 weeks of HFD feeding, there were no differences in the prevalence of aortic atherosclerotic lesion and total lesion areas between LDLR^{-/-} mice with CagA⁺ *H. pylori* infection with GW4869 treatment and non-infected LDLR^{-/-} control mice (Figures 6I–N). No significant effects of DMSO (vehicle for GW4869) on aortic ROS formation or aortic atherosclerotic burden were observed in hyperlipidemic LDLR^{-/-} mice with CagA⁺ *H. pylori* infection (Figures 6A–N). Treatment with GW4869 had no significant effect on atherosclerosis in hyperlipidemic LDLR^{-/-} mice without CagA⁺ *H. pylori* infection (Supplementary Figure 3). These data suggest that CagA⁺ *H. pylori* infection leads to significant endothelial dysfunction and increased atherosclerosis through CagA-containing exosomes-mediated ROS formation.

DISCUSSION

The data from the present study demonstrated: (1) CagA⁺ *H. pylori* achieved gastric colonization more effectively than CagA⁻ *H. pylori*; (2) CagA⁺ *H. pylori* infection induced endothelial dysfunction and promoted atherosclerosis; (3) exosomes from the serum of mice with CagA⁺ *H. pylori* infection, and exosomes from conditioned media of GES-1 co-cultured with CagA⁺ *H. pylori* significantly increased intracellular ROS and decreased endothelial function that were prevented with NAC treatment; and (4) NAC or GW4869 treatment effectively prevented aortic ROS production and aortic endothelial dysfunction in mice with CagA⁺ *H. pylori* infection. Importantly, these effects appear specific to CagA⁺ *H. pylori* and were not evident following CagA⁻ *H. pylori* infection. Collectively, these data suggest that CagA⁺ *H. pylori* infection impairs endothelial function through ROS production induced by CagA-containing exosomes.

The finding that CagA⁺ *H. pylori* colonized gastric mucosa more effectively than CagA⁻ *H. pylori* may provide an explanation for the clinical observation that over 90% of *H. pylori* patients are infected with the CagA⁺ *H. pylori* strain. Colonization in gastric epithelial cells is the critical initial event for *H. pylori* invasion and survival, and subsequent pathological changes in vasculature and other organ systems. With pH values as low as 1.5–2.5, the stomach fluid has been recognized as a natural antibiotic barrier (21). To colonize and survive in gastric mucous, bacteria have to overcome the extremely acidic and hypoxic environment. *H. pylori* in general has established multiple mechanisms to adapt and encounter the challenges in the stomach (22). However, CagA protein in CagA⁺ *H. pylori* may help their gastric colonization and promote persistent infection. Although some data shows that CagA⁺ *H. pylori* may be more susceptible to re-exposure to acidic environment (at pH 3.0) than CagA⁻ *H. pylori* in culture, CagA expression could increase the acid-tolerance and resistance capabilities of *H. pylori* (23), enabling the bacteria to survive under the acidic conditions of the stomach. CagA⁺ *H. pylori* delivers CagA through a T4SS into gastric epithelial cells. The translocated CagA then dysregulates the homeostatic signal transduction of gastric

epithelial cells involved in chronic inflammation and malignancy by changing cell polarity, apoptosis, and proliferation (24). In addition, CagA could activate host cell survival and antiapoptotic pathways to enhance self-renewal of gastric epithelium, helping sustain *H. pylori* infection (25). CagA could abrogate human β -defensin-3 expression via EGFR dephosphorylation, enhancing the ability to achieve persistent gastric infection of CagA⁺ *H. pylori* (24).

Compared to those with CagA⁻ *H. pylori* infection, patients with CagA⁺ *H. pylori* infection have a much higher incidence of CVDs, including atherosclerosis (26–30). Endothelial dysfunction is a key contributing factor for CVDs including atherosclerosis. The present study showed that infection with CagA⁺ *H. pylori*, not CagA⁻ *H. pylori*, significantly impaired endothelial function in C57BL/6 mice, and promoted the development of early atherosclerosis in hyperlipidemic LDLR^{-/-} mice. Atherosclerosis is characterized by chronic inflammation with increased ROS formation (31, 32). CagA⁺ *H. pylori* infection produces persistent low-grade systematic inflammation with increased production of pro-inflammatory cytokines, including CRP, IL-6, and IL-18 (33, 34). Immune-mediated responses targeting self-antigens may play an important role in atherosclerosis (35, 36). Interestingly, CagA has been proposed as an antigen that could activate autoimmune mechanisms. The anti-CagA antibodies are able to react with both bacterial CagA and proteins in medium and large arteries (35). Thus, anti-CagA antibodies may cross-react with proteins in vascular smooth muscle cells, fibroblast-like cells, and other cells that are involved in the initiation and progression of atherosclerosis (37). In addition, gut microbiota plays an important role in the development of atherosclerosis, and there is a relationship between gastric and intestinal microbiome and *H. pylori* infection. It has been demonstrated that there are significant differences in the diversity and number of gut microbiota between *H. pylori* infected and uninfected individuals (38, 39). It will be important to determine if CagA⁺ *H. pylori* infection could impair the population and balance of gut microbiota more than CagA⁻ *H. pylori* infection, thus leading to endothelial dysfunction and atherosclerosis.

The present study showed that CagA⁺ *H. pylori*, but not CagA⁻ *H. pylori*, infection significantly increased the level of aortic ROS in mice. This is consistent with the concept that CagA⁺ *H. pylori*, not CagA⁻ *H. pylori*, infection attenuates endothelial function and promotes the development of early atherosclerosis, and may provide an explanation for the clinical findings that patients with CagA⁺ *H. pylori* infection have significantly increased risk for atherosclerosis as compared with those with CagA⁻ *H. pylori* infection. This finding is also consistent with the results from our previous study with human subjects that *H. pylori* infection selectively increases the risk of carotid atherosclerosis for male patients younger than 50 years of age (40). A recent study, using a large database of 208,196 patients, reveals that there is a significant decrease in composite endpoints for CAD and death for younger patients (<65 years old) with early *H. pylori* eradication therapy, but not for older patients (≥ 65 years old) or control subjects (41). Further studies are needed to address the important question why

H. pylori infection selectively increases the risk of atherosclerosis for young males.

Exosomes are critically involved in cell function and disease development through direct and indirect cell-cell communications and the transfer of bioactive substances including proteins and microRNAs (42, 43). There are extensive interactions between exosomes and ROS. Exosomes can increase or decrease ROS production through various mechanisms, and ROS can regulate exosomes production and their contents as extensively summarized in a recent review by Bodega and colleagues (44). Study shows that PKH67-labeled CagA-containing exosomes readily enter HUVECs, and significantly inhibited cellular function (10). In the present study, serum exosomes from mice with CagA⁺ *H. pylori* infection, and exosomes from conditioned media of human GES-1 co-cultured with CagA⁺ *H. pylori* increased intracellular ROS production and inhibited the function of endothelial cells. In both situations, the effects of CagA⁺ *H. pylori* infection were effectively prevented with NAC treatment. Inhibition of exosomes release with GW4869 effectively prevented aortic ROS production and aortic endothelial dysfunction in mice as well as atherosclerotic burden in hyperlipidemic LDLR^{-/-} mice with CagA⁺ *H. pylori* infection. One may argue that GW4869 is a non-specific inhibitor of exosomes release, and thus the effect of GW4869 on atherosclerosis in mice with CagA⁺ *H. pylori* infection might be non-specific. However, our previous study showed that GW4869 treatment had no effect on endothelial function in mice without *H. pylori* infection (10). In the present study, no significant effect of GW4869 on atherosclerosis was observed in hyperlipidemic LDLR^{-/-} mice without CagA⁺ *H. pylori* infection. Collectively, these data support a mechanism whereby CagA⁺ *H. pylori* infection impairs endothelial function through CagA-containing exosomes-induced ROS production. Soluble components from *H. pylori*, including CagA, VacA, urease, and neutrophil activating factor A (NapA), could conceivably enter the circulation through exosomes, and trigger inflammatory responses and oxidative stress (45). Exosomal CagA from *H. pylori*-infected gastric epithelial cells has been shown to induce macrophage foam cell formation (46). Further studies are needed to define the specific molecule(s) in the exosomes that contributes to ROS production in endothelial cells and the consequent impairments in cellular function.

There are many factors that are important for *H. pylori* infection and the specific strains of infection, including (but not limited to) geographic locations and dietary habits. The prevalence of *H. pylori* infection varies significantly in the globe due to substantial differences in the population, culture, individual lifestyles, social and economic status, as well as environmental factors. Studies have shown that the prevalence of *H. pylori* infection are higher in Central/South America and Asia than other regions (47). However, the association between *H. pylori* infection and dietary habits remains inconsistent. It has been reported that intake of some uncooked vegetables and seafood, such as tomato, pepper, and mussels, correlates significantly with *H. pylori* infection (48). In contrast, no association is observed between *H. pylori* infection and intake of fruits, fish, legumes, honey, spices, meats, milk, and milk

products. A cross-sectional study has shown no relationship between *H. pylori* infection and dietary habits (49). Some data suggest that consumption of honey and green/black tea may be associated with decreased prevalence of *H. pylori* infection (50). Further studies are needed to determine if diet could play a different role in the infection of CagA⁺ *H. pylori* vs. CagA⁻ *H. pylori*.

It is very concerning that cardiovascular mortality has been increasing since 2010 especially for male subjects for unknown reasons (51). Studies suggest that *H. pylori* infection could be a significant risk factor for endothelial dysfunction, atherosclerosis, and CAD in young patients, and could provide a potential explanation for young patients who develop CAD without a clear etiology (41, 52). It is unclear why *H. pylori* infection does not increase the risk for atherosclerosis for patients older than 50 years. The pathophysiology of atherosclerosis is very complex and multifactorial that has not been fully understood. The data from the present study and our previous study (10) suggest that *H. pylori* infection could serve as a trigger to initiate the development of early atherosclerosis by compromising endothelial function at the initial phase of atherosclerosis. Other important factors including diabetes mellitus, hypertension, and hyperlipidemia may play a dominant role that could unmask the contribution of *H. pylori* infection to atherosclerosis in older patients. Further studies are needed to investigate the mechanism(s) on the selective effect of *H. pylori* infection on atherosclerosis in young populations. Clinically, it is reasonable to screen young male populations for *H. pylori* infection once a year and to treat them accordingly as an effective approach for early prevention of CVDs, especially premature atherosclerosis as the majority of patients with *H. pylori* infection are asymptomatic.

Study Limitations

The limitations in the present study include: (1) only male mice were used; (2) no studies were performed to determine the specific molecules in CagA-containing exosomes that could be primarily responsible for increasing ROS production and endothelial dysfunction and related mechanism(s); and (3) no studies were conducted to define the key pathway(s) that may significantly contribute to increased ROS levels in endothelial cells with CagA⁺ *H. pylori* infection.

CONCLUSION

The data suggested that CagA⁺ *H. pylori* colonized gastric mucosa more effectively than CagA⁻ *H. pylori*. CagA⁺ *H. pylori*, but not CagA⁻ *H. pylori*, infection induced endothelial dysfunction and promoted development of atherosclerosis through CagA-containing exosomes-mediated ROS formation.

DATA AVAILABILITY STATEMENT

The raw data supporting the conclusions of this article will be made available by the authors, without undue reservation.

ETHICS STATEMENT

The animal study was reviewed and approved by the Institutional Animal Care and Use Committee of the University of Missouri School of Medicine, Columbia, MO, United States.

AUTHOR CONTRIBUTIONS

ZL contributed to the conception and designed the study. XX, LZ, HW, FC, XL, YC, QZ, and MW contributed to the data collections and analysis. XX, LZ, HX, and WF contributed to the exosomes preparations and characterization. XX, LZ, LM-L, and MH contributed to the vascular function studies. XX and LZ drafted the manuscript. HH, D-PL, WF, LM-L, MH, CX, and ZL critically reviewed and interpreted the data and revised the manuscript. All authors contributed to the article and approved the submitted version.

REFERENCES

- Mentis A, Lehours P, Megraud F. Epidemiology and diagnosis of *Helicobacter pylori* infection. *Helicobacter*. (2015) 20(Suppl. 1):1–7. doi: 10.1111/hel.12250
- Eusebi LH, Zagari RM, Bazzoli F. Epidemiology of *Helicobacter pylori* infection. *Helicobacter*. (2014) 19(Suppl. 1):1–5. doi: 10.1111/hel.12165
- Covacci A, Censini S, Bugnoli M, Petracca R, Burrone D, Macchia G, et al. Molecular characterization of the 128-kDa immunodominant antigen of *Helicobacter pylori* associated with cytotoxicity and duodenal ulcer. *Proc Natl Acad Sci USA*. (1993) 90:5791–5. doi: 10.1073/pnas.90.12.5791
- Tummuru MK, Cover TL, Blaser MJ. Cloning and expression of a high-molecular-mass major antigen of *Helicobacter pylori*: evidence of linkage to cytotoxin production. *Infect Immun*. (1993) 61:1799–809. doi: 10.1128/iai.61.5.1799-1809.1993
- Hatakeyama M. *Helicobacter pylori* CagA – a bacterial intruder conspiring gastric carcinogenesis. *Int J Cancer*. (2006) 119:1217–23. doi: 10.1002/ijc.21831
- Shmueli H, Passaro DJ, Vaturi M, Sagie A, Pitlik S, Samra Z, et al. Association of CagA⁺ *Helicobacter pylori* infection with aortic atheroma. *Atherosclerosis*. (2005) 179:127–32. doi: 10.1016/j.atherosclerosis.2004.09.010
- Gimbrone MA Jr, Garcia-Cardena G. Endothelial cell dysfunction and the pathobiology of atherosclerosis. *Circ Res*. (2016) 118:620–36. doi: 10.1161/CIRCRESAHA.115.306301
- Pietrojusti A, Diomedes M, Silvestrini M, Cupini LM, Luzzi I, Gomez-Miguel MJ, et al. Cytotoxin-associated gene-A-positive *Helicobacter pylori* strains are associated with atherosclerotic stroke. *Circulation*. (2002) 106:580–4. doi: 10.1161/01.cir.0000023894.10871.2f
- Xiong X, Chen J, He M, Wu T, Yang H. *Helicobacter pylori* infection and the prevalence of hypertension in Chinese adults: the Dongfeng-Tongji cohort. *J Clin Hypertens (Greenwich)*. (2020) 22:1389–95. doi: 10.1111/jch.13928
- Xia X, Zhang L, Chi J, Li H, Liu X, Hu T, et al. *Helicobacter pylori* infection impairs endothelial function through an exosome-mediated mechanism. *J Am Heart Assoc*. (2020) 9:e014120. doi: 10.1161/JAHA.119.014120
- Zhang H, Deng T, Liu R, Ning T, Yang H, Liu D, et al. CAF secreted miR-522 suppresses ferroptosis and promotes acquired chemo-resistance in gastric cancer. *Mol Cancer*. (2020) 19:43. doi: 10.1186/s12943-020-01168-8
- Haney MJ, Klyachko NL, Zhao Y, Gupta R, Plotnikova EG, He Z, et al. Exosomes as drug delivery vehicles for Parkinson's disease therapy. *J Control Release*. (2015) 207:18–30. doi: 10.1016/j.jconrel.2015.03.033
- Zhang L, Liu H, Jia L, Lyu J, Sun Y, Yu H, et al. Exosomes mediate hippocampal and cortical neuronal injury induced by hepatic ischemia-reperfusion injury through activating pyroptosis in rats. *Oxid Med Cell Longev*. (2019) 2019:3753485. doi: 10.1155/2019/3753485

FUNDING

This work was supported by the US National Institutes of Health grant HL148196 (ZL).

ACKNOWLEDGMENTS

We thank Thomas Spencer for his technical help on the characterization of exosomes.

SUPPLEMENTARY MATERIAL

The Supplementary Material for this article can be found online at: <https://www.frontiersin.org/articles/10.3389/fcvm.2022.881372/full#supplementary-material>

- Guo H, Zhang J, Boudreau M, Meng J, Yin JJ, Liu J, et al. Intravenous administration of silver nanoparticles causes organ toxicity through intracellular ROS-related loss of inter-endothelial junction. *Part Fibre Toxicol*. (2016) 13:21. doi: 10.1186/s12989-016-0133-9
- Sayin VI, Ibrahim MX, Larsson E, Nilsson JA, Lindahl P, Bergo MO. Antioxidants accelerate lung cancer progression in mice. *Sci Transl Med*. (2014) 6:221ra15. doi: 10.1126/scitranslmed.3007653
- Cui Y, Liu L, Xiao Y, Li X, Zhang J, Xie X, et al. N-acetylcysteine differentially regulates the populations of bone marrow and circulating endothelial progenitor cells in mice with limb ischemia. *Eur J Pharmacol*. (2020) 881:173233. doi: 10.1016/j.ejphar.2020.173233
- Chai Y, Cao Z, Yu R, Liu Y, Yuan D, Lei L. Dexmedetomidine attenuates LPS-induced monocyte-endothelial adherence via inhibiting Cx43/PKC- α /NOX2/ROS signaling pathway in monocytes. *Oxid Med Cell Longev*. (2020) 2020:2930463. doi: 10.1155/2020/2930463
- Centa M, Ketelhuth DFJ, Malin S, Gistera A. Quantification of atherosclerosis in mice. *J Vis Exp*. (2019) 148:e59828. doi: 10.3791/59828
- Lau YS, Tian XY, Mustafa MR, Murugan D, Liu J, Zhang Y, et al. Boldine improves endothelial function in diabetic db/db mice through inhibition of angiotensin II-mediated BMP4-oxidative stress cascade. *Br J Pharmacol*. (2013) 170:1190–8. doi: 10.1111/bph.12350
- Thery C, Amigorena S, Raposo G, Clayton A. Isolation and characterization of exosomes from cell culture supernatants and biological fluids. *Curr Protoc Cell Biol*. (2006) Chapter 3:Unit 3.22. doi: 10.1002/0471143030.cb0322s30
- Singh A, Barnard TG. Surviving the acid barrier: responses of pathogenic *Vibrio cholerae* to simulated gastric fluid. *Appl Microbiol Biotechnol*. (2016) 100:815–24. doi: 10.1007/s00253-015-7067-2
- Ansari S, Yamaoka Y. Survival of *Helicobacter pylori* in gastric acidic territory. *Helicobacter*. (2017) 22:e12386. doi: 10.1111/hel.12386
- Karita M, Blaser MJ. Acid-tolerance response in *Helicobacter pylori* and differences between cagA⁺ and cagA⁻ strains. *J Infect Dis*. (1998) 178:213–9. doi: 10.1086/515606
- Backert S, Tegtmeyer N. Type IV secretion and signal transduction of *Helicobacter pylori* CagA through interactions with host cell receptors. *Toxins (Basel)*. (2017) 9:115. doi: 10.3390/toxins9040115
- Mimuro H, Suzuki T, Nagai S, Rieder G, Suzuki M, Nagai T, et al. *Helicobacter pylori* dampens gut epithelial self-renewal by inhibiting apoptosis, a bacterial strategy to enhance colonization of the stomach. *Cell Host Microbe*. (2007) 2:250–63. doi: 10.1016/j.chom.2007.09.005
- Wang B, Yu M, Zhang R, Chen S, Xi Y, Duan G. A meta-analysis of the association between *Helicobacter pylori* infection and risk of atherosclerotic cardiovascular disease. *Helicobacter*. (2020) 25:e12761. doi: 10.1111/hel.12761
- Rasmi Y, Rouhrai H, Khayati-Shal E, Shirpoor A, Saboori E. Association of endothelial dysfunction and cytotoxin-associated gene A-positive *Helicobacter*

- pylori* in patients with cardiac syndrome X. *Biomed J.* (2016) 39:339–45. doi: 10.1016/j.bj.2016.01.010
28. Gunn M, Stephens JC, Thompson JR, Rathbone BJ, Samani NJ. Significant association of cagA positive *Helicobacter pylori* strains with risk of premature myocardial infarction. *Heart.* (2000) 84:267–71. doi: 10.1136/heart.84.3.267
 29. Khodai Z, Vakili H, Ghaderian SM, Najari RA, Panah AS. Association of *Helicobacter pylori* infection with acute myocardial infarction. *Coron Artery Dis.* (2011) 22:6–11. doi: 10.1097/MCA.0b013e3283402360
 30. Mayr M, Kiechl S, Mendall MA, Willeit J, Wick G, Xu Q. Increased risk of atherosclerosis is confined to CagA-positive *Helicobacter pylori* strains: prospective results from the Bruneck study. *Stroke.* (2003) 34:610–5. doi: 10.1161/01.STR.0000058481.82639.EF
 31. Wu X, Zhang H, Qi W, Zhang Y, Li J, Li Z, et al. Nicotine promotes atherosclerosis via ROS-NLRP3-mediated endothelial cell pyroptosis. *Cell Death Dis.* (2018) 9:171. doi: 10.1038/s41419-017-0257-3
 32. Kattoor AJ, Pothineni NVK, Palagiri D, Mehta JL. Oxidative stress in atherosclerosis. *Curr Atheroscler Rep.* (2017) 19:42. doi: 10.1007/s11883-017-0678-6
 33. Ebrahimi A, Soofizadeh B, Ebrahimi F, Moaadab SY, Bonyadi M, Gojazadeh M, et al. Relationship between *Helicobacter pylori* cytotoxin-associated gene A protein with clinical outcomes in patients with rheumatoid arthritis. *Immunol Lett.* (2019) 211:49–52. doi: 10.1016/j.imlet.2019.05.014
 34. Figura N, Palazzuoli A, Vaira D, Campagna M, Moretti E, Iacoponi F, et al. Cross-sectional study: CagA-positive *Helicobacter pylori* infection, acute coronary artery disease and systemic levels of B-type natriuretic peptide. *J Clin Pathol.* (2014) 67:251–7. doi: 10.1136/jclinpath-2013-201743
 35. Franceschi F, Sepulveda AR, Gasbarrini A, Pola P, Silveri NG, Gasbarrini G, et al. Cross-reactivity of anti-CagA antibodies with vascular wall antigens: possible pathogenic link between *Helicobacter pylori* infection and atherosclerosis. *Circulation.* (2002) 106:430–4. doi: 10.1161/01.cir.0000024100.90140.19
 36. George J, Harats D, Shoenfeld Y. Autoimmunity in atherosclerosis. The role of autoantigens. *Clin Rev Allergy Immunol.* (2000) 18:73–86. doi: 10.1385/CRIAI:18:1:73
 37. Rozankovic PB, Huzjan AL, Cupic H, Bencic JJ, Basic S, Demarin V. Influence of CagA-positive *Helicobacter pylori* strains on atherosclerotic carotid disease. *J Neurol.* (2011) 258:753–61. doi: 10.1007/s00415-010-5824-9
 38. Klymiuk I, Bilgiler C, Stadlmann A, Thannesberger J, Kastner MT, Hogenauer C, et al. The human gastric microbiome is predicated upon infection with *Helicobacter pylori*. *Front Microbiol.* (2017) 8:2508. doi: 10.3389/fmicb.2017.02508
 39. Suarez-Jaramillo A, Baldeon ME, Prado B, Fornasini M, Cohen H, Flores N, et al. Duodenal microbiome in patients with or without *Helicobacter pylori* infection. *Helicobacter.* (2020) 25:e12753. doi: 10.1111/hel.12753
 40. Zhang L, Chen Z, Xia X, Chi J, Li H, Liu X, et al. *Helicobacter pylori* infection selectively increases the risk for carotid atherosclerosis in young males. *Atherosclerosis.* (2019) 291:71–7. doi: 10.1016/j.atherosclerosis.2019.10.005
 41. Wang JW, Tseng KL, Hsu CN, Liang CM, Tai WC, Ku MK, et al. Association between *Helicobacter pylori* eradication and the risk of coronary heart diseases. *PLoS One.* (2018) 13:e0190219. doi: 10.1371/journal.pone.0190219
 42. Pegtel DM, Gould SJ. Exosomes. *Annu Rev Biochem.* (2019) 88:487–514. doi: 10.1146/annurev-biochem-013118-111902
 43. Thery C, Zitvogel L, Amigorena S. Exosomes: composition, biogenesis and function. *Nat Rev Immunol.* (2002) 2:569–79. doi: 10.1038/nri855
 44. Bodega G, Alique M, Puebla L, Carracedo J, Ramirez RM. Microvesicles: ROS scavengers and ROS producers. *J Extracell Vesicles.* (2019) 8:1626654. doi: 10.1080/20013078.2019.1626654
 45. Jarzab M, Posselt G, Meisner-Kober N, Wessler S. *Helicobacter pylori*-derived outer membrane vesicles (OMVs): role in bacterial pathogenesis? *Microorganisms.* (2020) 8:1328. doi: 10.3390/microorganisms8091328
 46. Yang S, Xia YP, Luo XY, Chen SL, Li BW, Ye ZM, et al. Exosomal CagA derived from *Helicobacter pylori*-infected gastric epithelial cells induces macrophage foam cell formation and promotes atherosclerosis. *J Mol Cell Cardiol.* (2019) 135:40–51. doi: 10.1016/j.yjmcc.2019.07.011
 47. Peleteiro B, Bastos A, Ferro A, Lunet N. Prevalence of *Helicobacter pylori* infection worldwide: a systematic review of studies with national coverage. *Dig Dis Sci.* (2014) 59:1698–709. doi: 10.1007/s10620-014-3063-0
 48. Monno R, De Laurentiis V, Trerotoli P, Roselli AM, Ierardi E, Portincasa P. *Helicobacter pylori* infection: association with dietary habits and socioeconomic conditions. *Clin Res Hepatol Gastroenterol.* (2019) 43:603–7. doi: 10.1016/j.clinre.2018.10.002
 49. Assaad S, Chaaban R, Tannous F, Costanian C. Dietary habits and *Helicobacter pylori* infection: a cross sectional study at a Lebanese hospital. *BMC Gastroenterol.* (2018) 18:48. doi: 10.1186/s12876-018-0775-1
 50. Boyanova L, Ilieva J, Gergova G, Vladimirov B, Nikolov R, Mitov I. Honey and green/black tea consumption may reduce the risk of *Helicobacter pylori* infection. *Diagn Microbiol Infect Dis.* (2015) 82:85–6. doi: 10.1016/j.diagmicrobio.2015.03.001
 51. Tsao CW, Aday AW, Almarzooq ZI, Alonso A, Beaton AZ, Bittencourt MS, et al. Heart disease and stroke statistics-2022 update: a report from the American heart association. *Circulation.* (2022) 145:e153–639. doi: 10.1161/CIR.0000000000001052
 52. Mentias A, Hill E, Barakat AF, Raza MQ, Youssef D, Banerjee K, et al. An alarming trend: change in the risk profile of patients with ST elevation myocardial infarction over the last two decades. *Int J Cardiol.* (2017) 248:69–72. doi: 10.1016/j.ijcard.2017.05.011

Conflict of Interest: The authors declare that the research was conducted in the absence of any commercial or financial relationships that could be construed as a potential conflict of interest.

Publisher's Note: All claims expressed in this article are solely those of the authors and do not necessarily represent those of their affiliated organizations, or those of the publisher, the editors and the reviewers. Any product that may be evaluated in this article, or claim that may be made by its manufacturer, is not guaranteed or endorsed by the publisher.

Copyright © 2022 Xia, Zhang, Wu, Chen, Liu, Xu, Cui, Zhu, Wang, Hao, Li, Fay, Martinez-Lemus, Hill, Xu and Liu. This is an open-access article distributed under the terms of the Creative Commons Attribution License (CC BY). The use, distribution or reproduction in other forums is permitted, provided the original author(s) and the copyright owner(s) are credited and that the original publication in this journal is cited, in accordance with accepted academic practice. No use, distribution or reproduction is permitted which does not comply with these terms.



Abdominal Aortic Endothelial Dysfunction Occurs in Female Mice With Dextran Sodium Sulfate-Induced Chronic Colitis Independently of Reactive Oxygen Species Formation

OPEN ACCESS

Edited by:

Hong Chen,
Boston Children's Hospital
and Harvard Medical School,
United States

Reviewed by:

Kalpna Gupta,
University of California, Irvine,
United States
Cécile Oury,
University of Liège, Belgium

*Correspondence:

Zhenguo Liu
liuzheng@health.missouri.edu

† These authors have contributed
equally to this work

Specialty section:

This article was submitted to
Atherosclerosis and Vascular
Medicine,
a section of the journal
Frontiers in Cardiovascular Medicine

Received: 08 February 2022

Accepted: 04 March 2022

Published: 07 April 2022

Citation:

Wu H, Hu T, Zhang L, Xia X, Liu X,
Zhu Q, Wang M, Sun Z, Hao H, Cui Y,
Parrish AR, Li D-P, Hill MA, Xu C and
Liu Z (2022) Abdominal Aortic
Endothelial Dysfunction Occurs
in Female Mice With Dextran Sodium
Sulfate-Induced Chronic Colitis
Independently of Reactive Oxygen
Species Formation.
Front. Cardiovasc. Med. 9:871335.
doi: 10.3389/fcvm.2022.871335

Hao Wu^{1,2†}, Tingzi Hu^{1†}, Linfang Zhang¹, Xiujuan Xia¹, Xuanyou Liu¹, Qiang Zhu¹,
Meifang Wang¹, Zhe Sun³, Hong Hao¹, Yuqi Cui¹, Alan R. Parrish⁴, De-Pei Li¹,
Michael A. Hill³, Canxia Xu² and Zhenguo Liu^{1*}

¹ Center for Precision Medicine and Division of Cardiovascular Medicine, University of Missouri School of Medicine, Columbia, MO, United States, ² Department of Gastroenterology, Third Xiangya Hospital, Central South University, Changsha, China, ³ Dalton Cardiovascular Research Center, University of Missouri, Columbia, MO, United States, ⁴ Department of Medical Pharmacology and Physiology, University of Missouri School of Medicine, Columbia, MO, United States

Background and Objective: Inflammatory bowel disease (IBD) produces significant local and systemic inflammation with increased reactive oxygen species (ROS) formation. IBD Patients are at an increased risk for developing endothelial dysfunction and cardiovascular diseases. The present study tested the hypothesis that IBD impairs aortic endothelial function via ROS formation and investigate potential sex-related differences.

Methods and Results: Acute and chronic colitis models were induced in male and female C57BL/6 mice with dextran sodium sulfate (DSS) treatment. Aortic wall stiffness, endothelial function, and ROS levels, as well as serum levels of pro-inflammatory cytokines were evaluated. Acetylcholine (ACh)-induced endothelium-dependent relaxation of abdominal aorta without perivascular adipose tissue (PVAT) was significantly reduced in female mice, not males, with chronic colitis without a change in nitroglycerin-induced endothelium-independent relaxation. PVAT effectively preserved ACh-induced relaxation in abdominal aorta of female mice with chronic colitis. Aortic peak velocity, maximal intraluminal diameters, pulse wave velocity, distensibility and radial strain were preserved in mice with both acute and chronic colitis. Although pro-inflammatory cytokines levels were increased in mice with acute and chronic colitis, aortic ROS levels were not increased.

Conclusion: The data demonstrate that abdominal aortic endothelial function was attenuated selectively in female mice with chronic colitis independent of ROS formation. Further, PVAT played an important role in preserving endothelial function in female mice with chronic colitis.

Keywords: endothelial dysfunction, colitis, ROS, inflammatory bowel disease, aorta

INTRODUCTION

Inflammatory bowel disease (IBD), including Crohn's disease (CD) and ulcerative colitis (UC), is characterized by chronic and recurrent intestinal inflammation and is associated with significant extra-intestinal manifestations (EIMs) including arthropathy and arthritis, metabolic bone disease, skin disease, hepato-pancreato-biliary disease, renal disease, and cardiovascular disease (CVD) (1, 2). Several studies have suggested that patients with IBD are at an increased risk for developing CVD especially in young women (3, 4), however, the underlying mechanisms are poorly defined.

Endothelial dysfunction is closely associated with the development and progression of CVD including atherosclerosis and hypertension (5). Studies have shown that endothelium-dependent flow-mediated vasodilation is significantly decreased in patients with IBD (6). Microvascular endothelial dysfunction as measured using pulse arterial tonometry (PAT) has been reported in IBD patients with decreased PAT indices (7), and increased aortic stiffness (an indicator for vascular endothelial dysfunction and an independent predictor of cardiovascular events) (8). Reactive oxygen species (ROS) contribute to significant endothelial dysfunction and subsequent development and progression of CVD, especially atherosclerosis (9). IBD is a chronic and recurrent condition with significant local (intestine) and systemic inflammation, and significant increases in pro-inflammatory cytokines including tumor necrosis factor (TNF)- α , interleukin (IL)-1 β , and IL-6 (10). While this altered cytokine profile could be expected to increase ROS production, leading to endothelial dysfunction (11, 12) it is however, unclear if aortic endothelial function is impaired in IBD, and if there are sex-dependent differences.

Perivascular adipose tissue (PVAT) could release a variety of chemokines (including CCL2, CCL5, and CX3CL1) and adipocytokines that may have a significant impact on endothelial function via macrophage-mediated mechanism or anti-inflammatory activities (13, 14). It is known that aorta is heterogenous in its developmental origin, gene expression, and functionality (15). The present study was designed to test the hypothesis that experimental IBD leads to aortic endothelial cell dysfunction (thoracic and abdominal aorta) and excessive arterial stiffness through a mechanism related to increased ROS formation. There were four objectives: (1) to determine if IBD could decrease aortic endothelial function (as assessed by acetylcholine-mediated relaxation) both *in vivo* and *ex vivo*; (2) to determine if a sex difference was present in IBD-induced endothelial dysfunction; (3) to define the contribution of ROS formation to IBD-induced endothelial dysfunction; and (4) to investigate the role of PVAT in IBD-induced aortic endothelial

dysfunction. As IBD likely exhibits temporal relationships, both acute (7 days) and chronic (51 days) mouse models were used to achieve the objectives, using dextran sodium sulfate (DSS)-induced colitis in both male and female mice for the study.

MATERIALS AND METHODS

Animals

All animal experiments were conducted in accordance with the "Guide for the Care and Use of Laboratory Animals of US National Institutes of Health". The experimental protocols were reviewed and approved by the Institutional Animal Care and Use Committee of the University of Missouri, Columbia, MO, United States (protocol number 9227). Six-week-old C57BL/6 male and female mice were purchased from Jackson Laboratory (Bar Harbor, ME, United States), and were housed under standard laboratory conditions ($22 \pm 1^\circ\text{C}$, 12:12-h light/dark cycle).

Acute and Chronic DSS-Induced Colitis Mouse Models

Colitis was induced by oral administration of 2.5% DSS (MP Biomedicals, Santa Ana, CA, United States). DSS solution was made fresh every other day. Mice for the acute model were randomly assigned into four groups with 5–8 mice in each group, and for the chronic model 8–10 mice were included in each group: (1) female control, (2) female with DSS treatment, (3) male control, and (4) male with DSS treatment. For acute DSS-induced colitis, mice were treated for 7 days with DSS, and were euthanized on day 8 of DSS treatment. For chronic DSS-induced colitis, mice were treated with three cycles of DSS (7 days of treatment with 14 days of drinking water between each cycle) and subsequently euthanized on day 51 as described (16).

Assessment of Colitis Severity

All mice were weighed daily and assessed for stool consistency and fecal occult blood (Germaine Laboratories, San Antonio, TX, United States). The disease activity index (DAI) was obtained using a scoring system for each mouse as described (17). At the termination of each experiment colon length was measured from the ileocecal junction to the anal verge. Colon tissues were fixed in 10% formalin for 24 h, rehydrated in graded alcohol, hyalinized with xylene, embedded in paraffin, and cut into 5 μm thick tissue sections of. The colon tissue preparations were stained with hematoxylin and eosin (H&E), and examined using an upright microscope (Leica DM5500B, Wetzlar, Germany). The level of inflammation in colon tissue was determined using a scoring

system that included degrees of tissue damage and lamina propria inflammatory cell infiltration as described (16).

Analyses of Plasma Cytokines

After fully isoflurane anesthesia, retroorbital blood was collected in K3EDTA micro tubes (Sarstedt, Nümbrecht, Germany) and plasma separated by centrifugation (3,000 g for 10 min at 4°C). Plasma samples were kept at -80°C until analysis. The levels of plasma cytokines were determined by multiplex immunoassay with a BioPlex 200 Mouse Cytokine Array/Chemokine Array (Eve Technologies, Calgary, Canada) (18).

Blood Pressure Measurements

Blood pressure was measured non-invasively on conscious mice using a CODA volume pressure recording tail-cuff system (Kent Scientific Corporation, Torrington, CT, United States). Systolic, diastolic, and mean blood pressures were recorded.

TransAbdominal Ultrasound Imaging of Abdominal Aorta

Transabdominal ultrasound imaging of the abdominal aorta was conducted for each mouse at baseline and at days 8, 22, 36, and 50 after DSS treatment under general anesthesia with oxygen (1 L/min) and vaporized isoflurane (1.5% vol/vol). Adequate levels of anesthesia were confirmed by the absence of withdrawal reflexes via toe pinching. The animals were placed on a heated imaging stage in the supine position. Body temperature, heart rate, and respiratory rate were continuously monitored during imaging. Abdominal hair was removed by applying hair removal cream followed by cleaning with wet gauze prior to abdominal aorta measurements. Warm ultrasound gel was applied to the abdominal wall for placement of ultrasound probe (MS400, 18–38 MHz) to collect B-mode, M-mode, PW doppler mode, as well as ECG based Kilohertz Visualization (EKV) mode images, using a high-resolution ultrasound imaging system (Vevo 2100, FUJIFILM VisualSonics Inc., Bothell, WA, United States). Peak blood flow velocity within abdominal aorta was quantified using PW doppler mode. Maximal aortic intraluminal diameters (MILD) were measured using M mode. Pulse wave velocity (PWV), distensibility, and radial strain were measured in the abdominal aorta with EKV mode using VevoVasc software as described (19).

Aortic Endothelial Function Studies

Thoracic and abdominal aorta were carefully excised, dissected, and placed in ice-cold physiological saline solution (PSS) containing (in mM): 130 NaCl, 4.7 KCl, 1.18 KH₂PO₄, 1.17 MgSO₄, 14.9 NaHCO₃, 5.5 Glucose, 0.026 EDTA, and 1.6 CaCl₂, pH 7.4, gassed with 95% O₂ and 5% CO₂. Thoracic and abdominal aorta (with and without PVAT) were carefully cut into rings (2 mm in length) under a stereo-dissection microscope (20). The aortic rings were mounted to a multi-wire myograph system (620M; Danish Myo Technology, Aarhus, Denmark). The organ chambers were filled with 5 ml PSS at 37°C and aerated continuously with carbogen (95% O₂ + 5% CO₂). Based on vessel length/tension relationships, a preload tension of 10

and 12.5 mN/mm was applied to thoracic and abdominal aortic rings, respectively. The rings were allowed to equilibrate for 1 h with replacement of PSS every 20 min. To determine vascular contractility, aortic rings were incubated with high potassium PSS containing (in mM): 74.7 NaCl, 60 KCl, 1.18 KH₂PO₄, 1.17 MgSO₄, 14.9 NaHCO₃, 5.5 Glucose, 0.026 EDTA, and 1.6 CaCl₂ (pH 7.4). After adequate washout with PSS, a dose-response curve to endothelium-dependent vasodilator acetylcholine (Ach, 10⁻⁹ to 10⁻⁵ M, accumulative) and a dose-response curve to endothelium-independent vasodilator nitroglycerin (NTG, 10⁻⁹ to 10⁻⁵ M) for each aortic ring after submaximal precontraction with phenylephrine (PE, 10⁻⁶ M).

Measurement of ROS Formation Using Dihydroethidium Assay

Thoracic and abdominal aorta were cleaned of perivascular tissue (especially PVAT) and vertically embedded in Tissue-Tek optimal cutting temperature (OCT) compound (Sakura Finetek, Torrance, CA, United States), and frozen in liquid nitrogen immediately. Liver tissue was embedded in OCT compound and frozen in liquid nitrogen with subsequent assessment of whether ROS levels were increased in the liver of mice with chronic DSS-induced colitis. Frozen cross-sections (5 μm in thickness) of aorta and liver were prepared and incubated with 5 μM dihydroethidium (DHE; Molecular Probes, Eugene, OR, United States) for 15 min as described (21). Images were obtained using a fluorescence microscope (Olympus CKX53, Tokyo, Japan), and analyzed with Image J (NIH, Bethesda, MD, United States) software.

Statistical Analysis

All data were presented as mean ± SEM, and analyzed using an unpaired, two-tailed Student's *t*-test or two-way ANOVA followed by Bonferroni correction. All statistical analyses were conducted using Prism 8.0 software (GraphPad Software Inc., La Jolla, CA, United States). A two-sided *p* < 0.05 was considered statistically significant.

RESULTS

Assessment of Acute and Chronic DSS-Induced Colitis Models

All mice (both male and female) treated with 2.5% DSS for 7 days developed acute colitis (**Figure 1A**), as indicated by significant decreases in body weight (**Figure 1B**), colon length (**Figure 1C**), and significant increases in disease activity index (DAI) score (reflecting the severity of colitis) compared to control mice (**Figure 1D**). Increased colonic inflammation was also confirmed by histological analysis, showing mucosal erosions and lamina propria inflammatory cell infiltration in colon tissues of mice with acute colitis, compared to non-DSS treated mice (**Figure 1E**). In addition, plasma G-CSF, IL-6, and IL-17 were significantly increased in both female and male mice with acute colitis, while IFN-γ was only significantly increased in males (**Figure 1F**).

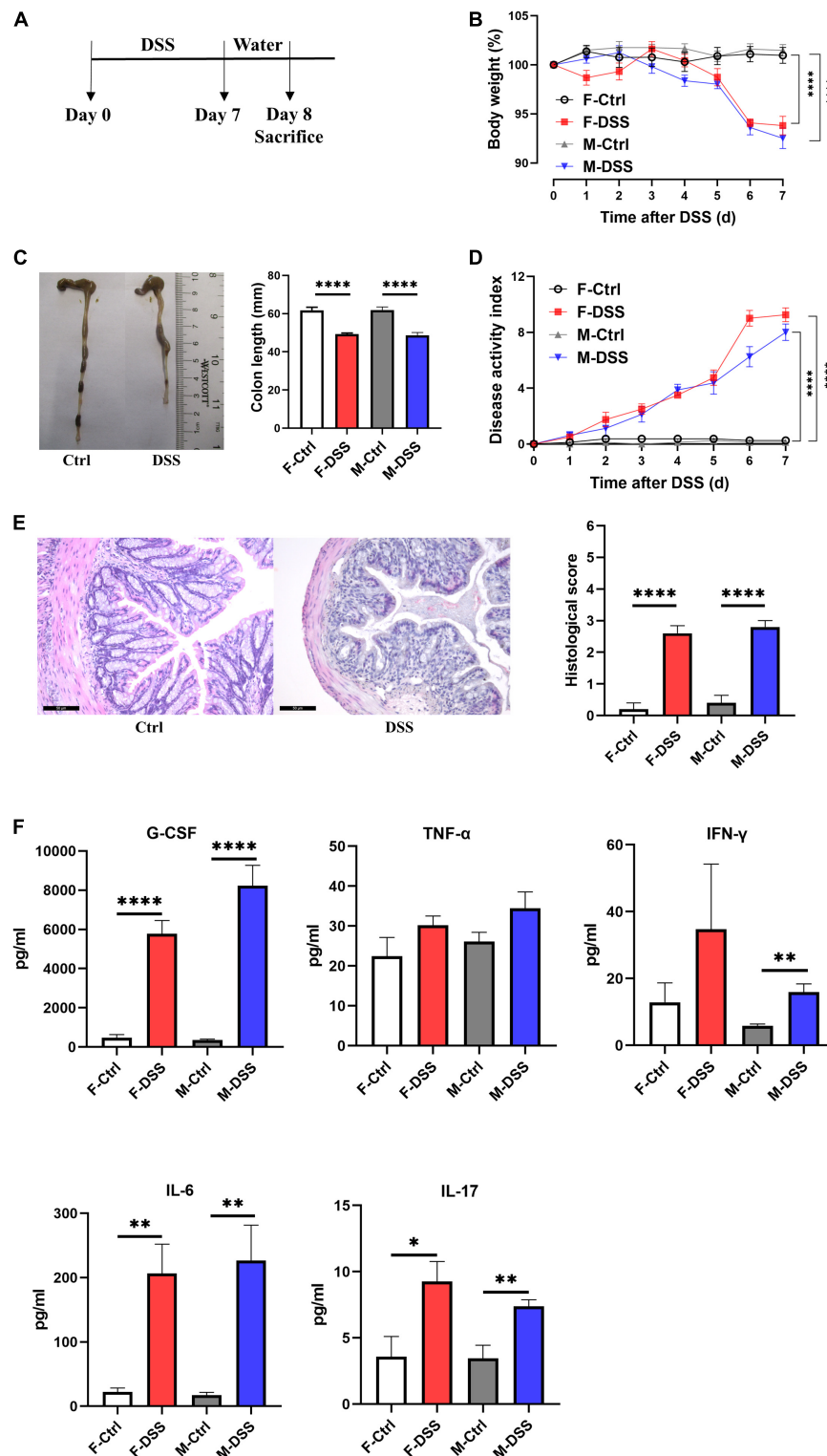


FIGURE 1 | Both female and male mice with acute DSS-induced colitis displayed significant inflammation in the colon and systemic inflammation. **(A)** Experimental scheme illustrating DSS treatment protocol for acute models. Changes in **(B)** body weight and **(D)** disease activity index (DAI) during DSS treatment. **(C)** Colon length and representative photographs for colon tissue in DSS-treated and control mice. **(E)** Representative images of H&E staining of colon tissue ($\times 200$; scale bar, 50 μm), and summary of histological score. **(F)** Levels of plasma cytokines in male and female mice with acute colitis model. Data are expressed as mean \pm SEM. * $p < 0.05$, ** $p < 0.01$, **** $p < 0.0001$, in unpaired 2-tailed Student's *t*-test **(B–F)**. *n* = 5–8 mice each group. F and M, female and male mice, respectively. G-CSF, granulocyte colony-stimulating factor; TNF- α , tumor necrosis factor alpha; IFN- γ , interferon gamma; IL, interleukin.

Chronically DSS-treated mice (3 cycles of 2.5% DSS for 7 days and interspaced with 14 days of drinking water) developed chronic colitis (**Figure 2A**), as demonstrated by significant decreases in colon length with fluctuating body weight (**Figure 2B**), enlarged mesenteric lymph nodes (**Figure 2C**), and fluctuating DAI scoring (**Figure 2D**), compared to control mice. Increased colonic inflammation was confirmed by histological analysis that showed marked tissue damage and lamina propria inflammatory cell infiltration in colon tissues of mice with chronic colitis, compared to the controls without DSS treatment (**Figure 2E**). For mice with chronic colitis, plasma G-CSF and IL-6 were significantly increased in both females and males, while TNF- α and IL-17 were increased only in females (**Figure 2F**).

Abdominal Aortic Peak Blood Flow Velocity, MILD, PWV, Distensibility, and Radial Strain Were Preserved in Both Male and Female Mice With Acute and Chronic Colitis

To determine if acute and chronic DSS-induced colitis could affect hemodynamics and arterial stiffness *in vivo*, transabdominal ultrasound imaging of abdominal aorta was conducted at baseline and day 8, 22, 36, and 50 after DSS administration (**Supplementary Figure 1**). Peak velocity was measured locally in the abdominal aorta using PW doppler mode images and MILD was measured using M-mode images, while PWV, distensibility and radial strain were measured by analyzing EKV data. There were no differences in peak velocity, MILD and PWV of abdominal aorta in either male and female mice with and without DSS-induced colitis (**Figures 3A–I**). Except in male mice at day 22 after DSS treatment, no differences in distensibility and radial strain were observed in abdominal aorta from either male or female mice with or without DSS-induced colitis (**Figures 3J–N**). There were no differences in heart rate, respiratory rate and blood pressure in either male and female mice with and without DSS-induced colitis (**Supplementary Figure 2**).

Aortic Endothelium-Dependent Vasodilation Was Preserved in Both Male and Female Mice With Acute Colitis

To determine if acute DSS-induced colitis could negatively affect aortic endothelial function in mice, endothelium-intact rings of both thoracic and abdominal aorta from both male and female mice were evaluated for endothelium-dependent and endothelium-independent relaxation after submaximal contraction with PE. There were no differences in Ach-induced endothelium-dependent relaxation (**Figure 4**) or NTG-induced endothelium-independent relaxation (**Supplementary Figure 5**) of thoracic and abdominal aorta in either male and female mice with and without acute DSS-induced colitis. No differences in PE-induced contraction were observed in either thoracic or abdominal aorta from either male or female mice with or without PVAT in acute DSS-induced colitis (**Supplementary Figure 3**).

Endothelium-Dependent Vasodilation Was Selectively Impaired in Abdominal Aorta in Female Mice With Chronic Colitis

To assess aortic endothelial function in chronic colitis, endothelium-intact rings of thoracic and abdominal aorta were precontracted sub-maximally with PE as above. Ach-induced endothelium-dependent relaxation (**Figures 5A–D**) and NTG-induced endothelium-independent relaxation (**Supplementary Figure 6A–D**) of thoracic aorta remained intact in both male and female mice with DSS-induced chronic colitis. However, Ach-induced endothelium-dependent relaxation of abdominal aorta was significantly reduced in female mice but not in male mice with chronic colitis mice (**Figures 5E,G**). The maximal relaxation in the control mice was $81.25 \pm 3.23\%$ that was significantly reduced to $66.94 \pm 3.00\%$ in chronic female colitis mice ($p = 0.006$, $n = 8$ mice per group). The EC₅₀ values (-Log[M]) for Ach-induced relaxation of abdominal aorta was significantly increased in female mice with chronic colitis over the control (6.63 ± 0.22 versus 7.26 ± 0.19 ; $p = 0.047$) (**Figure 5I**). In contrast, no differences were observed in NTG-induced endothelium-independent relaxation (**Supplementary Figure 6E–H**). No difference in PE-induced contraction was observed in either thoracic or abdominal aorta from either male or female mice with or without PVAT in chronic DSS-induced colitis (**Supplementary Figure 4**).

Perivascular Adipose Tissue Restored Endothelium-Dependent Vasodilation of Abdominal Aorta in Female Mice With Chronic Colitis

To determine if PVAT could have a significant impact on endothelial function in mice with chronic colitis, endothelium-intact rings of thoracic and abdominal aorta with or without PVAT were sub-maximally precontracted with PE. Ach-induced endothelium-dependent relaxation of abdominal aorta without PVAT was significantly reduced in female mice with chronic colitis (**Figure 5E**) without change in NTG-induced endothelium-independent relaxation (**Supplementary Figure 6E**). Interestingly, Ach-induced endothelium-dependent relaxation of abdominal aorta was preserved when PVAT was present (**Figure 5F**).

ROS Levels Remained Unchanged in Thoracic and Abdominal Aorta in Mice With Either Acute or Chronic Colitis

Both acute and chronic colitis trigger a systemic inflammation with increased ROS production. Thus, frozen aortic cross-sections were prepared for ROS measurement using DHE. To our surprise, there were no significant differences in ROS levels in fresh aortic cross-sections of either thoracic and abdominal aorta in male and female mice with acute or chronic colitis (**Figures 6A–D**), while ROS levels were significantly increased in the livers of both male and female mice with DSS-induced chronic colitis (**Supplementary Figure 7**).

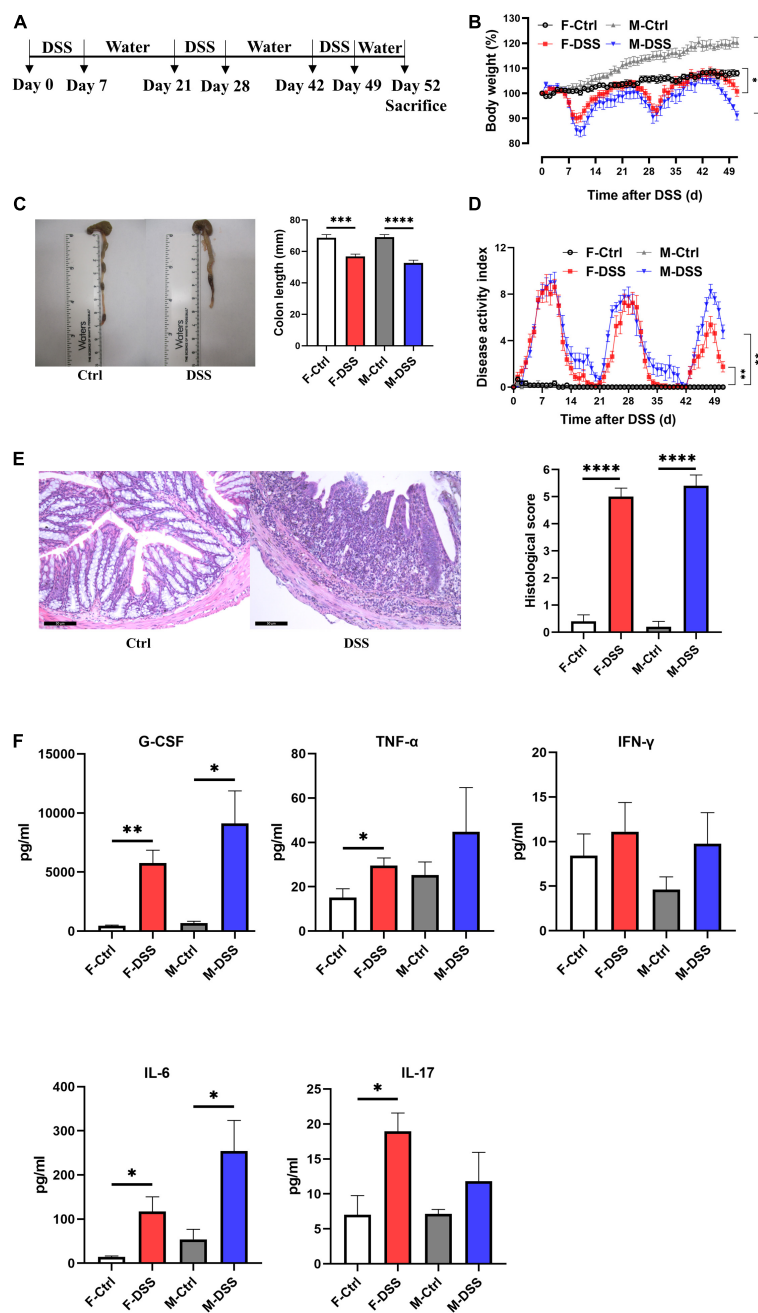


FIGURE 2 | Both female and male mice with chronic DSS-induced colitis displayed significant inflammation in the colon and systemic inflammation. **(A)** Experimental scheme illustrating the experimental protocol with treatment of DSS and water for chronic models. Changes in **(B)** body weight and **(D)** disease activity index (DAI) during DSS treatment. **(C)** Colon length and representative photographs for colon tissue in DSS-treated and control mice. **(E)** Representative images of H&E staining of colon tissue ($\times 200$; scale bar, 50 μm), and summary of histological score. **(F)** Levels of plasma cytokines in male and female mice with chronic colitis model. Results are expressed as mean \pm SEM. $^*p < 0.05$, $^{**}p < 0.01$, $^{***}p < 0.001$, $^{****}p < 0.0001$, in unpaired 2-tailed Student's *t*-test (**B–F**), $n = 5$ –8 mice each group. F and M, female and male mice, respectively. G-CSF, granulocyte colony-stimulating factor; TNF- α , tumor necrosis factor alpha; IFN- γ , interferon gamma; IL, interleukin.

DISCUSSION

In the present study, we demonstrated that: (1) DSS treatment successfully induced acute and chronic colitis in mice with significant increases in plasma pro-inflammatory cytokines; (2)

no significant changes in arterial stiffness was observed in either male and female mice with acute and chronic DSS-induced colitis; (3) no significant changes in endothelium-dependent and endothelium-independent relaxation of both thoracic and abdominal aorta were observed in either male and female mice

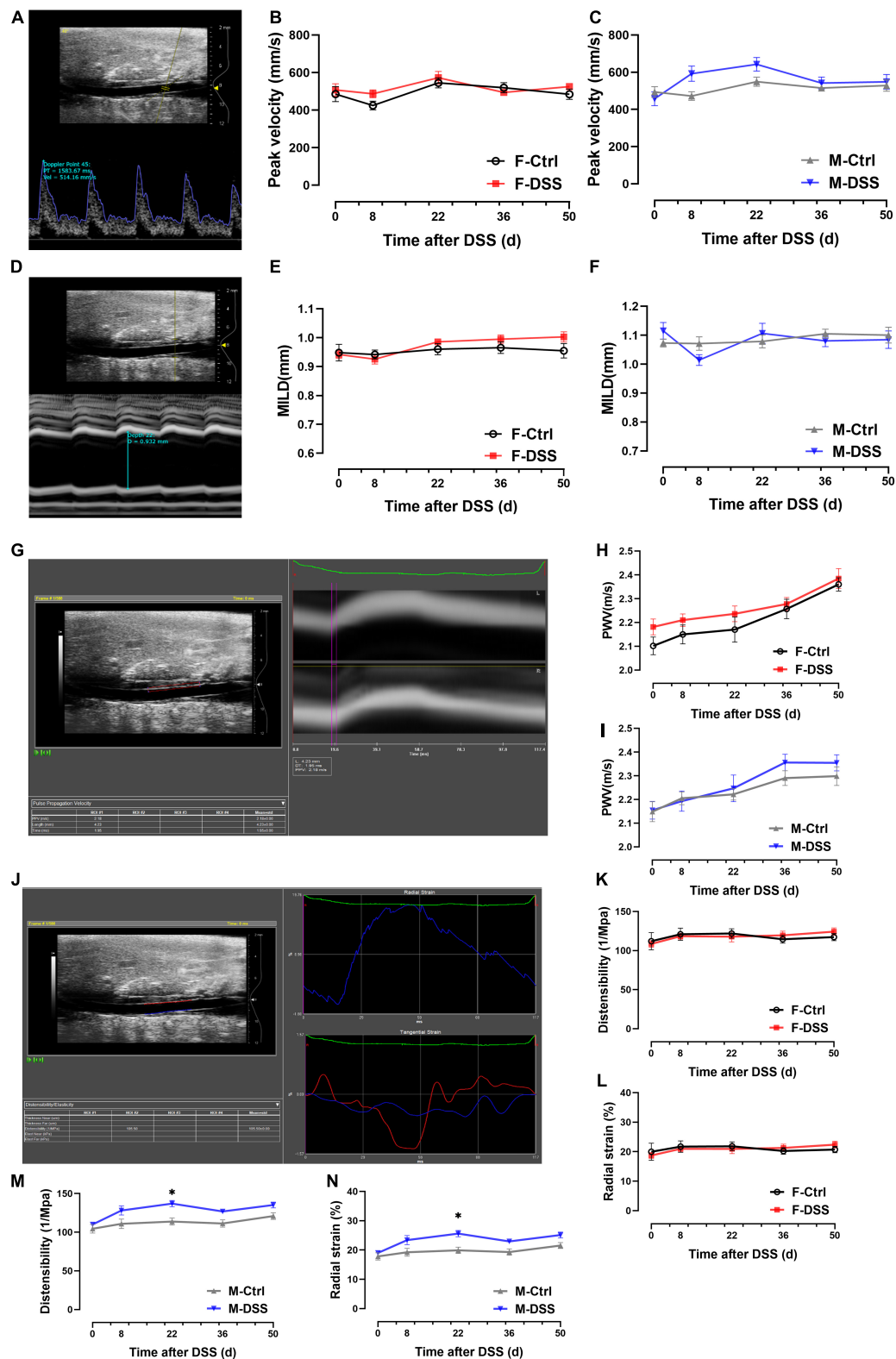
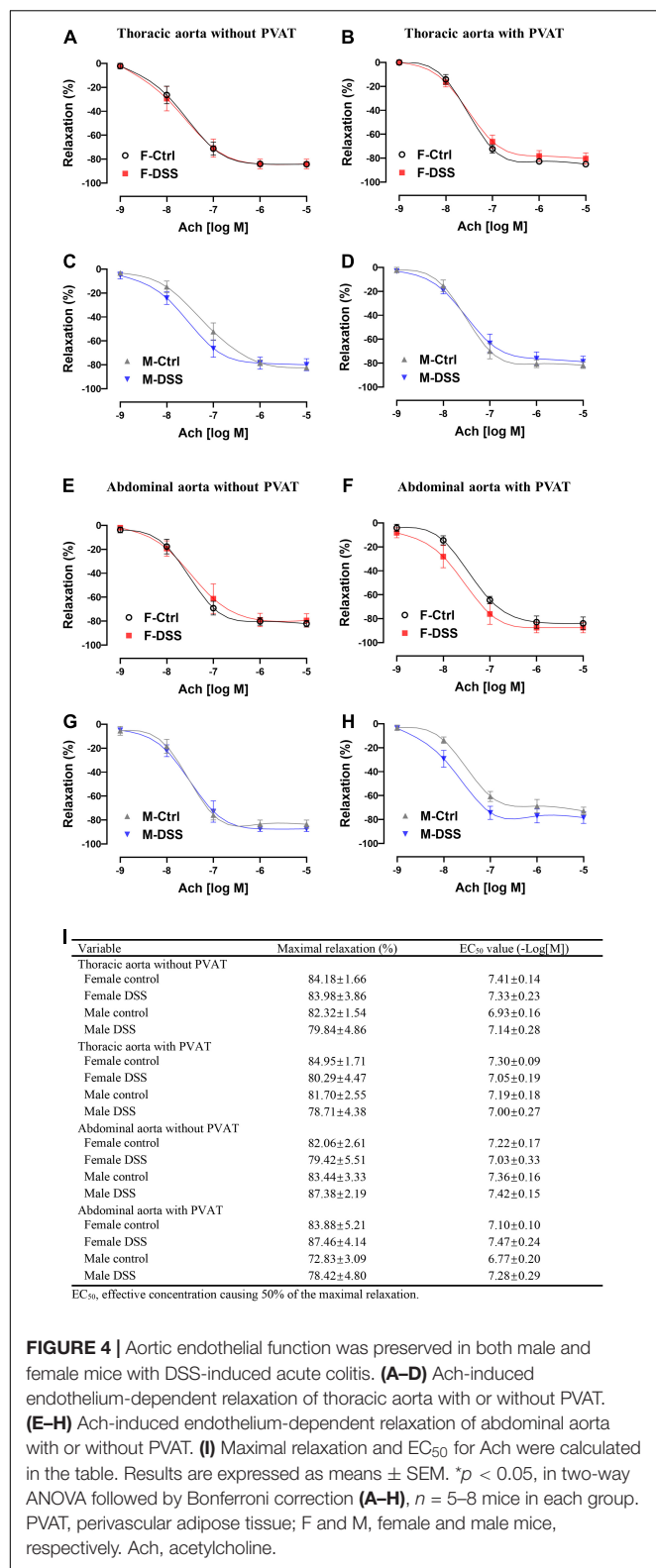
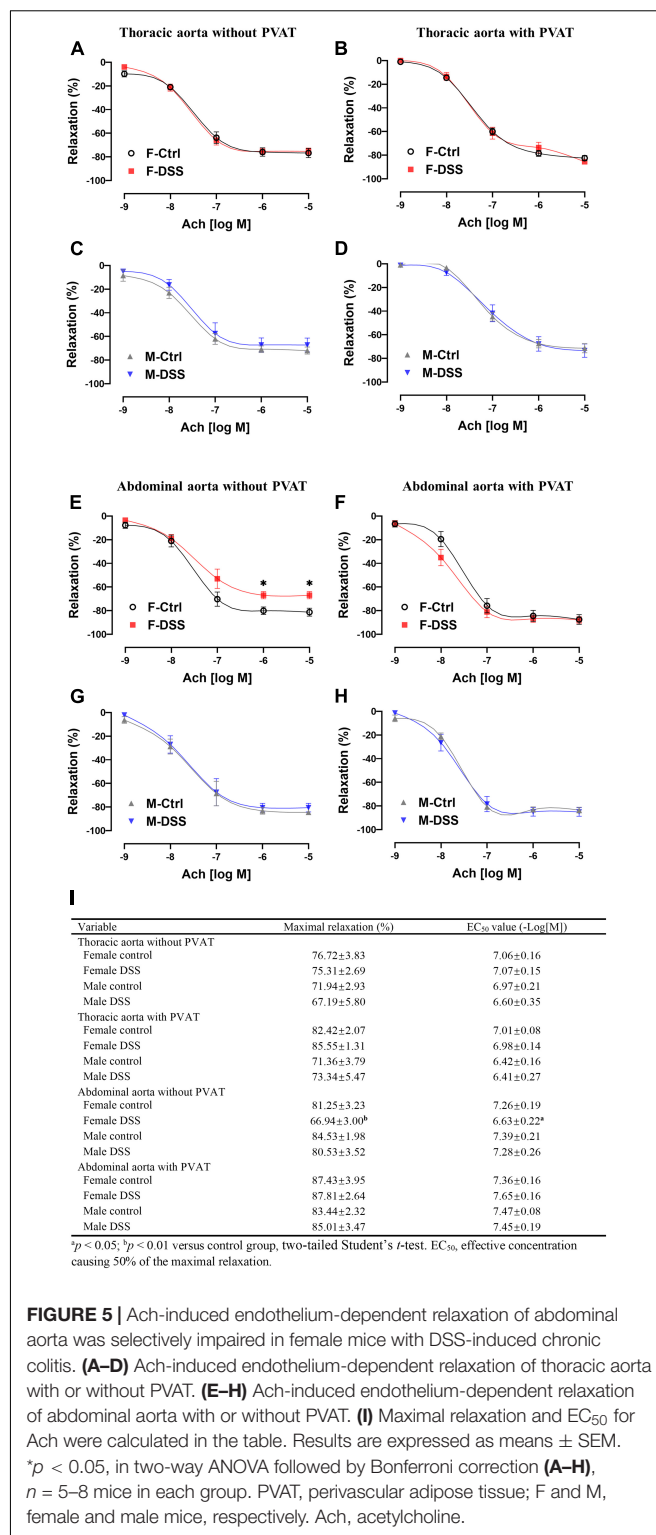


FIGURE 3 | No significant changes in hemodynamics and arterial stiffness of abdominal aorta were observed in both male and female mice with DSS-induced acute and chronic colitis. **(A–C)** Analysis of PW doppler mode images for peak velocity. **(D–F)** Analysis of M-mode images for MILD. **(G–I)** Analysis of EKV images for PWV. **(J–N)** Analysis of EKV images for distensibility and radial strain. Results are expressed as mean \pm SEM. * $p < 0.05$, in two-way ANOVA followed by Bonferroni correction **(E–N)**, $n = 6–8$ mice each group. F and M, female and male mice, respectively. MILD, maximal intraluminal diameter; PWV, pulse wave velocity.



with acute DSS-induced colitis; (4). endothelium-dependent relaxation was selectively impaired in the abdominal aorta of female mice with DSS-induced chronic colitis but not in



males; (5) PVAT preserved endothelium-dependent relaxation of abdominal aorta in female mice with chronic colitis; and (6) no changes in ROS levels were observed in either thoracic and abdominal aorta from male or female mice with acute or chronic colitis. These data suggest that endothelium-dependent

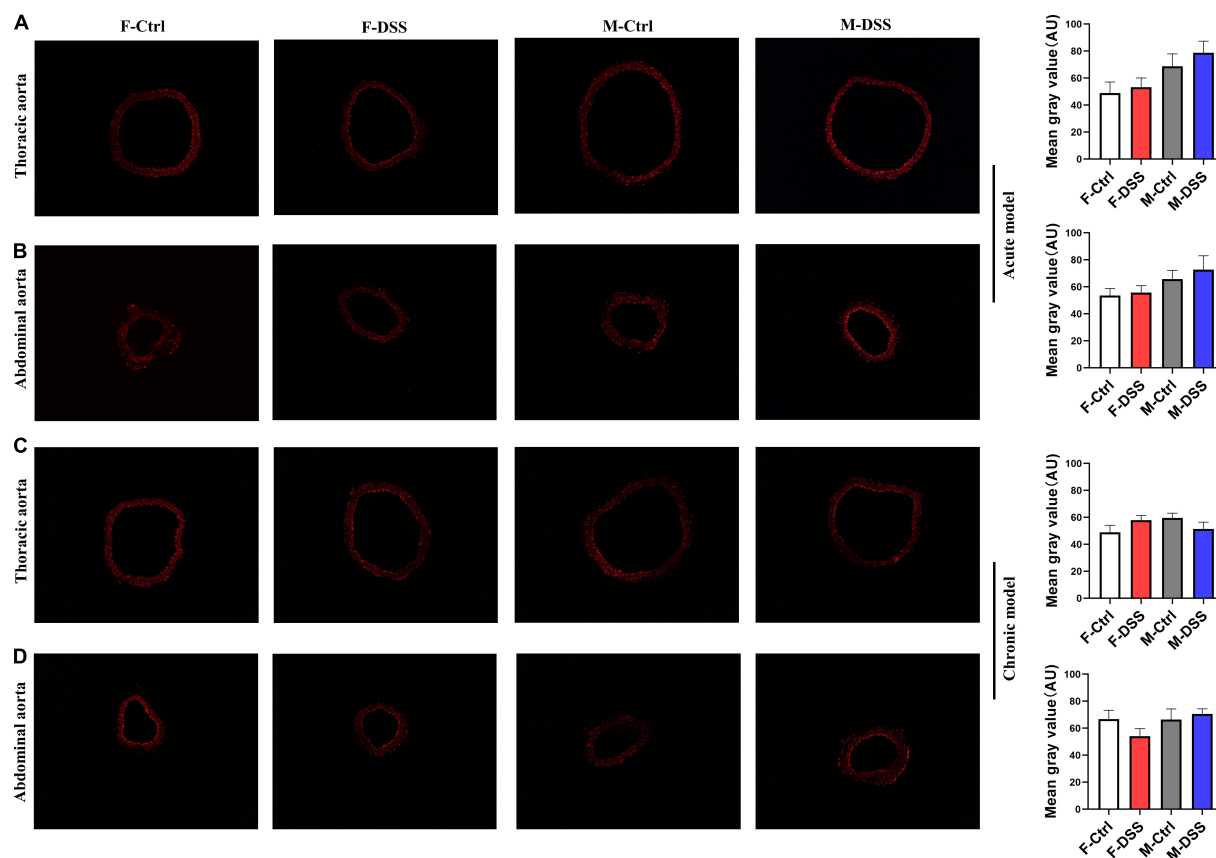


FIGURE 6 | Reactive oxygen species (ROS) levels remained unchanged in thoracic and abdominal aorta in mice with acute and chronic colitis in both female and male mice. Representative images of ROS in acute colitis model (A,B) and chronic colitis model (C,D) for thoracic and abdominal aortic rings using DHE staining ($\times 100$) and graph for quantification of ROS levels in the aortic rings. Results are expressed as means \pm SEM. * $p < 0.05$, in unpaired 2-tailed Student's *t*-test (A–D), $n = 5$ mice in each group. DHE, dihydroethidium. AU, arbitrary units. F and M, female and male mice, respectively.

relaxation is selectively attenuated in abdominal aorta of female mice with DSS-induced chronic colitis via a PVAT-associated mechanism that is independent of ROS formation.

Systemic inflammation and endothelial dysfunction are considered among the key factors that are critically involved in the development and progression of CVDs. IBD is characterized by chronic and recurrent inflammation of the gastrointestinal tract, and is associated with significant EIMs including non-infectious systemic inflammation and increased risk for CVD, especially in women (3, 4, 22). The data from the present study indeed showed plasma G-CSF, IL-6, and IL-17 levels to be significantly increased in both female and male mice with acute colitis, while IFN- γ was only significantly increased in males. For mice with chronic colitis, plasma G-CSF and IL-6 were significantly increased in both females and males, while TNF- α and IL-17 levels were selectively increased in female mice. These data confirmed that the plasma levels of pro-inflammatory cytokines were increased in mice with acute or chronic colitis.

Intact endothelial function is critical to normal vascular function. Studies have shown that the intestinal microvasculature of IBD patients with inflammatory flare exhibits significant endothelial dysfunction as evident by loss of Ach-induced

endothelium-dependent relaxation (23). Surprisingly, there are very limited data on defining the relationship between IBD and endothelial dysfunction in animal models. It has been shown that mice and rats with UC have a significant endothelial damage with increased vascular permeability and perivascular edema in colonic mucosa (24). Mice with DSS-induced colitis and T-cell transfer are reported to exhibit a significant decrease in retinal blood flow (25, 26). The data from the present study showed that *ex vivo* abdominal aortic endothelial function was significantly attenuated in female mice with DSS-induced chronic colitis, while the thoracic aortic endothelial function was preserved. The mechanism(s) for this finding is unclear at this point. It is known that thoracic and abdominal aorta are heterogeneous with different origins during embryogenesis (27). A recent study using different aortic segments and single-cell RNA-sequencing has shown that the cell populations in mouse aorta to be very diverse/heterogeneous. The composition of aortic cell populations, their gene expression profiles and intercellular signaling networks could dramatically and differentially change segmental aortic responses to changes in local and systematic conditions including hemodynamic and metabolic factors (including fats, ions, and glucose) (15). Further studies are

needed to define the mechanisms on the selective effect of DSS-induced chronic colitis on abdominal aorta and the apparent sex differences.

One of the interesting findings in the present study is that the endothelial function of abdominal aorta in female mice with DSS-induced chronic colitis is preserved *in vivo*, as is the *ex vivo* function of aortic rings with PVAT. In rodents, mesenteric arteries are surrounded with white adipose tissue, while the thoracic aorta is surrounded with brown adipose-like tissue and the PVAT of abdominal aorta is a mixture of white and brown adipose tissues (28). Historically, PVAT was usually removed from the vascular preparations for *ex vivo* vascular function studies. PVAT is juxtaposed to the vascular adventitia and is now considered to be important for vascular function. PVAT is comprised of dynamic cell populations including nerve terminals and immune cells in addition to adipocytes (29). These cells could directly communicate and interact with vascular cells including adventitial fibroblasts, vascular smooth muscle cells, and endothelial cells (28), thus participating in the regulation of vascular function. Clinical studies have demonstrated that perivascular nerve fiber subclasses are changed in colonic, mesenteric and submucosal blood vessels of IBD patients (30). Animal studies have shown that perivascular sensory neurotransmitter function of mesenteric arteries is profoundly impaired in an IL-10 knock out mouse colitis model (31). The findings in the present study suggests that abdominal aortic PVAT plays an important protective role in relation to endothelial function in female mice with DSS-induced chronic colitis. Further studies are needed to investigate the molecular mechanisms of PVAT in vascular endothelial function in different anatomical locations in IBD and sex difference.

There are significant sex differences in incidence and prevalence, clinical course, EIMs and response to therapies in IBD. Epidemiological studies have shown a greater predominance and severity of CD in women than in men, but a greater predominance and severity of UC in men than in women (32, 33). EIMs are diverse and commonly involve skin, joints, eye, liver and the cardiovascular system. Female IBD patients carry a higher risk of CVDs and anemia, while male patients have a higher risk of primary sclerosing cholangitis and primary ankylosing spondylitis (34–36). Several population studies have shown that women with IBD are at higher risk for acute arterial thrombotic events compared with men with IBD (3, 4). The mechanisms for sex differences in EIMs are unclear. Sex hormones not only affect gut-specific function, including gastric contractility, gastrointestinal transit, and sensitivity to pain (37), but are also important for endothelial function. Estrogen contributes significantly to the regulation of vasomotor activities through estrogen receptors α and β on endothelial cells and vascular smooth muscle cells (38). Physiological levels of testosterone are beneficial to cardiovascular system, while decreased serum levels of testosterone are associated with impaired endothelial function (39). The present study showed that endothelial function is impaired selectively in female mice with chronic colitis. As sexual dimorphism has been implicated in a number of vascular diseases, further studies, using female mice with oophorectomy or male mice with estrogen treatment, are needed to determine

if sex hormones contribute to the sex difference in endothelial function observed in mice with chronic colitis.

Significant production of a variety of pro-inflammatory cytokines occurs in IBD, both locally and systemically. In the present study, we observed that plasma TNF- α and IL-17 were selectively increased in female mice with chronic colitis. Increased levels of TNF- α could increase ROS production, and lead to endothelial dysfunction (11, 40). IL-17 is also a potent pro-inflammatory cytokine and activates RhoA/Rho-kinase, leading to endothelial dysfunction (41). However, the ROS levels in both thoracic and abdominal aorta were not increased in either male mice or females with acute and chronic DSS-induced colitis, suggesting that abdominal aortic endothelial dysfunction in female mice with DSS-induced chronic colitis may not be related to ROS formation. Further studies are warranted to explore the mechanism(s) by which abdominal aortic endothelial dysfunction occurs in female mice with chronic colitis.

In conclusion, the present study demonstrated that abdominal aortic endothelial function was attenuated selectively in female mice with DSS-induced chronic colitis independent of ROS formation, and PVAT played an important role in preserving endothelial function in female mice with chronic colitis.

DATA AVAILABILITY STATEMENT

The raw data supporting the conclusions of this article will be made available by the authors, without undue reservation.

ETHICS STATEMENT

The animal study was reviewed and approved by Institutional Animal Care and Use Committee of the University of Missouri.

AUTHOR CONTRIBUTIONS

HW, TH, and ZL contributed to conception and design of the study. HW, TH, MW, ZS, HH, and YC carried out the experiments. LZ and XX performed the statistical analysis. HW wrote the first draft of the manuscript. TH, XL, QZ, ZS, ARP, D-PL, MAH, and CX wrote sections of the manuscript. ZL supervised the project. All authors contributed to manuscript revision, read, and approved the submitted version.

FUNDING

The present work was partially supported by US NIH grants ES026200 and HL148196 (ZL).

SUPPLEMENTARY MATERIAL

The Supplementary Material for this article can be found online at: <https://www.frontiersin.org/articles/10.3389/fcvm.2022.871335/full#supplementary-material>

REFERENCES

- Ott C, Schölmerich J. Extraintestinal manifestations and complications in IBD. *Nat Rev Gastroenterol Hepatol*. (2013) 10:585–95. doi: 10.1038/nrgastro.2013.117
- Wu H, Hu T, Hao H, Hill MA, Xu C, Liu Z. Inflammatory bowel disease and cardiovascular diseases: a concise review. *Eur Heart J Open*. (2021) 2:oeab029. doi: 10.1093/ehjopen/oeab029
- Rungoe C, Basit S, Ranthe MF, Wohlfahrt J, Langholz E, Jess T. Risk of ischaemic heart disease in patients with inflammatory bowel disease: a nationwide Danish cohort study. *Gut*. (2013) 62:689–94. doi: 10.1136/gutjnl-2012-303285
- Kirchgesner J, Beaugerie L, Carrat F, Anderson NN, Jess T, Schwarzsinger M, et al. Increased risk of acute arterial events in young patients and severely active IBD: a nationwide French cohort study. *Gut*. (2018) 67:1261–8. doi: 10.1136/gutjnl-2017-314015
- Xu S, Ilyas I, Little PJ, Li H, Kamato D, Zheng X, et al. Endothelial dysfunction in atherosclerotic cardiovascular diseases and beyond: from mechanism to pharmacotherapies. *Pharmacol Rev*. (2021) 73:924–67. doi: 10.1124/pharmrev.120.000096
- Ozturk K, Guler AK, Cakir M, Ozen A, Demirci H, Turker T, et al. Pulse wave velocity, intima media thickness, and flow-mediated dilatation in patients with normotensive normoglycemic inflammatory bowel disease. *Inflamm Bowel Dis*. (2015) 21:1314–20. doi: 10.1097/MIB.0000000000000355
- Roifman I, Sun YC, Fedwick JP, Panaccione R, Buret AG, Liu H, et al. Evidence of endothelial dysfunction in patients with inflammatory bowel disease. *Clin Gastroenterol Hepatol*. (2009) 7:175–82. doi: 10.1016/j.cgh.2008.10.021
- Zanoli L, Ozturk K, Cappello M, Insera G, Geraci G, Tuttolomondo A, et al. Inflammation and aortic pulse wave velocity: a multicenter longitudinal study in patients with inflammatory bowel disease. *J Am Heart Assoc*. (2019) 8:e010942. doi: 10.1161/JAHA.118.010942
- Nowak WN, Deng J, Ruan XZ, Xu Q. Reactive oxygen species generation and atherosclerosis. *Arterioscler Thromb Vasc Biol*. (2017) 37:e41–52.
- Sands BE. Biomarkers of inflammation in inflammatory bowel disease. *Gastroenterology*. (2015) 149:1275–85.e2.
- Gao X, Belmadani S, Picchi A, Xu X, Potter BJ, Tewari-Singh N, et al. Tumor necrosis factor- α induces endothelial dysfunction in Lepr(db) mice. *Circulation*. (2007) 115:245–54. doi: 10.1161/CIRCULATIONAHA.106.650671
- Esteve E, Castro A, López-Bermejo A, Vendrell J, Ricart W, Fernández-Real J. Serum interleukin-6 correlates with endothelial dysfunction in healthy men independently of insulin sensitivity. *Diabetes Care*. (2007) 30:939–45. doi: 10.2337/dc06-1793
- Brown NK, Zhou Z, Zhang J, Zeng R, Wu J, Eitzman DT, et al. Perivascular adipose tissue in vascular function and disease: a review of current research and animal models. *Arterioscler Thromb Vasc Biol*. (2014) 34:1621–30. doi: 10.1161/ATVBAHA.114.303029
- Oikonomou EK, Antoniadou C. The role of adipose tissue in cardiovascular health and disease. *Nat Rev Cardiol*. (2019) 16:83–99. doi: 10.1038/s41569-018-0097-6
- He D, Mao A, Zheng CB, Kan H, Zhang K, Zhang Z, et al. Aortic heterogeneity across segments and under high fat/salt/glucose conditions at the single-cell level. *Natl Sci Rev*. (2020) 7:881–96. doi: 10.1093/nsr/nwaa038
- Wirtz S, Popp V, Kindermann M, Gerlach K, Weigmann B, Fichtner-Feigl S, et al. Chemically induced mouse models of acute and chronic intestinal inflammation. *Nat Protoc*. (2017) 12:1295–309. doi: 10.1038/nprot.2017.044
- Cooper HS, Murthy SN, Shah RS, Sedergran DJ. Clinicopathologic study of dextran sulfate sodium experimental murine colitis. *Lab Invest*. (1993) 69:238–49.
- Ogrodnik M, Zhu Y, Langhi LG, Tchkonja T, Krüger P, Fielder E, et al. Obesity-induced cellular senescence drives anxiety and impairs neurogenesis. *Cell Metab*. (2019) 29:1061–77.e8.
- Sharma N, Sun Z, Hill MA, Hans CP. Measurement of pulse propagation velocity, distensibility and strain in an abdominal aortic aneurysm mouse model. *J Vis Exp*. (2020) 156:e60515. doi: 10.3791/60515
- Chang L, Xiong W, Zhao X, Fan Y, Guo Y, Garcia-Barrio M, et al. Bmal1 in perivascular adipose tissue regulates resting-phase blood pressure through transcriptional regulation of angiotensinogen. *Circulation*. (2018) 138:67–79. doi: 10.1161/CIRCULATIONAHA.117.029972
- Wang Q, Zou MH. Measurement of reactive oxygen species (ROS) and mitochondrial ROS in AMPK knockout mice blood vessels. *Methods Mol Biol*. (2018) 1732:507–17. doi: 10.1007/978-1-4939-7598-3_32
- Harbord M, Annesse V, Vavricka SR, Allez M, Acosta MB, Boberg KM, et al. The first European evidence-based consensus on extra-intestinal manifestations in inflammatory bowel disease. *J Crohns Colitis*. (2016) 10:239–54. doi: 10.1093/ecco-jcc/jjv213
- Hatoum OA, Binion DG, Otterson MF, Gutterman DD. Acquired microvascular dysfunction in inflammatory bowel disease: loss of nitric oxide-mediated vasodilation. *Gastroenterology*. (2003) 125:58–69. doi: 10.1016/S0016-5085(03)00699-1
- Tolstanova G, Deng X, French SW, Lungu W, Paunovic B, Khomenko T, et al. Early endothelial damage and increased colonic vascular permeability in the development of experimental ulcerative colitis in rats and mice. *Lab Invest*. (2012) 92:9–21. doi: 10.1038/labinvest.2011.122
- Watts MN, Leskova W, Carter PR, Zhang S, Kosloski-Davidson M, Grisham MB, et al. Ocular dysfunction in a mouse model of chronic gut inflammation. *Inflamm Bowel Dis*. (2013) 19:2091–7. doi: 10.1097/MIB.0b013e318295fdb3
- Watts MN, Eshaq RS, Carter PR, Harris NR. Decreased retinal blood flow in experimental colitis; improvement by eye drop administration of losartan. *Exp Eye Res*. (2013) 115:22–6. doi: 10.1016/j.exer.2013.06.023
- Ruddy JM, Jones JA, Spinale FG, Ikonomidis JS. Regional heterogeneity within the aorta: relevance to aneurysm disease. *J Thorac Cardiovasc Surg*. (2008) 136:1123–30. doi: 10.1016/j.jtcvs.2008.06.027
- Chang L, Garcia-Barrio MT, Chen YE. Perivascular adipose tissue regulates vascular function by targeting vascular smooth muscle cells. *Arterioscler Thromb Vasc Biol*. (2020) 40:1094–109. doi: 10.1161/ATVBAHA.120.312464
- Saxton SN, Clark BJ, Withers SB, Eringa EC, Heagerty AM. Mechanistic links between obesity, diabetes, and blood pressure: role of perivascular adipose tissue. *Physiol Rev*. (2019) 99:1701–63. doi: 10.1152/physrev.00034.2018
- de Fontgalland D, Brookes SJ, Gibbins I, Wattoo DA. The neurochemical changes in the innervation of human colonic mesenteric and submucosal blood vessels in ulcerative colitis and Crohn's disease. *Neurogastroenterol Motil*. (2014) 26:731–44. doi: 10.1111/nmo.12327
- Norton CE, Grunz-Borgmann EA, Hart ML, Jones BW, Franklin CL, Boerman EM. Role of perivascular nerve and sensory neurotransmitter dysfunction in inflammatory bowel disease. *Am J Physiol Heart Circ Physiol*. (2021) 320:H1887–902. doi: 10.1152/ajpheart.00037.2021
- Lophaven SN, Lynge E, Burisch J. The incidence of inflammatory bowel disease in Denmark 1980–2013: a nationwide cohort study. *Aliment Pharmacol Ther*. (2017) 45:961–72. doi: 10.1111/apt.13971
- Bernstein CN, Wajda A, Svenson LW, MacKenzie A, Koehoorn M, Jackson M, et al. The epidemiology of inflammatory bowel disease in Canada: a population-based study. *Am J Gastroenterol*. (2006) 101:1559–68.
- Karmiris K, Avgerinos A, Tavernarakis A, Zeglinas C, Karatzas P, Koukouratos T, et al. Prevalence and characteristics of extra-intestinal manifestations in a large cohort of Greek patients with inflammatory bowel disease. *J Crohns Colitis*. (2016) 10:429–36. doi: 10.1093/ecco-jcc/jjv232
- Koutroubakis IE, Ramos-Rivers C, Regueiro M, Koutroumpakis E, Click B, Schwartz M, et al. Five-year period prevalence and characteristics of anemia in a large us inflammatory bowel disease cohort. *J Clin Gastroenterol*. (2016) 50:638–43. doi: 10.1097/MCG.0000000000000417
- Guerra I, Bujanda L, Castro J, Merino O, Tosca J, Camps B, et al. Clinical characteristics, associated malignancies and management of primary sclerosing cholangitis in inflammatory bowel disease patients: a multicenter retrospective cohort study. *J Crohns Colitis*. (2019) 13:1492–500. doi: 10.1093/ecco-jcc/jjz094
- Jiang Y, Greenwood-Van MB, Johnson AC, Travagli RA. Role of estrogen and stress on the brain-gut axis. *Am J Physiol Gastrointest Liver Physiol*. (2019) 317:G203–9. doi: 10.1152/ajpgi.00144.2019
- Mendelsohn ME, Karas RH. The protective effects of estrogen on the cardiovascular system. *N Engl J Med*. (1999) 340:1801–11. doi: 10.1056/nejm199906103402306
- Empen K, Lorbeer R, Dörr M, Haring R, Nauck M, Gläser S, et al. Association of testosterone levels with endothelial function in men: results from a

- population-based study. *Arterioscler Thromb Vasc Biol.* (2012) 32:481–6. doi: 10.1161/ATVBAHA.111.232876
40. Yuan S, Carter P, Bruzelius M, Vithayathil M, Kar S, Mason AM, et al. Effects of tumour necrosis factor on cardiovascular disease and cancer: a two-sample Mendelian randomization study. *EBioMedicine.* (2020) 59:102956. doi: 10.1016/j.ebiom.2020.102956
 41. Nguyen H, Chiasson VL, Chatterjee P, Kopriva SE, Young KJ, Mitchell BM. Interleukin-17 causes Rho-kinase-mediated endothelial dysfunction and hypertension. *Cardiovasc Res.* (2013) 97:696–704. doi: 10.1093/cvr/cvs422

Conflict of Interest: The authors declare that the research was conducted in the absence of any commercial or financial relationships that could be construed as a potential conflict of interest.

Publisher's Note: All claims expressed in this article are solely those of the authors and do not necessarily represent those of their affiliated organizations, or those of the publisher, the editors and the reviewers. Any product that may be evaluated in this article, or claim that may be made by its manufacturer, is not guaranteed or endorsed by the publisher.

Copyright © 2022 Wu, Hu, Zhang, Xia, Liu, Zhu, Wang, Sun, Hao, Cui, Parrish, Li, Hill, Xu and Liu. This is an open-access article distributed under the terms of the Creative Commons Attribution License (CC BY). The use, distribution or reproduction in other forums is permitted, provided the original author(s) and the copyright owner(s) are credited and that the original publication in this journal is cited, in accordance with accepted academic practice. No use, distribution or reproduction is permitted which does not comply with these terms.



Embracing Diversity, Equity, and Inclusion in the Scientific Community—Viewpoints of the Diversity, Equity, and Inclusion Committee of the North American Vascular Biology Organization

Mahdi Garelnabi^{1,2*}, Mitzy Cowdin^{1,3}, Yun Fang^{1,4}, Bandana Shrestha¹, Masuko Ushio-Fukai^{1,5}, Elena Aikawa^{1,6}, Garth Graham⁷, Grietje Molema^{1,8}, Hiromi Yanagisawa^{1,9} and Masanori Aikawa^{1,6*}

OPEN ACCESS

Edited by:

Masataka Sata,
Tokushima University, Japan

Reviewed by:

Ryuichi Morishita,
Osaka University, Japan
Minako Yamaoka-Tojo,
Kitasato University, Japan

*Correspondence:

Mahdi Garelnabi
mahdi_garelnabi@umt.edu
Masanori Aikawa
maikawa@bwh.harvard.edu

Specialty section:

This article was submitted to
Atherosclerosis and Vascular
Medicine,
a section of the journal
Frontiers in Cardiovascular Medicine

Received: 27 January 2022

Accepted: 31 January 2022

Published: 13 April 2022

Citation:

Garelnabi M, Cowdin M, Fang Y, Shrestha B, Ushio-Fukai M, Aikawa E, Graham G, Molema G, Yanagisawa H and Aikawa M (2022) Embracing Diversity, Equity, and Inclusion in the Scientific Community—Viewpoints of the Diversity, Equity, and Inclusion Committee of the North American Vascular Biology Organization. *Front. Cardiovasc. Med.* 9:863256. doi: 10.3389/fcvm.2022.863256

¹ Diversity, Equity, and Inclusion Committee, North American Vascular Biology Organization (NAVBO), Germantown, MD, United States, ² Department of Biomedical and Nutritional Sciences, University of Massachusetts, Lowell, MA, United States, ³ University of Texas Southwestern Medical Center, Dallas, TX, United States, ⁴ Section of Pulmonary and Critical Care, Department of Medicine, University of Chicago, Chicago, IL, United States, ⁵ Medical College of Georgia at Augusta University, Augusta, GA, United States, ⁶ Brigham and Women's Hospital, Harvard Medical School, Boston, MA, United States, ⁷ Healthcare and Public Health Partnerships, YouTube and Google Health, Playa Vista, CA, United States, ⁸ University Medical Center Groningen, Groningen, Netherlands, ⁹ Life Science Center for Survival Dynamics, TARA, University of Tsukuba, Tsukuba, Ibaraki, Japan

Recent increased visibility on racial issues in the United States elicited public outcry and a collective call for action. The social justice movement has facilitated energetic discussions about race, sexual orientation, and various issues of diversity, equity, and inclusion. This article discusses issues faced by people of color that we as scientists can address, as well as challenges faced by women and internationally trained scientists in the scientific community that need immediate attention. Moreover, we highlight various ways to resolve such issues at both institutional and individual levels. Silence and incremental solutions are no longer acceptable to achieving lasting social justice and ensure prosperous societies that work for all.

Keywords: African American, Asian American, Latinx, social justice, Native American, STEM women, diversity and inclusion

INTRODUCTION

Everyone deserves to live in dignity. However, reality is far from ideal, even in highly developed nations. Barriers to diversity, equity, and inclusion are major obstacles. The United States (US) recently faced an immediate need to address complex issues associated with the consequences of racism against people from the African-American and Asian-American communities. In addition to fundamental diversity issues, apathy may be another challenge. As the media's attention to racially charged events fades, attention shifts, particularly for those who are not directly affected. Lawmakers turn to other issues and potentially fail to act. Indeed, while the large-scale protests of summer 2020 have diminished, racial inequality and disparity remain inadequately unaddressed. Other diversity issues in the scientific community (e.g., gender, sexual orientation, culture, socioeconomic status, and religion) need equal attention. Recognizing such issues is only the

first step, and international organizations, governments, institutes, and individuals must work to understand problems, educate each other, and find solutions. Professional organizations must adopt strict, zero tolerance policies toward any form of racism and inequality.

As scientists, we should act swiftly to find solutions. The North American Vascular Biology Organization (NAVBO) has built a strong tradition of embracing and promoting diversity. In response to the need for justice, NAVBO launched the new Diversity, Equity, and Inclusion Committee and issued a Statement of Commitment to Diversity, Equity, and Inclusion^{1,2}. Here, the committee offers potential solutions to the various issues of diversity and inclusion the world and scientific communities face. Together, we can work to protect our core values and establish safe and compassionate environments.

I: OVERCOMING SOCIAL INJUSTICE AND MOVING FORWARD

Racial Inequality Is Real and Can Affect Public Health

Recent elevated visibility on the issues of racial injustice in the US has elicited public protests and a collective call for action³, prompting us to increase our fight against prejudice, ignorance, and indifference. We hope these protests end all forms of discrimination, not only against African-, Native-, and Asian-American people but also against other races and ethnicities, gender or gender identity, sex or sexual orientation, age, religion, culture, beliefs, national origin, immigration status, language proficiency, socioeconomic status, or intellectual or physical ability^{4,5,6} (1). NAVBO's moral convictions cannot tolerate discrimination. The positive side of recent events is that they created an opportunity for people of all backgrounds to unite and form transformational movements in many institutions in the US and around the globe, leading to the development of policies and legal frames designed to uproot all forms of inequality in society at large.

Study after study, from all angles, clearly show that many institutions suffer from biases and discrimination against African Americans and other people of color (1–5). In the US, most African Americans (92%), Latinx (78%), Native Americans (75%), and Asian Americans (61%) report experiencing racial discrimination (i.e., racial slurs, violence, threats, and harassment) at work and in schools. Institutions that honestly assessed their own racial fairness discovered concerns of inequality. For instance, an institutional assessment of the

American College of Physicians (ACP) reported that its membership applications considered race and religion, required citizenship in North America, and limited membership to English-language speakers in the first half of the 20th century (1). Gathering evidence from similar efforts by other groups would increase awareness of racial inequality. This is an important first step in establishing fair environments in the scientific community.

Racial injustice and disparity, including reduced access to employment, education, and crowded and substandard housing, affects public health and life expectancy in several ways. Discrimination causes adverse cognitive and emotional inadequacy, which can lead to lack of interest in healthy behaviors (e.g., sleep and exercise) and increased desire for unhealthy behaviors (e.g., alcoholism, drug abuse, and unhealthy food consumption) (6–8). Minorities have contracted COVID-19 far more often than the White populations. Recently published data show that African Americans disproportionately lost employment or income (9). Additionally, African Americans are more likely than White people to display vaccine hesitancy due to confidence and circumspection (10). As described by the Okorodudus, unfair treatment of young people by medical professionals may have led African Americans to distrust the entire medical system (11). Moreover, Albert et al. showed that health disparities are not merely differences in health status but rather an accumulated unfair practice in the healthcare system that can be modified for the well-being of the entire community (12). The social injustice and health disparities does not stop with African Americans, it is well documented in American Indian and Alaska Native people who have experienced health disparities when compared with other Americans. Lower life expectancy and disproportionate disease burden. They also experienced inadequate education, disproportionate poverty, discrimination in the delivery of health services, and cultural differences. All these issues are directly connected to socioeconomic difficulties (13).

The Role of Educational Institutions in Promoting Social Justice

Institutions of higher learning are critical platforms for fostering equality and promoting social justice. Accessibility to these institutions by people of color represents an important socioeconomical tool for supporting their communities. Because a college degree can alter a family's trajectory for generations, scholarships and other resources are important to the success of students from underrepresented communities. Thus, institutions should increase their financial commitment to diversity as a means to retain and graduate students of color (14). Updated curricula that highlight the historical struggle of African Americans and offer restorative approaches to expose the past head-on can provide avenues for a brighter future. Training is crucial to the success of underrepresented students.

Importantly, faculty should mirror the student body because the success of African American and other faculty of color helps ensure the success of students from underrepresented communities (15, 16). Institutions should provide resources

¹<https://www.navbo.org/about-us/policies>

²<https://www.navbo.org/archive/>

³<https://www.nytimes.com/2020/05/31/us/george-floyd-investigation.html>

⁴<https://www.cnn.com/2021/04/20/us/derek-chauvin-trial-george-floyd-deliberations/index.html>

⁵https://www.washingtonpost.com/national-security/george-floyd-police-officers-federal-charges-civil-rights/2021/05/07/c30fdb6-ac34-11eb-acd3-24b44a57093a_story.html

⁶<https://economictimes.indiatimes.com/news/international/world-news/us-president-joe-biden-to-america-after-floyd-verdict-we-cant-stop-here/articleshow/82185501.cms?from=mdr>

(e.g., adequate startup packages, mentorship, fair performance assessments) and tools that ensure the success of these faculty members. To retain faculty and trainees from underrepresented communities, institutional leadership must acknowledge and understand their experiences of racism (17). In addition, minority faculty require access to federal funding (2). Importantly, fair treatment by professional organizations helps ensure people of color that they can present their scientific work at conferences and symposia, chair scientific sessions, and compete for recognition (i.e., awards and recognitions), boosting their career and ensuring academic growth.

Professional organizations such as NAVBO should adopt strict policies and zero tolerance approaches to any form of racism or inequality, and work toward eliminating all forms of implicit bias in professional activities. Further, professional organizations must implement proactive methods to ensure fairness and support members of underrepresented communities. Dedicated committees that focus on programs and policies that promote diversity, equity, and inclusion can foster the success of faculty members from underrepresented communities. Some scientists, who do not understand how much underrepresented groups and minorities struggle, can unconsciously fall into implicit bias. Therefore, professional organizations must regularly conduct training programs and seminars on diversity and implicit biases and encourage scientists to increase diversity in their own institutions, research programs, and leadership positions. Notably, several studies indicate that diversity in the faculty or student body alone is not sufficient for resolving inequality. While many institutions have done a remarkable job diversifying their campuses, leadership often remains disproportionately dominated by white men (18).

We now recognize a greater need for reforming institutional practices in government, academia, sports, cultural societies, arts, etc. Inequality and injustice cannot be resolved without greater awareness, real efforts, and commitments from all sections of a society. It is not enough to merely issue statements that condemn injustice or simply post policies or statements on institutions' webpages. Our workforce should reflect the community. Identifying hidden discrimination in hiring, promotion, and access to resources is very important when implementing a fair workforce environment (**Figure 1**). Leaders, administrators, and educators of all backgrounds and at all levels need to act by adopting strategies with measurable outcomes.

Role of the National Institutes of Health

The US National Institutes of Health (NIH) is the largest public funding agency of biomedical and behavioral research worldwide. Its mission is to seek fundamental knowledge about the nature and behavior of living systems and then apply that knowledge to enhance health, lengthen life, and reduce illness and disability. In response to recent events that highlighted the reality of racial injustice in the US, the NIH issued a statement that recognizes systemic racism in biomedical research and strengthened its commitments to end structural racism in the biomedical workforce. The statement also acknowledged its

previous efforts have been insufficient⁷. The NIH is committed to developing new ways to support diversity, equity, and inclusion, and identifying and dismantling any policies and practices that may harm our workforce and our science (2).

The NIH recently launched UNITE, a new initiative that aims to identify and address structural racism within the NIH and the greater biomedical community⁷. Briefly, UNITE aims to establish an equitable culture within the biomedical research enterprise, reduce barriers to racial equity in its workforce, and advance health equity research to eliminate or lessen health disparities and inequities. UNITE also seeks to (i) identify critical elements that perpetuate structural racism and leads to a lack of diversity, equity, and inclusion in the biomedical enterprise; (ii) investigate and eliminate health disparities and inequities; (iii) change the organizational culture and structure of NIH to promote diversity, equity, and inclusion; (iv) coordinate NIH-wide efforts to ensure transparency, accountability, and sustainability of all UNITE efforts; and (v) evaluate NIH extramural policies and processes to identify and change cultures, practices, and structures to promote inclusivity and diversity within the extramural research ecosystem.

The NIH also promotes diversity, equity and inclusion by requiring the involvement of African American and other underrepresented people as presenters, a score-driving factor for R13 applications to support scientific conferences. This effort helps increase awareness of social injustice issues in science communities.

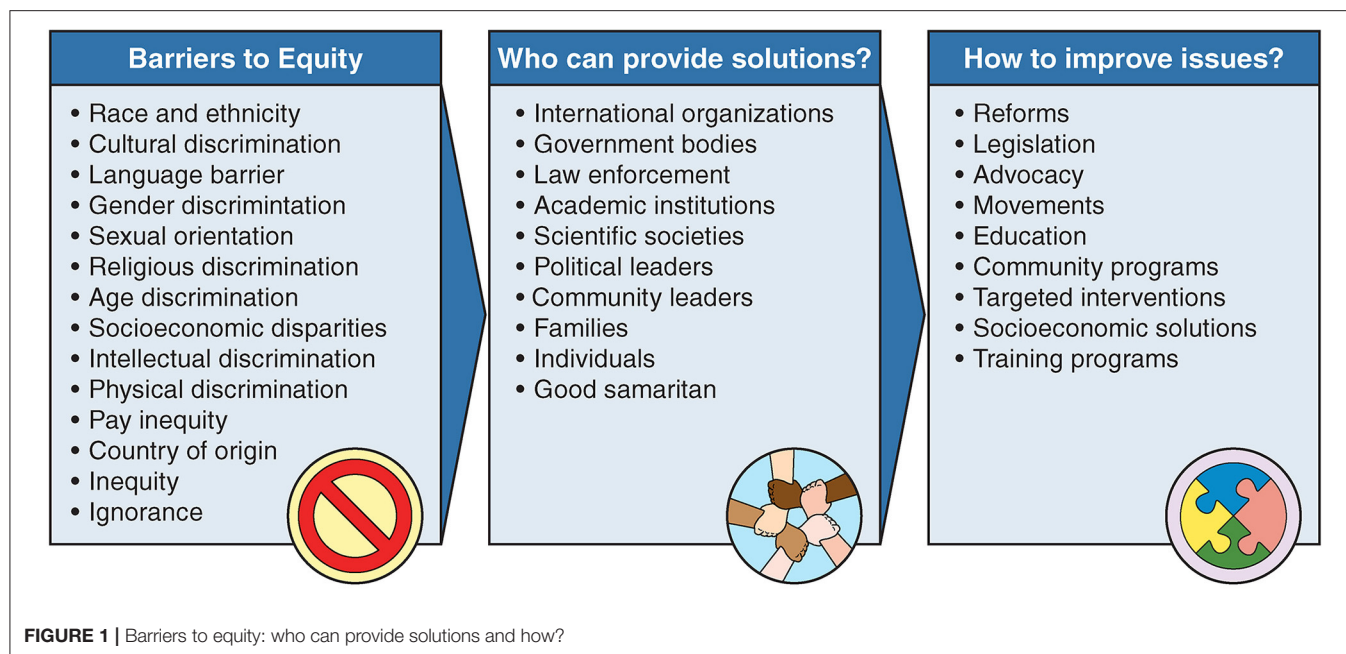
In addition to the NIH's efforts, collective action by all stakeholders (i.e., communities of scientific research, advocacy, clinical practice) and non-scientific communities, including the public, is crucial to ending systemic racism in the biomedical research workforce.

II: CHALLENGES IN CAREER DEVELOPMENT FOR WOMEN

The Underrepresentation of Women in Medicine Biological Sciences, and Science, Technology, Engineering, or Math

Although women's participation in biomedical sciences and other sciences, technology, engineering, and math (STEM) fields has increased, evidence suggests that women are still underrepresented in education, careers, and leadership positions (19). A large comprehensive bibliometric analysis of 1.5 million authors, led by systems scientist Albert-László Barabási, reported longitudinal gender gaps in academic publishing and significantly higher dropout rates in women (20). Particularly, women from racial and ethnic minority groups (e.g., African American, Hispanic, or indigenous) are insufficiently represented in various scientific professions and career levels. After graduating from high school, women are less likely than men to choose any of the STEM fields as a major in college. Women's representation in science decreases further at the graduate level, the transition to the workplace, and still further

⁷<https://www.nih.gov/ending-structural-racism/unite>



at senior and professorial levels⁸. Barriers to women's career progression partly explain their underrepresentation in faculty and leadership positions in medicine, biological sciences, and STEM. Importantly, women and men would share similar opportunities if the legal system supported them equally. Gender inequality should be recognized as a major social problem and a primary consideration for the members of our scientific community. A resolution of gender inequality will help improve women's education and careers and encourage more women to establish a career in science, benefitting society at large.

Understanding Barriers to Women's Career Development in Science

Evidence suggests that higher dropout rates for women in academic careers compared to men (20). Why? Barriers to career development for women are institutional, cultural, individual, and family-bounded. Institutional barriers include (i) lower-level professional positions, (ii) lower pay, (iii) dysfunctional legislations that hinder promotion, (iv) negative attitudes, and (v) limited access to networks and mentors (21). Other barriers include gender stereotypes, discrimination and harassment, and gender-role expectations. Self-recognized stereotyping and common biases seem to be the first obstacles for female graduates who begin a career in STEM. Such misconceptions include: (i) men are better than women in STEM fields; (ii) women are not interested in careers in science; and (iii) successful women behave in masculine ways. Gender bias may exist in peer review, job applications, recruitment, and promotions (22, 23). Responsibility for childcare or caring for an ill or aging family member is another typical barrier to women's career development. Frequently, men and women do not share

housework, childcare, and looking after the family's emotional well-being equally. Thus, many women scientists who strive to establish an independent career must balance work and family responsibilities, leading to career breaks or part-time appointments. A consequent reduction in publications has a negative impact on grant success rates and career development, resulting in job insecurity and reduced career retention.

Strategies to Overcome Barriers to Career Progression for Women

Mentoring and role-modeling programs help women develop a network with multiple mentoring relationships for degree and career success, in STEM (24). Mentoring programs can strengthen women's motivation and persistence in career pathways through (i) providing female role models; (ii) teaching women how to grow their mentor-mentee network; and (iii) introducing women to local mentors and sponsors. Training for issues related to stereotypes and unconscious biases, along with transparent recruitment and promotion processes, are required. Detailed plans to promote cultural shifts can ensure that women have equal access to opportunities and adequate paths to develop their career in science. Since most research appointments depend on active, independent grants with short-term contracts, women's pathways for promotion are often unclear^{9,10}.

Understanding a diversity-oriented working environment and identifying good mentors, collaborators, and peers can help women avoid isolation, stay connected with networks, and develop their careers in science. Organizations should train

⁸<https://www.nsf.gov/statistics/seind14/content/chapter-5/at05-15.pdf>

⁹<https://www.science.org/content/article/more-action-needed-retain-women-science>

¹⁰<https://publications.parliament.uk/pa/cm201314/cmselect/cmsctech/701/701.pdf>

employees on unconscious bias, diversity, and inclusion to encourage shifts in culture and improve strategies to recruit and retain female scientists. In addition, policies should promote an inclusive workplace and foster transparent promotion processes that ensure pay equity.

When facing such issues, female scientists should not struggle alone. Our institutions have a key responsibility to create safe working conditions that enable all employees to deliver high-quality work in an effective manner. Such environments have no place for workplace bullying or any other form of harassment (25). All personnel need active support to make our academic and research institutes gender-balanced at all the levels, from technical or administrative staff to junior investigators to full professor, provost, or institute director. Simply stated, diverse organizations perform better (26).

Any organization that is seriously interested in expanding gender diversity can instantly implement a “Zipper quota,” a method coined by Curt Rice¹¹. This method shortlists suitable women candidates and “zips” them together with a shortlist of suitable male candidates. Next, shortlisted candidates are selected by putting the first woman on the interview list, then the first man, followed by the 2nd woman, the 2nd man, and so on. Thus, any zipped list will yield a new shortlist for interviewing the best candidates. The strategy can be applied to recruitment for any position, and it provides recruitment committees with the exciting opportunity to interview the best female and best male candidates. In addition, the composition of recruitment committees can be established by “zipping” shortlists of its female and male members. This strategy minimizes the chances of selecting or promoting “the usual suspects;” instead, the best person is hired based on their own merits and the best scholars are promoted. Since women and men are equally smart and skilled, hiring qualified women will become part of the norm.

Imposter Syndrome

Imposter syndrome (i.e., doubting your own abilities) often hinders women’s success, and it can be generalized to any underrepresented group. Imposter syndrome internalizes thoughts that you are not good enough, do not belong, feel like a fraud, do not deserve the job or promotion. Additionally, you devalue your worth and think you have only succeeded due to luck, not because of your talent or qualifications. Imposter syndrome disproportionately affects minority groups and high-achieving women who struggle to accept their own accomplishments (25, 27). It persists throughout college and graduate school and into the working world, where women tend to judge their performance as worse than it is, while men judge their own performance as better. Even the most successful and accomplished women have this experience. Although imposter phenomenon is not an official diagnosis, psychologists and others acknowledge that it is a real and specific form of intellectual self-doubt. Imposter feelings generally include anxiety and depression, which greatly reduce confidence and cause women to consider leaving the field. Mentors who provide advice on how to deal with impostorism are especially helpful. Importantly

for women, overcoming imposter syndrome involves recording their accomplishments; visualizing and recognizing their success; talking to mentors, colleagues, or friends; removing doubt; becoming confident; realizing that no one is perfect, and reminding themselves that they are good at what they do.

Impact of COVID-19 on Women’s Career Development in Science

COVID-19 continues to spread around the world with unexpected consequences for health systems and global economies. Compared to men in science, the pandemic has greatly affected disadvantaged women, particularly in STEM (28–32). Women from diverse backgrounds have additional barriers during the pandemic, including homeschooling their children, general housework, and managing their paid workload. Therefore, women are less likely than men to attend STEM workplaces, submit manuscripts and grant applications, and start new projects. Because COVID-19 has caused budgetary restraint at some universities and academic medical centers, STEM jobs are at risk. Significantly reduced short-term contracts are held mainly by women (28). We hope that pandemic-related budget cuts do not influence ongoing equity programs. The future of women in STEM could be jeopardized if developments achieved in recent years are lost. Solving this issue requires consideration and discussion of how to mitigate the impact of COVID-19 on job security and career progression for women in medicine, biological sciences, and STEM.

III: LGBTQ+ IN STEM

Although social science research has made great strides in documenting and reporting the problems that racial minorities and women face in STEM, other sociodemographic minorities (e.g., sexual and gender minorities) have received less attention. This article refers to such minorities including but not limited to gay, lesbian, transgender, queer, non-binary, and asexual groups as LGBTQ+ (sometimes LGBTQ, LGBQ, or LGBT+, depending on context). These minorities are interesting in the context of inequality, but sampling limitations have prevented investigation into systemic inequalities faced by LGBTQ+ scientists. Recent studies report the climate surrounding LGBTQ+ individuals in STEM as significantly less pleasant compared to their heterosexual counterparts (32, 33). Specifically, sexual minorities were 7% less likely to finish a STEM degree compared to switching to a non-STEM major, although sexual minorities were more likely to participate in undergraduate research programs (34). In the workplace, up to 28% of LGBT scientist respondents have considered leaving their STEM workplace; transgender individuals were hardest hit, with nearly half having considered leaving; and 20% of transgender respondents frequently considered leaving (34, 35). Forty-nine percent of respondents agreed that there is an overall lack of awareness of LGBT+ issues in STEM. Notably, however, 70% of respondents reported that the working environment for LGBT+ scientists was improving (35).

¹¹<http://curt-rice.com/about/>

IV: FIRST GENERATION IN STEM

Being a first-generation (“first-gen”) scientist comes with its own unique challenges. First-gen students are those whose parents did not acquire any higher education after high school or the equivalent (36). These students often do not know how to navigate the college application process, especially for graduate school. Disadvantages facing first-gen students include (i) inability to speak to their parents and/or guardians about college resources, (ii) navigating college applications, and (iii) applying for grants or scholarships. These disadvantages are compounded for first-gen students from underrepresented racial groups, who may experience discrimination, racism, and language barriers while dealing with the hurdles of the college application process (37). In fact, Latinx students comprise a significantly larger portion of first-gen students (38). First-gen students are less likely to pursue an undergraduate or graduate degree due to many factors, but notably many must work one or more jobs to pay for college. Therefore, first-gens cannot fully devote themselves to extracurricular activities and gain experience to pursue graduate education (**Figure 2**) (38–40).

V: CHALLENGES OF INTERNATIONALLY TRAINED SCHOLARS

Barriers in Communication and Grant Writing

While this section focuses on how young international students can overcome difficulties and succeed, we also wish to increase awareness of the challenges foreign-born scientists experience in a new country, particularly the US. Discussing cultural differences and immigration restrictions can present fundamental challenges. Starting new careers as postdoctoral scientists and then moving into faculty positions in a new country are further compounded by cultural and language barriers. Although most postdocs and faculty members were educated in English and/or have acquired English language skills, developing effective communication skills across deep-rooted accents and vastly different cultural settings can be very difficult.

Alongside informal and social interactions, grant writing and presentation skills are critical to success in an academic career. Mastering such skills requires a great deal of practice and adaptation by foreign-trained scholars. When writing competitive grants, such scholars encounter differences in language and cultural communication styles, which often hinder the process and logical flow of ideas. Some languages, such as Japanese, are indirect and less clear compared with American-style English (e.g., the concept of “conclusion first”). Understanding differences in writing styles plays a substantial role in shaping grant applications, leading to successful funding that is a deciding factor for achieving career milestones.

Cultural Differences

International scholars, whose cultural backgrounds are vastly different from Western nations such as the US, sometimes think they will seem too bold, straightforward, or even disrespectful

to superiors and authority figures if they speak up without permission or hesitation. Some people misinterpret cultural and language barriers as a lack of confidence or initiative, or as intention to challenge people or propose solutions. Potentially, such misinterpretations can harm one's growth and career. International scholars benefit tremendously when they learn and adapt to Western or American cultures, which encourage innovation, proactive thinking, and self-promotion. In a rapidly evolving research landscape marked by new and emerging technologies, gaining courage to “jump on a moving train” may be critical for scientists from nations where more careful approaches are common or respected. Compared to other nationalities, Americans tend to be goal-oriented, a characteristic that may help speed actions and favor competitive environments. Asian scientists may take a more process-oriented, step-by-step approach that does not necessarily win competitions. Notably, blending new experiences and skills with the strengths they learned at home can strengthen their career prospects.

Having completed their doctoral degrees abroad, most international scientists' first encounter with the American academic system is as a postdoctoral fellow. Thus, they must navigate vastly different academic institutional policies and systems. Foreign scholars, particularly women, are often young adults venturing into family responsibilities, which add to the burden of acclimating to a new country with different norms. From deciphering amenities (e.g., finding good housing, setting up utilities and bank accounts, working out transportation options and schooling for children) to familiarizing themselves with distinctly different work cultures in a completely new environment can overwhelm some international trainees. Moreover, the rigors of academia (e.g., challenging experiments and long hours, working toward multiple publications, and writing successful grants) exponentially compound the challenges faced by international scholars. Some institutions have international societies or postdoctoral associations that can help with setting up some accommodations, but such support groups are relatively rare. Thus, many internationally trained scientists struggle alone. These challenges drive our efforts to share our views with young international scholars.

Beyond postdocs, similarly challenging scenarios confront the larger spectrum of international scholars who enter the academic system in the US, either early as doctoral students or later as faculty members. Regardless of where international scholars begin their journey, early steps to successfully assimilate into the new academic system and way of life can make a large difference. Learning to communicate effectively, think beyond one's limitations, and open up to new opportunities can be very beneficial. Importantly, students must learn to network, be openminded and proactive, and take a multidisciplinary approach to introduce themselves and their work to their new community. International students and postdocs must do their due diligence in finding the right doctoral lab and mentor and seek to match not only the science and academic experiences that interest them, but also the culture of the lab and the mentoring history of the principal investigator (PI). Importantly, she/he should recognize that a mentor–mentee relationship works both ways. Proactive communication helps a



FIGURE 2 | How can we be part of the solution.

PI understand each trainee's goals and makes a mentor–mentee team productive. Since grants are paramount in shaping one's academic career, international scholars should strive to develop their scientific communication skills and grant writing styles. The importance of guiding international scholars to various grant opportunities cannot be stressed enough. Administrative offices or leadership departments may help identify funding opportunities, and grant writing classes can help students write competitive applications for institutional, regional, and national funding.

Navigating visas to maintain legal status to live and work in the US is a significant liability for international scholars. International students begin their US journey with F-1 student visas, then optional practical training (OPT) visas, and finally

J-1 (exchange visitors) or H-1B (specialty occupations) visas. Most international postdoctoral researchers have a J-1 visa until they are eligible to apply for a self- or employer-sponsored green card. Some institutions may not support postdocs' H-1B visa or green card applications, adding the pressure on internationally trained scientists who wish to develop careers in the US¹². Visa restrictions and requirements are complex, expensive, and may risk work–life status, creating stress. Depending on the flexibility and understanding of mentors and institutions that sponsor them, this vulnerability can limit available opportunities. Academic research institutions have administrative services dedicated to international students,

¹²<https://www.ncbi.nlm.nih.gov/books/NBK268781/>

postdocs, and faculty members. International scholars should familiarize themselves with such resources and utilize them appropriately for routing daunting, meticulous, and time-sensitive visa transitions.

CONCLUSIONS

Silence is no longer acceptable when social injustice issues become intolerable in our progressive scientific society. The May 2020 murder of George Floyd in Minneapolis, Minnesota, led to worldwide protests of police brutality, racism, and lack of accountability toward African Americans, opening a wide door for an overall review of the issues of social justice and equality beyond racism in the US and around the globe. Attempts to address disparities in health care, education, judicial systems, and the spectrum of workplaces have been an ongoing demand for several decades. Using technology to document violations and social media to spread awareness of prejudices has helped increase awareness in all institutions, including those in the scientific community. This article discussed social justice issues relevant to African- and Asian-Americans, women, and LGBTQ+ as well as challenges faced by international scholars. Importantly, we provide future perspectives to resolve these self-made social determinants (Figure 2). While increased awareness is a critical first step, it is not enough. We must act together, as individuals and

as institutions, to introduce real changes that establish and provide inclusive, fair, and safe environments to all. NAVBO's commitment to diversity, equity, and inclusion strongly supports these goals.

DATA AVAILABILITY STATEMENT

The original contributions presented in the study are included in the article/supplementary material, further inquiries can be directed to the corresponding author/s.

AUTHOR CONTRIBUTIONS

MG and MA assembled the materials and coordinated the efforts. All authors contributed to the design and writing of this article.

ACKNOWLEDGMENTS

The authors would like to acknowledge the administrative support received from Ms. Bernadette Englert, the Executive Officer of NAVBO, and the members of the NAVBO Council for reviewing this paper. We like to recognize Dr. Keith Mitchell, Dr. Francine Coston, Dr. Valerie Stone, Ms. Cinamon Blair and Mr. Stephen John "Jay" Skelton for their editorial review of the first section (social justice) of this article. We also thank Ms. Karen Williams for professional English editing.

REFERENCES

- Serchen J, Doherty R, Atiq O, Hilden D. Racism and health in the United States: a policy statement from the American College of Physicians. *Ann Intern Med.* (2020) 173:556-7. doi: 10.7326/M20-4195
- Stevens KR, Masters KS, Imoukhuede PI, Haynes KA, Setton LA, Cosgriff-Hernandez E, et al. Fund black scientists. *Cell.* (2021) 184:561-5. doi: 10.1016/j.cell.2021.01.011
- Trotochaud K. Ethical issues and access to healthcare. *J Infus Nurs.* (2006) 29:165-70. doi: 10.1097/00129804-200605000-00007
- Cleveland Manchanda EC, Macias-Konstantopoulos WL. Tackling gender and racial bias in academic emergency medicine: the perceived role of implicit bias in Faculty Development. *Cureus.* (2020) 12:e11325. doi: 10.7759/cureus.11325
- Maupin J, Kaikow F, Kenik J, Sheehy A, Sterken D. Assessing perspectives on systemic racism in an academic hospital medical group: the ARCH Project. *WMJ.* (2021) 120:S66-9.
- Paradies Y, Ben J, Denson N, Elias A, Priest N, Pieterse A, et al. Racism as a determinant of health: a systematic review and meta-analysis. *PLoS ONE.* (2015) 10:e0138511. doi: 10.1371/journal.pone.0138511
- Churchwell K, Elkind MSV, Benjamin RM, Carson AP, Chang EK, Lawrence W, et al. Call to action: structural racism as a fundamental driver of health disparities: a presidential advisory from the American Heart Association. *Circulation.* (2020) 142:e454-68. doi: 10.1161/CIR.0000000000000936
- Ramirez-Valles J. Public health has an equity problem: a Latinx's voice. *Front Public Health.* (2020) 8:559352. doi: 10.3389/fpubh.2020.559352
- Sparks JR, Kebbe M, Flanagan EW, Beyl RA, Altazan AD, Yang S, et al. Impact of COVID-19 stay-at-home orders on health behaviors and anxiety in black and white Americans. *J Racial Ethn Health Disparities.* (2021) 19:1-5. doi: 10.1007/s40615-021-01131-3
- Liu R, Li GM. Hesitancy in the time of coronavirus: temporal, spatial, and sociodemographic variations in COVID-19 vaccine hesitancy. *SSM Popul Health.* (2021) 15:100896. doi: 10.1016/j.ssmph.2021.100896
- Okorodudu DO, Okorodudu DE. An issue of trust-vaccinating Black patients against COVID-19. *Lancet Respir Med.* (2021) 9:228-9. doi: 10.1016/S2213-2600(21)00002-3
- Albert MA, Carnethon MR, Watson KE. Disparities in cardiovascular medicine. *Circulation.* (2021) 143:2319-20. doi: 10.1161/CIRCULATIONAHA.121.055565
- Indian Health Service. Available online at: <https://www.ihs.gov/newsroom/factsheets/disparities/> (accessed December 15, 2021).
- James GB, Jr. *The perception of black male students of black faculty/staff involvement in mentorship at a predominantly white institution (Masters Theses)*, Eastern Illinois University, Lincoln Avenue Charleston, IL (2015).
- Bush M. *Lack Of Black Faculty Leads To Fewer Mentors For African-American Students In WNC.* (2018). Available online at: <https://www.bpr.org/post/lack-black-faculty-leads-fewer-mentors-african-american-students-wnc#stream/0> (accessed December 15, 2021).
- Ambrose AJ, Andaya JM, Yamada S, Maskarinec GG. Social justice in medical education: strengths and challenges of a student-driven social justice curriculum. *Hawaii J Med Public Health.* (2014) 73:244-50.
- Grubbs V. Diversity, equity, and inclusion that matter. *N Engl J Med.* (2020) 383:e25. doi: 10.1056/NEJMp2022639
- Kezar AJ. *Rethinking Leadership in a Complex, Multicultural, and Global Environment: New Concepts and Models for Higher Education.* Sterling, VA: Stylus Publishing, LLC (2009).
- Celebrating women in science. *Nat Cell Biol.* (2018) 20:993. doi: 10.1038/s41556-018-0190-4
- Huang J, Gates AJ, Sinatra R, Barabási AL. Historical comparison of gender inequality in scientific careers across countries and disciplines. *Proc Natl Acad Sci USA.* (2020) 117:4609-16. doi: 10.1073/pnas.1914221117

21. Coe IR, Wiley R, Bekker L-G: Organisational best practices towards gender equality in science and medicine. *Lancet*. (2019) 393:587–93. doi: 10.1016/S0140-6736(18)33188-X
22. Holman L, Stuart-Fox D, Hauser CE. The gender gap in science: how long until women are equally represented? *PLoS Biol*. (2018) 16:e2004956. doi: 10.1371/journal.pbio.2004956
23. Shannon G, Jansen M, Williams K, Cáceres C, Motta A, Odhiambo A, et al. Gender equality in science, medicine, and global health: where are we at and why does it matter? *Lancet*. (2019) 393:560–9. doi: 10.1016/S0140-6736(18)33135-0
24. González-Pérez S, Mateos de Cabo R, Sáinz M. Girls in STEM: is it a female role-model thing? *Front Psychol*. (2020) 11:2204. doi: 10.3389/fpsyg.2020.02204
25. National Research Council (US) Panel on Race, Ethnicity, and Health in Later Life. 2, Racial and Ethnic Identification, Official Classifications, and Health Disparities. In: Anderson NB, Bulatao RA, Cohen B, editors. *Critical Perspectives on Racial and Ethnic Differences in Health in Late Life*. Washington, DC: National Academies Press (US) (2004).
26. Nielsen MW, Alegria S, Börjeson L, Etzkowitz H, Falk-Krzesinski HJ, Joshi A, et al. Gender diversity leads to better science. *PNAS*. (2017) 114:1740–2. doi: 10.1073/pnas.1700616114
27. National Academies of Sciences, Engineering, and Medicine; Health and Medicine Division; Board on Population Health and Public Health Practice; Committee on Community-Based Solutions to Promote Health Equity in the United States. 2, The State of Health Disparities in the United States. In: Baciú A, Negussie Y, Geller A, et al., editors. *Communities in Action: Pathways to Health Equity*. Washington, DC: National Academies Press (US) (2017).
28. Speer JE, Lyon M, Johnson J. Gains and losses in virtual mentorship: a descriptive case study of undergraduate mentees and graduate mentors in STEM research during the COVID-19 pandemic. *CBE Life Sci Educ*. (2021) 20:ar14. doi: 10.1187/cbe.20-06-0128
29. Wester ER, Walsh LL, Arango-Caro S, Callis-Duehl KL. Student engagement declines in STEM undergraduates during COVID-19-driven remote learning. *J Microbiol Biol Educ*. (2021) 22:22.1.50. doi: 10.1128/jmbe.v22i1.2385
30. Gebhard C, Regitz-Zagrosek V, Neuhauser HK, Morgan R, Klein SL. Impact of sex and gender on COVID-19 outcomes in Europe. *Biol Sex Differ*. (2020) 11:29. doi: 10.1186/s13293-020-00304-9
31. Punjani N, Ha A, Caputo J, Wang V, Wiechmann L, Chiasson MA, et al. Outcome disparities among men and women With COVID-19: an analysis of the New York City population cohort. *J Drugs Dermatol*. (2020) 19:960–7. doi: 10.36849/JDD.2020.5590
32. Lassale C, Gaye B, Hamer M, Gale CR, Batty GD. Ethnic disparities in hospitalisation for COVID-19 in England: the role of socioeconomic factors, mental health, and inflammatory and pro-inflammatory factors in a community-based cohort study. *Brain Behav Immun*. (2020) 88:44–9. doi: 10.1016/j.bbi.2020.05.074
33. Cech EA, Waidunas TJ. Systemic inequalities for LGBTQ professionals in STEM. *Sci Adv*. (2021) 7:933–48. doi: 10.1126/sciadv.abe0933
34. Hughes, Bryce E. Coming out in STEM: factors affecting retention of sexual minority STEM students. *Sci Adv*. (2018) 4:eao6373. doi: 10.1126/sciadv.aao6373
35. Institute of Physics, Royal Astronomical Society and the Royal Society of Chemistry. *Exploring the Workplace for LGBT+ Physical Scientists*. (2019). Available online at: https://www.rsc.org/globalassets/04-campaigning-outreach/campaigning/lgbt-report/lgbt-report_web.pdf (accessed December 15, 2021).
36. Chen X. *First-Generation Students in Postsecondary Education A Look at Their College Transcripts Postsecondary Education Descriptive Analysis Report*, Blacksburg, VA (1988).
37. Hossler D, Schmit J, Vesper N. *Going to College: How Social, Economic, and Educational Factors Influence the Decisions Students Make* (1999).
38. Verdin D, Godwin AF. *First in the Family: A Comparison of First-Generation and Non-First-Generation Engineering College Students* Custom Citation APA *First in the Family: A Comparison of First-Generation and Non-First-Generation Engineering College Students*, School of Engineering Education, Purdue University, West Lafayette, Indiana (2015).
39. Phinney JS, Haas K. The process of coping among ethnic minority first-generation college freshmen: a narrative approach. *J Soc Psychol*. (2003) 143:707–26. doi: 10.1080/00224540309600426
40. Michael F. Report of the APS ad-hoc committee on LGBT issues – presentation of findings and recommendations. *Bull Am Phys Soc*. (2016) 61:2.

Author Disclaimer: Contents of this article do not necessarily represent the official position of NAVBO. The authors of this article represent their own opinions.

Conflict of Interest: GG was employed by Healthcare and Public Health at Google/YouTube.

The remaining authors declare that the research was conducted in the absence of any commercial or financial relationships that could be construed as a potential conflict of interest.

Publisher's Note: All claims expressed in this article are solely those of the authors and do not necessarily represent those of their affiliated organizations, or those of the publisher, the editors and the reviewers. Any product that may be evaluated in this article, or claim that may be made by its manufacturer, is not guaranteed or endorsed by the publisher.

Copyright © 2022 Garelnabi, Cowdin, Fang, Shrestha, Ushio-Fukai, Aikawa, Graham, Molema, Yanagisawa and Aikawa. This is an open-access article distributed under the terms of the Creative Commons Attribution License (CC BY). The use, distribution or reproduction in other forums is permitted, provided the original author(s) and the copyright owner(s) are credited and that the original publication in this journal is cited, in accordance with accepted academic practice. No use, distribution or reproduction is permitted which does not comply with these terms.



Long-Term Effect of Febuxostat on Endothelial Function in Patients With Asymptomatic Hyperuricemia: A Sub-Analysis of the PRIZE Study

Tatsuya Maruhashi¹, Yukihiro Higashi^{1,2*}, Hisako Yoshida³, Atsushi Tanaka⁴, Kazuo Eguchi⁵, Hirofumi Tomiyama⁶, Kazuomi Kario⁷, Toru Kato⁸, Nozomu Oda⁹, Nobuhiro Tahara¹⁰, Mitsutoshi Oguri¹¹, Hirotaka Watada¹² and Koichi Node⁴ for the PRIZE Study Investigators

OPEN ACCESS

Edited by:

Federica Fogacci,
University of Bologna, Italy

Reviewed by:

Arrigo Francesco Cicero,
University of Bologna, Italy
Samuel Silvestre,
Universidade da Beira Interior,
Portugal
Taiji Nagaoka,
Nihon University, Japan

*Correspondence:

Yukihiro Higashi
yhigashi@hiroshima-u.ac.jp

Specialty section:

This article was submitted to
Atherosclerosis and Vascular
Medicine,
a section of the journal
Frontiers in Cardiovascular Medicine

Received: 24 February 2022

Accepted: 11 April 2022

Published: 28 April 2022

Citation:

Maruhashi T, Higashi Y,
Yoshida H, Tanaka A, Eguchi K,
Tomiyama H, Kario K, Kato T, Oda N,
Tahara N, Oguri M, Watada H and
Node K (2022) Long-Term Effect of
Febuxostat on Endothelial Function
in Patients With Asymptomatic
Hyperuricemia: A Sub-Analysis of the
PRIZE Study.
Front. Cardiovasc. Med. 9:882821.
doi: 10.3389/fcvm.2022.882821

¹ Department of Cardiovascular Regeneration and Medicine, Research Institute for Radiation Biology and Medicine, Hiroshima University, Hiroshima, Japan, ² Division of Regeneration and Medicine, Medical Center for Translational and Clinical Research, Hiroshima University Hospital, Hiroshima, Japan, ³ Department of Medical Statistics, Osaka City University Graduate School of Medicine, Osaka, Japan, ⁴ Department of Cardiovascular Medicine, Saga University, Saga, Japan, ⁵ Department of General Internal Medicine, Saitama Red Cross Hospital, Saitama, Japan, ⁶ Department of Cardiology, Tokyo Medical University, Tokyo, Japan, ⁷ Department of Medicine, Division of Cardiovascular Medicine, Jichi Medical University School of Medicine, Shimotsuke, Japan, ⁸ Department of Clinical Research, National Hospital Organization, Tochigi Medical Center, Utsunomiya, Japan, ⁹ Department of Cardiology, Hiroshima Prefectural Hospital, Hiroshima, Japan, ¹⁰ Division of Cardiovascular Medicine, Department of Medicine, Kurume University School of Medicine, Kurume, Japan, ¹¹ Department of Cardiology, Kasugai Municipal Hospital, Kasugai, Japan, ¹² Department of Metabolism and Endocrinology, Juntendo University Graduate School of Medicine, Tokyo, Japan

Background: Xanthine oxidase is involved in the production of uric acid and the generation of superoxide anion. We evaluated the long-term effect of febuxostat, a non-purine selective xanthine oxidase inhibitor, on endothelial function in patients with asymptomatic hyperuricemia.

Methods: In the PRIZE study, patients with hyperuricemia were randomly assigned to either add-on febuxostat treatment (febuxostat group) or non-pharmacologic hyperuricemia treatment (control group). Among the 514 participants, endothelial function was assessed in 41 patients in the febuxostat group and 38 patients in the control group by flow-mediated vasodilation (FMD) of the brachial artery at the beginning of the study and after 12 and/or 24 months of treatment (63 men; median age, 68.0 years).

Results: The least squares mean concentration of serum uric acid was significantly lower in the febuxostat group than in the control group at 6 months (mean between-group difference [febuxostat group - control group], -2.09 mg/dL [95% confidence interval (CI), -2.520 to -1.659]; $P < 0.001$), 12 months (mean between-group difference, -2.28 mg/dL [95% CI, -2.709 to -1.842]; $P < 0.001$), and 24 months (mean between-group difference, -2.61 mg/dL [95% CI, -3.059 to

−2.169]; $P < 0.001$). No significant differences were found between groups in the least squares mean estimated percentage change in FMD at 12 months (mean between-group difference, −0.56% [95% CI, −1.670 to 0.548]; $P = 0.319$) and at 24 months (mean between-group difference, −0.60% [95% CI, −1.886 to 0.685]; $P = 0.357$).

Conclusion: Febuxostat treatment did not alter endothelial function assessed by FMD during a 2-year study period in patients with asymptomatic hyperuricemia.

Keywords: xanthine oxidase, xanthine oxidase inhibitor, febuxostat, flow-mediated vasodilation, endothelial function, hyperuricemia

INTRODUCTION

Endothelial dysfunction is regarded as the initial step in the pathogenesis of atherosclerosis and plays a critical role in progression to cardiovascular complications (1, 2). In addition, endothelial function has been shown to be an independent predictor of future cardiovascular events (3, 4). Therefore, it is important to select an appropriate intervention that will effectively improve or augment endothelial function to prevent cardiovascular events in the management of patients with cardiovascular disorders.

Xanthine oxidase (XO) has been regarded as one of the major oxidase enzymes involved in the generation of reactive oxygen species (ROS) (5, 6). During purine metabolism catalyzed by XO, not only uric acid but also superoxide anion ($O_2^{\cdot-}$) is generated concomitantly (7). Therefore, generation of ROS and production of uric acid are simultaneously increased with an increase in XO activity. ROS are involved in endothelial dysfunction by decreasing nitric oxide (NO) bioavailability through increasing NO inactivation and decreasing NO production *via* endothelial NO synthase uncoupling (2, 5). Although it remains unclear whether hyperuricemia is causally related to endothelial dysfunction in humans, experimental studies have indicated the possibility that hyperuricemia *per se* causes endothelial dysfunction through increasing inflammation or oxidative stress (8–10). Therefore, XO inhibitors have been expected to augment endothelial function by decreasing the generation of ROS and lowering serum uric acid levels (11, 12). Febuxostat is a non-purine selective XO inhibitor (13, 14). The short-term effect of febuxostat on endothelial function in humans has been investigated in a few studies (15–17). However, little information exists regarding the long-term effect of febuxostat on endothelial function in patients with asymptomatic hyperuricemia.

The PRIZE (program of vascular evaluation under uric acid control by xanthine oxidase inhibitor, febuxostat: multicenter, randomized controlled) study was a prospective, multicenter study conducted to evaluate the inhibitory effect of febuxostat on the progression of carotid artery intima-media thickness (IMT) over a 2-year follow-up period (18). In that study, flow-mediated vasodilation (FMD) of the brachial artery, an index of endothelial function, was measured in a subset of participants. Therefore, we carried out the present study as a pre-specified sub-analysis of the PRIZE study to evaluate the long-term effect of febuxostat treatment on endothelial function assessed by FMD of the brachial artery in patients with asymptomatic hyperuricemia.

MATERIALS AND METHODS

Study Design and Patients

The rationale and design of the PRIZE study (University Hospital Medical Information Network Center: ID 000012911) have been described previously (18, 19). In brief, the PRIZE study was a multicenter, prospective, randomized, open-label and blinded-endpoint trial carried out at 48 Japanese institutions. Eligible patients were at least 20 years of age and had asymptomatic hyperuricemia with a serum uric acid level >7.0 mg/dL and a maximum IMT of the common carotid artery (CCA) ≥ 1.1 mm, defined as a carotid arterial plaque in the guidelines of the Japan Society of Ultrasonics in Medicine and the Japan Academy of Neurosonology (20). Patients who had taken any serum uric acid-lowering agents within the 8-week period before assessment of eligibility, those who had gouty tophus, and those who had had symptoms of gouty arthritis within 1 year before assessment of eligibility were excluded. Other exclusion criteria are described elsewhere (19).

Between May 2014 and June 2016, a total of 514 patients with asymptomatic hyperuricemia were enrolled and randomly assigned in a 1:1 ratio to either add-on febuxostat treatment (febuxostat group: $n = 257$) or non-pharmacologic hyperuricemia treatment (control group: $n = 257$). Randomization was stratified on the basis of age, sex, presence or absence of type 2 diabetes, serum uric acid level (<8.0 or ≥ 8.0 mg/dL), and maximum CCA-IMT (<1.3 or ≥ 1.3 mm) (19). Treatment of patients in the febuxostat group was initially started with febuxostat at a dose of 10 mg daily. The dose could be increased to 20 mg daily at 1 month and 40 mg daily at 2 months. Febuxostat 40 mg daily was the targeted maintenance dose. At 3 months or later, febuxostat could be further increased up to 60 mg daily. When serum uric acid levels decreased to ≤ 2.0 mg/dL during the study period, the maintenance dose of febuxostat was decreased by 20 mg. Participants were followed up annually for 2 years.

The primary endpoint of the PRIZE study was the percentage change in mean CCA-IMT from baseline to 24 months after treatment. Carotid ultrasound examinations were performed at the beginning of treatment and after 12 and 24 months of treatment. Exploratory endpoints included percentage changes in FMD of the brachial artery from baseline to 12 and 24 months of treatment (19). In some participating institutions, measurement of FMD of the brachial artery was optional. Among a total of 514 patients, serial measurement of FMD was performed in 41 patients in the febuxostat group and 38 patients in the

control group at the beginning of the study and after 12 and/or 24 months of treatment. The data for these 79 patients from 10 institutions were analyzed in the present study. This sub-study is a pre-specified analysis (19). The study protocol was approved by the local institutional review boards and independent ethics committees at all sites. The study protocol conforms to the ethical guidelines of the 1975 Declaration of Helsinki. Written informed consent for participation in the study was obtained from all subjects.

Study Protocol

All assessments were performed in the morning, after overnight fasting, in a quiet, dark, and air-conditioned room (constant temperature of 22 to 25°C). Subjects were kept in the supine position throughout the study. A 23-gauge polyethylene catheter was inserted into the left deep antecubital vein to obtain blood samples. The vascular response to reactive hyperemia in the brachial artery was used for the assessment of endothelium-dependent FMD. FMD measurements were performed by skilled and trained physicians or sonographers without detailed knowledge of the baseline clinical characteristics of the subjects.

Measurement of Flow-Mediated Vasodilation

The same protocol for measurement of FMD in the brachial artery was used at all study sites. FMD was measured with the same ultrasound instrument specialized for FMD measurement in all institutions. A high-resolution linear artery transducer was coupled to computer-assisted analysis software (UNEXEF18G, UNEX Co, Nagoya, Japan) that used an automated edge detection system for measurement of brachial artery diameter. Detailed information on measurement of FMD of the brachial artery is provided in the online-only Data Supplement. In brief, FMD was measured by using a protocol in which an occlusion cuff placed around the forearm was inflated to 50 mm Hg above systolic blood pressure for 5 min to induce reactive hyperemia. Percentage of FMD [(Peak diameter - Baseline diameter)/Baseline diameter] was used for analysis (21). Intra-observer variability (coefficient of variation) was 10.1–11.2% (22).

Statistical Analysis

All reported probability values were 2-sided, and a probability value of <0.05 was considered statistically significant. Continuous variables are summarized as mean and standard deviation for normally distributed continuous variables or median (interquartile range [IQR]) for skewed ones. The Shapiro-Wilk test was used to evaluate normality. For between-group comparisons of continuous values, Student's *t*-test and the Wilcoxon test were used according to their respective distributions. Categorical variables are presented as frequencies and percentages and were compared by means of the χ^2 test. We used a mixed-effects model to estimate changes in serum uric acid and percentage changes in FMD over time by treatment (febuxostat group vs. control group). To estimate group differences in serum uric acid and percentage changes in FMD, models included treatment, follow-up time, and a

treatment \times follow-up time interaction term. The model for percentage changes in FMD included covariates of age, sex, serum uric acid levels at each time point, and FMD at baseline. The data were processed using R 4.0.1. (R Foundation for Statistical Computing, Vienna, Austria).

RESULTS

Baseline Clinical Characteristics

The baseline clinical characteristics of the subjects are summarized in **Table 1**. Of the 79 patients (mean age, 67.3 years; SD, 10.3 years), 63 (79.7%) were men, and 16 (20.3%) were women. Seventy-six (96.2%) had hypertension, 40 (50.6%) had dyslipidemia, 20 (25.3%) had diabetes mellitus, 11 (13.9%) were current smokers, 1 (1.3%) had previous gouty arthritis, 7 (8.9%) had previous myocardial infarction, 4 (5.1%) had stroke, and 10 (12.7%) had heart failure. There was no significant difference between the febuxostat group and the control group in any of the variables at baseline. In the febuxostat group, 11 (26.8%) patients received 10 mg, 15 (36.6%) received 20 mg, 3 (7.3%) received 30 mg, 7 (17.1%) received 40 mg, and 1 (2.4%) received 60 mg daily as the final adjusted dose of febuxostat.

Serum Uric Acid Level Control

Baseline serum uric acid levels were 7.67 mg/dL [95% confidence interval [CI], 7.38 to 7.96 mg/dL] in the febuxostat group and 7.51 mg/dL [95% CI, 7.21 to 7.82 mg/dL] in the control group. Significant differences in the serum uric acid levels were seen between the two groups at 6, 12, and 24 months (**Figure 1**). The least squares means of serum uric acid were lower in the febuxostat group than in the control group at 6 months (5.29 mg/dL [95% CI, 5.00 to 5.59] vs. 7.38 mg/dL [95% CI, 7.07 to 7.69]; mean between-group difference [febuxostat group - control group], -2.09 mg/dL [95% CI, -2.52 to -1.66]; $P < 0.001$), 12 months (5.24 mg/dL [95% CI, 4.94 to 5.54] vs. 7.51 mg/dL [95% CI, 7.20 to 7.83]; mean between-group difference, -2.28 mg/dL [95% CI, -2.71 to -1.84]; $P < 0.001$), and 24 months (4.76 mg/dL [95% CI, 4.46 to 5.07] vs. 7.38 mg/dL [95% CI, 7.06 to 7.70]; mean between-group difference, -2.61 mg/dL [95% CI, -3.06 to -2.17]; $P < 0.001$).

Endothelial Function

Baseline FMD values were $5.34\% \pm 2.61\%$ in the febuxostat group and $4.59\% \pm 2.73\%$ in the control group. Estimated percentage changes in FMD from baseline at 12 and 24 months in the febuxostat group and control group are shown in **Figure 2**. There were no significant differences between the febuxostat group and control group in the least squares means of estimated percentage changes in FMD at 12 months (-0.38% [95% CI, -1.07 to 0.31] vs. 0.18% [95% CI, -0.64 to 1.00]; mean between-group difference, -0.56% [95% CI, -1.67 to 0.55]; $P = 0.319$) and 24 months (-0.46% [95% CI, -1.28 to 0.37] vs. 0.14% [95% CI, -0.70 to 0.98]; mean between-group difference, -0.60% [95% CI, -1.89 to 0.69]; $P = 0.357$).

Diabetic complications accounted for 20 (25.3%) of the 79 cases: 9 in the febuxostat group and 11 in the control group. We

TABLE 1 | Subject clinical characteristics.

Variable	All	Control group	Febuxostat group	P-value
	(n = 79)	(n = 38)	(n = 41)	
Age, y (mean \pm SD)	67.3 \pm 10.3	67.4 \pm 10.5	67.1 \pm 10.2	0.898
Male, n (%)	63 (79.7)	30 (78.9)	33 (80.5)	1.000
Body mass index, kg/m ² (median [IQR])	25.1 (22.6–27.1)	25.5 (23.3–27.1)	24.8 (22.3–26.4)	0.298
Systolic blood pressure, mm Hg (mean \pm SA)	130.4 \pm 14.7	130.2 \pm 15.1	130.6 \pm 14.5	0.886
Diastolic blood pressure, mm Hg (mean \pm SA)	75.7 \pm 10.1	76.7 \pm 10.9	74.7 \pm 9.4	0.383
Current smoker, n (%)	11 (13.9)	2 (5.3)	9 (22.0)	0.069
Comorbidities, n (%)				
Hypertension	76 (96.2)	36 (94.7)	40 (97.6)	0.947
Dyslipidemia	40 (50.6)	20 (52.6)	20 (48.8)	0.907
Diabetes mellitus	20 (25.3)	11 (28.9)	9 (22.0)	0.649
Previous gouty arthritis	1 (1.3)	0 (0)	1 (2.4)	1.000
Previous myocardial infarction	7 (8.9)	3 (7.9)	4 (9.8)	1.000
Prior PCI	6 (7.6)	3 (7.9)	3 (7.3)	1.000
CABG	0 (0)	0 (0)	0 (0)	NA
Stroke	4 (5.1)	2 (5.3)	2 (4.9)	1.000
Heart failure	10 (12.7)	4 (10.5)	6 (14.6)	0.834
Medication, n (%)				
Antihypertensive drugs	78 (98.7)	37 (97.4)	41 (100)	0.970
ARBs	52 (65.8)	25 (65.8)	27 (65.9)	1.000
ACE inhibitors	10 (12.7)	5 (13.2)	5 (12.2)	1.000
Calcium channel blockers	57 (72.2)	27 (71.1)	30 (73.2)	1.000
β -blockers	28 (35.4)	17 (44.7)	11 (26.8)	0.100
Diuretics	23 (29.1)	12 (31.6)	11 (26.8)	0.829
Lipid-lowering drugs	34 (43.0)	16 (42.1)	18 (43.9)	1.000
Statins	33 (41.8)	15 (39.5)	18 (43.9)	0.865
Ezetimibe	4 (5.1)	1 (2.6)	3 (7.3)	0.663
Antiplatelet drugs	27 (34.2)	13 (34.2)	14 (34.1)	1.000
Aspirin	23 (29.1)	10 (26.3)	13 (31.7)	0.780

SD indicates standard deviation; IQR, interquartile range; PCI, percutaneous coronary intervention; CABG, coronary artery bypass grafting; ARB, angiotensin receptor blocker; ACE, angiotensin-converting enzyme; NA, not applicable.

examined the interaction between the presence and absence of diabetic complications and found no interaction in the present model (p for interaction = 0.886) (**Figure 3**).

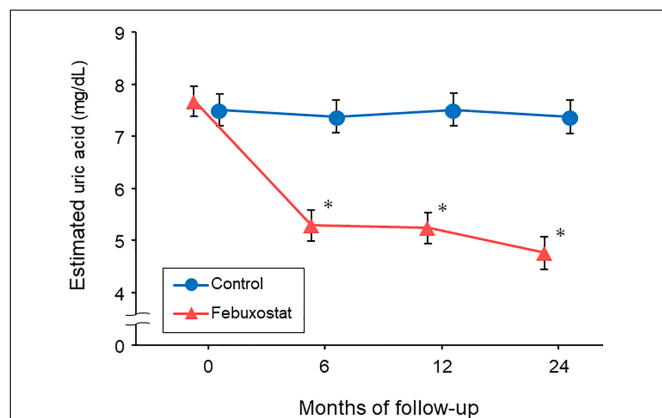


FIGURE 1 | Changes in estimated serum uric acid levels in the febuxostat group and the control group. The mixed-effects model included treatment, follow-up time, and a treatment \times follow-up time interaction term.* $P < 0.05$ vs. control group at each time point.

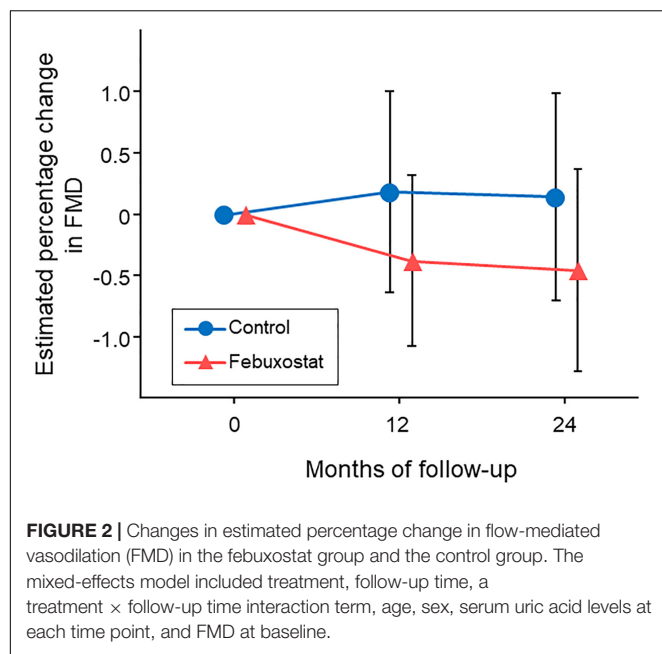
Relationship Between Serum Uric Acid Levels and Flow-Mediated Vasodilation

There was no significant difference in the relationship between estimated percentage change in FMD and serum uric acid levels at 24 months between the febuxostat group and control group (P for interaction = 0.550, P for treat = 0.687) (**Figure 4**). In addition, there was no significant difference in the relationship between estimated percentage change in FMD and change in serum uric acid levels at 24 months between the two groups (P for interaction = 0.066, P for treat = 0.126) (**Figure 5**).

DISCUSSION

The results of the present study demonstrated that 24 months of febuxostat treatment did not alter endothelial function assessed by FMD of the brachial artery in patients with asymptomatic hyperuricemia. To our knowledge, this is the first study in which the long-term effect of febuxostat treatment on endothelial function was investigated in patients with hyperuricemia.

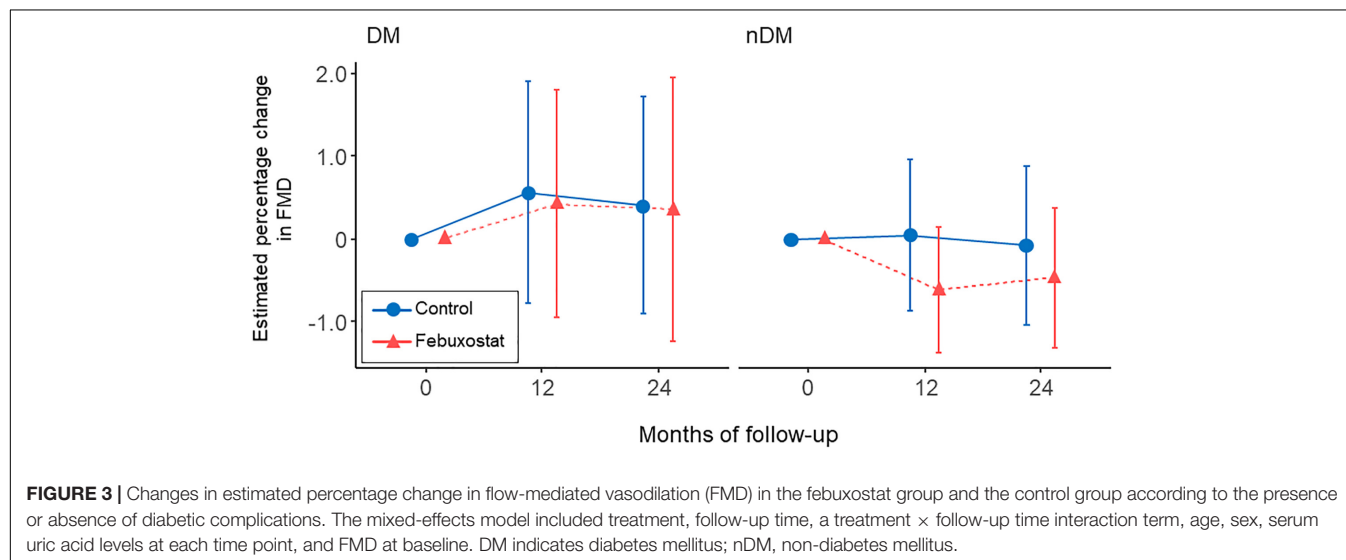
NO is directly inactivated by $O_2^{\cdot-}$ that is concomitantly generated in the process of purine metabolism catalyzed by XO. Direct reaction of NO with $O_2^{\cdot-}$ results in the



formation of peroxynitrite, a highly potent oxidant (6, 23). Tetrahydrobiopterin, an essential cofactor required for catalytic activity of endothelial NO synthase (eNOS), is oxidized to the biologically inactive form by peroxynitrite, leading to eNOS uncoupling with reduced NO formation and increased $O_2^{\cdot-}$ production (24). Therefore, NO bioavailability is decreased by $O_2^{\cdot-}$ generated in the process of purine metabolism catalyzed by XO through increased NO inactivation and/or decreased NO production, resulting in endothelial dysfunction. Experimental studies have indicated the possibility that uric acid *per se* causes endothelial dysfunction by being absorbed into endothelial cells through uric acid transporters and increasing inflammation or oxidative stress in endothelial cells (8, 9). Considering those putative mechanisms underlying endothelial dysfunction

in patients with hyperuricemia, XO inhibitors are expected to ameliorate endothelial function through decreasing the generation of ROS and lowering serum uric acid levels in patients with hyperuricemia. Indeed, treatment with allopurinol, an XO inhibitor, has been shown clinically to improve endothelial function assessed by FMD (25, 26). Febuxostat is a non-purine selective XO inhibitor that is officially approved for treatment of patients with asymptomatic hyperuricemia in Japan. Febuxostat has been shown to have a stronger inhibitory effect than that of allopurinol on XO (27). In addition, febuxostat is expected to have antioxidative and antiatherosclerotic effects that are superior to those of allopurinol (28). Therefore, febuxostat potentially has a more beneficial effect than allopurinol on endothelial function in patients with hyperuricemia.

The short-term effect of febuxostat on endothelial function in humans has been investigated in a few studies. Tsuruta et al. reported that 4 weeks of febuxostat treatment improved endothelial function assessed by FMD in patients with hyperuricemia on hemodialysis (15), whereas Nakata et al. reported that endothelial function assessed by peripheral artery tonometry deteriorated after 3 months of febuxostat treatment in patients with hyperuricemia (16). Hays et al. reported that 6 weeks of febuxostat treatment did not improve coronary endothelial function assessed by magnetic resonance imaging in patients with stable coronary artery disease (17). Taken together, it remains controversial whether short-term febuxostat treatment ameliorates endothelial function in humans. Moreover, the long-term effect of febuxostat treatment on endothelial function remains unclear. In the present study, we showed that FMD was not improved at 12 and 24 months after febuxostat treatment in patients with asymptomatic hyperuricemia. Our findings support the main results of the PRIZE study. The PRIZE study showed that 24 months of febuxostat treatment did not delay the progression of carotid IMT in patients with asymptomatic hyperuricemia (18). These findings suggest that long-term febuxostat treatment has little antiatherosclerotic effect in patients with hyperuricemia. Although the precise



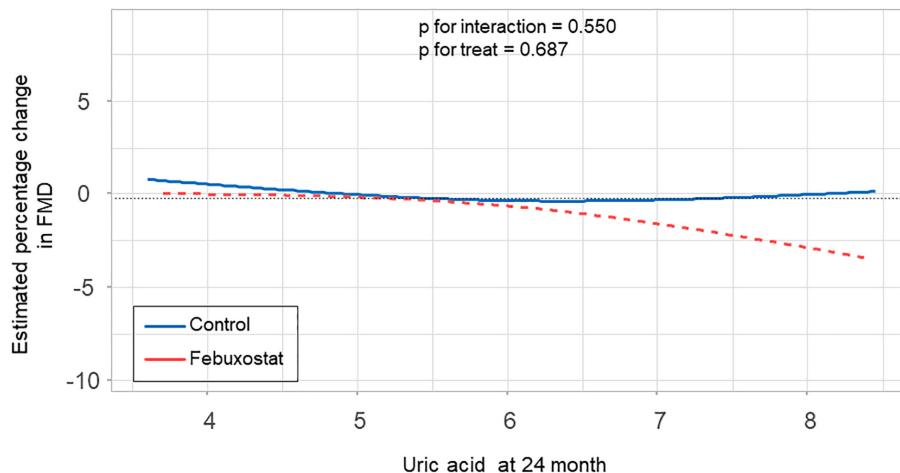


FIGURE 4 | Relationship between estimated percentage change in flow-mediated vasodilation (FMD) and serum uric acid levels at 24 months in the febuxostat group and the control group adjusted for baseline FMD.

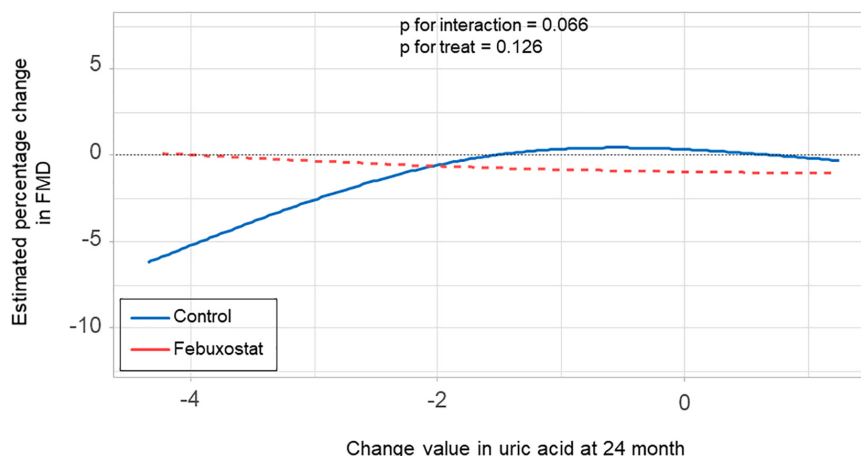


FIGURE 5 | Relationship between estimated percentage change in flow-mediated vasodilation (FMD) and change in serum uric acid levels at 24 months in the febuxostat group and the control group adjusted for baseline FMD.

reasons for the ineffectiveness of febuxostat treatment on endothelial function are unclear, one possible explanation is that the final doses of febuxostat were lower than expected. In the present study, 40 mg daily was a targeted maintenance dose of febuxostat. However, only 8 (19.5%) of 41 patients in the febuxostat group received febuxostat at ≥ 40 mg daily after 24 months. Therefore, we cannot exclude the possibility that the doses of febuxostat were inadequate to exert beneficial effects on endothelial function independent of the urate-lowering effect. Further studies are needed to determine whether adequate doses of febuxostat ameliorate endothelial function in patients with asymptomatic hyperuricemia.

A major limitation of the present study is the small sample size. Since this study was a sub-analysis, and FMD was a voluntary measurement parameter in the PRIZE study, the number of study subjects was relatively small. If the present results were obtained by a simple group comparison at 24 months, the

power would be 20~25% at best, and although the power is expected to be a little higher due to the mixed effects model used in this study, the number of cases is too small to be considered robust. Further studies with larger numbers of participants are needed to confirm the long-term effect of febuxostat on endothelial function in patients with asymptomatic hyperuricemia. Since most of the study's participants were men, the results of the present study may not be generalizable to female subjects with asymptomatic hyperuricemia (29). Moreover, all of the participants were Japanese. Therefore, the results may not be generalizable to other populations. A large proportion of the patients in the present study had comorbidities such as hypertension, dyslipidemia and diabetes mellitus as well as a smoking habit and a history of cardiovascular diseases, all of which are associated with endothelial dysfunction. Although there was no statistical difference in the prevalence of those comorbidities between the febuxostat group and control group,

we cannot deny the possibility that those comorbidities affected the results of the present study.

CONCLUSION

In patients with asymptomatic hyperuricemia, 24 months of febuxostat treatment did not alter endothelial function. The results of the present study do not support the use of febuxostat for ameliorating endothelial function in this population.

DATA AVAILABILITY STATEMENT

The raw data supporting the conclusions of this article will be made available by the authors, without undue reservation.

ETHICS STATEMENT

The study protocol was approved by the local institutional review boards and independent ethics committees at all sites.

PRIZE STUDY INVESTIGATORS

Principal Investigator: Koichi Node (Saga University, Saga, Japan).

PRIZE Steering Committee: Toyoaki Murohara (Nagoya University Graduate School of Medicine, Nagoya, Japan); Teruo Inoue (Dokkyo Medical University, Mibu, Japan); Masataka Sata (Tokushima University Graduate School, Tokushima, Japan); Mitsuru Ohishi (Kagoshima University, Kagoshima, Japan).

PRIZE Executive Committee: Kotaro Yokote (Chiba University Graduate School of Medicine, Chiba, Japan); Kazuomi Kario (Jichi Medical University School of Medicine, Shimotsuke, Japan); Hirotaka Watada (Juntendo University Graduate School of Medicine, Tokyo, Japan); Ichihiro Shimomura (Osaka University, Graduate School of Medicine, Suita, Japan); Munehide Matsuhisa (Tokushima University Graduate School, Tokushima, Japan); Yoshihiro Fukumoto (Kurume University School of Medicine, Kurume, Japan); Koji Maemura (Nagasaki University Graduate School of Biomedical Sciences, Nagasaki, Japan); Yusuke Ohya (University of the Ryukyus, Okinawa, Japan).

PRIZE Site Investigators: Yuichi Akasaki (Kagoshima University, Kagoshima, Japan); Junya Ako (Kitasato University School of Medicine, Sagamihara, Japan); Hirohisa Amano (Dokkyo Medical University, Mibu, Japan); Kazutaka Aonuma (Graduate School of Comprehensive Human Sciences, University of Tsukuba, Tsukuba, Japan); Yutaka Aoyama (Nagoya Daini Red Cross Hospital, Nagoya, Japan); Hirofumi Arai (Kameda Medical Center, Komogawa, Japan); Kuniya Asai (Nippon Medical School, Tokyo, Japan); Machiko Asaka (Saga University, Saga, Japan); Yoshifumi Awaji (Nagoya Ekisaikai Hospital, Nagoya, Japan); Noriko Ban (Chiba Aoba Municipal Hospital, Chiba, Japan); Toshiaki Ban (Isumi Medical Center, Isumi,

Japan); Yasuko K Bando (Nagoya University Graduate School of Medicine, Nagoya, Japan); Hiroyuki Daida (Juntendo University Graduate School of Medicine, Tokyo, Japan); Shunsuke Eguchi (Japanese Red Cross Nagoya Daini Hospital, Nagoya, Japan); Mami Enomoto (Graduate School of Comprehensive Human Sciences, University of Tsukuba, Tsukuba, Japan); Yuichi Fujii (Hiroshima General Hospital of West Japan Railway Company, Hiroshima, Japan); Akinori Fujikake (Dokkyo Medical University Saitama Medical Center, Koshigaya, Japan); Masanori Fujimoto (Graduate School of Medicine, Chiba University, Chiba, Japan); Tomohiro Fujisaka (Osaka Medical College, Takatsuki, Japan); Shuichi Fujita (Osaka Medical College, Takatsuki, Japan); Satoki Fukae (Nagasaki University Graduate School of Biomedical Sciences, Nagasaki, Japan); Daiju Fukuda (Tokushima University Graduate School of Biomedical Sciences, Tokushima, Japan); Mieko Fukui (Kimitsu Chuo Hospital, Kisarazu, Japan); Yuhei Goriki (Miyazaki Medical Association Hospital, Miyazaki, Japan); Shuichi Hamasaki (Kagoshima City Hospital, Kagoshima, Japan); Tomoya Hara (Tokushima University Graduate School of Biomedical Sciences, Tokushima, Japan); Hiroshi Hasegawa (Chiba University Graduate School of Medicine, Chiba, Japan); Kenichi Hashimoto (National Defense Medical College, Tokorozawa, Japan); Mitsumasa Hata (Sekino Hospital, Tokyo, Japan); Shiro Hata (Sasebo City General Hospital, Sasebo, Japan); Ryo Hayashida (Nagoya University Graduate School of Medicine, Nagoya, Japan); Akihiro Higashi (Dokkyo Medical University Saitama Medical Center, Koshigaya, Japan); Seiichiro Higuchi (Graduate School of Medicine, Chiba University, Chiba, Japan); Akihiro Honda (Kurume University School of Medicine, Kurume, Japan); Satoshi Hoshida (Jichi Medical University School of Medicine, Shimotsuke, Japan); Masaaki Hoshiga (Osaka Medical College, Takatsuki, Japan); Junko Hotchi (Tokushima University Graduate School of Biomedical Sciences, Tokushima, Japan); Sachiyo Igata (Kurume University School of Medicine, Kurume, Japan); Yumi Ikehara (University of the Ryukyus, Nishihara, Japan); Teruo Inoue (Dokkyo Medical University, Mibu, Japan); Youhei Inoue (Miyazaki Medical Association Hospital, Miyazaki, Japan); Hiroko Ishigami (Nagoya Daini Red Cross Hospital, Nagoya, Japan); Masaharu Ishihara (Hyogo College of Medicine, Nishinomiya, Japan); Hideki Ishii (Nagoya University Graduate School of Medicine, Nagoya, Japan); Tetsuya Ishikawa (Dokkyo Medical University Saitama Medical Center, Koshigaya, Japan); Takashi Ishimatsu (Nagasaki University Graduate School of Biomedical Sciences, Nagasaki, Japan); Yusuke Ishiyama (Jichi Medical University School of Medicine, Shimotsuke, Japan); Takahide Ito (Osaka Medical College, Takatsuki, Japan); Ayumi Ito (Nagoya Daini Red Cross Hospital, Nagoya, Japan); Toshiaki Kadokami (Fukuoka Saiseikai Futsukaichi Hospital, Chikushino, Japan); Haruo Kamiya (Japanese Red Cross Nagoya Daiichi Hospital, Nagoya, Japan); Soichiro Kashihara (Fukuoka Saiseikai Futsukaichi Hospital, Chikushino, Japan); Yoshihiro Kawamura (Kasugai Municipal Hospital, Kasugai, Japan); Kazuo Kitagawa (Tokyo Women's Medical University, Tokyo, Japan); Yoshio Kobayashi (Chiba University Graduate School of Medicine, Chiba, Japan); Satoshi Kodera (Asahi General Hospital, Asahi,

Japan); Seiji Koga (Nagasaki University Graduate School of Biomedical Sciences, Nagoya, Japan); Hisashi Koide (Chiba University Graduate School of Medicine, Chiba, Japan); Yuji Koide (Nagasaki University Graduate School of Biomedical Sciences, Nagasaki, Japan); Hiroshi Koiwaya (Miyazaki Medical Association Hospital, Miyazaki, Japan); Hiroki Kojima (Nagoya University Graduate School of Medicine, Nagoya, Japan); Eri Komai (Graduate School of Medicine, Chiba University, Chiba, Japan); Takaaki Komatsu (Dokkyo Medical University Saitama Medical Center, Koshigaya, Japan); Shingo Kono (Kobe City Medical Center General Hospital, Kobe, Japan); Takashi Kono (Graduate School of Medicine, Chiba University, Chiba, Japan); Yoshiaki Kubota (Nippon Medical School, Tokyo, Japan); Akio Kuroda (Institute of Advanced Medical Sciences, Tokushima University, Tokushima, Japan); Takanori Kuroyanagi (Dokkyo Medical University Saitama Medical Center, Koshigaya, Japan); Akifumi Kushiya (The Institute for Adult Diseases, Asahi Life Foundation, Tokyo, Japan); Kenya Kusunose (Tokushima University Graduate School of Biomedical Sciences, Tokushima, Japan); Tatsuya Maruhashi (Graduate School of Biomedical and Health Sciences, Hiroshima University, Hiroshima, Japan); Kazuo Matsunaga (Imari Arita Kyoritsu Hospital, Matsuura, Japan); Tomomi Matsuura (Tokushima University Graduate School of Biomedical Sciences, Tokushima, Japan); Takafumi Mayama (Graduate School of Medicine, Chiba University, Chiba, Japan); Daigo Mine (Saga-Ken Medical Centre Koseikan, Saga, Japan); Masatoshi Miyamura (Osaka Medical College, Takatsuki, Japan); Ryota Morimoto (Nagoya University Graduate School of Medicine, Nagoya, Japan); Hideaki Morita (Osaka Medical College, Takatsuki, Japan); Hidekazu Nagano (Chiba University Graduate School of Medicine, Chiba, Japan); Hidemitsu Nakagawa (Nozaki Tokushukai Hospital, Daito, Japan); Katsunori Nakamura (Ryukyu University Hospital, Nishihara, Japan); Ryo Nakamura (Fukuoka Saiseikai Futsukaichi Hospital, Chikushino, Japan); Ikuko Nakamura (Saga-Ken Medical Centre Koseikan, Saga, Japan); Hitoshi Nakashima (National Hospital Organization Kagoshima Medical Center, Kagoshima, Japan); Mamoru Nanasato (Japanese Red Cross Nagoya Daini Hospital, Nagoya, Japan); Isao Nishi (National Hospital Organization Kasumigaura Medical Center, Tsuchiura, Japan); Shinichi Niwano (Kitasato University School of Medicine, Sagami, Japan); Shuichi Nomura (Hiroshima General Hospital of West Japan Railway Company, Hiroshima, Japan); Nozomu Oda (Graduate School of Biomedical and Health Sciences, Hiroshima University, Hiroshima, Japan); Shio Oguchi (Kasugai Municipal Hospital, Kasugai, Japan); Mitsutoshi Oguri (Kasugai Municipal Hospital, Kasugai, Japan); Arihide Okahara (Saga-Ken Medical Centre Koseikan, Saga, Japan); Masaaki Okutsu (Nozaki Tokushukai Hospital, Daito, Japan); Fumitake Ozaki (Dokkyo Medical University Saitama Medical Center, Koshigaya, Japan); Michishige Ozeki (Osaka Medical College, Takatsuki, Japan); Tomoko Saisu (Tokyo Medical University, Tokyo, Japan); Yuichi Saito (Chiba University Hospital, Chiba, Japan); Makoto Saitoh (Nishio Municipal Hospital, Nishio, Japan); Yosuke Saka (Kasugai Municipal Hospital, Kasugai, Japan); Yoshihiko Sakai (Dokkyo Medical University Saitama Medical Center, Koshigaya, Japan); Kazushi Sakane (Osaka

Medical College, Takatsuki, Japan); Ikki Sakuma (Graduate School of Medicine, Chiba University, Chiba, Japan); Shakya Sandeep (Asahi General Hospital, Asahi, Japan); Hiroaki Sano (Nagoya Ekisaikai Hospital, Nagoya, Japan); Hisakuni Sekino (Sekino Hospital, Tokyo, Japan); Yuka Senoo (Nagoya Daini Red Cross Hospital, Nagoya, Japan); Kensaku Shibata (Osaka Medical College, Takatsuki, Japan); Yoshisato Shibata (Miyazaki Medical Association Hospital, Miyazaki, Japan); Takahisa Shibata (Isumi Medical Center, Isumi, Japan); Akina Shiga (Graduate School of Medicine, Chiba University, Chiba, Japan); Kazuki Shiina (Tokyo Medical University, Tokyo, Japan); Michio Shimabukuro (Tokushima University Graduate School of Biomedical Sciences, Tokushima, Japan); Yusaku Shimbo (Nagoya University Graduate School of Medicine, Nagoya, Japan); Wataru Shimizu (Nippon Medical School, Tokyo, Japan); Masahisa Shimpō (Jichi Medical University School of Medicine, Shimotsuke, Japan); Takeshi Soeki (Tokushima University Graduate School of Biomedical Sciences, Tokushima, Japan); Koichi Sohmiya (Osaka Medical College, Takatsuki, Japan); Hiroyuki Suzuki (Nagoya Daini Red Cross Hospital, Nagoya, Japan); Susumu Suzuki (Nagoya University Graduate School of Medicine, Nagoya, Japan); Makoto Suzuki (Kameda Medical Center, Kamogawa, Japan); Nobuhiro Tahara (Kurume University School of Medicine, Kurume, Japan); Tazu Tahara (The Institute for Adult Diseases, Asahi Life Foundation, Tokyo, Japan); Sadako Takahashi (Jichi Medical University School of Medicine, Shimotsuke, Japan); Bonpei Takase (National Defense Medical College, Tokorozawa, Japan); Kaoru Takegami (Saga-Ken Medical Centre Koseikan, Saga, Japan); Tomoko Takiguchi (Kimitsu Chuo Hospital, Kisarazu, Japan); Tomonobu Takikawa (Kasugai Municipal Hospital, Kasugai, Japan); Ai Tamura (Graduate School of Medicine, Chiba University, Chiba, Japan); Tomoaki Tanaka (Chiba University Graduate School of Medicine, Chiba, Japan); Akihito Tanaka (Nagoya University Graduate School of Medicine, Nagoya, Japan); Hiroyuki Tanaka (Niko Clinic, Takeo, Japan); Jun Tanigawa (Osaka Medical College, Takatsuki, Japan); Daisuke Tanimura (Nagoya Ekisaikai Hospital, Nagoya, Japan); Yosuke Tatami (Nagoya University Graduate School of Medicine, Nagoya, Japan); Takashi Terano (Chiba Aoba Municipal Hospital, Chiba, Japan); Fumio Terasaki (Osaka Medical College, Takatsuki, Japan); Tomoyuki Tobushi (Fukuoka Saiseikai Futsukaichi Hospital, Chikushino, Japan); Seiko Tokoi (Dokkyo Medical University, Mibu, Japan); Toshiyuki Tsubouchi (Nozaki Tokushukai Hospital, Daito, Japan); Daigaku Uchida (Hotaruno Central Clinic, Kisarazu, Japan); Tomohiro Ueda (Hiroshima General Hospital of West Japan Railway Company, Hiroshima, Japan); Rie Ueno (Tokushima University Graduate School of Biomedical Sciences, Tokushima, Japan); Hiromi Ueno (Jichi Medical University School of Medicine, Shimotsuke, Japan); Chikara Ueyama (Gifu Prefectural Tajimi Hospital, Tajimi, Japan); Tetsuzo Wakatsuki (Tokushima University Graduate School of Biomedical Sciences, Tokushima, Japan); Tomohiko Watanabe (Osaka Medical College, Takatsuki, Japan); Masato Watarai (Anjo Kosei Hospital, Anjo, Japan); Isao Yaguchi (Dokkyo Medical University Saitama Medical Center, Koshigaya, Japan); Ayumu Yajima (Saga University, Saga, Japan); Jiko Yamada (Tokyo Medical

University, Tokyo, Japan); Kyohei Yamamoto (Chiba Aoba Municipal Hospital, Chiba, Japan); Sachiko Yamauchi (Ryukyu University Hospital, Nishihara, Japan); Yohei Yamauchi (Osaka Medical College, Takatsuki, Japan); Naoto Yokota (Yokota Naika, Miyazaki, Japan); Tomohiko Yoshida (Chiba Aoba Municipal Hospital, Chiba, Japan); Goro Yoshioka (Miyazaki Medical Association Hospital, Miyazaki, Japan).

Members of the Data and Safety Monitoring Board: Hiroyuki Daida (Juntendo University Graduate School of Medicine, Tokyo, Japan); Junya Ako (Kitasato University School of Medicine, Sagamihara, Japan); Kazuo Kitagawa (Tokyo Women's Medical University, Tokyo, Japan).

Members of the Clinical Events Committee: Wataru Shimizu (Nippon Medical School, Tokyo, Japan); Yoshio Kobayashi (Chiba University Graduate School of Medicine, Chiba, Japan); Masaharu Ishihara (Hyogo College of Medicine, Nishinomiya, Japan).

Imaging Core Laboratory: Tsukuba Echo Core Laboratory. LLC; Tomoko Ishizu (Tsukuba University, Tsukuba, Japan).

Monitoring: Shinichiro Ueda (Clinical Research Management Center, University of the Ryukyus, Okinawa, Japan).

Audit Team: Clinical Research Support Center, University of the Ryukyus, Okinawa, Japan.

Trial Secretariat: Atsushi Tanaka (Saga University, Saga, Japan); Jun-ichi Oyama (Saga University, Saga, Japan); Mikiko Kagiya (Saga University, Saga, Japan); Nouvelle Place Inc., Tokyo, Japan; Organization for Clinical Medicine Promotion, Tokyo, Japan.

AUTHOR CONTRIBUTIONS

YH and TM drafted the article and conception of this study. HY performed the statistical analysis. KE, HT, KK, TK, NO,

NT, MO, and HW measured the FMD. AT and KN revised the article critically for important intellectual content. All authors contributed to the article and approved the submitted version.

FUNDING

This work was funded by Teijin Pharma Limited, Japan, and KN received the funding.

ACKNOWLEDGMENTS

We thank the members of the Data and Safety Monitoring Board: Hiroyuki Daida (Juntendo University Graduate School of Medicine, Tokyo, Japan); Junya Ako (Kitasato University School of Medicine, Sagamihara, Japan); and Kazuo Kitagawa (Tokyo Women's Medical University, Tokyo, Japan), and the Clinical Events Committee: Wataru Shimizu (Nippon Medical School, Tokyo, Japan); Yoshio Kobayashi (Chiba University Graduate School of Medicine, Chiba, Japan); and Masaharu Ishihara (Hyogo College of Medicine, Nishinomiya, Japan). We also thank Satoko Michiyama (Hiroshima University, Hiroshima, Japan) for excellent secretarial assistance.

SUPPLEMENTARY MATERIAL

The Supplementary Material for this article can be found online at: <https://www.frontiersin.org/articles/10.3389/fcvm.2022.882821/full#supplementary-material>

REFERENCES

- Ross R. Atherosclerosis—an inflammatory disease. *N Engl J Med.* (1999) 340:115–26.
- Higashi Y, Noma K, Yoshizumi M, Kihara Y. Endothelial function and oxidative stress in cardiovascular diseases. *Circ J.* (2009) 73:411–8. doi: 10.1253/circj.cj-08-1102
- Lerman A, Zeiher AM. Endothelial function: cardiac events. *Circulation.* (2005) 111:363–8. doi: 10.1161/01.CIR.0000153339.27064.14
- Matsuzawa Y, Kwon TG, Lennon RJ, Lerman LO, Lerman A. Prognostic value of flow-mediated vasodilation in brachial artery and fingertip artery for cardiovascular events: a systematic review and meta-analysis. *J Am Heart Assoc.* (2015) 4:e002270. doi: 10.1161/JAHA.115.002270
- Cai H, Harrison DG. Endothelial dysfunction in cardiovascular diseases: the role of oxidant stress. *Circ Res.* (2000) 87:840–4. doi: 10.1161/01.res.87.10.840
- Forstermann U, Xia N, Li H. Roles of vascular oxidative stress and nitric oxide in the pathogenesis of atherosclerosis. *Circ Res.* (2017) 120:713–35. doi: 10.1161/CIRCRESAHA.116.309326
- Berry CE, Hare JM. Xanthine oxidoreductase and cardiovascular disease: molecular mechanisms and pathophysiological implications. *J Physiol.* (2004) 555(Pt 3):589–606. doi: 10.1113/jphysiol.2003.055913
- Sugihara S, Hisatome I, Kuwabara M, Niwa K, Maharani N, Kato M, et al. Depletion of uric acid due to SLC22A12 (URAT1) loss-of-function mutation causes endothelial dysfunction in hypouricemia. *Circ J.* (2015) 79:1125–32. doi: 10.1253/circj.CJ-14-1267
- Sanchez-Lozada LG, Soto V, Tapia E, Avila-Casado C, Sautin YY, Nakagawa T, et al. Role of oxidative stress in the renal abnormalities induced by experimental hyperuricemia. *Am J Physiol Renal Physiol.* (2008) 295:F1134–41. doi: 10.1152/ajprenal.00104.2008
- Maruhashi T, Hisatome I, Kihara Y, Higashi Y. Hyperuricemia and endothelial function: from molecular background to clinical perspectives. *Atherosclerosis.* (2018) 278:226–31. doi: 10.1016/j.atherosclerosis.2018.10.007
- Cicero AFG, Fogacci F, Kuwabara M, Borghi C. Therapeutic strategies for the treatment of chronic hyperuricemia: an evidence-based update. *Medicina.* (2021) 57:58. doi: 10.3390/medicina57010058
- Strilchuk L, Fogacci F, Cicero AF. Safety and tolerability of available urate-lowering drugs: a critical review. *Expert Opin Drug Saf.* (2019) 18:261–71. doi: 10.1080/14740338.2019.1594771
- Kamatani N, Fujimori S, Hada T, Hosoya T, Kohri K, Nakamura T, et al. An allopurinol-controlled, randomized, double-dummy, double-blind, parallel between-group, comparative study of febuxostat (TMX-67), a non-purine-selective inhibitor of xanthine oxidase, in patients with hyperuricemia including those with gout in Japan: phase 3 clinical study. *J Clin Rheumatol Pract Rep Rheumat Musculoskelet Dis.* (2011) 17(4 Suppl. 2):S13–8. doi: 10.1097/RHU.0b013e31821d36cc
- Cicero AFG, Fogacci F, Cincione RI, Tocci G, Borghi C. Clinical effects of xanthine oxidase inhibitors in hyperuricemic patients. *Med Princ Pract Int J Kuwait Univ Health Sci Centre.* (2021) 30:122–30. doi: 10.1159/000512178

15. Tsuruta Y, Kikuchi K, Tsuruta Y, Sasaki Y, Moriyama T, Itabashi M, et al. Febuxostat improves endothelial function in hemodialysis patients with hyperuricemia: a randomized controlled study. *Hemodial Int Int Symp Home Hemodial.* (2015) 19:514–20. doi: 10.1111/hdi.12313
16. Nakata T, Ikeda S, Koga S, Yonekura T, Tsuneto A, Doi Y, et al. Randomized, open-label, cross-over comparison of the effects of benzbromarone and febuxostat on endothelial function in patients with hyperuricemia. *Int Heart J.* (2020) 61:984–92. doi: 10.1536/ihj.20-114
17. Hays AG, Iantorno M, Schar M, Lai S, Czarny M, Breton E, et al. The influence of febuxostat on coronary artery endothelial dysfunction in patients with coronary artery disease: a phase 4 randomized, placebo-controlled, double-blind, crossover trial. *Am Heart J.* (2018) 197:85–93. doi: 10.1016/j.ahj.2017.11.006
18. Tanaka A, Taguchi I, Teragawa H, Ishizaka N, Kanzaki Y, Tomiyama H, et al. Febuxostat does not delay progression of carotid atherosclerosis in patients with asymptomatic hyperuricemia: a randomized, controlled trial. *PLoS Med.* (2020) 17:e1003095. doi: 10.1371/journal.pmed.1003095
19. Oyama J, Tanaka A, Sato Y, Tomiyama H, Sata M, Ishizu T, et al. Rationale and design of a multicenter randomized study for evaluating vascular function under uric acid control using the xanthine oxidase inhibitor, febuxostat: the PRIZE study. *Cardiovasc Diabetol.* (2016) 15:87. doi: 10.1186/s12933-016-0409-2
20. Kinoshita M, Yokote K, Arai H, Iida M, Ishigaki Y, Ishibashi S, et al. Japan atherosclerosis society (JAS) guidelines for prevention of atherosclerotic cardiovascular diseases 2017. *J Atheroscler Thromb.* (2018) 25:846–984. doi: 10.5551/jat.GL2017
21. Corretti MC, Anderson TJ, Benjamin EJ, Celermajer D, Charbonneau F, Creager MA, et al. Guidelines for the ultrasound assessment of endothelial-dependent flow-mediated vasodilation of the brachial artery: a report of the international brachial artery reactivity task force. *J Am Coll Cardiol.* (2002) 39:257–65. doi: 10.1016/s0735-1097(01)01746-6
22. Tomiyama H, Higashi Y, Takase B, Node K, Sata M, Inoue T, et al. Relationships among hyperuricemia, metabolic syndrome, and endothelial function. *Am J Hypertens.* (2011) 24:770–4. doi: 10.1038/ajh.2011.55
23. Bartsaghi S, Radi R. Fundamentals on the biochemistry of peroxynitrite and protein tyrosine nitration. *Redox Biol.* (2018) 14:618–25. doi: 10.1016/j.redox.2017.09.009
24. Forstermann U, Sessa WC. Nitric oxide synthases: regulation and function. *Eur Heart J.* (2012) 33:829–37; 37a–d. doi: 10.1093/eurheartj/ehs001
25. Xin W, Mi S, Lin Z. Allopurinol therapy improves vascular endothelial function in subjects at risk for cardiovascular diseases: a meta-analysis of randomized controlled trials. *Cardiovasc Ther.* (2016) 34:441–9. doi: 10.1111/1755-5922.12215
26. Cicero AFG, Pirro M, Watts GF, Mikhailidis DP, Banach M, Sahebkar A. Effects of allopurinol on endothelial function: a systematic review and meta-analysis of randomized placebo-controlled trials. *Drugs.* (2018) 78:99–109. doi: 10.1007/s40265-017-0839-5
27. Becker MA, Schumacher HR Jr, Wortmann RL, MacDonald PA, Eustace D, Palo WA, et al. Febuxostat compared with allopurinol in patients with hyperuricemia and gout. *N Engl J Med.* (2005) 353:2450–61. doi: 10.1056/NEJMoa050373
28. Sezai A, Soma M, Nakata K, Hata M, Yoshitake I, Wakui S, et al. Comparison of febuxostat and allopurinol for hyperuricemia in cardiac surgery patients (NU-FLASH Trial). *Circ J.* (2013) 77:2043–9. doi: 10.1253/circj.cj-13-0082
29. Fogacci F, Borghi C, Di Micoli A, Degli Esposti D, Cicero AFG. Inequalities in enrollment of women and racial minorities in trials testing uric acid lowering drugs. *Nutr Metab Cardiovasc Dis.* (2021) 31:3305–13. doi: 10.1016/j.numecd.2021.09.011

Conflict of Interest: YH received honoraria and grants from Teijin, Boehringer Ingelheim, MSD, Sanofi, AstraZeneca, Kyowa Hakko Kirin, Takeda, Astellas, Daiichi Sankyo, Mochida, Nihon Kohden, Shionogi, Nippon Sigmax, Sanwa Kagaku Kenkyusho, Unex, and Kao; honoraria from Radiometer, Omron, Sumitomo Dainippon, Otsuka, Torii, Kowa, Fujiyaku, Amgen, Nippon Shinyaku, Itamar, Bayer, Eli Lilly, and Ono. AT received honoraria from Boehringer Ingelheim and research funding from GlaxoSmithKline. HT received funds from Omron Health Care Company, Asahi Calpis Wellness Company and Teijin Pharma Company. HW received honoraria for lectures for Mitsubishi Tanabe Pharma, Dainippon Sumitomo Pharma, Sanwa Kagaku, Takeda, Sanofi, Kowa, Merck Sharp; and Dohme, Boehringer Ingelheim, Eli Lilly, and Novo Nordisk, and research activities for Takeda, Boehringer Ingelheim, Kissei Pharma, Novo Nordisk, Mitsubishi Tanabe Pharma, Lifescan Japan, Dainippon Sumitomo Pharma, Kyowa Kirin, and Merck Sharp; and Dohme. KN received research grants from Asahi Kasei, Astellas, Bayer, Boehringer Ingelheim, Mitsubishi Tanabe, Teijin, and Terumo; scholarships from Astellas, Bayer, Bristol-Myers Squibb, Daiichi Sankyo, Daiichi Sankyo Healthcare, Takeda, and Teijin; and personal fees from Astellas, AstraZeneca, Bayer, Boehringer Ingelheim, Daiichi Sankyo Healthcare, Eli Lilly, Kowa, Mitsubishi Tanabe, MSD, Novartis, Ono, Takeda, and Teijin.

The remaining authors declare that the research was conducted in the absence of any commercial or financial relationships that could be construed as a potential conflict of interest.

Publisher's Note: All claims expressed in this article are solely those of the authors and do not necessarily represent those of their affiliated organizations, or those of the publisher, the editors and the reviewers. Any product that may be evaluated in this article, or claim that may be made by its manufacturer, is not guaranteed or endorsed by the publisher.

Copyright © 2022 Maruhashi, Higashi, Yoshida, Tanaka, Eguchi, Tomiyama, Kario, Kato, Oda, Tahara, Oguri, Watada and Node. This is an open-access article distributed under the terms of the Creative Commons Attribution License (CC BY). The use, distribution or reproduction in other forums is permitted, provided the original author(s) and the copyright owner(s) are credited and that the original publication in this journal is cited, in accordance with accepted academic practice. No use, distribution or reproduction is permitted which does not comply with these terms.



Prognostic Impact of Multiple Lymphocyte-Based Inflammatory Indices in Acute Coronary Syndrome Patients

Qiuxuan Li[†], Xiaoteng Ma[†], Qiaoyu Shao, Zhiqiang Yang, Yufei Wang, Fei Gao, Yujie Zhou, Lixia Yang* and Zhijian Wang*

OPEN ACCESS

Edited by:

Xiang Xie,
First Affiliated Hospital of Xinjiang
Medical University, China

Reviewed by:

Süleyman Ergün,
Julius Maximilian University of
Würzburg, Germany
Aleksandra Djokovic,
University Medical Center, Serbia
Ana Teresa Timoteo,
Hospital de Santa Marta, Portugal

*Correspondence:

Zhijian Wang
zjwang1975@hotmail.com
Lixia Yang
ylx966@163.com

[†]These authors have contributed
equally to this work

Specialty section:

This article was submitted to
Atherosclerosis and Vascular
Medicine,
a section of the journal
Frontiers in Cardiovascular Medicine

Received: 12 November 2021

Accepted: 18 February 2022

Published: 03 May 2022

Citation:

Li Q, Ma X, Shao Q, Yang Z, Wang Y,
Gao F, Zhou Y, Yang L and Wang Z
(2022) Prognostic Impact of Multiple
Lymphocyte-Based Inflammatory
Indices in Acute Coronary Syndrome
Patients.
Front. Cardiovasc. Med. 9:811790.
doi: 10.3389/fcvm.2022.811790

Beijing Key Laboratory of Precision Medicine of Coronary Atherosclerotic Disease, Department of Cardiology, Beijing Anzhen Hospital, Clinical Center for Coronary Heart Disease, Beijing Institute of Heart Lung and Blood Vessel Disease, Capital Medical University, Beijing, China

Background: The aim of this study was to evaluate the prognostic values of five lymphocyte-based inflammatory indices (platelet-lymphocyte ratio [PLR], neutrophil-lymphocyte ratio [NLR], monocyte-lymphocyte ratio [MLR], systemic immune inflammation index [SII], and system inflammation response index [SIRI]) in patients with acute coronary syndrome (ACS).

Methods: A total of 1,701 ACS patients who underwent percutaneous coronary intervention (PCI) were included in this study and followed up for major adverse cardiovascular events (MACE) including all-cause death, non-fatal ischemic stroke, and non-fatal myocardial infarction. The five indices were stratified by the optimal cutoff value for comparison. The association between each of the lymphocyte-based inflammatory indices and MACE was assessed by the Cox proportional hazards regression analysis.

Results: During the median follow-up of 30 months, 107 (6.3%) MACE were identified. The multivariate COX analysis showed that all five indices were independent predictors of MACE, and SIRI seemingly performed best (Hazard ratio [HR]: 3.847; 95% confidence interval [CI]: [2.623–5.641]; $p < 0.001$; C-statistic: 0.794 [0.731–0.856]). The addition of NLR, MLR, SII, or SIRI to the Global Registry of Acute Coronary Events (GRACE) risk score, especially SIRI (C-statistic: 0.699 [0.646–0.753], $p < 0.001$; net reclassification improvement [NRI]: 0.311 [0.209–0.407], $p < 0.001$; integrated discrimination improvement [IDI]: 0.024 [0.010–0.046], $p < 0.001$), outperformed the GRACE risk score alone in the risk predictive performance.

Conclusion: Lymphocyte-based inflammatory indices were significantly and independently associated with MACE in ACS patients who underwent PCI. SIRI seemed to be better than the other four indices in predicting MACE, and the combination of SIRI with the GRACE risk score could predict MACE more accurately.

Keywords: acute coronary syndrome, percutaneous coronary intervention, lymphocyte-based inflammatory indices, GRACE risk score, major adverse cardiovascular events

INTRODUCTION

In previous studies, vulnerable plaques are generally considered to be the typical feature of acute coronary syndrome (ACS). Acute events caused by thrombosis after plaque rupture are considered to be the leading cause of death in patients with coronary artery disease (1). In recent years, plaque erosion has also been demonstrated to be one of the important causes of ACS (2–4). Compared with those with plaque rupture, patients with plaque erosion are more likely to develop non-ST segment elevation myocardial infarction (5). However, for patients with ST segment elevation myocardial infarction (STEMI), plaque rupture is still the major pathological factor in most patients (6).

The application of percutaneous coronary intervention (PCI) and the upgrading of interventional technologies and devices have significantly reduced the incidence of major adverse cardiovascular events (MACE), thereby improving the prognosis of patients with ACS (7). However, ACS patients undergoing PCI are still at high risk, and recurrent or persistent angina symptoms are still a thorny problem. By instantaneous wave-free ratio assessment, nearly one-quarter of patients still had residual ischemia after stent implantation (8), and 10.7% of patients were re-hospitalized within 30 days after procedure (9). Therefore, accurate and comprehensive risk assessment is particularly important in treatment decision-making for high-risk patients.

Inflammation plays an important role in the formation and development of atherosclerosis, and has been identified as a key harmful mediator and pathogenic factor of ischemia-reperfusion injury in STEMI patients (5, 10). Inflammatory cells like white blood cells and inflammation-related indices, such as platelet-lymphocyte ratio (PLR) and neutrophil-lymphocyte ratio (NLR), can affect the prognosis of ACS patients (11). These indices can be combined with the Global Registry of Acute Coronary Events (GRACE) risk score, the SYNERGY between PCI with TAXUS and cardiac surgery (SYNTAX) score, and other scores to improve the risk stratification ability for ACS patients (12). Two novel inflammatory markers, systemic immune inflammation index (SII) and system inflammation response index (SIRI), consisting of three blood routine markers, were first used to predict the prognosis of cancer (13, 14). Recently, their association with cardiovascular disease has attracted much attention. Studies have found that they can be used as risk stratification indices and predict adverse events (15). However, few studies have compared their predictive abilities with indices such as NLR. The lymphocyte-based inflammatory indices have attracted our attention because of their simple source and low cost. If they can

predict the prognosis of ACS patients undergoing PCI, they will be good tools for stratifying patients at high risk.

The GRACE risk scoring system (16), which is widely used to predict the cumulative risk of death or myocardial infarction (MI) in ACS patients (17), includes age, heart rate, systolic blood pressure, creatinine, chronic heart failure, cardiac arrest at admission, ST-segment deviation, and elevated cardiac enzymes, but fails to involve any biological indicator. Therefore, we explored the ability of lymphocyte-based inflammatory indices in combination with the GRACE risk score to assess prognosis.

In this study, we evaluated the ability of five lymphocyte-based inflammatory indices including PLR, NLR, monocyte-lymphocyte ratio (MLR), SII, and SIRI to predict the long-term prognosis, and to improve the value of the GRACE risk score for risk stratification of ACS patients undergoing PCI.

METHOD

Study Design and Baseline Characteristics

This was a single-center prospective observational study based on cardiovascular center from Beijing Anzhen Hospital, Capital Medical University, which included 1,770 patients who underwent PCI for ACS between June 2016 and November 2017. We excluded 65 patients with at least one of the following conditions: prior coronary artery bypass grafting, acute and/or chronic infection, autoimmune diseases, known malignancy, Killip class > II, left ventricular ejection fraction < 30%, or renal dysfunction with creatinine clearance < 30 ml/min. Four patients were also excluded because of missing follow-up data despite at least four separate attempts to contact them. Finally, 1,701 patients were included in the analysis. All patients participating in the study were in line with the diagnostic criteria of ACS set by the American College of Cardiology Foundation/American Heart Association (ACC/AHA). This study was performed in accordance with the Helsinki Declaration of Human Rights and was approved by the institutional review board of Beijing Anzhen Hospital, Capital Medical University (IRB number: 2016034x).

Measurements

Demographics, lifestyle, and clinical history were collected through standard questionnaires on admission. Body mass index was calculated based on height and weight [a ratio of weight to height squared (kg/m^2)] of the patients on admission. The first peripheral venous blood after 12 h of fasting was obtained after admission at the hospital. Routine laboratory data and discharge medications were collected from the electronic medical system.

The counts of lymphocyte, platelet, neutrophil, and monocyte were measured in the Central Laboratory of Beijing Anzhen Hospital. In this study, the lymphocyte-based inflammatory indices included: PLR (platelet/lymphocyte), NLR (neutrophil/lymphocyte), MLR (monocyte/lymphocyte), SII (platelet* neutrophil/lymphocyte), and SIRI (neutrophil* monocyte/lymphocyte) (15, 18). The GRACE risk score was analyzed as a numerical value and calculated according to the GRACE risk model by using a computer program (<http://www.outcomes-umassmed.org/grace>).

Abbreviations: ACS, acute coronary syndrome; CI, confidence interval; GRACE, Global Registry of Acute Coronary Events; IDI, integrated discrimination improvement; IQR, interquartile range; MACE, major adverse cardiovascular events; MLR, monocyte-lymphocyte ratio; MI, myocardial infarction; NRI, net reclassification improvement; NLR, neutrophil-lymphocyte ratio; PCI, percutaneous coronary intervention; PLR, platelet-lymphocyte ratio; PPV, positive predictive value; SYNTAX, SYNERGY between PCI with TAXUS and cardiac surgery; SII, systemic inflammatory reaction index; SIRI, systemic inflammatory response index.

Definition of Clinical Endpoints and Follow-Up

The primary endpoint of this study was the composite of all-cause death, non-fatal ischemic stroke, and non-fatal MI. Ischemic stroke was defined as ischemic cerebral infarction, clinically documented on brain computed tomography or magnetic resonance imaging. MI was defined as the appearance of new pathological Q waves in two or more contiguous leads, or the level of cardiac enzymes/markers exceeding the upper limit with either ischemic symptoms or electrocardiogram (ECG) implicating ischemia. However, within 1 week after the PCI, only new pathological Q-wave MI was defined as adverse event. The end of follow-up was the date of the first non-fatal MI or non-fatal ischemic stroke or all-cause death occurrence. If more than one event occurred, the most severe event was chosen (death > stroke > MI). Patients were followed up since the date of one month after discharge and every six months thereafter by telephone. Trained personnel who never knew the baseline data of patients achieved the telephone contact.

Statistical Analysis

Statistical analyses were performed using the R, version 3.6.3 software (R Foundation for Statistical Computing, Vienna, Austria) and SPSS 24.0 (IBM Corporation, Chicago, IL). All statistical tests were two-tailed and $p < 0.05$ was considered statistically significant. Categorical variables were expressed as the percentage (number) tested with the chi-square test. Continuous variables were presented as mean with standard deviation or median with interquartile range (IQR). The normal distributions of the continuous variables were investigated by Kolmogorov-Smirnov test or histograms. Data with normal distribution were compared by ANOVA, otherwise by Kruskal-Wallis H tests. Receiver operating characteristic curves were used to calculate the cutoff values. The lymphocyte-based inflammatory indices were statistically analyzed as categorical variables according to the optimal cutoff values that were determined by Youden's index (sensitivity + specificity - 1). Univariate and multivariate Cox proportional hazards regression models were used to estimate the hazard ratio (HR) and 95% confidence interval (CI). The cumulative risk of the endpoint over time was presented graphically using Kaplan-Meier curve, and log-rank test was used to compare the two groups. To further evaluate the discrimination performance, the sensitivity, positive predictive value (PPV), and C-statistics were calculated, and C-statistics were compared pair-wise. Sensitivity refers to the probability of a positive laboratory test in a confirmed patient, and PPV refers to the probability of actual disease in a population with a positive laboratory test (19). To evaluate the ability of lymphocyte-based inflammatory indices to improve the predictive value of the GRACE risk model, we added these indices to the GRACE risk score as new models and performed net reclassification improvement (NRI) and integrated discrimination improvement (IDI) statistical analyses.

RESULT

Cohort Demographics

The mean age of the 1,701 patients at baseline was 60 ± 10 years, and 76.7% were men ($n = 1,305$). Among the 1,701 patients, more than one-half of the patients had hypertension (63.6%, $n = 1,082$), 46.0% ($n = 783$) had diabetes, 79.9% ($n = 1,359$) had dyslipidemia, and 12.8% ($n = 218$) were diagnosed as STEMI. During the median follow-up of 30 months (IQR, 30–36 months), 107 (6.3%) patients had MACE. Compared with those without event, patients with MACE had higher fasting plasma glucose levels, high-sensitivity C-reactive protein levels and SYNTAX score, but lower left ventricular ejection fraction. Also, patients with MACE had higher rate of aspirin and angiotensin-converting enzyme inhibitor (ACEI)/angiotensin II receptor blocker (ARB) use at discharge.

We sorted out the relevant variables of the GRACE risk model. Except creatinine and cardiac arrest, other GRACE variables were significantly different between patients with and without MACE. Compared with those without MACE, patients with MACE had higher GRACE risk scores, and had higher levels of NLR, PLR, MLR, SII, and SIRI. Baseline characteristics of the study population are summarized in **Table 1**.

Lymphocyte-Based Inflammatory Indices as Independent Predictors of MACE

The results of univariate and multivariate Cox proportional hazards regression analyses of lymphocyte-based inflammatory indices predicting MACE are summarized in **Table 2**. The univariate COX analysis showed higher rates of MACE corresponding to higher PLR (HR: 2.234; 95% CI: 1.530–3.264; $p < 0.001$), NLR (HR: 2.852; 95% CI: 1.951–4.169; $p < 0.001$), MLR (HR: 2.641; 95% CI: 1.794–3.887; $p < 0.001$), SII (HR: 3.055; 95% CI: 2.079–4.490; $p < 0.001$), and SIRI (HR: 3.847; 95% CI: 2.623–5.641; $p < 0.001$). In the multivariate COX analysis, the associations of PLR (HR: 1.768; 95% CI: 1.186–2.636; $p = 0.005$), NLR (HR: 1.767; 95% CI: 1.163–2.685; $p = 0.008$), MLR (HR: 1.795; 95% CI: 1.185–2.719; $p = 0.006$), SII (HR: 2.241; 95% CI: 1.471–3.414; $p < 0.001$), and SIRI (HR: 2.561; 95% CI: 1.681–3.902; $p < 0.001$) with MACE remained significant. As shown in **Figure 1**, Kaplan-Meier curves showed that the patients with higher lymphocyte-based inflammatory indices had higher incidences of MACE (all log-rank $p < 0.001$) (**Supplementary Table 1**).

Comparisons Among Various Lymphocyte-Based Inflammatory Indices

The comparisons among various lymphocyte-based inflammatory indices for predicting MACE are shown in **Table 3**. We observed that the sensitivity of MLR was the highest (59.1%), and the PPV of SIRI was the highest (13.4%). The C-statistics of the lymphocyte-based inflammatory indices were 0.692 [0.611–0.773] for PLR, 0.739 [0.666–0.812] for NLR, 0.729 [0.654–0.805] for MLR, 0.754 [0.682–0.825] for SII, and 0.794 [0.731–0.856] for SIRI. According to pair-wise comparison of the C-statistics, SIRI seemingly performed best.

TABLE 1 | Baseline characteristics of study population by major adverse cardiovascular events (MACE).

Variable	Total study population	No such event	MACE	P value
	N = 1,701	N = 1,594	N = 107	
Male, n (%)	1,305 (76.7)	1,227 (77.0)	78 (72.9)	0.334
BMI (kg/m ²)	25.7 ± 9.6	25.7 ± 9.4	25.3 ± 11.4	0.218
Current smoking, n (%)	754 (44.3)	709 (44.5)	45 (42.1)	0.625
Hypertension, n (%)	1082 (63.6)	1107 (63.2)	75 (70.1)	0.150
Diabetes, n (%)	783 (46.0)	731 (45.9)	52 (48.6)	0.582
Dyslipidemia, n (%)	1359 (79.9)	1268 (79.5)	91 (85.0)	0.170
Previous MI, n (%)	325 (19.1)	294 (18.4)	31 (29.0)	0.007
Previous PCI, n (%)	338 (19.9)	304 (19.1)	34 (31.8)	0.001
CKD, n (%)	737 (43.3)	684 (42.9)	53 (49.5)	0.181
Type of ACS				
UA, n (%)	1267 (74.5)	1196 (75.0)	71 (66.4)	0.046
NSTEMI, n (%)	216 (12.7)	193 (12.1)	23 (21.5)	0.005
STEMI, n (%)	218 (12.8)	205 (12.9)	13 (12.1)	0.831
GRACE variables				
Age (years)	60 ± 10	59 ± 10	64 ± 12	<0.001
HR (bpm)	68 ± 9	68 ± 9	73 ± 10	<0.001
SBP (mmHg)	130 ± 16	130 ± 16	134 ± 18	0.006
Creatinine (μmol/L)	70.3 [62.1–79.6]	70.3 [62.0–79.4]	70.2 [63.2–81.3]	0.432
Heart failure, n (%)	115 (6.8)	89 (5.6)	26 (24.3)	<0.001
ST-segment deviation, n (%)	298 (17.5)	269 (16.9)	29 (27.1)	0.007
Elevated cardiac enzymes/markers, n (%)	434 (25.5)	398 (25.0)	36 (33.6)	0.046
Cardiac arrest, n (%)	2 (0.1)	2 (0.1)	0 (0.0)	1.000
GRACE risk score	103 ± 38	102 ± 37	121 ± 44	<0.001
Laboratory data				
Triglycerides (mmol/L)	1.45 [1.01–2.06]	1.44 [1.00–2.04]	1.54 [1.12–2.28]	0.120
Total cholesterol (mmol/L)	4.15 ± 0.99	4.14 ± 0.99	4.24 ± 1.02	0.309
HDL-C (mmol/L)	1.03 ± 0.23	1.04 ± 0.23	1.00 ± 0.25	0.128
LDL-C (mmol/L)	2.44 ± 0.81	2.44 ± 0.81	2.51 ± 0.80	0.337
FPG (mmol/L)	5.78 [5.23–6.92]	5.78 [5.22–6.87]	6.12 [5.33–7.45]	0.018
hsCRP (mg/L)	1.34 [0.64–3.42]	1.32 [0.62–3.23]	2.86 [1.16–7.14]	<0.001
LVEF (%)	65 [60–68]	65 [60–68]	60 [53–66]	<0.001
30–39, n (%)	21 (1.2)	16 (1.0)	5 (4.7)	
40–49, n (%)	74 (4.4)	61 (3.8)	13 (12.1)	
≥50, n (%)	1606 (94.4)	1517 (95.2)	89 (83.2)	
Angiographic and procedural results				
Left-main/multi-vessel disease, n (%)	1,441 (84.7)	1347 (84.5)	94 (87.9)	0.352
Proximal LAD disease, n (%)	850 (50.0)	790 (49.6)	60 (56.1)	0.192
SYNTAX score	20 ± 11	20 ± 11	24 ± 12	<0.001
DES, n (%)	1397 (82.1)	1307 (82.0)	90 (84.1)	0.580
BRS, n (%)	97 (5.7)	91 (5.7)	6 (5.6)	0.965
DCB, n (%)	82 (4.8)	76 (4.8)	6 (5.6)	0.923
Discharge medications				
Aspirin, n (%)	1685 (99.1)	1586 (99.5)	99 (92.5)	<0.001
P2Y12 inhibitors, n (%)	1701 (100)	1594 (100)	107 (100)	/
Statins, n (%)	1701 (100)	1594 (100)	107 (100)	/
ACEI/ARBs, n (%)	821 (48.3)	748 (46.9)	73 (68.2)	<0.001
β-blockers, n (%)	1197 (70.4)	1123 (70.5)	74 (69.2)	0.777
Lymphocyte-based inflammatory indices				
PLR	118.06 [94.15–150.00]	117.20 [93.61–148.66]	137.74 [100.00–172.31]	0.002
NLR	2.26 [1.72–2.97]	2.22 [1.70–2.92]	2.91 [2.05–3.80]	<0.001

(Continued)

TABLE 1 | Continued

Variable	Total study population	No such event	MACE	P value
	N = 1,701	N = 1,594	N = 107	
MLR	0.20 [0.16–0.26]	0.20 [0.15–0.26]	0.25 [0.19–0.32]	<0.001
SII	468.00 [339.94–644.45]	461.51 [336.50–630.71]	613.42 [423.45–938.94]	<0.001
SIRI	0.80 [0.55–1.17]	0.78 [0.55–1.12]	1.20 [0.81–1.77]	<0.001

ACEI, angiotensin converting enzyme inhibitor; ACS, acute coronary syndrome; ARB, angiotensin II receptor blocker; BMI, body mass index; BRS, bioresorbable scaffold; CKD, chronic kidney disease; DCB, drug coated balloon; DES, drug eluting stent; FPG, fasting plasma glucose; GRACE, global registry of acute coronary events; HDL-C, high-density lipoprotein-cholesterol; HR, heart rate; HsCRP, high-sensitive C-reactive protein; LAD, left anterior descending branch; LDL-C, low-density lipoprotein-cholesterol; LVEF, left ventricular ejection fraction; MLR, monocyte-lymphocyte ratio; MI, myocardial infarction; NLR, neutrophil-lymphocyte ratio; NSTEMI, non-ST segment elevation myocardial infarction; PCI, percutaneous coronary intervention; PLR, platelet-lymphocyte ratio; SBP, systolic blood pressure; STEMI, ST segment elevation myocardial infarction; SII, systemic inflammatory reaction index; SIRI, systemic inflammatory response index; SYNTAX, Synergy between PCI with TAXus and cardiac surgery; UA, unstable angina.

TABLE 2 | The univariate and multivariate Cox proportional hazards analyses of lymphocyte-based inflammatory indices predicting MACE.

	Univariate		Multivariate*	
	HR (95% CI)	P Value	HR (95% CI)	P Value
PLR	2.234 (1.530–3.264)	<0.001	1.768 (1.186–2.636)	0.005
NLR	2.852 (1.951–4.169)	<0.001	1.767 (1.163–2.685)	0.008
MLR	2.641 (1.794–3.887)	<0.001	1.795 (1.185–2.719)	0.006
SII	3.055 (2.079–4.490)	<0.001	2.241 (1.471–3.414)	<0.001
SIRI	3.847 (2.623–5.641)	<0.001	2.561 (1.681–3.902)	<0.001

*Adjusted for GRACE risk score, past MI, past PCI, type of ACS, FPG, hsCRP, LVEF, SYNTAX score, use of aspirin and ACEI/ARBs at discharge.

Abbreviations as in **Table 1**.

Combinations of Lymphocyte-Based Inflammatory Indices With the GRACE Risk Score

To assess whether the combinations of lymphocyte-based inflammatory indices with the GRACE risk score could improve the predictive ability, we built six models with the GRACE risk score numerically incorporated into the models (**Table 4**). Compared with the basic model, the risk models consisting of the GRACE risk score and lymphocyte-based inflammatory indices had superior discrimination performance for MACE. We observed that the C-statistics increased significantly after adding NLR (0.668 [0.612–0.724], $p = 0.018$), MLR (0.672 [0.619–0.725], $p = 0.010$), SII (0.680 [0.627–0.733], $p = 0.005$), and SIRI (0.699 [0.646–0.753], $p < 0.001$) to the GRACE risk score. Among the five new models, the model with the GRACE risk score in combination with SIRI had the best reclassification significance with NRI of 31.1% ($p < 0.001$) and IDI of 2.4% ($p < 0.001$).

DISCUSSION

In this observational study, we evaluated the prognostic values of five lymphocyte-based inflammatory indices in ACS patients who underwent PCI for the first time. Lymphocyte-based inflammatory indices are readily available in clinical practice. We observed that the five indices were significantly and

independently associated with MACE in ACS patients. Through univariate and multivariate analysis, SIRI showed the highest C-statistics (0.794; 0.699), affirming the predictive value of SIRI. Although the C-statistic of SIRI was higher in univariate analysis, it did not mean that the predictive value of SIRI alone was higher. In multivariate analysis, multiple influencing or confounding factors were comprehensively considered.

In previous studies, NLR attracted the most attention from researchers. A number of studies showed that NLR promoted the development of atherosclerosis. Choi et al. found that NLR > 2.8 was an independent predictor of adverse cardiovascular events in patients with CAD undergoing PCI (20). Our study had a similar result that NLR ≥ 2.83 could predict the occurrence of MACE. The study of XU et al. showed a significant increase in 2-year adverse cardiovascular events in patients with left main and/or three-vessel disease when NLR ≥ 3.39 (21). An increase in neutrophils can promote oxidative damage to the vessel wall, while a decrease in lymphocytes can also exacerbate oxidative and inflammatory damage, both of which are associated with increased stiffness of the arteries (22, 23). NLR has been shown to be independently associated with coronary artery calcification, which increases the risk of CAD (24). Of note, even after receiving dual antiplatelet therapy, ACS patients with high NLR levels still have poor platelet inhibition, which promotes thrombosis and increases the risk of recurrent ischemic events (25).

Elevated PLR levels may be related to inflammatory activation and pro-thrombotic status in patients with ACS due to megakaryocyte proliferation and relative prothrombotic status (26). Li and colleagues observed that PLR significantly increased in elderly patients, resulting in poor prognosis (27). The study of Trakarnwijit et al. showed that PLR was an independent risk factor for CAD in patients aged 55 years and above, but was negatively associated with CAD in younger patients (28). The mean age of patients in our study was 60 ± 10 years, and we found that PLR has a limited prognostic value in ACS patients. Based on the results of our study, we do not recommend using PLR alone to predict cardiovascular outcomes, but we may consider combining PLR with other indices for risk stratification. The study of Liu et al. indicated that PLR-NLR combination could better predict the prognosis of acute MI and had higher sensitivity than PLR or NLR alone (29).

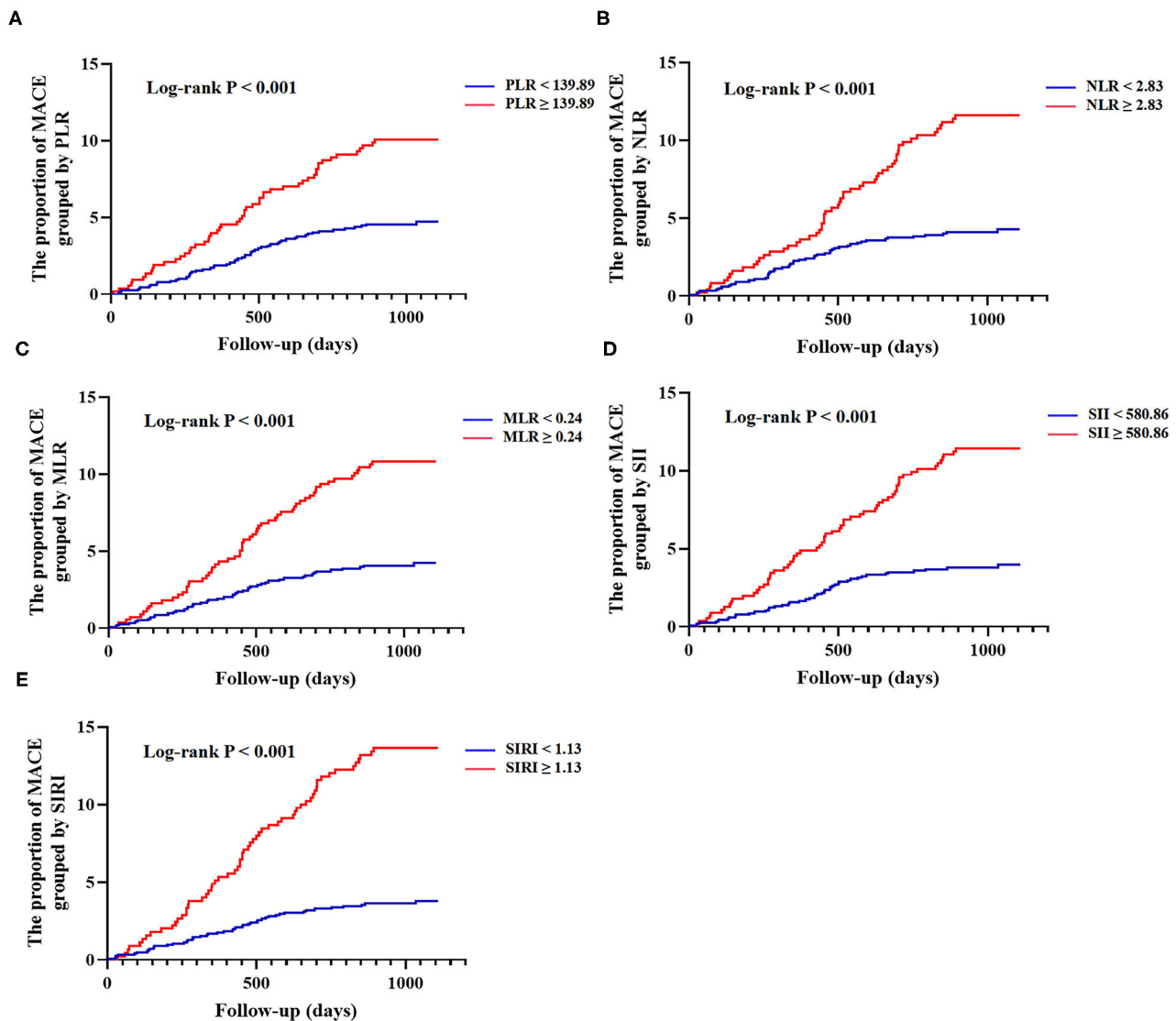


FIGURE 1 | Kaplan-Meier curves of lymphocyte-based inflammatory indices and cumulative incidence of major adverse cardiovascular events (MACE) at follow-up. **(A)** Grouped by platelet-lymphocyte ratio (PLR) (<139.89 vs. ≥ 139.89); **(B)** Grouped by neutrophil-lymphocyte ratio (NLR) (<2.83 vs. ≥ 2.83); **(C)** Grouped by monocyte-lymphocyte ratio (MLR) (<0.24 vs. ≥ 0.24); **(D)** Grouped by systemic immune inflammation index (SII) (<580.86 vs. ≥ 580.86); **(E)** Grouped by system inflammation response index (SIRI) (<1.13 vs. ≥ 1.13). MACE was defined as a composite of all-cause death, non-fatal ischemic stroke, and non-fatal myocardial infarction.

One study showed that MLR was independently associated with CAD and could be used to predict coronary lesion severity (30). The study of Song et al. yielded similar results (31). As one of the most important inflammatory cells, monocytes are directly involved in the formation and development of atherosclerosis. Monocytes adhere to vascular endothelium and differentiate into macrophages, and then transform into foam cells by ingesting oxidized lipoprotein, which can activate various inflammatory signal factors and oxidized free radicals in plaque (32, 33). It is encouraging that therapies targeting monocytes, macrophages, and foam cells are available to treat atherosclerosis (34).

SII and SIRI were originally used to evaluate the prognosis of tumors. In recent years, SII and SIRI have been shown to be good predictors of CAD. In fact, SII and SIRI are more comprehensive because both are a combination of three inflammatory cells compared to the other three indices. Therefore, it is not surprising that SII and SIRI outperformed the other three indices in predicting cardiovascular outcomes. Of note, in addition to neutrophil and lymphocyte, the other component included in SII is platelet, while in SIRI it is monocyte. Monocyte may be more closely related to the development of atherosclerosis than platelet. SII was shown to be positively correlated with SYNTAX score (35, 36), which could be used for CAD risk stratification

TABLE 3 | Comparisons among various lymphocyte-based inflammatory indices.

A.					
Discrimination ability	PLR	NLR	MLR	SII	SIRI
Cutoff value	139.89	2.83	0.24	580.86	1.13
Sensitivity (%)	48.9	52.8	59.1	58.2	56.4
Positive predictive value (%)	9.9	11.4	10.9	11.3	13.4
C-statistic (95% CI)	0.692 [0.611–0.773]	0.739 [0.666–0.812]	0.729 [0.654–0.805]	0.754 [0.682–0.825]	0.794 [0.731–0.856]
B.					
Comparison	C-statistic				P Value
	Difference				
NLR VS. PLR	0.047			0.128	
NLR VS. MLR	0.010			0.402	
MLR VS. PLR	0.037			0.218	
SII VS. PLR	0.061			0.042	
SII VS. NLR	0.014			0.317	
SII VS. MLR	0.024			0.283	
SIRI VS. PLR	0.101			0.013	
SIRI VS. NLR	0.054			0.044	
SIRI VS. MLR	0.064			0.018	
SIRI VS. SII	0.040			0.114	

(A) The discrimination ability of five lymphocyte-based inflammatory indices; (B) The pair-wise comparison of C-statistics among five lymphocyte-based inflammatory indices. Abbreviations as in **Table 1**.

TABLE 4 | Discrimination performance of GRACE risk score plus lymphocyte-based inflammatory indices in predicting MACE.

Model	C-Statistic (95% CI)	P value	NRI	P value	IDI	P value
GRACE	0.624 [0.566–0.682]	ref	ref		ref	
GRACE + PLR	0.656 [0.602–0.710]	0.057	0.199 [0.104–0.297]	<0.001	0.009 [0.002–0.024]	<0.001
GRACE + NLR	0.668 [0.612–0.724]	0.018	0.250 [0.148–0.341]	<0.001	0.015 [0.004–0.030]	<0.001
GRACE + MLR	0.672 [0.619–0.725]	0.010	0.245 [0.143–0.342]	0.002	0.011 [0.002–0.027]	0.002
GRACE + SII	0.680 [0.627–0.733]	0.005	0.268 [0.162–0.361]	<0.001	0.015 [0.005–0.031]	<0.001
GRACE + SIRI	0.699 [0.646–0.753]	<0.001	0.311 [0.209–0.407]	<0.001	0.024 [0.010–0.046]	<0.001

Abbreviations as in **Table 1**.

and prognostic prediction after PCI. Jin and colleagues found that the high rates of stroke and all-cause death corresponded to high levels of SII and SIRI, while the high risk of MI was only independently related to high SIRI (15). In the present study, we demonstrated that the predictive ability of SIRI for MACE was better than SII.

The GRACE scoring system is relatively common, standardized, and authoritative. The GRACE risk score combined with other indicators (such as platelet reactivity, hemoglobin A1c, and red blood cell distribution width) had a better predictive value than the GRACE risk score alone (37–39). One of our purposes is to explore the ability of five indicators to improve the GRACE score. Previous studies showed that adding neutrophil count to the GRACE risk score increased the C-statistic (0.698 vs. 0.796, $p < 0.001$), and enhanced the

NRI (0.637, $p = 0.020$) and IDI (0.180, $p < 0.001$) (40). Similar results were obtained by Zhou et al., where the GRACE risk score combined with NLR improved the C-statistic (0.69 vs. 0.77) (41). In our study, adding NLR to the GRACE risk score also increased the C-statistic (0.624 vs. 0.668), as well as enhanced the levels of NRI (0.250, $p < 0.001$) and IDI (0.015, $p < 0.001$). However, few studies investigated whether the addition of the other four indices, particularly SII and SIRI (higher predictive value in univariate analysis), improves the predictive ability of the GRACE risk score. In our study, for the first time, we added five lymphocyte-based inflammatory indices to the GRACE risk score, further illustrating their respective predictive ability, and we found that the addition of NLR, MLR, SII, or SIRI to the GRACE risk score, especially SIRI, outperformed the GRACE risk score alone in the risk predictive performance.

LIMITATION

The present study has some limitations. First, this was a single-center study with a relatively small sample size. Second, our study was limited to Chinese subjects, and thus the conclusion requires further validation before extending to other ethnic groups. Third, our study did not investigate the correlation between the lymphocyte-based inflammatory indices with the severity of CAD in ACS patients, which needs to be explored in subsequent studies.

CONCLUSION

The values of $PLR \geq 139.89$, $NLR \geq 2.83$, $MLR \geq 0.24$, $SII \geq 580.86$, and $SIRI \geq 1.13$ were significantly and independently associated with MACE in ACS patients who underwent PCI. SIRI seemed to be better than the other four indices in predicting MACE, and the combination of SIRI with the GRACE risk score could predict MACE more accurately. In the future, we can add the SIRI as a categorical variable to the GRACE risk score to complement the inflammation deficit. As for the classification threshold or the score weight in the GRACE scoring system of SIRI, further exploration is required.

DATA AVAILABILITY STATEMENT

The raw data supporting the conclusions of this article will be made available by the authors, without undue reservation.

REFERENCES

- Pasterkamp G, den Ruijter HM, Libby P. Temporal shifts in clinical presentation and underlying mechanisms of atherosclerotic disease. *Nat Rev Cardiol.* (2017) 14:21–9. doi: 10.1038/nrcardio.2016.166
- Libby P, Pasterkamp G, Crea F, Jang IK. Reassessing the mechanisms of acute coronary syndromes. *Circ Res.* (2019) 124:150–60. doi: 10.1161/CIRCRESAHA.118.311098
- Yonetsu T, Jang IK. Advances in intravascular imaging: new insights into the vulnerable plaque from imaging studies. *Korean Circ J.* (2018) 48:1–15. doi: 10.4070/kcj.2017.0182
- Partida RA, Libby P, Crea F, Jang IK. Plaque erosion: a new *in vivo* diagnosis and a potential major shift in the management of patients with acute coronary syndromes. *Eur Heart J.* (2018) 39:2070–6. doi: 10.1093/eurheartj/ehx786
- Eisen A, Giugliano RP, Braunwald E. Updates on acute coronary syndrome: a review. *JAMA Cardiol.* (2016) 1:718–30. doi: 10.1001/jamacardio.2016.2049
- Higuma T, Soeda T, Abe N, Yamada M, Yokoyama H, Shibutani S, et al. A combined optical coherence tomography and intravascular ultrasound study on plaque rupture, plaque erosion, and calcified nodule in patients with ST-segment elevation myocardial infarction: incidence, morphologic characteristics, and outcomes after percutaneous coronary intervention. *JACC Cardiovasc Interv.* (2015) 8:1166–76. doi: 10.1016/j.jcin.2015.02.026
- Hoole SP, Bambrough P. Recent advances in percutaneous coronary intervention. *Heart.* (2020) 106:1380–6. doi: 10.1136/heartjnl-2019-315707
- Jeremias A, Davies JE, Maehara A, Matsumura M, Schneider J, Tang K, et al. Blinded physiological assessment of residual ischemia after successful angiographic percutaneous coronary intervention: the DEFINE PCI study. *JACC Cardiovasc Interv.* (2019) 12:1991–2001. doi: 10.1016/j.jcin.2019.05.054

ETHICS STATEMENT

The studies involving human participants were reviewed and approved by the Institutional Review Board of Beijing Anzhen Hospital, Capital Medical University (IRB number: 2016034x). The patients/participants provided their written informed consent to participate in this study.

AUTHOR CONTRIBUTIONS

All authors were involved in the conception and design of the study, the collection, analysis, interpretation of the data, reviewed the final manuscript, read, and approved the final manuscript.

FUNDING

This work was supported by China Postdoctoral Science Foundation (2021M692253), Beijing Postdoctoral Research Foundation (2021-ZZ-023), and Beijing Municipal Administration of Hospitals' Mission Plan (SML20180601).

SUPPLEMENTARY MATERIAL

The Supplementary Material for this article can be found online at: <https://www.frontiersin.org/articles/10.3389/fcvm.2022.811790/full#supplementary-material>

- Biswas S, Dinh D, Lucas M, Duffy SJ, Brennan AL, Liew D, et al. Incidence and predictors of unplanned hospital readmission after percutaneous coronary intervention. *J Clin Med.* (2020) 9: E3242. doi: 10.3390/jcm9103242
- Crea F, Libby P. Acute coronary syndromes: the way forward from mechanisms to precision treatment. *Circulation.* (2017) 136:1155–66. doi: 10.1161/CIRCULATIONAHA.117.029870
- Haybar H, Pezeshki SMS, Saki N. Evaluation of complete blood count parameters in cardiovascular diseases: an early indicator of prognosis? *Exp Mol Pathol.* (2019) 110:104267. doi: 10.1016/j.yexmp.2019.104267
- Budzianowski J, Pieszko K, Burchardt P, Rzezniczak J, Hiczkiewicz J. The role of hematological indices in patients with acute coronary syndrome. *Dis Markers.* (2017) 2017:3041565. doi: 10.1155/2017/3041565
- Hu B, Yang XR, Xu Y, Sun YF, Sun C, Guo W, et al. Systemic immune-inflammation index predicts prognosis of patients after curative resection for hepatocellular carcinoma. *Clin Cancer Res.* (2014) 20:6212–22. doi: 10.1158/1078-0432.CCR-14-0442
- Qi Q, Zhuang L, Shen Y, Geng Y, Yu S, Chen H, et al. A novel systemic inflammation response index (SIRI) for predicting the survival of patients with pancreatic cancer after chemotherapy. *Cancer.* (2016) 122:2158–67. doi: 10.1002/cncr.30057
- Jin Z, Wu Q, Chen S, Gao J, Li X, Zhang X, et al. The associations of two novel inflammation indexes, SIRI and SIRI with the risks for cardiovascular diseases and all-cause mortality: a ten-year follow-up study in 85,154 individuals. *J Inflamm Res.* (2021) 14:131–40. doi: 10.2147/JIR.S283835
- Eagle KA, Lim MJ, Dabbous OH, Pieper KS, Goldberg RJ, Van de Werf F, et al. A validated prediction model for all forms of acute coronary syndrome: estimating the risk of 6-month postdischarge death in an international registry. *JAMA.* (2004) 291:2727–33. doi: 10.1001/jama.291.22.2727
- Fox KA, Dabbous OH, Goldberg RJ, Pieper KS, Eagle KA, Van de Werf F, et al. Prediction of risk of death and myocardial infarction

- in the six months after presentation with acute coronary syndrome: prospective multinational observational study (GRACE). *BMJ*. (2006) 333:1091. doi: 10.1136/bmj.38985.646481.55
18. Gao X, Liu Y, Tian Y, Rao C, Shi F, Bu H, et al. Prognostic value of peripheral blood inflammatory cell subsets in patients with acute coronary syndrome undergoing percutaneous coronary intervention. *J Int Med Res*. (2021) 49:3000605211010059. doi: 10.1177/03000605211010059
 19. Monaghan TF, Rahman SN, Agudelo CW, Wein AJ, Lazar JM, Everaert K, et al. Foundational statistical principles in medical research: sensitivity, specificity, positive predictive value, and negative predictive value. *Medicina*. (2021) 57:503. doi: 10.3390/medicina57050503
 20. Choi DH, Kobayashi Y, Nishi T, Kim HK, Ki YJ, Kim SS, et al. Combination of mean platelet volume and neutrophil to lymphocyte ratio predicts long-term major adverse cardiovascular events after percutaneous coronary intervention. *Angiology*. (2019) 70:345–51. doi: 10.1177/0003319718768658
 21. Xu N, Tang XF, Yao Y, Zhao X, Chen J, Gao Z, et al. Predictive value of neutrophil to lymphocyte ratio in long-term outcomes of left main and/or three-vessel disease in patients with acute myocardial infarction. *Catheter Cardiovasc Interv*. (2018) 91:551–7. doi: 10.1002/ccd.27495
 22. Li Y, Chen X, Huang L, Lu J. Association between neutrophil-lymphocyte ratio and arterial stiffness in patients with acute coronary syndrome. *Biosci Rep*. (2019) 39:BSR20190015. doi: 10.1042/BSR20190015
 23. Mozos I, Malainer C, Horbanczuk J, Gug C, Stoian D, Luca CT, et al. Inflammatory markers for arterial stiffness in cardiovascular diseases. *Front Immunol*. (2017) 8:1058. doi: 10.3389/fimmu.2017.01058
 24. Serrano CV Jr., de Mattos FR, Pitta FG, Nomura CH, de Lemos J, Ramires JAF, et al. Association between neutrophil-lymphocyte and platelet-lymphocyte ratios and coronary artery calcification score among asymptomatic patients: data from a cross-sectional study. *Mediators Inflamm*. (2019) 2019:6513847. doi: 10.1155/2019/6513847
 25. Verdoia M, Nardin M, Gioscia R, Negro F, Marcolongo M, Suryapranata H, et al. Higher neutrophil-to-lymphocyte ratio (NLR) increases the risk of suboptimal platelet inhibition and major cardiovascular ischemic events among ACS patients receiving dual antiplatelet therapy with ticagrelor. *Vascul Pharmacol*. (2020) 132:106765. doi: 10.1016/j.vph.2020.106765
 26. Li H, Zhou Y, Ma Y, Han S, Zhou L. The prognostic value of the platelet-to-lymphocyte ratio in acute coronary syndrome: a systematic review and meta-analysis. *Kardiol Pol*. (2017) 75:666–73. doi: 10.5603/KP.a2017.0068
 27. Li L, Ma Y, Geng XB, Tan Z, Wang JH, Cui C, et al. Platelet-to-lymphocyte ratio relates to poor prognosis in elderly patients with acute myocardial infarction. *Aging Clin Exp Res*. (2021) 33:619–24. doi: 10.1007/s40520-020-01555-7
 28. Trakarnwijitr I, Li B, Adams H, Layland J, Garlick J, Wilson A. Age modulates the relationship between platelet-to-lymphocyte ratio and coronary artery disease. *Int J Cardiol*. (2017) 248:349–54. doi: 10.1016/j.ijcard.2017.06.127
 29. Liu J, Ao W, Zhou J, Luo P, Wang Q, Xiang D. The correlation between PLR-NLR and prognosis in acute myocardial infarction. *Am J Transl Res*. (2021) 13:4892–9.
 30. Ji H, Li Y, Fan Z, Zuo B, Jian X, Li L, et al. Monocyte/lymphocyte ratio predicts the severity of coronary artery disease: a syntax score assessment. *BMC Cardiovasc Disord*. (2017) 17:90. doi: 10.1186/s12872-017-0507-4
 31. Song FH, Zheng YY, Tang JN, Wang W, Guo QQ, Zhang JC, et al. A correlation between monocyte to lymphocyte ratio and long-term prognosis in patients with coronary artery disease after PCI. *Clin Appl Thromb Hemost*. (2021) 27:1076029621999717. doi: 10.1177/1076029621999717
 32. Chistiakov DA, Bobryshev YV, Orekhov AN. Macrophage-mediated cholesterol handling in atherosclerosis. *J Cell Mol Med*. (2016) 20:17–28. doi: 10.1111/jcmm.12689
 33. Kavurma MM, Rayner KJ, Karunakaran D. The walking dead: macrophage inflammation and death in atherosclerosis. *Curr Opin Lipidol*. (2017) 28:91–8. doi: 10.1097/MOL.0000000000000394
 34. Liu H, Zhan F, Wang Y. Evaluation of monocyte-to-high-density lipoprotein cholesterol ratio and monocyte-to-lymphocyte ratio in ischemic stroke. *J Int Med Res*. (2020) 48:300060520933806. doi: 10.1177/0300060520933806
 35. Candemir M, Kiziltunc E, Nurkoc S, Sahinarslan A. Relationship between Systemic Immune-Inflammation Index (SII) and the severity of stable coronary artery disease. *Angiology*. (2021) 72:575–81. doi: 10.1177/0003319720987743
 36. Fan W, Zhang Y, Gao X, Liu Y, Shi F, Liu J, et al. The prognostic value of a derived neutrophil-lymphocyte ratio in patients with acute coronary syndrome undergoing percutaneous coronary intervention. *Clin Appl Thromb Hemost*. (2021) 27:10760296211034579. doi: 10.1177/10760296211034579
 37. Li S, Liu H, Liu J, Wang H. Improved predictive value of GRACE risk score combined with platelet reactivity for 1-year cardiovascular risk in patients with acute coronary syndrome who underwent coronary stent implantation. *Platelets*. (2016) 27:650–7. doi: 10.3109/09537104.2016.1153618
 38. Liu XJ, Wan ZF, Zhao N, Zhang YP, Mi L, Wang XH, et al. Adjustment of the GRACE score by HemoglobinA1c enables a more accurate prediction of long-term major adverse cardiac events in acute coronary syndrome without diabetes undergoing percutaneous coronary intervention. *Cardiovasc Diabetol*. (2015) 14:110. doi: 10.1186/s12933-015-0274-4
 39. Zhao N, Mi L, Liu X, Pan S, Xu J, Xia D, et al. Combined value of red blood cell distribution width and global registry of acute coronary events risk score for predicting cardiovascular events in patients with acute coronary syndrome undergoing percutaneous coronary intervention. *PLoS One*. (2015) 10:e0140532. doi: 10.1371/journal.pone.0140532
 40. Zhang S, Wan Z, Zhang Y, Fan Y, Gu W, Li F, et al. Neutrophil count improves the GRACE risk score prediction of clinical outcomes in patients with ST-elevation myocardial infarction. *Atherosclerosis*. (2015) 241:723–8. doi: 10.1016/j.atherosclerosis.2015.06.035
 41. Zhou D, Wan Z, Fan Y, Zhou J, Yuan Z, A. combination of the neutrophil-to-lymphocyte ratio and the GRACE risk score better predicts PCI outcomes in Chinese Han patients with acute coronary syndrome. *Anatol J Cardiol*. (2015) 15:995–1001. doi: 10.5152/AnatolJCardiol.2015.6174

Conflict of Interest: The authors declare that the research was conducted in the absence of any commercial or financial relationships that could be construed as a potential conflict of interest.

Publisher's Note: All claims expressed in this article are solely those of the authors and do not necessarily represent those of their affiliated organizations, or those of the publisher, the editors and the reviewers. Any product that may be evaluated in this article, or claim that may be made by its manufacturer, is not guaranteed or endorsed by the publisher.

Copyright © 2022 Li, Ma, Shao, Yang, Wang, Gao, Zhou, Yang and Wang. This is an open-access article distributed under the terms of the Creative Commons Attribution License (CC BY). The use, distribution or reproduction in other forums is permitted, provided the original author(s) and the copyright owner(s) are credited and that the original publication in this journal is cited, in accordance with accepted academic practice. No use, distribution or reproduction is permitted which does not comply with these terms.



Mechanical Strain Induces Transcriptomic Reprogramming of Saphenous Vein Progenitors

Davide Maselli^{1,2†}, Gloria Garoffolo^{3†}, Giada Andrea Cassanmagnago^{4,5}, Rosa Vono¹, Matthijs S. Ruiter³, Anita C. Thomas², Paolo Madeddu², Maurizio Pesce^{3†} and Gaia Spinetti^{1*†}

¹ IRCCS MultiMedica, Milan, Italy, ² Translational Health Sciences, Bristol Medical School, University of Bristol, Bristol, United Kingdom, ³ Unità di Ingegneria Tissutale Cardiovascolare, Centro Cardiologico Monzino IRCCS, Milan, Italy, ⁴ IRCCS Humanitas Research Hospital, Rozzano, Italy, ⁵ Department of Biomedical Sciences, Humanitas University, Pieve Emanuele, Italy

OPEN ACCESS

Edited by:

Shizuka Uchida,
Aalborg University
Copenhagen, Denmark

Reviewed by:

Alban Longchamp,
Centre Hospitalier Universitaire
Vaudois (CHUV), Switzerland
Margreet R. De Vries,
Leiden University Medical
Center, Netherlands

*Correspondence:

Gaia Spinetti
gaia.spinetti@multimedica.it

†These authors have contributed
equally to this work and share first
authorship

‡These authors share senior
authorship

Specialty section:

This article was submitted to
Atherosclerosis and Vascular
Medicine,
a section of the journal
Frontiers in Cardiovascular Medicine

Received: 02 March 2022

Accepted: 28 April 2022

Published: 27 May 2022

Citation:

Maselli D, Garoffolo G,
Cassanmagnago GA, Vono R,
Ruiter MS, Thomas AC, Madeddu P,
Pesce M and Spinetti G (2022)
Mechanical Strain Induces
Transcriptomic Reprogramming of
Saphenous Vein Progenitors.
Front. Cardiovasc. Med. 9:884031.
doi: 10.3389/fcvm.2022.884031

Intimal hyperplasia is the leading cause of graft failure in aortocoronary bypass grafts performed using human saphenous vein (SV). The long-term consequences of the altered pulsatile stress on the cells that populate the vein wall remains elusive, particularly the effects on saphenous vein progenitors (SVPs), cells resident in the vein adventitia with a relatively wide differentiation capacity. In the present study, we performed global transcriptomic profiling of SVPs undergoing uniaxial cyclic strain *in vitro*. This type of mechanical stimulation is indeed involved in the pathology of the SV. Results showed a consistent stretch-dependent gene regulation in cyclically strained SVPs vs. controls, especially at 72 h. We also observed a robust mechanically related overexpression of Adhesion Molecule with Ig Like Domain 2 (AMIGO2), a cell surface type I transmembrane protein involved in cell adhesion. The overexpression of AMIGO2 in stretched SVPs was associated with the activation of the transforming growth factor β pathway and modulation of intercellular signaling, cell-cell, and cell-matrix interactions. Moreover, the increased number of cells expressing AMIGO2 detected in porcine SV adventitia using an *in vivo* arterialization model confirms the upregulation of AMIGO2 protein by the arterial-like environment. These results show that mechanical stress promotes SVPs' molecular phenotypic switching and increases their responsiveness to extracellular environment alterations, thus prompting the targeting of new molecular effectors to improve the outcome of bypass graft procedure.

Keywords: saphenous vein progenitors, intimal hyperplasia, bypass graft, mechanosensitivity, AMIGO2

INTRODUCTION

Bypass grafting surgery is the main treatment for coronary artery disease, which represents the leading cause of morbidity and mortality in the industrialized western world (1, 2). Every year about one million surgical revascularization procedures are performed worldwide, and the saphenous vein (SV) remains the most widely used conduit as bypass graft (3). The reasons for this preference are the ease and rapid SV harvesting technique and its relatively higher length compared to radial or mammary arteries, which ensures enough supply for "multi-vessel" pathology (4). However, up to 20–50% of vein grafts will require intervention within 5 years due to the development of graft

stenosis caused by intimal hyperplasia (IH) (5, 6). A better understanding of the development and progression of vein graft disease is crucial for the development of new treatments. The causes of the progressive thickening of the tunica intima of SVs, used as a coronary bypass graft, leading to IH can be partially identified in surgical mismanagement at the time of harvesting, for which recently has been introduced “no-touch” harvesting technique (7). A better outcome in terms of SV graft patency has been also observed when coronary artery bypass graft surgery is performed in off-pump mode (8). However, IH represents a long-term consequence of vein adaptation to coronary blood flow (8) consisting of a change from a constant pressure (5–10 mmHg) and a steady flow, to a counter pulsed 120/80 mmHg and pulsatile flow, with a circumferential strain of 10–15% (9, 10). Under these conditions, wall shear stress on the endothelial monolayer increases by four times, and the quasi-steady venous flow rises to a mean flow rate of 250 ml/min (10). Opposite to arteries, the SV wall is incompressible at high pressures resulting in a blood flow rate in SV bypass graft 5–10 times higher than in arterial bypass graft (11–13). As a consequence, the cells in the tunica media of the vessel are exposed to severe stretching causing an increase in proliferation, changes in the extracellular matrix, and phenotype switching (14–16). There is an increasing number of evidence about the detrimental effect of mechanical stress on the tunica adventitia and strain-related activation of cells dwelling in the proximity of the *vasa vasorum* of the SV’ bypass graft (17–20). In particular, it has been observed that paracrine signals, established in an arterial-like pressure setting, might activate a multipotent population of cells, known as saphenous vein progenitors (SVPs), which uphold differentiation capacity in aged cardiovascular patients (21). Of note, we recently showed that mechanical straining of SV-derived smooth muscle cells (SMCs) determines their transition from a contractile to a secretory phenotype with associated release of the matricellular protein Thrombospondin-1 (TSP-1), which consequently induces the migration and proliferation of cells with SVP phenotype (19). Given the importance of tissue mechanics for the progression of vein graft disease and the potential role of SVP in SV remodeling, in this study, we aimed to assess the strain-related modification of SVPs. Using an RNAseq-based approach we evaluated whether mechanical strain could induce a specific phenotypic modification of SVPs. To investigate stress-related phenotypic changes we exposed primarily isolated SVPs to *in vitro* uniaxial mechanical strain. Genome-wide transcriptional alterations were examined using RNA-seq and analyzed for specific function/gene regulations.

MATERIALS AND METHODS

Ethics

The experimental investigation on human-derived SVPs was approved by the local Ethical Committee at Centro Cardiologico Monzino, IRCCS. Twelve patients recruited for the study were, females or males undergoing surgical removal of saphenous vein because of varicosity. All tissues used in the study are surgical leftovers. Exclusion criteria include concomitant neoplastic, infectious, connective tissue or inflammatory diseases,

pregnancy. The Research Ethics Committee approved the study which was performed according to the ethical principles recorded in the 1964 Declaration of Helsinki and later amendments. All the subjects gave written informed consent to participate. The main clinical characteristics of the participants are included in **Supplementary Table 1**.

Isolation of SVPs

Isolation of cells for *in vitro* experiments was performed as previously described, using two consecutive immunomagnetic selections to obtain CD31^{negative}/CD34^{positive} homogenous cell populations from saphenous vein, known as SVPs (21). After saphenectomy, veins were washed in PBS containing Penicillin/Streptomycin 100 U/mL (PBS + P/S). Saphenous vein walls were finely shredded using scissors and digested with Liberase Blendzyme 2 (Roche) diluted 2 mg/ml in Dulbecco Modified Eagle’s Medium (DMEM, GIBCO) for 4h at 37°C. The minced tissue was serially filtered through 70 μ m, 40 μ m, and 30 μ m cell strainers using PBS + P/S and then centrifuged at 300xg for 10 min at room temperature. SVPs were isolated as a result of two consecutive magnetic beads-assisted cell sorting (MACS, MiltenyiBiotec) using a MACS MS column, according to manufacturer’s instructions. First selection was performed using CD31 magnetic beads (MiltenyiBiotec), in which the negative fraction (CD31^{negative}) was retained and subjected to a second magnetic sorting performed with CD34 magnetic beads (MiltenyiBiotec). After that, CD31^{negative}/CD34^{positive} cell fraction was centrifuged and resuspended in endothelial growth medium EGM-2 (Lonza). SVPs were plated on fibronectin/gelatin-coated plate (0.1% fibronectin - 0.4% gelatin in PBS) 3×10^3 cells/cm² and cultured at 37°C in a cell culture incubator with 5% CO₂. Culture medium was replaced twice a week and once cells reached 80% confluency, they were trypsinized and split 1:3. Cells used in RNA-seq were between passage 3 and 5.

Immunocytochemical Characterization

To validate the identity of isolated SVPs we performed immunocytochemical characterization of the cultured cells for expression of neural/glial antigen 2 (NG2), platelet derived growth factor receptor- β (PDGFR β), GATA Binding Protein 4 (GATA4), CD31, CD146 and α -smooth muscle actin (α -SMA) (**Supplementary Figure 1**). SVPs were seeded at 5×10^3 cells/cm² on fibronectin/gelatin-coated plate chamber slides, after 24 hours (h) cells were washed with PBS and fixed with 4% PFA in PBS for 15 min at room temperature. When required (GATA4 and α -SMA), the cells were permeabilized with 0.1% Triton X-100 (Sigma-Aldrich) in PBS for 10 min at room temperature. Non-specific staining was blocked with 5% Fetal Bovine Serum (FBS) (GIBCO) in PBS for 30 min at room temperature. Following elimination of excess serum, the cells were exposed to the unconjugated primary antibodies at 4°C for 16 h: NG2 (1:100, Millipore AB-5320), PDGFR β (1:50, Santa Cruz SC-339), GATA4 (1:100, Abcam ab61767), CD31 (1:100, R&D BBA7), CD146 (1:100, Abcam ab75769), α -SMA (1:200, Dako M0851). After washing in PBS, the appropriate fluorescent secondary antibody (Alexa Fluor) diluted 1:200 in PBS was added to the cells

for 60 min at 37°C. Nuclei were stained with DAPI (Thermo Fisher Scientific) 1 µg/ml for 10 min at room temperature. Photos of random fields were taken at 20x magnification with Zeiss Observer Z1 inverted microscope.

In vitro Mechanical Stimulation of SVPs

To investigate the effect of mechanical strain on cultured cells, SVPs were subjected to cyclic strain using the FlexCell Tension Plus FX-5000T system. Before cell seeding, six-well uniaxial Bioflex plates were surface-coated with human fibronectin (10 µg/ml) in PBS after covalent crosslinking with a crosslinking reagent (sulfo-succinimidyl 6-(4'-azido-2'-nitrophenylamino) hexanoate; Sulfo-SANPAH) at 0.2 mg/ml in Hepes 50 mM (pH 8.5), photo-activated by exposure to UV-light (365 nm). Cells were subjected to uniaxial cyclic deformation protocol (0–10% deformation, 1 Hz frequency), for 24 and 72 h [according to a protocol established in (19)], while static controls were provided by seeding an equal amount of cells, under the same atmospheric conditions, but without mechanical stimulation (**Supplementary Figures 2A,B**). For imaging of mechanically stimulated SVPs, cells were fixed after 72 h of uniaxial cyclic straining with 4% PFA in PBS, and thereafter stained with Phalloidin-TRITC (1:500, Sigma) and DAPI 1 µg/ml (Thermo Fisher Scientific) at room temperature for 1 h.

Total RNA Isolation

For RNA-Seq analysis, total RNA was extracted from 5 different donors using RNeasy Mini kit (Qiagen). Cultured SVPs, approximately 4×10^5 to 5×10^5 cells per well, were resuspended in 700 µl of QIAzol Lysis Reagent (Qiagen) and residual DNA was removed by on-column DNase digestion. Total RNA was purified following the manufacturer's instructions and quantified by using NanoDrop-1000 spectrophotometer before integrity assessment with Agilent 2100 Bioanalyzer (RNA Integrity Number values >8).

RNA-Seq on *in vitro* Mechanical Stimulated SVPs

Next-generation sequencing experiments, including samples quality control and bioinformatics analysis, were performed by Genomix4life S.R.L. (Baronissi, Salerno, Italy). Indexed libraries were prepared from 500 ng/ea purified RNA with TruSeqStranded total RNA Sample Prep Kit (Illumina) according to the manufacturer's instructions. Libraries were quantified using the Agilent 2100 Bioanalyzer (Agilent Technologies) and Qubit fluorometer (Invitrogen Co.), then pooled such that each index-tagged sample was present in equimolar amounts, with a final concentration of the pooled samples of 2 nM. The pooled samples were subject to cluster generation and sequencing using an Illumina HiSeq 2,500 System (Illumina) in a 2 × 100 paired-end format at a final concentration of 8 pmol. The raw sequence files generated (.fastq files) underwent quality control analysis using FastQC (<http://www.bioinformatics.babraham.ac.uk/projects/fastqc/>) and the quality checked reads were trimmed with cutadapt v.1.10 and then aligned to the human genome (hg38 assembly) using STAR v.2.5.2, with standard parameters. Differentially expressed mRNAs were identified

using DESeq2 v.1.12. Gene annotation was obtained for all known genes in the human genome, as provided by GenCode (GRCh38.p7 release 25). Using the reads mapped to the genome, we calculated the number of reads mapping to each transcript with HT Seq-count v.0.6.1. These raw read counts were then used as input to DESeq2 for calculation of normalized signal for each transcript in the samples, and differential expression was reported as Fold Change along with associated adjusted *p*-values (computed according to Benjamini-Hochberg). Raw data of RNA-Seq that support the findings of this publication have been deposited in NCBI's Gene Expression Omnibus (22) and are accessible through GEO Series accession number GSE192712 (<https://www.ncbi.nlm.nih.gov/geo/query/acc.cgi?acc=GSE192712>).

RNA-Seq Data Pre-processing and Analysis

Upon inspection of quality control features with FastQC (version 0.11.8) [Andrews (2010). FastQC: a quality control tool for high throughput sequence data. Available online at: <http://www.bioinformatics.babraham.ac.uk/projects/fastqc>] and MultiQC (version 1.8), the raw sequencing reads were trimmed to remove adaptor contaminations, using Cutadapt (version 1.18) with the following parameters: cutadapt-a AGATCGGAAGAGCACACGTCTGAACTCCAGTCA -A AGATCGGAAGAGCGTCGTGTAGGGAAAGAGTGT -trim-n -pair-filter=any -minimum-length 20. Genome contamination screening was performed through FastQ Screen (version v0.14.0). The sequencing reads were, then, aligned to GENCODE's human reference genome (GRCh38 primary assembly v31) and quantified at the gene level using STAR (version 2.7.3a), with default parameters and allowing up to 3 mismatches.

Evaluation of sequencing alignment data was performed through Qualimap application (v.2.2.2-dev) (23), using the following analysis types: Multi-sample BAM QC, RNA-seq QC, and Counts QC.

RNA-Seq analysis was performed using DESeq2 package (version 1.22.2) (24) in the R software (version 3.6.3) [R Core Team (2020). R: A language and environment for statistical computing. R Foundation for Statistical Computing, Vienna, Austria. URL <https://www.R-project.org/>]. Samples were normalized for sequencing depth and RNA composition according to DESeq2 median of ratios method. Differential gene expression analysis was performed on genes that passed genefilter/DESeq2 independent filtering procedure ($\alpha = 0.05$). Genes showing a BH-adjusted *p*-value ≤ 0.05 and $\log_2\text{FoldChange} > 1.5$ or $\log_2\text{FoldChange} < -1.5$ were considered differentially expressed (DEGs).

For visualization purposes, counts were transformed using DESeq2 regularized log-transformation. DESeq2 plotPCA function was used for PCA analysis. Samples correlations were computed using the cor.dat function from the stats package (version 3.6.3). Heatmaps were plotted using the pheatmap package (version 1.0.12) [RaivoKolde (2019). pheatmap: Pretty Heatmaps. R package version 1.0.12. <https://CRAN.R-project.org/package=pheatmap>] and volcano plots with

the EnhancedVolcano package (version 1.4.0) [Kevin Blighe, Sharmila Rana and Myles Lewis (2019). EnhancedVolcano: Publication-ready volcano plots with enhanced coloring and labeling. R package version 1.4.0. <https://github.com/kevinblighe/EnhancedVolcano>] (BH-adjusted p -value cutoff = 0.05, FC cutoff = 1.5).

Motif-based TF prediction was performed in Cytoscape (version 3.8.0) running iRegulon App (25) on the complete set of differentially expressed genes in the dynamic vs. static conditions, with the following parameters: Motif collection = 10 K (9,713 PWMs), Track collection = 1,120 ChIP-seq tracks (ENCODE raw signals), min NEScore = 2, ROC threshold for AUC calculation (% = 3), max FDR = 0.05, Motif rankings database = 20 kb centered around TSS (7 species), Track rankings database = 20 kb centered around TSS (ChIP-seq derived).

DEGs from each contrast and the corresponding logFCs and adjusted p -values were uploaded to Ingenuity Pathways Analysis (IPA) software (version 60467501) (QIAGEN Inc.) (26). Core Analysis was performed using default settings: only protein-protein interaction networks, upstream regulators networks and Diseases and Biological Functions enriched pathways involving AMIGO2 were considered, along with evaluation of the IPA TGF- β signaling canonical pathway. Bubble plots were produced using ggplot2 package (version 3.3.2) [H. Wickham. ggplot2: Elegant Graphics for Data Analysis. Springer-Verlag New York, 2016.] in R.

Pathway enrichment analysis on DEGs at 24 h and 72 h was performed using Metascape (27) (Express Analysis), only pathways involving AMIGO2 gene were considered.

Porcine *in vivo* Model of Vein Graft Remodeling

In vivo studies were performed with Large White-Landrace cross pigs (weight 25 to 30 kg) using the saphenous vein-to-carotid artery interposition grafting model previously described (28). This investigation was performed in accordance with the Home Office Guidance on the operation of the Animals (Scientific Procedures) Act 1986 (HMSO, London, UK; PPL numbers 30/2585 and 30/3064) and was compliant with the EU Directive 2010/63/EU and principles stated in the Guide for the Care and Use of Laboratory Animals (Institute of Laboratory Animal Resources, 1996).

The animals were subjected to unilateral or bilateral autologous saphenous vein (SV) into common carotid artery bypass grafting. In brief, pigs were anesthetized with ketamine (Ketaset, 100 mg/mL), intubated, and maintained on 1–3% halothane under spontaneous ventilation. The animal was heparinized by intravenous administration of 100 IU/kg of heparin. The long saphenous vein was harvested from the hind leg using the “no touch” technique (29), rinsed in a saline solution containing 2 IU/mL heparin and 50 μ g/mL glyceryl trinitrate, and stored in the same solution at room temperature until needed. A 3-cm length of the vein was placed as an interposition graft to the internal carotid artery using continuous 7/0 Surgipro sutures. The flow was re-established and checked using a hand-held Doppler flow meter (Multidoplex II (model MD2), Huntleigh

Diagnostics Ltd, Cardiff, UK), and the animals were given antibiotic (ampicillin) and analgesic (buprenorphine) before and during recovery. The pigs were anesthetized and the SV grafts were collected at the established time points (1, 3, 7, 14, and 90 days), followed by euthanasia using an intra-cardiac overdose of pentobarbital. The grafts were fixed in 4% paraformaldehyde for 16 h and then embedded in paraffin for immunohistochemical analyses. Paraffin-embedded tissue sections were dehydrated and after blocking with 6% BSA for 1 h, incubated for 16 h at 4°C with the primary antibodies: AMIGO2 (1:100, Abcam ab84416) and α -SMA (1:150, Dako M0851) to enable the identification between the medial and adventitial layer. Subsequently, sections were incubated with appropriate secondary antibodies diluted 1:200 for 1 h at room temperature. Nuclei were stained with DAPI 1 μ g/mL for 10 min at room temperature. Digital images were obtained using an ApoTome fluorescence microscope or LSM-710 confocal scanning microscope (both Carl Zeiss, Germany). Cells positive for AMIGO2, counted in 3 fields *per* section, were expressed as a percentage of cells in the whole adventitia. Measurements and quantifications were performed using ImageJ (version 1.46r, National Institutes of Health, USA). Differences between time points were analyzed in GraphPad Prism 5 using ANOVA with Newman-Keuls *post hoc* test, with a significance level of 0.05.

Ex vivo Mechanical Stimulation of Human SV

SV segments for *ex vivo* culture were supplied from the Department of Cardiovascular Surgery at Centro Cardiologico Monzino. The veins were obtained from patients undergoing coronary artery bypass operations under protocols approved by the Ethical Committees of the Centro Cardiologico Monzino (Italy). Mechanical stimulation of SVs was performed using a custom-made bioreactor tailored to reproduce the coronary mechanics. SV were harvested with a “no-touch” technique (7) and stored at 4°C in DMEM supplemented with 10% FBS, 1% L-Glutamine, and 1% P/S. The *ex vivo* culture system exploited for veins stimulation was designed by Dipartimento di Elettronica, Informazione e Bioingegneria, Politecnico di Milano and Unità di Ingegneria Tissutale of Centro Cardiologico Monzino-IRCCS in Milan (30). This culture system allowed mimicking the arterial-like stimulation with a circumferential strain applied to the SV wall typical of the coronary circulation (31). Briefly, the arterial-like flow is accomplished in 4 independent phases: i) a loading step, ii) a pulsatile stimulation step, iii) an unloading step, and iv) a recirculation step. In the first phase, the vessel is filled with DMEM, 10% FBS, 1% L-Glutamine, and 1% P/S. During the pulsatile step, the medium is put under oscillating pressure between 80 mmHg and 120 mmHg and in the third phase the medium flows out of the vessels. The fourth phase is necessary to replace the medium inside the vein, thus maintaining stable nutrients and oxygen supply (17). The culture system was placed in a standard incubator at 37°C in a 5% CO₂ atmosphere and for a culture period of 14 days. Then, SV segments were unmounted from the culture system, fixed in formalin 37% for 16 h, and then embedded in paraffin for immunohistochemical

analyses. In brief, tissue sections were subjected to heat-induced antigen retrieval with 10 mM Sodium Citrate buffer pH 6.0 at 94°C for 30 min. Non-specific binding was blocked with 20% goat serum (Sigma-Aldrich) for 30 min at room temperature. Following the elimination of excess serum, the sections were exposed to the unconjugated primary antibodies at 4°C for 16 h: CD34 (1:50, R&D AF7227), AMIGO2 (1:200, Abcam ab84416), CD31 (1:50, R&D BBA7). After washing in PBS, the appropriate fluorescent secondary antibody (Alexa Fluor) diluted 1:200 in PBS was added to the cells for 60 min at 37°C. Nuclei were stained with DAPI (Thermo Fisher Scientific) 1 µg/ml for 10 min at room temperature. Photos were taken at 20x magnification with Zeiss Observer Z1 inverted microscope and reconstructed using Photoshop (Adobe) to obtain the adventitia-lumen image.

RESULTS

Cyclic Uniaxial Strain Induces Changes in the Transcriptome of Human SVPs

To assess the effect of mechanical stress on SVP transcriptome, we subjected cells to cyclic uniaxial strain (defined as dynamic, dyn, from now on) for 24 and 72 h compared to standard culture (static, stat) and performed RNA-Seq. This *in vitro* system allowed us to identify the early alterations in the transcription, underscoring the mechanisms associated. First, we conducted an unsupervised clustering of the results based on the top 100 most variables expressed genes in the different culture conditions. This analysis and principal component analysis (PCA) showed no stretch-related groupings among replicates (**Supplementary Figures 3A,B**). However, since the sequencing depth allowed us to quantify the expression of 28,624 genes that represent <50% of the ones annotated for *Homo sapiens* and include genes expressed at low levels, results may be non-consistent when performing differential expression analysis. Therefore, we next conducted a selection of genes expressed at reliable levels according to DESeq2 independent filtering procedure. The four datasets resulting from this filtering were paired in four comparisons to perform the differential expression analysis as follows: 1) 24 h dyn vs. 24 h stat, and 2) 72 h dyn vs. 72 h stat assessed the effect of strain at the two different time points 24 and 72 h; 3) 72 h stat vs. 24 h stat, and 4) 72 h dyn vs. 24 h dyn evaluated the effect of time on the culture conditions. These comparisons led to the following number of differentially expressed genes (DEGs): 1) 103 DEGs (24 h dyn vs. 24 h stat), 2) 819 DEGs (72 h dyn vs. 72 h stat), 3) 245 DEGs (72 h stat vs. 24 h stat), and 4) 72 DEGs in (72 h dyn vs. 24 h dyn) (**Supplementary Table 2**). We used hierarchical cluster analysis to assess the relationships between the DEGs in the four experimental conditions (**Figure 1**). As shown, the heatmaps built using the four different datasets indicated a major prevalence of DEGs in the static vs. dynamic conditions at 72 h. In addition, coherent differential regulation of genes was already observed at an earlier time point in dynamically strained vs. control cells for 24 h (**Figure 1A**). Moreover, a time-dependent effect both in static and dynamic conditions was observed (**Figures 1B,C**). The higher number of DEGs resulting

from the comparison between dynamic vs. static conditions at 72 h prompted us to further analyze the identity of the top-score genes up/downmodulated in this specific condition and to explore whether these genes were represented already at the earlier time point (24 h of stimulation). To this aim, we listed the 10 most up-regulated and the 10 most down-regulated genes in the 72 h dyn vs. 72 h stat condition (**Table 1**). These genes can be easily visualized in a volcano plot displaying the 819 DEGs arranged by fold change and Benjamini-Hochberg (BH)-adjusted *p*-value (**Figure 2**), they all had significantly higher expression (at least 1.5-fold more) than static controls along with a significant *p*-value (BH-adjusted *p*-value ≤ 0.05). In addition, **Table 2** shows the top regulated DEGs in the 24 h dyn vs. 24 h stat conditions. Only five genes were present in the top regulated lists at both time points representing candidates consistently regulated by mechanical stress in SVPs: Adhesion Molecule with Ig Like Domain 2 (*AMIGO2*), Serine/threonine-protein kinase 38-like (*STK38L*), Caveolae Associated Protein 4 (*CAVIN4*), Growth differentiation factor 5 (*GDF5*) and Polypeptide N-acetylgalactosaminyltransferase 15 (*GALNT15*) (**Table 3**).

Characterization of AMIGO2 Regulation Induced by Mechanical Stress in SVPs

Among the genes that appear to be involved in vascular biology/pathology, our interest focused on *AMIGO2*, a gene encoding for a cell surface type I transmembrane receptor, which is a member of a novel class of leucine-rich repeat (LRR) and Ig superfamily proteins (32). *AMIGO2* was identified for the first time in 2003, as an adhesion molecule necessary for the development of the axonal tract of neurons (33). Later, numerous other studies have reported *AMIGO2* expression in gastrointestinal tract cancers, revealing its anti-apoptotic and cell adhesion activities which bestow to the tumor cells a higher metastasis formation capacity (34–38). Therefore, considering that cell adhesion and migration are two of the main mechanisms involved in the reorganization of the SV wall during the formation of the neointima, we explored the putative functions of *AMIGO2* in mechanically stimulated SVPs and the signaling that may lie upstream of its differential expression at a transcriptional level.

First, we validated the RNA-Seq results using RT-qPCR on the same RNA pools used to perform the RNA-seq and on RNAs isolated from SVPs of different patients subjected to uniaxial strain. Results confirmed the overexpression of *AMIGO2* in the SVPs when mechanically stimulated (**Figure 3**).

We then investigated the regulation of *AMIGO2* in SVPs under mechanical stress by examining the DEGs in all data sets, taking into consideration the *AMIGO2*-associated expression processes, the interactions with other proteins, and the biological functions in which it is putatively involved. First, through iRegulon motif-based prediction we identified 8 transcription factors (TFs) potentially involved in *AMIGO2* expression regulation. Hierarchical clustering showed a partial grouping among SVPs samples after 24 h of strain, which becomes robust when considering the samples cultured for 72 h (**Figure 4**). Interestingly, 5 out of 8 TFs were related

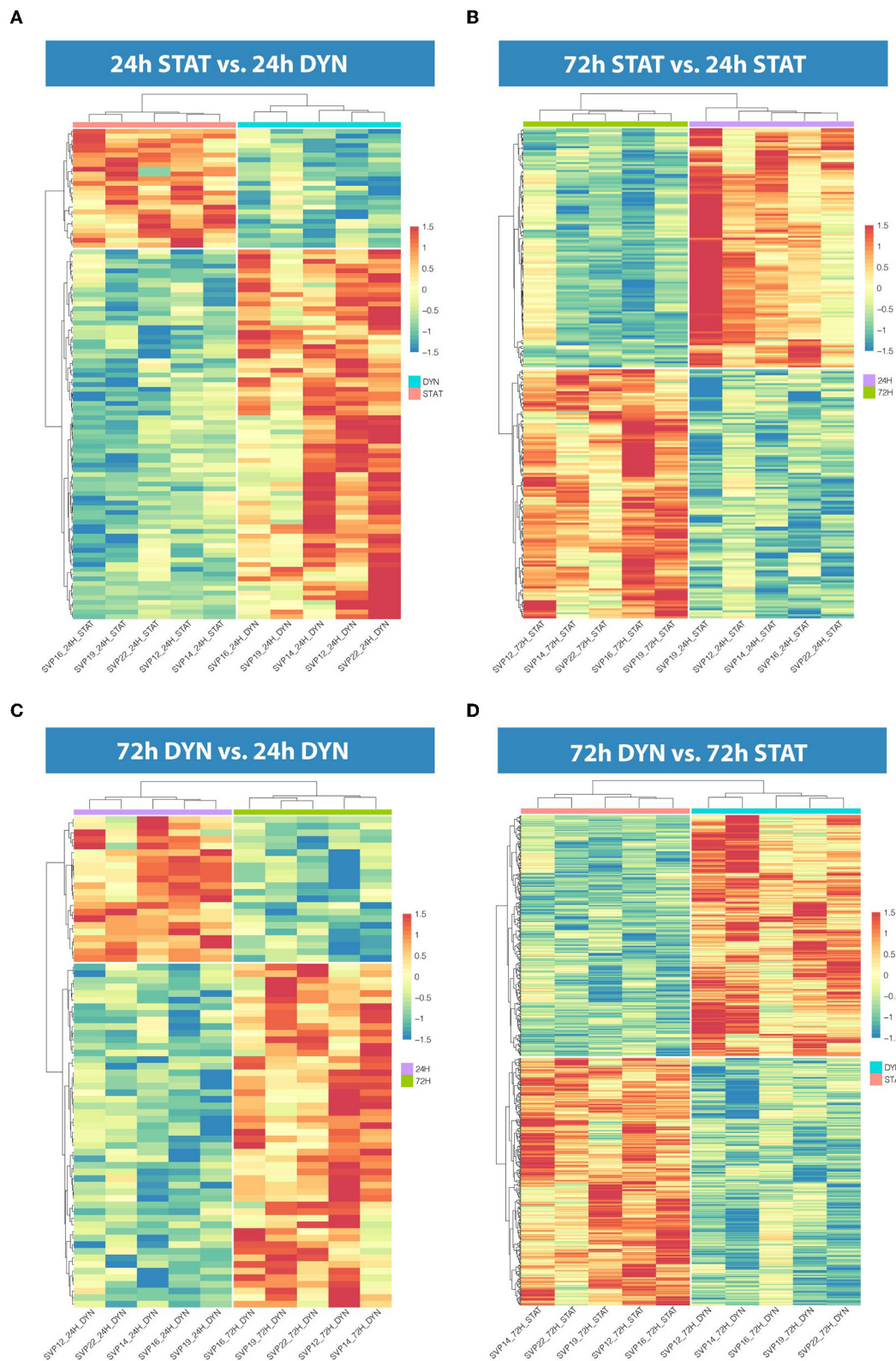
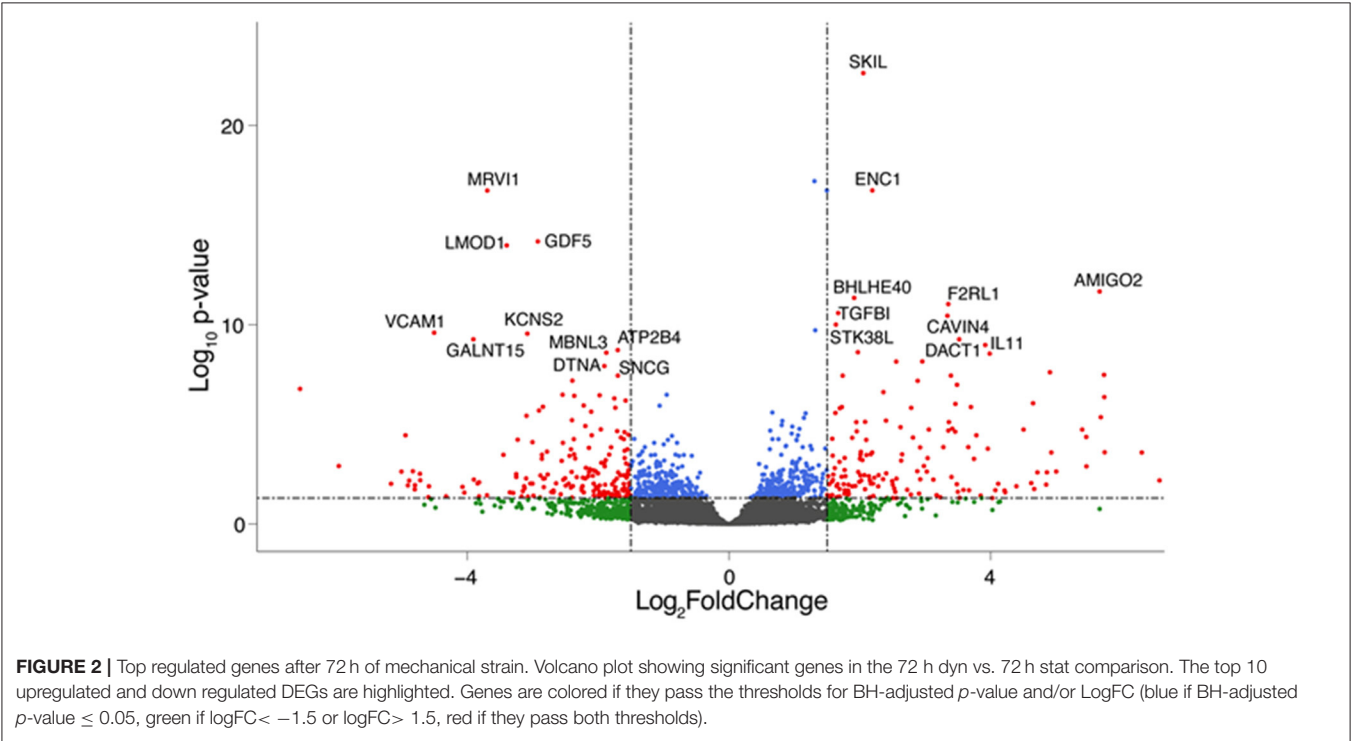


FIGURE 1 | Hierarchical clustering in the four comparisons. **(A)** Heatmap representation showing 103 DEGs in 24 h dyn vs. 24 h stat. **(B)** Heatmap representation showing 245 DEGs in 72 h stat vs. 24 h stat. **(C)** Heatmap representation showing 72 DEGs in 72 h dyn vs. 24 h dyn. **(D)** Heatmap representation showing 819 DEGs in 72 h dyn vs. 72 h stat. For all heatmaps BH-adjusted p -value ≤ 0.05 .

TABLE 1 | Top scored DEGs 72 h dyn vs. 72 h stat.

Top10 up-regulated DEGs – 72 h ON vs. 72 h OFF			Top10 down-regulated DEGs – 72 h ON vs. 72 h OFF		
Gene	Log ₂ FoldChange	P-value BH-adjusted	Gene	Log ₂ FoldChange	P-value BH-adjusted
SKIL	2.05	2.35E-23	MRV1	−3.69	1.84E-17
ENC1	2.19	1.82E-17	GDF5	−2.92	6.60E-15
AMIGO2	5.66	2.14E-12	LOMD1	−3.39	1.04E-14
BHLHE40	1.91	4.50E-12	VCAM1	−4.51	2.52E-10
F2RL1	3.35	9.19E-12	KCNS2	−3.08	2.79E-10
TGFB1	1.66	2.58E-11	GALNT15	3.91	5.39E-10
CAVIN4	3.33	3.55E-11	ATP2B4	−1.70	1.87E-09
STK38L	1.63	9.84E-11	MBNL3	−1.87	2.53E-09
DACT1	3.51	5.39E-10	DTNA	−1.90	1.18E-08
IL11	3.91	1.04E-09	SNCG	−1.70	3.58E-08



to transforming growth factor β (TGF- β) pathways (*RUNX1*, *PRDM1*, *SOX4*, *PPARG*, and *SMAD3*), known for modulating mesenchymal phenotype acquisition (39–43). The TF *CBFB* acts in coordination with *RUNX1* regulating the transcription of several genes, one of which is *NOTCH3* (44). *FOXD1* mediates gene expression of the cell during the reprogramming process (45). These activities combined with the negative effect of stretching on *TEF* expression suggest the switching of SVPs toward a proliferative phenotype (46). For a better understanding the effects of the mechanical stretching on the TGF- β pathway, we performed Ingenuity Pathway Analysis (IPA) at both 24 h dyn vs. 24 h stat (**Supplementary Figure 4**) and 72 h dyn vs. 72 h stat conditions (**Figure 5**). Through

pathway enrichment analysis for TGF- β signaling at 72 h dyn vs. 72 h stat, we were able to identify 36 genes associated with the TGF- β pathway that were down-regulated and 45 genes up-regulated (**Supplementary Figure 5**). To show relevant relationships between modulated genes we performed IPA analysis in the complete dataset. The topmost identified networks are shown in **Figures 6A,B**. In both comparisons 24 h dyn vs. 24 h stat and 72 h dyn vs. 72 h stat, *AMIGO2* expression was predicted to be controlled by *NR3C1*, the human glucocorticoid receptor gene, and *NEUROG1*, a regulator of neural progenitors’ differentiation (47, 48). Connections were also found for the mesenchymal oncogenes *FUS-DDIT3* at both time points and for *RASSF1* at 72 h (49, 50).

TABLE 2 | Top scored DEGs 24 h dyn vs. 24 h stat.

Top10 up-regulated DEGs – 24 h ON vs. 24 h OFF			Top10 down-regulated DEGs – 24 h ON vs. 24 h OFF		
Gene	Log ₂ FoldChange	P-value BH-adjusted	Gene	Log ₂ FoldChange	P-value BH-adjusted
CAVIN4	2.91	1.23E-04	ACKR4	–2.32	1.23E-04
AMIGO2	4.49	1.23E-04	GALNT15	–2.55	5.76E-04
EDN1	2.91	1.58E-04	ANKRD33B	–2.48	8.57E-03
KIA A 1755	2.68	4.60E-04	PDE7B	–1.55	1.46E-02
MIR503HG	2.73	5.75E-04	IFIT1	–1.67	1.46E-02
SMAD7	1.58	7.37E-04	FAM107A	–3.44	1.92E-02
TSPAN2	3.17	8.21E-04	TOX	–1.76	2.89E-02
COL7A1	2.42	1.23E-03	CENPP	–1.52	3.12E-02
STK38L	1.73	1.71E-03	ZNF367	–1.74	3.80E-02
ANGPTL4	1.62	2.78E-03	GDF5	–1.54	4.41E-02

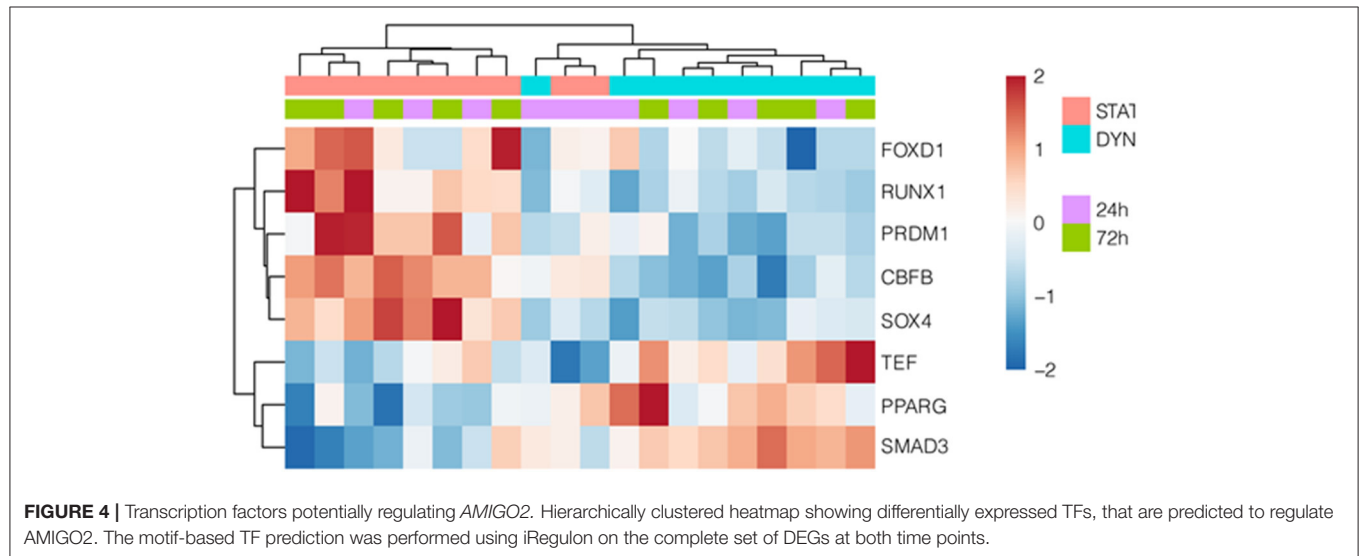
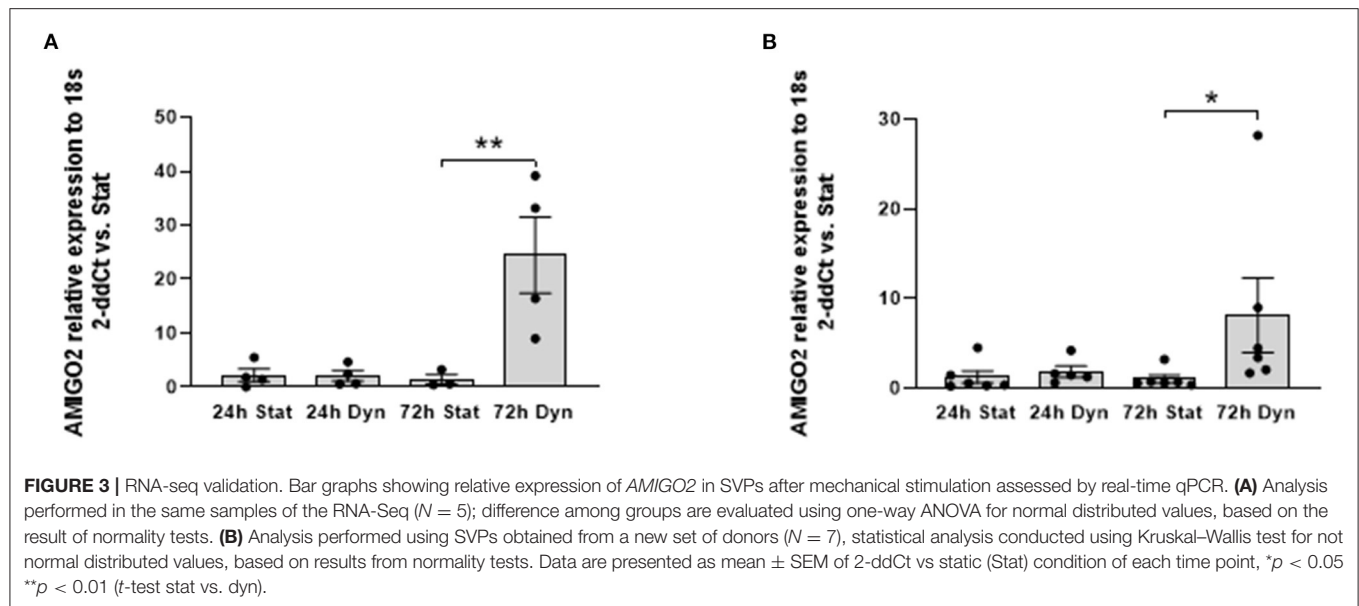
TABLE 3 | DEGs consistently regulated by mechanical stress.

Gene	Gene ID	Function	Log ₂ FoldChange	
			24 h	72 h
AMIGO2	347902	This gene encodes a cell receptor involved in axon extension and migration. Also described as a pro-survival factor in endothelial cells subjected to hypoxia and regulator of tumor cell adhesion and formation of metastases.	4.49	5.66
STK38L	23012	The encoded protein is a serine/threonine kinase 38 like, implicated in neuronal cytoskeletal development, neurite outgrowth and synaptic remodeling.	1.73	1.63
CAVIN4	347273	Cavin-4 protein modulates the morphology of formed caveolae, results activated the extracellular signal-regulated kinase pathway, influencing skeletal muscle differentiation, and to activate RhoA pathway, modulating cardiac function.	2.91	3.33
GDF5	8200	This is one of the earliest genes expressed in the embryonic joint interzone, fated to give rise to joint tissues. Gdf5-lineage mesenchymal stromal/stem cells are involved in cartilage repair.	–1.54	–2.92
GALNT15	117248	The encoded protein catalyzes the initial reaction in O-linked oligosaccharide biosynthesis	–2.55	–3.9

AMIGO2 Expression Is Associated With a Mechanical Strain-Mediated Phenotypic Shift in SVPs

To gain further insight into mechanical strain-associated changes in SVPs in relation to *AMIGO2* we analyzed the human protein-protein interaction networks by IPA (**Figures 7A,B**). In the 24 h dyn vs. 24 h stat comparison, *AMIGO2* was found connected to NFκB complex which was predicted up-regulated by the modulation of DEGs present in the network. After 72 h of culture, the specific modulation of several genes, including *AMIGO2*, suggested an interaction with Akt, which was predicted to be inhibited as a result of the stretch-dependent changes in the transcriptional profile of SVPs. This finding was in contrast with what has been reported in *AMIGO2*'s activation mechanism in endothelial cells (ECs) (36), and suggests that in SVPs *AMIGO2* could operate through different pathways, independent of PDK-Akt. Next, the effect of mechanical strain on the molecular and cellular functions of SVPs has been closely examined via Gene Ontology (GO) analysis of the 24 h dyn vs. 24 h stat

and 72 h dyn vs. 72 h stat conditions. **Table 4** shows the top 5 enriched pathways involving *AMIGO2*. The topmost function in SVPs stretched cells was cell-matrix adhesion (p -value 7.72×10^{-10}), along with chemotaxis (p -value 6.92×10^{-10}) and cell-cell adhesion via plasma-membrane adhesion molecules (p -value 2.07×10^{-10}), describing a potential switching of the SVPs phenotype toward migration. Ultimately, diseases and biological function-related pathways involving *AMIGO2* were obtained through IPA (**Figures 8A,B**). We observed an increase in the number of functions identified prolonging mechanical stress from 24 to 72 h. For example, the Cell Death and Survival macro-category after 24 h addressed only the regulation of apoptosis and necrosis, but after 72 h we also detected activation of cell viability and cell survival pathways. Of note, the cancer-related biofunctions were the most associated with *AMIGO2* at both time points, reflecting its potential role in tissue invasion and remodeling (34, 35, 37, 38). Thus, the investigations performed with iRegulon and IPA as well as the *AMIGO2*-related GO findings shed a light on how mechanical stress could produce a phenotypic switching in the SVPs, mediating their activation and

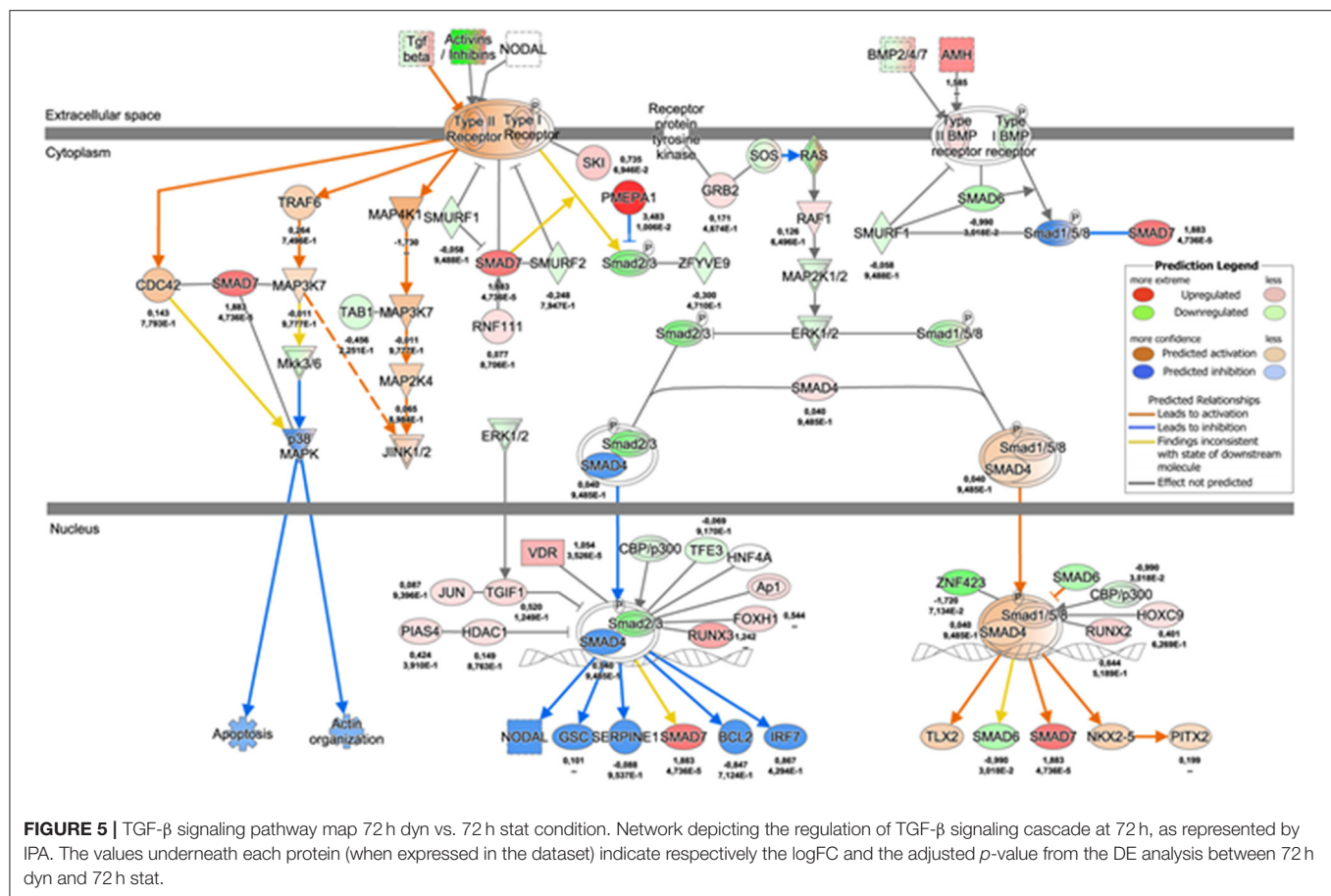


increasing their responsiveness to modifications occurring in the extracellular environment.

Arterial-Like Mechanic of SV Induces an Increase of *AMIGO2* Positive Cells Only in Long Term *in vivo* Model

Given that the cyclic mechanical stress on SVPs produced a significant overexpression of *AMIGO2* at the transcription level, we explored the effect of pulsatile coronary flow on *AMIGO2* protein expression. This was assessed in two experimental systems that we previously used to validate Thrombospondin-1 as a relevant target of mechanical stress in the human SV arterIALIZATION process (19). These consisted of an *in vivo* SV arterIALIZATION model, performed by surgical SV interposition

into carotid arteries in pigs, and of direct stimulation of human SVs using a coronary pulse duplicator that allows reproducing the mechanical conditions of the coronary circulation *in vitro*. Immunofluorescence staining was used to quantify the percentage of *AMIGO2* positive cells in pig SV native conduits (T0) and at 1, 7, 14, and 90 days after grafting into the carotid artery (Figure 9A). < 40% of the cells in the SV adventitia expressed *AMIGO2* at T0 ($37.13 \pm 5.84\%$, $N = 3$) (Figure 9B). This percentage remained relatively unaffected during the following 7 days after surgery. On day 14, the percentage reached almost 70% of the total cells of the adventitia ($69.35 \pm 3.52\%$, $N = 4$), but this was not statistically different from the previous time points. Only at day 90 post-surgery, we observed a significant increase of *AMIGO2* positive cells compared to T0, day 1, and day 7. In addition, we successfully



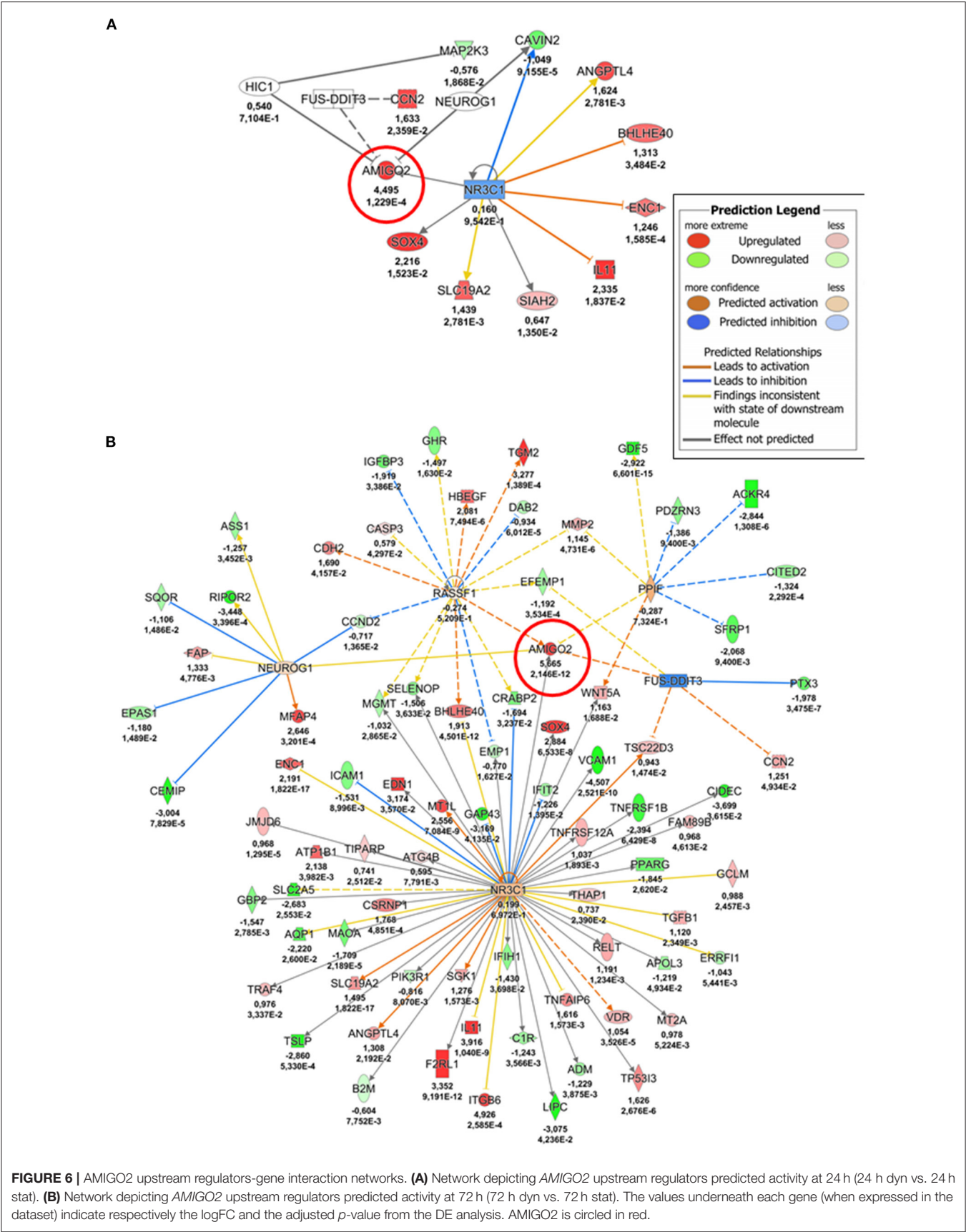
identified numerous AMIGO2 expressing cells in human SV, both in the untapped conduit (T0) and following the application of a pulsatile pressure regimen for 14 days in *ex vivo* culture (Figure 9C). It is interesting to note that in both experiments AMIGO2 expression was not restricted to the adventitia layer, but was also detected in several cells in the tunica media, as well as ECs. Particularly significant was the detection of AMIGO2/CD34 positive cells in the proximity of the *vasa vasorum*, where the SVPs are normally localized (21). The quantification of AMIGO2 expression in SVs from 4 different donors did not highlight any significant difference in the comparison T0 vs. Day 14 (data not shown). These data consolidate AMIGO2 as an important effector in the response to pathologic mechanical stress. Thus, despite the early AMIGO2 upregulation driven by the mechanical strain at 24 and 72 h in the SVPs, the protein increase in the adventitia appears to be delayed when the entire vein wall undergoes pulsatile arterial flow.

DISCUSSION

In this study, we showed for the first time that mechanical strain specifically alters the transcriptomic profile of human SVPs. The validation of the identified molecules and the further investigation of the molecular mechanisms associated with vein arterialization in specific cells is fundamental to developing

targeted preventive and curative strategies to combat the failure of bypass grafts.

The existing causal relationship between arterial hemodynamic and IH in vein grafts is long known and well-established (51). Experimental evidence demonstrated that when dissected veins are re-anastomosed to venous circulation they do not develop IH (52), while vein grafts transposed from the arterial circulation back to the venous flow exhibited the regression of IH (53, 54). Therefore, mechanical stress resulting from the coronary flow pattern is sufficient for the molecular setting of IH. Further validation of the detrimental role of coronary mechanical load on the integrity of the SV wall is provided by the significant reduction in IH and beneficial effects on vessel compliance exerted by external stenting or photochemical tissue passivation (20, 55). Recently we demonstrated the role of mechanical forces in the pathologic evolution of the human SV, identifying phenotypic switching of resident smooth muscle cells and the activation of TGF- β /Thrombospondin-1 signaling in the SV medial layer as the nexus between the fibrotic activation of vessel-resident cells and non-physiologic vessel perfusion (19). We also demonstrated that coronary flow mechanics endured by the SV induces progressive recruitment of SVPs from the adventitia and transition toward the medial layer. In the current study, we assessed the mechanical sensitivity of the SVPs themselves which, like resident smooth muscle cells, were



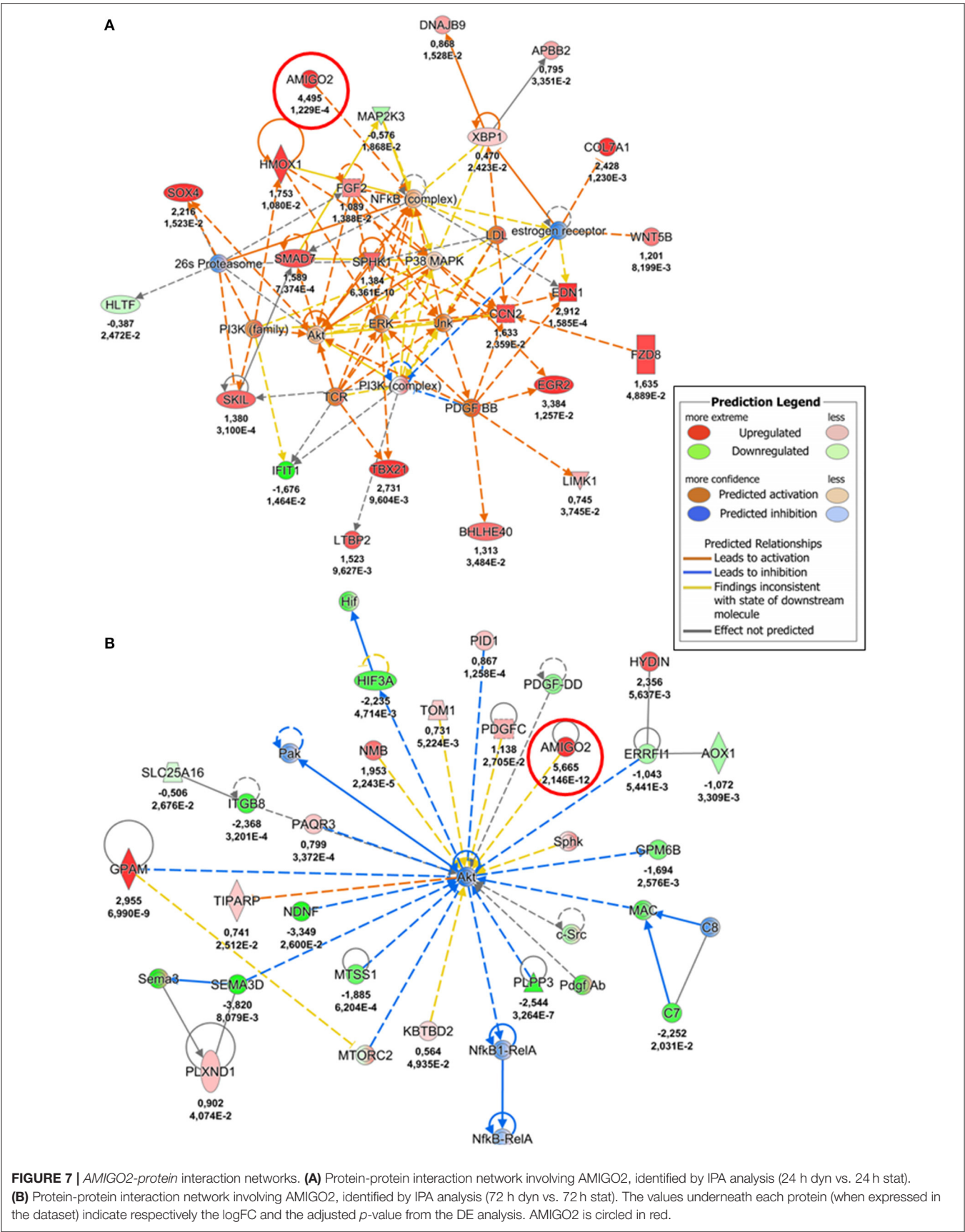


TABLE 4 | AMIGO2 related pathways regulation.

Term	Description	–Log10 value
GO:0098742	Cell-cell adhesion via plasma-membrane adhesion molecules	2.07
GO:0007160	Cell-matrix adhesion	7.72
GO:0044089	Positive regulation of cellular component biogenesis	3.74
GO:0006935	Chemotaxis	6.92
GO:0051962	Positive regulation of nervous system development	4.88

responsive to mechanical stress and thus may participate in the pathologic programming of the vein wall.

Using a platform that enables us to perform uniaxial strain *in vitro*, we subjected human primary culture amplified SVPs to a cyclic elongation pattern with a nominal deformation (10%) and a frequency (1 Hz) compatible with the predicted uniaxial strain component acting in SV wall (19). We then conducted a genome-wide RNA-Seq analysis to observe whether this stimulus was sufficient to elicit a robust change in SVPs gene expression. Through the analysis of DEGs in the four comparisons, two times of stimulation (24/72 h) and two experimental conditions (static/dynamic), we identified the 72 h dyn vs. 72 h stat as the most powerful in terms of transcriptomic alterations, with 819 DEGs. Interestingly, the variation in the transcriptome of SVPs subjected to mechanical stimulation occurred progressively and led to the identification of a few transcripts that were robustly up/downmodulated by mechanical treatment, highlighting them as “top scores” in the differentially expressed genes with possible important roles in SV pathologic programming.

Interestingly, this transcriptomic alteration is SVP-specific and potentially occurs before the phenotypic changes induced by paracrine signaling (17, 19). Moreover, SVP response to mechanical strain is similar to what has been observed in smooth muscle cells and ECs when comparable mechanical stress was applied (56). Several studies have demonstrated that cyclic strain exerts an effect on cellular proliferation, but there is no agreement with regard of this effect increases or reduces cell mitosis (56). Our results showed the activation in SVPs of apoptosis and necrosis pathways after 24 h with the addition of necrosis of epithelial tissue, neuronal cell death, cell viability, and cell survival pathways after 72 h of mechanical stress. This rather conflicting data would require further analysis. However, in the physiological environment of SV subjected to arterial flow, the paracrine signaling seems to generate a positive effect on SVPs proliferation, mainly through TGF- β and TSP-1 (19).

Among the DEGs, we found particularly interesting the upregulation of *AMIGO2* for its putative role in intercellular communication and cell migratory activity, one of the functions which appear to be activated in SVPs by mechanical straining. *AMIGO2* was first described in the development and survival of the nervous system, although following studies discovered numerous activities related to its expression in different cell phenotypes (33–38). *AMIGO2* belongs to the leucine-rich repeat (LRR) protein superfamily. LRR proteins share a common

structural framework of 20 to 30 amino acids rich in the hydrophobic amino acid leucine (57). This family includes intracellular, extracellular, and membrane proteins with a wide range of functions such as cell adhesion, signaling, extracellular matrix assembly, RNA processing, and immune response. *AMIGO2* acts as a cell adhesion molecule involved in signal transduction and, like other LRR proteins, functions mainly through homophilic and heterophilic interactions with proteins of the same family, i.e. *AMIGO* and *AMIGO3* (32, 34). It has been reported that in ECs and in gastric adenocarcinoma cell lines the inhibition of *AMIGO2* affected the ability to adhere to extracellular matrix components (34, 36). Moreover, Hossain et al. demonstrated the presence of *AMIGO2* in human microvascular ECs and pericytes, pointing to an interaction between these cells in vascular remodeling (58). In mechanically stressed SVPs the up-regulation of *AMIGO2* could confer a firmer adhesion to adhesion substrates but also enhance their sensitivity to modifications of the extracellular matrix. Since mechanical strain during IH induces the remodeling of LLR proteins (such as biglycan, versican, and decorin) (59–62), *AMIGO2* could participate in SVP migration across the SV wall as observed in our previous study. This hypothesis is further supported by our GO analysis performed to identify the top regulated molecular functions enriched with *AMIGO2* showing that in stretched SVPs cell-matrix adhesion, chemotaxis, and cell-cell adhesion via plasma-membrane adhesion molecules pathways were significantly up-regulated compared to static cultures, and by our unpublished evidences showing that mechanically strained-SVPs have a higher migratory mobility (Garoffolo et al., in preparation). Moreover, this finding is coherent to the invasive behavior that *AMIGO2* expression provides to tumor cells in the formation of metastasis (34, 35, 37, 38). Furthermore, a protein belonging to the LLR family, TSP-1, was already described as SVP's migration drive r (19). Notably, motif-based prediction of TFs potentially regulating *AMIGO2* revealed the presence of 5 TFs involved in TGF- β pathway. Previous studies reported that arterial-mimicking pressure elevates the expression of TGF- β in the SV and that TGF- β directly influences both ECs and SVPs, increasing the expression of SMC/mesenchymal differentiation markers and proliferation (19, 63). In addition, the presence of *AMIGO2* positive cells in the tunica media and not only the adventitia of the *ex vivo* stimulated human SVs and of *in vivo* arterialized pig SVs strongly suggest the involvement of the protein in a fibrotic process of the vessel wall controlled by mechanical-dependent

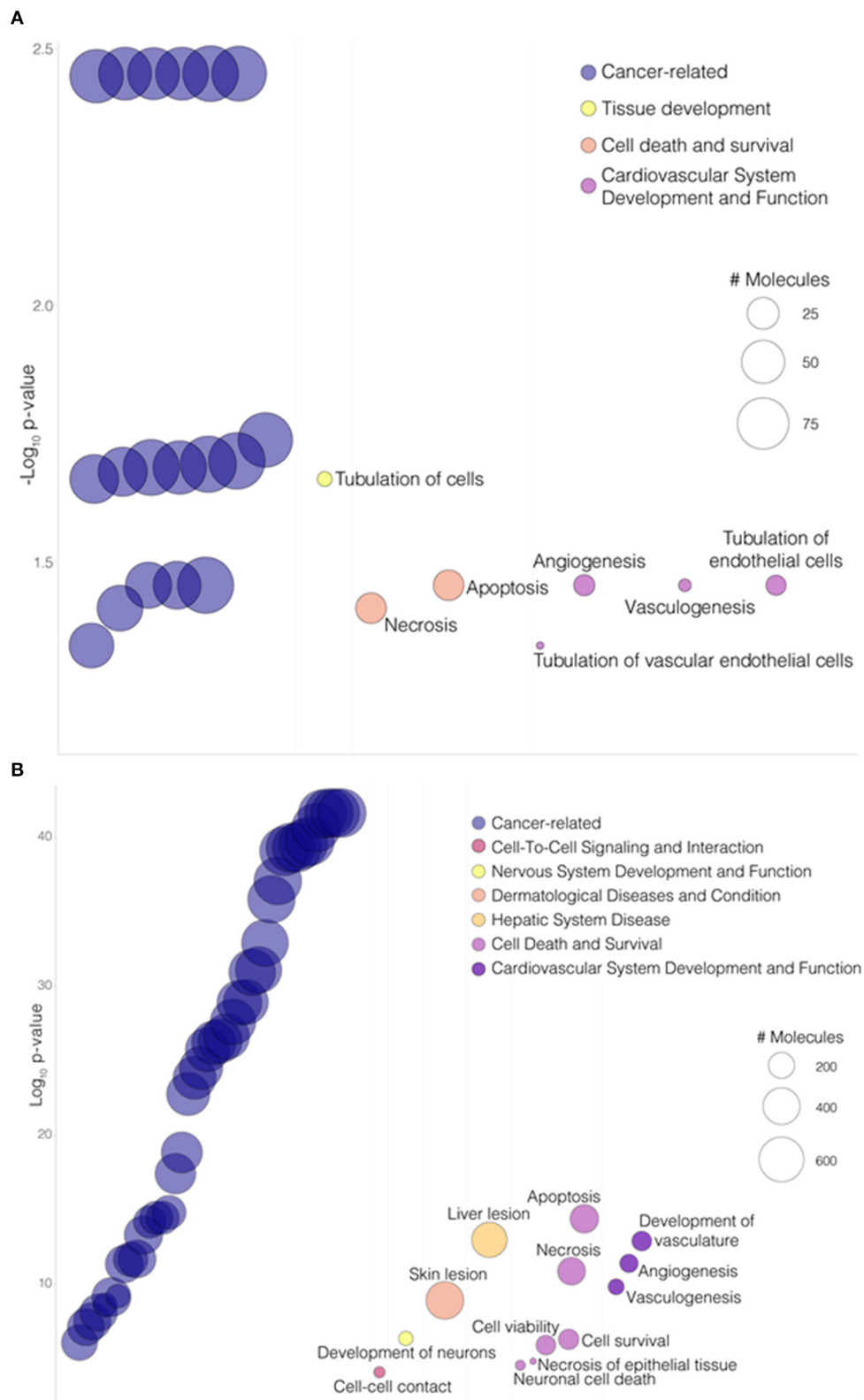


FIGURE 8 | AMIGO2 associated functions. **(A)** Bubbleplot portraying a selection of “Diseases and Biological Functions” enriched pathways involving AMIGO2 from IPA analysis, in the 24 h dyn vs. 24 h stat comparison. **(B)** Bubbleplot portraying a selection of “Diseases and Biological Functions” enriched pathways involving AMIGO2 from IPA analysis, in the 72 h dyn vs. 72 h stat comparison. Pathways are organized by macro-categories on the x-axis and ordered by $-\log_{10}$ BH-adjusted p -value on the y-axis. The bubble size is proportional to the number of molecules involved in the pathway.

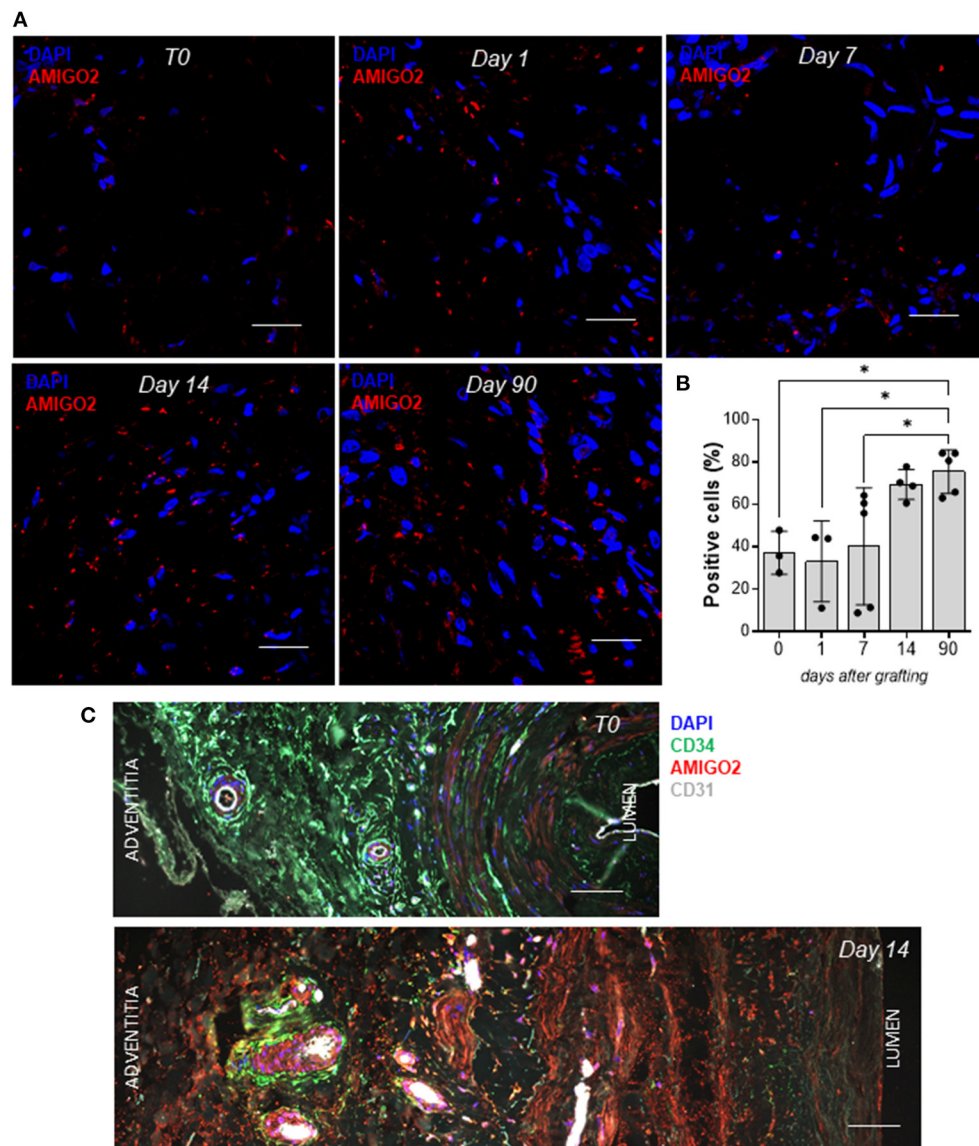


FIGURE 9 | AMIGO2 expression in vein graft remodeling. **(A)** Confocal microscopy analysis of paraffin-embedded porcine SVs for AMIGO2 (red) expression, nuclei are labeled with DAPI. Scale bar indicates 20 μm . **(B)** Bar graphs showing the percentage of AMIGO2 positive cells in porcine SV adventitia after grafting into the carotid artery (T0: $N = 3$, Day 1: $N = 3$, Day 7: $N = 5$, Day 14: $N = 4$, Day 90: $N = 5$; all data shown as Mean \pm SEM, * = $p < 0.05$). **(C)** Confocal microscopy analysis of paraffin-embedded human SVs for CD34 (green), AMIGO2 (red), CD31 (white), nuclei are labeled with DAPI. Scale bar indicates 50 μm .

pathways. Finally, we believe it would be worthy to investigate if the proneuronal transcription factor NEUROG1 (64) and the glucocorticoid receptor NR3C1 (48) play a role in the SVs differentiation toward intimal hyperplasia onset in the context of mechanical stress.

In summary, our results concur to a better understanding of the mechanisms underlying the SV remodeling and reveal a novel target for future investigations. In particular, new studies are warranted to assess the regulation of AMIGO2 within the combination of mechanical and paracrine stimuli,

such as TGF- β , to support the relevance of mechanically activated pathways in the onset and the progression of vein graft disease.

DATA AVAILABILITY STATEMENT

The datasets presented in this study can be found in online repositories. The names of the repository/repository and accession number(s) can be found below: <https://www.ncbi.nlm.nih.gov/GSE192712>.

ETHICS STATEMENT

This study was reviewed and approved by the Local Ethical Committee at Centro Cardiologico Monzino, IRCCS. All subjects gave their written informed consent to participate. The animal study was performed in accordance with the Home Office Guidance on the Operation of the Animals (Scientific Procedures) Act 1986 (HMSO, London, UK; PPL numbers 30/2585 and 30/3064) and was compliant with the EU Directive 2020/63/EU and principles stated in the Guide for the Care and Use of Laboratory Animals (Institute of Laboratory Animal Resources, 1996).

AUTHOR CONTRIBUTIONS

DM, GG, AT, MR, and RV performed experiments and analyzed data. GC analyzed data. MP, PM, and GS conceived the study. DM and GS wrote the paper. All authors contributed to the article and approved the submitted version.

REFERENCES

- Head SJ, Milojevic M, Taggart DP, Puskas JD. Current practice of state-of-the-art surgical coronary revascularization. *Circulation*. (2017) 136:1331–45. doi: 10.1161/CIRCULATIONAHA.116.022572
- Raja SG, Haider Z, Ahmad M, Zaman H. Saphenous vein grafts: To use or not to use? *Hear Lung Circ*. (2004) 13:150–6. doi: 10.1016/j.hlc.2004.03.013
- Osgood MJ, Hocking KM, Voskresensky I V., Li FD, Komalavilas P, Cheung-Flynn J, Brophy CM. Surgical vein graft preparation promotes cellular dysfunction, oxidative stress, and intimal hyperplasia in human saphenous vein. *J Vasc Surg*. (2014). 60: 202–11. doi: 10.1016/j.jvs.2013.06.004
- Locker C, Schaff H V, Dearani JA, Joyce LD, Park SJ, Burkhardt HM, et al. Multiple arterial grafts improve late survival of patients undergoing coronary artery bypass graft surgery: analysis of 8,622 patients with multivessel disease. *Circulation*. (2012) 126:1023–30. doi: 10.1161/CIRCULATIONAHA.111.084624
- Shukla N, Jeremy JY. Pathophysiology of saphenous vein graft failure: A brief overview of interventions. *Curr Opin Pharmacol*. (2012) 12:114–20. doi: 10.1016/j.coph.2012.01.001
- Wallitt EJW, Jevon M, Hornick PI. Therapeutics of Vein Graft Intimal Hyperplasia: 100 Years On. *Ann Thorac Surg*. (2007) 84:317–23. doi: 10.1016/j.athoracsurg.2007.02.035
- Dashwood MR, Tsui JC. “No-touch” saphenous vein harvesting improves graft performance in patients undergoing coronary artery bypass surgery: a journey from bedside to bench. *Vascul Pharmacol*. (2013) 58:240–50. doi: 10.1016/j.vph.2012.07.008
- Davies MG, Hagen PO. Reprinted Article “pathophysiology of vein graft failure: a review.” *Eur J Vasc Endovasc Surg*. (2011) 42. S19–29. doi: 10.1016/j.ejvs.2011.06.013
- Bouten CVC, Dankers PYW, Driessen-Mol A, Pedron S, Brizard AMA, Baaijens FPT. Substrates for cardiovascular tissue engineering. *Adv Drug Deliv Rev*. (2011) 63:221–41. doi: 10.1016/j.addr.2011.01.007
- Malek AM, Alper SL, Izumo S. Hemodynamic shear stress and its role in atherosclerosis. *J Am Med Assoc*. (1999) 282:2035–42. doi: 10.1001/jama.282.21.2035
- Davies MG, Klyachkin ML, Dalen H, Massey MF, Svendsen E, Hagen PO. The integrity of experimental vein graft endothelium-implications on the etiology of early graft failure. *Eur J Vasc Surg*. (1993) 7:156–65. doi: 10.1016/S0950-821X(05)80756-X
- Tai NR, Salacinski HJ, Edwards A, Hamilton G, Seifalian AM. Compliance properties of conduits used in vascular reconstruction. *Br J Surg*. (2000) 87:1516–24. doi: 10.1046/j.1365-2168.2000.01566.x

FUNDING

Funding/financial support was obtained from the Italian Ministry of Health, Ricerca Corrente to the IRCCS MultiMedica and Ricerca Finalizzata 2011 (project code: RF-2011-02346867) and was also supported by the Heart Research UK grant ‘Targeting pericytes for halting pulmonary hypertension in infants with congenital heart disease’ (R102602).

ACKNOWLEDGMENTS

We would like to thank Genomix4Life S.r.l., especially the technical team, for their support.

SUPPLEMENTARY MATERIAL

The Supplementary Material for this article can be found online at: <https://www.frontiersin.org/articles/10.3389/fcvm.2022.884031/full#supplementary-material>

- Fry DL. Acute vascular endothelial changes associated with increased blood velocity gradients. *Circ Res*. (1968) 22:165–97. doi: 10.1161/01.RES.22.2.165
- Newby AC, Zaltsman AB. Molecular mechanisms in intimal hyperplasia. *J Pathol*. (2000) 190:300–9. doi: 10.1002/(SICI)1096-9896(200002)190:3<300::AID-PATH596>3.0.CO;2-I
- Ward AO, Caputo M, Angelini GD, George SJ, Zakkar M. Activation and inflammation of the venous endothelium in vein graft disease. *Atherosclerosis*. (2017) 265:266–74. doi: 10.1016/j.atherosclerosis.2017.08.023
- O’Callaghan CJ, Williams B. Mechanical strain-induced extracellular matrix production by human vascular smooth muscle cells: role of TGF- β 1. *Hypertension*. (2000) 36:319–24. doi: 10.1161/01.HYP.36.3.319
- Prandi F, Piola M, Soncini M, Colussi C, D’Alessandra Y, Penza E, et al. Adventitial vessel growth and progenitor cells activation in an ex vivo culture system mimicking human saphenous vein wall strain after coronary artery bypass grafting. *PLoS ONE*. (2015) 10:e0117409. doi: 10.1371/journal.pone.0117409
- McGeachie J, Campbell P, Prendergast F. Vein to artery grafts. A quantitative study of revascularization by vasa vasorum and its relationship to intimal hyperplasia. *Ann Surg*. (1981) 194:100–7. doi: 10.1097/0000658-198107000-00018
- Garoffolo G, Ruiter MS, Piola M, Broschi M, Thomas AC, Agrifoglio M, et al. Coronary artery mechanics induces human saphenous vein remodelling via recruitment of adventitial myofibroblast-like cells mediated by thrombospondin-1. *Theranostics*. (2020) 10:2597–611. doi: 10.7150/thno.40595
- Salinas HM, Khan SI, McCormack MC, Fernandes JR, Gfrerer L, Watkins MT, Redmond RW, Austen WG. Prevention of vein graft intimal hyperplasia with photochemical tissue passivation. *J Vasc Surg*. (2017) 65:190–196. doi: 10.1016/j.jvs.2015.11.049
- Campagnolo P, Cesselli D, Al Haj Zen A, Beltrami AP, Kränkel N, Katare R, et al. Human adult vena saphena contains perivascular progenitor cells endowed with clonogenic and proangiogenic potential. *Circulation*. (2010) 121:1735–45. doi: 10.1161/CIRCULATIONAHA.109.899252
- Edgar R, Domrachev M, Lash AE. Gene expression omnibus: NCBI gene expression and hybridization array data repository. *Nucleic Acids Res*. (2002) 30:207–10. doi: 10.1093/nar/30.1.207
- Ewels P, Magnusson M, Lundin S, Källér M. MultiQC: Summarize analysis results for multiple tools and samples in a single report. *Bioinformatics*. (2016) 32:3047–8. doi: 10.1093/bioinformatics/btw354

24. Love MI, Huber W, Anders S. Moderated estimation of fold change and dispersion for RNA-seq data with DESeq2. *Genome Biol.* (2014) 15:550. doi: 10.1186/s13059-014-0550-8
25. Janky R, Verfaillie A, Imrichová H, van de Sande B, Standaert L, Christiaens V, et al. iRegulon: From a Gene List to a Gene Regulatory Network Using Large Motif and Track Collections. *PLoS Comput Biol.* (2014) 10:e1003731. doi: 10.1371/journal.pcbi.1003731
26. Krämer A, Green J, Pollard J, Tugendreich S. Causal analysis approaches in ingenuity pathway analysis. *Bioinformatics.* (2014) 30:523–30. doi: 10.1093/bioinformatics/btt703
27. Zhou Y, Zhou B, Pache L, Chang M, Khodabakhshi AH, Tanaseichuk O, et al. Metascape provides a biologist-oriented resource for the analysis of systems-level datasets. *Nat Commun.* (2019) 10:1–10. doi: 10.1038/s41467-019-09234-6
28. Angelini GD, Bryan AJ, Williams HMJ, Morgan R, Newby AC. Distention promotes platelet and leukocyte adhesion and reduces short-term patency in pig arteriovenous bypass grafts. *J Thorac Cardiovasc Surg.* (1990) 99:433–9. doi: 10.1016/S0022-5223(19)36973-9
29. Thomas AC, Wyatt MJ, Newby AC. Reduction of early vein graft thrombosis by tissue plasminogen activator gene transfer. *Thromb Haemost.* (2009) 102:145–52. doi: 10.1160/TH08-11-0772
30. Piola M, Ruiter M, Vismara R, Mastrullo V, Agrifoglio M, Zanobini M, et al. Full mimicking of coronary hemodynamics for ex-vivo stimulation of human saphenous veins. *Ann Biomed Eng.* (2017) 45:884–97. doi: 10.1007/s10439-016-1747-7
31. Piola M, Prandi F, Bono N, Soncini M, Penza E, Agrifoglio M, et al. compact and automated ex vivo vessel culture system for the pulsatile pressure conditioning of human saphenous veins. *J Tissue Eng Regen Med.* (2016) 10:E204–15. doi: 10.1002/term.1798
32. Kuja-Panula J, Kiiltomäki M, Yamashiro T, Rouhiainen A, Rauvala H, AMIGO. a transmembrane protein implicated in axon tract development, defines a novel protein family with leucine-rich repeats. *J Cell Biol.* (2003) 160:963–73. doi: 10.1083/jcb.200209074
33. Ono T, Sekino-Suzuki N, Kikkawa Y, Yonekawa H, Kawashima S. Alivin 1, a novel neuronal activity-dependent gene, inhibits apoptosis and promotes survival of cerebellar granule neurons. *J Neurosci.* (2003) 23:5887–96. doi: 10.1523/JNEUROSCI.23-13-05887.2003
34. Rabenau KE, O'Toole JM, Bassi R, Kotanides H, Witte L, Ludwig DL, et al. DEGA/AMIGO-2, a leucine-rich repeat family member, differentially expressed in human gastric adenocarcinoma: effects on ploidy, chromosomal stability, cell adhesion/migration and tumorigenicity. *Oncogene.* (2004) 23:5056–67. doi: 10.1038/sj.onc.1207681
35. Tsoi LC, Qin T, Slate EH, Zheng WJ. Consistent Differential Expression Pattern (CDEP) on microarray to identify genes related to metastatic behavior. *Acta Vet Scand.* (2011) 53:438. doi: 10.1186/1471-2105-12-438
36. Park H, Lee S, Shrestha P, Kim J, Park JA, Ko Y, et al. AMIGO2, a novel membrane anchor of PDK1, controls cell survival and angiogenesis via Akt activation. *J Cell Biol.* (2015) 211:619–37. doi: 10.1083/jcb.2015.03113
37. Kanda Y, Osaki M, Onuma K, Sonoda A, Kobayashi M, Hamada J, et al. Amigo2-upregulation in tumour cells facilitates their attachment to liver endothelial cells resulting in liver metastases. *Sci Rep.* (2017) 7:1–13. doi: 10.1038/srep43567
38. Nakamura S, Kanda M, Shimizu D, Tanaka C, Inokawa Y, Hattori N, et al. AMIGO2 expression as a potential prognostic biomarker for gastric cancer. *Anticancer Res.* (2020) 40:6713–21. doi: 10.21873/anticancer.14694
39. Kim W, Barron DA, Martin RS, Chan KS, Tran LL, Yang F, et al. RUNX1 is essential for mesenchymal stem cell proliferation and myofibroblast differentiation. *Proc Natl Acad Sci U S A.* (2014) 111:13389–6394. doi: 10.1073/pnas.1407097111
40. Romagnoli M, Belguisse K, Yu Z, Wang X, Landesman-Bollag E, Seldin DC, et al. Epithelial-to-mesenchymal transition induced by TGF- β 1 is mediated by blimp-1-dependent repression of BMP-5. *Cancer Res.* (2012) 72:6268–78. doi: 10.1158/0008-5472.CAN.12-2270
41. Peng X, Liu G, Peng H, Chen A, Zha L, Wang Z. SOX4 contributes to TGF- β -induced epithelial–mesenchymal transition and stem cell characteristics of gastric cancer cells. *Genes Dis.* (2018) 5:49–61. doi: 10.1016/j.gendis.2017.12.005
42. Kim SG, Kim HA, Jong HS, Park JH, Kim NK, Hong SH, et al. The endogenous ratio of Smad2 and Smad3 influences the cytostatic function of Smad3. *Mol Biol Cell.* (2005) 16:4672–83. doi: 10.1091/mbc.e05-01-0054
43. Reka AK, Kurapati H, Narala VR, Bommer G, Chen J, Standiford TJ, et al. Peroxisome proliferator-activated receptor- γ activation inhibits tumor metastasis by antagonizing smad3-mediated epithelial–mesenchymal transition. *Mol Cancer Ther.* (2010) 9:3221–32. doi: 10.1158/1535-7163.MCT-10-0570
44. Malik N, Yan H, Moshkovich N, Palangat M, Yang H, Sanchez V, et al. The transcription factor CBFB suppresses breast cancer through orchestrating translation and transcription. *Nat Commun.* (2019) 10:1–15. doi: 10.1038/s41467-019-10102-6
45. Koga M, Matsuda M, Kawamura T, Sogo T, Shigeno A, Nishida E, et al. Foxd1 is a mediator and indicator of the cell reprogramming process. *Nat Commun.* (2014) 5:1–9. doi: 10.1038/ncomms4197
46. Yang J, Wang B, Chen H, Chen X, Li J, Chen Y, Yuan D, Zheng S. Thyrotroph embryonic factor is downregulated in bladder cancer and suppresses proliferation and tumorigenesis via the AKT/FOXOs signalling pathway. *Cell Prolif.* (2019) 52: e12560. doi: 10.1111/cpr.12560
47. Palma-Gudiel H, Córdova-Palamera A, Leza JC, Fañanás L. Glucocorticoid receptor gene (NR3C1) methylation processes as mediators of early adversity in stress-related disorders causality: a critical review. *Neurosci Biobehav Rev.* (2015) 55:520–35. doi: 10.1016/j.neubiorev.2015.05.016
48. MuhChyi C, Juliandi B, Matsuda T, Nakashima K. Epigenetic regulation of neural stem cell fate during corticogenesis. *Int J Dev Neurosci.* (2013) 31:424–33. doi: 10.1016/j.ijdevneu.2013.02.006
49. Bennani-Baiti IM. Epigenetic and epigenomic mechanisms shape sarcoma and other mesenchymal tumor pathogenesis. *Epigenomics.* (2011) 3:715–32. doi: 10.2217/epi.11.93
50. Pérez-Mancera PA, Sánchez-García I. Understanding mesenchymal cancer: The liposarcoma-associated FUS-DDIT3 fusion gene as a model. *Semin Cancer Biol.* (2005) 15:206–14. doi: 10.1016/j.semcancer.2005.01.006
51. Owens CD. Adaptive changes in autogenous vein grafts for arterial reconstruction: Clinical implications. *J Vasc Surg.* (2010) 51:736–46. doi: 10.1016/j.jvs.2009.07.102
52. Brody WR, Angeli WW, Kosek JC. Histologic fate of the venous coronary artery bypass in dogs. *Am J Pathol.* (1972) 66:111–30.
53. Davies MG, Fulton GJ, Svendsen E, Hagen PO. Time course of the regression of intimal hyperplasia in experimental vein grafts. *Cardiovasc Pathol.* (1999) 8:161–8. doi: 10.1016/S1054-8807(98)00029-5
54. Fann JJ, Sokoloff MH, Sarris GE, Yun KL, Kosek JC, Miller DC. The reversibility of canine vein-graft arterIALIZATION. *Circulation.* (1990) 82:IV9–18.
55. Moodley L, Franz T, Human P, Wolf MF, Bezuidenhout D, Scherman J, et al. Protective constriction of coronary vein grafts with knitted nitinol. *Eur J Cardio-thoracic Surg.* (2013) 44:64–71. doi: 10.1093/ejcts/ezs670
56. Riha GM, Lin PH, Lumsden AB, Yao Q, Chen C. Roles of hemodynamic forces in vascular cell differentiation. *Ann Biomed Eng.* (2005) 33:772–9. doi: 10.1007/s10439-005-3310-9
57. Bella J, Hindle KL, McEwan PA, Lovell SC. The leucine-rich repeat structure. *Cell Mol Life Sci.* (2008) 65:2307–33. doi: 10.1007/s00018-008-8019-0
58. Hossain S, Ahmed MU, Alam S, Watanabe A, Harashima A, Yonekura H, Yamamoto H. Expressions and roles of AMIGO gene family in vascular endothelial cells. *Int J Biosci Biochem Bioinforma.* (2012) 10:1–5. doi: 10.7763/IJBBS.2012.V2.58
59. Scott L, Kerr A, Haydock D, Merrilees M. Subendothelial proteoglycan synthesis and transforming growth factor beta distribution correlate with susceptibility to atherosclerosis. *J Vasc Res.* (1997) 34:365–77. doi: 10.1159/000159245
60. Hocking AM, Shinomura T, McQuillan DJ. Leucine-rich repeat glycoproteins of the extracellular matrix. *Matrix Biol.* (1998) 17:1–19. doi: 10.1016/S0945-053X(98)90121-4

61. Lee RT, Yamamoto C, Feng Y, Potter-Perigo S, Briggs WH, Landschulz KT, et al. Mechanical strain induces specific changes in the synthesis and organization of proteoglycans by vascular smooth muscle cells. *J Biol Chem.* (2001) 276:13847–51. doi: 10.1074/jbc.M010556200
62. Kenagy RD, Kikuchi S, Evanko SP, Ruiter MS, Piola M, Longchamp A, et al. Versican is differentially regulated in the adventitial and medial layers of human vein grafts. *PLoS ONE.* (2018) 13:e0204045. doi: 10.1371/journal.pone.0204045
63. Cooley BC, Nevado J, Mellad J, Yang D, St. Hilaire C, Negro A, Fang F, Chen G, San H, Walts AD, et al. TGF- β signaling mediates endothelial-to-mesenchymal transition (EndMT) during vein graft remodeling. *Sci Transl Med.* (2014) 6:227ra34. doi: 10.1126/scitranslmed.3006927
64. Sun Y, Nadal-Vicens M, Misono S, Lin MZ, Zubiaga A, Hua X, et al. Neurogenin promotes neurogenesis and inhibits glial differentiation by independent mechanisms. *Cell.* (2001) 104:365–76. doi: 10.1016/s0092-8674(01)00224-0

Conflict of Interest: The authors declare that the research was conducted in the absence of any commercial or financial relationships that could be construed as a potential conflict of interest.

Publisher's Note: All claims expressed in this article are solely those of the authors and do not necessarily represent those of their affiliated organizations, or those of the publisher, the editors and the reviewers. Any product that may be evaluated in this article, or claim that may be made by its manufacturer, is not guaranteed or endorsed by the publisher.

Copyright © 2022 Maselli, Garoffolo, Cassanmagnago, Vono, Ruiter, Thomas, Madeddu, Pesce and Spinetti. This is an open-access article distributed under the terms of the Creative Commons Attribution License (CC BY). The use, distribution or reproduction in other forums is permitted, provided the original author(s) and the copyright owner(s) are credited and that the original publication in this journal is cited, in accordance with accepted academic practice. No use, distribution or reproduction is permitted which does not comply with these terms.



OPEN ACCESS

EDITED BY

Pasqualino Sirignano,
Sapienza University of Rome, Italy

REVIEWED BY

Wei Guo,
Chinese PLA General Hospital, China
Gabriele Pagliariccio,
Azienda Usl Teramo, Italy

*CORRESPONDENCE

Tiehao Wang
tiehao.wang@wchscu.cn
Bin Huang
xgwkhb@126.com

†These authors have contributed
equally to this work

SPECIALTY SECTION

This article was submitted to
Atherosclerosis and Vascular Medicine,
a section of the journal
Frontiers in Cardiovascular Medicine

RECEIVED 10 June 2022

ACCEPTED 01 August 2022

PUBLISHED 19 August 2022

CITATION

Zhou Y, Wang J, Zhao J, Yuan D,
Weng C, Wang T and Huang B (2022)
The effect of percutaneous vs.
cutdown access in patients after
Endovascular aortic repair (SWEET):
Study protocol for a single-blind,
single-center, randomized controlled
trial. *Front. Cardiovasc. Med.* 9:966251.
doi: 10.3389/fcvm.2022.966251

COPYRIGHT

© 2022 Zhou, Wang, Zhao, Yuan,
Weng, Wang and Huang. This is an
open-access article distributed under
the terms of the [Creative Commons
Attribution License \(CC BY\)](#). The use,
distribution or reproduction in other
forums is permitted, provided the
original author(s) and the copyright
owner(s) are credited and that the
original publication in this journal is
cited, in accordance with accepted
academic practice. No use, distribution
or reproduction is permitted which
does not comply with these terms.

The effect of percutaneous vs. cutdown access in patients after Endovascular aortic repair (SWEET): Study protocol for a single-blind, single-center, randomized controlled trial

Yuhang Zhou^{1,2†}, Jiarong Wang^{1†}, Jichun Zhao¹, Ding Yuan¹,
Chengxin Weng¹, Tiehao Wang^{1*} and Bin Huang^{1*}

¹Department of Vascular Surgery, West China Hospital, Sichuan University, Chengdu, China, ²West China School of Medicine, West China Hospital, Sichuan University, Chengdu, China

Background: Endovascular abdominal aortic repair (EVAR) and thoracic endovascular aortic repair (TEVAR) have become the first-line treatment for aortic diseases, but current evidence is uncertain regarding whether a percutaneous approach has better outcomes than cutdown access, especially for patient-centered outcomes (PCOs). This study is designed to compare these outcomes of percutaneous access vs. cutdown access after endovascular aortic repair.

Method: The SWEET study is a randomized, controlled, single-blind, single-center non-inferiority trial with two parallel groups in two cohorts respectively. After eligibility screening, subjects who meet the inclusion criteria will be divided into Cohort EVAR or Cohort TEVAR according to clinic interviews. And then participants in two cohorts will be randomly allocated to either intervention groups receiving percutaneous access endovascular repair or controlled groups receiving cutdown access endovascular repair separately. Primary clinician-reported outcome (ClinRO) is access-related complication, and primary patient-centered outcome (PCO) is time back to normal life. Follow-up will be conducted at 2 weeks, 1 month, 3 months postoperatively.

Discussion: The choice of either percutaneous or cutdown access may not greatly affect the success of EVAR or TEVAR procedures, but can influence the quality of life and patient-centered experience. Given the very low evidence for ClinROs and few data for PCOs, comparison of the percutaneous vs. cutdown access EVAR and TEVAR is essential for both patient-centered care and clinical decision making in endovascular aortic repair.

Trial registration: Chinese Clinical Trial Registry ChiCTR2100053161 (registered on 13th November, 2021).

KEYWORDS

percutaneous, cutdown, access, endovascular aortic repair, randomized controlled trial

Introduction

Aortic diseases consist of degenerative, inflammatory, traumatic, infectious and congenital disorders, among which aortic aneurysm and aortic dissection are two common and life-threatening diseases. In terms of abdominal aortic aneurysm alone, the worldwide prevalence in people aged 75 to 79 was 2,275 per 100,000 in 2010 (1). Alarming, 34% patients died before reaching a hospital or during first admission once aneurysm ruptured (2). As for aortic dissection, the pre-hospital and in-hospital mortality was even higher, and reached 39% (2). Therefore, timely and correct intervention is quite essential. According to the European Society for Vascular Surgery (ESVS) 2019 guidelines for abdominal aortic aneurysm and 2017 guidelines for thoracic aortic diseases, endovascular abdominal aortic repair (EVAR) or thoracic endovascular aortic repair (TEVAR) is the first-line treatment option for aortic diseases when the anatomy is appropriate, and this recommendation is Class I with level of evidence A (3, 4).

Endovascular intervention techniques continue to evolve, and it is now feasible to obtain percutaneous femoral artery access and close the arterial puncture site with a vascular closure device remotely. Compared with conventional cutdown access, percutaneous procedure was reported to have potential advantages, involving lower risks of access site infection and lymphorrhagia, as well as shorter operation time (5). However, endovascular aortic repairs usually require large-profile sheath in the femoral arteries, which can carry challenges to percutaneous access closure, especially in patients with calcified or small femoral arteries (6, 7). Failure in percutaneous closure can lead to surgical repair. The risk-benefit balance in the choice of access procedures is still uncertain.

Most previous data were mainly based on cohort studies of different periods with low level of evidence (8). Only four randomized controlled trials (RCTs) were published comparing two types of access during EVAR, but all trials were judged to have low or very low certainty of evidence with high risk of bias (9–12). In addition, no RCTs have been published comparing two types of access in TEVAR. Though the recent meta-analysis revealed comparable access complication rates between two access procedures, it is noteworthy that no studies reported patient-centered outcomes (PCOs), for instance, patient's experience and quality of life after surgery (13). Considering its relatively small impact on prognosis and large impact on quality of life, PCOs may be a new perspective to shed light on the selection of access procedures in EVAR or TEVAR.

Given the current gap in evidence, this study intends to design a single-center, parallel, non-inferiority, randomized controlled trial in a 1:1 ratio, comparing both clinician-reported outcomes (ClinROs) and PCOs between percutaneous vs. cutdown access in patients after Endovascular aortic repair (SWEET) in two cohorts (EVAR and TEVAR).

Materials and methods

Study setting

The SWEET trial is a single-center study conducted at West China Hospital, Sichuan University in Chengdu, China. The protocol is reported in accordance with the Standard Protocol Items: Recommendations for Interventional Trials (SPIRIT) guidelines (14). The SPIRIT checklist is shown in [Supplementary Table S1 \(Supplementary Material\)](#). The trial was registered in the Chinese Clinical Trial Registry (registration number: ChiCTR2100053161) on 13th November, 2021.

Participants

Recruitment

The participant characteristics derived from the PICO framework are presented in [Supplementary Table S2 \(Supplementary Material\)](#). Eligible patients with an indication for endovascular aortic repair will be informed concisely about the study by the attending resident. Subsequently, a trained research nurse will provide the consent and inform the patient in detail prior to the procedure. After careful consideration by the patient and relatives, the informed consent form will be signed prior to randomization in case of participation. Withdrawal from the study is permitted at any time for any reason, and it will not cause any consequence. To encourage participation, we will provide priority or fast track for outpatient appointments, follow-up assessment and consultation. If extra transportation costs are incurred due to the study, they will be paid by the sponsor.

Eligibility criteria

The study population consists of two independent cohorts: Cohort EVAR and TEVAR. The inclusion criteria of participants in Cohort EVAR are as follows: a. patient scheduled for EVAR because of abdominal aorto-iliac artery aneurysm or dissection, b. patient has signed informed consent. The inclusion criteria of participants in Cohort TEVAR are similar: a. patient scheduled for TEVAR because of thoracic aortic aneurysm or type B aortic dissection, b. patient has written informed consent.

The following exclusion criteria are applicable to both Cohort EVAR and TEVAR: a. emergent cases with ruptured or impending rupture aortic diseases, b. subjects with heavily calcified common femoral artery (more than 70% circumferential calcification).

Sample size

As no previous studies reported PCOs, we used the incidence of access site complications to estimate the sample size of the

SWEET trial. According to previous studies, the incidence of access site complications in percutaneous EVAR was 7.64%, compared with 11.81% in cutdown EVAR (13). We estimated the number of patients needed in this non-inferiority trial with non-inferiority margin of 0.10 (bilateral α 5%, power 80%) by PASS 15.0 software, and 54 patients are required for percutaneous and cutdown EVAR group, respectively. To allow for 10% drop out, 60 patients will be recruited per group, i.e., 120 for Cohort EVAR.

Previous TEVAR studies lacked solid data in above aspects, however, the relevant data of transcatheter aortic valve implantation (TAVI) can be used for reference due to their similar surgical approach (15). The incidence of access site complications was 8.7% in percutaneous TAVI and 8.5% in cutdown TAVI (16). The sample size was calculated with non-inferiority margin of 0.15 (bilateral α 5 %, power 80 %), 45 patients are required for percutaneous and cutdown TEVAR group separately. Fifty patients will be recruited each group allowing for 10% drop out, and the number of subjects in Cohort TEVAR is 100. Therefore, the total sample size of the SWEET trial is 220. The whole calculation process can be found in [Supplementary Tables S3, S4 \(Supplementary Material\)](#).

Intervention

In the percutaneous EVAR or TEVAR group, access is obtained through puncture of the common femoral artery deployment of two ProGlide devices (Abbott Vascular, Santa Clara, Calif) using a Preclose technique. The technique consists of deploying the needles of the first ProGlide device 30° medially or laterally from the midline. The second ProGlide needles are then deployed vertically from the first device, and then 16Fr sheath is inserted in the percutaneous access in EVAR and 18Fr sheath is used in TEVAR. When endovascular aortic repair is finished, the pretied knot and sutures of both devices are tightened and form knots by using the closure device remotely to achieve hemostasis. Pressuring and bandaging the puncture site gently also help stop bleeding. After percutaneous closure, it is necessary to observe whether the distal artery pulse well.

In the cutdown EVAR or TEVAR group, a 5-cm longitudinal incision is positioned in the groin area and common femoral artery is controlled by vessel loops. Femoral access is obtained through puncture under direct vision. After endovascular repair, the femoral artery is repaired thoroughly by a running 6-0 prolene suture. The subcutaneous tissue and skin are then sutured in standard fashion layer by layer.

Assignment of intervention

Cohort EVAR and TEVAR in the SWEET trial are designed as a parallel randomized controlled, single-blind, single-center

non-inferiority trial in a 1:1 ratio. The flow diagram for the study is outlined in [Figure 1](#). After eligibility screening, eligible subjects in the two cohorts will be randomly allocated to either intervention groups receiving percutaneous access endovascular aortic repair or control groups receiving cutdown access endovascular aortic repair separately. As for patients who require brachial artery access in Cohort TEVAR, the assignment will be based on their femoral artery access, independent of the approach for upper extremity access.

Block randomization stratified by age and body mass index (BMI) using permuted blocks of random sizes will be performed with 1:1 allocation in both cohorts. Randomization sequence is generated by SPSS 26.0 statistical software by a biostatistician. The block size will be concealed until the primary endpoints are analyzed. An independent research coordinator will be responsible for keeping the sequentially numbered allocation sequence list, and will inform the surgeons about the assigned access procedure prior to intervention. To avoid performance bias, every surgeon must have had 10 or more ProGlide procedures, and experience of at least 20 surgical cutdowns to expose the access artery is also needed.

Obviously, trial participants and operating team cannot be blinded to the allocation. The data will be entered into the computer in separate tables by employees outside the research team so that the analysts can analyze data without knowing the allocation information. Therefore, only data analysts are blinded in this study.

Outcome measures

The endpoints or composites in the SWEET trial are classified as ClinROs and PCOs. Cohort EVAR and TEVAR share the same primary and secondary endpoints. Primary and secondary outcomes will be assessed at 2 weeks, 1 month, and 3 months after surgery. An overview of the clinical outcome measures based on the SPIRIT recommendations is provided in [Table 1](#).

Primary outcomes

The primary ClinRO endpoint is access-related complications assessed in-hospital, 2 weeks and 1 month after surgery. The definition of access-related complications includes

- Access-site infection: inflammation of the groin presenting redness, swelling or exudation and requiring consecutive oral or intravenous antibiotics therapy.
- Bleeding/hematoma: fresh oozing blood or old blood stains seen on wound dressing/blood accumulation around the access site.
- Access-related arterial injury: arterial injuries requiring endarterectomy or patching due to the access technique.

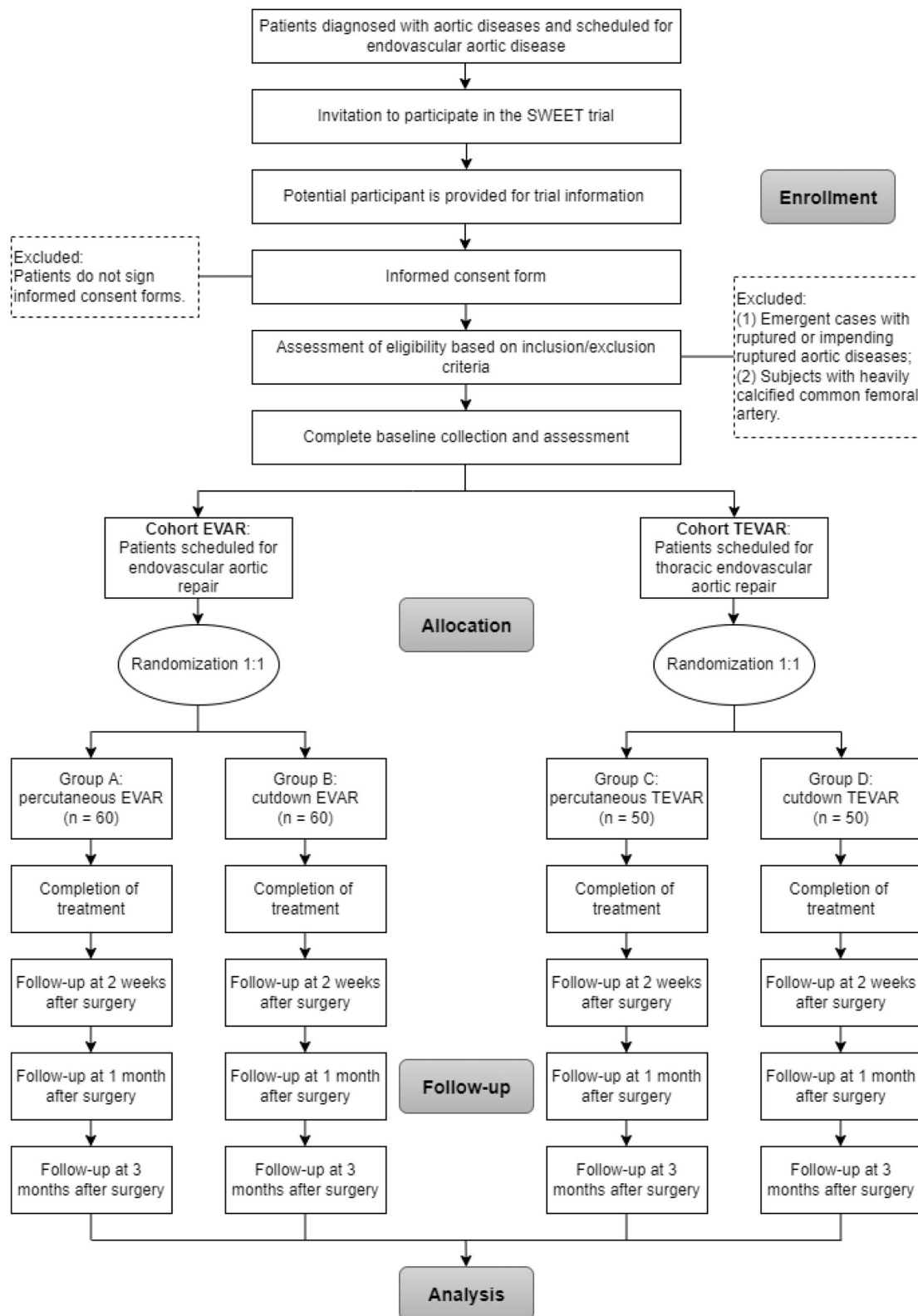


FIGURE 1
Flow of participants randomly assigned to percutaneous groups and cutdown groups.

TABLE 1 SPIRIT schedule for the SWEET randomized controlled trial.

Timepoint	Pre-study		Study visit	Follow-up		
	Enrollment	Baseline/ Allocation	Treatment	2-week after surgery	1-month after surgery	3-month after surgery
	-T1	0	T1	T2	T4	T5
Enrollment						
Eligibility screen	x					
Informed consent	x					
Clinical interviews		x				
Allocation		x				
Interventions			x			
Assessments						
<i>Primary ClinRO endpoint</i>						
Access-related complications			x	x	x	
Access site infection			x	x	x	
Bleeding/ hematoma			x	x	x	
Access-related arterial injury			x	x	x	
Femoral artery occlusion			x	x	x	
Pseudoaneurysm			x	x	x	
Lymphorrhagia/seroma			x	x	x	
Access-related nerve injury			x	x	x	
Wound dehiscence			x	x	x	
<i>Primary PCO endpoint</i>						
Time back to normal life/work				x	x	x
<i>Secondary ClinRO endpoints</i>						
Operative time			x			
Length of hospital stay			x	x	x	
30-day limb graft occlusion			x	x	x	
30-day overall complications			x	x	x	
30-day mortality			x	x	x	
<i>Secondary PCO endpoints</i>						
Quality of life scores				x	x	
Duration of access-related pain				x	x	x

- Femoral artery occlusion: femoral artery thrombosis presenting as distal artery pulse poorly requiring thrombectomy.
- Pseudoaneurysm: false aneurysm at the site of arterial injury presenting as a painful and pulsatile mass.
- Lymphorrhagia/seroma: swelling at access site caused by damage to lymphatic duct during access obtaining.
- Access-related nerve injury: nerve injuries presenting as persistent paresthesia of the thigh due to the access technique.
- Wound dehiscence: a partial or complete separation of previously close access wound edges.

The primary PCO endpoint is time (days) back to normal life/work assessed at 2 weeks by telephone interview and checked

at 1 month and 3 months in outpatient clinics after surgery. To determine the outcomes that patients care most, we conducted a preliminary survey in 50 patients who received EVAR or TEVAR prior to our trial, and recovery time back to normal life or work represented the major PCO endpoint.

Secondary outcomes

The secondary ClinRO endpoints will be assessed in-hospital, 2 weeks and 1 month postoperatively, involving

- Operative time (minutes): defined as duration of whole EVAR or TEVAR procedure.
- Length of hospital stay (days): defined as the period of time a patient remains in hospital.

- 30-day limb graft occlusion: defined as a complete limb occlusion regardless of symptoms or lumen stenosis of more than 50% detected by image examination within 30 days postoperatively (17).
- 30-day overall complications: defined as all systemic or local complications within 30 days postoperatively, whether related to the access or not.
- 30-day mortality: defined as all-cause deaths occurring in the intervention population within 30 days postoperatively.

The secondary PCO endpoints involve quality of life scores and duration of access-related pain, which will be assessed simultaneously with the primary PCO endpoint.

- Quality of life scores: participants' perception of physical and mental health from various aspects over time, scored with European Quality of Life 5 Dimensions (EQ-5D) questionnaire.
- Duration of access-related pain (days): length of participants' unpleasant sensory and emotional experience associated with access wound.

Withdraw and dropout

Patients who agreed to participate in the trial can quit the study at any time for any reason without any consequences. After withdrawal, the subjects will not be replaced by others and their randomization number will not be re-used. Subjects are considered as dropout if they are lost to follow-up within 1-month postoperatively or they withdraw from the study.

Data collection and management

Data collection methods

Baseline data required are shown in [Supplementary Table S5 \(Supplementary Material\)](#). Age, sex, BMI, comorbidity etc., should be collected before assignment to achieve maximum balance between groups. Anatomical characteristics of aortic aneurysm, aortic dissection and access artery that have potential impact on treatment success and prognosis should also be routinely measured by the operating team with computed tomography angiography (CTA). In particular, the heavily calcified femoral artery, defined as an estimated over 50% area of calcification in the superficial surface, needs more attention of investigator (7). So does the severe tortuous iliac artery, which is defined as any portion of iliac artery with tortuous angle more than 90° so that visually doubled or more on a single slice of axial CTA (18).

All patients after surgery will be examined for access-related complications during the everyday ward rounds and dressing changes. After discharge, the remaining primary and secondary outcomes can be gotten by telephone interviews

and outpatient re-examination over several months. Quality of life scores will be quantified by EQ-5D questionnaire during follow-up, which reduces the variability in life quality assessment by various researchers. The EQ-5D questionnaire evaluates overall quality of life from 5 dimensions of mobility, self-care, usual activities, pain/discomfort, anxiety/depression, with each dimension ranging level 1 to 5. And its reliability and validity have been verified in many studies (19, 20).

Data management and confidentiality

In this trial, all data will be entered into the computer and several databases will be established. Modifications to data of the database will be documented. Moreover, data management personnel will use the mobile hard disk to back up the data of the databases once a month. Statisticians and supervisors will conduct regular data verification.

All written materials concerning to the study, including informed consent, medical history, surgical records, etc., will be securely stored in file cabinets. All random assignment, data collection, and follow-up management containing participant information will be conducted in the form of a web spreadsheet, which can only be accessed and edited with specific permissions. Participants' information will not be disclosed outside of this study without their written consent.

Statistical methods

Analysis population

As Cohort EVAR and Cohort TEVAR were powered and randomized separately, the statistical analysis of both cohorts is planned to be reported separately. The analysis populations of this trial involve modified intention-to-treat (ITT) and per-protocol (PP) populations. The modified ITT is determined after randomization and when the patient started endovascular aortic repair, hence all patients who indeed receive endovascular aortic repair are involved in the primary analysis within the respective access group as originally allocated. In this trial, the modified ITT will be the main analysis set for the summary of both ClinROs and PCOs data. Both ITT and PP analysis are required for test of non-inferiority, and PP analysis serves as a sensitivity analysis. The non-inferiority margin was predetermined at 10%, and the non-inferiority test will be evaluated as a two-sided test at $\alpha = 0.05$. When non-inferiority is reached, ITT is further tested for superiority.

Analysis of primary and secondary outcomes

Generalized linear model (GLM) will be used to compare continuous primary and secondary endpoints, and further adjustment for age, gender, BMI and femoral artery calcification will be performed by multivariate GLM analysis. Logistic

regression using generalized estimating equations (GEE) will be applied to compare categorical primary and secondary endpoints. Using multivariate GEE models, the subsequent analysis will be adjusted for age, gender, BMI and femoral artery calcification. The access-related complications are counted and analyzed by the number of femoral accesses instead of the number of patients.

To address heterogeneity among study population, pre-specified subgroup analyses will be performed in the following populations: heavily calcified femoral artery vs. lightly calcified femoral artery, tortuous iliac artery vs. non-tortuous iliac artery, obesity or overweight vs. normal weight, smoking vs. none, elderly or octogenarian vs. younger population.

Handling of missing data

Missing data for baseline covariates will be addressed by multiple imputation in overall adjusted analyses, but those patients will not be included in the corresponding subgroup analysis.

Monitoring

Data monitoring

Data Monitoring Committee (DMC), completely independent of the research team, will monitor the validity of data through reviewing interim analysis related to primary outcomes. And the interim analysis would be conducted by an independent statistician after 50% participants have been randomly assigned and completed a 3-month follow-up. The DMC will also make recommendations for the amendments of the study protocol according to the results of interim analysis.

Harms

Adverse events are defined as any unfavorable and unintended experience happening to participants during hospitalization and follow-up, whether they are considered to be related to the intervention or not. The presence of underlying disease at enrollment will not be reported as an adverse event, but any increase in the severity of the underlying disease will be considered an adverse event. Details of all adverse events reported voluntarily by participants or observed by investigators will be recorded on the case record forms, such as start date, end date, action taken, results etc.

Any event leading to death, prolonged or renewed hospitalization, disability or permanent damage could be described as a serious adverse event, which should be reported to the ethics committee timely. The principal investigator is required to conduct periodic cumulative reviews of all adverse events and, if necessary, convene meetings to assess the risks and benefits of the study.

Auditing

The DMC initial meeting will be held early stage of study, and the agenda contains familiarizing study background, reviewing study protocol, and setting a deadline of interim analysis report etc. Every 6 months, DMC will review enrollment data, adverse events data, validity and completeness of study data with unlimited access. If necessary, the DMC may request additional analysis beyond the interim analysis or an unscheduled security meeting to further understand the efficacy and safety of the trial.

Ethics considerations and dissemination

Ethics approval

Ethics approval has been obtained from the Ethics Committee on Biomedical Research, West China Hospital of Sichuan University (approval number: 2021-1316) on 8th November 2021. Informed consent will be obtained from all participants, and the trial will be conducted in compliance with the Declaration of Helsinki and other regulations.

Protocol amendments

The protocol of SWEET trial may be amended during the progress of the trial, and any major amendments will be notified to the accredited medical research ethics committee and competent authority. Any revision in the informed consent forms will also be updated to the patients. Major amendments are defined as any change to the protocol that is likely to affect the conduct or management of the trial, safety of the patients or intervention details. Potential major amendments may include sample size adjustment based on actual clinical outcome difference between two groups, newly added outcomes and adjustment in statistical methods.

Ancillary and post-trial care

Participants will be compensated 2,000 yuan once primary wound adverse events occur. The primary wound adverse events are defined as access-site infection, bleeding/hematoma, access-related arterial injury, femoral artery occlusion, pseudoaneurysm, lymphorrhagia/seroma, access-related nerve injury and wound dehiscence during postoperative care in hospital or follow-up. China Postdoctoral Science Foundation will be responsible for the compensation.

Dissemination policy

The study has been registered in a public trial registry (www.chictr.org.cn). At the end of the SWEET trial, the principal investigator will write a summary concerning the main results and present it at annual congress or forum of vascular surgery

in China. Simultaneously, related articles will be prepared for publication in an international authoritative journal. After approval by the principal investigator, all abstracts and publications concerning the primary and secondary outcomes from the trial could be submitted.

Discussion

With the accelerated development of minimally invasive technology, the treatment for aortic diseases has undoubtedly entered the era of endovascular therapy. In line with the newest ESVS clinical guidelines, EVAR or TEVAR is the first-line option for aortic diseases with appropriate anatomy (3, 4). However, there is no consensus in vascular surgery community regarding the choice of access in endovascular aortic repair. In Sweden, 42% of all EVAR used percutaneous access in 2013, while 21% still used cutdown access simultaneously (21). The lack of high-quality evidence was the main reason for this phenomenon.

Previous cohort studies comparing percutaneous vs. cutdown EVAR or TEVAR demonstrated that percutaneous access had better outcomes on access site infection, wound healing and lymphorrhagia/seroma, while performed worse on pseudoaneurysm (8). However, those cohort studies analyzed patients from different periods with unequal treatment protocol and few studies reported standard deviation (SD) of continuous outcomes. Even though previous four RCTs compared percutaneous and cutdown access, their level of evidence is not high enough due to their outcomes measures, selection of reported results and inadequate sample size (9–12). Our trial uses access-related complications as the composite primary ClinRO endpoint, which contains infection, bleeding/hematoma, arterial injury, artery occlusion, pseudoaneurysm, lymphorrhagia/seroma, nerve injury, wound dehiscence. And this makes the primary outcome measures more statistically and clinically representative.

Patient-centered experience has been overlooked and rarely reported in studies, let alone as primary outcome. Uhlmann et al. evaluated access-related pain postoperatively by visual analog scale (VAS) and reported percutaneous EVAR did better in this aspect, however, solid data reflecting the quality of life and patient-centered experience were still lacking (10). Neither did the PiERO trial (9). PCO endpoints in the SWEET trial includes recovery time back to normal life, quality of life scores quantified by EQ-5D questionnaire and duration of access-related pain, which will fill in the blank.

Calcified femoral artery, tortuous iliac artery, obesity and inguinal scar were considered as risk factors for failure of percutaneous access EVAR (7, 22–24). Conversely, some researchers found that obesity and calcified femoral artery had no significant impact on the procedure success (25, 26). All these controversies were based on single-center experience or retrospective studies. The PEVAR trial stringently exclude

patients with the any risk factor to ensure a highly homogeneous study population, but it also limited real-world applicability of the results (11). As for remaining trials, although selection criteria were wider, screening of participants were still limited by femoral artery calcification, previous femoral artery surgery, obesity and other conditions (9, 10). Our trial further broadens the selection criteria and plans pre-specified subgroup analysis based on population who break through these limitations. According to the results of the subgroup analysis, we hope to explore which part of the population would be suitable for and benefit from percutaneous endovascular aortic repair.

The choice of either percutaneous or cutdown access may not greatly affect the success of EVAR or TEVAR procedures, but can influence the quality of life and patient-centered experience. Given the very low evidence for ClinROs and few data for PCOs, comparison of the percutaneous vs. cutdown access EVAR and TEVAR is essential for both patient-centered care and clinical decision making in endovascular aortic repair.

Ethics statement

The studies involving human participants were reviewed and approved by Ethics Committee on Biomedical Research, West China Hospital of Sichuan University. The patients/participants provided their written informed consent to participate in this study.

Author contributions

YZ and JW contributed to the conception and design of the trial and drafted the manuscript. JW, JZ, and DY will recruit and screen the participants. YZ, JW, CW, TW, and BH will participate in data collection and analysis. JZ, DY, TW, and BH provided supervision support. All authors contributed to the critical revisions and final approval of the manuscript.

Funding

The study is funded by the 69th batch of general support from China Postdoctoral Science Foundation (2021M692284). The funders have no role in study design, data collection, management and analysis, and decision to publish of the manuscript.

Conflict of interest

The authors declare that the research was conducted in the absence of any commercial or financial relationships

that could be construed as a potential conflict of interest.

Publisher's note

All claims expressed in this article are solely those of the authors and do not necessarily represent those of their affiliated organizations, or those of the publisher, the editors and the reviewers. Any product that may be evaluated in this article, or

claim that may be made by its manufacturer, is not guaranteed or endorsed by the publisher.

Supplementary material

The Supplementary Material for this article can be found online at: <https://www.frontiersin.org/articles/10.3389/fcvm.2022.966251/full#supplementary-material>

References

1. Sampson UK, Norman PE, Fowkes FG, Aboyans V, Song Y, Harrell FE Jr, et al. Estimation of global and regional incidence and prevalence of abdominal aortic aneurysms 1990 to 2010. *Global heart*. (2014) 9:159–70. doi: 10.1016/j.heart.2013.12.009
2. Landenhed M, Engström G, Gottsäter A, Caulfield MP, Hedblad B, Newton-Cheh C, et al. Risk profiles for aortic dissection and ruptured or surgically treated aneurysms: a prospective cohort study. *J Am Heart Assoc*. (2015) 4:e001513. doi: 10.1161/JAHA.114.001513
3. Riambau V, Böckler D, Brunkwall J, Cao P, Chiesa R, Coppi G, et al. Editor's choice-management of descending thoracic aorta diseases: clinical practice guidelines of the European society for vascular surgery (Esvs). *Eur J Vasc Endovasc Surg*. (2017) 53:4–52. doi: 10.1016/j.ejvs.2017.03.009
4. Wanhainen A, Verzini F, Van Herzeele I, Allaire E, Bown M, Cohnert T, et al. Editor's choice-European society for vascular surgery (Esvs) 2019 clinical practice guidelines on the management of abdominal aorto-iliac artery aneurysms. *Eur J Vasc Endovasc Surg*. (2019) 57:8–93. doi: 10.1016/j.ejvs.2020.09.004
5. Hajibandeh S, Hajibandeh S, Antoniou SA, Child E, Torella F, Antoniou GA. Percutaneous access for endovascular aortic aneurysm repair: a systematic review and meta-analysis. *Vascular*. (2016) 24:638–48. doi: 10.1177/1708538116639201
6. Rijkée MP, Statius van Eps RG, Wever JJ, van Overhagen H, van Dijk LC, Knippenberg B. Predictors of failure of closure in percutaneous evar using the prostar xl percutaneous vascular surgery device. *Eur J Vasc Endovasc*. (2015) 49:45–9. doi: 10.1016/j.ejvs.2014.10.017
7. Mousa AY, Campbell JE, Broce M, Abu-Halimah S, Stone PA, Hass SM, et al. Predictors of percutaneous access failure requiring open femoral surgical conversion during endovascular aortic aneurysm repair. *J Vasc Surg*. (2013) 58:1213–9. doi: 10.1016/j.jvs.2013.04.065
8. Vierhout BP, Pol RA, El Mounni M, Zeebregts CJ. Editor's choice-arteriotomy closure devices in evar, tevar, and tavr: a systematic review and meta-analysis of randomised clinical trials and cohort studies. *Eur J Vasc Endovasc Surg*. (2017) 54:104–15. doi: 10.1016/j.ejvs.2017.03.015
9. Vierhout BP, Pol RA, Ott MA, Pierie MEN, van Andringa de Kempenaer TMG, Hissink RJ, et al. Randomized Multicenter Trial on Percutaneous Versus Open Access in Endovascular Aneurysm Repair (Piero). *J Vasc Surg*. (2019) 69:1429–36. doi: 10.1016/j.jvs.2018.07.052
10. Uhlmann ME, Walter C, Taher F, Plimon M, Falkensammer J, Assadian A. Successful percutaneous access for endovascular aneurysm repair is significantly cheaper than femoral cutdown in a prospective randomized trial. *J Vasc Surg*. (2018) 68:384–91. doi: 10.1016/j.jvs.2017.12.052
11. Nelson PR, Kracjer Z, Kansal N, Rao V, Bianchi C, Hashemi H, et al. A multicenter, randomized, controlled trial of totally percutaneous access versus open femoral exposure for endovascular aortic aneurysm repair (the pevar trial). *J Vasc Surg*. (2014) 59:1181–93. doi: 10.1016/j.jvs.2013.10.101
12. Torsello GB, Kasprzak B, Klenk E, Tessarek J, Osada N, Torsello GF. Endovascular suture versus cutdown for endovascular aneurysm repair: a prospective randomized pilot study. *J Vasc Surg*. (2003) 38:78–82. doi: 10.1016/S0741-5214(02)75454-2
13. Antoniou GA, Antoniou SA. Editor's choice-percutaneous access does not confer superior clinical outcomes over cutdown access for endovascular aneurysm repair: meta-analysis and trial sequential analysis of randomised controlled trials. *Eur J Vasc Endovasc Surg*. (2021) 61:383–94. doi: 10.1016/j.ejvs.2020.11.008
14. Chan AW, Tetzlaff JM, Gotzsche PC, Altman DG, Mann H, Berlin JA, et al. SPIRIT 2013 explanation and elaboration: guidance for protocols of clinical trials. *BMJ*. (2013) 346:e7586. doi: 10.1136/bmj.e7586
15. Baxter RD, Hansen SK, Gable CE, DiMaio JM, Shutze WP, Gable DR. Outcomes of open versus percutaneous access for patients enrolled in the great registry. *Ann Vasc Surg*. (2021) 70:370–7. doi: 10.1016/j.avsg.2020.06.033
16. Abdelaziz HK, Megaly M, Debski M, Rahbi H, Kamal D, Saad M, et al. Meta-analysis comparing percutaneous to surgical access in trans-femoral transcatheter aortic valve implantation. *Am J Cardiol*. (2020) 125:1239–48. doi: 10.1016/j.amjcard.2020.01.021
17. Bogdanovic M, Stackelberg O, Lindström D, Ersryd S, Andersson M, Roos H, et al. Limb graft occlusion following endovascular aneurysm repair for infrarenal abdominal aortic aneurysm with the zenith alpha, excluder, and endurant devices: a multicentre cohort study. *Eur J Vasc Endovasc Surg*. (2021) 62:532–9. doi: 10.1016/j.ejvs.2021.05.015
18. Taudorf M, Jensen LP, Vogt KC, Grønvall J, Schroeder TV, Lönn L. Endograft limb occlusion in evar: iliac tortuosity quantified by three different indices on the basis of preoperative CTA. *Eur J Vasc Endovasc Surg*. (2014) 48:527–33. doi: 10.1016/j.ejvs.2014.04.018
19. Janssen MF, Bonsel GJ, Luo N. Is Eq-5d-5l Better Than Eq-5d-3l? a head-to-head comparison of descriptive systems and value sets from seven countries. *PharmacoEconomics*. (2018) 36:675–97. doi: 10.1007/s40273-018-0623-8
20. Welie AG, Stolk E, Mukuria C, Belay YB, Krahn MD, Sander B, et al. Reliability and validity of using Eq-5d-5l among healthy and adolescents with major mental health disorders in Ethiopia. *Eur J Health Econ*. (2022). doi: 10.1007/s10198-021-01412-y
21. Wanhainen A. Commentary on 'a randomized controlled trial of the fascia suture technique compared with a suture-mediated closure device for femoral arterial closure after endovascular aortic repair'. *Eur J Vasc Endovasc Surg*. (2015) 49:174. doi: 10.1016/j.ejvs.2014.11.001
22. Traul DK, Clair DG, Gray B, O'Hara PJ, Ouriel K. Percutaneous endovascular repair of infrarenal abdominal aortic aneurysms: a feasibility study. *J Vasc Surg*. (2000) 32:770–6. doi: 10.1067/mva.2000.107987
23. Nehler MR, Lawrence WA, Whitehill TA, Charette SD, Jones DN, Krupski WC. Iatrogenic vascular injuries from percutaneous vascular suturing devices. *J Vasc Surg*. (2001) 33:943–7. doi: 10.1067/mva.2001.115002
24. Teh LG, Sieunarine K, van Schie G, Goodman MA, Lawrence-Brown M, Prendergast FJ, et al. Use of the percutaneous vascular surgery device for closure of femoral access sites during endovascular aneurysm repair: lessons from our experience. *Eur J Vasc Endovasc Surg*. (2001) 22:418–23. doi: 10.1053/ejvs.2001.1495
25. Smith ST, Timaran CH, Valentine RJ, Rosero EB, Clagett GP, Arko FR. Percutaneous access for endovascular abdominal aortic aneurysm repair: can selection criteria be expanded? *Ann Vasc Surg*. (2009) 23:621–6. doi: 10.1016/j.avsg.2008.09.002
26. Etezadi V, Katzen BT, Naiem A, Johar A, Wong S, Fuller J, et al. Percutaneous suture-mediated closure versus surgical arteriotomy in endovascular aortic aneurysm repair. *J Vasc Interv Radiol*. (2011) 22:142–7. doi: 10.1016/j.jvir.2010.10.008



OPEN ACCESS

EDITED BY

Johannes A. Schmid,
Medical University of Vienna, Austria

REVIEWED BY

Svetlana Khaiboullina,
University of Nevada, Reno,
United States
Mabruka Alfaidi,
LSU Health Sciences
Center—Shreveport, United States

*CORRESPONDENCE

Jun-ichi Abe
jabe@mdanderson.org
Scott E. Evans
seevans@mdanderson.org
Nhat-Tu Le
nhle@houstonmethodist.org

†PRESENT ADDRESSES

Yin Wang,
Department of Experimental Radiation
Oncology, The University of Texas MD
Anderson Cancer Center, Houston, TX,
United States
Hang Thi Vu,
Center for Genomic and Precision
Medicine, Institute of Biosciences and
Technology, Texas A&M University,
Houston, TX, United States
Loka Reddy Velatooru,
Department of Dermatology, The
University of Texas MD Anderson
Cancer Center, Houston, TX,
United States
Masaki Imanishi,
Department of Pharmacology,
Tokushima University Graduate School
of Biomedical Science,
Tokushima, Japan
Tamlyn N. Thomas,
Cardiovascular Research Institute,
University of Rochester, Rochester, NY,
United States
Di Zhao,
Department of Experimental Radiation
Oncology MD Anderson Cancer
Center, Houston, TX, United States

†These authors have contributed
equally to this work

§These authors share senior authorship

SPECIALTY SECTION

This article was submitted to
Atherosclerosis and Vascular Medicine,
a section of the journal
Frontiers in Cardiovascular Medicine

RECEIVED 08 October 2021

ACCEPTED 21 July 2022

PUBLISHED 23 August 2022

MAGI1 inhibits interferon signaling to promote influenza A infection

Yin Wang^{1†}, Jun-ichi Abe^{1*†}, Khanh M. Chau^{2†},
Yongxing Wang^{3†}, Hang Thi Vu^{1†}, Loka Reddy Velatooru^{2†},
Fahad Gulraiz³, Masaki Imanishi^{1†},
Venkata S. K. Samanthapudi¹, Minh T. H. Nguyen²,
Kyung Ae Ko¹, Ling-Ling Lee¹, Tamlyn N. Thomas^{1†},
Elizabeth A. Olmsted-Davis², Sivareddy Kotla¹, Keigi Fujiwara¹,
John P. Cooke², Di Zhao^{1†}, Scott E. Evans^{3*§} and Nhat-Tu Le^{2*§}

¹Department of Cardiology, The University of Texas MD Anderson Cancer Center, Houston, TX, United States, ²Department of Cardiovascular Sciences, Center for Cardiovascular Regeneration, Houston Methodist Research Institute, Houston, TX, United States, ³Department of Pulmonary Medicine, The University of Texas MD Anderson Cancer Center, Houston, TX, United States

We have shown that membrane-associated guanylate kinase with inverted domain structure-1 (MAGI1), a scaffold protein with six PSD95/DiscLarge/ZO-1 (PDZ) domains, is involved in the regulation of endothelial cell (EC) activation and atherogenesis in mice. In addition to causing acute respiratory disease, influenza A virus (IAV) infection plays an important role in atherogenesis and triggers acute coronary syndromes and fatal myocardial infarction. Therefore, the aim of this study is to investigate the function and regulation of MAGI1 in IAV-induced EC activation. Whereas, EC infection by IAV increases MAGI1 expression, MAGI1 depletion suppresses IAV infection, suggesting that the induction of MAGI1 may promote IAV infection. Treatment of ECs with oxidized low-density lipoprotein (OxLDL) increases MAGI1 expression and IAV infection, suggesting that MAGI1 is part of the mechanistic link between serum lipid levels and patient prognosis following IAV infection. Our microarray studies suggest that MAGI1-depleted ECs increase protein expression and signaling networks involve in interferon (IFN) production. Specifically, infection of MAGI1-null ECs with IAV upregulates expression of signal transducer and activator of transcription 1 (STAT1), interferon b1 (IFNb1), myxovirus resistance protein 1 (MX1) and 2'-5'-oligoadenylate synthetase 2 (OAS2), and activate STAT5. By contrast, MAGI1 overexpression inhibits *Ifnb1* mRNA and MX1 expression, again supporting the pro-viral response mediated by MAGI1. MAGI1 depletion induces the expression of MX1 and virus suppression. The data suggests that IAV suppression by MAGI1 depletion may, in part, be due to MX1 induction. Lastly, interferon regulatory factor 3 (IRF3) translocates to the nucleus in the absence of IRF3 phosphorylation, and IRF3 SUMOylation is abolished in MAGI1-depleted ECs. The data suggests that MAGI1 inhibits IRF3 activation by maintaining IRF3 SUMOylation. In summary, IAV infection occurs in ECs in a MAGI1 expression-dependent manner by inhibiting anti-viral

responses including STATs and IRF3 activation and subsequent MX1 induction, and MAGI1 plays a role in EC activation, and in upregulating a pro-viral response. Therefore, the inhibition of MAGI1 is a potential therapeutic target for IAV-induced cardiovascular disease.

KEYWORDS

IAV, MAGI1, MX1, interferon signaling, IRF3, EC inflammation

Highlights

- IAV infection increases MAGI1 expression.
- MAGI1 depletion upregulates anti-viral response including STATs and IRF3 activation and inhibits EC infection by IAV.
- OxLDL induces MAGI1 expression and amplifies IAV infection in ECs.
- Anti-viral effects of MAGI1 depletion is at least partially depends on MX1 induction.
- De-SUMOylation and the consequent activation of IRF3 are induced by MAGI1 depletion.
- MAGI1 plays a crucial role in both accelerating EC activation and IAV infection.

Introduction

Whereas, three types of influenza viruses (A, B, and C) (1), negative-strand RNA viruses belonging to the *Orthomyxoviridae*

family, infect humans, seasonal flu epidemics are usually caused by influenza A virus (IAV) (2, 3), which targets epithelial cells in the human respiratory tract. The gap between the airspace and the capillary ECs is $\sim 0.5\ \mu\text{m}$, and alveolar wall cells and capillary ECs are separated only by the basal lamina and so that the endothelium is likely to be also exposed to free virus particles during IAV infection (4). According to some studies, IAV infects ECs *in vivo*, in association with development of flu symptom (5–8). However, other studies have suggested that ECs indirectly contribute to the pathogenesis of virus infection through control of the local inflammatory milieu in the lungs (9, 10). Indeed, some studies implicate EC function in IAV pathogenesis; i.e., in addition to causing acute respiratory disease IAV may trigger acute coronary syndromes and fatal myocardial infarction (11–15). Also, IAV infection of the vascular wall and/or increased levels of circulating pro-inflammatory cytokines may contribute to atherosclerotic lesion progression (16, 17). However, the molecular pathway by which IAV promotes atherogenesis has not been identified so that these processes may simply share common risk factors (10, 17).

The severity of IAV infection depends on the host inflammatory response. During inflammation, EC activation is a key step. Our previous studies showed that MAGI1 depletion prevents EC activation induced by pro-atherogenic type of flow (18–20). MAGI1, a scaffold protein with six PDZ domains, one guanylate kinase domain, and two WW (rsp5) domains flanked by the first and second PDZ domains, localizes to the tight and adherens junctions (20–22). A genome-wide association study revealed a strong association between MAGI1 locus and various chronic inflammatory diseases including Crohn's disease, in which MAGI1-dependent maintenance of the tight seal of the gastrointestinal tract is compromised (23). Indeed, we also showed that MAGI1 plays a critical role in regulating EC permeability (19).

Although the role of MAGI1 in EC activation has been reported (18–20), its role in IAV-induced EC activation is unknown. The aim of the study was to test the hypothesis that MAGI1 drives EC activation after IAV infection, and that this process promotes IAV-mediated cardiovascular disease.

Abbreviations: DAPI, 4',6-diamidino-2-phenylindole; ECs, endothelial cells; GAPDH, glyceraldehyde-3-phosphate dehydrogenase; HULECs, human lung microvascular ECs; HUVECs, human umbilical vein ECs; IAV, influenza A virus; ICAM-1, intercellular adhesion molecule 1; IFN, interferon; IFIH1, interferon-induced helicase C domain-containing protein 1; IPA, ingenuity pathway analysis; IRF3, interferon regulatory factor 3; ISG, IFN-stimulated genes; ISRE, interferon-stimulated response element; M2, matrix protein 2; MAGI1, membrane-associated guanylate kinase with inverted domain structure-1; MAVS, mitochondrial antiviral signaling protein; MOI, multiplicities of infection; MX1, myxovirus resistance protein 1; OAS2, 2'-5'-oligoadenylate synthetase 2; PARP9, poly(ADP-ribose) polymerase family member 9; PBM, PDZ binding motif; PBS, phosphate buffered saline; NP, nucleoprotein; OxLDL, oxidized low-density lipoprotein; PDZ, PSD95/DiscLarge/ZO-1; PTEN, phosphatase and tension homolog; qRT-PCR, quantitative reverse-transcriptase polymerase chain reaction; RIPA, radioimmunoprecipitation assay buffer; SDS, sodium dodecyl sulfate; SDS-PAGE, SDS polyacrylamide gel electrophoresis; STAT1/2, signal transducer and activator of transcription 1/2; siRNA, small interfering RNA; VCAM-1, vascular cell adhesion molecule 1.

Experimental procedures

Mice

All mice were fed a normal diet and housed in a room with an ambient temperature of 22°C and a 12-h light/12-h dark cycle in a pathogen-free environment at the Texas A&M Institute of Biosciences and Technology. MAGI1^{-/-} (homozygous knocked out) mice were generated and characterized as we have previously described (20). C57BL/6 mice were purchased from the Jackson Laboratory (Bar Harbor, ME). First, MAGI1^{-/-} mice were crossed with C57BL/6 mice to generate MAGI1^{+/-} (heterozygous) mice, which were then used to generate MAGI1^{-/-} and the wild type (WT) littermate control mice. All procedures on mice were approved by the Institutional Care and Use Committees of the Texas A&M Institute of Biosciences and Technology (2014-0231, 2017-0154) and The University of Texas MD Anderson Cancer Center (00001652, 00001109).

Cells

HUVECs were isolated through a collagenase digestion of the endothelium of human umbilical cord veins and were grown on culture dishes coated with 0.2% gelatin type A (MP Biomedicals, Solon, OH, USA) in Endothelial Cell Medium (ECM, Catalog #1001, Science Cell, San Diego, CA, USA). HUVEC isolation was approved by the Houston Methodist Research Institute (HMRI) Institutional Review Board (IRB, permit No. Pro00020559). Mouse lung ECs were isolated as we have performed and described previously (17, 22, 23). Mouse lung EC isolation was approved by the HMRI Institutional Animal Care and Use Committee (IACUC, permit No. IS00006725). Briefly, lungs were harvested from 6 to 8 weeks old mice, washed thoroughly in cold PBS, minced finely with scissors, then digested by collagenase. Sheep anti-rat PECAM-1-conjugated Dynabeads (Catalog #11035, Invitrogen, Carlsbad, CA, USA) were prepared and used to isolate mouse lung ECs. Mouse lung ECs were cultured in DMEM (Catalog #SH30243.0, Hyclone, Logan, UT, USA) supplemented with 20% FBS (Catalog #F2442, Sigma-Aldrich, Saint Louis, MO), 1% EC growth supplement (Promo Cell, Heidelberg, Germany), 25 mM HEPES buffer (Catalog #25-060-CI, Corning, Manassas, VA, USA), 1% non-essential amino acid solution (Catalog #25-025-CI, Corning, Manassas, VA, USA), 100 mg/ml heparin (Catalog #67457037399, Mylan Institutional, Rockford, IL, USA) and 1% penicillin/streptomycin solution (Catalog #30-002-CI, Corning, Manassas, VA, USA). HULECs (ATCC, CRL-3244, Manassas, VA, USA) were cultured in MCDB 131 medium (Catalog #10372019, Thermo Fisher Scientific (Waltham, MA, USA) supplemented with Microvascular Endothelial Cell Growth Kit-BBE (Catalog #PCS-110-040, ATCC, Manassas, VA, USA) containing 0.2% bovine brain extract, 5 ng/mL rh EGF,

10 mM L-glutamine, 0.75 Unit/mL heparin sulfate, 1 µg/mL hydrocortisone, 50 µg/mL ascorbic acid and 5% FBS.

Influenza A viral infection

For *in vitro* influenza A viral infection, as previously described (24), frozen stocks of mouse-adapted influenza A/Hong Kong/8/68 virus (H3N2) were diluted 1:1000 in 1x PBS and viral inocula (multiplicities of infection [MOI] of 0.1) were added to EC monolayer. For heat inactivation: influenza virus stocks were incubated for 30 min at 22.0, 35.0, 38.3, 43.7, 49.6, 55.6, 61.3, 66.7, and 70°C in a T-Gradient thermal cycler (Biometra, Göttingen, Germany) and subsequently stored at -80°C until *in vitro* infection (24, 25).

Gene expression profiling

Gene expression profiling was performed as we have previously described (20). Briefly, HUVECs were transfected with either control siRNA (siCont) or MAGI1 siRNA (siMAGI1), and total RNA was isolated approximately 48 h post-transfection using RNeasy Plus Micro Kit (Cat# 74034, QIAGEN, Germantown, MD) with DNA digestion. Total RNA was then hybridized using a GeneChip Human Transcriptome Array 2.0 (Affymetrix, Santa Clara, CA). The array data was analyzed using the Transcriptome Analysis Console 3.0 (Affymetrix) followed by data normalization using Tukey's biweight average algorithm. Significance was determined using unpaired ANOVA ($P < 0.05$) as we have previously described (20). The differential expression data were analyzed using Ingenuity Pathway Analysis (IPA) (application build 377306M [2016-03-16] and content version 27216297 [2016-03-16]; QIAGEN). All molecular interactions and relationships were based on curated findings in the literature stored in the Ingenuity Knowledge Base (QIAGEN).

siRNA-mediated MAGI1 depletion and transient MAGI1 overexpression

The siRNA sequence corresponding to nucleotides 843-857 of human MAGI1 coding sequence (5'-GGACCCUUCUCAGAAGUCCCCUCAA) (20) that specifically targets human MAGI1 for degradation was obtained from Sigma-Aldrich (Burlington, MA, USA). Authenticated siRNA sequence targeting human MX1 was obtained from Santa Cruz Biotechnology (Santa Cruz, Dallas, TX, USA). Non-target siRNA sequence (control) was obtained from Thermo Fisher Scientific (Waltham, MA, USA). siRNA-mediated MAGI1 depletion and transient MAGI1 overexpression were performed as we have previously described (20).

RNA extracts and qRT-PCR

Studies were performed 48 h after siRNA transfection, as indicated in each corresponding figure. Total RNA was then extracted using the PureLink RNA mini-Kit (Thermo Fisher Scientific; Waltham, MA, USA). cDNAs were synthesized using the iScript cDNA synthesis Kit (Bio-Rad, Hercules, CA 94547, USA). Mixtures for qRT-PCR reactions (10 μ L) contained cDNA synthesized from 20 ng of total RNA, 5 μ L of iQ SYBR Green Supermix (Bio-Rad, Hercules, CA 94547, USA), and 0.5 μ M each forward and reverse primer. qRT-PCR reactions were carried out at 95°C for 3 min followed by 40 cycles of denaturation at 95°C for 10 s, 60°C for 15 s, and 72°C for 30 s. qRT-PCR data acquisition was carried out using the CFX Connect Real-Time PCR Detection System (Bio-Rad, Hercules, CA 94547, USA). The comparative C_t ($2^{-\Delta\Delta C_t}$) method was used to relatively quantified changes in mRNA expression of samples, in which cycle threshold (C_t) values of target genes were normalized to that of the reference genes (26). All qRT-PCR primers were obtained from Sigma-Aldrich. The sequences of qRT-PCR primers were listed in the [Supplementary Table 1](#).

Protein extracts and immunoblotting

The cells were lysed on ice in RIPA buffer (50 mM Tris-HCl, pH 7.4, 150 mM NaCl, 1 mM ethylenediaminetetraacetic acid, 1% Nonidet P-40, 0.1% sodium dodecyl sulfate, 0.25% sodium deoxycholate) containing protease and phosphatase inhibitors (Sigma-Roche, Mannheim, Germany) (20). Cell lysates were briefly sonicated and then centrifuged at 16,000 $\times g$ for 10 min at 4°C to remove any debris. Cell extracts were mixed with SDS gel loading buffer and loaded on SDS-PAGE gels and separated proteins were transferred to nitrocellulose membranes. The membranes were probed with antibodies that specifically recognize proteins of interest. Some samples were analyzed by using the automated capillary electrophoresis Western analysis (Wes) system (ProteinSimple, San Jose, CA, USA) as we have performed previously (27).

Antibodies and reagents

The following antibodies were purchased: MAGI1 (Catalog #M5691, Sigma-Aldrich, St. Louis, MO, USA), STAT1 (Catalog #ab103813, Abcam, Cambridge, MA, USA), MX1 (Catalog #sc-271024, Santa Cruz Biotechnology, Dallas, TX, USA), phospho-STAT1 Y701 (Catalog #9167S, Cell Signaling, Danvers, MA, USA), IRF3 (Catalog #ab76409, Abcam, Cambridge, MA, USA), phospho-IRF3 S396 (Catalog #29047, Cell Signaling, Danvers, MA, USA), GAPDH (Catalog #ab9484, Abcam, Cambridge, MA, USA), b-actin (Catalog #4970, Cell Signaling, Danvers, MA, USA), NP (Catalog #sc-80481, Santa Cruz, Biotechnology,

Dallas, TX, USA), and M2 (Catalog #sc32238, Santa Cruz, Biotechnology, Dallas, TX, USA).

OxLDL preparation

LDL at 0.2 mg/mL was incubated with 5 mM CuSO₄ at 37°C for 24 h. The oxidation reaction was stopped by the addition of 20 mM EDTA. The preparations were concentrated by cone filtration and followed by dialyzed and sterilized by filtration through a 0.22 μ m filter. The extent of oxidation of the LDL preparation was determined by measuring Thiobarbituric acid reactive substance (TBARS, Catalog #10009055; Cayman Chemicals, Ann Arbor, MI, USA). Another control LDL sample was processed in parallel, without CuSO₄ addition. The results showed that OxLDL contained 14 nmol/mg protein and LDL contained 1 TBARS/mg protein.

Human IFN- β in cell culture supernates

ECs were transfected with either siCont or siMAGI1. Approximately after 48 h of transfection, conditioned medium was collected and levels of IFN β were measured using the human IFN- β Quantikine ELISA kit (Catalog #DIFNB0, R&D Systems, MN, USA).

Immunofluorescent staining

At the end of experiment, the cells were quickly washed twice with warm PBS, fixed with 4% paraformaldehyde in PBS for 15 min, and permeabilized with 0.2% Triton X-100 in PBS for 10 min. The cells were then incubated with a blocking solution (5% goat serum and 0.1% NP-40 in PBS) for 60 min at room temperature and incubated with the primary antibodies (IRF3 or NP) overnight at 4°C. Next, the cells were washed three times with PBS and incubated with fluorescently labeled secondary antibodies for 1 h at room temperature then were counterstained with 4',6-diamidino-2-phenylindole (DAPI) to identify nuclei at room temperature. Imaging was done using an Olympus FV1200 multiphoton-confocal dual microscope (Olympus, Tokyo, Japan).

Statistical analysis

First, we performed Shapiro-Wilk test for checking the normality of each group, and we performed an ordinary one-way ANOVA followed by Fisher's LSD testing for multiple group comparisons or unpaired student *t*-test with only the data that passed these normality tests. If the data did not pass the normality test, we performed Brown-Forsythe and Welch

ANOVA or unpaired t-test with Welch's correction tests using the Prism software (GraphPad Software). *P*-values <0.05 were considered statistically significant.

Data availability

The microarray data and MAGI1 sequence were deposited in the NCBI's Gene Expression Omnibus database (accession GSE95066) and GenBank (accession KY651081), respectively. All other data, analytic methods, and study materials that support the findings of this study are available in the Data supplement or from the corresponding authors upon reasonable request.

Results

IAV infection increases MAGI1 expression and MAGI1 depletion suppresses IAV infection

To determine if MAGI1 expression in ECs in response to IAV infection promotes atherogenesis, we infected primary HUVECs with IAV. Given that the umbilical vein carries oxygenated blood, which is completely different from the systemic venous blood, HUVEC is the preferred *in vitro* cell culture system for determining the molecular mechanism of EC activation-induced atherogenesis (28). HUVECs infected with heat-inactivated virus was used as the mock control. After 24 h of infection, the cells were lysed, total RNA was extracted and analyzed by qRT-PCR to determine relative changes in *Magi1* mRNA expression levels (Figure 1A). Neither phosphate-buffered saline (PBS, vehicle control) nor the heat-inactivated virus (mock treatment control) had an effect, whereas the IAV infected cells increased *Magi1* mRNA expression level. We next knocked down MAGI1 by transfecting HUVECs with either the small interfering RNA (siRNA) that specifically targets *Magi1* mRNA for degradation (siMAGI1) or the siRNA negative control (siCont). After 48 h of siRNA transfection, the cells were infected with either IAV or mock control. After 24 h of virus infection, the cells were lysed, and total RNA was extracted and analyzed by qRT-PCR to determine relative changes in viral nucleoprotein (NP) mRNA expression levels. With the heat-inactivated IAV mock infection, there was no difference between siMAGI1 and siCont samples in the level of viral NP mRNA expression (Figure 1B). Conversely, infecting HUVECs transfected with siMAGI1 with live virus drastically downregulates the viral NP mRNA expression level relative to that of the siCont (Figure 1B). Studies of the cells themselves using immunofluorescence staining for the influenza NP protein showed similar results (Figures 1C,D).

Because MAGI1 induces EC activation (20), we investigated whether IAV activated ECs through upregulation of MAGI1 by determining relative changes in mRNA expression level of intercellular adhesion molecule 1 (ICAM-1), a marker of EC activation, using qRT-PCR in MAGI1-depleted HUVECs with or without virus infection. IAV infection increased *Icam-1* mRNA expression level and knocking down MAGI1 prevented this virus induced upregulation of *Icam-1* expression (Figure 1E). These results indicate that MAGI1 is essential to IAV infection, and in addition, mediates the activation of ECs by the virus. Interestingly, 24 h after virus infection, vascular cell adhesion molecule 1 (*Vcam-1*) mRNA expression was downregulated (Supplementary Figure 2).

We speculated that other pathological conditions in ECs also upregulate MAGI1 expression. IAV induces acute respiratory disease and the association between serum lipid levels and prognosis after severe acute respiratory syndrome coronavirus 2 (SARS-CoV-2) and influenza virus has been reported (29–34). Therefore, we investigated the role of MAGI1 in HUVECs and in human lung endothelial cells (HULECs) and found that OxLDL increased MAGI1 expression in both HUVECs and HULECs (Figures 2A,B). Furthermore, we also found that the pre-treatment of EC with OxLDL increased IAV infection (Figure 2C). Taken together, these data suggest a possible role for MAGI1 in IAV-associated cardiovascular and acute respiratory disease in dyslipidemia patients through driving virus infection.

MAGI1 depletion upregulates IFN signaling

To gain insights into the biological relevance of the reduced MAGI1 expression in ECs, we transfected HUVECs with either siCont or siMAGI1. Approximately 48 h after transfection, the cells were lysed, total RNA were extracted and transcriptionally profiled. A set of genes in the siMAGI1-treated ECs with Significant Differential Gene Expression (absolute fold-change >2, *p*-value <0.05) was submitted to IPA (QIAGEN, Redwood City, CA) for core analysis. We identified 252 genes that were differentially expressed in siMAGI1-transfected ECs compared to that in siCont-transfected ECs. Using Fisher's Exact Test enrichment analysis for curated gene sets categorized by biological function and disease, we find that gene sets categorized as Dermatological-Disease and Conditions, Antimicrobial Response, Inflammatory Response, and Infectious Disease are the top four most significant groups ($-\log[P] > 20$, Figure 3A). The gene enrichment calculations and predicted biological gene effects, based upon directional expression changes and literature-substantiated causal relationships, indicated that the gene expression pattern will reduce viral infection in siMAGI1-transfected ECs compared to that in siCont-transfected ECs and that 45

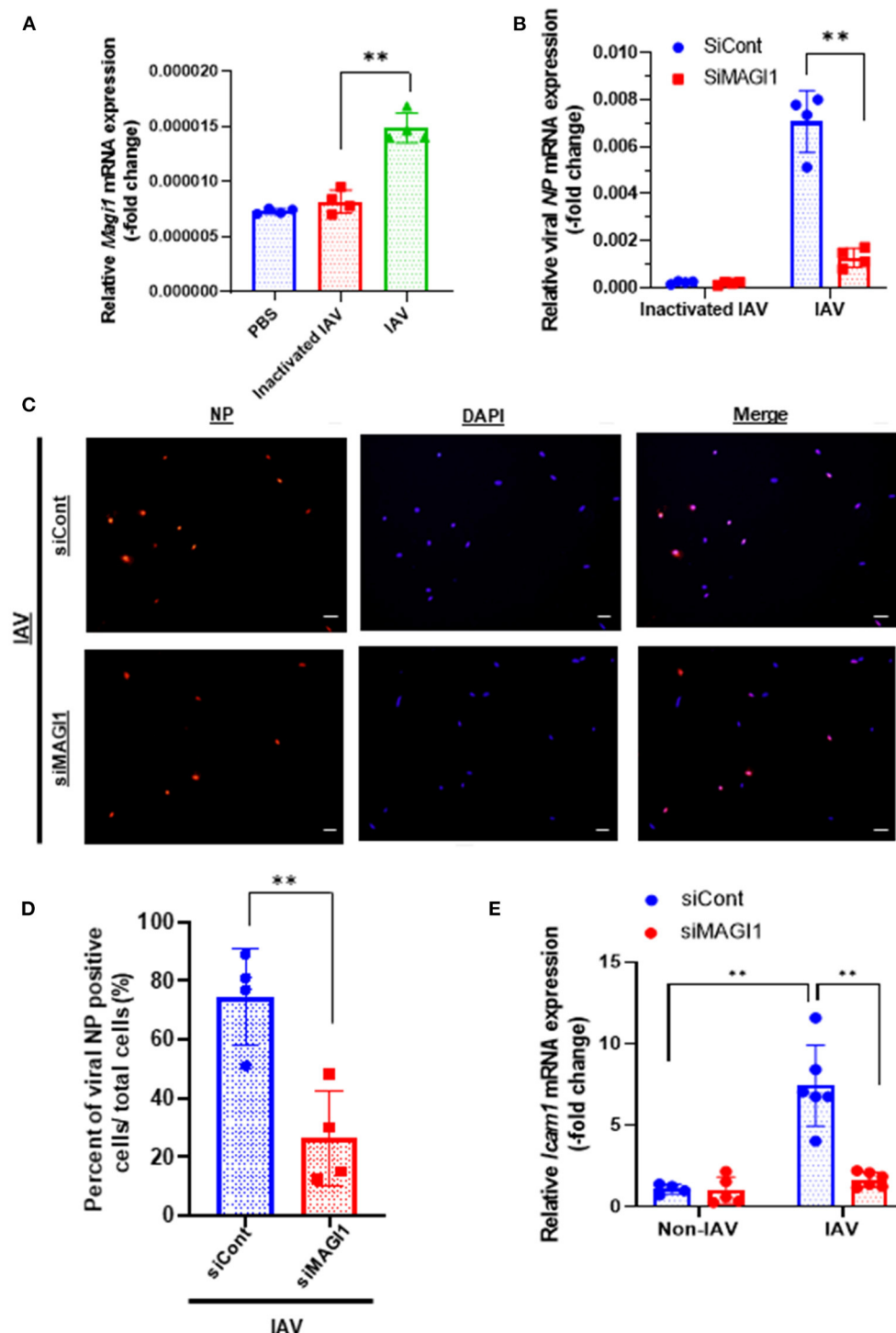


FIGURE 1

IAV infection increases MAGI1 expression and MAGI1 depletion suppresses IAV infection and inhibits EC inflammation. (A) HUVECs were infected with IAV, heat-inactivated virus, or treated with PBS for 24 h. Total RNA was extracted and qRT-PCR was performed. Relative changes in *Magi1* mRNA expression was calculated using the comparative C_t ($2^{-\Delta\Delta C_t}$) method. Ct values of *Magi1* were normalized to that of *Gapdh* (26). Each group passed the Shapiro-Wilk normality test, then one-way ANOVA followed by Turkey's multiple comparisons test were performed using the Prism software (GraphPad Software). The graph shows mean \pm SD ($n = 4$). $**p < 0.01$. (B) HUVECs were transfected with either siCont or siMAGI1. After 48 h of transfection, the cells were infected with IAV or heat-inactivated virus for 24 h. Total RNA was extracted then qRT-PCR was performed. Relative changes in the viral NP mRNA expression was calculated using the comparative C_t ($2^{-\Delta\Delta C_t}$) method. Ct values of the viral NP (Continued)

FIGURE 1 (Continued)

were normalized to that of the 18S ribosomal RNA (26). Each group passed the Shapiro-Wilk normality test, then two-way ANOVA followed by Turkey's multiple comparisons test were performed using the Prism software (GraphPad Software). The graph shows mean \pm SD ($n = 3$). $**p < 0.01$. (C) HUVECs were transfected with either siCont or siMAGI1. After 48 h of transfection, the cells were infected with IAV and immunofluorescence staining for the viral NP protein (red) and DAPI staining for the nucleus (blue) were performed. Scale bars: 20 μ M. (D) We analyzed a total of 30–120 cells per 2–3 fields per dish to determine the percentage of NP positive cells in a blinded manner. Each group passed the Shapiro-Wilk normality test, then unpaired student t -test was performed using the Prism software (GraphPad Software). The graph shows mean \pm SD ($n = 4$). $**p < 0.01$. (E) HUVECs were transfected with either siCont or siMAGI1. After 48 h of transfection, the cells were infected or not infected with IAV for 24 h. Total RNA was extracted, and qRT-PCR was performed. Relative changes in *Icam-1* mRNA expression was calculated using the comparative C_t ($2^{-\Delta\Delta C_t}$) method. Ct values of *Icam-1* were normalized to that of *gapdh* (26). Each group passed the Shapiro-Wilk normality test, then two-way ANOVA followed by Turkey's multiple comparisons test was performed using the Prism software (GraphPad Software). The graph shows mean \pm SD ($n = 4-6$). $**p < 0.01$.

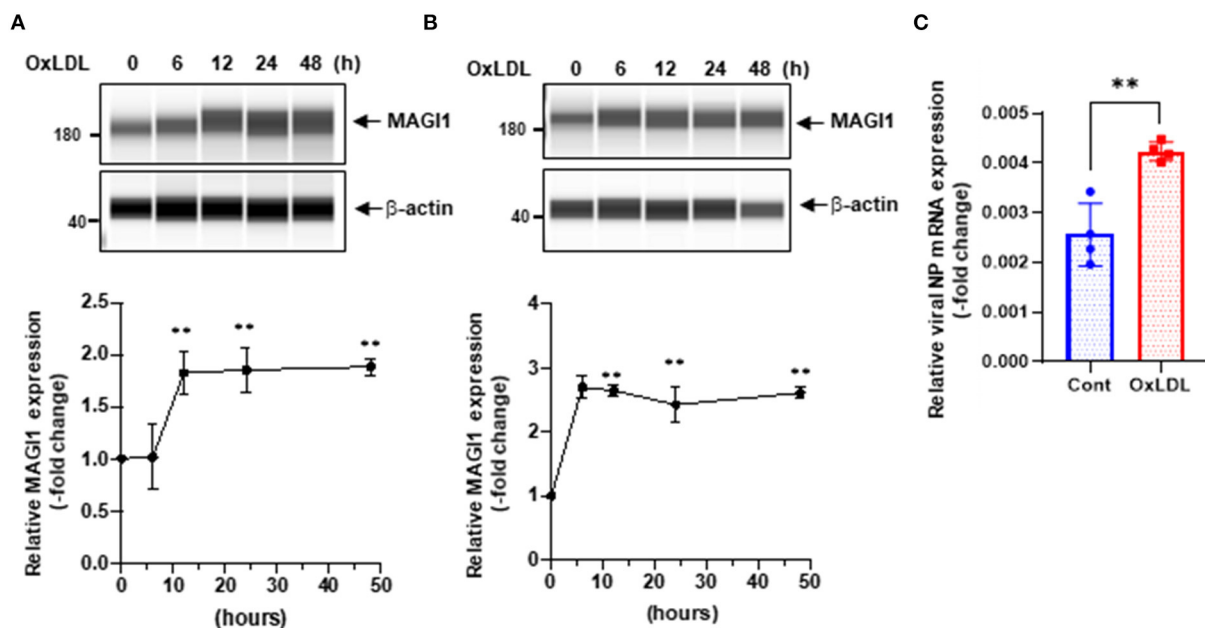


FIGURE 2

OxLDL increases MAGI1 expression and enhances IAV infection in ECs. (A,B) HUVECs (A) and HULECs (B) were pre-treated with OxLDL (10 μ g/mL) for the indicated times. Upper: relative changes in MAGI1 protein expression were analyzed using the automated capillary electrophoresis Western analysis (Wes) system (ProteinSimple, San Jose, CA, USA) (27). Lower (densitometric quantification): relative changes in MAGI1 protein expression after OxLDL treatment. Fold increases are shown after normalization with β -actin at each time point. Quantification was performed using Image J. Each group passed the Shapiro-Wilk normality test, then one-way ANOVA followed by Turkey's multiple comparisons test was performed using the Prism software (GraphPad Software). The graph shows mean \pm SD ($n = 3$). $**P < 0.01$. (C) HUVECs were pre-treated with OxLDL (10 μ g/mL) for 24 h then infected with IAV for another 24 h. Total RNA was extracted then qRT-PCR was performed. Relative changes in the viral NP mRNA expression were calculated using the comparative C_t ($2^{-\Delta\Delta C_t}$) method. Ct values of the viral NP were normalized to that of the 18S ribosomal RNA (26). Each group passed the Shapiro-Wilk normality test, then an unpaired student t -test was performed using the Prism software (GraphPad Software). The graph shows mean \pm SD ($n = 4$). $**p < 0.01$.

of the 82 genes had the measurement direction consistent with decreased viral infection (z -score, -2.7 ; $P = 5.6E-23$) (Supplementary Table 2). The high z -score predicts that MAGI1 depletion will down-regulate the expression of genes belonging to the viral infection category.

Figure 3B is the graphical summary constructed by the algorithm based on machine learning techniques to prioritize and connect entities identified by IPA. It shows the relationship which may not yet be connected by findings in the QIAGEN Knowledge Graph and suggests that MAGI1 depletion induces strong antiviral responses and IFN signaling by increasing *Ifih1*

(interferon-induced helicase C domain-containing protein 1), *Irf* (interferon regulatory factor) 3/7, *Parp9* (poly(ADP-ribose) polymerase family member 9), *Stat* (signal transducer and activator of transcription) 1/2, *Mavs* (mitochondrial antiviral signaling protein), *Eif2ak2* (eukaryotic translation initiation factor 2 alpha kinase), and *Ifng* (interferon gamma).

The predicted biological gene expression affected by MAGI1 depletion is shown as heat maps (Supplementary Figure 1). The results show the unique and strong downregulation of infectious disease category (Supplementary Figure 1) including viral infection (z -score, -2.7 ; $P = 5.6E-23$,

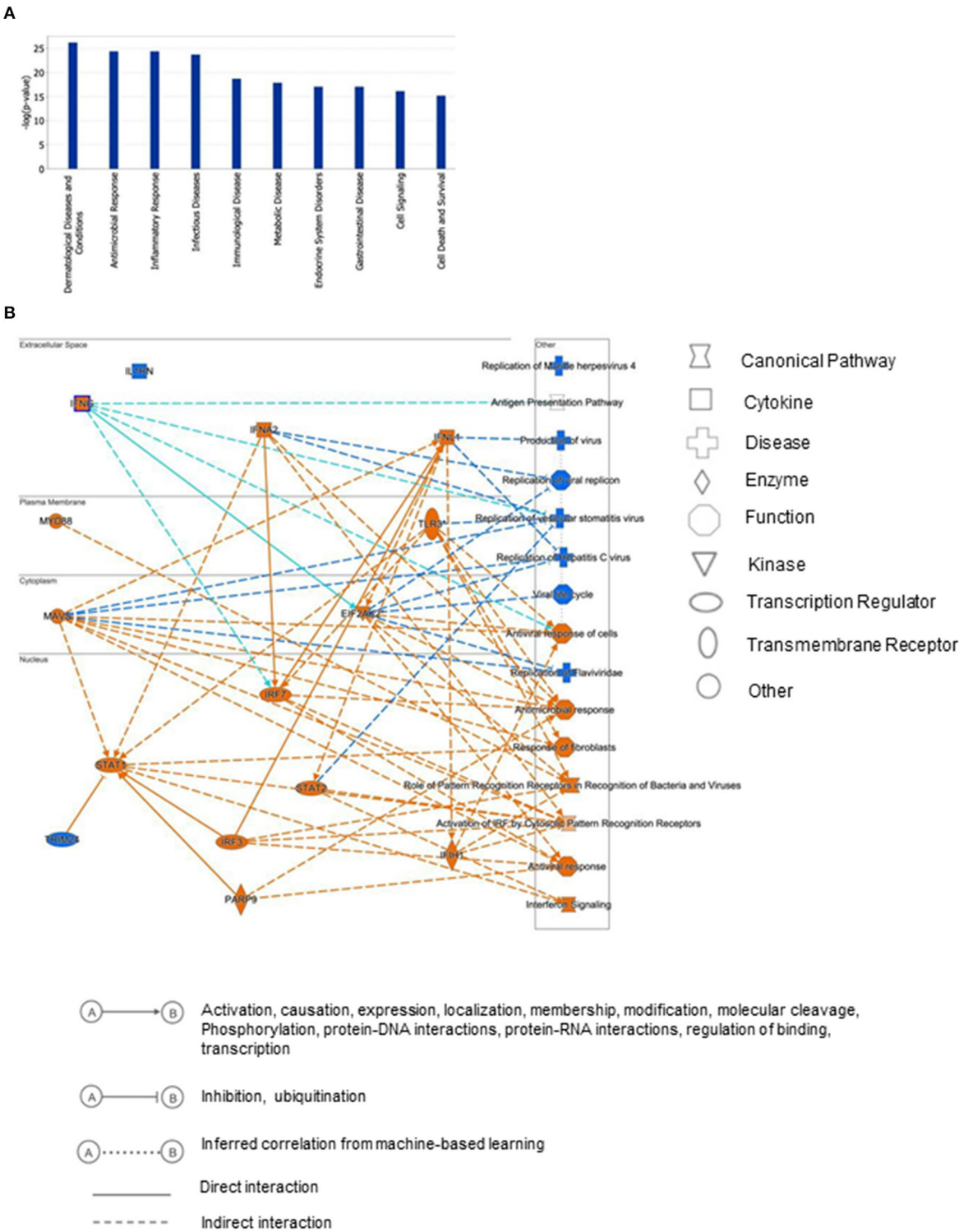


FIGURE 3
Differential gene expression profiles between siMAGI1 vs. siCont-treated ECs. **(A)** Statistical significance of the IPA-determined biological function and disease gene enrichment in siMAGI1-treated ECs calculated by the right-tailed Fisher exact test and presented as $-\log(P)$ value. A larger value on the y-axis represents greater significance. A total of 252 genes were differentially expressed in siMAGI1-transfected ECs compared to that in siCont-transfected ECs ($P < 0.05$; absolute fold change > 2). The p -value, calculated by the Fischer's exact test, reflects the likelihood that the association among a set of genes in the data set and a related biological function is significant. **(B)** Graphical summary of IPA results showing significant predictor genes that are related to antiviral response.

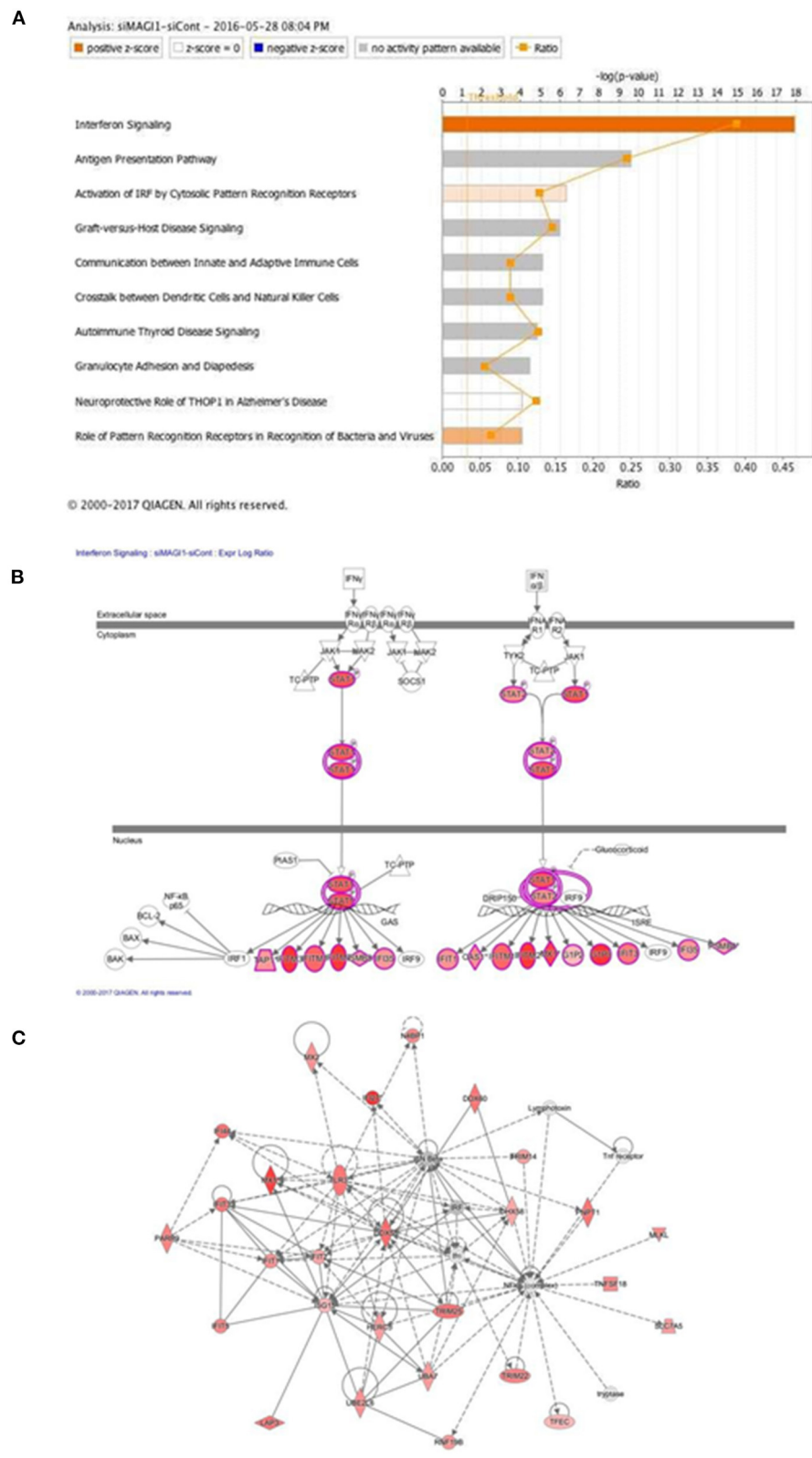


FIGURE 4
IFN signaling is the top-rank enriched IPA canonical pathway. **(A)** IPA-based identification of canonical pathways ($-\log[P] > 5$) associated with differentially expressed genes in HUVECs transfected with siMAG11 vs. siCont. The bar chart indicates the $-\log(P)$ value of the significance of (Continued)

FIGURE 4 (Continued)

enrichment of each category. (B) Induction of IFN signaling in MAGI1-depleted ECs. Pathway models of IFN signaling in ECs based on data in the Ingenuity Knowledge Base are shown. Expression of genes in red is higher in siMAGI1-treated ECs compared to that in siCont-treated ECs. (C) Gene enrichment analyses (right-tailed Fisher exact test) according to the IPA downstream effects analysis identified Antimicrobial Response, Inflammatory Response, and Infectious Diseases as the highest scoring IPA interaction networks. Green and red symbols denote genes with lower and higher expression, respectively, in siMAGI1-treated ECs compared to that in siCont-treated ECs. The arrows with solid lines indicate direct (usually physical) interactions between two molecules in the direction of the arrow. Whereas, arrows with dashed lines denote indirect interactions (e.g., molecule/gene X affects molecule/gene Y). The abbreviations shown are defined in [Supplementary Table 6](#).

[Supplementary Table 2](#)), replication of virus (z-score, -4.1 ; $P = 1.97\text{E-}24$, [Supplementary Table 3](#)), infection of mammalia (z-score, -3.6 ; $P = 9.1\text{E-}17$, [Supplementary Table 4](#)), and production of virus (z-score, -3.1 ; $P = 3.1\text{E-}07$, [Supplementary Table 5](#); [Supplementary Figure 1B](#)). We also find that IFN signaling is the top-ranked enriched IPA canonical pathway, which comprises of 36 genes, 14 of which are expressed at higher levels and thereby supporting the prediction that this pathway activation is increased in siMAGI1-transfected ECs compared to that in siCont-transfected ECs (z-score, 3.7 ; $P = 1.1\text{E-}18$) ([Figures 4A,B](#); [Supplementary Table 6](#)). Following the IPA generated network, which optimizes the interconnectivity of differentially expressed genes under the constraint of the maximal network size, we carried out Fisher's Exact Test gene set function and disease enrichment analysis to predict biological functions that are expected to be affected by a given interaction network. The gene set function and disease enrichment of the top ranked interaction networks, based on the number of interconnected differentially expressed genes, were Antimicrobial Response, Inflammatory Response, and Infectious Diseases (differentially expressed genes, 28) ([Figure 4C](#); [Supplementary Table 7](#)). As demonstrated in our network analysis ([Figure 4C](#)), although the expression of antiviral response-related genes, including *Mx1*, *Mx2*, and *Ddx58*, were upregulated in MAGI1-depleted ECs, NF- κ B expression did not exceed the gene expression significance threshold.

To verify key microarray results, we performed qRT-PCR using HUVECs transfected with siCont or siMAGI1 and evaluated relative changes in mRNA expression level of *Magi1*, *Mx1*, *Ifnb1*, *Ifna1*, *Ifng*, *Stat1*, *Stat5a*, and *Stat5b*. Knocking down MAGI1 increases mRNA expression level of *Ifnb1*, *Mx1* and *Stat1*, but decreases mRNA expression level of *Ifng*. MAGI1 depletion did not alter mRNA levels of *Ifna1*, *Stat5a*, and *Stat5b* ([Figure 5A](#)). To determine the anti-viral effects by MAGI1 depletion, we also evaluated *Oas2*, another anti-viral molecule that can cause viral RNA degradation and inhibition of viral replication (35) and find that depletion of MAGI1 by siRNA upregulated *Oas2* mRNA expression ([Figure 5B](#)). Although the goal of this study is to investigate the role of MAGI1 in IAV-associated cardiovascular diseases, we also treated HUVECs with siCont or siMAGI1 and quantified *Ifnb1* mRNA expression and observed a clear increase in *Ifnb1* mRNA expression ([Supplementary Figures 2B,C](#)), indicating that the yin-yang

form of correlation between *Magi1* and *Ifnb1* expressions is not specific to HUVECs.

We also confirmed key microarray results using immunoblotting to detect protein expression level. STAT1 protein expression was augmented by MAGI1 depletion ([Figure 5C](#)). Total STAT5 activity (p-STAT5 T694 represents total STAT5 activity including total STAT5 expression) was increased by siMAGI1 transfection ([Figure 5C](#)). We have also shown that the level of secreted IFN β in conditioned medium from siMAGI1-transfected ECs was increased compared to that from siCont-transfected ECs ([Figure 5D](#)). These data suggest that MAGI1 depletion differentially affects IFN signaling both in mRNA and protein levels.

To clarify the role of MAGI1 in IFN signaling, we performed two types of overexpression studies. First, we overexpressed MAGI1 and measured the relative changes in *Ifnb1* mRNA expressions. In ECs overexpressing MAGI1, *Ifnb1* mRNA expression levels were decreased ([Figures 5E,F](#)). Next, we determined if MAGI1 overexpression altered MX1 expression and observed little change (data not shown). Therefore, we stimulated ECs overexpressing MAGI1 with a low dose of IFN (200 U/mL), and observed a decreased MX1 expression ([Figure 5G](#)). It is unclear why *Ifnb1* mRNA and MX1 protein expression respond differently to MAGI1 overexpression; however, it is possible that IFN-mediated signaling such as p90RSK activation may potentiate the inhibitory effects of MAGI1 on MX1 expression through promoting MAGI1 post-translational modification (20). These data support a role for MAGI1 in promoting viral infection in ECs.

Knocking down MAGI1 suppresses IAV infection partially through increasing MX1 expression

Since MX1 exerts broad antiviral activity against several strains of viruses including IAV (36–38), we tested whether the MAGI1 depletion-induced virus suppression could be due to increased MX1 expression. HUVECs were transfected with siCont, siMX1, siMAGI1, or siMX1+siMAGI1 and then infected with IAV. We extracted total RNA from these cells and performed qRT-PCR to detect relative changes in viral NP mRNA expressions. Cell lysates were also immunoblotted

for MX1 protein expression. Knocking down MAGI1 increased MX1 expression. However, depletion of MX1 exerted no effect on MAGI1 expression (Figures 6A,B). Since we also noted the reduced MX1 expression by MAGI1 overexpression only occurs under IFN stimulation (Figure 5G), these data have suggested that MAGI1 is an upstream signaling event for regulating MX1 expression in ECs. The depletion of MAGI1 by siMAGI1 increased MX1 expression (Figure 6B), and the partial significant inhibition of MX1 expression after siMX1 transfection was due to the incomplete transfection efficiency by siMX1. We also observed that siMX1 reversed the anti-viral effects induced by siMAGI1, suggesting that siMAGI1-mediated induction of MX1 plays a meaningful role in siMAGI1-mediated anti-viral response. However, siMAGI1 leads to the inhibition of influenza infection (Figure 6C), which was in part due to the induction of MX1. In fact, in addition to MX1, we also found that the depletion of MAGI1 by siMAGI1 upregulated *Oas2* mRNA expression (Figure 5B). Furthermore, we also found the upregulation of *Ifnb1* (Figures 5A,B) and *Stat1* (Figures 5A,C) expression, STAT5 activation (Figure 5C), and IRF3 nuclear translocation (Figure 7B) which played a significant role in developing anti-viral response (Figure 7E) (39–42). Therefore, siMAGI1 can induce anti-viral effects not only through MX1 but also by induction of other anti-viral molecules (Figure 7E).

The *Mx1* gene in C57BL/6 mice contains a large deletion, which creates the MX1 null phenotype, a condition that increases susceptibility of this mouse strain to IAV (43, 44). We took advantage of this fact (i.e., *Mx1* null condition in C57BL/6 mice) to further determine if MAGI1 depletion in mice lacking MX1 still inhibits IAV infection. Mouse ECs were isolated from the lungs of *Magi1*^{−/−} and WT littermate control mice and cultured to confluence on gelatin-coated plates. The cells were then infected with virus for 24 h. Total mRNA was extracted from the infected cells, and relative changes in viral NP mRNA expression levels were determined by qRT-PCR (Figure 6D). No difference in NP mRNA expression was found between WT and *Magi1*^{−/−} mouse ECs. Whereas, we showed that NP mRNA burden is correlated with viral burden and infectivity (24), these results indicate that MX1 promotes the inhibition of virus replication caused by MAGI1 depletion.

Knocking down MAGI1 promotes IRF3 nuclear translocation and de-SUMOylation without affecting IRF3 phosphorylation

MAGI1 depletion in human lung epithelial cells increases phosphorylation of IRF3, an upstream transcriptional regulator of IFN genes, at S396, which triggers IRF3 translocation into the nucleus and activation IFN- β signaling (45, 46). Following activation in the cytoplasm, IRF3 translocate into

the nucleus and promotes the transcription of IFN- α and - β and IFN-stimulated genes by binding to the interferon-stimulated response element (ISRE) (47, 48). However, it is still not clear if ECs respond in the same manner. To address this question, we treated HUVECs with either siMAGI1 or siCont and detected IRF3 S396 phosphorylation and nuclear translocation. According to immunoblot analysis, similar levels of IRF3 phosphorylation at S396 was observed in control and MAGI1-depleted cells (Figures 5C, 7A,C). By contrast, IRF3 nuclear translocation was clearly observed in MAGI1-depleted HUVECs while the cytoplasmic staining was prevalent in cells treated with siCont (Figure 7B), suggesting that IRF3 nuclear translocation is involved in siMAGI1-mediated upregulation of IFN expression. Kubota et al. showed that virus infection enhances IRF3 SUMOylation, thereby attenuating IFN production (49). This finding has led us to investigate the potential role of MAGI1 on IRF3 SUMOylation. After 48 h of either siMAGI1 or siCont transfection, we lysed the cells and immuno-precipitated IRF3 with the antibody that specifically recognizes this protein. IgG antibody was used as a negative control. We then utilized immunoblotting to assess SUMOylated IRF3 using the antibody that recognizes only SUMO1. We found a significant decrease in IRF3 SUMOylation by MAGI1 depletion (Figures 7C,D), suggesting the upregulation of IRF3 transcriptional activity as described previously (49). These data suggest that MAGI1 depletion increased IRF3 transcriptional activity *via* downregulated IRF3 SUMOylation and promoted IRF3 nuclear translocation, which may be independent of IRF3 phosphorylation (Figure 7E).

Discussion

In this study, we find that IAV infection and OxLDL pre-treatment upregulate MAGI1 expression in ECs. Influenza replication is increased by OxLDL pre-treatment. Whereas, MAGI1 depletion decreased virus replication, suggesting the crucial role of IAV-induced MAGI1 expression in promoting IAV infection in hypercholesterolemia patients. In MAGI1-depleted ECs, we also noted heightened anti-viral events such as upregulation of IFN signaling and response-related gene expression including MX1 and OAS2. Lastly, we find that MAGI1 depletion inhibits IRF3 SUMOylation, which subsequently induces IRF3 activation. Our results suggest that IAV and/or OxLDL-induced MAGI1 expression accelerates virus infection in ECs and that MAGI1 depletion effectively inhibits this process. The data collectively provides insights into the role of MAGI1 in influenza infection as well as associated cardiovascular disease observed in dyslipidemia patients (11–15).

This study is the first to show that IAV infection increases MAGI1 expression in cultured ECs and that MAGI1 depletion suppresses IAV replication by increasing MX1 expression, a

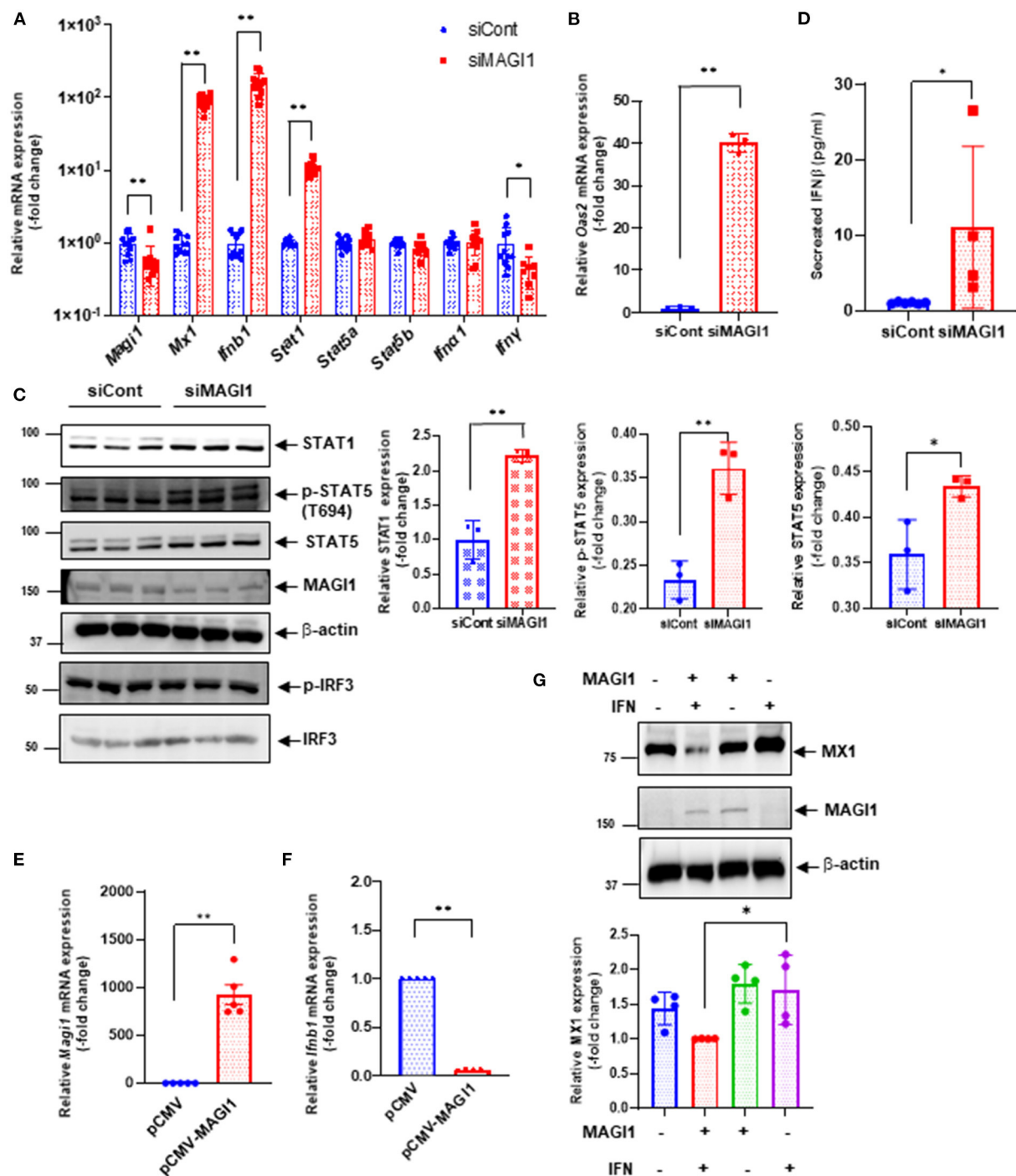


FIGURE 5

MAGI1 suppresses IFN signaling in ECs. (A) HUVECs were transfected with either siCont or siMAGI1. After 48 h of transfection, total RNA was extracted then qRT-PCR was performed. Relative changes in *Magi1*, *Mx1*, *Ifnb1*, *Ifna1*, *Ifng1*, *Stat1*, *Stat5a*, and *Stat5b* expression were calculated using the comparative C_t ($2^{-\Delta\Delta C_t}$) method. C_t values of each target gene were normalized to that of the *Gapdh* (26). Each group passed the Shapiro-Wilk normality test, then an unpaired student *t*-test was performed using the Prism software (GraphPad Software). The graph shows mean \pm SD ($n = 11$). ** $p < 0.01$, * $p < 0.05$. (B) HUVECs were transfected with either siCont or siMAGI1. After 48 h of transfection, total RNA was extracted then qRT-PCR was performed. Relative changes in *Oas2* mRNA expression were calculated using the comparative C_t ($2^{-\Delta\Delta C_t}$) method. C_t values of *Oas2* were normalized to that of the *Gapdh* (26). Each group passed the Shapiro-Wilk normality test, then an unpaired student *t*-test was performed using the Prism software (GraphPad Software). The graph shows mean \pm SD ($n = 3$). ** $p < 0.01$. (C) HUVECs were transfected with either siCont or siMAGI1. After 48 h of transfection, cell lysates were analyzed by immunoblotting with each specific antibody as indicated.

(Continued)

FIGURE 5 (Continued)

The graphs represent densitometry data from 3 independent gels, one of which is shown in the left panel. Each group passed the Shapiro-Wilk normality test, then an unpaired student *t*-test was performed using the Prism software (GraphPad Software). The graph shows mean \pm SD, *n* = 3, ***P* < 0.01, and **P* < 0.05. Uncropped figures were provided in the supplements. (D) HUVECs were transfected with either siCont or siMAGI1. After 48 h of transfection, conditioned medium was collected and levels of IFN β were measured. Each group passed the Shapiro-Wilk normality test, then an unpaired student *t*-test was performed using the Prism software (GraphPad Software). The graph shows mean \pm SD, *n* = 4–6, **P* < 0.05. (E,F) HUVECs were transfected with either the pCMV-MAGI1 or the pCMV-2B backbone construct (control) (20). After 24 h of transfection, total RNA was extracted then qRT-PCR was performed. Relative changes in *Magi1* (E) and *Irfn1* (F) mRNA expression were calculated using the comparative *C_t* ($2^{-\Delta\Delta C_t}$) method. *C_t* values of each target gene were normalized to that of the *gapdh* (26). At least, one of the groups did not pass the Shapiro-Wilk normality test, we performed an unpaired *t*-test with Welch's correction using the Prism software (GraphPad Software). The graph shows mean \pm SD, *n* = 5, ***P* < 0.01. (G) HUVECs were transfected with either the pCMV-MAGI1 or the pCMV-2B backbone construct (control) (20). After 24 h of transfection, the cells were treated with IFN (200 U/mL) for 6 h, and immunoblotting was performed with each specific antibodies as indicated. The graph (lower) represents densitometry data from 4 independent gels, one of which is shown in the top panel. Each group passed the Shapiro-Wilk normality test, then one-way ANOVA followed by Turkey's multiple comparisons test was performed using the Prism software (GraphPad Software). The graph shows mean \pm SD (*n* = 4). **p* < 0.05.

process that appears to induce IFN production. Indeed, others have shown that increased MX1 expression induces IFN- β production (46). The consensus PDZ-binding motif ESEV (glu-ser-glu-val) (PBM) in NS1 protein of IAV binds the PDZ domain of various proteins. MAGI1 has six PDZ domains, thus, it is possible that the binding between the virus NS1 PBM and MAGI1 plays a major role in viral infection and replication (48, 50). Since we find that virus infection upregulated MAGI1 expression, this increased MAGI1 expression provides a favorable environment for virus to replicate and thereby forming a positive feedback loop. Thus, MAGI1 depletion should break this cycle and suppress virus infection and replication. Our results have supported this model. In this study, we have also shown that knocking down MX1 impairs MAGI1 depletion-mediated IAV suppression. Moreover, the impaired virus infection caused by MAGI1 depletion was not detected in cultured lung ECs derived from C57BL/6 mice that are known to carry a truncated *Mx1* gene, which results in the MX1 null phenotype. The anti-viral effect of MX1 *in vivo* was clearly demonstrated using mouse models with and without MX1 expression (51). Together, these results suggest that MAGI1 depletion mediates the suppression of IAV infection, at least in part, by increasing MX1 expression. We also find upregulation of a broad range of IFN signaling network-related molecules (Figure 4) including the increase of STAT1 and *Oas2* expression and STAT5 activity (Figure 5), revealing how the depletion of MAGI1 can induce a strong anti-viral response (Figure 7E).

IRF3, a key transcriptional regulator of type I interferon, regulates the transcription of IFN- β and IFN-stimulated genes by binding the ISRE in their promoters. Upon viral infection, IRF3 in the cytoplasm of the infected cells is phosphorylated by the kinases TBK1 and IKK ϵ , and undergoes a conformational change and homo-dimerization, which permits its translocation to the nucleus where it binds the ISRE of target genes (46, 47). Knocking down MAGI1 specifically in lung epithelial cells causes IRF3 S396 phosphorylation and increased IFN production (46). Interestingly, although we found a clear IRF3 nuclear translocation after MAGI1

depletion, we did not detect significant increases of IRF3 phosphorylation under the same condition (Figures 7A,B). This led us to investigate other types of IRF3 post-translational modifications, and we found a significant decrease of IRF3 SUMOylation induced by MAGI1 depletion (Figures 7C,D). Since the activation of IRF3 by attenuating IRF3 SUMOylation has been reported (49), the decrease of IRF3 SUMOylation by siMAGI1 transfection can induce IRF3 nuclear translocation and transcriptional activity. Of note, we have reported that the similar effect of p53 SUMOylation in ECs cultured under disturbed flow leading to p53 nuclear export (52). Therefore, both p53 and IRF3 SUMOylation may be important to restrain these proteins in the cytoplasm, and after losing this modification, p53 and IRF3 translocate to the nucleus. Furthermore, we have previously reported that de-SUMOylation enzyme of sentrin/SUMO-specific protease 2 (SEN2) regulates MAGI1 SUMOylation and de-SUMOylation of MAGI1 induced by SEN2 promotes MAGI1 nuclear translocation and subsequent EC activation (20). Therefore, MAGI1 may inhibit IRF3 SUMOylation by modulating SEN2 function. Future studies will be necessary to clarify these issues.

EC activation is a major cause of cardiovascular disease. Our study revealed upregulation of ICAM-1 expression in IAV-infected ECs, indicating that virus infection activates ECs, and increasing the risk of cardiovascular dysfunction in influenza patients. In our recent study, we have shown that MAGI1 plays a major role in atherogenesis by inducing pro-inflammatory signaling in ECs (20). The role of MAGI1 in EC activation was confirmed by knock down studies, in which the virus induced ICAM-1 elevation was strongly inhibited. Together, these results show that MAGI1 could be the molecular link between IAV infection and cardiovascular disease. Furthermore, our current study shows that MAGI1 expression is upregulated under a pro-atherogenic, physiological perturbation i.e., OxLDL treatment (Figures 2A,B). More importantly, the pre-treatment of OxLDL upregulates virus infection in ECs (Figure 7C), suggesting that the induction of MAGI1 by OxLDL increases EC activation and accelerates virus infection by inhibiting

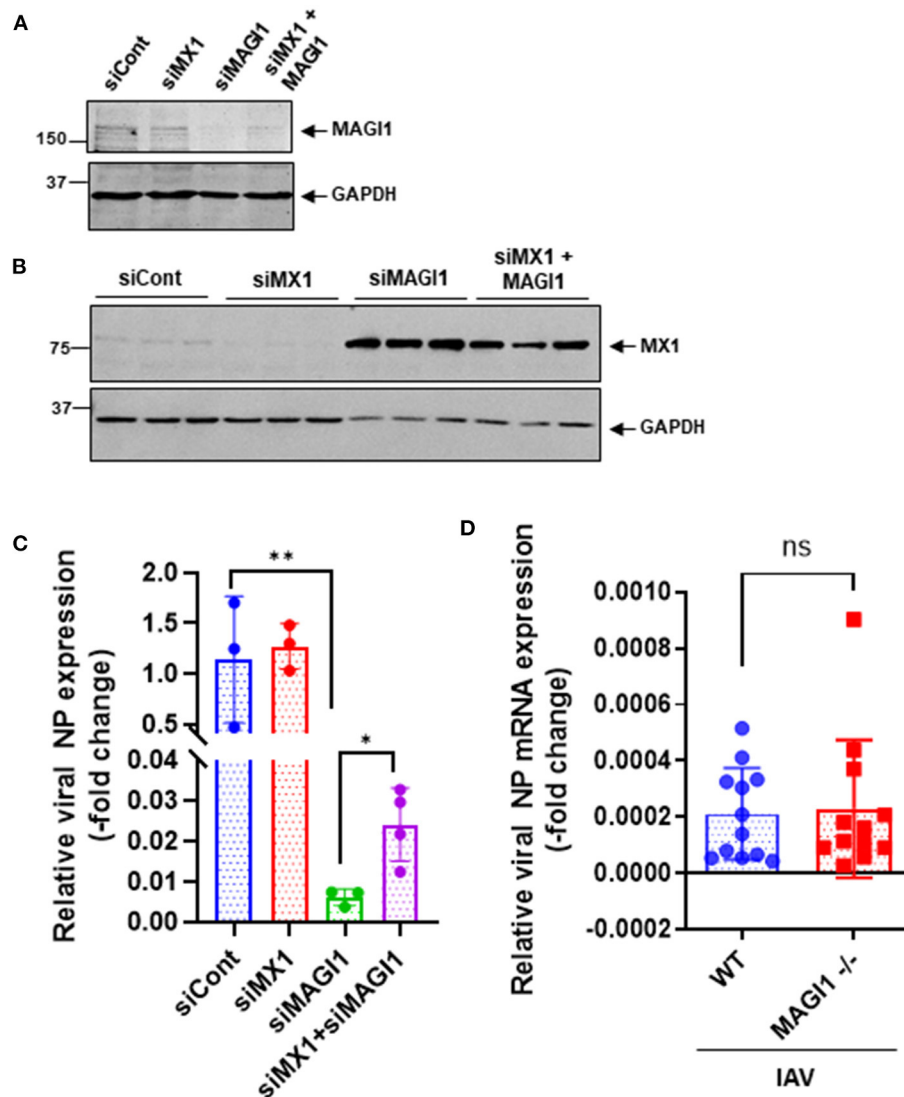


FIGURE 6

MX1 depletion reverses MAGI1 depletion-mediated suppression of IAV infection. (A,B) HUVECs were transfected with either siCont, siMX1, siMAGI1, or siMX1+siMAGI1. After 48 h of transfection, cell lysates were analyzed by immunoblotting with each specific antibody as indicated. Gels are representative of 3 independent experiments. (C) HUVECs were transfected with either siCont, siMX1, siMAGI1, or siMX1+siMAGI1. After 48 h of transfection, the cells were infected with IAV for 24 h. Total RNA was extracted then qRT-PCR was performed. Relative changes in the viral NP mRNA expression were calculated using the comparative C_t ($2^{-\Delta\Delta C_t}$) method. C_t values of the viral NP were normalized to that of the 18S ribosomal RNA (26). Each group passed the Shapiro-Wilk normality test, then one-way ANOVA followed by Turkey's multiple comparisons test was performed using the Prism software (GraphPad Software). The graph shows mean \pm SD ($n = 3-4$). $**p < 0.01$, $*p < 0.05$. (D) Mouse lung ECs were isolated from *Magi1*^{-/-} and littermate wild type (WT) control mice and cultured. The cells were infected with IAV for 24 h. Total RNA was extracted then qRT-PCR was performed. Relative changes in the viral NP mRNA expression were calculated using the comparative C_t ($2^{-\Delta\Delta C_t}$) method. C_t values of the viral NP were normalized to that of the 18S ribosomal RNA (26). Each group passed the Shapiro-Wilk normality test, then an unpaired student *t*-test was performed using the Prism software (GraphPad Software). The graph shows mean \pm SD, $n = 11$. NS: not significant.

IAV-mediated anti-viral responses (Figure 7E). It has been reported that IL-1 β stimulation induces VCAM-1 expression rapidly and temporally although sustaining ICAM-1 expression over 24–72 h (53). Therefore, the inhibition of VCAM-1 expression in our study may be due to a counter-response

to the initial increase of VCAM-1 expression induced by influenza A.

In addition to MAGI1, which has six PDZ domains, there are other PDZ domain-containing proteins—Dlg1, MAGI2, MAGI3, Scribble, Lin7C, PDLIM2 and PSD-95 - are potential

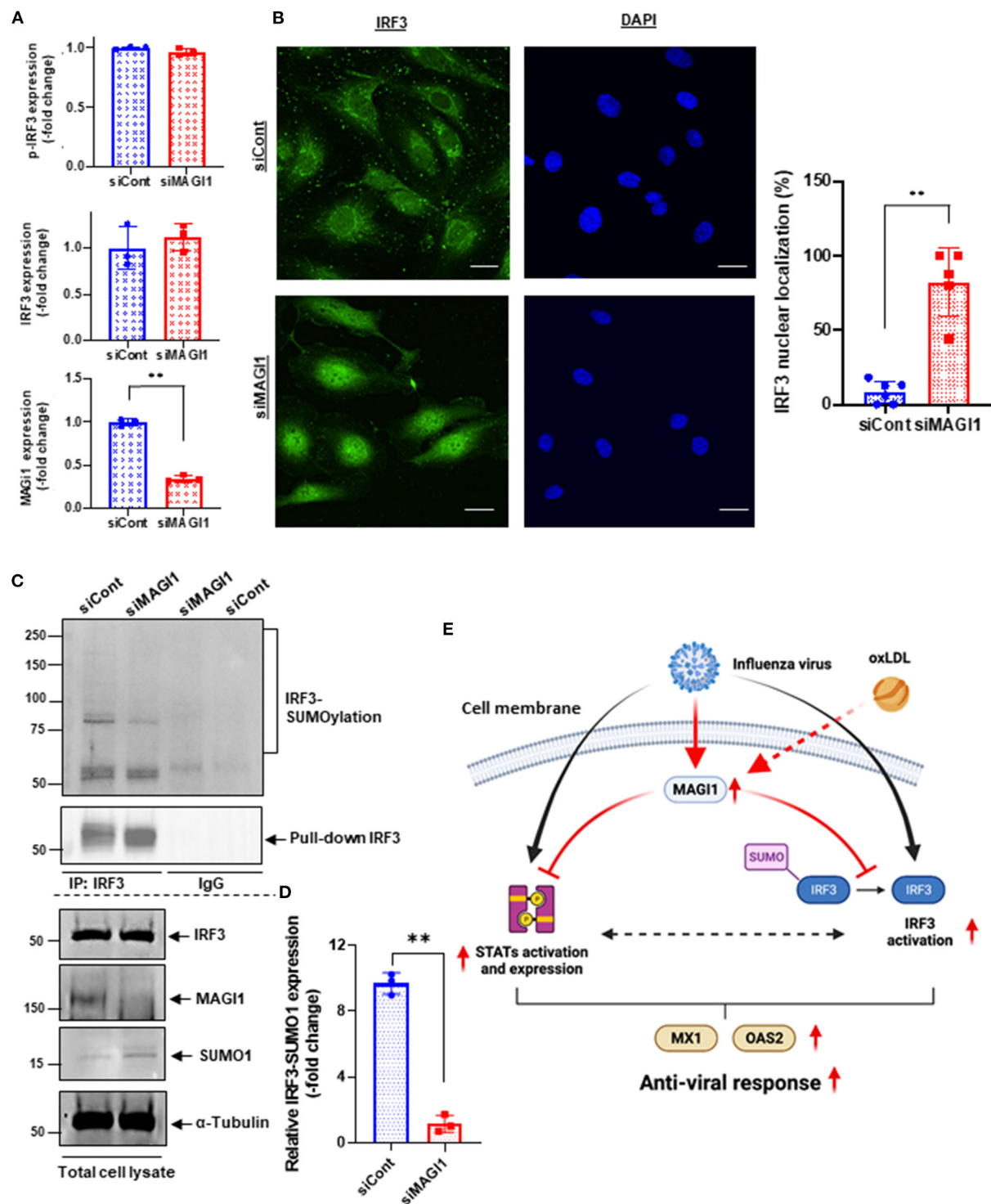


FIGURE 7

MAGI1 depletion promotes IRF3 nuclear translocation and de-SUMOylation without affecting IRF3 S396 phosphorylation. (A) HUVECs were transfected with either siCont or siMAGI1. After 48 h of transfection, cell lysates were analyzed by immunoblotting with each specific antibody as indicated. The graphs represent densitometry data from 3 independent gels, one of which is shown in Figure 5C. Each group passed the Shapiro-Wilk normality test, then an unpaired student *t*-test was performed using the Prism software (GraphPad Software). The graphs show mean \pm SD, *n* = 3, ***P* < 0.01. (B) HUVECs were transfected with either siCont or siMAGI1. After 48 h of transfection, immunofluorescence staining for IRF3 protein (green) and DAPI staining for the nuclei (blue) were performed. Scale bars: 20 μ M. Robust IRF3 nuclear translocation

(Continued)

FIGURE 7 (Continued)

noted in siMAGI1-transfected cells. The percentages of cells with nuclear staining were quantified by counting the cells with the mean intensity of IRF3 staining in the nucleus \geq mean intensity of IRF3 cytoplasmic staining by each dish ($n = 5-6$) in a blinded manner. **(C)** HUVECs were transfected with either siCont or siMAGI1. After 48 h of transfection, cell lysates were immuno-precipitated IRF3 with the antibody that specifically recognizes this protein then immunoblotting with the antibody that recognizes SUMO1 to detect IRF3 SUMOylation (20). IgG antibody was used as a negative control. Total cell lysates were immunoblotted with each specific antibody as indicated. **(D)** The graphs represent densitometry data from 3 independent gels, one of which is shown in shown in **(C)**. Median intensities of IRF3 SUMOylation were calculated after subtracting the background, which is median intensities of IgG control. Each group passed the Shapiro-Wilk normality test, then an unpaired student *t*-test with Welch's correction was performed using the Prism software (GraphPad Software). The graph shows mean \pm SD, $n = 3$, $**P < 0.01$. **(E)** The scheme depicts the relationship between MAGI1 and IFN signaling. IAV infection induces anti-viral responses including STATs and IRF3 activation and subsequent MX1 and OAS2 induction. For efficient infection of IAV to ECs, IAV induces MAGI1 expression, resulting in inhibition of anti-viral responses by inhibiting STATs and IRF3 activation. Especially, MAGI1 inhibits IRF3 de-SUMOylation and subsequent IRF3 activation. Importantly, OxLDL also upregulates MAGI1 expression and promotes IAV infection, which may explain the relationship between hypercholesterolemia and IAV infection in patients. The scheme was generated using BioRender.

targets of the NS1 protein of IAV that has the consensus PDZ-binding motif, ESEV (glu-ser-glu-val) (PBM). Indeed, PBM association with Scribble and Dlg1 promotes virus infection (48). Our study shows that MAGI1 also promotes virus infection, presumably *via* its interaction with PBM. Since MAGI1 depletion robustly inhibits IAV infection, MAGI1's role in supporting virus infection is larger than that of Scribble and Dlg1.

In conclusion, we have found that MAGI1 is involved in IAV infection of ECs. Previously, we have reported the crucial role of MAGI1 in EC activation and subsequent atherogenesis (20). In the current report, we found that IAV infection increases MAGI1 expression and enhances virus infection by inhibiting various anti-viral responses including STATs and IRF3 activation and induction of MX1 and OAS2 (Figure 7E). We also find that MAGI1 inhibits IRF3 de-SUMOylation, resulting in inhibiting IRF3 activation. These data suggest the crucial role of MAGI1 in inhibiting IAV-mediated anti-viral responses, and the induction of MAGI1 by OxLDL and IAV infection itself can accelerate further virus infection and promote severe EC activation (Figure 7E). Thus, MAGI1 as a promotor of both EC activation and virus infection, is a potential therapeutic target for influenza virus infection.

Data availability statement

The datasets presented in this study can be found in online repositories. The microarray data and MAGI1 sequence were deposited in the NCBI's Gene Expression Omnibus database (accession GSE95066) and GenBank (accession KY651081), respectively.

Ethics statement

The animal study was reviewed and approved by the Institutional Care and Use Committees of the Texas A&M Institute of Biosciences and Technology and The University of Texas MD Anderson Cancer Center.

Author contributions

YinW performed experiments, analyzed data, and drafted manuscript. J-iA planned and oversaw the project, funded research, performed data analysis, and wrote the manuscript. KC, YongW, HV, LR, and FG performed experiments. MI, VS, MN, KK, L-LL, and TT supported the experiments and interpretation of the data. EO-D, JC, SK, and KF contributed to the interpretation of the data and edited the manuscript. SE and N-TL planned and generated the study design, obtained funding, interpreted data, and wrote the manuscript. All authors contributed to the article and approved the submitted version.

Funding

This study was partially supported by funding's from the National Institutes of Health (NIH) to J-iA, N-TL, and JC (HL149303), J-iA (AI156921), JC (HL148338 and HL157790), N-TL (HL-134740), and SE (HL144805).

Acknowledgments

All authors would like to thank Dr. Henry J. Pownall (Houston Methodist Research Institute) for a critical reading of this manuscript.

Conflict of interest

The authors declare that the research was conducted in the absence of any commercial or financial relationships that could be construed as a potential conflict of interest.

Publisher's note

All claims expressed in this article are solely those of the authors and do not necessarily represent those of their affiliated organizations, or those of the publisher, the editors and the

reviewers. Any product that may be evaluated in this article, or claim that may be made by its manufacturer, is not guaranteed or endorsed by the publisher.

Supplementary material

The Supplementary Material for this article can be found online at: <https://www.frontiersin.org/articles/10.3389/fcvm.2022.791143/full#supplementary-material>

SUPPLEMENTARY FIGURE 1

Heat maps based on Ingenuity Downstream Effects Analysis (Diseases and Functions analysis). The maps show the functional hierarchy for differential gene expression in siMAGI1-transfected HUVECs with the significance and predicted activity state of gene sets identified by the Ingenuity Knowledge Base. The color-coded scales above both heat maps reflect the direction of change for each function based on activation z-scores (orange, upregulation; blue, downregulation; white, z-score of 0; gray, not available). (A) The level 1 squares in this heat map (high-level functional categories) indicate the functions predicted to increase or decrease with MAGI1 depletion. The size of each box reflects the *P*-value (the larger the box, the smaller the *P*-value). The *P*-values for the Infectious Disease categories are within the six highest category. The z-score for the Infectious Disease category is predicted to decrease with MAGI1 depletion. (B) The hierarchical heat map of the level 1 category Infectious Disease.

SUPPLEMENTARY FIGURE 2

Magi1, *Vcam1*, and *Ifnβ1* mRNA expression. (A) HUVECs were transfected with either siCont or siMAGI1. Approximately after 48 h of transfection, the cells were infected or not infected with IAV for 24 h.

Total RNA was extracted then qRT-PCR was performed. Relative changes in *Vcam1* mRNA expression were calculated using the comparative C_t ($2^{-\Delta\Delta C_t}$) method. C_t values of *Vcam1* mRNA expression were normalized to that of *Gapdh* (26). Each group passed the Shapiro-Wilk normality test, then two-way ANOVA followed by Turkey's multiple comparisons test was performed using the Prism software (GraphPad Software). The graph shows mean \pm SD ($n = 3$). $**p < 0.01$. (B,C) HUVECs were transfected with either siCont or siMAGI1. Approximately after 48 h of transfection, total RNA was extracted then qRT-PCR was performed. Relative changes in *Magi1* (B) and *Ifnβ1* (C) mRNA expression were calculated using the comparative C_t ($2^{-\Delta\Delta C_t}$) method. C_t values of each target gene were normalized to that of β -actin (26). At least, one of the groups did not pass the Shapiro-Wilk normality test, we performed an unpaired *t*-test with Welch's correction using the Prism software (GraphPad Software). The graph shows mean \pm SD, $n = 3$, $**P < 0.01$.

SUPPLEMENTARY TABLE 1

Oligonucleotide sequences.

SUPPLEMENTARY TABLE 2

Viral infection.

SUPPLEMENTARY TABLE 3

Replication of virus.

SUPPLEMENTARY TABLE 4

Infection of mammalia.

SUPPLEMENTARY TABLE 5

Production of virus.

SUPPLEMENTARY TABLE 6

Interferon signaling.

SUPPLEMENTARY TABLE 7

Antimicrobial response, inflammatory response, and infectious diseases.

References

- ReferencesDou D, Revol R, Ostbye H, Wang H, Daniels R. Influenza A virus cell entry, replication, virion assembly and movement. *Front Immunol.* (2018) 9:1581. doi: 10.3389/fimmu.2018.01581
- Eisfeldt AJ, Neumann G, Kawaoka Y. Influenza A virus isolation, culture and identification. *Nat Protoc.* (2014) 9:2663–81. doi: 10.1038/nprot.2014.180
- Flerlage T, Boyd DF, Meliopoulos V, Thomas PG, Schultz-Cherry S. Influenza virus and SARS-CoV-2: pathogenesis and host responses in the respiratory tract. *Nat Rev Microbiol.* (2021) 19:425–41. doi: 10.1038/s41579-021-00542-7
- Piantadosi CA, Schwartz DA. The acute respiratory distress syndrome. *Ann Intern Med.* (2004) 141:460–70. doi: 10.7326/0003-4819-141-6-200409210-00012
- Sugiyama MG, Gamage A, Zyla R, Armstrong SM, Advani S, Advani A, et al. Influenza virus infection induces platelet-endothelial adhesion which contributes to lung injury. *J Virol.* (2016) 90:1812–23. doi: 10.1128/JVI.02599-15
- Hiyoshi M, Indalao IL, Yano M, Yamane K, Takahashi E, Kido H, et al. Influenza A virus infection of vascular endothelial cells induces GSK-3beta-mediated beta-catenin degradation in adherens junctions, with a resultant increase in membrane permeability. *Arch Virol.* (2015) 160:225–34. doi: 10.1007/s00705-014-2270-5
- Armstrong SM, Wang C, Tigdi J, Si X, Dumpit C, Charles S, et al. Influenza infects lung microvascular endothelium leading to microvascular leak: role of apoptosis and claudin-5. *PLoS ONE.* (2012) 7:e47323. doi: 10.1371/journal.pone.0047323
- Short KR, Kroeze E, Fouchier RM, Kuiken T. Pathogenesis of influenza-induced acute respiratory distress syndrome. *Lancet Infect Dis.* (2014) 14, 57–69. doi: 10.1016/S1473-3099(13)70286-X
- Yang Y, Tang H. Aberrant coagulation causes a hyper-inflammatory response in severe influenza pneumonia. *Cell Mol Immunol.* (2016) 13:432–42. doi: 10.1038/cmi.2016.1
- Fong IW. New perspectives of infections in cardiovascular disease. *Curr Cardiol Rev.* (2009) 5:87–104. doi: 10.2174/157340309788166679
- Hebsur S, Vakil E, Oetgen WJ, Kumar PN, Lazarous DF. Influenza and coronary artery disease: exploring a clinical association with myocardial infarction and analyzing the utility of vaccination in prevention of myocardial infarction. *Rev Cardiovasc Med.* (2014) 15:168–75. doi: 10.3909/ricm0692
- Ludwig A, Lucero-Obusan C, Schirmer P, Winston C, Holodniy M. Acute cardiac injury events ≤ 30 days after laboratory-confirmed influenza virus infection among U.S. veterans, 2010–2012. *BMC Cardiovasc Disord.* (2015) 15:109. doi: 10.1186/s12872-015-0095-0
- Vejpongsa P, Kitkungvan D, Madjid M, Charitakis K, Anderson HV, Arain S, et al. Outcomes of acute myocardial infarction in patients with influenza and other viral respiratory infections. *Am J Med.* (2019) 132:1173–81. doi: 10.1016/j.amjmed.2019.05.002
- Kytomaa S, Hegde S, Claggett B, Udell JA, Rosamond W, Temte J, et al. Association of influenza-like illness activity with hospitalizations for heart failure: the atherosclerosis risk in communities study. *JAMA Cardiol.* (2019) 4:363–9. doi: 10.1001/jamacardio.2019.0549
- Haidari M, Wyde PR, Litovsky S, Vela D, Ali M, Casscells SW, et al. Influenza virus directly infects, inflames, and resides in the arteries of atherosclerotic and normal mice. *Atherosclerosis.* (2010) 208:90–6. doi: 10.1016/j.atherosclerosis.2009.07.028
- Tejaro JR, Walsh KB, Cahalan S, Fremgen DM, Roberts E, Scott F, et al. Endothelial cells are central orchestrators of cytokine amplification during influenza virus infection. *Cell.* (2011) 146:980–91. doi: 10.1016/j.cell.2011.08.015
- Bazaz R, Marriott HM, Francis SE, Dockrell DH. Mechanistic links between acute respiratory tract infections and acute coronary syndromes. *J Infect.* (2013) 66:1–17. doi: 10.1016/j.jinf.2012.09.009
- Abe RJ, Savage H, Imanishi M, Banerjee P, Kotla S, Paez-Mayorga J, et al. Corrigendum: p90RSK-MAGI1 module controls endothelial permeability by post-translational modifications of magi1 and hippo pathway. *Front Cardiovasc Med.* (2021). doi: 10.3389/fcvm.2021.663486

19. Abe RJ, Savage H, Imanishi M, Banerjee P, Kotla S, Paez-Mayorga J, et al. 90RS.K-MAGI1 module controls endothelial permeability by post-translational modifications of MAGI1 and hippo pathway. *Front Cardiovasc Med.* (2020) 7:542485. doi: 10.3389/fcvm.2020.542485
20. Abe JI, Ko KA, Kotla S, Wang Y, Paez-Mayorga J, Shin IJ, et al. MAGI1 as a link between endothelial activation and ER stress drives atherosclerosis. *JCI Insight.* (2019) 4:e125570. doi: 10.1172/jci.insight.125570
21. Dobrosotskaya I, Guy RK, James GL. MAGI-1, a membrane-associated guanylate kinase with a unique arrangement of protein-protein interaction domains. *J Biol Chem.* (1997) 272:31589–97. doi: 10.1074/jbc.272.50.31589
22. Hirabayashi S, Tajima M, Yao I, Nishimura W, Mori H, Hata Y, et al. JAM4, a junctional cell adhesion molecule interacting with a tight junction protein, MAGI-1. *Mol Cell Biol.* (2003) 23:4267–82. doi: 10.1128/MCB.23.12.4267–4282.2003
23. Alonso A, Domenech E, Julia A, Panes J, Garcia-Sanchez V, Mateu PN, et al. Identification of risk loci for Crohn's disease phenotypes using a genome-wide association study. *Gastroenterology.* (2015) 148:794–805. doi: 10.1053/j.gastro.2014.12.030
24. Kirkpatrick CT, Wang Y, Leiva Juarez MM, Shivshankar P, Pantaleon Garcia J, Plumer AK, et al. Inducible lung epithelial resistance requires multisource reactive oxygen species generation to protect against viral infections. *MBio.* (2018) 9:e00696–18. doi: 10.1128/mBio.00696-18
25. Jonges M, Liu WM, Van Der Vries E, Jacobi R, Pronk I, Boog C, et al. Influenza virus inactivation for studies of antigenicity and phenotypic neuraminidase inhibitor resistance profiling. *J Clin Microbiol.* (2010) 48:928–40. doi: 10.1128/JCM.02045-09
26. Wong ML, Medrano JF. Real-time PCR for mRNA quantitation. *Biotechniques.* (2005) 39:75–85. doi: 10.2144/05391RV01
27. Paez-Mayorga J, Chen AL, Kotla S, Tao Y, Abe RJ, He ED, et al. Ponatinib activates an inflammatory response in endothelial cells via ERK5 SUMOylation. *Front Cardiovasc Med.* (2018) 5:125. doi: 10.3389/fcvm.2018.00125
28. Onat D, Brillon D, Colombo PC, Schmidt AM. Human vascular endothelial cells: a model system for studying vascular inflammation in diabetes and atherosclerosis. *Curr Diab Rep.* (2011) 11:193–202. doi: 10.1007/s11892-011-0182-2
29. Aparisi A, Iglesias-Echeverria C, Ybarra-Falcon C, Cusacovich I, Uribarri A, Garcia-Gomez M, et al. Low-density lipoprotein cholesterol levels are associated with poor clinical outcomes in COVID-19. *Nutr Metab Cardiovasc Dis.* (2021) 31:2619–27. doi: 10.1016/j.numecd.2021.06.016
30. Nguyen M, Bourredjem A, Piroth L, Bouhemad B, Jalil A, Pallot G, et al. High plasma concentration of non-esterified polyunsaturated fatty acids is a specific feature of severe COVID-19 pneumonia. *Sci Rep.* (2021) 11:10824. doi: 10.1038/s41598-021-90362-9
31. Masana L, Correig E, Ibarretxe D, Anoro E, Arroyo JA, Jerico C, et al. Low HDL and high triglycerides predict COVID-19 severity. *Sci Rep.* (2021) 11:7217. doi: 10.1038/s41598-021-86747-5
32. Van Kerkhove MD, Vandemaële KA, Shinde V, Jaramillo-Gutierrez G, Koukounari A, Donnelly CA, et al. Risk factors for severe outcomes following 2009 influenza A (H1N1) infection: a global pooled analysis. *PLoS Med.* (2011) 8:e1001053. doi: 10.1371/journal.pmed.1001053
33. Anderson, M. R, Geleris, J, Anderson, D. R, Zucker, J, Nobel, Y. R, Freedberg, D. Ferrante, A. Anderson, M. R, et al. (2020). Body mass index and risk for intubation or death in SARS-CoV-2 infection : a retrospective cohort study. *Ann Intern Med* 173, 782–790. doi: 10.7326/M20-3214
34. Tartof SY, Qian L, Hong V, Wei R, Nadjafi RF, Fischer H, et al. Obesity and mortality among patients diagnosed with COVID-19: results from an integrated health care organization. *Ann Intern Med.* (2020) 173:773–81. doi: 10.7326/M20-3742
35. Mahony R, Gargan S, Roberts R, Bourke N, Keating SE, Bowie AG, et al. A novel anti-viral role for STAT3 in IFN- α signalling responses. *Cell Mol Life Sci.* (2017) 74:1755–64. doi: 10.1007/s00018-016-2435-3
36. Collet B, Boudinot P, Benmansour A, Secombes CJ. An Mx1 promoter-reporter system to study interferon pathways in rainbow trout. *Dev Comp Immunol.* (2004) 28:793–801. doi: 10.1016/j.dci.2003.12.005
37. Verhelst J, Parthoens E, Schepens B, Fiers W, Saelens X. Interferon-inducible protein Mx1 inhibits influenza virus by interfering with functional viral ribonucleoprotein complex assembly. *J Virol.* (2012) 86:13445–55. doi: 10.1128/JVI.01682-12
38. Wisskirchen C, Ludersdorfer TH, Muller DA, Moritz E, Pavlovic J. Interferon-induced antiviral protein MxA interacts with the cellular RNA helicases UAP56 and URH49. *J Biol Chem.* (2011) 286:34743–51. doi: 10.1074/jbc.M111.251843
39. Baturcam E, Vollmer S, Schluter H, Maciewicz RA, Kurian N, Vaarala O, et al. MEK inhibition drives anti-viral defence in RV but not RSV challenged human airway epithelial cells through AKT/p70S6K/4E-BP1 signalling. *Cell Commun Signal.* (2019) 17:78. doi: 10.1186/s12964-019-0378-7
40. Raftery N, Stevenson NJ. Advances in anti-viral immune defence: revealing the importance of the IFN JAK/STAT pathway. *Cell Mol Life Sci.* (2017) 74:2525–35. doi: 10.1007/s00018-017-2520-2
41. Islam S, Espitia CM, Persky DO, Carew JS, Nawrocki ST. Targeting JAK/STAT signaling antagonizes resistance to oncolytic reovirus therapy driven by prior infection with HTLV-1 in models of T-cell lymphoma. *Viruses.* (2021) 13. doi: 10.3390/v13071406
42. Perry AK, Chen G, Zheng D, Tang H, Cheng G. The host type I interferon response to viral and bacterial infections. *Cell Res.* (2005) 15:407–22. doi: 10.1038/sj.cr.7290309
43. Verhelst J, Spitaels J, Nurnberger C, De Vlioger D, Ysenbaert T, Staeheli W, et al. Functional comparison of Mx1 from two different mouse species reveals the involvement of loop L4 in the antiviral activity against influenza A viruses. *J Virol.* (2015) 89:10879–90. doi: 10.1128/JVI.01744-15
44. Staeheli P, Grob R, Meier E, Sutcliffe JG, Haller O. Influenza virus-susceptible mice carry Mx genes with a large deletion or a nonsense mutation. *Mol Cell Biol.* (1988) 8:4518–23. doi: 10.1128/mcb.8.10.4518-4523.1988
45. Al Hamrashdi M, Brady G. Regulation of IRF3 activation in human antiviral signaling pathways. *Biochem Pharmacol.* (2022) 200:115026. doi: 10.1016/j.bcp.2022.115026
46. Kumar M, Liu H, Rice AP. Regulation of interferon-beta by MAGI-1 and its interaction with influenza A virus NS1 protein with ESEV PBM. *PLoS ONE.* (2012) 7:e41251. doi: 10.1371/journal.pone.0041251
47. Bakshi S, Taylor J, Strickson S, McCartney T, Cohen P. Identification of TBK1 complexes required for the phosphorylation of IRF3 and the production of interferon beta. *Biochem J.* (2017) 474:1163–74. doi: 10.1042/BCJ20160992
48. Fitzgerald KA, McWhirter SM, Faia KL, Rowe DC, Latz E, Golenbock DT, et al. IKKepsilon and TBK1 are essential components of the IRF3 signaling pathway. *Nat Immunol.* (2003) 4:491–6. doi: 10.1038/ni921
49. Kubota T, Matsuoka M, Chang TH, Tailor P, Sasaki T, Tashiro M, et al. Virus infection triggers SUMOylation of IRF3 and IRF7, leading to the negative regulation of type I interferon gene expression. *J Biol Chem.* (2008) 283:25660–70. doi: 10.1074/jbc.M804479200
50. Gonzalez-Mariscal L, Dominguez-Calderon A, Raya-Sandino A, Ortega-Olvera JM, Vargas-Sierra O, Martinez-Revollar G, et al. Tight junctions and the regulation of gene expression. *Semin Cell Dev Biol.* (2014) 36:213–23. doi: 10.1016/j.semdb.2014.08.009
51. Moritoh K, Yamauchi H, Asano A, Yoshii K, Kariwa H, Takashima I, et al. Generation of congenic mouse strains by introducing the virus-resistant genes, Mx1 and Oas1b, of feral mouse-derived inbred strain MSM/Ms into the common strain C57BL/6J. *Jpn J Vet Res.* (2009) 57:89–99. doi: 10.14943/jjvr.57.2.89
52. Heo KS, Lee H, Nigro P, Thomas T, Le NT, Chang E, et al. PKCzeta mediates disturbed flow-induced endothelial apoptosis via p53 SUMOylation. *J Cell Biol.* (2011) 193:867–84. doi: 10.1083/jcb.201010051
53. Scholz D, Devaux B, Hirche A, Potzsch B, Kropp B, Schaper W, et al. Expression of adhesion molecules is specific and time-dependent in cytokine-stimulated endothelial cells in culture. *Cell Tissue Res.* (1996) 284:415–23. doi: 10.1007/s004410050602

CITATION

Wang Y, Abe J-i, Chau KM, Wang Y, Vu HT, Reddy Velatooru L, Gulraiz F, Imanishi M, Samanthapudi VSK, Nguyen MTH, Ko KA, Lee L-L, Thomas TN, Olmsted-Davis EA, Kotla S, Fujiwara K, Cooke JP, Zhao D, Evans SE and Le N-T (2022) MAGI1 inhibits interferon signaling to promote influenza A infection. *Front. Cardiovasc. Med.* 9:791143. doi: 10.3389/fcvm.2022.791143

COPYRIGHT

© 2022 Wang, Abe, Chau, Wang, Vu, Reddy Velatooru, Gulraiz, Imanishi, Samanthapudi, Nguyen, Ko, Lee, Thomas, Olmsted-Davis, Kotla, Fujiwara, Cooke, Zhao, Evans and Le. This is an open-access article distributed under the terms of the [Creative Commons Attribution License \(CC BY\)](https://creativecommons.org/licenses/by/4.0/). The use, distribution or reproduction in other forums is permitted, provided the original author(s) and the copyright owner(s) are credited and that the original publication in this journal is cited, in accordance with accepted academic practice. No use, distribution or reproduction is permitted which does not comply with these terms.



OPEN ACCESS

EDITED BY

Masanori Aikawa,
Brigham and Women's Hospital and
Harvard Medical School, United States

REVIEWED BY

Ahmed Ismaeel,
University of Kentucky, United States
Carson Hoffmann,
Emory University, United States

*CORRESPONDENCE

Guillaume Mahé
maheguillaume@yahoo.fr

SPECIALTY SECTION

This article was submitted to
Atherosclerosis and Vascular Medicine,
a section of the journal
Frontiers in Cardiovascular Medicine

RECEIVED 11 May 2022

ACCEPTED 18 July 2022

PUBLISHED 09 September 2022

CITATION

Métairie A, Tollenaere Q, Lanéelle D, Le
Faucheur A, Le Pabic E, Omarjee L and
Mahé G (2022) Simplification of
ankle-brachial-index measurement
using Doppler-waveform classification
in symptomatic patients suspected of
lower extremity artery disease.
Front. Cardiovasc. Med. 9:941600.
doi: 10.3389/fcvm.2022.941600

COPYRIGHT

© 2022 Métairie, Tollenaere, Lanéelle,
Le Faucheur, Le Pabic, Omarjee and
Mahé. This is an open-access article
distributed under the terms of the
[Creative Commons Attribution License](#)
(CC BY). The use, distribution or
reproduction in other forums is
permitted, provided the original
author(s) and the copyright owner(s)
are credited and that the original
publication in this journal is cited, in
accordance with accepted academic
practice. No use, distribution or
reproduction is permitted which does
not comply with these terms.

Simplification of ankle-brachial-index measurement using Doppler-waveform classification in symptomatic patients suspected of lower extremity artery disease

Antoine Métairie¹, Quentin Tollenaere¹, Damien Lanéelle²,
Alexis Le Faucheur³, Estelle Le Pabic⁴, Loukman Omarjee¹ and
Guillaume Mahé^{1,3,4,5*}

¹Vascular Medicine Unit, CHU Rennes, Rennes, France, ²Vascular Medicine Unit, CHU
Caen-Normandie, Caen, France, ³University of Rennes, Rennes, France, ⁴CHU Rennes, Inserm,
Clinical Investigation Center (CIC), Rennes, France, ⁵Pôle Imagerie Médicale et Explorations
Fonctionnelles, Hôpital Pontchaillou, Rennes, France

Objectives: Ankle-brachial index (ABI) is commonly used for screening lower extremity peripheral artery disease (PAD) according to the international guidelines. Arterial Doppler waveform recordings is a tool to diagnose and assess PAD severity. We hypothesized that ABI measurement could be simplified by measuring only the pressure where the best arterial flow is recorded. The aim of this study was to evaluate the concordance between ABI performed according to the American Heart Association guidelines (AHA-ABI) and ABI measured according to best arterial waveform (FLOW-ABI).

Design: This was a monocentric cross-sectional study.

Methods: We included patients with exertional limb symptoms suspected of PAD. Arterial Doppler waveforms and ABI were acquired on both lower extremities at the pedis and tibial posterior arteries. Each arterial waveform was classified using the Saint-Bonnet classification. Concordances were analyzed with the kappa coefficient (confidence interval 95%). Exercise PAD study was registered n° NCT03186391.

Results: In total, one hundred and eighty-eight patients (62+/-12 years and 26.8+/-4.5 kg/m²) with exertional limb symptoms were included from May 2016 to June 2019. On each extremity, FLOW-ABI had excellent concordance for the diagnosis of PAD with the AHA-ABI with a kappa of 0.95 (95% CI: 0.90, 0.99) in the right extremity and 0.91 (95% CI: 0.86, 0.97) in the left extremity.

Conclusion: There is almost perfect concordance between AHA-ABI and FLOW-ABI. Thus, ABI can be simplified into five pressure measurements instead of seven in patient suspected of PAD with exertional limb symptoms. The question remains in patients with chronic limb ischemia.

KEYWORDS

lower extremity artery disease, Doppler waveforms, ankle-brachial index, peripheral arterial disease, claudicant

Introduction

Lower extremity peripheral artery disease (PAD) is one of the most common diseases with a major cardiovascular morbidity-mortality, particularly in developed countries (1). Its prevalence is estimated around 236 million persons worldwide in 2015 (1, 2), with a growth trend. The estimated prevalence in Europe and the United States of America is between 3 and 10% according to the different studies and increases with age (between 15 and 20% over 70 years old) (3).

One of the recommended diagnostic means is the measurement of the ankle-brachial index (ABI) at rest by dividing the highest of the two arterial pressures of the two ankle arteries by the highest brachial pressure between both arms (4–8). To be considered as pathological, a cutoff equal to 0.90 and below was retained (4, 5). In addition to its diagnostic utility, ABI has a prognostic interest with, when pathological, more than doubling of the 10-year rates of coronary events, cardiovascular mortality, and total mortality (9, 10). Guidelines about ABI were proposed in 2012 by the *American Heart Association* to standardize the procedure (11). The ABI is based on counterclockwise sequence of seven measures of pressure. This specific sequence to measure ABI is not done in clinical practice due to several barriers including the measurement duration, lack of reimbursement, and staff availability (12). Indeed, the average time for an ABI measurement is around 5 min for a trained physician and without considering the resting time before the measurement (12) whereas the primary care physician consultation time is limited (16 min in 2006 in France to <10 min in numerous countries) (13–16). A simplification (i.e., shorter duration) in the measurement could be interesting for the diffusion and the use of this diagnostic method.

The arterial flow analysis of the Doppler waveform is as well an interesting tool for the arterial hemodynamic evaluation (7, 17, 18) and can be an interesting diagnostic tool in particular populations such as patients with chronic kidney disease and diabetes (19) where the ABI value can be falsely elevated due to arterial calcifications (20).

We hypothesized that the highest arterial pressure in each extremity is located on the distal artery with the best arterial Doppler waveform; thus, ABI measurement might be simplified by measuring only five pressures instead of the seven as proposed by the AHA and other international guidelines (6, 7, 11, 21).

The main objective of this study was to analyze the concordance for the diagnosis of PAD between the ABI

measured with the AHA method (AHA-ABI) and ABI measured considering the pressure in the artery with the best Doppler waveform (FLOW-ABI) to simplify the measurement in clinical practice.

Materials and methods

Study design and population

This is a retrospective study on consecutive patients suspected of PAD with exertional limb pain referred between May 2016 and June 2019 to our vascular center in the University Hospital of Rennes, France (22).

The study was approved by an institutional review board from the University Hospital of Rennes (12, 17). All participants gave written informed consent. The study protocol conforms to the ethical guidelines of the 1975 Declaration of Helsinki. The exercise PAD study was registered with the American National Institutes of Health database under reference n° NCT03186391.

Patients were included if they had full data available including arterial Doppler waveform and ABI measurements available for both extremities.

Demographic characteristics

We collected all the medical history including age, sex, body mass index, comorbidities, and medications (statins, antihypertension treatment, anticoagulant, or antiplatelet).

Doppler waveform analysis and ABI measurement

Patients were at rest in a comfortable temperature room (20–22°C) for at least 20 min, in a supine position prior to testing (23). Arterial Doppler waveforms were described for each artery of the limbs before pressure measurements with a hand-held Doppler probe (8 MHz; Basic Atys Medical, Soucieu en Jarrest, France). Arterial Doppler waveforms were described using the Saint-Bonnet Classification as recommended by the French Vascular Teachers of Vascular Medicine (7, 17, 18). This classification provides a superior categorization rate when compared to other classifications (24). A normal flow consists of a multiphasic curve (N or A among Saint-Bonnet) (8, 17). In the case of an arterial lesion, the arterial waveform is modified depending on the degree of arterial lumen stenosis allowing the assessment of the severity of the disease and the state of collateral arteries. Saint-Bonnet classification ranges from type N to E until 0 where N stands for normal, type E describes the type of waveforms recorded in highly pathological

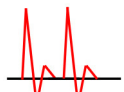
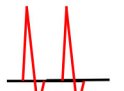
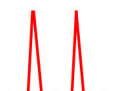
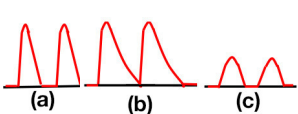





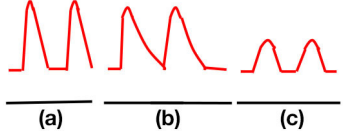

Abbreviations: ABI, ankle-brachial pressure index at rest; PAD, lower extremity peripheral artery disease; TPA, tibial posterior artery (RTPA, right TPA; LTPA, left TPA); DPA, dorsalis pedis artery (RDPA, right DPA; LDPA, left DPA).

arteries, and 0 describes an occluded artery. In the simplified classification, there are six types: Saint-Bonnet N to Saint-Bonnet A (considered as a normal flow), Saint-Bonnet B, Saint-Bonnet CD, Saint-Bonnet E, and Saint-Bonnet 0 (no flow). The classification was developed to homogenize the Doppler arterial flow description (17). Table 1 depicts the classification and its

equivalence to the classification proposed by the Society for Vascular Medicine (SVM) and Society for Vascular Ultrasound (SVU) consensus (25, 26).

The AHA-ABI was calculated as proposed by AHA guidelines: “During the sequence of measurement, the first measurement should be repeated at the end of the sequence

TABLE 1 Equivalence between Saint-Bonnet classification and SVM/SVU classification.

Saint-Bonnet classification	Doppler waveforms	SVM/SVU classification
Arterial waveform with high resistive flow		
Saint-Bonnet N		Multiphasic (Triphasic), high resistive with sharp peak, and rapid upstroke
Saint-Bonnet A		Multiphasic (Biphasic), high resistive with sharp peak, and rapid upstroke
Saint-Bonnet B		Monophasic, high resistive with sharp peak, and rapid upstroke
Saint-Bonnet CD		Monophasic, high resistive, (a) Dampened (b) Dampened, and prolonged upstroke (c) Dampened, and prolonged upstroke
Saint-Bonnet E		Monophasic, high resistive, dampened, and prolonged upstroke
Saint-Bonnet 0		Absent
Arterial waveforms with intermediate or low resistive flow		
Saint-Bonnet N-CF		Monophasic, intermediate resistive with sharp peak, and rapid upstroke
Saint-Bonnet A-CF		Monophasic, intermediate resistive with sharp peak, and rapid upstroke
Saint-Bonnet B-CF		Monophasic, low resistive with sharp peak, and rapid upstroke.
Saint-Bonnet CD-CF		Monophasic, low resistive, (a) Dampened (b) Dampened, and prolonged upstroke (c) Dampened, and prolonged upstroke
Saint-Bonnet E-CF		Monophasic, low resistive, dampened, and prolonged upstroke

Please refer to validation papers for both classifications (17, 25). SVM means Society for Vascular Medicine. SVU means Society for Vascular Ultrasound.

and both results averaged to temper the white coat effect of the first measurement, except if the difference between the 2 measurements of the first arm exceeds 10 mmHg. In that case, the first measurement should be disregarded and only the second measurement should be considered. For example, when the counterclockwise sequence — right arm, right posterior tibial artery (RPTA), right dorsalis pedis artery (RDPA), left posterior tibial artery (LPTA), left dorsalis pedis artery (LDPA), left brachial artery — is used, the measurement of the right arm should be repeated at the end of the sequence and both results obtained at the right arm should be averaged unless the difference between the 2 measurements of the right arm exceeds 10 mm Hg. In this case, only the second measurement of right arm pressure should be considered” (11, 12).

The FLOW-ABI was obtained by dividing the pressure of the lower extremity artery with the best Doppler waveforms by the highest brachial pressure between both arms. In the case of similar Doppler waveform between the posterior tibial artery (PTA) and the dorsalis pedis artery (DPA), we used the posterior tibial artery by default.

The last three types (CD, E, and O) were grouped together due to their small numbers to have a significantly large group for comparison.

Statistical analyses

The results are expressed as mean \pm standard deviation in the case of normal distribution (Shapiro–Wilk test) or in median [25th centile and 75th centile] in the other cases. The Kruskal–Wallis test (KW) was used for the comparisons between the ankle blood pressures and the Saint-Bonnet Doppler waveform types, analyzing independently each limb. The concordance between the AHA-ABI and the FLOW-ABI for the diagnosis of PAD was assessed using the Kappa coefficient expressed with a confidence interval of 95% for the right and left limbs. A second analysis was performed in a subgroup of limbs that had different Doppler waveform types. The Landis and Koch interpretation of kappa values was used: 0.21–0.40: fair; 0.41–0.60: moderate, 0.61–0.80: substantial; >0.80: almost perfect (27). Correlations

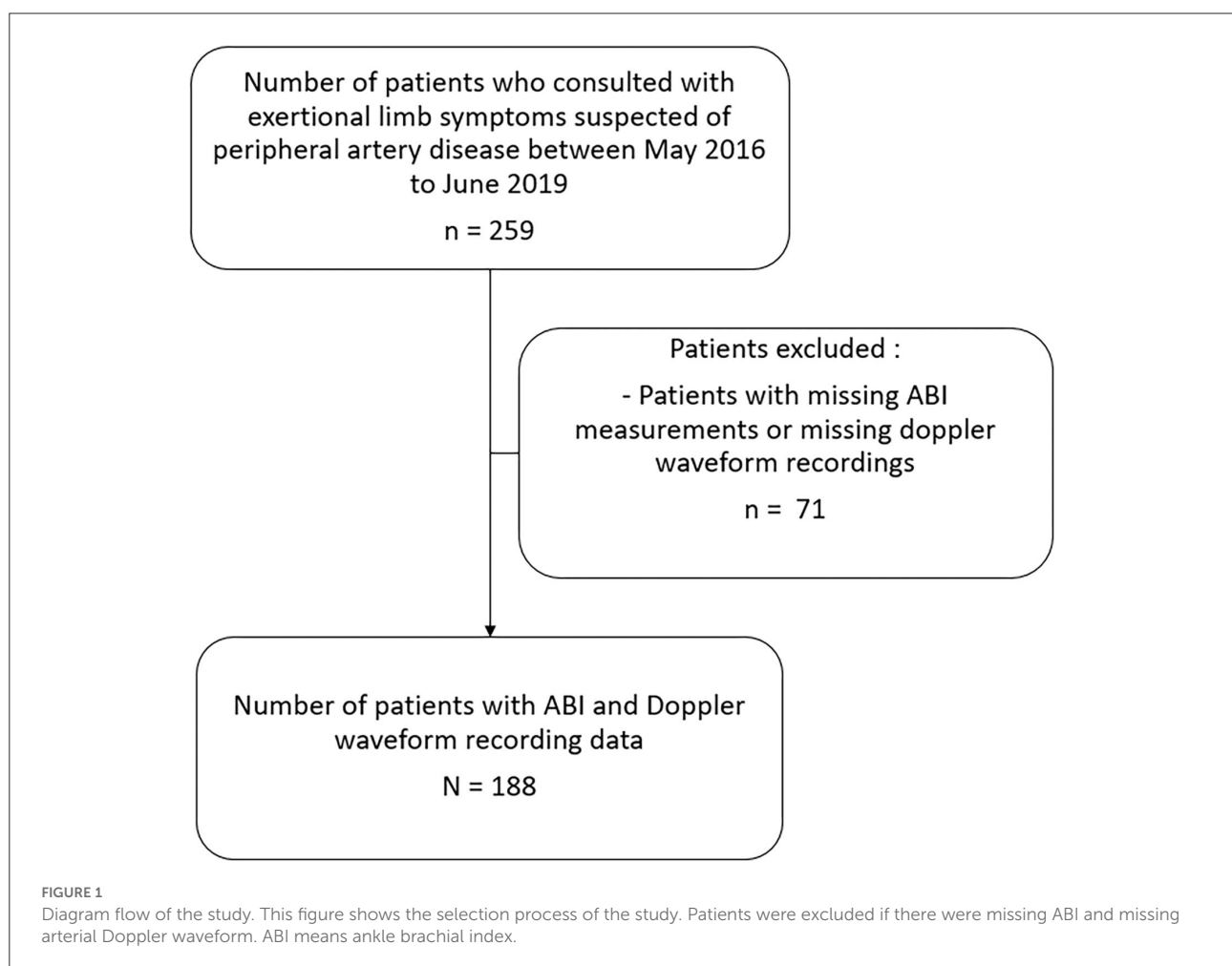


TABLE 2 Characteristics of the study population.

Clinical characteristics	<i>n</i> = 188
Male, <i>n</i> = 188	152 (80.9%)
Age (years), <i>n</i> = 188	62 ± 12
BMI (kg/m ²), <i>n</i> = 187	26.83 ± 4.52
Comorbidities, (history of), no. (%)	
Hypertension, <i>n</i> = 188	128 (68.1%)
Dyslipidemia, <i>n</i> = 188	127 (67.6%)
Diabetes mellitus, <i>n</i> = 188	38 (20.2%)
Tobacco, <i>n</i> = 182	
Active	74 (40.7%)
Stopped >6 months	80 (44.0%)
Never	28 (15.4%)
Vascular bypass, <i>n</i> = 184	27 (14.7%)
Vascular angioplasty, <i>n</i> = 182	56 (30.8%)
Myocardial infarction, <i>n</i> = 181	59 (32.6%)
Stroke (ischemic, hemorrhagic, or transient), <i>n</i> = 180	21 (11.7%)
Diuretics, <i>n</i> = 188	45 (23.9%)
ACEI/A2RA, <i>n</i> = 188	113 (60.1%)
Beta blockers, <i>n</i> = 188	62 (33.0%)
Calcium channel blockers, <i>n</i> = 188	48 (25.5%)
VKA, <i>n</i> = 188	12 (6.4%)
Oral anticoagulants, <i>n</i> = 188	8 (4.3%)
Antiplatelet agents (Aspirin or Clopidogrel), <i>n</i> = 188	147 (78.2%)
Statins, <i>n</i> = 188	118 (62.8%)
Fibrates, <i>n</i> = 188	4 (2.1%)

BMI, body mass index; ACEI, angiotensin-converting enzyme inhibitors; A2RA, angiotensin II receptor antagonists; VKA, vitamin K antagonists.

between ABI-AHA and FLOW-ABI were assessed with the Spearman's correlation coefficient. The significance level used for all statistical tests was <0.05 . All analyses were performed with SAS software, v.9.4[®] (SAS Institute, Cary, NC, USA).

Results

Among 259 patients suspected of PAD with exertional limb symptoms, 188 patients were included as shown in [Figure 1](#). Patients were excluded if there were missing limb artery pressures and Doppler waveforms for both arteries in each limb ($n = 71$).

Baseline characteristics are presented in [Table 2](#). The average age was 62 ± 12 years old and most of them were males (80.9%). The mean AHA-ABI was 0.88 ± 0.30 for the right limbs and 0.88 ± 0.26 for left limbs.

The Doppler waveforms were the same between ipsilateral limbs arteries in 138/188 in the right limb (73.4%) and 143/188 in the left limb (76.1%).

[Figure 2](#) shows the mean distal arterial pressure by artery on each leg according to the Doppler waveform (using the Saint-Bonnet classification).

Significant difference between the best Doppler waveform type (N according to the Saint-Bonnet classification) and the pressures from the arteries classed in the three last types of the classification (CD, E, and 0 among the Saint-Bonnet classification) was found with a p -value < 0.05 for each artery of each limb. However, no statistical difference appears between the arteries classified N and A ($p > 0.05$). When the N pressures are compared with the ones classified B, only the two tibial posterior arteries are significantly different.

The analysis of the concordance between the AHA-ABI and the FLOW-ABI shows an excellent concordance rating PAD/no PAD with a kappa value equal to 0.95 (95% CI: 0.90, 0.99) for the right limb and 0.91 (95% CI: 0.86, 0.97) for the left limb. The contingency tables are reported in [Table 3](#). We obtain respectively for the right and left limbs only 5 (2.7%) and 8 (4.3%) discordant diagnosis between AHA-ABI and FLOW-ABI (please refer to [Supplementary materials: Supplementary Tables 1, 2](#)). When analyzing only the limbs with different Doppler waveforms, a perfect concordance was found for the right and left limbs. The kappa values were equal to 1.00 (95% CI: 1.00, 1.00) for the right limb and 1.00 (95% CI: 1.00, 1.00) for the left limb.

Medians of differences of ABI value between the two methods were 0.09 (IC 95%: 0.06, 0.16) for the right limb and 0.13 (IC 95%: 0.10, 0.16) for the left limb excluding one patient with outlier values. Indeed, one patient with diabetes had different values according to the two methods (0.45 vs. 1.57). The discordant patients' values are available in [Supplemental materials](#).

We found a high correlation between AHA-ABI and FLOW-ABI on both lower extremities ([Figure 3](#)) with a Spearman's correlation coefficient of 0.96 for the right and 0.88 for the left (p -value < 0.0001). For the limbs with different waveforms, coefficients of correlation between AHA-ABI and FLOW-ABI were 0.99 and 0.99 for the right and left limbs, respectively.

Discussion

Ankle-brachial index is an important diagnostic tool for PAD, but it is a time-consuming method with seven measures of pressure to perform when clinicians follow the AHA guidelines (23). To our knowledge, this study is the first that tries to simplify the ABI measurement to improve its use in clinical practice. We demonstrate an almost perfect concordance (kappa > 0.90) between AHA-ABI and FLOW-ABI for both lower extremities suggesting that both measurements can be used in

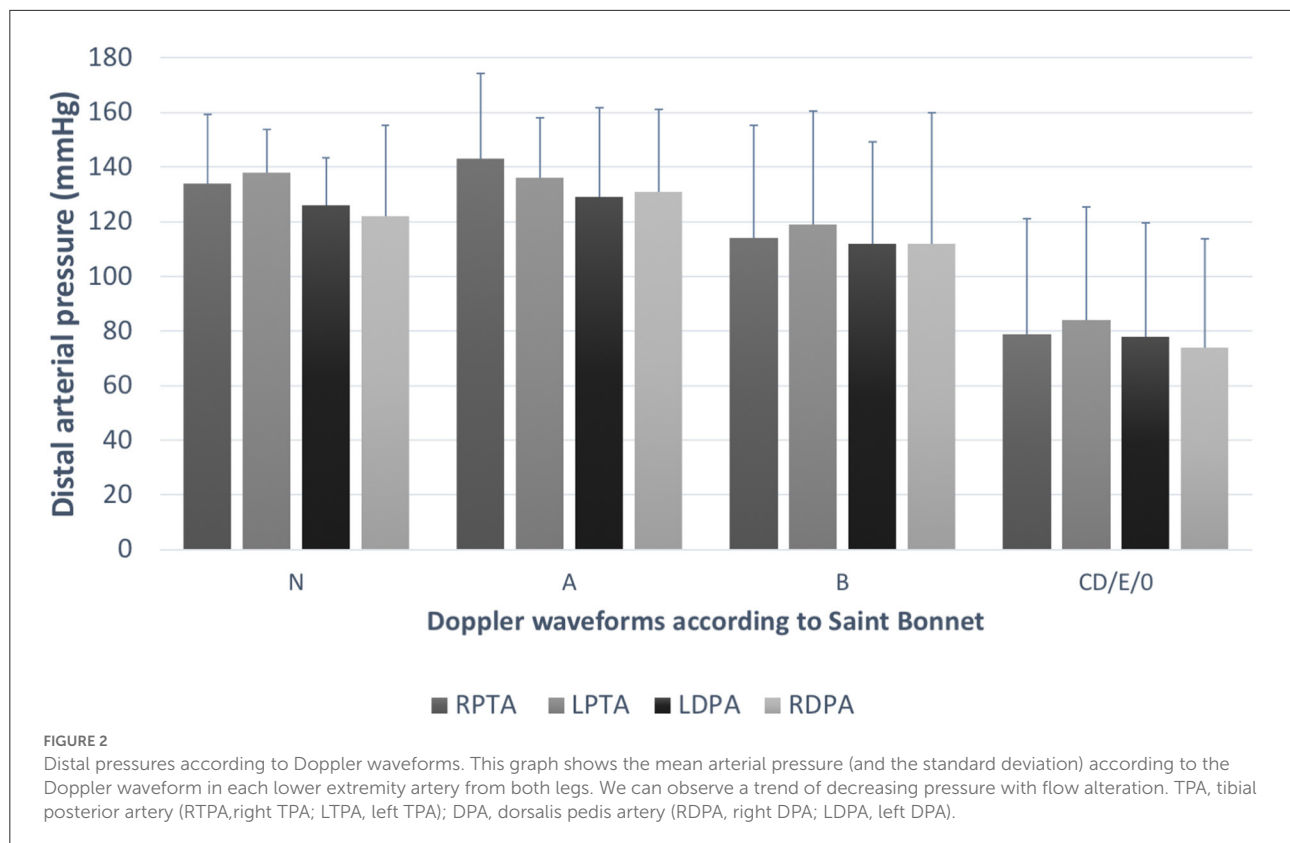


TABLE 3 Contingency tables between AHA-ABI and FLOW-ABI.

Total limbs							
Right (n = 188)		AHA-ABI		Left (n = 188)		AHA-ABI	
		PAD	No PAD			PAD	No PAD
FLOW-ABI	PAD	106	5	FLOW-ABI	PAD	103	8
	No PAD	0	77		No PAD	0	77

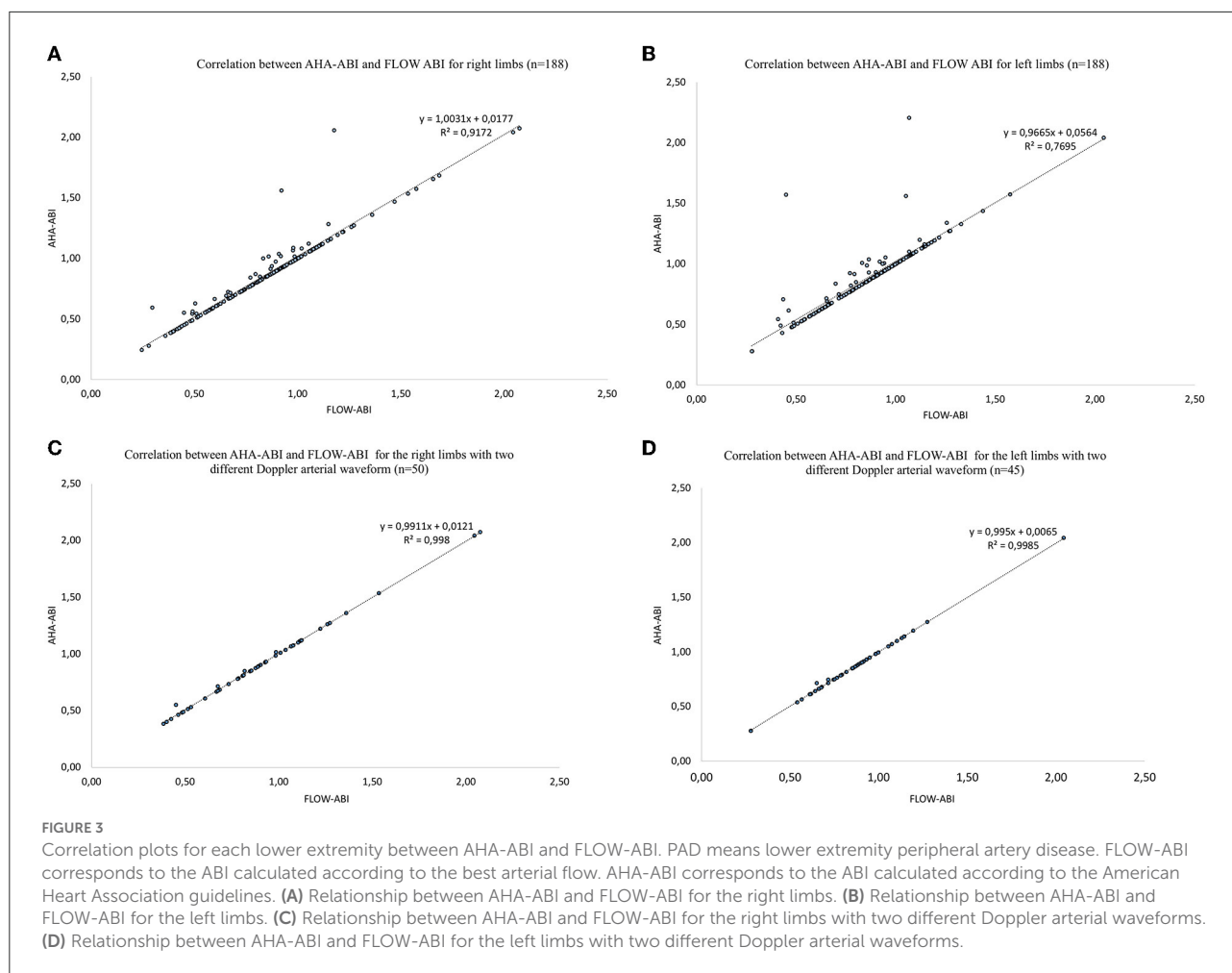
Limbs with different types of Doppler waveforms according to Saint-Bonnet							
Right (n = 50)		AHA-ABI		Left (n = 45)		AHA-ABI	
		PAD	No PAD			PAD	No PAD
FLOW-ABI	PAD	28	0	FLOW-ABI	PAD	29	0
	No PAD	0	22		No PAD	0	16

FLOW-ABI corresponds to the ABI calculated according to the best arterial flow. AHA-ABI corresponds to the ABI calculated according to the American Heart Association guidelines. PAD means lower extremity peripheral artery disease.

clinical practice in patients suspected of PAD. Furthermore, it is important to note that discrepancies appear for only five right (2.7%) and eight left (4.3%) limbs. These discrepancies were in the usual variability (≤ 0.15) of the measure for 8 out of 13 (11, 28, 29). Of interest, the second analysis of limbs that had different Doppler waveforms types strengthens the results

of the present result since the kappa value reached 1.00 for both limbs.

This result may have a strong impact in clinical practice by permitting the measurement of only one artery on each limb, the one with the best Doppler waveform, saving time and allowing the increased use of ABI, in particular among



general practitioners. Indeed, physicians from various countries have not adopted, in common practice, this measurement in primary care practices (30, 31). The PAD Awareness, Risk, and Treatment New Resources for Survival (PARTNERS) program made evidence that physicians admitted the utility of ABI for screening the PAD but three main barriers were identified: the lack of time, staff availability, and reimbursement (12). The measurement time is a key point in the daily use of this test. The mean time for an ABI measurement was recently reported around 5 min by a trained vascular physician (32) without taking into account the 10-min rest time recommended (8). Another study found a mean time for ABI measurement by general practitioners around 17 min among more than 13,000 patients (33). Furthermore, this time constraint has an impact for vascular physicians who practice ABI several times a day. Considering a measurement time of 1 min per artery (34), measuring only five pressures instead of seven could save 2 min per patient, with similar accuracy. During a busy day, this could represent

more than 30 min per day corresponding to more patients who can be seen.

The other interest of simplifying the ABI measurement might be about the education of medical students and residents. Indeed, studies have demonstrated that learning how to measure ABI is challenging (34) and not sustained (35). We hypothesize that this simplified method might improve the performance of medical students and residents to perform ABI, but this remains to be studied.

Moreover, this study confirms that the best pressure matches with the best Doppler waveform and conversely. This supports the importance of harmonization and definition of the arterial Doppler waveforms using a standardized classification. Indeed, various papers from different countries (USA, China, and France) found heterogeneity in Doppler waveform descriptions if no classification was used (7, 26, 36–38). This work was made possible by the use of the Saint-Bonnet classification that is recommended by the French Vascular Medicine Teachers (CEMV, College des

Enseignants de Médecine Vasculaire) and the French Vascular Medicine and Surgery Societies (SFMV, SCVE) (7). Other classifications exist but a recent paper has shown that the Saint-Bonnet classification provides a superior categorization rate when compared to other classifications (24). Furthermore, the Saint-Bonnet classification was also associated with the functional status of patients with suspected PAD (31). In July 2020, the American Society for Vascular Medicine and Society for Vascular Ultrasound proposed a consensus (25, 26) about the description of arterial (and venous) Doppler waveforms to alleviate confusion. They developed this nomenclature based on the flow direction, the phasicity, and resistance. This description gathers the terms needed to use common language to be clinically useful. This consensus is of great interest, but studies about the use of the SVM/SVU consensus should be performed to confirm its utility in clinical practice.

Limits

Our study has several limitations. First, the present results were found in patients with exertional limb symptoms and suspected of PAD. Thus, we cannot ascertain that similar results will be found in asymptomatic patients or in patients with critical limb ischemia. Second, the use of the posterior tibial artery by default in case of similar waveform categorization may be a bias. However, there is a trend in clinical practice to measure more pressure on the posterior tibial artery than on dorsalis pedis artery. Furthermore, although the artery caliber between both arteries does not appear significantly different in several studies (39, 40), there is a trend for an augmented prevalence of stenosis on the dorsalis pedis artery vs. the posterior tibial artery (40). Third, we followed the AHA procedure to measure the ABI except for the measurement of the brachial pressure that was measured with an automatic blood pressure monitor (Carescap Dinamap V100; GE Healthcare) as previously done in other papers (7, 22, 32). We are confident with our results since (i) Montgomery and Gardner (41) found no statistical difference between Doppler measurement and automatic measurement at the brachial level, and (ii) this is suggested by the French guidelines (7). Fourth, we did not study the reproducibility of the FLOW-ABI measurement, but this was not the aim of this study. However, the intra-observer coefficient in our team to perform AHA-ABI is 9.4% as previously reported (34). The reproducibility of the FLOW-ABI remains to be studied. Fifth, we had a small sample size of patients with diabetes, and data about chronic kidney disease (CKD) status was unknown in this population whereas ABI can be falsely elevated in diabetic and patients with CKD (42). Therefore, the results of this study should be used with cautious in these patients.

Finally, this technique requires a machine that allows the visualization of the Doppler waveform. The price may be an issue in its development as well as the time required to train physicians on the machine's use and waveform interpretation and classification.

Conclusion

Our study shows that ABI measurement using FLOW-ABI is as accurate as the AHA-ABI method for the diagnosis of PAD. The FLOW-ABI might replace the AHA-ABI in patients with exertional limb symptoms and suspected of PAD. Further studies with an external validation of these criteria seem useful to confirm our findings in a global population and the benefit in practice.

Data availability statement

The raw data supporting the conclusions of this article will be made available by the authors, without undue reservation.

Ethics statement

The studies involving human participants were reviewed and approved by Institutional Review Board from the University Hospital of Rennes (12, 17). The patients/participants provided their written informed consent to participate in this study.

Author contributions

Study design: AM, GM, and ALF. Data collection: AM, QT, GM, and LO. Data analysis: AM, ELP, DL, and GM. Writing: AM and GM. All authors contributed to the article and approved the submitted version.

Conflict of interest

The authors declare that the research was conducted in the absence of any commercial or financial relationships that could be construed as a potential conflict of interest.

Publisher's note

All claims expressed in this article are solely those of the authors and do not necessarily represent those

of their affiliated organizations, or those of the publisher, the editors and the reviewers. Any product that may be evaluated in this article, or claim that may be made by its manufacturer, is not guaranteed or endorsed by the publisher.

References

- Criqui MH, Aboyans V. Epidemiology of peripheral artery disease. *Circ Res.* (2015) 116:1509–26. doi: 10.1161/CIRCRESAHA.116.303849
- Song P, Rudan D, Zhu Y, Fowkes FJI, Rahimi K, Fowkes FGR, et al. Global, regional, and national prevalence and risk factors for peripheral artery disease in 2015: an updated systematic review and analysis. *Lancet Glob Health.* (2019) 7:e1020–30. doi: 10.1016/S2214-109X(19)30255-4
- Fowkes FGR, Rudan D, Rudan I, Aboyans V, Denenberg JO, McDermott MM, et al. Comparison of global estimates of prevalence and risk factors for peripheral artery disease in 2000 and 2010: a systematic review and analysis. *Lancet.* (2013) 382:1329–40. doi: 10.1016/S0140-6736(13)61249-0
- Grenon SM, Gagnon J, Hsiang Y. Ankle–Brachial index for assessment of peripheral arterial disease. *N Engl J Med.* (2009) 361:e40. doi: 10.1056/NEJMvcm0807012
- WINSOR T. Influence of arterial disease on the systolic blood pressure gradients of the extremity. *Am J Med Sci.* (1950) 220:117–26.
- Aboyans V, Ricco J-B, Bartelink M-LEL, Björck M, Brodmann M, Cohnert T, et al. editor's choice - 2017 esc guidelines on the diagnosis and treatment of peripheral arterial diseases, in collaboration with the European society for vascular surgery (ESVS). *Eur J Vasc Endovasc Surg.* (2018) 55:305–68. doi: 10.1016/j.ejvs.2017.07.018
- Mahé G, Boge G, Bura-Rivière A, Chakfé N, Constans J, Goueffic Y, et al. Disparities between international guidelines (AHA/ESC/ESVS/ESVM/SVS) concerning lower extremity arterial disease: consensus of the french society of vascular medicine (SFMV) and the French society for vascular and endovascular surgery (SCVE). *Ann Vasc Surg.* (2021) 72:1–56. doi: 10.1016/j.avsg.2020.11.011
- Gerhard-Herman MD, Gornik HL, Barrett C, Barshes NR, Corriere MA, Drachman DE, et al. 2016 AHA/ACC guideline on the management of patients with lower extremity peripheral artery disease: executive summary: a report of the American college of cardiology/american heart association task force on clinical practice guidelines. *J Am Coll Cardiol.* (2017) 69:1465–508. doi: 10.1016/j.jacc.2016.11.008
- Ankle brachial index combined with framingham risk score to predict cardiovascular events and mortality: a meta-analysis. *JAMA.* (2008) 300:197–208. doi: 10.1001/jama.300.2.197
- Hiatt WR, Hoag S, Hamman RF. Effect of diagnostic criteria on the prevalence of peripheral arterial disease. *Circulation.* (1995) 91:1472–9. doi: 10.1161/01.CIR.91.5.1472
- Aboyans V, Criqui MH, Abraham P, Allison MA, Creager MA, Diehm C, et al. Measurement and interpretation of the ankle-brachial index: a scientific statement from the American heart association. *Circulation.* (2012) 126:2890–909. doi: 10.1161/CIR.0b013e318276fbc8
- Mohler ER, Treat-Jacobson D, Reilly MP, Cunningham KE, Miani M, Criqui MH, et al. Utility and barriers to performance of the ankle-brachial index in primary care practice. *Vasc Med.* (2004) 9:253–60. doi: 10.1191/1358863x04vm5590a
- Deveugele M, Derese A, Brink-Muinen A. van den, Bensing J, Maeseneer JD. Consultation length in general practice: cross sectional study in six European countries. *BMJ.* (2002) 325:472. doi: 10.1136/bmj.325.7362.472
- Iacobucci G. GP appointments last less than five minutes for half the world's population. *BMJ.* (2017) 359:5172. doi: 10.1136/bmj.j5172
- Irving G, Neves AL, Dambha-Miller H, Oishi A, Tagashira H, Verho A, et al. International variations in primary care physician consultation time: a systematic review of 67 countries. *BMJ Open.* (2017) 7:e017902. doi: 10.1136/bmjopen-2017-017902
- Deveugele M, Derese A, De Bacquer D, van den Brink-Muinen A, Bensing J, De Maeseneer J. Consultation in general practice: a standard operating procedure? *Patient Educ Couns.* (2004) 54:227–33. doi: 10.1016/S0738-3991(03)00239-8
- Mahé G, Boulon C, Désormais I, Lacroix P, Bressollette L, Guilmot JL, et al. College of the French vascular medicine teachers (CEMV) statement: arterial Doppler waveforms analysis (simplified Saint-Bonnet classification). *J Med Vasc.* (2018) 43:255–61. doi: 10.1016/j.jdmv.2018.05.002
- Mahé G, Boulon C, Desormais I, Lacroix P, Bressollette L, Guilmot J-L, et al. Statement for Doppler waveforms analysis. *VASA.* (2017) 46:337–45. doi: 10.1024/0301-1526/a000638
- Norgren L, Hiatt WR, Dormandy JA, Nehler MR, Harris KA, Fowkes FGR. Inter-society consensus for the management of peripheral arterial disease (TASC II). *Eu J Vasc Endovasc Surg.* (2007) 33:S1–S75. doi: 10.1016/j.ejvs.2006.09.024
- Brownrigg JRW, Schaper NC, Hinchliffe RJ. Diagnosis and assessment of peripheral arterial disease in the diabetic foot. *Diab Med.* (2015) 32:738–47. doi: 10.1111/dme.12749
- Halliday A, Bax JJ. The 2017 ESC guidelines on the diagnosis and treatment of peripheral arterial diseases, in collaboration with the European society for vascular surgery (ESVS). *Eu J Vasc Endovasc Surg.* (2018) 55:301–2. doi: 10.1016/j.ejvs.2018.03.004
- Stivalet O, Paisant A, Belabbas D, Omarjee L, Le Faucheur A, Landreau P, et al. Exercise testing criteria to diagnose lower extremity peripheral artery disease assessed by computed-tomography angiography. *PLoS ONE.* (2019) 14:e0219082. doi: 10.1371/journal.pone.0219082
- Chaudru S, de Müllenheim P-Y, Le Faucheur A, Kaladji A, Jaquinandi V, Mahé G. Training to perform ankle-brachial index: systematic review and perspectives to improve teaching and learning. *Eur J Vasc Endovasc Surg.* (2016) 51:240–7. doi: 10.1016/j.ejvs.2015.09.005
- Guilcher A, Lanéelle D, Hoffmann C, Guillaumat J, Constans J, Bressollette L, et al. Comparison of the use of arterial doppler waveform classifications in clinical routine to describe lower limb flow. *J Clin Med.* (2021) 10:e464. doi: 10.3390/jcm10030464
- Kim ES, Sharma AM, Scissons R, Dawson D, Eberhardt RT, Gerhard-Herman M, et al. Interpretation of peripheral arterial and venous Doppler waveforms: a consensus statement from the society for vascular medicine and society for vascular ultrasound. *Vasc Med.* (2020) 25:484–506. doi: 10.1177/1358863X20937665
- Wen C, Gao M, Fu Y, Zhao R, Tong Y, Scissons R, et al. high variability of arterial Doppler waveform descriptions exists in China. *Vasc Med.* (2020) 25:221–2. doi: 10.1177/1358863X20903808
- Landis JR, Koch GG. The measurement of observer agreement for categorical data. *Biometrics.* (1977) 33:159–74.
- Nicoloff AD, Taylor LM, Sexton GJ, Schuff RA, Edwards JM, Yeager RA, et al. Homocysteine and progression of atherosclerosis study investigators. Relationship between site of initial symptoms and subsequent progression of disease in a prospective study of atherosclerosis progression in patients receiving long-term treatment for symptomatic peripheral arterial disease. *J Vasc Surg.* (2002) 35:38–46. doi: 10.1067/mva.2002.120381
- Cronenwett JL, Warner KG, Zelenock GB, Whitehouse WM Jr, Graham LM, Lindenauer SM, et al. Intermittent claudication: current results of non-operative management. *Arch Surg.* (1984) 119:430–6. doi: 10.1001/archsurg.1984.01390160060012
- Collins TC, Suarez-Almazor M, Petersen NJ. An absent pulse is not sensitive for the early detection of peripheral arterial disease. *Fam Med.* (2006) 38:5. Available online at: <https://fammedarchives.blob.core.windows.net/imagesandpdfs/fmhub/fm2006/January/Tracie38.pdf>
- Hageman D, Pesser N, Gommans LNM, Willigendael EM, Sambeek MRHM. van, Huijbers E, et al. Limited adherence to peripheral arterial disease guidelines and suboptimal ankle brachial index reliability in dutch primary care. *Eu J Vasc Endovasc Surg.* (2018) 55:867–73. doi: 10.1016/j.ejvs.2018.02.011

Supplementary material

The Supplementary Material for this article can be found online at: <https://www.frontiersin.org/articles/10.3389/fcvm.2022.941600/full#supplementary-material>

32. Catillon F, Tuffier S, Guilcher A, Tollenaere Q, Métairie A, Miossec A, Mauger C. Proficiency of medical students at obtaining pressure measurement readings using automated ankle and toe measuring devices for diagnosis of lower extremity peripheral artery disease. *Annals Vasc Surg.* (2019) 65:183–8. doi: 10.1016/j.avsg.2019.10.092
33. Bendermacher BL, Teijink JA, Willigendael EM, Bartelink M-L, Peters RJ, Langenberg M, et al. Applicability of the ankle-brachial-index measurement as screening device for high cardiovascular risk: an observational study. *BMC Cardiovasc Disord.* (2012) 12:59. doi: 10.1186/1471-2261-12-59
34. Donnou C, Chaudru S, Stivalet O, Paul E, Charasson M, Selli J-M, et al. How to become proficient in performance of the resting ankle-brachial index results of the first randomized controlled trial. *Vascular Medicine.* (2018) 23:109. doi: 10.1177/1358863X17740993
35. Omarjee L, Donnou C, Chaudru S, Locher C, Paul E, Charasson M, et al. Impact of an educational intervention on ankle-brachial index performance among medical students and fidelity assessment at 6 months. *Ann Vasc Surg.* (2019) 56:246–53. doi: 10.1016/j.avsg.2018.07.044
36. Lanéelle D, Scissons R, Mahé G. Inter-observer reliability of a 4-item Doppler ultrasound waveforms classification. *Vasa.* (2020) 49:518–9. doi: 10.1024/0301-1526/a000906
37. Omarjee L, Stivalet O, Hoffmann C, Scissons R, Bressollette L, Mahé G, et al. Heterogeneity of Doppler waveform description is decreased with the use of a dedicated classification. *Vasa.* (2018) 47:471–4. doi: 10.1024/0301-1526/a000724
38. Zhao R, Lanéelle D, Gao M, Fu Y, Tong Y, Scissons R, Wen C, Mahé G. Inter-rater reliability of 4-item arterial doppler waveform classification system for description of arterial doppler waveforms. *Front Cardiovasc Med.* (2020) 7:8274. doi: 10.3389/fcvm.2020.584274
39. Czyzewska D, Ustymowicz A, Krysiuk K, Witkowski P, Zonenberg M, Dobrzycki K, et al. Ultrasound assessment of the caliber of the arteries in the lower extremities in healthy persons – the dependency on age, sex and morphological parameters of the subjects. *J Ultrason.* (2012) 12:420–7. doi: 10.15557/JoU.2012.0030
40. Lorbeer R, Grotz A, Dörr M, Völzke H, Lieb W, Kühn J-P, et al. Reference values of vessel diameters, stenosis prevalence, and arterial variations of the lower limb arteries in a male population sample using contrast-enhanced MR angiography. *PLoS ONE.* (2018) 13:e0197559. doi: 10.1371/journal.pone.0197559
41. Montgomery PS, Gardner AW. Comparison of three blood pressure methods used for determining ankle/brachial index in patients with intermittent claudication. *Angiology.* (1998) 49:723–8. doi: 10.1177/000331979804901003
42. AbuRahma AF, Adams E, AbuRahma J, Mata LA, Dean LS, Caron C, et al. Critical analysis and limitations of resting ankle-brachial index in the diagnosis of symptomatic peripheral arterial disease patients and the role of diabetes mellitus and chronic kidney disease. *J Vasc Surg.* (2020) 71:937–45. doi: 10.1016/j.jvs.2019.05.050



OPEN ACCESS

EDITED BY

Tatsuya Iso,
Gunma University of Health
and Welfare, Japan

REVIEWED BY

Isabelle Vila,
Université de Montpellier, France
Ping Lin,
Southwest University, China

*CORRESPONDENCE

Daiju Fukuda
daiju.fukuda@omu.ac.jp;
daiju.fukuda@tokushima-u.ac.jp

SPECIALTY SECTION

This article was submitted to
Atherosclerosis and Vascular Medicine,
a section of the journal
Frontiers in Cardiovascular Medicine

RECEIVED 22 February 2022

ACCEPTED 15 August 2022

PUBLISHED 13 September 2022

CITATION

Nishimoto S, Sata M and Fukuda D
(2022) Expanding role
of deoxyribonucleic acid-sensing
mechanism in the development
of lifestyle-related diseases.
Front. Cardiovasc. Med. 9:881181.
doi: 10.3389/fcvm.2022.881181

COPYRIGHT

© 2022 Nishimoto, Sata and Fukuda.
This is an open-access article
distributed under the terms of the
[Creative Commons Attribution License](#)
(CC BY). The use, distribution or
reproduction in other forums is
permitted, provided the original
author(s) and the copyright owner(s)
are credited and that the original
publication in this journal is cited, in
accordance with accepted academic
practice. No use, distribution or
reproduction is permitted which does
not comply with these terms.

Expanding role of deoxyribonucleic acid-sensing mechanism in the development of lifestyle-related diseases

Sachiko Nishimoto^{1,2}, Masataka Sata² and Daiju Fukuda^{2,3*}

¹Faculty of Clinical Nutrition and Dietetics, Konan Women's University, Kobe, Japan, ²Department of Cardiovascular Medicine, Tokushima University Graduate School of Biomedical Sciences, Tokushima, Japan, ³Department of Cardiovascular Medicine, Osaka Metropolitan University, Osaka, Japan

In lifestyle-related diseases, such as cardiovascular, metabolic, respiratory, and kidney diseases, chronic inflammation plays a causal role in their pathogenesis; however, underlying mechanisms of sterile chronic inflammation are not well-understood. Previous studies have confirmed the damage of cells in these organs in the presence of various risk factors such as diabetes, dyslipidemia, and cigarette smoking, releasing various endogenous ligands for pattern recognition receptors. These studies suggested that nucleic acids released from damaged tissues accumulate in these tissues, acting as an endogenous ligand. Undamaged DNA is an integral factor for the sustenance of life, whereas, DNA fragments, especially those from pathogens, are potent activators of the inflammatory response. Recent studies have indicated that inflammatory responses such as the production of type I interferon (IFN) induced by DNA-sensing mechanisms which contributes to self-defense system in innate immunity participates in the progression of inflammatory diseases by the recognition of nucleic acids derived from the host, including mitochondrial DNA (mtDNA). The body possesses several types of DNA sensors. Toll-like receptor 9 (TLR9) recognizes DNA fragments in the endosomes. In addition, the binding of DNA fragments in the cytosol activates cyclic guanosine monophosphate (GMP)-adenosine monophosphate (AMP) synthase (cGAS), resulting in the synthesis of the second messenger cyclic GMP-AMP (cGAMP). The binding of cGAMP to stimulator of interferon genes (STING) activates NF- κ B and TBK-1 signaling and consequently the production of many inflammatory cytokines including IFNs. Numerous previous studies have demonstrated the role of DNA sensors in self-defense through the recognition of DNA fragments derived from pathogens. Beyond the canonical role of TLR9 and cGAS-STING, this review describes the role of these DNA-sensing mechanism in the inflammatory responses caused by endogenous DNA fragments, and in the pathogenesis of lifestyle-related diseases.

KEYWORDS

DNA-sensing mechanism, chronic inflammation, atherosclerosis, metabolic diseases, COPD, TLR9, STING, CKD

Introduction

An organism needs to efficiently detect and resolve continual pathogenic attacks to maintain host-survival and homeostasis. The innate immune system protects the host from pathogenic infection by employing pattern recognition receptors (PRRs), which recognize pathogen-associated molecular patterns (PAMPs) and coordinate appropriate host defense mechanisms. PRRs include Toll-like receptors (TLRs), retinoic acid-inducible gene I-like receptors (RLRs), and NOD-like receptors (NLRs). After binding to their respective ligands, these receptors are activated, which results in the release of cytokines and chemokines. These first immune responses recruit antigen-presenting cells and leukocytes at the site of infection and induce subsequent adaptive immunity.

Toll-like receptors, which are the most familiar PRRs, are evolutionarily conserved and recognize various components came from bacteria, fungi, and viruses. There are 10 members of the TLR family in humans. Classically, most TLRs are categorized into two sub-groups. The first comprises TLR1, TLR2, TLR4, TLR5, TLR6, and TLR11 which are primarily expressed on the cell surface, and their function is to recognize the components of microbial membranes (1). The other sub-group is composed of TLR3, TLR7, TLR8, and TLR9. These TLRs are expressed intracellularly in vesicles [e.g., lysosomes, endosomes, and the endoplasmic reticulum (ER)] and recognize microbial nucleic acids (2–5). In the past, numerous studies have examined the downstream signaling related to TLRs and demonstrated that it requires the recruitment of several adaptor proteins, which lead to the activation of the nuclear factor-kappa B (NF- κ B) and interferon (IFN) regulatory factor (IRF) pathways, accelerating inflammatory responses (2). In addition to TLRs which recognize nucleic acid, cytoplasmic DNA sensors have been known. In particular, stimulator of interferon genes (STING) which recognizes second messenger cyclic guanosine monophosphate-adenosine monophosphate (GMP-AMP) (cGAMP) generated from cyclic GMP-AMP synthase (cGAS) activated by DNA fragments in the cytosol have been well-studied (6–9). RNA sensors in the cytosol, such as RLRs also have been known (10, 11). Numerous studies have reported that multiple pathways related to inflammation, such as IRFs, NF- κ B, and inflammasomes, are activated after these DNA sensors bind to their ligands (12).

Non-communicable diseases (NCDs) are a major contributor to the global burden of disease and account for up to 72% of worldwide deaths (13). Chronic low-grade inflammation, characterized by persistent elevated concentrations of circulating pro-inflammatory cytokines, has been associated with the development of both age and diet-related NCDs, including obesity, cardiometabolic diseases, respiratory and auto-immune diseases, and many cancers (14–16). Recent studies have demonstrated that PRR signaling contributes not only to innate immune responses but also to

the pathogenesis of various inflammatory diseases. Especially, the TLR9 signaling and STING signaling have attracted much attention, because emerging evidence suggested their roles in the pathogenesis of lifestyle-related diseases. Lifestyle-related diseases are a group of diseases that onset and progression closely link with lifestyle and behavior factor(s), such as dietary habits, physical activities, rest, smoking, alcohol consumption, etc. Especially cardiovascular diseases, metabolic disorders, respiratory diseases including chronic obstructive pulmonary disease (COPD), chronic kidney diseases (CKD) are focused as major lifestyle-related diseases, that are a health threat to humans in recent decades (17–19). Beyond the canonical role of TLR9 and cGAS-STING in antimicrobial and antiviral immunity, the functional roles of TLR9 and cGAS-STING to lifestyle-related diseases has emerged from recent expanding evidence. This review briefly summarizes the role of TLR9 and STING signaling in the pathogenesis of inflammation caused by self-derived DNA fragments. This review also highlights the roles of the DNA sensing system in the pathophysiology of lifestyle-related diseases and discusses its potential as a therapeutic target for these diseases.

Deoxyribonucleic acid damage in lifestyle-related diseases

Sterile chronic inflammation is recognized as a shared mechanism of vascular diseases and metabolic diseases; however, the molecular mechanisms of sterile chronic inflammation remain a major medical problem that is yet to be solved. Though the mechanisms which cause DNA damage is multifactorial (20), DNA damage has been reported to play a crucial role in the development of these diseases (21, 22). Previous studies demonstrated that higher oxidative stress (23) and lower oxygen pressure (24) related to pathologic condition in unhealthy lifestyles and metabolic risk factors cause the deterioration of the cells in the vascular system and tissue of the metabolic organs. Subsequently, damaged genomic DNA and mitochondrial DNA (mtDNA) (25–29) are released and/or accumulated within the body (14, 30–32). We previously reported the accumulation of DNA fragments in macrophages, which infiltrate into atherosclerotic lesions and adipose tissue by using immune-electron microscopy and inflammatory activation of macrophages by DNA fragments (17–19). These results suggested that pro-inflammatory activation of macrophages by DNA damage play a key role in the pathophysiology of cardiometabolic diseases (33).

In developed countries, chronic kidney disease (CKD) is the most commonly attribute to diabetes and hypertension. The progression of CKD is associated with adverse clinical outcomes, including end-stage renal disease (ESRD), cardiovascular disease, and increased mortality (34–36). In the kidney, tubular cells contain enriched mitochondria to prepare for higher

energy consumption. Recent studies highlight a pathogenic role of mitochondrial damage in the development of kidney disease. In fact, several kidney diseases such as diabetic nephropathy, tubulo-nephritis, and CKD show elevated mtDNA levels not only in the plasma but also in the urine (37–39). A recent study showed that urinary mtDNA levels have no significant association with the rate of worsening of renal function in non-diabetic CKD, although the levels correlate with baseline renal function, proteinuria, and the severity of histological damage (40).

Chronic obstructive pulmonary disease is a respiratory disorder characterized by irreversible limited expiratory airflow and abnormal inflammation. Etiologically, cigarette smoking (CS) is a major risk factor for COPD (41). Here, the impaired function of alveolar macrophages is a notable factor (42). CS-induced abnormal inflammatory responses amplify protease expression and oxidative stress, which accelerate COPD pathogenesis (43, 44). These processes further damage lung cells, including epithelial, vascular, and inflammatory cells, thus altering the lung microenvironment and enhancing the release of endogenous ligands. In fact, previous *in vitro* and *in vivo* studies have demonstrated that CS increased mtDNA damage (45, 46).

Deoxyribonucleic acid damage is also a potential marker of inflammatory diseases. The presence of extracellular DNA, which is named as cell-free DNA (cfDNA), has been known for a long time (47). Furthermore, recent studies have reported positive correlations between circulating cfDNA levels and the disease condition such as traumas (48–50), sepsis (51), cancer (52) or inflammatory diseases including autoimmune diseases (53–57), ESRD (58, 59), and neurodegenerative diseases (60). Recent clinical studies also have shown positive correlations between plasma cfDNA levels and the development of cardiometabolic disorders in humans. A clinical study that used coronary computed tomographic (CT) angiography demonstrated that patients with severe coronary artery disease had significantly higher levels of plasma double-stranded DNA and nucleosomes than those in the control group (61). Our previous study that used optical coherence tomography also revealed a positive correlation between cfDNA levels in the target artery and the inflammatory features of plaque in the target lesion of patients with acute myocardial infarction (17). In addition, we demonstrated that obese individuals presented higher cfDNA levels in the plasma and that the severity of abdominal adiposity and insulin resistance positively correlated with plasma levels of cfDNA (33). Similarly, several studies have reported that CS triggered DNA damage, releasing self-derived DNA into the plasma and alveolar space (62, 63). Thus, DNA damage and cfDNA has drawn increasing attention as a causal factor which initiates and accelerates vascular and metabolic diseases (20, 32).

Therefore, investigating pro-inflammatory roles of endogenous DNA fragments released from the host and the

mechanisms by which endogenous DNA fragments accelerates inflammation associated with lifestyle-related diseases have become a research topic of great interest.

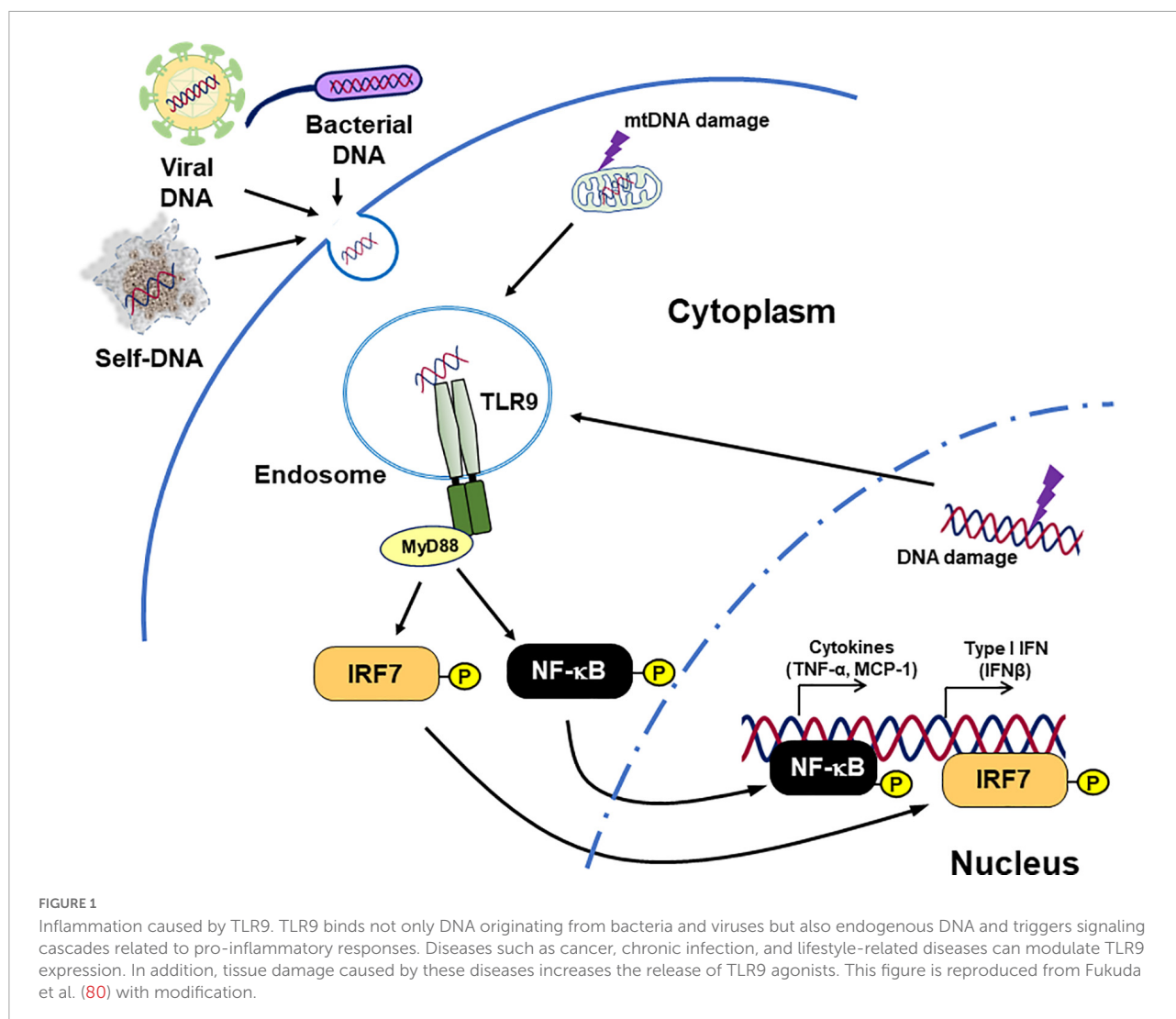
Activation of toll-like receptor 9 and cyclic GMP-AMP synthase-stimulator of interferon genes

Toll-like receptor 9 is a well-studied DNA-sensing TLR. It recognizes unmethylated CpG motif-containing DNA fragments and induces innate immune response (64). After binding with ligands, TLR9 activates inflammatory pathways such as myeloid differentiation primary response 88 (MyD88)–IRF7 pathway and MyD88–NF- κ B pathway, resulted in the production of type I IFN and inflammatory cytokines (Figure 1; 45, 65–67).

The cGAS-STING pathway is originally known as cytosolic DNA sensor machinery which recognizes pathogen-derived DNA, thus regulating the innate immune response (6, 68–70). STING ligates with cGAMP which is generated by cGAS activated with DNA fragments presented in the cytoplasm. Subsequently, STING activates NF- κ B and IRF3, inducing IFNs and other pro-inflammatory cytokines (Figure 2; 7–9, 68, 71, 72).

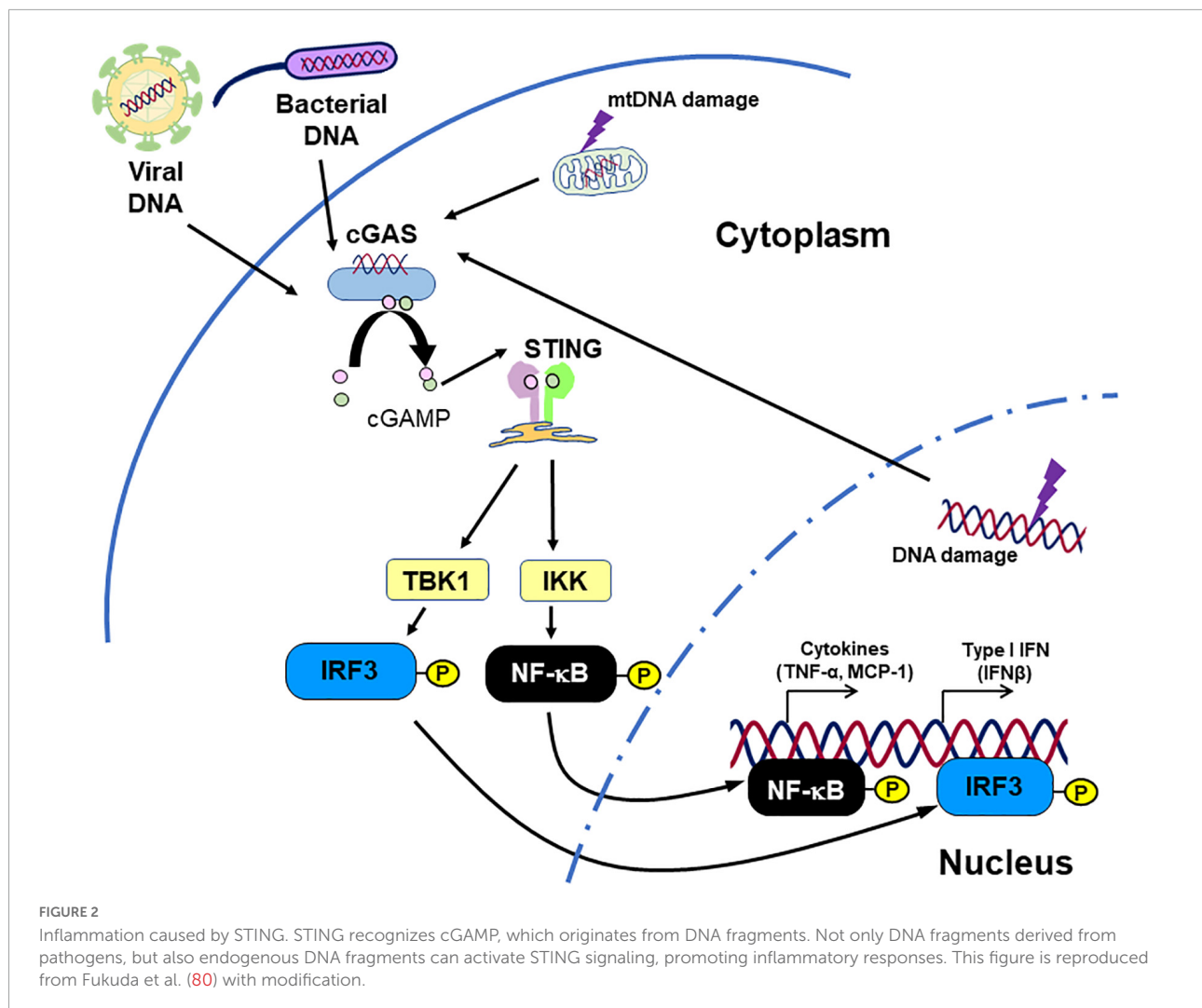
The role of deoxyribonucleic acid sensor in metabolic diseases

Due to lifestyle changes, the prevalence of obesity is increasing worldwide. This condition has close link with multiple metabolic abnormalities, including insulin resistance, and hepatic steatosis. Chronic sterile inflammation in metabolic organs plays a central role in the pathology of obesity and its associated complications. The mechanisms by which obesity promotes inflammation in metabolic organs are still undefined. However, obesity disturb the balance of the hypertrophy and the proliferation of adipocytes, angiogenesis, and the role of immune cells (24, 73, 74) because of higher oxidative stress, lower oxygen pressure (23), and excess inflammation, initiating cellular degeneration in adipose tissue (75–77). Here, local and/or systemic adipocyte-derived factors are suggested to participate in multiple pathways which accelerate inflammation within adipose tissue (77). Thus, many studies have been investigating the contribution of TLRs (78, 79). Recent studies, including our own, have demonstrated that among adipocyte-derived factors, self-derived DNA fragments released from metabolic organs promote chronic sterile inflammation by acting as endogenous ligands for DNA sensors.



We previously demonstrated that obesity caused by a high fat diet (HFD)-feeding increased plasma single-stranded DNA (ssDNA) levels in mice. Similarly, patients with visceral obesity, determined by CT, showed higher plasma ssDNA levels compared with the non-obese control. Furthermore, we reported that plasma ssDNA levels have a positive correlation with insulin resistance as determined by HOMA-IR, in humans (33). We also investigated the role of TLR9 in adipose tissue inflammation as it is one of the major receptors of nucleic acids (2). At first, we confirmed that HFD-induced obesity promotes TLR9 expression in the visceral fat. To explore the role of TLR9 in obese condition, we employed diet-induced obesity mouse model. TLR9 deficiency decreases macrophage accumulation into the visceral fat along with the reduction of inflammation in the adipose tissue and the inhibition of the development of obesity-induced insulin resistance (33). Similarly, pharmacological blocking of TLR9 with iODN2088, a specific inhibitory oligonucleotide for TLR9, in HFD-fed wild-type mice suppressed inflammation in adipose tissue

and ameliorated insulin sensitivity. In contrast, restoration of TLR9 only in BM aggravated insulin resistance in HFD-fed TLR9 deficient mice. In agreement with *in vivo* studies, our *in vitro* studies revealed that DNA fragments released from obese adipocytes partially promoted pro-inflammatory activation of macrophages *via* TLR9 signaling. Our results indicate that obesity overstimulates the innate immune system by increasing both ligand and receptor levels. In tandem, these results suggest a link between TLR9 and obesity-associated insulin resistance. Simultaneously, these results suggested that cfDNA-TLR9 signaling can be a potential therapeutic target for insulin resistance in obese subjects. Other TLR9 ligands, such as HMGB1, might also participate in TLR9 activation in obese subjects (81). However, a previous study reported opposite results. In that study, the authors demonstrated the protective role of TLR9 in the development of insulin resistance by showing the exacerbation of insulin resistance and pro-inflammatory activation of macrophages in TLR9 deficient mice (82). Further studies are needed to explore



the function of TLR9 in the pathogenesis of obesity-induced insulin resistance.

Recent evidence has also demonstrated the contribution of TLR9 signaling to the pathogenesis of non-alcoholic fatty liver disease (NAFLD) (27). A preclinical study using a mouse model reported that TLR9 signaling activated by mtDNA accelerates the progression of hepatocyte damage and liver fibrosis, and that a TLR7/9 antagonist ameliorated the development of hepatic steatosis. As with animal studies, clinical studies have revealed that patients with non-alcoholic steatohepatitis (NASH) exhibits higher mtDNA levels compared to the controls (83, 84). Metabolic stresses caused by fat accumulation in the liver are thought to induce hepatocyte damage, leading to the release and accumulation of endogenous DNA fragments. DNA fragment-induced TLR9 activation might be an important driver of inflammatory responses in this widespread liver disease. Thus, TLR9 activation caused by self-derived DNA may be one of the molecular mechanisms of NAFLD.

In addition to TLR9, the expression of signaling molecules related to STING pathway is enhanced in metabolic organs in obese mouse models (85–87). For instance, the activation of cGAS–cGAMP–STING pathway by mtDNA derived from adipose tissues promoted chronic sterile inflammation in adipose tissue and contributed to the development of insulin resistance (87, 88). The activation of STING signaling in pancreatic β -cells was also documented in genetically obese mice such as db/db mice, suggesting that STING signaling is involved in the pathophysiology of type 2 diabetes (T2D) which is characterized by dysfunction of pancreatic β -cells (89).

Resembling TLR9, a number of studies have reported the role of STING signaling in the disease processes in NAFLD (90–92). The excess of fat accumulation in the liver triggers mitochondria dysfunction and mtDNA damage in hepatocytes (93). The activation of STING induced by these mtDNA fragments increases production of type I IFN (90, 91), accelerating oxidative stress and inflammation as hepatic diseases develop (94). In fact, genetically deficiency of STING

ameliorated non-alcoholic steatohepatitis and insulin resistance in wild-type mice (90, 91). Here, Kupffer cells, a type of macrophage in the liver, are suggested to play a pivotal role. Kupffer cells increase the expression of inflammatory molecules such as TNF- α and interleukin-6 in the response to released mtDNA from hepatocytes, which accelerates disease processes (91). Furthermore, some clinical studies have shown potential contribution of STING signaling in patients with NAFLD by linking the release of mtDNA and the progression inflammation and fibrosis in the liver (92, 95).

Lifestyle and dietary changes tend to enlarge the number of patients with obesity and its complications worldwide. This could result in more attention being directed toward the role of TLR9 and STING signaling in the development of metabolic diseases, such as insulin resistance and hepatic diseases and advances being made in new therapeutic strategies. To explore the function of DNA sensors in the pathogenesis of metabolic diseases further studies are warranted.

The role of deoxyribonucleic acid sensors in vascular diseases

Chronic inflammation in the vascular system initiates impairment of endothelial function, accelerating atherogenic process (96). Efficient intervention to risk factors such as dyslipidemia, T2D, and hypertension decreases cardiovascular events, although significant residual risk is still concerned (97). This also indicates that molecular and cellular mechanisms of atherogenesis are not completely understood.

Accumulating evidence demonstrates the participation of innate immune system in the process of vascular inflammation despite its multifactorial etiology (98). A variety of cells in arterial lesions, including endothelial cells, macrophages, and dendritic cells express PRRs, including TLRs (99–102). TLR9 plays a crucial role in atherosclerosis development. Several studies have demonstrated that the stimulation of TLR9 signaling accelerates pro-inflammatory activation of macrophages and dendritic cells (103–105). In addition, we found that ODN1826, a TLR9 agonist, partially through p38 MAPK signaling, increased the expression of pro-inflammatory molecules in apolipoprotein E-deficient (ApoE KO) macrophages (17). Previous studies have revealed the damage of vascular cells in atherosclerotic lesions (106–108), suggesting the release of various endogenous ligands for TLRs (109). In our *in vivo* study, genetic deletion of TLR9 suppressed atherogenesis in ApoE KO mice which received angiotensin II infusion (17). The blockade of TLR9 with the administration of iODN2088, an inhibitory oligodeoxynucleotide specific to TLR9, reduced atherosclerotic lesion development when compared to the control group in the same mouse model. Both genetical and pharmacological TLR9 blocking also abated

the inflammatory features of atherosclerotic plaques at both the RNA and protein levels, while restoration of TLR9 in the bone marrow exacerbated atherogenesis in TLR9-deficient ApoE KO mice. These findings suggest that TLR9 has pro-atherogenic roles (17). Similarly, another study reported pharmacological blockade of TLR9 by IRS869 mitigated atherosclerotic lesion development and shifted macrophage polarization to the anti-inflammatory M2 phenotype (110). Pro-atherogenic properties of TLR9 was also reported by showing impaired reendothelialization and advanced atherosclerotic plaques in ApoE KO mice which received the administration of TLR9 agonist (111). Furthermore, we demonstrated that TLR9 contributes to the impairment of blood flow recovery in the ischemic limb by using a hind-limb ischemia model (18). TNF- α released from accumulated macrophages *via* TLR9 signaling played an important role. All these studies suggest that TLR9 activation enhances inflammatory responses and accelerates the development of vascular diseases.

Several groups have reported incongruous results by reporting that TLR9 has anti-atherogenic effects (112–114). Koulis et al. (114) demonstrated anti-atherogenic role of TLR9 by showing that TLR9-deficient ApoE KO mice exhibited increased inflammation in the plaque along with an increase in blood lipid levels. They also reported that the administration of CpG-ODN1668, a TLR9 agonist, suppressed atherosclerotic lesion development in ApoE KO mice. Thus, the role of TLR9 which have been reported is discrepant. Interestingly, a previous study reported conflicting roles of TLR9 activation depending on the concentration of its ligand (115). Therefore, the difference between the mouse model and experimental methods might result in the variance in the levels of ligands, which explains the discrepancy reported in previous studies. Further investigations are needed to clarify the effects of TLR9 on atherosclerosis.

A number of previous studies have investigated the role of cGAS-STING pathway as a major cytosolic DNA sensor and demonstrated its activation in response not only to pathogen-derived DNA but also endogenous DNA (6, 68–70). Amongst others, we have described the role of STING in the pathogenesis of atherosclerosis. To explore direct evidence of the contribution of STING signaling in vascular inflammation and subsequent atherogenesis, we first attempted to detect the presence of DNA damage in mouse atherosclerotic lesions by using WTD-fed ApoE KO mice, one of the widely used hypercholesterolemic mouse models, because released endogenous DNA initiates the production of STING ligands (19). The results of western blotting and immune-electron microscopy demonstrated the expression of γ H2AX, a DNA damage marker, and the accumulation of DNA fragments in macrophages, respectively. Furthermore, we demonstrated the presence of cGAMP, a direct agonist of STING, in the atherosclerotic aorta of this mouse model using liquid chromatograph–mass spectrometry. Therefore, we deleted STING in ApoE KO mice to investigate

its role in atherogenesis. Genetic deletion of STING decreased atherogenesis and attenuated the inflammatory features of the vasculature. Pharmacological blocking of STING using C-176 also decreased atherogenesis in the aorta compared to that in control groups. In contrast, its BM-specific expression promotes atherosclerotic lesion progression in ApoE KO mice. These results suggest causal roles of STING in the pathogenesis of atherosclerosis development. Additionally, a recent study showed that the genetic deficiency of IRF3, which is an adaptor molecule in downstream of STING signaling, attenuated the progression and the vulnerability of atherosclerotic plaques in ApoE KO mice (116). Similarly, administration of IFN- β , which is a downstream molecule of STING signaling, promotes atherogenesis in hypercholesterolemic mouse models (117). In our study, STING deficiency reduced the expression of IFN- β in the aorta of ApoE KO mice (19), which is consistent with these results. We further demonstrated that both cGAMP and mtDNA promoted the expression of inflammatory molecules, such as IFN- β , in both mouse and human macrophages (19). In addition, we demonstrated the expression of STING and cGAMP in atherosclerotic plaques collected by carotid endarterectomy, the levels of which were significantly higher in atherosclerotic lesions than control samples purchased from a tissue bank (19).

Recently, one study reported causal role of STING signaling in the pathogenesis of aortic disease (118). Genetic deletion of STING significantly decreased the aortic diameter, dissection, and aortic aneurysm formation in a mouse model. The underlying mechanisms included damage and release of DNA fragments from smooth muscle cells, and activation of macrophages by these DNA fragments. They also showed the inhibitory effects of C-176, a specific STING inhibitor, in their mouse model, suggesting the contribution of STING signaling to aortic aneurysm formation. The results of these studies suggest that the activation of STING signaling promotes vascular inflammation and that it could be a potential therapeutic focus for vascular diseases.

Contribution of STING to the development of vascular diseases has been also suggested in humans. The gain-of-function mutation in STING is reported to have close link with vasculopathy observed in STING-associated vasculopathy with onset in infancy (SAVI), which is a rare familial autoinflammatory disease (119–121). Enhanced IFN- β transcription in peripheral blood mononuclear cells in SAVI patients is thought to be one of the mechanisms involved (115). In contrast, one study reported protective effect of single-nucleotide polymorphism R293Q on STING on cardiovascular disease associated with obesity (122, 123). Evidence regarding the contribution of cGAS–cGAMP–STING signaling to vascular diseases is still limited; however, the results of recent studies suggest that STING signaling contributes to the pathogenesis of vascular diseases.

Thus, the role thought to be played by TLR9 and cGAS–cGAMP–STING signaling is expanding to vascular diseases in

addition to the innate immune system. Further investigation of the role of these signaling in the development of vascular diseases would improve the understanding of the pathogenesis of atherosclerosis and might stimulate the development of new therapeutic approaches.

The role of deoxyribonucleic acid sensor in kidney diseases

The roles of TLRs in inflammation observed in kidney diseases have been established in both animal models and patients. Several studies have confirmed the association between the TLR9 gene and CKD (124, 125). A human study demonstrated that patients with ESRD showed significant upregulation of TLR2 and TLR4, but not TLR7 or TLR9, in monocytes (126). On the other hand, polymorphisms of TLR9 have been confirmed to be associated with CKD in the Han Chinese population (124). A following study showed that the -1237T/C SNP of the TLR9 gene is significantly associated with ESRD in this population and that -1237T/C may be involved in the development of ESRD through transcriptional modulation of TLR9 (125). Therefore, TLR9 may play a critical role in the development of CKD.

Chronic kidney diseases is manifested by chronic inflammation, with continuous, unsuccessful injury-repair cycles and following fibrosis. These processes involve the activation of macrophages (127). Previous studies have reported the leading role of chronic inflammation and macrophage polarization in the progression of CKD. An animal study demonstrated that systemic exposure to CpG-DNA 1668, one of the TLR9 ligand, increases CD11b + /Ly6Chi macrophages and induces classically activated renal M1 macrophages that enhance intrarenal inflammation and disease progression of Alport nephropathy and other types of chronic kidney diseases (128). Activation of TLR9 induces accumulation of M1 macrophages and increased expression of pro-inflammatory cytokines in the renal interstitial compartment (129). Several studies also have explored the role of TLR9 using experimental acute kidney injury (AKI). Previous studies indicated that TLR9 does not contribute to the development of ischemic AKI by showing that TLR9 deficient mice were not protected against ischemic AKI (130, 131). In contrast, Han et al. reported that renal proximal tubular TLR9 activation exacerbates ischemic AKI by accelerating renal tubular inflammation, apoptosis as well as necrosis *via* NF- κ B and caspase activation after ischemia-reperfusion injury, which leads to the development of AKI (132–134). The fibrosis of the kidney is another feature of AKI. One animal study using a mouse AKI-CKD transition model demonstrated that attenuation of CKD in the TLR9 deficient mice mainly relies on the effects of TLR9 on macrophages (129). In this study, TLR9 deficiency decreases the number of leukocyte and macrophage in the kidney following ischemia-reperfusion injury.

Chronic kidney diseases is associated with accelerated atherosclerosis progression and high incidence of cardiovascular events (135–138). An animal study using 5/6 nephrectomy or unilateral nephrectomy in ApoE KO mice demonstrated that CKD markedly accelerates atherogenesis in ApoE KO mice (136). They suggested that the CKD models which employed ApoE KO mouse are a useful tool to explore the mechanisms of uremic atherosclerosis. Due to a typical oxidative stress, CKD has emerged as a particularly strong risk factor for CVD (135). Thrombotic events are more likely to occur in patients with CKD, as well as in ApoE KO mice with CKD (138), suggesting that the plaques in CKD possess vulnerable features. A recent study using ApoE KO mice demonstrated that induction of CKD increases the release of mtDNA because of oxidative stress-induced mitochondrial damage, which activates the cGAS-STING pathway and subsequently induces type 1 IFN response in vascular smooth muscle cells (138). Interestingly, a recent study which used diabetic mouse models such as db/db mice and KKAY mice has reported that self-DNA-activated cGAS-STING pathway can be a new mechanism causing inflammation in the kidneys in diabetic condition (139). Alleviating type 1 IFN *via* cGAS-STING pathway may become a potential treatment strategy against diabetic kidneys as well as CKD-associated cardiovascular diseases.

These studies demonstrate that activation of the DNA sensors contributes to the development of kidney diseases, suggesting potential new therapeutic targets for preventing the progression of AKI, CKD, and diabetic kidney diseases. However, how DNA sensors affects CKD progression remains unclear. Further studies are needed.

The role of deoxyribonucleic acid sensor in chronic obstructive pulmonary disease

Chronic obstructive pulmonary disease is a respiratory disorder characterized by irreversible limited expiratory airflow and aberrant inflammation. Inflammation plays a pivotal role in the pathogenesis of COPD (140, 141). The underlying molecular mechanisms are not completely understood; however, recent evidence has suggested that the innate immune system partially contributes to its pathogenesis (124, 142). Previous studies have determined the expression and function of TLRs in the development of COPD (143, 144).

The expression of TLR9 in the lungs (145) and its contribution to the pathogenesis of COPD have been reported (146). Foronjy et al. (147) demonstrated that genetic deletion of TLR9 prevents the development of CS-induced COPD in mice. The authors reported that in addition to inflammatory cells, epithelial cells play a pivotal role in COPD development. This is logical because the epithelium of the airways acts as the first line of defense against pathogens through the process of

using a variety of receptors, such as TLRs. In immune responses, reactive-oxygen species (ROS) production is beneficial in the process of self-defense (148), and its accumulation is evident in patients with COPD (149). The overproduction of ROS is intended to abolish invading pathogens, meanwhile it can induce unwanted cellular damage. Excess ROS can directly initiate an inflammatory response and negatively affect tissue function and cellular structure (150). A previous study reported that ROS-induced mtDNA release stimulates immune cells because of TLR9 activation (151). The role and mechanism of activation of TLR9 in the development of COPD remain unclear; however, recent studies have reported that TLR9 polymorphisms are associated with both lung dysfunction and COPD (152, 153). Further study is required to understand the pathophysiology of COPD and develop novel therapeutic strategies that target TLR9.

Some viral-related innate immune mediators, such as RIG1, MDA5, LGP2, STING, and DAI are expressed in the lung tissue and bronchi of patients with COPD (154). Host-derived DNA fragments may act as pro-inflammatory signals for pulmonary inflammation (155). Recent data indicated the role of DAMPs in COPD (156) and many studies have attempted to reveal the relationship between STING and its ligand in the development of this particular disease (157). Nascimento et al. (62) showed that mouse CS-exposure promotes self-DNA release, which correlates with a neutrophil influx into the bronchoalveolar space *via* STING signaling. In a mouse model, acute CS exposure increased the self-DNA content in the alveolar space and accelerated the inflammatory response through the cGAS-STING pathway (62). Deslee et al. (158) demonstrated the nucleic-acid oxidation in alveolar fibroblasts of patients with severe emphysema. Similarly, CS exposure to mice accumulated nucleic acid oxidation in alveolar fibroblasts time dependently. DNase I treatment also reduced CS-induced lung inflammation (159). On the other hand, several previous studies have suggested that the suppression of cGAS-STING pathway and lower IFN levels are associated with a poor immune response to pathogens in patients with COPD (160, 161). These impeded STING-related immune responses may cause immune compromise in patients. Therefore, targeting the DNA-sensing mechanism such as STING is a double-edged sword. Further studies are needed to establish potential therapeutic strategies in lung diseases.

Conclusion

The detection of exogenous DNA is the most fundamental function of the innate immune system and is the first line of self-defense in the human body (67). This system promotes inflammation against endogenous DNA fragments, as well as exogenous DNA, under certain circumstances. The underlying mechanism by which DNA-sensing mechanisms cause an unwanted immune response to host-derived DNA remains

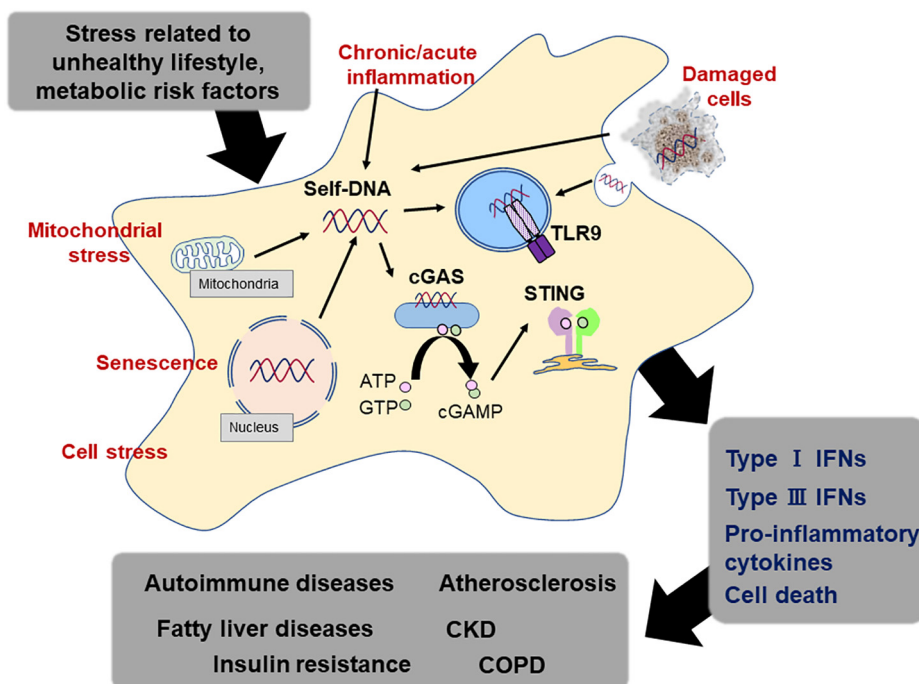


FIGURE 3

DNA sensing system and lifestyle-related diseases. Endogenous DNA fragments activate the DNA sensing mechanism, which participates in the activation of the immune response. Immune response caused by endogenous DNA fragments via DNA sensors such as TLR9 and STING accelerates sterile inflammation, leading to the development of lifestyle-related diseases, such as atherosclerosis, metabolic diseases, and pulmonary diseases.

completely unknown. In this review, we synthesized findings from a very large and rapidly growing body of research investigating associations between DNA-sensing mechanism and the development of lifestyle-related diseases (80). The evidence suggests that host-derived DNA fragment including mtDNA potentially works as a stimulator of TLR9 and/or cGAS-STING pathway under a certain circumstance, accelerating chronic inflammation (Figure 3). Although there are increasing number of studies, remaining discrepancies of the results may attribute to the study design such as experiment duration, types of agonists and antagonists, and animal background. Furthermore, methods of preparing DNA sample from blood or culture medium and quantification of the amount, sequences of DNA fragments which have higher potential as exogenous ligands for DNA sensors, and the origin of DNA fragments should be established to elucidate the importance of this system as a therapeutic target in the future.

As previous studies have demonstrated, risk factors, such as obesity, T2D, and dyslipidemia, induce tissue damage, which suggests the release of exogenous ligands, including nucleic acids. Therefore, controlling these risk factors by using the combination of medical treatment and a healthy lifestyle is indispensable in regulating inflammation caused by DNA-sensing mechanisms.

From the view of drug development, identifying the crosstalk between TLR9, cGAS-STING, and other types of

DNA sensors of specific cell type in each stage of diseases will also help developing effective treatment in the future. Indeed, several animal studies have suggested that the administration of inhibitors for DNA sensors including TLR9 and STING attenuates the development of several lifestyle-related diseases such as insulin resistance, hepatic diseases, and atherosclerosis. However, DNA-sensing mechanism basically functions as self-defense. Further studies are needed to establish therapeutic strategies targeting this system. In addition, several studies have mentioned the crosstalk between TLR9 and cGAS-STING in response to DNA damage related with infectious diseases and some pathological conditions. In a mouse model of malarial infection, cGAS-STING pathway has been shown to induce suppressor of cytokine signaling (SOCS)1/3 to downregulate TLR9 signaling (162, 163). Deb et al. reported that triggering of the cGAS-STING pathway in plasmacytoid dendritic cells can induce expression of SOCS molecules, leading to inhibit the TLR9 pathway-mediated IFN production (162). In contrast, a synergistic role of TLR9 and STING by has also been reported in animal models such as acute peripheral tissue trauma models or other chemically induced lung injury (164, 165). Here, mtDNA activates neutrophils through both cGAS-STING and TLR9 pathways and leads to an increase in the production of neutrophil elastase and extracellular neutrophil-derived DNA in neutrophil extracellular traps, resulting in acceleration of subsequent sterile inflammation. At *in vitro* level, a study using

cell lines such as human monocyte and human pDC has shown that a particular type of ODN can induce a strong cGAS-STING-dependent IFN response (166), suggesting that we need careful interpretation of the results derived from *in vitro* experiments which employed CpG-ODNs for distinguishing between TLR9- and cGAS-dependent effects. Until now, the number of studies which examined the crosstalk between multiple signal pathways related to innate immune systems in lifestyle-related diseases. Therefore, further detailed studies about the differences in the temporal and spatial expression and function of these innate immune signals in lifestyle-related diseases will help us to clarify the pathogenic roles of these DNA sensors in these diseases and provide evidence for further prevention and therapeutics.

In summary, DNA sensors, such as TLR9 and cGAS-STING, participate in the development of lifestyle-related diseases such as vascular, metabolic, kidney, and pulmonary diseases. These findings also highlight the potential benefits of transitioning to a healthy lifestyle to decrease disease risk. Further studies are required to understand the stimuli and mechanisms by which one of the most essential immune systems can play a harmful role, and to establish well-tolerated methods targeting DNA-sensing mechanism for these lifestyle-related diseases.

Author contributions

All authors listed have made a substantial, direct, and intellectual contribution to the work, and approved it for publication.

References

1. Kawai T, Akira S. The role of pattern-recognition receptors in innate immunity: update on Toll-like receptors. *Nat Immunol.* (2010) 11:373–84.
2. Takeuchi O, Akira S. Pattern recognition receptors and inflammation. *Cell.* (2010) 140:805–20.
3. Yamamoto M, Takeda K. Current views of toll-like receptor signaling pathways. *Gastroenterol Res Pract.* (2010) 2010:240365.
4. Yang L, Seki E. Toll-like receptors in liver fibrosis: cellular crosstalk and mechanisms. *Front Physiol.* (2012) 3:138. doi: 10.3389/fphys.2012.00138
5. Blasius AL, Beutler B. Intracellular toll-like receptors. *Immunity.* (2010) 32:305–15.
6. Barber GN. STING-dependent cytosolic DNA sensing pathways. *Trends Immunol.* (2014) 35:88–93.
7. Barber GN. STING: infection, inflammation and cancer. *Nat Rev Immunol.* (2015) 15:760–70.
8. Cai X, Chiu YH, Chen ZJ. The cGAS-cGAMP-STING pathway of cytosolic DNA sensing and signaling. *Mol Cell.* (2014) 54:289–96.
9. Chen Q, Sun L, Chen ZJ. Regulation and function of the cGAS-STING pathway of cytosolic DNA sensing. *Nat Immunol.* (2016) 17:1142–9.
10. Loo YM, Gale M Jr. Immune signaling by RIG-I-like receptors. *Immunity.* (2011) 34:680–92.
11. Schlee M. Master sensors of pathogenic RNA - RIG-I like receptors. *Immunobiology.* (2013) 218:1322–35. doi: 10.1016/j.imbio.2013.06.007
12. Okude H, Ori D, Kawai T. Signaling through nucleic acid sensors and their roles in inflammatory diseases. *Front Immunol.* (2020) 11:625833. doi: 10.3389/fimmu.2020.625833
13. Global Burden of Disease 2016 Causes of Death Collaborators. Global, regional, and national age-sex specific mortality for 264 causes of death, 1980–2016: a systematic analysis for the Global Burden of Disease Study 2016. *Lancet.* (2017) 390:1151–210. doi: 10.1016/S0140-6736(17)32152-9
14. Hotamisligil GS. Inflammation, metaflammation and immunometabolic disorders. *Nature.* (2017) 542:177–85.
15. Bennett JM, Reeves G, Billman GE, Sturmberg JP. Inflammation-nature's way to efficiently respond to all types of challenges: implications for understanding and managing "the epidemic" of chronic diseases. *Front Med.* (2018) 5:316. doi: 10.3389/fmed.2018.00316
16. Calder PC, Bosco N, Bourdet-Sicard R, Capuron L, Delzenne N, Doré J, et al. Health relevance of the modification of low grade inflammation in ageing (inflammageing) and the role of nutrition. *Ageing Res Rev.* (2017) 40:95–119. doi: 10.1016/j.arr.2017.09.001
17. Fukuda D, Nishimoto S, Aini K, Tanaka A, Nishiguchi T, Kim-Kaneyama JR, et al. Toll-like receptor 9 plays a pivotal role in angiotensin ii-induced atherosclerosis. *J Am Heart Assoc.* (2019) 8:e010860. doi: 10.1161/JAHA.118.010860
18. Nishimoto S, Aini K, Fukuda D, Higashikuni Y, Tanaka K, Hirata Y, et al. Activation of toll-like receptor 9 impairs blood flow recovery after hind-limb ischemia. *Front Cardiovasc Med.* (2018) 5:144. doi: 10.3389/fcvm.2018.00144

Funding

This work was partially supported by JSPS Kakenhi Grants (Number 20K19695 to SN, Number 19K08584 to DF, and Number 19H03654 to MS), Bristol-Myers Squibb Research Grants (DF), The 2022 Osaka Metropolitan University Strategic Research Promotion Project (Priority Research) (DF), The Uehara Memorial Foundation (DF), Takeda Science Foundation (MS), and the Vehicle Racing Commemorative Foundation (MS). The funders had no role in the study design, data collection and analysis, or preparation of the manuscript.

Conflict of interest

The authors declare that the research was conducted in the absence of any commercial or financial relationships that could be construed as a potential conflict of interest.

Publisher's note

All claims expressed in this article are solely those of the authors and do not necessarily represent those of their affiliated organizations, or those of the publisher, the editors and the reviewers. Any product that may be evaluated in this article, or claim that may be made by its manufacturer, is not guaranteed or endorsed by the publisher.

19. Pham PT, Fukuda D, Nishimoto S, Kim-Kaneyama JR, Lei XF, Takahashi Y, et al. a cytosolic DNA sensor, plays a critical role in atherogenesis: a link between innate immunity and chronic inflammation caused by lifestyle-related diseases. *Eur Heart J*. (2021) 42:4336–48. doi: 10.1093/eurheartj/ehab249
20. Shah NR, Mahmoudi M. The role of DNA damage and repair in atherosclerosis: a review. *J Mol Cell Cardiol*. (2015) 86:147–57.
21. Ballinger SW, Patterson C, Knight-Lozano CA, Burow DL, Conklin CA, Hu Z, et al. Mitochondrial integrity and function in atherogenesis. *Circulation*. (2002) 106:544–9.
22. Włodarczyk M, Nowicka G. Obesity, DNA damage, and development of obesity-related diseases. *Int J Mol Sci*. (2019) 20:1146.
23. Furukawa S, Fujita T, Shimabukuro M, Iwaki M, Yamada Y, Nakajima Y, et al. Increased oxidative stress in obesity and its impact on metabolic syndrome. *J Clin Invest*. (2004) 114:1752–61.
24. Sung HK, Doh KO, Son JE, Park JG, Bae Y, Choi S, et al. Adipose vascular endothelial growth factor regulates metabolic homeostasis through angiogenesis. *Cell Metab*. (2013) 17:61–72.
25. Fetterman JL, Holbrook M, Westbrook DG, Brown JA, Feeley KP, Bretón-Romero R, et al. Mitochondrial DNA damage and vascular function in patients with diabetes mellitus and atherosclerotic cardiovascular disease. *Cardiovasc Diabetol*. (2016) 15:53.
26. Kawane K, Tanaka H, Kitahara Y, Shimaoka S, Nagata S. Cytokine-dependent but acquired immunity-independent arthritis caused by DNA escaped from degradation. *Proc Natl Acad Sci USA*. (2010) 107:19432–7. doi: 10.1073/pnas.1010603107
27. Saito Y, Hikita H, Nozaki Y, Kai Y, Makino Y, Nakabori T, et al. DNase II activated by the mitochondrial apoptotic pathway regulates RIP1-dependent non-apoptotic hepatocyte death via the TLR9/IFN- β signaling pathway. *Cell Death Differ*. (2019) 26:470–86. doi: 10.1038/s41418-018-0131-6
28. Takahashi A, Loo TM, Okada R, Kamachi F, Watanabe Y, Wakita M, et al. Downregulation of cytoplasmic DNases is implicated in cytoplasmic DNA accumulation and SASP in senescent cells. *Nat Commun*. (2018) 9:1249. doi: 10.1038/s41467-018-03555-8
29. Zhang B, Davidson MM, Hei TK. Mitochondria regulate DNA damage and genomic instability induced by high LET radiation. *Life Sci Space Res*. (2014) 1:80–8.
30. Libby P. Inflammation in atherosclerosis. *Nature*. (2002) 420:868–74.
31. Oka T, Hikoso S, Yamaguchi O, Taneike M, Takeda T, Tamai T, et al. Mitochondrial DNA that escapes from autophagy causes inflammation and heart failure. *Nature*. (2012) 485:251–5. doi: 10.1038/nature10992
32. Shimizu I, Yoshida Y, Suda M, Minamino T. DNA damage response and metabolic disease. *Cell Metab*. (2014) 20:967–77.
33. Nishimoto S, Fukuda D, Higashikuni Y, Tanaka K, Hirata Y, Murata C, et al. Obesity-induced DNA released from adipocytes stimulates chronic adipose tissue inflammation and insulin resistance. *Sci Adv*. (2016) 2:e1501332. doi: 10.1126/sciadv.1501332
34. Matsushita K, Coresh J, Sang Y, Chalmers J, Fox C, Guallar E, et al. Estimated glomerular filtration rate and albuminuria for prediction of cardiovascular outcomes: a collaborative meta-analysis of individual participant data. *Lancet Diabetes Endocrinol*. (2015) 3:514–25.
35. Astor BC, Matsushita K, Gansevoort RT, van der Velde M, Woodward M, Levey AS, et al. Lower estimated glomerular filtration rate and higher albuminuria are associated with mortality and end-stage renal disease. A collaborative meta-analysis of kidney disease population cohorts. *Kidney Int*. (2011) 79:1331–40.
36. van der Velde M, Matsushita K, Coresh J, Astor BC, Woodward M, Levey A, et al. Lower estimated glomerular filtration rate and higher albuminuria are associated with all-cause and cardiovascular mortality. A collaborative meta-analysis of high-risk population cohorts. *Kidney Int*. (2011) 79:1341–52.
37. Whitaker RM, Stallons LJ, Kneff JE, Alge JL, Harmon JL, Rahn JJ, et al. Urinary mitochondrial DNA is a biomarker of mitochondrial disruption and renal dysfunction in acute kidney injury. *Kidney Int*. (2015) 88:1336–44.
38. Wei PZ, Kwan BC, Chow KM, Cheng PM, Luk CC, Li PK, et al. Urinary mitochondrial DNA level is an indicator of intra-renal mitochondrial depletion and renal scarring in diabetic nephropathy. *Nephrol Dial Transplant*. (2018) 33:784–8. doi: 10.1093/ndt/gfx339
39. Chang CC, Chiu PF, Wu CL, Kuo CL, Huang CS, Liu CS, et al. Urinary cell-free mitochondrial and nuclear deoxyribonucleic acid correlates with the prognosis of chronic kidney diseases. *BMC Nephrol*. (2019) 20:391. doi: 10.1186/s12882-019-1549-x
40. Wei Z, Kwan BC-H, Chow KM, Cheng PM-S, Luk CC-W, Lai K-B, et al. Urinary mitochondrial DNA level as a biomarker of tissue injury in non-diabetic chronic kidney diseases. *BMC Nephrol*. (2018) 19:367. doi: 10.1186/s12882-018-1178-9
41. Salvi S. Tobacco smoking and environmental risk factors for chronic obstructive pulmonary disease. *Clin Chest Med*. (2014) 35:17–27.
42. Sethi S, Mallia P, Johnston SL. New paradigms in the pathogenesis of chronic obstructive pulmonary disease II. *Proc Am Thorac Soc*. (2009) 6:532–4.
43. Calverley PMA, Walker P. Chronic obstructive pulmonary disease. *Lancet*. (2003) 362:1053–61.
44. Sethi S, Murphy TF. Infection in the pathogenesis and course of chronic obstructive pulmonary disease. *N Engl J Med*. (2008) 359:2355–65.
45. Kaisho T, Tanaka T. Turning NF- κ B and IRFs on and off in DC. *Trends Immunol*. (2008) 29:329–36. doi: 10.1016/j.it.2008.03.005
46. Yao H, Yang SR, Kode A, Rajendrasozhan S, Caito S, Adenuga D, et al. Redox regulation of lung inflammation: role of NADPH oxidase and NF- κ B signalling. *Biochem Soc Trans*. (2007) 35:1151–5.
47. Gould TJ, Lysov Z, Liaw PC. Extracellular DNA and histones: double-edged swords in immunothrombosis. *J Thromb Haemost*. (2015) 13:S82–91. doi: 10.1111/jth.12977
48. Simmons JD, Lee Y-L, Mulekar S, Kuck JL, Brevard SB, Gonzalez RP, et al. Elevated levels of plasma mitochondrial DNA DAMPs are linked to clinical outcome in severely injured human subjects. *Ann Surg*. (2013) 258:591–8. doi: 10.1097/SLA.0b013e3182a4ea46
49. Gu X, Yao Y, Wu G, Lv T, Luo L, Song Y. The plasma mitochondrial DNA is an independent predictor for post-traumatic systemic inflammatory response syndrome. *PLoS One*. (2013) 8:e72834. doi: 10.1371/journal.pone.0072834
50. Aswani A, Manson J, Itagaki K, Chiazza F, Collino M, Wupeng WL, et al. Scavenging circulating mitochondrial DNA as a potential therapeutic option for multiple organ dysfunction in trauma hemorrhage. *Front Immunol*. (2018) 9:891. doi: 10.3389/fimmu.2018.00891
51. Yamanouchi S, Kudo D, Yamada M, Miyagawa N, Furukawa H, Kushimoto S. Plasma mitochondrial DNA levels in patients with trauma and severe sepsis: time course and the association with clinical status. *J Crit Care*. (2013) 28:1027–31. doi: 10.1016/j.jccr.2013.05.006
52. Singel KL, Grzankowski KS, Khan A, Grimm MJ, D'Auria AC, Morrell K, et al. Mitochondrial DNA in the tumour microenvironment activates neutrophils and is associated with worse outcomes in patients with advanced epithelial ovarian cancer. *Br J Cancer*. (2019) 120:207–17. doi: 10.1038/s41416-018-0339-8
53. Mosca M, Giuliano T, Cuomo G, Doveri M, Tani C, Curcio M, et al. Cell-free DNA in the plasma of patients with systemic sclerosis. *Clin Rheumatol*. (2009) 28:1437–40.
54. Arneth B. Systemic lupus erythematosus and DNA degradation and elimination defects. *Front Immunol*. (2019) 10:1697. doi: 10.3389/fimmu.2019.01697
55. Duvvuri B, Lood C. Cell-Free DNA as a biomarker in autoimmune rheumatic diseases. *Front Immunol*. (2019) 10:502. doi: 10.3389/fimmu.2019.00502
56. Rykova E, Sizikov A, Roggenbuck D, Antonenko O, Bryzgalov L, Morozkin E, et al. Circulating DNA in rheumatoid arthritis: pathological changes and association with clinically used serological markers. *Arthritis Res Ther*. (2017) 19:85. doi: 10.1186/s13075-017-1295-z
57. Swarup V, Rajeswari MR. Circulating (cell-free) nucleic acids—a promising, non-invasive tool for early detection of several human diseases. *FEBS Lett*. (2007) 581:795–9. doi: 10.1016/j.febslet.2007.01.051
58. Atamaniuk J, Kopecky C, Skoupy S, Säemann MD, Weichhart T. Apoptotic cell-free DNA promotes inflammation in haemodialysis patients. *Nephrol Dial Transplant*. (2012) 27:902–5. doi: 10.1093/ndt/gfr695
59. Coimbra S, Rocha S, Nascimento H, Valente MJ, Catarino C, Rocha-Pereira P, et al. Cell-free DNA as a marker for the outcome of end-stage renal disease patients on haemodialysis. *Clin Kidney J*. (2021) 14:1371–8.
60. Wilkins HM, Weidling IW, Ji Y, Swerdlow RH. Mitochondria-derived damage-associated molecular patterns in neurodegeneration. *Front Immunol*. (2017) 8:508. doi: 10.3389/fimmu.2017.00508
61. Borissoff JJ, Joosen IA, Versteijlen MO, Brill A, Fuchs TA, Savchenko AS, et al. Elevated levels of circulating DNA and chromatin are independently associated with severe coronary atherosclerosis and a prothrombotic state. *Arterioscler Thromb Vasc Biol*. (2013) 33:2032–40. doi: 10.1161/ATVBAHA.113.301627
62. Nascimento M, Gombault A, Lacerda-Queiroz N, Panek C, Savigny F, Sbeity M, et al. Self-DNA release and STING-dependent sensing drives inflammation to cigarette smoke in mice. *Sci Rep*. (2019) 9:14848. doi: 10.1038/s41598-019-51427-y
63. Giordano L, Gregory AD, Pérez Verdaguer M, Ware SA, Harvey H, DeWallace E, et al. Extracellular release of mitochondrial DNA: triggered by

cigarette smoke and detected in COPD. *Cells*. (2022) 11:369. doi: 10.3390/cells11030369

64. Hemmi H, Takeuchi O, Kawai T, Kaisho T, Sato S, Sanjo H, et al. Toll-like receptor recognizes bacterial DNA. *Nature*. (2000) 408:740–5.

65. Latz E, Schoenemeyer A, Visintin A, Fitzgerald KA, Monks BG, Knetter CF, et al. TLR9 signals after translocating from the ER to CpG DNA in the lysosome. *Nat Immunol*. (2004) 5:190–8. doi: 10.1038/ni1028

66. Kawasaki T, Kawai T. Toll-like receptor signaling pathways. *Front Immunol*. (2014) 5:461. doi: 10.3389/fimmu.2014.00461

67. Akira S, Uematsu S, Takeuchi O. Pathogen recognition and innate immunity. *Cell*. (2006) 124:783–801.

68. Ishikawa H, Barber GN. STING is an endoplasmic reticulum adaptor that facilitates innate immune signalling. *Nature*. (2008) 455:674–8.

69. Zhong B, Yang Y, Li S, Wang YY, Li Y, Diao F, et al. The adaptor protein MITA links virus-sensing receptors to IRF3 transcription factor activation. *Immunity*. (2008) 29:538–50.

70. Sauer JD, Sotelo-Troha K, von Moltke J, Monroe KM, Rae CS, Brubaker SW, et al. The N-ethyl-N-nitrosourea-induced Goldenticket mouse mutant reveals an essential function of Sting in the in vivo interferon response to Listeria monocytogenes and cyclic dinucleotides. *Infect Immun*. (2011) 79:688–94. doi: 10.1128/IAI.00999-10

71. Wu J, Sun L, Chen X, Du F, Shi H, Chen C, et al. Cyclic GMP-AMP is an endogenous second messenger in innate immune signaling by cytosolic DNA. *Science*. (2013) 339:826–30.

72. Ishikawa H, Ma Z, Barber GN. STING regulates intracellular DNA-mediated, type I interferon-dependent innate immunity. *Nature*. (2009) 461:788–92. doi: 10.1038/nature08476

73. Hotamisligil GS. Inflammation and metabolic disorders. *Nature*. (2006) 444:860–7.

74. Hotamisligil GS, Erbay E. Nutrient sensing and inflammation in metabolic diseases. *Nat Rev Immunol*. (2008) 8:923–34.

75. Strissel KJ, Stancheva Z, Miyoshi H, Perfield JW II, DeFuria J, Jick Z, et al. Adipocyte death, adipose tissue remodeling, and obesity complications. *Diabetes*. (2007) 56:2910–8.

76. Murano I, Barbatelli G, Parisani V, Latini C, Muzzonigro G, Castellucci M, et al. Dead adipocytes, detected as crown-like structures, are prevalent in visceral fat depots of genetically obese mice. *J Lipid Res*. (2008) 49:1562–8. doi: 10.1194/jlr.M800019-JLR200

77. Rigamonti A, Brennand K, Lau F, Cowan CA. Rapid cellular turnover in adipose tissue. *PLoS One*. (2011) 6:e17637. doi: 10.1371/journal.pone.0017637

78. Fresno M, Alvarez R, Cuesta N. Toll-like receptors, inflammation, metabolism and obesity. *Arch Physiol Biochem*. (2011) 117:151–64.

79. Engin AB. Adipocyte-macrophage cross-talk in obesity. *Adv Exp Med Biol*. (2017) 960:327–43.

80. Fukuda D, Pham, PT, Sata, M. Emerging roles of the innate immune system regulated by DNA sensors in the development of vascular and metabolic diseases. *J Atheroscler Thromb*. (2022) 29:297–307.

81. Guzmán-Ruiz R, Ortega F, Rodríguez A, Vázquez-Martínez R, Díaz-Ruiz A, García-Navarro S, et al. Alarmin high-mobility group B1 (HMGB1) is regulated in human adipocytes in insulin resistance and influences insulin secretion in β -cells. *Int J Obes*. (2014) 38:1545–54. doi: 10.1038/ijo.2014.36

82. Hong CP, Yun CH, Lee GW, Park A, Kim YM, Jang MH. TLR9 regulates adipose tissue inflammation and obesity-related metabolic disorders. *Obesity*. (2015) 23:2199–206. doi: 10.1002/oby.21215

83. Kamfar S, Alavian SM, Houshmand M, Yadegarazari R, Seifi Zarei B, Khalaj A, et al. Liver mitochondrial DNA copy number and deletion levels may contribute to nonalcoholic fatty liver disease susceptibility. *Hepat Mon*. (2016) 16:e40774. doi: 10.5812/hepatmon.40774

84. Garcia-Martinez I, Santoro N, Chen Y, Hoque R, Ouyang X, Caprio S, et al. Hepatocyte mitochondrial DNA drives nonalcoholic steatohepatitis by activation of TLR9. *J Clin Invest*. (2016) 126:859–64. doi: 10.1172/JCI83885

85. Reilly SM, Chiang SH, Decker SJ, Chang L, Uhm M, Larsen MJ, et al. An inhibitor of the protein kinases TBK1 and IKK- ϵ improves obesity-related metabolic dysfunctions in mice. *Nat Med*. (2013) 19:313–21. doi: 10.1038/nm.3082

86. Zhao P, Wong KI, Sun X, Reilly SM, Uhm M, Liao Z, et al. TBK1 at the crossroads of inflammation and energy homeostasis in adipose tissue. *Cell*. (2018) 172:731–43.e12. doi: 10.1016/j.cell.2018.01.007

87. Bai J, Cervantes C, Liu J, He S, Zhou H, Zhang B, et al. DsbA-L prevents obesity-induced inflammation and insulin resistance by suppressing the mtDNA release-activated cGAS-cGAMP-STING pathway. *Proc Natl Acad Sci USA*. (2017) 114:12196–201. doi: 10.1073/pnas.1708744114

88. Mao Y, Luo W, Zhang L, Wu W, Yuan L, Xu H, et al. IRF3 triggers endothelial inflammation in response to free fatty acid-induced mitochondrial damage in diet-induced obesity. *Arterioscler Thromb Vasc Biol*. (2017) 37:920–9.

89. Hu HQ, Qiao JT, Liu FQ, Wang JB, Sha S, He Q, et al. The STING-IRF3 pathway is involved in lipotoxic injury of pancreatic β cells in type 2 diabetes. *Mol Cell Endocrinol*. (2020) 518:110890. doi: 10.1016/j.mce.2020.110890

90. Luo X, Li H, Ma L, Zhou J, Guo X, Woo SL, et al. Expression of STING Is increased in liver tissues from patients with NAFLD and promotes macrophage-mediated hepatic inflammation and fibrosis in mice. *Gastroenterology*. (2018) 155:1971–84.e4. doi: 10.1053/j.gastro.2018.09.010

91. Yu Y, Liu Y, An W, Song J, Zhang Y, Zhao X. STING-mediated inflammation in Kupffer cells contributes to progression of nonalcoholic steatohepatitis. *J Clin Invest*. (2019) 129:546–55. doi: 10.1172/JCI121842

92. Wang X, Rao H, Zhao J, Wee A, Li X, Fei R, et al. STING expression in monocyte-derived macrophages is associated with the progression of liver inflammation and fibrosis in patients with nonalcoholic fatty liver disease. *Lab Invest*. (2020) 100:542–52. doi: 10.1038/s41374-019-0342-6

93. Begriche K, Igoudjil A, Pessayre D, Fromenty B. Mitochondrial dysfunction in NASH: causes, consequences and possible means to prevent it. *Mitochondrion*. (2006) 6:1–28. doi: 10.1016/j.mito.2005.10.004

94. Zhai Y, Qiao B, Gao F, Shen X, Vardanian A, Busuttil RW, et al. Type I, but not type II, interferon is critical in liver injury induced after ischemia and reperfusion. *Hepatology*. (2008) 47:199–206.

95. Akazawa Y, Nakashima R, Matsuda K, Okamoto K, Hirano R, Kawasaki H, et al. Detection of DNA damage response in nonalcoholic fatty liver disease via p53-binding protein 1 nuclear expression. *Mod Pathol*. (2019) 32:997–1007. doi: 10.1038/s41379-019-0218-8

96. Libby P. Inflammation in atherosclerosis. *Arterioscler Thromb Vasc Biol*. (2012) 32:2045–51.

97. Aday AW, Ridker PM. Targeting residual inflammatory risk: a shifting paradigm for atherosclerotic disease. *Front Cardiovasc Med*. (2019) 6:16. doi: 10.3389/fcvm.2019.00016

98. Hansson GK, Libby P, Schönbeck U, Yan ZQ. Innate and adaptive immunity in the pathogenesis of atherosclerosis. *Circ Res*. (2002) 91:281–91.

99. Roshan MH, Tambo A, Pace NP. The Role of TLR2, TLR4, and TLR9 in the pathogenesis of atherosclerosis. *Int J Inflamm*. (2016) 2016:1532832.

100. Xu XH, Shah PK, Faure E, Equils O, Thomas L, Fishbein MC, et al. Toll-like receptor-4 is expressed by macrophages in murine and human lipid-rich atherosclerotic plaques and upregulated by oxidized LDL. *Circulation*. (2001) 104:3103–8. doi: 10.1161/hc5001.100631

101. Scholtes VP, Versteeg D, de Vries JP, Hoefer IE, Schoneveld AH, Stella PR, et al. Toll-like receptor 2 and 4 stimulation elicits an enhanced inflammatory response in human obese patients with atherosclerosis. *Clin Sci*. (2011) 121:205–14. doi: 10.1042/CS20100601

102. Snodgrass RG, Huang S, Choi IW, Rutledge JC, Hwang DH. Inflammasome-mediated secretion of IL-1 β in human monocytes through TLR2 activation; modulation by dietary fatty acids. *J Immunol*. (2013) 191:4337–47. doi: 10.4049/jimmunol.1300298

103. Sorrentino R, Morello S, Chen S, Bonavita E, Pinto A. The activation of liver X receptors inhibits toll-like receptor-9-induced foam cell formation. *J Cell Physiol*. (2010) 223:158–67. doi: 10.1002/jcp.22022

104. Lee JG, Lim EJ, Park DW, Lee SH, Kim JR, Baek SH. A combination of Lox-1 and Nox1 regulates TLR9-mediated foam cell formation. *Cell Signal*. (2008) 20:2266–75. doi: 10.1016/j.cellsig.2008.08.022

105. Niessner A, Sato K, Chaikof EL, Colmegna I, Goronzy JJ, Weyand CM. Pathogen-sensing plasmacytoid dendritic cells stimulate cytotoxic T-cell function in the atherosclerotic plaque through interferon- α . *Circulation*. (2006) 114:2482–9. doi: 10.1161/CIRCULATIONAHA.106.642801

106. Littlewood TD, Bennett MR. Apoptotic cell death in atherosclerosis. *Curr Opin Lipidol*. (2003) 14:469–75.

107. Isner JM, Kearney M, Bortman S, Passeri J. Apoptosis in human atherosclerosis and restenosis. *Circulation*. (1995) 91:2703–11.

108. Martinet W, Schrijvers DM, De Meyer GR. Necrotic cell death in atherosclerosis. *Basic Res Cardiol*. (2011) 106:749–60.

109. Zheng Y, Gardner SE, Clarke MC. Cell death, damage-associated molecular patterns, and sterile inflammation in cardiovascular disease. *Arterioscler Thromb Vasc Biol*. (2011) 31:2781–6.

110. Ma C, Ouyang Q, Huang Z, Chen X, Lin Y, Hu W, et al. Toll-like receptor 9 inactivation alleviated atherosclerotic progression and inhibited macrophage polarized to M1 phenotype in ApoE $^{-/-}$ mice. *Dis Mark*. (2015) 2015:909572. doi: 10.1155/2015/909572

111. Krogmann AO, Lüsebrink E, Steinmetz M, Asdonk T, Lahrmann C, Lütjohann D, et al. Proinflammatory stimulation of toll-like receptor 9 with high dose CpG ODN 1826 impairs endothelial regeneration and promotes atherosclerosis in mice. *PLoS One*. (2016) 11:e0146326. doi: 10.1371/journal.pone.0146326
112. Waibler Z, Anzaghe M, Konur A, Akira S, Müller W, Kalinke U. Excessive CpG 1668 stimulation triggers IL-10 production by cDC that inhibits IFN- α responses by pDC. *Eur J Immunol*. (2008) 38:3127–37. doi: 10.1002/eji.200838184
113. Bouaziz JD, Calbo S, Maho-Vaillant M, Saussine A, Bagot M, Bensussan A, et al. 10 produced by activated human B cells regulates CD4(+) T-cell activation in vitro. *Eur J Immunol*. (2010) 40:2686–91. doi: 10.1002/eji.201040673
114. Koulis C, Chen YC, Hausding C, Ahrens I, Kyaw TS, Tay C, et al. Protective role for Toll-like receptor-9 in the development of atherosclerosis in apolipoprotein E-deficient mice. *Arterioscler Thromb Vasc Biol*. (2014) 34:516–25.
115. Wu J, Cui H, Dick AD, Liu L. TLR9 agonist regulates angiogenesis and inhibits corneal neovascularization. *Am J Pathol*. (2014) 184:1900–10. doi: 10.1016/j.ajpath.2014.03.001
116. Liu H, Cheng WL, Jiang X, Wang PX, Fang C, Zhu XY, et al. Ablation of interferon regulatory factor 3 protects against atherosclerosis in apolipoprotein E-deficient mice. *Hypertension*. (2017) 69:510–20. doi: 10.1161/HYPERTENSIONAHA.116.08395
117. Goossens P, Gijbels MJ, Zerneck A, Eijgelaar W, Vergouwe MN, van der Made I, et al. Myeloid type I interferon signaling promotes atherosclerosis by stimulating macrophage recruitment to lesions. *Cell Metab*. (2010) 12:142–53. doi: 10.1016/j.cmet.2010.06.008
118. Luo W, Wang Y, Zhang L, Ren P, Zhang C, Li Y, et al. Critical role of cytosolic DNA and its sensing adaptor STING in aortic degeneration, dissection, and rupture. *Circulation*. (2020) 141:42–66. doi: 10.1161/CIRCULATIONAHA.119.041460
119. Jeremiah N, Neven B, Gentili M, Callebaut I, Maschalidis S, Stolzenberg MC, et al. Inherited STING-activating mutation underlies a familial inflammatory syndrome with lupus-like manifestations. *J Clin Invest*. (2014) 124:5516–20. doi: 10.1172/JCI79100
120. Liu Y, Jesus AA, Marrero B, Yang D, Ramsey SE, Sanchez GAM, et al. Activated STING in a vascular and pulmonary syndrome. *N Engl J Med*. (2014) 371:507–18. doi: 10.1056/NEJMoa1312625
121. Munoz J, Rodière M, Jeremiah N, Rieux-Laucat F, Oojageer A, Rice GI, et al. Stimulator of interferon genes-associated vasculopathy with onset in infancy: a mimic of childhood granulomatosis with polyangiitis. *JAMA Dermatol*. (2015) 151:872–7. doi: 10.1001/jamadermatol.2015.0251
122. Hamann L, Ruiz-Moreno JS, Szwed M, Mossakowska M, Lundvall L, Schumann RR, et al. STING SNP R293Q is associated with a decreased risk of aging-related diseases. *Gerontology*. (2019) 65:145–54.
123. Hamann L, Szwed M, Mossakowska M, Chudek J, Puzianowska-Kuznicka M. First evidence for STING SNP R293Q being protective regarding obesity-associated cardiovascular disease in age-advanced subjects - a cohort study. *Immun Ageing*. (2020) 17:7. doi: 10.1186/s12979-020-00176-y
124. Lu KC, Yang HY, Lin YF, Kao SY, Lai CH, Chu CM, et al. The T-1237C polymorphism of the Toll-like receptor-9 gene is associated with chronic kidney disease in a Han Chinese population. *Tohoku J Exp Med*. (2011) 225:109–16. doi: 10.1620/tjem.225.109
125. Yang HY, Lu KC, Lee HS, Huang SM, Lin YF, Wu CC, et al. Role of the functional Toll-Like receptor-9 promoter polymorphism (-1237T/C) in increased risk of end-stage renal disease: a case-control study. *PLoS One*. (2013) 8:e58444. doi: 10.1371/journal.pone.0058444
126. Gollapudi P, Yoon JW, Gollapudi S, Pahl MV, Vaziri ND. Leukocyte toll-like receptor expression in end-stage kidney disease. *Am J Nephrol*. (2010) 31:247–54.
127. Engel JE, Chade AR. Macrophage polarization in chronic kidney disease: a balancing act between renal recovery and decline?. *Am J Physiol Renal Physiol*. (2019) 317:F1409–13. doi: 10.1152/ajprenal.00380.2019
128. Ryu M, Kulkarni OP, Radomska E, Miosge N, Gross O, Anders HJ. Bacterial CpG-DNA accelerates Alport glomerulosclerosis by inducing an M1 macrophage phenotype and tumor necrosis factor- α -mediated podocyte loss. *Kidney Int*. (2011) 79:189–98. doi: 10.1038/ki.2010.373
129. Zheng H, Zhang Y, Li L, Zhang R, Luo Z, Yang Z, et al. Depletion of toll-like receptor-9 attenuates renal tubulointerstitial fibrosis after ischemia-reperfusion injury. *Front Cell Dev Biol*. (2021) 9:641527. doi: 10.3389/fcell.2021.641527
130. Li X, Yun Z, Tan Z, Li S, Wang D, Ma K, et al. The role of Toll-like receptor (TLR) 2 and 9 in renal ischemia and reperfusion injury. *Urology*. (2013) 81:1379.e15–20.
131. Bakker PJ, Scantlebury AM, Butter LM, Claessen N, Teske GJ, van der Poll T, et al. TLR9 mediates remote liver injury following severe renal ischemia reperfusion. *PLoS One*. (2015) 10:e0137511. doi: 10.1371/journal.pone.0137511
132. Han SJ, Li H, Kim M, Shlomchik MJ, Lee HT. Kidney proximal tubular TLR9 exacerbates ischemic diabetic kidney injury. *J Immunol*. (2018) 201:1073–85.
133. Jang HR, Rabb H. Immune cells in experimental acute kidney injury. *Nat Rev Nephrol*. (2015) 11:88–101.
134. Forni LG, Darmon M, Ostermann M, Oudemans-van Straaten HM, Pettit V, Prowle JR, et al. Renal recovery after acute kidney injury. *Intensive Care Med*. (2017) 43:855–66.
135. Drüeke TB, Massy ZA. Atherosclerosis in CKD: differences from the general population. *Nat Rev Nephrol*. (2010) 6:723–35.
136. Bro S, Bentzon JF, Falk E, Andersen CB, Olgaard K, Nielsen LB. Chronic renal failure accelerates atherogenesis in apolipoprotein E-deficient mice. *J Am Soc Nephrol*. (2003) 14:2466–74. doi: 10.1097/01.asn.0000088024.72216.2e
137. Yang K, Du C, Wang X, Li F, Xu Y, Wang S, et al. Indoxyl sulfate induces platelet hyperactivity and contributes to chronic kidney disease-associated thrombosis in mice. *Blood*. (2017) 129:2667–79. doi: 10.1182/blood-2016-10-744060
138. Bi X, Du C, Wang X, Wang XY, Han W, Wang Y, et al. Mitochondrial damage-induced innate immune activation in vascular smooth muscle cells promotes chronic kidney disease-associated plaque vulnerability. *Adv Sci*. (2021) 8:2002738. doi: 10.1002/adv.202002738
139. Myakala K, Jones BA, Wang XX, Levi M. Sacubitril/valsartan treatment has differential effects in modulating kidney disease in db/db mice and KKAY mice compared with valsartan treatment. *Am J Physiol Renal Physiol*. (2021) 320:F1133–51. doi: 10.1152/ajprenal.00614.2020
140. Barnes PJ. Cellular and molecular mechanisms of chronic obstructive pulmonary disease. *Clin Chest Med*. (2014) 35:71–86.
141. Di Stefano A, Caramori G, Ricciardolo FL, Capelli A, Adcock IM, Donner CF. Cellular and molecular mechanisms in chronic obstructive pulmonary disease: an overview. *Clin Exp Allergy*. (2004) 34:1156–67.
142. Holt PG, Strickland DH, Wikström ME, Jahnsen FL. Regulation of immunological homeostasis in the respiratory tract. *Nat Rev Immunol*. (2008) 8:142–52.
143. Doz E, Noulin N, Boichot E, Guénon I, Fick L, Le Bert M, et al. Cigarette smoke-induced pulmonary inflammation is TLR4/MyD88 and IL-1R1/MyD88 signaling dependent. *J Immunol*. (2008) 180:1169–78.
144. Geraghty P, Dabo AJ, D'Armiento J. TLR4 protein contributes to cigarette smoke-induced matrix metalloproteinase-1 (MMP-1) expression in chronic obstructive pulmonary disease. *J Biol Chem*. (2011) 286:30211–8. doi: 10.1074/jbc.M111.238824
145. Schneberger D, Caldwell S, Kanthan R, Singh B. Expression of Toll-like receptor 9 in mouse and human lungs. *J Anat*. (2013) 222:495–503.
146. Nadigel J, Préfontaine D, Baglioni CJ, Maltais F, Bourbeau J, Eidelman DH, et al. Cigarette smoke increases TLR4 and TLR9 expression and induces cytokine production from CD8(+) T cells in chronic obstructive pulmonary disease. *Respir Res*. (2011) 12:149. doi: 10.1186/1465-9921-12-149
147. Foronjy RF, Salathe MA, Dabo AJ, Baumlín N, Cummins N, Eden E, et al. TLR9 expression is required for the development of cigarette smoke-induced emphysema in mice. *Am J Physiol Lung Cell Mol Physiol*. (2016) 311:L154–66. doi: 10.1152/ajplung.00073.2016
148. Song JH, Ahn JH, Kim SR, Cho S, Hong EH, Kwon BE, et al. Manassantin B shows antiviral activity against coxsackievirus B3 infection by activation of the STING/TBK-1/IRF3 signalling pathway. *Sci Rep*. (2019) 9:9413. doi: 10.1038/s41598-019-45868-8
149. Zuo L, Hallman AH, Yousif MK, Chien MT. Oxidative stress, respiratory muscle dysfunction, and potential therapeutics in chronic obstructive pulmonary disease. *Front Biol*. (2012) 7:506–13. doi: 10.1007/s11515-012-1251-x
150. Zuo L, Zhou T, Pannell BK, Ziegler AC, Best TM. Biological and physiological role of reactive oxygen species—the good, the bad and the ugly. *Acta Physiol*. (2015) 214:329–48. doi: 10.1111/apha.12515
151. Lai JH, Wu DW, Wu CH, Hung LF, Huang CY, Ka SM, et al. Mitochondrial CMPK2 mediates immunomodulatory and antiviral activities through IFN-dependent and IFN-independent pathways. *iScience*. (2021) 24:102498. doi: 10.1016/j.isci.2021.102498
152. Berenson CS, Kruzel RL, Wrona CT, Mammen MJ, Sethi S. Impaired innate COPD alveolar macrophage responses and toll-like receptor-9 polymorphisms. *PLoS One*. (2015) 10:e0134209. doi: 10.1371/journal.pone.0134209
153. Pabst S, Bradler O, Gillissen A, Nickenig G, Skowasch D, Grohe C. Toll-like receptor-9 polymorphisms in sarcoidosis and chronic obstructive pulmonary disease. *Adv Exp Med Biol*. (2013) 756:239–45. doi: 10.1007/978-94-007-4549-0_30

154. D'Anna SE, Maniscalco M, Carriero V, Gnemmi I, Caramori G, Nucera F, et al. Evaluation of innate immune mediators related to respiratory viruses in the lung of stable COPD patients. *J Clin Med.* (2020) 9:1807. doi: 10.3390/jcm9061807
155. Pouwels SD, Faiz A, den Boef IE, Gras R, van den Berge M, Boezen HM, et al. Genetic variance is associated with susceptibility for cigarette smoke-induced DAMP release in mice. *Am J Physiol Lung Cell Mol Physiol.* (2017) 313:L559–80. doi: 10.1152/ajplung.00466.2016
156. Pouwels SD, Heijink IH, ten Hacken NH, Vandenabeele P, Krysko DV, Nawijn MC, et al. DAMPs activating innate and adaptive immune responses in COPD. *Mucosal Immunol.* (2014) 7:215–26.
157. Yu L, Liu P. Cytosolic DNA sensing by cGAS: regulation, function, and human diseases. *Signal Transduct Target Ther.* (2021) 6:170.
158. Deslee G, Adair-Kirk TL, Betsuyaku T, Woods JC, Moore CH, Gierada DS, et al. Cigarette smoke induces nucleic-acid oxidation in lung fibroblasts. *Am J Respir Cell Mol Biol.* (2010) 43:576–84.
159. King PT, Sharma R, O'Sullivan KM, Callaghan J, Dousha L, Thomas B, et al. Deoxyribonuclease 1 reduces pathogenic effects of cigarette smoke exposure in the lung. *Sci Rep.* (2017) 7:12128. doi: 10.1038/s41598-017-12474-5
160. García-Valero J, Olloquequi J, Montes JF, Rodríguez E, Martín-Satué M, Texidó L, et al. Deficient pulmonary IFN- β expression in COPD patients. *PLoS One.* (2019) 14:e0217803. doi: 10.1371/journal.pone.0217803
161. Qin H, Huang G, Gao F, Huang B, Wang D, Hu X, et al. Diminished stimulator of interferon genes production with cigarette smoke-exposure contributes to weakened anti-adenovirus vectors response and destruction of lung in chronic obstructive pulmonary disease model. *Exp Cell Res.* (2019) 384:111545.
162. Yu X, Cai B, Wang M, Tan P, Ding X, Wu J. Cross-regulation of two type I interferon signaling pathways in plasmacytoid dendritic cells controls anti-malaria immunity and host mortality. *Immunity.* (2016) 45:1093–107. doi: 10.1016/j.immuni.2016.10.001
163. Deb P, Dai J, Singh S, Kalyoussef E, Fitzgerald-Bocarsly P. Triggering of the cGAS-STING pathway in human plasmacytoid dendritic cells inhibits TLR9-mediated IFN production. *J Immunol.* (2020) 205:223–36.
164. Temizoz B, Kuroda E, Ohata K, Jounai N, Ozasa K, Kobiyama K, et al. TLR9 and STING agonists synergistically induce innate and adaptive type-II IFN. *Eur J Immunol.* (2015) 45:1159–69. doi: 10.1002/eji.201445132
165. Liu L, Mao Y, Xu B, Zhang X, Fang C, Ma Y. Induction of neutrophil extracellular traps during tissue injury: involvement of STING and Toll-like receptor 9 pathways. *Cell Prolif.* (2019) 52:e12579–12579.
166. Bode C, Poth JM, Fox M, Schulz S, Klinman DM, Latz E, et al. Cytosolic d-type CpG-oligonucleotides induce a type I interferon response by activating the cGAS-STING signaling pathway. *Eur J Immunol.* (2021) 51:1686–97. doi: 10.1002/eji.202048810



OPEN ACCESS

EDITED BY

Hiromi Yanagisawa,
University of Tsukuba, Japan

REVIEWED BY

Hong Jin,
Karolinska Institutet, Sweden
Jeroen Essers,
Erasmus Medical Center, Netherlands

*CORRESPONDENCE

Claudia Goettsch
cgoettsch@ukaachen.de

SPECIALTY SECTION

This article was submitted to
Atherosclerosis and Vascular Medicine,
a section of the journal
Frontiers in Cardiovascular Medicine

RECEIVED 01 June 2022

ACCEPTED 15 August 2022

PUBLISHED 20 September 2022

CITATION

Heuschkel MA, Babler A, Heyn J,
van der Vorst EPC, Steenman M,
Gesper M, Kappel BA, Magne D,
Gouëffic Y, Kramann R,
Jahnen-Dechent W, Marx N, Quillard T
and Goettsch C (2022) Distinct role
of mitochondrial function and protein
kinase C in intimal and medial
calcification *in vitro*.
Front. Cardiovasc. Med. 9:959457.
doi: 10.3389/fcvm.2022.959457

COPYRIGHT

© 2022 Heuschkel, Babler, Heyn, van
der Vorst, Steenman, Gesper, Kappel,
Magne, Gouëffic, Kramann,
Jahnen-Dechent, Marx, Quillard and
Goettsch. This is an open-access
article distributed under the terms of
the [Creative Commons Attribution
License \(CC BY\)](#). The use, distribution
or reproduction in other forums is
permitted, provided the original
author(s) and the copyright owner(s)
are credited and that the original
publication in this journal is cited, in
accordance with accepted academic
practice. No use, distribution or
reproduction is permitted which does
not comply with these terms.

Distinct role of mitochondrial function and protein kinase C in intimal and medial calcification *in vitro*

Marina A. Heuschkel¹, Anne Babler², Jonas Heyn¹,
Emiel P. C. van der Vorst^{3,4,5,6}, Marja Steenman⁷,
Maren Gesper¹, Ben A. Kappel¹, David Magne⁸,
Yann Gouëffic⁹, Rafael Kramann^{2,10,11},
Willi Jahnen-Dechent¹², Nikolaus Marx¹, Thibaut Quillard^{7,13}
and Claudia Goettsch^{1*}

¹Department of Internal Medicine I—Cardiology, Medical Faculty, RWTH Aachen University, Aachen, Germany, ²Institute of Experimental Medicine and Systems Biology, University Hospital, RWTH Aachen, Aachen, Germany, ³Interdisciplinary Center for Clinical Research, Institute for Molecular Cardiovascular Research, RWTH Aachen University, Aachen, Germany, ⁴Department of Pathology, Cardiovascular Research Institute Maastricht, Maastricht University Medical Centre, Maastricht, Netherlands, ⁵Institute for Cardiovascular Prevention (IPEK), Ludwig-Maximilians-University Munich, Munich, Germany, ⁶DZHK (German Centre for Cardiovascular Research), Partner Site Munich Heart Alliance, Munich, Germany, ⁷L'institut Du Thorax, Inserm UMR 1087, CNRS, INSERM, France and Nantes Université, Nantes, France, ⁸ICBMS UMR CNRS 5246, Université Claude Bernard Lyon 1, Villeurbanne, France, ⁹Department of Vascular Surgery, Vascular Center, Groupe Hospitalier Paris Saint-Joseph, Paris, France, ¹⁰Department of Nephrology and Clinical Immunology, University Hospital RWTH Aachen, Aachen, Germany, ¹¹Department of Internal Medicine, Nephrology and Transplantation, Erasmus Medical Center, Rotterdam, Netherlands, ¹²Biointerface Laboratory, Helmholtz Institute for Biomedical Engineering, RWTH Aachen University, Aachen, Germany, ¹³PHY-OS Laboratory, INSERM UMR 1238, Nantes University of Medicine, Nantes, France

Introduction: Vascular calcification (VC) is a major risk factor for cardiovascular morbidity and mortality. Depending on the location of mineral deposition within the arterial wall, VC is classified as intimal and medial calcification. Using *in vitro* mineralization assays, we developed protocols triggering both types of calcification in vascular smooth muscle cells (SMCs) following diverging molecular pathways.

Materials and methods and results: Human coronary artery SMCs were cultured in osteogenic medium (OM) or high calcium phosphate medium (CaP) to induce a mineralized extracellular matrix. OM induces osteoblast-like differentiation of SMCs—a key process in intimal calcification during atherosclerotic plaque remodeling. CaP mimics hyperphosphatemia, associated with chronic kidney disease—a risk factor for medial calcification. Transcriptomic analysis revealed distinct gene expression profiles of OM and CaP-calcifying SMCs. OM and CaP-treated SMCs shared 107 differentially regulated genes related to SMC contraction and metabolism. Real-time extracellular efflux analysis demonstrated decreased mitochondrial respiration and glycolysis in CaP-treated SMCs compared to increased mitochondrial respiration without altered glycolysis in OM-treated SMCs. Subsequent kinome and *in silico* drug repurposing analysis (Connectivity Map) suggested

a distinct role of protein kinase C (PKC). *In vitro* validation experiments demonstrated that the PKC activators prostratin and ingenol reduced calcification triggered by OM and promoted calcification triggered by CaP.

Conclusion: Our direct comparison results of two *in vitro* calcification models strengthen previous observations of distinct intracellular mechanisms that trigger OM and CaP-induced SMC calcification *in vitro*. We found a differential role of PKC in OM and CaP-calcified SMCs providing new potential cellular and molecular targets for pharmacological intervention in VC. Our data suggest that the field should limit the generalization of results found in *in vitro* studies using different calcification protocols.

KEYWORDS

vascular calcification, vascular smooth muscle cells, drug repurposing, mitochondrial function, matrix mineralization, protein kinase C

Introduction

Cardiovascular diseases are the leading cause of death worldwide (1). Vascular calcification (VC) is a significant risk factor for cardiovascular morbidity and mortality in patients with end-stage renal disease, diabetes, and atherosclerosis (2). However, no pharmaceutical therapy is available to prevent or halt VC progression.

Based on the deposition site of minerals within the arterial wall, VC can be classified into two main types: intimal calcification observed in advanced atherosclerotic plaques and medial calcification lacking lipid deposits, most prevalent in end-stage renal disease and diabetes (3).

Historically, VC is regarded as a degenerative process including cell and tissue inflammation, degeneration, and remodeling, ultimately resulting in extracellular matrix (ECM) mineral deposition. Alternatively, calcification of both the tunica intima and tunica media is considered a cell-autonomous process reminiscent of osteogenesis (4). Vascular smooth muscle cells (SMCs) are the most abundant cell type in the arterial vessel wall and contribute to VC through osteochondrogenic transdifferentiation, characterized by the expression of osteogenic markers, elaboration of a mineralization competent extracellular matrix, and shedding of calcifying extracellular vesicles (3, 5).

Although both intimal and medial calcification results in ectopic calcification, it seems likely that they are triggered by different initiating and propagating molecular mechanisms (3). The variety of factors triggering VC development is reflected in various experimental *in vivo* and *in vitro* models (6). For example, osteogenic medium, commonly used to differentiate mesenchymal stem cells to osteoblasts, induces marked phenotypic changes of SMCs characterized by a loss of contractile markers and increased expression of bone-related

genes. This mimics osteoblastogenesis in intimal calcification, a key process in atherosclerotic plaque remodeling (7, 8). On the other hand, a medium enriched in phosphate mimics the hyperphosphatemia associated with the pathophysiology of chronic kidney disease (CKD), which is a prevalent risk factor for medial calcification (9–11). Therefore, this study investigates and comparatively analyzes two different calcification protocols reflecting intimal and medial calcification. We hypothesize that distinct mineralization protocols alter specific intracellular mechanisms associated with SMC transdifferentiation and extracellular matrix mineralization.

Materials and methods

Human primary vascular smooth muscle cells

Human coronary artery SMCs (PromoCell, pSMCs) were grown in SMC growth medium 2 (SMC-GM2, PromoCell) supplemented with Smooth Muscle Cell Growth Medium 2 Supplement Mix (Promocell) consisting of 0.5 ng/ml epidermal growth factor, 5 µg/ml insulin, 2 ng/ml basic fibroblast growth factor, 1% penicillin/streptomycin (P/S), and 5% fetal bovine serum (FBS) at 37°C in humidified 5% CO₂. Cells were used between passages 3 and 9 from at least three independent cell donors.

Immortalized vascular smooth muscle cells

To generate immortalized SMC (iSMC) lines, primary human coronary artery SMCs were cultured in Dulbecco's

Modified Eagle Medium (DMEM, Thermo Scientific) with 4.5 g/L glucose, 10% FBS, 1% P/S at 37°C in humidified 5% CO₂ (Thermo Fisher) and immortalized using SV40LT and HTERT. Retroviral particles were produced by transient transfection of HEK293T cells using TransIT-LT (Mirus). Two types of amphotropic particles were generated by co-transfection of plasmids pBABE-puro-SV40-LT (Addgene) or xlox-dNGFR-TERT (Addgene) in combination with a packaging plasmid pUMVC (Addgene) and a pseudotyping plasmid pMD2.G (Addgene). Retroviral particles were 100x concentrated using Retro-X concentrator (Clontech) 48 h post-transfection. Cell transduction was initiated by incubating the target cells with the retroviral supernatants for 48 h. After 7 days, the infected cells were selected with 2 µg/ml puromycin for 72 h.

Calcification assays and visualization

pSMCs and iSMCs were cultured in the presence of either control medium (CM, DMEM, 10% FBS, 1% P/S), osteogenic medium [OM, consisting of CM supplemented with 10 nM dexamethasone (Sigma-Aldrich), 10 mM β-glycerol phosphate (Sigma-Aldrich) and 100 µM l-ascorbate phosphate (Sigma-Aldrich)], or CaP [consisting of CM supplemented with 1.8 mM CaCl₂ (ROTH) and 0.9 mM Na₂HPO₄/NaH₂PO₄ (ROTH)] to reach a final concentration of 3 mM calcium and 2 mM phosphate. The concentrations of CaP aim to mimic the calcium and phosphate serum levels in CKD patients of 9.1 ± 0.7 mg/dL (2.27 mM) and 5.3 ± 1.4 mg/dL (1.72 mM) respectively (12). Media exchange was performed twice weekly.

Mineralized matrix formation was assessed by Alizarin Red S staining. Cell cultures were fixed with 4% paraformaldehyde (PFA) and stained with 2% (w/v) Alizarin Red S (pH 4.2, Sigma-Aldrich) for 30 min at room temperature. Excess dye was removed by washing with distilled water and imaged under a light microscope (EVOS® FL Cell Imaging System). The staining was quantified by Alizarin Red S elution from the extracellular matrix using 100 mM cetylpyridinium chloride (Sigma-Aldrich) in water for 20 min at 37°C. Absorption was measured at 570 nm in a spectrophotometer (TECAN).

Stimulation of vascular smooth muscle cells

Cells were stimulated with PD184352 (Sigma-Aldrich), prostratin (Sigma-Aldrich), ingenol,3,20-dibenzoate (Enzo LifeSciences), L690,330 (Tocris), fluticasone propionate (Sigma), or Go6983 (Tocris) dissolved in dimethylsulfoxide

(DMSO) or water (for L690,330). An equal amount of the vehicle (1:1,000) was used as solvent control.

Cell viability

Cell viability was assessed using the AlamarBlue assay (Thermo Scientific), according to the manufacturer's protocol. Upon entering the viable cell, resazurin—the active compound of AlamarBlue—is reduced to resorufin that is assessed by fluorescence at Ex₅₆₀ nm/Em₅₉₀ nm.

Furthermore, cell viability was assessed by a live/dead fluorescence-based cell assay using fluorescein diacetate (FDA) and propidium iodide (PI). Staining of cells was performed using a mixture of 0.5 µg/ml FDA (Sigma-Aldrich) and (0.05 µg/ml PI), (Sigma-Aldrich) in PBS for 30 s. Cells treated with 0.5% Triton X-100 (Sigma-Aldrich) for 2 min served as a positive control for cell death. Following staining, cells were washed with PBS and examined by fluorescence microscopy. Image J v2.0 software was employed for quantification. Fluorescence images were converted into single-channel 8-bit grayscale images, and the threshold was adjusted to measure the mean gray values. FDA mean fluorescence intensity was divided by the corresponding PI mean fluorescence intensity to calculate the FDA/PI ratio at day 0 and day 7.

Activity of tissue non-specific alkaline phosphatase

Tissue non-specific alkaline phosphatase (TNAP) activity was measured in cells using the Alkaline Phosphatase Activity Colorimetric Assay Kit (BioVision) according to the manufacturer's protocol and normalized to the total protein amount assessed by bicinchoninic acid (BCA) assay (Thermo Scientific).

Ribonucleic acid preparation and real-time polymerase chain reaction

Total RNA was isolated using TRIzol reagent (Life Technologies). Reverse transcription was performed using the High capacity cDNA Reverse Transcription Kit (Life Technologies), according to the manufacturer's protocol. The gene expression levels were quantified by TaqMan-based real-time PCR reactions (Life Technologies). The used TaqMan probes are listed in **Supplementary Table 1**. The expression levels were normalized to RPLP0. Results were calculated using the ΔΔCt method and presented as fold increase relative to control.

Gene expression analysis

300 ng of total RNA from calcifying and control pSMCs were processed using the GeneChip WT PLUS Reagent Kit (Affymetrix, Inc., Santa Clara, CA, United States) following the manufacturer's protocol to yield purified biotinylated sense-stranded cDNA. Hybridization was performed to Clariom D Human Arrays using the GeneChip Hybridization, Wash & Stain Kit (Affymetrix, Inc., Santa Clara, CA, United States) and Fluidics Station 450 for 16 h at 45°C. Arrays were scanned using Affymetrix GeneChip Scanner 3000 controlled by GeneChip Command Console (AGCC) version 4.0 to produce CEL intensity files. The raw data were analyzed using the Transcriptome Analysis Console software (TAC4.0, ThermoFisher Scientific, United States) with default parameters for gene-level expression analysis based on the annotation Hg38 clariom_D_Human.r1.na36.hg38.a1.transcript.csv. SST-RMA was applied for normalization and summarization. Values are defined as log₂ scaled normalized gene level expression values.

Microarray data have been deposited in NCBI's GEO and are accessible through GEO Series accession number GSE211752.

Heatmaps and volcano plots were generated using the R statistical software environment. Heatmaps were visualized using the heatmap.2 function in the ggplot package and volcano plots were generated with the EnhancedVolcano package version 1.4.0 (13). The ConsensusPathDB database¹ was used for pathway over-representation analysis, employing the canonical pathways from the Kyoto Encyclopedia of Genes and Genomes (KEGG) and Reactome. Pathways with a *p*-value < 0.05 were considered to be significantly enriched in a gene set of interest.

Western blot analysis

Cells were lysed with RIPA buffer (Thermo Scientific) containing protease and phosphatase inhibitor (Roche). Protein concentration was measured using the BCA assay (Thermo Scientific) according to the manufacturer's instructions. 15 µg protein was separated in 8% polyacrylamide gel, transferred to a nitrocellulose membrane, and incubated overnight with OXPHOS (1:1000, Abcam, ab110413) and human beta-actin (1:10,000; Sigma-Aldrich, A2228). Bound antibodies were then detected using HRP-conjugated secondary antibody (anti-mouse: #7076, Cell Signaling) and visualized by enhanced Super Signal West blotting substrate (ThermoFisher Scientific) with a ChemiDocTM MP Imaging System and the software Image Lab version 6.0. Protein bands were quantified by FIJI (ImageJ) software (Version 1.53c), and normalized to the loading control beta-actin.

¹ <http://consensuspathdb.org>

Collagen contraction assay

1.5×10^5 cells per mL were embedded in collagen gels from rat tail collagen type 1 (R&D system). 200 µL of the cell suspension was combined with 100 µL of 3 mg/mL Cultrex Rat Collagen I and 12 µL of filtered 1 M NaOH for each gel. Subsequently, 250 µL of the cell-populated collagen gel was transferred to each well of a 24-well dish and incubated at room temperature for 20 min to induce collagen polymerization. CM was added to each well, and the polymerized collagen gel was gently detached from the plate edges. After 24 h, the media was changed to CM, OM, or CaP. Each condition was analyzed in triplicates. Images of the collagen gels were obtained after 5 days. The average contraction values were analyzed by area measurement with imageJ expressed as % reduction in gel diameter compared to the gel diameters without cells.

(Immuno) fluorescence imaging

Cells were washed with PBS, fixed in 4% PFA for 15 min, and permeabilized for 10 min in 0.5% [v/v] Triton X-100 (Sigma Aldrich). After blocking in 1% bovine serum albumin (BSA), fixed and permeabilized SMCs were incubated with anti-human alpha-smooth muscle actin (α-SMA; 1:200, Dako, M0851), TOM20 (1:200, Proteintech, 11802-1-AP), alpha-tubulin (α-tubulin, 1:25, Cell Signaling, 2144S), calponin (1:50, Thermo Scientific, MA5-32061), mouse IgG control (DAKO, X0931), or rabbit IgG control (R&D systems, AB-105-C). Subsequently, after washing Alexa Fluor 594 (1:1000, Thermo Scientific, R37115) or 488 (1:1000, Life Technologies, A32723) labeled secondary antibody was applied. Nuclei were counterstained with 2.5 µg/ml 4',6-Diamidino-2-phenylindole dihydrochloride (DAPI, Carl Roth), and slides were covered using a mounting medium (Dako).

For mitochondrial visualization, cells were labeled with 300 nM MitoTrackerRed FM (ThermoFisher Scientific) in serum-free CM at 37°C for 30 min. Nuclear staining was performed with 1 µM Hoechst 33,342 solution (Thermo Scientific). Images were acquired using a Leica DMI6000B inverted fluorescence microscope.

Real-time extracellular flux analysis

Mitochondrial respiration of cells was characterized by Seahorse XFe96 Flux Analyzer (Agilent) using the Seahorse XF Mito Stress Test Kit (Agilent). This technique allows real-time measurements of the oxygen consumption rate (OCR) and glycolysis (ECAR) in living cells. Cells were seeded into XF96 cell culture microplates (Agilent) at ~5,000 cells per well. Cells were then cultured for 7 days in CM, OM, or CaP with media change at day 3. One day before the assay, XFe96 Sensor Cartridge (Agilent) was hydrated with water overnight

at 37°C in a CO₂-free incubator. Cells were washed with DMEM supplemented with 10 mM glucose, 2 mM L-glutamine, and 1 mM pyruvate, pH 7.4, and incubated in a CO₂-free incubator at 37°C for 1 h. The Sensor Cartridge was loaded with different inhibitors from the Seahorse Mito Stress Kit to block the respiratory chain [oligomycin (1 µM), carbonyl cyanide-4 (trifluoromethoxy) phenylhydrazone (FCCP, 0.5 µM), and a mixture of rotenone/antimycin A (0.5 µM)]. The general protocol of the measurements includes three baseline measurements with mix (3 min)/measure (3 min) followed by the injection of port A (oligomycin). Afterward, respiration was measured three times with mix (3 min)/measure (3 min) with the injection of ports B (FCCP) and C (rotenone/antimycin) with the same measurement cycle of three times mix/measure.

The activity of respiratory chain complexes in mitochondria was analyzed in permeabilized cells by Seahorse XFe96 Flux Analyzer. The assay allows direct measurement and overview of respiratory chain activity by adding different substrates to the complexes (14). The measurement was performed as previously described (15). Briefly, cells were washed once with mannitol and sucrose (MAS) buffer [220 mM mannitol, 70 mM sucrose, 10 mM KH₂PO₄, 5 mM MgCl₂, 2 mM N-(2-Hydroxyethyl)piperazine-N'-(2-ethanesulfonic acid) (HEPES) and 1 mM Ethylene Glycol Tetraacetic Acid]. Afterward, MAS buffer supplemented with 4 mM adenosine 5'-diphosphate sodium salt (ADP; Sigma-Aldrich) and 10 µg/ml saponin (Sigma-Aldrich) was added to the cells in a final volume of 180 µl/well. The activity of respiratory chain complexes I, II, and IV was analyzed by adding substrates sequentially during the measurement. To analyze complex I, 10 mM pyruvate (Sigma-Aldrich) and 1 mM malate (Sigma-Aldrich) were directly added to MAS buffer containing ADP and saponin. To inhibit complex I, 20 µM rotenone (Sigma-Aldrich; final concentration 2 µM) was injected *via* port A of XFe96 sensor cartridge. Afterward, 100 mM succinate (Sigma-Aldrich; final concentration 10 mM) for complex II was added *via* port B. Port C and D were loaded with 20 µM antimycin A (Sigma-Aldrich; final concentration 2 µM; port C) as complex II inhibitor and with 1 mM N,N,N',N'-Tetramethyl-p-phenylenediamine (TMPD, final concentration 0.1 mM, Sigma-Aldrich; port D) together with 100 mM ascorbic acid (Sigma-Aldrich; final concentrations: 10 mM; port D) to analyze the activity of complex IV. The measurement protocol includes no equilibration step and cycles of two times mix (0.5 min)/wait (0.5 min)/measure (2 min) between injections.

Phospho kinase array

Tyrosine kinase (PTK) and Serine-Threonine kinase (STK) profiles were determined using the PamChip® peptide tyrosine kinase and Ser/Thr Kinase assay microarray systems on PamStation®12, respectively (PamGene International). Each PTK-PamChip® and STK-PamChip® array contains 196 and

144 individual phospho-site(s). Serum-starved (0.1% FBS, 16 h) iSMCs were cultured for 24 h in CM, OM, or CaP (0.1% FBS), washed once in ice-cold PBS, and lysed for 15 min on ice using M-PER Mammalian Extraction Buffer containing Halt Phosphatase Inhibitor and EDTA-free Halt Protease Inhibitor Cocktail (1:100 each; Thermo Scientific). Lysates were centrifuged for 15 min at 16,000 × *g* at 4°C. Protein quantification was performed with Pierce™ Coomassie Plus (Bradford) Assay according to the manufacturer's instructions.

Pamgene International B.V. supplied all reagents used for PTK and STK activity profiling. For the PTK assay, 7.0 µg of protein was applied per array and assayed using the standard protocol supplied by Pamgene. Initially, to prepare the PTK Basic Mix, the freshly frozen lysate was added to 4 µL of 10 × protein PTK reaction buffer (PK), 0.4 µL of 100 × (BSA), 0.4 µL of 1 M dithiothreitol (DTT) solution, 4 µL of 10 × PTK additive, 4 µL of 4 mM ATP and 0.6 µL of monoclonal anti-phosphotyrosine FITC-conjugated detection antibody (clone PY20). The total volume of the PTK Basic Mix was adjusted to 40 µL by adding distilled water. Before loading the PTK Basic Mix on the array, a blocking step was performed, applying 30 µL of 2% BSA to the middle of every array and washing with PTK solution for PamChip® preprocessing. Next, 40 µL of PTK Basic Mix was applied to each array of the PamChips®. Then, the microarray assays were run for 94 cycles. An image was recorded by a CCD camera PamStation®12 at kinetic read cycles 32–93 at 10, 50, and 200 ms and end-level read cycle at 10, 20, 50, 100, and 200 ms.

For the STK assay, 1.0 µg of protein and 400 µM ATP were applied per array with an antibody mix to detect the phosphorylated Ser/Thr. The spot intensity at each time point was quantified (and corrected for local background) using the BioNavigator software version 6.3 (PamGene International). Upstream Kinase Analysis, a functional scoring method (PamGene), was used to rank kinases based on combined specificity scores (based on peptides linked to a kinase, derived from six databases) and sensitivity scores (based on treatment-control differences) (16).

In silico drug repurposing analysis

The common genes between OM and CaP-calcified SMCs from the transcriptomics datasets were used as the gene expression signature for drug repurposing analysis using the web-based tool Connectivity Map (CMap²) (17). The two different lists of up and down-regulated genes were submitted in the "Query" of CMap tool against the Touchstone reference dataset of gene expression (L1000) to compare the query gene set with compounds reference perturbation signatures (January 2021). The compounds were ranked according to the CMap

² <https://clue.io/>

score (tau score). A negative score indicated that the compound had a potentially reversed gene signature profile. A positive score indicated that the compound potentially mimics the input gene-phenotype. Compounds with a tau score $<$ or $>$ 70 and a p -value $<$ 0.05 were considered for further investigation. The sum of the compound tau score in OM and CaP signatures was used to rank the compounds.

Human carotid artery specimens and transcriptomic analysis

The human biocollection and transcriptomic analysis have been published previously (18). From February 2008 to December 2015, atheromatous plaques were harvested and collected from patients undergoing carotid endarterectomy in the Department of Vascular Surgery at Nantes University Hospital. Healthy arteries free of atherosclerotic lesions were obtained from organ donors. Sample collection and handling were performed under the Medical and Ethical Committee guidelines in Nantes, France, and written informed consent was obtained from all patients and organ donors. The experimental protocol was approved by the Agence de Biomédecine (research protocol #PFS09-014, authorized on Dec 23, 2009, by the Agence de Biomédecine, France). Legal and ethical authorizations were granted by the French Research Ministry (n° DC-2008-402), the National Commission for Computerized Information and Liberties (CNIL, n° 1520735 v 0), and the local ethical committee (GNEDS).

The atherosclerotic plaques were fixed in 10% formalin for 24–48 h, decalcified in Sakura TDE 30 fluid, and embedded in paraffin. Sections (4 μ m thickness) were stained with hematoxylin-eosin (HE). Whole sections were imaged with a NanoZoomer digital slide scanner (Hamamatsu Photonics, Hamamatsu, Japan).

Samples for RNA processing were harvested and immediately snap-frozen in liquid nitrogen or stored in All-protect Tissue Reagent (Qiagen). Total RNA was extracted using Macherey Nagel NucleoSpin columns (Macherey Nagel). RNA was hybridized to Agilent Human Gene Expression Microarrays. Fluorescence values corresponding to raw expression data were extracted using Feature Extraction Software (Agilent). Positive and negative control probes were removed. Non-linear effects, such as background or saturation, were corrected by Lowess against a median profile of all samples. Values of replicate probes were averaged. Genes differentially expressed between atherosclerotic and healthy arteries were identified using Significance Analysis of Microarrays, with an FDR = 0% (19). Microarray data have been deposited in NCBI's Gene Expression Omnibus (GEO) and are accessible through GEO Series accession number GSE100927.

Human coronary artery plaque single-cell ribonucleic acid sequencing data analysis

Single-cell RNA sequencing data from human coronary artery plaques were previously published (20) (GEO Series accession number GSE131778) and plotted using the web-based tool PlaqView³ (21). In brief, diseased specimens from the right coronary artery with atherosclerotic lesions ranging from mild, non-calcified plaques to more advanced lesions with areas of calcification of four cardiac transplant recipients were dissociated and subjected to single-cell RNA sequencing (20). The clinical characteristics of the patients included in the study were previously described and included written consent prior to the procedure (20).

Mouse artery specimens and transcriptomic analysis

Data used in this study were previously published (22) and are available in NCBI's GEO (accession number GSE159833). We used publically available RNA sequence data of the artery of *Apoe*-deficient mice as a model for atherosclerotic intimal calcification and a 5/6 nephrectomy-induced CKD model for medial calcification. Briefly, *Apoe*-deficient mice were fed a chow diet for 16 months to induce atherosclerotic intimal calcifications. 8-week-old C57BL/6 mice were subjected to subtotal 5/6 nephrectomy using a two-step method and fed a diet containing 2% phosphate and water containing 0.45% NaCl for 4 weeks after 5/6 nephrectomy to induce medial calcification. 8-week-old C57BL/6 mice fed a chow diet were used as control. RNA sequencing data were available for two samples per group. Data were extracted and differentially regulated genes (Log2 fold change $<$ -0.5 or $>$ 0.5 ; $p <$ 0.05) in *Apoe*-deficient mice or CKD group compared to the control group were identified using the web-application GREIN (GEO RNA-seq Experiments Interactive Navigator⁴) (23).

Statistical analysis

Statistical analyses were performed using the GraphPad Prism program (Prism Software Inc., Version 8). Data are presented as mean \pm SD; n indicates the number of independent experiments. For comparison between two groups, unpaired Student's t -test was performed. For comparison among three or

³ <http://plaqviewv2.uvadcos.io/>

⁴ <http://www.ilincs.org/apps/grein/>

more treatment groups, one-way ANOVA followed by Dunnett posttest was performed. In case of unequal variance detected by *F*-test, unpaired Student's *t*-test with Welch's correction was used. A *p*-value of less than 0.05 was considered significant.

Results

Characterization of osteogenic medium and calcium phosphate-induced calcification

First, we examined the calcification profile of primary smooth muscle cells (pSMCs) cultured with osteogenic media (OM) or calcium phosphate media (CaP). Calcification occurred in both media yet differed concerning amount and kinetics. Alizarin red S staining and quantification showed that calcification was 3.0 fold increased at day 21 in OM ($p = 0.008$) and 2.5 fold increased at day 7 in CaP ($p = 0.010$) (Figures 1A,B). Calcification was first observed after 14 days of culture in OM and after 5 days in CaP, respectively (Supplementary Figures 1A,B). OM and CaP did not affect cell viability at day 14 and 7, respectively (Figures 1C,D). Next, we assessed mRNA levels of the osteogenic markers ALPL and RUNX2 at early time points. ALPL mRNA (7.2 fold, $p = 0.037$) and RUNX2 mRNA (2.8 fold, $p = 0.044$) was up-regulated in OM

at day 7, while in CaP-calcified SMCs, we observed a 1.3 fold increase of RUNX2 mRNA ($p = 0.010$) and no change in ALPL mRNA at day 3 (Figures 1E–H). Tissue alkaline phosphatase (TNAP) activity increased 3.7-fold ($p = 0.010$) in OM but not in CaP on day 14 (Supplementary Figure 1C). We performed a collagen gel contraction assay to compare the effects of OM and CaP in SMC contractility. When placed into a collagen gel, SMCs exert traction forces to remodel their local environment, reducing the gel area by consolidating collagen fibrils (24). Control SMCs contracted the gels by 52% of the initial area over 5 days (Figure 1I). OM significantly decreased the % of the initial collagen gel size compared to CM (-1.4 fold, $p = 0.049$), while CaP tended to increase the gel size (1.2 fold, $p = 0.193$).

Osteogenic medium and calcium phosphate-calcifying primary vascular smooth muscle cells display distinct gene expression

To study the underlying molecular mechanisms driving the different VC models, we analyzed the transcriptome of CaP and OM-calcified pSMCs on days 3 and 7, respectively, aiming to achieve comparable early calcification time points corresponding to one-third of the time required to achieve

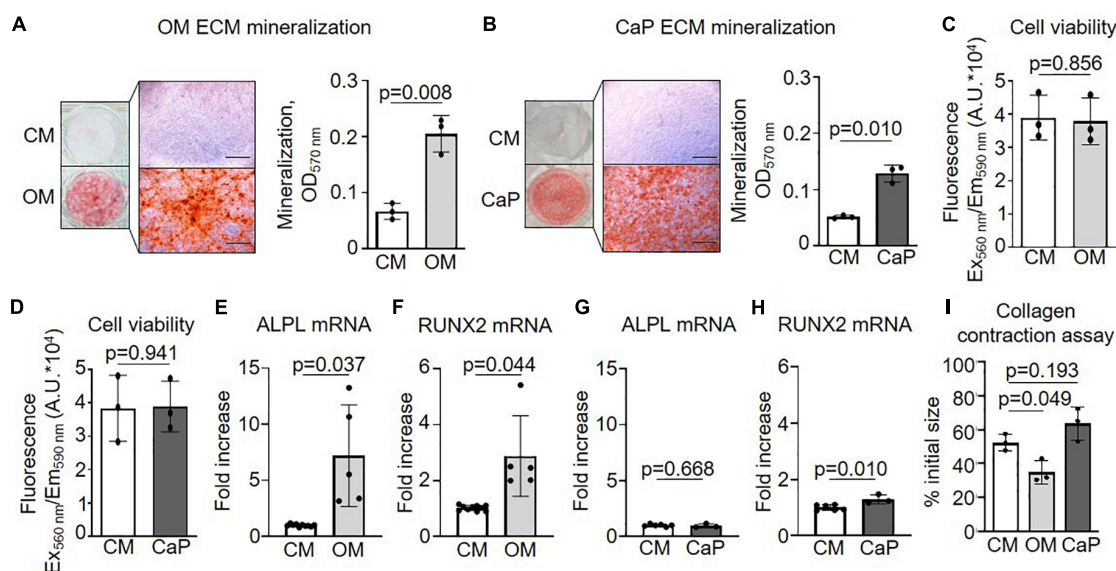


FIGURE 1

Characterization of osteogenic medium (OM) and calcium phosphate (CaP)-induced calcification of primary coronary artery smooth muscle cells (pSMCs). (A) pSMCs were cultured in control medium (CM) and OM for 21 days or (B) CaP for 7 days. Representative images of extracellular matrix (ECM) mineralization were detected by alizarin red S staining and eluted staining quantified by assessing the optical density at 570 nm. Scale bar: 1,000 μ m. $n = 3$ (C) Effect of OM and (D) CaP-induced calcification on cell viability assessed by AlamarBlue assay (Fluorescence Ex₅₆₀ nm/Em₅₉₀ nm) on day 21 for OM and day 7 for CaP. $n = 3$. (E–H) ALPL and RUNX2 mRNA expression for (E,F) OM-calcified pSMCs (day 7) and (G,H) for CaP-calcified pSMCs (day 3). (I) Collagen contraction assay at day 5. $n = 3$ –5. Error bars indicate \pm SD. Each n indicates an independent pSMC donor. Unpaired *t*-test and one-way ANOVA with Dunnett's *post hoc* test for I.

calcification with the respective protocols (**Supplementary Figure 1**). Applying a fold-change cut-off of 1.5 identified 1,557 differentially regulated genes in OM-calcified pSMCs and 941 genes in CaP-calcified pSMCs compared to control media (CM) (**Figures 2A–C** and **Supplementary Table 2**).

Pathway over-representation analysis of the OM-regulated genes highlighted the enrichment of elastic fiber formation,

elastic fiber structural molecules, and metabolism pathways (**Supplementary Table 3**). In CaP, the top over-represented pathways were phosphatidylinositol signaling system, regulation of pyruvate dehydrogenase complex, and SMC contraction (**Supplementary Table 4**).

We combined the transcriptomics datasets of the differentially regulated genes from OM and CaP-calcified

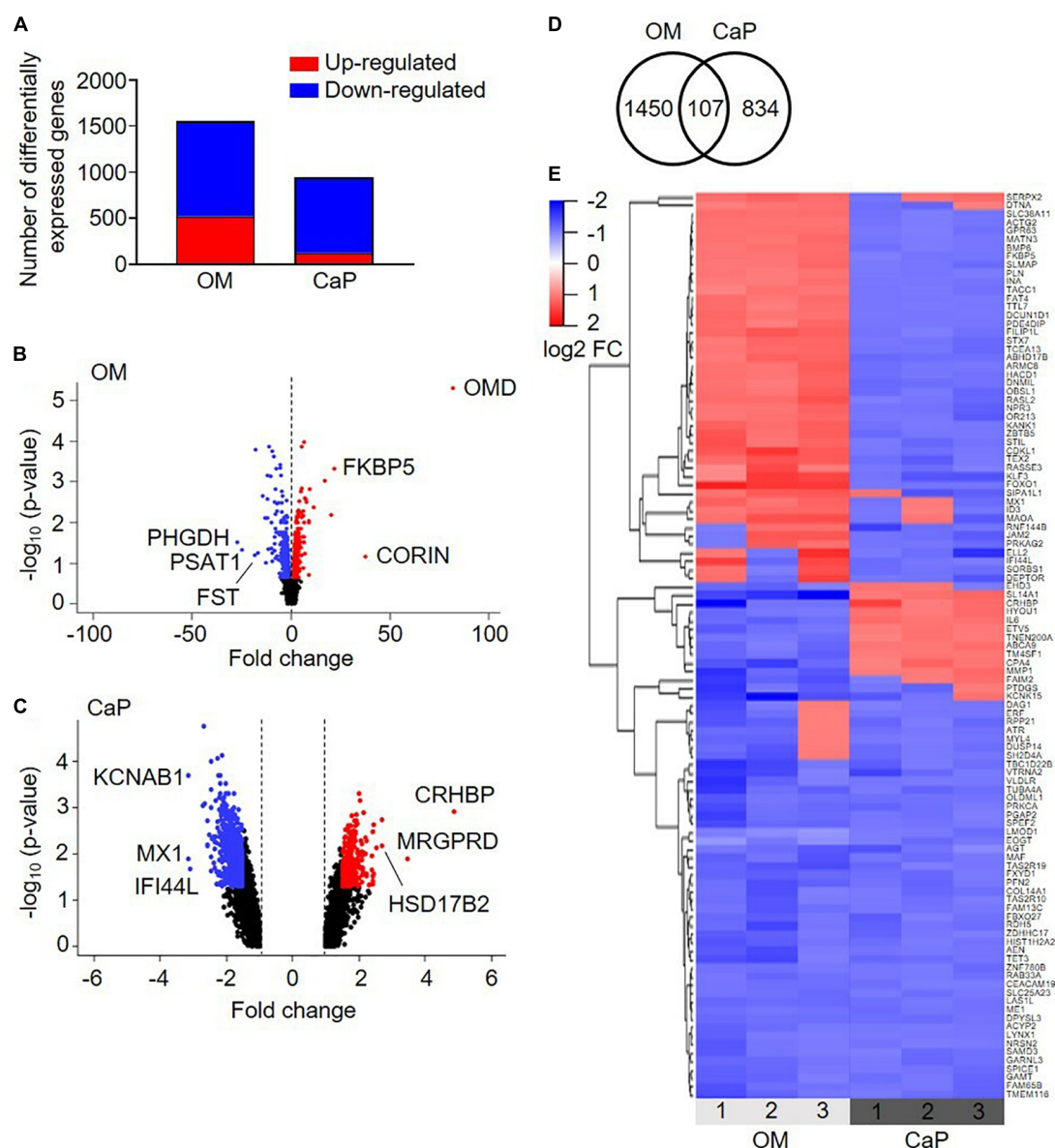


FIGURE 2

Transcriptional profiling of osteogenic (OM) and calcium phosphate (CaP)-calcified primary coronary artery smooth muscle cells (pSMCs). **(A)** Number of up-regulated (red) and down-regulated (blue) genes from OM and CaP-calcified pSMCs compared to control (CM). Cut-off FC 1.5. **(B,C)** Volcano plots of the differentially expressed genes in OM and CaP-calcified pSMCs, respectively, compared to CM. Plotted on the x-axis is the fold change between calcified and CM pSMCs. Plotted on the y-axis is the $-\log_{10}(p\text{-value})$. Significant differentially expressed genes are divided into up-regulated (red dots) and down-regulated (blue dots) genes, while non-significant genes are shown in black. The top three up- and downregulated genes are named. **(D)** The Venn diagram shows overlapping differentially expressed genes between OM and CaP-calcified pSMCs. **(E)** Heatmap presenting the expression profiles of the 107 common genes. Genes with a fold change $\geq \pm 1.5$ and a $p\text{-value} < 0.05$ are considered differentially expressed. $n = 3$ independent primary SMC donors.

pSMCs and found 107 genes shared between the two data sets (**Figure 2D**). 1/3 of the genes showed similar gene expression, while 2/3 exhibited a distinct gene regulation cluster (**Figure 2E**). Pathways associated with the over-represented genes included muscle contraction, SMC contraction, and epithelial growth factor receptor (EGFR) transactivation by gastrin (**Supplementary Table 5**). These data suggested that OM and CaP-calcified pSMCs displayed distinct gene profiles driving calcification along distinct pathways.

Establishment and characterization of an immortalized vascular smooth muscle cell model

We generated an immortalized SMC line (iSMC) to avoid the intrinsic biological variability associated with primary SMCs. Validation of the iSMC phenotype revealed expression levels of the contraction marker calponin and SMC markers α -SMA and α -tubulin similar to pSMCs (**Supplementary Figure 2**). Characterization of OM and CaP-calcified iSMCs related to TNAP activity (**Supplementary Figure 3A**), ECM mineralization (**Supplementary Figures 3B,C**), mRNA expression of the osteogenic markers ALPL and RUNX2 (**Supplementary Figures 3D–F**), cell viability (**Supplementary Figures 3H–J**), and contraction properties (**Supplementary Figure 3K**) showed similar results in iSMCs compared to primary SMCs.

Osteogenic medium and calcium phosphate-calcifying vascular smooth muscle cells display a different mitochondrial function profile

Metabolism and pyruvate dehydrogenase complexes were two pathways highlighted in our over-representation analysis. Both pathways inform about mitochondrial function and, thus about, cell health (25). Mitochondria are critically required in energy-demanding functions, and the mitochondrial matrix is rich in calcium (26), which has been shown to trigger calcification (27). Therefore, we investigated the effect of OM or CaP on the morphology and bioenergetics of mitochondria. MitoTracker and TOM20 staining showed no difference in the mitochondria phenotype in calcifying iSMCs (**Figure 3A**). However, we observed different alterations in mitochondrial function for OM and CaP-calcifying iSMCs using real-time extracellular flux analysis to evaluate the mitochondrial respiration and glycolysis by simultaneous time-course measurement of the oxygen consumption rate (OCR) and extracellular acidification rate (ECAR), respectively. Compared to CM, CaP decreased the basal respiration (-62% , $p < 0.001$), the ATP production (-67% , $p < 0.001$), maximum

respiration (-66% , $p < 0.001$), non-mitochondrial respiration (-49% , $p = 0.002$), and proton leakage (-28% , $p = 0.032$) in iSMCs (**Figures 3B–G**). On the other hand, OM increased maximal respiration ($+ 22\%$, $p = 0.005$), non-mitochondrial respiration ($+ 32\%$, $p = 0.006$), and proton leakage ($+ 36\%$, $p = 0.010$) compared to CM. Glycolysis was 2.3-fold decreased in CaP-calcified iSMCs compared to CM ($p = 0.029$), while OM did not alter glycolysis (**Figures 3H,I**).

To further explore the mechanisms associated with the metabolic impact of OM and CaP, we evaluated single mitochondrial complex function (**Supplementary Figure 4A**). Through mitochondrial efflux analysis, we observed that OM-calcified iSMCs displayed increased complex I OCR ($+ 39\%$, $p = 0.025$), and IV OCR ($+ 47\%$, $p = 0.011$) OCR, while CaP-calcified iSMCs showed a tendency to reduced complex III (-29% , $p = 0.071$) and IV (-32% , $p = 0.068$) (**Supplementary Figures 4B–E**).

Drug repurposing

We performed a drug repurposing analysis using the Cmap database to identify novel compounds targeting VC and to verify the hypothesis that they would work differently in our *in vitro* models. Cmap analysis matches a specific disease's transcriptomic profiles (differentially induced and repressed genes) with a signature profile associated with compounds. We independently scored the common gene profiles of OM and CaP datasets (**Figure 4A**). When a compound signature reversely correlates with the differentially expressed genes, the compound is considered a potential repositioning candidate. If it correlates positively, it is considered a molecular mimic of the observed phenotype (17).

Consequently, we focused on the compounds with the highest connectivity and retained those with a tau score > 70 or < -70 in both OM and CaP datasets, which resulted in 12 overlapping candidate compounds (**Figure 4B** and **Table 1**). Interestingly, no compound displayed simultaneous negative connectivity for OM and CaP. Two out of 12 compounds exhibited positive connectivity for OM and CaP-calcified iSMCs. Ten out of 12 compounds displayed inverse connectivity (three compounds: negative connectivity for OM, positive connectivity for CaP; seven compounds: positive connectivity for OM, negative connectivity for CaP) (**Table 1**), highlighting the distinct regulation among the same genes.

Next, we calculated the distance of tau scores from OM and CaP and selected the top five compounds for further *in vitro* validation. Among the top five compounds were two protein kinase C (PKC) activators –prostratin and ingenol –which are predicted to promote calcification in CaP and inhibit calcification in OM. In line with the findings, results from the phospho-kinase array analysis from OM and CaP-treated iSMCs

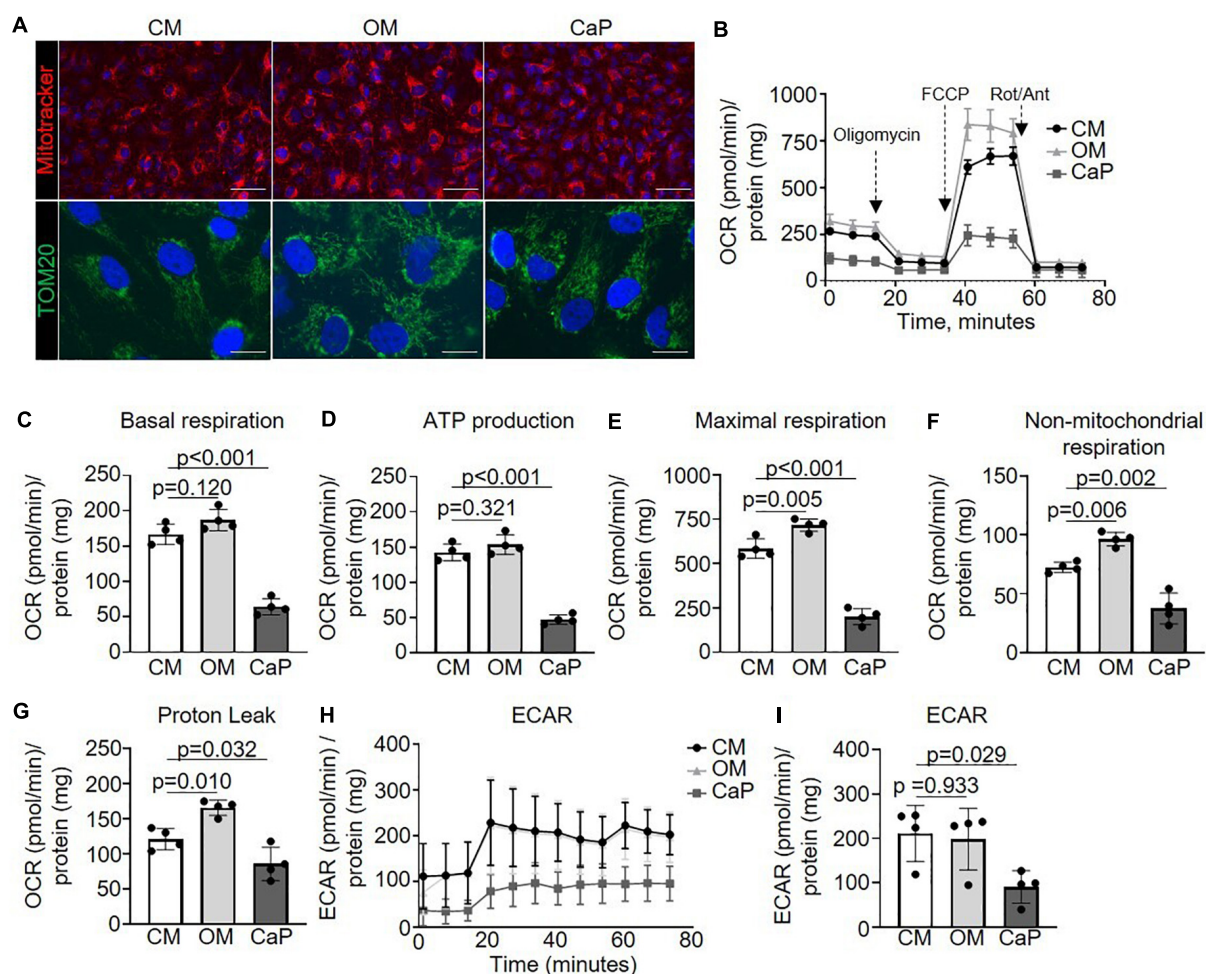


FIGURE 3

Mitochondrial respiration increases in osteogenic medium (OM) and attenuates in calcium phosphate (CaP)-calcified vascular smooth muscle cells (SMC) immortalized SMCs (iSMCs) were cultured for 7 days in control medium (CM), OM or CaP. (A) Representative images of live iSMCs for the mitochondria-specific dye MitoTracker Red (red) and nuclear Hoeschst staining (blue) and immunofluorescence for TOM20 (green) with DAPI nuclear staining (blue). $n = 3$, scale bar: 75 μm and 10 μm , respectively. (B) Mitochondrial oxygen consumption rates (OCR) of OM and CaP-calcified iSMCs subjected to the XF Mito Stress Test measured using the Seahorse XF96 flux analyzer, with sequential injections of mitochondrial effectors [oligomycin, carbonyl cyanide-4 (trifluoromethoxy) phenylhydrazone (FCCP) and rotenone (Rot), antimycin (Ant)] at time points indicated by the downward arrows. $n = 4$. (C) Basal respiration, (D) ATP production, (E) Maximal respiration, (F) Non-mitochondrial respiration, (G) Proton leak, (H,I) Extracellular acidification rate (ECAR) and quantification. OCR and ECAR were normalized to protein content. Error bars indicate \pm SD. Each n indicates an independent replicate. One-way ANOVA with Dunnett's *post hoc* test.

also indicated a differential role of the PKC signaling pathway in the calcification process (**Supplementary Figures 5A–C**). OM and CaP-treated SMCs shared nine differentially regulated serine/threonine kinases and 64 differentially regulated tyrosine kinases (**Supplementary Figure 5A**).

Subsequently, we performed *in vitro* experiments to validate the role of PKC. Both prostratin and ingenol decreased ECM mineralization in OM (-2.9 fold, $p = 0.001$ and -5.6 fold, $p = 0.005$, respectively) (**Figure 4C** and **Supplementary Figure 6A**), which was abolished by the PKC inhibitor Go6983 (**Figure 4D** and **Supplementary Figure 6B**), supporting the predicted effect from the *in silico* analysis.

In CaP-calcified iSMCs prostratin and ingenol increased ECM mineralization ($+1.8$ fold, $p = 0.002$ and $+1.5$ fold, $p = 0.034$) (**Figure 4E** and **Supplementary Figure 6C**) which was abolished by the PKC inhibitor Go6983 (**Figure 4F** and **Supplementary Figure 6D**).

Regarding the other repurposable compound candidates, the MEK inhibitor PD-184352 displayed no effect on ECM matrix mineralization of both OM and CaP models (**Supplementary Figures 7A,B**). Using the glucocorticoid receptor agonist fluticasone, which was predicted to increase OM and decrease CaP-induced SMC phenotype, we observed increased ECM mineralization when used as

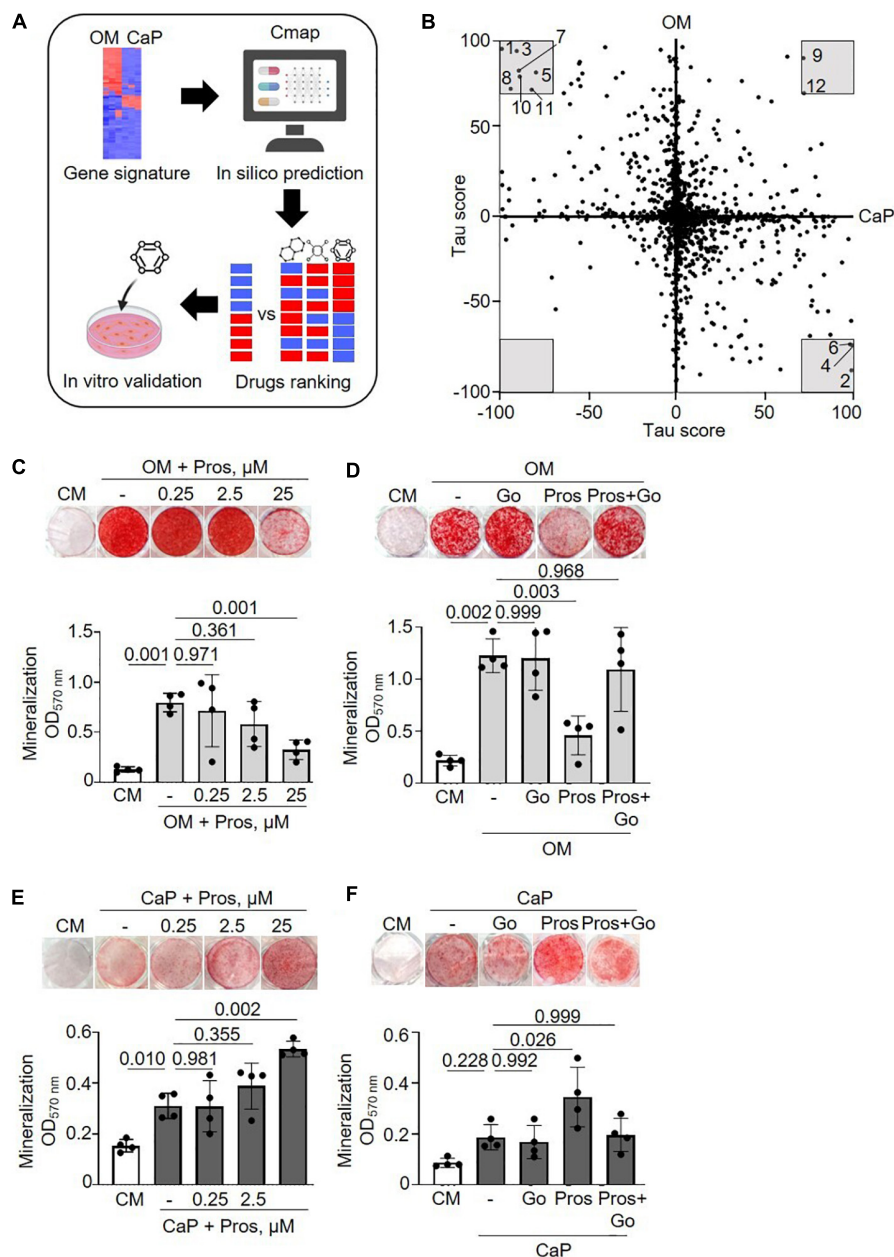


FIGURE 4

Drug repurposing of osteogenic medium (OM) and calcium phosphate (CaP) gene signatures. (A) Scheme of the method. Created with <https://Biorender.com> (B) Scatter plot with predicted effects of drugs on OM and CaP-induced calcification. Gray area—drugs with predicted tau score < or > 70. 1: PD-184352, 2: Prostratin, 3: Fluticasone, 4: Ingenol, 5: L-690330, 6: Phorbol 12-myristate 13-acetate (PMA), 7: Halometasone, 8: Sunitinib, 9: MLN-2238, 10: Hydrocortisone, 11: Benztropine, 12: Puromycin. (C,D) Effect of the protein kinase C (PKC) activator prostratin (Pros) and the PKC inhibitor Go6983 (Go) in OM and (E,F) in CaP-calcified immortalized vascular smooth muscle cells (iSMCs). iSMCs were cultured in control medium (CM) and OM for 14 days or CaP for 7 days with different concentrations of prostratin (0.25, 2.5, and 25 μM). Go (100 nM) was combined with 25 μM prostratin. Representative images of extracellular matrix mineralization (top) detected by alizarin red S staining and quantification of eluted staining (bottom). $n = 4-5$. C-H, DMSO (1:1,000) was used as solvent control in CM, OM, and CaP groups. Error bars indicate \pm SD. Each n indicates an independent replicate. One-way ANOVA with Dunnett's *post hoc* test.

a dexamethasone substitute in OM and no effect on CaP-calcified iSMCs (Supplementary Figures 7C,D). Finally, L-690330, an inositol monophosphatase inhibitor, prevented ECM mineralization in both OM and CaP-treated cells

(Supplementary Figures 7E,F). In summary, we validated two out of five candidates (Supplementary Figure 7G). The tested compounds did not interfere with cell viability (Supplementary Figures 8A–L).

TABLE 1 Repurposable drug candidates with tau score < or > 70 sorted by the sum of tau scores in osteogenic media (OM) and calcium phosphate media (CaP) gene signature (tau distance).

No.	Drug	OM	CaP	Tau distance	Function
1	PD-184352	95.3	−98.8	194.1	MEK inhibitor
2	Prostratin	−87.2	99.5	186.7	PKC activator
3	Fluticasone	94.1	−90.3	184.5	Glucocorticoid receptor agonist
4	Ingenol	−73.0	99.7	172.7	PKC activator
5	L-690330	82.9	−89.0	172.0	Inositol monophosphatase inhibitor
6	PMA	−72.4	98.8	171.2	PKC activator
7	Halometasone	79.5	−88.6	168.1	Glucocorticoid receptor agonist
8	Sunitinib	72.6	−93.8	166.4	FLT3 inhibitor
9	MLN-2238	90.0	72.3	162.3	Proteasome inhibitor
10	Hydrocortisone	81.9	−79.4	161.4	Glucocorticoid receptor agonist
11	Benzatropine	72.1	−81.8	153.9	Acetylcholine receptor antagonist
12	Puromycin	72.6	70.2	142.8	Protein synthesis inhibitor

Transcriptome-wide comparison of the gene signature of *in vitro* calcification models with mouse and human calcified arteries

Finally, we compared our *in vitro* OM and CaP gene signature with the gene signature of mouse and human calcified arteries to evaluate the relevance of each model and the common genes involved in both *in vitro* and *in vivo* calcification.

We used human carotid atherosclerotic lesions from the ECLAGEN biocollection that displayed calcification as detected by histology (Figure 5A; 18). Transcriptome analysis of all sets of genes showed a panel of 25 common genes that were differentially expressed in both *in vitro* models and diseased carotid arteries (Figures 5B,C and Supplementary Tables 6, 7). Nine common genes were upregulated in calcified carotid lesions and 16 down-regulated (Figure 5D). DAVID analysis identified four main enriched gene ontology (GO) clusters, including GO terms like muscle contraction, cytoskeleton, cytoplasm, mitochondria, membrane, protein binding, nucleotide-binding, and transcription regulation (28). Furthermore, an additional 287 and 120 regulated genes were shared between human lesions and OM and CaP models, respectively, suggesting that both models share molecular features related to plaque calcification.

Furthermore, we used publically available single-cell RNA sequencing data from the human coronary artery to localize the 107 common genes between OM and CaP-calcified pSMCs to specific cell clusters. 102 from the 107 genes were present in the 9,798 cells that were previously annotated to 14 cell clusters (20; Supplementary Figure 9). Considering only genes that were expressed in at least 20% of the cells revealed 53 genes whose highest expression was detected in the SMC, pericyte 1, fibromyocyte, and fibroblast cell clusters (Supplementary Table 8).

Next, we used publically available transcriptome data from an *Apoe*^{−/−} and CKD mouse model to address intimal and medial calcification. Intersecting differentially regulated genes from OM and CaP-calcified pSMCs and *Apoe*^{−/−} and CKD mice revealed 26 genes shared between the four data sets (Supplementary Figure 10A). Considering differentially regulated genes, OM shared 42.7% of its genes with *Apoe*^{−/−} mice and 23.0% with CKD mice. CaP shares 39.7% of its genes with *Apoe*-deficient mice and 20.4% with CKD mice (Supplementary Figure 10B).

Discussion

Vascular calcification comprises mineral deposition in the tunica media or the tunica intima, associated with distinct risk factors and clinical outcomes (29). Intimal calcification generally correlates with atherosclerosis plaque burden, hyperlipidemia, and chronic arterial inflammation. In contrast, medial calcification is a non-occlusive process that leads to increased vascular stiffness and reduced vascular compliance, frequently associated with diabetes and chronic kidney disease (3). To our knowledge, this work compares for the first time different *in vitro* SMC calcification protocols mimicking intimal and medial calcification, respectively. By deploying different *in vitro* models, our results support the hypothesis that different molecular pathways trigger intimal and medial calcification.

It is a widely accepted concept that the development of VC is associated with phenotypic transdifferentiation of SMCs, resulting in SMCs with osteoblast-like characteristics (30). Our data corroborate published findings, demonstrating that TNAP activity and ALPL mRNA levels are induced in OM-calcified SMCs (31). Interestingly, TNAP was not regulated in CaP-calcified SMCs, consistent with previous

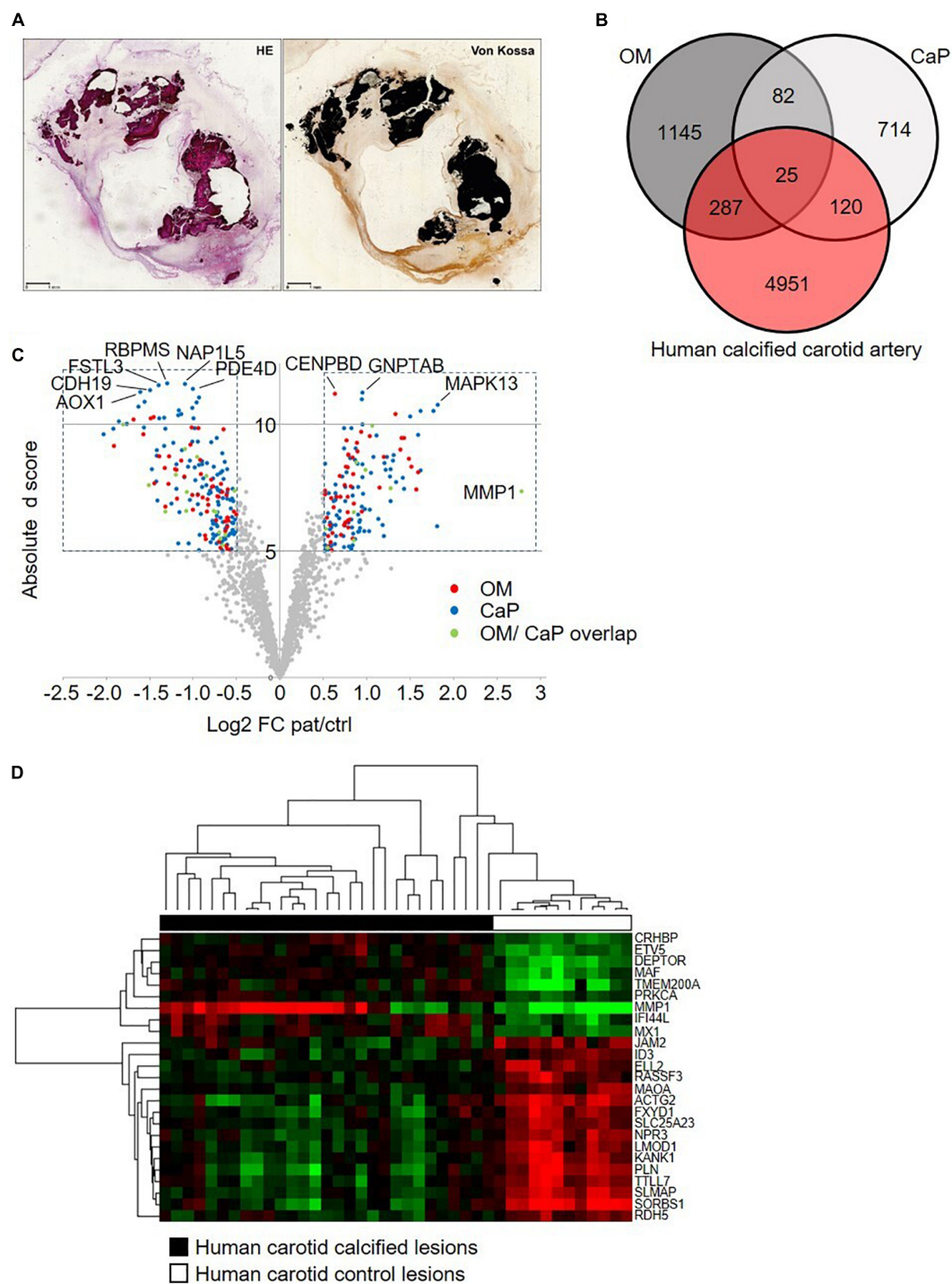


FIGURE 5

Comparative transcriptome analysis across human carotid artery and *in vitro* models. **(A)** Serial sections of a resin embedded carotid lesion [hematoxylin eosin staining (HE) and von Kossa staining] Bar: 1 mm. **(B)** Venn diagram comparing the osteogenic media (OM)-treated primary coronary artery smooth muscle cells (pSMCs) and calcium phosphate (CaP)-treated pSMCs gene signatures to the human calcified carotid artery gene signature. **(C)** The volcano plot of the human calcified carotid artery dataset displays only the OM and CaP gene signature genes. Plotted on the x-axis is the log₂ of the fold change (FC) between the calcified and control carotid artery. Plotted on the y-axis is the absolute *d* score obtained through Significant Analysis of Microarrays (*T*-statistic value). Significant differentially expressed genes (Absolute *d* score > 5, Log₂ FC < -0.5 or > 0.5) are indicated in red (OM genes), blue (CaP genes), or green (shared between OM and CaP). Non-differentially expressed genes are shown in gray. **(D)** Hierarchical clustering of the 25 differential regulated genes that are common between carotid artery, OM-calcified pSMCs, and CaP-calcified pSMCs. Green, black and red corresponds to lower, median and higher gene expression values, respectively.

reports demonstrating repression of TNAP activity and mRNA expression in CaP-calcified SMCs at early calcification time points (32). Moreover, TNAP was not present in extracellular vesicles isolated from CaP-calcified SMCs (33). This suggests that CaP-induced calcification is independent of TNAP-mediated osteogenesis.

Changes in the transcriptional profile of SMCs have been reported during osteogenic differentiation (34, 35). Our gene expression analysis revealed distinct molecular regulation in mRNA profiles in response to OM or CaP-induced calcification. OM and CaP share less than 12% of their differentially regulated genes. Those shared genes between OM and CaP-calcified SMCs highlighted enrichment of genes encoding proteins for smooth muscle contraction and were mostly oppositely regulated. Based on a functional collagen contraction assay, we observed that SMC contraction dynamics were oppositely affected by OM and CaP-induced calcification, where OM displayed higher contraction rates than control. One of the primary functions of SMCs is maintaining vascular tone and regulating blood pressure *via* their contractile properties (36). Upon biological stress signals or vascular injury, SMCs undergo a phenotypic modulation associated with higher proliferation rates, migration, and altered contractile marker expression (37).

Our transcriptomics pathway enrichment analysis revealed alterations in the metabolism pathway in OM-calcified SMCs and changes in the pyruvate dehydrogenase complex in CaP-calcified SMCs. The pyruvate dehydrogenase complex is central in regulating energy metabolism and mitochondrial function (38). Furthermore, mitochondrial dysfunction has been associated with VC progression (39). Therefore, we investigated whether OM and CaP-induced SMC calcification was related to alterations in mitochondrial bioenergetic properties. We observed that CaP-calcified SMCs showed apparent impairment of mitochondria phosphorylation parameters, raising the question of whether high concentrations of CaP directly attenuate mitochondrial function. Calcium is considered an important regulator of mitochondrial metabolism, and isolated mitochondria increase ATP production upon stimulation with low calcium levels (40). Conversely, higher concentrations of CaP result in mitochondrial calcium overload and attenuated oxidative phosphorylation. Recent studies attribute this adverse effect to intramitochondrial calcium phosphate granules (41, 42). In calcified SMCs a shift from mitochondria phosphorylation toward a glycolytic breakdown of glucose was previously described (43). This change is similar to the Warburg effect, frequently observed in cancer cells. Notably, the reduction of mitochondrial respiration in CaP-calcified SMCs was also accompanied by a decrease in glycolysis, which was not observed in OM-calcified SMCs. In a murine model of phosphate-induced VC, others also demonstrated that decreased mitochondrial phosphorylation precedes

decreased glycolytic capacity (44). This suggests that in CaP-calcified SMCs, glycolysis might not compensate for deficient mitochondrial ATP production.

Furthermore, we found that treating SMC with OM enhanced maximal respiratory rate. Others have shown that the transdifferentiation of mesenchymal stem cells into osteoblasts is also linked to increased mitochondrial respiration and that human aortic SMCs displayed elevated basal respiration after β -glycerolphosphate treatment, a component of OM (26, 45). Therefore, the increased oxidative phosphorylation in OM-calcified SMCs potentially highlights a mitochondrial response to maintain the high energy demands of ECM synthesis, remodeling, and contraction. Nevertheless, the exact mechanisms underlying mitochondrial dysfunction during VC have yet to be elucidated. Current literature suggests mitochondrial dysfunction as both a cause and consequence of VC (46). Previous data demonstrated a diffuse tubulin cytoskeleton and a more apparent actin cytoskeleton in OM-calcified SMCs (47). Interestingly, there is evidence from yeasts that cytoskeletal changes can be transmitted to mitochondria, resulting in functional modification of the organelle (48, 49). Whether the observed cytoskeleton alterations and mitochondrial functional changes are linked in OM or CaP-calcified SMCs remains to be further investigated.

Although significant progress has been made in understanding VC pathology, VC remains a disease without therapy. Drug repurposing may indeed identify novel therapeutic use for existing drugs. This *in silico* approach was applied in cardiovascular disease and COVID-19 (50–52). In this study, the drug repositioning pipeline revealed a differential role of PKC in VC. We validated those results using prostratin and ingenol, specific PKC activators. As predicted, the PKC activators reduced calcification in OM and increased it in CaP *in vitro*. Concomitantly, the PKC signaling was shown in our kinome array as differentially regulated in OM and CaP-calcified SMC, suggesting that although oppositely regulated, the PKC signaling pathway is involved in both intimal and medial calcification.

Indeed, increasing evidence suggests that PKC is potentially involved in the process of CVD. PKC δ expression was induced in human atherosclerotic plaques from the mammary artery compared to control tissue (53). PKC β deficient mice or treatment with the PKC β inhibitor ruboxistaurin decreased the atherosclerotic lesion size in Apoe-deficient mice (54). Additionally, inhibition of PKC resulted in a dose-dependent inhibition of dexamethasone-induced osteogenic differentiation and ECM calcium deposit in human mesenchymal stem cells (55). Other studies suggested that PKC α suppresses bone formation (56, 57). This is in line with our results demonstrating that the PKC activators ingenol and prostratin inhibit OM-mediated SMC calcification. Contrary to our results, in human SMCs calcified using 2 mM calcium and

5 mM β -glycerophosphate, deletion or inhibition of PKC α increased ECM mineralization (58). Others also showed that PKC α and δ phosphorylation was decreased in phosphate-induced calcification of SMCs and aortas through osteogenic signaling and cytoskeleton disruption (59). Although our results indicate opposite regulation between PKC and VC in CaP-mediated calcification, it is important to mention that we identified and used compounds to activate all PKC isoforms since prostratin and ingenol have little PKC isoform selectivity.

While *in vitro* models have proven to be important in biological research, it remains challenging to translate the results to human conditions. Mapping the common differentially regulated genes from OM and CaP-calcified SMCs to single-cell RNAseq data from human coronary arteries showed that most of the genes were present in the cell clusters annotated for SMCs, pericytes, fibromyocytes, and fibroblasts. Those clusters also contained the osteogenic markers TNFRSF11B (20), ALPL, and MSX2. Differentially regulated genes from OM and CaP and the gene signature of human calcified carotid arteries shared only 25 genes. The observed transcriptional dissimilarities *in vitro* and *in vivo* are expected since the atherosclerotic plaque consists of multiple interacting cell types with crosstalk to the ECM that may drive different transcriptional changes (60). Using two different vascular beds—coronary artery SMCs and carotid arteries—might further explain the diverse mRNA profiles. Previously, it has been shown that the calcification propensity is highly dependent on the heterogeneity of SMCs from different vascular beds underlying different calcification mechanisms (61).

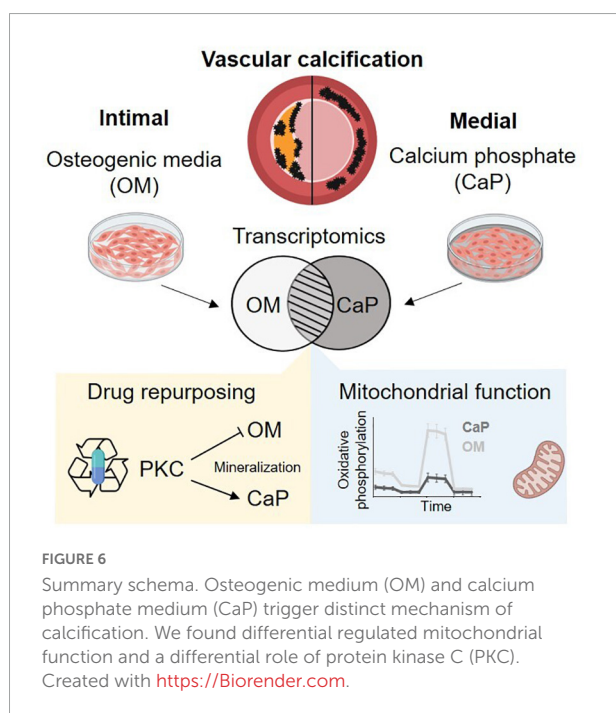
Our study has limitations. VC is a complex disease caused by many risk factors, such as diabetes, chronic kidney disease, and aging, and multiple cell types and differentiation pathways are involved that our study did not address. Moreover, while differentiating micro and macrocalcification is crucial to atherosclerotic plaque vulnerability (62), the *in vitro* SMC models cannot discriminate between the two calcifications morphologies. Spotty microcalcification within the intimal atherosclerotic plaque promotes plaque vulnerability, while macrocalcification is discussed to stabilize the plaque (63). The sheet-like medial calcifications cause increased vascular stiffness and reduced vessel compliance (62). Those differences in the clinical consequences between medial and intimal calcification underline future efforts to adopt the calcification disease models to study the underlying mechanisms. Furthermore, *in vitro* cell culture models do not recapitulate the interplay of different cell types and the crosstalk with the ECM that is important for developing micro- and macrocalcification. Previously, it was shown that the calcification morphology and density depend on the plaques' collagen content (64). Previously, our group reported that integrating different omic layers can yield novel molecular pathways that are not visible at a single level in cardiovascular calcification (65). Here, only one single molecular layer at one timepoint was accessed through transcriptomics and further used in the *in silico* drug repurposing analysis. It is well-acknowledged that not one single model can imitate the disease environment (6). The rationale of selecting the most suitable *in vitro* vascular calcification model may allow a precise understanding of the data and elaborate the initial development of novel drugs for the treatment. In the future, *in vivo* validation is needed to support the differential mechanisms of calcification in the tunica intimal and media.

Conclusion

Our results strengthen previous observations that OM and CaP-induced SMC calcification *in vitro* is triggered by different mechanisms (Figure 6). We found a differential role of PKC in OM and CaP-calcified SMCs, providing new opportunities for therapeutic investigation. Our data suggest that the field should limit the generalization of results found in *in vitro* studies. Proper method reporting of *in vitro* calcification protocols could lead to a better understanding of the potential mediators of VC and yield significant insights into the pathophysiological mechanism of intimal and medial calcification.

Data availability statement

The datasets presented in this study can be found in online repositories. The names of the repository/repositories and accession number(s) can be found in the article.



Ethics statement

The studies involving human participants were reviewed and approved by Nantes University Ethical Committee (GNEDS). The patients/participants provided their written informed consent to participate in this study.

Author contributions

CG and TQ conceptualized and designed the study. TQ, RK, and NM contributed to the study design and the discussion of the results. MH, AB, JH, EvdV, and MG performed the experiments. MH and MS performed the statistical analysis. BK, DM, YG, and WJ-D contributed to the interpretation and the discussion of the results. MH created the figures and wrote the first draft of the manuscript with assistance from CG, JH, and AB. CG, WJ-D, and TQ revised the manuscript. All authors contributed and reviewed the manuscript and approved the final version.

Funding

This work was funded by the “Deutsche Forschungsgemeinschaft” (DFG, German Research Foundation) [GO1801/5-1 to CG and Transregional Collaborative Research Centre (TRR 219; Project-ID 322900939) to CG, WJ-D, RK, and NM], a research grant from the European Union’s Horizon 2020 research and innovation program under the Marie Skłodowska-Curie grant agreement No. 722609, INTRICARE (to CG, WJ-D, and NM), and a grant from the European Research Area Network on Cardiovascular Diseases (ERA-NET CVD JTC2017, Microexploration project; BMBF 01KL1801) to CG and DM. EvdV received financial support from the Interdisciplinary Center for Clinical Research within the faculty of Medicine at the RWTH Aachen University. TQ received financial support from the Fondation de l’Avenir (Paris, France), the University Hospital of Nantes (Nantes, France), and the Fédération Française de Cardiologie (Paris, France).

References

- Lozano R, Naghavi M, Foreman K, Lim S, Shibuya K, Aboyans V, et al. Global and regional mortality from 235 causes of death for 20 age groups in 1990 and 2010: A systematic analysis for the global burden of disease study 2010. *Lancet*. (2012) 380:2095–128. doi: 10.1016/s0140-6736(12)61728-0
- Virani SS, Alonso A, Aparicio HJ, Benjamin EJ, Bittencourt MS, Callaway CW, et al. Heart disease and stroke statistics—2021 update. *Circulation*. (2021) 143:e254–743. doi: 10.1161/cir.0000000000000950
- Lanzer P, Boehm M, Sorribas V, Thiriet M, Janzen J, Zeller T, et al. Medial vascular calcification revisited: Review and perspectives. *Eur Heart J*. (2014) 35:1515–25. doi: 10.1093/eurheartj/ehu163
- Durham AL, Speer MY, Scatena M, Giachelli CM, Shanahan CM. Role of smooth muscle cells in vascular calcification: Implications in atherosclerosis and arterial stiffness. *Cardiovasc Res*. (2018) 114:590–600. doi: 10.1093/cvr/cvy010
- Goettsch C, Hutcheson JD, Aikawa M, Iwata H, Pham T, Nykjaer A, et al. Sortilin mediates vascular calcification via its recruitment into extracellular vesicles. *J Clin Investigat*. (2016) 126:1323–36. doi: 10.1172/jci80851
- Herrmann J, Babic M, Tolle M, van der Giet M, Schuchardt M. Research models for studying vascular calcification. *Int J Mol Sci*. (2020) 21:2204. doi: 10.3390/ijms21062204

Acknowledgments

This work was supported by the Genomics Facility, a core facility of the Interdisciplinary Center for Clinical Research (IZKF) Aachen within the Faculty of Medicine at RWTH Aachen University. We thank Lin Gan for her support. We are most grateful to the GenoBIRD Core Facility for its technical support. We also thank Carine Montagne, Flavien Gautron, and Manon Pondjikli for the management of biocollections, which was funded by the Allocation Nationale de Recherche (ANR) for physiopathology and by an inter-regional Program Hospitalier de Recherche Clinique (PHRC). **Figures 4A, 6** were created with Biorender.

Conflict of interest

The authors declare that the research was conducted in the absence of any commercial or financial relationships that could be construed as a potential conflict of interest.

The reviewer JE declared a shared affiliation with one of the author RK to the handling editor at the time of review.

Publisher’s note

All claims expressed in this article are solely those of the authors and do not necessarily represent those of their affiliated organizations, or those of the publisher, the editors and the reviewers. Any product that may be evaluated in this article, or claim that may be made by its manufacturer, is not guaranteed or endorsed by the publisher.

Supplementary material

The Supplementary Material for this article can be found online at: <https://www.frontiersin.org/articles/10.3389/fcvm.2022.959457/full#supplementary-material>

7. Steitz SA, Speer MY, Curinga G, Yang HY, Haynes P, Aebersold R, et al. Smooth muscle cell phenotypic transition associated with calcification: Upregulation of Cbfa1 and downregulation of smooth muscle lineage markers. *Circ Res.* (2001) 89:1147–54. doi: 10.1161/hh2401.101070
8. Shioi S, Nishizawa Y, Jono S, Koyama H, Hosoi M, Morii H. Beta glycerophosphate accelerates calcification in cultured bovine vascular smooth muscle cells. *Arteriosclerosis Thrombosis Vasc Biol.* (2003) 15:2003–9.
9. Jono S, McKee MD, Murry CE, Shioi A, Nishizawa Y, Mori N, et al. Phosphate regulation of vascular smooth muscle cell calcification. *Circ Res.* (2000) 87:1–8.
10. Hruska KA, Mathew S, Lund R, Qiu P, Pratt R. Hyperphosphatemia of chronic kidney disease. *Kidney Int.* (2008) 74:148–57. doi: 10.1038/ki.2008.130
11. Moe SM, Chen NX. Mechanisms of vascular calcification in chronic kidney disease. *J Am Soc Nephrol.* (2008) 19:213–6. doi: 10.1681/ASN.2007080854
12. Kim GH, Choi BS, Cha DR, Chee DH, Hwang E, Kim HW, et al. Serum calcium and phosphorus levels in patients undergoing maintenance hemodialysis: A multicentre study in Korea. *Kidney Res Clin Pract.* (2014) 33:52–7. doi: 10.1016/j.krcp.2013.12.003
13. Wickham H. *Ggplot2- Elegant Graphics for Data Analysis*. 2nd ed. Cham: Springer (2016). p. 260.
14. Salabei JK, Gibb AA, Hill BG. Comprehensive measurement of respiratory activity in permeabilized cells using extracellular flux analysis. *Nat Protoc.* (2014) 9:421–38. doi: 10.1038/nprot.2014.018
15. Gesper M, Nonnast ABH, Kumowski N, Stoehr R, Schuett K, Marx N, et al. Gut-derived metabolite indole-3-propionic acid modulates mitochondrial function in cardiomyocytes and alters cardiac function. *Front Med (Lausanne).* (2021) 8:648259. doi: 10.3389/fmed.2021.648259
16. Chirumamilla CS, Fazil M, Perez-Novo C, Rangarajan S, de Wijn R, Ramireddy P, et al. Profiling activity of cellular kinases in migrating T-cells. *Methods Mol Biol.* (2019) 1930:99–113. doi: 10.1007/978-1-4939-9036-8_13
17. Subramanian A, Narayan R, Corsello SM, Peck DD, Natoli TE, Lu X, et al. A next generation connectivity map: L1000 platform and the first 1,000,000 profiles. *Cell.* (2017) 171:1437–52.e17. doi: 10.1016/j.cell.2017.10.049
18. Steenman M, Espitia O, Maurel B, Guyomarch B, Heymann MF, Pistorius MA, et al. Identification of genomic differences among peripheral arterial beds in atherosclerotic and healthy arteries. *Sci Rep.* (2018) 8:3940. doi: 10.1038/s41598-018-22292-y
19. Tusher VG, Tibshirani R, Chu G. Significance analysis of microarrays applied to the ionizing radiation response. *Proc Natl Acad Sci U S A.* (2001) 98:5116–21. doi: 10.1073/pnas.091062498
20. Wirka RC, Wagh D, Paik DT, Pjanic M, Nguyen T, Miller CL, et al. Atheroprotective roles of smooth muscle cell phenotypic modulation and the Tcf21 disease gene as revealed by single-cell analysis. *Nat Med.* (2019) 25:1280–9. doi: 10.1038/s41591-019-0512-5
21. Ma WF, Hodonsky CJ, Turner AW, Wong D, Song Y, Mosquera JV, et al. Enhanced Single-Cell RNA-Seq workflow reveals coronary artery disease cellular cross-talk and candidate drug targets. *Atherosclerosis.* (2022) 340:12–22. doi: 10.1016/j.atherosclerosis.2021.11.025
22. Han Y, Zhang J, Huang S, Cheng N, Zhang C, Li Y, et al. MicroRNA-223-3p inhibits vascular calcification and the osteogenic switch of vascular smooth muscle cells. *J Biol Chem.* (2021) 296:100483. doi: 10.1016/j.jbc.2021.100483
23. Mahi NA, Najafabadi MF, Pilarczyk M, Kouril M, Medvedovic M, Grein: An interactive web platform for re-analyzing geo RNA-Seq data. *Sci Rep.* (2019) 9:7580. doi: 10.1038/s41598-019-43935-8
24. Travis JA, Hughes MJ, Wong JM, Wagner WD, Geary RL. Hyaluronan enhances contraction of collagen by smooth muscle cells and adventitial fibroblasts: Role of CD44 and implications for constrictive remodeling. *Circ Res.* (2001) 88:77–83. doi: 10.1161/01.res.88.1.77
25. Zhang H, Alder NN, Wang W, Szeto H, Marcinek DJ, Rabinovitch PS. Reduction of elevated proton leak rejuvenates mitochondria in the aged cardiomyocyte. *Elife.* (2020) 9:e60827. doi: 10.7554/eLife.60827
26. Alesutan I, Moritz F, Haider T, Shouxuan S, Gollmann-Tepekoylu C, Holfeld J, et al. Impact of beta-glycerophosphate on the bioenergetic profile of vascular smooth muscle cells. *J Mol Med.* (2020) 98:985–97. doi: 10.1007/s00109-020-01925-8
27. Bonucci E, Sadun R. Experimental calcification of the myocardium. Ultrastructural and histochemical investigations. *Am J Pathol.* (1973) 71:167–92.
28. Huang DW, Sherman BT, Lempicki RA. Bioinformatics enrichment tools: Paths toward the comprehensive functional analysis of large gene lists. *Nucleic Acids Res.* (2009) 37:1–13. doi: 10.1093/nar/gkn923
29. Zhu D, Mackenzie NC, Farquharson C, Macrae VE. Mechanisms and clinical consequences of vascular calcification. *Front Endocrinol (Lausanne).* (2012) 3:95. doi: 10.3389/fendo.2012.00095
30. Fakhry M, Roszkowska M, Briolay A, Bougault C, Guignandon A, Diaz-Hernandez JJ, et al. TNAP stimulates vascular smooth muscle cell trans-differentiation into chondrocytes through calcium deposition and BMP-2 activation: Possible implication in atherosclerotic plaque stability. *Biochim Biophys Acta Mol Basis Dis.* (2017) 1863:643–53. doi: 10.1016/j.bbdis.2016.12.003
31. Goettsch C, Strzelecka-Kiliszek A, Bessueille L, Quillard T, Mechtaouf L, Pikula S, et al. TNAP as a therapeutic target for cardiovascular calcification - a discussion of its pleiotropic functions in the body. *Cardiovasc Res.* (2020) 118:84–96. doi: 10.1093/cvr/cvaa299
32. Villa-Bellosta R. Synthesis of extracellular pyrophosphate increases in vascular smooth muscle cells during phosphate-induced calcification. *Arterioscler Thromb Vasc Biol.* (2018) 38:2137–47. doi: 10.1161/ATVBAHA.118.311444
33. Kapustin AN, Chatrou ML, Drozdov I, Zheng Y, Davidson SM, Soong D, et al. Vascular smooth muscle cell calcification is mediated by regulated exosome secretion. *Circ Res.* (2015) 116:1312–23. doi: 10.1161/CIRCRESAHA.116.305012
34. Alves DAM, Eijken M, van de Peppel J, van Leeuwen JPTM. Calcifying vascular smooth muscle cells and osteoblasts: Independent cell types exhibiting extracellular matrix and biomineralization-related mimics. *BMC Genomics.* (2014) 15:965. doi: 10.1186/1471-2164-15-965
35. Rukov JL, Gravesen E, Mace ML, Hofman-Bang J, Vinther J, Andersen CB, et al. Effect of chronic uremia on the transcriptional profile of the calcified aorta analyzed by RNA sequencing. *Am J Physiol Renal Physiol.* (2016) 310:F477–91. doi: 10.1152/ajprenal.00472.2015
36. Lacolley P, Regnault V, Nicoletti A, Li Z, Michel JB. The vascular smooth muscle cell in arterial pathology: A cell that can take on multiple roles. *Cardiovasc Res.* (2012) 95:194–204. doi: 10.1093/cvr/cvs135
37. Owens G, Kumar MS, Wamhoff BR. Molecular regulation of vascular smooth muscle cell differentiation in development and disease. *Physiol Rev.* (2004) 84:767–801.
38. Park S, Jeon JH, Min BK, Ha CM, Thoudam T, Park BY, et al. Role of the pyruvate dehydrogenase complex in metabolic remodeling: Differential pyruvate dehydrogenase complex functions in metabolism. *Diabetes Metab J.* (2018) 42:270–81. doi: 10.4093/dmj.2018.0101
39. Lee SJ, Lee IK, Jeon JH. Vascular calcification-new insights into its mechanism. *Int J Mol Sci.* (2020) 21:2685. doi: 10.3390/ijms21082685
40. Fink BD, Bai F, Yu L, Sivitz WI. Regulation of ATP production: Dependence on calcium concentration and respiratory state. *Am J Physiol Cell Physiol.* (2017) 313:C146–53. doi: 10.1152/ajpcell.00086.2017
41. Malyala S, Zhang Y, Strubbe JO, Bazil JN. Calcium phosphate precipitation inhibits mitochondrial energy metabolism. *PLoS Comput Biol.* (2019) 15:e1006719. doi: 10.1371/journal.pcbi.1006719
42. Strubbe-Rivera JO, Schrad JR, Pavlov EV, Conway JE, Parent KN, Bazil JN. The mitochondrial permeability transition phenomenon elucidated by cryo-em reveals the genuine impact of calcium overload on mitochondrial structure and function. *Sci Rep.* (2021) 11:1037. doi: 10.1038/s41598-020-80398-8
43. Ma WQ, Sun XJ, Zhu Y, Liu NF. PDK4 promotes vascular calcification by interfering with autophagic activity and metabolic reprogramming. *Cell Death Dis.* (2020) 11:991. doi: 10.1038/s41419-020-03162-w
44. Rashdan NA, Sim AM, Cui L, Phadwal K, Roberts FL, Carter R, et al. Osteocalcin regulates arterial calcification via altered WNT signaling and glucose metabolism. *J Bone Miner Res.* (2020) 35:357–67. doi: 10.1002/jbmr.3888
45. Shum LC, White NS, Mills BN, Bentley KL, Eliseev RA. Energy metabolism in mesenchymal stem cells during osteogenic differentiation. *Stem Cells Dev.* (2016) 25:114–22. doi: 10.1089/scd.2015.0193
46. Phadwal K, Vrahnas C, Ganley IG, MacRae VE. Mitochondrial dysfunction: Cause or consequence of vascular calcification? *Front Cell Dev Biol.* (2021) 9:611922. doi: 10.3389/fcell.2021.611922
47. Rogers MA, Maldonado N, Hutcheson JD, Goettsch C, Goto S, Yamada I, et al. Dynamin-related protein 1 inhibition attenuates cardiovascular calcification in the presence of oxidative stress. *Circ Res.* (2017) 121:220–33. doi: 10.1161/CIRCRESAHA.116.310293
48. Gourlay CW, Carpp LN, Timpson P, Winder SJ, Ayscough KR. A role for the actin cytoskeleton in cell death and aging in yeast. *J Cell Biol.* (2004) 164:803–9. doi: 10.1083/jcb.200310148
49. Green DR, Kroemer G. The pathophysiology of mitochondrial cell death. *Science.* (2004) 305:626–9. doi: 10.1126/science.1099320

50. Ridker PM, Everett BM, Thuren T, MacFadyen JG, Chang WH, Ballantyne C, et al. Antiinflammatory therapy with canakinumab for atherosclerotic disease. *N Engl J Med.* (2017) 377:1119–31. doi: 10.1056/NEJMoa1707914
51. Nidorf SM, Fiolet ATL, Mosterd A, Eikelboom JW, Schut A, Opstal TSJ, et al. Colchicine in patients with chronic coronary disease. *N Engl J Med.* (2020) 383:1838–47. doi: 10.1056/NEJMoa2021372
52. Galindez G, Matschinske J, Rose TD, Sadegh S, Salgado-Albarrán M, Späth J, et al. Lessons from the Covid-19 pandemic for advancing computational drug repurposing strategies. *Nat Computat Sci.* (2021) 1:33–41. doi: 10.1038/s43588-020-00007-6
53. Lin CS, Lin FY, Ho LJ, Tsai CS, Cheng SM, Wu WL, et al. Pkcdelta signalling regulates SR-A and CD36 expression and foam cell formation. *Cardiovasc Res.* (2012) 95:346–55. doi: 10.1093/cvr/cvs189
54. Harja E, Chang JS, Lu Y, Leitges M, Zou YS, Schmidt AM, et al. Mice deficient in PKCbeta and apolipoprotein E display decreased atherosclerosis. *FASEB J.* (2009) 23:1081–91. doi: 10.1096/fj.08-120345
55. Liu J, Someren E, Mentink A, Licht R, Dechering K, van Blitterswijk C, et al. The effect of PKC activation and inhibition on osteogenic differentiation of human mesenchymal stem cells. *J Tissue Eng Regen Med.* (2010) 4:329–39. doi: 10.1002/term.242
56. Nakura A, Higuchi C, Yoshida K, Yoshikawa H. Pkcalpha suppresses osteoblastic differentiation. *Bone.* (2011) 48:476–84. doi: 10.1016/j.bone.2010.09.238
57. Galea GL, Meakin LB, Williams CM, Hulin-Curtis SL, Lanyon LE, Poole AW, et al. Protein kinase Calpha (PKCalpha) regulates bone architecture and osteoblast activity. *J Biol Chem.* (2014) 289:25509–22. doi: 10.1074/jbc.M114.580365
58. Borland SJ, Morris TG, Borland SC, Morgan MR, Francis SE, Merry CLR, et al. Regulation of vascular smooth muscle cell calcification by syndecan-4/FGF-2/PKCalpha signalling and cross-talk with TGFbeta. *Cardiovasc Res.* (2017) 113:1639–52. doi: 10.1093/cvr/cvx178
59. Lee K, Kim H, Jeong D. Protein kinase C regulates vascular calcification via cytoskeleton reorganization and osteogenic signaling. *Biochem Biophys Res Commun.* (2014) 453:793–7. doi: 10.1016/j.bbrc.2014.10.026
60. Bardeesi ASA, Gao J, Zhang K, Yu S, Wei M, Liu P, et al. A novel role of cellular interactions in vascular calcification. *J Transl Med.* (2017) 15:95. doi: 10.1186/s12967-017-1190-z
61. Espitia O, Chatelais M, Steenman M, Charrier C, Maurel B, Georges S, et al. Implication of molecular vascular smooth muscle cell heterogeneity among arterial beds in arterial calcification. *PLoS One.* (2018) 13:e0191976.
62. Hutcheson JD, Goettsch C, Rogers MA, Aikawa E. Revisiting cardiovascular calcification: A multifaceted disease requiring a multidisciplinary approach. *Semin Cell Dev Biol.* (2015) 46:68–77. doi: 10.1016/j.semcdb.2015.09.004
63. Libby P, Aikawa M. Stabilization of atherosclerotic plaques: New mechanisms and clinical targets. *Nat Med.* (2002) 8:1257–62. doi: 10.1038/nm1102-1257
64. Hutcheson JD, Goettsch C, Bertazzo S, Maldonado N, Ruiz JL, Goh W, et al. Genesis and growth of extracellular-vesicle-derived microcalcification in atherosclerotic plaques. *Nat Mater.* (2016) 15:335–43. doi: 10.1038/nmat4519
65. Heuschkel MA, Skenteris NT, Hutcheson JD, van der Valk DD, Bremer J, Goody P, et al. Integrative multi-omics analysis in calcific aortic valve disease reveals a link to the formation of amyloid-like deposits. *Cells.* (2020) 9:2164. doi: 10.3390/cells9102164



OPEN ACCESS

EDITED BY

Masanori Aikawa,
Brigham and Women's Hospital
and Harvard Medical School,
United States

REVIEWED BY

Liming Yu,
The University of Texas Health Science
Center at San Antonio, United States
Mabruka Alfaidi,
LSU Health Sciences Center
Shreveport, United States

*CORRESPONDENCE

Hanjoong Jo
hjo@emory.edu

SPECIALTY SECTION

This article was submitted to
Atherosclerosis and Vascular Medicine,
a section of the journal
Frontiers in Cardiovascular Medicine

RECEIVED 27 June 2022

ACCEPTED 29 August 2022

PUBLISHED 30 September 2022

CITATION

Demos C, Johnson J, Andueza A,
Park C, Kim Y, Villa-Roel N, Kang D-W,
Kumar S and Jo H (2022) Sox13 is
a novel flow-sensitive transcription
factor that prevents inflammation by
repressing chemokine expression
in endothelial cells.
Front. Cardiovasc. Med. 9:979745.
doi: 10.3389/fcvm.2022.979745

COPYRIGHT

© 2022 Demos, Johnson, Andueza,
Park, Kim, Villa-Roel, Kang, Kumar and
Jo. This is an open-access article
distributed under the terms of the
[Creative Commons Attribution License](#)
(CC BY). The use, distribution or
reproduction in other forums is
permitted, provided the original
author(s) and the copyright owner(s)
are credited and that the original
publication in this journal is cited, in
accordance with accepted academic
practice. No use, distribution or
reproduction is permitted which does
not comply with these terms.

Sox13 is a novel flow-sensitive transcription factor that prevents inflammation by repressing chemokine expression in endothelial cells

Catherine Demos¹, Janie Johnson¹, Aitor Andueza¹,
Christian Park¹, Yerin Kim¹, Nicolas Villa-Roel¹,
Dong-Won Kang¹, Sandeep Kumar¹ and Hanjoong Jo^{1,2*}

¹Wallace H. Coulter Department of Biomedical Engineering, Georgia Institute of Technology, Emory University, Atlanta, GA, United States, ²Division of Cardiology, Department of Medicine, Emory University, Atlanta, GA, United States

Atherosclerosis is a chronic inflammatory disease and occurs preferentially in arterial regions exposed to disturbed blood flow (d-flow) while the stable flow (s-flow) regions are spared. D-flow induces endothelial inflammation and atherosclerosis by regulating endothelial gene expression partly through the flow-sensitive transcription factors (FSTFs). Most FSTFs, including the well-known Kruppel-like factors KLF2 and KLF4, have been identified from *in vitro* studies using cultured endothelial cells (ECs). Since many flow-sensitive genes and pathways are lost or dysregulated in ECs during culture, we hypothesized that many important FSTFs in ECs *in vivo* have not been identified. We tested the hypothesis by analyzing our recent gene array and single-cell RNA sequencing (scRNAseq) and chromatin accessibility sequencing (scATACseq) datasets generated using the mouse partial carotid ligation model. From the analyses, we identified 30 FSTFs, including the expected *KLF2/4* and novel FSTFs. They were further validated in mouse arteries *in vivo* and cultured human aortic ECs (HAECs). These results revealed 8 FSTFs, *SOX4*, *SOX13*, *SIX2*, *ZBTB46*, *CEBPβ*, *NFIL3*, *KLF2*, and *KLF4*, that are conserved in mice and humans *in vivo* and *in vitro*. We selected *SOX13* for further studies because of its robust flow-sensitive regulation, preferential expression in ECs, and unknown flow-dependent function. We found that siRNA-mediated knockdown of *SOX13* increased endothelial inflammatory responses even under the unidirectional laminar shear stress (ULS, mimicking s-flow) condition. To understand the underlying mechanisms, we conducted an RNAseq study in HAECs treated with *SOX13* siRNA under shear conditions (ULS vs. oscillatory shear mimicking d-flow). We found 94 downregulated and 40 upregulated genes that changed in a shear- and *SOX13*-dependent manner. Several cytokines, including *CXCL10* and *CCL5*, were the most strongly upregulated genes in HAECs treated with *SOX13* siRNA. The robust induction of *CXCL10* and *CCL5* was further validated by qPCR and ELISA

in HAECs. Moreover, the treatment of HAECs with Met-CCL5, a specific CCL5 receptor antagonist, prevented the endothelial inflammation responses induced by siSOX13. In addition, SOX13 overexpression prevented the endothelial inflammation responses. In summary, SOX13 is a novel conserved FSTF, which represses the expression of pro-inflammatory chemokines in ECs under s-flow. Reduction of endothelial SOX13 triggers chemokine expression and inflammatory responses, a major proatherogenic pathway.

KEYWORDS

shear-sensitive TF, Sox13, CCL5, CXCL10, endothelium, inflammation

Introduction

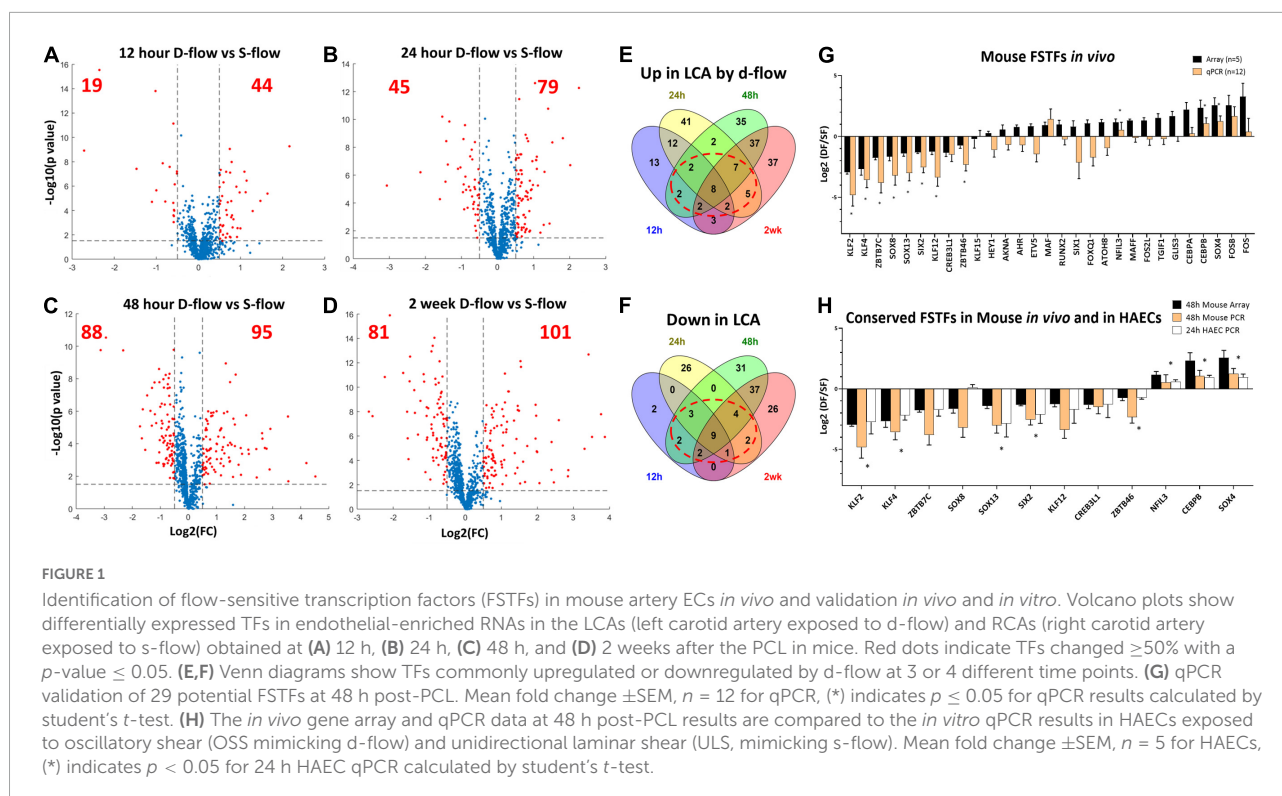
Atherosclerosis is a leading cause of death worldwide as the major underlying cause of myocardial infarction, stroke, and peripheral arterial disease (1). Atherosclerotic plaques preferentially develop in curved or branched arterial regions exposed to disturbed flow (d-flow), characterized by low and oscillatory shear stress (OSS). In contrast, artery regions exposed to stable flow (s-flow) with characteristic unidirectional, high laminar shear stress (ULS) are protected from the disease (2–6). D-flow and s-flow are recognized by mechanosensors, which trigger a wide spectrum of different endothelial responses. While s-flow/ULS promotes a healthy endothelial phenotype, d-flow/OSS induces atherosclerosis development and progression (7–11) by regulating gene expression on a genome-wide scale (9, 12–17). Transcription factors regulated in a flow-sensitive manner (FSTFs) play a key role in genome-wide gene expression by driving transcription of flow-sensitive genes (9, 10, 13, 15, 18).

Many FSTFs, such as Kruppel-like factors (KLF2 and KLF4), are well-known to regulate the expression of hundreds of target genes and numerous anti- or pro-atherogenic pathways (14, 19–23). KLF2 overexpression in static ECs induces key flow-sensitive pathways, demonstrating the importance of FSTFs in ECs (24). Other FSTFs include NF- κ B, AP-1, and YAP/TAZ, which regulate inflammatory signaling, proliferation, and migration in response to d-flow/OSS in endothelial cells (ECs) (25–29). These well-known FSTFs have been mostly identified from ECs cultured *in vitro* (26), while similar *in vivo* studies are lacking. Since ~45% of flow-sensitive genes identified *in vivo* are estimated to be dysregulated or lost in ECs during culture *in vitro* (17, 30), we hypothesized that some important, highly sensitive FSTFs active under *in vivo* conditions had yet to be discovered.

To identify novel FSTFs in artery ECs *in vivo*, we re-analyzed two independent datasets that we previously reported using our mouse partial carotid ligation (PCL) model, the d-flow-induced mouse model of atherosclerosis (12, 13). In the PCL model (Figure 1), three of the four caudal branches

(left external carotid, internal carotid, and occipital artery) of the left common carotid artery (LCA) are ligated, leaving the superior thyroid artery patent. In the same animal, the contralateral right carotid artery (RCA) with characteristic ULS continues to be exposed to s-flow and serves as a control. The PCL causes d-flow with characteristic OSS in the LCA, rapidly inducing robust atherosclerosis within 2 weeks, directly demonstrating a causal relationship between d-flow and atherosclerosis (31, 32). To understand the mechanisms of flow-induced atherosclerosis, we previously carried out a gene array study using endothelial-enriched “bulk” RNAs from the LCAs and RCAs obtained at four-time points (12 h, 24 h, 48 h, and 2 weeks) after the PCL surgery (12). In addition, we performed a single-cell RNA sequencing (scRNAseq) and single-cell Assay for Transposase-Accessible Chromatin with high-throughput sequencing (scATACseq) using the LCA and RCA RNAs obtained at 2-day and 2-week post-PCL time points (13). The scRNAseq and scATACseq studies showed that d-flow induces genome- and epigenome-wide changes in gene expression, reprogramming endothelial cells from the healthy atheroprotective phenotype to pro-inflammatory and pro-atherogenic phenotypes, including the transition of ECs to mesenchymal (EndMT) and immune cell-like (EndICLT) cells (13).

Here, we re-analyzed the *in vivo* datasets from the PCL studies (gene array, scRNAseq, and scATACseq datasets) and found several novel FSTFs, including SOX13, that are conserved in mouse artery ECs *in vivo* and human aortic ECs (HAECs) *in vitro*. SRY (Sex Determining Region Y)-box transcription factor 13 (SOX13) is a member of the SoxD subfamily of the SRY-related high mobility group (HMG) box (Sox) transcription factors and is involved in the regulation of embryonic development and the determination of cell fate (33). SOX13 is also known as islet cell antibody 12 (ICA12), as it is a type-1 diabetes autoantigen. Critically, SOX13 binds with TCF1 competitively to β -catenin, thereby indirectly preventing TCF1/ β -catenin targets from being transcribed in embryonic tissues (34). SOX13 has also been studied in various cancers where many functions are related to stem cell fate determination



(35–38). SOX13 protein expression is high in embryonic arterial walls, suggesting part of the developmental role is in arteriogenesis (39, 40). SOX13 flow sensitivity has not previously been reported, nor has a role in atherosclerosis emerged. To examine SOX13 functional effects and transcriptional targets under flow, we further conducted RNAseq and functional studies using HAECs treated with SOX13 siRNA (siSOX13) or overexpression plasmid under shear conditions. The results show that SOX13 is a novel FSTF induced by s-flow and represses the expression of cytokines CCL5 and CXCL10, preventing endothelial inflammation. The loss of SOX13, in contrast, dramatically induces the expression of the cytokines, leading to robust endothelial inflammation.

Results

Identification and validation of novel factors regulated in a flow-sensitive manner in mouse artery endothelial cells *in vivo* and in cultured human aortic endothelial cells

To identify FSTFs in mouse artery ECs *in vivo*, we first re-analyzed our genome-wide transcriptome data using the EC-enriched bulk RNAs from the mouse PCL study (12). The

gene array dataset (GSE182291) was comprised of transcript expression results of LCAs (exposed to d-flow) and RCAs (contralateral s-flow) obtained at four-time points: 12 h, 24 h, 48 h, and 2 weeks post-PCL. We first cross-checked the list of human TFs (41) to our mouse gene array data and found 973 TFs detected at least at the one-time point. Then, we determined differential expression in LCA vs. RCA at each time point to identify TFs that changed by flow by $\geq 50\%$ with a p -value ≤ 0.05 , representing our definition of FSTFs. The total number of FSTFs at each time point was 63 at 12 h, 124 at 24 h, 183 at 48 h, and 182 at 2 weeks, totaling 323 unique FSTFs changing at least at one time-point (Figures 1A–D). Of the 323, 8 upregulated and 9 downregulated FSTFs changed in the consistent direction by d-flow at all four time-points (Figures 1E,F). In addition, we found 20 upregulated and 14 downregulated TFs that changed consistently in three time points. Of those, we removed any TFs that changed in the opposite direction at any time point. Through the analyses, we found 30 FSTFs that changed consistently in one direction, up or down, at more than 3 time points in mouse artery ECs.

Next, we validated the gene array data of these 30 potential FSTFs by qPCR using additional RNA samples obtained from LCAs and RCAs at 48 h post-PCL (Figure 1G). We confirmed the flow sensitivity of 12 of 29 potential FSTFs, while one (*TCF23*) was not detectable by qPCR. Next, we examined mRNA expression in HAECs to determine if the mouse FSTFs were also conserved in human ECs and flow-sensitive

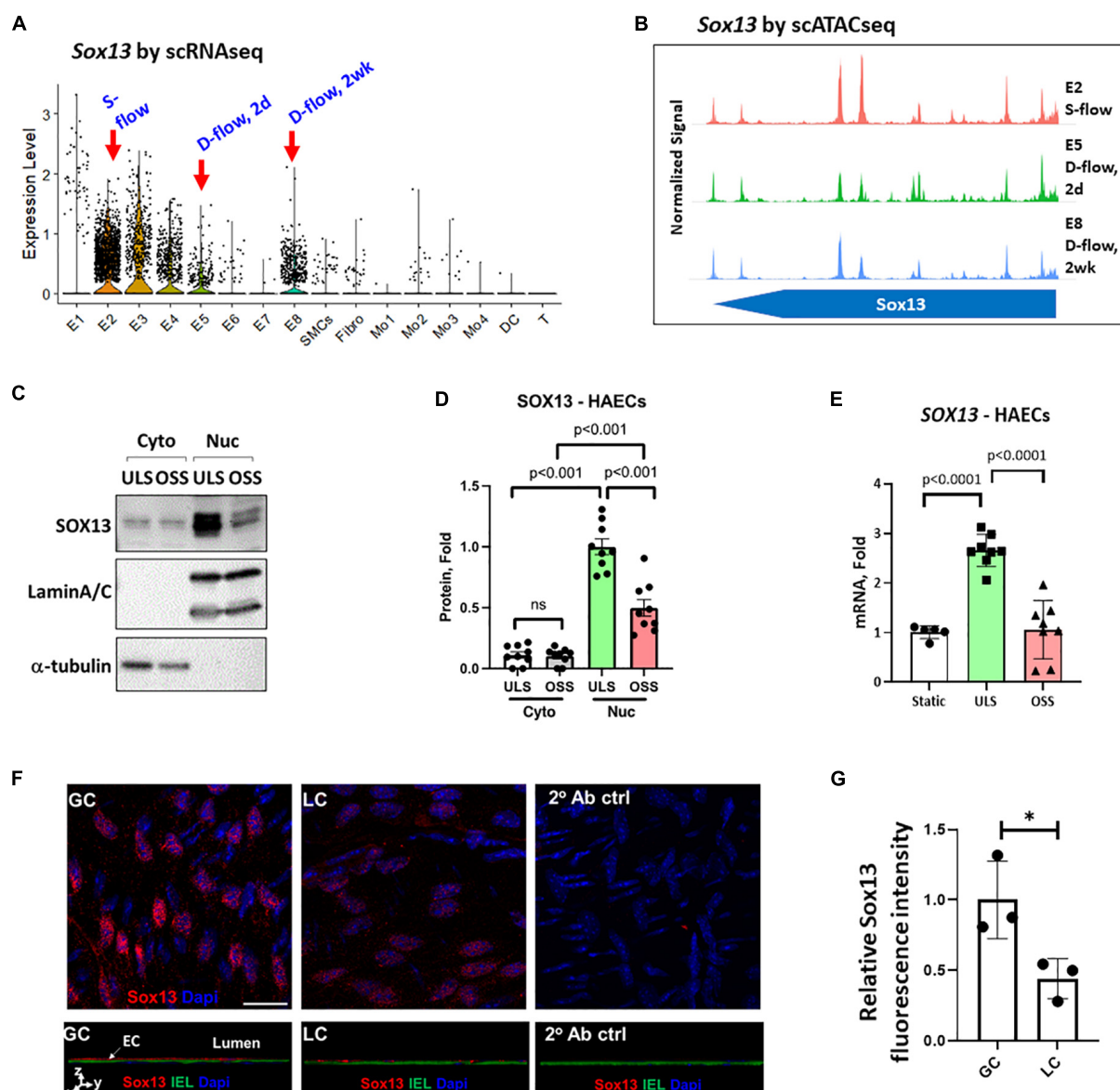


FIGURE 2

Validation of SOX13 flow sensitivity in ECs. (A) Violin plot shows *SOX13* expression profile in our published scRNAseq data obtained from the mouse LCAs and RCAs at the 2-day (acute) or 2 weeks (chronic) post-PCL (partial carotid ligation) surgery. E2 represents a healthy EC cluster exposed to s-flow in RCA. E5 and E8 are EC clusters exposed to acute and chronic d-flow, respectively. (B) Chromatin accessibility plot of *Sox13* gene was obtained by re-analyzing the published scATACseq data using the same mouse PCL model. E2 (s-flow), E5 (acute d-flow), and E8 (chronic d-flow) showed a time-dependent closure of *SOX13* accessibility by d-flow in ECs. (C–E) HAECs exposed to ULS or OSS for 24 h were lysed, fractionated into the cytoplasmic (cyto) and nuclear (nuc) fractionations, and western blot analyzed using antibodies to SOX13, laminA/C, and α-tubulin (C) and quantified (D). Mean±SEM, $n = 5$, p -values calculated by student's t -test. (E) Shows *SOX13* qPCR from a similar HAEC shear study, Mean±SEM, $n = 8$, p -values calculated by student's t -test. (F) Shows immunofluorescence staining of Sox13 of mouse GC (greater curvature exposed to stable flow) and LC (lesser curvature exposed to disturbed flow) naturally in the aortic arch. The bottom panels show orthogonal views, showing SOX13 expression above the internal elastic lamina (IEL). DAPI shows nuclei. (G) Shows the quantitation of SOX13 expression. Mean±SEM, $n = 3$ mice, $p \leq 0.05$ by student's t -test.

in vitro. In HAECs subjected to ULS (mimicking s-flow) or OSS (mimicking d-flow) for 24 h, we validated the expression of 8 of the 12 TFs that were regulated by flow in a consistent manner (Figure 1H). Five upregulated FSTFs by ULS were *KLF2*, *KLF4*, *SOX13*, *SIX2*, and *ZBTB46*, and 3 upregulated

by OSS were *NFIL3*, *CEBPβ*, and *SOX4* (Figure 1H). *KLF2*, *KLF4*, *ZBTB46*, and *SOX4* (42–45) were previously shown to be FSTFs in ECs, demonstrating the validity of our approach. In contrast, *SOX13*, *SIX2*, *CEBPβ*, and *NFIL3* are novel potential FSTFs.

Validation of Sox13 as a flow-sensitive transcription factor by re-analyzing the *in vivo* single-cell RNA sequencing and single-cell assay for transposase-accessible chromatin with high-throughput sequencing datasets of mouse artery endothelial cells

We also re-analyzed our published scRNAseq data from the mouse PCL study to further validate the flow sensitivity of *Sox13*, *Six2*, *Cebpb*, and *Nfil3*. Four groups were represented in this study: RCA/s-flow or LCA/d-flow for 2 days or 2 weeks each. *Sox13* showed a strong flow sensitivity and preferential expression in ECs compared to other artery wall cell types (smooth muscle cells, immune cells, and fibroblasts) (Figure 2A). Briefly, the E1 cluster consisted of ECs present in all 4 conditions (2d-RCA, 2d-LCA, 2wk-RCA, and 2wk-LCA). E1–E4 consisted of ECs exposed to s-flow conditions (2d-RCA and 2wk-RCA). The majority of E5 and E7 clusters consisted of ECs exposed to acute d-flow (2d-LCA). E6 and E8 exclusively consisted of ECs exposed to chronic d-flow (2wk-LCA). *Sox13* expression was significantly higher in the healthy EC subpopulation (E2) found in s-flow-exposed RCAs compared to the pro-atherogenic, d-flow-exposed EC subpopulations (E5 and E8) (13). Although E5 (acute d-flow) expressed lower *Sox13* levels than E8 (chronic d-flow), both ECs showed significantly lower levels compared to E2 (s-flow condition). We also re-analyzed the scATACseq data and found that *Sox13* chromatin accessibility was more open (indicating higher gene transcription activity) in the healthy E2 under the s-flow condition compared to the pro-atherogenic E5 and E8 populations under the acute (2-day) and chronic (2-week) d-flow conditions, respectively (Figure 2B and Supplementary Table 1). The scATACseq and the scRNAseq data analyses further support the mouse gene array data and HAEC validation results (Figure 1), demonstrating that *Sox13* is indeed a novel FSTF in ECs. Therefore, we decided to focus on studying SOX13 further in this study.

Stable flow induces SOX13 expression in the nucleus of human aortic endothelial cells and in mouse aortic endothelial cells

We examined the effect of shear on SOX13 protein expression in the cytoplasmic and nuclear fractions in HAECs. SOX13 protein was predominantly expressed in the nucleus, and exposure to ULS significantly increased the expression in the nuclear fraction compared to the static or OSS conditions (Figures 2C,D). ULS exposure also significantly increased *SOX13* mRNA expression compared to OSS and

static conditions in HAECs (Figure 2E). These data further demonstrated that SOX13 protein is primarily expressed in the nucleus, as expected for a TF, under s-flow conditions in HAECs.

Furthermore, we examined Sox13 protein in mouse aortic arch regions in an immunofluorescence staining study using the greater curvature (GC) exposed to stable flow and lesser curvature (LC) exposed to disturbed flow intrinsically. The staining result (Figures 2F,G) clearly demonstrated the specific staining of Sox13 above the internal elastic layer (IEL), demonstrating a higher SOX13 expression in the endothelial layer in the aorta naturally exposed to stable flow in GC than disturbed flow in LC region. This result further supports that Sox13 protein expression is higher in the naturally stable flow region than the unstable flow region in mouse aorta *in vivo*.

SOX13 knockdown induces cytokine and chemokine expression in human aortic endothelial cells

To determine how SOX13 regulates EC function, we first knocked down SOX13 with two pooled siRNAs to SOX13 (siSOX13). Treatment of HAECs with the siSOX13 effectively reduced *SOX13* mRNA (Figure 3A) and nuclear SOX13 protein levels under the static or flow conditions (Figures 3B–F). As controls, we measured the shear-dependent expression of *KLF2*, *KLF4*, and *VCAM1* under the ULS and OSS conditions in HAECs treated with siSOX13 and control siRNA (siCtrl) (Figures 3G–I). As expected, the ULS exposure decreased the expression of *VCAM1* while increasing *KLF2* and *KLF4* compared to the OSS condition. Interestingly, we found that *VCAM1* mRNA and protein expression was increased by siSOX13 compared to siCtrl, indicating potential endothelial inflammation even under the ULS condition. In contrast, *KLF2* and *KLF4* did not significantly change by the siSOX13 treatment under the ULS condition.

To explore the underlying mechanism of SOX13 knockdown effect, we next conducted RNA sequencing (RNAseq) analysis in four groups of HAECs treated with siSOX13 or siCtrl and ULS or OSS conditions: (1) siCtrl ULS, (2) siSOX13 ULS, (3) siCtrl OSS, and (4) siSOX13 OSS. HAECs were transfected with siSOX13 or siCtrl for 24 h, then subjected to ULS or OSS for an additional 24 h, and the total RNA was analyzed by RNAseq ($n = 4$). To identify the genes (GSE207087) regulated by a flow- and siSOX13-dependent manner, we screened for differentially expressed genes that changed by $\geq 50\%$ with a p -value of ≤ 0.05 between the four groups. The gene list was further filtered to remove low-abundance genes with ≤ 50 mean total counts/sample in all groups.

First, a comparison between the siCtrl OSS and siCtrl ULS showed 369 downregulated and 211 upregulated genes by OSS under the basal (siCtrl) condition (Figure 4A).

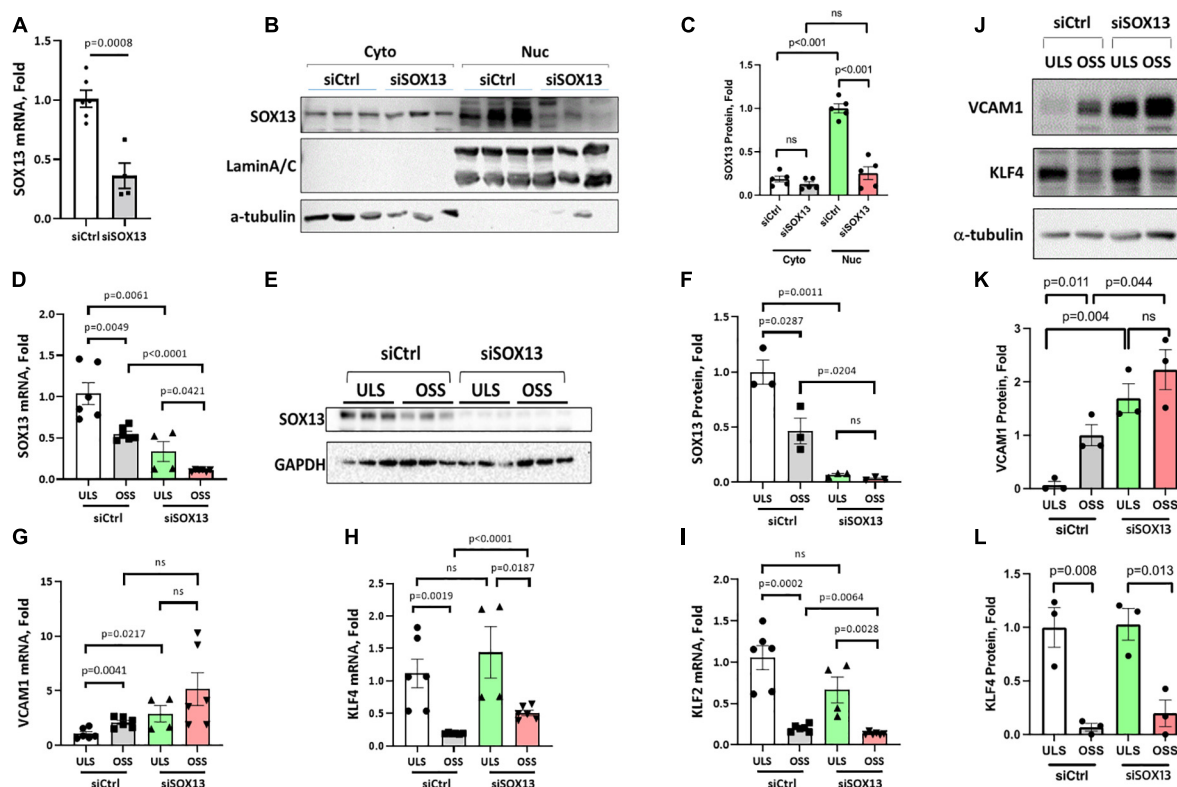


FIGURE 3

siSOX13 knockdown of SOX13 in HAECs. (A–C) Static HAEC study. HAECs were treated with siSOX13 vs. siCtrl for 48 h, and analyzed by qPCR (A) and western blot using cytoplasmic and nuclear fractions with SOX13 antibody (B) and quantified (C). (D–L) Shear study. HAECs treated with siSOX13 vs. siCtrl for 48 h were exposed to ULS or OSS for another 24 h, and analyzed for SOX13 by qPCR (D), western blot of whole cell lysate (E,F). Additional qPCR assays for VCAM1, KLF4, and KLF2 (G–I) and western blots for VCAM1 and KLF4 (J,L) were conducted. Mean±SEM, $n = 4-6$ (F,I) or 3 (K,L) are shown, and p -values calculated by student's t -test.

Next, we identified SOX13-dependent genes under the ULS condition. siSOX13 treatment under ULS condition downregulated 430 genes while upregulating 343 genes compared to the siCtrl ULS (Figure 4B), demonstrating the major impact of SOX13 knockdown on ULS-dependent gene expression. siSOX13 treatment under the OSS condition also downregulated 392 and upregulated 397 genes compared to the siCtrl OSS (Figure 4C), demonstrating the robust effect of SOX13 knockdown in this acute OSS condition. The comparison between siSOX13 OSS and siSOX13 ULS showed 200 upregulated and 156 downregulated genes (Figure 4D).

We next examined which genes were commonly upregulated or downregulated by OSS (vs. ULS) or siSOX13 (vs. siCtrl) conditions in HAECs by comparing the differentially expressed gene lists as shown in the Venn diagrams (Figures 4E,F). The comparison revealed 94 genes commonly downregulated by OSS (siCtrl OSS vs. siCtrl ULS) or siSOX13 under ULS conditions (siSOX13 ULS vs. siCtrl ULS) (Figure 4E). This 94 gene list (Figure 4G) contained SOX13 (as expected by siSOX13 treatment), AQP1 (a predicted SOX13

gene target) (46), THBD, and NOS3. We next found 40 genes commonly upregulated by OSS (siCtrl OSS vs. siCtrl ULS) or siSOX13 under ULS conditions (siSOX13 ULS vs. siCtrl ULS) (Figure 4F). Interestingly, the 40 gene list (Figure 4H) included many cytokines and chemokines, CXCL1, CXCL2, CXCL6, CXCL8, CSF3, IL6, and CCL2. In addition, we found the top 20 most upregulated genes by SOX13 knockdown regardless of the shear conditions. The 20 gene list contained additional cytokines and chemokines, including CCL5 and CXCL10 (Figure 4I). These results suggest that SOX13 is an FSTF regulating cytokine and chemokine expression in ECs.

Flow- and SOX13-dependent biological processes

To predict the role of SOX13 and its target genes in endothelial function and atherosclerosis, we conducted a gene ontology (GO) analysis using the commonly regulated gene lists (Figures 4G,I). The GO analysis of the 94 commonly

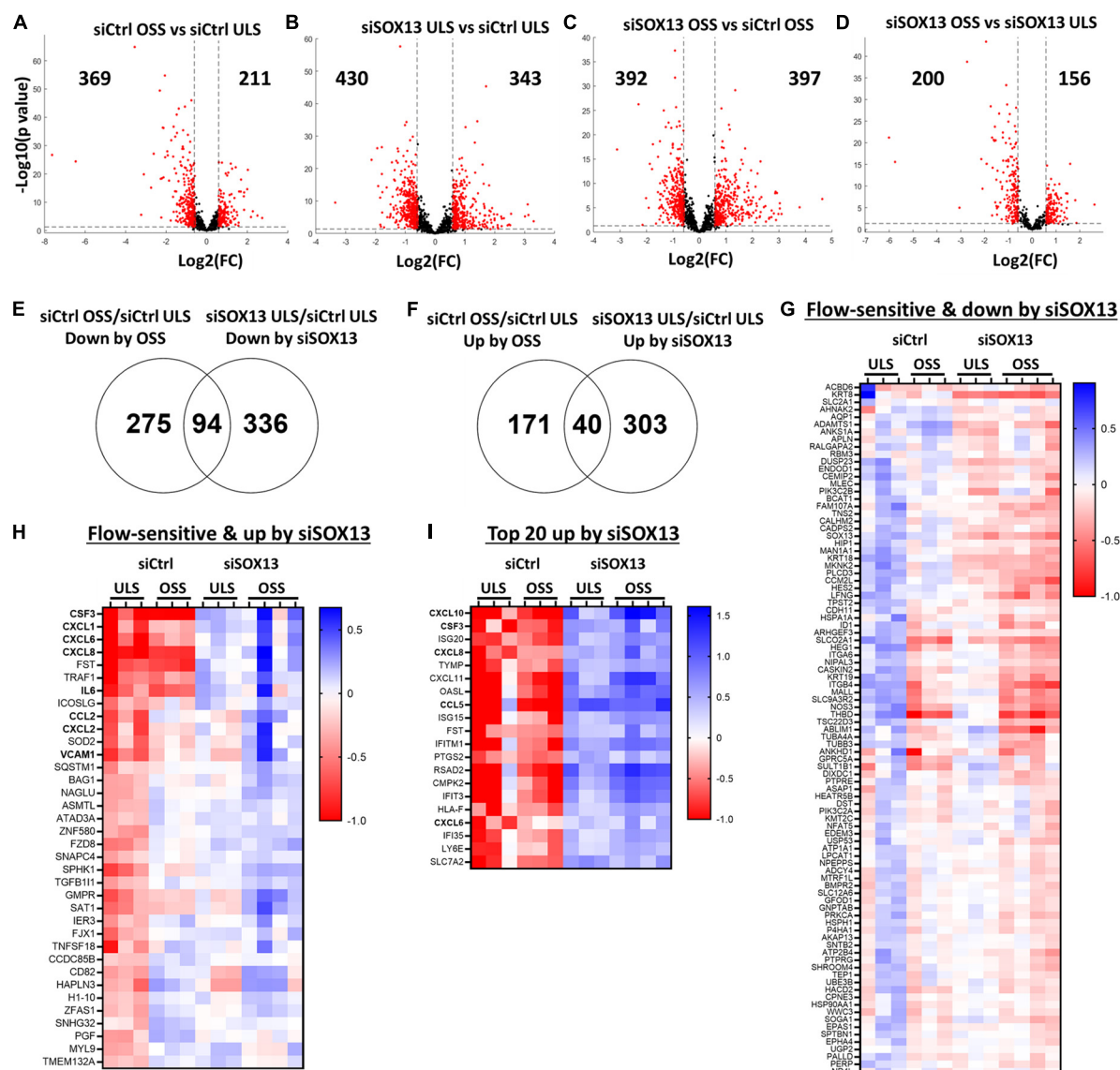


FIGURE 4

Shear-dependent and SOX13-dependent gene expression in HAECs by RNAseq analysis. HAECs treated with siSOX13 or siCtrl for 24 h were exposed to OSS or ULS for another 24 h, and total RNAs were analyzed by RNAseq. (A–D) Shows differential gene expression by comparing the four groups: (1) siCtrl OSS, (2) siSOX13 OSS, (3) siCtrl LSS, and (4) siSOX13 LSS. The number of significantly downregulated (left) or upregulated (right) genes by $\geq 50\%$ with a p -value ≤ 0.05 (shown as red dots) are indicated in each volcano plot. (E,F) Venn diagrams show commonly downregulated genes by OSS or siSOX13 (E) and upregulated genes by OSS or siSOX13 in ULS condition (F). (G,H) Heat map of the 94 commonly downregulated genes by OSS or siSOX13 in ULS condition (G) and the 40 commonly upregulated by OSS or by siSOX13. (I) Heatmap of top 20 genes upregulated by siSOX13 regardless of shear conditions.

downregulated genes by OSS or siSOX13 under the ULS condition (Figure 4H) showed that biological processes related to development, anatomical structure, blood vessel morphogenesis, and cell fate were enriched (Figure 5A), known SOX13-dependent processes (33, 39, 47, 48). In contrast, the GO analysis of the 40 genes upregulated by OSS and SOX13 knockdown under ULS conditions (Figure 4I) showed enrichment of 25 biological processes (Figure 5B). Interestingly, 17 of the 25 enriched biological

processes were related to inflammation, including inflammatory response, cytokine-mediated signaling, response to chemokine leukocyte migration, and leukocyte chemotaxis. In addition, the GO analysis of the top 20 most upregulated genes by the siSOX13 treatment, regardless of the shear conditions, revealed the predominant enrichment of immune cell infiltration processes, including migration and chemotaxis of monocytes and T-cells (Figure 5C). These results strongly suggest that the reduction of SOX13 by either

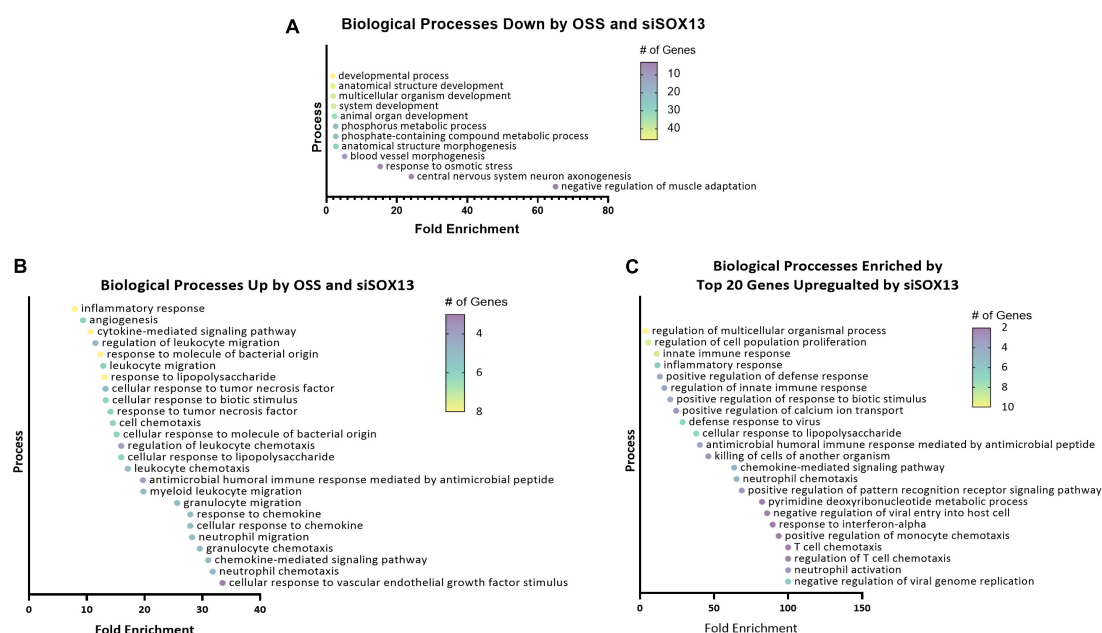


FIGURE 5

Gene ontology analysis of shear-dependent and SOX13-dependent genes. Biological processes enriched by the 94 commonly downregulated genes by OSS or siSOX13 in ULS condition (A), the 40 commonly upregulated by OSS or by siSOX13 (B), and the top 20 genes upregulated by siSOX13 regardless of shear conditions (C) are shown. All biological processes listed were significant by *p*-value.

OSS or siSOX13 triggers a strong pro-inflammatory response, a d-flow-induced and pro-atherogenic pathway (49–53), by inducing the expression of cytokines and chemokines in ECs.

SOX13 regulates pro-inflammatory chemokine expression in endothelial cells

Our heat map and GO analyses (Figures 4, 5) showed that loss of SOX13 strongly induced pro-inflammatory chemokines and cytokines. To validate the results, we conducted a qPCR analysis on 10 of the most interesting potential targets identified from the analyses, using SOX13 and AQP1 as positive controls (Figure 6A). We found that treatment with siSOX13 under the ULS condition induced expression of CXCL1, CXCL6, CXCL8 (IL8), CXCL10, IL6, CCL2 (MCP1), CCL5, and CSF3 in HAECs. Interestingly, CCL5 and CXCL10 mRNAs were two of the most dramatically upregulated chemokines by siSOX13.

Although CCL5 and CXCL10 expression did not change significantly in HAECs in response to LSS or OSS for a 24 h period, *in vitro*, they rapidly responded to SOX13 knockdown. Upon analysis of our scRNAseq and gene array data, both CCL5 and CXCL10 expression increase dramatically at the longer term, 2 week time point (Supplementary Figure 1). Flow-dependent expression does not occur *in vivo* in the 2 day

and shorter time points, consistent with the short-term 24 h *in vitro* shear results.

To further validate chemokine expression due to SOX13 knockdown, we measured CCL5 and CXCL10 protein levels by ELISA in the conditioned media (CM). Under both the static and shear conditions, siSOX13 treatment dramatically induced the expression of CCL5 and CXCL10 compared to siCtrl, further confirming the SOX13 knockdown effect on these chemokines (Figures 6B–E).

Next, we tested whether overexpression of SOX13 can prevent pro-inflammatory gene expression. Transfection with SOX13 overexpression plasmid in HAECs induced SOX13 and AQP1 mRNA expression as expected (Figures 7A–C). We found that SOX13 overexpression decreased the expression of the chemokines and cytokines, including CCL5 and CXCL10 (Figure 7C). We further validated that the protein levels of CCL5 and CXCL10 were decreased in the CM by SOX13 overexpression compared to the RFP control (Figures 7D,E). Together, these results demonstrated that SOX13 knockdown strongly induced, while overexpression reduced cytokine and chemokine expression in HAECs.

SOX13 knockdown increases endothelial inflammation via CCL5

To functionally test the SOX13 effect on EC inflammation, we performed THP1 monocyte adhesion assays using HAECs

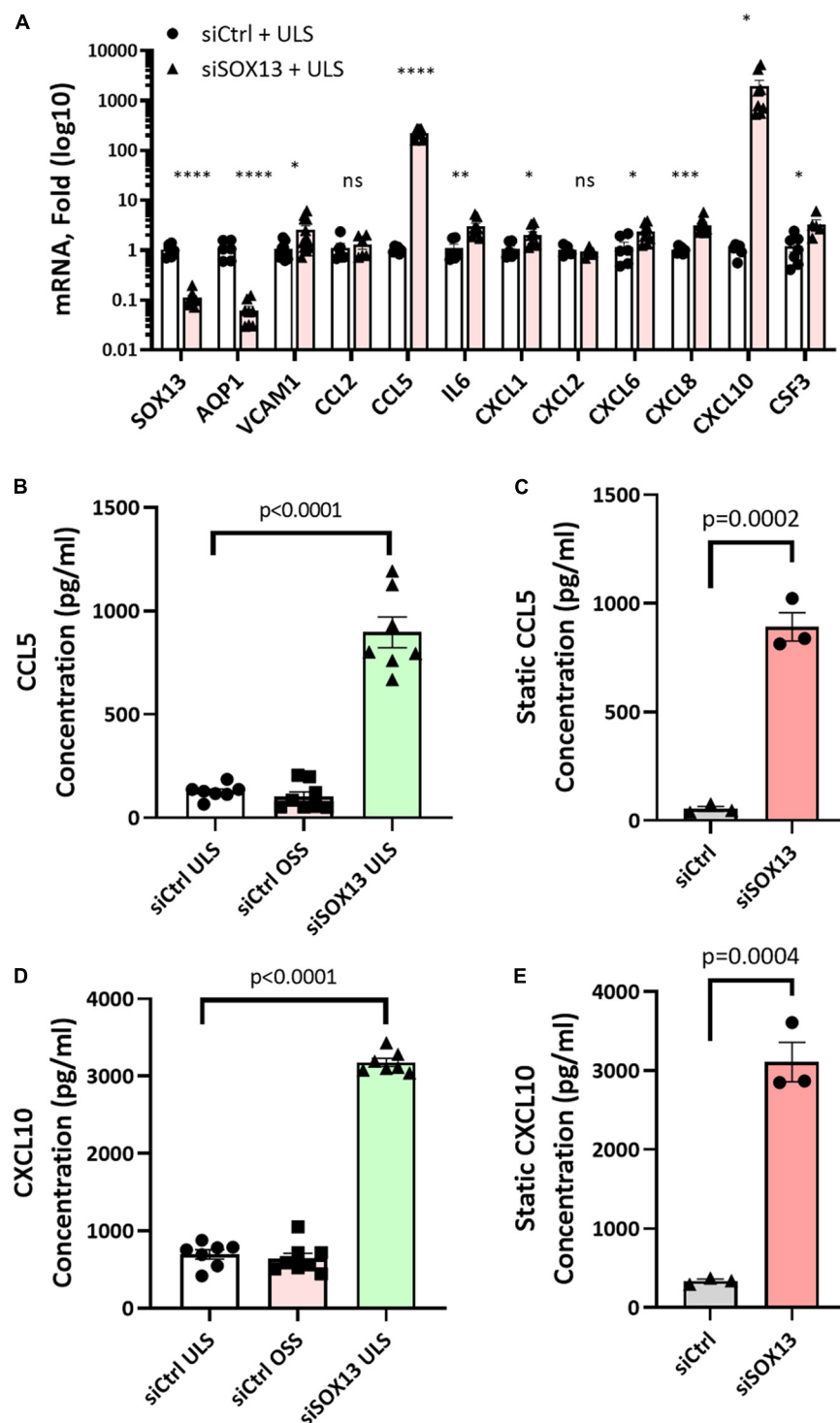


FIGURE 6

Validation of SOX13 targets by qPCR and ELISA. HAECs treated with siSOX13 or siCtrl for 24 h were exposed to OSS or ULS for another 24 h, and total RNAs were analyzed by RNAseq to validate the top SOX13-dependent targets (A) $n = 4-7$, Mean \pm SEM are shown. * $p \leq 0.05$, ** $p \leq 0.01$, *** $p \leq 0.001$, and **** $p \leq 0.0001$ as determined by student's t -test. The conditioned media from HAECs treated with siSOX13 and shear (B,D) or static (C,E) conditions were analyzed by ELISA quantification of CCL5 (B,C) or CXCL10 (D,E). Mean \pm SEM are shown, p -values determined by student's t -test.

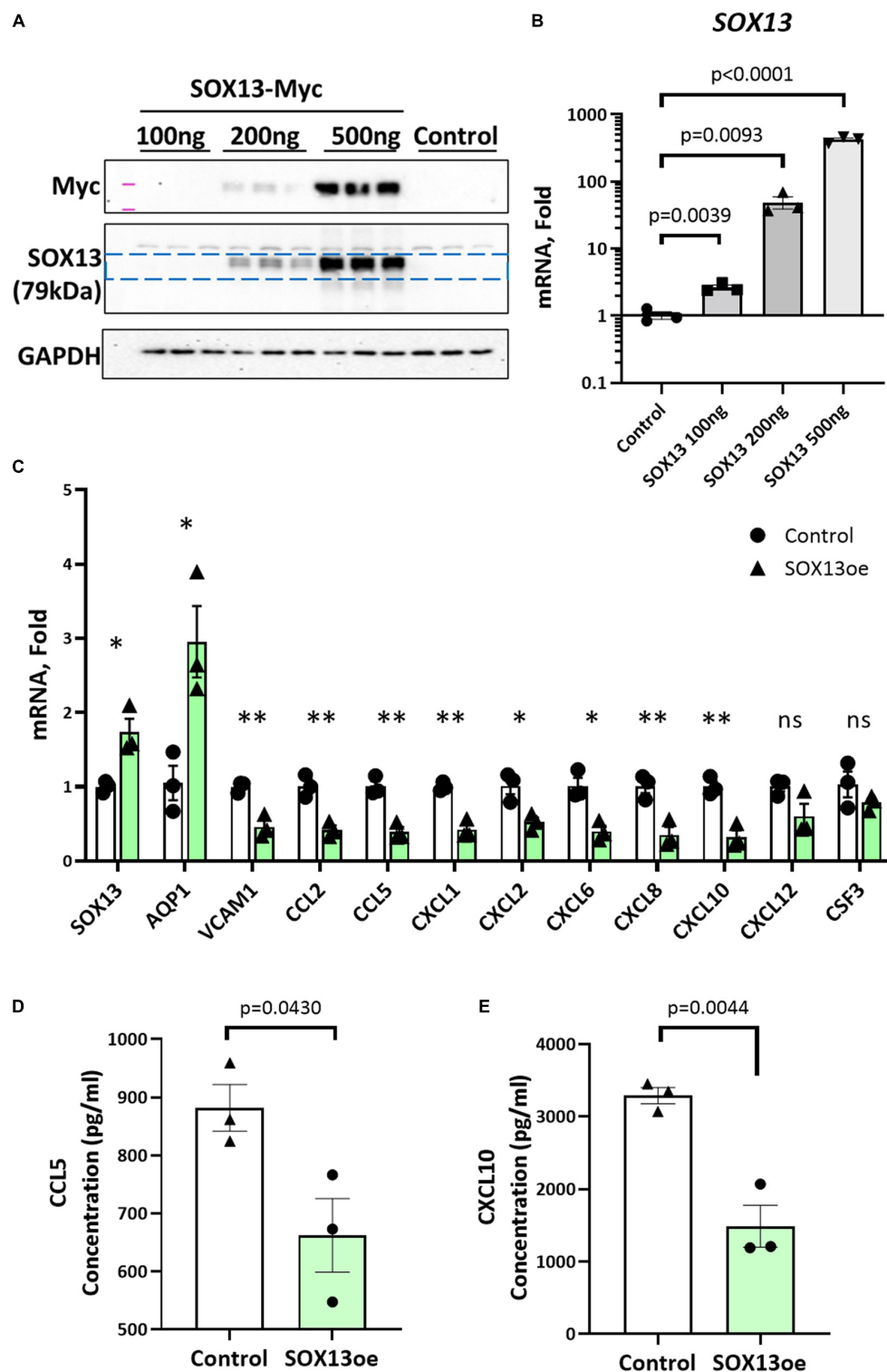


FIGURE 7

SOX13 plasmid overexpression reduces inflammatory markers and chemokine expression. (A) Western blot of whole cell lysate and (B) qPCR of SOX13 plasmid concentration curve in static HAECs after 48h compared to GFP control plasmid. (C) qPCR analysis of SOX13 targets following 48 h static SOX13 or GFP control overexpression in HAECs at a concentration of 200 ng, using SOX13 and AQP1 as positive controls. $n = 3$, Mean \pm SEM are shown. * $p \leq 0.05$, ** $p \leq 0.01$ as determined by student's t -test. (D) ELISA quantification of CCL5 and (E) CXCL10 in the conditioned media from static HAECs, 48 h following SOX13 or control plasmid transfection. Mean \pm SEM are shown, $n = 3$, p -values determined by student's t -test.

treated with siSOX13, SOX13 overexpression, and shear. First, we found that overexpression of SOX13 reduced the OSS-dependent increase in monocyte adhesion to HAECs (**Figure 8A**), demonstrating the role of SOX13 in the OSS condition. Next, we found that siSOX13 increased monocyte adhesion to HAECs under the ULS condition (**Figure 8B**). Since CCL5 was the most strongly induced chemokine by siSOX13, we used the specific CCL5 antagonist MetCCL5 to test if it can prevent siSOX13-induced monocyte adhesion. First, MetCCL5 was added to the media during ULS exposure for 1 day to inhibit CCL5 acting on ECs. Following the shear, monocytes were added to the CM, containing any residual amount of MetCCL5 following the 24h shear, and the number of adhered monocytes was quantified. In this condition, MetCCL5 treatment prevented monocyte adhesion to HAECs induced by siSOX13 in the ULS condition (**Figure 8C**). MetCCL5 serves as a specific CCL5 antagonist by binding to the CCL5 receptor on monocytes, leading to inhibition of atherosclerosis in mouse models (54, 55), but its effect on ECs is unknown. Therefore, we tested whether the inhibitory effect of MetCCL5 on monocyte adhesion (**Figure 8C**) was mediated at the level of ECs. To this end, we added MetCCL5 to the HAECs during ULS for 1 day. Then the CM was removed, HAECs were washed and replaced with fresh media containing THP1 monocytes, and adhered monocytes were counted. MetCCL5 still prevented monocyte adhesion to HAECs treated with siSOX13 and ULS (**Figure 8D**). These results suggest that SOX13 knockdown induced chemokine expression, including CCL5, which increased monocyte adhesion to ECs. Our results show that MetCCL5 prevented monocyte adhesion to HAECs by directly blocking the CCL5 effect on HAECs.

Discussion

Here, we identified novel FSTFs, including SOX13, in mouse artery ECs by re-analyzing the *in vivo* gene array, scRNAseq, and scATACseq datasets and validated them in HAECs *in vitro*. We further showed that SOX13 is induced by s-flow or ULS and decreased by d-flow or OSS. While the SOX13 knockdown dramatically induced expression of pro-inflammatory cytokines and chemokines, including CCL5 and CXCL10, SOX13 overexpression caused anti-inflammatory responses. Importantly, the CCL5 antagonist MetCCL5 prevented monocyte adhesion induced by SOX13 knockdown under shear conditions. These results reveal that SOX13, induced by s-flow but reduced by d-flow, is a potent anti-inflammatory FSTF, which represses pro-inflammatory chemokine and cytokine expression in ECs.

Several FSTFs, including KLF2/4, have been previously identified in cultured ECs, including human umbilical vein ECs (HUVECs). While these FSTFs have been critical to understanding flow-sensitive gene regulation, endothelial

function, and vascular pathophysiology, some FSTFs may have not been identified because they were lost or dysregulated in ECs under *in vitro* culture. It was estimated that approximately 45% of all flow-sensitive genes are dysregulated or lost in cultured ECs compared to *in vivo* ECs (17, 56, 57). It is possible that those lost or dysregulated genes during culture are highly flow-sensitive ones, including FSTFs. Therefore, we hypothesized that we could discover novel FSTFs by examining *in vivo* gene array and scRNAseq datasets obtained from our PCL studies. Indeed, our present study revealed 12 FSTFs *in vivo*. We determined that 8 of these mouse FSTFs (*KLF2*, *KLF4*, *SOX4*, *ZBTB46*, *SOX13*, *SIX2*, *NFIL3*, and *CEBPβ*) were conserved in human ECs (HAECs) and showed consistent flow-sensitivity. *KLF2/4* are best characterized FSTFs (14, 43), while *SOX4* and *ZBTB46* were also reported as FSTFs (44, 45), confirming the validity of our approach. *SOX13*, *SIX2*, *NFIL3*, and *CEBPβ* are potentially novel FSTFs identified in this study. Interestingly, our scRNAseq data analysis showed that *SOX13* is preferentially expressed in ECs but not in other arterial wall cell types (smooth muscle cells, immune cells, and fibroblasts). Further, our scATACseq analysis showed that chromatin accessibility of the *SOX13* gene, including the promoter region, was highly accessible (indicating a high gene transcriptional activity) under the s-flow condition compared to the d-flow condition in mouse carotid arteries *in vivo*. This indicates that flow regulates *SOX13* at the transcriptional level. At the protein level, *SOX13* protein is found predominantly in the nucleus. *In vivo*, *Sox13* immunofluorescence staining indicates higher intensity in the s-flow-exposed greater curvature of the aortic arch compared to the d-flow-exposed lesser curvature. Also, *SOX13* function in flow-dependent endothelial biology was unknown. Based on these, we decided to characterize the role of *SOX13* as a novel FSTF.

SOX13 plays an important role in arterial development, T-cell differentiation, and cell fate determination (33, 40, 58). Dysregulation of *SOX13* is involved in cancer development (35, 38, 59–61), but its role in atherosclerosis and flow-dependent function in adult ECs was unknown. *SOX13* can act as a TF that directly binds to its DNA binding motif (47) or as a cofactor binding to other TFs such as T-Cell Factor1 (TCF1) to indirectly regulate gene transcription (53). To determine how *SOX13* induced by ULS regulates endothelial function, we performed the RNAseq study in HAECs treated with siSOX13 under the ULS condition compared to the OSS condition. From the study, we identified two distinct classes of *SOX13* target genes: (1) 40 OSS-induced genes that were also upregulated by siSOX13 in the ULS condition (**Figure 4H**) and (2) 94 downregulated genes by OSS or siSOX13 (**Figure 4G**). Interestingly, the 40 OSS- or siSOX13-induced genes (including cytokines and chemokines) lacked the *SOX13* DNA binding motifs, whereas 70 of the 94 downregulated genes (including developmental genes and the known target *AQP1*) (39, 48, 62–64) contained the *SOX13* binding motifs as determined by a MEME motif analysis (65)

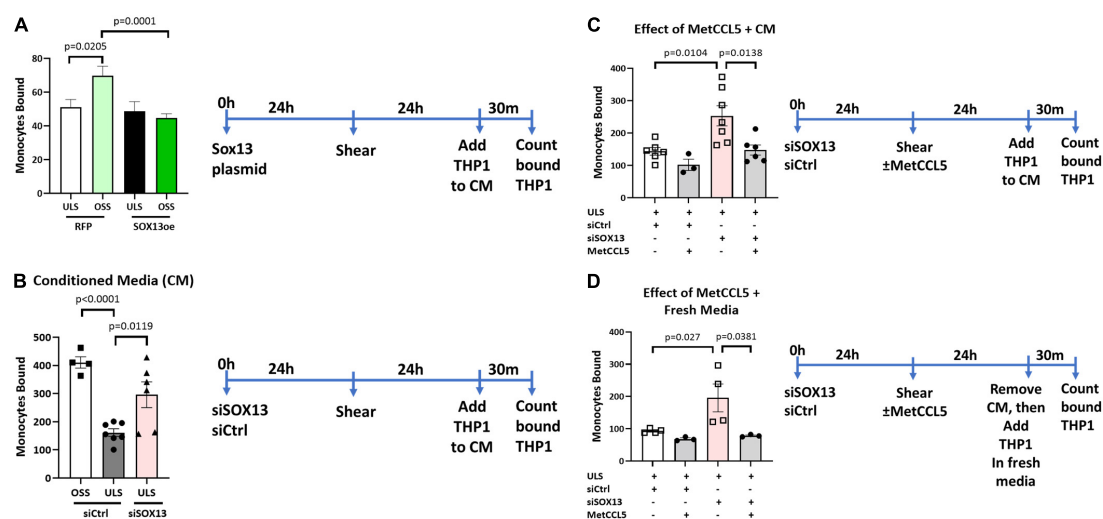


FIGURE 8

Monocyte adhesion induced by siSOX13 is prevented by treating HAEs with MetCCL5. **(A)** HAEs overexpressing SOX13 or RFP control were exposed to OSS or ULS for another 24 h. Following shear, THP1 monocytes were added to the conditioned media (CM), and adhered monocytes were counted. **(B)** HAEs treated with siSOX13 or siCtrl were exposed to OSS or ULS for another 24 h. Following shear, THP1 monocytes were added to the CM, and adhered monocytes were counted. **(C,D)** HAEs treated with siSOX13 or siCtrl were exposed to OSS or ULS in the presence or absence of MetCCL5 for another 24 h. Following shear, THP1 monocytes were added to the CM, and adhered monocytes were counted. **(C)** In panel **(D)**, following shear, CM was removed, HAEs were washed with fresh medium, THP1 monocytes were added to the CM, and adhered monocytes were counted. Mean \pm SEM are shown, $n = 3$ to 7, p -values determined by one-way ANOVA.

and comparison to a SOX13 ChIPseq dataset (46). These results suggest that SOX13 regulates its gene targets through direct and indirect mechanisms.

It was particularly interesting that many of the 40 OSS- and siSOX13-induced genes were pro-inflammatory cytokines and chemokines, a novel finding with a potential therapeutic implication. Of those, we validated the dramatic upregulation of CCL5 and CXCL10 by qPCR and ELISA induced by siSOX13 in the ULS condition. In contrast, SOX13 overexpression significantly reduced the expression of CCL5 and CXCL10 mRNA and protein. CCL5 (C-C motif ligand 5, also known as RANTES) and CXCL10 (C-X-C motif chemokine ligand 10) are two well-known cytokines that promote monocyte recruitment and macrophage maturation to atherosclerotic plaques (66–69). Increased serum levels of CCL5 and CXCL10 are associated with human atherosclerotic plaque progression and stability, and the inhibition of either cytokine reduced atherosclerosis in animal models (70, 71).

CXCL10 is a specific T-cell effector and is important in recruiting T-cells to atherosclerotic lesions (70). Interestingly, treatment with CXCL10 neutralizing antibody reduced the size and stability of atherosclerotic plaques in the carotid cuff model of atherosclerosis in ApoE^{-/-} mice (70). CCL5 is found on EC surfaces deposited by activated platelets and produced by other arterial cells, such as smooth muscle cells and macrophages, but the role of ECs as a source of CCL5 is unclear (71). CCL5 recruits monocytes to inflamed endothelium in early atherosclerotic lesions (71). The CCL5

antagonist MetCCL5 inhibits monocyte binding to ECs and reduces mouse atherosclerotic plaque development (54, 55, 72). These literatures demonstrate that both CXCL10 and CCL5 play critical roles in atherosclerosis development, and their inhibition is an effective anti-atherogenic approach.

The present study demonstrated that CXCL10 and CCL5 are regulated by shear stress in a SOX13-dependent manner and that Sox13 appears to play a dominant repressor role in flow-dependent chemokine expression. Our scRNAseq data analysis showed that CCL5 and CXCL10 expression was upregulated in a time-dependent manner by d-flow. CCL5 expression was increased by 2- and 15-fold at 2 days (E5 vs. E2) and 2 weeks (E8 vs. E2) post-PCL, respectively (Supplementary Figure 1A). CXCL10 expression was increased only in the 2-week, but not in 2-day, post-PCL time point by 3.5-fold (Supplementary Figure 1B). In addition, the gene array data analysis showed a similar chronic flow-dependent response with a significant increase only at the 2-week post-PCL time point, increasing 24-fold for CCL5 and 19-fold for CXCL10 expression, but no significant change at 12, 24, and 48 h time points (Supplementary Figures 1C,D). The mechanism for this relatively slow, chronic d-flow-dependent induction of these cytokines is unclear, but may be related to a gradual loss of SOX13 over time below a threshold level, contributing to an overall endothelial cellular status change. In support of this notion, we recently showed that chronic d-flow induces endothelial reprogramming, including endothelial to mesenchymal transition (EndMT) and endothelial to immune

TABLE 1 Mouse qPCR primer sequences.

Mouse gene	Forward sequence	Reverse sequence
m_Ahr	CTGGTTGTACAGCAGATGCCT	CGGTCTTCTGTATGGATGAGCTC
m_Akna	AGGACCTGTCTCCTTGCCAGAT	GAGACCTCTTGGGCTTTCCTCA
m_Atoh8	CAACGGAGATCAAAGCCCTGCA	CTTCTGCCCATAGGAGTAGCAC
m_Cebpa	GCAAAGCCAAGAAGTCGGTGGA	CCTTCTGTTCGGTCTCCACGTT
m_Cebpb	CAACCTGGAGACGCAGCACAAG	GCTTGAACAAGTTCCGCAGGGT
m_Creb3l1	AGCCTTGTGCTTCGTTCTGGTG	CATCGTAGAACAGTAGGCTTCGG
m_Etv5	GCAGGAATACCATGACCCACTG	AGGATGACTGGCAGTTAGGCAC
m_Fos	GGGAATGGTGAAGACCGTGTC	GCAGCCATCTTATTCGGTTCCC
m_Fosb	ACCTGTCTTCGGTGGACTCCTT	TGGCTGGTTGTGATTGCGGTGA
m_Fosl2	AGGAGGAGAAGCGTCGAATCCG	CCAGACTTCTCCTCTTCCAGCT
m_Foxq1	CAACGAGTACCTCATGGCAAG	GCATCCAGTAGTTGTCTTGCC
m_Glis3	GGACCCATTTCACCTCCAGCAA	CAAAGTCGTGGACACCAGAGAC
m_Hey1	CCAACGACATCGTCCCAGGTTT	CTGCTTCTCAAAGGCACTGGGT
m_Klf12	CCTTTCATAGCCAGAGCAGTAC	TGGCGTCTGTGCTCTCAATGC
m_Klf15	ACACCAAGAGCAGCCACCTCAA	GCCTTGACAACTCATCTGAGCG
m_Klf2	CACCTAAAGGCGCATCTGCGTA	GTGACCTGTGTGCTTTCGGTAG
m_Klf4	CTATGCAGGCTGTGGCAAAACC	TTGCGGTAGTGCCTGGTCAGTT
m_Maf	AGGAGGTGATCCGACTGAAGCA	TCTCTGCTTGAGGTGGTCTAC
m_Maff	ACCTGTCCGATGAAGCGTGAT	TAGCCGCGGTCTTGAGTGTGC
m_Nfil3	CAGGACTACCAGACATCCAAGG	AGGACACCTCTGACATACGGA
m_Runx2	CCTGAACCTGCACCAAGTCCT	TCATCTGGCTCAGATAGGAGGG
m_Six1	AGGTCAGCAACTGGTTTAAAGAACC	GAGTTGATTCTGCTTGTGGAGG
m_Six2	CACGCAAGTCAGCAACTGGTTC	ACTTGCCACTGCCATTGAGCGA
m_Sox13	CCTATTAGCCCATTCCTGCA	CTTGCTGTGAGGTTCACTGGT
m_Sox4	GATCTCCAAGCGGTAGGCAAA	GTAGTCAGCCATGTGCTTGAGG
m_Sox8	CGCATCTCCATAACGCAGAGCT	TCTTCCTTCGCCTTGGCTGGTA
m_Tcf23	GCTGGAGCAATCACAGACTGAG	TGACGAAGCGTCTTCACCCGAG
m_Tgfr1	CAGATTCTGCGAGACTGGCTGT	CGGGCGTTGATGAACCAGTTAC
m_Zbtb46	CACCGTCACTCACTTGGACA	GCAGCTGACATCACCTCGAT
m_Zbtb7c	GAGAAGCCGTACATGTGCAGCA	CACGAACTTGGCGTTGCAGTGA

cell-like transition (EndICLT), taking 2 weeks post-PCL (13). Interestingly, we found that *CCL5* and *CXCL10* expression did not show a significant flow-dependent response in HAECs by LSS or OSS conducted over a 24 h period. However, *CCL5* and *CXCL10* expression was dramatically induced if SOX13 was knockdown by siSOX13. The lack of flow sensitivity of the *CCL5* and *CXCL10* in the short-term *in vitro* experiment agrees with the *in vivo* data (Supplementary Figure 1). Due to a technical limitation of exposing HAECs to shear *in vitro* for 2 weeks, for an extended period, we did not test the shear response of *CCL5* and *CXCL10* under a similar chronic condition. Taken together, we propose that d-flow gradually reduces SOX13 expression over time below a threshold level, triggering strong *CCL5* and *CXCL10* expression through an indirect mechanism in ECs. Interestingly, neither *CCL5* nor *CXCL10* contains the SOX13 DNA binding motif in the promoter regions. Therefore, we hypothesize that SOX13 plays a dominant repressor role. Even relatively small amounts of SOX13 may bind to another

TF, such as NF- κ B, preventing its binding and activation of *CCL5* transcription. However, under the d-flow or SOX13 knockdown conditions, the SOX13-bound TF such as NF- κ B could be released from SOX13 and bind to the *CCL5* promoter, increasing its transcription. Interestingly, *CCL5* and *CXCL10* are known transcriptional targets of NF- κ B family members (73). It would be interesting to test whether the loss of SOX13 would activate the NF- κ B pathway leading to chemokine induction.

We showed that loss of SOX13 induced monocyte adhesion to ECs in the *CCL5*-dependent manner. We found that siSOX13 dramatically induced *CCL5* protein release by HAECs, even under ULS conditions, as measured by ELISA in the conditioned media. The *CCL5* antagonist, MetCCL5, is known to bind to the *CCL5* receptors on monocytes, preventing its activation (55). Our study tested if MetCCL5 could inhibit monocyte adhesion by blocking the *CCL5* receptors on HAECs (Figure 8). Our result suggests that not only monocytes but also ECs mediate the

anti-inflammatory effect, a key anti-atherogenic mechanism, of MetCCL5.

In conclusion, we found several novel FSTFs from *in vivo* mouse artery ECs that are conserved in cultured human aortic ECs. Of these, we show that SOX13 is increased under *s-flow* conditions, repressing the expression of pro-inflammatory cytokines CCL5 and CXCL10. Loss of SOX13 by *d-flow* or siRNA induces endothelial inflammation by increasing CCL5 and CXCL10 expression, and MetCCL5 prevents the pro-inflammatory effects. SOX13, CCL5, and CXCL10 are potential atherogenic therapeutic targets.

Materials and methods

Mice and partial carotid ligation surgery

Eight-week-old C57Bl/6 male mice (Jackson lab) were maintained and cared for in accordance with the National Institutes of Health (NIH) guidelines in our AAALAC-accredited experimental animal facility at Emory University under a controlled environment ($21 \pm 2^\circ\text{C}$, $50 \pm 10\%$ relative humidity, and a 12 h light: 12 h dark cycle with lights on at 0700h EST). All mouse studies were approved by the Institutional Animal Care and Use Committee at Emory University and were in accordance with the established guidelines and regulations consistent with federal assurance. PCL surgery was performed under anesthesia by ligating 3 of 4 caudal branches of LCA (left external carotid, internal carotid, and occipital artery) using 6–0 silk suture, leaving the superior thyroid artery patent. The presence of low and oscillatory shear was confirmed by ultrasonography as we previously described (32, 74).

In vivo gene array dataset, single-cell RNA sequencing, and single-cell assay for transposase-accessible chromatin with high-throughput sequencing datasets using the mouse partial carotid ligation study

The gene array data (GSE182291) used in this study was previously reported by us (12). Briefly, endothelial-enriched RNAs obtained from the LCAs and RCAs, following the PCL surgery at 12 h, 24 h, 48 h, and 2 weeks were subjected to whole-genome microarray analysis using the Affymetrix HT_MG-430_PM. For this study, 10 week-old male C57/BL6 mice from Jackson Lab ($n = 5$ each) were used.

The scRNAseq data set (Bioproject # PRJNA646233) and scATACseq data set (Bioproject # PRJNA646233) used in this study were previously reported by us (13). Briefly, intraluminally

obtained single cells or single nuclei obtained from the LCAs and RCAs, following PCL at 2 days or 2 weeks, were used for scRNAseq and scATACseq. For this study, 10-week-old male C57/BL6 mice from Jackson Lab ($n = 10$ each for scRNAseq and $n = 12$ each for scATACseq) were used. The sequencing results were analyzed for gene expression analysis by violin plot and chromatin accessibility assay at the genes of interest using the R-packages as we described (13). Gene ontology analysis and functional pathway analysis Gene ontology analysis was performed using PANTHER.

Human aortic endothelial cells

Human aortic endothelial cells obtained from (Cell Applications Lot#: 2463) were cultured in a complete medium (MCDB 131, 10% FBS, 1% Pen-Strep, 1% L-glutamine, 1% ECGS, 15 ng/mL IGF-1, 1 mg/mL hydrocortisone, 50 mg/mL ascorbic acid, 5 ng/mL VEGF, 5 ng/mL EGF, 5 ng/mL FGF) (13, 75). The medium was refreshed every 3 days and cells were used through passage 7.

Cone and plate viscometer

For *in vitro* flow experiments, we exposed confluent cells to steady unidirectional flow (*s-flow*, 15 dyn/cm²) or bidirectional oscillatory flow (*d-flow*, $+5/-4$ dyn/cm² at 1 Hz) to mimic *in vivo* flow profiles using the cone-and-plate viscometer for 24- or 48-h experiments (75). In brief, a cone controlled by a stepping motor is placed in a standard 10 cm tissue culture dish containing confluent HAEC monolayer. The cone was rotated unidirectionally or bidirectionally at different velocities to generate *s-flow* and *d-flow* conditions, respectively. Under these conditions, *s-flow* induces anti-inflammatory KLF2 (Krüppel-like factor 2) expression and *d-flow* generates inflammatory signaling at levels resembling those observed *in vivo* (76–78).

RNA extraction from cells for quantitative RT-PCR and RNAseq

For RNA collection, cells were lysed with Qiazol and total RNA was purified using the Qiagen miREasy kit (74004) or Zymo Direct-zol Miniprep kit (R2052) (13, 75). RNA was quantified by Nanodrop and was reverse transcribed for use in a two-step qRT-PCR using the High-Capacity cDNA Reverse Transcription Kit (Applied Biosystems 4368814).

RNAseq data analyses

For RNAseq, HAECs were collected in Qiazol lysis reagent and processed for RNA isolation using miRNeasy Mini Kit

TABLE 2 Human qPCR primer sequences.

Gene	Forward sequence	Reverse sequence
AHR	GTCGTCTAAGGTGTCTGCTGGA	CGCAAACAAAGCCAACTGAGGTG
AKNA	CTCTGGCAACAGTGAGGTGGAG	GGAGAGACTTCACACTGAGGTAC
AQP1	TATGCGTGCTGGCTACTACCGA	GGTTAATCCCACAGCCAGTGTAG
ATOH8	AGCCTTCGAGGCGCTCAGGAA	TCGGCACTGTAGTCAAGGTCAG
BTG2	GCAGAGGCTTAAGGTCTTCAGC	TGGTTGATGCGAATGCAGCGGT
CCL5	CCTGCTGCTTTGCCACATTGC	ACACACTTGGCGGTTCTTTCCG
CEBPA	AGGAGGATGAAGCCAAGCAGCT	AGTGCGCGATCTGGAAGTGCAG
CEBPβ	AGAAGACCGTGGACAAGCACAG	CTCCAGGACCTTTGTGCTGCGT
CREB3L1	GCCTTGCTGCTTTGTTCTGGTGC	CCGTCACTCGTAGAATAGGAGGC
CSF3	AAGGTCGTGCTGGCATTCTG	AGCTGTGATCAGTGGTTGGG
CX3CL1	ACAGCACCGGTGTGACGAAA	AACAGCCTGTGCTGTCTCGTCT
CXCL1	AGCTTGCCCTCAATCCTGCATCC	TCCTTCAGGAACGCCACCAGT
CXCL10	GGTGAGAAGAGATGTCTGAATCC	GTCCATCCTTGAAGCACTGCA
CXCL11	AGCAGTGAAAGTGGCAGAT	TTGGGATTTAGGCATCGT
CXCL2	CATCGAAAAGATGCTGAAAAATG	TTCAGGAACAGCCACCAATA
CXCL3	AAAATCATCGAAAAGATACTGAACAAG	GTAAGGGCAGGGACCAC
CXCL6	GGGAAGCAAGTTTGCTGGACC	AAACTGCTCCGCTGAAGACTGG
CXCL8/ IL8	GAGAGTGATTGAGAGTGGAACAC	CACAACCCCTCTGCACCCAGTTT
DHX58	ATGACCACCTGGAGATGCCTGA	CATTGTAGCGCCTCAGGTGAAG
EMCN	GCAAGCACTTCAGCAACCAGCC	GGATCTGCCTTCCAGCACATTC
ETV5	GTGTTGTGCCTGAGAGACTGGA	CGACCTGTCCAGGCAATGAAGT
FAM107A	GCTCATCAAGCCCAAGAAGCTG	TCTGGCTTGCTGTCCACACCAA
FOS	GCCTCTCTTACTACCACTCACC	AGATGGCAGTGACCGTGGAAT
FOSB	TCTGTCTTCGGTGGACTCCTTC	GTTGCACAAGCCACTGGAGGTC
FOSL2	AAGAGGAGGAGAAGCGTCGCAT	GCTCAGCAATCTCCTTCTGCAG
FOXQ1	CCTACTCGTACATCGCGTCCAT	TCGTTGAGCGAAAAGGTTGTGGC
GLIS3	AAGCCAGGTCTCTACAGCATGC	ACTCAAGGTCTGTGGACGCCAAA
HEY1	TGTCTGAGCTGAGAAGGCTGGT	TTCAGGTGATCCACGGTCATCTG
HLA-F	GCTGCTGTGATGTGGAGGAAGA	GTATGTTCTGTGAGGCACAAGTGC
IFI35	CACGATCAACATGGAGGAGTGC	GGCAGGAAATCCAGTGACCAAC
IFI6	TGATGAGCTGGTCTGCGATCCT	GTAGCCCATCAGGGCACCATA
IFIT3	CCTGGAATGCTTACGGCAAGCT	GAGCATCTGAGAGTCTGCCCAA
IFITM1	GGCTTCATAGCATTTCGCTACTC	AGATGTTCAAGGCACTTGCGCGT
IL1β	CCACAGACCTTCCAGGAGAATG	GTGCAGTTCAAGTATCGTACAGG
IL3	CTTCGAAGGCCAAACCTGGA	ATGGATTGGATGTGCGGTGG
ISG20	ACACGTCCACTGACAGGCTGTT	ATCTTCCACCGAGCTGTGTCCA
KLF12	CCTTTCCATAGCCAGAGCAGTAC	CTGGCGTCTTGTGCTCTCAATAC
KLF15	GTGAGAAGCCCTTCGCCTGCA	ACAGGACACTGGTACGGCTTCA
KLF2	ATGACCACCAACCATTGCAC	ACACCTCTCAGCTGTTTCCA
KLF4	CATCTCAAGGCACACCTGCGAA	TCGGTCGCATTTTGGCACTGG
Lpar1	GGCTATGTTTCGCCAGAGGACTA	GGAGTCCAGCAGATGATAAAGGC
MAF	AGAAGTTGGTGAGCAGCGGCTT	CACTGATGGCTCCAACCTGCGA
MAFF	CTGTGCGACGAGGCGCTGATG	AGCCACGGTTTTTGTAGTGTGCG
Map4k4	CAACATCTCGCTCCCCTGTT	CCTGGGCTCAATACTGGTGG
MCP1/ CCL2	AGAATCACCAGCAGCAAGTGTCC	TCCTGAACCCACTTCTGCTTGG
MFAP5	GGGTCAATAGTCAACGAGGAGAC	GCCAAGTCATCTGTGGAAGGTG
MX2	AAAAGCAGCCCTGTGAGGCATG	GTGATCTCCAGGCTGATGAGCT
NFIL3	TGGAGAAGACGAGCAACAGGTC	CTTGTGTGGCAAGGCAGAGGAA
OASL	GTGCCTGAAACAGGACTGTTGC	CCTCTGCTCCACTGTCAAGTGG

(Continued)

TABLE 2 (Continued)

Gene	Forward sequence	Reverse sequence
PTGS2	CGGTGAAACTCTGGCTAGACAG	GCAAACCGTAGATGCTCAGGGA
SIX1	AGGTCAGCAACTGGTTAAGAACC	GAGGAGAGAGTTGGTTCTGCTTG
SIX2	CACACAGGTCAGCAACTGGTTC	TCATCCTCCGAGCTGCCTAACA
SOX13	CCGAAACAGCAGCCACATCAAG	CTGCTTCTCCTGGTTGGTCATG
SOX4	GACATGCACAACGCCGAGATCT	GTAGTCAGCCATGTGCTTGAGG
SOX8	GACCAGTACCCGCACCTG	GCTTCTCGCTCTCGCTCA
TCF23	CCTCCTCAGGCACTGTGTTT	CTCTGGCCTTCTCTGTGAC
TCF7L2	GAATCGTCCCAGAGTGATGTCG	TGCACTCAGCTACGACCTTTGC
TGIF1	GGATTGGCTGTATGAGCACCGT	GCCATCCTTTCTCAGCATGTACG
TXNIP	CAGCAGTGCAAACAGACTTCGG	CTGAGGAAGCTCAAAGCCGAAC
ZBTB46	AGCAGGTGGAAGATGACAGCCG	TGCTGGCTTCGGTGACGACACA
ZBTB7C	GGAGAAGCCATACATGTGCACC	ACGAACCTGGCGTTGCAGTGGA

TABLE 3 Antibodies used for western blotting and immunostaining.

Antibody	Species	Cat. No.	Company	RRID	Concentration
GAPDH	Rabbit	sc-25778	Santa Cruz Technologies	RRID:AB_10167668	1:2500
Myc-tag	Mouse	2276S	Cell Signaling Technology	RRID:AB_331783	1:1000
SOX13	Rabbit	18902-1-AP	Proteintech	RRID:AB_10642149	1:500
Lamin A/C	Rabbit	2032S	Cell Signaling Technology	RRID:AB_2136278	1:500
α -Tubulin	Rabbit	2144S	Cell Signaling Technology	RRID:AB_2210548	1:1000

(Qiagen 217004). Following quality checks, library was prepared and RNA sequenced at Novogene ($n = 4$ per group). The data was processed with Partek and R package RSubread from Bioconductor, to identify differentially expressed genes, as described (79). Potential direct targets of SOX13 TF binding motifs were examined with USC Genome Browser and a MEME motif analysis (65) and comparison to a SOX13 ChIPseq dataset (46).

Quantitative RT-PCR for validation of mRNAs

Quantitative Real-time PCR (qPCR) was performed on selected genes using Brilliant II SYBR Green QPCR Master Mix (Stratagene) with custom-designed primers on a Real-Time PCR System (ABI StepOne Plus) (17). All qPCR results were normalized based on 18S RNA expression in the respective sample. Fold changes were determined using the $\Delta\Delta C_t$ method (80). Mouse qPCR primers are detailed in Table 1. Human primer sequences are detailed in Table 2.

Protein assay and western blotting

Cells were collected and lysed in RIPA buffer, and analyzed by western blot as we described (13, 75). Briefly,

protein concentration was determined with Pierce BCA assay, and Western blot was conducted using Immobilon Western Chemiluminescent HRP (EMD Millipore) and quantified using the Thermo Fisher iBright Imaging system. Nuclear and cytoplasmic fractionation was performed using HAEC lysates with NE-PER® Nuclear and Cytoplasmic Extraction Reagents (Thermo Fisher Scientific 78833) per the manufacturer's instruction. Antibodies used are listed in Table 3.

Treatment of human aortic endothelial cells with SOX13 siRNA, overexpression plasmid, or MetCCL5

For siRNA knockdown transfections, Oligofectamine (Thermo Fisher Scientific 12252011) was used as a transfection reagent as we reported (13). The siRNAs were purchased from Integrated DNA Technologies (hs.Ri.SOX13.13.1, hs.Ri.SOX13.13.2 and Negative control: 51-01-14-04). The two SOX13 dsRNA sequences were pooled and treated at a final concentration of 50nM to achieve a robust knockdown. For plasmid transfections, Lipofectamine 3000 (Thermo Fisher Scientific 15338030) was used as we reported (13). SOX13-myc-DDK-tagged (Origene RC210697) was used with a GFP- or RFP-(for monocyte adhesion assay) expressing plasmid with the same backbone as a control (pCMV backbone from Addgene #11153).

MetCCL5 (R&D 335-RM-025) was added to the fresh media at a concentration of 50ng/ml at the beginning of the 24 h shear exposure.

Monocyte adhesion assay

Monocyte binding was determined using THP-1 monocytes (ATCC TIB-202, [RRID:CVCL_0006](#)) as we reported (75). In brief, THP-1 cells (1.5×10^5 cells/mL) were labeled with a fluorescent dye 2-,7-bis(carboxyethyl)-5 (6)-carboxyfluorescein-AM (BCECF) (Thermo Fisher Scientific B1150; 1 mg/mL) in serum-free RPMI medium (Thermo Fisher Scientific 11875093) for 30 min at 37°C. After exposure to flow or transfection treatments, BCECF-loaded THP-1 cells were added directly to the ECs to the conditioned medium. In some studies, the CM was removed, HAECs were washed with fresh medium, before adding the THP1 cells. After a 30-min incubation at 37°C under no-flow conditions, unbound monocytes were removed by washing the endothelial dishes 2× with HBSS, and cells with bound monocytes were fixed with 4% Paraformaldehyde (Sigma Aldrich 47608) for 10 min. Bound monocytes were quantified by counting the cells under a fluorescent microscope.

Statistical analysis

Statistical analyses were performed using GraphPad Prism software. All of the n numbers represent biological replicates. Error bars depict the standard error of means (SEMs). The datasets were analyzed for normality using the Shapiro–Wilk test ($p < 0.05$) and equal variance using the *F*-test ($p > 0.05$). Data that followed a normal distribution and possessed equal variance were analyzed using a two-tailed Student *t*-test or one-way analysis of variance (ANOVA) where appropriate. The statistical analysis for scRNAseq differential gene expression analysis was performed using Partek Genomics Suite, GSA (Gene Specific Analysis) (13). This algorithm is a statistical modeling approach used to test for differential expression of genes or transcripts in Partek Flow. GSA can consider the following response distributions: Normal, Lognormal, Lognormal with shrinkage, Negative Binomial, Poisson, and ANOVA. Moreover, it also performs multivariate analysis to see which factors influence that gene.

Data availability statement

The datasets presented in this study can be found in online repositories. The names of the repository/repositories

and accession number GSE207087 can be found in the article/[Supplementary material](#).

Ethics statement

The animal study was reviewed and approved by the Emory University IACUC.

Author contributions

CD, SK, D-WK, and HJ conceptualized and planned the experiments. CD, JJ, AA, CP, YK, NV-R, SK, and D-WK performed the experiments. CD, AA, CP, YK, NV-R, and SK analyzed the results. CD and HJ wrote the first draft and edited the final manuscript with input from all authors. All authors approved the submitted version.

Funding

This work was supported by funding from the National Institutes of Health grants HL119798, HL139757, and HL151358 to HJ. HJ was also supported by Wallace H. Coulter Distinguished Faculty Professorship.

Conflict of interest

The authors declare that the research was conducted in the absence of any commercial or financial relationships that could be construed as a potential conflict of interest.

Publisher's note

All claims expressed in this article are solely those of the authors and do not necessarily represent those of their affiliated organizations, or those of the publisher, the editors and the reviewers. Any product that may be evaluated in this article, or claim that may be made by its manufacturer, is not guaranteed or endorsed by the publisher.

Supplementary material

The Supplementary Material for this article can be found online at: <https://www.frontiersin.org/articles/10.3389/fcvm.2022.979745/full#supplementary-material>

References

- Libby P. The changing landscape of atherosclerosis. *Nature*. (2021) 592:524–33.
- Gimbrone MA Jr., Garcia-Cardena G. Vascular endothelium, hemodynamics, and the pathobiology of atherosclerosis. *Cardiovascular Pathol.* (2013) 22:9–15.
- Sun L, Rajamannan NM, Sucusky P. Defining the role of fluid shear stress in the expression of early signaling markers for calcific aortic valve disease. *PLoS One*. (2013) 8:e84433. doi: 10.1371/journal.pone.0084433
- Malek AM, Alper SL, Izumo S. Hemodynamic shear stress and its role in atherosclerosis. *JAMA*. (1999) 282:2035–42.
- Davies PF, Dewey CF Jr., Bussolari SR, Gordon EJ, Gimbrone MA Jr. Influence of hemodynamic forces on vascular endothelial function. In vitro studies of shear stress and pinocytosis in bovine aortic cells. *J Clin Invest.* (1984) 73:1121–9. doi: 10.1172/JCI11298
- Texon M. The hemodynamic concept of atherosclerosis. *Bull N Y Acad Med.* (1960) 36:263–74.
- Ando J, Yamamoto K. Effects of shear stress and stretch on endothelial function. *Antioxid Redox Signal.* (2011) 15:1389–403.
- Dunn J, Simmons R, Thabet S, Jo H. The role of epigenetics in the endothelial cell shear stress response and atherosclerosis. *Int J Biochem Cell Biol.* (2015) 67:167–76.
- Kwak BR, Bäck M, Bochaton-Piallat M-L, Caligiuri G, Daemen MJAP, Davies PF, et al. Biomechanical factors in atherosclerosis: mechanisms and clinical implications†. *Eur Heart J.* (2014) 35:3013–20.
- Tarbell JM, Shi Z-D, Dunn J, Jo H. Fluid mechanics, arterial disease, and gene expression. *Annu. Rev. Fluid Mech.* (2014) 46:591–614.
- Demos CJ, Tamargo IA, Jo H. Biomechanical regulation of endothelial function in atherosclerosis. In: Ohayon J, Finet G, Pettigrew RI editors. *Biomechanics of Coronary Atherosclerotic Plaque*. (Cambridge, MA: Academic Press) (2020). p. 3–47.
- Kumar S, Sur S, Perez J, Demos C, Kang DW, Kim CW, et al. Atorvastatin and blood flow regulate expression of distinctive sets of genes in mouse carotid artery endothelium. *Curr Top Membr.* (2021) 87:97–130. doi: 10.1016/bs.ctm.2021.08.004
- Andueza A, Kumar S, Kim J, Kang D-W, Mumme HL, Perez JJ, et al. Endothelial reprogramming by disturbed flow revealed by single-cell RNA and chromatin accessibility study. *Cell Rep.* (2020) 33:108491. doi: 10.1016/j.celrep.2020.108491
- Sangwung P, Zhou G, Nayak L, Chan ER, Kumar S, Kang D-W, et al. KLF2 and KLF4 control endothelial identity and vascular integrity. *JCI Insight.* (2017) 2:e91700. doi: 10.1172/jci.insight.91700
- Simmons RD, Kumar S, Jo H. The role of endothelial mechanosensitive genes in atherosclerosis and omics approaches. *Arch Biochem Biophys.* (2016) 591:111–31. doi: 10.1016/j.abb.2015.11.005
- Dunn J, Qiu H, Kim S, Jingo D, Hoffman R, Kim CW, et al. Flow-dependent epigenetic DNA methylation regulates endothelial gene expression and atherosclerosis. *J Clin Invest.* (2014) 124:3187–99.
- Ni C-W, Qiu H, Rezvan A, Kwon K, Nam D, Son DJ, et al. Discovery of novel mechanosensitive genes in vivo using mouse carotid artery endothelium exposed to disturbed flow. *Blood*. (2010) 116:e66–73. doi: 10.1182/blood-2010-04-278192
- Chiu J-J, Chien S. Effects of disturbed flow on vascular endothelium: pathophysiological basis and clinical perspectives. *Physiol Rev.* (2011) 91:327–87. doi: 10.1152/physrev.00047.2009
- Boon RA, Horrevoets AJG. Key transcriptional regulators of the vasoprotective effects of shear stress. *Hamostaseologie.* (2009) 29:39–43.
- Dekker RJ, van Soest S, Fontijn RD, Salamanca S, de Groot PG, VanBavel E, et al. Prolonged fluid shear stress induces a distinct set of endothelial cell genes, most specifically lung Krüppel-like factor (KLF2). *Blood*. (2002) 100:1689–98. doi: 10.1182/blood-2002-01-0046
- Fledderus JO, van Thienen JV, Boon RA, Dekker RJ, Rohlena J, Volger OL, et al. Prolonged shear stress and KLF2 suppress constitutive proinflammatory transcription through inhibition of ATF2. *Blood*. (2007) 109:4249–57. doi: 10.1182/blood-2006-07-036020
- Lee JS, Yu Q, Shin JT, Sebza E, Bertozzi C, Chen M, et al. Klf2 is an essential regulator of vascular hemodynamic forces in vivo. *Dev Cell.* (2006) 11:845–57. doi: 10.1016/j.devcel.2006.09.006
- SenBanerjee S, Lin Z, Atkins GB, Greif DM, Rao RM, Kumar A, et al. KLF2 is a novel transcriptional regulator of endothelial proinflammatory activation. *J Exp Med.* (2004) 199:1305–15.
- Dekker RJ, Boon RA, Rondaij MG, Kragt A, Volger OL, Elderkamp YW, et al. KLF2 provokes a gene expression pattern that establishes functional quiescent differentiation of the endothelium. *Blood*. (2006) 107:4354–63. doi: 10.1182/blood-2005-08-3465
- Rausch V, Bostrom JR, Park J, Bravo IR, Feng Y, Hay DC, et al. The hippo pathway regulates caveolae expression and mediates flow response via caveolae. *Curr Biol.* (2019) 29:242–255.e6. doi: 10.1016/j.cub.2018.11.066
- Niu N, Xu S, Xu Y, Little PJ, Jin ZG. Targeting mechanosensitive transcription factors in atherosclerosis. *Trends Pharmacol Sci.* (2019) 40:253–66.
- Wang L, Luo J-Y, Li B, Tian XY, Chen L-J, Huang Y, et al. Integrin-YAP/TAZ-JNK cascade mediates atheroprotective effect of unidirectional shear flow. *Nature*. (2016) 540:579. doi: 10.1038/nature20602
- Wung BS, Cheng JJ, Hsieh HJ, Shyy YJ, Wang DL. Cyclic strain-induced monocyte chemotactic protein-1 gene expression in endothelial cells involves reactive oxygen species activation of activator protein 1. *Circ Res.* (1997) 81:1–7. doi: 10.1161/01.res.81.1.1
- Burke SJ, Lu D, Sparer TE, Masi T, Goff MR, Karlstad MD, et al. NF-κB and STAT1 control CXCL1 and CXCL2 gene transcription. *Am J Physiol Endocrinol Metab.* (2014) 306:E131–49. doi: 10.1152/ajpendo.00347.2013
- Topper JN, Gimbrone MA Jr. Blood flow and vascular gene expression: fluid shear stress as a modulator of endothelial phenotype. *Mol Med Today.* (1999) 5:40–6.
- Nam D, Ni CW, Rezvan A, Suo J, Budzyn K, Llanos A, et al. Partial carotid ligation is a model of acutely induced disturbed flow, leading to rapid endothelial dysfunction and atherosclerosis. *Am. J Physiol Heart Circ Physiol.* (2009) 297:H1535–43. doi: 10.1152/ajpheart.00510.2009
- Nam D, Ni CW, Rezvan A, Suo J, Budzyn K, Llanos A, et al. A model of disturbed flow-induced atherosclerosis in mouse carotid artery by partial ligation and a simple method of RNA isolation from carotid endothelium. *J Vis Exp.* (2010) 40:1861. doi: 10.3791/1861
- Lefebvre V. The SoxD transcription factors – Sox5, Sox6, and Sox13 – are key cell fate modulators. *Int J Biochem Cell Biol.* (2010) 42:429–32. doi: 10.1016/j.biocel.2009.07.016
- Spidale NA, Sylvia K, Narayan K, Miu B, Frascoli M, Melichar HJ, et al. Interleukin-17-producing γδ T cells originate from SOX13⁺ progenitors that are independent of γδTCR signaling. *Immunity.* (2018) 49:857–872.e5.
- Nelson SR, Roche S, Cotter M, Garcia PA, Reitmeier D, Zollbrecht E, et al. Genomic profiling and functional analysis of let-7c miRNA-mRNA interactions identify SOX13 to be involved in invasion and progression of pancreatic cancer. *J Oncol.* (2020) 2020:2951921. doi: 10.1155/2020/2951921
- Liang Z, Xu J, Gu C. Novel role of the SRY-related high-mobility-group box D gene in cancer. *Semin Cancer Biol.* (2020) 67:83–90. doi: 10.1016/j.semcancer.2019.07.011
- He Z, Ruan X, Liu X, Zheng J, Liu Y, Liu L, et al. FUS/circ_002136/miR-138-5p/SOX13 feedback loop regulates angiogenesis in Glioma. *J Exp Clin Cancer Res.* (2019) 38:65. doi: 10.1186/s13046-019-1065-7
- Feng M, Fang F, Fang T, Jiao H, You S, Wang X, et al. Sox13 promotes hepatocellular carcinoma metastasis by transcriptionally activating Twist1. *Lab Invest.* (2020) 100:1400–10. doi: 10.1038/s41374-020-0445-0
- Roose J, Korver W, Oving E, Wilson A, Wagenaar G, Markman M, et al. High expression of the HMG box factor Sox-13 in arterial walls during embryonic development. *Nucleic Acids Res.* (1998) 26:469–76. doi: 10.1093/nar/26.2.469
- Argentaro A, Olsson J, Critcher R, McDowall SG, Harley VR. Genomic characterisation and fine mapping of the human SOX13 gene. *Gene.* (2000) 250:181–9. doi: 10.1016/s0378-1119(00)00157-8
- Lambert SA, Jolma A, Campitelli LF, Das PK, Yin Y, Albu M, et al. The human transcription factors. *Cell.* (2018) 172:650–65.
- Huddleson JP, Ahmad N, Srinivasan S, Lingrel JB. Induction of KLF2 by fluid shear stress requires a novel promoter element activated by a phosphatidylinositol 3-kinase-dependent chromatin-remodeling pathway. *J Biol Chem.* (2005) 280:23371–9. doi: 10.1074/jbc.M413839200
- Villarreal G Jr., Zhang Y, Larman HB, Gracia-Sancho J, Koo A, García-Cardena G. Defining the regulation of KLF4 expression and its downstream transcriptional targets in vascular endothelial cells. *Biochem Biophys Res Commun.* (2010) 391:984–9. doi: 10.1016/j.bbrc.2009.12.002
- Wang Y, Sun H-Y, Kumar S, Puerta MDM, Jo H, Rezvan A. ZBTB46 is a shear-sensitive transcription factor inhibiting endothelial cell proliferation via

gene expression regulation of cell cycle proteins. *Lab Invest.* (2018) 99:305–18. doi: 10.1038/s41374-018-0060-5

45. Cheng, CK, Lin X, Pu Y, Tse JKY, Wang Y, Zhang C-L, et al. SOX4 is a novel phenotypic regulator of endothelial cells in atherosclerosis revealed by single-cell analysis. *J Adv Res.* (2022) doi: 10.1016/j.jare.2022.02.017.
46. Partridge EC, Chhetri SB, Prokop JW, Ramaker RC, Jansen CS, Goh S-T, et al. Occupancy maps of 208 chromatin-associated proteins in one human cell type. *Nature.* (2020) 583:720–8. doi: 10.1038/s41586-020-2023-4
47. Kasimiotis H, Myers MA, Argentaro A, Martin S, Fida S, Ferraro T, et al. Sex-determining region Y-related protein SOX13 is a diabetes autoantigen expressed in pancreatic islets. *Diabetes.* (2000) 49:555–61. doi: 10.2337/diabetes.49.4.555
48. Melichar HJ, Narayan K, Der SD, Hiraoka Y, Gardiol N, Jeannot G, et al. Regulation of gammadelta versus alphabeta T lymphocyte differentiation by the transcription factor SOX13. *Science.* (2007) 315:230–3. doi: 10.1126/science.1135344
49. Turner MD, Nedjai B, Hurst T, Pennington DJ. Cytokines and chemokines: at the crossroads of cell signalling and inflammatory disease. *Biochim Biophys Acta.* (2014) 1843:2563–82. doi: 10.1016/j.bbamer.2014.05.014
50. Gencer S, Evans BR, van der Vorst EPC, Döring Y, Weber C. inflammatory chemokines in atherosclerosis. *Cells.* (2021) 10:226.
51. Su W, Zhao Y, Wei Y, Zhang X, Ji J, Yang S. Exploring the pathogenesis of psoriasis complicated with atherosclerosis via microarray data analysis. *Front Immunol.* (2021) 12:667690. doi: 10.3389/fimmu.2021.667690
52. Munjal A, Khandia R. Atherosclerosis: orchestrating cells and biomolecules involved in its activation and inhibition. *Adv Protein Chem Struct Biol.* (2020) 120:85–122. doi: 10.1016/bs.apcsb.2019.11.002
53. Alberts-Grill N, Rezvan A, Son DJ, Qiu H, Kim CW, Kemp ML, et al. Dynamic immune cell accumulation during flow-induced atherogenesis in mouse carotid artery: an expanded flow cytometry method. *Arterioscler Thromb Vasc Biol.* (2012) 32:623–32. doi: 10.1161/ATVBAHA.111.242180
54. Veillard NR, Kwak B, Pelli G, Mulhaupt F, James RW, Proudfoot AE, et al. Antagonism of RANTES receptors reduces atherosclerotic plaque formation in mice. *Circ Res.* (2004) 94:253–61. doi: 10.1161/01.RES.0000109793.17591.4E
55. Projahn D, Simsekylmaz S, Singh S, Kanzler I, Kramp BK, Langer M, et al. Controlled intramyocardial release of engineered chemokines by biodegradable hydrogels as a treatment approach of myocardial infarction. *J Cell Mol Med.* (2014) 18:790–800. doi: 10.1111/jcmm.12225
56. Kaiser D, Freyberg MA, Friedl P. Lack of hemodynamic forces triggers apoptosis in vascular endothelial cells. *Biochem Biophys Res Commun.* (1997) 231:586–90.
57. Blackman BR, Garcia-Cardena G, Gimbrone JMA. A new in vitro model to evaluate differential responses of endothelial cells to simulated arterial shear stress waveforms. *J Biomech Eng.* (2002) 124:397–407. doi: 10.1115/1.1486468
58. Marfil V, Moya M, Pierreux CE, Castell JV, Lemaigre FP, Real FX, et al. Interaction between Hhex and SOX13 modulates Wnt/TCF activity. *J Biol Chem.* (2010) 285:5726–37. doi: 10.1074/jbc.M109.046649
59. Tang J, Tian Z, Liao X, Wu G. SOX13/TRIM11/YAP axis promotes the proliferation, migration and chemoresistance of anaplastic thyroid cancer. *Int J Biol Sci.* (2021) 17:417–29. doi: 10.7150/ijbs.54194
60. Du F, Li X, Feng W, Qiao C, Chen J, Jiang M, et al. SOX13 promotes colorectal cancer metastasis by transactivating SNAI2 and c-MET. *Oncogene.* (2020) 39:3522–40. doi: 10.1038/s41388-020-1233-4
61. Bie LY, Li D, Wei Y, Li N, Chen XB, Luo SX. SOX13 dependent PAX8 expression promotes the proliferation of gastric carcinoma cells. *Artif Cells Nanomed Biotechnol.* (2019) 47:3180–7. doi: 10.1080/21691401.2019.1646751
62. Wang Y, Risteovski S, Harley VR. SOX13 exhibits a distinct spatial and temporal expression pattern during chondrogenesis, neurogenesis, and limb development. *J Histochem Cytochem.* (2006) 54:1327–33. doi: 10.1369/jhc.6A6923.2006
63. Daigle M, Roumaud P, Martin LJ. Expressions of Sox9, Sox5, and Sox13 transcription factors in mice testis during postnatal development. *Mol Cell Biochem.* (2015) 407:209–21.
64. Baroti T, Schillinger A, Wegner M, Stolt CC. Sox13 functionally complements the related Sox5 and Sox6 as important developmental modulators in mouse spinal cord oligodendrocytes. *J Neurochem.* (2016) 136:316–28. doi: 10.1111/jnc.13414
65. Bailey TL, Johnson J, Grant CE, Noble WS. The MEME suite. *Nucleic Acids Res.* (2015) 43:W39–49.
66. Hillyer P, Male D. Expression of chemokines on the surface of different human endothelia. *Immunol Cell Biol.* (2005) 83:375–82.
67. Zernecke A, Shagdarsuren E, Weber C. Chemokines in atherosclerosis: an update. *Arterioscler Thromb Vasc Biol.* (2008) 28:1897–908.
68. van den Borne P, Quax PH, Hoefer IE, Pasterkamp G. The multifaceted functions of CXCL10 in cardiovascular disease. *BioMed Res Int.* (2014) 2014:893106.
69. Li J, Ley K. Lymphocyte migration into atherosclerotic plaque. *Arterioscler Thromb Vasc Biol.* (2015) 35:40–9.
70. Segers D, Lipton JA, Leenen PJM, Cheng C, Tempel D, Pasterkamp G, et al. Atherosclerotic Plaque stability is affected by the chemokine CXCL10 in both mice and humans. *Int J Inflam.* (2011) 2011:936109.
71. Jongstra-Bilen J, Tai K, Althagafi MG, Siu A, Scipione CA, Karim S, et al. Role of myeloid-derived chemokine CCL5/RANTES at an early stage of atherosclerosis. *J Mol Cell Cardiol.* (2021) 156:69–78. doi: 10.1016/j.jmcc.2021.03.010
72. Proudfoot AEI, Power CA, Hoogwerf AJ, Montjovent M-O, Borlat F, Offord RE, et al. Extension of recombinant human RANTES by the retention of the initiating methionine produces a potent antagonist (*). *J Biol Chem.* (1996) 271:2599–603. doi: 10.1074/jbc.271.5.2599
73. Farina FM, Serio S, Hall IF, Zani S, Cassanmagnago GA, Climent M, et al. The epigenetic enzyme DOT1L orchestrates vascular smooth muscle cell-monocyte crosstalk and protects against atherosclerosis via the NF- κ B pathway. *Eur Heart J.* (2022) 43:ehac097. doi: 10.1093/eurheartj/ehac097
74. Son DJ, Kumar S, Takabe W, Kim CW, Ni CW, Alberts-Grill N, et al. The atypical mechanosensitive microRNA-712 derived from pre-ribosomal RNA induces endothelial inflammation and atherosclerosis. *Nat Commun.* (2013) 4:3000. doi: 10.1038/ncomms4000
75. Williams D, Mahmoud M, Liu R, Andueza A, Kumar S, Kang DW, et al. Stable flow-induced expression of KLK10 inhibits endothelial inflammation and atherosclerosis. *Elife.* (2022) 11:e72579. doi: 10.7554/eLife.72579
76. Dardik A, Chen L, Frattini J, Asada H, Aziz F, Kudo FA, et al. Differential effects of orbital and laminar shear stress on endothelial cells. *J Vasc Surg.* (2005) 41:869–80. doi: 10.1016/j.jvs.2005.01.020
77. Ali MH, Schumacker PT. Endothelial responses to mechanical stress: where is the mechanosensor? *Crit Care Med.* (2002) 30:S198–206.
78. Boo YC, Jo H. Flow-dependent regulation of endothelial nitric oxide synthase: role of protein kinases. *Am J Physiol.* (2003) 285:C499–508.
79. Chen Y, Lun AT, Smyth GKJF. From reads to genes to pathways: differential expression analysis of RNA-Seq experiments using Rsubread and the edgeR quasi-likelihood pipeline. *F1000Res.* (2016) 1438:5. doi: 10.12688/f1000research.8987.2
80. Schmittgen TD, Livak KJ. Analyzing real-time PCR data by the comparative C(T) method. *Nat Protoc.* (2008) 3:1101–8. doi: 10.1038/nprot.2008.73



OPEN ACCESS

EDITED BY

Ryuichi Morishita,
Osaka University, Japan

REVIEWED BY

Christine Espinola-Klein,
Johannes Gutenberg University
Mainz, Germany
Håkan Wallen,
Karolinska Institutet (KI), Sweden

*CORRESPONDENCE

Loes H. Willems
loes.h.willems@radboudumc.nl

†These authors share senior authorship

SPECIALTY SECTION

This article was submitted to
Atherosclerosis and Vascular Medicine,
a section of the journal
Frontiers in Cardiovascular Medicine

RECEIVED 28 June 2022

ACCEPTED 20 September 2022

PUBLISHED 06 October 2022

CITATION

Willems LH, Thijssen DHJ, Groh LA,
Kooijman NI, Ten Cate H, Spronk HMH,
Donders ART, van der
Vijver-Coppen RJ, van Hoek F,
Nagy M, Reijnen MMPJ and Warlé MC
(2022) Dual pathway inhibition as
compared to acetylsalicylic acid
monotherapy in relation to endothelial
function in peripheral artery disease, a
phase IV clinical trial.
Front. Cardiovasc. Med. 9:979819.
doi: 10.3389/fcvm.2022.979819

COPYRIGHT

© 2022 Willems, Thijssen, Groh,
Kooijman, Ten Cate, Spronk, Donders,
van der Vijver-Coppen, van Hoek,
Nagy, Reijnen and Warlé. This is an
open-access article distributed under
the terms of the [Creative Commons
Attribution License \(CC BY\)](#). The use,
distribution or reproduction in other
forums is permitted, provided the
original author(s) and the copyright
owner(s) are credited and that the
original publication in this journal is
cited, in accordance with accepted
academic practice. No use, distribution
or reproduction is permitted which
does not comply with these terms.

Dual pathway inhibition as compared to acetylsalicylic acid monotherapy in relation to endothelial function in peripheral artery disease, a phase IV clinical trial

Loes H. Willems^{1*}, Dick H. J. Thijssen^{2,3}, Laszlo A. Groh¹,
Nina I. Kooijman¹, Hugo Ten Cate^{4,5}, Henri M. H. Spronk⁴,
A. Rogier T. Donders⁶, Rozemarijn J. van der Vijver-Coppen¹,
Frank van Hoek¹, Magdolna Nagy^{4†}, Michel M. P. J. Reijnen^{7,8†}
and Michiel C. Warlé^{4†}

¹Department of Surgery, Radboud University Medical Center, Nijmegen, Netherlands, ²Department of Physiology, Radboud Institute for Health Sciences, Radboud University Medical Center, Nijmegen, Netherlands, ³Research Institute for Sport and Exercise Sciences, Liverpool John Moores University, Liverpool, United Kingdom, ⁴Departments of Internal Medicine and Biochemistry, Maastricht University Medical Center (MUMC) and Cardiovascular Research Institute Maastricht (CARIM) School for Cardiovascular Diseases, Maastricht, Netherlands, ⁵Center for Thrombosis and Haemostasis, Gutenberg University Medical Center, Mainz, Germany, ⁶Department for Health Evidence, Radboud Institute for Health Sciences, Radboud University Medical Center, Nijmegen, Netherlands, ⁷Department of Surgery, Rijnstate Hospital, Arnhem, Netherlands, ⁸Multi-Modality Medical Imaging Group, Faculty of Science and Technology, University of Twente, Enschede, Netherlands

Objective: Dual pathway inhibition (DPI) by combining acetylsalicylic acid (ASA) with low-dose rivaroxaban has been shown to reduce cardiovascular events in patients with peripheral arterial disease (PAD) when compared to ASA monotherapy. A potential explanation is that inhibition of factor Xa improves endothelial function through crosstalk between coagulation and inflammatory pathways, subsequently attenuating the occurrence of cardiovascular events. We hypothesize that the addition of rivaroxaban to ASA in PAD patients leads to improved endothelial function.

Design: An investigator-initiated, multicentre trial investigating the effect of DPI on endothelial function.

Methods: Patients, diagnosed with PAD, were enrolled in two cohorts: cohort A (Rutherford I-III) and cohort B (Rutherford IV-VI). Participants received ASA monotherapy for a 4-weeks run-in period, followed by 12 weeks of DPI. Macro- and microvascular endothelial dysfunction were studied by measuring carotid artery reactivity upon sympathetic stimulus and by measuring plasma endothelin-1 concentrations, respectively. All measurements were performed during the use of ASA (baseline) and after 12 weeks of DPI.

Results: 159 PAD patients (111 cohort A, 48 cohort B) were enrolled. Twenty patients discontinued study drugs early. Carotid artery constriction upon sympathetic stimulation at baseline (ASA) and after 12 weeks of DPI was similar

in the total group, 22.0 vs. 22.7% ($p = 1.000$), and in the subgroups (Cohort A 22.6 vs. 23.7%, $p = 1.000$; cohort B 20.5 vs. 20.5%, $p = 1.000$), respectively. The mean concentration of plasma endothelin-1 at baseline and after 12 weeks of DPI did not differ, 1.70 ± 0.5 vs. 1.66 ± 0.64 pmol/L ($p = 0.440$) in the total group, 1.69 ± 0.59 vs. 1.62 ± 0.55 pmol/L in cohort A ($p = 0.202$), and 1.73 ± 0.53 vs. 1.77 ± 0.82 pmol/L in cohort B ($p = 0.682$), respectively.

Conclusion: Macro- and microvascular endothelial dysfunction, as reflected by carotid artery reactivity and plasma endothelin-1 concentrations, are not influenced in PAD patients by addition of low-dose rivaroxaban to ASA monotherapy for 12 weeks.

Trial registration: <https://clinicaltrials.gov/ct2/show/NCT04218656>.

KEYWORDS

peripheral arterial disease, aspirin, rivaroxaban, factor Xa inhibitors, endothelial cells, vascular endothelium

Introduction

Patients with peripheral arterial disease (PAD) are at high risk of developing cardiovascular events (1, 2), for which single antiplatelet therapy (SAPT) is indicated (3, 4). Recently, the COMPASS trial demonstrated that dual pathway inhibition (DPI), where acetylsalicylic acid (ASA) is combined with low-dose rivaroxaban (2.5 mg twice daily), reduces the rate of major adverse cardiovascular (MACE) and limb (MALE) events, compared to ASA monotherapy (5). The VOYAGER-PAD trial confirmed these findings in PAD patients, who underwent peripheral revascularization (6). The precise mechanism underlying the benefit of rivaroxaban in PAD patients is currently unclear.

Rivaroxaban is an oral inhibitor of factor Xa, the first enzyme in the “common pathway” of the coagulation cascade. Besides this prominent role in the coagulation cascade, previous literature demonstrates that factor Xa can activate protease-activated receptors (PAR) on the surface of endothelial cells in the inner lining of the arterial wall. By binding to PAR, factor Xa is capable of modulating inflammatory pathways, contributing to vascular inflammation, leukocyte migration and endothelial dysfunction (7–9).

Endothelial dysfunction contributes to the development and progression of atherosclerosis (10) and is generally present years before the patient develops symptomatic disease (11). Other risk factors for developing atherosclerotic disease have also been related to endothelial dysfunction, including hypertension (12), hyperlipidaemia (13), diabetes mellitus (14), and aging (15). Presence of endothelial dysfunction, independent from disease state and other risk factors, is strongly related to the occurrence of MACE (16–18) and MALE (16, 17). Risk-reducing interventions for atherosclerosis, such as physical activity and lipid-lowering drug therapy, have been shown to improve

endothelial dysfunction (19–21). Rivaroxaban may therefore potentially improve endothelial function, thus contributing to the previously demonstrated reduction in MACE in PAD patients.

A simple and non-invasive test has been developed and validated to assess macrovascular endothelial function by measuring carotid artery reactivity (CAR) in response to a sympathetic stimulus. The CAR response was proven to be strongly related to cardiovascular risk, closely related to coronary artery endothelial function, and independently predictive for the 1-year occurrence of MACE in PAD patients (22, 23). Microvascular endothelial dysfunction, on the other hand, has been strongly related to plasma concentrations of endothelin-1 (ET-1) (24). ET-1 is a potent vasoconstrictor peptide (25) and has been suggested to be a potential target for treating microvascular endothelial dysfunction in atherosclerosis (26).

In this study, we hypothesize that DPI, by combining ASA with low-dose rivaroxaban for 12 weeks, reduces macro- and microvascular endothelial dysfunction in symptomatic PAD patients.

Materials and methods

This is an investigator-initiated, non-randomized, multicenter parallel trial of two clinical cohorts investigating the effect of DPI (ASA with low-dose rivaroxaban) on endothelial function in PAD patients. The study was approved by the regional ethics committee and the local directory boards. The study was conducted in accordance with the latest revision of the Declaration of Helsinki and Good Clinical Practice regulations and is registered at [ClinicalTrials.gov](https://clinicaltrials.gov) on January 6th, 2020 (NCT04218656) and at the Dutch Trial Register on September 22nd, 2020 (NL8908). Written informed consent was

obtained from all participants. The protocol has been published previously (27).

Participants

Patients with lower extremity PAD and an indication for SAPT according to the current guidelines (3, 4) were recruited. Based on the severity of PAD, patients were divided into cohort A (intermittent claudication, Rutherford I-III) and cohort B (chronic limb-threatening ischemia (CLTI), Rutherford IV-VI), where the highest Rutherford classification recorded for a patient (either now or in the past) was used to allocate a patient into one of the two cohorts (28). Patients with an increased bleeding risk, severe renal impairment, systemic treatment with CYP3A4 inhibitors/inducers, concomitant treatment with other anticoagulants, and known hypersensitivity to ASA/rivaroxaban were excluded. A detailed description of the in- and exclusion criteria can be found in our previously published protocol (27).

Procedures

Eligible patients received low-dose (80–100 mg once daily) ASA monotherapy during a 4-weeks run-in period. After 4 weeks, medication adherence was evaluated by interview (T1). Participants with an adherence below 80% were excluded and replaced. Patients who dropped out before T1 and did not fulfill the run-in period were considered non-adherent and were replaced. Subsequently, at T1, participants were prescribed DPI by ASA (100 mg once daily) plus low-dose rivaroxaban (2.5 mg twice daily) for 12 weeks. After these 12 weeks (T2), DPI was discontinued, and participants could resume SAPT. During study participation, the occurrence of severe adverse events (SAE) was recorded, including myocardial infarction, stroke, acute limb ischemia (ALI), deterioration of PAD as classified by Rutherford (28), need for peripheral revascularization, lower extremity amputation, major bleeding and death.

Outcomes

The primary outcome was a change in macrovascular endothelial dysfunction represented by a change in the proportion of participants with a constrictive CAR response upon sympathetic stimulus from T1 (ASA monotherapy) to T2 (after 12 weeks of DPI). The secondary outcome is a change in microvascular endothelial dysfunction represented by a change in mean plasma ET-1 level from T1 to T2.

We explored changes in the activation of the common pathway by measuring markers of thrombin generation, including thrombin:antithrombin (TAT) complexes and

prothrombin fragment 1+2 (F1.2). Additionally, activated coagulation factor XI in complex with its natural inhibitor antithrombin (FXIa:AT) was measured, in order to assess for changes in activation of the intrinsic pathway (positive feedback loop mechanism).

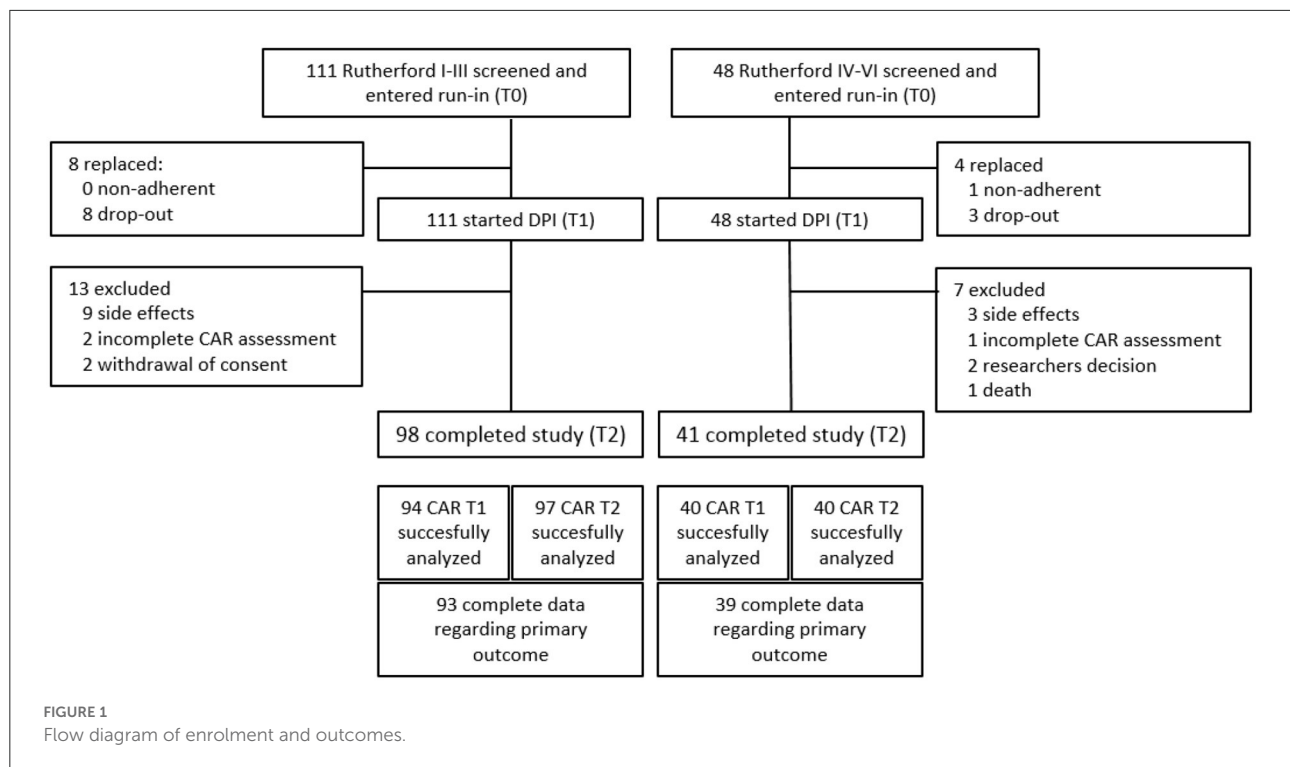
The carotid artery reactivity test

The CAR test assesses endothelial function by measuring the change in diameter of the common carotid artery in response to a sympathetic stimulus (cold pressor test). The common carotid artery was visualized using Philips Lumify ultrasound device (Philips Healthcare, Best, The Netherlands) with a L12-4 MHz linear array probe, during a 30 second baseline, and during a subsequent 3 mins of sympathetic stimulation by hand in ice water immersion. The common carotid artery diameter was measured with semi-automatic custom-designed edge-detection and wall-tracking software by an investigator, blinded for the test moment (T1 or T2). The area under the curve (AUC) relative to baseline was calculated. A net positive AUC represents a dilatory response, and a net negative AUC represents a constrictive response. Additionally, the peak change percentage dilatation or constriction (CAR%) was computed as the mean diameter over a 10-sec interval—excluding control interval—most deviating from baseline diameter, relative to baseline.

To limit the influence of external factors on the CAR test, participants were instructed 1) not to eat or drink anything except for water in the 6 h preceding their appointment, 2) not to have beverages with caffeine, alcohol, or any products that are high in vitamin C in the 18 h preceding their appointment, and 3) not to do heavy exercise training in the 24 h preceding their appointment. Each patient underwent endothelial testing twice, at T1 and at T2. Time of appointment was generally between 9 and 12 AM and was equal for both T1 and T2.

Blood sampling

Venous blood samples were collected by venipuncture in 10 ml Lithium-Heparin (Vacuette) tubes. Platelet poor plasma was prepared by centrifuging whole blood at 2,500 g for 10 mins followed by a second centrifugation step at 2,500 g for 20 mins, both at room temperature. The platelet poor plasma was stored at -80°C until further analysis. Plasma concentrations of ET-1 were quantified using commercial ELISA kits (R&D, Minneapolis (Minnesota), United States of America). Plasma concentrations of TAT and FXIa:AT were quantified by in-house developed ELISA methods as described previously (29) and F1.2 was quantified using commercially available assays (EnzygnostTM F1+2, Siemens Healthineers, The Hague, the Netherlands).



Statistical analyses

This study was powered to detect a relative reduction in the proportion of patients with CAR constriction when switching from ASA to DPI of ~40%. Based on previous literature, the expected prevalence of CAR constriction at baseline was 40% in cohort A (intermittent claudication) and 60% in cohort B (CLTI) (22). With an alpha of 5%, a power of 80%, and allowing for a drop-out rate of 5%, the final sample size was 159 participants (111 in cohort A and 48 in cohort B).

Change in proportion of participants with CAR constriction from T1 to T2 was compared using McNemar's Z-test, 2-sided equality. Differences in CAR% and plasma ET-1 levels from T1 to T2 was analyzed using the paired sample *t*-test. Differences in plasma concentrations of the coagulation markers TAT, F1.2 and FXIa:AT were explored using the Wilcoxon signed ranks test.

Categorical and continuous baseline variables are recorded as percentage and mean, respectively. SAEs were reported as numbers. Analyses are performed using IBM SPSS statistics 25. *p* values below 0.05 were considered significant.

Results

Enrolment and baseline characteristics

Between June 2020 and August 2021, 159 patients with symptomatic PAD were enrolled, with an additional 12 patients

being enrolled to replace participants with an adherence below 80% at T1 (Figure 1). In total, 111 patients with intermittent claudication (cohort A) and 48 patients with CLTI (cohort B) completed the run-in period and were started on DPI. Of these, 20 discontinued the trial. The most common reasons for not continuing the trial were side effects associated with the study medication (Figure 1). Baseline characteristics are shown in Table 1. The mean age of the participants was 67 years and 66% were male. Most patients used ASA as SAPT (64.8%) before study participations, while 35.2% used clopidogrel.

Endothelial function

The CAR response was successfully assessed in 134/139 patients after a 4-weeks run-in period of ASA monotherapy (T1) and in 137/139 patients after 12 weeks of DPI (T2). Complete paired assessment was obtained of 132 participants, 93 in Cohort A and 39 in cohort B (Figure 1). The numbers of patients with a CAR dilatory response and a CAR constrictive response at T1 and T2, respectively, are presented in Table 2. The proportion of patients with a constrictive CAR response at T1 and T2 was similar in the total group, 22.0 vs. 22.7% ($p = 1.000$), respectively. Subsequent analysis on cohort A and cohort B revealed comparable trends in constrictive response rates, 22.6 vs. 23.7% ($p = 1.000$) for cohort A and 20.5 vs. 20.5% ($p = 1.000$) for cohort B, respectively. Consistent with

TABLE 1 Baseline characteristics of the patients that successfully completed the run-in period.

	All, <i>n</i> = 159	Cohort A, <i>n</i> = 111	Cohort B, <i>n</i> = 48
Age (mean \pm SD)	67 \pm 8	67 \pm 8	68 \pm 9
Male (<i>n</i> , %)	105 (66.0)	77 (69.4)	28 (58.3)
BMI (mean \pm SD)	26.8 \pm 4.6	27.1 \pm 4.7	26.1 \pm 4.2
Tobacco use (<i>n</i> , %)			
Current	52 (32.7)	31 (27.9)	21 (43.8)
Former	98 (61.6)	74 (66.7)	24 (50.0)
Never	9 (5.7)	6 (5.4)	3 (6.3)
Alcohol use (<i>n</i> , %)			
Never	43 (27.0)	29 (26.1)	14 (29.2)
Rarely	17 (10.7)	11 (9.9)	6 (12.5)
Monthly	14 (8.8)	13 (11.7)	1 (2.1)
Weekly	46 (28.9)	33 (29.7)	13 (27.1)
Daily	39 (24.5)	25 (22.5)	14 (29.2)
Previous intervention for PAD (<i>n</i> , %)	105 (66.0)	64 (57.7)	41 (85.4)
Endovascular revascularization	100 (62.9)	64 (57.7)	36 (75.0)
Thrombendarterectomy	12 (7.5)	(4.5)	7 (14.6)
Bypass surgery	18 (11.3)	6 (5.4)	12 (25.0)
Lower extremity amputation	5 (3.1)	0 (0.0)	5 (10.4)
Amputation of toe(s)	3 (1.9)	0 (0.0)	3 (6.3)
Thrombolysis	2 (1.3)	0 (0.0)	2 (4.2)
Embolectomy	1 (0.6)	0 (0.0)	1 (2.1)
Comorbidity (<i>n</i> , %)			
Hypertension	114 (71.7)	79 (71.2)	35 (72.9)
Hyperlipidaemia	71 (44.7)	51 (45.9)	20 (41.7)
Ischaemic heart disease	50 (31.4)	33 (29.7)	17 (35.4)
CVA/TIA	20 (12.6)	12 (10.8)	8 (16.7)
Diabetes mellitus	52 (32.7)	36 (32.4)	16 (33.3)
Asthma/COPD	42 (26.4)	30 (27.0)	12 (25.0)
Medication before study participation (<i>n</i> , %)			
Acetylsalicylic acid	103 (64.8)	75 (67.7)	28 (58.3)
Clopidogrel	56 (35.2)	36 (32.4)	20 (41.7)
Lipid lowering drugs	146 (91.8)	102 (91.9)	44 (91.7)
Antihypertensive drugs	117 (73.6)	82 (73.9)	35 (72.9)

Cohort A: intermittent claudication, Rutherford I-III. Cohort B: chronic limb-threatening ischaemia, Rutherford IV-VI.
 BMI, body mass index; PAD, peripheral arterial disease; CVA, cerebrovascular accident; TIA, transient ischaemic attack; COPD, chronic obstructive pulmonary disease.

this, the peak change in percentage of carotid artery diameter revealed no differences between T1 and T2 with a mean CAR% of 1.92 ± 2.88 vs. 1.69 ± 3.09 ($p = 0.510$) in the total group, 2.03 ± 2.98 vs. 1.71 ± 2.96 in cohort A ($p = 0.442$), and 1.66 ± 2.64 vs. 1.63 ± 3.42 in cohort B ($p = 0.969$), respectively (Table 3).

The mean plasma ET-1 levels at T1 and T2 did not differ significantly and were 1.70 ± 0.57 vs. 1.66 ± 0.64 pg/mL ($p = 0.440$) for the total group, 1.69 ± 0.59 vs. 1.62 ± 0.55 pg/mL ($p = 0.202$) for cohort A, and 1.73 ± 0.53 vs. 1.77 ± 0.82 pg/mL ($p = 0.682$) for cohort B (Table 3).

Coagulation activity

In vivo coagulation activity of the common and intrinsic pathway was measured at T1 and T2 (Table 4). The mean plasma concentration of TAT and F1.2 significantly decreased with DPI compared to ASA monotherapy, 1.13 ± 3.37 vs. 0.99 ± 3.82 μ g/L ($p = 0.013$) and 386.43 ± 204.41 vs. 258.24 ± 153.79 pmol/L ($p < 0.001$), at T1 and T2 respectively. There was no significant difference in FXIa:AT levels between T1 and T2, 17.68 ± 25.69 vs. 16.90 ± 21.59 pM ($p = 0.949$).

Adverse events

In total, 18 SAEs were experienced by 16 patients (Supplementary Table S1). The two patients who experienced ALI had a second severe adverse event: one underwent a peripheral transluminal angioplasty of the iliac arteries, while the other decided for a palliative policy and died. Both patients used ASA before study participation and suffered from ALI during the run-in phase. The other 14 SAEs occurred during DPI treatment (Supplementary Table S1).

Possible side effects were reported by 31 participants, 4 of whom reported two possible side effects. The onset of the possible side effects was during DPI treatment for 28 of 31 participants. The most common side effects were minor bleeding problems ($n = 11$), skin rash ($n = 6$) and gastro-intestinal complaints ($n = 5$). Thirteen participants withdrew from study participation because of possible side effects of study medication (ASA 1, rivaroxaban 12).

Discussion

In this study we investigated the potential impact of switching ASA monotherapy to DPI, by combining ASA with low-dose rivaroxaban, on macro- and microvascular endothelial dysfunction in patients with PAD and observed no differences. While the addition of rivaroxaban resulted in suppression of markers of thrombin formation, demonstrating an overall anticoagulant effect, the carotid artery response upon sympathetic stimulation and plasma ET-1 concentrations were similar after 4 weeks of ASA monotherapy and after 12 weeks of DPI.

TABLE 2 Total patients with a CAR dilatatory response and a constrictive response at the test moments T1 and T2.

All participants, <i>n</i> = 132		CAR response at T2, after 12 weeks of dual pathway inhibition		
		Dilatation	Constriction	Total
CAR response at T1, after 4 weeks of ASA monotherapy	Dilatation	80	23	103
	Constriction	22	7	29
	Total	102	30	132
Cohort A, <i>n</i> = 93		CAR response at T2, after 12 weeks of dual pathway inhibition		
		Dilatation	Constriction	Total
CAR response at T1, after 4 weeks of ASA monotherapy	Dilatation	55	17	72
	Constriction	16	5	21
	Total	71	22	93
Cohort B, <i>n</i> = 39		CAR response at T2, after 12 weeks of dual pathway inhibition		
		Dilatation	Constriction	Total
CAR response at T1, after 4 weeks of ASA monotherapy	Dilatation	25	6	31
	Constriction	6	2	8
	Total	31	8	39

Cohort A: intermittent claudication, Rutherford I-III. Cohort B: chronic limb-threatening ischaemia, Rutherford IV-VI.
CAR, carotid artery reactivity; ASA, acetylsalicylic acid.

Classically, macrovascular endothelial dysfunction was angiographically determined by detecting endothelium-dependent vasodilatation of the coronary arteries as response to an increase of endothelium derived nitric oxide by infusion of acetylcholine (30) or blood flow increasing medication (31). Due to risks related to the invasive character of these methods, non-invasive detection of endothelial dysfunction by vascular ultrasound gained interest. In this study, the CAR in response to cold pressor testing (sympathetic stimulus) was used. The CAR test is a simple, non-invasive test using an easy accessible vascular bed to assess macrovascular endothelial function. The CAR test closely relates to coronary artery endothelial function as tested by the classical invasive methods and has shown to be strongly related to cardiovascular risk in the population of peripheral arterial disease (22). Endothelial functions such as modulation of vascular tone, thrombogenicity and inflammation, are regulated by molecules, amongst which ET-1 (32). Plasma concentrations of ET-1 strongly relate to microvascular endothelial function (24) and are therefore an easy target to evaluate changes in its function. Previous research has even suggested ET-1 as a potential for treating microvascular endothelial dysfunction in atherosclerosis (26).

To our best knowledge, this study is the first to investigate changes in endothelial function by antithrombotic drugs. Previous literature has addressed the effect of lipid-lowering drugs on endothelial dysfunction. The impaired endothelial-dependent responses (i.e., nitric-oxide mediated vasodilatation),

present in patients with hypercholesterolemia, can be reversed by lowering cholesterol levels using lipid-lowering therapies. This effect can already be observed after 1 month and persists with continued therapy (20, 33, 34). Furthermore, other cardiovascular risk reducing interventions have been shown to improve endothelial function. Exercise training augments endothelial dependent vasodilatation, provoked by acetylcholine infusion, in both coronary vessels and resistance vessels in atherosclerotic patients (19). The same effect can be observed by non-invasive methods of measuring endothelial dysfunction. Buckley et al. demonstrated significant improvements in vascular health after a 12-week physical activity program in patients with cardiovascular risk factors and in patients with manifest cardiovascular disease, with reversed carotid artery constriction in response to sympathetic stimulus and increased brachial artery flow-mediated dilatation (21, 35).

Improved endothelial dysfunction thus correlates with a reduction in cardiovascular risk factors and might subsequently reduce the occurrence of MACE. This is in line with the results of van Mil et al. who demonstrated that patients with a constrictive CAR response have a 4-fold increased risk of developing MACE and a 2-fold increased risk for clinical deterioration, in patients with manifest PAD. Low-dose rivaroxaban in addition to ASA has been shown to reduce the occurrence of myocardial infarction, stroke, ALI and cardiovascular death, in patients with PAD (5, 6). The current study, however, could not confirm an improvement in

TABLE 3 The effect of DPI on endothelial dysfunction as represented by the CAR response, CAR%, and plasma endothelin-1 levels.

	T1 (ASA)	T2 (DPI)	<i>p</i>
CAR response, constriction, <i>n</i> (%)	<i>McNemar's test</i>		
All	29 (22.0)	30 (22.7)	1.000
Cohort A	21 (22.6)	22 (23.7)	1.000
Cohort B	8 (20.5)	8 (20.5)	1.000
CAR%, mean \pm SD	<i>Paired sample t-test</i>		
All	1.92 \pm 2.88	1.69 \pm 3.09	0.510
Cohort A	2.03 \pm 2.98	1.71 \pm 2.96	0.442
Cohort B	1.66 \pm 2.64	1.63 \pm 3.42	0.969
Plasma endothelin-1, pg/mL, mean \pm SD	<i>Paired sample t-test</i>		
All	1.70 \pm 0.57	1.66 \pm 0.64	0.440
Cohort A	1.69 \pm 0.59	1.62 \pm 0.55	0.202
Cohort B	1.73 \pm 0.53	1.77 \pm 0.82	0.682

Cohort A: intermittent claudication, Rutherford I-III. Cohort B: chronic limb-threatening ischaemia, Rutherford IV-VI.
 CAR, carotid artery reactivity; SD, standard deviation; ASA, acetylsalicylic acid; DPI, dual pathway inhibition.

TABLE 4 The effect of DPI on activation of the common and intrinsic pathway of coagulation.

	T1 (ASA)	T2 (DPI)	<i>p</i>
TAT, μ g/L, mean \pm SD	1.13 \pm 3.37	0.99 \pm 3.82	0.013
F1,2, pmol/L, mean \pm SD	386.43 \pm 204.41	258.24 \pm 153.79	<0.001
FXIa:AT, pM, mean \pm SD	17.68 \pm 25.69	16.90 \pm 21.59	0.949

TAT, thrombin:antithrombin; F1,2, fragment 1+2; FXI:aAT, factorXI:antithrombin; SD, standard deviation; ASA, acetylsalicylic acid; DPI, dual pathway inhibition.

endothelial function underlying this benefit of rivaroxaban in PAD patients.

Rivaroxaban is an oral inhibitor of factor Xa, which plays a crucial role in the coagulation cascade by cleaving prothrombin, yielding the active thrombin. During this process, a fragment of prothrombin called F1,2 is released next to thrombin itself. Thrombin activates the intrinsic pathway through a positive feedback loop mechanism converting FXI into its active metabolite FXIa (36). Both thrombin and FXIa will be rapidly bound by antithrombin in circulation, generating TAT and FXI:AT, respectively. Treatment with rivaroxaban thus leads to a decrease in generation of active thrombin, coinciding with a decrease of TAT, FXIa, FXI:AT and F1,2. Since active thrombin is only present in circulation for a very short time, TAT, FXI:AT and F1,2 are acknowledge as more useful measures for thrombin level in the blood. A significant decrease in markers of thrombin generation is observed in participants at T2 compared to T1. This is consistent with the addition of rivaroxaban to ASA

monotherapy and provides a strong indication that the negative findings regarding endothelial function in our study were not caused by non-adherence to medication. Since other studies on anticoagulants failed to show a clinical benefit on MACE in both the short- and long-term follow-up, it is highly unlikely that the clinical benefit of rivaroxaban is fully explained by its effect on coagulation (37).

In addition to its role in the coagulation cascade, factor Xa has been identified as a direct agonist of PAR-1 leading to thrombin independent platelet activation and thrombus formation. By inhibiting factor Xa, rivaroxaban can attenuate platelet aggregation, in addition to its antithrombotic effect (7, 8, 38, 39). In mice, administration of rivaroxaban for 20 weeks reduced thrombus formation and atherosclerotic plaque destabilization (38, 40). In humans, platelet aggregation and thrombus formation under arterial flow conditions are attenuated in the presence of rivaroxaban, but thrombus regression has not been investigated (38).

Morphological improvement of atherosclerotic lesions has also been shown with dietary treatment in monkeys, and this improvement coincides with restoration of endothelial function (41). Since morphological improvement of atherosclerotic lesions has only been observed with long-term (20 weeks) treatment with rivaroxaban, the interventional period of 12-weeks DPI in the current study, might be too short to establish improved endothelial function. However, the clinical benefit of rivaroxaban as observed in the COMPASS and VOYAGER-PAD trial, is not delayed, but visible from study onset. Therefore, if improving endothelial dysfunction underlies the clinical benefit of rivaroxaban in PAD patients, one would expect to see some signs of improvement within a 12-week period of DPI.

Future research should address other possible long-term PAR-related benefits of rivaroxaban in humans, such as the capability of rivaroxaban to regress atherosclerotic plaques (42), and whether this relates to other (easily measurable) elements of PAR inhibition, such as improved endothelial function (after >12 weeks of rivaroxaban) or reduced vascular inflammation.

The strengths of this study are mainly related to its straightforward approach. By establishing a run-in period of ASA monotherapy, followed by 12 weeks of DPI, we could compare both antithrombotic strategies using paired assessments. Furthermore, the study protocol has been pre-published, facilitating replicability. There are also limitations that should be addressed. The prevalence of endothelial dysfunction, represented by CAR constriction, was lower than anticipated. While we predicted that 40% of the participants with claudication, and 60% of the participants with CLTI would show a constrictive response, in our study, the prevalence of CAR constriction varied between 20 and 25% in both cohorts. The expected high prevalence of CAR constriction was based

on the CAVIPAD study, in which the CAR response was evaluated in 172 patients with PAD (22). A lower proportion of constrictive CAR in our study can be explained by our relatively strict in- and exclusion criteria. By selecting patients solely on SAPT, we implicitly may have excluded most patients with more severe (i.e., acute coronary syndrome in the past year, multivessel disease) concomitant coronary artery disease, and patients with a recent vascular intervention. Also, patients with a current malignancy and patients with a glomerular filtration rate below 30 were excluded. This might have led to the selection of a relatively “healthy” cohort of PAD patients. In addition, we classified patients into cohort A or B, based on their highest Rutherford classification ever, rather than on current classification. Therefore, patients in cohort B, might not have been as severely diseased as the patients with CLTI in the CAVIPAD study. A prevalence of 20–25% CAR constriction is in line with other studies that determined the CAR response in patients with atherosclerosis. The COVAS study, and the study by Buckley et al. both found a prevalence of 24% CAR constriction in respectively 50 patients with various expressions of atherosclerosis and 95 patients with coronary artery disease (35, 43). Another limitation is the relatively high drop-out rate. By replacing all participants that dropped out before starting DPI, we endeavored to obtain as much paired assessments of the primary and secondary outcomes as possible. Another 20 patients, however, dropped out during 12 weeks of DPI. Noteworthy, is the high number of side effects reported to the study team, which mainly underlies the high drop-out rate. Possible side effects of low-dose rivaroxaban were reported by 28 (17.6%) participants, and for 12 (7.5%) participants, these side effects were such that a stop in study medication was requested. The high occurrence of side effects should be considered when prescribing DPI in PAD patients. Last, some patients experienced peripheral revascularization during their DPI treatment. An eventual improvement of mobility with subsequent improvement in endothelial function, was not corrected for. As the number of patients undergoing revascularization was relatively small we believe that this was not a relevant source of bias, although a certain influence cannot be ruled out.

In conclusion, macro- and microvascular endothelial dysfunction, as determined by determining the CAR response and measuring plasma ET-1 concentrations, is not influenced by addition of low-dose rivaroxaban to ASA monotherapy during 12 weeks in PAD patients.

Data availability statement

The raw data supporting the conclusions of this article will be made available by the authors, without undue reservation.

Ethics statement

The studies involving human participants were reviewed and approved by Medical Research Ethics Committee Oost-Nederland. The patients/participants provided their written informed consent to participate in this study.

Author contributions

LW, DT, ARD, MR, and MW contributed to the concept of the study and the study design. LW, NK, RV-C, FH, MR, and MW contributed to the data collection. LW, LG, ARD, and MN contributed to the data analyses. LW, DT, LG, HT, HS, MN, MR, and MW contributed to the data interpretation. LW wrote the first version of the manuscript. All authors read, revised, and approved the final manuscript.

Funding

This work was supported by Bayer B.V. (Grant Number 21065). The funder was not involved in the study design, collection, analysis, interpretation of data, the writing of this article or the decision to submit it for publication.

Acknowledgments

The authors thank Daphne van Veen for research coordination and assistance in the Rijnstate hospital.

Conflict of interest

The authors declare that the research was conducted in the absence of any commercial or financial relationships that could be construed as a potential conflict of interest.

Publisher's note

All claims expressed in this article are solely those of the authors and do not necessarily represent those of their affiliated organizations, or those of the publisher, the editors and the reviewers. Any product that may be evaluated in this article, or claim that may be made by its manufacturer, is not guaranteed or endorsed by the publisher.

Supplementary material

The Supplementary Material for this article can be found online at: <https://www.frontiersin.org/articles/10.3389/fcvm.2022.979819/full#supplementary-material>

References

1. Steg PG, Bhatt DL, Wilson PWF, D'Agostino R Sr, Ohman EM, Röther J, et al. REACH Registry Investigators. one-year cardiovascular event rates in outpatients with atherothrombosis. *JAMA*. (2007) 297:1197–206. doi: 10.1001/jama.297.11.1197
2. Bhatt DL, Eagle KA, Ohman EM, Hirsch AT, Goto S, Mahoney EM, et al. REACH Registry investigators. comparative determinants of 4-year cardiovascular event rates in stable outpatients at risk of or with atherothrombosis. *JAMA*. (2010) 304:1350–7. doi: 10.1001/jama.2010.1322
3. Aboyans V, Ricco JB, Bartelink MEL, Björck M, Brodmann M, Cohnert T, et al. 2017 ESC Guidelines on the Diagnosis and Treatment of Peripheral Arterial Diseases, in collaboration with the European Society for Vascular Surgery (ESVS): Document covering atherosclerotic disease of extracranial carotid and vertebral, mesenteric, renal, upper and lower extremity arteries. Endorsed by: the European Stroke Organization (ESO) The Task Force for the Diagnosis and Treatment of Peripheral Arterial Diseases of the European Society of Cardiology (ESC) and of the European Society for Vascular Surgery (ESVS). *Eur Heart J*. (2018) 39:763–816. doi: 10.1093/eurheartj/ehx095
4. Gerhard-Herman MD, Gornik HL, Barrett C, Barshes NR, Corriere MA, Drachman DE, et al. AHA/ACC guideline on the management of patients with lower extremity peripheral artery disease: executive summary: a report of the american college of cardiology/american heart association task force on clinical practice guidelines. *Circulation*. (2017) 135:e686–725. doi: 10.1161/CIR.0000000000000501
5. Anand SS, Bosch J, Eikelboom JW, Connolly SJ, Diaz R, Widimsky P, et al. COMPASS investigators. Rivaroxaban with or without aspirin in patients with stable peripheral or carotid artery disease: an international, randomised, double-, placebo-controlled trial. *Lancet*. (2018) 391:219–29. doi: 10.1016/S0140-6736(17)32409-1
6. Bonaca MP, Bauersachs RM, Anand SS, Debus ES, Nehler MR, Patel MR, et al. Rivaroxaban in peripheral artery disease after revascularization. *n Engl J Med*. (2020) 382:1994–2004. doi: 10.1056/NEJMoa2000052
7. Borissoff JI, Spronk HM, ten Cate H. The hemostatic system as a modulator of atherosclerosis. *n Engl J Med*. (2011) 364:1746–60. doi: 10.1056/NEJMra1011670
8. Spronk HM, de Jong AM, Crijns HJ, Schotten U, Van Gelder IC, Ten Cate H. Pleiotropic effects of factor Xa and thrombin: what to expect from novel anticoagulants. *Cardiovasc Res*. (2014) 101:344–51. doi: 10.1093/cvr/cvt343
9. Esmon CT. Targeting factor Xa and thrombin: impact on coagulation and beyond. *Thromb Haemost*. (2014) 111:625–33. doi: 10.1160/TH13-09-0730
10. Lerman A, Zeiher AM. Endothelial function: cardiac events. *Circulation*. (2005) 111:363–8. doi: 10.1161/01.CIR.0000153339.27064.14
11. Shechter M, Shechter A, Koren-Morag N, Feinberg MS, Hirsch L. Usefulness of brachial artery flow-mediated dilation to predict long-term cardiovascular events in subjects without heart disease. *Am J Cardiol*. (2014) 113:162–7. doi: 10.1016/j.amjcard.2013.08.051
12. Panza JA, Quyyumi AA, Brush JE. Epstein Abnormal endothelium-dependent vascular relaxation in patients with essential hypertension. *n Engl J Med*. (1990) 323:22–7. doi: 10.1056/NEJM199007053230105
13. Casino PR, Kilcoyne CM, Quyyumi AA, Hoeg JM, Panza JA. The role of nitric oxide in endothelium-dependent vasodilation of hypercholesterolemic patients. *Circulation*. (1993) 88:2541–7. doi: 10.1161/01.CIR.88.6.2541
14. Mäkimattila S, Virkamäki A, Groop PH, Cockcroft J, Utriainen T, Fagerudd J, et al. Chronic hyperglycemia impairs endothelial function and insulin sensitivity via different mechanisms in insulin-dependent diabetes mellitus. *Circulation*. (1996) 94:1276–82. doi: 10.1161/01.CIR.94.6.1276
15. Celermajer DS, Sorensen KE, Spiegelhalter DJ, Georgakopoulos D, Robinson J, Deanfield JE. Aging is associated with endothelial dysfunction in healthy men years before the age-related decline in women. *J Am Coll Cardiol*. (1994) 24:471–6. doi: 10.1016/0735-1097(94)90305-0
16. Bonetti PO, Lerman LO, Lerman A. Endothelial dysfunction: a marker of atherosclerotic risk. *Arterioscler Thromb Vasc Biol*. (2003) 23:168–75. doi: 10.1161/01.ATV.0000051384.43104.FC
17. Schächinger C, Britten MB, Zeiher AM. Prognostic impact of coronary vasodilator dysfunction on adverse long-term outcome of coronary heart disease. *Circulation*. (2000) 101:1899–906. doi: 10.1161/01.CIR.101.16.1899
18. Perticone F, Ceravolo R, Pujia A, Ventura G, Iacopino S, Scozzafava A, et al. Prognostic significance of endothelial dysfunction in hypertensive patients. *Circulation*. (2001) 104:191–6. doi: 10.1161/01.CIR.104.2.191
19. Hambrecht R, Wolf A, Gielen S, Linke A, Hofer J, Erbs S, et al. Effect of exercise on coronary endothelial function in patients with coronary artery disease. *n Engl J Med*. (2000) 342:454–60. doi: 10.1056/NEJM200002173420702
20. Treasure CB, Klein JL, Weintraub WS, Talley JD, Stillabower ME, Kosinski AS, et al. Beneficial effects of cholesterol-lowering therapy on the coronary endothelium in patients with coronary artery disease. *n Engl J Med*. (1995) 332:481–7. doi: 10.1056/NEJM199502233320801
21. Buckley BJR, Watson PM, Murphy RC, Graves LEF, Whyte G, Thijssen DHJ. Carotid artery function is restored in subjects with elevated cardiovascular disease risk after a 12-week physical activity intervention. *Can J Cardiol*. (2019) 35:23–6. doi: 10.1016/j.cjca.2018.10.015
22. Van Mil ACCM, Pouwels S, Wilbrink J, Warlé MC, Thijssen DHJ. Carotid artery reactivity predicts events in peripheral arterial disease patients. *Ann Surg*. (2019) 269:767–73. doi: 10.1097/SLA.0000000000002558
23. van Mil AC, Hartman Y, van Oorschot F, Heemels A, Bax N, Dawson EA, et al. Correlation of carotid artery reactivity with cardiovascular risk factors and coronary artery vasodilator responses in asymptomatic, healthy volunteers. *J Hypertens*. (2017) 35:1026–34. doi: 10.1097/HJH.0000000000001274
24. Kaski JC, Elliott PM, Salomone O, Dickinson K, Gordon D, Hann C, et al. Concentration of circulating plasma endothelin in patients with angina and normal coronary angiograms. *Br Heart J*. (1995) 74:620–4. doi: 10.1136/hrt.74.6.620
25. Yanagisawa M, Kurihara H, Kimura S, Tomobe Y, Kobayashi M, Mitsui Y, et al. A novel potent vasoconstrictor peptide produced by vascular endothelial cells. *Nature*. (1988) 332:411–5. doi: 10.1038/332411a0
26. Naya M, Aikawa T, Manabe O, Obara M, Koyanagawa K, Katoh C, et al. Elevated serum endothelin-1 is an independent predictor of coronary microvascular dysfunction in non-obstructive territories in patients with coronary artery disease. *Heart Vessels*. (2021) 36:917–23. doi: 10.1007/s00380-020-01767-x
27. Willems LH, Thijssen DHJ, Donders ART, van der Vijver-Coppen RJ, Groh LA, Reijnen MMPJ, et al. A protocol for DUAL pathway inhibition (low-dose rivaroxaban and aspirin) as compared to aspirin only to improve endothelial function in peripheral artery disease. *Med Case Rep Study Protocols*. (2021) 2:e0163. doi: 10.1097/MD9.0000000000000163
28. Rutherford RB, Baker JD, Ernst C, Johnston KW, Porter JM, Ahn S, et al. Recommended standards for reports dealing with lower extremity ischemia: revised version. *J Vasc Surg*. (1997) 26:517–38. doi: 10.1016/S0741-5214(97)70045-4
29. Govers-Riemsag JWP, Smid M, Cooper JA, Bauer KA, Rosenberg RD, Hack CE, et al. The plasma kallikrein-kinin system and risk of cardiovascular disease in men. *J Thromb Haemost*. (2007) 5:1896–903. doi: 10.1111/j.1538-7836.2007.02687.x
30. Ludmer PL, Selwyn AP, Shook TL, Wayne RR, Mudge GH, Alexander RW, et al. Paradoxical vasoconstriction induced by acetylcholine in atherosclerotic coronary arteries. *n Engl J Med*. (1986) 315:1046–51. doi: 10.1056/NEJM198610233151702
31. Cox DA, Vita JA, Treasure CB, Fish RD, Alexander RW, Ganz P, et al. Atherosclerosis impairs flow-mediated dilation of coronary arteries in humans. *Circulation*. (1989) 80:458–65. doi: 10.1161/01.CIR.80.3.458
32. Chia PY, Teo A, Yeo TW. Overview of the Assessment of endothelial function in humans. *Front Med*. (2020) 7:542567. doi: 10.3389/fmed.2020.542567
33. Stroes ES, Koomans HA, de Bruin TW, Rabelink TJ. Vascular function in the forearm of hypercholesterolaemic patients off and on lipid-lowering medication. *Lancet*. (1995) 346:467–71. doi: 10.1016/S0140-6736(95)91322-X
34. O'Driscoll G, Green D, Taylor RR. Simvastatin, an HMG-coenzyme A reductase inhibitor, improves endothelial function within 1 month. *Circulation*. (1997) 95:1126–31. doi: 10.1161/01.CIR.95.5.1126
35. Buckley BJ, Thijssen DHJ, Murphy RC, Graves LEF, Cochrane M, Gillison F, et al. Pragmatic evaluation of a coproduced physical activity referral scheme: a UK quasi-experimental study. *BMJ Open*. (2020) 10:e034580. doi: 10.1136/bmjopen-2019-034580
36. Gailani D, Broze GJ Jr. Factor XI activation in a revised model of blood coagulation. *Science*. (1991) 253:909–12. doi: 10.1126/science.1652157
37. Warfarin Antiplatelet Vascular Evaluation Trial Investigators, Anand S, Yusuf S, Xie C, Pogue J, Eikelboom J, et al. Oral anticoagulant and antiplatelet therapy and peripheral arterial disease. *n Engl J Med*. (2007) 357:217–27. doi: 10.1056/NEJMoa065959
38. Petzold T, Thienel M, Dannenberg L, Mourikis P, Helten C, Ayhan A, et al. Rivaroxaban reduces arterial thrombosis by inhibition of FXa-driven

platelet activation *via* protease activated receptor-1. *Circ Res.* (2020) 126:486–500. doi: 10.1161/CIRCRESAHA.119.315099

39. Jurk K, Rothenaicher KF, Groß K, Rossmann H, Weißer G, Schmidtman I, et al. Differential inhibition of platelet reactivity by dual therapy with aspirin and low-dose rivaroxaban in peripheral arterial disease: a pilot study. *Front Cardiovasc Med.* (2022) 9:865166. doi: 10.3389/fcvm.2022.865166

40. Hara T, Fukuda D, Tanaka K, Higashikuni Y, Hirata Y, Nishimoto S, et al. Rivaroxaban, a novel oral anticoagulant, attenuates atherosclerotic plaque progression and destabilization in ApoE-deficient mice. *Atherosclerosis.* (2015) 242:639–46. doi: 10.1016/j.atherosclerosis.2015.03.023

41. Harrison DG, Armstrong ML, Freiman PC, Heistad DD. Restoration of endothelium-dependent relaxation by dietary treatment of atherosclerosis. *J Clin Invest.* (1987) 80:1808–11. doi: 10.1172/JCI113276

42. Posthuma JJ, Posma JJN, van Oerle R, Leenders P, van Gorp RH, Jaminon AMG, et al. Targeting coagulation factor Xa promotes regression of advanced atherosclerosis in apolipoprotein-e deficient mice. *Sci Rep.* (2019) 9:3909. doi: 10.1038/s41598-019-40602-w

43. Willems LH, Nagy M, Ten Cate H, Spronk HMH, Groh LA, Leentjens J, et al. Sustained inflammation, coagulation activation and elevated endothelin-1 levels without macrovascular dysfunction at 3 months after COVID-19. *Thromb Res.* (2022) 209:106–14. doi: 10.1016/j.thromres.2021.11.027



OPEN ACCESS

EDITED BY
Pasqualino Sirignano,
Sapienza University of Rome, Italy

REVIEWED BY
Ren Junhong,
Peking University, China
Hongpeng Zhang,
Chinese PLA General Hospital, China
Gioele Simonte,
Hospital of Santa Maria della
Misericordia in Perugia, Italy

*CORRESPONDENCE
Tiehao Wang
wangth31@163.com
Bin Huang
xgwkhb@126.com

†These authors have contributed
equally to this work and share first
authorship

SPECIALTY SECTION
This article was submitted to
Atherosclerosis and Vascular Medicine,
a section of the journal
Frontiers in Cardiovascular Medicine

RECEIVED 16 September 2022
ACCEPTED 27 October 2022
PUBLISHED 09 November 2022

CITATION
Shen Y, Wang J, Zhao J, Yuan D,
Wang T and Huang B (2022) DANCER:
Study protocol of a prospective,
non-randomized controlled trial for
crossed limb versus standard limb
configuration in endovascular
abdominal aortic aneurysm repair.
Front. Cardiovasc. Med. 9:1046200.
doi: 10.3389/fcvm.2022.1046200

COPYRIGHT
© 2022 Shen, Wang, Zhao, Yuan, Wang
and Huang. This is an open-access
article distributed under the terms of
the [Creative Commons Attribution
License \(CC BY\)](#). The use, distribution
or reproduction in other forums is
permitted, provided the original
author(s) and the copyright owner(s)
are credited and that the original
publication in this journal is cited, in
accordance with accepted academic
practice. No use, distribution or
reproduction is permitted which does
not comply with these terms.

DANCER: Study protocol of a prospective, non-randomized controlled trial for crossed limb versus standard limb configuration in endovascular abdominal aortic aneurysm repair

Yinzhi Shen^{1†}, Jiarong Wang^{2†}, Jichun Zhao², Ding Yuan²,
Tiehao Wang^{2*} and Bin Huang^{2*}

¹West China School of Medicine, Sichuan University, Chengdu, China, ²Department of Vascular Surgery, West China Hospital, Sichuan University, Chengdu, China

Background: Hostile anatomy, especially severely angulated neck and tortuous iliac arteries, has always been a conundrum in endovascular aneurysm repair (EVAR). Crossed limb (CL) graft, also called the “ballerina technique,” has been utilized to address this problem by facilitating gate cannulation. In terms of short and long-term outcomes, correlated studies have made inconsistent conclusions and this issue remains controversial. Based on a previous cohort study conducted in our center, we aim to prospectively compare the safety and efficacy between CL and standard limb (SL) configuration in patients receiving EVAR.

Methods: This is a prospective, single-center, non-randomized controlled trial. A total of 275 patients who meet the inclusion criteria will be enrolled and allocated with a 4:11 ratio of CL to SL, which is based on results of our previous study. All patients will receive same perioperative management and postoperative medications. All EVAR procedures will be performed under standard protocol, utilizing Endurant II or IIs Stent Graft. The configuration of the graft stent will be decided by surgeons and confirmed by final angiography. The primary outcome is 3-year freedom from major adverse limb-graft events (MALEs). Endpoints will be assessed at the following time points: 1, 6, 12, 24, and 36 months.

Discussion: To our best knowledge, this crossed vs. standard Configuration in Endovascular Repair (DANCER) trial is the first non-randomized controlled trial to compare these two graft configurations in EVAR. The main aim is to compare the MALEs between two groups at 3 years postoperatively. This trial will hopefully provide high-level evidence for employing CL in EVAR.

Clinical trial registration: [www.chictr.org.cn], identifier [ChiCTR2100053055].

KEYWORDS

non-randomized controlled trial, crossed limb, standard limb, EVAR, abdominal aortic aneurysm

Introduction

Abdominal aortic aneurysm (AAA) is a pathological, localized dilation of abdominal aorta (1), characterized by decreased smooth muscle cells, extracellular matrix breakdown, inflammatory cell infiltration and endothelial dysfunction (2). The prevalence of AAA increases with age, estimated to be 1.3–1.7% in 65-year-old men (3, 4). Many patients with AAA are asymptomatic and mostly diagnosed after incidental imaging or, in the worst case, rupture (1). With mortality up to 85%, AAA rupture is an important death cause in adults, which renders AAA one of the most important diseases in vascular surgery (5). Both the Society for Vascular Surgery and the European Society for Vascular Surgery have recommended endovascular aneurysm repair (EVAR) as the preferred treatment modality for AAA in certain patients (6, 7). Compared with traditional open surgical repair, EVAR has the advantage of minimal invasiveness and shorter procedure time (8). Nevertheless, EVAR performed in patients with hostile anatomy could be technically challenging and more likely to induce postoperative complications. A large number of studies concluded that hostile proximal neck is associated with a higher rate of type I endoleak, secondary procedure and mortality in the short and long term after the procedure (9–11). Similarly, distal aortoiliac tortuosity has been revealed to be related with higher graft-related complications (12–14). To resolve this problem, great innovations have been made in the past few decades and one of them, crossed limb (CL), was raised in 2002 for patients with severely angulated neck. This ballet-dancer-like configuration could facilitate gate cannulation and theoretically avoid graft disconnection and endoleaks (15). By now, this technology has been widely applied in clinical practice.

For efficacy of the CL in practice, however, related studies have drawn inconsistent conclusions, which makes the

true effect of CL doubtful. By analysis of computed fluid dynamics, CL showed a tendency to prevent stent thrombosis, accompanied by tolerance for higher wall shear stress and helicity characteristics (16, 17). On the contrary, long-term fatigue and displacement implications were revealed by the same studies and another one demonstrated that it was the angle of the aneurysm neck other than the configuration that affected hemodynamic index (18). Similar controversial outcomes were observed in clinical trials. Two retrospective cohort trials showed that CL group had a longer procedural time and more type II endoleak compared with standard limb (SL) groups; however, technical success rate, postoperative complications, reintervention and overall survival were comparable (19, 20). This result was mirrored in the latest meta-analysis with no significant difference found in perioperative mortality, endoleak or limb occlusion. This study concluded that CL did not confer inferior clinical outcomes compared to SL in the medium term (21).

To further explore this issue, we conducted a cohort study in 2021, which suggested that no significant evidence was found to favor either configuration in terms of adverse limb events, endoleak, reintervention or overall survival (22). A trend toward a lower risk of type IB endoleak was observed in the CL group after stratification by large aneurysm sac or tortuous iliac artery. On the other hand, CL incurred a higher risk of reintervention and adverse limb events in patients with angulated aneurysmal neck. As commented by editors, our previous study showed interesting results and had the advantage of significant enrolled patients and sufficient time of follow up. However, it was subject to its retrospective, observational nature and other limitations. To elucidate this problem, a prospective study with a uniform reporting standard and careful design is required accordingly (23). Therefore, the utility of CL configuration requires further investigation, which propels us to launch this study.

This prospective, single-center, non-randomized controlled trial aims to compare the safety and efficacy of CL vs. SL configuration in EVAR patients, which could provide high-level evidence for choice of optimal stent graft configuration.

Abbreviations: AAA, abdominal aortic aneurysm; AP, anterior-posterior; CL, crossed limb; DANCER, crossed vs. standard Configuration in Endovascular Repair; EVAR, endovascular aneurysm repair; LR, left-right; MALEs, major adverse limb-graft events; SL, standard limb; SPIRIT, Standard Protocol Items: Recommendations for Interventional Trials.

The primary outcome of interest is 3-year freedom from major adverse limb-graft events (MALEs).

Hypothesis to be tested

In AAA patients who receive EVAR, CL is not inferior to SL configuration in terms of safety and efficacy in the short and long term.

Materials and methods

Study design and approvals

This study is a prospective, single-center, non-randomized controlled study conducted in West China Hospital. This protocol is developed according to Standard Protocol Items: Recommendations for Interventional Trials (SPIRIT) 2013 Statement for study protocols of clinical trials (24). The SPIRIT checklist has been completed in additional file 1.

Recruitment and enrollment

We recruit patients diagnosed with infrarenal AAA (Figure 1) from 1st December 2021. The eligibility criteria for inclusion and exclusion are shown in Table 1. Adult patients with indicated infrarenal AAA (diagnosed with ICD I71.3 and I71.4) and suitable iliofemoral anatomy are included in our study. Excluded are patients who could not tolerate perioperative medications and patients expected to receive reintervention. Both groups of patients share general inclusion or exclusion criteria.

We will recruit patients by putting up posters and advertising online to meet the expected enrollment. In addition, we provide fast-track follow-up for patients who are willing to participate in our study. Figure 2 shows the schedule of enrollment, interventions and assessments, following the template provided by SPIRIT (24).

Allocations of intervention

Based on the anatomic features of the aneurysm by intraoperative imaging, surgeons will determine whether to adopt CL or SL configuration. When both configurations are feasible, surgeons will assign the limb configuration based on covariate adaptive matching between the two groups. The major matched covariates are as follows: age, gender and aneurysm diameter. Both surgeons and participants are not blinded to the interventions, and only statisticians who analyze the data are blinded.

The CL and SL configurations are defined as crossed or uncrossed limb grafts in anteroposterior view of the final angiogram, respectively. CL is further subdivided into anterior-posterior (AP) cross and left-right (LR) cross, which correspond to ≥ 50 and $< 50\%$ overlapped areas between two limb grafts in the angiogram. SL is similarly subdivided into AP parallel and LR parallel with the same definition.

The included patients will receive the same perioperative management, including blood pressure control, analgesia and medication with antiplatelets and statins. In interventional operating room, both common femoral arteries will be used for percutaneous or cut down access. After administration of 0.5 mg/kg unfractionated heparin, graft stents are placed in accordance with instruction for use by an experienced surgeon of vascular surgery. Treatment procedures are performed under a standard protocol. The Endurant II or IIs Stent Graft (Medtronic, Minneapolis, Minn) is used for repair.

Postoperative medications include antiplatelet monotherapy (aspirin 100 mg once a day or clopidogrel 75 mg once a day) and statins. Patients are expected to take these medications all life unless severe adverse event occurs. Anticoagulants, such as low molecular weight heparin or direct oral anticoagulants, will be used according to surgeons' decision.

Follow-up

After the procedure, all included patients will receive follow-up in outpatient clinics at 1, 6, and 12 months and annually thereafter. The required routine examinations include history taking, physical examination, blood biochemical index and duplex ultrasound. All biological specimens will be processed in routine procedure and not be used in ancillary or other studies. The computed tomography angiography will be performed to search for detailed information if any adverse event, especially endoleak or limb thrombosis, is found by duplex ultrasound. Patients who are unable to return to the outpatient clinic will be suggested to undergo duplex ultrasonography or computed tomography in local medical institutions, which will send medical records and images back to researchers. For patients who fail to finish the expected follow-up, telephone interview or WeChat message will be used instead to record survival status and postoperative adverse events. Due to no additional harm induced by the trial, all adverse events will be processed according to normal treatment procedure and patients will not automatically quit the group or receive additional compensation.

Patients are defined as dropout if the following events occur: (1) Fail to complete the expected follow-up and could not obtain image or medical records: a subject is considered lost to follow-up if they could not be contacted *via* five attempts by telephone or WeChat message. (2) Make withdrawal consent: all

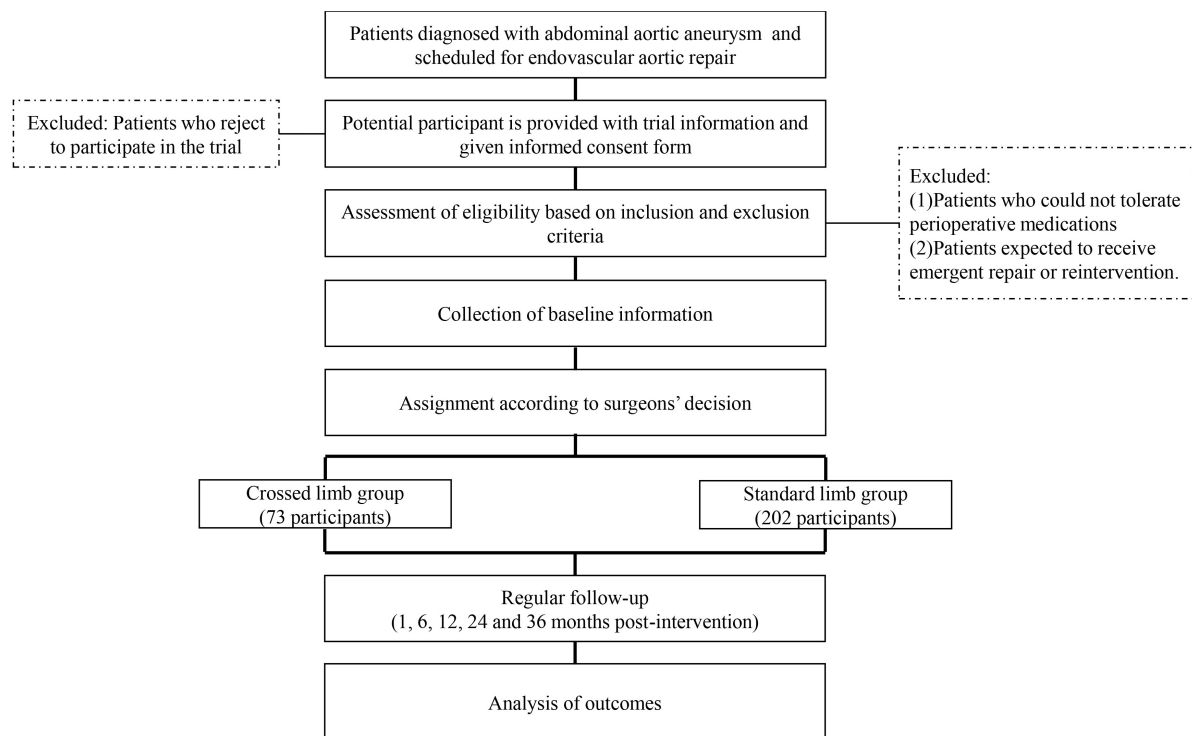


FIGURE 1

The procedure of screening, randomization and follow-up in the DANCER trial.

TABLE 1 Inclusion and exclusion criteria for participants.

Inclusion

Patients are considered eligible if they meet all of the following criteria:

1. Men or non-pregnant women aged ≥ 18 years and with sufficient life expectancy to complete all the processes of the study.
2. Diagnosed with infrarenal abdominal aortic aneurysm (according to ICD I71.3 and I71.4) and indicated for surgical intervention.
3. Local anatomy of bilateral femoral and iliac arteries allows for guide wire passing.
4. Provide written informed consent and agree to participate in the study.
5. Placement of iliac endografts is required during the procedure.

Exclusion

Patients shall be excluded from the trial if they meet any of the following criteria:

1. Unable to tolerate contrast agents, antiplatelets or anticoagulants.
2. Recorded with previous primary repair for AAA, no matter EVAR or open surgical repair.

AAA, abdominal aortic aneurysm; EVAR, endovascular aneurysm repair.

participants have the right to withdraw from the study at any time for any reason without obstruction.

Outcomes of interest

The primary outcome is 3-year freedom from MALEs, which involves type IB/III endoleak and limb occlusion. Type IB endoleak is defined as persistent direct flow in the aneurysm sac due to inadequate distal seal of the stent graft. Type III endoleak is defined as persistent direct flow resulting from stent graft component separation or fabric tear. Limb occlusion is defined as a total occlusion occurring in limb grafts, regardless

of symptoms, or an invasively treated stenosis resulting from thrombus formation ($> 50\%$ lumen reduction).

The secondary outcomes involve 3-year freedom from type IA endoleak and 3-year freedom from aortic reintervention. Type IA endoleak is defined as persistent direct flow in the aneurysm sac due to inadequate proximal seal of the stent graft. Aortic reintervention refers to any secondary surgical procedure related to the index EVAR.

Other outcomes consist of three aspects: intraoperative technical outcomes (operation time, radiation exposure time, dosage of contrast medium and technical success rate); short-term postoperative outcomes (length of stay in intensive care unit or vascular ward, acute kidney injury, 30-day overall



	Study Period						
	Enrollment	Allocation	Post allocation				Close-out
Time point	-t1	0	t1 (1month)	t2 (6months)	t3 (12months)	t4 (24 months)	36 months after operation
Enrollment:							
Eligibility screen	X						
Informed consent	X						
Preoperative management	X						
Allocation		X					
Intervention:							
Crossed limb							
Standard limb							
Assessments:							
Demographic & anatomical details	X	X					
Primary outcomes			X	X	X	X	X
Secondary outcomes			X	X	X	X	X
Other outcomes			X	X	X	X	X

FIGURE 2
The schedule of enrollment, interventions and assessments.

morbidity, 30-day major adverse cardiac events, 30-day all-cause mortality); long-term outcomes (renal function decline, occurrence of type I/II/III endoleak or stent migration, freedom from major adverse cardiac events, aneurysm related death, overall survival).

Detailed information for outcomes is listed in **Table 2**.

Data collection

Figure 1 shows the flow diagram of the trial. Once patients are admitted, baseline data will be collected for both groups, including demographic characteristics, comorbidities and anatomical variables. The demographics are collected from history taking and hospital information system. The comorbidity is evaluated by the Charlson Comorbidity Index to quantify its severity. Anatomical variables are as follows: length of aneurysm neck, oversizing ratio in proximal neck and distal limb, neck angulation, maximum diameter of aneurysm sac, intramural thrombus load of aneurysmal sac, iliac tortuosity, common iliac artery aneurysm and distal iliac calcification. We will report reasons for withdrawal for each group and compare the reasons qualitatively. Details of the procedure, consisting of operation time, radiation exposure time and contrast medium dosage, are recorded immediately after the operations. At preoperative and postoperative evaluation (24, 48, and 72 h),

laboratory examinations will be conducted and corresponding results will be collected from the laboratory information system.

Quality control

The study staff have received systematic training for recording all baseline information before initiation of the project, with a special focus on recording comorbidity and measuring parameters of AAA. Pamphlets with protocols for history taking and definitions for related comorbidity have been distributed to the staff. By computed tomography angiography, all the diameters are measured from the minor axis of axial cuts or from planes perpendicular to the centerline in reformatted slices. Two researchers will independently complete the measurement and when more than 10% differences occur, a senior member will arbitrate and give final result. Medical staffs will strictly follow the standard procedure of AAA treatment in our hospital and provide the same perioperative management or nursing care for all patients.

Sample size calculation

We calculate the sample size for this study based on the results of our previous study (22), in which 11.5 and 7.9% of

TABLE 2 Detailed information for outcomes.

Outcomes	Definition
Primary outcome	
3-year freedom from MALEs	Free of type IB, III endoleak and limb occlusion within 3 years
Secondary outcomes	
3-year freedom from type IA endoleak	Free of type I endoleak within 3 years
3-year freedom from aortic reintervention	Free of any reintervention related to the index EVAR within 3 years
Other outcomes	
Intraoperative technical outcome	
technical success rate	Freedom from surgical conversion or mortality, type I or III endoleaks, or graft limb obstruction after the deployment of devices
Short-term postoperative outcomes	
Acute kidney injury	Serum creatinine elevates by 0.3 mg/dL or 50% compared with baseline within 48 h; or urine less than 0.5 mL/kg/h for more than 6 h
30-day morbidity	The existence of any adverse event within 30 days, consisting of infection, pseudoaneurysm, deep venous thrombosis, hypoalbuminemia, hemorrhage, embolism, stroke, buttock ischemia and systematic complications such as pulmonary, cardiac, cerebral and bowel events
30-day MACEs	Diagnosed with myocardial infarction, chronic cardiac failure, or receive repeat revascularization or died within 30 days
Long-term outcomes	
Renal function decline	Diagnosed with chronic renal failure and could not be attributed to other known causes
Type I endoleak	Endoleak due to inadequate proximal or distal seal of the stent graft
Type II endoleak	Endoleak originating from collateral vessels
Type III endoleak	Endoleak resulting from stent graft component separation or fabric tear
Stent migration	Migration from original position for more than 5 mm
Aneurysm related death	All deaths from secondary aneurysm rupture after repair, death within 30 days of any reintervention attributable to the aneurysm or death from other aneurysm-related causes (including graft infection or fistula)

MALEs, major adverse limb-graft events; EVAR, endovascular aneurysm repair; MACEs, major adverse cardiac events.

patients suffered from adverse limb events in CL and SL groups, respectively. In this trial, we hypothesize that the freedom from adverse limb events in the CL group is not inferior to that in the SL group. The predetermined non-inferiority margin on the risk difference scale (8) is set to 0.15 between the two groups. The type I and II error rates are set to 0.05 and 0.2, respectively. As the intraoperative choice of limb configuration is difficult to randomize, the ratio of enrolled patients between the CL and SL groups is set to 4:11 based on our previous cohort study (22). After accounting for a 20% rate of dropout, it is calculated that 73 subjects are needed for the CL group, and this value is 202 in the SL group. All calculations are performed by PASS 15 software.

Statistical analysis

Categorical data is expressed as number and rate, while continuous data is expressed as means \pm standard deviation if they are normally distributed or median with interquartile range otherwise. Student's *t*-test or Mann-Whitney *U*-test

is used for univariate analysis of continuous data. χ^2 -test or Fisher's exact test is used for categorical data. For primary analyses, multivariate logistic regression is used to calculate adjusted odds ratio and 95% confidence interval for short-term outcomes. Cox proportional hazard regression analysis and marginal structural model are adopted to assess the association between limb configuration and time-to-event outcomes.

The propensity score to undergo CL or SL is estimated by logistic regression model based on demographic and anatomic information. Inverse probability of treatment weighting adjusted analyses are performed to achieve weighted balance with standardized differences < 0.10 . Sensitivity analysis is conducted to stabilize the weights by truncating the non-overlapping tails of the propensity score distributions which below or above the 1st and 99th percentiles. Subgroup analysis is conducted in terms of large aneurysm sac, severely angulated neck, tortuous iliac arteries and iliac landing zone (whether using bell-bottom iliac stent graft). In addition, this analysis will be carried out in AP and LR subgroups. R studio Version

1.2.1335¹ and Empower (X&Y solutions, Inc., Boston, MA)² are utilized for statistical analysis.

Patient and public involvement

Patients are also included in the design of the crossED vs. stANDARD Configuration in Endovascular Repair (DANCER). We conducted a preliminary survey in AAA patients who would receive EVAR to investigate the preferred follow-up modality and clinical outcomes they care most. Subsequent improvements were made accordingly.

Discussion

AAA is a localized dilation of infrarenal abdominal aorta. As a degenerative disease (25), it is common in the elderly population, with an estimated prevalence rate of 3.3% in men aged 65–74 years (26). AAA rupture is the most emergent case and has a high mortality rate even after immediate surgery (27). Therefore, prophylactic repair, either conducted by open surgery or EVAR, plays an important role in the treatment. EVAR has been recommended as a first-line modality for AAA (6, 7) and is widely applied in clinical practice. However, local vascular anatomy, in most cases referred to proximal neck, aneurysm sac, or aortoiliac arteries (Figure 3) (8), determines a successful EVAR performance, achieving sufficient sealing and fixation of anchoring segments (28). It could otherwise be technically challenging for the procedure, especially when cannulating contralateral gate of the endograft. Moreover, these anatomic predictors have a negative influence on postoperative outcomes. Angulated neck is found to be a predictor for sac enlargement (29), which is closely linked with postoperative aortic rupture (30). Sac remodeling, with a close connection with endoleaks, reintervention and mortality, may be affected by hostile neck and AAA volume (31). There is mounting evidence proving that patients with these hostile anatomical features could suffer from postoperative adverse events more commonly (32–35). As a result, for patients with hostile anatomy and serious comorbidities, clinicians may face a dilemma, as both EVAR and open surgery repair could be inapplicable.

Described by Ramaiah et al. in 2002 first (15), CL technique (Figure 4) is a useful adjunct to solve this problem by connecting ipsilateral guidewire to contralateral gate, arranging the limb graft just like a ballerina. It is expected to facilitate the procedure and, furthermore, reduce graft gate disconnection and endoleak. The true effect of CL, however, on postoperative outcomes has yet to be elucidated and currently no indications or contraindications have been described. This

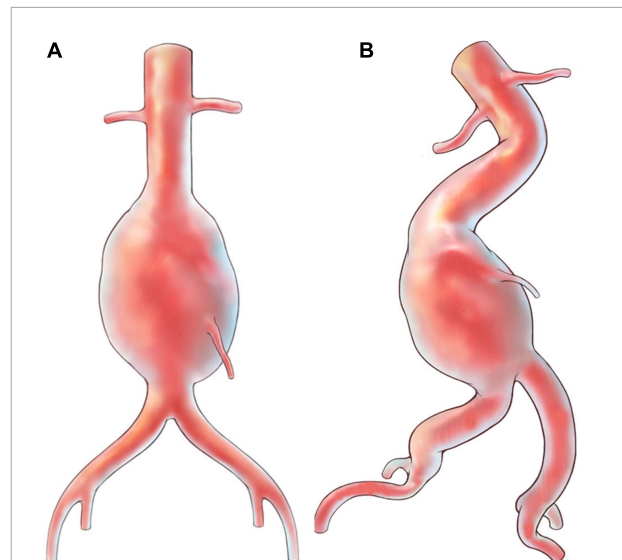


FIGURE 3
Illustrations for abdominal aortic aneurysm with hostile anatomy. (A) Aneurysm with "normal" appearance; (B) aneurysm with angulated neck and tortuous iliac arteries.

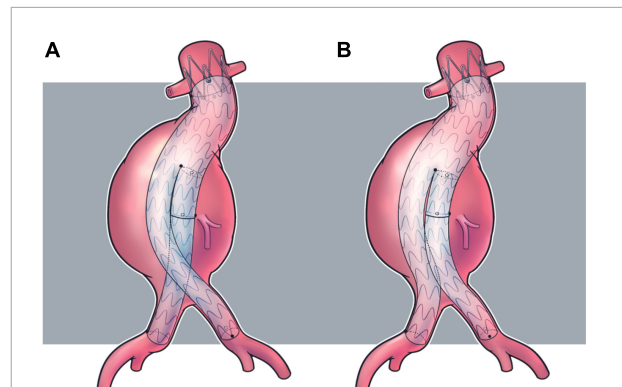


FIGURE 4
Illustrations for stent graft configuration. (A) Crossed limb; (B) standard limb.

is a challenging issue for research because involved patients are always characterized by complicated anatomical conditions, which could induce considerable selection bias. Additionally, randomized controlled trials, with the highest evidence level, could be extremely difficult to conduct, as the performance of CL or SL is mainly based on anatomy and surgeons' experience. Related studies, mainly cohort studies, have made inconsistent conclusions on this issue. Several studies revealed no difference in perioperative death, short or long term endoleak, limb graft occlusion, aneurysm sac expansion, reintervention or overall survival (19, 20), which was confirmed by a recent meta-analysis (21). While in our previous cohort study, which was characterized by the largest sample size and additional subgroup analysis, patients with large aneurysm sac and tortuous iliac

¹ <http://www.R-project.org>

² www.empowerstats.com

arteries encountered fewer type I endoleaks in the CL group (22). This conclusion was consistent with a recent hemodynamic study revealing that this non-standard configuration could sustain higher wall shear stress and helicity characteristics (16, 17). However, it was questioned that it may be modified delivering system, instead of CL, that improved prognosis (36). Moreover, other computational analyses did not conclude likewise. Georgakarakos et al. revealed that the displacement force, one of the targets that CL aims at, was only slightly affected by the CL configuration and this effect could be blunted by concomitant modifications of the stent (37). Qing et al. studied the hemodynamic performance of these two configurations and concluded that the main factor affecting the index was the angle of aneurysm neck, while configuration had little effect on hemodynamics (18).

Several limitations exist in our study. Firstly, this is a non-randomized controlled trial and therefore it could not provide higher level of evidence like randomized one. However, as discussed above, we believe that this is the most suitable research type for this issue and could draw convincing conclusions similarly. Secondly, we conduct this trial in a single center in West China Hospital, which is a tertiary medical center and receive many patients with complex medical problems. This may cause heterogeneity and whether this conclusion could be generalized to the world is uncertain. The large sample number we anticipated, however, could make up for this problem partly.

Currently, the true effect of CL on clinical outcomes is still a matter of debate. The lack of a higher level of evidence, especially prospective clinical trials in this scenario, prevents its elucidation. Therefore, the main aim of our present trial is to compare the safety and efficacy between CL and SL configuration in patients receiving EVAR with Endurant II or IIs Stent Graft. Moreover, two spatial subclassifications of CL and SL, AP and LR, will be further investigated. This will hopefully provide high-level evidence for limb graft placement in AAA patients, especially in those with hostile anatomy.

Ethics statement

The trial was approved by the Ethics Committee on Biomedical Research, West China Hospital of Sichuan

University (approval number: 202–1353) on 8th November 2021 and registered in the Chinese Clinical Trial Registry (registration number: ChiCTR2100053055) on 10th November 2021. The studies involving human participants were reviewed and approved by Ethics Committee on Biomedical Research, West China Hospital of Sichuan University. The patients/participants will all provide their written informed consent to participate in this study.

Author contributions

JZ was the project leader. YS and JW wrote the manuscript of the protocol. JW was responsible for calculating the sample size and performing data analysis. BH and TW contributed to devise the study concept. All authors contributed to patient recruitment, data collection and EVAR performance, read, and approved the final manuscript.

Funding

This work was supported by the Sichuan Province Science and Technology Support Program (Grant nos. 2022YFS0366, 2022YFS0187, 2022YFS0359, 2022YFS0361).

Conflict of interest

The authors declare that the research was conducted in the absence of any commercial or financial relationships that could be construed as a potential conflict of interest.

Publisher's note

All claims expressed in this article are solely those of the authors and do not necessarily represent those of their affiliated organizations, or those of the publisher, the editors and the reviewers. Any product that may be evaluated in this article, or claim that may be made by its manufacturer, is not guaranteed or endorsed by the publisher.

References

1. Sakalihasan N, Limet R, Defawe OD. Abdominal aortic aneurysm. *Lancet*. (2005) 365:1577–89. doi: 10.1016/s0140-6736(05)66459-8
2. Sun J, Deng H, Zhou Z, Xiong X, Gao L. Endothelium as a potential target for treatment of abdominal aortic aneurysm. *Oxid Med Cell Longev*. (2018) 2018:6306542. doi: 10.1155/2018/6306542
3. Svensjö S, Björck M, Gürtelschmid M, Djavani Gidlund K, Hellberg A, Wanhainen A. Low prevalence of abdominal aortic aneurysm among 65-year-old
4. swedish men indicates a change in the epidemiology of the disease. *Circulation*. (2011) 124:1118–23. doi: 10.1161/circulationaha.111.030379
4. Jacomelli J, Summers L, Stevenson A, Lees T, Earnshaw JJ. Impact of the first 5 years of a national abdominal aortic aneurysm screening programme. *Br J Surg*. (2016) 103:1125–31. doi: 10.1002/bjs.10173
5. Czerny M, Beyersdorf F. Abdominal aortic aneurysm. *Dtsch Arztebl Int*. (2020) 117:811–2. doi: 10.3238/arztebl.2020.0811

6. Chaikof EL, Dalman RL, Eskandari MK, Jackson BM, Lee WA, Mansour MA, et al. The society for vascular surgery practice guidelines on the care of patients with an abdominal aortic aneurysm. *J Vasc Surg.* (2018) 67:2–77.e2. doi: 10.1016/j.jvs.2017.10.044
7. Wanhainen A, Verzini F, Van Herzele I, Allaire E, Bown M, Cohnert T, et al. Editor's choice - European society for vascular surgery (ESVS) 2019 clinical practice guidelines on the management of abdominal aorto-iliac artery aneurysms. *Eur J Vasc Endovasc Surg.* (2019) 57:8–93. doi: 10.1016/j.ejvs.2018.09.020
8. Kim HO, Yim NY, Kim JK, Kang YJ, Lee BC. Endovascular aneurysm repair for abdominal aortic aneurysm: a comprehensive review. *Korean J Radiol.* (2019) 20:1247–65. doi: 10.3348/kjr.2018.0927
9. Antoniou GA, Georgiadis GS, Antoniou SA, Kuhan G, Murray DA. Meta-analysis of outcomes of endovascular abdominal aortic aneurysm repair in patients with hostile and friendly neck anatomy. *J Vasc Surg.* (2013) 57:527–38. doi: 10.1016/j.jvs.2012.09.050
10. Bernardini G, Litterscheid S, Torsello GB, Torsello GF, Beropoulos E, Özdemir-van Brunschot DA. Meta-analysis of safety and efficacy of endovascular aneurysm repair in aneurysm patients with severe angulated infrarenal neck. *PLoS One.* (2022) 17:e0264327. doi: 10.1371/journal.pone.0264327
11. van Schaik TG, Meekel JP, de Bruin JL, Yeung KK, Blankenstein JD. Identifying high risk for proximal endograft failure after EVAR in patients suitable for both open and endovascular elective aneurysm repair. *J Vasc Surg.* (2022) 76:1261–9. doi: 10.1016/j.jvs.2022.06.001
12. Gallitto E, Gargiulo M, Faggioli G, Pini R, Mascoli C, Freyrie A, et al. Impact of iliac artery anatomy on the outcome of fenestrated and branched endovascular aortic repair. *J Vasc Surg.* (2017) 66:1659–67. doi: 10.1016/j.jvs.2017.04.063
13. Coulston J, Baigent A, Selvachandran H, Jones S, Torella F, Fisher R. The impact of endovascular aneurysm repair on aortoiliac tortuosity and its use as a predictor of iliac limb complications. *J Vasc Surg.* (2014) 60:585–9. doi: 10.1016/j.jvs.2014.03.279
14. Wyss TR, Dick F, Brown LC, Greenhalgh RM. The influence of thrombus, calcification, angulation, and tortuosity of attachment sites on the time to the first graft-related complication after endovascular aneurysm repair. *J Vasc Surg.* (2011) 54:965–71. doi: 10.1016/j.jvs.2011.04.007
15. Ramaiah VG, Thompson CS, Shafique S, Rodriguez JA, Ravi R, DiMugno L, et al. Crossing the limbs: a useful adjunct for successful deployment of the aneurysm stent-graft. *J Endovasc Ther.* (2002) 9:583–6. doi: 10.1177/152660280200900505
16. Ashraf F, Ambreen T, Park CW, Kim DI. Comparative evaluation of balloon-type and conventional stent graft configurations for endovascular aneurysm repair: a CFD analysis. *Clin Hemorheol Microcirc.* (2021) 78:1–27. doi: 10.3233/ch-200996
17. Shek TL, Tse LW, Nabovati A, Amon CH. Computational fluid dynamics evaluation of the cross-limb stent graft configuration for endovascular aneurysm repair. *J Biomech Eng.* (2012) 134:121002. doi: 10.1115/1.4007950
18. Qing M, Qiu Y, Wang J, Zheng T, Yuan DA. Comparative Study on the hemodynamic performance within cross and non-cross stent-grafts for abdominal aortic aneurysms with an angulated neck. *Front Physiol.* (2021) 12:795085. doi: 10.3389/fphys.2021.795085
19. Georgiadis GS, Georgakarakos EI, Antoniou GA, Trellopoulos G, Argyriou C, Nikolopoulos ES, et al. Clinical outcomes after Crossed-Limb Vs. Conventional endograft configuration in endovascular AAA repair. *J Endovasc Ther.* (2013) 20:853–62. doi: 10.1583/13-4286mr.1
20. Dattani N, Wild J, Sidloff D, Fishwick G, Bown M, Choke E, et al. Outcomes following limb crossing in endovascular aneurysm repairs. *Vasc Endovasc Surg.* (2015) 49:52–7. doi: 10.1177/1538574415587512
21. Kontopodis N, Galanakis N, Ioannou CV, Tsetis D, Georgiadis GS, Antoniou GA. Meta-analysis of the crossed versus standard limb configuration in endovascular aneurysm repair. *Ann Vasc Surg.* (2022) 80:358–69. doi: 10.1016/j.avsg.2021.10.037
22. Wang J, Zhao J, Ma Y, Huang B, Yang Y, Yuan D, et al. Editor's choice - mid term outcomes of Crossed Limb Vs. Standard Limb configuration in endovascular abdominal aortic aneurysm repair: a propensity score analysis. *Eur J Vasc Endovasc Surg.* (2021) 61:579–88. doi: 10.1016/j.ejvs.2021.01.018
23. van den Berg JC. The crossed legs, “Ballerina” (or “Johnnie Walker”) configuration: a solution or bottle neck in endovascular aneurysm repair? *Eur J Vasc Endovasc Surg.* (2021) 61:589–90. doi: 10.1016/j.ejvs.2021.01.041
24. Chan AW, Tetzlaff JM, Götzsche PC, Altman DG, Mann H, Berlin JA, et al. SPIRIT 2013 explanation and elaboration: guidance for protocols of clinical trials. *BMJ.* (2013) 346:e7586. doi: 10.1136/bmj.e7586
25. Sakalihasan N, Michel JB, Katsargyris A, Kuivaniemi H, Defraigne JO, Nchimi A, et al. Abdominal aortic aneurysms. *Nat Rev Dis Primers.* (2018) 4:34. doi: 10.1038/s41572-018-0030-7
26. Grøndal N, Sogaard R, Lindholt JS. Baseline prevalence of abdominal aortic aneurysm, peripheral arterial disease and hypertension in men aged 65–74 years from a Population Screening Study (Viva Trial). *Br J Surg.* (2015) 102:902–6. doi: 10.1002/bjs.9825
27. Acher C, Acher CW, Castello Ramirez MC, Wynn M. Operative mortality and morbidity in ruptured abdominal aortic aneurysms in the endovascular age. *Ann Vasc Surg.* (2020) 66:70–6. doi: 10.1016/j.avsg.2019.10.073
28. Stather PW, Wild JB, Sayers RD, Bown MJ, Choke E. Endovascular aortic aneurysm repair in patients with hostile neck anatomy. *J Endovasc Ther.* (2013) 20:623–37. doi: 10.1583/13-4320mr.1
29. Schanzer A, Greenberg RK, Hevelone N, Robinson WP, Eslami MH, Goldberg RJ, et al. Predictors of abdominal aortic aneurysm sac enlargement after endovascular repair. *Circulation.* (2011) 123:2848–55. doi: 10.1161/circulationaha.110.014902
30. Wyss TR, Brown LC, Powell JT, Greenhalgh RM. Rate and predictability of graft rupture after endovascular and open abdominal aortic aneurysm repair: data from the EVAR trials. *Ann Surg.* (2010) 252:805–12. doi: 10.1097/SLA.0b013e3181fcb44a
31. van Rijswijk RE, Jebbink EG, Zeebregts CJ, Reijnen MA. Systematic review of anatomic predictors of abdominal aortic aneurysm remodeling after endovascular repair. *J Vasc Surg.* (2022) 75:1777–85. doi: 10.1016/j.jvs.2021.11.071
32. Mathlouthi A, Locham S, Dakour-Aridi H, Black JH, Malas MB. Impact of suprarenal neck angulation on endovascular aneurysm repair outcomes. *J Vasc Surg.* (2020) 71:1900–6. doi: 10.1016/j.jvs.2019.08.250
33. Qayyum H, Hansrani V, Antoniou GA. Prognostic role of severe infrarenal aortic neck angulation in endovascular aneurysm repair. *Eur J Vasc Endovasc Surg.* (2021) 62:409–21. doi: 10.1016/j.ejvs.2021.05.014
34. Oliveira NFG, Gonçalves FB, Hoeks SE, Josee van Rijn M, Ultee K, Pinto JP, et al. Long-term outcomes of standard endovascular aneurysm repair in patients with severe neck angulation. *J Vasc Surg.* (2018) 68:1725–35. doi: 10.1016/j.jvs.2018.03.427
35. Hobo R, Kievit J, Leurs LJ, Buth J. Influence of severe infrarenal aortic neck angulation on complications at the proximal neck following endovascular AAA repair: a Eurostar Study. *J Endovasc Ther.* (2007) 14:1–11. doi: 10.1583/06-1914.1
36. Kakkos SK, Tsolakis IA, Zampakis P. Re: “Midterm outcomes of Crossed Limb Vs. Standard Limb configuration in endovascular abdominal aortic aneurysm repair: a propensity score analysis”. *Eur J Vasc Endovasc Surg.* (2021) 62:661. doi: 10.1016/j.ejvs.2021.06.035
37. Georgakarakos E, Xenakis A, Manopoulos C, Georgiadis GS, Tsangaris S, Lazarides MK. Modeling and computational analysis of the hemodynamic effects of crossing the limbs in an aortic endograft (“Ballerina” Position). *J Endovasc Ther.* (2012) 19:549–57. doi: 10.1583/12-3820.1



OPEN ACCESS

EDITED BY

Xuebin Qin,
Tulane University, United States

REVIEWED BY

Fengming Liu,
Shandong University, China
Min Cheng,
Weifang Medical University, China

*CORRESPONDENCE

Liang Qiu
liangqiu@jxutcm.edu.cn
Jun Yu
jun.yu@temple.edu

[†]These authors share first authorship

SPECIALTY SECTION

This article was submitted to
Atherosclerosis and Vascular Medicine,
a section of the journal
Frontiers in Cardiovascular Medicine

RECEIVED 19 August 2022

ACCEPTED 01 November 2022

PUBLISHED 24 November 2022

CITATION

Tang L, Kuang C, Shan D, Shi M, Li J,
Qiu L and Yu J (2022) The ethanol
extract of *Edgeworthia gardneri* (Wall.)
Meisn attenuates macrophage foam
cell formation and atherogenesis in
ApoE^{-/-} mice.
Front. Cardiovasc. Med. 9:1023438.
doi: 10.3389/fcvm.2022.1023438

COPYRIGHT

© 2022 Tang, Kuang, Shan, Shi, Li, Qiu
and Yu. This is an open-access article
distributed under the terms of the
[Creative Commons Attribution License](#)
(CC BY). The use, distribution or
reproduction in other forums is
permitted, provided the original
author(s) and the copyright owner(s)
are credited and that the original
publication in this journal is cited, in
accordance with accepted academic
practice. No use, distribution or
reproduction is permitted which does
not comply with these terms.

The ethanol extract of *Edgeworthia gardneri* (Wall.) Meisn attenuates macrophage foam cell formation and atherogenesis in ApoE^{-/-} mice

Le Tang^{1,2†}, Cuifang Kuang^{1,2†}, Dan Shan^{1,2,3}, Min Shi^{1,2},
Jiangsheng Li^{1,2}, Liang Qiu^{1,2*} and Jun Yu^{3*}

¹Centre for Translational Medicine, Jiangxi University of Chinese Medicine, Nanchang, China,

²Jiangxi Key Laboratory of Traditional Chinese Medicine for Prevention and Treatment of Vascular Remodeling Diseases, Jiangxi University of Chinese Medicine, Nanchang, China, ³Department of Cardiovascular Sciences and Centre for Metabolic Disease Research, Lewis Katz School of Medicine, Temple University, Philadelphia, PA, United States

Introduction: Atherosclerotic cardiovascular disease is the leading cause of death worldwide. The *Edgeworthia gardneri* (Wall.) Meisn is a Tibetan medicine commonly used to prepare herbal tea to alleviate the local people's metabolic diseases. However, the anti-atherosclerotic effect of ethanol extract of the flower of *E. gardneri* (Wall.) Meisn (EEEG) and its underlying mechanism remain unknown.

Methods: EEGE was used to treat low-density lipoprotein (ox-LDL)-induced macrophages to detect macrophage foaming, cholesterol binding and uptake, and lipid transport-related gene expression. EEGE treated ApoE^{-/-} mice fed a high-fat diet for 16 weeks to detect atherosclerotic plaque area, macrophage infiltration, and liver and small intestine lipid transport-related gene expression.

Results: EEGE inhibited macrophage-derived foam cell formation induced by oxidized low-density lipoprotein (ox-LDL) by reducing CD36-mediated lipoprotein uptake. EEGE significantly alleviated atherosclerosis in ApoE^{-/-} mice fed a high-fat diet for 16 weeks. EEGE treatment significantly decreased atherosclerotic plaque area, macrophage infiltration, and increased collagen content. Moreover, EEGE treatment significantly downregulated mRNA expression of hepatic *Srb1* and intestinal *Npc1l1* and increased expression of hepatic *Cyp7a1*.

Conclusion: Our study highlighted that EEGE played a role in attenuating atherosclerotic plaque formation by reducing macrophage foam cell formation.

KEYWORDS

Edgeworthia gardneri (Wall.) Meisn, macrophage, foam cell, atherosclerosis, CD36

Introduction

According to the World Health Organization statistics, cardiovascular disease will affect 23.6 million people worldwide by 2030. Atherosclerosis (AS) has become the leading cause of death in patients with cardiovascular disease and the primary pathological basis of cardiovascular disease. The pathogenic mechanism underlying AS is complex and closely related to abnormal lipid metabolism, vascular endothelial injury, genetic factors, and hemodynamic changes. At present, antioxidant, lipid-regulating, and antiplatelet drugs are commonly used to treat AS. Lipid-lowering drugs such as statins, fibrates, ezetimibe, and PCSK9 inhibitors are mainly used to prevent and treat AS in clinical practice. Although they slow down the disease progression, these drugs can only reduce the mortality of cardiovascular diseases by 30% and may lead to complications and adverse reactions, such as respiratory tract infection, muscle pain, low back pain, joint pain, and other side effects caused by ezetimibe (1). Given the adverse reactions associated with current AS management, safer and more effective anti-atherosclerotic drugs are urgently needed.

In the process of AS occurrence, oxidized low-density lipoprotein (ox-LDL) is continually uptaken by macrophages. When the intracellular cholesterol far exceeds the scavenging capacity, significant cholesterol will accumulate in the macrophages and transform them into foam cells (1). The foam cell formation is a fundamental step in initiating and developing atherosclerosis plaque (2). The scavenger receptors SR-A1, SR-B1, and CD36 expressed in the macrophage are responsible for binding to and taking up ox-LDL. ATP-binding cassette transporters like ABCA1 and ABCG1 are members of the ABC superfamily of transmembrane transporters, which mediate cholesterol efflux to apolipoprotein A1 (apoA1) and high-density lipoprotein (HDL) (3). Therefore, attempts to reduce foam cells may be a potential therapeutic strategy for inhibiting early-stage atherosclerosis pathogenesis (4).

The *Edgeworthia gardneri* (Wall.) Meisn (EG) belongs to Family Thymelaeaceae Genus *Edgeworthia* Meisn. The dry flower bud of EG is a widely recognized Tibetan medicine because of its long-term use, pollution-free drug source, and unique efficacy. It is known as one of the “Eighteen Treasures of Qinghai Tibet” in China. The flower of EG contains flavonoids, polysaccharides, volatile oils, fatty acids, triterpenes, and nitrogen-containing compounds. It has been used to prepare herbal tea to alleviate metabolic diseases (5). Previous researches have shown that EG has anti-hyperglycemia, anti-insulin resistance, and anti-adipogenesis activities, and the underlying mechanisms may be related to α -glucosidase and α -amylase inhibition, IRS1/GSK3 β /FoxO1 and PPAR γ / β signaling pathway activation, and gut microbiota modulation (6–10). However, the anti-atherosclerotic potential effect of EG and its underlying mechanism have not been reported.

Here, we evaluated the effect of ethanol extract of flower of *Edgeworthia gardneri* (EEEG) on atherosclerosis in an ApoE^{−/−} mice fed a high-fat diet (HFD). The effect and mechanism of EEEG on promoting reverse cholesterol transport (RCT) and inhibiting foam cell formation were also investigated.

Materials and methods

Materials and chemicals

The EG was purchased from Zangxi Tang (Tibet, China), and a voucher specimen (No.GH827) was deposited in the Jiangxi University of Chinese Medicine, Nanchang, China. MTT (M1020), Dimethyl sulfoxide (D8370), Trypsin (T8150), Oil red O powder (O8020), high sugar Dulbecco's modified Eagle's medium (DMEM) (12100-500), and PMI 1640 medium (31,800) were purchased from Solarbio (Beijing, China). Fetal Bovine Serum (FBS) (CC-4101A) was purchased from Lonza (Walkersville, MD, USA). Human oxidized low-density lipoprotein (ox-LDL, yb-002) and fluorescently labeled oxidized low-density lipoprotein (yb-0010) were obtained from Yiyuan Biology (Guangzhou, China). Bodipy TM493/503(D3922) was purchased from Invitrogen (Carlsbad, CA, USA). Rat anti-mouse CD68 antibody (MCA1957) or Monoclonal anti-alpha-smooth muscle-FITC antibody (F3777) was purchased from Bio-Rad (Kidlington, USA) or Sigma-Aldrich (St. Louis, MO, USA). Rabbit Polyclonal Anti-CYP7A1 antibody (TA351400) was purchased from Origene. Blood lipid test kits were purchased from Nanjing Jiancheng Bioengineering Institute.

Animals and treatment

Forty-six 6–8-week-old male ApoE^{−/−} mice (20–22 g) were purchased from Nanjing Biomedical Research Institute of Nanjing University [Certificate of Conformity No. SCXK (Su) 2015-0001]. Mice were housed in IVC cages (temperature 20–26°C, humidity 40–70%) under alternating 12 h light and 12 h dark conditions and given adequate food. The animal experiments were approved by the Ethics Review Committee of the Jiangxi University of Chinese Medicine. Mice fed a high-fat diet were randomly divided into four groups ($n = 11$ or 12): HFD group treated with 100 μ L sterile PBS (0.01 M); HFD group treated with low (1 g/kg of body weight), medium (2 g/kg of body weight), and high doses (4 g/kg of body weight) of EEEG solution, respectively. All mice were administered orally with PBS or EEEG once a day for 16 weeks and then sacrificed after fasting for 8 h. Blood samples were collected. The full-length aorta and heart specimens were fixed in 4% PFA.

Preparation of *Edgeworthia gardneri* ethanol extract

The EG (2.7 kg) was extracted three times with 60% ethanol (total volume 9 L) for 2 h. The combined extracts were concentrated under reduced pressure and extracted with petroleum ether, petroleum ether extracts were obtained, and the residue was partitioned into H₂O and extracted with 30% ethanol. After that, 30% ethanol extract was obtained. Then the 30% EEG was dissolved in dimethyl sulfoxide (DMSO) and PBS to get a stock solution for cell and animal experiments, respectively.

The EEG was qualitatively and quantitatively analyzed by HPLC using a Waters Acquity TM Ultra Performance LC system (Waters Corporation, Milford, MA, USA) in conjunction with a Waters HSS T3 TM (150 × 2.1 mm, 1.8 μm) column. The column temperature was maintained at a constant 25°C. The mobile phase flow rate was 0.8 ml/min. The mobile phase consists of acetonitrile (solvent A) and H₂O (solvent B), and both A and B contain 0.1% methanol. The elution procedure was set as performed as described before (10): 0–1 min, 1% A; 1.1–8 min, 1% A; 8.1–10 min, 99% A; and 10.1–12 min, 1% A. Results were shown in [Supplementary Figure 1](#).

Isolation of mouse bone marrow-derived macrophages

L929 cells were cultured in RPMI 1640 medium and incubated in a humidified atmosphere (5% CO₂; 37°C) for 5 days. The culture media was then collected and centrifuged at 1,000 rpm for 5 min, and the supernatant was harvested as the L929 conditioned medium.

Eight-week-old male C57BL/6 mice were sacrificed and immersed in 75% ethanol solution for 5 min for sterilization. Bilateral femurs were separated and washed in the macrophage starvation medium. Then the ends of the femurs were cut off, and the bone marrow in the femurs was flushed out with DMEM. Cells were centrifuged at 3,000 rpm for 5 min and suspended in DMEM supplemented with 10% fetal bovine serum, 100 U/mL penicillin, and 100 U/mL streptomycin. Cells were then placed in 10-cm dishes and incubated in a humidified atmosphere (5% CO₂, 37°C) for 72 h. Floating cells in the medium were collected and centrifuged. The harvested cells were resuspended with an L929 conditioned medium and adhered to the cell dish, followed by replacing the medium with a fresh medium.

BMDM viability assay

BMDMs were transferred into 96-well-plates (4 × 10⁴ cells/well) and incubated for 5 days. Then, 200 μL of medium

containing different concentrations of EEG (0.1, 1, 10, 100, and 200 μg/ml) was added to each well and incubated for 24 h. After washing twice with PBS, 200 μL of MTT solution (1 mg/mL) was added to each well and incubated for 4 h. Finally the MTT solution was removed, followed by adding 100 μL of DMSO to each well and incubated for 10 min. The absorbance of all samples was measured at 490 nm.

Foam cell formation assay

Cells or full-length aortas fixed in 4% paraformaldehyde (PFA) solution were washed three times with PBS, rinsed with the 60% isopropyl alcohol solution for 1 min, and stained with freshly prepared Oil red O working solution for 15 min. Cells or full-length aortas were rinsed briefly with 60% isopropyl alcohol and carefully rinsed with distilled water. Then, cells or full-length aortas were observed under the microscope and photographed. The average Oil red O positive areas were calculated relative to the number of cells.

Raw 264.7 cells were inoculated in the 24-well-plates (1 × 10⁵ cells/well) and incubated at 37°C for 24 h. Then, the Raw 264.7 cells were treated with 80 μg/ml of ox-LDL for 24 h, followed by washing twice with PBS. 200 μL of BODIPY working solution (1 μg/ml) was added to each well, incubated in the dark for 20 min at 37°C, and washed with acidic PBS (pH 2.7; 25 mM Glycine; 3% BSA) for 5 min. After that, Raw 264.7 cells were fixed in 4% PFA solution for 15 min and washed three times with PBS, followed by staining with DAPI (1:1,000) staining solution for 3 min and washing with PBS for 3 times. Cells were observed by laser confocal fluorescence microscopy and photographed. The average fluorescence intensity was quantified by Image J and calculated as the total area of green fluorescence intensity relative to the number of cells.

THP-1 cells (human myeloid leukemia mononuclear cells) were cultured in the 24-well-plates (3 × 10⁵ cells/well) in 1640 medium, and cells were incubated with 80 μg/ml ox-LDL for 24 h, simultaneous intervention with 1 μM rosiglitazone and intervention with 1 μg/mL EEG for 24 h. Cells fixed in 4% paraformaldehyde (PFA) solution were washed three times with PBS, rinsed with the 60% isopropyl alcohol solution for 1 min, and stained with freshly prepared Oil red O working solution for 15 min. Cells were rinsed briefly with 60% isopropyl alcohol and carefully rinsed with distilled water. Then, cells were observed under the microscope and photographed. The average Oil red O positive area was calculated as the total area of Oil red O relative to the number of cells.

Analysis of Dil-oxLDL binding and uptake

Binding assay: BMDM cells which covered the bottom of 12-well-plates were stimulated with EEG and Dil-oxLDL at

4°C for 30, 60, 90, and 120 min, respectively (11). Uptake assay: BMDM cells were stimulated with EEEG and Dil-oxLDL for 2, 4, and 6 h, respectively (11).

Cells were washed 4 times with acidic PBS for 5 min, digested with trypsin for 5 min, and centrifuged at 1,000 rpm for 3 min. Cell pellets were suspended in PBS, transferred to the sample tube, and analyzed by flow cytometry.

Histopathological staining and immunofluorescence analysis

The collected aortic roots fixed in 4% PFA were washed with PBS. The samples were then embedded in an optimal cutting temperature compound, frozen in liquid nitrogen, and cut into serial 10 µm-thick cryosections from the aortic root to the apex. A series of sections were collected on a stereomicroscope slide and stained with Oil red O, hematoxylin-eosin, and Masson's trichrome (Solarbio, China).

The sections stained with Oil red O were counterstained with hematoxylin-eosin for 30 s. After washing with tap water for 2 min, the sections were mounted with glycerin and gelatin and photographed using Nikon 4,500 digital camera. The sizes of atherosclerotic plaque and collagen fibers were determined using Image J software.

Frozen sections rinsed with PBS solution for 15 min were blocked in a solution containing 5% donkey serum, 0.5% bovine serum albumin (BSA), and 0.03% Triton X-100 for 1 h and the sections were incubated with primary anti-CD68 (1:250) or anti-α-SMA mouse antibody (1:500) overnight at 4°C, respectively. After rinsing with PBS solution for 15 min, the sections were incubated with fluorescence-conjugated secondary antibody for 1 h and stained with 4,6-diamidino-2-phenylindole (DAPI) for 3 min. After removing the DAPI solution, sections were photographed using fluorescence microscopy, and the average fluorescence intensity was quantified by Image J and calculated as the total area of fluorescence intensity relative to the plaque area.

Quantitative RT-PCR

Total RNA from cells or tissues was extracted using Trizol reagents. cDNA was synthesized using PrimeScript™ RT reagent Kit (Takara, Kyoto, Japan) following the manufacturer's instructions. Real-time PCR was performed following the SYBR® Premix Ex Taq™ II (Takara, Kyoto, Japan). The primer sequences are shown in [Supplementary Table 1](#). *β-actin* was used as the internal control.

Western blotting

Tissues were homogenized with 150 µl of RIPA lysis buffer. The lysis buffer was then centrifuged (12,000 rpm, 15 min, 4°C). Protein was quantified in the supernatant using a BCA protein assay kit. The primary antibodies of CYP7A1 (TA351400, Origene), were used. Approximately 40 µg of total protein was resolved by sodium dodecyl sulfate-polyacrylamide gel electrophoresis, electroblotted onto 0.45-µm polyvinylidene fluoride membranes, and probed overnight at 4°C. Membranes were incubated with secondary horseradish peroxidase-antibodies (anti-mouse or anti-rabbit) for 1 h at room temperature. Immunoblots were detected with Image Studio.

Determination of serum lipid profiles

Lipid profiles, including total cholesterol (TCHO), triglycerides (TG), low-density lipoprotein-cholesterol (LDL-C), and high-density lipoprotein-cholesterol (HDL-C) were measured using commercially available kits with a multifunctional enzyme marker according to the manufacturer's instructions.

Statistical analysis

All values were expressed as the mean ± S.E.M and analyzed using GraphPad Prism 9.0.2 software (San Diego, CA, USA). One-way analysis of variance (ANOVA) followed by Dunnett's test was used to evaluate statistical differences among groups. A value of $P < 0.05$ described a statistically significant difference.

Results

EEEG inhibits ox-LDL-induced macrophage foam cell formation

To determine the non-cytotoxic dose range, freshly isolated mouse BMDMs were treated with different concentrations (0.1, 1, 10, 100, and 200 µg/mL) of EEEG for 24 h. As shown in [Figure 1A](#), EEEG did not induce cell death at all concentrations tested. The concentrations of 100 µg/mL or lower were used for all the following experiments. Macrophages can uptake the excess lipids, differentiate into lipid-laden foam cells, and promote the progression of atherosclerosis (12). To investigate the effect of EEEG on macrophage foam cell formation, BMDM cells were pretreated with vehicle, or 0.1, 1, 10, and 100 µg/mL of EEEG for 24 h, followed by ox-LDL loading. The result showed ([Figures 1B,C](#)) that EEEG significantly reduced macrophage foam cell formation

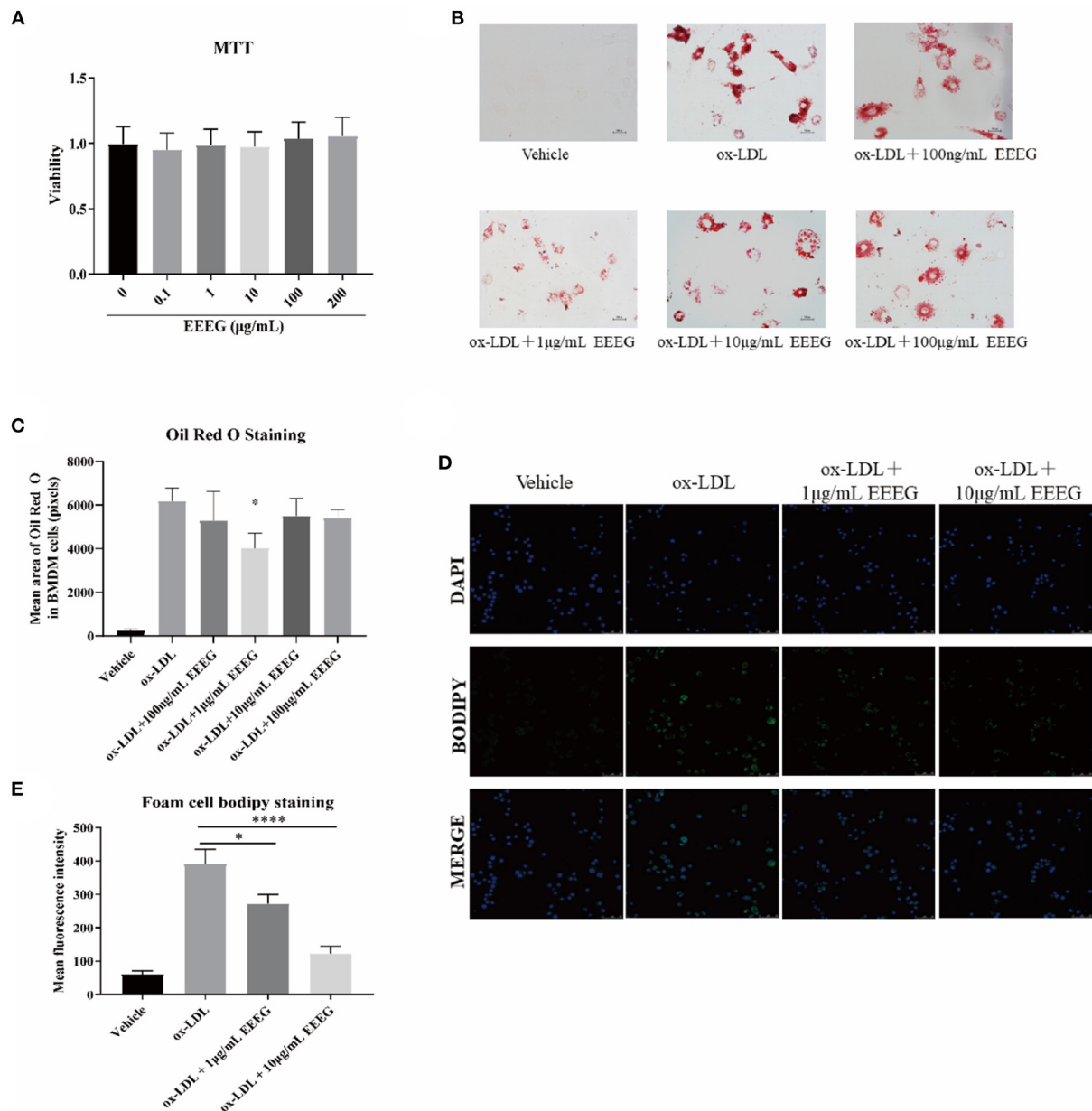


FIGURE 1
EEEG treatment reduces macrophage foam cell formation. **(A)** Effect of EEG treatment on BMDM viability. **(B)** Foam cell formation assayed by oil-red-O staining. Cells were incubated for 24 h with ox-LDL in the presence or absence of EEG, followed by Oil red O staining. **(C)** Quantification of ox-LDL uptake by macrophages. **(D)** BODIPY staining of RAW 264.7 cells. Cells were incubated for 24 h with ox-LDL in the presence or absence of EEG, followed by BODIPY staining. **(E)** Quantification of BODIPY fluorescence staining. Data are expressed as mean \pm s.e.m.. Statistical analysis was based on Graphpad Prism 9.0.2 software and a value of $P < 0.05$ was considered statistically significant. One-way ANOVA with Student Neuman-Keuls *post-hoc* test was performed to compare the data between multiple groups, * $p < 0.05$, **** $p < 0.0001$ vs. ox-LDL.

compared with vehicle control. Similarly, BODIPY staining showed that EEG (1 and 10 $\mu\text{g/mL}$) significantly inhibited ox-LDL-induced intracellular lipid droplets accumulation in RAW264.7 macrophages (Figures 1D,E). These results suggested that EEG effectively inhibited minimally modified lipid accumulation and macrophage foam cell formation.

EEEG treatment reduces macrophage uptake of ox-LDL

The intracellular cholesterol transport is essential for maintaining cholesterol homeostasis and depends on cholesterol binding, uptake, and efflux (13). To determine which biological

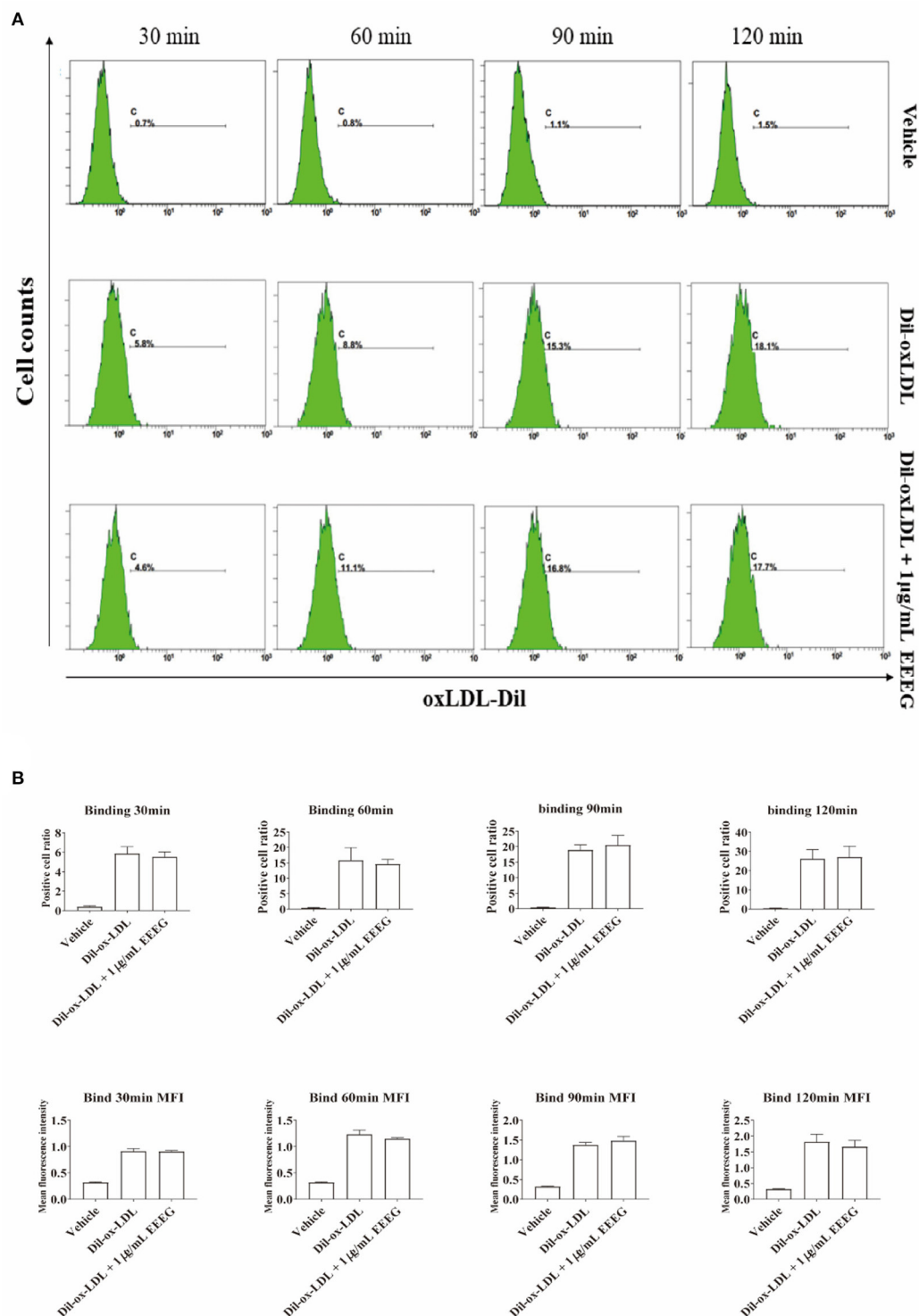


FIGURE 2

EEEG treatment does not influence the surface-binding of oxLDL to macrophages. **(A)** Representative histogram plots of DiI-ox-LDL binding by macrophages. Cells were incubated for 30, 60, and 90 min with DiI-ox-LDL in the presence or absence of EEFG, followed by flow cytometry. **(B)** Quantification of the percentage of positive cells and mean fluorescence intensity values. DiI-ox-LDL-fluorescence is shown on the Y-axis and macrophages on the X-axis. Data are expressed as mean \pm s.e.m., Statistical analysis was based on Graphpad Prism 9.0.2 software and a value of $P < 0.05$ was considered statistically significant. One-way ANOVA with Student Neuman-Keuls *post-hoc* test was performed to compare the data between multiple groups.

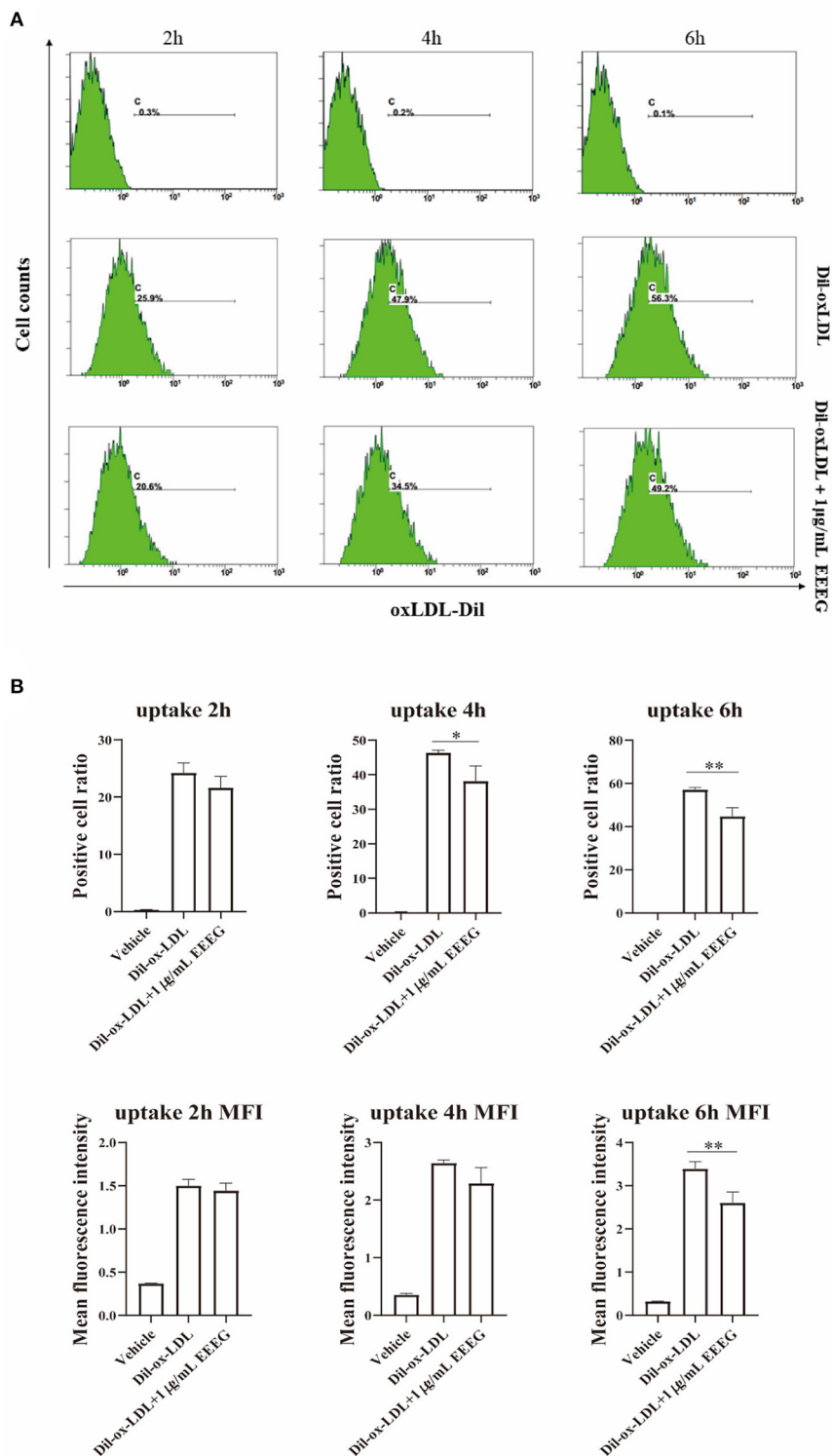


FIGURE 3
EEFG inhibits the uptake of oxidized low-density lipoprotein by macrophages. **(A)** Representative histogram plots of Dil-ox-LDL binding by macrophages. Cells were incubated for 2, 4, and 6 h with Dil-ox-LDL in the presence or absence of EEFG, followed by flow cytometry. **(B)** Quantification of the percentage of positive cells and mean fluorescence intensity values. Dil-ox-LDL-fluorescence is shown on the Y-axis and macrophage numbers on the X-axis. Data are expressed as mean \pm s.e.m., Statistical analysis was based on Graphpad Prism 9.0.2 software and a value of $P < 0.05$ was considered statistically significant. One-way ANOVA with Student Neuman-Keuls *post-hoc* test was performed to compare the data between multiple groups, * $p < 0.05$, ** $p < 0.01$ vs. ox-LDL.

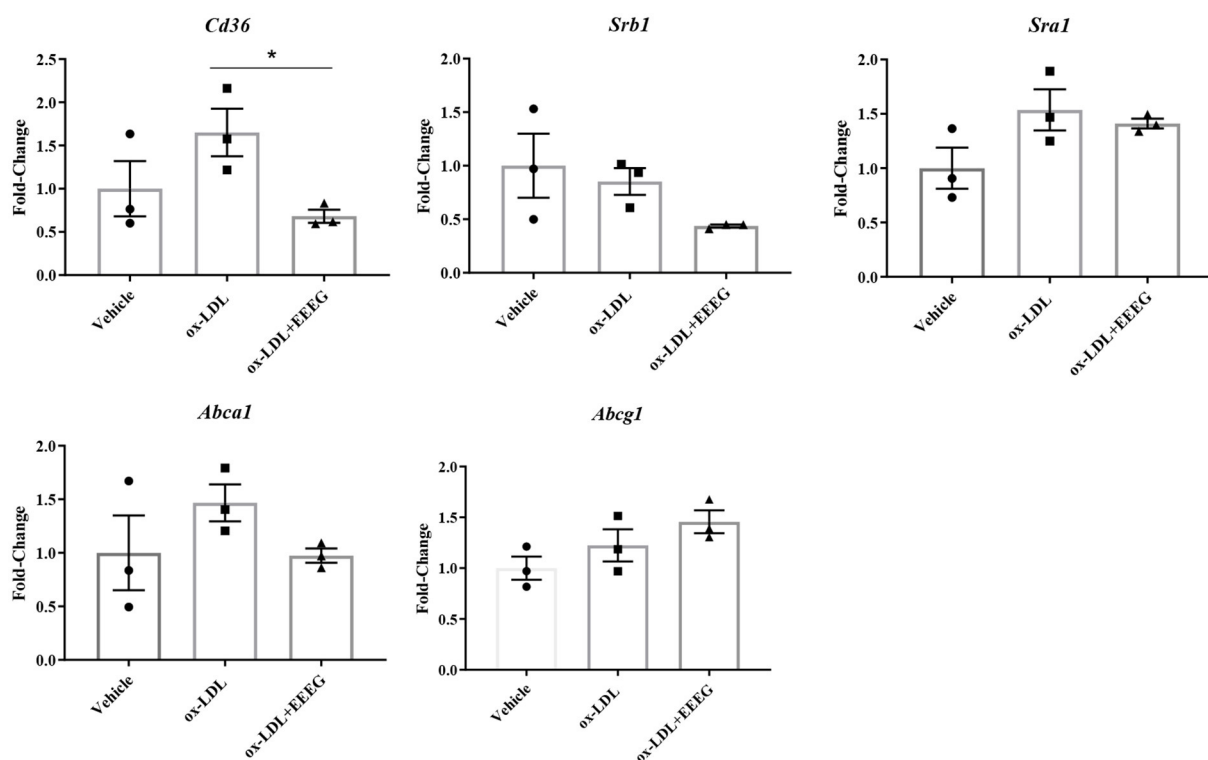


FIGURE 4
EEEG treatment reduces expression levels of genes involved in ox-LDL uptake. Expression levels of cholesterol homeostasis-related genes involved in uptake and efflux of ox-LDL in BMDM. Data are expressed as mean \pm s.e.m., Statistical analysis was based on Graphpad Prism 9.0.2 software and a value of $P < 0.05$ was considered statistically significant. One-way ANOVA with Student Neuman-Keuls *post-hoc* test was performed to compare the data between multiple groups, * $p < 0.05$.

processes are affected by EEG during the foam cell formation, cholesterol binding and uptake were evaluated by flow cytometry. As shown in **Figures 2A,B**, compared to vehicle control, EEG (1 μ g/mL) treatment did not change the surface Dil fluorescent intensity after Dil-oxLDL incubation up to 120 min. This result indicated that EEG did not affect cholesterol binding in macrophages. Next, BMDMs were treated with Dil-oxLDL+EEEG for 2, 4, and 6 h, respectively. The results showed that compared with the Dil-oxLDL group, the number of positive cells in the Dil-oxLDL+EEEG group was significantly reduced at 4 and 6 h. The mean fluorescence intensity of the Dil-oxLDL+EEEG group was also significantly lower than that of the Dil-oxLDL alone group at 6 h (**Figures 3A,B**), indicating that EEG reduced macrophage foam cell formation by decreasing uptake of ox-LDL.

EEEG reduces the expression of genes essential for ox-LDL uptake

Scavenger receptors and cholesterol transporters ABCA1 and ABCG1 are essential for cholesterol uptake and efflux (13).

To examine the levels of gene expression involved in cholesterol uptake and efflux in BMDM cells before and after EEG treatment, quantitative RT-PCR was used to detect the mRNA levels of *Cd36*, *Sra1*, *Srb1*, *Abca1*, and *Abcg1*. Consistent with the previous results (**Figures 3A,B**), the expression levels of *Cd36* was significantly decreased after EEG treatment (**Figure 4**). There was no significant difference in the expression of *Sra1*, *Srb1*, *Abca1*, and *Abcg1* mRNA expression in the EEG group compared with those in the vehicle control group. These results strongly suggested that EEG may reduce the formation of foam cells by inhibiting cholesterol uptake but not cholesterol efflux *via* down-regulating scavenger receptors' expression levels of CD36. To evaluate whether the inhibitory effect of EEG on foam cell formation was dependent on CD36. THP-1 cells were treated with PPAR- γ agonist, Rosiglitazone (RSG), PPAR- γ is essential for basal expression of CD36 (14), and the result showed a significant increase in lipid droplets in the ox-LDL + RSG group compared with ox-LDL group. After treatment with 1 μ g/mL of EEG, a significant reduction in lipid droplets was observed in the ox-LDL + RSG + EEG group compared with ox-LDL + RSG group (**Supplementary Figure 2**), indicating that reduction of uptake of ox-LDL by EEG may be dependent on CD36.

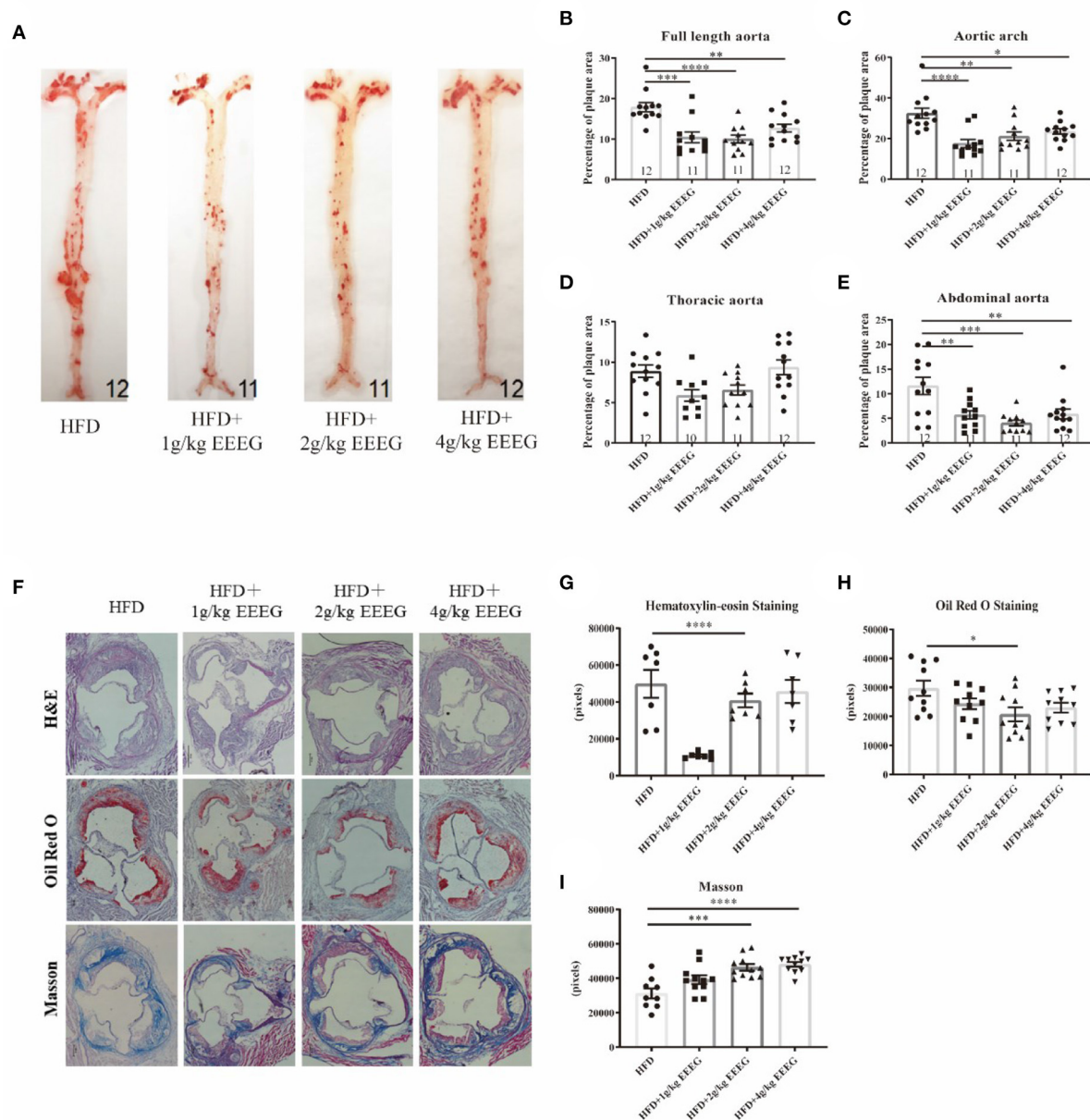


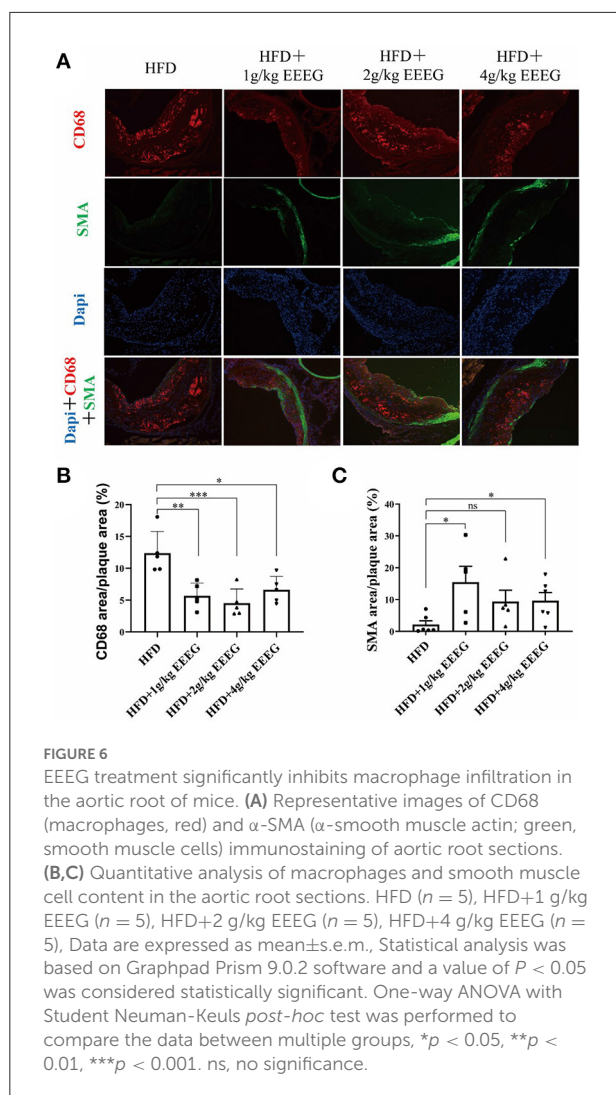
FIGURE 5

EEEG reduces atherosclerotic plaque areas in HFD-fed ApoE^{-/-} mice. (A) Representative images of Oil-Red-O staining of entire aortas including the aortic arch, thoracic, and abdominal regions. (B–E) Quantitative analysis of aorta lesion areas stained with Oil-Red-O. (F) Representative images of H&E, Oil-Red-O, and Masson staining of aortic root. (G–I) Quantitative analysis of aortic root section lesion areas stained with H&E, Oil-Red-O, and Masson. HFD ($n = 12$), HFD+1 g/kg EEG ($n = 11$), HFD+2 g/kg EEG ($n = 11$), HFD+4 g/kg EEG ($n = 12$). Data are expressed as mean \pm s.e.m., Statistical analysis was based on Graphpad Prism 9.0.2 software and a value of $P < 0.05$ was considered statistically significant. One-way ANOVA with Student Neuman-Keuls *post-hoc* test was performed to compare the data between multiple groups, * $p < 0.05$, ** $p < 0.01$, *** $p < 0.001$, **** $p < 0.0001$ vs. HFD.

EEEG treatment attenuates atherosclerotic plaque formation in HFD-fed ApoE^{-/-} mice

Macrophage foam cell formation is a hallmark of atherosclerosis (15). Since EEGE effectively inhibited lipid

uptake and foam cell formation *in vitro*, we thus hypothesized that it might attenuate atherogenesis. To test this hypothesis, ApoE^{-/-} mice were fed with HFD and treated with vehicle, 1, 2, or 4 g/kg of EEGE for 16 weeks. Full-length aorta and aortic roots were collected and stained with Oil red O, hematoxylin-eosin, and Masson's trichrome. As shown in Figure 5, the area



of plaques from mice treated with EEG was significantly lower than in vehicle treated mice. The size of plaques in mice administrated with 1 and 2 g/kg of EEG was smaller in the aortic arch and abdominal aorta compared with mice fed with the vehicle. Consistently, the plaque area in the aortic roots from mice treated with 1 g/kg of EEG was also markedly smaller than that in mice fed with vehicle (Figures 5A,B). In addition, collagen fiber contents in the aortic roots of mice treated with EEG significantly increased as compared to those in mice fed with vehicle (Figures 5C,D). These results indicated that EEG inhibits atherosclerotic plaque formation and enhances plaque stability in ApoE^{-/-} mice.

EEEG inhibits macrophage content in atherosclerotic plaque

Next, the cellular composition of the plaques was examined by immunofluorescence staining. As shown in Figure 6,

treatment with 1, 2, and 4 g/kg of EEG significantly attenuated CD68⁺ macrophages in aortic roots by ~95.4, 56.2, and 86.1%, respectively, compared to vehicle-treated mice. Interestingly, α -SMA positive cells increased by 725, 256, and 304% in 1, 2, and 4 g/kg of EEG-treated mice. Together with the collagen staining, as shown in Figures 5F–I, our results suggested that EEG treatment promoted a more stable plaque phenotype in atherogenic mice.

EEEG treatment reduces cholesterol absorption in HFD-fed ApoE^{-/-} mice

As shown in Supplementary Figure 3, EEG significantly decreased serum levels of LDL-C, but did not change the serum levels of TC, TG, and HDL-C. Reverse cholesterol transport involves removing excess cholesterol from plaque and transporting it to the liver for degradation into bile acids (16). The expression levels of genes essential for cholesterol transport and metabolism in the liver and intestine were detected to examine whether EEG treatment influenced the cholesterol transport and metabolism in HFD-fed ApoE^{-/-} mice. The results showed that both 2 g/kg and 4 g/kg of EEG treatment significantly reduced hepatic *Srb1* mRNA expression levels; 1 g/kg of EEG significantly up-regulated hepatic Cyp7a1 mRNA expression levels compared with the vehicle group. In addition, both 2 g/kg and 4 g/kg of EEG significantly up-regulated hepatic Cyp7a1 protein expression levels compared with the vehicle group (Figures 7A,C). No significant difference in mRNA expression of *Abcg5/8* was observed between the EEG group and vehicle group (Figure 7A). Furthermore, 2 g/kg of EEG treatment significantly promoted *Npc1l1* expression in the intestine. EEG did not change the intestinal *Abcg5/8* mRNA expression levels compared with the vehicle group (Figure 7B). These results showed that EEG might effectively inhibit cholesterol absorption and promote cholesterol metabolism.

Discussion

Atherosclerotic cardiovascular disease is the leading cause of death in humans. Statins have significant lipid-lowering effects but are unsuitable for all patients with high cholesterol and can cause serious side effects. The flower of *E. gardneri* (Wall.) Meisn is commonly used in beverages to prevent and treat diabetes and cardiovascular disease in Tibet (9). For the first time, the present study shows that EEG had an anti-atherosclerotic effect in apoE-deficient mice by restraining macrophage foam cell formation.

Foaming macrophages with subsequent fatty streaks formation contribute to the steady growth of atherosclerotic plaques (4). New drugs that inhibit macrophage-derived foam cell formation have important scientific significance for reducing the morbidity and mortality of the atherosclerotic

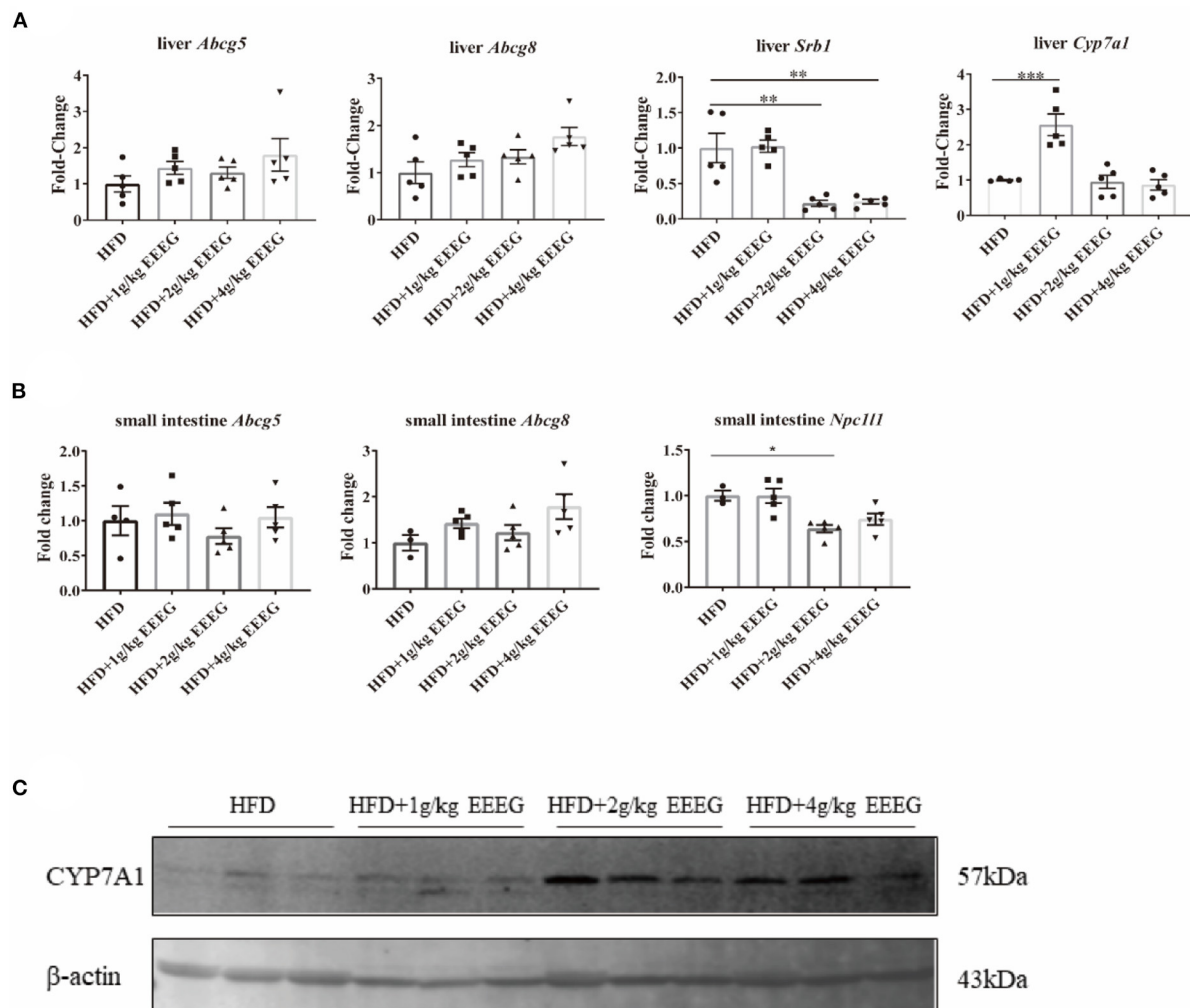


FIGURE 7
EEEG reduces cholesterol absorption in the liver and small intestine of mice. **(A)** RT-qPCR analysis of *Abcg5*, *Abcg8*, *Srb1*, and *Cyp7a1* gene expression in liver. **(B)** RT-qPCR analysis of *Abcg5*, *Abcg8*, and *Npc1l1* gene expression in the small intestine. **(C)** Expression of CYP7A1 in the liver of each group of mice analyzed by Western blotting. Data are expressed as mean \pm s.e.m., Statistical analysis was based on Graphpad Prism 9.0.2 software and a value of $P < 0.05$ was considered statistically significant. One-way ANOVA with Student Neuman-Keuls *post-hoc* test was performed to compare the data between multiple groups, * $p < 0.05$, ** $p < 0.01$, *** $p < 0.001$.

cardiovascular disease. Various medicinal plants have been shown to possess anti-atherogenic properties by interfering with foam cell development (17). Some herbal extracts, such as *Allium sativum* or *Ocimum basilicum*, can inhibit foam cell formation in human macrophages by reducing scavenger receptor activity *in vitro* (18, 19). Other extracts, such as *Cassia occidentalis* and *Moringa oleifera*, are tested to hinder the development of foam cells in animals (20, 21). Furthermore, a growing body of evidence has shown that bioactive components of medicinal plants, such as flavonoids, gossypetin, and lycopene, suppress foam cell formation by regulating cholesterol transporter, lectin-like oxidized low-density lipoprotein receptor-1, acyl CoA cholesterol acyltransferase activity, and neutral cholesteryl

ester hydrolase activity (22–24). This study demonstrated that the EEGG ameliorated ox-LDL-induced foam cell formation in RAW264.7 cells and bone marrow-derived macrophages. The flower of *E. gardneri* (Wall.) Meisn mainly contains flavonoids, coumarins, phenylpropan, triterpenoids, volatile oils, and other components. Flavonoids are among the key medicinal ingredients found in the flower of *E. gardneri* (Wall.) Meisn (25–27). Therefore, we speculated that flavonoids in the flower of *E. gardneri* (Wall.) Meisn played an important role in inhibiting the formation of foam cells, and further studies are warranted to confirm.

Macrophage cholesterol homeostasis is maintained by balancing the influx and efflux pathways. Cholesterol influx

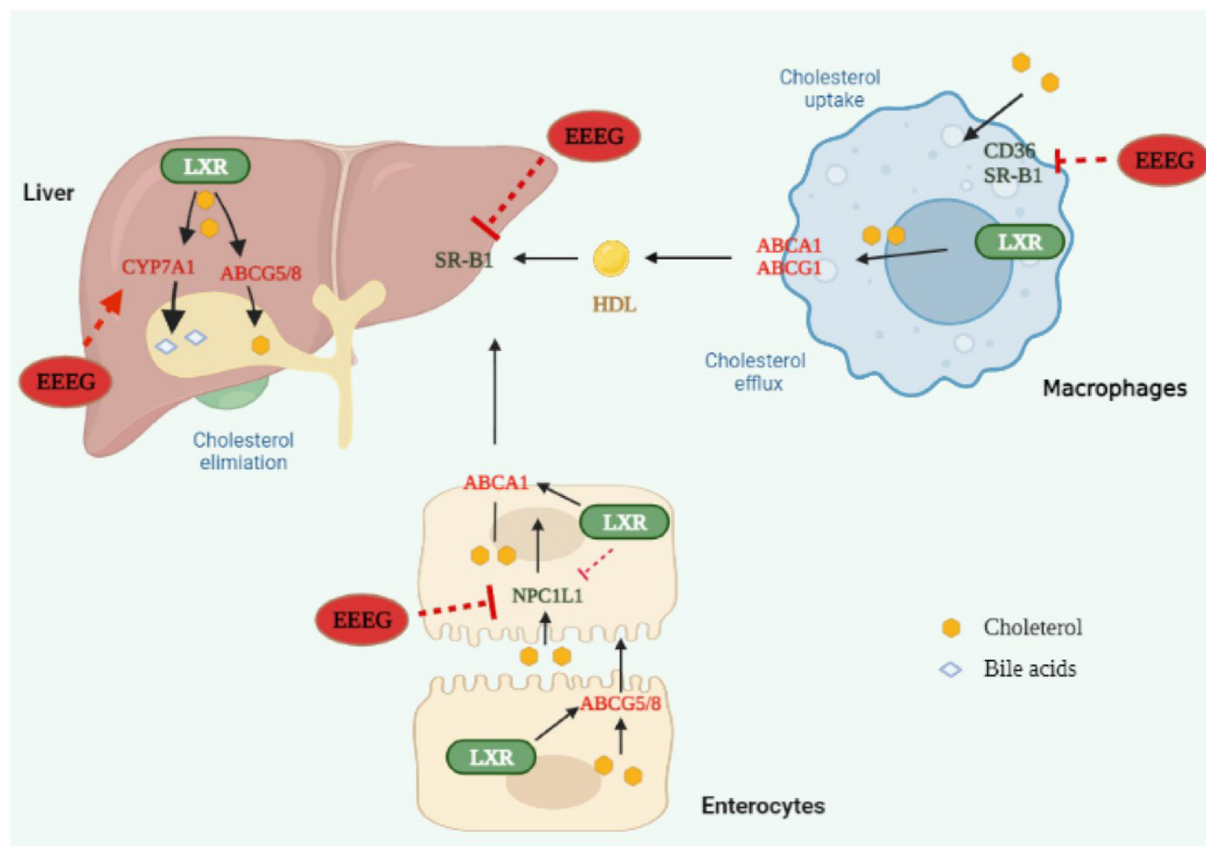


FIGURE 8
 Edgeworthia gardneri (Wall.) Meisn attenuates atherogenesis in mice by inhibiting macrophage foam cell formation via decreasing CD36-mediated ox-LDL uptake. EEEG inhibited macrophage-derived foam cell formation induced by oxidized low-density lipoprotein (ox-LDL) by reducing CD36-mediated lipoprotein uptake. Furthermore, EEEG treatment significantly downregulated mRNA expression of hepatic *Srebp1* and intestinal *Npc1l1* and increased expression of hepatic *Cyp7a1*, which may promote the reverse cholesterol transport and decrease the serum levels of cholesterol. In conclusion, EEEG may play a role in attenuating atherosclerotic plaque formation by reducing macrophage foam cell formation.

occurs by binding and uptake of neutral and modified lipoproteins mediated by SR-A and CD36. In contrast, cholesterol efflux is regulated by lipid-poor ApoA1 or HDL by ABCA1 and ABCG1, respectively (28). Decreased expression of SR-A and CD36 or increased expression of ABCA1 and ABCG1 block foam cell formation in macrophages (29, 30). Previous studies demonstrate that ox-LDL uptake by macrophages is prevented by herbal extracts, such as *Syzygium cumini* leaf extract, *Rubus coreanus* fruit extract, and medicinal plant decoctions (31–33). Here, we observed the EEEG reduced the uptake of Dil-ox-LDL by macrophages but had no noticeable effect on the binding of Dil-ox-LDL. In accordance with this result, expression of CD36 was markedly decreased, and expression of SR-A tended to be down-regulated by the EEEG. The expression of CD36 is tightly regulated by PPAR- γ in response to the stimuli (34). Therefore, we used the PPAR- γ agonist, Rosiglitazone to evaluate whether the inhibitory effect of EEEG on foam cell formation was dependent on

CD36. After treatment with 1 μ g/mL of EEEG, a significant reduction in lipid droplets was observed in the ox-LDL + RSG + EEEG group compared with ox-LDL + RSG group, and there was no significant difference between ox-LDL + EEEG group and ox-LDL + RSG + EEEG group (Supplementary Figure 2). The expressions of ABCA1 and ABCG1 were not altered in the macrophages. Collectively, these data implied that the EEEG inhibited macrophage-derived foam cell formation by decreasing uptake of ox-LDL via reducing expression of CD36. How EEEG reduces CD36 expression remains to be elusive.

As shown in Figure 5, the EEEG attenuated atherosclerotic plaque size and lipid content (oil-red-O staining) in ApoE $^{-/-}$ mice. EEEG treatment significantly decreased the macrophage-positive area in the aortic sinuses in HFD-fed ApoE $^{-/-}$ mice. Macrophage-derived foam cell formation plays a critical role in the early event of atherogenesis (35). The decreased macrophage-positive area and lipid content suggest EEEG may inhibit inflammation and lipid loading in atherogenesis *in vivo*.

Collagen fibers are the main component of atherosclerotic lesions and are used as an index to evaluate plaque stability (36). The EEEG treatment increased the number of vascular smooth muscle cells and the amount of collagen fiber, indicating that the EG may stabilize atherosclerotic plaque. However, its underlying mechanism still needs to be uncovered.

Reverse cholesterol transport is a pathway that transports cholesterol from peripheral tissues to the liver and intestine for excretion (37). *Srb1*, *Abcg5/8*, and *Cyp7a1* are involved in the uptake of cholesteryl esters, cholesterol excretion, and cholesterol metabolism in the liver, respectively. In contrast, intestinal sterol transporters *Abcg5/8* and *Npc1l1* are involved in the excretion of cholesterol from enterocytes into the lumen and absorption of cholesterol from the lumen into enterocytes, respectively. In this study, the medium and high doses of EEEG decreased the mRNA expression of hepatic *Srb1* and intestinal *Npc1l1*. The low dose of EEEG increased the mRNA expression of hepatic *Cyp7a1*. Together, we inferred from the results that EEEG inhibited the uptake of cholesteryl esters in the liver and intestine and promoted the transformation of cholesterol into bile acid in the liver, which was dependent on the dose of EEEG.

In conclusion, our study demonstrated that EEEG decreased CD36-mediated ox-LDL uptake and macrophage foam cell formation ultimately inhibited atherosclerosis (Figure 8). This study shed light on understanding the anti-atherosclerotic effect and mechanism of the flower of *E. gardneri* (Wall.) Meisn.

Data availability statement

The original contributions presented in the study are included in the article/Supplementary material, further inquiries can be directed to the corresponding authors.

Ethics statement

The animal study was reviewed and approved by Ethics Review Committee of the Jiangxi University of Chinese Medicine.

Author contributions

LT performed the experiment. CK performed the data analyses and wrote the manuscript. DS, MS, and JL contributed

significantly to analysis and manuscript preparation. LQ contributed to the conception of the study. JY helped perform the analysis with constructive discussions. All authors contributed to the article and approved the submitted version.

Funding

This research was supported by the National Natural Science Foundation of China (82160791 and 81860090), Natural Science Foundation of Jiangxi Province (20202BABL206007), Scientific Research Foundation of the Education Department of Jiangxi Province (GJJ190677), Ph.D. Research Startup Foundation of Jiangxi University of Traditional Chinese Medicine (2019WBZR009), Jiangxi Key Laboratory of Traditional Chinese Medicine for Prevention and Treatment of Vascular Remodeling Related Diseases (20202BCD42014), and Traditional Chinese Medicine Science and Technology Planning Project of Jiangxi Provincial Health and Family Planning Commission (2018B141).

Conflict of interest

The authors declare that the research was conducted in the absence of any commercial or financial relationships that could be construed as a potential conflict of interest.

Publisher's note

All claims expressed in this article are solely those of the authors and do not necessarily represent those of their affiliated organizations, or those of the publisher, the editors and the reviewers. Any product that may be evaluated in this article, or claim that may be made by its manufacturer, is not guaranteed or endorsed by the publisher.

Supplementary material

The Supplementary Material for this article can be found online at: <https://www.frontiersin.org/articles/10.3389/fcvm.2022.1023438/full#supplementary-material>

References

1. Steinbrecher UP, Parthasarathy S, Leake DS, Witztum JL, Steinberg D. Modification of low density lipoprotein by endothelial cells involves lipid

peroxidation and degradation of low density lipoprotein phospholipids. *Proc Natl Acad Sci U S A*. (1984) 81:3883–7. doi: 10.1073/pnas.81.12.3883

2. Moore KJ, Tabas I. Macrophages in the pathogenesis of atherosclerosis. *Cell*. (2011) 145:341–55. doi: 10.1016/j.cell.2011.04.005
3. Ye D, Lammers B, Zhao Y, Meurs I, Van Berkel TJ, Van Eck M. ATP-binding cassette transporters A1 and G1, HDL metabolism, cholesterol efflux, and inflammation: important targets for the treatment of atherosclerosis. *Curr Drug Targets*. (2011) 12:647–60. doi: 10.2174/138945011795378522
4. Poznyak AV, Nikiforov NG, Starodubova AV, Popkova TV, Orekhov AN. Macrophages and foam cells: brief overview of their role, linkage, and targeting potential in atherosclerosis. *Biomedicines*. (2021) 9:1221. doi: 10.3390/biomedicines9091221
5. Yan LS, Cheng BC, Zhang SF, Luo G, Zhang C, Wang QG, et al. Tibetan medicine for diabetes mellitus: overview of pharmacological perspectives. *Front Pharmacol*. (2021) 12:748500. doi: 10.3389/fphar.2021.748500
6. Gao D, Zhang YL, Yang FQ, Li F, Zhang QH, Xia ZN. The flower of *Edgeworthia gardneri* (Wall) Meisn suppresses adipogenesis through modulation of the AMPK pathway in 3T3-L1 adipocytes. *J Ethnopharmacol*. (2016) 191:379–86. doi: 10.1016/j.jep.2016.06.059
7. Zhang Y, Yan LS, Ding Y, Cheng BCY, Luo G, Kong J, et al. *Edgeworthia gardneri* (Wall) Meisn water extract ameliorates palmitate induced insulin resistance by regulating IRS1/GSK3 β /FoxO1 signaling pathway in human HepG2 hepatocytes. *Front Pharmacol*. (2019) 10:1666. doi: 10.3389/fphar.2019.01666
8. Zhao DG, Zhou AY, Du Z, Zhang Y, Zhang K, Ma YY. Coumarins with α -glucosidase and α -amylase inhibitory activities from the flower of *Edgeworthia gardneri*. *Fitoterapia*. (2015) 107:122–7. doi: 10.1016/j.fitote.2015.10.012
9. Gao D, Zhang YL, Xu P, Lin YX, Yang FQ, Liu JH, et al. *In vitro* evaluation of dual agonists for PPAR γ / β from the flower of *Edgeworthia gardneri* (wall) Meisn. *J Ethnopharmacol*. (2015) 162:14–9. doi: 10.1016/j.jep.2014.12.034
10. Zhang Z, Xu H, Zhao H, Geng Y, Ren Y, Guo L, et al. *Edgeworthia gardneri* (Wall.) Meisn water extract improves diabetes and modulates gut microbiota. *J Ethnopharmacol*. (2019) 239:111854. doi: 10.1016/j.jep.2019.111854
11. Pearson T, Wattis JA, O'Malley B, Pickersgill L, Blackburn H, Jackson KG, et al. Mathematical modelling of competitive LDL/VLDL binding and uptake by hepatocytes. *J Math Biol*. (2009) 58:845–80. doi: 10.1007/s00285-008-0205-z
12. Remmerie A, Scott CL. Macrophages and lipid metabolism. *Cell Immunol*. (2018) 330:27–42. doi: 10.1016/j.cellimm.2018.01.020
13. Dergunov AD, Savushkin EV, Dergunova IV, Litvinov DY. Significance of cholesterol-binding motifs in ABCA1, ABCG1, and SR-B1 structure. *J Membr Biol*. (2018) 252:1–20. doi: 10.1007/s00232-018-0056-5
14. Moore KJ, Rosen ED, Fitzgerald ML, Randow F, Andersson LP, Altschuler D, et al. The role of PPAR-gamma in macrophage differentiation and cholesterol uptake. *Nat Med*. (2001) 7:41–7. doi: 10.1038/83328
15. Wang D, Yang Y, Lei Y, Tzvetkov NT, Liu X, Yeung AWK, et al. Targeting foam cell formation in atherosclerosis: therapeutic potential of natural products. *Pharmacol Rev*. (2019) 71:596–670. doi: 10.1124/pr.118.017178
16. Sierksma A, Grobbee DE, Hendriks H. Vascular and biochemical effects of moderate alcohol consumption: mechanisms of protection against cardiovascular disease. In: *Comprehensive Handbook of Alcohol Related Pathology*. Vol. 2 (2005). p. 911–919. doi: 10.1016/b978-012564370-2/50073-8
17. Gholipour S, Sewell RDE, Lorigooini Z, Rafieian-Kopaei M. Medicinal plants and atherosclerosis: a review on molecular aspects. *Curr Pharm Des*. (2018) 24:3123–31. doi: 10.2174/1381612824666180911121525
18. Bravo E, Amrani S, Aziz M, Harnafi H, Napolitano M. *Ocimum basilicum* ethanolic extract decreases cholesterol synthesis and lipid accumulation in human macrophages. *Fitoterapia*. (2008) 79:515–23. doi: 10.1016/j.fitote.2008.05.002
19. Morihara N, Ide N, Weiss N. Aged garlic extract inhibits homocysteine-induced scavenger receptor CD36 expression and oxidized low-density lipoprotein cholesterol uptake in human macrophages *in vitro*. *J Ethnopharmacol*. (2011) 134:711–6. doi: 10.1016/j.jep.2011.01.021
20. Fidèle N, Joseph B, Emmanuel T, Théophile D. Hypolipidemic, antioxidant and anti-atherosclerogenic effect of aqueous extract leaves of *Cassia. occidentalis* Linn (Caesalpinaceae) in diet-induced hypercholesterolemic rats. *BMC Complement Altern Med*. (2017) 17:76. doi: 10.1186/s12906-017-1566-x
21. Chumark P, Khunawat P, Sanvarinda Y, Phornchirasilp S, Morales NP, Phivthong-Ngam L, et al. The *in vitro* and *ex vivo* antioxidant properties, hypolipidaemic and antiatherosclerotic activities of water extract of *Moringa oleifera* Lam. leaves. *J Ethnopharmacol*. (2008) 116:439–46. doi: 10.1016/j.jep.2007.12.010
22. Dong P, Pan L, Zhang X, Zhang W, Wang X, Jiang M, et al. Hawthorn (*Crataegus pinnatifida* Bunge) leave flavonoids attenuate atherosclerosis development in apoE knock-out mice. *J Ethnopharmacol*. (2017) 198:479–88. doi: 10.1016/j.jep.2017.01.040
23. Chen JH, Tsai CW, Wang CP, Lin HH. Anti-atherosclerotic potential of gossypetin via inhibiting LDL oxidation and foam cell formation. *Toxicol Appl Pharmacol*. (2013) 272:313–24. doi: 10.1016/j.taap.2013.06.027
24. Singh S, Changkija S, Mudgal R, Ravichandran V. Bioactive components to inhibit foam cell formation in atherosclerosis. *Mol Biol Rep*. (2022) 49:2487–501. doi: 10.1007/s11033-021-07039-9
25. Pan, X., Xia Z, Lin Y. Chemical constituents from *Edgeworthia gardneri* (Thymelaeaceae). *Biochem Syst Ecol*. (2012) 45:148–50. doi: 10.1016/j.bse.2012.07.031
26. Nan CY, Zhu JX, Jiang W, Zhong GY, Li M. Chemical constituents from *Edgeworthia gardneri* Flos. *J Chin Med Mat*. (2017) 40:1618–21.
27. Dong JL, Huang W, Ran MH, Liu JM, Hospital WN. Chemical constituents from *Edgeworthia gardneri* and their antioxidant activities. *Chin Tradit Patent Med*. (2019) 41:1578–82.
28. Ghosh S. Macrophage cholesterol homeostasis and metabolic diseases: critical role of cholesteryl ester mobilization. *Expert Rev Cardiovasc Ther*. (2014) 9:329–40. doi: 10.1586/erc.11.16
29. Kunjathoor VV. Scavenger receptors class A-I/II and CD36 are the principal receptors responsible for the uptake of modified low density lipoprotein leading to lipid loading in macrophages. *J Biol Chem*. (2002) 277:49982–8. doi: 10.1074/jbc.M209649200
30. Meurs I, Out R, Van Berkeo TJ, van Eck M. Role of the ABC transporters ABCA1 and ABCG1 in foam cell formation and atherosclerosis. *Future Lipidol*. (2008) 3:675–87. doi: 10.2217/17460875.3.6.675
31. Bhandary B, Lee GH, So BO, Kim SY, Kim MG, Kwon JW, et al. *Rubus coreanus* inhibits oxidized-LDL uptake by macrophages through regulation of JNK activation. *Am J Chinese Med*. (2012) 40:967–78. doi: 10.1142/S0192415X12500711
32. Dos Santos MM, de Souza Prestes A, de Macedo GT, Ferreira SA, Souza Vargas JL, Schüler LC, et al. *Syzygium cumini* leaf extract protects macrophages against the oxidized LDL-induced toxicity: A promising atheroprotective effect. *Biomed Pharmacother*. (2021) 142:111196. doi: 10.1016/j.biopha.2020.111196
33. Checkouri E, Ramin-Mangata S, Diotel N, Viranaicken W, Marodon C, Reignier F, et al. Protective effects of medicinal plant decoctions on macrophages in the context of atherosclerosis. *Nutrients*. (2021) 13:280. doi: 10.3390/nu13010280
34. Chawla A, Barak Y, Nagy L, Liao D, Tontonoz P, Evans RM. PPAR-gamma dependent and independent effects on macrophage-gene expression in lipid metabolism and inflammation. *Nat Med*. (2001) 7:48–52. doi: 10.1038/83336
35. haik-Dasthagirisahab YB, Mekasha S, He X, Gibson FC 3rd, Ingalls RR. Signaling events in pathogen-induced macrophage foam cell formation. *Pathog Dis*. (2016) 74:ftw074. doi: 10.1093/femspd/ftw074
36. Halvorsen B, Otterdal K, Dahl TB, Skjelland M, Gullestad L, Øie E, et al. Atherosclerotic plaque stability—what determines the fate of a plaque? *Prog Cardiovasc Dis*. (2009) 51:183–94. doi: 10.1016/j.pcad.2008.09.001
37. Ohashi R, Mu H, Wang X, Yao Q, Chen C. Reverse cholesterol transport and cholesterol efflux in atherosclerosis. *QJM*. (2005) 98:845–56. doi: 10.1093/qjmed/hci136



OPEN ACCESS

EDITED BY

Ha Won Kim,
Augusta University, United States

REVIEWED BY

Motoi Okada,
Asahikawa Medical University, Japan
Mehmet Murat Koseoglu,
Augusta University, United States

*CORRESPONDENCE

Robert M. Graham
b.graham@victorchang.edu.au

SPECIALTY SECTION

This article was submitted to
Atherosclerosis and Vascular Medicine,
a section of the journal
Frontiers in Cardiovascular Medicine

RECEIVED 28 September 2022

ACCEPTED 16 November 2022

PUBLISHED 06 December 2022

CITATION

Bax M, Romanov V, Junday K,
Giannoulitou E, Martinac B,
Kovacic JC, Liu R, Iismaa SE and
Graham RM (2022) Arterial dissections:
Common features and new
perspectives.
Front. Cardiovasc. Med. 9:1055862.
doi: 10.3389/fcvm.2022.1055862

COPYRIGHT

© 2022 Bax, Romanov, Junday,
Giannoulitou, Martinac, Kovacic, Liu,
Iismaa and Graham. This is an
open-access article distributed under
the terms of the [Creative Commons
Attribution License \(CC BY\)](https://creativecommons.org/licenses/by/4.0/). The use,
distribution or reproduction in other
forums is permitted, provided the
original author(s) and the copyright
owner(s) are credited and that the
original publication in this journal is
cited, in accordance with accepted
academic practice. No use, distribution
or reproduction is permitted which
does not comply with these terms.

Arterial dissections: Common features and new perspectives

Monique Bax^{1,2}, Valentin Romanov^{1,2}, Keerat Junday^{1,2},
Eleni Giannoulitou^{1,2}, Boris Martinac^{1,2}, Jason C. Kovacic^{1,2,3,4},
Renjing Liu^{1,2}, Siiri E. Iismaa^{1,2} and Robert M. Graham^{1,2,3*}

¹Victor Chang Cardiac Research Institute, Darlinghurst, NSW, Australia, ²UNSW Medicine and Health, UNSW Sydney, Kensington, NSW, Australia, ³St. Vincent's Hospital, Darlinghurst, NSW, Australia, ⁴Icahn School of Medicine at Mount Sinai, Cardiovascular Research Institute, New York, NY, United States

Arterial dissections, which involve an abrupt tear in the wall of a major artery resulting in the intramural accumulation of blood, are a family of catastrophic disorders causing major, potentially fatal sequelae. Involving diverse vascular beds, including the aorta or coronary, cervical, pulmonary, and visceral arteries, each type of dissection is devastating in its own way. Traditionally they have been studied in isolation, rather than collectively, owing largely to the distinct clinical consequences of dissections in different anatomical locations – such as stroke, myocardial infarction, and renal failure. Here, we review the shared and unique features of these arteriopathies to provide a better understanding of this family of disorders. Arterial dissections occur commonly in the young to middle-aged, and often in conjunction with hypertension and/or migraine; the latter suggesting they are part of a generalized vasculopathy. Genetic studies as well as cellular and molecular investigations of arterial dissections reveal striking similarities between dissection types, particularly their pathophysiology, which includes the presence or absence of an intimal tear and vasa vasorum dysfunction as a cause of intramural hemorrhage. Pathway perturbations common to all types of dissections include disruption of TGF- β signaling, the extracellular matrix, the cytoskeleton or metabolism, as evidenced by the finding of mutations in critical genes regulating these processes, including *LRP1*, collagen genes, fibrillin and TGF- β receptors, or their coupled pathways. Perturbances in these connected signaling pathways contribute to phenotype switching in endothelial and vascular smooth muscle cells of the affected artery, in which their physiological quiescent state

is lost and replaced by a proliferative activated phenotype. Of interest, dissections in various anatomical locations are associated with distinct sex and age predilections, suggesting involvement of gene and environment interactions in disease pathogenesis. Importantly, these cellular mechanisms are potentially therapeutically targetable. Consideration of arterial dissections as a collective pathology allows insight from the better characterized dissection types, such as that involving the thoracic aorta, to be leveraged to inform the less common forms of dissections, including the potential to apply known therapeutic interventions already clinically available for the former.

KEYWORDS

arterial dissection, aortic dissection, spontaneous coronary artery dissection (SCAD), cervical artery dissection (CeAD), TGF- β , extracellular matrix, vascular smooth muscle cells (VSMCs), endothelial cells (ECs)

Arterial features define vulnerability to dissections

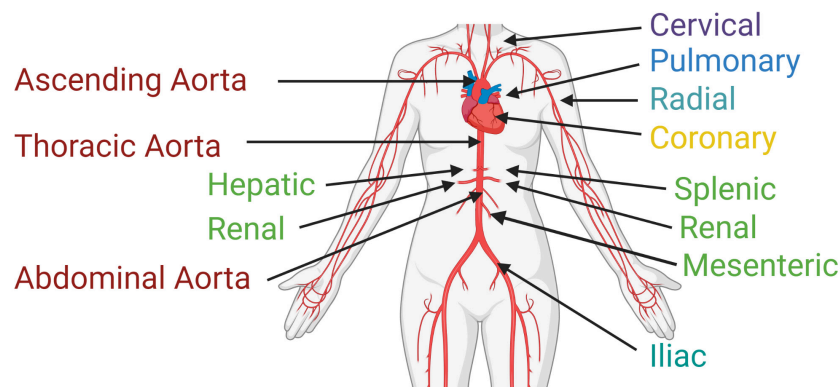
An arterial dissection is a structural failure of an arterial wall that results in an intramural bleed, which forms an intramural hematoma (IMH) that dissects the vessel wall. As the IMH expands it causes the ipsilateral vessel wall to bulge into the vessel lumen toward the contralateral wall, which in smaller diameter vessels leads to obstruction of blood flow. This obstruction prevents tissue perfusion causing ischemia and/or infarction. If the dissection is accompanied by an intimal tear, obstruction of the true lumen can be due to the IMH causing a thrombus that extends into and occludes the true lumen or can give rise to emboli that occlude distal arterial branches, resulting in micro-infarcts. The one exception to IMH-induced luminal occlusion is dissection of the aorta, which has a very large diameter, wherein the most concerning complication is not obstruction of blood flow or embolic events, but extension of the dissection into the pericardial space resulting in a hemopericardium that can cause pericardial tamponade, or extension of the dissection into a smaller diameter branch, such as a renal artery, resulting in renal ischemia or infarction. Dissections occur in medium and large arteries; with occurrences decreasing with diminishing arterial size (**Figure 1**). Clinically, dissections are often categorized by anatomical location. This localization predates the medical specialty best-relating to the dissection – aortic and coronary artery dissections, which cause heart failure, are the focus of cardiologists; cervical dissections, which lead to migraines,

or in severe cases, stroke, are the focus of neurologists. Despite the growth of vascular medicine as a specialty that bridges these anatomic regions, few reviews to date have considered these conditions collectively as a spectrum of diseases. Undeniable similarities between arterial dissections implicate common disease mechanisms. Aortic dissection, one of the best studied arterial dissection types, is associated with dysfunction of interlinked TGF- β signaling pathways, and disruption of extracellular matrix (ECM) structure, cytoskeletal function and vascular smooth muscle cell metabolism (1). Combining this research with increasing knowledge from other types of dissections and with heritable diseases commonly associated with arterial dissections will provide insight for better therapeutic intervention and prevention, which are severely lacking in many of these lesser understood dissection disorders.

Dissections are thought to originate in two of the three arterial layers – in the innermost layer, composed of an endothelial cell (EC) monolayer (*tunica intima*; intima), and in the thick muscular middle layer (*tunica media*; media) composed of concentric layers of vascular smooth muscle cells (VSMCs) and ECM that together form the lamellar unit (2). The outermost layer, an ECM coating (*tunica adventitia*; adventitia) is not a site of dissection-initiation (**Figure 2**).

These arterial layers vary anatomically. As muscular arteries branch further away from the heart their thickness decreases because of a decreasing number of lamellar units within the *tunica media*. This muscular layer provides the mechanical qualities – distensibility and elasticity – of a vessel. Without these properties, the vessel would lack compliance, resulting in excessive pressure within the vessel that would impair the ejection of blood from the heart. These large conduit arteries are also referred to as elastic arteries, owing to their high levels of elasticity facilitated by an abundance of elastin-rich ECM. As vessel size decreases, the amount of ECM, relative to VSMCs, is reduced. Medium-sized vessels are thus referred to as

Abbreviations: ECs, endothelial cells; VSMC, vascular smooth muscle cell; AD, aortic dissection; SCAD, spontaneous coronary artery dissection; CeAD, cervical artery dissection; WGS, whole genome sequencing; FMD, fibromuscular dysplasia; IMH, intramural hematoma; ECM, extracellular matrix.



Artery	Intimal Medial Thickness (mm)	Reported Incidence Rates	References
Ascending Aorta	1.48	Most Common 10 cases/100,000 person-years (thoracic); Ascending more common than descending	Bae 2003 Saliba 2015 Roberts 1991
Descending Aorta	1.39		
Abdominal Aorta	1.24	Least Common Aortic Dissection Subtype	Sumbul 2019 Roberts 1991
Coronary Artery	0.75	Less Common 2.7 cases/100,000 person-years	Fayad 2000 Kronzer 2020
Cervical Artery	0.66	Less Common 2.6 cases/100,000 person-years	Eigenbrodt 2007 Lee 2006
Renal Artery	0.50	Rare Estimated 1-2% arterial dissections	Leertouwer 1999 Jha 2020
Pulmonary Artery	0.16	Very Rare ~150 cases reported	Li 2012 Fernando 2019

FIGURE 1

Arterial dissections are reported in large- and medium-sized arteries throughout the body at varying frequencies within the population. The risk of dissection varies with sex and age. Reported incidences correlate with average intimal medial thickness. Created with [BioRender.com](https://www.biorender.com).

muscular arteries (or distributing arteries). As arteries branch further into resistance vessels, the media is further reduced (3). Dissections have not been reported in resistance vessels. Branching of arteries adds complexity in vascular structure, contributing to arterial microenvironments. For example, non-linear vessel morphology, including divergent junctions or bifurcations, exposes differing arterial regions to varying blood flow forces (shear stress).

Elastic and muscular arteries require vasa vasorum

Larger arteries that exceed 29 lamellar units or are > 5 mm in thickness (with the exception of the coronary arteries) have vasa vasorum, which are required for perfusion and oxygenation of the arterial wall (4). Functionally, vasa vasorum are end arteries, terminating close to the adventitial-medial layer and are drained by postcapillary venules (5, 6). The vasa vasorum capillary bed is highly irregular, forming kinks, twists, and outpouchings (7, 8). Typically, vasa vasorum perfuse only the outer two-thirds of the medial layer, the inner third being oxygenated by diffusion

from the lumen. However, under pathological conditions, such as atherosclerotic plaque-formation where there is a barrier to oxygenation *via* luminal diffusion, vasa vasorum can extend inward toward the lumen to also perfuse the subendothelial *tunica media* (9, 10). While medial vasa vasorum are required for perfusion of the *media* in muscular arteries, such as the thoracic aorta, muscular veins and the pulmonary artery, thinner-walled vessels, such as the abdominal aorta, only have adventitial vasa vasorum, which are not essential for perfusion and integrity of the medial layer (11).

Flow in medial vasa vasorum has been largely understudied except in the aorta, so the physiology of vasa vasorum flow remains unclear. It is unknown, for example, if and to what extent flow in medial vasa vasorum is supported by their own VSMCs and/or pericytes, and whether or not flow in the vasa vasorum is dependent on compressive forces, such as peristaltic pressure of the media resulting from VSMC contraction (11, 12). The scale and structure of the vasa vasorum confer several interesting microfluidic properties: (1) Flow of blood through these vessels will mostly be laminar, as viscous forces dominate over inertial forces at these scales, as evident from **Reynolds Number** (Re, below), however, both eddies and to some extent

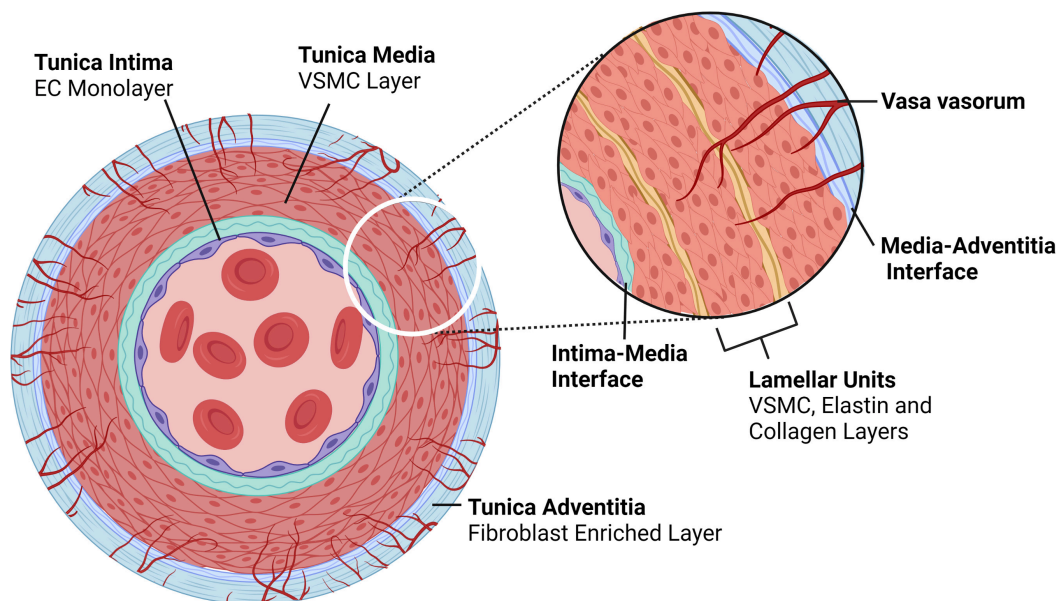


FIGURE 2

Typical architecture of medium to large, elastic and muscular arteries. Arteries comprise of three layers – the tunica intima is the innermost layer consisting of an endothelial monolayer; abluminal this monolayer is an ECM membrane located between the intima and the media, the latter being the second layer of the artery. The tunica media is concentrically layered with lamellar units of VSMCs bounded by elastin- and collagen-rich fibers. In larger arteries, the media is perfused by capillaries known as vasa vasorum, which enter the media through the outermost layer, the tunica adventitia; an ECM and fibroblast-rich layer. Created with [BioRender.com](https://www.biorender.com).

turbulence can be induced following intimal failure, leading to flow disturbances;

$$Re = \frac{\rho v L}{\mu}$$

where ρ is fluid density, v is fluid velocity and L is vessel length, and μ is fluid viscosity.

(2) The **circumferential stress** (σ , below), derived from Laplace's Equation, acts perpendicular to the radius of the lumen. For small vessels circumferential stress is relatively low, as it scales directly with internal pressure. This acts to dilate the vessel, the radius of the lumen and the thickness of the vessel wall (13, 14). Vasa vasorum lumens range from $\sim 2 \mu\text{m}$ to $329 \mu\text{m}$, with an average luminal size of $\sim 40 \mu\text{m}$ (15). A vessel of this size should accommodate the pressure moving through an artery, at diastole, without failing. As such, failure of the vasa vasorum by pressure overload is unlikely, unless the surrounding environment no longer provides the required compressive forces;

$$\sigma = \frac{P r}{w}$$

where P is internal pressure, r is lumen radius and w is wall thickness.

Placing the above relationship into context, arteries on average, have an inner lumen that is 25 times larger than that of the vasa vasorum. To reduce stress within the arterial wall, the wall thickness must increase. The average arterial wall can

be 150 times thicker than the average wall thickness of the vasa vasorum (assuming wall thickness of an average arteriole) (16).

(3) To a certain extent, the vasa vasorum can be expected to exhibit viscoelasticity to accommodate the sudden rise in pressure, which results in rapid, non-linear dilation of the lumen that tapers off if the pressure is maintained. The extent to which the vasa vasorum is compressed or dilated depends on the surrounding tissue, including the ECM and its constituents exhibit both viscoelastic and strain-stiffening behavior (17);

(4) The flow of blood through the vasa vasorum, from the adventitia to the media, scales directly with pressure, as given by the **Hagen-Poiseuille Equation** (below) and inversely with length of the vessel, i.e., the longer the vessel, the lower the flow rate (Q). The high degree of tortuosity of the vasa vasorum has several effects: while the vessels are better protected from longitudinal strains, the increase in vessel length increases the pressure required to drive blood from their entry point in the adventitia to their termination in the media and on to the postcapillary venules;

$$Q = \frac{\pi r^4 \Delta P}{8 \mu L}$$

where, r is vessel radius, ΔP is pressure difference, μ is viscosity and L is vessel length.

(5) The localization of vasa vasorum in the outermost section of the media is proposed to be a function of the compressive pressure exerted by the surrounding matrix and the

underlying luminal pressure (18). The extent to which the vasa vasorum propagate axially through the media depends on the pressure drop across the vessel (ΔP = pressure at inlet – pressure at outlet) and the point at which luminal pressure overcomes the necessary pressure to drive blood throughout the length of the vessel (pressure at lumen > pressure at outlet).

Anatomical differences in vasa vasorum are evident. The coronary arteries, while relatively thin walled, are exposed to large cyclical deformations, owing to the movement of the heart. Cyclical compression of vasa vasorum significantly reduces flow rate within the vessels, reducing nutrient exchange and oxygen delivery. As such, it is unsurprising that the density of vasa vasorum in coronary arteries is higher than that of carotid or renal arteries and is almost 10 times greater than that of the femoral arteries. In the case of the femoral artery, a high density of vasa vasorum is not required as its vasa vasorum do not undergo cyclical compression and, as such, are able to maintain relatively constant blood flow with fewer branches and with slightly larger luminal diameters (~22%) (19).

There are also structural and site-specific differences between the vasa vasorum of different arteries. The endothelial-surface-fraction (endothelial surface area/vessel wall volume) of the coronary artery vasa vasorum exceeds that of renal or femoral arteries by threefold, while the vascular-area-fraction (vasa vasorum area/vessel wall area) of the coronary artery vasa vasorum is roughly twice as high (20). Accordingly, the vasa vasorum within the coronary arteries are designed to withstand higher pressures, permitting greater perfusion than the vasa vasorum of other arteries. Disruption of blood flow through the vasa vasorum has been shown to increase tissue stiffness leading to detachment of the layers near the adventitial-medial border. This suggests that the vasa vasorum play a vital role in aortic wall integrity (15). As tissue stiffens, the artery is less efficient at dampening oscillations and pulsatility arising from systolic and diastolic phases of the heart, resulting in greater flow instability. This instability can be characterized by the **Womersley number** (α , below) representing the ratio of unsteady forces to viscous forces (21). The Womersley number is very small in the vasa vasorum (0.1), indicating that viscous forces dominate within these vessels and are well dampened from pulsatility. In contrast, main arteries are exposed to pulsatility that is approximately 100 times larger than for vasa vasorum (22). For example, the Womersley number for the ascending aorta, thoracic aorta, abdominal aorta and the femoral artery are 17.8, 12.1, 7.38, and 3.14, respectively (23).

$$\alpha = \frac{D_m}{2} \sqrt{\frac{\rho 2\pi f}{\mu}}$$

where D_m is the diameter of the vessel, ρ is fluid density, f is heart rate and μ is blood viscosity.

Theoretically, to allow vasa vasorum blood flow in the absence of a supporting muscular layer requires that the distending forces or hydrostatic pressure within the vasa

vasorum exceed the compressive forces in the media (12, 24). The efficacy with which arteries maintain the appropriate level of distensibility and elasticity to allow appropriate flow – both at the tissue and cellular level – is subject to the appropriate ECM composition and, thus, physical properties, as well as structural, and metabolic proteins. Expression of these proteins is influenced by environmental factors, such as sex, aging, and lifestyle.

Endothelial cells are the first layer of defense in arteries

The EC monolayer forming the intima is the first line of protection against infection and injury, acting as a selectively permeable barrier to prevent toxin- and pathogen-entry into tissues, and is an important interface between the immune system and its cognate perfused tissues. Critical to vascular function, ECs are one of the main factors governing vascular tone (25). EC communication with the underlying VSMCs modulates vasodilation *via* the gaseous messenger nitric oxide (NO) secreted following VSMC contraction. NO signaling by ECs has been shown to regulate not only VSMC contractility, but also ECM composition (26), as well as inhibiting platelet aggregation (27) and regulating VSMC metabolism and proliferation (28, 29).

Of particular relevance to arterial dissections, ECs also play a key role in mediating the response to injury. ECs and megakaryocytes are the only cells that produce the glycoprotein, von Willebrand factor (vWF), a carrier protein for factor VIII required for blood coagulation (30). Following damage to the intima, vWF binds to platelet membrane glycoproteins and exposes ECM to mediate platelet adhesion leading to clot formation. The majority (95%) of vWF is secreted constitutively by ECs, however, 5% is retained by ECs and stored in cellular vesicles known as Weibel–Palade bodies, ready for localized release if required (31). EC-derived extracellular vesicles are important in mediating VSMC activation. Extracellular vesicles derived from rat ECs that were subjected to serum depletion were found to alter the VSMC proteome by upregulating VSMC stress responses as well as cellular metabolism (32).

Endothelial cell identity is fluid

The body is estimated to contain $2.54 \pm 1.05 \times 10^{12}$ ECs (33). Under physiological conditions quiescent ECs have an average lifespan of approximately 6 years and account for only ~0.1% of the daily turnover of all cells (34, 35). Under conditions of growth or injury, ECs are activated, becoming “synthetic” or “secretory,” through upregulation of proliferative and secretory pathways [(36); Figure 3]. There are many subtypes of activated ECs, perhaps best defined by the inducing stimulus. Activation can be induced by blood vessel growth

(angiogenesis) through growth factor signaling, such as by fibroblast growth factors (FGF) and vascular endothelial growth factor (VEGF), which upregulate proliferative, migratory, and invasive processes. Disturbances in blood flow force (shear stress), and inflammation (acute and chronic) can activate ECs. These activated cells upregulate inflammatory processes, including expression of inflammatory proteins such as VCAM1 and ICAM1, which promote immune cell infiltration (36, 37). Recent hypotheses propose that this inflammatory type of EC dysfunction occurs in response to SARS-CoV-2 infection (38).

Anatomy and sex influence endothelial cell identity

Quiescent ECs vary anatomically. A recent single cell sequencing analysis, which allowed the development of the first murine endothelial atlas, studied over 32,000 cells from 11 anatomical regions and identified 78 subclasses of ECs based on their transcriptome (39). This work confirmed earlier findings from DNA microarray analysis of ECs originating from different tissues and vessel types (40). These studies found that ECs group by vessel type, such as artery and vein, and also showed heterogeneity amongst cell types. Interestingly, ECs were found to have upregulation of pathways that were relevant to their anatomical origin – for example, ECs from the blood-brain barrier were upregulated for solute transport processes, while ECs derived from the liver and spleen, organs that filter and protect from pathogens, were upregulated for scavenging and immuno-regulating processes (40). Anatomical region and vascular type variations in ECs are not surprising given differences in the stimuli to which these cells are exposed. A study of human umbilical vein ECs from the same donor displayed variation in both their proteomes and lipidomes following exposure to differing shear stress (5 vs. 15 dynes/cm²) (41). These differences may represent potential anatomical vulnerabilities, rendering ECs from certain arteries more susceptible to particular stressors than others.

Endothelial cell populations also differ on the basis of sex. A comparison of umbilical vein EC transcriptomes between boy-girl twin pairs at birth indicated sex-specific differences in a number of pathways, such as enrichment in females for epithelial to mesenchymal transition and hypoxia, and in males the unfolded protein response and protein secretion (42). The same comparison was made in human adults (from the general population) and sex differences were again found, though some pathways were different, suggesting a sex hormone (rather than sex chromosome) effect whereby females had an enrichment for estrogen response pathways (early and late), while males had an increase in TGF- β pathway transcripts (42). These variables could contribute to risk of vascular diseases – including dissections – positively or negatively. Defining what is a healthy baseline EC expression profile will likely provide important insight into vascular diseases.

Vascular smooth muscle cells are essential for structure in medium to large arteries

Under normal physiological conditions, VSMCs are contractile cells with a spindle-shaped morphology, reinforced by a well-ordered array of cytoskeletal proteins, including myosin heavy chain 11 (MYH11), α -smooth muscle actin (ACTA2), calponin (CNN1), and transgelin (TAGLN). Cellular contractility places a large metabolic demand on VSMCs. Yet, despite the advantage of oxidative phosphorylation in terms of energy economy, VSMCs use a combination of both oxidative phosphorylation and glycolytic metabolism to an almost equal extent when measured at rest (43). It is hypothesized that this acts to buffer energy depletion and prevent an ATP crisis (44), but persistent use of aerobic glycolysis (i.e., the Warburg effect) is also consistent with continued proliferation of VSMCs, even in adulthood. Despite these high energy demands, VSMCs are relatively long lived with a half-life of 270 – 400 days (45).

Vascular smooth muscle cell identity is also fluid

Like ECs, VSMCs can also undergo phenotypic switching from the physiological contractile phenotype to a highly proliferative synthetic cellular state in response to certain cues, such as injury (Figure 3). Under stress conditions, expression of cytoskeletal proteins, including MYH11, ACTA2, CNN1, and TAGLN, is reduced as cells switch from the contractile to a synthetic state. Earlier research defined synthetic VSMCs as cells that assume a more rounded morphology and have increased proliferative, secretory and migratory properties (46). Phenotype switching to the synthetic state coincides with a metabolic shift to increased reliance on glycolysis (47). Molecular triggers such as PDGF-BB, TGF- β , actin A, retinoids, angiotensin II, TNF- α , IGF-I, -II, endothelin-1, and NO as well as reactive oxygen species and a reduced glutathione (GSH) redox status, can all modulate the activation state of VSMCs (46, 48, 49). Activation can also be mediated by shear stress – synthetic VSMCs supplemented with media from ECs, even under low physiological stress (12 dynes/cm²), will upregulate contractile markers (50). VSMC phenotype has also been shown to be regulated epigenetically and the capacity for phenotypic modulation appears to be conserved across species, having been demonstrated in rats, pigs, cows, and humans (46, 51, 52).

Increased understanding of VSMC phenotypic switching has led to the traditional binary classification of contractile and synthetic being reconsidered, since it is now clear that synthetic VSMCs can transdifferentiate into several different lineages, including foam cells, macrophage-like VSMCs, myofibroblast-like VSMCs and osteoblast-like VSMCs [reviewed in (53)]. The field has been aware that these synthetic subtypes exist (51), however, it is only with recent technologies, such as advanced lineage tracing and single cell RNA-Seq, that they



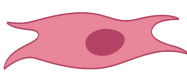




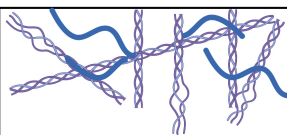
	Endothelial Cells	Vascular Smooth Muscle Cells	Fibroblasts	Extracellular Matrix
Quiescent	 <ul style="list-style-type: none"> • Monolayer in intima • Permeable barrier-forming • Control vascular tone • Control inflammatory response • Low turnover (6 year average) • Predominantly glycolytic • Vary with sex and anatomy 	 <ul style="list-style-type: none"> • Multilayer in media • Contractile • Modulate vasa vasorum blood flow within the media • Low turn over (~1 year half-life) • Aerobic respiration • Vary with sex and anatomy 	 <ul style="list-style-type: none"> • Main component of adventitia • ↓ ECM production and maintenance 	 <ul style="list-style-type: none"> • Required in all artery layers • Well organized • Determine artery distensibility and elasticity • Elastic and collagen fibers
Activated	 <ul style="list-style-type: none"> • ↓ Function as barrier-forming • ↑ Motility • ↑ Proliferation • ↑ ECM production 	 <ul style="list-style-type: none"> • ↓ Function as contractile cells • ↑ Motility • ↑ Proliferation • ↑ ECM production • ↑ Glycolysis • Activated state varies depending on activation type 	 <ul style="list-style-type: none"> • ↓ Function • ↑ Motility • ↑ Proliferation • ↑ ECM production • Activated fibroblasts can differentiate to myofibroblasts 	 <ul style="list-style-type: none"> • Disorganized depositions • Alter mechanical properties • Influences identity of surrounding cells

FIGURE 3

Phenotypic changes in the cellular and extracellular components of the artery in response to injury/infection. Created with [BioRender.com](https://www.biorender.com).

have been explored in detail. Single cell sequencing analysis of aortic tissue indicated that the tunica media consists of five VSMC-like clusters, which are grouped according to their gene expression profiles and indicate pathways associated with contraction, stress responses, and cell cycling (with both low and high contractile protein expression), and also fibroblasts (54). The capacity of VSMCs to regulate these processes is well documented to be perturbed in many vascular diseases, particularly atherosclerosis [reviewed in (55)], but to date has not been well explored in terms of its involvement in arterial dissection pathophysiology. VSMC phenotype switching has been described as a pathological mechanism of aortic dissections (56), though importantly, this phenomenon is yet to be considered for other arterial dissection types, such as spontaneous coronary artery dissection (SCAD) or cervical artery dissection (CeAD). How synthetic VSMCs are activated in arterial dissections may differ between dissection subtypes in other vasculopathies and this knowledge is likely critical for understanding how and why these various vasculopathies occur.

Signaling from ECs is important for VSMC phenotype switching. VSMCs never exist *in vivo* without some proximity to ECs. Although separated by the internal elastic lamina, this layer offers little resistance to direct chemical communication between these cells as it is fenestrated, or discontinuous and fibrous (57). It has long been established that interactions between ECs and VSMCs affect cell morphology and proliferation of both these cell types (58). Studies of bovine aortic VSMC and EC co-cultured but separated by a permeable polyethylene terephthalate membrane, mimicking the internal elastic lamina, indicated a 56% increase in VSMC proliferation when VSMCs were co-cultured opposite ECs compared to

VSMC-only cultures. Notably, the VSMCs co-cultured with ECs retained a spindle shape, whereas VSMC-only cultures were epithelioid in appearance (58), consistent with a contractile and synthetic phenotype, respectively (46). It is not clear how well these co-cultures reflect *in vivo* conditions where VSMCs vary in proximity to the ECs of the intima and vasa vasorum, however, 3D cultures of VSMCs and ECs may provide insights into their relationship in the context of phenotype modulation.

Anatomy and sex influence vascular smooth muscle cell identity

Like ECs, VSMCs vary based on anatomical location and between sexes. Reduced intimal-medial thickness, owing to a lower abundance of VSMC is observed in females (59, 60). Single cell RNA transcriptome analysis demonstrated sex-specific differences in the expression of collagen in murine aortic-derived VSMCs (54). More recently, a single cell study also highlighted that key drivers of atherosclerosis differ between sexes – unique VSMC phenotype-modulating mechanisms underpinning an increased risk of atherosclerotic lesion development in females (61). Collectively, these data highlight that like ECs, in both health and disease VSMC identity is highly nuanced with regards to the influence of sex.

The extracellular matrix provides the structural qualities of the vasculature

It would be remiss to discuss the cells of the vasculature without also considering the most abundant feature of the arterial cell landscape – the ECM. A fascinating, dynamic

environment, it is irrefutably a major player of the vasculature and is as important as the ECs and VSMCs themselves. The ECM accounts for up to 60% of the dry weight of a large vessel (2). Critical to the structure and function of the arterial wall, the ECM provides elasticity and distensibility, and acts to provide critical signals, both directly by interacting with adhesion molecules such as integrins, and indirectly, as a reservoir for signaling factors. ECM composition differs within the vessel wall, including that adjacent to ECs, in the lamellae formed by VSMCs, as well as at the interface between the contractile and non-contractile layers (intima-media and media-adventitia). Differences in ECM composition are critical for providing the specific mechanical and biochemical properties required to facilitate appropriate signaling for each unique microenvironment of the vessel wall, and for maintenance of arterial homeostasis (62).

There are two major macromolecules within the arterial ECM: elastic fibers and collagen fibers. Elastic fibers comprise a diverse range of ECM species, including elastin, fibrillin, microfibril-associated glycoprotein-1, latent TGF- β , decorin, biglycan, versican, microfibrillar-associated protein, tropoelastin, lysyl oxidase, fibulin, vitronectin, amyloid, collagens, and endostatin (63). Elastin is attributed with providing distensibility in the vessels and distributing stress onto collagen (64). Encoded by *ELN*, elastin is the major component of elastic fibers. Like collagen, elastin is also expressed variably in different anatomical locations (3). Decreases in elastin expression during development have been shown to result in thickening of lamellar units and increased abundance of VSMCs, which is thought to compensate for the reduced elasticity normally provided by the elastin in the ECM layer of the lamellae. Elastin insufficiency has been linked to hypertension in later life in both mice and humans (65).

Collagen fibers are comprised of bundles of collagen fibrils, which are formed from collagen triple helix bundles (each collagen triple helix being made up of three collagen chains). Collagen is the most abundant protein in mammals. There are many types of collagen chains – over 44 chains have been recognized (66). Different collagen types provide different mechanical properties, such as stiffness or elasticity (67). In arteries, collagen is the greatest facilitator of the contractile changes that occur and is attributed with defining the stiffness of vessels (64). The abundance of total collagen and collagen subtypes in the vasculature is not universal (67, 68), with differences in variables such as anatomy, sex, ethnicity and age still to be cataloged.

The extracellular matrix is essential to cellular identity

The ensemble of ECM proteins, known as the matrisome, encompasses 300 different proteins that provide the elegant and complex extracellular environment required to maintain cellular identity (66, 69). Both VSMCs and ECs contribute to

the generation and modification of the arterial ECM, which is established during development, and has low turnover in adult life, except for alterations with aging, disease, and injury. For example, once established at birth, elastin turnover is thought to be only 1% per annum (70). Experiments as early as the 1980s showed that altering the ECM on which VSMCs are grown drastically changes the morphology of VSMCs, highlighting the importance of consistency in the ECM. Male rat aortic VSMCs change their phenotype, including their shape, attachment, and spread *in vitro*, with alterations in fibronectin, laminin, collagen IV or peptide coating (71). Even changes to the conformation of collagen can influence cellular phenotype: collagen 1 in its fibrillar form promotes a contractile VSMC phenotype, whereas monomeric collagen 1 activates VSMC proliferation, indicative of encouraging a synthetic phenotype (72). Elastin is similarly essential – in cultured primary porcine VSMCs, elastin reduces proliferation and migration in an inverse dose-dependent manner, while in ECs, proliferation was only reduced once elastin reached a threshold concentration (10 mg/mL) (73). Additionally, homozygous elastin knock-out-derived murine VSMCs express reduced levels of contractile myofilament-associated proteins, including ACTA2, CNN1 and TAGLN. The mechanisms driving this shift in phenotype have led to the finding that elastin can activate a G protein-coupled pathway leading to the inhibition of adenylate cyclase, which causes a reduction in cAMP levels and stimulates actin polymerization (74).

The mechanical properties of the arterial ECM modulate cellular phenotypes. Increased extracellular stiffness has been shown to influence an array of cellular properties, including focal adhesion expression and cytoskeletal structure (75, 76). Stiffness also influences expression of plasticity proteins. A study into the effects of altered substrate stiffness on mesenchymal stem cells (vascular progenitors) found that expression of the Yamanaka factors' Nanog, Sox2, and Oct4, decreased with increased stiffness (77). This same study also found that reduced stiffness resulted in a more relaxed nucleus, leading to the speculation that this allowed for an increase in euchromatin that facilitated increased pluripotency gene expression (77). Interestingly, increased motility in the presence of a stiffer substrate, a response known as durotaxis, has been shown when VSMCs were plated on fibronectin, but not laminin, and an inverse relationship has been shown in a recent study comparing migration of VSMCs on collagen (migration decreased with increased stiffness) and fibronectin (again, migration increased with an increase in substrate stiffness) (78, 79). Together these studies suggest the effects of extracellular substrate stiffness rely not only on the mechanical properties of VSMCs but also on ECM composition.

The ECM provides a critical reservoir for growth factors and signaling compounds, such as TGF- β . TGF- β signaling is fundamental in mediating both EC and VSMC proliferation, cell death, migration and adhesion, cytoskeletal organization,

as well as in regulating the ECM itself (80). This signaling is nuanced – eliciting differing effects depending on cell type, concentration, and receptor presence (81). In ECs, for example, TGF- β binding to the TGF- β receptor 2 (TGF β R2) and the ALK5 complex elicits downstream SMAD2/3 signaling, which inhibits proliferation and migration and, thereby, maintains quiescence. Conversely TGF- β interaction with the TGF- β R 2 and the ALK1 complex activates SMAD1/5 signaling, stimulating proliferation and migration (82). TGF- β is stored in a latent form in the ECM. Under normal physiological conditions, latent TGF- β is activated by cleavage of its propeptide (latency-associated protein) by furin. This activation occurs *via* a number of mechanisms, the primary being integrin activation (80).

Anatomy and sex influence arterial extracellular matrix

Given the complex variability in arterial cell identity, it is unsurprising that arterial ECMs vary beyond simple differences in abundances of collagen fibers and elastin fibers. The overall composition of the ECM varies in different anatomical regions – as aforementioned, expression of the ECM in ECs and VSMCs varies throughout the vascular tree. A microarray study of blood vessels harvested post-mortem indicated distinct differences in mRNA expression of ECM protein-encoding genes. Thus, ECM proteins, including collagen subtypes 5 α 1/2, 4 α 1 and 4 α 2, as well as many ECM interacting proteins, such as integrins, were found to be differentially expressed across anatomical regions, with a distinct partitioning when grouped by vessel size (83).

Given the differing functional requirements of the layers of the artery, vascular ECM must also vary in composition at the microenvironment level. The interfaces of the arterial layers must facilitate the coalescence of two differing cell types, which differ in function, and, therefore, structure. Endothelial ECM is characterized by great asymmetry in its composition – the luminal surface of ECs lacks the structural components of collagen and elastin fibers. Instead, the extracellular space is covered in a fragile mesh-like layer of polysaccharides, proteoglycans, glycoproteins and glycosaminoglycans, termed the glycocalyx, that appropriately translates to “sweet husk.” This layer, which appears almost as a fur lining, retains hyaluronan and heparan sulfate to create a hydrostatic pressure gradient (84). It plays an important role in preventing pathogen entry, and facilitating the diffusion of required nutrients (85). On the reverse, intramural side of ECs, the intimal-medial interface must facilitate the interactions of ECs with the contractile VSMCs of the media. Similarly, the ECM of the media, so integral to facilitating pulsatility, must coordinate the recurring units of VSMCs, yet it must also permit reticulation of vasa vasorum from the adventitia into the media.

Further to this complexity, artery composition and stiffness also varies based on sex and aging. Artery size varies with sex;

average female arteries are smaller than their male counterparts (86, 87). Arterial stiffness increases with age. Rates of change are, however, sex-dependent such that arterial stiffening accelerates after the onset of menopause, reversing the trend in women, who, relative to men, have more compliant vessels (88, 89). This phenomenon is also observed in non-human primates (90). This relationship has been attributed to sex hormone levels such as estrogen and progesterone, which are lower in men, and which decrease in menopausal women. Progesterone and estrogen have been demonstrated to alter ECM deposition by VSMCs *in vitro*, thus reduced ECM regulation by these hormones is suspected to contribute to this increased arterial stiffness (91). However, a recent study of 339 women found that the arterial stiffness increase that occurred within the year following their final menses did not correlate with either estrogen or follicle stimulating hormone levels, though this study did not examine progesterone levels (92).

Arterial cells and extracellular matrix dysfunction prime arteries for dissection

Arterial dissections occur when arterial structure is compromised, and, except for aortic dissections, development of an IMH prevents perfusion by the artery. Dissection falls into two categories (Figure 4): (1) an IMH forms within the media, while the intima remains intact, or (2) the integrity of the intimal layer is compromised resulting in the formation of a false lumen due to blood flowing into the medial layer of the artery from the true lumen, resulting in an IMH. It is not clear if this tear in the intima is a primary event or is secondary to expansion of an existing IMH, however, angiography, which requires the use of a thin guidewire for catheter placement has been known to cause an iatrogenic intimal tear and/or to exacerbate a spontaneous dissection.

Collectively, the localization of dissections within arteries implicates perturbations of ECs, VSMCs and/or arterial ECM in the etiology of arterial dissections. Schievink and colleagues, proposed in their 1994 review that primary arteriopathies are the result of single ECM protein mutations, the phenotypes of which are predicated on the distribution (and abundance) of ECM expression in different organs (93). Based on these considerations, it seems reasonable to hypothesize that the composition of different arteries is predicated on their mechanical requirements, and that dysfunction in critical ECM components at an anatomical position will predispose the vascular structure to dissection at such locations. It could also be speculated that the subtypes of dissection correlate with a specific Achilles’ heel of arterial architecture *i.e.*, that the various ECM compositions at different cellular interfaces of the artery (EC-EC, EC-VSMC, VSMC-VSMC, and EC-ECM

layer, VSMC-ECM layer) serve as points of mechanical weakness when compromised by aberrant protein expression, with such weakness predisposing to dissection. Extending this notion, perturbations in EC and VSMC function, particularly VSMC contractility, may similarly compromise arterial integrity and contribute to susceptibility to dissection.

Spontaneous arterial dissections

Spontaneous arterial dissections occur both in association with connective tissue diseases as well as independently, in otherwise seemingly healthy individuals. A commonly held hypothesis is that spontaneous arterial dissection events occur according to a two-hit model – requiring a genetic burden to predispose an individual to a dissection, and an environmental trigger to precipitate the event. Many of the pathways and genes that have been associated with spontaneous arterial dissections are shared amongst different dissection types, as discussed below.

Spontaneous arterial dissections may occur in many different anatomical locations, such as the cervical arteries and aorta, or there may be multiple dissections in one area, such as in multiple branches of the coronary artery (94). This strongly suggests that there are likely mechanistic subtypes of arterial dissection. Simultaneous artery dissections have been reported – one case study reported seven arterial dissections within 24 h of hospital admission in both iliac arteries, inferior mesenteric, renal, splenic and celiac arteries (95). Although no phenotypic features of connective tissue diseases were evident, genetic screening of the 28 vascular dissection and aneurysm-associated genes (a connective tissue disease panel) identified a variant in *COL3A1* (c.3199A > T, Ser1067Cys). The clinical significance of this variant is unknown; these amino acids differ only in one functional group whereby an alcohol in serine is replaced by a thiol group in cysteine (95). As there were other family members who were also homozygous for this variant with no history of vasculopathy, further investigation, such as whole genome sequencing (WGS) and cellular and molecular studies, is needed to elucidate the mechanisms causing this extreme phenotype.

Importantly, there are reports of family members carrying variable penetrance risk variants, who have no notable disease features and who have not suffered from a dissection (1, 96, 97). Whether there is a protective genetic element present in these individuals, or if the right positive environmental cues (or lack of negative environmental cues) are also present, is unclear. Future integration of WGS information to determine polygenic risk scores for dissection may be helpful for these individuals. The asymptomatic state yields hope that therapeutic intervention, to upregulate protective cellular processes, once defined, could prevent future dissections in family members at risk, and those at risk of recurrent dissections.

Diseases affecting vascular extracellular matrix are associated with increased risk of arterial dissections

Increased risk of arterial dissections in a number of diseases that affect vascular integrity suggests a genetic predisposition to dissections. Patients with connective tissue syndromes including Ehlers–Danlos, Marfan syndrome, Loeys–Dietz, Alport, as well as those with osteogenesis imperfecta (brittle bone disease), polycystic kidney disease, and fibromuscular dysplasia (FMD), commonly report dissections in the aorta, coronaries, and/or cervical arteries. Pathogenic variants causing these conditions are overwhelmingly ECM-related (Table 1). Sexual dimorphism is reported in many of these conditions – for example in a study of vascular Ehlers–Danlos patients, men were more common in the aortic dissection cohorts, while women dominated in the SCAD and CeAD Ehlers–Danlos cohorts. While larger studies are needed to further validate these findings (98), this theme of sex-related differences is prominent among the different types of arterial dissection.

Aortic dissections

The aorta is the largest artery in the body, and the most common artery to dissect. It is subjected to the highest pressure of any artery, being the first to receive ejected, oxygenated blood from the heart. It is estimated that 1–2% of all deaths in the Western world are caused by weak and defective aortic structure (99). Thoracic aortic dissections are the most common catastrophic vascular structural failure, exceeding that of ruptured abdominal aortic aneurysms. Taking into account cases that are lethal prior to hospital admission, the annual prevalence of aortic dissections is 15 cases per 100,000 people (100).

Aortic dissection pathology

There are numerous clinical classification systems for aortic dissections. Traditional anatomical-based classification systems remain popular – namely the ternary DeBakey system (101) and the binary Stanford system (102), both of which classify dissections according to the extent of involvement of the ascending and/or descending aorta. Aortic dissections are also commonly classified by their anatomical locations into thoracic and abdominal regions. The majority (62.3%) of aortic dissections occur in the ascending portion of the aorta and are considered thoracic aortic dissections (103). Newer classification systems have been proposed, some of which consider features of pathology (e.g., where, within the vessel wall, the dissection forms; if the dissection was iatrogenic, and if atherosclerotic plaques were present) that provide useful information for understanding the underlying mechanisms. However, these have not yet been widely adopted

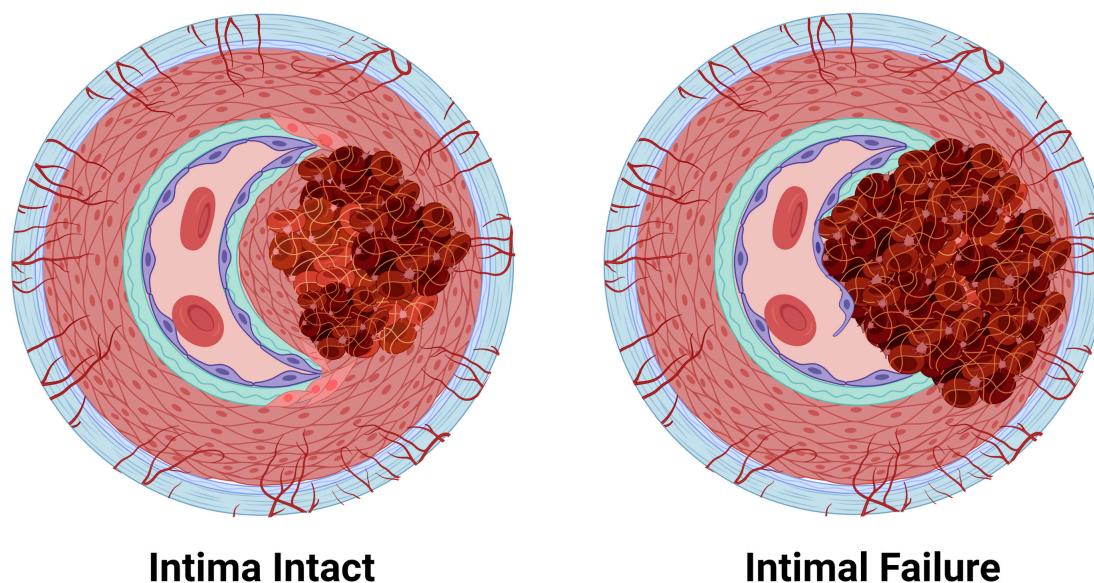


FIGURE 4

The two pathologies of arterial dissections: bleeding within the tunica media results in intramural hematoma formation with separation of the tunica media layer to create a false lumen that causes occlusion of the true lumen of the vessel, thereby preventing tissue perfusion. Some dissection events are associated with tunica intima tearing (intimal failure). Created with [BioRender.com](https://www.biorender.com/).

(104, 105). It has been proposed that dissections occur at areas of the aorta subjected to the largest pressure changes; a notion supported by computational flow predictions (106). Vasa vasorum dysfunction is also increasingly recognized as being central in aortic dissection pathogenesis (107). This is strongly evidenced by a porcine study wherein occlusion of aortic vasa vasorum was sufficient to cause aortic dissection (108). Further investigations into vasa vasorum dysfunction are urgently needed.

Conditions and risk factors associated with aortic dissection

As the most common type of arterial dissection, aortic dissections are also the most well-defined in terms of associated risks. Sexual dimorphism is evident with males accounting for 67.5% of cases (109). Women who experience an aortic dissection tend to be older. Analysis of the International Registry of Acute Aortic Dissections revealed that of patients under 50 years old, males represented 80% of cases, however, this divergence steadily drops with age, reaching an almost 1:1 male:female ratio in patients over 75 years old (103). Notably, this study also showed dissection location partitioned with age – the mean age of patients suffering from an ascending aortic dissection was significantly younger than those who developed other aortic dissections.

Hypertension is a strongly linked risk factor for aortic dissections. In a Swedish study of thoracic and abdominal aortic dissections, hypertension was present in 86% of individuals (109). Smoking, which has been linked to hypertension, as

well as general vascular damage, is also a high risk factor (110, 111). It is unclear whether this association is due to smoking causing hypertension, arterial damage, or both, and/or to another explanation entirely. Other agents that cause vascular injury have also been linked to aortic dissection including infections, such as syphilis (112). Though now rare, in cases of syphilis where the infection has been ongoing for more than 10 years, cardiovascular sequelae, including aortic dissection, are common, (113, 114). An increase in aortic dissections following COVID-19 infections has been reported and long term effects of infection are yet to be fully realized (115). Rare cases of aortic dissection have also been reported in people with ankylosing spondylitis, an inflammatory autoimmune condition that often causes aortitis (116).

Genetics and molecular mechanisms of aortic dissections

Perturbations in a number of pathways have been implicated in aortic dissections – TGF- β signaling, ECM, VSMC contractility, and VSMC metabolism (117). Importantly, these pathways are critical in cellular identity and phenotype switching in VSMCs, which we postulate precedes all forms of arterial dissection. The genetics of aortic dissections are subject to regular review. It is not the intent of this review to provide an exhaustive update, but rather a comparison for a holistic view of arterial dissections. By comparing findings with the growing wealth of knowledge provided by genetic and cellular studies, we can begin to elucidate the underlying disease mechanisms shared by all arterial dissections. Moreover,

TABLE 1 Arterial dissection associated conditions.

Condition	Description	Genes with pathogenic variants	Prevalence	Sexual dimorphism	Dissection associated	References
Ehlers–Danlos (EDS)	CTD; hyperextendable joints, hyperextensible skin, easy bruising, abnormal scarring; vascular EDS subtype, and in 17% 13 non-vascular EDS have vascular involvement	<i>COL1A1, COL1A2, COL5A1, COL5A2, COL3A1, COL12A, ADAMTS2, PLOD1, FKBP14, TNXB, CHST14, DSE, B4GALT7, B3GALT6, SLC39A13, ZNF469, PRDM5, CIR, CIS, AEBP1</i>	1:5,000	Dissection types vary by gender	CeAD, aortic, SCAD	(98, 264–268)
Marfan syndrome	CTD; affects the ocular, skeletal, and cardiovascular systems with varying severity	<i>FBN1</i>	1:5,000–1:10,000	Sex related burden (pregnancy increases aortic root dilation)	CeAD, aortic, SCAD, PA	(109, 157, 220, 269–272)
Loeys–Dietz syndrome	CTD; affects the skin, skeletal and cardiovascular system	<i>TGFBR1, TGFBR2, SMAD3, TGFB2</i>	Less than 1:10,000	NA	CeAD, aortic, SCAD	(273–275)
Alport syndrome	Affects the renal, auditory and ocular systems. Hypertension increases risk of cardiovascular events 1000 fold.	<i>COL4A3, COL4A4, COL4A5</i>	1:10,000	X-linked in 85% cases	Aortic, SCAD	(276–279)
Fibromuscular dysplasia	Abnormal (dysplastic) cell growth in medium-sized arteries causing tortuosity	<i>PHACTR1</i>	Up to 6.6% population (potential kidney donors)	90% patients female; male patients significantly associated with CeAD	CeAD, SCAD	(157, 166, 171, 280, 281)
Polycystic kidney disease	Kidney cyst formation, cardiovascular	<i>PKD1, PKD2</i>	10M people globally	NA	CeAD, Aortic, SCAD, iliac	(34, 175, 282–284)
Osteogenesis imperfecta	Brittle bones disease	<i>COL1A1, COL1A2, BMP1, CRTAP, LEPRE1, PPIB, TMEM38B, SERPINH1, FKBP10, PLOD2, WNT1, CREB3L1</i>	1:20,000	NA	CeAD, aortic, SCAD	(229, 285–289)

contrasting the differences in these dissection subtypes can direct our understanding of the susceptibility of specific anatomical locations to dissection.

Transforming growth factor β signaling dysfunction

Given the well-established link between TGF- β signaling dysfunction and disease-associated aortic dissections, such as in Marfan Syndrome, it is unsurprising that several members of this pathway have been implicated in spontaneous aortic dissections as well as connective tissue diseases. Variants that have been associated with thoracic aortic dissection (through syndromic affiliations, such as Loeys–Dietz) include two of the three isoforms of TGF- β (*TGFB2*-3), both TGF- β receptors, *TGFBR1* and *TGFBR2*, and TGF- β -latent transforming growth factor β -binding protein 1 and 3 (*LTBP1*, *LTBP3*) (118–120). Protein-protein interaction analysis has implicated TGF- β 1 as a central protein in aortic dissections (121), though variants in *TGFB1*, *per se*, have not been identified in patients.

The downstream effectors of TGF- β signaling, such as the SMAD family, have also been linked to aortic dissections. *SMAD3* is regarded as a definitive causal gene for thoracic aortic dissections (122). *SMAD2*, *SMAD4* and *SMAD6*, which signal through c-Jun/c-Fos (123), are also associated with aortic dissections (1, 118, 120, 124, 125). *ZFYVE9*, encoding zinc finger FYVE domain-containing protein 9, which recruits SMAD proteins and is involved in TGF- β signaling, has been associated with aortic dissections through recent whole exome sequencing studies (121). Similarly, *LRP1* has recently been associated with acute aortic dissections (126). Loss of *LRP1* recapitulates Marfan syndrome disease mechanisms, wherein TGF- β is prematurely released from the ECM. Interestingly, loss of *LRP1* upregulates the JNK1/2-c-Jun-Fra-2 signaling pathway in myofibroblasts (127), a pathway also affected in aortic dissections.

Mutant forkhead box E3 (*FOXE3*) has been identified to predispose to aortic dissections (128). Not a lot is known about

the role of FOXE3, a transcription factor better known for its critical role in lens epithelial cell proliferation and survival. In mouse lens epithelial cells, forced persistent expression of *FOXE3* during development alters the cytoskeleton and the ECM, and causes prolonged upregulation of TGF- β 3 and CTGF expression (129). *FOXE3*-deficient mice have increased VSMC apoptosis, as well as increased aortic pressure, and rupture (128). Methionine adenosyltransferase 2A (*MAT2A*) (130), another aortic dissection risk-associated gene, has previously been suggested to be a VSMC metabolism gene, however, recent work in hepatic stellate cells has also identified *MAT2A* as a downstream target of TGF- β . Upregulation of TGF- β 1 increased *MAT2A* concentration *via* p65 phosphorylation, with subsequent increased expression of both *ACTA2* and *COL1A1* (131).

Extracellular matrix dysfunction in aortic dissections

Variants in an array of collagen subtypes are associated with aortic dissections, including eleven collagen genes: (*COL1A1*, *COL1A2*, *COL3A1*, *COL4A1*, *COL4A5*, *COL5A1*, *COL5A2*, *COL9A1*, *COL9A2*, *COL11A1*, and *COL18A1*) (1, 118, 120, 121, 124, 125, 132, 133). Variants in a range of quintessential ECM proteins are also involved, including EGF-containing fibulin-like extracellular matrix protein 2 (*EFEMP2*), microfibril associated protein 5 (*MFAP5*), lysyl oxidase (*LOX*), elastin (*ELN*), and fibrillin (*FBN*)-1 and -2 (121, 134, 135).

Dysregulation of the ECM is a regularly occurring theme in aortic dissection-associated variants. Downregulation of the hsa-miR-29 family, which has been shown to increase collagen levels, including in cardiac fibrosis where it has been shown to increase collagen1A1, 1A2, 3A, and fibrillin-1 mRNA expression in regions affected by myocardial infarction in mice (136), was detected in aortic tissue of dissection patients compared to healthy controls (132). A decrease in HDAC6 protein levels has also been detected in aortic tissue of dissection patients compared to coronary artery disease patients, whereas mRNA levels of ECM proteins were found to be increased, including *COL3A1* and *COL1A2*, matrix metalloproteinase 2 (*MMP2*), tissue inhibitor of metalloproteinases 2 (*TIMP2*), periostin (*POSTN*) and connective tissue growth factor (*CTGF*). This ECM regulation of matrix secretion is thought to involve HDAC6 deacetylation of H3K23 (137). *MMP1* (total) and *MMP9* (total and active) levels have been shown to be increased in aortic dissection tissues compared to controls (138).

Suppressor of cytokine signaling 3 (*SOC3*) is a more recent gene to be implicated in the pathogenesis of aortic dissections. In a mouse model of aortic dissection induced by minipump administration of the lysyl oxidase inhibitor, β -aminopropionitrile (BAPN, 150 mg/kg/day), and the vasoconstrictor, angiotensin II (1,000 ng/kg/min), it was found that knockout of *SOC3*, an activator of JAK/STAT and negative regulator of Janus kinases/signal transducer, led to a decrease in aortic dissections (139). Aortae from *SOC3* knockouts

had increased tensile strength, likely due to an increased deposition of total collagen, which was significantly higher in the adventitia. This suggests that increased tensile strength reduces the incidence of dissections (139). Additionally, levels of several ECM-associated proteins have been found to be decreased in aortic dissection tissue, including HSP27, SOD3 and osteoglycin (140).

Cytoskeletal dysfunction in aortic dissection

Proteins of the cytoskeleton, as well as cell adhesion-associated proteins that anchor vascular cells to the vascular ECM, feature heavily in the proteins that are associated with aortic dissection. Altered expression of VSMC intracellular contractile proteins, including MYH11, myosin light-chain kinase (encoded by *MYLK*) that phosphorylates myosin light chain, *ACTA2*, and *TAGLN* have been associated with aortic dissections. In addition, *ACTA2* mRNA has been found to be increased in aortic tissue of dissection patients (137), suggestive of cells undergoing phenotypic changes. An early proteomics study also implicated an upregulation of *ACTA2* protein with concomitant decrease in *TAGLN* protein in aortic tissues from patients post-dissection compared to controls (140). Talin-1, which tethers the ECM to the cytoskeleton by tethering actin to integrin, and is involved in the regulation of focal adhesions, integrin signaling, proliferation and migration, has been shown to be downregulated in aortic dissection tissue compared to normal controls (141, 142). Variants in the cell adhesion neurogenic locus notch homolog protein 1 gene, *NOTCH1*, are associated with aortic dissection/aneurysm (143). Moreover, protein levels of *NOTCH1* have been shown to be reduced in thoracic aortic dissection tissue, despite an upregulation of *NOTCH1* mRNA (144). Collectively, the altered expression of these cytoskeletal proteins is suggestive of cellular activation and remodeling.

Dysfunction in the regulation of cytoskeleton proteins has also been associated with aortic dissections. A zinc finger protein, four and a half LIM protein 1 (encoded by *FHL1*), which regulates the structure and formation of myosin filaments (122, 145), was found *via* proteomics to be decreased in aortic tissue (140). This has also been independently corroborated in Western blot analyses of aortic tissue from dissection sufferers, which found a 2.5-fold decrease in *FHL1* level in patients compared to controls. Importantly, immunohistochemistry revealed this decrease was most pronounced in the area of the media surrounding the tear when compared to the intima and adventitia (122). In the myoblast C2C12 cell line, *FHL1* has been observed to potentiate the effects of TGF- β (146). In non-diseased vessels, *FHL1* has been observed to increase with increased blood pressure (147), and has been shown to be increased in rat VSMCs following treatment with hypertrophic stimuli (148). siRNA knockdown of *FHL1* in rat VSMCs caused a decrease in cell proliferation, which was not associated with apoptosis (122). Together these data suggest that *FHL1* plays

a role in VSMC plasticity (contractility/synthetic identity), though the exact role of this protein in VSMC phenotype regulation, and its role in vascular dissection will require further investigation. Similarly, variants of Unc-51-like kinase 4 (*ULK4*), a pseudokinase thought to remodel the cytoskeleton, have been linked to aortic dissections (126), with variants in *ULK4* having also been linked to hypertension (149, 150).

Metabolic dysfunction in aortic dissection

Metabolic changes are reported to precede aortic dissections, and a number of genes associated with aortic dissections are linked to metabolism (125). *DAB2IP*, encoding disabled homolog 2-interacting protein, which is involved in cell growth and survival and has been associated with aortic dissection as well as abdominal aortic aneurysms (121, 151). mRNA expression of both *CREBBP* (encoding CREB-binding protein) and *EP300* (encoding histone acetyltransferase p300), both of which regulate cAMP-associated genes, was found to be downregulated in patient aortic dissection tissue compared to healthy controls (121). Interestingly, the aforementioned study by Liao et al. (140) focused on the role of oxidative stress as a mitigating pathway for aortic dissection (140), which is further supported by the recent identification of mitochondrial dysfunction being modulated by ECM stiffness in Marfan syndrome-associated aortic aneurysm formation (152).

Variants in the glucose transport 10 protein, Glut10 (encoded by *SLC2A10*), have been associated with a Marfan syndrome-like disease pathology that is seen in arterial tortuosity syndrome, another disease associated with aortic dissections. (100, 153). Variants in *SLC2A10* lead to a decreased density of Glut10 transporters, which causes ECM disarray and subsequent inappropriate TGF- β signaling, as well as oxidative stress (154). Notably, pathogenic variants in glut10 have been shown to alter angiogenesis (155). *CBS* encoding cystathionine-beta-synthase, has been categorized as a low-risk gene for aortic dissection (120). Variants in *CBS* are associated with the metabolic condition, homocystinuria, which, similar to pathogenic *SLC2A10* variants, can result in a Marfan syndrome-like disease pathology. Conversely, Group V secreted phospholipase A2 (sPLA₂-V) is believed to play a protective role against aortic dissection. Increasing downstream mobilization of sPLA₂-V substrates has been shown to rescue an angiotensin II infused murine model of aortic dissection. Thus, increasing dietary oleic acid and linoleic acid, which are normally mobilized by sPLA₂-V, eliminated spontaneous dissection observed in 45% of sPLA₂ knockout mice (*Pla2g5*^{-/-}) (156).

Spontaneous coronary artery dissection

The coronary artery, which supplies blood to the heart itself, is the only artery to perfuse its cognate tissue, the myocardium,

during the relaxation phase of the cardiac cycle (diastole) rather than in systole. As with other muscular vessels, the outer layer of the coronary tunica media is perfused by vasa vasorum that originate from sites of branching of the coronary vessels (9) with little if any contribution from vasa interna (8). Dissection of the coronary artery results in an acute coronary syndrome (myocardial infarction or unstable angina) or death (157). As with all dissections, advances in their detection, via CT or MR angiography and direct intravascular imaging modalities (intravascular ultrasound and optical coherence tomography), have increased the diagnosis of spontaneous coronary artery dissections (SCAD) that were previously likely to be markedly underdiagnosed. It is now estimated that up to 4% of acute coronary syndromes are caused by a coronary artery dissection (158).

Spontaneous coronary artery dissection pathology

Most dissections in the coronary artery (~70%) do not present with an intimal flap, indicating that IMH formation from vasa vasorum rupture is likely central to SCAD pathophysiology. There is a correlation between areas of the coronary artery that are more susceptible to dissection and a lower vasa vasorum density; the left anterior descending coronary artery (60% of dissection cases) has a density of 1.2×10^{-5} vasa vasorum/ μm^2 , compared to the left circumflex (38% of dissection cases), which has 1.88×10^{-5} vasa vasorum/ μm^2 , and the right coronary artery, (7% of dissection cases) that has a density of 2.14×10^{-5} vasa vasorum/ μm^2 (157, 159). One study has reported increased vascularization in the adventitia of post-mortem sections following fatal dissections compared to nonobstructive coronary artery disease patient sections (160). While it is unclear if this preceded or was a consequence of the SCAD, increased vascularization of this outermost layer may be due to a localized dysfunction, such as an increase in ischaemic areas within the media, which would promote angiogenesis in vasa vasorum (9).

Spontaneous coronary artery dissection associated conditions and risk activities

There is a distinct sexual dimorphism in SCAD incidence with 82–98% of cases occurring in women aged between 45 and 52 years (157, 161, 162). An estimated one third of myocardial infarctions in women under 50 are caused by SCAD. Risk of recurrence of SCAD has been reported to be up to 30% (163), although a recent prospective observational study only reported recurrence in 2% of cases over a median follow-up of over 2 years (164). The risk factors associated with SCAD are similar to those for aortic dissections. Hypertension and migraine are found commonly in SCAD survivors, being present in 45 and 43% of cases, respectively (94, 161). FMD is common in SCAD patients. SCAD and FMD share many of the same risk loci; FMD being reported in 45–86% of cases (165, 166).

Such marked overlap suggests SCAD may be a manifestation of FMD specific to the coronaries, although it is intriguing that the classical vessel beading of FMD is not observed in the coronary arteries of SCAD patients (167). Inflammatory disorders and infections are rarely associated with SCAD. For example, like aortic dissections, there is anecdotal evidence that SCAD can occur in association with tertiary syphilis (168, 169). In addition, SCAD has been reported in a recently recovered COVID patient (negative nasal swab, positive for COVID-19 IgG antibodies) (170).

Spontaneous coronary artery dissection genetics and molecular mechanisms

Though little research has been done investigating the molecular mechanisms of SCAD, a number of genomic studies have been undertaken (97, 163, 171, 172), which indicate that genetic risk for SCAD can result from variants in multiple genes. The common nature of these variants suggests SCAD is likely a polygenic disease and requires an additional environmental stress for a dissection to occur. A meta-analysis of case control studies identified the first risk locus as the A-allele of rs9349379, a single nucleotide polymorphism located in an intron in the *PHACTR1/EDN* gene, which was found with a frequency of 0.72 in SCAD cases compared to 0.56 in controls (OR 1.67; $p < 6.67 \times 10^{-21}$). Identification of this locus sparked debate over the level of endothelial involvement in SCAD as the rs9340379 locus is located in an intronic region of *PHACTR1*, which is also a putative enhancer of the upstream gene encoding endothelin 1 (*EDN1*) (171), an endothelially expressed potent vasoconstrictor peptide. A clinical study has attributed deficient EC function to a difference in vascular function observed in SCAD patients, however, it failed to consider the role of VSMCs in the decreased peripheral arterial tone (vasoconstriction/dilation) observed in SCAD patients (173). Conversely, coronary blood flow studies suggest that endothelial dysfunction is not a principal cause of coronary artery dissection (174). Given the involvement of VSMCs in other vascular dissection disorders, it is unlikely that deficits in endothelial function alone would cause all SCADs, however, cellular studies will be critical in understanding how these two cell types contribute to the pathophysiology of coronary dissections. More recently, several other potential genetic risk loci have been identified as a result of WGS studies and genome wide association studies (GWAS), as detailed as follows.

Transforming growth factor β signaling dysfunction in spontaneous coronary artery dissection

Proteins directly and indirectly involved in the TGF- β signaling pathway have been strongly implicated in SCAD pathophysiology. Recently, a targeted and genome-wide analysis of a cohort of 91 SCAD patients revealed an enrichment of TGF- β when rare variant collapsing analysis was performed (172). Variants in *TGFB2* and *SMAD3*, as well as *PKD1* have been

associated with SCAD in WGS analyses (175). Additionally, variants in *FBN1* have been associated with SCAD in a GWAS, as well as from WGS analysis, which identified two likely pathogenic variants (97, 172). Fibrillin has also been proposed as a SCAD biomarker, being elevated in SCAD patients compared to other acute coronary syndrome patients and healthy controls (176). However, fibrillin 1 is not specific for SCAD as it has also been found to be elevated in other vasculopathies including aortic and cervical dissections (177).

Variants in SCAD-associated genes, *TBX2*, a T-box transcription factor; *YY1API*, yin yang 1 (YY1)-associated protein 1; *FIIR*, encoding junctional adhesion molecule-A (JAM-A), and *LRP1*, which is also associated with aortic dissections, have been shown to affect cellular proliferation through pathways downstream of TGF- β (175, 178–182). *GLI3*, which was identified as a gene linked to SCAD in the Carss et al. (175) patient cohort, has also been thought to be linked to TGF- β signaling. Encoding a transcription factor in the sonic hedgehog pathway, *GLI3* is suggested to be a repressor of TGF- β -dependent hedgehog pathway activation, which is critical for proliferation and cellular identity (183, 184).

Extracellular matrix dysfunction in spontaneous coronary artery dissection

Similar to aortic dissections, collagen variants have been associated with SCAD based on a recent whole exome sequencing study (185). Variants of a rare and disruptive nature (being pathogenic or likely pathogenic) were found to be enriched in a cohort of 130 SCAD patients in the ECM structural constituent conferring tensile strength pathway (GO:00300200), which included *COL1A1*, *COL1A2*, *COL3A1*, *COL4A1*, *COL5A1*, *COL5A2*, *COL6A1*, *COL12A1* and *COL27A1*. Variants in *COL3A1* and *COL4A1* were also identified by Tarr et al. (172). Carss et al. (175) highlighted variants in other genes, including *COL18A1* and *COL4A2*, and SRY-Box transcription factor 9 encoded by *SOX9* (186), as having possible associations with SCAD, however, they did not reach their required significance thresholds, but scored highly and were plausibly associated with SCAD. This same study also identified that variants in the gene for the protein transport protein, *SEC24B*, were SCAD-associated, with expression of *SEC24B* having since been found to be involved in collagen export (187).

A number of ECM glycoprotein genes have also been associated with SCAD via GWAS studies, including *ECM1* and *ADAMTSL4* (97, 163, 188). *ECM1* is associated with cellular migration and cellular phenotype transition, and has been shown to inhibit activation of TGF- β (189, 190). *ADAMTSL4* binds with fibrillin-1, and accelerates the biogenesis of microfibrils (191). Turley and coworkers also suggested that a secreted protein, encoded by *C1orf54*, is associated with SCAD; *C1orf54* has previously been linked to carotid artery aneurysm, although the function of this protein is still unknown (97).

FMR1 has been linked to SCAD. Premutations in this gene, which encodes fragile X mental retardation protein (FMRP), are thought to increase susceptibility to dissections, since FMRP is involved in regulating the ECM and cytoskeleton (192). Impaired cytoskeletal protein-function has been shown in embryonic fibroblasts of *FMRP* knockout mice (193), and increased plasma levels of MMP9 are observed in Fragile X patients as compared to healthy controls (194). Of note, hypertension is also common in patients with Fragile X syndrome, though the mechanism for this is unclear (195).

SCAD studies have also identified pathogenic variants of *ABCC6* (or loci associated with this gene) in patients (172, 188). Encoding ATP Binding Cassette Subfamily C Member 6, variants in this gene cause *pseudoxanthoma elasticum*, a connective tissue disorder that affects vision, skin and the cardiovascular system to varying degrees (196, 197); cardiovascular sequelae occurring later than cutaneous and ophthalmological manifestations (198). It is thought that an increased degradation of elastin, as well as the presence of calcium/phosphorus deposits contribute to this arterial pathology (199). Transmission electron microscopy imaging of the dermis of *pseudoxanthoma elasticum* patients showed irregular and clumped elastic fibers, as well as disorganized collagen, with some studies finding that collagen fibers are also misaligned (200, 201). Carotid arteries of these patients have been shown to have an increased intima/media thickness, and peripheral arteries (intracranial carotid, and arteries of the limbs) show precocious calcification (202).

Cytoskeletal dysfunction in spontaneous coronary artery dissection

Similar to aortic dissections, pathogenic variants in the talin 1 gene, *TLN1*, have been identified in a SCAD family cohort, along with 10 sporadic cases (203). Recent molecular studies have linked *PHACTR1*, *LRP1*, fibrillin 1, and talin 1 through indirect association; these proteins all commonly interact with integrins, acting to bridge the cell and the ECM (97, 163). Variants in cytoskeletal proteins including myosin light-chain kinase (encoded by *MYLK*), which phosphorylates myosin light chain, *MYH11*, and *MYLK2*, have also been linked to SCAD (172, 175). *NFATC1*, which encodes nuclear factor of activated T cells c1, is a transcription factor downstream of *LRP1*; its signaling regulates the extracellular bone morphogenetic protein-binding endothelial regulator pathway (204), and has been associated with modulation of VSMC cellular identity (205).

HDAC9, encoding histone deacetylase 9, was implicated in SCAD as a highly ranked gene in collapsing analysis by Carss and colleagues (175). *HDAC9* is associated with prevention of calcification in the media whereby *HDAC9* knockdown has been shown to increase calcification, and its overexpression *via* adenovirus reduced calcification in cultured murine VSMCs as well as in a mouse calcification model of high phosphate

treatment (206). An *HDAC9* variant is also associated with large vessel stroke (207). Importantly, *HDAC9* has been shown to repress contractile protein gene expression in murine aortic tissue (208).

Metabolic dysfunction in spontaneous coronary artery dissection

A likely pathogenic variant in *ALDH18A1*, which encodes aldehyde dehydrogenase 18 family member A1, also known as pyrroline-5-carboxylate synthetase (P5CS) (209), was identified in a cohort of 91 SCAD cases (172). Variants in *ALDH18A1* have been reported to cause *cutis laxa*, a rare connective tissue disorder associated with abnormal ECM. *Cutis laxa* is also linked to the aortic dissection-associated genes, *EFEMP2* (fibulin 4), *SLC2A10*, *ELN*, and the related genes, *FBLN5*, *LTBP4* (210). A variant in *ALDH18A1* has been found to reduce cellular arginine, and dietary arginine supplementation of a *cutis laxa* patient carrying this variant has been shown to attenuate disease symptoms. Importantly in the context of SCAD, arginine is critical for both ECM and NO synthesis (209).

A variant in *TSR1*, a ribosome maturation factor, was identified in a predominantly male Chinese Han SCAD cohort (211). However, patients with atherosclerosis were not excluded from this study so the implications of this finding are not yet clear, and they have yet to be replicated (212). In support of this finding, however, is the identification that variants in other protein synthesizing genes have been associated with SCAD, including mitochondrial ribosomal protein S21 (*MRPS21*) and peptidyl-glycine alpha-amidating monooxygenase (*PAM*) (175). Variants in two VSMC proliferation genes, *ARNTL* and *LINC00310*, have also been associated with SCAD. These genes encode the circadian clock regulating transcription factor, aryl hydrocarbon receptor nuclear translocator-like protein 1, and a long non-coding RNA, respectively (97, 175, 213, 214).

Cervical artery dissections

Cervical artery dissections (CeADs), encompassing dissections of the carotid and vertebral arteries, can present as migraine, or can cause a stroke, which may be fatal (215). Improvements in non-invasive imaging have led to increased reporting of these dissections in stroke patients. CeADs are believed to be the cause of up to 25% of strokes in young and middle-aged adults (under 50) (216). The prevalence of these dissections is now estimated to be at least 5 cases per 100,000 individuals (217), and more than half of CeAD patients will develop a stroke (218).

Cervical artery dissection pathology

As with aortic dissections and SCAD, CeADs present with an IMH, that may or may not be associated with an intimal flap, with pseudoaneurysms also being found. In some cases that

involve an intimal tear, the endothelium is described as being irregular (218). Interestingly, in an etiological investigation into connective tissue disorders in 65 cervical artery dissection patients, 55% displayed ultrastructural aberrations in collagen, similar to those seen in Ehlers-Danlos syndrome, with only 5% of the patients having clinical manifestations of skin, joint or skeletal abnormalities. These findings strongly implicate vascular-specific ECM defects as an important component of disease etiology (219). This notion is reinforced by reports of cystic medial necrosis/mucopolysaccharide accumulation in the tissue of patients (220), and the recent identification of an ECM signature in recurrent CeAD patient skin biopsies detected by proteomics analysis (221). A post-mortem histology study performed on the superficial temporal artery of CeAD patients described an increase in vasa vasorum density, as well as the presence of micro-hematomas in CeAD patients compared to cadaver controls (222), although it remains unclear if these findings precede or are merely secondary to the dissection.

Cervical artery dissection associated conditions and risk factors

In a study of CeAD patients, sexual dimorphism was evident with 57% patients in the study being male. Interestingly, females who accounted for the remaining 43% were significantly younger with an average age of 42.5 years, compared to 47.5 years for male patients (223). It is unclear to what extent referral bias contributed to this divergence in patient populations, however, this follows the same trend of age-based gender risk observed in aortic dissection and SCAD (109, 161). A history of a cerebral aneurysm has been reported in almost 1 in 5 CeAD patients (18.2%), suggesting a common genetic risk (224).

Hypertension (225) and migraine are known risk factors for CeAD (226, 227). Acute infection increases the risk of CeAD, with acute infection 1 month prior to CeAD having been reported in nearly one third (31.9%) of cases, compared to 13.5% of controls (228). The frequency of infection was lower in those with a single artery dissection (odds ratio, 2.1) than in those with multiple arteries affected (odds ratio, 6.4) (228). As with aortic dissections and SCAD, again there are case studies linking syphilis infection with CeAD (113, 114). Developmental defects in the neural crest, resulting in congenital heart defects, are thought to link heart development with CeAD (229).

Cervical artery dissection genetics and molecular mechanisms

The genetic risk factors for CeAD are less well studied compared to aortic dissection and SCAD, with few WGS and GWAS studies being reported to date. Nonetheless, gene variants that increase the risk of CeAD follow a similar theme to those of aortic dissection and SCAD, including associations with TGF- β signaling, ECM and cytoskeletal protein genes, and metabolism associated genes. Variants in *TGFBR2* (230,

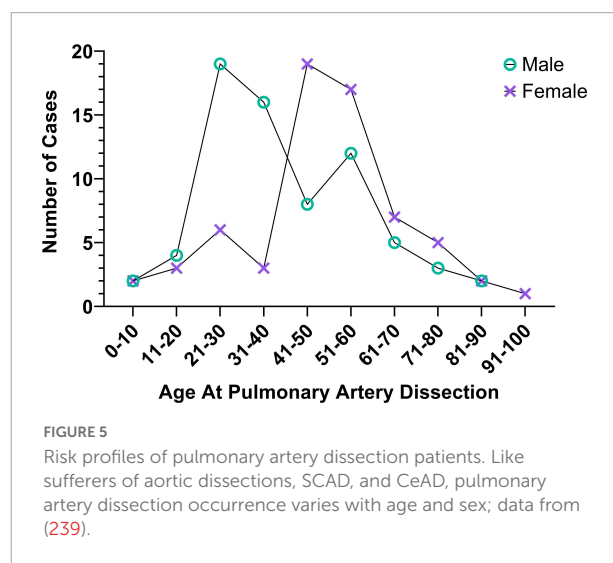
231), dual specificity protein phosphatase 22 (*DUSP22*), (232), *LRP1* and *PHACTR1* have all been associated with an increased risk of CeAD (233). Variants in ECM protein genes associated with CeAD include those for *COL3A1*, *COL4A1*, and *COL5A2* and *FBN1* (230, 232, 234, 235). Proteomic analysis of skin punch biopsies from patients with recurrent CeAD implicates ECM proteins whereby comparison of the proteomes of six recurrent CeAD patients with those 12 healthy controls that detected increases in perlecan, laminin- β 2 (encoded by *HSPG2* and *LAMB2*, respectively) and *COL12A1*, and decreases were detected in *COL1A2*, *COL4A2* as well as *ELN* and microfibril associated protein 5 (*MFAP5*), respectively. Western blot analysis of these biopsy samples also revealed a decrease in *COL1A1* (221).

Variants in the genes for both intercellular adhesion molecule 1 (*ICAM1*) and cytoskeletal alpha-1-syntrophin (*SNTA1*) have also been associated with CeAD (232, 236), whereas associations between CeAD and metabolism involve variants in methylenetetrahydrofolate reductase (*MTHFR*), which regulates homocysteine levels (231), and alterations in homocysteine are associated with thrombosis and atherosclerosis that occur with deficiencies in folate, vitamin B₆ and vitamin B₁₂ (237). This is of interest as methionine adenosyltransferase 1A is an aortic dissection-associated protein and is also modulated by folate; low plasma folate levels were found to increase the risk of cervical artery dissection in a cohort of 39 patients (238).

Rarer arterial dissections

Pulmonary artery dissections

The pulmonary artery is responsible for perfusion of the lungs and, uniquely, is the only artery to carry deoxygenated



blood. A recent comprehensive literature review found only 150 reported cases of pulmonary artery (PA) dissections (239). As with many of the dissection disorders, detection of PA dissections has increased exponentially since the first identification described post-mortem in 1842 (239, 240), presumably due to better diagnostic technologies. Patients diagnosed antemortem have a survival rate of 70.5% – a stark contrast to early reports, which deemed the condition almost certainly fatal. Increased reporting correlated with increased antemortem reporting (239), suggesting the condition has been previously underreported due to a surprisingly high survival rate coupled with a low detection rate and that PA dissections are not as ultra-rare as once thought.

Like other dissection events, PA dissections occur most commonly in the young to middle aged with three quarters of PA dissections patients being 21–60 years (239). Sexual dimorphism is less apparent in PA dissections, with a slight tendency to occur more frequently in males than females (ratio 1.1:1). However, as with the aforementioned arterial dissection types, cases diverge with both age and gender (109, 161, 223) where males represented 76% of cases in the age group 21–30, while females represented 70% of cases in the age group 41–50 (Figure 5).

Although the pathology of PA dissections is not well studied, dissections occur both with and without an intimal tear (240–242). In addition, post-mortem pathology of one patient indicated accumulation of acid mucopolysaccharides in the media, and degeneration and disorientation of the elastic medial layer (240); mucopolysaccharide deposition in the media having also been reported in a pregnancy-associated rupture of a dissecting aneurysm (243). These findings suggest that PA dissections and dissecting aneurysms may result from cystic medial necrosis and, in this regard, it is of interest that the pulmonary artery is richly endowed with medial vasa vasorum, which are required for perfusion and integrity of the medial layer. It is also noted that PA dissections are difficult to discern from dissecting pulmonary aneurysms (244–246).

Pulmonary hypertension is the strongest linked risk factor for PA dissections, with an estimated 50% of patients suffering from pulmonary hypertension and, independently, 9.8% from systemic hypertension (239, 242). Following hypertension, the next most common risk factor, yet far less mentioned in case studies, is a strong link to congenital heart disease; such abnormalities also predisposing to pulmonary aneurysms (229, 245, 247). To date, no genetic studies have been performed for PA dissections.

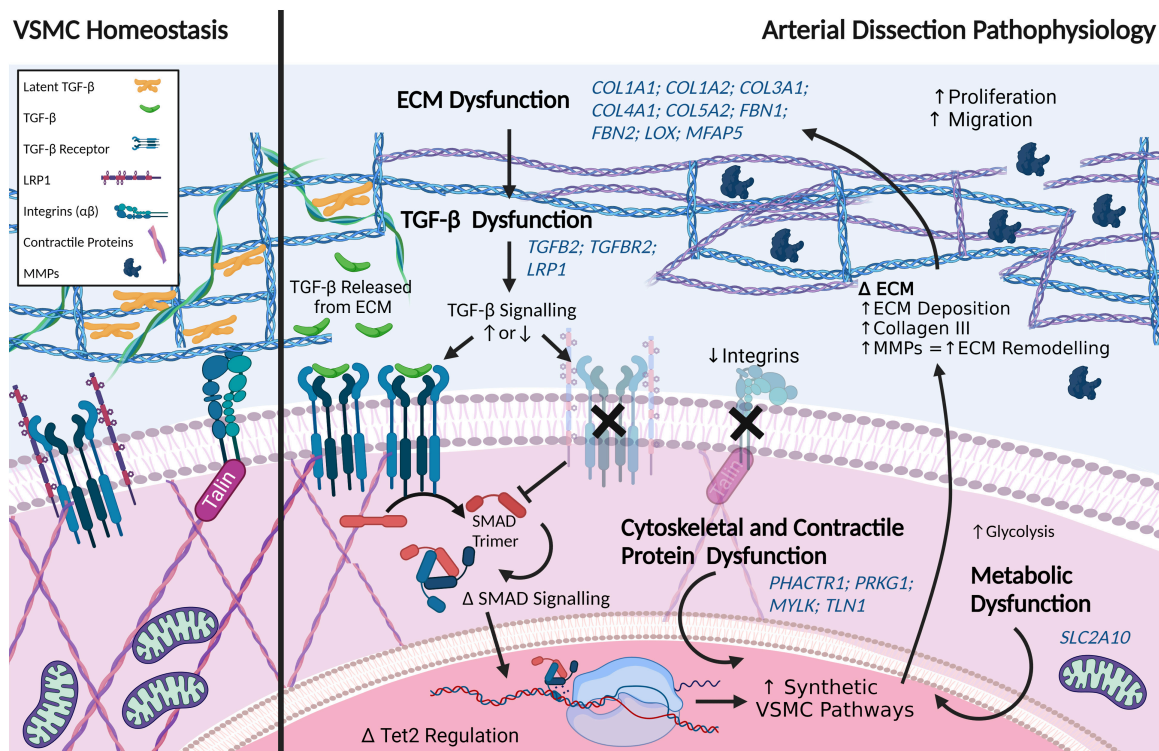


FIGURE 6

Pathways perturbed in arterial dissections include the extracellular matrix (ECM), TGF-β, signaling, cellular contraction/cytoskeleton, and metabolism. Dysregulation in any number of these pathways can drive vascular smooth muscle cells (VSMCs) toward a more synthetic phenotype. Variants in the same genes (italicized in blue) belonging to these pathways have been commonly identified in at least two types of arterial dissections. Created with [BioRender.com](https://www.biorender.com).

Renal and visceral artery dissections

Primary dissections of renal and visceral arteries (including the splenic, hepatic and mesenteric) are relatively uncommon, but they may occur secondary to extension of thoracic aortic dissections. It is possible, therefore, that these dissections represent extreme phenotypes, which may be instructive. Importantly, understanding the mechanisms underlying these rarer forms of dissection may provide insights into the pathogenesis of these diseases. Renal dissections are the second most common cause of renal infarct after embolism (248). They are classified into three groups based on cause (1) iatrogenic, (2) agonal (associated with renal failure, cirrhosis, and/or sepsis), or (3) spontaneous. Asymptomatic visceral dissections often produce few or no symptoms (249), suggesting that similar to SCAD and CeAD, these dissections are underdiagnosed.

Diagnosis of renal and visceral artery dissections typically only occurs if a computed tomography scan is performed as traditional imaging methods are not sensitive enough to detect a dissection, again suggesting that this is an under-diagnosed condition (250). This difficulty in detecting renal and visceral dissection may also explain why the first case of renal artery dissection was not reported until 1944 (251). Moreover, a quarter of renal artery dissections are only diagnosed at autopsy (250). As with other dissections, detection requires visualization of either an intimal flap and/or an intramural hematoma or both (252, 253).

Renal artery dissections predominantly occur in men at a 10:1 male to female ratio (250). Likewise, mesenteric and splenic artery dissections occur much more commonly in men (>80% of cases) (254, 255). Hypertension is linked to renal

TABLE 2 Common features of arterial dissections.

Features	Aortic dissections	SCAD	CeAD	Pulmonary
Pathology				
Intramural haematoma and intimal failure	(100)	(157)	(218)	(241)
Altered vasa vasorum	(108)	(160)	(222)	
Risk factors				
Sexual dimorphism	67.5% male age related dimorphism (109)	84% women (161)	57% male age related dimorphism (223)	Age related dimorphism (239)
Average age of dissection	63 years old (103)	51.1 years old (161)	45.3 years old (223)	44.8 years old (239)
Hypertension	(109)	(161)	(225)	(239, 242)
Migraine		(94, 188)	(227)	
Infection/Inflammation	(112)	(168)	(228)	Some evidence, (244)
Connective tissue disorders	(100)	(166)	(219)	(240)
Examples of shared disease associated genes/pathways				
ECM	<i>COL1A1</i>	(Limited data) (132, 133)	(172);	(221)
	<i>COL1A2</i>	(Limited data) (132)	(172, 185)	(221)
	<i>COL3A1</i>	(121)	(172, 175, 185)	(234)
	<i>COL4A1</i>	(Limited data) (132)	(172, 185)	(230)
	<i>COL5A2</i>	(125)	(172, 185)	(232)
	<i>FBN1</i>	(121, 290)	(97, 172, 291)	(230)
	<i>FBN2</i>	(121)	(172)	
	<i>LOX</i>	(135)	(175)	
	<i>MFAP5</i>	(134)	(172)	(221)
TGF- β pathways	<i>LRP1</i>	(121, 126)	(97, 172, 188)	(233, 292)
	<i>TGFBR2</i>	(121)		(230)
	<i>TGFB2</i>	(119)	(Likely pathogenic) (175)	
Cytoskeletal/Contractile pathways	<i>PHACTR1</i>		(97, 171, 188)	(233)
	<i>MYLK</i>	(121, 125)	(175)	
	<i>PRKG1</i>	(293)	(172)	
	<i>TLN1</i>	(142)	(203)	
VSMC metabolism	<i>SLC2A10</i>	(1)	(172)	

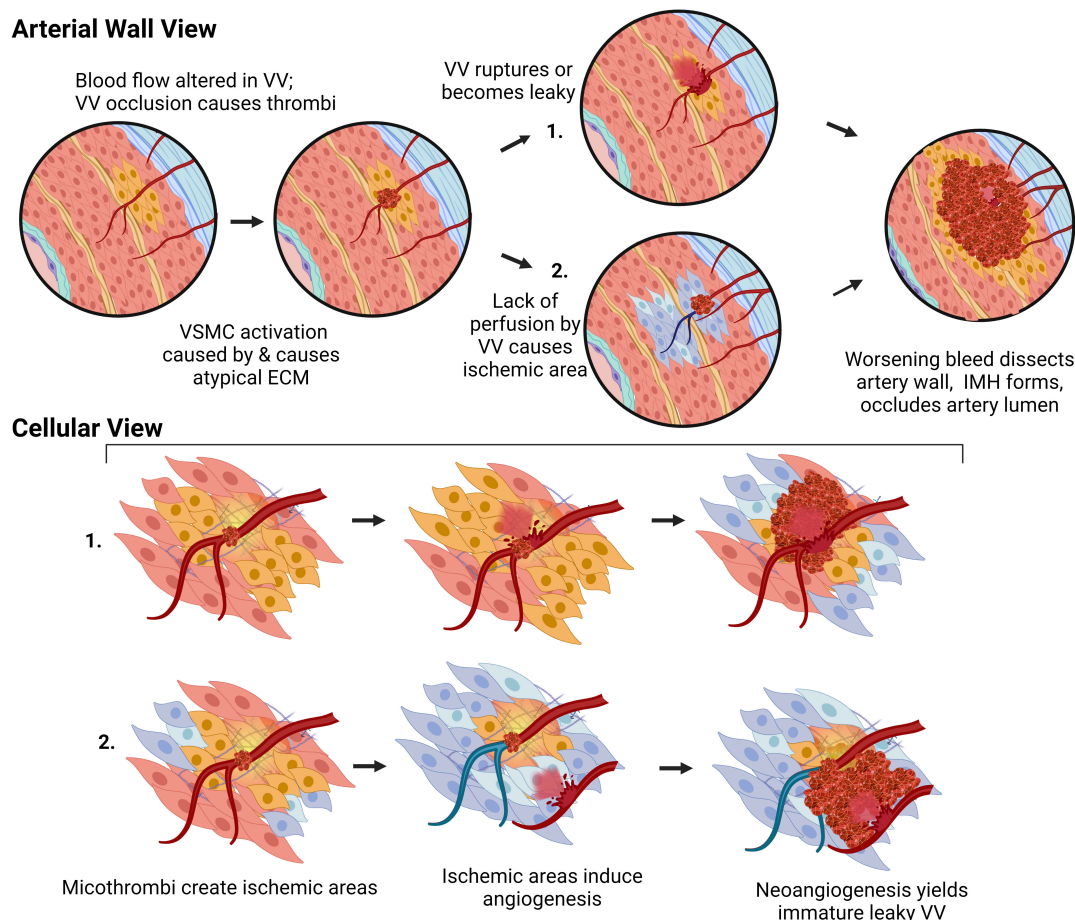


FIGURE 7

Proposed mechanism for arterial dissections. Atypical ECM deposition, activation of VSMC or EC will perturb vasa vasorum (VV) blood flow, leading to either their spontaneous rupture, or an area of ischemia encouraging growth of immature leaky vessels prone to bleed and, thus the development of an intramural hematoma, which impairs luminal blood flow resulting in tissue ischemia and/or infarction. Created with BioRender.com.

dissections and visceral artery dissections (256). Unlike many other types of dissections, the presence of atherosclerosis is not considered a basis to exclude spontaneous arterial dissection in renal or visceral dissection diagnosis (257, 258). Similar to PA dissections, no genetic studies have been performed for renal or visceral artery dissections.

Discussion – Common features of dissections

By considering arterial dissections as a collective, we gain insight into both the commonalities and unique features of this devastating family of vascular disorders (Table 1). Despite differing consequences of arterial dissections – from myocardial infarction to stroke – the pathological presentation of dissections is consistent: arterial dissections present as an IMH (with or without an intimal flap). Common risk factors

for arterial dissection patients include hypertension, tortuous vessels, and/or a history of vascular infection. Currently, there are no specific preventative therapeutics for arterial dissections, however, patients are often prescribed therapies such as the angiotensin II blocker, losartan, not only to manage hypertension (113, 114, 153, 228), but also because of its unique reverse-remodeling properties, which other antihypertensive agents such as angiotensin converting enzyme inhibitors lack. In Marfan syndrome, for example, the pathological changes in the aortic root are thought to be related to angiotensin II receptor 1 (ART1) signaling and the reverse-remodeling effects of losartan are mediated by blocking ART1 signaling and downstream TGF- β signaling (259). Targeted delivery of TGF- β inhibitory peptides has also recently been suggested as a potential future therapeutic for SCAD (260). Importantly, these stimuli are known to alter cellular identity, increasing cellular activation in ECs and VSMCs, and to alter the ECM (36, 46). The risk of arterial dissections is influenced by both sex and age, being

more common in one gender than the other at different ages. This age-gender risk also varies depending on the anatomical location of the arterial bed involved. Vascular aging and sex contribute to differences in the arteries of men and women – particularly differences in stiffness and distensibility (90), but even at the molecular cellular level, in ECs, VSMCs, and the ECM. These differences undoubtedly contribute to differences in risk-demographics for various types of arterial dissections. β -blocking drugs, particularly the β 1-adrenergic receptor blocker, metoprolol, are commonly used in the management of arterial dissections, both as anti-hypertensive agents and to reduce vessel shear stress. Moreover, in an observational study, β -blocking drugs (metoprolol or bisoprolol) have been shown to reduce SCAD recurrences (261).

The commonalities link to mechanistic findings associated with arterial dissections. Perturbations in TGF- β signaling, the ECM, the cytoskeleton, and metabolism, are described in both spontaneous and syndromic dissections. In spontaneous dissections, variants in genes associated with these pathways including *PHACTR1*, *LRP1*, *SLC2A10*, *FBN1*, *COL3A1*, *COL4A1*, and *COL5A2* are common to at least two, if not three, arterial dissection subtypes (Figure 6 and Table 2). Importantly, dysfunction in these pathways is associated with vascular cell activation and subsequent phenotype switching. Phenotype switching has been described in aortic dissections (56, 117), but has not yet been a central theme in the pathophysiology of other arterial dissections. Nonetheless, we postulate that vascular cell phenotype switching can account for the pathology of arterial dissection: changes in vascular ECM can cause and be caused by cellular activation. Altered mechanical strength in the vasculature caused by altered VSMCs or ECM forces will likely affect vasa vasorum blood flow. Altered forces may cause occlusion of the vasa vasorum leading to ischemia and necrosis of the tunica media, particularly in arteries with low vasa vasorum density. Notably, vasa vasorum occlusion in porcine models has been shown to be sufficient to cause ischemia and dissection of the aorta (108), and reduced density of vasa vasorum inversely correlates with an increased risk of dissection in the coronary arteries (157, 159). Areas of ischemia will increase the likelihood of immune cell infiltration, which has been found in post-mortem arterial dissection tissues (222, 262). Moreover, areas of ischemia will, similar to atherosclerosis, stimulate neo-angiogenesis leading to proliferation of vasa vasorum. Histological evidence for increased abundance of vasa vasorum is reported in SCAD and CeAD (160, 222). This may be of significance since newly formed vasa vasorum lack a functional muscular layer (11) and are notoriously weak and leaky (263). Occlusion of vasa vasorum alone, or the growth of new still leaky vasa vasorum are potential sources of bleeding within the artery wall, IMH formation and vessel

wall dissection. Similarly, endothelial phenotype switching from quiescent cells to activated phenotypes would weaken the endothelial barrier - in the intima or arteries and/or in the vasa vasorum, *per se* - again being a likely cause of bleeding and IMH formation (Figure 7). While more studies are needed to address these hypotheses, cellular activation represents a strong under-explored mechanism in arterial dissections, and, potentially, is an important therapeutic target.

Author contributions

MB and VR researched the literature and wrote the manuscript with input from KJ, EG, BM, JK, RL, SI, and RG. All authors contributed to the article and approved the submitted version.

Funding

This work was supported in part by grants from the Cardiac Society of Australia and New Zealand; the St. Vincent's Clinic Foundation; the Catholic Archdiocese of Sydney; Perpetual Philanthropy; and SCAD Research Inc. EG supported by a NSW Health Early Mid-Career Fellowship, a NSW Health Early Mid-Career Cardiovascular Grant, and a National Heart Foundation of Australia Future Leader Fellowship (101204). The funders were not involved in the study design, collection, analysis, interpretation of data, the writing of this article or the decision to submit it for publication.

Conflict of interest

The authors declare that the research was conducted in the absence of any commercial or financial relationships that could be construed as a potential conflict of interest.

Publisher's note

All claims expressed in this article are solely those of the authors and do not necessarily represent those of their affiliated organizations, or those of the publisher, the editors and the reviewers. Any product that may be evaluated in this article, or claim that may be made by its manufacturer, is not guaranteed or endorsed by the publisher.

References

- Pinar D, Jones GT, Milewicz DM. Genetics of thoracic and abdominal aortic diseases: aneurysms, dissections, and ruptures. *Circ Res.* (2019). 124:588–606. doi: 10.1161/CIRCRESAHA.118.312436
- Wolinsky H, Glagov S. A lamellar unit of aortic medial structure and function in mammals. *Circ Res.* (1967) 20:99–111. doi: 10.1161/01.RES.20.1.99
- Leloup AJA, Van Hove CE, Heykers A, Schrijvers DM, De Meyer GRY, Franssen P. Elastic and muscular arteries differ in structure, basal no production and voltage-gated Ca²⁺-Channels. *Front Physiol.* (2015) 6:375. doi: 10.3389/fphys.2015.00375
- Wolinsky H, Glagov S. Nature of species differences in the medial distribution of aortic vasa vasorum in mammals. *Circ Res.* (1967) 20:409–21. doi: 10.1161/01.RES.20.4.409
- Gössl M, Malyar NM, Rosol M, Beighley PE, Ritman EL. Impact of coronary vasa vasorum functional structure on coronary vessel wall perfusion distribution. *Am J Physiol.* (2003) 285:H2019–26. doi: 10.1152/ajpheart.00399.2003
- Mulligan-Kehoe MJ, Simons M. Vasa vasorum in normal and diseased arteries. *Circulation.* (2014) 129:2557–66. doi: 10.1161/CIRCULATIONAHA.113.007189
- Lametschwandtner A, Minnich B, Kachlik D, Setina M, Stingl J. Three-dimensional arrangement of the vasa vasorum in explanted segments of the aged human great saphenous vein: scanning electron microscopy and three-dimensional morphometry of vascular corrosion casts. *Anat Rec.* (2004) 281A:1372–82. doi: 10.1002/ar.a.20098
- Patzelt M, Kachlik D, Stingl J, Sach J, Stibor R, Benada O, et al. Morphology of the vasa vasorum in coronary arteries of the porcine heart: a new insight. *Ann Anat.* (2019) 223:119–26. doi: 10.1016/j.aanat.2019.02.006
- Williams JK, Heistad DD. Structure and function of vasa vasorum. *Trends Cardiovasc Med.* (1996) 6:53–7. doi: 10.1016/1050-1738(96)00008-4
- Xu J, Lu X, Shi G-P. Vasa vasorum in atherosclerosis and clinical significance. *Int J Mol Sci.* (2015) 16:11574–608. doi: 10.3390/ijms160511574
- Williams JK, Armstrong ML, Heistad DD. Blood flow through new microvessels: factors that affect regrowth of vasa vasorum. *Am J Physiol.* (1988) 254:H126–32. doi: 10.1152/ajpheart.1988.254.1.H126
- Dobrin B. Mechanical properties of arteries. *Physiol Rev.* (1978) 58:64. doi: 10.1152/physrev.1978.58.2.397
- Basford JR. The Law of Laplace and its relevance to contemporary medicine and rehabilitation. *Arch Phys Med Rehabil.* (2002) 83:1165–70. doi: 10.1053/apmr.2002.33985
- Burton AC. On the physical equilibrium of small blood vessels. *Am J Physiol.* (1951) 164:319–29. doi: 10.1152/ajplegacy.1951.164.2.319
- Phillippi JA. On vasa vasorum: a history of advances in understanding the vessels of vessels. *Sci Adv.* (2022) 8:eab6364. doi: 10.1126/sciadv.abl6364
- Cao X, Maharjan S, Ashfaq R, Shin J, Zhang YS. Bioprinting of small-diameter blood vessels. *Engineering.* (2021) 7:832–44. doi: 10.1016/j.eng.2020.03.019
- Dessalles CA, Leclech C, Castagnino A, Barakat AI. Integration of substrate- and flow-derived stresses in endothelial cell mechanobiology. *Commun Biol.* (2021) 4:764. doi: 10.1038/s42003-021-02285-w
- Ritman E, Lerman A. The dynamic vasa vasorum. *Cardiovasc Res.* (2007) 75:649–58. doi: 10.1016/j.cardiores.2007.06.020
- Galili O, Herrmann J, Woodrum J, Sattler KJ, Lerman LO, Lerman A. Adventitial vasa vasorum heterogeneity among different vascular beds. *J Vasc Surg.* (2004) 40:529–35. doi: 10.1016/j.jvs.2004.06.032
- Hildebrandt HA, Gössl M, Mannheim D, Versari D, Herrmann J, Spendlove D, et al. Differential distribution of vasa vasorum in different vascular beds in humans. *Atherosclerosis.* (2008) 199:47–54. doi: 10.1016/j.atherosclerosis.2007.09.015
- Stalder AE, Frydrychowicz A, Russe MF, Korvink JG, Hennig J, Li K, et al. Assessment of flow instabilities in the healthy aorta using flow-sensitive MRI. *J Magnet Reson Imaging.* (2011) 33:839–46. doi: 10.1002/jmri.22512
- Doutel E, Galindo-Rosales FJ, Campo-Deaño L. Hemodynamics challenges for the navigation of medical microbots for the treatment of CVDs. *Materials.* (2021) 14:7402. doi: 10.3390/ma14237402
- San O, Staples AE. An improved model for reduced-order physiological fluid flows. *J Mech Med Biol.* (2012) 12:1250052. doi: 10.1142/S0219519411004666
- Gössl M, Rosol M, Malyar NM, Fitzpatrick LA, Beighley PE, Zamir M, et al. Functional anatomy and hemodynamic characteristics of vasa vasorum in the walls of porcine coronary arteries: vasa vasorum in coronary arteries. *Anat Rec.* (2003) 272A:526–37. doi: 10.1002/ar.a.10060
- Stary HC, Blankenhorn DH, Chandler B, Glagov S, William I, Richardson M, et al. A definition of the intima of human arteries and of its atherosclerosis-prone regions. A report from the committee on vascular lesions of the council on arteriosclerosis, American heart association. *Circulation.* (1992) 85:15. doi: 10.1161/01.cir.85.1.391
- Myers PR, Tanner MA. Vascular endothelial cell regulation of extracellular matrix collagen: role of nitric oxide. *ATVB.* (1998) 18:717–22. doi: 10.1161/01.ATV.18.5.717
- Radomski M, Palmer R, Moncada S. Modulation of platelet aggregation by an L-arginine-nitric oxide pathway. *Trends Pharmacol Sci.* (1991) 12:87–8.
- Garg UC, Hassid A. Nitric oxide-generating vasodilators and 8-bromo-cyclic guanosine monophosphate inhibit mitogenesis and proliferation of cultured rat vascular smooth muscle cells. *J Clin Invest.* (1989) 83:1774–7. doi: 10.1172/JCI114081
- Sarkar R, Meinberg EG, Stanley JC, Gordon D, Clinton Webb R. Nitric oxide reversibly inhibits the migration of cultured vascular smooth muscle cells. *Circ Res.* (1996) 78:225–30. doi: 10.1161/01.RES.78.2.225
- Peyvandi F, Garagiola I, Baronciani L. Role of von Willebrand factor in the haemostasis. *Blood Transfus.* (2011) 9(Suppl. 2):s3–8. doi: 10.2450/2011.002S
- Sadler JE. Biochemistry and genetics of von willebrand factor. *Annu Rev Biochem.* (1998) 67:395–424. doi: 10.1146/annurev.biochem.67.1.395
- Boyer MJ, Kimura Y, Akiyama T, Baggett AY, Preston KJ, Scalia R, et al. Endothelial cell-derived extracellular vesicles alter vascular smooth muscle cell phenotype through high-mobility group box proteins. *J Extracell Vesicles.* (2020) 9:1781427. doi: 10.1080/20013078.2020.1781427
- Bianconi E, Piovesan A, Facchin F, Beraudi A, Casadei R, Frabetti F, et al. An estimation of the number of cells in the human body. *Ann Hum Biol.* (2013) 40:463–71. doi: 10.3109/03014460.2013.807878
- Bergmann O, Zdunek S, Felker A, Salehpour M, Alkass K, Bernard S, et al. Dynamics of cell generation and turnover in the human heart. *Cell.* (2015) 161:1566–75. doi: 10.1016/j.cell.2015.05.026
- Sender R, Milo R. The distribution of cellular turnover in the human body. *Nat Med.* (2021) 27:45–8. doi: 10.1038/s41591-020-01182-9
- Waitkus M, Harris D, DiCorleto P, Mathew AV, Pennathur S. Mechanisms of Endothelial Activation. In: Mackay IR, Rose NR, Diamond B, Davidson A editors. *Encyclopedia of Medical Immunology.* New York, NY: Springer New York (2014). p. 693–703. doi: 10.1007/978-0-387-84828-0_176
- Pober JS, Sessa WC. Evolving functions of endothelial cells in inflammation. *Nat Rev Immunol.* (2007) 7:803–15. doi: 10.1038/nri2171
- Escher R, Breakey N, Lämmle B. Severe COVID-19 infection associated with endothelial activation. *Thromb Res.* (2020) 190:62. doi: 10.1016/j.thromres.2020.04.014
- Paik DT, Tian L, Williams IM, Rhee S, Zhang H, Liu C, et al. Single-cell RNA-seq unveils unique transcriptomic signatures of organ-specific endothelial cells. *Circulation.* (2020) 142:1848–62. doi: 10.1161/CIRCULATIONAHA.119.041433
- Kalucka J, de Rooij LPMH, Goveia J, Rohlenova K, Dumas SJ, Meta E, et al. Single-cell transcriptome atlas of murine endothelial cells. *Cell.* (2020) 180:764–779.e20. doi: 10.1016/j.cell.2020.01.015
- Venturini G, Malagrino PA, Padilha K, Tanaka LY, Laurindo FR, Dariolli R, et al. Integrated proteomics and metabolomics analysis reveals differential lipid metabolism in human umbilical vein endothelial cells under high and low shear stress. *Am J Physiol.* (2019) 317:C326–38. doi: 10.1152/ajpcell.00128.2018
- Hartman RJG, Kapteijn DMC, Haitjema S, Bekker MN, Mokry M, Pasterkamp G, et al. Intrinsic transcriptomic sex differences in human endothelial cells at birth and in adults are associated with coronary artery disease targets. *Sci Rep.* (2020) 10:12367. doi: 10.1038/s41598-020-69451-8
- Yang M, Chadwick AE, Dart C, Kamishima T, Quayle JM. Bioenergetic profile of human coronary artery smooth muscle cells and effect of metabolic intervention. *PLoS One.* (2017) 12:e0177951. doi: 10.1371/journal.pone.0177951
- Shi J, Yang Y, Cheng A, Xu G, He F. Metabolism of vascular smooth muscle cells in vascular diseases. *Am J Physiol.* (2020) 319:H613–31. doi: 10.1152/ajpheart.00220.2020
- Neese RA, Misell LM, Turner S, Chu A, Kim J, Cesar D, et al. Measurement in vivo of proliferation rates of slow turnover cells by 2H₂O labeling of the deoxyribose moiety of DNA. *Proc Natl Acad Sci USA.* (2003) 99:15345–50. doi: 10.1073/pnas.232551499

46. Rensen SSM, Doevendans PAFM, van Eys GJJM. Regulation and characteristics of vascular smooth muscle cell phenotypic diversity. *Neth Heart J*. (2007) 15:100–8. doi: 10.1007/BF03085963
47. Chiong M, Cartes-Saavedra B, Norambuena-Soto I, Mondaca-Ruff D, Morales PE, Garc a-a-Miguel M, et al. Mitochondrial metabolism and the control of vascular smooth muscle cell proliferation. *Front Cell Dev Biol*. (2014) 2:72. doi: 10.3389/fcell.2014.00072
48. Izawa K, Okada M, Sumitomo K, Nakagawa N, Aizawa Y, Kawabe J, et al. Impaired glutathione redox system paradoxically suppresses angiotensin II-induced vascular remodeling. *PLoS One*. (2014) 9:e108115. doi: 10.1371/journal.pone.0108115
49. Madamanchi NR, Vendrov A, Runge MS. Oxidative stress and vascular disease. *Arterioscler Thromb Vasc Biol*. (2005) 25:29–38. doi: 10.1161/01.ATV.0000150649.39934.13
50. Tsai M-C, Chen L, Zhou J, Tang Z, Hsu T-F, Wang Y, et al. Shear stress induces synthetic-to-contractile phenotypic modulation in smooth muscle cells via peroxisome proliferator-activated receptor α/δ activations by prostacyclin released by sheared endothelial cells. *Circ Res*. (2009) 105:471–80. doi: 10.1161/CIRCRESAHA.109.193656
51. Frid MG, Moiseeva EP, Stenmark KR. Multiple phenotypically distinct smooth muscle cell populations exist in the adult and developing bovine pulmonary arterial media in vivo. *Circ Res*. (1994) 75:669–81. doi: 10.1161/01.RES.75.4.669
52. Liu R, Jin Y, Tang WH, Qin L, Zhang X, Tellides G, et al. Ten-eleven translocation-2 (TET2) is a master regulator of smooth muscle cell plasticity. *Circulation*. (2013) 128:2047–57. doi: 10.1161/CIRCULATIONAHA.113.002887
53. Sorokin V, Vickneson K, Kofidis T, Woo CC, Lin XY, Foo R, et al. Role of vascular smooth muscle cell plasticity and interactions in vessel wall inflammation. *Front Immunol*. (2020) 11:599415. doi: 10.3389/fimmu.2020.599415
54. Pedroza AJ, Tashima Y, Shad R, Cheng P, Wirka R, Churovich S, et al. Single-cell transcriptomic profiling of vascular smooth muscle cell phenotype modulation in marfan syndrome aortic aneurysm. *Arterioscler Thromb Vasc Biol*. (2020) 40:2195–211. doi: 10.1161/ATVBAHA.120.314670
55. Liu R, Leslie KL, Martin KA. Epigenetic regulation of smooth muscle cell plasticity. *Biochim Biophys Acta*. (2015) 1849:448–53. doi: 10.1016/j.bbaggm.2014.06.004
56. Wang L, Zhang J, Fu W, Guo D, Jiang J, Wang Y. Association of smooth muscle cell phenotypes with extracellular matrix disorders in thoracic aortic dissection. *J Vasc Surg*. (2012) 56:1698.e–709.e. doi: 10.1016/j.jvs.2012.05.084
57. Hill MA, Nourian Z, Ho I-L, Clifford PS, Martinez-Lemus L, Meininger GA. Small artery elastin distribution and architecture-focus on three dimensional organization. *Microcirculation*. (2016) 23:614–20. doi: 10.1111/micc.12294
58. Fillinger MF, O'Connor SE, Wagner RJ. The effect of endothelial cell coculture on smooth muscle cell proliferation. *Vasc Surg*. (1993) 17:1058–68. doi: 10.1016/0741-5214(93)90676-D
59. Erbel R. Aortic dimensions and the risk of dissection. *Heart*. (2006) 92:137–42. doi: 10.1136/hrt.2004.055111
60. Kablak-Ziemicka A, Przewlocki T, Tracz W, Pieniazek P, Musialek P, Sokolowski A. Gender differences in carotid intima-media thickness in patients with suspected coronary artery disease. *Am J Cardiol*. (2005) 96:1217–22. doi: 10.1016/j.amjcard.2005.06.059
61. Hartman RJG, Owsiany K, Ma L, Koplev S, Hao K, Slenders L, et al. Sex-stratified gene regulatory networks reveal female key driver genes of atherosclerosis involved in smooth muscle cell phenotype switching. *Circulation*. (2021) 143:713–26. doi: 10.1161/CIRCULATIONAHA.120.051231
62. Yurdagul A, Finney AC, Woolard MD, Orr AW. The arterial microenvironment: the where and why of atherosclerosis. *Biochem J*. (2016) 473:1281–95. doi: 10.1042/BJ20150844
63. Kielty CM, Sherratt MJ, Shuttleworth CA. Elastic fibres. *J Cell Sci*. (2002) 115:2817.
64. Wagenseil JE, Mecham RP. Vascular extracellular matrix and arterial mechanics. *Physiol Rev*. (2009) 89:957–89. doi: 10.1152/physrev.00041.2008
65. Brooke B. New insights into elastin and vascular disease. *Trends Cardiovasc Med*. (2003) 13:176–81. doi: 10.1016/S1050-1738(03)00065-3
66. Naba A, Clauser KR, Hoersch S, Carr SA, Hynes RO. The matrisome: in silico definition and in vivo characterization by proteomics of normal and tumor extracellular matrices. *Mol Cell Proteomics*. (2012) 11:M111.014647. doi: 10.1074/mcp.M111.014647
67. Wittig C, Szulcek R. Extracellular matrix protein ratios in the human heart and vessels: how to distinguish pathological from physiological changes? *Front Physiol*. (2021) 12:708656. doi: 10.3389/fphys.2021.708656
68. Basu P, Sen U, Tyagi N, Tyagi S. Blood flow interplays with elastin: collagen and MMP: TIMP ratios to maintain healthy vascular structure and function. *Vasc Health Risk Manag*. (2010) 2010:215–28. doi: 10.2147/VHRM.S9472
69. Kelleher CM, McLean SE, Mecham RP. *Vascular Extracellular Matrix and Aortic Development: Current Topics in Developmental Biology*. Amsterdam: Elsevier (2004). p. 153–88. doi: 10.1016/S0070-2153(04)62006-0
70. Starcher BC. Elastin and the lung. *Thorax*. (1986) 41:577–85. doi: 10.1136/thx.41.8.577
71. Hedin U, Bottger BA, Forsberg E, Johansson S, Thyberg J. Diverse effects of fibronectin and laminin on phenotypic properties of cultured arterial smooth muscle cells. *J Cell Biol*. (1988) 107:307–19. doi: 10.1083/jcb.107.1.307
72. Ichii T, Koyama H, Tanaka S, Kim S, Shioi A, Okuno Y, et al. Fibrillar collagen specifically regulates human vascular smooth muscle cell genes involved in cellular responses and the pericellular matrix environment. *Circ Res*. (2001) 88:460–7. doi: 10.1161/01.RES.88.5.460
73. Ito S, Ishimaru S, Wilson SE. Inhibitory effect of type I collagen gel containing alpha-elastin on proliferation and migration of vascular smooth muscle and endothelial cells. *Cardiovasc Surg*. (1997) 5:176–83. doi: 10.1016/s0967-2109(97)00004-5
74. Karnik SK. A critical role for elastin signaling in vascular morphogenesis and disease. *Development*. (2003) 130:411–23. doi: 10.1242/dev.00223
75. Sazonova OV, Lee KL, Isenberg BC, Rich CB, Nugent MA, Wong JY. Cell-cell interactions mediate the response of vascular smooth muscle cells to substrate stiffness. *Biophys J*. (2011) 101:622–30. doi: 10.1016/j.bpj.2011.06.051
76. Smith LR, Cho S, Discher DE. Stem cell differentiation is regulated by extracellular matrix mechanics. *Physiology*. (2018) 33:16–25. doi: 10.1152/physiol.00026.2017
77. Gerardo H, Lima A, Carvalho J, Ramos JRD, Couceiro S, Travasso RDM, et al. Soft culture substrates favor stem-like cellular phenotype and facilitate reprogramming of human mesenchymal stem/stromal cells (hMSCs) through mechanotransduction. *Sci Rep*. (2019) 9:9086. doi: 10.1038/s41598-019-45352-3
78. Hartman CD, Isenberg BC, Chua SG, Wong JY. Vascular smooth muscle cell durotaxis depends on extracellular matrix composition. *Proc Natl Acad Sci USA*. (2016) 113:11190–5. doi: 10.1073/pnas.1611324113
79. Rickel AP, Sanyour HJ, Leyda NA, Hong Z. Extracellular matrix proteins and substrate stiffness synergistically regulate vascular smooth muscle cell migration and cortical cytoskeleton organization. *ACS Appl Biol Mater*. (2020) 3:2360–9. doi: 10.1021/acsabm.0c00100
80. Goumans M-J, ten Dijke P. TGF- β signaling in control of cardiovascular function. *Cold Spring Harb Perspect Biol*. (2018) 10:a022210. doi: 10.1101/cshperspect.a022210
81. Shi M, Zhu J, Wang R, Chen X, Mi L, Walz T, et al. Latent TGF- β structure and activation. *Nature*. (2011) 474:343–9. doi: 10.1038/nature10152
82. van Meeteren LA, ten Dijke P. Regulation of endothelial cell plasticity by TGF- β . *Cell Tissue Res*. (2012) 347:177–86. doi: 10.1007/s00441-011-1222-6
83. Chi J-T, Chang HY, Haraldsen G, Jahnsen FL, Troyanskaya OG, Chang DS, et al. Endothelial cell diversity revealed by global expression profiling. *Proc Natl Acad Sci USA*. (2003) 100:10623–8. doi: 10.1073/pnas.1434429100
84. Gaudette S, Hughes D, Boller M. The endothelial glycocalyx: structure and function in health and critical illness. *J Vet Emerg Crit Care*. (2020) 30:117–34. doi: 10.1111/vec.12925
85. M ckl L. The emerging role of the mammalian glycocalyx in functional membrane organization and immune system regulation. *Front Cell Dev Biol*. (2020) 8:253. doi: 10.3389/fcell.2020.00253
86. Bons LR, Rueda-Ochoa OL, El Ghoul K, Rohde S, Budde RP, Leening MJ, et al. Sex-specific distributions and determinants of thoracic aortic diameters in the elderly. *Heart*. (2020) 106:133–9. doi: 10.1136/heartjnl-2019-315320
87. Sheifer SE, Canos MR, Weinfurt KP, Arora UK, Mendelsohn FO, Gersh BJ, et al. Sex differences in coronary artery size assessed by intravascular ultrasound. *Am Heart J*. (2000) 139:649–52. doi: 10.1016/S0002-8703(00)90043-7
88. Kehmeier MN, Walker AE. Sex differences in large artery stiffness: implications for cerebrovascular dysfunction and Alzheimer's disease. *Front Aging*. (2021) 2:791208. doi: 10.3389/fragi.2021.791208
89. Waddell TK, Dart AM, Gatzka CD, Cameron JD, Kingwell BA. Women exhibit a greater age-related increase in proximal aortic stiffness than men. *J Hypertens*. (2001) 19:2205–12. doi: 10.1097/00004872-200112000-00014

90. Vatner SE, Zhang J, Vyzas C, Mishra K, Graham RM, Vatner DE. Vascular stiffness in aging and disease. *Front Physiol.* (2021) 12:762437. doi: 10.3389/fphys.2021.762437
91. Natoli AK, Medley TL, Ahimastos AA, Drew BG, Thearle DJ, Dilley RJ, et al. Sex steroids modulate human aortic smooth muscle cell matrix protein deposition and matrix metalloproteinase expression. *Hypertension.* (2005) 46:1129–34. doi: 10.1161/01.HYP.0000187016.06549.96
92. Samargandy S, Matthews KA, Brooks MM, Barinas-Mitchell E, Magnani JW, Janssen I, et al. Arterial stiffness accelerates within 1 year of the final menstrual period: the SWAN Heart study. *Arterioscler Thromb Vasc Biol.* (2020) 40:1001–8. doi: 10.1161/ATVBAHA.119.313622
93. Schievink WI, Michels VV, Piepgras DG. Neurovascular manifestations of heritable connective tissue disorders. A review. *Stroke.* (1994) 25:889–903. doi: 10.1161/01.STR.25.4.889
94. McGrath-Cadell L, McKenzie P, Emmanuel S, Muller DWM, Graham RM, Holloway CJ. Outcomes of patients with spontaneous coronary artery dissection. *Open Heart.* (2016) 3:e000491. doi: 10.1136/openhrt-2016-000491
95. Amitai Komem D, Sukenik Halevy R, Griton Y, Shnaker A, Levy Y, Weissmann J, et al. A Rare case of 7 simultaneous arterial dissections and review of the literature. *Vasc Endovascular Surg.* (2019) 53:617–22. doi: 10.1177/1538574419864783
96. Shalata A, Mahroom M, Milewicz DM, Limin G, Kassam F, Badarna K, et al. Fatal thoracic aortic aneurysm and dissection in a large family with a novel MYLK gene mutation: delineation of the clinical phenotype. *Orphanet J Rare Dis.* (2018) 13:41. doi: 10.1186/s13023-018-0769-7
97. Turley TN, O'Byrne MM, Kosel ML, de Andrade M, Gulati R, Hayes SN, et al. Identification of susceptibility loci for spontaneous coronary artery dissection. *JAMA Cardiol.* (2020) 5:929. doi: 10.1001/jamacardio.2020.0872
98. Pepin MG, Schwarze U, Rice KM, Liu M, Leistritz D, Byers PH. Survival is affected by mutation type and molecular mechanism in vascular Ehlers–Danlos syndrome (EDS type IV). *Genet Med.* (2014) 16:881–8. doi: 10.1038/gim.2014.72
99. Lindsay ME, Dietz HC. Lessons on the pathogenesis of aneurysm from heritable conditions. *Nature.* (2011) 473:308–16. doi: 10.1038/nature10145
100. Nienaber CA, Clough RE, Sakalihasan N, Suzuki T, Gibbs R, Mussa F, et al. Aortic dissection. *Nat Rev Dis Prim.* (2016) 2:16053. doi: 10.1038/nrdp.2016.53
101. De Bakey ME, Henly WS, Cooley DA, Morris GC, Crawford ES, Beall AC. Surgical management of dissecting aneurysms of the aorta. *J Thorac Cardiovasc Surg.* (1965) 49:130–49. doi: 10.1016/S0022-5223(19)33323-9
102. Daily PO, Trueblood HW, Stinson EB, Wuerflein RD, Shumway NE. Management of acute aortic dissections. *Ann Thorac Surg.* (1970) 10:237–47. doi: 10.1016/S0003-4975(10)65594-4
103. Hagan PG, Nienaber CA, Isselbacher EM, Bruckman D, Karavite DJ, Russman PL, et al. The international registry of acute aortic dissection (IRAD): new insights into an old disease. *JAMA.* (2000) 283:897. doi: 10.1001/jama.283.7.897
104. Lempel JK, Frazier AA, Jeudy J, Kligerman SJ, Schultz R, Ninalowo HA, et al. Aortic arch dissection: a controversy of classification. *Radiology.* (2014) 271:848–55. doi: 10.1148/radiol.14131457
105. Qanadli SD, Malekzadeh S, Villard N, Jouannic A-M, Bodenmann D, Tozzi P, et al. A new clinically driven classification for acute aortic dissection. *Front Surg.* (2020) 7:37. doi: 10.3389/fsurg.2020.00037
106. Fritridge R, Thompson M. (Eds.). *Mechanisms of Vascular Disease: A Reference Book for Vascular Specialists.* Adelaide, SA: University of Adelaide Press (2011).
107. Haverich A, Boyle EC. Aortic dissection is a disease of the vasa vasorum. *JTCVS Open.* (2021) 5:30–2. doi: 10.1016/j.jxon.2020.12.012
108. Angouras D, Sokolis DP, Dosios T, Kostomitsopoulos N, Boudoulas H, Skalkas G, et al. Effect of impaired vasa vasorum flow on the structure and mechanics of the thoracic aorta: implications for the pathogenesis of aortic dissection. *Eur J Cardiothor Surg.* (2000) 17:468–73. doi: 10.1016/s1010-7940(00)00382-1
109. Landenhed M, Engström G, Gottsäter A, Caulfield MP, Hedblad B, Newton-Cheh C, et al. Risk profiles for aortic dissection and ruptured or surgically treated aneurysms: a prospective cohort study. *J Am Heart Assoc.* (2015) 4:e001513. doi: 10.1161/JAHA.114.001513
110. Aune D, Schlesinger S, Norat T, Riboli E. Tobacco smoking and the risk of abdominal aortic aneurysm: a systematic review and meta-analysis of prospective studies. *Sci Rep.* (2018) 8:14786. doi: 10.1038/s41598-018-32100-2
111. Kihara T, Yamagishi K, Iso H, Tamakoshi A. Passive smoking and mortality from aortic dissection or aneurysm. *Atherosclerosis.* (2017) 263:145–50. doi: 10.1016/j.atherosclerosis.2017.06.022
112. Stansal A, Mirault T, Rossi A, Dupin N, Bruneval P, Bel A, et al. Recurrent tamponade and aortic dissection in syphilis. *Ann Thorac Surg.* (2013) 96:e111–3. doi: 10.1016/j.athoracsur.2013.05.096
113. Bourazza A, Kerouache A, Reda R, Mounach J, Mosseddaq R. Méningovascularite d'origine syphilitique : étude de cinq cas. *Rev Neurol.* (2008) 164:369–73. doi: 10.1016/j.neurol.2007.12.007
114. Marangi A, Moretto G, Cappellari M, Micheletti N, Tomelleri G, Bovi P. Bilateral internal carotid artery dissection associated with prior syphilis: a case report and review of the literature. *Neuropsychiatr Dis Treat.* (2016) 12:1351–4. doi: 10.2147/NDT.S106845
115. Wu J, Mamas MA, Mohamed MO, Kwok CS, Roebuck C, Humberstone B, et al. Place and causes of acute cardiovascular mortality during the COVID-19 pandemic. *Heart.* (2021) 107:113–9. doi: 10.1136/heartjnl-2020-317912
116. Yuan S-M. Cardiovascular involvement of ankylosing spondylitis: report of three cases. *Vascular.* (2009) 17:342–54. doi: 10.2310/6670.2009.00023
117. Milewicz DM, Trybus KM, Guo D, Sweeney HL, Regalado E, Kamm K, et al. Altered smooth muscle cell force generation as a driver of thoracic aortic aneurysms and dissections. *Arterioscler Thromb Vasc Biol.* (2017) 37:26–34. doi: 10.1161/ATVBAHA.116.303229
118. Faggion Vinholo T, Brownstein AJ, Ziganshin BA, Zafar MA, Kuivaniemi H, Body SC, et al. Genes associated with thoracic aortic aneurysm and dissection: 2019 update and clinical implications. *Aorta.* (2019) 07:099–107. doi: 10.1055/s-0039-3400233
119. Boileau C, Guo D-C, Hanna N, Regalado ES, Detaint D, Gong L, et al. TGFβ2 mutations cause familial thoracic aortic aneurysms and dissections associated with mild systemic features of Marfan syndrome. *Nat Genet.* (2012) 44:916–21. doi: 10.1038/ng.2348
120. Takeda N, Komuro I. Genetic basis of hereditary thoracic aortic aneurysms and dissections. *J Cardiol.* (2019) 74:136–43. doi: 10.1016/j.jcc.2019.03.014
121. Wang Z, Zhuang X, Chen B, Wen J, Peng F, Liu X, et al. 99-case study of sporadic aortic dissection by whole exome sequencing indicated novel disease-associated genes and variants in Chinese population. *Biomed Res Int.* (2020) 2020:1–12. doi: 10.1155/2020/7857043
122. Weng J, Liao M, Zou S, Bao J, Zhou J, Qu L, et al. Downregulation of FHL1 expression in thoracic aortic dissection: implications in aortic wall remodeling and pathogenesis of thoracic aortic dissection. *Ann Vasc Surg.* (2011) 25:240–7. doi: 10.1016/j.avsg.2010.10.001
123. Zhang Y, Feng X-H, Derynck R. Smad3 and Smad4 cooperate with c-Jun/c-Fos to mediate TGF-β-induced transcription. *Nature.* (1998) 394:6. doi: 10.1038/29814
124. Brownstein A, Kostiuik V, Ziganshin B, Zafar M, Kuivaniemi H, Body S, et al. Genes associated with thoracic aortic aneurysm and dissection: 2018 update and clinical implications. *Aorta.* (2018) 06:013–020. doi: 10.1055/s-0038-1639612
125. Michel J-B, Jondeau G, Milewicz DM. From genetics to response to injury: vascular smooth muscle cells in aneurysms and dissections of the ascending aorta. *Cardiovasc Res.* (2018) 114:578–89. doi: 10.1093/cvr/cvy006
126. Guo D, Grove ML, Prakash SK, Eriksson P, Hostetler EM, LeMaire SA, et al. Genetic variants in LRP1 and ULK4 are associated with acute aortic dissections. *Am J Hum Genet.* (2016) 99:762–9. doi: 10.1016/j.ajhg.2016.06.034
127. Schnieder J, Mamazhakypov A, Birnhuber A, Wilhelm J, Kwapiszewska G, Ruppert C, et al. Loss of LRP1 promotes acquisition of contractile-myofibroblast phenotype and release of active TGF-β1 from ECM stores. *Matrix Biol.* (2020) 88:69–88. doi: 10.1016/j.matbio.2019.12.001
128. Kuang S-Q, Medina-Martinez O, Guo D, Gong L, Regalado ES, Reynolds CL, et al. FOXE3 mutations predispose to thoracic aortic aneurysms and dissections. *J Clin Invest.* (2016) 126:948–61. doi: 10.1172/JCI83778
129. Landgren H, Blixt A, Carlsson P. Persistent FoxE3 expression blocks cytoskeletal remodeling and organelle degradation during lens fiber differentiation. *Invest Ophthalmol Vis Sci.* (2008) 49:4269–77. doi: 10.1167/iovs.08-2243
130. Guo D, Gong L, Regalado ES, Santos-Cortez RL, Zhao R, Cai B, et al. MAT2A mutations predispose individuals to thoracic aortic aneurysms. *Am J Hum Genet.* (2015) 96:170–7. doi: 10.1016/j.ajhg.2014.11.015
131. Wang K, Fang S, Liu Q, Gao J, Wang X, Zhu H, et al. TGF-β1/p65/MAT2A pathway regulates liver fibrogenesis via intracellular SAM. *EBioMedicine.* (2019) 42:458–69. doi: 10.1016/j.ebiom.2019.03.058
132. Liao M, Zou S, Weng J, Hou L, Yang L, Zhao Z, et al. A microRNA profile comparison between thoracic aortic dissection and normal thoracic aorta indicates the potential role of microRNAs in contributing to thoracic aortic dissection pathogenesis. *J Vasc Surg.* (2011) 53:1341.e–9.e. doi: 10.1016/j.jvs.2010.11.113

133. Rahkonen O, Su M, Hakovirta H, Koskivirta I, Hormuzdi SG, Vuorio E, et al. Mice with a deletion in the first intron of the Col1a1 gene develop age-dependent aortic dissection and rupture. *Circ Res.* (2004) 94:83–90. doi: 10.1161/01.RES.0000108263.74520.15
134. Barbier M, Gross M-S, Aubart M, Hanna N, Kessler K, Guo D-C, et al. MFAP5 loss-of-function mutations underscore the involvement of matrix alteration in the pathogenesis of familial thoracic aortic aneurysms and dissections. *Am J Hum Genet.* (2014) 95:736–43. doi: 10.1016/j.ajhg.2014.10.018
135. Guo D, Regalado ES, Gong L, Duan X, Santos-Cortez RLP, Arnaud P, et al. LOX mutations predispose to thoracic aortic aneurysms and dissections. *Circ Res.* (2016) 118:928–34. doi: 10.1161/CIRCRESAHA.115.307130
136. van Rooij E, Sutherland LB, Thatcher JE, DiMaio JM, Naseem RH, Marshall WS, et al. Dysregulation of microRNAs after myocardial infarction reveals a role of miR-29 in cardiac fibrosis. *Proc Natl Acad Sci USA.* (2008) 105:13027–32. doi: 10.1073/pnas.0805038105
137. Guo X, Fang Z-M, Wei X, Huo B, Yi X, Cheng C, et al. HDAC6 is associated with the formation of aortic dissection in human. *Mol Med.* (2019) 25:10. doi: 10.1186/s10020-019-0080-7
138. Zhang X, Wu D, Choi JC, Minard CG, Hou X, Coselli JS, et al. Matrix metalloproteinase levels in chronic thoracic aortic dissection. *J Surg Res.* (2014) 189:348–58. doi: 10.1016/j.jss.2014.03.027
139. Hirakata S, Aoki H, Ohno-Urabe S, Nishihara M, Furusho A, Nishida N, et al. Genetic deletion of Socs3 in smooth muscle cells ameliorates aortic dissection in mice. *JACC Basic Transl Sci.* (2020) 5:126–44. doi: 10.1016/j.jacbs.2019.10.010
140. Liao M, Liu Z, Bao J, Zhao Z, Hu J, Feng X, et al. A proteomic study of the aortic media in human thoracic aortic dissection: implication for oxidative stress. *J Thorac Cardiovasc Surg.* (2008) 136:65.e–72.e. doi: 10.1016/j.jtcvs.2007.11.017
141. Gough RE, Gault BT. The tale of two talins - two isoforms to fine-tune integrin signalling. *FEBS Lett.* (2018) 592:2108–25. doi: 10.1002/1873-3468.13081
142. Wei X, Sun Y, Wu Y, Zhu J, Gao B, Yan H, et al. Downregulation of Talin-1 expression associates with increased proliferation and migration of vascular smooth muscle cells in aortic dissection. *BMC Cardiovasc Disord.* (2017) 17:162. doi: 10.1186/s12872-017-0588-0
143. Proost D, Vandeweyer G, Meester JAN, Saleminck S, Kempers M, Ingram C, et al. Performant mutation identification using targeted next-generation sequencing of 14 thoracic aortic aneurysm genes. *Hum Mutat.* (2015) 36:808–14. doi: 10.1002/humu.22802
144. Zou S, Ren P, Nguyen M, Coselli JS, Shen YH, LeMaire SA. Notch signaling in descending thoracic aortic aneurysm and dissection. *PLoS One.* (2012) 7:e52833. doi: 10.1371/journal.pone.0052833
145. McGrath MJ, Cottle DL, Nguyen M-A, Dyson JM, Coghill ID, Robinson PA, et al. Four and a half LIM protein 1 binds myosin-binding protein C and regulates myosin filament formation and sarcomere assembly. *J Biol Chem.* (2006) 281:7666–83. doi: 10.1074/jbc.M512552200
146. Lee JY, Lori D, Wells DJ, Kemp PR. FHL1 activates myostatin signalling in skeletal muscle and promotes atrophy. *FEBS Open Bio.* (2015) 5:753–62. doi: 10.1016/j.fob.2015.08.011
147. Amirak E, Zakkar M, Evans PC, Kemp PR. Perfusion of veins at arterial pressure increases the expression of KLF5 and cell cycle genes in smooth muscle cells. *Biochem Biophys Res Commun.* (2010) 391:818–23. doi: 10.1016/j.bbrc.2009.11.145
148. Kaplan-Albuquerque N, Bogaert YE, Van Putten V, Weiser-Evans MC, Nemenoff RA. Patterns of gene expression differentially regulated by platelet-derived growth factor and hypertrophic stimuli in vascular smooth muscle cells. *J Biol Chem.* (2005) 280:19966–76. doi: 10.1074/jbc.M500917200
149. Eysers PA. Marveling at the Incredible ULK4. *Structure.* (2020) 28:1181–3. doi: 10.1016/j.str.2020.10.005
150. Juhola J, Oikonen M, Magnussen CG, Mikkilä V, Siitonen N, Jokinen E, et al. Childhood physical, environmental, and genetic predictors of adult hypertension: the cardiovascular risk in young finns study. *Circulation.* (2012) 126:402–9. doi: 10.1161/CIRCULATIONAHA.111.085977
151. Gretarsdottir S, Baas AF, Thorleifsson G, Holm H, den Heijer M, de Vries J-PPM, et al. Genome-wide association study identifies a sequence variant within the DAB2IP gene conferring susceptibility to abdominal aortic aneurysm. *Nat Genet.* (2010) 42:692–7. doi: 10.1038/ng.622
152. Oller J, Gabandé-Rodríguez E, Ruiz-Rodríguez MJ, Desdín-Micó G, Aranda JF, Rodríguez-Díez R, et al. Extracellular tuning of mitochondrial respiration leads to aortic aneurysm. *Circulation.* (2021) 143:2091–109. doi: 10.1161/CIRCULATIONAHA.120.051171
153. Callewaert B, De Paeppe A, Coucke P. *Arterial Tortuosity Syndrome*. Seattle, WA: University of Washington (1993).
154. Zoppi N, Chiarelli N, Cinquina V, Ritelli M, Colombi M. GLUT10 deficiency leads to oxidative stress and non-canonical $\alpha\text{v}\beta 3$ integrin-mediated TGF β signalling associated with extracellular matrix disarray in arterial tortuosity syndrome skin fibroblasts. *Hum Mol Genet.* (2015) 24:679–87. doi: 10.1093/hmg/ddv382
155. Coucke PJ, Willaert A, Wessels MW, Callewaert B, Zoppi N, De Backer J, et al. Mutations in the facilitative glucose transporter GLUT10 alter angiogenesis and cause arterial tortuosity syndrome. *Nat Genet.* (2006) 38:452–7. doi: 10.1038/ng1764
156. Watanabe K, Taketomi Y, Miki Y, Kugiyama K, Murakami M. Group V secreted phospholipase A2 plays a protective role against aortic dissection. *J Biol Chem.* (2020) 295:10092–111. doi: 10.1074/jbc.RA120.013753
157. Graham RM, McGrath-Cadell L, Muller DWM, Holloway CJ. The mystery and enigma of spontaneous coronary artery dissection. *Heart Lung Circ.* (2018) 27:401–5. doi: 10.1016/S1443-9506(18)30060-X
158. Nishiguchi T, Tanaka A, Ozaki Y, Taruya A, Fukuda S, Taguchi H, et al. Prevalence of spontaneous coronary artery dissection in patients with acute coronary syndrome. *Eur Heart J.* (2016) 5:263–70. doi: 10.1177/2048872613504310
159. Panchagnula K, Punja R, Punja D, Suryavanshi C. A comparative study of vasa vasorum density among coronary arteries. *Artery Res.* (2018) 22:36. doi: 10.1016/j.artres.2018.04.002
160. Kwon T-G, Gulati R, Matsuzawa Y, Aoki T, Guddeti RR, Herrmann J, et al. Proliferation of coronary adventitial vasa vasorum in patients with spontaneous coronary artery dissection. *JACC Cardiovasc Imaging.* (2016) 9:2. doi: 10.1016/j.jcmg.2015.11.030
161. Franke KB, Nerlekar N, Marshall H, Psaltis PJ. Systematic review and meta-analysis of the clinical characteristics and outcomes of spontaneous coronary artery dissection. *Int J Cardiol.* (2021) 322:34–9. doi: 10.1016/j.ijcard.2020.08.076
162. Okura T, Takahashi K, Sakaue T, Ueda S, Enomoto D, Yamamoto D, et al. A case of spontaneous coronary artery dissection with early de novo recurrence. *J Cardiol Cases.* (2019) 20:1–3. doi: 10.1016/j.jccase.2019.01.006
163. Saw J, Starovoytov A, Humphries K, Sheth T, So D, Minhas K, et al. Canadian spontaneous coronary artery dissection cohort study: in-hospital and 30-day outcomes. *Eur Heart J.* (2019) 40:1188–97. doi: 10.1093/eurheartj/ehz007
164. Garcia-Guimaraes M, Masotti M, Sanz-Ruiz R, Macaya F, Roura G, Nogales JM, et al. Clinical outcomes in spontaneous coronary artery dissection. *Heart.* (2022) 108:1530–8. doi: 10.1136/heartjnl-2022-320830
165. Georges A, Yang M-L, Berrandou T-E, Bakker MK, Dikilitas O, Kiando SR, et al. Genetic investigation of fibromuscular dysplasia identifies risk loci and shared genetics with common cardiovascular diseases. *Nat Commun.* (2021) 12:6031. doi: 10.1038/s41467-021-26174-2
166. Iismaa SE, Hesselton S, McGrath-Cadell L, Muller DW, Fatkin D, Giannoulatos E, et al. Spontaneous coronary artery dissection and fibromuscular dysplasia: vasculopathies with a predilection for women. *Heart Lung Circ.* (2020) 30:27–35. doi: 10.1016/j.hlc.2020.05.110
167. Michelis KC, Olin JW, Kadian-Dodov D, d'Escamard V, Kovacic JC. Coronary artery manifestations of fibromuscular dysplasia. *J Am Coll Cardiol.* (2014) 64:1033–46. doi: 10.1016/j.jacc.2014.07.014
168. Hayes SN, Kim ESH, Saw J, Adlam D, Arslanian-Engoren C, Economy KE, et al. Spontaneous coronary artery dissection: current state of the science: a scientific statement from the american heart association. *Circulation.* (2018) 137:e523–57. doi: 10.1161/CIR.0000000000000564
169. Rafiq A, Pokharel P, Krim NR. Rare case of asymptomatic spontaneous coronary artery dissection. *J Cardiol Cases.* (1999) 13:149–52. doi: 10.1016/j.jccase.2016.01.004
170. Cannata S, Birkinshaw A, Sado D, Dworakowski R, Pareek N. Spontaneous coronary artery dissection after COVID-19 infection presenting with ST segment elevation. *Eur Heart J.* (2020) 41:4602–4602. doi: 10.1093/eurheartj/ehaa813
171. Adlam D, Olson TM, Combaret N, Kovacic JC, Iismaa SE, Al-Hussaini A, et al. Association of the PHACTR1/EDN1 genetic locus with spontaneous coronary artery dissection. *J Am Coll Cardiol.* (2019) 73:58–66. doi: 10.1016/j.jacc.2018.09.085
172. Tarr I, Hesselton S, Iismaa SE, Rath E, Monger S, Troup M, et al. Exploring the genetic architecture of spontaneous coronary artery dissection using whole-genome sequencing. *Circ Genom Precis Med.* (2022) 15:10–1161. doi: 10.1161/CIRCGEN.121.003527
173. Mori R, Macaya F, Sara JD, Taya T, Mejia-Renteria H, Gonzalo N, et al. Non-invasive assessment of endothelial function in patients with spontaneous coronary artery dissection: a case-control study. *Int J Cardiol.* (2020) 1:10–42. doi: 10.1016/j.ijcard.2020.04.049

174. Waterbury TM, Tweet MS, Hayes SN, Prasad A, Lerman A, Gulati R. Coronary endothelial function and spontaneous coronary artery dissection. *Eur Heart J*. (2020) 9:90–5. doi: 10.1177/2048872618795255
175. Carss KJ, Baranowska AA, Armisen J, Webb TR, Hamby SE, Premawardhana D, et al. Spontaneous coronary artery dissection: insights on rare genetic variation from genome sequencing. *Circ Genom Precis Med*. (2020) 13:e003030. doi: 10.1161/CIRCGEN.120.003030
176. Hui P, Bai Y, Su X, Quan N, Qiao B, Zheng Y, et al. The value of plasma fibrillin-1 level in patients with spontaneous coronary artery dissection. *Int J Cardiol*. (2020) 302:150–6. doi: 10.1016/j.ijcard.2019.12.015
177. Marshall LM, Carlson EJ, O'Malley J, Snyder CK, Charbonneau NL, Hayflick SJ, et al. Thoracic aortic aneurysm frequency and dissection are associated with fibrillin-1 fragment concentrations in circulation. *Circ Res*. (2013) 113:1159–68. doi: 10.1161/CIRCRESAHA.113.301498
178. Boucher P, Li W-P, Matz RL, Takayama Y, Auwerx J, Anderson RGW, et al. LRP1 Functions as an atheroprotective integrator of TGF β and PDGF signals in the vascular wall: implications for Marfan syndrome. *PLoS One*. (2007) 2:e448. doi: 10.1371/journal.pone.0000448
179. Fahey J, Ramalison M, White A. Identifying genetic causes of spontaneous coronary artery dissection by whole genome sequencing in related individuals. *J Am Coll Cardiol*. (2018) 71:A123. doi: 10.1016/S0735-1097(18)30664-8
180. Guo D, Duan X-Y, Regalado ES, Mellor-Crummey L, Kwartler CS, Kim D, et al. Loss-of-Function mutations in YY1AP1 lead to grange syndrome and a fibromuscular dysplasia-like vascular disease. *Am J Hum Genet*. (2017) 100:21–30. doi: 10.1016/j.ajhg.2016.11.008
181. Li J, Ballim D, Rodriguez M, Cui R, Goding CR, Teng H, et al. The anti-proliferative function of the TGF- β 1 signaling pathway involves the repression of the oncogenic TBX2 by its homologue TBX3. *J Biol Chem*. (2014) 289:35633–43. doi: 10.1074/jbc.M114.596411
182. Wang Y, Lui W-Y. Transforming growth factor- β 1 attenuates junctional adhesion molecule-A and contributes to breast cancer cell invasion. *Eur J Cancer*. (2012) 48:3475–87. doi: 10.1016/j.ejca.2012.04.016
183. Katoh Y, Katoh M. Hedgehog signaling, epithelial-to-mesenchymal transition and miRNA (Review). *Int J Mol Med*. (1998) 22:271–5. doi: 10.3892/ijmm_00000019
184. Matissek SJ, Elswa SF. GLI3: a mediator of genetic diseases, development and cancer. *Cell Commun Signal*. (2020) 18:54. doi: 10.1186/s12964-020-00540-x
185. Zekavat SM, Chou EL, Zekavat M, Pampana A, Paruchuri K, Lino Cardenas CL, et al. Fibrillar collagen variants in spontaneous coronary artery dissection. *JAMA Cardiol*. (2022) 7:396. doi: 10.1001/jamacardio.2022.0001
186. Bell DM, Leung KKH, Ng LJ, Zhou S, Ling W, Sham MH, et al. SOX9 directly regulates the type-II collagen gene. *Nat Genet*. (1997) 16:174–8.
187. Lu C-L, Ortmeier S, Brudvig J, Moretti T, Cain J, Boyadjiev SA, et al. Collagen has a unique SEC24 preference for efficient export from the endoplasmic reticulum. *Traffic*. (2021) 23:91–3. doi: 10.1111/tra.12826
188. Saw J, Yang M-L, Trinder M, Tcheandjieu C, Xu C, Starovoytov A, et al. Chromosome 1q21.2 and additional loci influence risk of spontaneous coronary artery dissection and myocardial infarction. *Nat Commun*. (2020) 11:4432. doi: 10.1038/s41467-020-17558-x
189. Fan W, Liu T, Chen W, Hammad S, Longerich T, Hausser I, et al. ECM1 prevents activation of transforming growth factor β , hepatic stellate cells, and fibrogenesis in mice. *Gastroenterology*. (2019) 157:1352–1367.e13. doi: 10.1053/j.gastro.2019.07.036
190. Lee K, Nam K, Oh S, Lim J, Kim RK, Shim D, et al. ECM1 regulates tumor metastasis and CSC-like property through stabilization of β -catenin. *Oncogene*. (2015) 34:6055–65. doi: 10.1038/onc.2015.54
191. Gabriel LAR, Wang LW, Bader H, Ho JC, Majors AK, Hollyfield JG, et al. ADAMTSL4, a secreted glycoprotein widely distributed in the eye, binds fibrillin-1 microfibrils and accelerates microfibril biogenesis. *Invest Ophthalmol Vis Sci*. (2012) 53:461. doi: 10.1167/iovs.10-5955
192. McKenzie FJ, Tassanakijpanich N, Epps KC, March SK, Hagerman RJ. Spontaneous coronary artery dissection in females with the fragile X FMR1 premutation. *JACC Case Rep*. (2020) 2:40–4. doi: 10.1016/j.jaccas.2019.11.058
193. Nolze A, Schneider J, Keil R, Lederer M, Hüttelmaier S, Kessels MM, et al. FMRP regulates actin filament organization via the armadillo protein p0071. *RNA*. (2013) 19:1483–96. doi: 10.1261/rna.037945.112
194. Dziembowska M, Pretto DI, Janusz A, Kaczmarek L, Leigh MJ, Gabriel N, et al. High MMP-9 activity levels in fragile X syndrome are lowered by minocycline. *Am J Med Genet*. (2013) 161:1897–903. doi: 10.1002/ajmg.a.36023
195. Ramírez-Cheyne JA, Duque GA, Ayala-Zapata S, Saldarriaga-Gil W, Hagerman P, Hagerman R, et al. Fragile X syndrome and connective tissue dysregulation. *Clin Genet*. (2019) 95:262–7. doi: 10.1111/cge.13469
196. Bergen AAB, Plomp AS, Schuurman EJ, Terry S, Breuning M, Dauwerse H, et al. Mutations in ABCC6 cause pseudoxanthoma elasticum. *Nat Genet*. (2000) 25:228–31. doi: 10.1038/s41436-020-00945-6
197. Verschuere S, Navassiolava N, Martin L, Nevalainen PI, Coucke PJ, Vanakker OM. Reassessment of causality of ABCC6 missense variants associated with pseudoxanthoma elasticum based on Sherloc. *Genet Med*. (2021) 23:131–9. doi: 10.1038/s41436-020-00945-6
198. Germain DP. Pseudoxanthoma elasticum. *Orphanet J Rare Dis*. (2017) 12:85. doi: 10.1186/s13023-017-0639-8
199. Bartstra JW, Spiering W, van den Ouweland JMW, Mali WPTM, Janssen R, de Jong PA. Increased elastin degradation in pseudoxanthoma elasticum is associated with peripheral arterial disease independent of calcification. *J Clin Med*. (2020) 9:2771. doi: 10.3390/jcm9092771
200. de Almeida HL Jr, de Almeida MG, Jorge VM, de Abreu LB. Ultrastructural aspects of pseudoxanthoma elasticum. *An Bras Dermatol*. (2017) 92:527–30. doi: 10.1590/abd1806-4841.20175972
201. Kiss N, Fésüs L, Bozsányi S, Szeri F, Van Gils M, Szabó V, et al. Nonlinear optical microscopy is a novel tool for the analysis of cutaneous alterations in pseudoxanthoma elasticum. *Lasers Med Sci*. (2020) 35:1821–30. doi: 10.1007/s10103-020-03027-w
202. Kranenburg G, de Jong PA, Mali WP, Attrach M, Visseren FLJ, Spiering W. Prevalence and severity of arterial calcifications in pseudoxanthoma elasticum (PXE) compared to hospital controls. Novel insights into the vascular phenotype of PXE. *Atherosclerosis*. (2017) 256:7–14. doi: 10.1016/j.atherosclerosis.2016.11.012
203. Turley TN, Theis JL, Sundsbak RS, Evans JM, O'Byrne MM, Gulati R, et al. Rare missense variants in TLN1 are associated with familial and sporadic spontaneous coronary artery dissection. *Circ Genom Precis Med*. (2019) 12:173–82. doi: 10.1161/CIRCGEN.118.002437
204. Lockyer P, Mao H, Fan Q, Li L, Yu-Lee L-Y, Eissa NT, et al. LRP1-dependent BMPER signaling regulates lipopolysaccharide-induced vascular inflammation. *Arterioscler Thromb Vasc Biol*. (2017) 37:1524–35. doi: 10.1161/ATVBAHA.117.309521
205. Johnson EN, Lee YM, Sander TL, Rabkin E, Schoen FJ, Kaushal S, et al. NFATc1 mediates vascular endothelial growth factor-induced proliferation of human pulmonary valve endothelial cells. *J Biol Chem*. (2003) 278:1686–92. doi: 10.1074/jbc.M210250200
206. He P, Yu H, Jiang L, Chen Z, Wang S, Macrae VE, et al. Hdac9 inhibits medial artery calcification through down-regulation of osterix. *Vasc Pharmacol*. (2020) 132:106775. doi: 10.1016/j.vph.2020.106775
207. The International Stroke Genetics Consortium [ISGC], The Wellcome Trust Case Control Consortium 2 (WTCCC2), Bellenguez C, Bevan S, Gschwendtner A, Spencer CCA, et al. Genome-wide association study identifies a variant in HDAC9 associated with large vessel ischemic stroke. *Nat Genet*. (2012) 44:328–33. doi: 10.1038/ng.1081
208. Lino Cardenas CL, Kessinger CW, Cheng Y, MacDonald C, MacGillivray T, Ghoshhajra B, et al. An HDAC9-MALAT1-BRG1 complex mediates smooth muscle dysfunction in thoracic aortic aneurysm. *Nat Commun*. (2018) 9:1009. doi: 10.1038/s41467-018-03394-7
209. Martinelli D, Häberle J, Rubio V, Giunta C, Hausser I, Carrozzo R, et al. Understanding pyrroline-5-carboxylate synthetase deficiency: clinical, molecular, functional, and expression studies, structure-based analysis, and novel therapy with arginine. *J Inher Metab Dis*. (2012) 35:761–76. doi: 10.1007/s10545-011-9411-8
210. Berk DR, Bentley DD, Bayliss SJ, Lind A, Urban Z. Cutis laxa: a review. *J Am Acad Dermatol*. (2012) 66:e1–842. doi: 10.1016/j.jaad.2011.01.004
211. Sun Y, Chen Y, Li Y, Li Z, Li C, Yu T, et al. Association of TSR1 variants and spontaneous coronary artery dissection. *J Am Coll Cardiol*. (2019) 74:167–76. doi: 10.1016/j.jacc.2019.04.062
212. Grond-Ginsbach C, Böckler D, Newton-Cheh C. Pathogenic TSR1 gene variants in patients with spontaneous coronary artery dissection. *J Am Coll Cardiol*. (2019) 74:177–8. doi: 10.1016/j.jacc.2019.06.005
213. Li J, Peng W, Du L, Yang Q, Wang C, Mo Y. The oncogenic potentials and diagnostic significance of long non-coding RNA LINC00310 in breast cancer. *J Cell Mol Med*. (2018) 22:4486–95. doi: 10.1111/jcmm.13750
214. Takaguri A, Sasano J, Akihiro O, Satoh K. The role of circadian clock gene BMAL1 in vascular proliferation. *Eur J Pharmacol*. (2020) 872:172924. doi: 10.1016/j.ejphar.2020.172924

215. von Babo M, De Marchis GM, Sarikaya H, Stapf C, Buffon F, Fischer U, et al. Differences and similarities between spontaneous dissections of the internal carotid artery and the vertebral artery. *Stroke*. (2013) 44:1537–42. doi: 10.1161/STROKEAHA.113.001057
216. Debette S, Leys D. Cervical-artery dissections: predisposing factors, diagnosis, and outcome. *Lancet Neurol*. (2009) 8:668–78. doi: 10.1016/S1474-4422(09)70084-5
217. Menon RK, Norris JW. Cervical arterial dissection. *Ann N Y Acad Sci*. (2008) 1142:200–17. doi: 10.1196/annals.1444.015
218. Wu Y, Wu F, Liu Y, Fan Z, Fisher M, Li D, et al. High-resolution magnetic resonance imaging of cervicocranial artery dissection: imaging features associated with stroke. *Stroke*. (2019) 50:3101–7. doi: 10.1161/STROKEAHA.119.026362
219. Brandt T, Orberk E, Weber R, Werner I, Busse O, Müller BT, et al. Pathogenesis of cervical artery dissections: association with connective tissue abnormalities. *Neurology*. (2001) 57:24–30. doi: 10.1212/WNL.57.1.24
220. Liebeskind DS, Saver JL. *Cervicocephalic Arterial Dissections, in: Neurological Therapeutics: Principles and Practice*. London: CRC Press (2003).
221. Mayer-Suess L, Pechlaner R, Barallobre-Barreiro J, Boehme C, Toell T, Lynch M, et al. Extracellular matrix protein signature of recurrent spontaneous cervical artery dissection. *Neurology*. (2020) 95:e2047–55. doi: 10.1212/WNL.00000000000010710
222. Volker W, Dittich R, Grewe S, Nassenstein I, Csiba L, Herczeg L, et al. The outer arterial wall layers are primarily affected in spontaneous cervical artery dissection. *Neurology*. (2011) 76:1463–71.
223. Arnold M, Kappeler L, Georgiadis D, Berthet K, Keserue B, Bousser MG, et al. Gender differences in spontaneous cervical artery dissection. *Neurology*. (2006) 67:1050–2. doi: 10.1212/01.wnl.0000237341.30854.6a
224. Majamaa K, Portimajärvi H, Sotaniemi KA, Myllylä VV. Familial aggregation of cervical artery dissection and cerebral aneurysm. *Stroke*. (1994) 25:1704–5. doi: 10.1161/01.STR.25.8.1704
225. Pezzini A. Arterial hypertension as risk factor for spontaneous cervical artery dissection. A case-control study. *J Neurol Neurosurg Psychiatry*. (2006) 77:95–7. doi: 10.1136/jnnp.2005.063107
226. D'Anglejan-Chatillon J, Ribeiro V, Mas JL, Youl BD, Bousser MG. Migraine—a risk factor for dissection of cervical arteries. *Headache*. (1989) 29:560–1. doi: 10.1111/j.1526-4610.1989.hed2909560.x
227. De Giuli V, Grassi M, Lodigiani C, Patella R, Zedde M, Gandolfo C, et al. Association between migraine and cervical artery dissection: the Italian project on stroke in young adults. *JAMA Neurol*. (2017) 74:512. doi: 10.1001/jamaneurol.2016.5704
228. Guillon B, Berthet K, Benslamia L, Bertrand M, Bousser M-G, Tzourio C. Infection and the risk of spontaneous cervical artery dissection: a case-control study. *Stroke*. (2003) 34:e79–81. doi: 10.1161/01.STR.0000078309.56307.5C
229. Schievink WI, Mokri B, Piepgras DG, Gittenberger-de Groot AC. Intracranial aneurysms and cervicocephalic arterial dissections associated with congenital heart disease. *Neurosurgery*. (1996) 39:685–90. doi: 10.1097/00006123-199610000-00006
230. Grond-Ginsbach C, Brandt T, Kloss M, Aksay SS, Lyrer P, Traenka C, et al. Next generation sequencing analysis of patients with familial cervical artery dissection. *Eur Stroke J*. (2017) 2:137–43. doi: 10.1177/2396987317693402
231. Ruiz-Franco A, Barboza MA, Jara-Prado A, Canizales-Quinteros S, Leon-Mimila P, Arguëlles-Morales N, et al. TGFBR2 mutation and MTHFR-C677T polymorphism in a Mexican mestizo population with cervico-cerebral artery dissection. *J Neurol*. (2016) 263:1066–73. doi: 10.1007/s00415-016-8101-8
232. Grond-Ginsbach C, Chen B, Pjontek R, Wiest T, Jiang Y, Burwinkel B, et al. Copy number variation in patients with cervical artery dissection. *Eur J Hum Genet*. (2012) 20:1295–9. doi: 10.1038/ejhg.2012.82
233. Debette S, Kamatani Y, Metso TM, Kloss M, Chauhan G, Engelter ST, et al. Common variation in PHACTR1 is associated with susceptibility to cervical artery dissection. *Nat Genet*. (2015) 47:78–83. doi: 10.1038/ng.3154
234. Debette S, Markus HS. The genetics of cervical artery dissection: a systematic review. *Stroke*. (2009) 40:e459–66. doi: 10.1161/STROKEAHA.108.534669
235. von Pein F, Välikilä M, Schwarz R, Morcher M, Klima B, Grau A, et al. Analysis of the COL3A1 gene in patients with spontaneous cervical artery dissections. *J Neurol*. (2002) 249:862–6. doi: 10.1007/s00415-002-0745-x
236. Longoni M, Grond-Ginsbach C, Grau AJ, Genius J, Debette S, Schwanninger M, et al. The ICAM-1 E469K gene polymorphism is a risk factor for spontaneous cervical artery dissection. *Neurology*. (2006) 66:1273. doi: 10.1212/01.wnl.0000208411.01172.0b
237. Varga EA, Sturm AC, Misita CP, Moll S. Homocysteine and MTHFR mutations: relation to thrombosis and coronary artery disease. *Circulation*. (2005) 111:e289–93. doi: 10.1161/01.CIR.0000165142.37711.E7
238. Arauz A, Hoyos L, Cantú C, Jara A, Martínez L, García I, et al. Mild hyperhomocysteinemia and low folate concentrations as risk factors for cervical arterial dissection. *Cerebrovasc Dis*. (2007) 24:210–4. doi: 10.1159/000104479
239. Fernando DMG, Thilakarathne SMNK, Wickramasinghe CU. Pulmonary artery dissection—a review of 150 cases. *Heart Lung*. (2019) 48:428–35. doi: 10.1016/j.hrtlung.2019.02.007
240. Shilkin KB, Low LP, Chen BTM. Dissecting aneurysm of the pulmonary artery. *J. Pathol*. (1969) 98:25–9. doi: 10.1002/path.1710980104
241. Inayama Y, Nakatani Y, Kitamura H. Pulmonary artery dissection in patients without underlying pulmonary hypertension. *Histopathology*. (2001) 38:435–42. doi: 10.1046/j.1365-2559.2001.01129.x
242. Khattar RS. Pulmonary artery dissection: an emerging cardiovascular complication in surviving patients with chronic pulmonary hypertension. *Heart*. (2005) 91:142–5. doi: 10.1136/hrt.2004.045799
243. Green NJ, Rollason TP. Pulmonary artery rupture in pregnancy complicating patent ductus arteriosus. *Heart*. (1992) 68:616–8. doi: 10.1136/hrt.68.12.616
244. Best J. Dissecting aneurysm of the pulmonary artery with multiple cardiovascular abnormalities and pulmonary hypertension. *Med J Aust*. (1967) 2:1129–30. doi: 10.5694/j.1326-5377.1967.tb27334.x
245. Park HS, Chamrath MR, Lamus D, Saboo SS, Sutphin PD, Kalva SP. Pulmonary artery aneurysms: diagnosis & endovascular therapy. *Cardiovasc Diagn Ther*. (2018) 8:350–61. doi: 10.21037/cdt.2018.04.01
246. Senbaklavaci Ö, Kaneko Y, Bartunek A, Brunner C, Kurkciyan E, Wunderbaldinger P, et al. Rupture and dissection in pulmonary artery aneurysms: incidence, cause, and treatment—review and case report. *J Thorac Cardiovasc Surg*. (2001) 121:1006–8. doi: 10.1067/mtc.2001.112634
247. Mohammad K, Sahlol M, Egiebor O, Sadikot RT. Idiopathic pulmonary artery dissection: a case report. *J Med Case Rep*. (2009) 3:7426. doi: 10.4076/1752-1947-3-7426
248. Yoon K, Song S-Y, Lee CH, Ko B-H, Lee S, Kang BK, et al. Spontaneous renal artery dissection as a cause of acute renal infarction: clinical and MDCT findings. *J Korean Med Sci*. (2017) 32:605. doi: 10.3346/jkms.2017.32.4.605
249. Matsuo R, Ohta Y, Ohya Y, Kitazono T, Irie H, Shikata T, et al. Isolated dissection of the celiac artery: a case report. *Angiology*. (2000) 51:603–7. doi: 10.1177/000331970005100710
250. Renaud S, Leray-Moragues H, Chenine L, Canaud L, Vernhet-Kovacsik H, Canaud B. Spontaneous renal artery dissection with renal infarction. *Clin Kidney J*. (2012) 5:261–4. doi: 10.1093/ckj/sfs047
251. Bumpus HC. A case of renal hypertension. *J Urol*. (1944) 52:295–9. doi: 10.1016/S0022-5347(17)70262-5
252. Gandhi SP, Patel K, Pal BC. Isolated spontaneous renal artery dissection presented with flank pain. *Case Rep Radiol*. (2015) 2015:1–5. doi: 10.1155/2015/896706
253. Vaidya S, Dighe M. Spontaneous celiac artery dissection and its management. *Radiol Case*. (2010) 4:30–3. doi: 10.3941/jrcr.v4i4.408
254. Garrett HE. Options for treatment of spontaneous mesenteric artery dissection. *J Vasc Surg*. (2014) 59:1433–9.e1-2. doi: 10.1016/j.jvs.2014.01.040
255. Lee SI, Kim JJ, Yang HJ, Lee K. Spontaneous dissection of celiac trunk with concurrent splenic artery dissection. *Clin Exp Emerg Med*. (2015) 2:256–9. doi: 10.15441/ceem.15.030
256. Jha A, Afari M, Koulouridis I, Bhat T, Garcia L. Isolated renal artery dissection: a systematic review of case reports. *Cureus*. (2020) 12:e6960. doi: 10.7759/cureus.6960
257. Richer J, Hill HL, Wang Y, Yang M-L, Hunker KL, Lane J, et al. A novel recurrent COL5A1 genetic variant is associated with a dysplasia-associated arterial disease exhibiting dissections and fibromuscular dysplasia. *Arterioscler Thromb Vasc Biol*. (2020) 40:2686–99. doi: 10.1161/ATVBAHA.119.313885
258. Takayama T, Miyata T, Shirakawa M, Nagawa H. Isolated spontaneous dissection of the splanchnic arteries. *J Vasc Surg*. (2008) 48:329–33. doi: 10.1016/j.jvs.2008.03.002
259. Milewicz DM, Ramirez F. Therapies for thoracic aortic aneurysms and acute aortic dissections: old controversies and new opportunities. *Arterioscler Thromb Vasc Biol*. (2019) 39:126–36. doi: 10.1161/ATVBAHA.118.310956

260. Weldy CS, Murtha R, Kim JB. Dissecting the genomics of spontaneous coronary artery dissection. *Circ Genom Precis Med.* (2022) 15:e003867. doi: 10.1161/CIRCGEN.122.003867
261. Saw J, Humphries K, Aymong E, Sedlak T, Prakash R, Starovoytov A, et al. Spontaneous coronary artery dissection—clinical outcomes and risk of recurrence. *J Am Coll Cardiol.* (2017) 70:1148–58. doi: 10.1016/j.jacc.2017.06.053
262. Margaritis M, Saini F, Baranowska-Clarke AA, Parsons S, Vink A, Budgeon C, et al. Vascular histopathology and connective tissue ultrastructure in spontaneous coronary artery dissection: pathophysiological and clinical implications. *Cardiovasc Res.* (2021) 118:cvab183. doi: 10.1093/cvr/cvab183
263. Sedding DG, Boyle EC, Demandt JAF, Sluimer JC, Dutzmann J, Haverich A, et al. Vasa vasorum angiogenesis: key player in the initiation and progression of atherosclerosis and potential target for the treatment of cardiovascular disease. *Front Immunol.* (2018) 9:706. doi: 10.3389/fimmu.2018.00706
264. Malfait F, Castori M, Francomano CA, Giunta C, Kosho T, Byers PH. The Ehlers–Danlos syndromes. *Nat Rev Dis Prim.* (2020) 6:64. doi: 10.1038/s41572-020-0194-9
265. D'hondt S, Van Damme T, Malfait F. Vascular phenotypes in nonvascular subtypes of the Ehlers–Danlos syndrome: a systematic review. *Genet Med.* (2018) 20:562–73. doi: 10.1038/gim.2017.138
266. Demmler JC, Atkinson MD, Reinhold EJ, Choy E, Lyons RA, Brophy ST. Diagnosed prevalence of Ehlers–Danlos syndrome and hypermobility spectrum disorder in Wales, UK: a national electronic cohort study and case-control comparison. *BMJ Open.* (2019) 9:e031365. doi: 10.1136/bmjopen-2019-031365
267. Chu LC, Johnson PT, Dietz HC, Brooke BS, Arnaoutakis GJ, Black JH, et al. Vascular complications of Ehlers–Danlos syndrome: CT findings. *Am J Roentgenol.* (2012) 198:482–7. doi: 10.2214/AJR.11.6603
268. Murphy-Ryan M, Psychogios A, Lindor NM. Hereditary disorders of connective tissue: a guide to the emerging differential diagnosis. *Genet Med.* (2010) 12:344–54. doi: 10.1097/GIM.0b013e3181e074f0
269. Harry D. Marfan syndrome. In: Adam MP, Ardinger HH, Pagon RA, Wallace SE, Bean LJ, Mirzaa G, et al. editors. *GeneReviews*®. Seattle, WA: University of Washington, Seattle (1993).
270. ten Dijke P, Arthur HM. Extracellular control of TGFβ signalling in vascular development and disease. *Nat Rev Mol Cell Biol.* (2007) 8:857–69. doi: 10.1038/nrm2262
271. Smalcelj A, Brida V, Samarzija M, Matana A, Margetic E, Drinkovic N. Pressure pulmonary artery aneurysm. *Texas Heart Inst J.* (2005) 32:6.
272. Renard M, Muiño-Mosquera L, Manalo EC, Tufa S, Carlson EJ, Keene DR, et al. Sex, pregnancy and aortic disease in Marfan syndrome. *PLoS One.* (2017) 12:e0181166. doi: 10.1371/journal.pone.0181166
273. MacCarrick G, Black JH, Bowdin S, El-Hamamsy I, Frischmeyer-Guerrero PA, Guerrero AL, et al. Loeys–Dietz syndrome: a primer for diagnosis and management. *Genet Med.* (2014) 16:576–87. doi: 10.1038/gim.2014.11
274. Rienhoff HY, Yeo C, Morissette R, Khrebtukova I, Melnick J, Luo S, et al. A mutation in TGFβ 3 associated with a syndrome of low muscle mass, growth retardation, distal arthrogryposis and clinical features overlapping with Marfan and Loeys–Dietz syndrome. *Am J Med Genet.* (2013) 161:2040–6. doi: 10.1002/ajmg.a.36056
275. Malhotra A, Westesson P-L. Loeys–Dietz syndrome. *Pediatr Radiol.* (2009) 39:1015–1015. doi: 10.1007/s00247-009-1252-3
276. Hertz JM, Thomassen M, Storey H, Flinter F. Clinical utility gene card for: alport syndrome. *Eur J Hum Genet.* (2012) 20:713–713. doi: 10.1038/ejhg.2011.237
277. Kruegel J, Rubel D, Gross O. Alport syndrome—insights from basic and clinical research. *Nat Rev Nephrol.* (2013) 9:170–8. doi: 10.1038/nrneph.2012.259
278. Anuwatworn A, Sethi P, Steffen K, Jonsson O, Petrasko M. Spontaneous coronary artery dissection: a rare manifestation of alport syndrome. *Case Rep Cardiol.* (2017) 2017:1–3. doi: 10.1155/2017/1705927
279. Patel J, Abt P, Cheng K, Aurigemma G, Rosenthal L. Type A dissection in a patient with alport syndrome. *Circ Cardiovasc Imaging.* (2020) 13:e010701. doi: 10.1161/CIRCIMAGING.120.010701
280. Gornik HL, Persu A, Adlam D, Aparicio LS, Azizi M, Boulanger M, et al. First International Consensus on the diagnosis and management of fibromuscular dysplasia. *Vasc Med.* (2019) 24:164–89. doi: 10.1177/1358863X18821816
281. Talarowska P, Dobrowolski P, Klisiewicz A, Kostera-Pruszycki A, Członkowska A, Kurkowska-Jastrzębska I, et al. High incidence and clinical characteristics of fibromuscular dysplasia in patients with spontaneous cervical artery dissection: the ARCADIA-POL study. *Vasc Med.* (2019) 24:112–9. doi: 10.1177/1358863X18811596
282. Haruta S, Gunji K, Kawamura T, Hiroshima K. Generalized vascular dissection on pathological examination in a patient with polycystic kidney disease and acute aortic dissection. *J Natl Med Assoc.* (2019) 111:563–8. doi: 10.1016/j.jnma.2019.04.008
283. Krishnappa V, Vinod P, Deverakonda D, Raina R. Autosomal dominant polycystic kidney disease and the heart and brain. *Cleve Clin J Med.* (2017) 84:471–81. doi: 10.3949/ccjm.84a.16107
284. Chapin HC, Caplan MJ. The cell biology of polycystic kidney disease. *J Cell Biol.* (2010) 191:701–10. doi: 10.1083/jcb.201006173
285. Sillence DO, Senn A, Danks DM. Genetic heterogeneity in osteogenesis imperfecta. *J Med Genet.* (1979) 16:101–16. doi: 10.1136/jmg.16.2.101
286. Marini JC, Forlino A, Bächinger HP, Bishop NJ, Byers PH, Paepe AD, et al. Osteogenesis imperfecta. *Nat Rev Dis Prim.* (2017) 3:17052. doi: 10.1038/nrdp.2017.52
287. Forlino A, Marini JC. Osteogenesis imperfecta. *Lancet.* (2016) 387:1657–71. doi: 10.1016/S0140-6736(15)00728-X
288. Balasubramanian M, Verschuere A, Kleevens S, Luyckx I, Perik M, Schirwani S, et al. Aortic aneurysm/dissection and osteogenesis imperfecta: four new families and review of the literature. *Bone.* (2019) 121:191–5. doi: 10.1016/j.bone.2019.01.022
289. Chougui K, Addab S, Palomo T, Morin SN, Veilleux L, Bernstein M, et al. Clinical manifestations of osteogenesis imperfecta in adulthood: an integrative review of quantitative studies and case reports. *Am J Med Genet.* (2020) 182:842–65. doi: 10.1002/ajmg.a.61497
290. LeMaire SA, McDonald M-LN, Guo D, Russell L, Miller CC, Johnson RJ, et al. Genome-wide association study identifies a susceptibility locus for thoracic aortic aneurysms and aortic dissections spanning FBN1 at 15q21.1. *Nat Genet.* (2011) 43:996–1000. doi: 10.1038/ng.934
291. Giuliani L, Di Toro A, Disabella E, Grasso M, Serio A, Urtis M, et al. P5539Genetic heterogeneity of spontaneous coronary artery dissection (SCAD). *Eur Heart J.* (2019) 40:ehz746.0485. doi: 10.1093/eurheartj/ehz746.0485
292. Daghas I, Sargurupremraj M, Danning R, Gormley P, Malik R, Amouyel P, et al. Migraine, stroke, and cervical arterial dissection: shared genetics for a triad of brain disorders with vascular involvement. *Neurol Genet.* (2022) 8:00. doi: 10.1212/NXG.0000000000000653
293. Guo D, Regalado E, Casteel DE, Santos-Cortez RL, Gong L, Kim JJ, et al. Recurrent gain-of-function mutation in PRKG1 causes thoracic aortic aneurysms and acute aortic dissections. *Am J Hum Genet.* (2013) 93:398–404. doi: 10.1016/j.ajhg.2013.06.019



OPEN ACCESS

EDITED BY

Masanori Aikawa,
Brigham and Women's Hospital and Harvard
Medical School, United States

REVIEWED BY

Masuko Ushio-Fukai,
Augusta University, United States
Noemi Rotllan Vila,
Sant Pau Institute for Biomedical Research,
Spain

*CORRESPONDENCE

Marjo M. P. C. Donners
✉ Marjo.donners@maastrichtuniversity.nl

SPECIALTY SECTION

This article was submitted to
Atherosclerosis and Vascular Medicine,
a section of the journal
Frontiers in Cardiovascular Medicine

RECEIVED 21 June 2022

ACCEPTED 13 January 2023

PUBLISHED 27 January 2023

CITATION

van der Vorst EPC, Maas SL, Theodorou K,
Peters LJF, Jin H, Rademakers T, Gijbels MJ,
Rousch M, Jansen Y, Weber C, Lehrke M,
Lebherz C, Yildiz D, Ludwig A, Bentzon JF,
Biessen EAL and Donners MMPC (2023)
Endothelial ADAM10 controls cellular response
to oxLDL and its deficiency exacerbates
atherosclerosis with intraplaque hemorrhage
and neovascularization in mice.
Front. Cardiovasc. Med. 10:974918.
doi: 10.3389/fcvm.2023.974918

COPYRIGHT

© 2023 van der Vorst, Maas, Theodorou, Peters,
Jin, Rademakers, Gijbels, Rousch, Jansen,
Weber, Lehrke, Lebherz, Yildiz, Ludwig,
Bentzon, Biessen and Donners. This is an
open-access article distributed under the terms
of the [Creative Commons Attribution License](#)
(CC BY). The use, distribution or reproduction in
other forums is permitted, provided the original
author(s) and the copyright owner(s) are
credited and that the original publication in this
journal is cited, in accordance with accepted
academic practice. No use, distribution or
reproduction is permitted which does not
comply with these terms.

Endothelial ADAM10 controls cellular response to oxLDL and its deficiency exacerbates atherosclerosis with intraplaque hemorrhage and neovascularization in mice

Emiel P. C. van der Vorst^{1,2,3,4,5}, Sanne L. Maas^{2,3}, Kosta Theodorou¹,
Linsey J. F. Peters^{1,2,3}, Han Jin¹, Timo Rademakers¹,
Marion J. Gijbels^{1,6,7}, Mat Rousch¹, Yvonne Jansen⁴,
Christian Weber^{4,5,8}, Michael Lehrke⁹, Corinna Lebherz⁹,
Daniela Yildiz^{10,11}, Andreas Ludwig¹⁰, Jacob F. Bentzon^{12,13},
Erik A. L. Biessen^{1,2} and Marjo M. P. C. Donners^{1*}

¹Department of Pathology, Cardiovascular Research Institute Maastricht (CARIM), Maastricht University Medical Center, Maastricht, Netherlands, ²Institute for Molecular Cardiovascular Research (IMCAR), RWTH Aachen University Hospital, Aachen, Germany, ³Interdisciplinary Centre for Clinical Research (IZKF), RWTH Aachen University Hospital, Aachen, Germany, ⁴Institute for Cardiovascular Prevention (IPEK), Ludwig Maximilian University of Munich, Munich, Germany, ⁵German Centre for Cardiovascular Research (DZHK), Partner Site Munich Heart Alliance, Munich, Germany, ⁶Department of Molecular Genetics, Cardiovascular Research Institute Maastricht (CARIM), Maastricht University Medical Center, Maastricht, Netherlands, ⁷Department of Medical Biochemistry, Amsterdam UMC, Locatie AMC, Amsterdam, Netherlands, ⁸Department of Biochemistry, Cardiovascular Research Institute Maastricht (CARIM), Maastricht University Medical Center, Maastricht, Netherlands, ⁹Department of Internal Medicine I, RWTH Aachen University Hospital, Aachen, Germany, ¹⁰Institute of Molecular Pharmacology, RWTH Aachen University Hospital, Aachen, Germany, ¹¹Institute of Experimental and Clinical Pharmacology and Toxicology, PZMS, ZHMB, Saarland University, Homburg, Germany, ¹²Experimental Pathology of Atherosclerosis Laboratory, Spanish National Center for Cardiovascular Research (CNIC), Madrid, Spain, ¹³Atherosclerosis Research Unit, Department of Clinical Medicine, Aarhus University, Aarhus, Denmark

Introduction: The transmembrane protease A Disintegrin And Metalloproteinase 10 (ADAM10) displays a “pattern regulatory function,” by cleaving a range of membrane-bound proteins. In endothelium, it regulates barrier function, leukocyte recruitment and angiogenesis. Previously, we showed that ADAM10 is expressed in human atherosclerotic plaques and associated with neovascularization. In this study, we aimed to determine the causal relevance of endothelial ADAM10 in murine atherosclerosis development *in vivo*.

Methods and results: Endothelial *Adam10* deficiency (*Adam10^{eko}*) in Western-type diet (WTD) fed mice rendered atherogenic by adeno-associated virus-mediated PCSK9 overexpression showed markedly increased atherosclerotic lesion formation. Additionally, *Adam10* deficiency was associated with an increased necrotic core and concomitant reduction in plaque macrophage content. Strikingly, while intraplaque hemorrhage and neovascularization are rarely observed in aortic roots of atherosclerotic mice after 12 weeks of WTD feeding, a majority of plaques in both brachiocephalic artery and aortic root of *Adam10^{eko}* mice contained these features, suggestive of major plaque destabilization. *In vitro*, ADAM10 knockdown in human coronary artery endothelial cells (HCAECs) blunted the shedding of lectin-like oxidized LDL (oxLDL) receptor-1 (LOX-1) and increased endothelial inflammatory

responses to oxLDL as witnessed by upregulated ICAM-1, VCAM-1, CCL5, and CXCL1 expression (which was diminished when *LOX-1* was silenced) as well as activation of pro-inflammatory signaling pathways. LOX-1 shedding appeared also reduced *in vivo*, as soluble LOX-1 levels in plasma of *Adam10^{ecko}* mice was significantly reduced compared to wildtypes.

Discussion: Collectively, these results demonstrate that endothelial ADAM10 is atheroprotective, most likely by limiting oxLDL-induced inflammation besides its known role in pathological neovascularization. Our findings create novel opportunities to develop therapeutics targeting atherosclerotic plaque progression and stability, but at the same time warrant caution when considering to use ADAM10 inhibitors for therapy in other diseases.

KEYWORDS

a disintegrin and metalloproteinase 10, atherosclerosis, endothelial cells, intraplaque hemorrhage, neovascularization, inflammatory signaling, LOX-1

1. Introduction

Atherosclerosis is a lipid-driven chronic inflammatory disease, which manifests in regions with disturbed flow in the medium- and large-sized arteries. The initiation of atherosclerosis is characterized by endothelial cell activation and dysfunction, leading to the disruption of the endothelial barrier function and the active recruitment of leukocytes into the vessel wall (1).

A crucial mechanism to regulate cell signaling and subsequent cellular responses, like cell recruitment, is proteolytic processing of transmembrane proteins, also referred to as (ectodomain) shedding. The A Disintegrin And Metalloproteinase (ADAM) family is involved in the shedding of numerous cell surface proteins, e.g., adhesion molecules, chemokines and cytokine receptors (2). One of the most prominent ADAM family members, ADAM10, has previously been reported to be implicated in several physiological and pathological processes, e.g., tumor growth and metastasis (2, 3). It is ubiquitously expressed, constitutively active in all vascular cells and deficiency of *Adam10* results in embryonic lethality at stage E9.5, when the vascular system develops (4). Indeed, and as a master regulator of Notch, ADAM10 is well known to have an important role in cardiovascular development (5, 6) and to limit sprouting angiogenesis and pathological neovascularization in developing mouse retina (7–9). Additionally, ADAM10 can regulate endothelial permeability and leukocyte transmigration by cleaving vascular endothelial cadherin (VE-Cadherin) (10, 11) and intracellular adhesion molecule-1 (ICAM-1) (12). ADAM10 has a large repertoire of substrates, many of which are involved in the pathogenesis of atherosclerosis, including lectin-like oxidized low-density lipoprotein (oxLDL) receptor 1 (LOX-1) (3, 13). Previously, we have shown that ADAM10 is expressed in human atherosclerotic arteries, correlating with plaque progression (11). In a conditional knockout mouse model, we demonstrated that deficiency of *Adam10* in myeloid cells did not affect atherosclerotic lesion size, but enhanced plaque stability by increasing fibrosis (14). ADAM10 was also expressed in plaque endothelium and associated with neovascularization (11). However, whether endothelial ADAM10 contributes in the pathogenesis of atherosclerosis or this increased expression reflects a disease-related response, e.g., an attempt to dampen/limit plaque neovascularization has not been investigated so far.

Here, we used the model of adeno-associated virus-mediated proprotein convertase subtilisin/kexin type 9 (PCSK9) gene transfer in mice deficient in endothelial *Adam10* (15–17), to investigate the causal role of endothelial ADAM10 in atherosclerosis development. We report that the absence of endothelial ADAM10 severely aggravates atherosclerotic plaque formation in mice. Moreover, while plaque granulocyte and collagen content remained unchanged, lesions of mice with endothelial *Adam10* deficiency had larger necrotic cores and concomitant lower macrophage content. Strikingly, lesions from *Adam10* deficient mice contained intraplaque microvessels and showed clear signs of intraplaque hemorrhage. These features have never been observed before at such early time point (12 weeks) in murine aortic root atherosclerotic lesions of Western type diet (WTD) fed mice (18). Knockdown of *ADAM10* in human coronary artery endothelial cells (HCAECs) challenged with oxidized low-density lipoprotein (oxLDL) resulted in a more severe pro-inflammatory, hence more pro-atherogenic, phenotype, in agreement with significantly reduced LOX-1 shedding.

2. Materials and methods

2.1. Animals

Mouse experiments were approved by the Animal Ethics Committee of Maastricht University, Netherlands (permit number 2013-009), and were performed in compliance with the Dutch government guidelines. Female endothelial specific (*Tie2-Cre*) *Adam10* knockout (*Adam10^{ecko}*) and wildtype (*Adam10^{wt}*) littermate control mice on a mixed genetic background were previously described (7) and generously provided by Dr. C. Blobel (New York, USA).

2.2. Baseline vessel morphometry

Left carotid arteries were collected from female wildtype and *Adam10^{ecko}* mice (aged 10–12 weeks; *n* = 7 and 8, respectively), fixed

overnight in 1% paraformaldehyde and embedded in paraffin. Cross-sections (4 μm) were cut and four sections (100 μm apart) were stained with Movat's stain to visualize the elastic laminae. Pictures were taken using a Leica DM3000 light microscope and sections were analyzed in a blinded manner using computerized morphometry (Leica QWin V3). For each mouse, total vessel area (area within external elastic lamina), medial area (area between internal and external elastic lamina), and lumen area (area within internal elastic lamina) were measured at 100 μm distance from the aortic arch.

2.3. Atherosclerotic lesion induction and analysis

Female wildtype and *Adam10^{ecto}* mice (aged 10–12 weeks; $n = 16$ and 14, respectively) were rendered prone to atherosclerosis by a single intravenous injection of adeno-associated virus serotype 8 containing D377Y-murine PCSK9 [AAV-PCSK9; 1×10^{11} vector genomes per mouse; as described previously (15)], followed by western type diet (WTD) feeding (0.25% cholesterol; Special Diets Services, Witham, Essex, UK). Blood was collected from the tail vein for analyses of plasma lipids at baseline (before WTD) and after 1, 3, 6, 9, and 12 weeks of WTD feeding after 4 h fasting. After 12 weeks of WTD feeding, mice were anesthetized, euthanized, and perfused with PBS containing nitroprusside (0.1 mg/ml, Sigma-Aldrich, Seelze, Germany). Mouse hearts and the brachiocephalic trunk (BC) of the right carotid artery were excised and fixed overnight in 1% paraformaldehyde. Serial paraffin sections of the aortic root were cut (4 μm) and stained with hematoxylin and eosin (H&E, Sigma) for morphometric analysis of lesion size, plaque, necrotic core area (defined as acellular regions) and plaque phenotype staging. Total plaque areas were obtained by averaging morphometric measurements of five representative H&E sections (20 μm apart) of the aortic root and five representative H&E sections (20 μm apart) of the BC. Plaque phenotype characterization was determined as previously described (19), with slight modifications. Plaques were classified as early (foam cell rich, but lacking a necrotic core), moderately advanced (containing a fibrotic cap and often a necrotic core, but no medial macrophage infiltration) and advanced lesions, typified by medial macrophage infiltrates, elastic lamina degradation and more pronounced necrosis and fibrosis. For each mouse, the aortic valves (three per mouse) was scored by an experienced pathologist in a blinded manner based on above described characteristics using a 0–5 scale (0–1: early, 2–3: moderate, 4–5: advanced; each valve was scored on the cross sections with the most advanced plaque stage) and these results were used to determine the percentages of the different stages. Martius, Scarlet and Blue (MSB) staining was used for semi-quantitative analyses of fibrin deposits (severity score of 1–5, average of 5 sections). Atherosclerotic lesions were further characterized for macrophage (MAC3, clone M3/84, 1:200, BD Biosciences, New Jersey, USA), granulocyte (Ly6G, clone 1A8, BD) and collagen (Sirius Red, Sigma) content. Minimal cap thickness was measured at the thinnest point of the fibrous cap. A polarization filter and birefringence color discrimination were used to differentiate various collagen structures (ranging from loosely patched—immature—thin collagen, to tightly packed—mature—thick collagen fibers), as described by MacKenna et al. (20). Additionally, sections were analyzed for microvessels (CD31, clone MEC13.3, 1:25, BD), apoptosis [Cleaved

Caspase-3 (Asp175, 1:100, Cell Signaling #9661)], and alpha smooth muscle actin (αSMA ; clone 1A4, 1:3000, Sigma). Cell nuclei were counterstained with hematoxylin. Immunofluorescent staining of erythrocytes in atherosclerotic lesions was performed using anti-TER-119 antibodies (1:500, Biolegend); cell nuclei were stained with DAPI. Pictures were taken using a Leica DM3000 light microscope and sections were analyzed in a blinded manner using computerized morphometry (Leica QWin V3). Necrotic core was defined as cell and nucleus free plaque area, containing cholesterol clefts.

2.4. Blood lipid analyses

Blood was collected at the start ($t = 0$) and after 1, 3, 6, 9, and 12 weeks of WTD. Plasma was separated by centrifugation ($2100 \times g$, 10 min, 4°C), and stored at -80°C until further use. Plasma cholesterol and triglycerides were determined using standard enzymatic kits (Cholesterol FS[®]10; Triglycerides FS 5[®] Ecoline; Diagnostic Systems GmbH, Holzheim, Germany) according to the manufacturer's instructions.

2.5. Cell culture

Human Primary Coronary Artery Endothelial Cells (HCAECs; CC-2585), EGM-2 Bulletkit medium (CC-3162) and ReagentPack Subculture Reagents (CC-5034) were purchased from Lonza. Cells were kept at 37°C and 5% CO_2 under sterile conditions in a humidified incubator. Subculturing and medium refreshing were performed according to the manufacturer's protocol. For *ADAM10* silencing studies, cells were transfected with either 20 nM negative control siRNA (Negative Control DsiRNA, Cat. nr. 51-01-14-03, Integrated DNA Technologies) or 20 nM *ADAM10* siRNA duplex mix (TriFECTa[®] Kit DsiRNA Duplex, Integrated DNA Technologies) consisting of the following duplexes: hs.Ri.ADAM10.13.1 (5'-rArUrCrArCrUrUrCrArArGrArArGrUrArArArGrCTA-3' and 5'-rUrArGrCrUrUrUrArCrUrUrCrUrArGrUrUrGrArArGrUrGrArUrGrU-3'), hs.Ri.ADAM10.13.2 (5'-rGrUrCrArUrGrUrUrArArArGrCrGrArUrUrGrArUrArCrAAT-3' and 5'-rArUrUrGrUrArUrCrArArUrCrGrCrUrUrUrArArCrArUrGrArCrUrG-3'), and hs.Ri.ADAM10.13.3 (5'-rCrArUrGrGrUrGrArArArCrGrCrArUrArArGrArUrCrAAT-3' and 5'-rArUrUrGrArUrUrCrUrUrArUrGrCrGrUrUrUrCrArCrCrArUrGrArA-3'). For *LOX-1* silencing studies, cells were transfected with either 20 nM negative control siRNA (Negative Control DsiRNA, Cat. nr. 51-01-14-03, Integrated DNA Technologies) or 20 nM *LOX-1* siRNA (Silencer Select, Ambion). Transfection was performed via siPORT[™] NeoFX[™] Transfection Agent according to the manufacturer's protocol (Invitrogen by Life Technologies). Cells were transfected for 24 h (for double knockdown of *ADAM10* and *LOX-1*, both siRNA complexes were combined) and the transfection efficiency was evaluated by qPCR. Cells were optionally treated with 25 $\mu\text{g}/\text{ml}$ oxLDL 24 h before evaluating the impact of *ADAM10* silencing.

2.6. Flow cytometry analyses

Absolute circulating leukocyte subset numbers were determined by flow cytometry calibrated using Trucount Beads (BD). Blood was

collected at the start ($t = 0$) and after 12 weeks of WTD. Erythrocytes were removed by incubation with erylisis buffer (155 mM NH_4Cl and 10 mM KHCO_3). Leukocytes were defined as CD45^+ (Biolegend), T-lymphocytes as $\text{CD45}^+ \text{CD3}^+$ (eBioscience) NK1.1^- (BD), NK cells as $\text{CD45}^+ \text{CD3}^- \text{NK1.1}^+$, B-lymphocytes as $\text{CD45}^+ \text{CD3}^- \text{NK1.1}^- \text{B220}^+$ (BD) granulocytes as $\text{CD45}^+ \text{CD3}^- \text{NK1.1}^- \text{B220}^- \text{CD11b}^+$ (BD) Ly6G^+ (BD), and monocytes as $\text{CD45}^+ \text{CD3}^- \text{NK1.1}^- \text{B220}^- \text{CD11b}^+ \text{Ly6G}^-$. Data were acquired using a FACS Canto II (BD Bioscience) and analyzed with FACSdiva software (BD Bioscience).

To measure protein expression of vascular adhesion molecule-1 (VCAM-1) and ICAM-1 on the cell surface of HCAECs, flow cytometric analysis was performed 24 h after transfection with ADAM10 siRNA (with or without LOX-1 siRNA). Cells were also simultaneously stimulated with or without 25 $\mu\text{g}/\text{ml}$ oxLDL. The HCAECs were then harvested and stained for VCAM-1 (eBioscience) and ICAM-1 (eBioscience).

2.7. RNA isolation and cDNA synthesis

Total RNA isolation from cell culture samples was performed by commercially available RNA isolation kit from Zymoresearch (Direct-zol microprep kit) according to the manufacturer's protocol. The quality (A_{260}/A_{280}) and the quantity ($\text{ng}/\mu\text{L}$) of the RNA was measured by NanoPhotometer N60/N50 (Implen). A ratio of ~ 2 for A_{260}/A_{280} was accepted as good quality RNA. RNA samples were diluted to the same concentration and the cDNA synthesis was performed *via* the commercially available iScript cDNA synthesis kit from Bio-Rad according to the manufacturer's protocol.

2.8. PCR

Quantitative real-time PCR was performed using PowerUpTM SYBRTM Green Master Mix (Life Technologies), according to the manufacturer's protocol. Real-time PCR reactions with the primer pair for ADAM10 (5'TTGCCCTCCTCTAAACCACTTCCA-3' and 5'AGGCAGTAGGAAGAACCAAGGCAA-3') or for ADAM17 (5'GGGAAGTGACTTAGCAGATG-3' and 5'CTAGATTACCTTCA CCTTACC-3') were performed using the ViiA7 Real Time PCR system (Life Technologies). Gene expression was normalized to Beta Actin according to the $\Delta\Delta\text{Ct}$ method.

2.9. RNA preparation and sequencing

Snap frozen aortic arches from atherosclerotic *Adam10^{wt}* and *Adam10^{cko}* mice were pooled (three pools of two aortic arches) and RNA was extracted as described above. Library construction was done by using Oligo(dT) magnetic beads to select mRNA with poly(A) tail or hybridize the rRNA with DNA probe and digest the DNA/RNA hybrid strand, followed by DNase I reaction to remove DNA probe. After purification, the target RNA was obtained. The target RNA and reverse transcription was fragmented to double-strand cDNA (dscDNA) by N6 random primer, which was followed by end repair of the dscDNA with phosphate at 5' end and stickiness "A" at 3' end, and ligation and adaption with stickiness "T" at 3' end to the dscDNA. Two specific primers are used to amplify the ligation product, and

the PCR product was denatured by heat and the single-strand DNA is cyclized by splint oligo and DNA ligase followed by sequencing on the prepared library. Samples were sequenced by BGISEQ-500 system.

2.10. RNA-sequencing data analysis

Raw sequences were aligned to the murine reference cDNA (GRCm39.v107) obtained from the Ensembl using kallisto (v0.48.0) (21). Transcript abundances were aggregated into gene level by the R package tximport (v1.22.0) (22). Genes with an average read count below 5 were removed. In addition, only protein-coding genes were included, resulting in 14,980 genes for differential expression analysis.

Based on the raw read counts, gene differential expression analysis was performed by the R package DESeq2 (v1.34.0) (23) with the parameter alpha set as 0.05. The Benjamini-Hochberg procedure was used to adjust the p -values to decrease the false discovery rate. We set \log_2 fold change > 0 (up-regulation) or < 0 (down-regulation) as well as a significance level of adjusted p -value = 0.05 as the thresholds for significantly differentially expressed genes (DEGs). Raw read counts were normalized using the variance stabilizing transformation provided in the DESeq2 package for heatmap visualization.

We associated gene differential expression with biological functions by gene set overrepresentation analysis (GSEA) and gene set enrichment analysis (GSEA) (24). For GSEA, we analyzed the significantly up-/down-regulated genes separately to associated DEGs with Gene Ontology annotation terms. GSEA was performed on the list of all analyzed genes sorted based on \log_2 fold change from high to low based on hallmark gene sets obtained from the Molecular Signatures Database. Both analyses were performed using the R package clusterprofiler (v4.2.2) (25). P -values were corrected by the Benjamini-Hochberg procedure.

The raw sequencing data analyzed in this study have been deposited into the Gene Expression Omnibus (GEO) with the accession number GSE209602.

2.11. ELISA

LOX-1, CCL5, and CXCL1 levels in supernatant were measured with the LOX-1/OLR1 Human ELISA kit (ThermoFisher), ELISA Deluxe set human CCL5 (Biolegend) and Human GROa uncoated ELISA kit (ThermoFisher), respectively. LOX-1 was measured in murine plasma using the Mouse LOX-1/OLR1 ELISA kit (ThermoFisher).

2.12. Kinase activity profiling

Kinase profiles were determined using the PamChip[®] peptide based tyrosine kinase (PTK) and the PamChip[®] Ser/Thr Kinase (STK) microarray system on PamStation[®]12 (PamGene International, 's-Hertogenbosch, Netherlands). Each PTK-PamChip[®] array contains 196 individual phospho-site(s) that are peptide sequences derived from substrates for Tyrosine kinases. Each STK-PamChip[®] array contains 144 individual phospho-site(s) that are peptide sequences derived from substrates for Ser/Thr kinases. Peptide phosphorylation is visualized by detection of the fluorescent signal emitted after binding of the FITC-conjugated antibody to

the phosphorylation site. HCAECs were transfected and stimulated with/without oxLDL as described above and subsequently washed once in ice-cold PBS, with 4 biological replicates per condition, and lysed for 15 min on ice using M-PER Mammalian Extraction Buffer containing Halt Phosphatase Inhibitor and EDTA-free Halt Protease Inhibitor Cocktail (1:100 each; Thermo Fischer Scientific). Lysates were centrifuged for 15 min. at $16,000 \times g$ at 4°C in a pre-cooled centrifuge. Protein quantification was performed with PierceTM Coomassie Plus (Bradford) Assay according to the manufacturer's instructions.

For the PTK assay, $10.0 \mu\text{g}$ and for the STK assay, $2.0 \mu\text{g}$ of protein was applied per array ($N = 4$ per condition) and carried out using the standard protocol supplied by Pamgene International B.V. Images were recorded by a CCD camera PamStation[®] 12. The spot intensity at each time point was quantified (and corrected for local background) using the BioNavigator software version 6.3 (PamGene International, 's-Hertogenbosch, Netherlands). Upstream Kinase Analysis (UKA) (26), a functional scoring method (PamGene) was used to rank kinases based on combined specificity scores (based on peptides linked to a kinase, derived from 6 databases) and sensitivity scores (based on treatment-control differences).

Over-representation analyses (ORA) of the Kyoto Encyclopedia of Genes and Genomes (KEGG) database for the kinases with significant differences from control were performed using the ClusterProfiler R-package (27). The list of kinases of interest contains the kinases with higher Median Final Scores (> 1.2). The p -values were adjusted for multiple comparisons by false discovery rate (FDR).

2.13. Statistics

Data are expressed as mean \pm standard error of the mean (SEM). Statistical analysis was performed using GraphPad Prism version 9.1.1 (GraphPad Software, Inc., San Diego, CA, USA). Outliers were identified using the ROUT = 1 method. Gaussian distribution was tested via the D'Agostino-Pearson omnibus normality test, while homogeneity of variance by Levene's test. Significance was tested using either Student's t -test (with Welch correction as required) or Mann-Whitney U -test for normally and non-normally distributed data, respectively, unless stated otherwise. A two-tailed p -value < 0.05 was considered statistically significant.

3. Results

3.1. Endothelial *Adam10* deficiency significantly augments atherosclerosis development

To investigate the causal impact of endothelial ADAM10 in atherosclerosis, *Adam10^{wt}* and *Adam10^{cko}* mice were rendered atherogenic via adeno-associated virus (AAV) aided murine PCSK9 gene transfer (15), followed by WTD feeding for 12 weeks. As expected, WTD feeding resulted in a prominent increase in plasma cholesterol and triglycerides levels, though no differences were observed between both ADAM10 genotypes (Figure 1A). Additionally, endothelial *Adam10* deficiency had no effect on general leukocyte numbers in the blood before or after 12 weeks of WTD feeding (Supplementary Figure 1A). At baseline, i.e., under

normolipidemic conditions, there was no indication for any large vessel abnormalities, based on left carotid artery morphometry (Supplementary Figures 1B, C). Furthermore, body weight after 12 weeks of WTD feeding was not changed between groups (Supplementary Figure 1D).

Although ADAM10 expression in human atherosclerosis positively correlates with disease progression and endothelial *Adam10* knockdown is known to reduce leukocyte recruitment (13), endothelial *Adam10* deficiency resulted in a remarkable 45% increase in atherosclerotic plaque size in the aortic root, compared to wildtype controls (Figures 1B, C). Besides this significant increase in plaque size, *Adam10^{cko}* mice also showed a noteworthy increase in plaque progression (Figure 1D). In addition, plaque expansion and progression in *Adam10^{cko}* mice was associated with a significantly increased (50%) relative necrotic core content (Figure 1E), with a concomitant decrease in relative macrophage content (Figure 1F), while the absolute macrophage area and cleaved Caspase-3 area were unchanged (Supplementary Figures 1E, F). In contrast, granulocyte (Figure 1G) and total collagen (Figure 1H) contents were unchanged between both genotypes. Collagen fibers in *Adam10^{cko}* plaques were more mature (Figure 1I) and minimal cap thickness increased (Figure 1J).

Interestingly, endothelial *Adam10* deficiency also significantly increased the plaque area in the brachiocephalic trunk of the right carotid artery (BC), a site where lesion development generally is less progressed than in the aortic root (Figure 2A). This is also the only site in mice where advanced lesions incidentally were seen to display signs of plaque rupture or intraplaque hemorrhage (IPH) (18). Interestingly, overt fibrin deposits, reflective of IPH associated thrombus formation, were found in 5 out of 8 *Adam10^{cko}* mice, while only minor fibrin deposits were seen in 2 out of 8 *Adam10^{wt}* mice (Figure 2B).

3.2. Aortic root plaques of *Adam10^{cko}* mice show overt intraplaque hemorrhage and neovascularization

Remarkably, further examination revealed that atherosclerotic plaques in the aortic root from *Adam10^{cko}* mice were also rich in IPH and neovessels, which to our knowledge is the first report at this site, especially at this relatively early time point (12 weeks WTD, i.e., ~ 22 weeks of age, Figures 3A, B). This IPH consisted mainly of erythrocytes (in contrast to the fibrin deposits observed in the brachiocephalic artery) was confirmed by TER-119 staining for erythrocytes (Figure 3C) and shown to be present in a striking 62% of *Adam10^{cko}* mice, significantly higher compared to *Adam10^{wt}* mice, which did not contain any hemorrhages at all (Figure 3B). IPHs were not only observed near the abluminal side of the intima (Figures 3A, C), but also more closely to the lumen (Figure 3D). Intraplaque microvessels, which are most likely functional based on the presence of intraluminal erythrocytes, were sixfold more frequent in aortic root plaques of *Adam10^{cko}* mice (Figures 3A, E). Moreover, aortic root plaques of *Adam10^{cko}* mice contained intraplaque CD31⁺ α SMA⁺ cell clusters, which may represent (immature) vessels or sites of endothelial-to-mesenchymal transition (28) (Figures 3F–H). While ADAM10 is known to control angiogenic processes in a non-atherosclerotic setting (7–9), these observations clearly indicate not only a protective role for ADAM10 in plaque neovascularization,

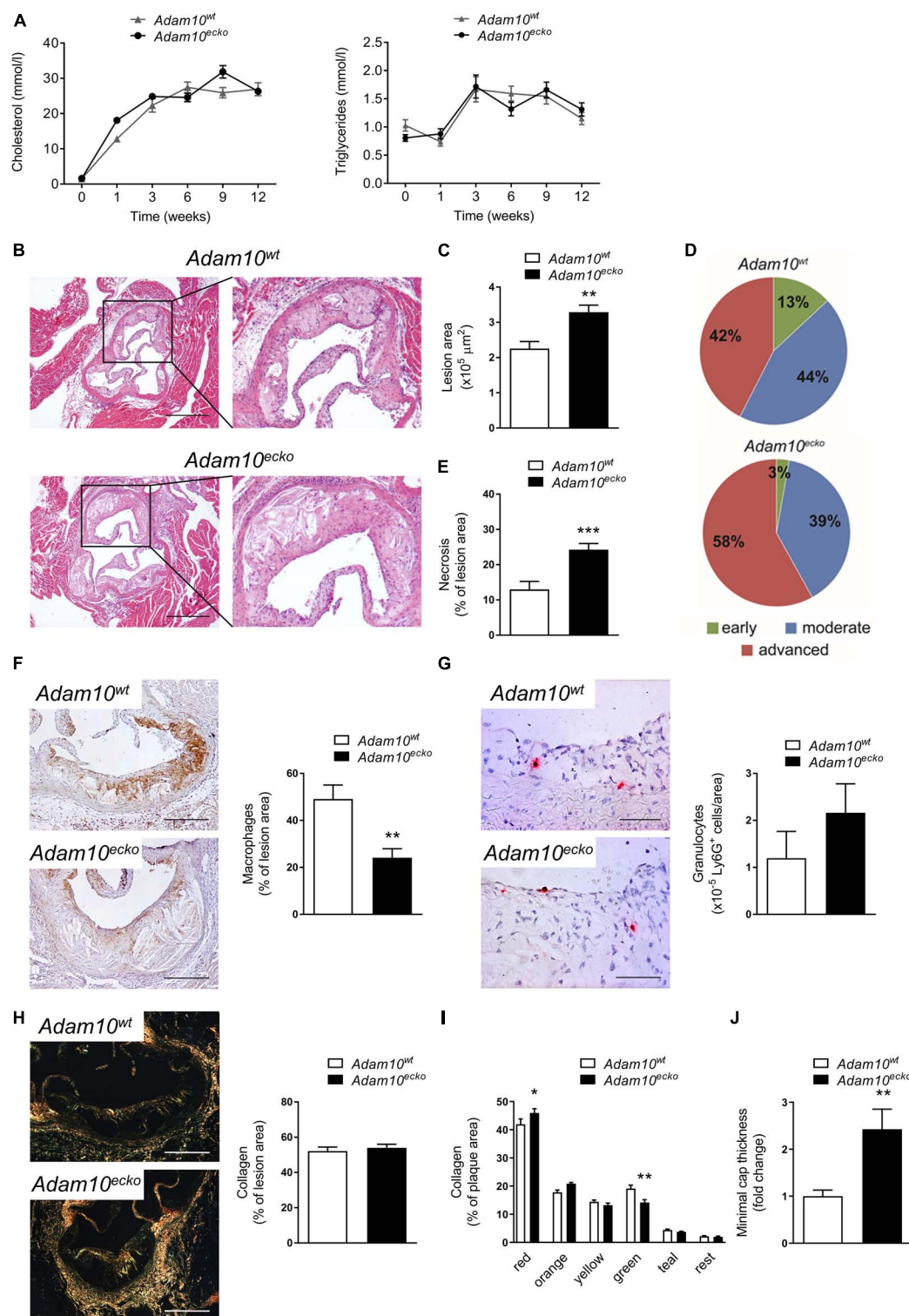
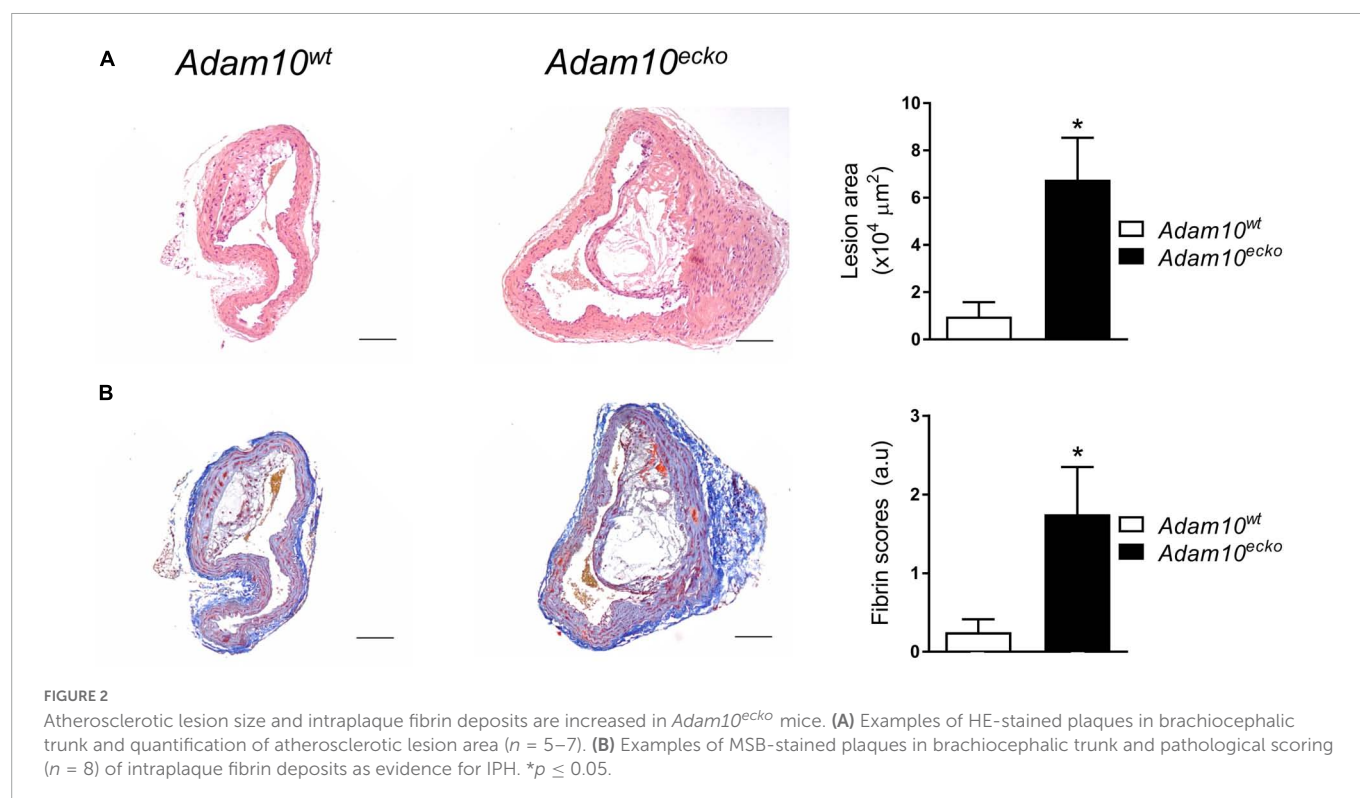


FIGURE 1

Adam10^{cko} significantly increases atherosclerotic lesion formation and intraplaque necrosis. Endothelial *Adam10* deficient (*Adam10^{cko}*) and wildtype mice (*Adam10^{wt}*) mice were rendered hyperlipidemic by AAV8-PCSK9 gene transfer, followed by 12 week western type diet feeding. (A) Plasma cholesterol and triglyceride levels ($n = 13-16$). (B–D) Atherosclerotic lesion area (B,C) and plaque stage quantification (D) in the aortic root (H&E staining, $n = 13-15$; scale bar, 400 μm). Indicated percentages reflect the total number of valves (three per mouse) that are classified as belonging to the respective plaque stage. (E) Quantification of necrotic core area ($n = 13-16$). (F–H) Representative images of (immuno)histological stainings for macrophages (F, MAC3⁺; $n = 12-14$; scale bar, 200 μm), granulocytes (G, Ly6G⁺, $n = 13-16$; scale bar, 100 μm) and total collagen (H, Sirius Red imaged with polarized light; $n = 13-16$; scale bar, 200 μm) in aortic root atherosclerotic plaques with quantification. (I) Quantification of different collagen fibers in the plaques, ranging from thick—mature collagen (red), to loosely packed—thin collagen fibers (green) ($n = 13-16$). Sidak's multiple comparison test was conducted to determine the statistical significance between the two groups. (J) Quantification of minimal cap thickness ($n = 13-15$). * $p \leq 0.05$; ** $p \leq 0.01$; *** $p \leq 0.001$.



but also in atherosclerosis development and progression, suggesting a crucial role of endothelial ADAM10 in maintaining endothelial quiescence/homeostasis.

3.3. Atherosclerotic plaques from *Adam10^{ecko}* mice demonstrate a more inflamed phenotype

In order to examine the underlying mechanisms by which endothelial specific *Adam10* deficiency affects the atherosclerotic vessel, we mapped the changes in transcriptional makeup by bulk RNA-sequencing of aortic arches from atherosclerotic *Adam10^{ecko}* and *Adam10^{wt}* mice. We detected 181 differentially expressed genes (DEGs), of which 103 genes were significantly up- and 78 genes downregulated upon endothelial *Adam10* deficiency (Figures 4A, B). Albeit bulk-sequencing has limitations over single-cell plaque analysis (29) as it cannot specify the cell-origin of the detected genes, we did detect well-known endothelial specific genes, e.g., von Willebrand factor, which is a known marker of endothelial dysfunction involved in platelet and leukocyte adhesion (30, 31), to be highly upregulated in plaques of *Adam10^{ecko}* mice. Interestingly, although not specific for endothelium, another highly upregulated gene *Arhgap45* has been suggested to negatively regulate endothelial barrier function (32). Over-representation analysis (ORA) revealed enrichment of GO pathways involved in inflammation, immune cell activation and cell adhesion in *Adam10^{ecko}* mice (Figure 4C), of which the latter process involves DEGs both relevant for leukocyte adhesion to endothelium as well as endothelial integrity and cell-cell adhesion. In line with the GSEA results, GSEA also clearly demonstrates an increase in inflammatory response and inflammatory signaling pathways like IL-6-JAK-STAT3 signaling in plaques from *Adam10^{ecko}* mice compared to *Adam10^{wt}* mice

(Figure 4D). Combined, these results suggest that mice with an endothelial *Adam10* deficiency have plaques with a more inflamed phenotype.

3.4. ADAM10 silencing induces pro-atherogenic phenotype in HCAECs upon oxLDL stimulation

To further investigate the underlying mechanisms by which ADAM10 affects endothelial cells in an atherogenic environment, we silenced *ADAM10* in HCAECs (Supplementary Figure 2A), which did not result in a compensatory upregulation of its closely related family member *ADAM17* (Supplementary Figure 2B), and challenged them with pro-atherogenic oxLDL. Since the adhesion molecules ICAM-1 and VCAM play an important role in atherogenesis and are known substrates of ADAM-proteases (12, 33), the effect of *ADAM10* silencing on their surface expression was evaluated. Though ADAM10 was previously shown to regulate ICAM-1 cleavage (12), at least in TNF-stimulated human umbilical vein endothelial cells, we did not find differences in unstimulated cells. However, oxLDL exposure led to increased ICAM-1/VCAM-1 surface expression (Figure 5A), suggesting an enhanced response to oxLDL in *ADAM10* deficient endothelial cells. The more pro-inflammatory and pro-atherogenic phenotype of oxLDL-stimulated HCAECs after silencing *ADAM10* was further substantiated by the observed increased secretion of the chemokines CXCL1 and CCL5 compared to control oxLDL treated HCAECs (Figure 5B). Furthermore, kinomic analysis confirmed that *ADAM10* silencing induced pro-inflammatory signaling in oxLDL treated HCAECs, exemplified by amongst others increased phosphorylation of p38 and Src (Figure 5C). Furthermore KEGG analysis demonstrated that *ADAM10* silencing results in increased PI3K-Akt and MAPK

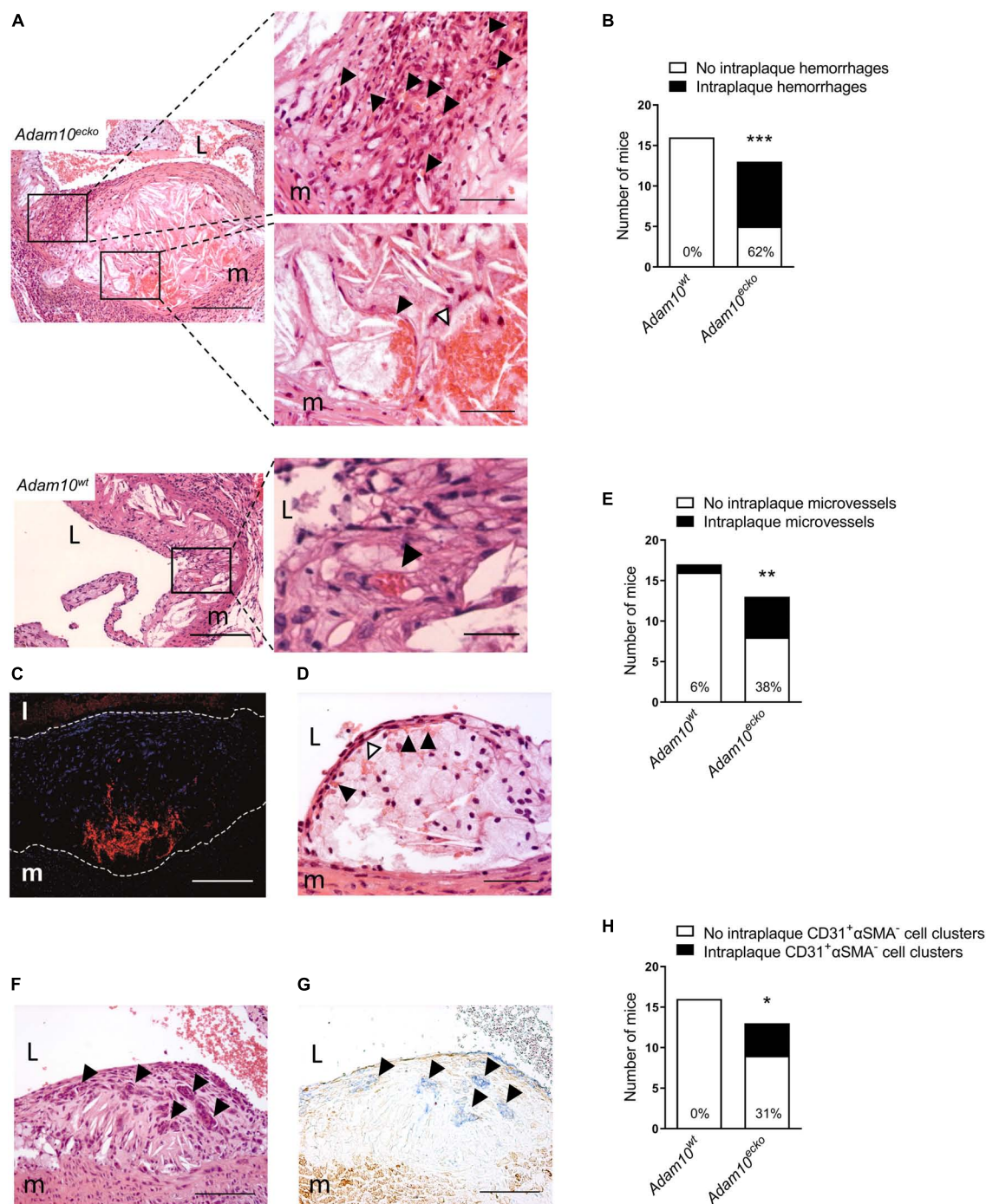


FIGURE 3

Atherosclerotic lesions of *Adam10^{ecko}* mice display several plaque destabilizing features. (A) *Adam10^{ecko}* left panel: Atherosclerotic lesion in the aortic root containing pronounced intraplaque hemorrhage and microvessels of an *Adam10^{ecko}* mouse (H&E, scale bar, 400 μ m). *Adam10^{ecko}* upper right detail panel: Detail of multiple small microvessels containing erythrocytes (indicated with black arrowheads) in aortic root lesion (H&E, scale bar, 200 μ m). *Adam10^{ecko}* lower right detail panel: Detail of a large microvessel containing erythrocytes (indicated with black arrowhead) and intraplaque hemorrhage (indicated with white arrowhead) at the plaque base in the aortic root (H&E, scale bar, 50 μ m). *Adam10^{wt}* left panel: Atherosclerotic lesion in the aortic root of an *Adam10^{wt}* mouse containing a microvessel (H&E, scale bar, 400 μ m). *Adam10^{wt}* right detail panel: Detail of the microvessel containing erythrocytes (indicated with black arrowhead) in aortic root lesion (H&E, scale bar, 50 μ m). (B) Quantification of intraplaque hemorrhage in aortic root of *Adam10^{wt}* and *Adam10^{ecko}* mice after 12 weeks on western type diet. (C) Immunofluorescence staining of erythrocytes (TER-119, red) in the atherosclerotic intima (cell nuclei, DAPI, blue) of an adjacent slide shown in panel (A; scale bar, 100 μ m). Lesion borders are indicated with dashed lines. (D) Atherosclerotic lesions containing intraplaque hemorrhage (indicated with white arrowheads) possibly originating from neovessels from the luminal side of the aorta (indicated with black arrowheads; H&E, scale bar, 100 μ m). (E) Quantification of intraplaque microvessels in aortic root of *Adam10^{wt}* and *Adam10^{ecko}* mice after 12 weeks on western type diet. (F,G) Clusters of cells (indicated with black arrowheads) within an atherosclerotic lesion of an *Adam10^{ecko}* mouse (F, H&E, scale bar, 100 μ m), which are positive for CD31 (G, blue, indicated by black arrowheads) and negative for α -SMA (G, brown; scale bar, 100 μ m). (H) Quantification of intraplaque CD31⁺αSMA⁻ cell clusters in aortic root of *Adam10^{wt}* and *Adam10^{ecko}* mice after 12 weeks on western type diet. L, lumen; m, media. Fisher's exact test was conducted to determine the statistical significance between the two groups. * $P \leq 0.05$; ** $P \leq 0.01$; *** $P \leq 0.001$.

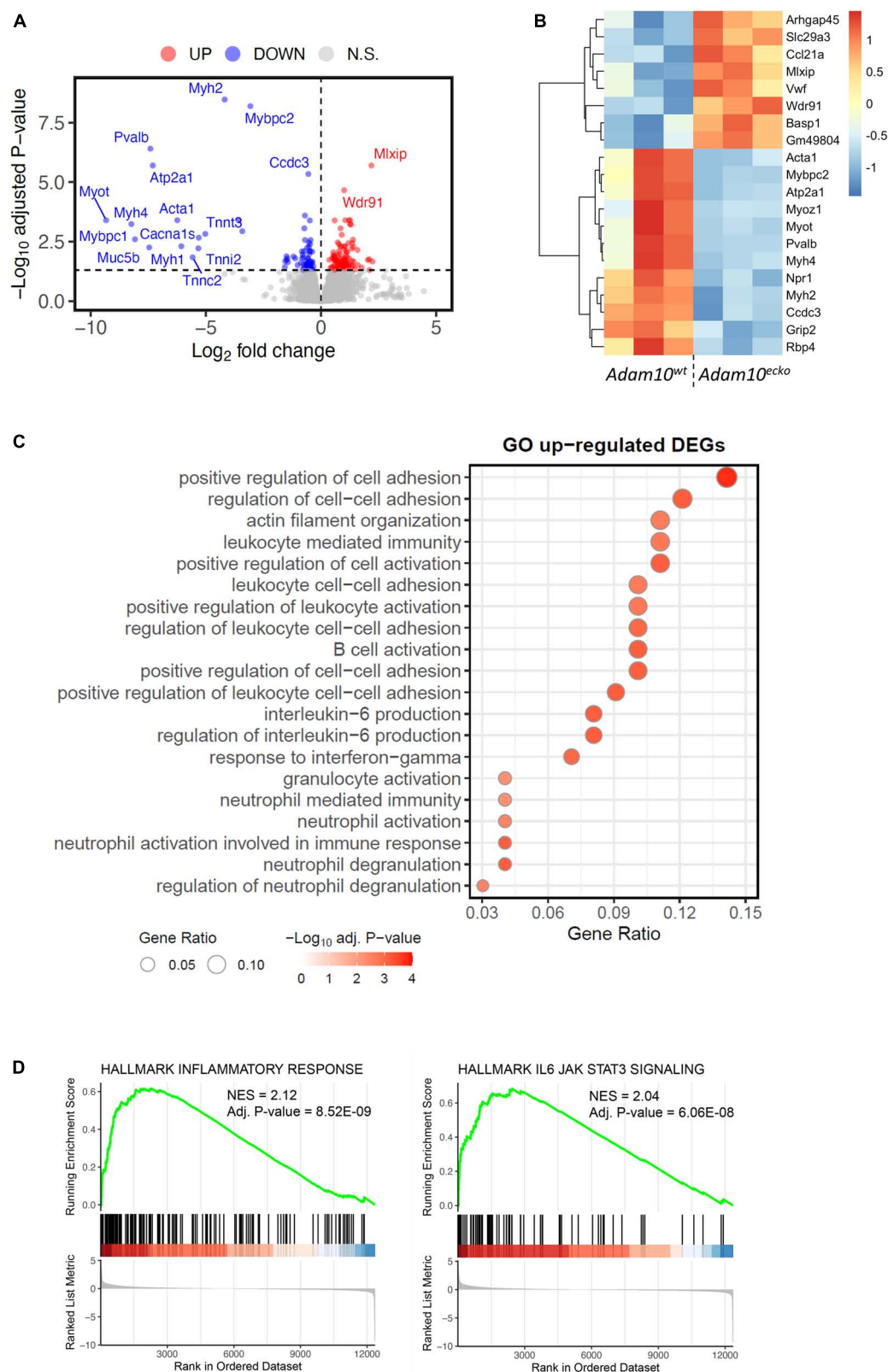


FIGURE 4

RNA-sequencing demonstrates an inflammatory genetic profile in vessels from *Adam10^{cko}* mice. (A) Volcano plot visualizing up-/downregulated genes in *Adam10^{cko}* vs. *Adam10^{wt}* mice. Horizontal line represents adjusted *p*-value of 0.05, while vertical lines represent \log_2 FC of 0. N.S., not-significant.

(B) Heatmap of top 20 most differentially expressed genes. Variance stabilizing transformed expression values are z-normalized per gene/row. (C) Gene ontology of vessels from *Adam10^{cko}* vs. *Adam10^{wt}* mice evaluated by GSEA. (D) GSEA figures showing the dysregulation of inflammatory responses and IL6-JAK-STAT3 signaling in *Adam10^{cko}* vs. *Adam10^{wt}* mice.

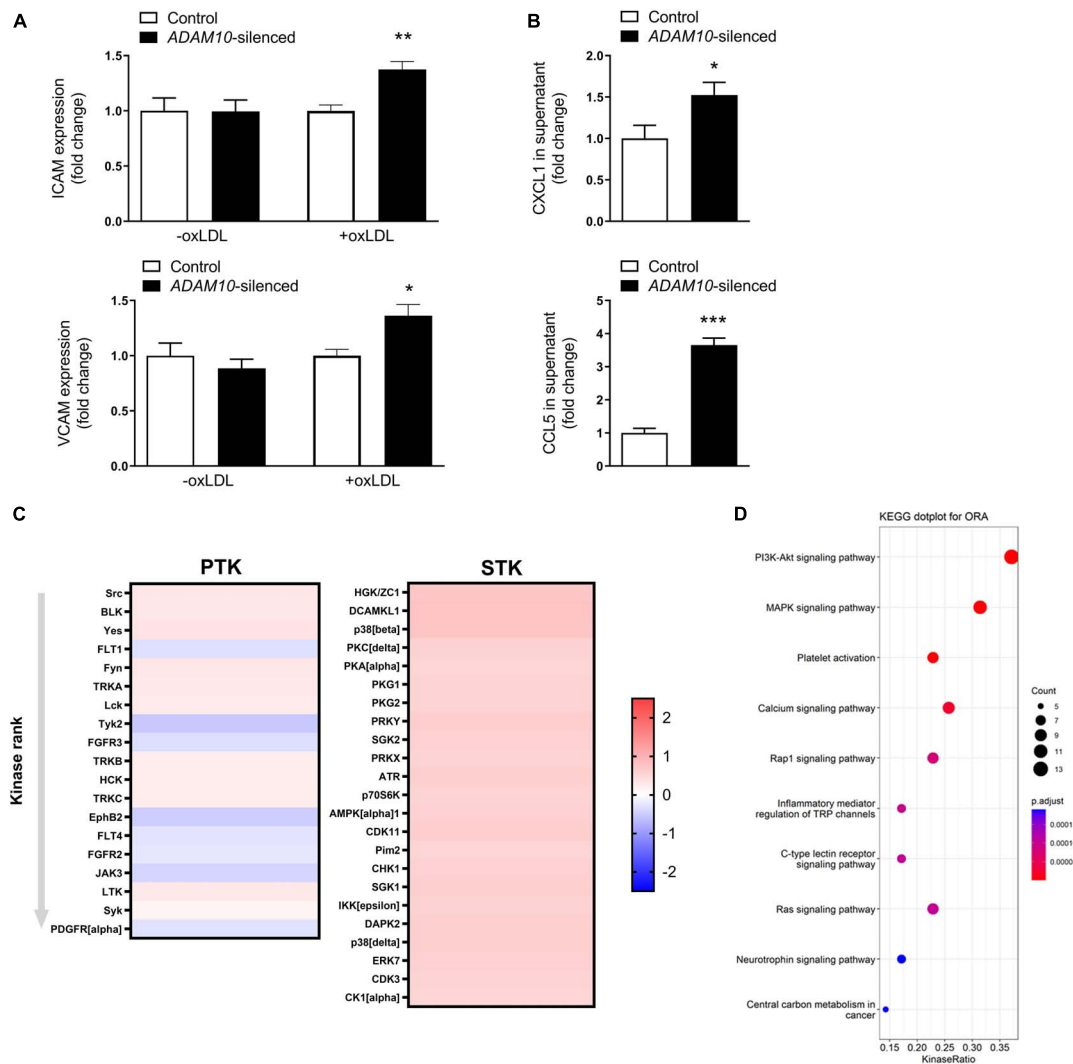


FIGURE 5

ADAM10 silencing results in a pro-inflammatory, pro-atherogenic phenotype in HCAECs. **(A)** Surface expression of ICAM and VCAM, measured by flow cytometry in control and *Adam10* silenced HCAECs stimulated with or without 25 μ g/ml oxLDL for 24 h ($n = 3-6$). Fold change has been determined for each condition by comparing to the respective control condition. **(B)** Quantification of soluble CCL5 and CXCL1 in supernatant of control and *ADAM10* silenced HCAECs stimulated with 25 μ g/ml oxLDL for 24 h, measured by ELISA ($n = 8-11$). **(C)** Kinomic analysis of control and *ADAM10* silenced HCAECs stimulated with 25 μ g/ml oxLDL for 30 min. Visualized is the heatmap of kinases that are up-regulated upon *ADAM10* silencing after oxLDL stimulation. Red color reflects increased phosphorylation, while blue color reflects decreased phosphorylation in *ADAM10* silenced HCAECs (fold change compared to scrambled control cells, $n = 4$). **(D)** Dot plot for over-representation analysis (ORA) of KEGG with significant differences from control using the PTK and STK dataset. Visualized are the top 10 of upregulated pathways in *ADAM10* silenced HCAECs, stimulated with 25 μ g/ml oxLDL for 30 min. * $p \leq 0.05$; ** $p \leq 0.01$; *** $p \leq 0.001$.

signaling, known downstream pathways of LOX-1 and mediators of ICAM and chemokine expression in mouse aortic endothelial cells (34, 35) (Figure 5D).

3.5. The inflammatory and pro-atherogenic phenotype of endothelial cells lacking *ADAM10* is LOX-1 dependent

Since the observed inflammatory effects in HCAECs upon *ADAM10* silencing seem to be dependent on oxLDL stimulation, we evaluated the shedding of the endothelial oxLDL receptor LOX-1, which is a known substrate of *ADAM10* (36), previously also shown to be involved in pro-inflammatory responses to oxLDL

in mouse aortic endothelial cells (35). Indeed, *ADAM10* silencing strongly decreased LOX-1 shedding in HCAECs, as evidenced by a decrease in soluble LOX-1 in the cells' culture medium (Figure 6A). To investigate whether LOX-1 is indeed causally involved in the observed inflammatory and pro-adhesion effects, we silenced *LOX-1* in combination with *ADAM10* in HCAECs. In line with our expectation, *LOX-1* silencing significantly reduced ICAM and VCAM expression after oxLDL stimulation of *ADAM10*-silenced HCAECs (Figure 6B). Additionally, also the secretion of CXCL1 and CCL5 in response to oxLDL stimulation is significantly reduced upon *LOX-1* silencing (Figure 6C). Importantly, we could confirm that LOX-1 shedding is also affected by endothelial *Adam10* deficiency *in vivo*, as soluble LOX-1 levels in the plasma were significantly reduced in *Adam10^{ecko}* mice (Figure 6D). In summary, reduced LOX-1 shedding in *ADAM10*-deficient endothelium may render these mice

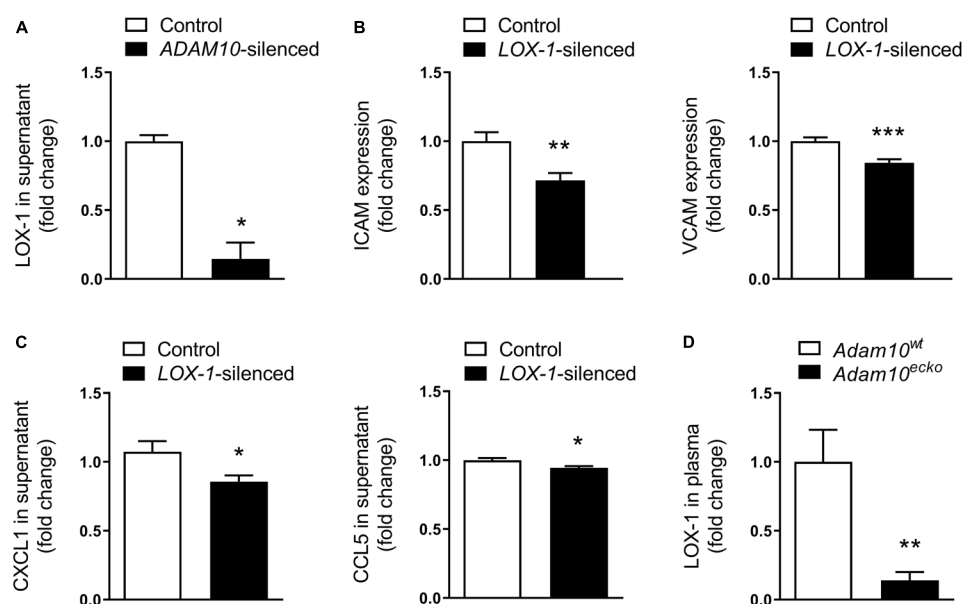


FIGURE 6

LOX-1 shedding is a key mediator in the observed pro-inflammatory and pro-atherogenic effects by endothelial ADAM10. (A) Quantification of soluble LOX-1 in supernatant of control and ADAM10 silenced HCAECs stimulated with 25 μ g/ml oxLDL for 24 h, measured by ELISA ($n = 3$). (B) Surface expression of ICAM and VCAM, measured by flow cytometry in control and LOX-1 silenced HCAECs (all conditions were additionally ADAM10 silenced) stimulated with or without 25 μ g/ml oxLDL for 24 h ($n = 9$). (C) Quantification of soluble CCL5 and CXCL1 in supernatant of control and LOX-1 silenced HCAECs (all conditions were additionally ADAM10 silenced) stimulated with 25 μ g/ml oxLDL for 24 h, measured by ELISA ($n = 15-22$). (D) Plasma LOX-1 levels in Adam10^{ecko} and Adam10^{wt} mice ($n = 11-14$). * $p \leq 0.05$; ** $p \leq 0.01$; *** $p \leq 0.001$.

more susceptible to oxLDL-induced inflammatory processes and atherosclerosis.

4. Discussion

This study is the first to establish that endothelial Adam10 deficiency significantly exacerbates atherosclerotic lesion formation and promotes plaque vulnerability in mice, with increased necrosis, IPH and neovascularization as most frequent features. These findings are in line with previous literature showing vascular abnormalities and increased (pathological) neovascularization in endothelial Adam10 deficient mice (7–9). However, they are in sharp contrast to the significantly reduced atherosclerosis development in mice with endothelial deficiency of Adam17, a family member with a large overlap in substrate repertoire (37).

Especially the observation of substantial IPHs and neovascularization in Adam10^{ecko} mice was to our knowledge unprecedented at this site and age of mice. In previous studies IPH and intraplaque microvessels were only detected in the carotid or brachiocephalic artery of aged (> 40 weeks) atherosclerosis-prone mice (38), upon prolonged WTD feeding of Apoe^{-/-} mice (> 40 weeks) (39), after surgical (40), pharmacological [focal mast cell activation (41)] intervention or with haploinsufficiency of a key extracellular matrix component (fibulin-1) (42). IPH has already been identified as critical factor in necrotic core expansion and plaque growth (43), features that we have also observed in Adam10^{ecko} mice. The decreased relative lesional macrophage content and necrotic core expansion are therefore likely the resultants of the more advanced plaque progression stage in Adam10^{ecko} mice. Whether this is causal in or secondary to the overt presence of intraplaque microvessels, which are known to provide a major portal for lipids,

leukocytes and cholesterol-rich erythrocytes into the atherosclerotic plaque (38, 44, 45), remains to be addressed. Besides this novel observation of tissue neovascularization under chronic inflammatory conditions, several lesions from Adam10^{ecko} mice also contained CD31⁺ α SMA⁺ cell clusters resembling hyperplastic endothelial cells, which were previously only observed in the intestines and kidneys of Adam10^{ecko} mice (7).

The broad pattern regulatory function of ADAM10 makes it challenging to pinpoint a single responsible key mediator for the observed phenotype in Adam10^{ecko} mice. Angiogenesis, the sprouting of new blood vessels from the existing vasculature, is a tightly regulated process which is induced by various stimuli, including pro-angiogenic growth factors, like vascular endothelial growth factor (VEGF), hypoxia, metabolic stress and inflammation (46). ADAM10 has already been shown to be able to regulate the angiogenic process through shedding of various key receptors, including VEGF receptor 2 (VEGFR2) and Notch (9, 11, 47). ADAM10-mediated Notch cleavage, for example, is a crucial step in Notch activation, which in endothelial cells limits tip cell selection and sprout formation, thereby reducing excessive sprouting and branching (48). Interestingly, interference with Notch signaling phenocopies the vascular abnormalities caused by ADAM10 deletion under baseline conditions (7–9), suggesting that reduced Notch signaling most likely underlies the pathological neovascularization in atherosclerotic lesions caused by endothelial Adam10 deficiency.

A second important mechanism potentially contributing to the profound plaque phenotype of endothelial Adam10 deficiency involves ADAM10's inflammation dampening functions. As highlighted in this and other studies (12), endothelial ADAM10 plays an important role in the cleavage of adhesion molecules, necessary for efficient transmigration. Thereby, a lack of ADAM10 results in increased and prolonged leukocyte adhesion to the vascular wall,

though eventually does not restrict leukocyte transmigration (12). Our RNAseq data indeed confirm that *Adam10^{eko}* atherosclerotic plaques are more inflammatory, with an enrichment in inflammatory signaling, immune cell activation and cell adhesion, which could reflect both leukocyte adhesion and angiogenic processes. Previously, we have demonstrated that endothelial ADAM10 is responsible for the shedding of LOX-1, thereby increasing the surface expression of this pro-atherogenic receptor for oxLDL (34, 35). It has already been shown in fibroblasts that increased *Lox-1* expression results in an increased expression of ICAM-1 and VCAM (49) and also in mouse aortic endothelial cells, enhanced LOX-1 signaling upregulated ICAM-1 and increased pro-inflammatory signaling via ERK1/2 and p38 (34, 35), we could confirm in HCAECs that *ADAM10* deficiency indeed reduced LOX-1 shedding and enhanced endothelial proinflammatory responses to oxLDL, including p38 activation and chemokine secretion. Interestingly, the fact that ADAM17 appeared not to be involved in LOX-1 cleavage (35) might explain, at least partly, the different impact on atherogenesis between endothelial *Adam10* and *Adam17* deficiency (37).

Taken together, this study demonstrates that endothelial ADAM10 is a protective factor in atherosclerosis, on the one hand by restraining plaque neovascularization and intraplaque hemorrhage, and on the other hand by limiting inflammation. While the ADAM10-Notch axis is a well-known master regulator of neovascularization, this study demonstrates a crucial role of ADAM10 in pro-inflammatory processes in endothelial cells, at least in part by regulating expression of leukocyte adhesion molecules and by controlling receptor availability for pro-atherogenic stimuli, as demonstrated for LOX-1. Although it remains to be determined to what extent endothelial ADAM10 can influence these vulnerable plaque features in humans, its overt expression in intraplaque microvessels in human plaques suggests an active regulatory function in humans as well (11).

Data availability statement

The raw data supporting the conclusions of this article will be made available by the authors, without undue reservation.

Ethics statement

The animal study was reviewed and approved by the Animal Ethics Committee of Maastricht University, Netherlands.

Author contributions

EV, EB, and MD: conceptualization. EV, KT, SM, and MD: methodology. EV, KT, SM, LP, HJ, TR, MG, MR, and YJ: formal

analysis and investigation. EV and KT: writing—original draft preparation. EB and MD: writing—review and editing. EV and MD: funding acquisition. CW, ML, CL, DY, AL, and JB: resources. MD: supervision. All authors contributed to the article and approved the submitted version.

Funding

This work was supported by the Dutch Heart Foundation (Dr. E. Dekker grant 20120T79) and the Limburg University Fund (SWOL; Professor's Fund) to MD, in part by DFG grant Lu869/8-1 to AL, the Cardiovascular Research Institute Maastricht (CARIM Ph.D.-award), the Alexander von Humboldt Foundation, a grant from the Interdisciplinary Center for Clinical Research within the faculty of Medicine at the RWTH Aachen University, the DZHK (German Centre for Cardiovascular Research) the BMBF (German Ministry of Education and Research), the NWO-ZonMw Veni (91619053), and the Fritz Thyssen Stiftung (Grant No. 10.20.2.043MN) to EV.

Acknowledgments

We would like to thank T. Woopen for excellent technical assistance.

Conflict of interest

The authors declare that the research was conducted in the absence of any commercial or financial relationships that could be construed as a potential conflict of interest.

Publisher's note

All claims expressed in this article are solely those of the authors and do not necessarily represent those of their affiliated organizations, or those of the publisher, the editors and the reviewers. Any product that may be evaluated in this article, or claim that may be made by its manufacturer, is not guaranteed or endorsed by the publisher.

Supplementary material

The Supplementary Material for this article can be found online at: <https://www.frontiersin.org/articles/10.3389/fcvm.2023.974918/full#supplementary-material>

References

1. Tabas I, Garcia-Cardena G, Owens G. Recent insights into the cellular biology of atherosclerosis. *J Cell Biol.* (2015) 209:13–22. doi: 10.1083/jcb.201412052
2. Drey Mueller D, Pruessmeyer J, Groth E, Ludwig A. The role of ADAM-mediated shedding in vascular biology. *Eur J Cell Biol.* (2012) 91:472–85. doi: 10.1016/j.ejcb.2011.09.003

3. van der Vorst E, Keijbeck A, de Winther M, Donners MM. A disintegrin and metalloprotease: molecular scissors in angiogenesis, inflammation and atherosclerosis. *Atherosclerosis*. (2012) 224:302–8. doi: 10.1016/j.atherosclerosis.2012.04.023
4. Jorissen E, Prox J, Bernreuther C, Weber S, Schwanbeck R, Serneels L, et al. The disintegrin/metalloproteinase ADAM10 is essential for the establishment of the brain cortex. *J Neurosci*. (2010) 30:4833–44. doi: 10.1523/JNEUROSCI.5221-09.2010
5. Hartmann D, de Strooper B, Serneels L, Craessaerts K, Herremans A, Annaert W, et al. The disintegrin/metalloprotease ADAM 10 is essential for Notch signalling but not for alpha-secretase activity in fibroblasts. *Hum Mol Genet*. (2002) 11:2615–24. doi: 10.1093/hmg/11.21.2615
6. Zhang C, Tian L, Chi C, Wu X, Yang X, Han M, et al. Adam10 is essential for early embryonic cardiovascular development. *Dev Dyn*. (2010) 239:2594–602. doi: 10.1002/dvdy.22391
7. Glomski K, Monette S, Manova K, De Strooper B, Saftig P, Blobel C. Deletion of Adam10 in endothelial cells leads to defects in organ-specific vascular structures. *Blood*. (2011) 118:1163–74. doi: 10.1182/blood-2011-04-348557
8. Alabi R, Glomski K, Haxaire C, Weskamp G, Monette S, Blobel C. ADAM10-dependent signaling through Notch1 and Notch4 controls development of organ-specific vascular beds. *Circ Res*. (2016) 119:519–31. doi: 10.1161/CIRCRESAHA.115.307738
9. Caolo V, Swennen G, Chalaris A, Wagenaar A, Verbruggen S, Rose-John S, et al. ADAM10 and ADAM17 have opposite roles during sprouting angiogenesis. *Angiogenesis*. (2015) 18:13–22. doi: 10.1007/s10456-014-9443-4
10. Schulz B, Pruessmeyer J, Maretzky T, Ludwig A, Blobel C, Saftig P, et al. ADAM10 regulates endothelial permeability and T-Cell transmigration by proteolysis of vascular endothelial cadherin. *Circ Res*. (2008) 102:1192–201. doi: 10.1161/CIRCRESAHA.107.169805
11. Donners M, Wolfs I, Olieslagers S, Mohammadi-Motahhari Z, Tchaikovski V, Heeneman S, et al. A disintegrin and metalloprotease 10 is a novel mediator of vascular endothelial growth factor-induced endothelial cell function in angiogenesis and is associated with atherosclerosis. *Arterioscler Thromb Vasc Biol*. (2010) 30:2188–95. doi: 10.1161/ATVBAHA.110.213124
12. Morsing S, Rademakers T, Brouns S, Stalborch A, Donners M, van Buul J. ADAM10-mediated cleavage of ICAM-1 is involved in neutrophil transendothelial migration. *Cells*. (2021) 10:232. doi: 10.3390/cells10020232
13. Dreymueller D, Theodorou K, Donners M, Ludwig A. Fine tuning cell migration by a disintegrin and metalloproteinases. *Med Inflamm*. (2017) 2017:9621724. doi: 10.1155/2017/9621724
14. van der Vorst E, Jeurissen M, Wolfs I, Keijbeck A, Theodorou K, Wijnands E, et al. Myeloid A disintegrin and metalloproteinase domain 10 deficiency modulates atherosclerotic plaque composition by shifting the balance from inflammation toward fibrosis. *Am J Pathol*. (2015) 185:1145–55. doi: 10.1016/j.ajpath.2014.11.028
15. Bjorklund M, Hollensen A, Hagensen M, Dagnaes-Hansen F, Christoffersen C, Mikkelsen J, et al. Induction of atherosclerosis in mice and hamsters without germline genetic engineering. *Circ Res*. (2014) 114:1684–9. doi: 10.1161/CIRCRESAHA.114.302937
16. Mahmoud M, Kim H, Xing R, Hsiao S, Mammoto A, Chen J, et al. TWIST1 integrates endothelial responses to flow in vascular dysfunction and atherosclerosis. *Circ Res*. (2016) 119:450–62. doi: 10.1161/CIRCRESAHA.116.308870
17. Theodorou K, van der Vorst E, Gijbels M, Wolfs I, Jeurissen M, Theelen T, et al. Whole body and hematopoietic ADAM8 deficiency does not influence advanced atherosclerotic lesion development, despite its association with human plaque progression. *Sci Rep*. (2017) 7:11670. doi: 10.1038/s41598-017-10549-x
18. Emini Veseli B, Perrotta P, De Meyer G, Roth L, Van der Donck C, Martinet W, et al. Animal models of atherosclerosis. *Eur J Pharmacol*. (2017) 816:3–13. doi: 10.1016/j.ejphar.2017.05.010
19. Gijbels M, van der Cammen M, van der Laan L, Emeis J, Havekes L, Hofker M, et al. Progression and regression of atherosclerosis in APOE3-Leiden transgenic mice: an immunohistochemical study. *Atherosclerosis*. (1999) 143:15–25. doi: 10.1016/S0021-9150(98)00263-9
20. MacKenna D, Omens J, Covell J. Left ventricular perimysial collagen fibers uncoil rather than stretch during diastolic filling. *Basic Res Cardiol*. (1996) 91:111–22. doi: 10.1007/BF00799683
21. Bray N, Pimentel H, Melsted P, Pachter L. Near-optimal probabilistic RNA-seq quantification. *Nat Biotechnol*. (2016) 34:525–7. doi: 10.1038/nbt.3519
22. Soneson C, Love M, Robinson M. Differential analyses for RNA-seq: transcript-level estimates improve gene-level inferences. *F1000Res*. (2015) 4:1521. doi: 10.12688/f1000research.7563.1
23. Love M, Huber W, Anders S. Moderated estimation of fold change and dispersion for RNA-seq data with DESeq2. *Genome Biol*. (2014) 15:550. doi: 10.1186/s13059-014-0550-8
24. Subramanian A, Tamayo P, Mootha V, Mukherjee S, Ebert B, Gillette M, et al. Gene set enrichment analysis: a knowledge-based approach for interpreting genome-wide expression profiles. *Proc Natl Acad Sci U.S.A.* (2005) 102:15545–50. doi: 10.1073/pnas.0506580102
25. Wu T, Hu E, Xu S, Chen M, Guo P, Dai Z, et al. clusterProfiler 4.0: A universal enrichment tool for interpreting omics data. *Innovation*. (2021) 2:100141. doi: 10.1016/j.xinn.2021.100141
26. Chirumamilla C, Fazil M, Perez-Novo C, Rangarajan S, de Wijn R, Ramireddy P, et al. Profiling Activity of Cellular Kinases in Migrating T-Cells. *Methods Mol Biol*. (2019) 1930:99–113. doi: 10.1007/978-1-4939-9036-8_13
27. Yu G, Wang L, Han Y, He Q. clusterProfiler: an R package for comparing biological themes among gene clusters. *OMICS*. (2012) 16:284–7. doi: 10.1089/omi.2011.0118
28. Evrard S, Lecce L, Michelis K, Nomura-Kitabayashi A, Pandey G, Purushothaman K, et al. Endothelial to mesenchymal transition is common in atherosclerotic lesions and is associated with plaque instability. *Nat Commun*. (2016) 7:11853. doi: 10.1038/ncomms11853
29. Li X, Wang C. From bulk, single-cell to spatial RNA sequencing. *Int J Oral Sci*. (2021) 13:36. doi: 10.1038/s41368-021-00146-0
30. Vischer U. von Willebrand factor, endothelial dysfunction, and cardiovascular disease. *J Thromb Haemost*. (2006) 4:1186–93. doi: 10.1111/j.1538-7836.2006.01949.x
31. Lip G, Blann A. von Willebrand factor: a marker of endothelial dysfunction in vascular disorders? *Cardiovasc Res*. (1997) 34:255–65. doi: 10.1016/S0008-6363(97)00039-4
32. Amado-Azevedo J, Reinhard N, van Bezu J, van Nieuw Amerongen G, van Hinsbergh V, Hordijk P. The minor histocompatibility antigen 1 (HMA1)/ArhGAP45 is a RacGAP and a novel regulator of endothelial integrity. *Vascul Pharmacol*. (2018) 101:38–47. doi: 10.1016/j.vph.2017.11.007
33. van der Vorst E, Weber C, Donners MA. Disintegrin and metalloproteases (ADAMs) in cardiovascular, metabolic and inflammatory diseases: aspects for theranostic approaches. *Thromb Haemost*. (2018) 118:1167–75. doi: 10.1055/s-0038-1660479
34. Mentrup T, Cabrera-Cabrera F, Schroder B. Proteolytic regulation of the lectin-like oxidized lipoprotein receptor LOX-1. *Front Cardiovasc Med*. (2020) 7:594441. doi: 10.3389/fcvm.2020.594441
35. Mentrup T, Theodorou K, Cabrera-Cabrera F, Helbig A, Happ K, Gijbels M, et al. Atherogenic LOX-1 signaling is controlled by SPPL2-mediated intramembrane proteolysis. *J Exp Med*. (2019) 216:807–30. doi: 10.1084/jem.20171438
36. Mitsuka H, Kume N, Hayashida K, Inui-Hayashida A, Aramaki Y, Toyohara M, et al. Interleukin 18 stimulates release of soluble lectin-like oxidized LDL receptor-1 (sLOX-1). *Atherosclerosis*. (2009) 202:176–82. doi: 10.1016/j.atherosclerosis.2008.04.002
37. van der Vorst E, Zhao Z, Rami M, Holdt L, Teupser D, Steffens S, et al. Contrasting effects of myeloid and endothelial ADAM17 on atherosclerosis development. *Thromb Haemost*. (2017) 117:644–6. doi: 10.1160/TH16-09-0674
38. Rademakers T, Douma K, Hackeng T, Post M, Sluimer J, Daemen M, et al. Plaque-associated vasa vasorum in aged apolipoprotein E-deficient mice exhibit proatherogenic functional features in vivo. *Arterioscler Thromb Vasc Biol*. (2013) 33:249–56. doi: 10.1161/ATVBAHA.112.300087
39. Eriksson E. Intravital microscopy on atherosclerosis in apolipoprotein e-deficient mice establishes microvessels as major entry pathways for leukocytes to advanced lesions. *Circulation*. (2011) 124:2129–38. doi: 10.1161/CIRCULATIONAHA.111.030627
40. Chen Y, Bui A, Diesch J, Manasseh R, Hausding C, Rivera J, et al. A novel mouse model of atherosclerotic plaque instability for drug testing and mechanistic/therapeutic discoveries using gene and microRNA expression profiling. *Circ Res*. (2013) 113:252–65. doi: 10.1161/CIRCRESAHA.113.301562
41. Bot I, de Jager S, Zernecke A, Lindstedt K, van Berkel T, Weber C, et al. Perivascular mast cells promote atherogenesis and induce plaque destabilization in apolipoprotein E-deficient mice. *Circulation*. (2007) 115:2516–25. doi: 10.1161/CIRCULATIONAHA.106.660472
42. Van der Donck C, Van Herck J, Schrijvers D, Vanhoutte G, Verhoye M, Blockx I, et al. Elastin fragmentation in atherosclerotic mice leads to intraplaque neovascularization, plaque rupture, myocardial infarction, stroke, and sudden death. *Eur Heart J*. (2015) 36:1049–58. doi: 10.1093/eurheartj/ehu041
43. Kolodgie F, Gold H, Burke A, Fowler D, Kruth H, Weber D, et al. Intraplaque hemorrhage and progression of coronary atheroma. *N Engl J Med*. (2003) 349:2316–25. doi: 10.1056/NEJMoa035655
44. Ishihara T, Sano J, Yamanami S, Yamashita Y, Takahashi M, Uchino F, et al. Foamy cells associated with phagocytosis of glutaraldehyde-treated red blood cells and red cell membranes. *Acta Pathol Jpn*. (1987) 37:627–37. doi: 10.1111/j.1440-1827.1987.tb00397.x
45. O'Brien K, McDonald T, Chait A, Allen M, Alpers C. Neovascular expression of E-selectin, intercellular adhesion molecule-1, and vascular cell adhesion molecule-1 in human atherosclerosis and their relation to intimal leukocyte content. *Circulation*. (1996) 93:672–82. doi: 10.1161/01.CIR.93.4.672
46. Mulligan-Kehoe M, Simons M. Vasa vasorum in normal and diseased arteries. *Circulation*. (2014) 129:2557–66. doi: 10.1161/CIRCULATIONAHA.113.007189
47. van Tetering G, van Diest P, Verlaan I, van der Wall E, Kopan R, Vooijs M. Metalloprotease ADAM10 is required for Notch1 site 2 cleavage. *J Biol Chem*. (2009) 284:31018–27. doi: 10.1074/jbc.M109.006775
48. Hellstrom M, Phng L, Hofmann J, Wallgard E, Coultas L, Lindblom P, et al. Dll4 signalling through Notch1 regulates formation of tip cells during angiogenesis. *Nature*. (2007) 445:776–80. doi: 10.1038/nature05571
49. Chen K, Chen J, Liu Y, Xie J, Li D, Sawamura T, et al. Adhesion molecule expression in fibroblasts: alteration in fibroblast biology after transfection with LOX-1 plasmids. *Hypertension*. (2005) 46:622–7. doi: 10.1161/01.HYP.0000179045.95915.b0



OPEN ACCESS

EDITED BY

Hiroki Aoki,
Kurume University, Japan

REVIEWED BY

Venkateswaran Subramanian,
University of Missouri, United States
Xiangqian Kong,
Shandong Provincial Hospital, China

*CORRESPONDENCE

Rong Wang
✉ rongw1986@xjtu.edu.cn
Sihai Zhao
✉ sihaizhao@xjtu.edu.cn

[†]These authors share first authorship

SPECIALTY SECTION

This article was submitted to Atherosclerosis and Vascular Medicine, a section of the journal Frontiers in Cardiovascular Medicine

RECEIVED 01 December 2022

ACCEPTED 27 February 2023

PUBLISHED 15 March 2023

CITATION

Fu W, Liu H, Wei P, Xia C, Yu Q, Tian K, Li Y, Liu E, Xu B, Miyata M, Wang R and Zhao S (2023) Genetic deficiency of protein inhibitor of activated STAT3 suppresses experimental abdominal aortic aneurysms. *Front. Cardiovasc. Med.* 10:1092555. doi: 10.3389/fcvm.2023.1092555

COPYRIGHT

© 2023 Fu, Liu, Wei, Xia, Yu, Tian, Li, Liu, Xu, Miyata, Wang and Zhao. This is an open-access article distributed under the terms of the [Creative Commons Attribution License \(CC BY\)](https://creativecommons.org/licenses/by/4.0/). The use, distribution or reproduction in other forums is permitted, provided the original author(s) and the copyright owner(s) are credited and that the original publication in this journal is cited, in accordance with accepted academic practice. No use, distribution or reproduction is permitted which does not comply with these terms.

Genetic deficiency of protein inhibitor of activated STAT3 suppresses experimental abdominal aortic aneurysms

Weilai Fu^{1,2†}, Haole Liu^{1†}, Panpan Wei^{1,3}, Congcong Xia^{1,3}, Qingqing Yu¹, Kangli Tian¹, Yankui Li², Enqi Liu¹, Baohui Xu⁴, Masaaki Miyata⁵, Rong Wang^{1*} and Sihai Zhao^{1,3*}

¹Institute of Cardiovascular Science, Translational Medicine Institute, Xi'an Jiaotong University Health Science Center, Xi'an, China, ²Department of Vascular Surgery, The Second Hospital of Tianjin Medical University, Tianjin, China, ³Laboratory Animal Center, Xi'an Jiaotong University Health Science Center, Xi'an, China, ⁴Department of Surgery, Stanford University School of Medicine, Stanford, CA, United States, ⁵School of Health Science, Faculty of Medicine, Kagoshima University, Kagoshima, Japan

Aim: Signal transducer and activator of transcription (STAT) signaling is critical for the pathogenesis of abdominal aortic aneurysms (AAAs). Though protein inhibitor of activated STAT3 (PIAS3) negatively modulates STAT3 activity, but its role in AAA disease remains undefined.

Method: AAAs were induced in PIAS3 deficient (PIAS3^{-/-}) and wild type (PIAS3^{+/+}) male mice *via* transient intra-aortic elastase infusion. AAAs were assessed by *in situ* measurements of infrarenal aortic external diameters prior to (day 0) and 14 days after elastase infusion. Characteristic aneurysmal pathologies were evaluated by histopathology.

Results: Fourteen days following elastase infusion, aneurysmal aortic diameter was reduced by an approximately 50% in PIAS3^{-/-} as compared to PIAS3^{+/+} mice. On histological analyses, PIAS3^{-/-} mice showed less medial elastin degradation (media score: 2.5) and smooth muscle cell loss (media score: 3.0) than those in PIAS3^{+/+} mice (media score: 4 for both elastin and SMC destruction). Aortic wall leukocyte accumulation including macrophages, CD4⁺ T cells, CD8⁺ T cells and B cells as well as mural neovessel formation were significantly reduced in PIAS3^{-/-} as compared to PIAS3^{+/+} mice. Additionally, PIAS3 deficiency also downregulated the expression levels of matrix metalloproteinases 2 and 9 by 61% and 70%, respectively, in aneurysmal lesion.

Conclusion: PIAS3 deficiency ameliorated experimental AAAs in conjunction with reduced medial elastin degradation and smooth muscle cell depletion, mural leukocyte accumulation and angiogenesis.

KEYWORDS

abdominal aortic aneurysm, protein inhibitor of activated STAT3, inflammation, macrophage, animal model

Introduction

Abdominal aortic aneurysm (AAA) is a lethal degenerative disease that is prevalent in older smoker men (1, 2). Inflammation is one of well-established pathophysiological mechanisms in the genesis of AAAs. For example, the circulating levels of inflammatory cytokines such as interleukin (IL)-6, IL-1 β , tumor necrosis factor (TNF)- α and other mediators were elevated in patients with AAAs and may mediate AAA formation and

progression (3–5). Inhibition of inflammatory cytokines effectively attenuated experimental AAA formation (6–8).

Janus kinase (JAK)/signal transducer and activator of transcription (STAT) signaling critically regulates inflammatory responses (9, 10). It is involved in cytokine production, immune cell recruitment, and initiation of adaptive responses (9, 11). Four JAKs (JAK1-JAK3 and tyrosine kinase 2) and seven STATs (STAT1-STAT4, STAT5a, STAT5b, and STAT6) are present in mammalian cells (12). JAK2/STAT3 signaling modulates cell proliferation as well as cell survival. Additionally, enhanced JAK2/STAT3 signaling activity has been reported in clinical AAA specimens (13).

Excessively activating JAK/STAT signaling leads to dysregulated immune responses and thus tissue damage. Several endogenous inhibitory proteins, such as protein inhibitor of activated STAT (PIAS) and suppressor of cytokine signaling (SOCS), are evolved to limit overwhelming inflammation due to augmented JAK/STAT activity. We previously showed that PIAS3 was reversely associated with atherosclerotic progression and inhibited inflammatory responses and smooth muscle cell (SMC) proliferation (14). AAA as a chronic inflammatory disease may share some common pathogenic pathways with atherosclerosis. The role PIAS3 plays in AAAs has not been clarified. Therefore, the present study was to investigate the influence of PIAS3 deficiency on experimental AAAs in the elastase-induced AAA model.

Materials and methods

Animals

PIAS3 gene (NM_001165949) is located on mouse chromosome 3 with fourteen exons (15). PIAS3 deficient (PIAS3^{-/-}) mice on C57BL/6 genetic background were created in Cyagen Biosciences (Suzhou) Inc (Taicang, Jiangsu, China) using the CRISPR/CAS9 technique. Briefly, the exons of 2–9 were selected as target sites, and two gRNAs with Cas9 mRNA were microinjected into zygotes for PIAS3 deficient mouse generation (Figure 1A). F0 founders were identified *via* PCR genotyping followed by DNA sequencing. Homozygotes (PIAS3^{-/-}) and wild type (PIAS3^{+/+}) littermates were screened and used for all experiments. The use and care of animals as well as all experimental procedures were reviewed and approved by the Laboratory Animal Administration Committee of Xi'an Jiaotong University (No. 2019–1178). All information on animals and related reagents were detailed in **Supplementary Table S1**.

Phenotyping of PIAS3 deficient mice

For PCR screening, tail tip samples were collected from <3 weeks old mice and genomic DNA was extracted by proteinase K digestion. Genotyping PCR primers were AAACAAGACTAAAG GAGTATGGGC (sense 1), TAGAGGAAGGGGAAGGGAAGTAAAG (antisense 1) and CTCAGACACTCGGAACTCATC (antisense 2).

For quantitative reverse transcription PCR (qRT-PCR) and Western blotting analyses, total RNA and proteins were extracted from aortas. The PIAS3 primers for qRT-PCR analysis were sense: ACCAAGAATGGAGCTGAGCC (sense) and TCTGGATT CCGGATCCCCCTT (antisense). Antibodies against PIAS3 and β -actin were obtained from Cell Signaling Technology (Danvers, MA, United States) and TransGen Biotech Co., Ltd (Beijing, China), respectively.

Experimental AAA modeling

Experimental AAAs were induced in PIAS3^{-/-} and PIAS3^{+/+} mice by transient luminal infusion of porcine pancreatic elastase (PPE, 1.5 units/mL in phosphate-buffered saline) in controlled infrarenal aortic segment as previously reported (16, 17). Briefly, 9–12 weeks old male mice were anesthetized by 2% isoflurane inhalation, and infrarenal aorta was exposed *via* a laparotomy. Infrarenal aorta was then infused with PPE solution *via* an aortotomy for 5 min under constant pressure as previously described (18). After the surgery, all mice were maintained in individual cages with free access to chow diet and water.

Measurement of abdominal aortic diameters

Prior to PPE infusion, infrarenal aorta was photographed with a digital camera. The diameter was measured using Images Plus3.0 ML (Motic Electric Group Co., Ltd, Xiamen, Fujian, China) and served the baseline level. On day 14 after PPE infusion, infrarenal aortic diameter for each mouse was measured by the same procedure prior to sacrifice and aorta was then harvested. A mouse with a more than 50% aortic dilation over the baseline was considered aneurysmal (18).

Analysis of medial elastin and SMCs

Mice were euthanized by carbon dioxide inhalation. PPE-infused aortic segment was collected, embedded in optimal cutting temperature media, and sectioned (6 μ m). Frozen sections were stained with hematoxylin and eosin (H & E) and Elastic van Gieson (EVG) stains, respectively, for the assessment of general morphology and elastin integrity. Aortic media elastin degradation was graded as I (mild) to IV (severe) on EVG-stained sections as previously reported (16–20). To evaluate SMC depletion, acetone-fixed frozen sections were stained with a goat anti-SMC α -actin antibody followed a standard biotin-streptavidin peroxidase procedure. Biotinylated donkey anti-goat IgG antibody and streptavidin-peroxidase conjugate were obtained from the Jackson ImmunoResearch Laboratories Inc., West Grove, PA, United States). AEC substrate kit for color development was purchased from Vector Laboratories Inc., Burlingame, CA, United States. Aortic medial SMC depletion was graded on a scale of I (mild) to IV (severe) as reported previously (20).

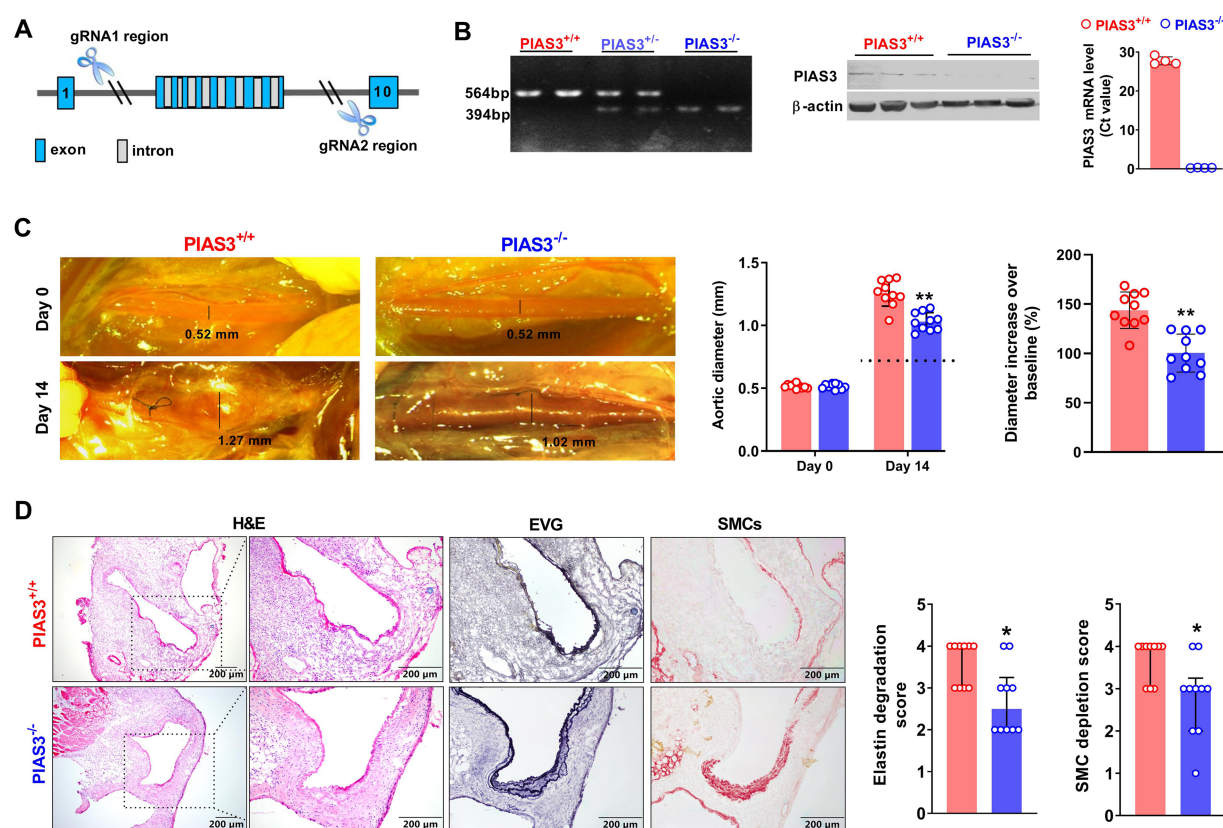


FIGURE 1

Genetic deficiency of PIAS3 suppresses experimental AAAs. (A): Strategy for generating PIAS3 deficient (PIAS3^{-/-}) mice by targeting exons 2-9 via the CRISPR/Cas9 technique. (B): Characterization of PIAS3^{-/-} mice by PCR genotyping, qRT-PCR and Western blotting analyses. (C): Representative aortic photographs and quantification of aortic diameters on day 0 and day 14 after elastase infusion. Dotted line indicates average aortic diameter after PBS infusion (approximately 0.8 mm). (D): Representative images of H&E, EVG and SMC α -actin staining as well as the semi-quantification (media and interquartile) of aneurysmal medial elastin and SMC destruction. Two-way ANOVA followed two group comparison (C) and non-parametric Mann-Whitney test (D). $N = 10$ for each group, * $p < 0.05$ and ** $p < 0.01$ as compared to PIAS3^{+/+} mice.

Analysis of aortic leukocytes

Acetone-fixed aortic frozen sections were stained with monoclonal antibodies against CD68 (macrophages), CD4⁺ T cells, CD8⁺ T cells and B cells (B220) (18). Sections were sequentially incubated with biotinylated goat anti-rat antibody (Vector Laboratories Inc), PBS, streptavidin-peroxidase conjugate (Jackson ImmunoResearch Laboratories Inc), PBS, peroxidase substrate AEC (Vector Laboratories Inc), counterstained with hematoxylin, mounted and cover-slipped. Aortic mural macrophage accumulation was graded on a scale of I (mild) to IV (severe) (20). CD4⁺ T cells, CD8⁺ T cells and B cells were quantitated as positively stained cells per aortic cross section (ACS) (20).

Immunostaining of aneurysmal matrix metalloproteinases

Matrix metalloproteinases (MMPs), particularly MMP2 and MMP9, contribute to the pathogenesis of AAAs. MMP2 and

MMP9 were assessed by immunostaining using goat anti-mouse polyclonal antibodies against MMP2 (AF1488) and MMP9 (AF909) (R & D Systems, Minneapolis, MN, United States) (Cite your JIR article). The expression levels were quantitated as the positively stained area per ACS using the image analysis software (WinRoof 6.5, Mitani Co. Ltd., Tokyo, Japan).

Analysis of mural angiogenesis

Angiogenesis was analyzed by immunostaining with rat anti-mouse CD31 monoclonal antibody (Clone 390, Biolegend Inc, San Diego, CA, United States) previously described. The neovessels number were counted under the microscope and reported as CD31-positive vessels per ACS (20, 21).

Statistical analysis

Prism 9.0 software was used for all statistical analyses. Continuous variables were expressed as mean and standard deviation (normal distribution) or media with interquartile (not

normal distribution). Student's *t* and nonparametric Mann-Whitney tests were used for normally and nonnormally distributed data, respectively. Two-way ANOVA followed by Sidak's multiple comparisons test was used for testing statistical difference for aortic diameters among groups. Statistical significance level was set at $p < 0.05$.

Results

Generation of PIAS3 knockout mice

As illustrated in **Figures 1A,B**, PIAS3 deficient mice were successfully generated by CRISPR/Cas9 techniques. PCR genotyping demonstrated the homozygotes of PIAS3 deficiency. qRT-PCR and Western blotting analysis further confirmed the deficiency of PIAS3 at mRNA and protein levels in PIAS3^{-/-} as compared to PIAS3^{+/+} mice.

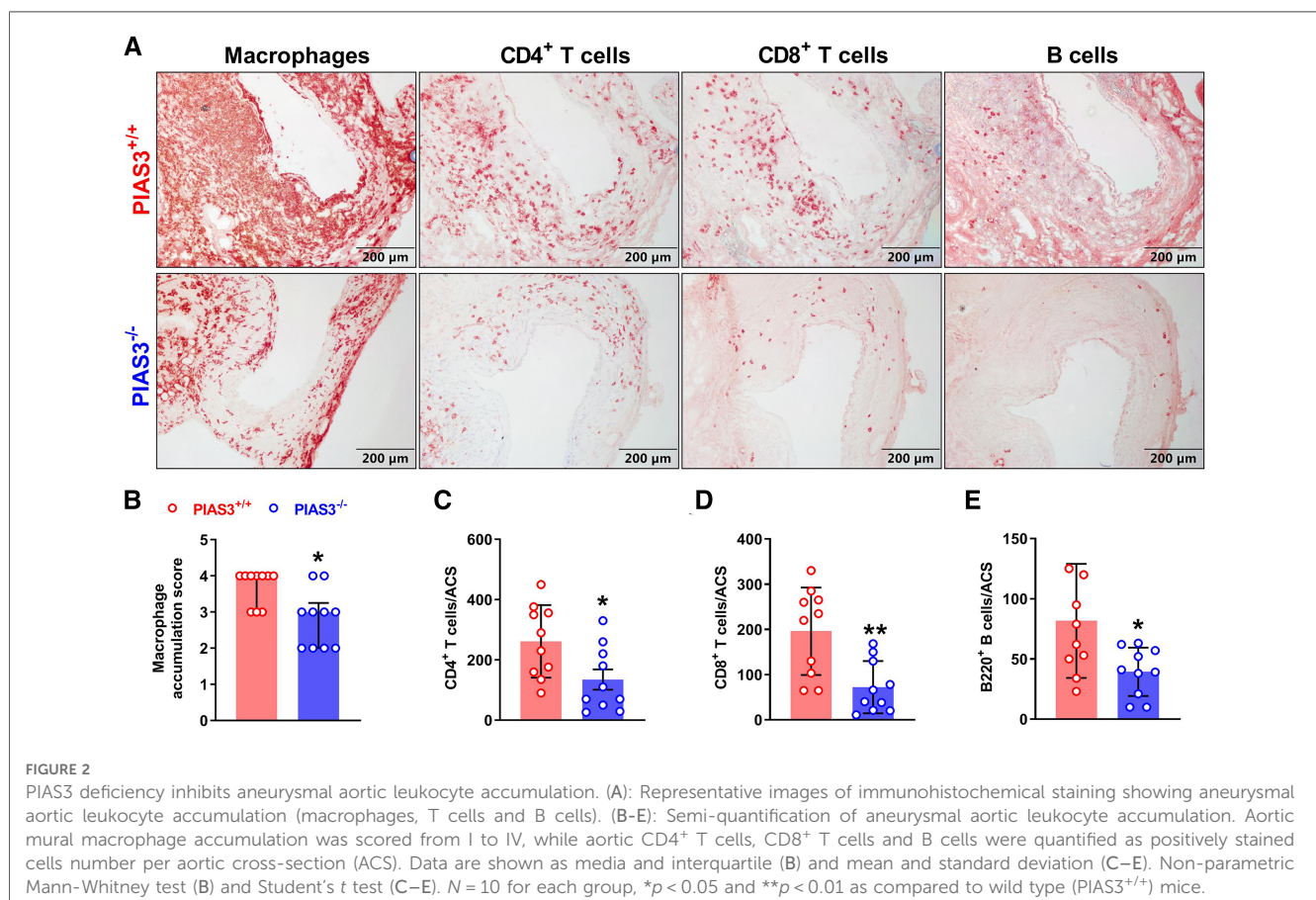
PIAS3 deficiency suppresses PPE-induced aortic dilation in mice

Intra-infrarenal aortic PPE infusion was conducted to induce AAAs in PIAS3^{+/+} and PIAS3^{-/-} mice. Experimental AAAs were

successfully induced in PIAS3^{+/+} mice (**Figure 1C**). PIAS3 deficiency significantly inhibited aortic expansion as compared to PIAS3^{+/+} mice. Aortic diameter on day 14 after PPE infusion were 1.03 ± 0.07 mm and 1.26 ± 0.10 mm for PIAS3^{-/-} and PIAS3^{+/+} mice, respectively (**Figure 1C**). After subtracting an average aortic dilation caused by PBS infusion (approximately 0.8 mm), PIAS3 deficiency reduced PPE-induced aortic expansion by approximately 50% (**Figure 1C**, middle panel). The diameter increase over the baseline was significantly less in PIAS3^{-/-} than that in PIAS3^{+/+} mice (**Figure 1C**, right panel).

PIAS3 deficiency ameliorates medial elastin degradation and SMC depletion

Histological analysis was performed in aneurysmal aortas. In H&E staining, PPE infusion induced a remarkable aortic dilation, predominant inflammatory cell infiltration, medial elastin degradation and SMC loss (**Figure 1D**, left panel). However, PIAS3^{-/-} mice were protective against the destruction of medial elastin and SMCs. In comparison with PIAS3^{+/+} mice, the integrity of medial elastin was relatively preserved in PIAS3^{-/-} mice, with significantly reduced elastin degradation score (**Figure 1D**, middle panel). Similar was true for medial SMCs (**Figure 1D**, right panel).



PIAS3 deficiency inhibits aortic leukocyte accumulation

In aortic immunostaining, the score for the accumulation of macrophages, identified by CD68-positive cells, was significantly lower in PIAS3^{-/-} than that in PIAS3^{+/+} mice (Figures 2A,B). Similarly, PIAS3 deficiency reduced the accumulation of CD4⁺ T cells, CD8⁺ T cells and B cells by approximately 50% (Figure 2).

PIAS3 deficiency reduces aortic MMP2 and MMP9 expression

MMP2 and MMP9 are contributors of PPE-induced AAAs (17, 22, 23). The levels of aortic MMP2 and MMP 9 were diminished in PIAS3^{-/-} as compared to PIAS3^{+/+} mice (Figure 3A). In semi-quantitative analysis, individual MMP positively stained areas were reduced by approximately 61% and 70% for MMP2 and MMP9, respectively, in PIAS3^{-/-} as compared to PIAS3^{+/+} mice (Figures 3B,C).

PIAS3 deficiency suppresses mural angiogenesis

Mural angiogenesis is involved in AAA pathogenesis (24–27). We thus determined whether the protective effect of PIAS3 deficiency on AAAs was associated with altered angiogenesis. In immunostaining of CD31, a maker of angiogenesis, the neovessels were significantly less in PIAS3^{-/-} than that in PIAS3^{+/+} mice (Figure 4, left panel), with a 40% reduction in mural neovessels in PIAS3^{-/-} mice (Figure 4, right panel).

Discussion

Inflammation is implicated in the initiation and evolution of AAAs (28). It leads to aortic medial elastin degradation, the apoptosis and dysfunction of vascular SMC by proteolytic enzymes, free radicals, cytokines, and other inflammatory products (29). JAK2/STAT3 signaling is a main intrinsic pathway for inflammation. It is involved in the creation and sustenance of inflammatory milieu by modulating the expression of cytokines, chemokines, and other mediators (30). In this study, we found that PIAS3 deficiency attenuated experimental AAAs induced by elastase infusion. There were less aneurysmal medial elastin and SMC destruction in PIAS3^{-/-} mice than those in PIAS3^{+/+} mice. Moreover, in comparison with PIAS3^{+/+} mice, aortic leukocyte infiltration, MMP expression and mural angiogenesis were attenuated in PIAS3^{-/-} mice. These results demonstrate that PIAS3 deletion ameliorated experimental AAAs by preserving SMCs, inhibiting aortic leukocyte infiltration, and decreasing angiogenesis.

It has been previously shown that JAK2/STAT3 signaling activity was involved in the pathogenesis of AAAs (13, 31, 32).

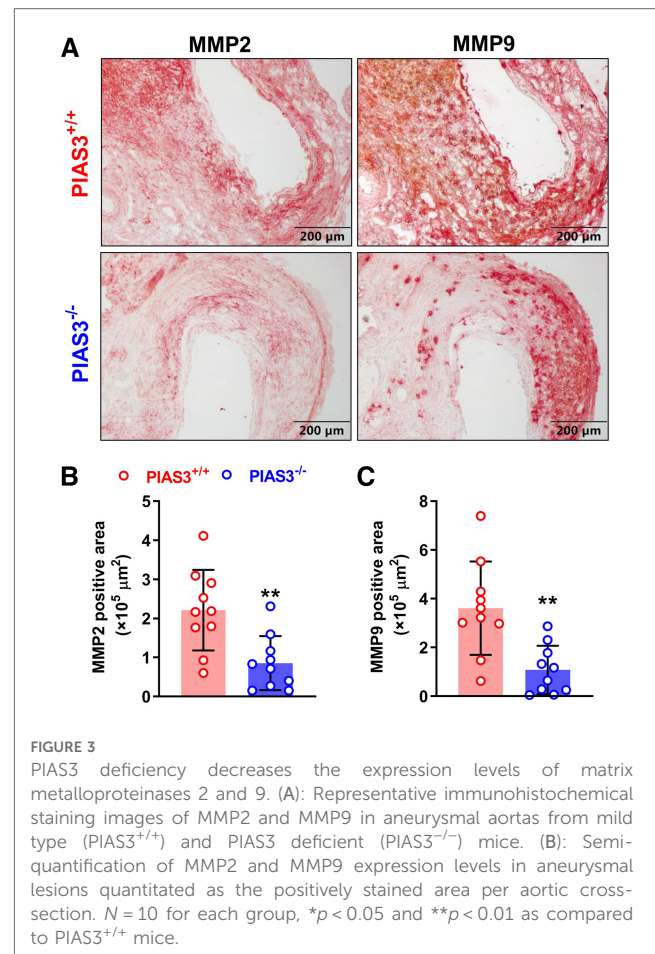


FIGURE 3

PIAS3 deficiency decreases the expression levels of matrix metalloproteinases 2 and 9. (A): Representative immunohistochemical staining images of MMP2 and MMP9 in aneurysmal aortas from mild type (PIAS3^{+/+}) and PIAS3 deficient (PIAS3^{-/-}) mice. (B): Semi-quantification of MMP2 and MMP9 expression levels in aneurysmal lesions quantitated as the positively stained area per aortic cross-section. *N* = 10 for each group, **p* < 0.05 and ***p* < 0.01 as compared to PIAS3^{+/+} mice.

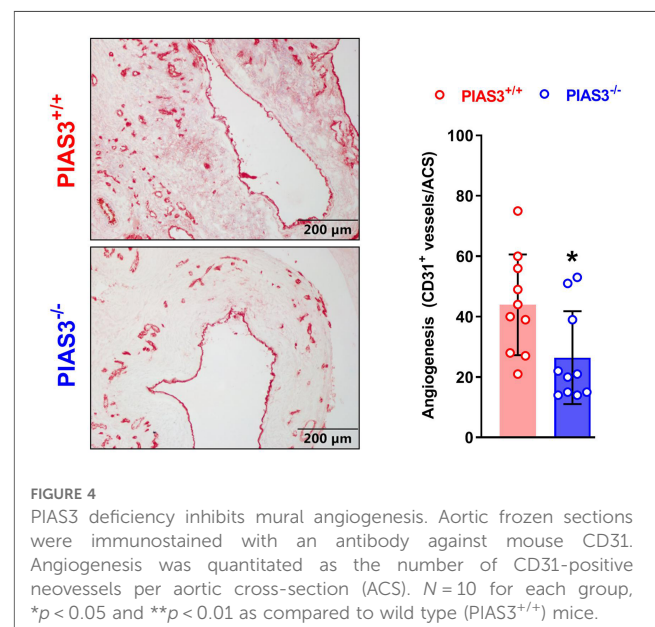


FIGURE 4

PIAS3 deficiency inhibits mural angiogenesis. Aortic frozen sections were immunostained with an antibody against mouse CD31. Angiogenesis was quantitated as the number of CD31-positive neovessels per aortic cross-section (ACS). *N* = 10 for each group, **p* < 0.05 and ***p* < 0.01 as compared to wild type (PIAS3^{+/+}) mice.

In human aortic tissues, JAK2/STAT3 expression levels were higher in aneurysmal than those in non-aneurysmal aortas (31). IL-6, a JAK2/STAT3 activator, was elevated in the human aneurysmal as compared to non-aneurysmal aortas (32, 33).

However, previously reported influence of STAT3 pathway components on AAAs varied. Disruption of STAT3 signaling in bone marrow-derived cells aggravated whereas myeloid cell-STAT3 deletion had limited effect on experimental AAAs (34). A STAT3 inhibitor attenuated angiotensin II-induced AAA progression in mice through inhibiting vascular inflammation and maintaining autophagy (35), whereas severe angiotensin II-induced AAAs were noted in mice overexpressing SOCS3, another negative regulator of JAK2/STAT3 signaling, in T lymphocytes in association with impaired IL-17 production (34). These discrepancies of STAT3 inhibition/activation concerning AAA progression might be resulted from differential influence on different vascular structural and immune cells. In SMC, the STAT3 inhibitor suppressed inflammation related signaling activation, such as JAK2/STAT3 and NF- κ B signaling, which ameliorated AAAs (35). In T cells, overexpression SOCS3 blocked STAT3 signaling activation, thereby significantly impeded Th17 development and decreased interleukin-17 production (34). Reduced IL-17 production is associated with severe vascular inflammation and enhanced susceptibility to aneurysms (36).

We previously found that PIAS3 was negatively associated with the JAK2/STAT3 activation and inflammatory responses in macrophages during atherosclerosis (14). Unexpectedly, the present study showed that PIAS3 deficiency attenuated PPE-induced AAA formation and reduced leukocyte infiltration in experimental AAA lesions. It is possible that chronic activation of STAT3 caused by PIAS3 deficiency may trigger tissue repair responses. In a recent study, SMC-specific SOCS3 deletion was protective against aortic dissection (37). Regionally activating STAT3 in the aorta may initiate host defense mechanisms thereby promoting SMC survival following vascular injury (37). Chronic activation of STAT3 evoked tissue repair responses by altering the phenotype of SMCs, macrophages, and fibroblasts, leading to enhancement of the tensile strength of the aortic wall (37). In addition, mural angiogenesis also contributes to AAA pathogenesis. In present study, PIAS3 deletion decreased aneurysmal mural angiogenesis, which might also result in the attenuation of AAA formation in PIAS3 deficient mice. PIAS3 has been shown to increase the levels of hypoxia-inducible factor (HIF)-1 α , a critical angiogenic transcription factor, by stabilizing HIF-1 protein (38). HIF-1 α /vascular endothelial growth factor (VEGF-A) pathway plays a vital role in the development of AAAs (39–43). Thus, angiogenesis inhibition by PIAS3 deficiency may be potentially attributed to low HIF-1 protein stability and thus reduced VEGF-A levels.

In conclusion, the present study demonstrated that genetic PIAS3 deficiency attenuated experimental AAAs in association with reduced medial elastin degradation, SMC depletion, leukocyte infiltration and aortic wall angiogenesis. Due to the limited aneurysmal tissues, the functions of MMPs and STAT3 were not determined in the present study. Further studies on the mechanism of PIAS3 regulating AAA will be conducted in the future.

Data availability statement

The original contributions presented in the study are included in the article/**Supplementary materials**, further inquiries can be directed to the corresponding author/s.

Ethics statement

The animal study was reviewed and approved by the Laboratory Animal Administration Committee of Xi'an Jiaotong University (No. 2019-1178).

Author contributions

SZ, RW, BX and MM are involved in the study design; SZ, EL and RW collected and analyzed data, as well as drafted the manuscript; WF, HL, CX, PW, KT, QY, YL and RW performed experiments; EL, BX, RW and SZ critically revised manuscript. All authors contributed to the article and approved the submitted version.

Funding

This work was partly supported by grants from the Natural Science Foundation of Shaanxi Province (2023-CX-PT-17, 2021PT-056, 2023-CX-PT-01), Natural Science Project of Xi'an Jiaotong University (YXJLRH2022073) and the National Natural Science Foundation of China (82170471).

Conflict of interest

The authors declare that the research was conducted in the absence of any commercial or financial relationships that could be construed as a potential conflict of interest.

Publisher's note

All claims expressed in this article are solely those of the authors and do not necessarily represent those of their affiliated organizations, or those of the publisher, the editors and the reviewers. Any product that may be evaluated in this article, or claim that may be made by its manufacturer, is not guaranteed or endorsed by the publisher.

Supplementary material

The Supplementary Material for this article can be found online at: <https://www.frontiersin.org/articles/10.3389/fcvm.2023.1092555/full#supplementary-material>.

References

- Tang W, Yao L, Roetker NS, Alonso A, Lutsey PL, Steenson CC, et al. Lifetime risk and risk factors for abdominal aortic aneurysm in a 24-year prospective study: the ariC study (atherosclerosis risk in communities). *Arterioscler, Thrombosis, and Vasc Biol.* (2016) 36(12):2468–77. doi: 10.1161/ATVBAHA.116.308147
- Takada M, Yamagishi K, Tamakoshi A, Iso H, Group JS. Body mass Index and mortality from aortic aneurysm and dissection. *J Atheroscler Thromb.* (2021) 28(4):338–48. doi: 10.5551/jat.57232
- Juvonen J, Surcel HM, Satta J, Teppo AM, Bloigu A, Syrjala H, et al. Elevated circulating levels of inflammatory cytokines in patients with abdominal aortic aneurysm. *Arterioscler, Thrombosis, and Vasc Biol.* (1997) 17(11):2843–7. doi: 10.1161/01.atv.17.11.2843
- Batra R, Suh MK, Carson JS, Dale MA, Meisinger TM, Fitzgerald M, et al. Il-1beta (interleukin-1beta) and tnfr-alpha (tumor necrosis factor-alpha) impact abdominal aortic aneurysm formation by differential effects on macrophage polarization. *Arterioscler, Thrombosis, and Vasc Biol.* (2018) 38(2):457–63. doi: 10.1161/ATVBAHA.117.310333
- Ouyang M, Wang M, Yu B. Aberrant mitochondrial dynamics: an emerging pathogenic driver of abdominal aortic aneurysm. *Cardiovasc Ther.* (2021) 2021:6615400. doi: 10.1155/2021/6615400
- Xiong W, MacTaggart J, Knispel R, Worth J, Persidsky Y, Baxter BT. Blocking tnfr-alpha attenuates aneurysm formation in a murine model. *J Immunol.* (2009) 183(4):2741–6. doi: 10.4049/jimmunol.0803164
- Isselbacher EM. Losartan for the treatment of marfan syndrome: hope fades. *J Am Coll Cardiol.* (2018) 72(14):1619–21. doi: 10.1016/j.jacc.2018.07.051
- Yu J, Morimoto K, Bao W, Yu Z, Okita Y, Okada K. Glucagon-Like peptide-1 prevented abdominal aortic aneurysm development in rats. *Surgery Today.* (2016) 46(9):1099–107. doi: 10.1007/s00595-015-1287-z
- Banerjee S, Biehl A, Gadina M, Hasni S, Schwartz DM. Jak-Stat signaling as a target for inflammatory and autoimmune diseases: current and future prospects. *Drugs.* (2017) 77(11):1261. (Vol 77, Pg 521, 2017) doi: 10.1007/s40265-017-0772-7
- O'Shea JJ. Targeting the jak/stat pathway for immunosuppression. *Ann Rheum Dis.* (2004) 63:67–71. doi: 10.1136/ard.2004.028290
- Garbers C, Aparicio-Siegmund S, Rose-John S. The il-6/Gp130/Stat3 signaling axis: recent advances towards specific inhibition. *Curr Opin Immunol.* (2015) 34:75–82. doi: 10.1016/j.coi.2015.02.008
- Kiu H, Nicholson SE. Biology and significance of the jak/stat signalling pathways. *Growth Factors.* (2012) 30(2):88–106. doi: 10.3109/08977194.2012.660936
- Liao MF, Xu J, Clair AJ, Ehrman B, Graham LM, Eagleton MJ. Local and systemic alterations in signal transducers and activators of transcription (stat) associated with human abdominal aortic aneurysms. *J Surg Res.* (2012) 176(1):321–8. doi: 10.1016/j.jss.2011.05.041
- Wang R, Zhang YJ, Xu LR, Lin Y, Yang XF, Bai L, et al. Protein inhibitor of activated Stat3 suppresses oxidized ldl-induced cell responses during atherosclerosis in apolipoprotein E-deficient mice. *Sci Rep-Uk.* (2016) 6:36790. doi: 10.1038/Srep36790
- Okazaki Y, Furuno M, Kasukawa T, Adachi J, Bono H, Kondo S, et al. Analysis of the mouse transcriptome based on functional annotation of 60,770 full-length cdnas. *Nature.* (2002) 420(6915):563–73. doi: 10.1038/nature01266
- Liu HL, Tian KL, Xia CC, Wei PP, Xu BY, Fu WL, et al. Kunming Mouse strain is less susceptible to elastase-induced abdominal aortic aneurysms. *Anim Model Exp Med.* (2022) 5(1):72–80. doi: 10.1002/ame2.12197
- Liu HL, Wei PP, Fu WL, Xia CC, Li YK, Tian KL, et al. Dapagliflozin ameliorates the formation and progression of experimental abdominal aortic aneurysms by reducing aortic inflammation in mice. *Oxid Med Cell Longev.* (2022) 2022:8502059. doi: 10.1155/2022/8502059
- Tian KL, Xia CC, Liu HL, Xu BY, Wei PP, Fu WL, et al. Temporal and quantitative analysis of aortic immunopathologies in elastase-induced mouse abdominal aortic aneurysms. *J Immunol Res.* (2021) 2021:6297332. doi: 10.1155/2021/6297332
- Xu BH, Iida Y, Glover KJ, Ge YB, Wang Y, Xuan HJ, et al. Inhibition of vegf (vascular endothelial growth factor)-a or its receptor activity suppresses experimental aneurysm progression in the aortic elastase infusion model. *Arterioscler Thromb Vasc.* (2019) 39(8):1652–66. doi: 10.1161/Atvbaha.119.312497
- Ikezo T, Shoji T, Guo J, Shen F, Lu HS, Daugherty A, et al. No effect of hypercholesterolemia on elastase-induced experimental abdominal aortic aneurysm progression. *Biomolecules.* (2021) 11(10):1434–48. doi: 10.3390/biom11101434
- Guo J, Shoji T, Ge Y, Zheng X, Li Y, Zhao S, et al. Treatment with the prolyl hydroxylase inhibitor jnj promotes abdominal aortic aneurysm progression in diabetic mice. *Eur J Vasc Endovasc Surg.* (2022) 63(3):484–94. doi: 10.1016/j.ejvs.2021.10.030
- Longo GM, Xiong W, Greiner TC, Zhao Y, Fiotti N, Baxter BT. Matrix metalloproteinases 2 and 9 work in concert to produce aortic aneurysms. *J Clin Investigation.* (2002) 110(5):625–32. doi: 10.1172/JCI15334
- Dhital S, Vyavahare NR. Nanoparticle-Based targeted delivery of pentagalloyl glucose reverses elastase-induced abdominal aortic aneurysm and restores aorta to the healthy state in mice. *PLoS one.* (2020) 15(3):e0227165. doi: 10.1371/journal.pone.0227165
- Zhang M, Sui W, Cheng C, Xue F, Tian Z, Cheng J, et al. Erythropoietin promotes abdominal aortic aneurysms in mice through angiogenesis and inflammatory infiltration. *Science Translational Med.* (2021) 13(603):eaa4959. doi: 10.1126/scitranslmed.aaz4959
- Lukasiewicz A, Reszec J, Kowalewski R, Chyczewski L, Lebkowska U. Assessment of inflammatory infiltration and angiogenesis in the thrombus and the wall of abdominal aortic aneurysms on the basis of histological parameters and computed tomography angiography study. *Folia Histochemica et Cytobiologica.* (2012) 50(4):547–53. doi: 10.5603/20323
- Satta J, Soini Y, Mosorin M, Juvonen T. Angiogenesis is associated with mononuclear inflammatory cells in abdominal aortic aneurysms. *Ann Chir Gynaecol.* (1998) 87(1):40–2.
- Thompson MM, Jones L, Nasim A, Sayers RD, Bell PR. Angiogenesis in abdominal aortic aneurysms. *Eur J Vasc Endovasc Surg.* (1996) 11(4):464–9. doi: 10.1016/s1078-5884(96)80183-3
- Shi J, Guo J, Li Z, Xu B, Miyata M. Importance of Nlrp3 inflammasome in abdominal aortic aneurysms. *J Atheroscler Thromb.* (2021) 28(5):454–66. doi: 10.5551/jat.RV17048
- Golledge J. Abdominal aortic aneurysm: update on pathogenesis and medical treatments. *Nat Rev Cardiol.* (2019) 16(4):225–42. doi: 10.1038/s41569-018-0114-9
- Hillmer EJ, Zhang HY, Li HS, Watowich SS. Stat3 signaling in immunity. *Cytokine Growth F R.* (2016) 31:1–15. doi: 10.1016/j.cytogfr.2016.05.001
- Xiao J, Wei ZJ, Chen X, Chen WQ, Zhang H, Yang CL, et al. Experimental abdominal aortic aneurysm growth is inhibited by blocking the Jak2/Stat3 pathway. *Int J Cardiol.* (2020) 312:100–6. doi: 10.1016/j.ijcard.2020.03.072
- Lindeman JH, Abdul-Hussien H, Schaapherder AF, Van Bockel JH, Von der Thüsen JH, Roelen DL, et al. Enhanced expression and activation of pro-inflammatory transcription factors distinguish aneurysmal from atherosclerotic aorta: il-6- and il-8-dominated inflammatory responses prevail in the human aneurysm. *Clinical Science.* (2008) 114(11):687–97. doi: 10.1042/CS20070352
- Harrison SC, Smith AJP, Jones GT, Swerdlow DI, Rampuri R, Bown MJ, et al. Interleukin-6 receptor pathways in abdominal aortic aneurysm. *Eur Heart J.* (2013) 34(48):3707–16. doi: 10.1093/eurheartj/ehs354
- Romain M, Taleb S, Dalloz M, Ponnuswamy P, Esposito B, Perez N, et al. Overexpression of Socs3 in T lymphocytes leads to impaired interleukin-17 production and severe aortic aneurysm formation in mice—brief report. *Arteriosclerosis, Thrombosis, and Vasc Biol.* (2013) 33(3):581–4. doi: 10.1161/ATVBAHA.112.300516
- Wu QY, Cheng Z, Zhou YZ, Zhao Y, Li JM, Zhou XM, et al. A novel Stat3 inhibitor attenuates angiotensin ii-induced abdominal aortic aneurysm progression in mice through modulating vascular inflammation and autophagy. *Cell Death Dis* (2020) 11(2):131. doi: 10.1038/s41419-020-2326-2
- Chandesris MO, Azarine A, Ong KT, Taleb S, Boutouyrie P, Mousseaux E, et al. Frequent and widespread vascular abnormalities in human signal transducer and activator of transcription 3 deficiency. *Circ Cardiovasc Genet.* (2012) 5(1):25–34. doi: 10.1161/CIRCGENETICS.111.961235
- Hirakata S, Aoki H, Ohno-Urabe S, Nishihara M, Furusho A, Nishida N, et al. Genetic deletion of Socs3 in smooth muscle cells ameliorates aortic dissection in mice. *Jacc-Basic Transl Sci.* (2020) 5(2):126–44. doi: 10.1016/j.jacpts.2019.10.010
- Nakagawa K, Kohara T, Uehata Y, Miyakawa Y, Sato-Ueshima M, Okubo N, et al. Pias3 enhances the transcriptional activity of hif-1alpha by increasing its protein stability. *Biochem Biophys Res Commun.* (2016) 469(3):470–6. doi: 10.1016/j.bbrc.2015.12.047
- Yu B, Wang X, Song Y, Xie G, Jiao S, Shi L, et al. The role of hypoxia-inducible factors in cardiovascular diseases. *Pharmacol Ther.* (2022) 238:108186. doi: 10.1016/j.pharmthera.2022.108186
- Kaneko H, Anzai T, Takahashi T, Kohno T, Shimoda M, Sasaki A, et al. Role of vascular endothelial growth factor-a in development of abdominal aortic aneurysm. *Cardiovasc Res.* (2011) 91(2):358–67. doi: 10.1093/cvr/cvr080
- Wang W, Xu B, Xuan H, Ge Y, Wang Y, Wang L, et al. Hypoxia-Inducible factor 1 in clinical and experimental aortic aneurysm disease. *J Vasc Surg.* (2018) 68(5):1538–50; e2. doi: 10.1016/j.jvs.2017.09.030
- Tedesco MM, Terashima M, Blankenberg FG, Levashova Z, Spin JM, Backer MV, et al. Analysis of in situ and ex vivo vascular endothelial growth factor receptor expression during experimental aortic aneurysm progression. *Arterioscler, Thromb, Vasc Biol.* (2009) 29(10):1452–7. doi: 10.1161/ATVBAHA.109.187757
- Nishibe T, Dardik A, Kondo Y, Kudo F, Muto A, Nishi M, et al. Expression and localization of vascular endothelial growth factor in normal abdominal aorta and abdominal aortic aneurysm. *Int Angiol.* (2010) 29(3):260–5.



OPEN ACCESS

EDITED BY

Masanori Aikawa,
Harvard Medical School, United States

REVIEWED BY

Nobuhiro Tahara,
Kurume University, Japan
Takehiro Funamizu,
Juntendo University, Japan

*CORRESPONDENCE

Kenichiro Otsuka
✉ otsuka.kenichiro@omu.acu.jp

[†]These authors have contributed equally to this work

SPECIALTY SECTION

This article was submitted to Atherosclerosis and Vascular Medicine, a section of the journal Frontiers in Cardiovascular Medicine

RECEIVED 11 November 2022

ACCEPTED 21 February 2023

PUBLISHED 17 March 2023

CITATION

Kitada R, Otsuka K and Fukuda D (2023) Role of plaque imaging for identification of vulnerable patients beyond the stage of myocardial ischemia.

Front. Cardiovasc. Med. 10:1095806.
doi: 10.3389/fcvm.2023.1095806

COPYRIGHT

© 2023 Kitada, Otsuka and Fukuda. This is an open-access article distributed under the terms of the [Creative Commons Attribution License \(CC BY\)](https://creativecommons.org/licenses/by/4.0/). The use, distribution or reproduction in other forums is permitted, provided the original author(s) and the copyright owner(s) are credited and that the original publication in this journal is cited, in accordance with accepted academic practice. No use, distribution or reproduction is permitted which does not comply with these terms.

Role of plaque imaging for identification of vulnerable patients beyond the stage of myocardial ischemia

Ryoko Kitada[†], Kenichiro Otsuka^{*†} and Daiju Fukuda

Department of Cardiovascular Medicine, Osaka Metropolitan University Graduate School, Osaka, Japan

Chronic coronary syndrome (CCS) is a progressive disease, which often first manifests as acute coronary syndrome (ACS). Imaging modalities are clinically useful in making decisions about the management of patients with CCS. Accumulating evidence has demonstrated that myocardial ischemia is a surrogate marker for CCS management; however, its ability to predict cardiovascular death or nonfatal myocardial infarction is limited. Herein, we present a review that highlights the latest knowledge available on coronary syndromes and discuss the role and limitations of imaging modalities in the diagnosis and management of patients with coronary artery disease. This review covers the essential aspects of the role of imaging in assessing myocardial ischemia and coronary plaque burden and composition. Furthermore, recent clinical trials on lipid-lowering and anti-inflammatory therapies have been discussed. Additionally, it provides a comprehensive overview of intracoronary and noninvasive cardiovascular imaging modalities and an understanding of ACS and CCS, with a focus on histopathology and pathophysiology.

KEYWORDS

chronic coronary syndrome, acute coronary syndrome, imaging, ischemia, atherosclerosis, plaque vulnerability, coronary microvascular dysfunction, inflammation

1. Introduction

Coronary artery disease (CAD) is a progressive disease that often first manifests as acute coronary syndrome (ACS). ACS is a life-threatening disease that affects approximately 1,045,000 people per year in the United States, leading to hospitalization and contributing to a remarkable economic and health care burden (1). In 2019, the European Society of Cardiology proposed the term chronic coronary syndrome (CCS) in the revised guidelines for stable CAD (2). It emphasizes that CCS is a chronic condition rather than the conventional “stable” angina or “stable” CAD. This paradigm shift calls for the early diagnosis, intervention, and continuous treatment of risk factors in patients with CCS to prevent cardiovascular events, including sudden death, ACS, and heart failure.

Clinical symptoms are an important aspect in diagnosing CCS (2). Although ACS often occurs as the first manifestation, noninvasive tests such as electrocardiography, echocardiography and elevated cardiac troponin levels can help in the diagnosis of ACS (3). Imaging modalities are highly useful for assessing the presence of CAD in patients with and without clinical symptoms based on clinical risk factors. The therapeutic goals of CCS include the lifelong prevention of ACS development and symptom reduction (2). While the primary percutaneous coronary intervention (PCI) strategy reportedly improves outcomes in patients with ST-segment elevation myocardial infarction (STEMI) (2), the

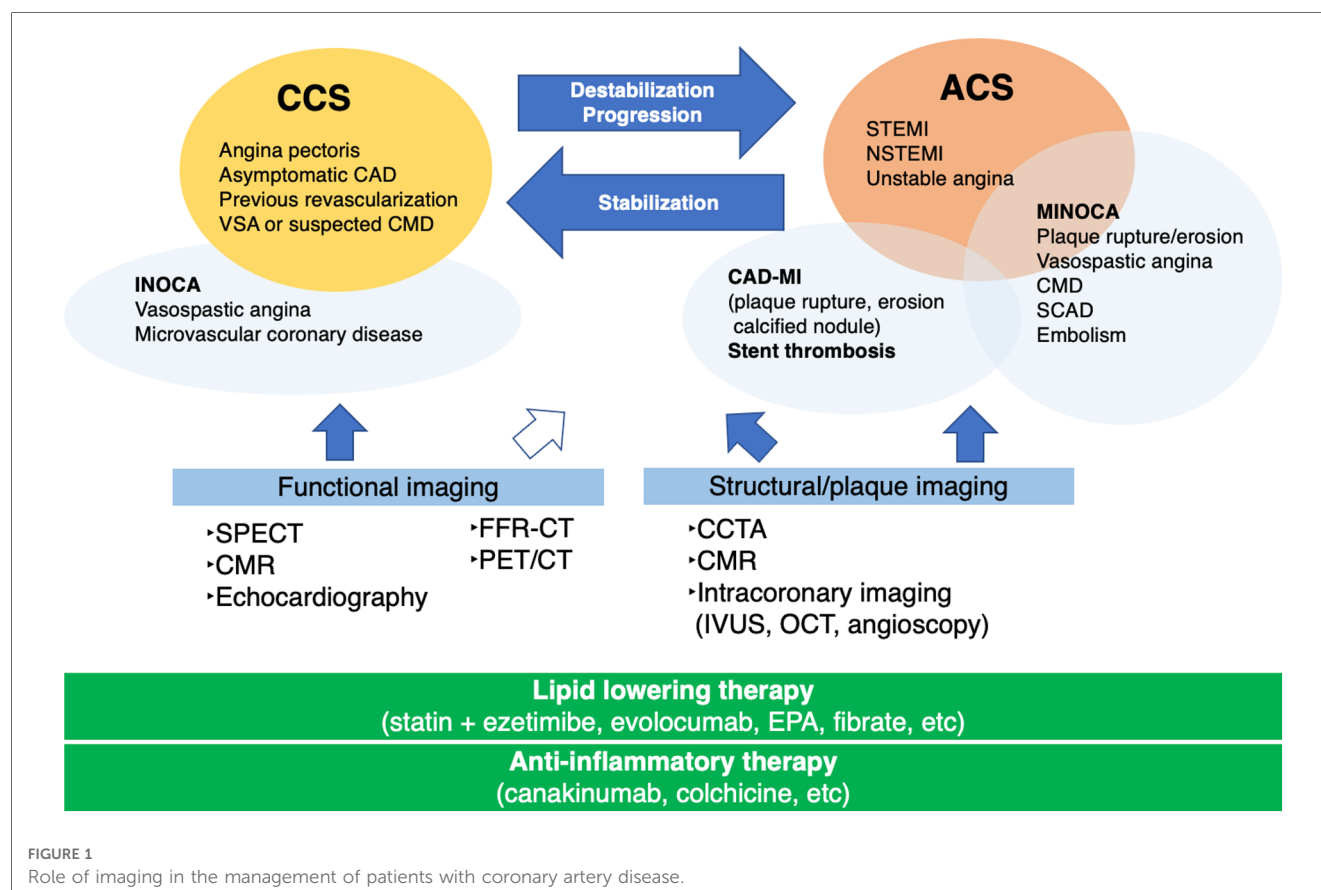
evaluation of myocardial ischemia, a surrogate marker of the disease, is central to determining indications for coronary revascularization in patients with CCS. The COURAGE (the Clinical Outcomes Utilizing Revascularization and Aggressive Drug Evaluation) trial demonstrated that PCI did not reduce the risk of death, nonfatal myocardial infarction (MI), or other major cardiovascular events (4). Subsequently, a sub-analysis demonstrated that a greater ischemic burden is associated with PCI benefits (5). To determine whether PCI is superior to optimized medical therapy (OMT) in patients with stable angina and a high ischemic burden the International Study of Comparative Health Effectiveness With Medical and Invasive Approaches (ISCHEMIA) trial was conducted at 320 institutions in 37 countries ($n = 5,179$). The ISCHEMIA trial compared the invasive (OMT + coronary revascularization) and conservative (OMT + invasive strategy, if necessary) strategies in patients with stable angina pectoris and moderate-to-severe myocardial ischemia ($>10\%$), while excluding patients with heart failure, left main coronary lesions, and chronic kidney disease (6). There was no statistically significant difference in the primary endpoint between the two groups during follow-up. The observations from these key clinical trials indicate the importance of OMT and coronary revascularization with their appropriate timing and indications.

The identification of underlying factors, such as coronary plaque burden, high-risk plaques, and coronary microvascular disease (CMD), is crucial for the management of patients with

CCS beyond the stage of myocardial ischemia. **Figure 1** illustrates the role of imaging and therapeutic targets in the management of patients with CAD. Imaging modalities are clinically useful in deciding the appropriate management of patients with CAD (2, 7–11). The development of noninvasive imaging technologies, such as coronary computed tomography angiography (CCTA) and cardiac magnetic resonance (CMR), has propelled our understanding of the features that accelerate subclinical CAD leading to ACS (12, 13). Intracoronary imaging has deepened our understanding of the mechanisms underlying coronary lesion destabilization in ACS (14, 15). Accurate prediction of coronary lesions leading to ACS requires a comprehensive assessment of plaque vulnerability, including plaque burden (16, 17), inflammatory status (18), coronary plaque mechanical stress (19, 20), and coronary microvascular function (21). These in turn determine the fate of coronary plaque rupture/erosion. In this study, we present a review highlighting the latest CAD knowledge and investigate the role and future perspective of coronary plaque imaging in the diagnosis and management of patients with CAD and clinical trials for lipid-lowering and anti-inflammatory therapies.

2. Pathophysiology of ACS

Understanding the pathogenesis of ACS largely relies on careful autopsy studies of sudden cardiac death. Fuster et al.



proposed the concept of ACS, including unstable angina, acute MI, and sudden cardiac death, and determined that plaque rupture-induced thrombus formation is linked to occlusion and severe stenosis of the coronary arteries (3, 22). The most common pathological cause of ACS is plaque rupture; postmortem studies conducted in the 1980s demonstrated that plaque rupture is found in the most fatal MIs (23, 24), indicating the presence of vulnerable plaques. Vulnerable plaques are typically characterized by a large central lipid core which is covered by a thin inflamed fibrous cap with few smooth muscle cells (25); chronic inflammation weakens the collagen structure of the fibrous caps (19, 26). In recent decades, attempts have been made to use imaging to identify precursor lesions that progress to ACS (16, 27–30) on the hypothesis that local therapeutic interventions may prevent plaque rupture-induced thrombosis. Increased plaque volume (31), thin fibrous caps (32), and microcalcifications (27, 33) detected on imaging modalities reportedly serve as independent predictors of ACS; however, ACS prediction remains challenging (34).

Plaque erosion is the second leading cause of ACS, is reportedly more common in women, and has fewer inflammatory cells and proteoglycan-rich lesions than a ruptured plaque (35–38). Superficial erosion-induced plaque thrombosis involves less macrophage-mediated inflammation, just as in the case of fibrous cap rupture. Superficial erosion is complicated by lesions with different epidemiologies and morphologies and involves a pathophysiological mechanism different from that of a fibrous cap rupture. Factors other than plaques, such as endothelial shear stress and neutrophil extracellular traps (NETosis) (37, 38), are thought to play a vital role in plaque erosion-induced thrombus formation. Furthermore, recent clinical studies have demonstrated that intimal healing following a silent plaque rupture/erosion plays a vital role in plaque progression (39, 40).

Following plaque rupture and erosion, calcified nodules are reportedly the least common cause of ACS ($\leq 5\%$). Calcified nodules are characterized by the eruption of calcified nodules with an underlying fibrocalcific plaque and minimal or no necrosis (25). ACS caused by plaque erosion or calcified nodules can cause non-occlusive thrombosis in the culprit lesion; however, plaque rupture-induced ACS is often accompanied by occlusive thrombosis.

3. Role of imaging in nonobstructive CAD

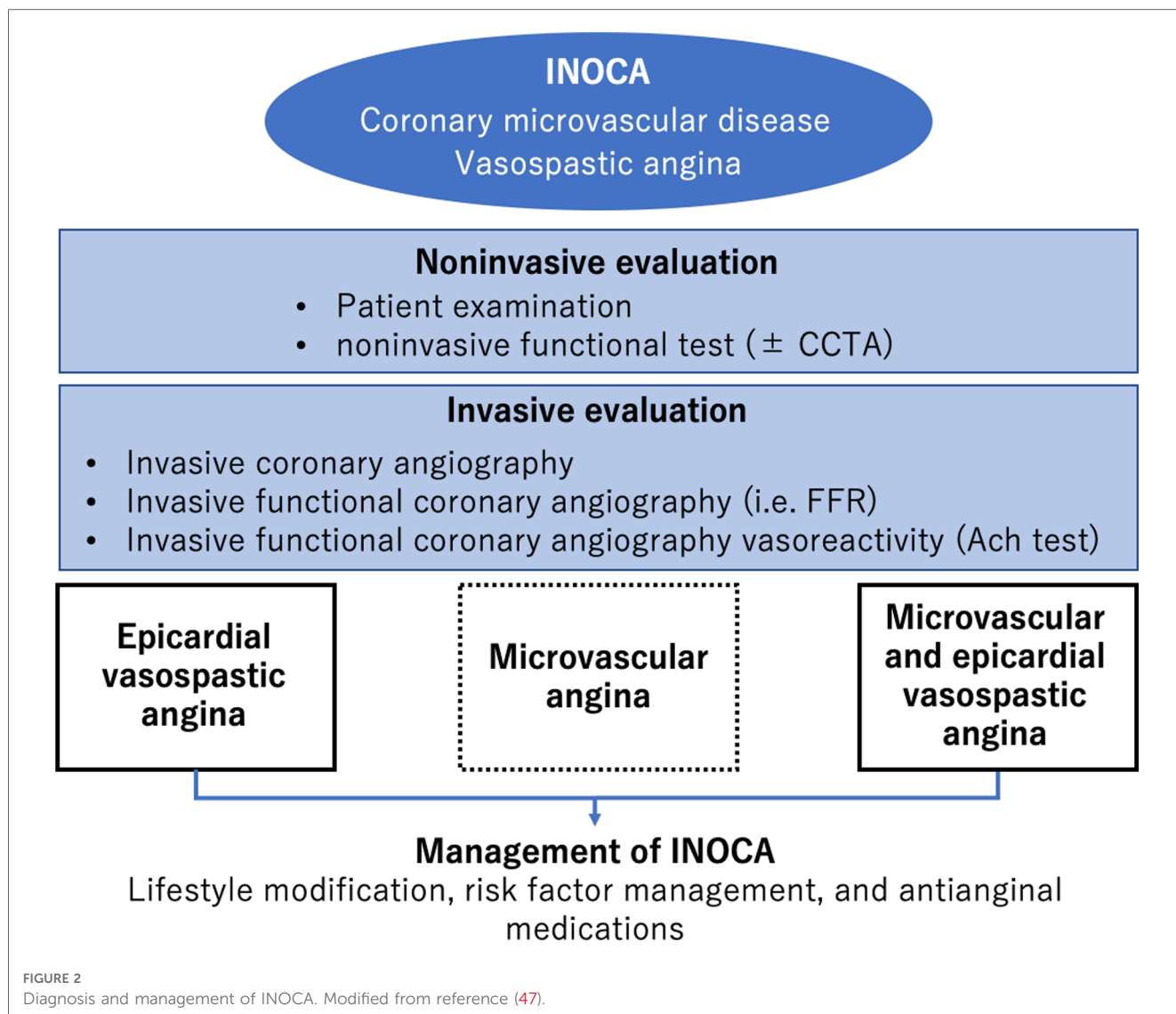
Approximately one-fifth of ACS cases occur despite the absence of coronary thrombi, suggesting that functional changes other than thrombus formation may contribute to its development. MI with nonobstructive coronary artery disease (MINOCA) is a condition in which MI is diagnosed based on elevated levels of cardiac enzymes and symptoms without evidence of obstructive coronary artery disease on invasive coronary angiography (ICA). The following three diagnostic criteria for MINOCA were proposed in a position paper by the European Society of Cardiology: (1) AMI criteria as defined by

the Third Universal Definition of Myocardial Infarction with clinical evidence of ischemic symptoms; (2) absence of $a > 50\%$ stenotic lesion in the major epicardial vessels; and (3) absence of other specific causes for the acute clinical symptoms (41). Various mechanisms have been postulated for the development of MINOCA, including plaque disruption, epicardial coronary vasospasm, coronary microvascular dysfunction, coronary embolism/thrombosis, CAD, spontaneous coronary artery dissection, and supply-demand mismatch (42). MINOCA occurs in 6%–8% of patients diagnosed with acute MI. MINOCA is more common in women and often presents as non-STEMI. Imaging modalities such as CMR and intravascular imaging are reportedly useful in investigating the underlying cause of MINOCA (42). Simultaneous assessment of CFR or coronary microvascular resistance and detection of ischemia is recommended during catheter laboratory testing in patients with ischemia with nonobstructive coronary arteries (INOCA) (43). Comprehensive assessment of the structure, ischemia, and CMD will help provide better CCS management (21, 44).

There is a growing interest in INOCA (12, 45, 46), a condition in which there is no significant stenosis in the epicardial coronary artery on ICA despite anginal symptoms and ischemic findings on noninvasive testing. **Figure 2** illustrates the diagnostic strategy for INOCA (47). The pathogenesis of vasospastic angina (VSA) involves abnormal endothelial function, that is, decreased production of nitric oxide by endothelial cells, which is a scenario encountered in CCS (38). VSA treatment includes smoking cessation and administration of calcium channel blockers and vasodilators. Another condition of INOCA is CMD, which is more common in women than in men and involves organic microvascular narrowing and coronary spasm (21). The diagnostic criteria of CMD are defined by the Coronary Vasomotor Disorders International Study (COVADIS) group (44): exertional chest pain or dyspnea, absence of obstructive CAD, objective evidence of myocardial ischemia on functional imaging, and CMD as determined by measuring CFR or coronary microvascular resistance (21). Coronary microcirculatory function can be indirectly assessed using noninvasive imaging modalities, including transthoracic doppler echocardiography (48, 49), CMR (50), and positron emission tomography (PET)/computed tomography (CT) (51, 52). Moreover, a comprehensive assessment of CFR and coronary microvascular resistance, in addition to ischemia detection, is recommended in the catheter laboratory when diagnosing INOCA (43).

4. Functional or structural imaging

Patients with a history of MI and anginal symptoms are reportedly at high risk of cardiovascular events and may require more intensive treatments (53). For patients with a high pretest probability, evaluation of myocardial ischemia is important for patient management. For several decades, physicians have largely depended on the identification of patients with myocardial ischemia to perform coronary revascularization (54). Functional imaging for identifying myocardial ischemia includes single



photon emission computed tomography (SPECT), PET/CT, stress echocardiography, or stress CMR. Although these imaging modalities are highly useful with high diagnostic accuracy for obstructive CAD in clinical practice, their ability to diagnose diffuse nonobstructive CAD is limited (55, 56).

CCTA is a noninvasive imaging technique that enables visualization of cardiac structures, coronary plaque structure and composition, and functional stenosis severity. **Table 1** summarizes the recent clinical trials investigating the utility of CCTA in patients with stable chest pain. CCTA reportedly offers a high negative predictive value for significant obstructive CAD and has become a first-line test for symptomatic patients with suspected CAD (59), asymptomatic patients with low-to-intermediate cardiovascular risk (59), and those with low pretest probability (2). The strength of CCTA is that it provides direct visualization of the entire coronary artery and determines the presence of nonobstructive CAD. In the PROMISE (A Randomized Comparison of Anatomic vs. Functional Diagnostic Testing Strategies in Symptomatic Patients with Suspected Coronary Artery Disease) trial which investigated stable

symptomatic outpatients referred for non-invasive evaluation of suspected CAD ($n = 10,003$), there was no significant difference between the two groups (randomized to anatomical testing with CCTA or functional testing) in the primary outcome (7). Further investigation demonstrated that CCTA had a higher discriminatory ability to predict outcomes than functional testing (57). This finding may be explained by the fact that CCTA enables the identification of nonobstructive diseases that develop into ACS and obstructive CAD requiring coronary revascularization (55, 56).

To test the hypothesis that an early invasive treatment strategy would reduce events in patients with moderate or greater ischemia rather than a conservative pharmacotherapeutic treatment strategy, the ISCHEMIA trial included cases of stable angina with documented moderate-to-severe ($\geq 10\%$) ischemia (6). Blinded CCTA was performed, and patients with left main coronary artery lesions were excluded. A total of 5,179 patients from a total of 8,518 were randomized, with 2,588 patients in the invasive treatment group and 2,591 in the conservative treatment group (mean age, 64 years; 40% had diabetes and 90% had anginal symptoms). The invasive treatment group consisted of

TABLE 1 Summary of the randomized controlled trials using CCTA in patients with stable chest pain.

Authors Reference	Year	Country, follow-up (years)	Study design, data source	Sample Size	Comparison	Primary endpoint	Outcome	Summary of findings				
U Hoffman et al. Reference (57)	2017	North America, 26.1 months	PROMISE trial, prospective observational study	9,102	CCTA vs. functional	A composite of time-to-MACE including death from any cause, MI, or hospitalization for unstable angina	CCTA vs. functional death, 137 (3.1%) vs. 132 (3.0%). Death, 62 (1.4%) vs. 66 (1.4%), MI, 26 (0.6%) vs. 31 (0.7%), Unstable angina, 52 (1.2%) vs. 41 (0.9%).	No difference in clinical outcome				
De Newby et al. Reference (8)	2018	Scotland, 4.8 y	SCOT-HEART trial, prospective observational study	4,138	SOC vs. SOC+CCTA	Death due to CAD or nonfatal MI	SOC vs. SOC +CCTA group 2.3% (48 patients) vs. 3.9% (81 patients)	The use of CCTA resulted in a significantly lower rate of death due to CAD or nonfatal MI.				
JM Lee et al. Reference (56)	2019	Korea, 5 y	The 3 V FFR-FRIENDS study,prospective observational study	299 (772 vessels)	High risk plaque characteristics ≥ 3 vs. <3 with FFR	VOCO (ischemia-driven target vessel revascularization, vessel-related MI, and cardiac death)	The cumulative incidence of VOCO at 5 years was 4.3%, 15.0%, and 10.7% among the deferred vessels with FFR >0.80 and ≥ 3 high-risk plaque characteristics, and stented vessels with FFR ≤ 0.80 , respectively.	Integration of both physiological stenosis severity and plaque vulnerability would provide better prognostic stratification of patients than the individual components alone.				
E Sorbets et al. Reference (53)	2020	45 countries, 5 y	CLARIFY registry, the prospective observational study	32,703	Prior MI vs. no prior MI Angina vs. no angina	CV death and nonfatal MI	<table><tr><td>Prior MI</td><td>CV death or non-fatal MI 9.1% vs. 6.4% (Prior MI) PCI 7.1% vs. 7.9%</td></tr><tr><td>Angina</td><td>CV death or non-fatal MI 9.8% vs. 7.5% (Angina) PCI 9.6% vs. 6.8%</td></tr></table>	Prior MI	CV death or non-fatal MI 9.1% vs. 6.4% (Prior MI) PCI 7.1% vs. 7.9%	Angina	CV death or non-fatal MI 9.8% vs. 7.5% (Angina) PCI 9.6% vs. 6.8%	Both angina and prior MI are easily identifiable high-risk groups
Prior MI	CV death or non-fatal MI 9.1% vs. 6.4% (Prior MI) PCI 7.1% vs. 7.9%											
Angina	CV death or non-fatal MI 9.8% vs. 7.5% (Angina) PCI 9.6% vs. 6.8%											
MJ Budoff et al. Reference (58)	2020	USA, 18 months	EVAPORATE trial, randomized, double-blind, placebo-controlled trial	80	Icosapent ethyl (IPE) vs. placebo	The change in LAP volume measured on CCTA	IPE vs. placebo Change in LAP -0.3 mm^3 vs 0.9 mm^3 ($p = 0.006$)	IPE significantly regressed the LAP volume on CCTA compared to the placebo.				

SOC, standard of care; CAD, coronary artery disease; CV, cardiovascular; MI, myocardial infarction; ACS, acute coronary syndrome; LAP, low-attenuation plaque; CCTA, coronary computed tomography angiography; VOCO, vessel-oriented composite outcome; PCI, percutaneous coronary intervention; FFR, fraction flow reserve.

patients who underwent diagnostic catheterization within approximately one month if the core laboratory demonstrated $\geq 10\%$ ischemia with exclusion of left main CAD on CCTA; PCI or CABG was performed within three months, if necessary. The conservative treatment group did not require imaging tests or invasive treatment but was continued on OMT, with a primary focus of controlling the patients' symptoms. The follow-up period for both groups was 3.3 years, with very high follow-up rates of 99.4% and 99.7%, respectively. These results suggest that OMT may be an appropriate option for patients with CCS who meet the inclusion criteria of the ISCHEMIA trial with SPECT and CCTA. Extended analysis will provide further insights into the appropriate management of patients with CCS (60).

5. Non-invasive plaque imaging

The utility of CCTA-guided management has been well-documented. The SCOT-HEART (Scottish Computed Tomography of the Heart) trial demonstrated that CCTA-guided therapy provides better clinical outcomes than standard therapy

does in patients with CCS (8). This can be explained by the effects of aspirin, statins, coronary revascularization, and lifestyle modifications through the identification of the presence of coronary atherosclerotic plaques on CCTA. **Figure 3** illustrates a representative CCTA image of a patient with chest pain, showing high-risk plaque features, which led to ACS. The ROMICAT-II (Multicenter Study to Rule Out Myocardial Infarction by Cardiac Computed Tomography) trial demonstrated that high-risk coronary plaque features, including positive remodeling, low-attenuation plaques (LAP), spotty calcification, and napkin-ring sign, were independent predictors of ACS; these serve as useful diagnostic tools to rule out ACS in clinical practice (62). Although the predictive value of high-risk plaque features is not high enough to predict long-term ACS prognosis, a recent clinical trial demonstrated that a LAP volume of $>4\%$ is the strongest predictor of clinical risk factors, plaque volume, and stenosis severity (17). CCTA-derived high-risk plaques are associated with an increased incidence of ACS even in patients without myocardial ischemia (55). The combination of fraction flow reserve-CT and coronary structural features may provide a comprehensive assessment of patients requiring coronary revascularization and future ACS events (63).

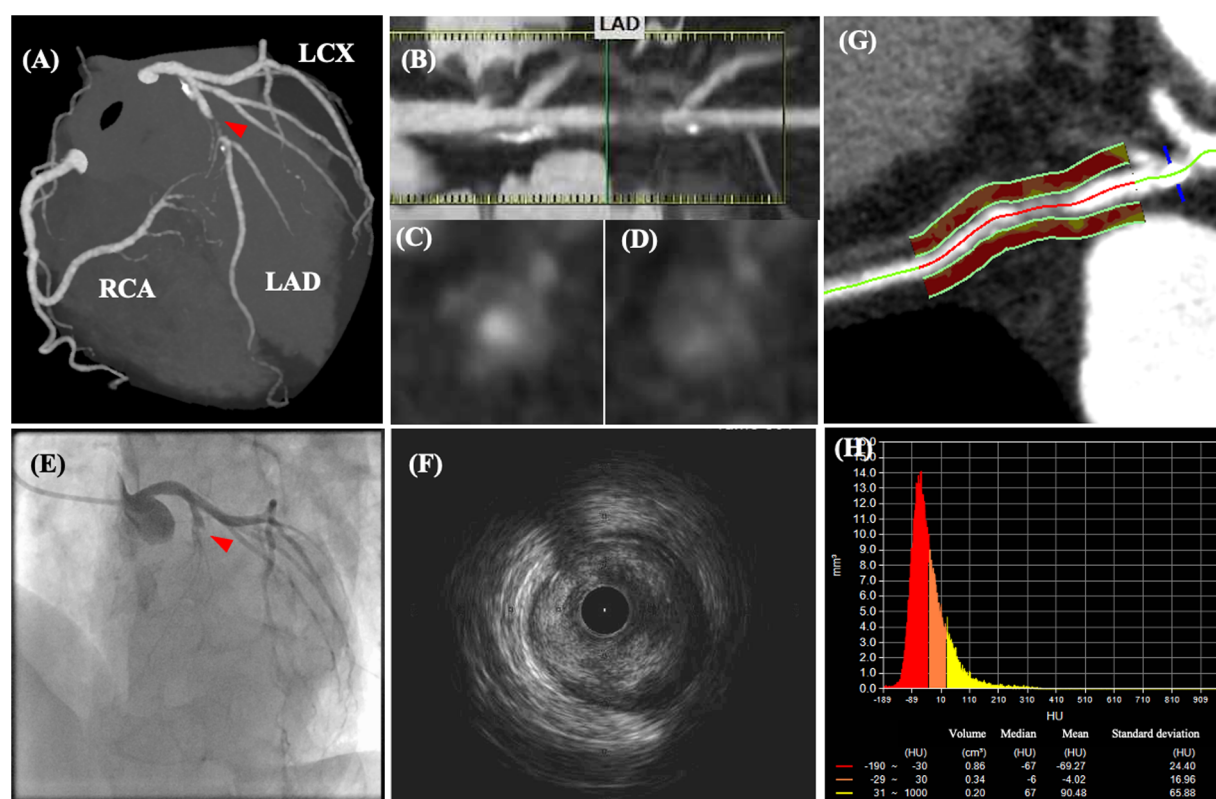


FIGURE 3

Coronary computed tomography angiography and angiographic images of a patient with acute chest pain. CCTA images of a patient with acute chest pain without ST-segment changes on electrocardiography. CCTA images (A–D) indicate 70–99% luminal stenosis with high-risk plaque features (positive remodeling, low-attenuation plaque, napkin ring sign, and spotty calcification) in the proximal left ascending coronary artery (LAD). After CCTA examination, the patient's chest pain worsened, and ST-segment elevation was detected. (E) Emergent coronary angiography revealed total occlusion of the LAD, which corresponded to the location of the high-risk plaque visualized on CCTA. (F) Intravascular ultrasonography revealed an intraluminal thrombus secondary to plaque rupture. (G,H) Post-hoc analysis demonstrated an increased pericoronary artery attenuation of >-70 HU. Modified from reference (61).

CMR can assess perfusion and wall motion abnormalities of the left ventricle and cardiac structures, serving as the gold standard noninvasive imaging technique for diagnosing cardiomyopathy (64, 65), myocarditis (66), MI, and mechanical complications of MI (67). CMR with late gadolinium enhancement also allows the visualization of scar tissue and enables differentiation of recent MI from prior MI (68). CMR with T1 mapping is an alternative method for assessing myocardial edema (69, 70). CMR is widely used to differentiate other diseases mimicking ACS, including Takotsubo cardiomyopathy (65, 71) and MI with MINOCA (42). CMR also allows visualization of coronary plaques by assessing the signal intensity (72, 73). Hyperintense plaques, defined as a plaque-to-myocardium signal intensity ratio of >1.4 , reportedly predicts ACS events in patients with suspected or known CAD (72). Daniel et al. demonstrated an association of intraplaque hemorrhage-related unstable carotid plaque features with stroke and myocardial infarction in 1,349 patients without a history of stroke or CAD with subclinical atherosclerosis. This indicates that the presence of intraplaque hemorrhage in the carotid arteries is associated with stroke and CAD development, independent of plaque size or cardiovascular risk factors (74, 75).

PET/CT imaging with a variety of radioactive tracer probes is used to identify and characterize arterial plaque burden at high risk for rupture and subsequent thromboembolic vessel occlusion (76). Peripheral vascular and coronary inflammation can be detected and quantified using 18-F-fluorodeoxyglucose (18F-FDG)-PET/CT (77). However, in approximately 50% of patients with ACS or MI, no local increase in coronary 18F-FDG uptake is observed. Thus, a less inflammatory but lipid-rich coronary plaque burden may account for a significant portion of the coronary plaque ruptures. Additionally, 18F-FDG-PET/CT scans may be negative in lipid-rich plaques because inflammation-induced macrophage infiltration, a major substrate for 18F-FDG uptake, is less pronounced in the surviving hypoxic cells. ^{18}F -fluoromisonidazole (FMISO) changes to a more reactive form and remains intracellular by covalently binding to intracellular molecules. Thus, while using 18F-FMISO to signal hypoxia, PET in combination with 18F-sodium fluoride (18F-NaF) can determine active calcification in the CAD process and microcalcifications (78, 79).

6. Intracoronary plaque imaging

ICA, the gold standard for assessing CAD severity, enables visualization of the coronary arterial lumen; however, its ability to assess the outer vessel walls is limited. Intravascular ultrasound (IVUS), optical coherence tomography (OCT), and angioscopy are used to elucidate the pathogenesis of ACS and progression of coronary atherosclerosis. The use of intracoronary imaging in PCI guidance is increasing (80), thereby revealing the post-interventional mechanisms of stent failure, including thrombosis and restenosis (81, 82). Dual antiplatelet therapy (DAPT) effectively prevents post-implantation stent thrombosis; however, bleeding is the primary, major complication of coronary

revascularization (83). Complex PCI involves intervention in patients with left main disease, multiple stent implantations, and severely calcified lesions, often requiring a longer duration of DAPT (84, 85). Clinical guidelines recommend the potential benefit of an antiplatelet-anticoagulation combination therapy or anticoagulation monotherapy (86). Furthermore, recent clinical studies have demonstrated that intracoronary imaging may beneficially affect the outcomes of patients who undergo PCI (87). Whether antiplatelet or anticoagulation therapy is effective in preventing device-oriented complications in patients undergoing complex PCI remains controversial.

IVUS assesses the coronary plaque morphology, arterial lumen, and vessel wall size, which improves our understanding of the pathogenesis of ACS (88–90). In addition to advances in the faster pullback of grayscale IVUS, virtual histology (VH-), integrated backscatter (IB-), and near-infrared spectroscopy (NIRS-) IVUSs allow the evaluation of atherosclerotic tissue characteristics. In the PROSPECT trial using VH-IVUS, 697 patients with ACS were studied; plaque volume of $>70\%$, VH-thin-capped fibroatheroma (TCFA), and minimal luminal area of $<4\text{ mm}^2$ were predictors of lesions associated with a 3-year incidence of major cardiovascular adverse events (MACE) (16). However, IVUS's (resolution: $100\text{--}200\text{ }\mu\text{m}$) ability to detect fibrous cap thickness in TCFA ($<65\text{ }\mu\text{m}$) is limited. NIRS-IVUS is an imaging technique based on near-infrared spectroscopy that assesses the probability of lipids being present as a chemogram (91). A multicenter prospective study investigating 1,563 patients showed that NIRS-IVUS enabled the identification of patients with a high probability of developing MACE (92). Over a mean follow-up of 732 days, the incidence of MACE in patients with $\text{maxLCBI4mm} \geq 400$ without significant stenosis was 13%, which was twice as high as that in patients without $\text{maxLCBI4mm} \geq 400$ (6%). These clinical studies indicate that the lipid/necrotic core burden may be a potential therapeutic target.

OCT uses near-infrared light to image the structures of the coronary vessel walls with a high resolution of $0\text{--}15\text{ }\mu\text{m}$ (93) (Figure 4). OCT can investigate tissue response and stent expansion or apposition during PCI; however, it requires blood clearing during procedures. Recent clinical trials have demonstrated the non-inferiority of OCT compared to IVUS and its superiority over ICA alone (94). This indicates that intravascular imaging-guided PCI has advantages over angiography-guided PCI in patients with ACS (95) and CCS (96). OCT aids in visualizing the microstructures of the coronary arterial walls, including the fibrous cap (97), lipid content (98, 99), calcification (100), macrophages (101, 102), cholesterol crystals (103, 104) and neovascularization (105–107). In the CLIMA study (108), Prati et al. investigated the prognostic value of OCT findings of lesions in the left descending coronary artery. In a total of 1,776 lipid plaques, the presence of MLA $<3.5\text{ mm}^2$, fibrous cap thickness $<75\text{ }\mu\text{m}$, lipid arc circumferential extension of $>180^\circ$, and OCT-defined macrophages were associated with an increased risk of the primary endpoint. Despite the substantial association between the presence of TCFA and MACE, OCT-TCFAs do not necessarily lead to ACS (99). Most thrombus formation associated with plaque rupture or erosion without

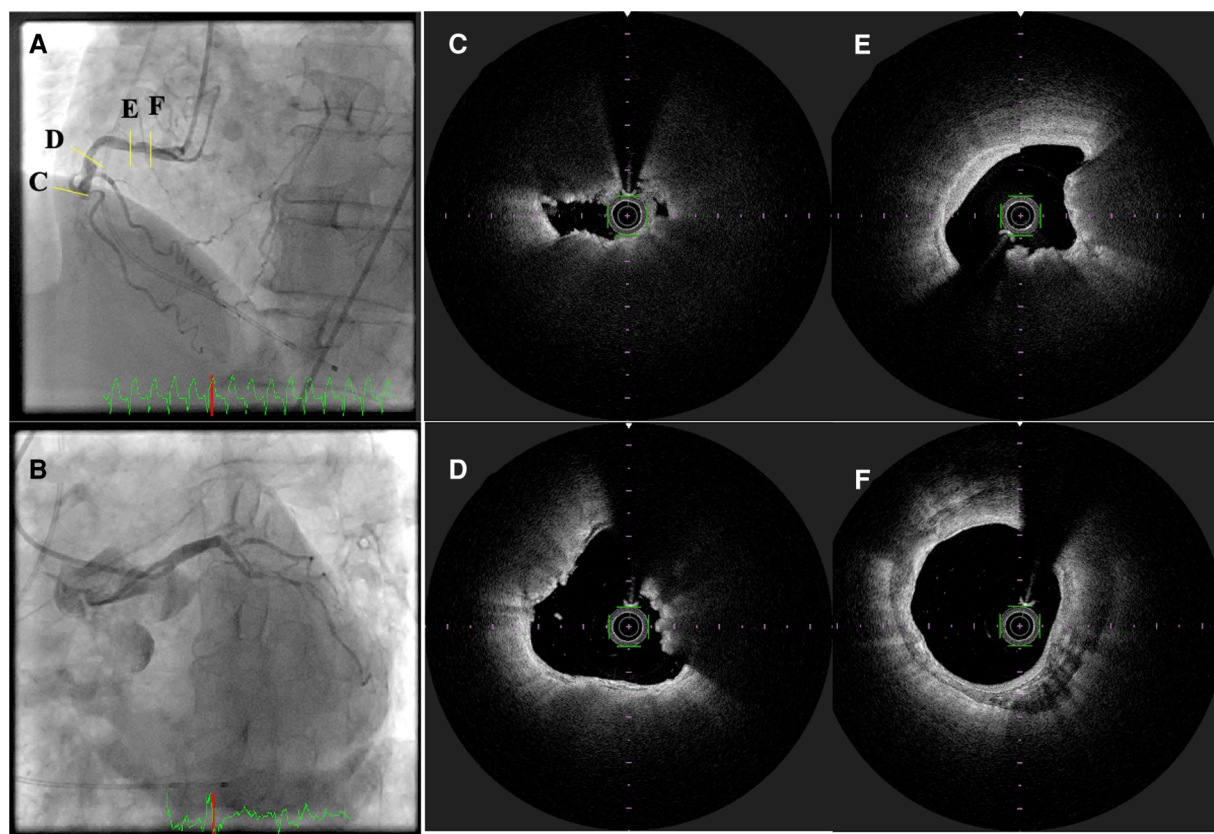


FIGURE 4

Optical frequency domain imaging of ST-segment elevation myocardial infarction. (A,B) Invasive coronary angiography revealed total occlusion of the mid-portion of the right coronary artery with collateral flow to the left descending coronary artery. (C–F) optical frequency domain imaging (OFDI) images after thrombectomy. (C) Thin capped fibroatheroma, (D,E) calcified nodules (yellow arrows), and (F) calcification.

clinical events is thought to be remodeled by vessel healing, followed by progression of the stenosis grade (40, 109). These findings have motivated the introduction of novel intracoronary imaging modalities, such as near-infrared autofluorescence and near-infrared fluorescence OCT (110), dual-modality OCT-IVUS (111), and polarization-sensitive (PS-) OCT (112, 113) to investigate the biological tissue components and comprehensive structures of coronary atherosclerosis (114, 115).

7. Lipid-lowering therapy in CAD

A meta-analysis of randomized clinical trials (RCT) investigating the effects of intensive lipid-lowering therapy found that statin therapy caused regression of the atherosclerotic disease burden (116). Other RCTs have also demonstrated that for patients at a higher risk of atherosclerosis, lower LDL cholesterol levels were better for plaque regression and CAD prognosis (117–119). Ezetimibe, a commonly used non-statin lipid-lowering drug, reduces LDL cholesterol levels by 13%–20%, with a low incidence of side effects. The IMPROVE-IT (Improved Reduction of Outcomes: Vytorin Efficacy International Trial) trial demonstrated that the addition of ezetimibe to statin therapy

resulted in a progressive reduction in LDL cholesterol levels and improved cardiovascular outcomes (118).

The role of imaging in the investigation of the effects of lipid-lowering therapies in patients with CAD is being increasingly recognized. In the FOURIER trials, Sabatine et al. demonstrated that PCSK9 inhibition with evolocumab, a monoclonal antibody, lowers the LDL cholesterol levels, leading to a reduced risk of cardiovascular events. The effect of alirocumab, a PCSK9 inhibitor, on the plaque volume and characteristics were evaluated in the PACMAN-AMI (Effects of the PCSK9 Antibody Alirocumab on Coronary Atherosclerosis in Patients With Acute Myocardial Infarction) randomized trial (15). The mean change in atherosclerotic volume assessed using IVUS was -2.13% in the alirocumab group and -0.92% in the placebo group. The change in the minimal fibrous capsule thickness was also more in the alirocumab group than in the placebo group, proving its plaque-reducing effect.

CCTA is an imaging modality widely used to study the pharmacological effects of changes in the plaque volume and composition. Budoff et al. demonstrated that icosapent ethyl reduced LAP volume (<50 HU) on CCTA over 18 months (58). Furthermore, in 857 patients undergoing serial CCTA imaging, van Rosendaal et al. investigated the compositional changes in the untreated, progressed coronary lesions, including low-

TABLE 2 Clinical trials targeting inflammatory pathways.

Authors References	Year	Country, follow-up (y)	Study design, data source	Sample size	Study population	Comparison	Primary endpoint	outcome	Summary of findings
PM Ridker et al. Reference (121)	2017	39 countries, 3.7 years	CANTOS, a randomized, double-blind trial	10,061	Stable CAD, persistent elevation of hsCRP (>2 mg/l)	Three doses of Canakinumab (IL-1 β antibody) 50 mg, 150 mg, 300 mg vs. placebo	Nonfatal MI, nonfatal stroke, or cardiovascular death	Placebo: 4.50 events per 100 person-years. 50 mg/150 mg/ 300 mg dose of canakinumab: 4.11/3.86/3.90 events per 100 person-years, respectively.	Canakinumab lowered the plasma CRP, IL-1 and IL-6 levels. Reduction in CV events.
PM Ridker et al. Reference (122)	2019	North America, 2.3 years	CIRT, a randomized, double-blind trial	4,786	Stable CAD and persistent evidence of inflammation, type 2 diabetes or metabolic syndrome	Low-dose (15–20 mg) methotrexate (a purine metabolism inhibitor) once per week vs. placebo	Nonfatal MI, nonfatal stroke, or cardiovascular death, hospitalization for unstable angina	Methotrexate group/placebo group: 201/207 patients. Incidence rate: 4.13/4.31 per 100 person-years (Methotrexate/ placebo)	Halted prematurely for futility. No change in plasma IL-1 β , IL-6 and hsCRP levels. No reduction in CV events
JC Tardif et al. Reference (123)	2019	12 countries, 22.6 months	COLCOT, A randomized, double-blind trial	4,745	Recent MI (<30 days)	Low-dose (0.5 mg/day) colchicine (a tubulin disrupter) vs. placebo	A composite of death from CV, resuscitated cardiac arrest, MI, stroke, or urgent hospitalization.	Colchicine/placebo incidence: 5.5%/7.1%	Reduction in CV death and CV events. Increase in pneumonia
SM Nidorf et al. Reference (124)	2013	Australia, 36 months	LoDoCo, a prospective, randomized, observer- blinded trial	532	Stable CAD	Low-dose (0.5 mg/day) colchicine plus usual care or standard care alone	The composite incidence of ACS, out-of-hospital cardiac arrest, or non-cardioembolic ischemic stroke.	Colchicine /placebo: 5.3%/16%	Colchicine effectively prevents cardiovascular events in patients with stable coronary disease.
Nidorf SM et al. Reference (125)	2020	Australia, Netherlands, 28.6 months	LoDoCo2, A randomized, controlled, double-blind trial	5,522	Chronic CAD	Low-dose (0.5 mg/day) colchicine plus usual care or standard care plus placebo	A composite of CV death, spontaneous MI, ischemic stroke, or ischemia-driven coronary revascularization.	Colchicine group/placebo group 6.8%/9.6% (Incidence, 2.5 vs. 3.6 events per 100 person-years)	Reduction in CV events

ACS, acute coronary syndrome; CAD, coronary artery disease; CV, cardiovascular; MI, myocardial infarction; hsCRP, high-sensitive C-reactive protein; IL, interleukin.

attenuation (−30 to 75 HU), fibro-fatty (76–130 HU), fibrous (131–350 HU), low-density calcium (351–700 HU), high-density calcium (701–1,000), and 1 K (1,000 HU) plaques (11). Serial CCTA imaging demonstrated that statin therapy is associated with a decrease in low-attenuation and fibrofatty plaques and a greater progression of high-density calcium and 1 K plaques. Taken together, CCTA is a useful imaging modality that assesses coronary structures and disease burden and its changes in response to OMT and lifestyle modifications.

8. Anti-inflammatory therapy and future perspectives of imaging

Although experimental studies have demonstrated a causal relationship between vascular inflammation and atherosclerosis, until recently, no robust evidence has suggested that anti-inflammatory therapy can prevent adverse cardiovascular outcomes (120). **Table 2** summarizes the recent clinical trials that have investigated the effects of anti-inflammatory therapy in patients with CAD. In the CANTOS (Canakinumab Antiinflammatory Thrombosis Outcome Study) trial which evaluated the effects of inflammation-targeted therapy in patients with stable CAD at residual inflammatory risk, high doses of canakinumab produced a 15% reduction in MACE and a 17% reduction in cardiovascular events (121). The CIRT trial, a prospective RCT consisting of 4,786 patients with stable atherosclerosis and diabetes or metabolic syndrome, demonstrated that low-dose methotrexate did not reduce MACE (122). However, low-dose methotrexate reduces plasma IL-1 β , IL-6, and CRP levels, supporting the concept that adequate inhibition of the innate immune pathway is necessary to ensure long-term cardiovascular benefits.

COLCOT and LoDoCo2 are two large clinical trials that provided and confirmed the hypothesis that repurposed colchicine is an effective anti-inflammatory agent in atherosclerosis (123, 125). Colchicine is an antimicrotubule agent that inhibits tubulin polymerization and microfibrinolysis. Part of its anti-inflammatory effect is due to its inhibition of NLRP3 inflammasome formation, which indirectly suppresses IL-1 β activation and decreases the downstream IL-6 and CRP levels. The COLCOT trial included approximately 5,000 patients with ACS who either received colchicine at 0.5 mg/day or placebo. During the 2-year follow-up, the colchicine group showed a 23% reduction in cardiovascular events. These clinical trials provided evidence for the addition of anti-inflammatory therapy to standard medical regimens, and suggested the importance of imaging techniques to assess vascular inflammation and plaque stabilization (10, 126, 127).

Imaging of the inflammation for the risk stratification can determine patients at a higher risk of atherosclerotic cardiovascular disease (ASCVD). Although PET/CT enables assessment of the inflammatory status of the large aorta, pericoronary arteries, and carotid arteries, its clinical application remains limited (128–131). CCTA enables the measurement of epicardial adipose tissue volume and composition (132, 133). Recent software developments

have enabled pericoronary adipose tissue attenuation analysis (**Figure 3D**), which serves as a predictor of patient outcomes (18). In addition, degradation of collagen, a major component of fibrous caps, plays a pivotal role in coronary plaque healing (134). Microscopic polarization-sensitive (PS) OCT (112, 113) is used to assess plaque structure and tissue polarization. Catheter-based PS-OCT enables quantitative assessment of plaque characteristics, such as collagen, vascular smooth muscle cells, and macrophages, by measuring polarization properties (birefringence and depolarization) (135–137). Otsuka et al. demonstrated that fibrous caps of plaques in patients with ACS had lower birefringence than those of plaques in patients with stable CAD (138). These findings indicate fibrous cap integrity, which could be weakened by matrix metalloproteinases-induced collagen degradation. Further studies are warranted to determine whether polarimetric signatures provide additional value for diagnosing plaque stability beyond that provided by the coronary plaque structural features (82, 137–139).

9. Conclusions

The identification of patients with myocardial ischemia can guide the management of stable CAD, which contributes to appropriate coronary revascularization. Systemic and vascular inflammation are potential imaging targets to assess plaque vulnerability in patients at a higher risk of ASCVD events. Novel imaging technologies will open up new avenues for the assessment of plaque vulnerability beyond the stage of ischemia.

Author contributions

RK and KO drafted the manuscript. DF supervised this study and drafted the manuscript. All authors contributed to the article and approved the submitted version.

Funding

This work was partially supported by research grants from the Japanese Heart Foundation, the Konica Minolta Science and Technology Foundation, and KAKENHI (Nos: 20K22923 and 22K08109).

Acknowledgments

We would like to thank Editage (www.editage.com) for the English language editing.

Conflict of interest

The authors declare that the research was conducted in the absence of any commercial or financial relationships that could be construed as a potential conflict of interest.

Publisher's note

All claims expressed in this article are solely those of the authors and do not necessarily represent those of their affiliated

organizations, or those of the publisher, the editors and the reviewers. Any product that may be evaluated in this article, or claim that may be made by its manufacturer, is not guaranteed or endorsed by the publisher.

References

- Virani SS, Alonso A, Benjamin EJ, Bittencourt MS, Callaway CW, Carson AP, et al. Heart disease and stroke statistics-2020 update: a report from the American Heart Association. *Circulation*. (2020) 141:e139–e596. doi: 10.1161/CIR.0000000000000757
- Knuuti J, Wijns W, Saraste A, Capodanno D, Barbato E, Funck-Brentano C, et al. 2019 ESC guidelines for the diagnosis and management of chronic coronary syndromes. *Eur Heart J*. (2020) 41:407–77. doi: 10.1093/eurheartj/ehz425
- Fuster V, Kovacic JC. Acute coronary syndromes: pathology, diagnosis, genetics, prevention, and treatment. *Circ Res*. (2014) 114:1847–51. doi: 10.1161/CIRCRESAHA.114.302806
- Boden WE, O'Rourke RA, Teo KK, Hartigan PM, Maron DJ, Kostuk WJ, et al. Optimal medical therapy with or without PCI for stable coronary disease. *N Engl J Med*. (2007) 356:1503–16. doi: 10.1056/NEJMoa070829
- Shaw LJ, Berman DS, Maron DJ, Mancini GBJ, Hayes SW, Hartigan PM, et al. Optimal medical therapy with or without percutaneous coronary intervention to reduce ischemic burden: results from the clinical outcomes utilizing revascularization and aggressive drug evaluation (COURAGE) trial nuclear substudy. *Circulation*. (2008) 117:1283–91. doi: 10.1161/CIRCULATIONAHA.107.743963
- Maron DJ, Hochman JS, Reynolds HR, Bangalore S, O'Brien SM, Boden WE, et al. Initial invasive or conservative strategy for stable coronary disease. *N Engl J Med*. (2020) 382:1395–407. doi: 10.1056/NEJMoa1915922
- Douglas PS, Hoffmann U, Patel MR, Mark DB, Al-Khalidi HR, Cavanaugh B, et al. Outcomes of anatomical versus functional testing for coronary artery disease. *N Engl J Med*. (2015) 372:1291–300. doi: 10.1056/NEJMoa1415516
- SCOT-HEART Investigators, Newby DE, Adamson PD, Berry C, Boon NA, Dweck MR, et al. Coronary CT angiography and 5-year risk of myocardial infarction. *N Engl J Med*. (2018) 379:924–33. doi: 10.1056/NEJMoa1805971
- Hecht HS, Blaha MJ, Kazerooni EA, Cury RC, Budoff M, Leipsic J, et al. CAC-DRS: coronary artery calcium data and reporting system. An expert consensus document of the society of cardiovascular computed tomography (SCCT). *J Cardiovasc Comput Tomogr*. (2018) 12:185–91. doi: 10.1016/j.jcct.2018.03.008
- Vaidya K, Arnott C, Martínez GJ, Ng B, McCormack S, Sullivan DR, et al. Colchicine therapy and plaque stabilization in patients with acute coronary syndrome: a CT coronary angiography study. *JACC Cardiovasc Imaging*. (2018) 11:305–16. doi: 10.1016/j.jcmg.2017.08.013
- van Rosendaal AR, van den Hoogen IJ, Gianni U, Ma X, Tantawy SW, Bax AM, et al. Association of statin treatment with progression of coronary atherosclerotic plaque composition. *JAMA Cardiol*. (2021) 6:1257–66. doi: 10.1001/jamacardio.2021.3055
- Pasupathy S, Air T, Dreyer RP, Tavella R, Beltrame JF. Systematic review of patients presenting with suspected myocardial infarction and nonobstructive coronary arteries. *Circulation*. (2015) 131:861–70. doi: 10.1161/CIRCULATIONAHA.114.011201
- Abdelrahman KM, Chen MY, Dey AK, Virmani R, Finn AV, Khamis RY, et al. Coronary computed tomography angiography from clinical uses to emerging technologies: JACC state-of-the-art review. *J Am Coll Cardiol*. (2020) 76:1226–43. doi: 10.1016/j.jacc.2020.06.076
- Araki M, Park SJ, Dauerman HL, Uemura S, Kim JS, Di Mario C, et al. Optical coherence tomography in coronary atherosclerosis assessment and intervention. *Nat Rev Cardiol*. (2022) 19:684–703. doi: 10.1038/s41569-022-00687-9
- Räber L, Ueki Y, Otsuka T, Losdat S, Häner JD, Lonborg J, et al. Effect of alirocumab added to high-intensity statin therapy on coronary atherosclerosis in patients with acute myocardial infarction: the PacMan-AMI randomized clinical trial. *JAMA*. (2022) 327:1771–81. doi: 10.1001/jama.2022.5218
- Stone GW, Maehara A, Lansky AJ, de Bruyne B, Cristea E, Mintz GS, et al. A prospective natural-history study of coronary atherosclerosis. *N Engl J Med*. (2011) 364:226–35. doi: 10.1056/NEJMoa1002358
- Williams MC, Kwicinski J, Doris M, McElhinney P, D'Souza MS, Cadet S, et al. Low-attenuation noncalcified plaque on coronary computed tomography angiography predicts myocardial infarction: results from the multicenter SCOT-HEART trial (Scottish computed tomography of the HEART). *Circulation*. (2020) 141:1452–62. doi: 10.1161/CIRCULATIONAHA.119.044720
- Antonopoulos AS, Sanna F, Sabharwal N, Thomas S, Oikonomou EK, Herdman L, et al. Detecting human coronary inflammation by imaging perivascular fat. *Sci Transl Med*. (2017) (398):eal2658. doi: 10.1126/scitranslmed.aal2658
- Doradla P, Otsuka K, Nadkarni A, Villiger M, Karanasos A, Zandvoort LJC, et al. Biomechanical stress profiling of coronary atherosclerosis: identifying a multifactorial metric to evaluate plaque rupture risk. *JACC Cardiovasc Imaging*. (2020) 13:804–16. doi: 10.1016/j.jcmg.2019.01.033
- Adriaenssens T, Allard-Ratick MP, Thondapu V, Sugiyama T, Raffel OC, Barlis P, et al. Optical coherence tomography of coronary plaque progression and destabilization: JACC focus seminar Part 3/3. *J Am Coll Cardiol*. (2021) 78:1275–87. doi: 10.1016/j.jacc.2021.07.032
- Camici PG, d'Amati G, Rimoldi O. Coronary microvascular dysfunction: mechanisms and functional assessment. *Nat Rev Cardiol*. (2015) 12:48–62. doi: 10.1038/nrcardio.2014.160
- Fuster V, Badimon L, Badimon JJ, Chesebro JH. The pathogenesis of coronary artery disease and the acute coronary syndromes (1). *N Engl J Med*. (1992) 326:242–50. doi: 10.1056/NEJM199201233260406
- Burke AP, Farb A, Malcom GT, Liang YH, Smialek J, Virmani R. Coronary risk factors and plaque morphology in men with coronary disease who died suddenly. *N Engl J Med*. (1997) 336:1276–82. doi: 10.1056/NEJM199705013361802
- Virmani R, Kolodgie FD, Burke AP, Farb A, Schwartz SM. Lessons from sudden coronary death: a comprehensive morphological classification scheme for atherosclerotic lesions. *Arterioscler Thromb Vasc Biol*. (2000) 20:1262–75. doi: 10.1161/01.ATV.20.5.1262
- Yahagi K, Kolodgie FD, Otsuka F, Finn AV, Davis HR, Joner M, et al. Pathophysiology of native coronary, vein graft, and in-stent atherosclerosis. *Nat Rev Cardiol*. (2016) 13:79–98. doi: 10.1038/nrcardio.2015.164
- Burke AP, Kolodgie FD, Farb A, Weber DK, Malcom GT, Smialek J, et al. Healed plaque ruptures and sudden coronary death: evidence that subclinical rupture has a role in plaque progression. *Circulation*. (2001) 103:934–40. doi: 10.1161/01.CIR.103.7.934
- Motoyama S, Sarai M, Harigaya H, Anno H, Inoue K, Hara T, et al. Computed tomographic angiography characteristics of atherosclerotic plaques subsequently resulting in acute coronary syndrome. *J Am Coll Cardiol*. (2009) 54:49–57. doi: 10.1016/j.jacc.2009.02.068
- Ozaki Y, Okumura M, Ismail TF, Motoyama S, Naruse H, Hattori K, et al. Coronary CT angiographic characteristics of culprit lesions in acute coronary syndromes not related to plaque rupture as defined by optical coherence tomography and angioscopy. *Eur Heart J*. (2011) 32:2814–23. doi: 10.1093/eurheartj/ehr189
- Otsuka K, Fukuda S, Tanaka A, Nakanishi K, Taguchi H, Yoshikawa J, et al. Napkin-ring sign on coronary CT angiography for the prediction of acute coronary syndrome. *JACC Cardiovasc Imaging*. (2013) 6:448–57. doi: 10.1016/j.jcmg.2012.09.016
- Ahmadi A, Leipsic J, Blankstein R, Taylor C, Hecht H, Stone GW, et al. Do plaques rapidly progress prior to myocardial infarction? The interplay between plaque vulnerability and progression. *Circ Res*. (2015) 117:99–104. doi: 10.1161/CIRCRESAHA.117.305637
- Stone GW, Mintz GS, Virmani R. Vulnerable plaques, vulnerable patients, and intravascular imaging. *J Am Coll Cardiol*. (2018) 72:2022–6. doi: 10.1016/j.jacc.2018.09.010
- Kume T, Akasaka T, Kawamoto T, Okura H, Watanabe N, Toyota E, et al. Measurement of the thickness of the fibrous cap by optical coherence tomography. *Am Heart J*. (2006) 152:755.e1–e4. doi: 10.1016/j.ahj.2006.06.030
- Ehara S, Kobayashi Y, Yoshiyama M, Shimada K, Shimada Y, Fukuda D, et al. Spotty calcification typifies the culprit plaque in patients with acute myocardial infarction: an intravascular ultrasound study. *Circulation*. (2004) 110:3424–9. doi: 10.1161/01.CIR.0000148131.41425.E9
- Arbab-Zadeh A, Fuster V. The myth of the “vulnerable plaque”: transitioning from a focus on individual lesions to atherosclerotic disease burden for coronary artery disease risk assessment. *J Am Coll Cardiol*. (2015) 65:846–55. doi: 10.1016/j.jacc.2014.11.041
- Arbab-Zadeh A, Fuster V. From detecting the vulnerable plaque to managing the vulnerable patient: JACC state-of-the-art review. *J Am Coll Cardiol*. (2019) 74:1582–93. doi: 10.1016/j.jacc.2019.07.062
- Kolodgie FD, Burke AP, Farb A, Weber DK, Kutys R, Wight TN, et al. Differential accumulation of proteoglycans and hyaluronan in culprit lesions: insights into plaque erosion. *Arterioscler Thromb Vasc Biol*. (2002) 22:1642–8. doi: 10.1161/01.ATV.0000034021.92658.4C

37. Quillard T, Araújo HA, Franck G, Shvartz E, Sukhova G, Libby P. TLR2 And neutrophils potentiate endothelial stress, apoptosis and detachment: implications for superficial erosion. *Eur Heart J.* (2015) 36:1394–404. doi: 10.1093/eurheartj/ehv044
38. Crea F, Libby P. Acute coronary syndromes: the way forward from mechanisms to precision treatment. *Circulation.* (2017) 136:1155–66. doi: 10.1161/CIRCULATIONAHA.117.029870
39. Kubo T, Maehara A, Mintz GS, Doi H, Tsujita K, Choi SY, et al. The dynamic nature of coronary artery lesion morphology assessed by serial virtual histology intravascular ultrasound tissue characterization. *J Am Coll Cardiol.* (2010) 55:1590–7. doi: 10.1016/j.jacc.2009.07.078
40. Yamamoto MH, Yamashita K, Matsumura M, Fujino A, Ishida M, Ebara S, et al. Serial 3-vessel optical coherence tomography and intravascular ultrasound analysis of changing morphologies associated with lesion progression in patients with stable angina pectoris. *Circ Cardiovasc Imaging.* (2017) 10:1–9. doi: 10.1161/CIRCIMAGING.117.006347
41. Agewall S, Beltrame JF, Reynolds HR, Niessner A, Rosano G, Caforio ALP, et al. ESC Working group position paper on myocardial infarction with non-obstructive coronary arteries. *Eur Heart J.* (2017) 38:143–53. doi: 10.1093/eurheartj/ehw149
42. Tamis-Holland JE, Jneid H, Reynolds HR, Agewall S, Brilakis ES, Brown TM, et al. Contemporary diagnosis and management of patients with myocardial infarction in the absence of obstructive coronary artery disease: a scientific statement from the American Heart Association. *Circulation.* (2019) 139:e891–e908. doi: 10.1161/CIR.0000000000000670
43. Marinescu MA, Löffler AI, Ouellette M, Smith L, Kramer CM, Bourque JM. Coronary microvascular dysfunction, microvascular angina, and treatment strategies. *JACC Cardiovasc Imaging.* (2015) 8:210–20. doi: 10.1016/j.jcmg.2014.12.008
44. Shimokawa H, Suda A, Takahashi J, Berry C, Camici PG, Crea F, et al. Clinical characteristics and prognosis of patients with microvascular angina: an international and prospective cohort study by the coronary vasomotor disorders international study (COVADIS) group. *Eur Heart J.* (2021) 42:4592–600. doi: 10.1093/eurheartj/ehab282
45. Suda A, Takahashi J, Hao K, Kikuchi Y, Shindo T, Ikeda S, et al. Coronary functional abnormalities in patients with angina and nonobstructive coronary artery disease. *J Am Coll Cardiol.* (2019) 74:2350–60. doi: 10.1016/j.jacc.2019.08.1056
46. Reynolds HR, Picard MH, Spertus JA, Peteiro J, Lopez Sendon JL, Senior R, et al. Natural history of patients with ischemia and no obstructive coronary artery disease: the CIAO-ischemia study. *Circulation.* (2021) 144:1008–23. doi: 10.1161/CIRCULATIONAHA.120.046791
47. Kunadian V, Chieffo A, Camici PG, Berry C, Escaned J, Maas AHEM, et al. An EAPCI expert consensus document on ischaemia with non-obstructive coronary arteries in collaboration with European society of cardiology working group on coronary pathophysiology & microcirculation endorsed by coronary vasomotor disorders international study group. *Eur Heart J.* (2020) 41:3504–20. doi: 10.1093/eurheartj/ehaa503
48. Nakanishi K, Fukuda S, Shimada K, Miyazaki C, Otsuka K, Kawarabayashi T, et al. Prognostic value of coronary flow reserve on long-term cardiovascular outcomes in patients with chronic kidney disease. *Am J Cardiol.* (2013) 112:928–32. doi: 10.1016/j.amjcard.2013.05.025
49. Kubo T, Fukuda S, Hirata K, Shimada K, Maeda K, Komukai K, et al. Comparison of coronary microcirculation in female nurses after day-time versus night-time shifts. *Am J Cardiol.* (2011) 108:1665–8. doi: 10.1016/j.amjcard.2011.07.028
50. Zhou W, Lee JCY, Leung ST, Lai A, Lee T-F, Chiang JB, et al. Long-term prognosis of patients with coronary microvascular disease using stress perfusion cardiac magnetic resonance. *JACC Cardiovasc Imaging.* (2021) 14:602–11. doi: 10.1016/j.jcmg.2020.09.034
51. Naya M, Murthy VL, Foster CR, Gaber M, Klein J, Hainer J, et al. Prognostic interplay of coronary artery calcification and underlying vascular dysfunction in patients with suspected coronary artery disease. *J Am Coll Cardiol.* (2013) 61:2098–106. doi: 10.1016/j.jacc.2013.02.029
52. Gdowski MA, Murthy VL, Doering M, Monroy-Gonzalez AG, Slart R, Brown DL. Association of isolated coronary microvascular dysfunction with mortality and major adverse cardiac events: a systematic review and meta-analysis of aggregate data. *J Am Heart Assoc.* (2020) 9:e014954. doi: 10.1161/JAHA.119.014954
53. Sorbets E, Fox KM, Elbez Y, Danchin N, Dorian P, Ferrari R, et al. Long-term outcomes of chronic coronary syndrome worldwide: insights from the international CLARIFY registry. *Eur Heart J.* (2020) 41:347–56. doi: 10.1093/eurheartj/ehz660
54. Task Force on Myocardial Revascularization of the European Society of Cardiology (ESC) and the European Association for Cardio-Thoracic Surgery (EACTS), European Association for Percutaneous Cardiovascular Interventions (EAPCI), Wijns W, Kolh P, Danchin N, Di Mario C, Falk V, Folliguet T, et al. Guidelines on myocardial revascularization. *Eur Heart J.* (2010) 31:2501–55. doi: 10.1093/eurheartj/ehq277
55. Otsuka K, Fukuda S, Tanaka A, Nakanishi K, Taguchi H, Yoshiyama M, et al. Prognosis of vulnerable plaque on computed tomographic coronary angiography with normal myocardial perfusion image. *Eur Heart J Cardiovasc Imaging.* (2014) 15:332–40. doi: 10.1093/ehjci/jet232
56. Lee JM, Choi KH, Koo BK, Park J, Kim J, Hwang D, et al. Prognostic implications of plaque characteristics and stenosis severity in patients with coronary artery disease. *J Am Coll Cardiol.* (2019) 73:2413–24. doi: 10.1016/j.jacc.2019.02.060
57. Hoffmann U, Ferencik M, Udelson JE, Picard MH, Truong QA, Patel MR, et al. Prognostic value of noninvasive cardiovascular testing in patients with stable chest pain: insights from the PROMISE trial (prospective multicenter imaging study for evaluation of chest pain). *Circulation.* (2017) 135:2320–32. doi: 10.1161/CIRCULATIONAHA.116.024360
58. Budoff MJ, Bhatt DL, Kinninger A, Lakshmanan S, Muhlestein JB, Le VT, et al. Effect of icosapent ethyl on progression of coronary atherosclerosis in patients with elevated triglycerides on statin therapy: final results of the EVAPORATE trial. *Eur Heart J.* (2020) 41:3925–32. doi: 10.1093/eurheartj/ehaa652
59. Narula J, Chandrasekhar Y, Ahmadi A, Abbasa S, Berman DS, Blankstein R, et al. SCCT 2021 Expert consensus document on coronary computed tomographic angiography: a report of the society of cardiovascular computed tomography. *J Cardiovasc Comput Tomogr.* (2021) 15:192–217. doi: 10.1016/j.jcct.2020.11.001
60. Anthonopolos R, Maron DJ, Bangalore S, Reynolds HR, Xu Y, O'Brien SM, et al. Ischemia-EXTEND studies: rationale and design. *Am Heart J.* (2022) 254:228–33. doi: 10.1016/j.ahj.2022.09.009
61. Hojo K, Otsuka K, Kasayuki N. Plaque rupture after coronary CT angiography. *Eur Heart J.* (2022):ehac743. in press. doi: 10.1093/eurheartj/ehac743
62. Puchner SB, Liu T, Mayrhofer T, Truong QA, Lee H, Fleg JL, et al. High-risk plaque detected on coronary CT angiography predicts acute coronary syndromes independent of significant stenosis in acute chest pain: results from the ROMICAT-II trial. *J Am Coll Cardiol.* (2014) 64:684–92. doi: 10.1016/j.jacc.2014.05.039
63. Lee JM, Choi KH, Koo BK, Park J, Kim J, Hwang D, et al. Prognostic implications of plaque characteristics and stenosis severity in patients with coronary artery disease. *J Am Coll Cardiol.* (2019) 73:2413–24. doi: 10.1016/j.jacc.2019.02.060
64. Ingkanisorn WP, Kwong RY, Bohme NS, Geller NL, Rhoads KL, Dyke CK, et al. Prognosis of negative adenosine stress magnetic resonance in patients presenting to an emergency department with chest pain. *J Am Coll Cardiol.* (2006) 47:1427–32. doi: 10.1016/j.jacc.2005.11.059
65. Yamaura H, Ishikawa H, Otsuka K, Kasayuki N. Reverse takotsubo cardiomyopathy as a cause of acute chest pain in a young woman following COVID-19 vaccination. *Circ Cardiovasc Imaging.* (2022) 15:e013661. doi: 10.1161/CIRCIMAGING.121.013661
66. Ferreira VM, Schulz-Menger J, Holmvang G, Kramer CM, Carbone I, Sechtem U, et al. Cardiovascular magnetic resonance in nonischemic myocardial inflammation: expert recommendations. *J Am Coll Cardiol.* (2018) 72:3158–76. doi: 10.1016/j.jacc.2018.09.072
67. Tanimoto T, Imanishi T, Kitabata H, Nakamura N, Kimura K, Yamano T, et al. Prevalence and clinical significance of papillary muscle infarction detected by late gadolinium-enhanced magnetic resonance imaging in patients with ST-segment elevation myocardial infarction. *Circulation.* (2010) 122:2281–7. doi: 10.1161/CIRCULATIONAHA.109.935338
68. Kwong RY, Schussheim AE, Rekhraj S, Aletras AH, Geller N, Davis J, et al. Detecting acute coronary syndrome in the emergency department with cardiac magnetic resonance imaging. *Circulation.* (2003) 107:531–7. doi: 10.1161/01.cir.0000047527.11221.29
69. Taylor AJ, Salerno M, Dharmakumar R, Jerosch-Herold M. T1 mapping: basic techniques and clinical applications. *JACC Cardiovasc Imaging.* (2016) 9:67–81. doi: 10.1016/j.jcmg.2015.11.005
70. Kim HW, Jenista ER, Wendell DC, Azevedo CF, Campbell MJ, Darty SN, et al. Patients with acute myocarditis following mRNA COVID-19 vaccination. *JAMA Cardiol.* (2021) 6:1196–201. doi: 10.1001/jamacardio.2021.2828
71. Bossone E, Lyon A, Citro R, Athanasiadis A, Meimoun P, Parodi G, et al. Takotsubo cardiomyopathy: an integrated multi-imaging approach. *Eur Heart J Cardiovasc Imaging.* (2014) 15:366–77. doi: 10.1093/ehjci/jet167
72. Noguchi T, Kawasaki T, Tanaka A, Yasuda S, Goto Y, Ishihara M, et al. High-intensity signals in coronary plaques on noncontrast T1-weighted magnetic resonance imaging as a novel determinant of coronary events. *J Am Coll Cardiol.* (2014) 63:989–99. doi: 10.1016/j.jacc.2013.11.034
73. Matsumoto K, Ehara S, Hasegawa T, Sakaguchi M, Otsuka K, Yoshikawa J, et al. Localization of coronary high-intensity signals on T1-weighted MR imaging: relation to plaque morphology and clinical severity of angina pectoris. *JACC Cardiovasc Imaging.* (2015) 8:1143–52. doi: 10.1016/j.jcmg.2015.06.013
74. Bos D, Arshi B, van den Bouwhuisen QJA, Ikram MK, Selwaness M, Vernooij MW, et al. Atherosclerotic carotid plaque composition and incident stroke and coronary events. *J Am Coll Cardiol.* (2021) 77:1426–35. doi: 10.1016/j.jacc.2021.01.038
75. van der Toorn JE, Bos D, Ikram MK, Verwoert GC, van der Lugt A, Ikram MA, et al. Carotid plaque composition and prediction of incident atherosclerotic cardiovascular disease. *Circ Cardiovasc Imaging.* (2022) 15:e013602. doi: 10.1161/CIRCIMAGING.121.013602
76. Tarkin JM, Joshi FR, Rudd JHF. PET Imaging of inflammation in atherosclerosis. *Nat Rev Cardiol.* (2014) 11:443–57. doi: 10.1038/nrcardio.2014.80

77. Rudd JHF, Narula J, Strauss HW, Virmani R, Machac J, Klimas M, et al. Imaging atherosclerotic plaque inflammation by fluorodeoxyglucose with positron emission tomography: ready for prime time? *J Am Coll Cardiol.* (2010) 55:2527–35. doi: 10.1016/j.jacc.2009.12.061
78. Weck MR, Chow MWL, Joshi NV, Williams MC, Jones C, Fletcher AM, et al. Coronary arterial 18F-sodium fluoride uptake: a novel marker of plaque biology. *J Am Coll Cardiol.* (2012) 59:1539–48. doi: 10.1016/j.jacc.2011.12.037
79. Joshi NV, Vesey AT, Williams MC, Shah ASV, Calvert PA, Craighead FHM, et al. 18F-fluoride Positron emission tomography for identification of ruptured and high-risk coronary atherosclerotic plaques: a prospective clinical trial. *Lancet.* (2014) 383:705–13. doi: 10.1016/S0140-6736(13)61754-7
80. Maehara A, Matsumura M, Ali ZA, Mintz GS, Stone GW. IVUS-guided versus OCT-guided coronary stent implantation: a critical appraisal. *JACC Cardiovasc Imaging.* (2017) 10:1487–503. doi: 10.1016/j.jcmg.2017.09.008
81. Yamaji K, Ueki Y, Souteyrand G, Daemen J, Wiebe J, Nef H, et al. Mechanisms of very late bioresorbable scaffold thrombosis: the INVEST registry. *J Am Coll Cardiol.* (2017) 70:2330–44. doi: 10.1016/j.jacc.2017.09.014
82. Otsuka K, Villiger M, van Zandvoort LJC, Neleman T, Karanasos A, Dijkstra J, et al. Polarimetric signatures of vascular tissue response to drug-eluting stent implantation in patients. *JACC Cardiovasc Imaging.* (2020) 13:2695–6. doi: 10.1016/j.jcmg.2020.07.009
83. Valgimigli M, Frigoli E, Heg D, Tijssen J, Jüni P, Vranckx P, et al. Dual antiplatelet therapy after PCI in patients at high bleeding risk. *N Engl J Med.* (2021) 385:1643–55. doi: 10.1056/NEJMoa2108749
84. Giustino G, Chieffo A, Palmerini T, Valgimigli M, Feres F, Abizaid A, et al. Efficacy and safety of dual antiplatelet therapy after complex PCI. *J Am Coll Cardiol.* (2016) 68:1851–64. doi: 10.1016/j.jacc.2016.07.760
85. Otsuka K. Newer-generation drug-eluting stents in patients undergoing complex percutaneous coronary intervention. *JACC Asia.* (2021) 1:342–4. doi: 10.1016/j.jacasi.2021.09.001
86. Valgimigli M, Bueno H, Byrne RA, Collet JP, Costa F, Jeppsson A, et al. 2017 ESC focused update on dual antiplatelet therapy in coronary artery disease developed in collaboration with EACTS: the task force for dual antiplatelet therapy in coronary artery disease of the European society of cardiology (ESC) and of the European association for cardio-thoracic surgery (EACTS). *Eur Heart J.* (2018) 39:213–60. doi: 10.1093/eurheartj/ehx419
87. Groenland FTW, Neleman T, Kakar H, Scoccia A, des Plantes AC Z, Clephas PRD, et al. Intravascular ultrasound-guided versus coronary angiography-guided percutaneous coronary intervention in patients with acute myocardial infarction: a systematic review and meta-analysis. *Int J Cardiol.* (2022) 353:35–42. doi: 10.1016/j.ijcard.2022.01.021
88. Tanaka A, Kawarabayashi T, Nishibori Y, Sano T, Nishida Y, Fukuda D, et al. No-reflow phenomenon and lesion morphology in patients with acute myocardial infarction. *Circulation.* (2002) 105:2148–52. doi: 10.1161/01.cir.0000015697.59592.07
89. Fukuda D, Shimada K, Tanaka A, Kusuyama T, Yamashita H, Ehara S, et al. Comparison of levels of serum matrix metalloproteinase-9 in patients with acute myocardial infarction versus unstable angina pectoris versus stable angina pectoris. *Am J Cardiol.* (2006) 97:175–80. doi: 10.1016/j.amjcard.2005.08.020
90. Hong MK, Mintz GS, Lee CW, Kim YH, Lee SW, Song JM, et al. Comparison of coronary plaque rupture between stable angina and acute myocardial infarction: a three-vessel intravascular ultrasound study in 235 patients. *Circulation.* (2004) 110:928–33. doi: 10.1161/01.CIR.0000139858.69915.2E
91. Terada K, Kubo T, Kameyama T, Matsuo Y, Ino Y, Emori H, et al. NIRS-IVUS for differentiating coronary plaque rupture, erosion, and calcified nodule in acute myocardial infarction. *JACC Cardiovasc Imaging.* (2021) 14:1440–50. doi: 10.1016/j.jcmg.2020.08.030
92. Waksman R, Di Mario C, Torguson R, Ali ZA, Singh V, Skinner WH, et al. Identification of patients and plaques vulnerable to future coronary events with near-infrared spectroscopy intravascular ultrasound imaging: a prospective, cohort study. *Lancet.* (2019) 394:1629–37. doi: 10.1016/S0140-6736(19)31794-5
93. Bouma BE, Villiger M, Otsuka K, Oh WY. Intravascular optical coherence tomography [invited]. *Biomed Opt Express.* (2017) 8:2660–86. doi: 10.1364/BOE.8.002660
94. Kubo T, Shinke T, Okamura T, Hibi K, Nakazawa G, Morino Y, et al. Optical frequency domain imaging vs. intravascular ultrasound in percutaneous coronary intervention (OPINION trial): one-year angiographic and clinical results. *Eur Heart J.* (2017) 38:3139–47. doi: 10.1093/eurheartj/ehx351
95. Meneveau N, Souteyrand G, Motreff P, Caussin C, Amabile N, Ohlmann P, et al. Optical coherence tomography to optimize results of percutaneous coronary intervention in patients with non-ST-elevation acute coronary syndrome: results of the multicenter, randomized DOCTORS study (does optical coherence tomography optimize results of stenting). *Circulation.* (2016) 134:906–17. doi: 10.1161/CIRCULATIONAHA.116.024393
96. Ali ZA, Maehara A, Généreux P, Shlofmitz RA, Fabbiochi F, Nazif TM, et al. Optical coherence tomography compared with intravascular ultrasound and with angiography to guide coronary stent implantation (ILUMIEN III: OPTIMIZE PCI): a randomised controlled trial. *Lancet.* (2016) 388:2618–28. doi: 10.1016/S0140-6736(16)31922-5
97. Yonetsu T, Kakuta T, Lee T, Takahashi K, Kawaguchi N, Yamamoto G, et al. In vivo critical fibrous cap thickness for rupture-prone coronary plaques assessed by optical coherence tomography. *Eur Heart J.* (2011) 32:1251–9. doi: 10.1093/eurheartj/ehq518
98. Tanaka A, Imanishi T, Kitabata H, Kubo T, Takarada S, Tanimoto T, et al. Lipid-rich plaque and myocardial perfusion after successful stenting in patients with non-ST-segment elevation acute coronary syndrome: an optical coherence tomography study. *Eur Heart J.* (2009) 30:1348–55. doi: 10.1093/eurheartj/ehp122
99. Xing L, Higuma T, Wang Z, Aguirre AD, Mizuno K, Takano M, et al. Clinical significance of lipid-rich plaque detected by optical coherence tomography: a 4-year follow-up study. *J Am Coll Cardiol.* (2017) 69:2502–13. doi: 10.1016/j.jacc.2017.03.556
100. Sugiyama T, Yamamoto E, Fracassi F, Lee H, Yonetsu T, Kakuta T, et al. Calcified plaques in patients with acute coronary syndromes. *JACC Cardiovasc Interv.* (2019) 12:531–40. doi: 10.1016/j.jcin.2018.12.013
101. Tearney GJ, Yabushita H, Houser SL, Aretz HT, Jang IK, Schlendorf KH, et al. Quantification of macrophage content in atherosclerotic plaques by optical coherence tomography. *Circulation.* (2003) 107:113–9. doi: 10.1161/01.CIR.0000044384.41037.43
102. Phipps JE, Vela D, Hoyt T, Halaney DL, Mancuso JJ, Buja LM, et al. Macrophages and intravascular OCT bright spots: a quantitative study. *JACC Cardiovasc Imaging.* (2015) 8:63–72. doi: 10.1016/j.jcmg.2014.07.027
103. Otsuka K, Shimada K, Ishikawa H, Nakamura H, Katayama H, Takeda H, et al. Usefulness of pre- and post-stent optical frequency domain imaging findings in the prediction of periprocedural cardiac troponin elevation in patients with coronary artery disease. *Heart Vessels.* (2020) 35:451–62. doi: 10.1007/s00380-019-01512-z
104. Katayama Y, Tanaka A, Taruya A, Kashiwagi M, Nishiguchi T, Ozaki Y, et al. Feasibility and clinical significance of in vivo cholesterol crystal detection using optical coherence tomography. *Arterioscler Thromb Vasc Biol.* (2020) 40:220–9. doi: 10.1161/ATVBAHA.119.312934
105. Hasegawa T, Otsuka K, Iguchi T, Matsumoto K, Ehara S, Nakata S, et al. Serum n-3 to n-6 polyunsaturated fatty acids ratio correlates with coronary plaque vulnerability: an optical coherence tomography study. *Heart Vessels.* (2014) 29:596–602. doi: 10.1007/s00380-013-0404-4
106. Iguchi T, Hasegawa T, Otsuka K, Matsumoto K, Yamazaki T, Nishimura S, et al. Insulin resistance is associated with coronary plaque vulnerability: insight from optical coherence tomography analysis. *Eur Heart J Cardiovasc Imaging.* (2014) 15:284–91. doi: 10.1093/ehjci/jet158
107. Taruya A, Tanaka A, Nishiguchi T, Matsuo Y, Ozaki Y, Kashiwagi M, et al. Vasa vasorum restructuring in human atherosclerotic plaque vulnerability: a clinical optical coherence tomography study. *J Am Coll Cardiol.* (2015) 65:2469–77. doi: 10.1016/j.jacc.2015.04.020
108. Prati F, Romagnoli E, Gatto L, La Manna A, Burzotta F, Ozaki Y, et al. Relationship between coronary plaque morphology of the left anterior descending artery and 12 months clinical outcome: the CLIMA study. *Eur Heart J.* (2020) 41:383–91. doi: 10.1093/eurheartj/ehz520
109. Fracassi F, Crea F, Sugiyama T, Yamamoto E, Uemura S, Vergallo R, et al. Healed culprit plaques in patients with acute coronary syndromes. *J Am Coll Cardiol.* (2019) 73:2253–63. doi: 10.1016/j.jacc.2018.10.093
110. Ughi GJ, Wang H, Gerbaud E, Gardecki JA, Fard AM, Hamidi E, et al. Clinical characterization of coronary atherosclerosis with dual-modality OCT and near-infrared autofluorescence imaging. *JACC Cardiovasc Imaging.* (2016) 9:1304–14. doi: 10.1016/j.jcmg.2015.11.020
111. Ren J, Shishkov M, Villiger ML, Otsuka K, Nadkarni SK, Bouma BE. Single-catheter dual-modality intravascular imaging combining IVUS and OFDI: a holistic structural visualisation of coronary arteries. *EuroIntervention.* (2021) 17:e919–22. doi: 10.4244/EIJ-D-20-00990
112. de Boer JF, Hitznerberger CK, Yasuno Y. Polarization sensitive optical coherence tomography – A review [invited]. *Biomed Opt Express.* (2017) 8:1838–73. doi: 10.1364/BOE.8.001838
113. Nadkarni SK, Pierce MC, Park BH, de Boer JF, Whittaker P, Bouma BE, et al. Measurement of collagen and smooth muscle cell content in atherosclerotic plaques using polarization-sensitive optical coherence tomography. *J Am Coll Cardiol.* (2007) 49:1474–81. doi: 10.1016/j.jacc.2006.11.040
114. Bourantas CV, Jaffer FA, Gijzen FJ, Van Soest G, Madden SP, Courtney BK, et al. Hybrid intravascular imaging: recent advances, technical considerations, and current applications in the study of plaque pathophysiology. *Eur Heart J.* (2017) 38:400–12. doi: 10.1093/eurheartj/ehw097
115. Otsuka K, Villiger M, Nadkarni SK, Bouma BE. Intravascular polarimetry: clinical translation and future applications of catheter-based polarization sensitive optical frequency domain imaging. *Front Cardiovasc Med.* (2020) 7:146. doi: 10.3389/fcvm.2020.00146
116. Cholesterol Treatment Trialists' (CTT) Collaboration, Baigent C, Blackwell L, Emberson J, Holland LE, Reith C, et al. Efficacy and safety of more intensive lowering of LDL cholesterol: a meta-analysis of data from 170,000 participants in 26 randomised trials. *Lancet.* (2010) 376:1670–81. doi: 10.1016/S0140-6736(10)61350-5

117. Boekholdt SM, Hovingh GK, Mora S, Arsenault BJ, Amarenco P, Pedersen TR, et al. Very low levels of atherogenic lipoproteins and the risk for cardiovascular events: a meta-analysis of statin trials. *J Am Coll Cardiol.* (2014) 64:485–94. doi: 10.1016/j.jacc.2014.02.615
118. Cannon CP, Blazing MA, Giugliano RP, McCagg A, White JA, Theroux P, et al. Ezetimibe added to statin therapy after acute coronary syndromes. *N Engl J Med.* (2015) 372:2387–97. doi: 10.1056/NEJMoa1410489
119. Sabatine MS, Giugliano RP, Keech AC, Honarpour N, Wiviott SD, Murphy SA, et al. Evolocumab and clinical outcomes in patients with cardiovascular disease. *N Engl J Med.* (2017) 376:1713–22. doi: 10.1056/NEJMoa1615664
120. Libby P. The changing landscape of atherosclerosis. *Nature.* (2021) 592:524–33. doi: 10.1038/s41586-021-03392-8
121. Ridker PM, Everett BM, Thuren T, MacFadyen JG, Chang WH, Ballantyne C, et al. Antiinflammatory therapy with canakinumab for atherosclerotic disease. *N Engl J Med.* (2017) 377:1119–31. doi: 10.1056/NEJMoa1707914
122. Ridker PM, Everett BM, Pradhan A, MacFadyen JG, Solomon DH, Zaharris E, et al. Low-dose methotrexate for the prevention of atherosclerotic events. *N Engl J Med.* (2019) 380:752–62. doi: 10.1056/NEJMoa1809798
123. Tardif JC, Kouz S, Waters DD, Bertrand OF, Diaz R, Maggioni AP, et al. Efficacy and safety of low-dose colchicine after myocardial infarction. *N Engl J Med.* (2019) 381:2497–505. doi: 10.1056/NEJMoa1912388
124. Nidorf SM, Eikelboom JW, Budgeon CA, Thompson PL. Low-dose colchicine for secondary prevention of cardiovascular disease. *J Am Coll Cardiol.* (2013) 61:404–10. doi: 10.1016/j.jacc.2012.10.02
125. Nidorf SM, Fiolet ATL, Mosterd A, Eikelboom JW, Schut A, Opstal TSJ, et al. Colchicine in patients with chronic coronary disease. *N Engl J Med.* (2020) 383:1838–47. doi: 10.1056/NEJMoa2021372
126. Cecconi A, Vilchez-Tschischke JP, Mateo J, Sanchez-Gonzalez J, España S, Fernandez-Jimenez R, et al. Effects of colchicine on atherosclerotic plaque stabilization: a multimodality imaging study in an animal model. *J Cardiovasc Transl Res.* (2021) 14:150–60. doi: 10.1007/s12265-020-09974-7
127. Montarello NJ, Singh K, Sinhal A, Wong DTL, Alcock R, Rajendran S, et al. Assessing the impact of colchicine on coronary plaque phenotype after myocardial infarction with optical coherence tomography: rationale and design of the COCOMO-ACS study. *Cardiovasc Drugs Ther.* (2022) 36:1175–86. doi: 10.1007/s10557-021-07240-9
128. Vesey AT, Jenkins WS, Irkle A, Moss A, Sng G, Forsythe RO, et al. 18F-fluoride and 18F-fluorodeoxyglucose positron emission tomography after transient ischemic attack or minor ischemic stroke: case-control study. *Circ Cardiovasc Imaging.* (2017) 10:e004976. doi: 10.1161/CIRCIMAGING.116.004976
129. Fletcher AJ, Tew YY, Tzolos E, Joshi SS, Kaczynski J, Nash J, et al. Thoracic aortic 18F-sodium fluoride activity and ischemic stroke in patients with established cardiovascular disease. *JACC Cardiovasc Imaging.* (2022) 15:1274–88. doi: 10.1016/j.jcmg.2021.12.013
130. Ohshima K, Matsumoto Y, Shimokawa H. Coronary artery spasm and perivascular adipose tissue inflammation: insights from translational imaging research. *Eur Cardiol.* (2019) 14:6–9. doi: 10.15420/ecr.2019.3.2
131. Piri R, Gerke O, Høilund-Carlson PF. Molecular imaging of carotid artery atherosclerosis with PET: a systematic review. *Eur J Nucl Med Mol Imaging.* (2020) 47:2016–25. doi: 10.1007/s00259-019-04622-y
132. Mahabadi AA, Berg MH, Lehmann N, Kälsch H, Bauer M, Kara K, et al. Association of epicardial fat with cardiovascular risk factors and incident myocardial infarction in the general population: the Heinz Nixdorf Recall Study. *J Am Coll Cardiol.* (2013) 61:1388–95. doi: 10.1016/j.jacc.2012.11.062
133. Hwang IC, Park HE, Choi SY. Epicardial adipose tissue contributes to the development of non-calcified coronary plaque: a 5-year computed tomography follow-up study. *J Atheroscler Thromb.* (2017) 24:262–74. doi: 10.5551/jat.36467
134. Vergallo R, Crea F. Atherosclerotic plaque healing. *N Engl J Med.* (2020) 383:846–57. doi: 10.1056/NEJMra2000317
135. Villiger M, Otsuka K, Karanasos A, Doradla P, Ren J, Lippok N, et al. Coronary plaque microstructure and composition modify optical polarization: a new endogenous contrast mechanism for optical frequency domain imaging. *JACC Cardiovasc Imaging.* (2018) 11:1666–76. doi: 10.1016/j.jcmg.2017.09.023
136. Villiger M, Otsuka K, Karanasos A, Doradla P, Ren J, Lippok N, et al. Repeatability assessment of intravascular polarimetry in patients. *IEEE Trans Med Imaging.* (2018) 37:1618–25. doi: 10.1109/TMI.2018.2815979
137. van Zandvoort LJC, Otsuka K, Villiger M, Neleman T, Dijkstra J, Zijlstra F, et al. Polarimetric signatures of coronary thrombus in patients with acute coronary syndrome. *Circ J.* (2021) 85:1806–13. doi: 10.1253/circj.CJ-20-0862
138. Otsuka K, Villiger M, Karanasos A, van Zandvoort LJC, Doradla P, Ren J, et al. Intravascular polarimetry in patients with coronary artery disease. *JACC Cardiovasc Imaging.* (2020) 13:790–801. doi: 10.1016/j.jcmg.2019.06.015
139. Otsuka K, Villiger M, Nadkarni SK, Bouma BE. Intravascular polarimetry for tissue characterization of coronary atherosclerosis. *Circ Rep.* (2019) 1:550–7. doi: 10.1253/circrep.CR-19-0102



OPEN ACCESS

EDITED BY

Hiroshi Iwata,
Juntendo University, Japan

REVIEWED BY

Yuichi Chikata,
Juntendo University, Japan
François-Xavier Lapébie,
Centre Hospitalier Universitaire de
Toulouse, France

*CORRESPONDENCE

Guillaume Mahé
✉ maheguillaume@yahoo.fr

SPECIALTY SECTION

This article was submitted to
Atherosclerosis and Vascular Medicine,
a section of the journal
Frontiers in Cardiovascular Medicine

RECEIVED 13 June 2022

ACCEPTED 06 February 2023

PUBLISHED 21 March 2023

CITATION

Tollenaere Q, Métairie A, Le Pabic E, Le
Faucheur A and Mahé G (2023) Use of the
Walking Impairment Questionnaire and Walking
Estimated-Limitation Calculated by History
questionnaire to detect maximal walking
distance equal to or lower than 250 m in
patients with lower extremity arterial disease.
Front. Cardiovasc. Med. 10:968213.
doi: 10.3389/fcvm.2023.968213

COPYRIGHT

© 2023 Tollenaere, Métairie, Le Pabic, Le
Faucheur and Mahé. This is an open-access
article distributed under the terms of the
[Creative Commons Attribution License \(CC BY\)](#).
The use, distribution or reproduction in other
forums is permitted, provided the original
author(s) and the copyright owner(s) are
credited and that the original publication in this
journal is cited, in accordance with accepted
academic practice. No use, distribution or
reproduction is permitted which does not
comply with these terms.

Use of the Walking Impairment Questionnaire and Walking Estimated-Limitation Calculated by History questionnaire to detect maximal walking distance equal to or lower than 250 m in patients with lower extremity arterial disease

Quentin Tollenaere¹, Antoine Métairie¹, Estelle Le Pabic²,
Alexis Le Faucheur³ and Guillaume Mahé^{1,3*}

¹Vascular Medicine Unit, Centre Hospitalier Universitaire de Rennes, Rennes, France, ²CHU Rennes, Inserm, CIC 1414 (Clinical Investigation Center), Rennes, France, ³Univ Rennes, M2S – EA 7470, Rennes, France

Objective: The objective was to assess the accuracy and optimal threshold of the Walking Impairment Questionnaire (WIQ) and the Walking Estimated-Limitation Calculated by History (WELCH) questionnaire in identifying patients with a maximal walking distance (MWD) below or equal to 250 m.

Methods: This retrospective study screened 388 consecutive patients with suspected symptomatic lower extremity arterial disease (LEAD). Collected data included the patient's history, resting ankle-brachial index, WIQ, and WELCH. MWD was assessed with a treadmill test at 2 mph (3.2 km/h) with a 10% grade. An optimized threshold for detection of MWD \leq 250 m was determined for each questionnaire via receiver operating characteristic (ROC) curves. Subsequently, multivariate analysis was performed to build a new simple score to detect MWD \leq 250 m.

Results: The study included 297 patients (63 ± 10 years old). With a threshold of \leq 64%, the WIQ predicted MWD \leq 250 m with an accuracy of 71.4% (66.2, 76.5%). With a threshold of \leq 22, the WELCH predicted a treadmill walking distance of \leq 250 m with an accuracy of 68.7% (63.4, 74.0%). A new score with only four "yes or no" questions had an accuracy of 71.4% (66.3, 76.6%). Items on this new score consisted of the level of difficulty of walking 1 block, declared maximum walking distance, usual walking speed, and maximum duration of slow walking.

Conclusion: A WIQ score \leq 64% and a WELCH score \leq 22 help to predict a walking distance of \leq 250 m in a treadmill test at 2 mph (3.2 km/h) with a 10% grade. A 4-item score could be used for rapid evaluation of walking distance among patients with LEAD, but the validity of this 4-item score requires further confirmation studies.

KEYWORDS

lower extremity artery disease, peripheral artery disease, intermittent claudication, walking distance assessment, questionnaire, treadmill test

1. Introduction

Lower extremity arterial disease (LEAD) affects more than 230 million people worldwide (1). Walking distance is closely related to quality of life (QOL), as measured by QOL questionnaires in patients with LEAD. Maximal walking distance (or time) as established during treadmill walking is widely used as an index of walking impairment. The assessment of maximal walking distance (MWD) is also an issue in the Rutherford LEAD classification, where identification of the stage depends on the patient's ability to walk for 5 min at 2 mph at a 10% slope that corresponds to 267 m, rounded to 250 m (2). Vascular surgery societies recommend the Rutherford classification for clinical trials as well as in clinical practice (3). Furthermore, the American Medical Association, health insurance companies and public health regulation agencies, use walking distance to evaluate LEAD impairment for compensation schemes and from the perspective of health economics (4). Therefore, clinical measurements of MWD are useful in the prediction of patients' functional limitations, in the assessment of patients for surgery and endovascular procedures, and for the inclusion of patients in clinical trials.

Clinicians can assess the functional limitations of patients with LEAD by several means: standardized treadmill tests, a 6-min walking test, and more recently, global positioning system (GPS) recordings (5). Standardized treadmill tests are the only validated method for LEAD diagnosis and remain the gold standard. However, standardized treadmill testing is costly. Treadmill testing for angina costs around USD 500 per patient when considering staffing requirements (medical and clerical), equipment (charge per person), and overhead charges (room rental and utility costs), and it requires medical attention for around 20 min. Treadmill testing for LEAD suffers from the same limitations and is less commonly available (6).

A number of questionnaires, such as the Walking Impairment Questionnaire (WIQ) and the Walking Estimated-Limitation Calculated by History (WELCH) questionnaire, are readily accessible and represent tools of interest for estimating patients' impairment (7, 8). However, these questionnaires do not measure MWD and there is no simple known rule to determine a patient's walking distance from the results of such questionnaires. We hypothesize that from among the questions of the WIQ and the WELCH and measures of patient clinical characteristics, a subset of items could be selected that would accurately reflect MWD, with a focus on identifying patients with MWD lower than 250 m. This could be of interest to select patients for clinical trials and to assess the severity of claudication.

Therefore, the primary objective of this study was to determine which cut-off values of WIQ and WELCH scores predict a maximal walking distance equal to or lower than 250 m on the treadmill. The secondary objective was to determine which clinical variables or questions from the WIQ and the WELCH questionnaire best predict a MWD below or equal to 250 m.

2. Methods

2.1. Type of study

This was a cross-sectional, non-interventional, monocentric study based on a retrospective analysis of consecutive patients referred to the vascular unit of University Hospital, Rennes, France for exertional limb symptoms and suspected of having LEAD.

We recruited all 388 patients between 1 January 2017 and 1 September 2020. All patients consulted for treadmill MWD evaluation with an established or suspected diagnosis of LEAD.

The Exercise PAD cohort study is registered with the American National Institutes of Health database under reference n° NCT03186391. All patients signed an agreement explaining the research protocol and were treated in accordance with the Helsinki convention (9). The protocol was submitted to the local ethics committee of University Hospital of Rennes.

2.2. Inclusion and exclusion criteria

Patients were included in the data if they met the hemodynamic criterion for LEAD, i.e., a resting ankle-brachial index (ABI) below or equal to 0.90 or a difference between post-exercise ABI and resting ABI above 18.5% of resting ABI (10). Exclusion criteria were (i) inability to answer the WIQ or the WELCH questionnaire, (ii) interruption of the Strandness Test due to dyspnea or thoracic pain, (iii) interruption of the Strandness Test because the patient could not achieve a speed of 3.2 km/h (roughly 2 mph), and (iv) interruption of the Strandness Test because of purely rheumatologic pain (knee pain, for instance).

2.3. Study protocol

Patients underwent a physical examination, medical history (anamnesis), resting ABI measurement, a standard treadmill test, and post-exercise pressure measurements at a single appointment. We collected the following examination data: age; declared walking distance of pain onset; declared maximal walking distance before stopping; and tobacco consumption, graded as past if cessation occurred at least 6 months before examination or as ongoing if cessation occurred < 6 months before or the patient was currently smoking. We also measured weight and height. We completed the patient history on the basis of the patient's current drug prescriptions, the patient's recollection, and previous hospitalization reports or any other data available.

History data included diabetes status, defined by ongoing sugar-lowering treatment or HbA1c > 6.5%; dyslipidemia status, defined by ongoing statin treatment or declared dyslipidemia; hypertension, defined by current use of antihypertensive drugs; presence of vascular graft; presence of vascular stent; history of coronary heart disease or heart stenting or coronary bypass; history of carotid artery disease, graded as ischemic stroke, transient ischemic stroke, or asymptomatic carotid endarterectomy; and obstructive sleep apnea syndrome.

We asked the patient to spontaneously estimate their own walking distance at pain onset (“declared pain-onset walking distance”, DPWD) and maximal walking distance (“declared maximal walking distance”, DMWD).

We also administered a French version of the WIQ and the WELCH questionnaire to each patient before the exercise.

The Walking Impairment Questionnaire (WIQ) (7) is frequently used to evaluate the impairment of patients with LEAD. A trained physician administered the WIQ to the patients. The WIQ consists of three sets of questions: one regarding the level of difficulty of walking at an average speed, another regarding the level of difficulty of walking 100 m at increasing speeds, and the last regarding the level of difficulty of climbing increasing numbers of flights of stairs. Then, after a specific calculation, all these scores are rounded in the form of percentages and the WIQ score is the average of these three scores. The higher the score, the better the walking capacity of the patient.

The Walking Estimated-Limitation Calculated by History (WELCH) questionnaire (8) is also frequently used to assess the limitations of patients with LEAD. It consists of four questions; the first three relate to the amount of time before stopping at increasing speeds, and the last is a multiplier and compares the patient’s speed with that of their relatives. WELCH score varies between 0 and 100. The higher the score, the better the walking capacity of the patient.

Measurement of resting ABI was performed according to American Heart Association recommendations using a hand-held Doppler probe (8 MHz; Basic Atys Medical, Soucieu en Jarrest, France) by a trained vascular medicine physician, with the exception of brachial blood pressure measurements, which were taken using an automated oscillometric blood pressure monitor (Carescape Dinamap V100; GE Healthcare) (4, 11).

The patient was at rest for 10 min in a supine position, relaxed, head and heels supported by an examination desk. We controlled the room temperature at $21 \pm 1^\circ\text{C}$. We used the counterclockwise sequence for pressure measurement: right brachial artery, right posterior tibial artery, right dorsalis pedis artery, left posterior tibial artery, left dorsalis pedis artery, left brachial artery, and right brachial artery. We calculated the ABI by dividing the highest pressure at the lower limb (dorsalis pedis or posterior tibial pressure) by the highest pressure at the arm, as recommended.

We used a treadmill test (3.2 km/h, 10% slope) to determine MWD. Patients were asked to rate their pain on a 0–4 scale, and we stopped the treadmill test if the patient reached 4 on the pain scale or was unable to reach a speed of 3.2 km/h (around 2 mph), in accordance with recommendations (12). We also stopped the treadmill test if the patient experienced acute chest pain or major dyspnea, or when they had completed the 10-min test for a total distance of 525 m. Immediately after the treadmill test, within 1 min, we measured the post-exercise ankle-brachial index, as previously described.

2.4. Statistical analysis

Continuous variables are reported in the form mean \pm standard deviation (SD) or median, and categorical variables are reported as numbers (percentages).

Receiver Operating Characteristic (ROC) curves were drawn by plotting sensitivity against 1 minus specificity. The optimal threshold was defined as the threshold that maximized sensitivity + specificity, known as the Youden index. For declared walking distances, 250 m was used as a threshold.

Subsequently, we determined the area under the curve (AUC) of the WIQ and WELCH scores, maximal declared walking distance, and declared pain onset walking distance.

We used McNemar tests for 2 by 2 comparisons of the accuracy of the WELCH, the WIQ, and declared walking distance with their respective optimized thresholds.

We calculated the Pearson correlation between WIQ total score and MWD, and between WELCH score and MWD.

Logistic univariate regressions were used to identify the variables associated with MWD. All variables, such as age and sex, were converted to nominal binary variables, using the median value for continuous variables, with the exceptions of body mass index and tobacco consumption. The median value was rounded to the nearest multiple of 50 m for the declared walking distance variable.

For answers to the questionnaire, a step-by-step analysis was used to regroup the answers into groups that maximized AUC. Response options to the WELCH questionnaire were regrouped to create equal-size groups. For the WIQ, a sensitivity analysis was conducted to determine whether the regrouping of the response options into three groups (“no difficulty” in one group, “some difficulty” and “slight difficulty” in a second group, and “much difficulty” and “unable to do” in a third group) had an influence on the outcomes of the statistical analysis.

We did not use composite variables, such as the partial or complete results of the WIQ and combined questions of the WELCH questionnaire, as the aim of the research was not to overcomplicate pre-existing questionnaires. Post-exercise data, such as post-exercise ABI, were not plotted, because the aim of the research was to determine walking distance *ex ante*.

For the ABI, we compared the use of both the median value and a value of 0.90 as thresholds, as the latter is a criterion for LEAD. Both the best ABI and the worst ABI were plotted.

We used logistic univariate regressions over all collected data to identify the variables associated with MWD. We selected a lax *p*-value threshold of < 0.20 to identify variables of interest for further study in a multivariate model. The choice of a loose value of *p* threshold to identify variables associated with MWD allowed more variables to be tested in the multivariate model. Subsequently, a backward stepwise procedure was used to identify explanatory variables. We used a statistical threshold of 0.05 to eliminate variables one by one. We created a score using the multivariate coefficients of the statistically significant variables.

We simplified the score to a 1-digit scoring model by simply rounding the multivariate coefficients to the nearest natural number. Finally, we measured the performance of this model in terms of sensitivity, specificity, and area under the ROC curve.

We adopted a statistical significance threshold of 0.05 for all tests except the univariate model. A 95% confidence interval is reported for all estimates. We used the SAS[®] 9.4 software package (SAS Institute, Cary, NC, USA) for statistical analysis.

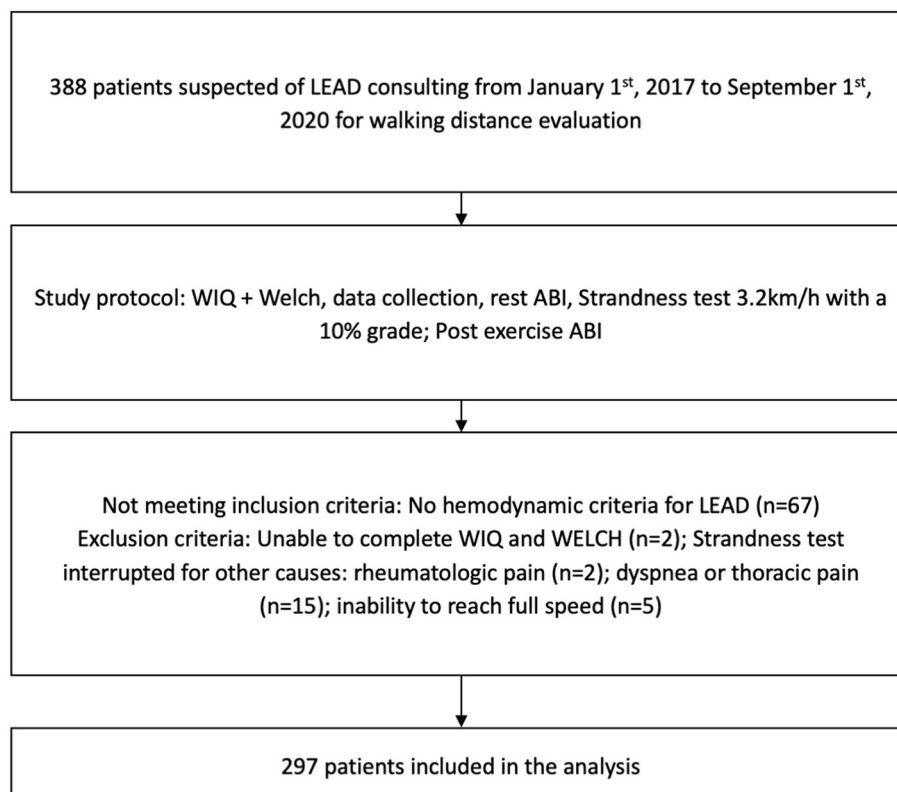


FIGURE 1

Flow chart with inclusion and exclusion criteria. LEAD, lower extremity arterial disease; WIQ, Walking Impairment Questionnaire; WELCH, Walking Estimated-Limitation Calculated by History; ABI, ankle-brachial index.

3. Results

3.1. Patients' demographic characteristics

We recruited 388 adult patients with suspected LEAD (Figure 1). Sixty-seven patients did not meet the hemodynamic criteria for LEAD and were not included. Twenty-four additional patients were excluded from the analysis because the treadmill test was interrupted for other causes than LEAD, e.g., dyspnea or thoracic pain ($n = 15$), inability to reach full speed ($n = 5$), or purely rheumatologic pain ($n = 2$). These last two patients both experienced knee pain that prevented them from walking and had a history of knee arthrosis. We excluded two additional patients due to missing data, as both were unable to answer the questions of the WIQ and the WELCH questionnaire. In total, we analyzed data from 297 patients.

Among the 297 patients included in the analysis, the mean age was 63 ± 10 years. A total of 83% were men, and the mean body mass index was 27.0 ± 4.4 kg/m². Twenty-six percent of patients had diabetes. Sample characteristics and data collected on a range of variables are detailed in Table 1. The mean WIQ score was $46 \pm 25\%$, and the mean WELCH score was 26 ± 19 .

A total of 185 patients did not complete the 250 m walking test; the remaining 112 patients completed it.

3.2. Correlations

The correlation coefficient representing correlation with MWD as measured on the treadmill was higher for the WELCH [with a correlation of 0.55 (0.46, 0.62)] and the WIQ [0.51 (0.42, 0.59)] than for the DMWD [with a correlation of 0.41 (0.31, 0.50)] and the DPWD [0.21 (0.10, 0.32)].

3.3. Optimized thresholds for detection of 250 m MWD for the WELCH and the WIQ

The AUC of the ROC curves was 0.78 (0.73, 0.83) for the WELCH and 0.74 (0.68, 0.80) for the WIQ. The optimal threshold for detection of a treadmill MWD ≤ 250 m was ≤ 22 for the WELCH and $\leq 64\%$ for the WIQ (Table 2).

With accuracies of 68.7% (63.4, 74.0%) and 71.4% (66.2, 76.5%) for the WELCH and the WIQ, respectively, using the

previously determined thresholds, WIQ and WELCH scores were more accurate for prediction of $MWD \leq 250$ m than the patients' declared maximal walking distance ($p = 0.02$) and their declared pain-onset walking distance ($p < 0.01$). There was no statistical difference in terms of accuracy between the WIQ and the WELCH.

3.4. Variables associated with walking ≤ 250 m

Among all variables, all questions of the WIQ and the WELCH questionnaire were individually associated with walking ≤ 250 m

TABLE 1 Population characteristics.

Variables	Population (n=297)
Age (years)	63.0 \pm 10.0
Male sex	247 (83%)
Body mass index (kg/m ²)	27.0 \pm 4.4
DPWD (m)	332 \pm 884
DMWD (m)	1,086 \pm 2,048
Diabetes	76 (26%)
Dyslipidemia	239 (81%)
Hypertension	233 (79%)
Current smoker or smoking cessation < 6 months	120 (41%)
Smoking cessation > 6 months	141 (48%)
Never smoked	34 (12%)
Lower limb graft or stent	109 (37%)
ACS or coronary stent or bypass	96 (32%)
History of ischemic stroke	29 (10%)
Sleep apnea syndrome	30 (10%)
Worst limb ABI	0.81 \pm 0.26
Resting ABI ≤ 0.90	195 (66%)
Best limb ABI	0.94 \pm 0.28
WIQ (%)	46 \pm 25
WELCH (points)	26 \pm 19

Results are presented in the form mean \pm standard deviation or number (proportion). ABI, ankle-brachial index; WIQ, Walking Impairment Questionnaire; WELCH, Walking Estimated-Limitation Calculated by History; ACS, acute coronary syndrome; DMWD, declared maximal walking distance; DPWD, declared pain-onset walking distance.

TABLE 2 Sensitivity and specificity, area under the receiver operating characteristic curve, AUC, and correlation with measured walking distance for WIQ score, WELCH score, and patients' estimates.

Score	Threshold	AUC	Sensitivity	Specificity	Accuracy	Correlation
WELCH	≤ 22	0.78 (0.73, 0.83)	69.7% (63.1, 76.4%)	67.0% (59.8, 74.1%)	68.7% (63.4, 74.0%)	0.55 (0.46, 0.62)
WIQ	$\leq 64\%$	0.74 (0.68, 0.80)	88.1% (83.4, 92.8%)	43.8% (37.3, 50.2%)	71.4% (66.2, 76.5%)	0.51 (0.42, 0.59)
DMWD	≤ 250 m	0.72 (0.66, 0.78)	46.5% (39.3, 53.7%)	76.8% (69.0, 84.6%)	57.9% (52.3, 63.5%)	0.41 (0.31, 0.50)
DPWD	≤ 250 m	0.56 (0.49, 0.63)	73.5% (67.2, 79.9%)	38.4% (31.7, 45.1%)	60.3% (54.7, 65.8%)	0.21 (0.10, 0.32)

AUC, area under the curve; DMWD, declared maximal walking distance; DPWD, declared pain-onset walking distance; WIQ, Walking Impairment Questionnaire; WELCH, Walking Estimated-Limitation Calculated by History. All variables are presented with a 95% confidence interval.

with $p < 0.20$ and were therefore included for further analysis (Tables 3, 4). As described previously, the response options for each WIQ item were regrouped to form three groups, and the response options for each WELCH item were regrouped to produce similarly sized groups.

In addition to these questionnaire items, the variables declared maximal walking distance, declared pain-onset walking distance, history of vascular graft or stenting or other vascular surgery of lower limbs, diabetes, resting ABI bilaterally ≤ 0.90 , worst ABI, and best ABI were associated with walking ≤ 250 m with a p -value below 0.20; all these variables were therefore included in the multivariate analysis.

In contrast, age above 66 years, female sex, obesity or overweight, dyslipidemia, hypertension, tobacco consumption, and coronary heart disease were not found to be significantly associated with walking ≤ 250 m.

3.5. Explanatory variables

All variables significantly associated with walking ≤ 250 m with $p \leq 0.20$ were included in a multivariate model with step-by-step analysis. This multivariate analysis showed that a subset of four items could be selected to predict $MWD \leq 250$ m accurately, with a high significance value ($p \leq 0.01$). Results and odds ratios are shown in Table 5.

Each explanatory variable was a WIQ or WELCH item with some answers regrouped. Neither pre-existing conditions nor risk factors such as age, diabetes, or smoking were identified as explanatory variables in our analysis.

The maximizing threshold for the calculated values was 1.95. We detail each variable of this intermediate score in Table 5. The higher the score, the greater the risk of walking ≤ 250 m. The distribution of the score according to the treadmill walking distance is presented in the Appendix.

3.6. Simplified scoring model

We simplified the score by setting a 1-digit scoring model, as shown in Table 6, with the values rounded to the nearest natural number. The optimal threshold for the 1-digit score was 2. Therefore, we declared patients with a simplified score of 3, 4, or 5 to be positive for $MWD \leq 250$ m, and patients with a simplified score of 2, 1, or 0 to be negative.

TABLE 3 Univariate analysis of questionnaire variables associated with walking ≤ 250 m.

Variable	OR (95% CI)	P
Level of difficulty of walking indoors (WIQ)		$p = 0.0005$
No difficulty	1	
Some difficulty/slight difficulty	3.21 (1.75, 5.89)	
Much difficulty/unable to do	7.39 (0.28, 195.75)	
Level of difficulty of walking 20 m (WIQ)		$p < 0.0001$
No difficulty	1	
Some difficulty/slight difficulty	3.62 (2.02, 6.48)	
Much difficulty/unable to do	7.98 (0.30, 211.63)	
Level of difficulty of walking 50 m (WIQ)		$p < 0.0001$
No difficulty	1	
Some difficulty/slight difficulty	3.32 (2.00, 5.51)	
Much difficulty/unable to do	19.36 (3.47, 108.05)	
Level of difficulty of walking 100 m (WIQ)		$p < 0.0001$
No difficulty	1	
Some difficulty/slight difficulty	2.61 (1.51, 4.50)	
Much difficulty/unable to do	18.96 (6.55, 54.90)	
Level of difficulty of walking 200 m (WIQ)		$p < 0.0001$
No difficulty	1	
Some difficulty/slight difficulty	2.80 (1.47, 5.36)	
Much difficulty/unable to do	9.09 (4.29, 19.27)	
Level of difficulty of walking 300 m (WIQ)		$p < 0.0001$
No difficulty	1	
Some difficulty/slight difficulty	3.38 (1.59, 7.19)	
Much difficulty/unable to do	7.52 (3.57, 15.82)	
Level of difficulty of walking 500 m (WIQ)		$p < 0.0001$
No difficulty	1	
Some difficulty/slight difficulty	4.21 (1.55, 11.39)	
Much difficulty/unable to do	11.27 (4.35, 29.19)	
Level of difficulty of walking one block slowly (WIQ)		$p = 0.0006$
No difficulty	1	
Some difficulty/slight difficulty	2.28 (1.39, 3.76)	
Much difficulty/unable to do	8.85 (1.52, 51.66)	
Level of difficulty of walking one block at average speed (WIQ)		$p < 0.0001$
No difficulty	1	
Some difficulty/slight difficulty	2.09 (1.25, 3.50)	
Much difficulty/unable to do	8.50 (3.17, 22.76)	
Level of difficulty of walking one block quickly (WIQ)		$p < 0.0001$
No difficulty	1	

(Continued)

TABLE 3 (Continued)

Variable	OR (95% CI)	P
Some difficulty/slight difficulty	1.85 (0.85, 4.04)	
Much difficulty/unable to do	4.89 (2.23, 10.75)	
Level of difficulty of jogging one block (WIQ)		$p = 0.0004$
No difficulty	1	
Some difficulty/slight difficulty	1.85 (0.43, 7.92)	
Much difficulty/unable to do	5.57 (1.44, 21.58)	
Level of difficulty of climbing one flight of stairs (WIQ)		$p = 0.0005$
No difficulty	1	
Some difficulty/slight difficulty	2.33 (1.41, 3.86)	
Much difficulty/unable to do	4.22 (1.51, 11.76)	
Level of difficulty of climbing two flights of stairs (WIQ)		$p < 0.0001$
No difficulty	1	
Some difficulty/slight difficulty	2.87 (1.63, 5.06)	
Much difficulty/unable to do	5.50 (2.75, 11.02)	
Level of difficulty of climbing three flights of stairs (WIQ)		$p < 0.0001$
No difficulty	1	
Some difficulty/slight difficulty	2.30 (1.10, 4.79)	
Much difficulty/unable to do	6.15 (3.06, 12.36)	
Maximal duration of a slow walk (WELCH)		$p < 0.0001$
"1 hour" or "3 hours or more"	1	
"Not possible," "30 seconds," "1 minute," "3 minutes," "10 minutes," or "30 minutes"	5.35 (3.05, 9.39)	
Maximal duration of a walk at a normal pace (WELCH)		$p < 0.0001$
"30 minutes," "1 hour," or "3 hours or more"	1	
"Not possible," "30 seconds," "1 minute," "3 minutes," or "10 minutes"	6.34 (3.63, 11.05)	
Maximal duration of a walk at a rapid pace (WELCH)		$p < 0.0001$
"10 minutes," "30 minutes," "1 hour," or "3 hours or more"	1	
"Not possible," "30 seconds," "1 minute," or "3 minutes"	4.99 (2.91, 8.54)	
Walking speed compared to relatives of same age (WELCH)		$p < 0.0001$
"A bit slower," "same speed," or "faster"	1	
"Much slower" or "moderately slower"	3.97 (2.40, 6.57)	

OR, odds ratio; CI, confidence interval; WIQ, Walking Impairment Questionnaire; WELCH, Walking Estimated-Limitation Calculated by History.

The area under the curve was 0.79 (0.74, 0.84) for the 1-digit score model. For the population, the sensitivity of the 1-digit model was 73.0% (66.6, 79.4%), specificity was 70.0% (62.7, 76.6%), and accuracy was 71.4% (66.3, 76.6%). The correlation

TABLE 4 Univariate analysis of variables other than items of the WIQ and WELCH.

Variable	OR (95% CI)	P
Age		<i>p</i> = 0.2959
≤66 years old	1	
>66 years old	1.30 (0.80, 2.12)	
Sex		<i>p</i> = 0.7844
Male	1	
Female	1.09 (0.58, 2.05)	
Body mass index (BMI)		<i>p</i> = 0.9785
< 25 kg/m ²	1	
25–30 kg/m ²	1.06 (0.61, 1.82)	
≥30 kg/m ²	1.05 (0.56, 1.96)	
DPWD (declared pain-onset walking distance)		<i>p</i> = 0.0021
≥400 m	1	
< 400 m	2.40 (1.37, 4.19)	
DMWD (declared maximal walking distance)		<i>p</i> < 0.0001
≥750 m	1	
<750 m	5.05 (2.98, 8.56)	
Diabetes		<i>p</i> = 0.0371
No	1	
Yes	1.83 (1.04, 3.24)	
Treated dyslipidaemia		<i>p</i> = 0.3866
Yes	1	
No	1.31 (0.71, 2.40)	
Treated hypertension		<i>p</i> = 0.2614
Yes	1	
No	0.72 (0.41, 1.27)	
Tobacco consumption		<i>p</i> = 0.6373
Never	1	
Yes, active	1.01 (0.46, 2.25)	
Previous (>6 months)	0.80 (0.37, 1.75)	
Vascular graft or stenting or other vascular surgery of lower limbs		<i>p</i> = 0.0062
No	1	
Yes	2.04 (1.22, 3.39)	
NSTEMI, STEMI, or coronary heart disease or ischemic or transient stroke or carotid endarterectomy		<i>p</i> = 0.8078
No	1	
Yes	1.06 (0.65, 1.72)	
Resting ankle-brachial index		<i>p</i> = 0.0168
One side or none ≤ 0.90	1	
Both sides ≤ 0.90	1.82 (1.11, 2.97)	

(Continued)

TABLE 4 (Continued)

Variable	OR (95% CI)	P
Best ankle-brachial index		<i>p</i> = 0.0006
≥0.98	1	
<0.98	2.32 (1.43, 3.76)	
Worst ankle-brachial index		<i>p</i> = 0.0033
≥0.90	1	
<0.90	2.07 (1.27, 3.36)	

NSTEMI, non-ST elevation myocardial infarction; STEMI, ST elevation myocardial infarction; OR, odds ratio; CI, confidence interval; WIQ, Walking Impairment Questionnaire; WELCH, Walking Estimated-Limitation Calculated by History.

coefficient representing the correlation between the simplified 1-digit score and MWD as measured by the treadmill test was -0.52 ($-0.60, -0.43$).

Receiver operating characteristic (ROC) curves are presented in **Figure 2**; these illustrate the fact that the simplified score can be as accurate as the WIQ and the WELCH.

4. Discussion

4.1. Main results

This study aimed to determine the threshold for scores on the WIQ and the WELCH that would best predict walking ≤ 250 m in a treadmill test (10%; 2 mph); to demonstrate that WIQ and WELCH scores are more accurate than patients' own estimates; and to construct a new scoring instrument based on the most discriminative elements among clinical variables and the items of each of these questionnaires.

The findings confirmed the threshold for WELCH score to predict whether a patient can walk 250 m or less. In a previous study, Abraham et al. found a cut-off of WELCH score equal to or lower than 25 to detect a walking distance of 257 m or less (8). In our study, with a threshold of 22, the measured sensitivity of the WELCH questionnaire was lower at 69.7% (63.1, 76.4%), but specificity was higher at 67.0% (59.8, 74.1%), consistent with a lower cut-off. We also identified a WIQ score threshold of 64% for prediction of a maximal walking distance of 250 m. This result is consistent with a previous study that found that an overall WIQ score of 42.5% or less identified low performers (i.e., LEAD patients with MWD < 160 m) with a sensitivity of 90% and specificity of 73% (13).

The results of the present study confirm the moderate correlation of WIQ score [0.51 (0.42, 0.59)] and WELCH score [0.55 (0.46, 0.62)] with MWD as assessed in the treadmill test in our population. Other clinical studies have found a “weak” correlation of these scores with objective measurement of walking distance, with correlation coefficients ranging from 0.33 (14) to 0.59 (15). The WIQ and the WELCH instruments were not constructed based on multivariate analysis to determine the questions of interest, and they were not designed to predict whether a patient can walk ≤ 250 m. Despite this, we found that the answers to WELCH and WIQ items were statistically

TABLE 5 Explanatory variables for 250 m treadmill test [odds ratios are presented in the form: odds ratio (95% confidence interval)].

Explanatory variable	Odds ratio (95% CI)	Score	P-value
During the last week, how difficult was it for you to walk 1 block, on level ground, at average speed without stopping to rest? ^a			0.006
No difficulty	1	0	
Some difficulty/slight difficulty	1.14 (0.58, 2.26)	0.13	
Much difficulty/unable to do	6.39 (1.90, 21.50)	1.85	
What maximum distance can you walk before stopping because the pain becomes unbearable?			0.007
Answer strictly above 750 m	1	0	
Answer below or equal to 750 m	2.39 (1.27, 4.49)	0.87	
Compared to the usual walking speed of your relatives, friends, or people of your own age, do you think that you personally usually walk... ^b			0.010
“A bit slower,” “same speed,” or “faster”	1	0	
“Much slower” or “moderately slower”	2.11 (1.20, 3.73)	0.75	
How long can you walk slowly (slower than the usual speed of relatives, friends, or other people of your own age) on level ground without stopping? ^b			0.006
“1 hour” or “3 hours or more”	1	0	
“Not possible,” “30 seconds,” “1 minute,” “3 minutes,” “10 minutes,” or “30 minutes”	2.59 (1.32, 5.09)	0.95	
Threshold when adding variables		>1.95	

^aFrom the WIQ (Walking Impairment Questionnaire).^bFrom the WELCH (Walking Estimated-Limitation Calculated by History).

CI, confidence interval.

TABLE 6 Simple 1-digit score with binary questions.

During the last week, how difficult was it for you to walk 1 block (100 m), on level ground, without stopping to rest?	No difficulty, some difficulty, or slight difficulty	0
	Much difficulty/unable to do	2
What maximum distance can you walk before stopping because the pain becomes unbearable?	Answers strictly above 750 m	0
	Answers below 750 m	1
Compared to the usual walking speed of your relatives, friends, or people of your own age, do you think that you personally usually walk...	“A bit slower,” “same speed,” or “faster”	0
	“Much slower” or “moderately slower”	1
How long can you walk slowly (slower than the usual speed of relatives, friends, or other people of your own age) on level ground without stopping?	“1 hour” or “3 hours or more”	0
	“Not possible,” “30 seconds,” “1 minute,” “3 minutes,” “10 minutes,” or “30 minutes”	1
Threshold for indication of walking ≤ 250 m	>2	
Area under the curve of simple 1-digit score	0.79 (0.74, 0.84)	
Accuracy	71.4% (66.3, 76.6%).	
Correlation coefficient	−0.52 (−0.60, −0.43).	

associated with walking ≤ 250 m. In the present study, when clinical data were included in the model, only items taken from the WELCH questionnaire and the WIQ, along with the patient's declared maximal walking distance, remained in the model. This result is consistent with other studies, as the use of questions soliciting self-estimates of speed or distance is already known to improve the performance of the WIQ and the WELCH questionnaire (16).

Known factors for walking impairment did not appear as explanatory variables. This means that, although present tobacco consumption (17), absence of statin treatment (18), diabetes (19), female sex (20), and high body mass index (21) negatively influence walking distance, these factors fail to discriminate between patients who can walk ≤ 250 m and those who can walk further.

Our results show that the use of a simple 1-digit scoring model consisting of only four simple questions could enable accurate

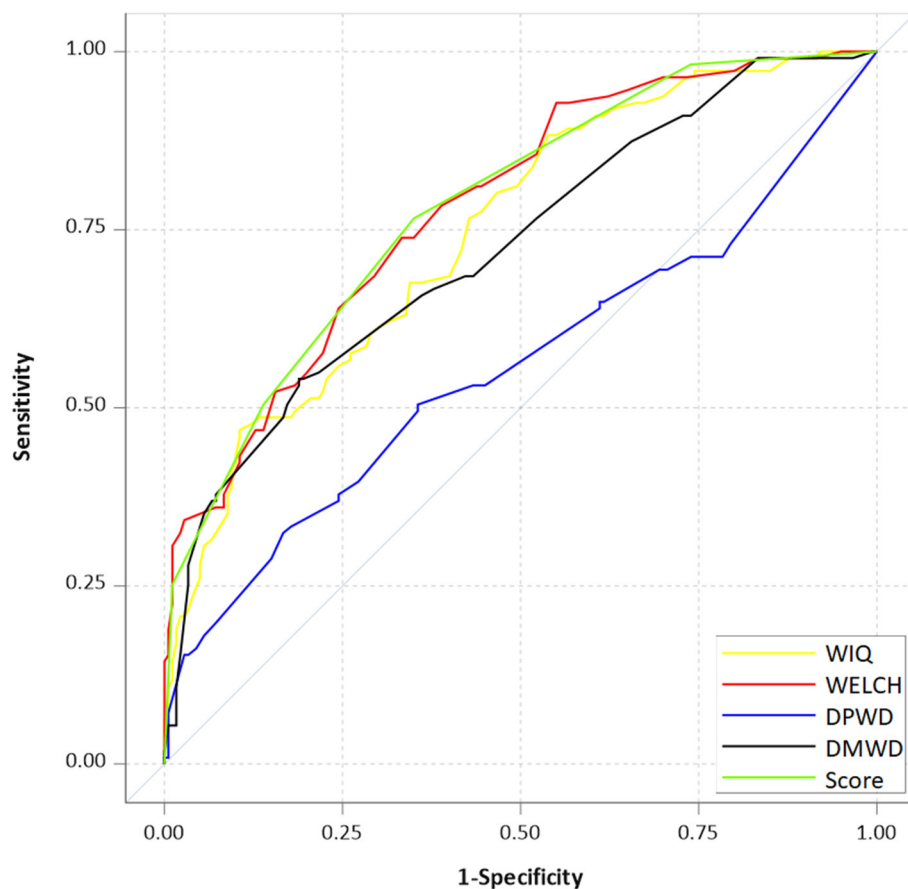


FIGURE 2

Receiver operating characteristic curves for questionnaires used to predict whether patients with LEAD can walk ≤ 250 m in a treadmill test. WIQ, Walking Impairment Questionnaire; WELCH, Walking Estimated-Limitation Calculated by History; DMWD, declared maximal walking distance; DPWD, declared pain-onset walking distance.

classification of patients in 73% of cases. These questions include the patient's own estimates, their average walking speed, the level of difficulty of walking 100 m at average speed, and the maximal duration of slow walking; they have only binary response options, as the options used in the WELCH questionnaire and the WIQ were regrouped. The 1-digit scoring model was significantly more accurate and more strongly correlated with the MWD than the patients' estimates. The correlation and accuracy of the 1-digit scoring model were similar to those of the WIQ and WELCH, but with a much simpler questionnaire. The use of existing questionnaires may also be helpful for further multicentric and international validation, as the WELCH and the WIQ each have validated versions in multiple languages.

4.2. Limitations

This study was retrospective. No external prospective validation study has been conducted with the simplified 4-item score. The questions were all presented as part of a questionnaire, with a logical path between questions, and results from the presentation of isolated questions might differ from results obtained from their presentation within

the questionnaire. Therefore, we advocate against the use of the simplified 4-item score before external and internal validation. Moreover, the study was conducted at a single center, in the French language; it was also conducted by doctors familiar with the WIQ and the WELCH. We intend to conduct further research to investigate these issues and mitigate these limitations.

All variables were evaluated only against a treadmill test at 3.2 km/h and 10% grade. We do not know what the results would be if they were evaluated against other treadmill protocols or a 6-min assessment or real-life assessment of walking distance. Moreover, we did not investigate whether WIQ scores, WELCH scores, or scores on the simple 1-digit model would reflect any increase or decrease in walking distance over time or after an intervention with good sensitivity. For instance, in previous studies, changes after revascularization have tended to be overestimated by WIQ and WELCH scores, which decrease to a greater extent than the objective change observed in treadmill tests (22).

The absence from the model of known factors for walking impairment, such as diabetes, age, and treatment for current conditions, as explanatory variables could be partly due to our study design. Our study population mostly consisted of patients receiving intensive treatment

in a referral center. The wider applicability of the results, especially to sub-groups such as elderly people, people with impaired cognition, obese people, or non-Caucasian groups, is questionable. The education levels of patients and data on their social status were not collected. The impact on the model of including age, ethnicity, and education could require additional research.

All questionnaires were administered by trained physicians. We did not investigate the role of care management nurses or whether the use of these scores can improve disease management. Communication between caregivers is known to be a key factor for disease management success (23).

Moreover, the definitions of dyslipidemia and hypertension that we used prevented us from drawing any conclusion regarding the effects of antihypertensive or lipid-lowering drugs.

A sensitivity analysis was conducted in which the response options for the WIQ and the WELCH questionnaire were regrouped in an alternative manner, with the option “unable to do” forming one group. The number of patients in the “unable to do” class was very small, ranging from 0 to 21, and the resulting scoring instrument was much more complicated, with seven different questions included. Interestingly, ABI was identified as an explanatory variable under that analysis.

We could not plot Doppler waveforms as relevant clinical data for the measurement of walking impairment, as these data were not available for all patients, although a study has shown that Doppler waveforms are associated with MWD (24). It remains to be examined whether the addition of this clinical measurement will improve the performance of this scoring model or not.

5. Conclusion

In conclusion, a WIQ score $\leq 64\%$ or a WELCH score ≤ 22 could help to predict a maximal walking distance equal to or lower than 250 m in a standardized treadmill test. A simplified score could be used for rapid evaluation of a patient's walking distance in a population of patients with LEAD. However, dedicated studies are still required before this 4-item score can be put into practice or used to pre-select patients.

References

1. Song P, Rudan D, Zhu Y, Fowkes FJI, Rahimi K, Fowkes FGR, et al. Global, regional, and national prevalence and risk factors for peripheral artery disease in 2015: an updated systematic review and analysis. *Lancet Glob Health*. (2019) 7:e1020–30. doi: 10.1016/S2214-109X(19)30045-4
2. Rutherford RB, Baker JD, Ernst C, Johnston KW, Porter JM, Ahn S, et al. Recommended standards for reports dealing with lower extremity ischemia: revised version. *J Vasc Surg*. (1997) 26:517–38. doi: 10.1016/S0741-5214(97)70045-4
3. Stoner MC, Calligaro KD, Chaer RA, Dietzek AM, Farber A, Guzman RJ, et al. Reporting standards of the Society for Vascular Surgery for endovascular treatment of chronic lower extremity peripheral artery disease: executive summary. *J Vasc Surg*. (2016) 64:227–8. doi: 10.1016/j.jvs.2016.03.432
4. Gerhard-Herman MD, Gornik HL, Barrett C, Barshes NR, Corriere MA, Drachman DE, et al. 2016 AHA/ACC guideline on the management of patients with lower extremity peripheral artery disease: A Report of the American College of

Data availability statement

The raw data supporting the conclusions of this article will be made available by the authors, without undue reservation.

Ethics statement

The studies involving human participants were reviewed and approved by Comité d’Ethique du Centre Hospitalier Universitaire de Rennes. The patients/participants provided their written informed consent to participate in this study.

Author contributions

QT and GM conceived and designed the analysis. QT, GM, and AM collected the data. ALF contributed analysis tools and EL performed the analysis. QT and GM wrote the paper, which was reviewed by AM, EL, and ALF. All authors contributed to the article and approved the submitted version.

Conflict of interest

The authors declare that the research was conducted in the absence of any commercial or financial relationships that could be construed as a potential conflict of interest.

Publisher's note

All claims expressed in this article are solely those of the authors and do not necessarily represent those of their affiliated organizations, or those of the publisher, the editors and the reviewers. Any product that may be evaluated in this article, or claim that may be made by its manufacturer, is not guaranteed or endorsed by the publisher.

- Cardiology/American Heart Association Task Force on Clinical Practice Guidelines. *Circulation*. (2017) 135:e686–e725. doi: 10.1161/CIR.0000000000000502
5. Le Faucheur A, Abraham P, Jaquinandi V, Bouyé P, Saumet JL, Noury-Desvaux B. Measurement of walking distance and speed in patients with peripheral arterial disease: a novel method using a global positioning system. *Circulation*. (2008) 117:897–904. doi: 10.1161/CIRCULATIONAHA.107.725994
6. Sabharwal N, Stoykova B, Taneja A, Lahiri A. A randomized trial of exercise treadmill ECG versus stress SPECT myocardial perfusion imaging as an initial diagnostic strategy in stable patients with chest pain and suspected CAD: Cost analysis. *J Nucl Cardiol*. (2007) 14:174–86. doi: 10.1016/j.nuclcard.2006.12.324
7. McDermott MM, Liu K, Guralnik JM, Martin GJ, Criqui MH, Greenland P. Measurement of walking endurance and walking velocity with questionnaire: validation of the walking impairment questionnaire in men and women with peripheral arterial disease. *J Vasc Surg*. (1998) 28:1072–81. doi: 10.1016/S0741-5214(98)70034-5
8. Abraham P, Godet R, Harbonnier M, Laneelle D, Leftheriotis G, Ouedraogo N. External validation of the “walking estimated limitation calculated by history”

- (WELCH) questionnaire in patients with claudication. *Eur J Vasc Endovasc Surg.* (2014) 47:319–25. doi: 10.1016/j.ejvs.2013.11.010
9. World Medical Association Declaration of Helsinki. Ethical principles for medical research involving human subjects. *JAMA.* (2013) 310:2191. doi: 10.1001/jama.2013.281053
 10. Stivalet O, Paisant A, Belabbas D, Omarjee L, Le Faucheur A, Landreau P, et al. Exercise testing criteria to diagnose lower extremity peripheral artery disease assessed by computed-tomography angiography. *PLoS ONE.* (2019) 14:e0219082. doi: 10.1371/journal.pone.0219082
 11. Mahé G, Boge G, Bura-Rivière A, Chakfé N, Constans J, Goueffic Y, et al. Disparities between international guidelines (AHA/ESC/ESVS/ESVM/SVS) concerning lower extremity arterial disease: consensus of the french society of vascular medicine (SFMV) and the french society for vascular and endovascular surgery (SCVE). *Ann Vasc Surg.* (2021) 72:1–56. doi: 10.1016/j.avsg.2020.11.011
 12. Denolin H. Guidelines for exercise testing and prescription, 4th edition edited by american college of sports medicine lea & febiger, philadelphia (1991) 314 pages, illustrated, \$15.00 isbn: 0-8121-1324-1. *Clin Cardiol.* (1992) 15:139–40. doi: 10.1002/clc.4960150224
 13. Sagar SP, Brown PM, Zelt DT, Pickett WL, Tranmer JE. Further clinical validation of the walking impairment questionnaire for classification of walking performance in patients with peripheral artery disease. *Int J Vasc Med.* (2012) 2012:190641. doi: 10.1155/2012/190641
 14. Nicolai SPA, Kruidenier LM, Rouwet EV, Graffius K, Prins MH, Teijink JAW. The walking impairment questionnaire: an effective tool to assess the effect of treatment in patients with intermittent claudication. *J Vasc Surg.* (2009) 50:89–94. doi: 10.1016/j.jvs.2008.12.073
 15. Ouedraogo N, Mahe G, Marchand J, Saïdi K, Leftheriotis G, Abraham P. Validation of a new simple questionnaire to “estimate ambulation capacity by history” (EACH) in patients with claudication. *J Vasc Surg.* (2011) 54:133–8. doi: 10.1016/j.jvs.2010.11.129
 16. Mahe G, Ouedraogo N, Marchand J, Vielle B, Picquet J, Leftheriotis G, et al. Self-reported estimation of usual walking speed improves the performance of questionnaires estimating walking capacity in patients with vascular-type claudication. *J Vasc Surg.* (2011) 54:1360–5. doi: 10.1016/j.jvs.2011.05.048
 17. Fritschi C, Collins EG, O’Connell S, McBurney C, Butler J, Edwards L. The effects of smoking status on walking ability and health-related quality of life in patients with peripheral arterial disease. *J Cardiovasc Nurs.* (2013) 28:380–6. doi: 10.1097/JCN.0b013e31824af587
 18. Mohler ER, Hiatt WR, Creager MA. Cholesterol reduction with atorvastatin improves walking distance in patients with peripheral arterial disease. *Circulation.* (2003) 108:1481–6. doi: 10.1161/01.CIR.0000090686.57897.F5
 19. Murabito JM, D’Agostino RB, Silbershatz H, Wilson PWF. Intermittent claudication: a risk profile from the framingham heart study. *Circulation.* (1997) 96:44–9. doi: 10.1161/01.CIR.96.1.44
 20. Barochiner J, Aparicio L, Waisman G. Challenges associated with peripheral arterial disease in women. *Vasc Health Risk Manag.* (2014) 10: 115–128. doi: 10.2147/VHRM.S45181
 21. Larsson UE, Reynisdottir S. The six-minute walk test in outpatients with obesity: reproducibility and known group validity. *Physiother Res Int.* (2008) 13:84–93. doi: 10.1002/pri.398
 22. Henni S, Ammi M, Semporé Y, Hersant J, Zegar G, Gourdier AS, et al. Treadmill measured vs. questionnaire estimated changes in walking ability in patients with peripheral artery disease. *Eur J Vasc Endovasc Surg.* (2019) 57:676–84. doi: 10.1016/j.ejvs.2018.11.015
 23. Ciccone MM, Aquilino A, Cortese F, Scicchitano P, Sassara M, Mola E, et al. Feasibility and effectiveness of a disease and care management model in the primary health care system for patients with heart failure and diabetes (Project Leonardo). *Vasc Health Risk Manag.* (2010) 6:297. doi: 10.2147/VHRM.S9252
 24. Miossec A, Tollenaere Q, Lanéelle D, Guilcher A, Métairie A, Le Pabic E, et al. Arterial doppler waveforms are independently associated with maximal walking distance in suspected peripheral artery disease patients. *Front Cardiovasc Med.* (2021) 8:608008. doi: 10.3389/fcvm.2021.608008

Appendix

TABLE A1 Distribution of scores on the 1-digit scoring instrument in the study population.

Score	Treadmill walking distance > 250 m	Treadmill walking distance \leq 250 m	Total
5	3 (6%)	51 (94%)	54
4	1 (25%)	3 (75%)	4
3	30 (27%)	81 (73%)	111
2	43 (52%)	40 (48%)	83
1	26 (72%)	10 (28%)	36
0	9 (100%)	0 (0%)	9
Total	112	185	297



OPEN ACCESS

EDITED BY

Masanori Aikawa,
Brigham and Women's Hospital, Harvard
Medical School, United States

REVIEWED BY

Robert N. Helsley,
University of Kentucky, United States
Alessia Di Costanzo,
Sapienza University of Rome, Italy

*CORRESPONDENCE

Arif Yurdagul
✉ arif.yurdagul@lsuhs.edu
Oren Rom
✉ oren.rom@lsuhs.edu

[†]These authors share senior authorship

SPECIALTY SECTION

This article was submitted to Atherosclerosis
and Vascular Medicine, a section of the journal
Frontiers in Cardiovascular Medicine

RECEIVED 05 December 2022

ACCEPTED 23 March 2023

PUBLISHED 02 May 2023

CITATION

Finney AC, Das S, Kumar D, McKinney MP, Cai B,
Yurdagul A Jr and Rom O (2023) The interplay
between nonalcoholic fatty liver disease and
atherosclerotic cardiovascular disease.
Front. Cardiovasc. Med. 10:1116861.
doi: 10.3389/fcvm.2023.1116861

COPYRIGHT

© 2023 Finney, Das, Kumar, McKinney, Cai,
Yurdagul and Rom. This is an open-access
article distributed under the terms of the
Creative Commons Attribution License (CC BY).
The use, distribution or reproduction in other
forums is permitted, provided the original
author(s) and the copyright owner(s) are
credited and that the original publication in this
journal is cited, in accordance with accepted
academic practice. No use, distribution or
reproduction is permitted which does not
comply with these terms.

The interplay between nonalcoholic fatty liver disease and atherosclerotic cardiovascular disease

Alexandra C. Finney¹, Sandeep Das¹, Dhananjay Kumar²,
M. Peyton McKinney¹, Bishuang Cai³, Arif Yurdagul Jr^{1,2*†}
and Oren Rom^{1,2*†}

¹Department of Pathology and Translational Pathobiology, Louisiana State University Health Shreveport, Shreveport, LA, United States, ²Department of Molecular and Cellular Physiology, Louisiana State University Health Shreveport, Shreveport, LA, United States, ³Division of Liver Diseases, Department of Medicine, Icahn School of Medicine at Mount Sinai, NY, United States

Therapeutic approaches that lower circulating low-density lipoprotein (LDL)-cholesterol significantly reduced the burden of cardiovascular disease over the last decades. However, the persistent rise in the obesity epidemic is beginning to reverse this decline. Alongside obesity, the incidence of nonalcoholic fatty liver disease (NAFLD) has substantially increased in the last three decades. Currently, approximately one third of world population is affected by NAFLD. Notably, the presence of NAFLD and particularly its more severe form, nonalcoholic steatohepatitis (NASH), serves as an independent risk factor for atherosclerotic cardiovascular disease (ASCVD), thus, raising interest in the relationship between these two diseases. Importantly, ASCVD is the major cause of death in patients with NASH independent of traditional risk factors. Nevertheless, the pathophysiology linking NAFLD/NASH with ASCVD remains poorly understood. While dyslipidemia is a common risk factor underlying both diseases, therapies that lower circulating LDL-cholesterol are largely ineffective against NASH. While there are no approved pharmacological therapies for NASH, some of the most advanced drug candidates exacerbate atherogenic dyslipidemia, raising concerns regarding their adverse cardiovascular consequences. In this review, we address current gaps in our understanding of the mechanisms linking NAFLD/NASH and ASCVD, explore strategies to simultaneously model these diseases, evaluate emerging biomarkers that may be useful to diagnose the presence of both diseases, and discuss investigational approaches and ongoing clinical trials that potentially target both diseases.

KEYWORDS

atherosclerosis, animal models, biomarkers, nonalcoholic fatty liver disease, nonalcoholic steatohepatitis, pathophysiology, therapeutics

1. Introduction

Despite the remarkable advances in interventional therapeutics, decades of basic science and clinical research, atherosclerotic cardiovascular disease (ASCVD) remains the leading cause of death worldwide (1). While the overarching pathoetiology largely arises from dyslipidemia, the imbalance of cholesterol and triglyceride lipids, numerous comorbidities complicate and exacerbate ASCVD (1). Of particular significance are metabolic- and obesity-related diseases, which have globally increased prevalence since the 1970s (2). Nonalcoholic fatty liver disease (NAFLD) and nonalcoholic steatohepatitis (NASH) are also

strongly associated with the metabolic syndrome (3), which currently afflicts approximately 90% of obese patients (4) and approximately 55% of individuals with type 2 diabetes (T2D) (5). Globally, the incidence of NAFLD has increased from 25% in 2005 to 32% today (6), highlighting an alarming trend in rising NAFLD burden. Despite this, no FDA-approved drug exists in the treatment of NAFLD/NASH. While NAFLD is associated with increased risk of liver-related mortality, the most common cause of death in patients with NAFLD, particularly those with the more severe NASH, is cardiovascular disease (CVD) (7–12). This, combined with the rising prevalence of both ASCVD and NAFLD has led to extensive discussion of the relationship between these two diseases. In 2022 alone, the increasingly transparent relationship between NAFLD/NASH and ASCVD has piqued interest between multiple scientific fields of expertise (13–17), culminating in a scientific statement from the American Heart Association (8).

Despite this acknowledgement, the specific mechanisms regulating the onset, crosstalk, and exacerbation of NAFLD and ASCVD remain unclear. The reasons for this are multifactorial: (1) there is no single established model to study NAFLD/NASH and ASCVD simultaneously, (2) since most patients with NAFLD/NASH and ASCVD are asymptomatic, diagnosis is often incidental and limited to routine blood screening (e.g., plasma lipids, liver transaminases) (18), calcium imaging (19), or less routinely, biopsy (20), and (3) clinical trials have remained limited in targeting either NASH or atherosclerosis, thus, it is unknown whether current clinical trials for NASH affect cardiovascular outcome or vice versa. For example, obeticholic acid, the most advanced drug candidate for NASH, causes hyperlipidemia, raising concerns about the possible adverse consequences on ASCVD (21). Furthermore, the effect of traditional therapies for ASCVD, e.g., statins, on NASH has shown inconsistent results in improving histological features of NASH (22, 23). Thus, strategies that simultaneously interrogate therapies for both NASH and ASCVD are necessary. This review will provide insight into each of these limitations, offering a comprehensive and current summary of our understanding regarding the relationship between NAFLD/NASH and ASCVD (Figure 1). Below, we (1) summarize the molecular drivers that regulate ASCVD and NAFLD/NASH, (2) discuss which animal models should be considered for evaluating translational interpretation of preclinical findings, (3) review emerging biomarkers for both NASH and atherosclerosis that may also serve as therapeutic strategies, and (4) examine potential limitations and caveats for the concurrent treatment of both NASH and ASCVD.

2. Pathophysiology of ASCVD and NAFLD/NASH

2.1. Mechanisms driving the initiation and progression of atherosclerosis

Most cases of myocardial infarction and stroke are caused by atherosclerosis, the fibrofatty plaques in the arterial branch of the

vascular tree (24). The formation of atherosclerotic plaques is driven primarily by the deposition of apolipoprotein (Apo)-B-containing lipoproteins in the subendothelial spaces of the intima that subsequently drive maladaptive, non-resolving inflammation (25). Thus, individuals with familial hypercholesterolemia, particularly in the low-density lipoprotein (LDL) fraction, are disposed to developing atherosclerotic plaques at an early age (26). Other risk factors include insulin resistance and metabolic syndrome (27). Advanced atherosclerotic plaques contain vast amounts of extracellular matrix (ECM) proteins, calcium minerals, and a large necrotic core formed from the death of lipoprotein-rich monocyte-derived macrophages. These advanced atherosclerotic plaques can impede blood flow to downstream tissues through occlusion of the vessel lumen, causing symptomatic ischemia (24). More frequently however, atherosclerotic plaques rupture and leak the highly thrombogenic contents from the necrotic core into the lumen, resulting in an occlusive thrombus. Deaths from ASCVD were declining over the last two decades as treating more individuals for high LDL (~28% in 1999–2002 to ~48% in 2005–2008) resulted in twice as many individuals successfully lowering their circulating LDL-cholesterol from ~15% to ~33% (28). Despite the advent of potent cholesterol-lowering medicines, such as statins and anti-proprotein convertase subtilisin/kexin type 9 (PCSK9)-blocking antibodies, ASCVD remains the leading cause of death worldwide. More troubling is the recent trend that life expectancy growth has begun to decline, with a substantial rise in CVD deaths having the most impact (29). Thus, a deeper understanding of the cellular and molecular mechanisms driving atherosclerosis is necessary to conceive novel therapeutic strategies.

2.1.1. Endothelial cell activation

LDL particles accumulate in the subendothelial intima due to increased endothelial cell permeability caused by disturbed blood flow (30). Apart from the antioxidant environment normally provided by the blood, LDL particles become oxidized (ox-LDL) by unmitigated reactive oxygen species (ROS) production, leading to its uptake by scavenger receptors (31, 32). Unlike the LDL receptor (LDLR), scavenger receptors undergo positive feedback that maintains persistent cellular uptake of ox-LDL (33). Endothelial cells that take up ox-LDL activate the proinflammatory transcription factor nuclear factor- κ B (NF- κ B) that drive the expression of adhesion molecules, such as intercellular adhesion molecule 1 (ICAM1) and vascular cell adhesion molecule 1 (VCAM1) (34). These adhesion molecules presented on the apical surface of endothelial cells bind circulating leukocytes and promote their entry into the vessel wall. The role of endothelial cell activation in promoting atherosclerosis is crucial, as atherosclerosis formation tends to only occur at sites of disturbed blood flow, such as curvatures, branch points, and bifurcations, and experimental strategies that prevent endothelial cell activation prevent atherosclerosis formation (30).

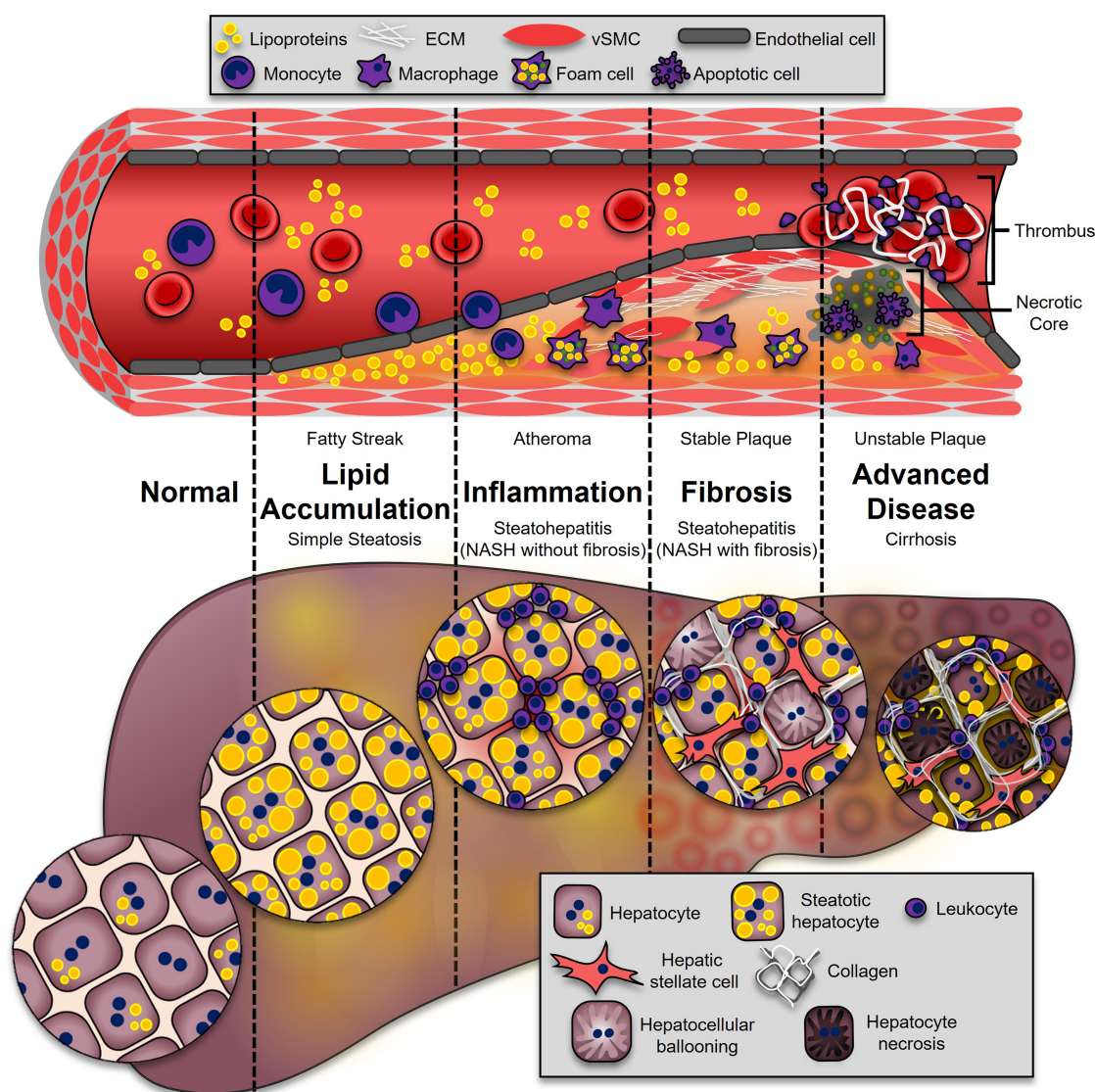


FIGURE 1

Progression of ASCVD and NASH. The onset of both ASCVD and NASH begins with dysregulated lipid metabolism, leading to their accumulation in the neointimal region of the artery (fatty streak), or the hepatocytes (simple hepatic steatosis). This process enhances inflammatory pathways in both diseases. During atherosclerosis, leukocytes adhere and transmigrate into the developing plaque, where they secrete additional cytokines and chemokines (atheroma). In the liver, leukocytes from the circulation accumulate, leading to NASH (NASH without fibrosis). These immune cells secrete soluble factors to activate collagen-producing cells: synthetic vascular smooth muscle cells (vSMCs) in atherosclerosis (stable plaque), and hepatic stellate cells in the liver (NASH with fibrosis). The most advanced stages of disease are associated with higher mortality. In atherosclerosis, advanced plaques with a large necrotic core and thin fibrous caps are prone to rupture (unstable plaque), which is highly thrombogenic. In the liver, excessive fibrosis and cell death leads to irreversible damage and loss of liver function (cirrhosis).

2.1.2. Vascular smooth muscle cell dedifferentiation and altered macrophage functions

Vascular smooth muscle cells (vSMCs) regulate blood pressure and vessel integrity under normal conditions (35). However, during early atherosclerosis, vSMCs undergo dedifferentiation whereby they lose canonical vSMC markers, such as α smooth muscle actin (α SMA) and transgelin (SM22), and reignite signaling pathways associated with development (36). Furthermore, dedifferentiated vSMCs begin to migrate, proliferate, and synthesize ECM proteins, thereby expanding the growing lesion

towards the lumen of the vessel. Interestingly, vSMCs produce a panoply of ECM proteins that can retain growth factors, cytokines, and chemokines (35). Whereas soluble growth factors and cytokines transmit potent signals rapidly, matrix-bound and immobilized factors resist internalization and degradation, sustaining their signaling capabilities and promoting fibroproliferative remodeling (37).

After endothelial cells are activated in regions of disturbed flow, monocytes infiltrate the subendothelial intima, where they differentiate into macrophages. These monocyte-derived macrophages ingest rampant amounts of ox-LDL, transforming

them into cholesterol-rich “foam cells” and compromising their beneficial immune cell functions (25). Macrophages are also highly susceptible to cell death owing to the intrinsic lipotoxic properties of ox-LDL that drive endoplasmic reticulum (ER) stress, resulting in their eventual death and release of damage-associated molecular patterns (DAMPs) in the surrounding microenvironment (38). Through various mechanisms, surrounding macrophages lose their ability to clear dying cells (termed “efferocytosis”), substantially expanding necrotic core areas and impairing the production of pro-resolving mediators, such as interleukin (IL)-10 and transforming growth factor beta (TGF β) (39, 40). Importantly, experimental strategies to restore efferocytosis in settings where it fails, mitigate atherosclerosis and even promote its regression (41–43).

2.1.3. Consequences of unmitigated atherosclerosis progression

Most acute cardiovascular events leading to myocardial infarction and stroke are caused by plaque rupture. During this process, highly thrombogenic material from the necrotic core, which is particularly rich in tissue factor, are released into the vessel lumen (24). Atheromas with relatively large necrotic cores and thin fibrous caps have often been considered “vulnerable” plaques, whereas “stable” plaques have much thicker fibrous caps (44). Macrophages and vSMCs are particularly sensitive to ox-LDL and undergo cell death, forming necrotic cores. An imbalance in fibrogenesis vs. fibrolysis impedes vSMC-dependent ECM synthesis and assembly and drives thinning of the protective fibrous cap. Inflammatory cells activated in the atherosclerotic milieu also possess robust levels of collagenases that degrade the collagen-rich fibrous cap. Structural weakening of the fibrous cap results in interfacial debonding, characterized as the physical separation of fibrillar matrix (45, 46). Notably, this phenomenon is frequently observed in ruptured atheromas (45, 46).

2.2. NAFLD: Onset, progression, and molecular drivers

NAFLD represents a range of liver pathologies beginning with excessive accumulation of lipids, particularly triglycerides, in hepatocytes (47). Additional findings of enhanced cytokine and chemokine production, inflammatory cell recruitment, and hepatocyte death characterize NASH, which may progress into fibrosis, cirrhosis, and liver failure. Importantly, NAFLD is emerging as a leading cause of liver disease, with 20%–30% of the individuals progressing to cirrhosis due to NASH (48, 49). Cardiometabolic disorders, such as insulin resistance and the metabolic syndrome, are risk factors contributing to the progression of NASH (50).

2.2.1. Hepatic steatosis and lipotoxicity

Increased caloric consumption is one of the leading causes of NAFLD, as excessive substrate overload or dysfunction in the ability of adipose tissue to store fats results in lipolysis (51). Consequently, circulating free fatty acids increase and are then taken up by secondary storage organs, particularly the liver,

through fatty acid transport protein 5 (FATP5) and the scavenger receptor CD36 (52, 53). This stimulates signaling pathways that ultimately drive intrahepatic triglyceride accumulation. In addition, *de novo* lipogenesis (DNL) promotes hepatic steatosis by converting carbohydrates into lipids. Thus, the three main pathways, (1) enhanced lipolysis from adipose tissue, (2) triglyceride synthesis from the dietary nutrients, and (3) the conversion of dietary sugars into fatty acids by DNL, drive hepatic steatosis. In this manner, the liver’s capacity to adequately process carbohydrates and fatty acids become impaired, and the formation of toxic lipid species, such as lysophosphatidylcholines, diacylglycerols, and ceramides, takes place (51). Consequently, these lipotoxic lipid species elicit a robust unfolded protein response (UPR) and ER stress that promote inflammasome activation and cell death.

Excess accumulation of intrahepatic fatty acids drives ER stress, uncouples mitochondria, and elevates ROS production by the mitochondria (54). Consequently, Jun N-terminal kinase (JNK) becomes activated and promotes intrinsic apoptosis through a caspase-2-BID signaling pathway (55). Also, fatty acid conversion to triglycerides increases the expression of death receptors and their cognate ligands, tumor necrosis factor alpha (TNF α) and Fas, to stimulate extrinsic cell death. Intrinsic or extrinsic apoptosis leads to the release of DAMPs that crosstalk with either resident or recruited macrophages to stimulate toll-like receptor (TLR)-dependent expression of multiple proinflammatory cytokines and chemokines.

2.2.2. Inflammation

A critical feature that distinguishes hepatic steatosis from NASH is the presence of hepatic inflammation, particularly of resident Kupffer cells and recruited monocyte-derived macrophages (56). Meta-analysis of RNA sequencing and single-cell RNA sequencing have revealed critical alterations in the myeloid compartment recruited to livers during NASH. Firstly, turnover and maintenance of embryonically-derived Kupffer cells are diminished during the progression of steatosis to NASH, likely due to lipotoxicity (57). Second, monocyte-derived macrophages recruited to the liver, which highly expresses *Trem2*, *Gpnmb*, *Cd9*, *Spp1*, and *Itgax*, genes associated with macrophages in NASH, accumulate in areas near desmin^{high} hepatic stellate cells, revealing their capability to crosstalk with hepatic stellate cells to drive hepatic fibrosis (58). Importantly, macrophages have been definitively proven to contribute to NASH, as depleting Kupffer cells from mice using liposomal clodronate, deleting the chemokine receptor C-C chemokine receptor type 2 (CCR2), or ablating bone marrow cells from mice using irradiation, mitigates the progression of steatosis to NASH (59–62).

Through a variety of mechanisms, macrophages in the liver exhibit a heightened state of inflammation and produce vast amounts of IL-1 β (63). Consequently, peroxisome proliferator-activated receptor alpha (PPAR α) becomes suppressed, and oxidation of fatty acids is impaired, ultimately leading to an accumulation of fatty acids (63). Fatty acids not only stimulate triglyceride production in hepatocytes, but they also stimulate

inflammatory responses in liver immune cells (56). The saturated fatty acids, palmitate and laurate, drive IL-1 β secretion by mediating NLRP3 inflammasome activation during NASH in a TLR2-dependent mechanism (56, 64, 65). Furthermore, palmitate activates NADPH oxidase 2 (NOX2) in hepatic macrophages and induces ROS production (66). Importantly, elevated levels of ROS directly stimulate TNF α expression. Also, macrophages from steatotic livers show enhanced production of toxic lipid mediators, particularly diacylglycerols and ceramides (56).

2.2.3. Hepatic stellate cell activation and fibrosis

Persistent deposition of ECM proteins, such as collagens, in the liver drive cirrhosis and liver failure. Excluding CVD, liver fibrosis is the major cause of liver-related mortality in patients with NASH (47, 50). Therefore, hepatic fibrosis is among the most important endpoints in clinical trials. Hepatic fibrosis is largely mediated by the activation of non-parenchymal hepatic stellate cells that leads to their dedifferentiation towards a myofibroblast phenotype, enabling them to robustly synthesize and deposit ECM proteins (67). Evolutionarily conserved developmental programs, including Notch, hedgehog, and Hippo-YAP-TAZ, are “reawakened” in acute liver injury to stimulate hepatocyte regeneration (67). However, growing research in these pathways has revealed that they also critically drive hepatic fibrosis during NASH. For example, transgenic overexpression of Notch in hepatocytes leads to enhanced osteopontin secretion, enhancing fibrosis through hepatic stellate cell activation (68, 69). Consistently, hepatocyte-specific inactivation of Notch signaling protects mice from developing NASH-induced hepatic fibrosis (69). Whereas Hedgehog signaling is inactive in normal livers, it becomes reactivated during NASH and enhanced Hedgehog activity correlates with disease severity and fibrosis staging (67, 70). In addition, Sonic Hedgehog and Indian Hedgehog activates hepatic stellate cells and drive ECM protein synthesis (71). Moreover, hepatocyte YAP and TAZ expression are intimately linked to liver fibrosis and positively correlate with NASH and deleting or silencing TAZ in hepatocytes lowers inflammation and fibrosis in a mouse model of NASH (72–74).

3. Concurrent modelling of NASH and atherosclerosis

To investigate the pathophysiology of NAFLD/NASH or ASCVD, multiple well-established animal models have been accepted by the scientific community and are commonly utilized for evaluating translational interpretation of preclinical findings. Below, we will discuss dietary models predominantly administered to mice, highlighting potential limitations of current application when investigating both NAFLD/NASH and ASCVD, as well as non-murine models that may have stronger translational potential but comprise their own set of limitations.

3.1. Diets in excess or deficiency: Which is ideal?

Given both NAFLD/NASH and ASCVD arise from dysregulated lipid metabolism and excessive lipid accumulation, the most appropriate models capitalize on genetic and/or dietary lipid loading with additional modifications to exacerbate disease, such as simple carbohydrates or cholesterol. Lipid profiling of mice demonstrates that the majority of their cholesterol is carried in high-density lipoprotein (HDL) particles, contrasting human lipid profile in which HDLs comprise only one-third of total cholesterol (75). Since elevated LDLs and very low-density lipoproteins (VLDLs) are direct contributors to atherogenesis (76), mice will therefore not spontaneously develop atherosclerotic lesions comparable to humans beyond the initial fatty streak (77). Thus genetic (*Ldlr*^{−/−} (78), and apolipoprotein E deficient [*Apoe*^{−/−}] mice 79, 80) or viral (PCSK9-AAV 81, 82) manipulation is required for mice to develop atherosclerosis. Implementing a combination of genetic dyslipidemia with dietary models to induce NASH permits simultaneous investigation of both NASH and atherosclerosis.

While administration of a high-fat diet in atherosclerotic models is well-established to induce hyperlipidemia and steatohepatitis (83–85), whether high-fat or Western diets are sufficient to elicit all components of NASH (hepatic steatosis, inflammation, and hepatocellular ballooning) and fibrosis remains unclear. Multiple studies report conflicting phenotypes in *Apoe*^{−/−} mice following a high-fat diet regimen. For example, Karavia and colleagues demonstrated that despite administration of a high-fat diet (21.2% fat) for 24 weeks, *Apoe*^{−/−} mice will accumulate less hepatic triglycerides compared with C57BL/6 mice fed the same diet (86). In contrast, others showed that only 8 weeks of high-fat diet in *Apoe*^{−/−} mice was sufficient to induce hepatocellular ballooning and hepatic fibrosis (87). Additional studies by Matsuzawa et al. found that 12–24 weeks of an “atherogenic diet” in C57BL/6J mice is sufficient to induce hepatocellular ballooning and hepatic fibrosis (88), while Zhang et al., induced steatohepatitis with fibrosis and hepatocellular carcinoma following 14 months of high-fat, high-cholesterol feeding in C57BL/6 mice (89). Furthermore, a study by Schierwagen et al. compared Western diet and methionine-choline deficient (MCD)-diet in *Apoe*^{−/−} mice, demonstrating significant fibrosis and hepatocellular ballooning in Western diet-fed mice after just 7 weeks (90). Comparisons between diet formulations used in the above studies show that while Karavia and colleagues utilized a Western-type diet, which contains 0.2% cholesterol (86, 91), Schierwagen et al. and Matsuzawa et al. utilized diets containing 1.25% cholesterol (88, 90). Furthermore, Trevaskis and colleagues first described the Amylin liver NASH (AMLN) diet, which contained 2% cholesterol and 40% fat from either partially hydrogenated vegetable oil or lard and induced murine steatohepatitis and fibrosis following 12 weeks feeding (92). Together, these studies highlight the fact that additional components of a high-fat or Western diet, mainly cholesterol, contribute to the NASH phenotype beyond excessive calories from fat (Table 1).

TABLE 1. Murine and non-murine models of NAFLD/NASH with or without atherosclerosis

Disease Model	Animal Model	Diet Source	Diet Components	Time on Diet	Phenotype	References
Murine models						
NAFLD	Mouse (C57BL/6J) <i>Apoe</i> ^{-/-}	Mucedola, Milan, Italy	Western-type Diet: 21.2% kCal from fat 0.2% cholesterol	24 weeks	Normal hepatic histology with no triglyceride accumulation noted	Karavia et al. (99)
NAFLD	Mouse (C57BL/6J)	Envigo	Fructose-palmitate diet (TD.160785): 190g/kg hydrogenated vegetable shortening 40g/kg anhydrous milk fat 0.2%–0.5% cholesterol 55% glucose/45% fructose w/w in the drinking water	16 weeks	Enhanced steatosis but no fibrosis	Wang et al. (76)
NASH	Mouse (C57BL/6J) <i>Apoe</i> ^{-/-}	No information provided	High-fat diet No additional information provided	8 weeks	Enhanced plasma AST/ALT, hepatic steatohepatitis, ballooning, and fibrosis	Lu et al. (100)
NASH	Mouse (C57BL/6J)	Oriental Yeast, Tokyo, Japan	Atherogenic diet: 14g fat 1.25% cholesterol High fat diet 60g fat 1.25% cholesterol	12–24 weeks	Enhanced steatosis, inflammation, and fibrosis observed in atherogenic and high fat diet combined, but not atherogenic diet alone	Matsuzawa et al. (101)
NASH	Mouse (C57BL/6J)	Research Diets, New Brunswick, NJ Envigo	High-fat diet (D12492): 60% fat 0.03% cholesterol Choline-deficient high fat diet (D05010402) 60% fat 0.03% cholesterol Choline deficient Western diet (TD.88137): 42% fat, 0.2% cholesterol	15 weeks	Enhanced steatosis. Inflammation only observed in Western diet. Fibrosis only observed in choline deficient high fat diet and Western diet.	Smati et al. (124)
NASH	Mouse (C57BL/6J)	Teklad	Fructose-palmitate-cholesterol (TD.140154): 190g/kg hydrogenated vegetable shortening 40g/kg anhydrous milk fat 1.25% cholesterol ~35% reduction in choline 55% glucose/45% fructose w/w in the drinking water	8–28 weeks	Enhanced steatohepatitis and fibrosis	Wang et al. (74)
NASH	Mouse (C57BL/6J)	Envigo	Fructose-palmitate diet (TD.160785): 190g/kg hydrogenated vegetable shortening 40g/kg anhydrous milk fat 1.25% cholesterol ~35% reduction in choline 55% glucose/45% fructose w/w in the drinking water	16 weeks	Enhanced steatohepatitis and fibrosis	Wang et al. (76)
NASH	Mouse (<i>Lep</i> ^{ob} / <i>Lep</i> ^{ob})	Research Diets, New Brunswick, NJ	High trans-fat, high fructose, high cholesterol diet (HTF): 40% kCal fat from vegetable shortening 22% w/w fructose 2% cholesterol	12 weeks for trans-fat diet	Enhanced hepatic steatosis and fibrosis	Trevaskis et al. (104)
NASH	Mouse (C57BL/6J)	Research Diets, New Brunswick, NJ	NASH diet (D17010103): 40% kCal fat with 50g/kg primex shortening (non-transfat), 122g/kg corn oil, partially hydrogenated 22% w/w fructose 2% cholesterol	24 weeks	Enhanced AST, ALT, and ALP, with enhanced steatohepatitis and fibrosis	Rom et al. (96, 97)
NASH-HCC	Mouse (C57BL/6J)	Specialty Feeds, Glenn Forrest, WA	High-fat/high-cholesterol diet: 43.7% fat 0.203% cholesterol	8–14 months	Enhanced AST, ALT, steatohepatitis, and fibrosis beginning at 8 months, and HCC observed by 10 months	Zhang et al. (102)

(Continued)

TABLE 1. (Continued)

Disease Model	Animal Model	Diet Source	Diet Components	Time on Diet	Phenotype	References
NASH and Atherosclerosis	Mouse (C56BL/6J) <i>Ldlr</i> ^{-/-} .Leiden	Research Diets, New Brunswick, NJ	High-fat diet (D12451): 45% kCal fat from lard 35% kCal carbohydrates from sucrose 0.01% w/w cholesterol Fast food diet: 41% kCal fat from milk fat 44% kcal carbohydrates from fructose 0.05% w/w cholesterol	28 weeks	Enhanced AST, ALT, hepatic steatohepatitis, fibrosis, and atherosclerosis	Van den Hoek et al. (86)
Non-murine models						
Coronary artery disease	Ossabaw pig	No information provided	Western diet: 38% kCal fat 1.5% cholesterol w/w	6 months	Significant increases in ALP, ALT, AST (but no liver histology noted), and coronary artery lesions compared with control diet	Matthan et al. (133)
NASH	Ossabaw pig	Purina TestDiet, Inc., Richmond, IN	Atherogenic diet: 46% kCal fat 20% kCal fructose 2% cholesterol 900 ppm choline Modified atherogenic diet: 43% kCal fat 17.8% fructose 2% cholesterol 700ppm choline	24 weeks	Enhanced AST and ALT, steatohepatitis, ballooning, and fibrosis in modified atherogenic diet group. Enhanced ALT and steatosis in atherogenic diet group.	Lee et al. (134)
NASH with fibrosis by NaNO ₂ injections	Wistar rat	Research Diets, New Brunswick, NJ	Choline deficient high fat diet (A06071302): 60% kcal fat 0.03% cholesterol 0.1% methionine Choline deficient NaNO ₂ injections: 10-30mg/kg	10 weeks, with NaNO ₂ administered following 4 weeks	Enhanced fibrosis	Schwabl et al. (126)
NASH and atherosclerosis	Japanese white rabbit	No information provided	High-fat and -cholesterol diet: 12% corn oil 0.75% cholesterol	9 months	Enhanced steatohepatitis, hepatic fibrosis, and aortic atheroma	Ogawa et al. (135)
NASH and atherosclerosis by aortic endothelial injury by balloon catheter	Rabbit	TestDiet, Saint Louis, MO	Cholesterol containing chow diet: 2.4% fat w/w 1% cholesterol	3 months	Enhanced hepatocyte ballooning and fibrosis. Atherosclerosis only enhanced with cholesterol diet and injury	Taylor et al. (139)
NASH	Cynomolgus monkey	Kunming Biomed International	High fat diet: 20% fat, 5% cholesterol	3 years	Enhanced steatohepatitis, fibrosis, and NAS score	Lyu et al. (142)
NASH	Cynomolgus monkey	Beijing Keao Xieli Feed Co., Ltd, Beijing, China	High fat high cholesterol diet: 10% lard 15% cholesterol	24 weeks	Enhanced steatohepatitis, hepatic ballooning, fibrosis, and NAS score	Jian et al. (143)
NASH	Cynomolgus monkey	Keao Xieli	High fat high cholesterol diet: 10% lard 1% cholesterol	16 weeks	Enhanced NAS score, steatosis, and fibrosis	Zang et al. (144)

Supplementation of a high-fat diet with cholesterol appears to be a major contributor to the pathogenesis of NASH. Analysis of liver biopsies from patients with NASH demonstrated that free cholesterol accumulation associates with hepatic steatosis and continues to increase with the progression of NASH (93). In addition, unlike triglycerides or free fatty acids, cholesterol loading is sufficient to deplete mitochondrial glutathione in hepatocytes resulting in sensitivity to inflammatory cytokines (94). Following extended high-fat, high-cholesterol feeding for 14 months, cholesterol induces gut microbiota dysbiosis, enhanced gut leakiness, endotoxemia, and bile acid biosynthesis in C57BL/6 mice, which result in NASH with fibrosis and HCC (89). However, the effects of dietary cholesterol and the risk of CVD

remains unclear (95). Since conventional atherogenic diets parallel human consumption of cholesterol (96, 97), but typically contain approximately one-tenth that of murine NASH diets (0.2% and 2%, respectively (83, 92)), excessive cholesterol supplementation may be inappropriate for the comparative studies of CVD and NASH together. Thus, other components such as dietary sugars may be considered when addressing models for concurrent NASH and ASCVD.

Since fructose largely replaced sucrose as a source of sweeteners in soft drinks in the 1970's, an association between high-fructose corn syrup consumption and obesity became increasingly observed (98). In addition, beyond increasing hepatic steatosis, fructose enhances aortic wall thickness and foam cell count in

Sprague-Dawley rats fed a high-fat diet (99). Van den Hoek and colleagues fed *Ldlr*^{-/-}.Leiden mice an obesogenic diet for 28 weeks containing 41% calories from fat, 0.05% cholesterol, and 44% calories from fructose (100), which recapitulated multiple aspects of NASH like inflammation (100), fibrosis (101), and circulating AST and ALT (102), as well as established atherosclerotic lesions (100). Since *Ldlr*^{-/-}.Leiden mice are susceptible to diet-induced obesity and metabolic syndrome compared with conventional *Ldlr*^{-/-} mice (103), this model proved effective in examining both fibrotic NASH and atherosclerosis (100). While normal consumption of fructose feeds into glycogen biosynthesis (104), excessive fructose consumption suppresses fatty acid β -oxidation (FAO) in the liver (105) and induces DNL by the induction of sterol regulatory element-binding protein-1 (SREBP1), acetyl-CoA carboxylase-1 (ACC1), and fatty acid synthase (FAS) (105, 106). By comparing the supplementation of fructose to glucose in humans and mice, Stanhope et al. and Softic et al. demonstrated that inhibition of FAO and induction of DNL are caused specifically by high intake of fructose, and not glucose (107–109). In the gastrointestinal tract, fructose deteriorates the gut barrier and promotes chronic inflammation by endotoxemia (110). Since endotoxemia is associated with liver disease and atherosclerosis (111, 112), the effects of fructose on the development of NAFLD/NASH and ASCVD may be due to chronic inflammation secondary to enhanced gastrointestinal permeability. Thus, the contribution of high-fructose intake for the concurrent development on NASH and atherosclerosis warrants further research.

Although diets with excess nutrients elicit NASH or ASCVD pathology, diets lacking key nutrients are an additional avenue for inducing disease. Choline and methionine deficiency diminishes VLDL assembly and reduces triglyceride clearance but results in weight loss (113), contrasting with typical weight gain associated with most human NASH. The MCD diet was previously viewed as a conventional NASH model; however, multiple groups demonstrated that MCD does not cause insulin resistance (114) and enhances weight loss despite hepatic steatosis (115), highlighting the disconnect between human disease characteristics and disease in MCD diet-fed mice. Since the MCD model clearly has its deficiencies in application with NASH pathology, researchers have developed modifications of this model to align the diet-induced phenotype more closely with human NASH. For example, the high-fat, choline-deficient diet induces steatosis, inflammation, and fibrosis over a 15-week period; however, it does not induce ballooning (116). Choline deficiency reduces pro-atherogenic VLDL assembly (113) but choline supplementation has no effect on atherosclerotic plaque area (117). The choline-deficient high-fat diet with no added choline but 0.1% methionine has approximately 0.03% cholesterol and induces steatohepatitis (116); however, to develop fibrosis the addition of 25 mg/kg NaNO₂ (118) is required to induce hypoxemia (119). Enhancing methionine to 0.2% does prevent weight loss while enhancing NASH and hepatic fibrosis (113). While enhancing liver fat accumulation, the choline-deficient high-fat diet actually attenuates fasting plasma insulin and improves glucose tolerance (120). Patients with NAFLD

develop hyperinsulinemia as a result of impaired whole-body insulin clearance, which may further drive hepatic steatosis (121). The positive correlation between hyperinsulinemia and atherosclerosis has been long-established (122). Therefore, models mimicking hyperinsulinemia, should be considered in appropriate models of both NASH and ASCVD.

3.2. Non-murine models

The utilization of mice for pathological modelling has its benefits. For example, mice gestate and grow rapidly, require small spaces for housing, are relatively inexpensive to care for, and are easily genetically manipulated. While numerous mouse models have been implemented to study NAFLD/NASH or ASCVD, each provides a unique set of limitations. For example, atheroprone mice must first be “humanized” with genetic manipulation to shift their endogenous plasma cholesterol composition. Furthermore, as outlined in section 2.1, many mouse models of NASH do not completely mimic all aspects of the human disease, particularly hepatocellular ballooning and fibrosis (123). Additionally, dietary models alone are insufficient to induce atherosclerosis in mice due to their plasma lipid composition (77). Therefore, the use of non-murine or large animal models that spontaneously develop atherosclerosis may provide a more accurate representation of both human NASH and ASCVD.

Porcine models of atherosclerosis are closely related to the human disease due to similar lipoprotein composition; thus, pigs do not require genetic modification to induce ASCVD (124). In addition to their use as an atherogenic model (125), miniature Ossabaw pigs develop metabolic syndrome with abnormal liver pathology indicative of NASH when fed a modified high-fat, low-choline diet for 24 weeks (126). However, pigs require larger housing facilities, utilize more resources, and are therefore not as cost-effective. Rabbits may be a useful alternative to pigs or mice because they require less resources than pigs and are able to develop NASH with fibrosis following 9 months of a modified diet containing 0.75% cholesterol and 12% corn oil (127). Rabbits were pivotal in the initial discovery of atherosclerosis in which the Russian physician Ignatowski observed aortic plaques in rabbits fed an enriched animal fat and protein diet (128). Since then, rabbits are widely used for atherosclerosis studies due to their similarities to human lipoproteins, and both diet-and genetically-induced atherosclerotic models have been implemented (129). Furthermore, 1% cholesterol-fed rabbits develop both atherosclerosis (130) and fibrotic NASH, representing a simple model to investigate both diseases simultaneously (131). However, rabbits show wide genetic variability compared with mice (129) and therefore require larger cohorts to observe meaningful differences between treatment groups. Perhaps the most translatable model of either NASH or atherosclerosis is the use of nonhuman primates. For example, cholesterol metabolism between humans and Baboons is remarkably similar (132), and baboons given a high-sugar, high-fat diet leads to weight gain and hyperlipidemia similar to humans (133). Cynomolgus monkeys given a diet containing 20% fat with 5% cholesterol developed NASH with fibrosis (134). In addition, a high-fat, high-cholesterol

(1%) diet can accelerate NASH in *Cynomolgus* monkeys with spontaneously-developed NASH symptoms (135, 136). However, the ethical considerations of these animals should be heavily weighed when deciding which models are the most appropriate. Despite their obvious similarities with humans, the advanced cognition of nonhuman primates sheds light on the moral obligations of scientific researchers (137).

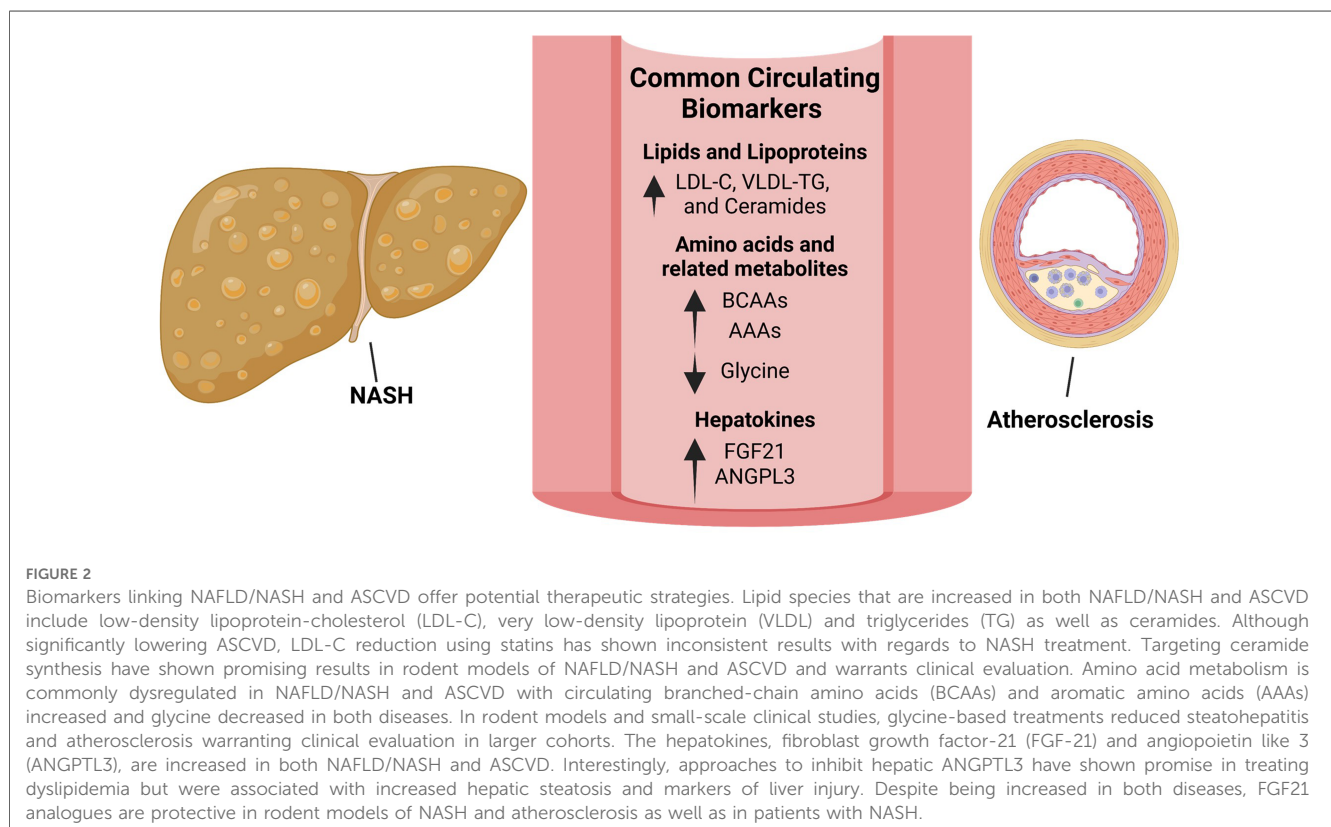
4. Emerging biomarkers linking NAFLD/NASH and ASCVD offer potential therapeutic strategies

The circulating levels of liver enzymes (aspartate transaminase [AST], and alanine transaminases [ALT]), other nonenzymatic proteins (albumin) and metabolites of heme (bilirubin) are routinely used to diagnose and monitor liver diseases, including NAFLD/NASH (138). While liver function tests are routinely preformed, their interpretation is often challenging and their relevance to CVD, the main cause of death in patients with NASH (7–12, 139–141) is limited. Furthermore, predictive biomarkers of NASH are lacking, resulting in invasive biopsy as the only method for diagnosis (51). Established biomarkers for CVD including C-reactive protein (CRP), cardiac troponins I and T, B-type natriuretic peptides, and D-dimer, are widely used for diagnosis and management of various CVDs including atherosclerosis, myocardial infarction, acute coronary syndrome, cardiac arrest, thrombosis, and ischemic cardiac diseases (142–144). Despite the wide use of these biomarkers for diagnosis and

monitoring, there remains a need to identify new pathological pathways and pertinent biomarkers that can be useful for concurrent diagnosis and monitoring of NAFLD and CVD. Herein, we explore established and newly identified biomarkers that are closely related to NAFLD/NASH and ASCVD (Figure 2).

4.1. Lipids, lipoproteins, and lipid peroxidation products

The liver is the major site of lipid and lipoprotein metabolism and regulates the production and clearance of all classes of lipoprotein particles (145). In addition, the liver regulates the metabolism of the major lipoprotein components including triglycerides and cholesterol (146, 147). Dysregulation of hepatic lipid metabolism leading to excess lipid accumulation is a hallmark feature of NAFLD which further promotes atherogenic dyslipidemia and the risk of ASCVD (147, 148). Thus, alteration in circulating lipoproteins in patients with NAFLD is considered an early biomarker to predict the risk of ASCVD. Preclinical and clinical reports showed that improvement in NAFLD improves dyslipidemia (149–151); however, statins or other lipid-lowering agents did not reduce the risk of cardiovascular mortality in patients with NAFLD (152). In contrast, pemafibrate, a PPAR α modulator that lowers triglycerides, VLDL, and cholesterol, did not reduce the incidence of cardiovascular events but lowered the incidence of NAFLD (153). These studies highlight the need to improve our understanding of the role of other lipid and non-lipid metabolites, not only as biomarkers linking these two diseases, but also as potential targets for concurrent therapy.



Enhanced influx of free fatty acids to the liver, oxidative stress and inflammatory stimuli promotes the synthesis of hepatic ceramides in NAFLD (154, 155). Ceramides are active lipid intermediates of the sphingolipid family that are produced mainly in the liver (156). Beyond their increased levels in the liver, circulating ceramides are elevated in animal models and patients with NAFLD (157, 158), particularly in those with NASH (159), where they are found mainly in VLDL and LDL particles (159, 160). Moreover, various ceramide species (mainly Cer16:0, Cer18:0 and Cer24:1) are consistently associated with adverse cardiovascular outcomes and mortality (161–163), and have been suggested as biomarkers for ASCVD beyond the currently existing risk factors (164). Ceramides are not only associated with ASCVD but can also increase atherosclerosis by promoting endothelial dysfunction (154, 165). Pharmacological (myriocin) and genetic (hepatic deletion of dihydroceramide desaturase-1) approaches targeting ceramide synthesis not only lowered hepatic steatosis and fibrosis (166, 167), but also reversed endothelial dysfunction and atherosclerosis in rodent models (168, 169).

In NAFLD, and particularly in NASH, hepatic mitochondrial dysfunction augments ROS production promoting lipid peroxidation, the oxidation of polyunsaturated fatty acids *via* lipid-peroxyl radical reaction (54, 170–172). Beyond enhanced hepatic lipid peroxidation, an increase in systemic markers of lipid peroxidation (e.g., malonaldehyde, MDA) is well-documented in both experimental models and in patients with NAFLD (173–175). Furthermore, higher circulating MDA in patients with NAFLD is associated with lower antioxidant capacity of HDL and subclinical atherosclerosis (176). Peroxidation of lipoproteins (mainly ox-LDL) plays critical roles in various steps of atherosclerosis development (177), including endothelial activation and dysfunction (178, 179), monocyte adhesion (180, 181), macrophage-foam cell formation (182–185), and proliferation and migration of vSMCs (186, 187). Indeed, circulating ox-LDL is a useful marker in predicting the risk of coronary artery diseases (CAD) (188) as well as NAFLD severity (189). In addition, circulating ox-LDL in the form of MDA-LDL is not only increased in individuals with NAFLD, but is also associated with high-risk atherosclerotic plaques in the same patients (190).

4.2. Amino acids

While dysregulated lipid metabolism in NAFLD/NASH and ASCVD has been extensively studied, recent evidence strongly suggests altered amino acid metabolism as a common factor in both diseases (83, 191–203). Gaggini et al. (192) found that most circulating amino acids were elevated among obese subjects with NAFLD and further increased in the presence of insulin resistance (IR) and obesity. Patients with more advanced liver damage and fibrosis had higher levels of the branched-chain amino acids (BCAAs, leucine, isoleucine and valine) (204) and aromatic amino acids (AAAs tryptophan, phenylalanine, and tyrosine) (192, 205). Furthermore, BCAAs and AAAs are consistently reported to be positively associated with increased

risk for ASCVD independent of hypertension and metabolic disease (206–209).

Despite the associations between elevated circulating amino acids and NAFLD or ASCVD, a causative role of BCAAs and AAAs remains unclear. In mice with NAFLD, BCAAs promote liver injury and apoptosis by downregulating lipid-induced autophagy (210). In contrast, BCAA supplementation to mice fed high-fat or choline-deficient, high-fat diets lowered hepatic steatosis and injury through suppression of hepatic lipogenic genes and modulation of intestinal microbiota-mediated production of acetic acid (211, 212). These contrasting effects may be due to specific BCAAs, since the adverse metabolic effects in obese mice appear to be mediated by isoleucine and valine but not by leucine, whose restriction aggravated hepatic steatosis (213). In addition, leucine protects against macrophage foam cell formation by inhibiting lipid biosynthesis, promoting cholesterol efflux and enhancing mitochondrial respiration (191, 197, 214, 215). Furthermore, *Apoe*^{−/−} mice supplemented with leucine showed enhanced hepatic cholesterol efflux, which effectively reduced circulating LDL and atherosclerosis (216). The effects of BCAAs on different cell types may differentially regulate the pathogenesis of atherosclerosis. For example, supraphysiological levels of BCAAs (6 mmol/L) enhanced ROS and activated endothelial cells (217). In contrast, physiological levels of leucine (0.2 mmol/L) protect against macrophage foam cell formation by inhibiting lipid biosynthesis, promoting cholesterol efflux and enhancing mitochondrial respiration (191, 197, 214, 215). Thus, future studies are warranted to clarify the causative role of exogenous BCAAs and determine the effects of individual BCAAs in NAFLD/NASH and ASCVD.

In individuals with histologically confirmed NAFLD, plasma phenylalanine was increased only in those with NASH, while tyrosine was increased in both patients with simple steatosis and NASH (218). Tyrosine and total AAAs were associated with NAFLD severity assessed by hepatocellular ballooning, inflammation and fibrosis in patients with NASH (192, 205). Also, serum AAAs were reported to be higher in patients with NASH, but when compared to patients with simple steatosis, only tryptophan was higher in those with NASH. In addition, serum tryptophan and tyrosine were positively correlated with total and LDL-cholesterol (219), suggesting that alterations in circulating AAAs are associated with the risk of NAFLD-associated CVD. Indeed, in a large cohort of adults Finns, circulating tyrosine was positively associated with subclinical atherosclerosis assessed by carotid intima-media thickness (IMT) (200). In addition, phenylalanine and tyrosine were associated with CAD, ischemic stroke, and cardiovascular events (220). While the above studies demonstrate increased circulating AAAs in NAFLD/NASH and ASCVD, studies addressing the causative role of altered AAA metabolism and the effects of individual AAAs in the development of these diseases are lacking.

Whereas circulating BCAAs and AAAs are increased, glycine, the simplest amino acid, is consistently reported to be lower in association with suppressed hepatic glycine biosynthetic genes (e.g., alanine-glyoxylate aminotransferase [AGXT] and serine hydroxymethyltransferase [SHMT]) and inversely associated with

the risk or severity of NAFLD/NASH, CVD and related cardiometabolic diseases in both mouse models and patients (83, 192, 195, 196, 199, 201, 221–225). While these reports highlight lower circulating glycine as an emerging biomarker for both NAFLD/NASH and ASCVD, studies in humans and mice support a causative role of reduced glycine availability and the potential of glycine-based treatment in both diseases (83, 199, 201). Glycine is a nonessential amino acid mainly synthesized in the liver (226). In patients and mice with NAFLD, glycine is a limiting substrate for *de novo* synthesis of glutathione (GSH), the most abundant endogenous antioxidant (83, 199). Therefore, the decrease in circulating glycine in NAFLD may be explained by insufficient hepatic production coupled with enhanced demand for GSH biosynthesis. Furthermore, glycine restriction aggravates atherosclerosis in *Apoe*^{−/−} mice (83, 195). Glycine or glycine-based treatments [e.g., serine, trimethylglycine (betaine) and a glycine-based tripeptide, DT-109] lowered hepatic steatosis, inflammation and fibrosis as well as atherosclerosis in various rodent models (83, 195, 227) and humans (199) through mechanisms involving hepatic GSH biosynthesis, enhanced fatty acid utilization, suppression of proinflammatory/fibrotic responses and modulation of the gut microbiome. In addition to glycine, glutamate, another component of GSH, is increased in NAFLD/NASH, which has been attributed to gamma-glutamyltransferase-mediated glutamate release during GSH transamination and upregulation of hepatic glutaminase-1 (192, 203). This, together with alternations in serine metabolism in NAFLD (192, 198), serve as a basis for the glutamate-serine-glycine (GSG) index, which recently emerged as a potential biomarker for the severity of NAFLD and fibrosis (192, 228).

4.3. Polyamines

Polyamines including putrescine, spermidine, and spermine are present in all living organisms. These aliphatic polycation compounds play a role in various biological events including maintenance of chromatin structure, gene transcription and translation, cell growth, and proliferation. The biological effects of polyamines are believed to be mediated by modulation of protein-protein and protein-DNA interactions (229–231). Emerging evidence suggests that polyamines modulate the risk of CVD, metabolic diseases, neurological disorders, and cancer (232–235). Nevertheless, the role of polyamine metabolism as a potential link between NAFLD/NASH and CVD remains to be explored.

Dysregulated metabolism of polyamines in NASH has been identified in human and rodent studies. A metabolomics-based study demonstrated that circulating spermidine was more than 2-fold lower in individuals with advanced NASH and fibrosis compared to those with the early disease (236). Alternations in polyamine metabolism during NASH could be attributed to the availability of S-adenosylmethionine (SAME), a universal methyl donor and a polyamine precursor. In NASH, glycine-N-methyltransferase (GNMT), which catalyzes the transfer of a methyl group from SAME to glycine, is reduced, promoting an increase

in SAME and subsequent accumulation of putrescine associated with enhanced lipid peroxidation (237). While changes in circulating putrescine in NAFLD/NASH have not been reported yet and the evidence for decreased spermidine is limited (236), a number of studies reported a protective role of spermidine in mouse models of NAFLD. In diet-induced obese mice, supplementation with spermidine lowered hepatic steatosis associated with downregulation of lipogenic genes and upregulation of genes driving FAO, including *Ppara* (233, 238). Also, spermidine ameliorated obesity-associated NAFLD in mice by increasing the phosphorylation of hepatic AMP-activated protein kinase (AMPK), which in turn inhibited the expression of the lipogenic genes *Srebf1c* and *Fas* (239). In addition, spermidine treatment restored the hypusination of translation factor EIF5A, which was decreased in NASH, leading to enhanced mitochondrial FAO and protection against diet-induced NASH in mice (240). While the studies above suggest dysregulated polyamine metabolism in NASH and indicate a protective role of spermidine, further research is needed to establish the use of polyamines as biomarkers for NAFLD/NASH.

With regards to CVD, the association with spermidine has been evaluated in a number of recent studies. In individuals with AMI, serum spermidine was associated with improved prognosis and reduced rates of major adverse cardiac events (241). On the other hand, a higher risk of stroke was found with an increasing baseline serum spermidine (242). Moreover, obese and overweight subjects were found to have higher serum spermidine along with increased atherogenic markers including triglycerides, total and LDL-cholesterol (243). While the above association studies appear to be conflicting, intervention studies in mouse models consistently demonstrated athero/cardioprotective properties of spermidine. In *Apoe*^{−/−} mice, spermidine supplementation lowered plaque lipid accumulation and necrotic cores. Spermidine triggered cholesterol efflux in autophagy-competent but not in autophagy-deficient VSMCs or macrophages lacking autophagy related 7 (*Atg7*) (244). In addition, spermidine and spermine protected against LDL oxidation resulting in reduced uptake of ox-LDL by macrophages (245). Furthermore, spermidine decreased cardiac hypertrophy and preserved diastolic function in old mice concomitant with enhanced cardiac autophagy, mitophagy and mitochondrial respiration. These cardioprotective effects were abolished in mice lacking *Atg5* in cardiomyocytes (232), supporting the notion that induction of autophagy by spermidine may be useful to prevent CVD. Interestingly, in humans, higher consumption of dietary spermidine was associated with lower CVD incidence (232). Together, while spermidine supplementation appears to be protective against NAFLD/NASH and CVD in mouse models, the use of spermidine or other polyamines as biomarkers and the therapeutic potential of spermidine in clinical settings warrant further research.

4.4. Oxalate

Oxalate is the ionic form of oxalic acid, and is an end-product of glyoxylate metabolism in the liver, which accounts for 80%–90%

of total circulating oxalate (246–248). The vast majority of oxalate (>90%) is eliminated through the kidneys (249, 250). Although humans have no enzymes capable of degrading oxalate (251), specific hepatic enzymes can prevent oxalate overproduction *via* the detoxification of glyoxylate to glycolate (by glycolate reductase/hydroxypyruvate reductase, GRHPR) or glycine (by AGXT) (252). Genetic defects in these enzymes result in primary hyperoxaluria, in which toxic levels of oxalate are produced by the liver (252). Furthermore, increased systemic oxalate can also be caused by impaired oxalate excretion in chronic kidney disease (250, 253). Beyond this, increased serum or urine oxalate has recently been linked with NAFLD/NASH (83, 248) and CVD (83, 248, 253, 254).

Suppression of glyoxylate detoxifying genes, particularly AGXT, has been consistently reported in both in humans and mice with NAFLD/NASH. Assessment of hepatic gene expression in patients who had undergone bariatric surgery revealed that AGXT is downregulated in those with NASH (255). In support, AGXT and GRHPR were recently reported to be downregulated in steatotic hepatocytes isolated from patients with NAFLD (248). Analysis of liver transcriptomic data from several cohorts of patients with various degrees of liver disease (steatosis, NASH, cirrhosis, and HCC) combined with data from mice with NAFLD or NASH revealed that AGXT was consistently downregulated in all human and mouse cohorts (83, 196, 248, 256). Furthermore, aggravated NASH and fibrosis in *Agxt*^{-/-} mice fed a NASH-inducing diet suggest a causative role of oxalate in NAFLD (83). Nevertheless, future studies evaluating the liver and circulating levels of oxalate in patients with NAFLD/NASH are warranted.

With regards to CVD, increased circulating oxalate has been associated with increased cardiovascular morbidity and mortality. Among hemodialysis patients, serum oxalate was positively associated with cardiovascular risk factors including elevated pulse wave velocity, central aortic systolic and diastolic blood pressures, and risk for cardiovascular events (253, 257). In patients with end-stage renal disease, increased circulating oxalate was not only associated with CVD events, but also with aggravated dyslipidemia (increased triglycerides and VLDL-cholesterol, and decreased HDL-cholesterol) and proatherogenic cytokines and chemokines (IL-6, TNF α , and monocyte chemoattractant protein-1) (254). In patients with significant CAD and normal kidney function, and in atherosclerotic *Apoe*^{-/-} mice, we found a significant decrease in the glycine to oxalate ratio aligned with downregulated hepatic AGXT. In mice deficient with both *Agxt* and *Apoe*, as well as in *Apoe*^{-/-} mice challenged with exogenous oxalate, atherosclerosis was increased with enhanced superoxide and CCL5 in atherosclerotic lesions. These effects were reversed by AAV-mediated overexpression of AGXT in livers of *Apoe*^{-/-} mice, indicating a causative role of oxalate overproduction in atherosclerosis (196). At the cellular level, oxalate was reported to induce mitochondrial dysfunction, oxidative stress and the release of proinflammatory chemokines and cytokines in endothelial cells, monocytes, and macrophages (196, 258–260). Together, the association between circulating oxalate, NAFLD/NASH and ASCVD should be further studied in larger cohorts including patients without kidney disease.

4.5. Hepatokines

The liver secretes various proteins known as hepatokines that can regulate systemic metabolic homeostasis through a crosstalk with other organs including skeletal muscle, adipose tissue, the central nervous system and blood vessels (261). In addition to their metabolic role, systemic alterations in hepatokines are implicated in several pathological conditions including IR, diabetes and CVD (261, 262); however, evidence regarding the role of hepatokines as modulators of atherosclerosis is limited.

Angiopoietin-like 3 (ANGPTL3) is a glycoprotein that is expressed and secreted primarily by the liver (263). Secreted ANGPTL3 binds lipoprotein lipase and inhibits its activity to hydrolyze lipoprotein triglycerides into fatty acids that are taken up by metabolic tissues. As a result, circulating triglycerides are increased (264, 265). Indeed, individuals with loss-of-function mutations in *ANGPTL3* have lower plasma triglycerides (266). In a cross-sectional investigation of obese subjects, both hepatic and plasma ANGPTL3 were higher in individuals with NAFLD and positively correlated with hepatic steatosis and histological markers of NASH (267). Among patients with various degrees of NAFLD, serum ANGPTL3 was increased in individuals with NASH, but not in those with simple steatosis (268). With regards to CVD, a study involving 1,493 MI cases and 3,231 controls demonstrated that individuals with lower plasma ANGPTL3 had a reduced risk of MI (269). In line, increased plasma ANGPTL3 was positively associated with the severity of coronary stenosis among patients with angina (270). Beyond its potential as a biomarker, the efficacy of ANGPTL3 inhibition has been studied extensively in preclinical and clinical settings. Both in *Ldlr*^{-/-} mice treated with antisense oligonucleotides (ASO) targeting *Angptl3* and in APOE*3Leiden.CETP mice treated with an antibody against ANGPTL3 (evinacumab), hypercholesterolemia, hypertriglyceridemia and atherosclerosis were significantly decreased (271, 272). Evinacumab also lowered fasting triglycerides and LDL-cholesterol in a phase I trial (271). In a phase IIb trial, administration of vupanorsen, an ASO targeting hepatic *ANGPTL3*, to patients with hypercholesterolemia and hypertriglyceridemia significantly reduced triglycerides together with a modest decrease in LDL-cholesterol. Unfortunately, at higher doses, vupanorsen administration was associated with increased hepatic fat, and over 3-fold elevations in ALT and AST (273). These studies highlight the potential complications in determining dosage for therapeutics like vupanorsen.

Fibroblast growth factor-21 (FGF-21) is a hormone primarily produced and secreted by the liver (274, 275). The hepatic expression and circulating levels of FGF21 are consistently reported to be higher in NAFLD, and are associated with enhanced hepatic necroinflammation and fibrosis (276–280). Furthermore, FGF21 was positively correlated with total cholesterol and triglycerides, and multivariate regression analysis indicated that FGF21 is an independent risk factor of CAD (281). Moreover, serum FGF21 predicted the incident of ASCVD events independent of NAFLD and other traditional cardiovascular risk factors (282, 283). Despite these findings indicating elevated circulating FGF21 as a common biomarker

for NAFLD and ASCVD, FGF21 is known for its protective properties in both diseases. An extensive body of literature have demonstrated the protective effects of recombinant FGF21 or FGF21 analogues in preclinical models of NASH (284, 285) and atherosclerosis (286, 287) as well as in patients with NASH (288, 289), serving as an attractive therapeutic marker for both diseases.

Fetuin-A, also known as $\alpha 2$ -Heremans-Schmid glycoprotein (AHSG), is synthesized and secreted predominantly by the liver and is among the first hepatokines identified to regulate metabolism through multiorgan crosstalk (290–292). Elevated fetuin-A levels are positively correlated with liver fat, patients with NAFLD, IR, and hepatic fibrosis (293–295). The link between fetuin-A, NAFLD and other metabolic disorders has sparked interest in its involvement in CVD; however, these studies yielded inconsistent results. In a case-cohort investigation, higher circulating fetuin-A was associated with MI and ischemic stroke after adjustment for confounders (296). In contrast, lower plasma fetuin-A, independent of traditional CVD risk factors, was found to be associated with increased CVD mortality among 1,620 patients with CAD (297). Therefore, while fetuin-A may serve as a potential biomarker in NAFLD, the conflicting findings above indicate that fetuin-A may not be a useful biomarker in ASCVD.

5. Dual-targeting of NASH and ASCVD: Limitations, caveats, and potential directions

Significant advances in our understanding of the mechanisms that drive NASH have led to the development of numerous of drug candidates that target different pathways in the pathogenesis of NASH. As extensively reviewed (298, 299), these candidates include drugs that target insulin/glucose homeostasis, lipid metabolism, proinflammatory/profibrotic responses, and the gut-liver axis, alongside pharmacological/surgical approaches aimed at lowering body weight. A limited number of drugs that demonstrated efficacy in phase IIb trials were or are currently evaluated in phase III trials. A few drugs approved for other metabolic diseases (e.g., T2D, and obesity) are evaluated as potential treatments for NAFLD/NASH in phase IV trials. While the current therapeutic pipeline in NASH (298, 299) and emerging approaches to treat ASCVD *via* modifying inflammation (300) have been comprehensively reviewed, in this section we discuss (1) potential cardiovascular consequences of promising drug candidates for NASH, and (2) the effects of commonly used (lipid-lowering) and new (anti-inflammatory) drugs for ASCVD on NASH.

5.1. Antidiabetic drugs for concurrent treatment of NASH and ASCVD

The prevalence of NAFLD and NASH in patients with T2D is higher than the general population and was estimated at 55% and 37%, respectively (5). As T2D is closely associated with NASH, a

number of antidiabetic drugs have been considered as potential treatments for NASH. Among these drugs, pioglitazone, a PPAR γ agonist and insulin sensitizer, is currently evaluated in a phase IV clinical trial for NASH (NCT00994682). Pioglitazone administered for 18 months to prediabetic or T2D patients with biopsy-proven NASH effectively lowered NAS and fibrosis scores while improving insulin sensitivity (300–302). However, pioglitazone treatment was associated with weight gain compared to placebo (302). Moreover, pioglitazone was associated with other adverse effects including enhanced risk of hospitalization for heart failure due to fluid retention (303–305). Despite this, accumulating evidence suggests a protective effect of pioglitazone on atherosclerosis-driven events including MI and ischemic stroke. In patients with impaired glucose tolerance or T2D, pioglitazone reduced carotid IMT (306, 307) and atherosclerotic plaque inflammation in association with decreased CRP and increased HDL-cholesterol (308, 309). Furthermore, pioglitazone treatment was associated with reduced total and LDL-cholesterol, triglycerides, and lipoprotein (a) (310–312). Therefore, the cardiovascular consequences of pioglitazone in patients with NASH warrant further research in long-term, large clinical trials.

Newer antidiabetic drug classes, including glucagon-like peptide 1 (GLP1) receptor agonists and sodium-glucose cotransporter-2 (SGLT2) inhibitors, have emerged as potential therapies for NASH. GLP1, an incretin secreted from intestinal L-cells, enhances glucose-stimulated insulin secretion and promotes satiety (313–316). Liraglutide is a GLP1 analogue known to lower body weight (317). In a phase II trial including overweight patients with biopsy-confirmed NASH, 48 weeks of liraglutide treatment was associated with higher rates of NASH resolution and attenuation of fibrosis (318). Stable isotope studies in patients treated with liraglutide, supported by lipid flux studies in human primary hepatocytes, demonstrated that liraglutide inhibits hepatic DNL (319), suggesting additional benefits beyond lowering body weight. Semaglutide, another GLP1 receptor agonist, has more pronounced body weight-lowering effects (320). In a phase II trial including patients with biopsy-confirmed NASH and fibrosis, semaglutide administered for 72 weeks led to a 13% reduction in body weight and was associated with higher rates of NASH resolution and improvement of fibrosis (321). With regards to ASCVD, liraglutide administered to patients with T2D has been consistently reported to improve circulating lipid profile (reduce triglycerides, total and LDL-cholesterol, and increase HDL-cholesterol) and reduce carotid IMT (322–324). The effects of semaglutide on atherosclerosis are currently being evaluated in phase IV trials (NCT03985384). Together, the above studies indicate the potential of GLP1 receptor agonists for concurrent treatment of NASH and ASCVD, which should be confirmed in long-term studies assessing cardiovascular outcomes in patients with NASH. Furthermore, considering that the expression of GLP1 receptor is not detected in livers (325, 326) and aortas (327) from mice, monkeys and humans, the mechanisms by which GLP1 receptor agonists protect against NASH and ASCVD, beyond lowering body weight, warrant further investigation.

SGLTs are membrane proteins that regulate nutrient transport across the intestinal epithelium and the proximal renal tubules.

While SGLT1 is expressed primarily in enterocytes and absorbs glucose from the gut lumen, SGLT2 is expressed in the proximal tubule and regulates glucose reabsorption from the glomerular filtrate (328). Thus, by decreasing renal glucose reabsorption and increasing urinary glucose excretion, SGLT2 inhibitors, such as empagliflozin, reduce hyperglycemia in patients with T2D (329). Empagliflozin has been evaluated for NAFLD treatment in phase IV trials (NCT02637973, NCT02686476, NCT02964715). In patients with T2D, empagliflozin administered for 20 weeks reduced circulating ALT and liver fat assessed by MRI-derived proton density fat fraction (MRI-PDFF) (330). Although including a small sample size ($n=9$), a study in patients with T2D and biopsy-proven NASH reported that empagliflozin treatment for 24 weeks improved histological components of NASH including steatosis, ballooning and fibrosis while reducing blood glucose, body weight and total cholesterol (331). Dapagliflozin, another SGLT2 inhibitor given to patients with T2D and NAFLD for 12 weeks, lowered circulating ALT and AST together with glucose and body weight. However, compared with placebo, reduction in hepatic fat was found when dapagliflozin was combined with omega-3 carboxylic acids, but not as a monotherapy (332). Also, although lowering body weight, dapagliflozin administered to insulin-resistant overweight/obese individuals for 12 weeks did not improve hepatic steatosis (333). However, when given to patients with T2D and NAFLD for 24 weeks, dapagliflozin lowered circulating ALT, hepatic steatosis and fibrosis assessed by MRI-PDFF and magnetic resonance elastography (MRE) (334). Interestingly, a recent phase II study including patients with NASH reported that 12 weeks of treatment with licogliflozin, a dual SGLT1/2 inhibitor, reduced circulating ALT and hepatic fat assessed by MRI-PDFF (335). Importantly, dramatic beneficial cardiovascular outcomes have been reported in T2D patients treated with SGLT2 inhibitors. In long-term and large phase III trials including patients with T2D with or at risk for ASCVD, treatment with empagliflozin or dapagliflozin was associated with lower rates of cardiovascular death (336, 337). Considering that SGLT2 is primarily expressed in the kidneys, the mechanisms by which SGLT2 inhibitors reduce the cardiovascular risk and directly affect the atherosclerotic plaque, beyond glucose- and body weight-lowering effects, are not completely clear (338, 339). Furthermore, whether long-term treatment with SGLT2 inhibitors concurrently lowers NASH and ASCVD remains unknown.

5.2. Targeting lipid metabolism for simultaneous treatment of NASH and ASCVD: Challenges and opportunities

Lipid overload is central to the pathogenesis of NASH. Fatty acids are supplied in excess to the liver *via* 1) enhanced flow from lipolysis of triglycerides in adipose tissue, and 2) increased synthesis from carbohydrates, primarily fructose, *via* DNL (50, 340). In addition to increased lipogenesis, fructose also suppresses hepatic FAO (109). Enhanced DNL coupled with impaired FAO result in the formation of lipotoxic species that

induce hepatic oxidative stress, proinflammatory and profibrotic responses to promote NASH (50, 341, 342). Therefore, pharmacological strategies aimed at inhibiting DNL or enhancing FAO can reduce hepatic lipotoxicity and attenuate NASH. Nevertheless, considering the major role of the liver as a regulator of systemic lipids, such approaches may have detrimental or beneficial effects on circulating lipids that may affect ASCVD.

In the initial step of fatty acid biosynthesis, acetyl-CoA is converted to malonyl-CoA by ACC (343). In phase II trials, patients with NASH treated for 12 weeks with the ACC inhibitor, firsocostat (GS-0976), showed reduced circulating ALT, hepatic steatosis and markers of fibrosis (344) mediated by inhibition of hepatic DNL assessed by heavy water labeling (345). However, similar to other ACC inhibitors [MK-4074 (346) or PF-05221304 (347)] treatment with firsocostat increased circulating triglycerides (344), which can be attributed to the upregulation of hepatic SREBP-1, enhanced VLDL production and impaired triglyceride clearance (348). While these findings raise concerns that targeting ACC may aggravate atherogenic dyslipidemia, co-administration of PF-05221304 with a diacylglycerol acyltransferase 2 inhibitor (PF-06865571), reduced liver fat assessed by MRI-PDFF and mitigated the increase in circulating triglycerides in patients with NAFLD (347). Nevertheless, the cardiovascular consequences of ACC inhibition either as a monotherapy or in combination with other drugs warrant further research in long-term clinical trials.

The conversion of acetyl-CoA and malonyl-CoA to palmitate is catalyzed by FAS, which controls the liver capacity to synthesize fatty acids through DNL (349). In a phase IIa trial including individuals with hepatic steatosis and fibrosis, treatment for 12 weeks with a FAS inhibitor, TVB-2640, dose-dependently decreased circulating ALT, AST and liver fat determined by MRI-PDFF. Importantly, TVB-2640 treatment significantly decreased circulating total and LDL-cholesterol. Although HDL-cholesterol was also decreased, lipidomics revealed beneficial effects including reduced triglycerides enriched in palmitate-containing species, diacylglycerols, bile acids and ceramides (350). Therefore, apart from the decrease in HDL-cholesterol, improved circulating lipid profile, reduced markers of hepatic steatosis and injury, indicate TVB-2640 as a promising candidate for dual treatment of NASH and ASCVD. Currently, TVB-2640 is evaluated in a phase IIb trial recruiting patients with NASH that will be treated for 52 weeks (NCT04906421). Longer-term studies are needed to determine the cardiovascular outcomes of TVB-2640 in patients with NASH.

The rate-limiting step in the synthesis of monounsaturated fatty acids is catalyzed by stearoyl-CoA desaturase 1 (SCD1) (351). The partial inhibitor of hepatic SCD1, aramchol, is a conjugate of cholic acid and arachidic acid, and is currently the most advanced drug candidate for NASH among those targeting hepatic DNL. In a 52-weeks, phase IIb trial including 247 patients with NASH, aramchol led to a time- and dose-dependent reduction in circulating ALT and AST. Histological analysis revealed that treatment with aramchol was associated with higher rates of NASH resolution and improvement in

fibrosis compared with placebo (352). Of note, no significant differences in circulating lipid profile were found between the groups (352, 353). While the cardiovascular outcomes of SCD1 inhibition have not been addressed in humans, loss of SCD1 in *Ldlr*^{-/-} mice (354) or its inhibition in *Ldlr*^{-/-} / *ApoB* 100/100 mice via ASO (355) enhanced atherosclerosis while reducing hepatic steatosis. Plans to test aramchol in the phase III/IV ARMOR trial (NCT04104321) in patients with biopsy-proven NASH and fibrosis for 5 years will shed light on the long-term effects of aramchol treatment on NASH and perhaps its cardiovascular consequences.

In addition to DNL inhibition, drugs that promote FAO can also lower hepatic lipotoxicity and NASH. This approach has been pursued by activation of key regulators of hepatic FAO, mainly PPAR α and PPAR β/δ . Among the three PPAR isotypes (PPAR α , PPAR β/δ and PPAR γ), PPAR α is the most abundant in hepatocytes where it acts as a master regulator of mitochondrial/peroxisomal FAO (356). In mice, hepatocyte-specific loss of PPAR α enhances steatohepatitis, which is aggravated in whole-body *Ppara*^{-/-} mice, indicating a protective role for both hepatic and extrahepatic PPAR α in NASH (357–359). Accordingly, the PPAR α agonist, Wy-14,643, lowers MCD diet-induced NASH and fibrosis in mice (360). Few clinical studies evaluated the effects of the PPAR α agonists, fibrates, in NASH. In patients with biopsy-confirmed NASH, treatment with fenofibrate for 48 weeks reduced circulating transaminases, triglycerides and glucose while increasing apolipoprotein A1. Histological assessment revealed improved hepatocellular ballooning, but no significant changes in steatosis, inflammation, and fibrosis (361). Interestingly, in patients with NASH and fibrosis, fenofibrate administered 2 weeks before the addition of the ACC inhibitor, firsocostat, not only mitigated hypertriglyceridemia, but also improved liver biochemistry compared to icosapent ethyl (Vascepa) (362). Pemafibrate, a selective PPAR α modulator, lowers NASH in mice fed the MCD or AMLN diet (363). In a phase II trial including 117 patients with NAFLD, pemafibrate administered for 48 weeks lowered circulating ALT and LDL-cholesterol. Although liver fat assessed by MRI-PDFF was not altered, MRE-based liver stiffness was significantly reduced (364). The concurrent improvement in plasma lipids and liver biochemistry suggest beneficial effects of PPAR α agonism in both NASH and ASCVD. Although this notion was supported by studies in *ApoE*^{-/-} (365) and *ApoE**3Leiden mice (366) in which fenofibrate reduced atherosclerosis, a multinational trial including over 10,000 patients with CVD, demonstrated that pemafibrate was not associated with lower incidence of cardiovascular events although NAFLD incidence was reduced (153).

PPAR β/δ is ubiquitously expressed, including in hepatocytes, Kupffer cells and hepatic stellate cells (367, 368). Studies in mice lacking PPAR β/δ indicated its roles in regulating hepatic FAO and antiinflammatory responses in Kupffer cells (369, 370). The dual PPAR α/δ agonist, elafibranor (GFT505), showed promising outcomes in preclinical NASH models (371) and in a phase IIb trial (372) in which 52 weeks of treatment with elafibranor led to higher rates of NASH resolution and reduction in fibrosis. Importantly, elafibranor not only decreased circulating

transaminases, but also lowered triglycerides and LDL-cholesterol, increased HDL-cholesterol and improved glycemic control, indicating significant improvement of overall cardiometabolic risk (372). These promising findings led to the evaluation of elafibranor in a phase III trial (RESOLVE IT) including over 2,000 patients with histologically confirmed NASH (NCT02704403). Unfortunately, results of the week 72 interim analysis revealed that elafibranor did not achieve NASH resolution without worsening of fibrosis, and the RESOLVE-IT trial was discontinued.

The beneficial effects of elafibranor and the PPAR γ agonist, pioglitazone, have raised interest in pan-PPAR agonism as a potential therapy for NASH. In preclinical studies, selective PPAR α (fenofibrate), PPAR γ (pioglitazone) and PPAR δ (GW501516) were compared to the pan-PPAR agonist, lanifibranor, and indicated that pan-PPAR agonism lowers experimental NASH by combining the beneficial effects of the three PPAR isotypes (373). Indeed, in a phase IIb trial including 247 patients with biopsy-proven NASH, lanifibranor administered for 24 weeks led to higher rates of NASH resolution and improvement in fibrosis compared with placebo. Importantly, in addition to lowering circulating transaminases, lanifibranor had beneficial effects on plasma lipid profile and glycemic control. Nevertheless, a mild increase in body weight (\approx 3%) was noted (374). Currently, the phase 3 NATiv3 trial (NCT04849728) is recruiting patients with NASH and fibrosis to assess the long-term efficacy of lanifibranor for up to 7 years. Findings from this study will provide important insight of the cardiometabolic consequences of pan-PPAR agonism in patients with NASH.

Statins reduce circulating cholesterol through inhibition of HMG-CoA reductase and remain the leading therapeutic in reducing the risk of cardiovascular events (375). Although dyslipidemia is a hallmark of both NAFLD/NASH and atherosclerosis, whether cholesterol-lowering by statin therapy improves NASH outcome remains inconsistent and thus is not a current recommendation for NASH management (376). Despite this, statin therapy may have pleiotropic beneficial effects for the treatment of NAFLD/NASH. In MCD diet-fed mice, fluvastatin reduces hepatic steatosis and improves inflammation and fibrosis through activation of PPAR α and its target genes enhancing FAO (377). Rosuvastatin blunts NASH-induced pro-inflammatory cytokine expression in livers from high-fat diet-fed STAM mice (378), while simvastatin reduces inflammation and fibrosis in *ApoE*^{-/-} mice fed a high-fat, high-cholesterol diet for 7 weeks with corresponding inhibition of Ras and Rho signaling (379). Treating obese mice with atorvastatin reduces cholesterol accumulation in isolated hepatocytes and reduces cholesterol-induced mitochondrial depletion of GSH (94), and atorvastatin is currently being evaluated in phase II trials for the treatment of NAFLD/NASH (NCT04679376). However, high-intensity atorvastatin therapy appears to enhance insulin secretion in patients with an increased risk of developing T2D (380). Since hyperinsulinemia is an early marker for metabolic disease (381) and is strongly associated with NAFLD (121), chronic use of statins in the treatment of NASH and ASCVD warrants further

investigation with potential contraindications. Furthermore, statin users appear to have higher caloric intake, which is associated with weight gain and complicates disease progression (382).

A potential complicating factor is the presence of genetic variants or single-nucleotide polymorphisms (SNPs). In particular, SNPs in patatin-like phospholipase domain-containing protein 3 (*PNPLA3*), or transmembrane 6 super family 2 (*TM6SF2*) are known as strong predictors of NAFLD risk independent of associated metabolic confounding factors, despite these variants promoting lipotoxicity (383). However, the presence of the *PNPLA* and *TM6SF2* variants reduces the risk of ASCVD in patients with NAFLD (384). In contrast, mutations in Angiopoietin-like 3 (*ANGPTL3*) lead to hypolipidemia (385), since circulating *ANGPTL3* inhibits lipoprotein lipase and is positively associated with NASH (386). Thus, therapeutics targeting *PNPLA3*, but not *ANGPTL3*, may be contraindicated should the outcome yield exacerbated ASCVD. These studies highlight the importance of identifying and considering genetic factors in both NAFLD and ASCVD which has been thoroughly discussed previously (14).

5.3. Ectopic fat as a potential link and therapeutic target in NAFLD/NASH and CVD

Patients with metabolic disease and obesity who have undergone bariatric surgery have marked improvement in insulin resistance (NCT03853590) and reduced risk of major cardiovascular events (387). Since previous studies demonstrated an association between bariatric surgery-induced weight loss and improved hepatic inflammation and fibrosis (388), a retrospective cohort study of nearly 1,200 patients with NAFLD and obesity was analyzed following bariatric surgery (389). Patients who received gastric bypass or sleeve gastrectomy demonstrated marked improvement in both adverse liver and cardiovascular outcomes (389). Since bariatric surgery effectively achieves weight loss in obese patients (390), the relationship between the effects of bariatric surgery and improved NASH and CVD outcome may be due to the effects of reducing visceral and ectopic adipose tissue. Although the risk of NASH and CVD rise with increasing BMI (391), ectopic fat [the storage of fat in non-adipose tissues (392)] and visceral fat [the storage of fat in the mediastinal and abdominal cavities (393)] appear to be a more reliable correlation between cardiometabolic disease compared with BMI alone (394). Similarly, CAD patients with normal BMI have enhanced visceral fat accumulation (395). Indeed, NAFLD patients with normal BMI have excessive visceral fat compared with non-NAFLD patients (396). The detrimental correlations between visceral fat, NASH and CVD are likely due in part to adipokine secretion, like TNF α (397), which mediates inflammatory responses locally and systemically. Independent of BMI, reducing visceral fat improves comorbidities of CVD and NASH (398). Consistent with this, calorie restriction improves NAFLD-related biomarkers such as transaminases, liver steatosis and fibrosis scores (399), as well as reducing the risk for atherosclerosis (400). The benefits for calorie restriction and improvement of NASH and ASCVD are multifactorial. Calorie

restriction (1) reduces adipokine release which attenuates systemic inflammatory signaling (401), (2) reduces serum lipids and comorbidities associated with disease exacerbation (e.g., hypertension) (400), (3) activates autophagy, which protects against hepatic steatosis and inflammation (402), and (4) activates various molecular pathways (e.g., AMPK) which are associated with protection against NASH and atherosclerosis (403, 404).

AMPK responds to energy demand by sensing the ratio of ATP to ADP/AMP. Activation of AMPK enhances catabolism and reduces anabolism, but additionally protects against oxidative stress-induced endothelial activation in atherosclerosis (405). AMPK additionally augments reverse cholesterol transport in atherosclerosis and polarizes macrophages to an M2 phenotype (404), which are associated with plaque stability and regression (406). In murine models of NAFLD, AMPK activation is inhibited due to overnutrition (407). Thus, activation of AMPK yields improvement in both CVD and NASH outcome in mouse models. Metformin activates AMPK, which reduces hepatic steatosis (408), and activation of AMPK with PF-06409577 reduces dyslipidemia and liver transaminases in rats and non-human primates (409). Another AMPK activator, PXL770, attenuates DNL, hepatic steatosis, inflammation, and ballooning in mouse NASH models (403). These effects may be due to inhibition of mTORC1, which is inhibited by AMPK through phosphorylation of raptor (410). mTOR activates lipogenesis by inducing SREBP-1c activation (411). Selective inhibition of mTORC1 by folliculin (FCLN) deletion protects against NASH by TFE3 transcription factor-induced inhibition of lipogenesis (412); however, the impact of FCLN deletion has not been investigated in atherosclerotic mice. While clinical trials for NASH are ongoing and activation of AMPK by PXL770 in mice improves atherosclerotic outcome (403, 413, 414), whether these results extend to human atherosclerotic patients has yet to be explored.

5.4. Lowering inflammation for dual-targeting of NASH and ASCVD

Since primary components of the pathophysiology of NASH and atherosclerosis involve the regulation of inflammatory cytokines, leukocyte response, and the crosstalk between these mediators (300, 415), systemic therapy reducing inflammation may yield benefits across both pathologies. Given the potent effects of IL-1 β signaling and its central role in inflammation, the monoclonal antibody targeting IL-1 β (canakinumab) has been implemented in the CANTOS phase III clinical trials (NCT01327846) for the treatment of CVD (416). It is well-established that the proinflammatory cytokine, IL-1 β , activates endothelial cells to express adhesion molecules, secrete chemokines, and vSMC proliferation to augment atherogenesis (417). Furthermore, IL-1 β gene expression increases in livers of mice fed a high-fat, high-cholesterol (1.25%) diet for 18 weeks, and deletion of IL-1 β reduces steatosis, inflammation, ballooning, and fibrosis in these mice (418). Thus far, the CANTOS trial has proved promising since inhibition of IL-1 β reduces the total number of serious cardiovascular events in patients with prior

MI history (416); however, it has not examined whether IL-1 β inhibition by canakinumab improves characteristics of NASH. Since deletion of IL-1 β reduces steatohepatitis, and fibrosis in mice fed a NASH-inducing diet (418), further investigation on the effects of canakinumab in human NASH are warranted. Such studies should also consider the potential risk of infection or sepsis considering that treatment with canakinumab was found to be associated with a higher incidence of fatal infection in the CANTOS trial (419).

While the effects of IL-1 β inhibition remain unexplored in NASH clinical trials, several preclinical and clinical studies have analyzed the potential benefits of targeting TNF α for NASH. Antibody therapy against TNF α yielded promising results with diet-induced NASH in mouse and rat models showing improvement in circulating AST, ALT, steatohepatitis, and fibrosis (420–422). However, retrospective studies of patients receiving anti-TNF α for immune-related diseases reported no reduction in the incidence of new onset NAFLD, NASH, or cirrhosis (423). While antagonism of TNF α with monoclonal antibodies yielded effective results in patients with rheumatoid arthritis (424) and inflammatory bowel disease (425), clinical trials for anti-TNF α in patients with chronic heart failure (RECOVER and RENAISSANCE) were terminated prematurely due to no observable benefit (426). Furthermore, the anti-TNF α monoclonal antibody CNT05048 (CNT) enhanced plasma triglycerides, VLDL, and atherosclerosis in *Ldlr*^{-/-} mice (427), suggesting the use of anti-TNF α antibodies for atherosclerosis may be contraindicated.

While the effects of targeting cytokines in NASH and ASCVD warrant further investigation, chemokine signaling appears to be a promising direction in targeting inflammation. Since mice fed a choline-deficient diet have enhanced hepatic CCR2 (60) and clinical trials demonstrated efficacy and safety with antagonism of CCR2 and CCR5 in patients with HIV (428), the CENTAUR clinical trial (NCT02217475) proceeded with the CCR2/CCR5 dual antagonist cenicriviroc over the course of 2 years (429). At the completion of this phase IIb trial, patients with NASH and fibrosis who received cenicriviroc demonstrated marked improvement in fibrosis without worsening of NASH (429). Despite the completion of phase II clinical trial, phase III (AURORA, NCT03028740) was terminated early due to lack of efficacy. CCL2 signals through its receptor CCR2, which is required for monocyte emigration from the bone marrow during an inflammatory response (430), and deletion of CCR2 significantly reduces atherosclerosis (431). Inhibition of CCR2 with the MLN1202 monoclonal antibody reduced the levels circulating CRP, a marker of cardiovascular risk (432). Although the effects of cenicriviroc on CVD were studied in an early clinical trial (NCT01474954), the trial was terminated due to low enrollment. Taken together, the effects of CCR2/CCR5 inhibition may improve some aspects of ASCVD; however, since activation of both CCR2 and CCR5 receptors directly activate hepatic stellate cells which promote hepatic fibrosis (433), further investigation on the effects of cenicriviroc on vSMCs are indicated to determine whether treatment affects atherosclerotic plaque stability.

5.5. Targeting fibrosis in NASH and atherosclerosis: A potential contraindication

Despite the numerous studies investigating the mechanisms behind NASH or ASCVD, those that utilize genetic manipulation often do so with subsequent onset of disease. These studies, while informative, may not be appropriate for identifying therapeutic targets since intervention of NASH and ASCVD does not occur until they become symptomatic. More advanced disease, both for NASH and ASCVD, involve the accumulation of fibrous tissue in the liver and vessels, respectively. In NASH, advanced fibrosis is correlated with worse prognosis (434). In contrast, fibrous or fibrocellular atherosclerotic plaques confer stability against plaque rupture and catastrophic events (435). Therefore, systemic targeting of fibrosis to improve NASH may be contraindicated for maintaining stable fibroatheromas. Currently, several clinical trials for the treatment of NASH seek to improve clinical outcome which includes lowering fibrosis (374, 436, 437). However, it is unknown whether these will affect cardiovascular morbidity and mortality.

PPARs regulate lipid homeostasis through transcriptional control of FAO and DNL (438). Since the relationship between dysregulated lipid metabolism and NASH or ASCVD is well-established, therapeutics targeting of PPARs may yield successful results. Indeed, the PPAR γ agonist pioglitazone and PPAR α fenofibrate reduced atherosclerosis and hepatic steatosis in mice lacking both ApoE and Farnesoid x receptor (FXR) (439), which modeled NASH and atherosclerosis simultaneously. FXR, a nuclear receptor responsible for bile acid and cholesterol synthesis, suppresses hepatic lipogenesis and VLDL assembly by attenuating SREBP1-c (440). In addition, FXR activity promotes PPAR α transcription through binding directly to the PPAR α reporter (441). Currently the non-steroidal FXR agonist Cilofexor is undergoing Phase II clinical trials for NASH treatment and has shown promising results in the reduction of hepatic steatosis, inflammation, and fibrosis (436). While deletion of FXR from *ApoE*^{-/-} mice enhanced atherosclerosis (442), it remains unknown if the anti-fibrotic effects of FXR in stellate cells is conserved in plaque associated vSMCs. Since Cilofexor primarily acts in the intestine (443), it may reduce the potential side effects of systemic FXR activation; however, further investigation on its effects on atherosclerotic plaques is warranted. FXR additionally induces FGF-19, which enhances cholesterol efflux and HDL assembly through modulation of hepatic ABCA1 and ApoA1 (444). Administration of the FGF-19 analog NGM282 reduces atherosclerosis in *ApoE*^{-/-} mice, enhances plasma HDL-cholesterol in healthy subjects (444), and improved NASH and fibrosis in phase II clinical trials (445). However, NGM282 increases plasma LDL-cholesterol (437), suggesting a potentially exacerbating factor in atherosclerosis. Furthermore, NGM282 reduces atherosclerotic fibrosis in mice (444), implicating the potential for plaque rupture with sustained therapy. In addition to NGM282, the synthetic bile acid obetacholic acid agonizes FXR and has been implemented in phase III clinical trials for the treatment of NASH (NCT02548351). Since patients receiving

obetacholic acid have enhanced circulating VLDL and LDL but reduced circulating HDL (21), its administration in the context of atherosclerosis may be contraindicated. Since these studies terminated at 72 weeks (21), the long-term effects of obetacholic acid on atherosclerosis remain unknown. Overall, the long-term effects of these NASH/fibrosis-targeting drugs must consider the potential effects on atherosclerotic plaque instability.

6. Concluding remarks and future directions

In this review, we highlighted our current gaps in knowledge with particular emphasis on modelling both diseases, common biomarkers and potential therapeutics, and the potential caveats we currently face by targeting specific aspects of each disease. In the past decade cardiovascular-related mortality rates are steadily increasing concomitant with a rapid rise in obesity and NAFLD/NASH incidences (1, 2), currently afflicting one-third of the population worldwide (6). Despite this prevalence, no FDA-approved drugs exist for the treatment of NASH. Since NASH serves as an independent risk factor for ASCVD, and individuals with NASH are at a greater risk of ASCVD-related mortality compared with liver-related mortality (7–12, 139–141), further understanding of the link between these two diseases is clearly indicated (8). Future studies establishing accepted models of NASH and atherosclerosis will provide a translational understanding of the relationship between NASH and ASCVD. By identifying new biomarkers shared between NASH and ASCVD, early detection and intervention will help to reverse the incline in NASH- and ASCVD-related mortality. Lastly, clinical trials seeking an effective therapeutic for NASH must heavily consider the potential influences on atherosclerotic plaque burden.

References

1. Tsao CW, Aday AW, Almarazooq ZI, Anderson CAM, Arora P, Avery CL, et al. Heart disease and stroke statistics-2023 update: a report from the American heart association. *Circulation*. (2023) 147(8):e93–621. doi: 10.1161/CIR.0000000000001123
2. Loos RJF, Yeo GSH. The genetics of obesity: from discovery to biology. *Nat Rev Genet*. (2022) 23(2):120–33. doi: 10.1038/s41576-021-00414-z
3. Marchesini G, Marzocchi R. Metabolic syndrome and NASH. *Clin Liver Dis*. (2007) 11(1):105–17; ix. doi: 10.1016/j.cld.2007.02.013
4. Younossi ZM, Koenig AB, Abdelatif D, Fazel Y, Henry L, Wymer M. Global epidemiology of nonalcoholic fatty liver disease-meta-analytic assessment of prevalence, incidence, and outcomes. *Hepatology*. (2016) 64(1):73–84. doi: 10.1002/jhep.28431
5. Younossi ZM, Golabi P, de Avila L, Paik JM, Srishord M, Fukui N, et al. The global epidemiology of NAFLD and NASH in patients with type 2 diabetes: a systematic review and meta-analysis. *J Hepatol*. (2019) 71(4):793–801. doi: 10.1016/j.jhep.2019.06.021
6. Riaz K, Azhari H, Charette JH, Underwood FE, King JA, Afshar EE, et al. The prevalence and incidence of NAFLD worldwide: a systematic review and meta-analysis. *Lancet Gastroenterol Hepatol*. (2022) 7(9):851–61. doi: 10.1016/S2468-1253(22)00165-0
7. Targher G, Byrne CD, Lonardo A, Zoppini G, Barbui C. Non-alcoholic fatty liver disease and risk of incident cardiovascular disease: a meta-analysis. *J Hepatol*. (2016) 65(3):589–600. doi: 10.1016/j.jhep.2016.05.013
8. Duell PB, Welty FK, Miller M, Chait A, Hammond G, Ahmad Z, et al. Nonalcoholic fatty liver disease and cardiovascular risk: a scientific statement from the American heart association. *Arterioscler Thromb Vasc Biol*. (2022) 42(6):e168–85. doi: 10.1161/ATV.0000000000000153
9. Stepanova M, Younossi ZM. Independent association between nonalcoholic fatty liver disease and cardiovascular disease in the US population. *Clin Gastroenterol Hepatol*. (2012) 10(6):646–50. doi: 10.1016/j.cgh.2011.12.039
10. Oni ET, Agatston AS, Blaha MJ, Fialkow J, Cury R, Sposito A, et al. A systematic review: burden and severity of subclinical cardiovascular disease among those with nonalcoholic fatty liver; should we care? *Atherosclerosis*. (2013) 230(2):258–67. doi: 10.1016/j.atherosclerosis.2013.07.052
11. Pais R, Giral P, Khan JF, Rosenbaum D, Housset C, Poynard T, et al. Fatty liver is an independent predictor of early carotid atherosclerosis. *J Hepatol*. (2016) 65(1):95–102. doi: 10.1016/j.jhep.2016.02.023
12. Targher G, Byrne CD, Tilg H. NAFLD and increased risk of cardiovascular disease: clinical associations, pathophysiological mechanisms and pharmacological implications. *Gut*. (2020) 69(9):1691–705. doi: 10.1136/gutjnl-2020-320622

Author contributions

AF designed the graphic in **Figure 1** and **Table 1**. AY and OR designed **Figure 2** with Biorender. All authors contributed to drafting and editing of the review. All authors contributed to the article and approved the submitted version.

Funding

This work was partly supported by the National Institutes of Health grants DK134011 and HL150233 (OR), HL145131 and HL167758 (AY), and DK115778 and GM147269 (BC); Collaborative Intramural Research Program (LSUHS and Ochsner Clinic Foundation, AY and OR); an American Heart Association Postdoctoral Fellowship 23POST1026505 (AF), and the LSUHS Center for Cardiovascular Diseases and Sciences Malcolm Feist Fellowships (AF).

Conflict of interest

The authors declare that the research was conducted in the absence of any commercial or financial relationships that could be construed as a potential conflict of interest.

Publisher's note

All claims expressed in this article are solely those of the authors and do not necessarily represent those of their affiliated organizations, or those of the publisher, the editors and the reviewers. Any product that may be evaluated in this article, or claim that may be made by its manufacturer, is not guaranteed or endorsed by the publisher.

13. Barbarroja N, Ruiz-Ponce M, Cuesta-Lopez L, Perez-Sanchez C, Lopez-Pedraza C, Arias-de la Rosa I, et al. Nonalcoholic fatty liver disease in inflammatory arthritis: relationship with cardiovascular risk. *Front Immunol.* (2022) 13:997270. doi: 10.3389/fimmu.2022.997270
14. Baratta F, D'Erasmo L, Bini S, Pastori D, Angelico F, Del Ben M, et al. Heterogeneity of non-alcoholic fatty liver disease (NAFLD): implication for cardiovascular risk stratification. *Atherosclerosis.* (2022) 357:51–9. doi: 10.1016/j.atherosclerosis.2022.08.011
15. Chew NWS, Chong B, Ng CH, Kong G, Chin YH, Xiao W, et al. The genetic interactions between non-alcoholic fatty liver disease and cardiovascular diseases. *Front Genet.* (2022) 13:971484. doi: 10.3389/fgene.2022.971484
16. Cazac GD, Lacatusu CM, Mihai C, Grigorescu ED, Onofriescu A, Mihai BM. New insights into non-alcoholic fatty liver disease and coronary artery disease: the liver-heart axis. *Life (Basel).* (2022) 12(8):1–25. doi: 10.3390/life12081189
17. Wang Z, Ye M, Zhang XJ, Zhang P, Cai J, Li H, et al. Impact of NAFLD and its pharmacotherapy on lipid profile and CVD. *Atherosclerosis.* (2022) 355:30–44. doi: 10.1016/j.atherosclerosis.2022.07.010
18. Galvin Z, Rajakumar R, Chen E, Adeyi O, Selzner M, Grant D, et al. Predictors of de novo nonalcoholic fatty liver disease after liver transplantation and associated fibrosis. *Liver Transpl.* (2019) 25(1):56–67. doi: 10.1002/lt.25338
19. Meng H, Ruan J, Yan Z, Chen Y, Liu J, Li X, et al. New progress in early diagnosis of atherosclerosis. *Int J Mol Sci.* (2022) 23(16):1–14. doi: 10.3390/ijms23168939
20. Spengler EK, Loomba R. Recommendations for diagnosis, referral for liver biopsy, and treatment of nonalcoholic fatty liver disease and nonalcoholic steatohepatitis. *Mayo Clin Proc.* (2015) 90(9):1233–46. doi: 10.1016/j.mayocp.2015.06.013
21. Siddiqui MS, Van Natta ML, Connelly MA, Vuppalanchi R, Neuschwander-Tetri BA, Tonascia J, et al. Impact of obeticholic acid on the lipoprotein profile in patients with non-alcoholic steatohepatitis. *J Hepatol.* (2020) 72(1):25–33. doi: 10.1016/j.jhep.2019.10.006
22. Nelson A, Torres DM, Morgan AE, Fincke C, Harrison SA. A pilot study using simvastatin in the treatment of nonalcoholic steatohepatitis: a randomized placebo-controlled trial. *J Clin Gastroenterol.* (2009) 43(10):990–4. doi: 10.1097/MCG.0b013e31819c392e
23. Bril F, Portillo Sanchez P, Lomonaco R, Orsak B, Hecht J, Tio F, et al. Liver safety of statins in prediabetes or T2DM and nonalcoholic steatohepatitis: post hoc analysis of a randomized trial. *J Clin Endocrinol Metab.* (2017) 102(8):2950–61. doi: 10.1210/clinem.2017-00867
24. Libby P, Buring JE, Badimon L, Hansson GK, Deanfield J, Bittencourt MS, et al. Atherosclerosis. *Nat Rev Dis Primers.* (2019) 5(1):56. doi: 10.1038/s41572-019-0106-z
25. Moore KJ, Sheedy FJ, Fisher EA. Macrophages in atherosclerosis: a dynamic balance. *Nat Rev Immunol.* (2013) 13(10):709–21. doi: 10.1038/nri3520
26. Hu P, Dharmayat KI, Stevens CAT, Sharabiani MTA, Jones RS, Watts GF, et al. Prevalence of familial hypercholesterolemia among the general population and patients with atherosclerotic cardiovascular disease: a systematic review and meta-analysis. *Circulation.* (2020) 141(22):1742–59. doi: 10.1161/CIRCULATIONAHA.119.044795
27. Fruchart JC, Nierman MC, Stroes ES, Kastelein JJ, Duriez P. New risk factors for atherosclerosis and patient risk assessment. *Circulation.* (2004) 109(23 Suppl 1):III15–9. doi: 10.1161/01.CIR.0000131513.33892.5b
28. Centers for Disease C, Prevention. Vital signs: prevalence, treatment, and control of high levels of low-density lipoprotein cholesterol—United States, 1999–2002 and 2005–2008. *MMWR Morb Mortal Wkly Rep.* (2011) 60(4):109–14.
29. Mehta NK, Abrams LR, Myrskylä M. US life expectancy stalls due to cardiovascular disease, not drug deaths. *Proc Natl Acad Sci U S A.* (2020) 117(13):6998–7000. doi: 10.1073/pnas.1920391117
30. Hahn C, Schwartz MA. Mechanotransduction in vascular physiology and atherogenesis. *Nat Rev Mol Cell Biol.* (2009) 10(1):53–62. doi: 10.1038/nrm2596
31. Miller YI, Choi SH, Wiesner P, Fang L, Harkewicz R, Hartvigsen K, et al. Oxidation-specific epitopes are danger-associated molecular patterns recognized by pattern recognition receptors of innate immunity. *Circ Res.* (2011) 108(2):235–48. doi: 10.1161/CIRCRESAHA.110.223875
32. Navab M, Anantharamaiah GM, Reddy ST, Van Lenten BJ, Ansell BJ, Fonarow GC, et al. The oxidation hypothesis of atherogenesis: the role of oxidized phospholipids and HDL. *J Lipid Res.* (2004) 45(6):993–1007. doi: 10.1194/jlr.R400001-JLR200
33. Moore KJ, Freeman MW. Scavenger receptors in atherosclerosis: beyond lipid uptake. *Arterioscler Thromb Vasc Biol.* (2006) 26(8):1702–11. doi: 10.1161/01.ATV.0000229218.97976.43
34. Yurdagul A Jr, Green J, Albert P, McInnis MC, Mazar AP, Orr AW. Alpha5beta1 integrin signaling mediates oxidized low-density lipoprotein-induced inflammation and early atherosclerosis. *Arterioscler Thromb Vasc Biol.* (2014) 34(7):1362–73. doi: 10.1161/ATVBAHA.114.303863
35. Yurdagul A Jr. Crosstalk between macrophages and vascular smooth muscle cells in atherosclerotic plaque stability. *Arterioscler Thromb Vasc Biol.* (2022) 42(4):372–80. doi: 10.1161/ATVBAHA.121.316233
36. Gomez D, Owens GK. Smooth muscle cell phenotypic switching in atherosclerosis. *Cardiovasc Res.* (2012) 95(2):156–64. doi: 10.1093/cvr/cvs115
37. Davies MJ, Richardson PD, Woolf N, Katz DR, Mann J. Risk of thrombosis in human atherosclerotic plaques: role of extracellular lipid, macrophage, and smooth muscle cell content. *Br Heart J.* (1993) 69(5):377–81. doi: 10.1136/hrt.69.5.377
38. Tabas I, Glass CK. Anti-inflammatory therapy in chronic disease: challenges and opportunities. *Science.* (2013) 339(6116):166–72. doi: 10.1126/science.1230720
39. Doran AC, Yurdagul A Jr, Tabas I. Efferocytosis in health and disease. *Nat Rev Immunol.* (2020) 20(4):254–67. doi: 10.1038/s41577-019-0240-6
40. Yurdagul A Jr, Doran AC, Cai B, Fredman G, Tabas IA. Mechanisms and consequences of defective efferocytosis in atherosclerosis. *Front Cardiovasc Med.* (2017) 4:86. doi: 10.3389/fcvm.2017.00086
41. Ampomah PB, Cai B, Sukka SR, Gerlach BD, Yurdagul A Jr, Wang X, et al. Macrophages use apoptotic cell-derived methionine and DNMT3A during efferocytosis to promote tissue resolution. *Nat Metab.* (2022) 4(4):444–57. doi: 10.1038/s42255-022-00551-7
42. Gerlach BD, Ampomah PB, Yurdagul A Jr, Liu C, Laurant MC, Wang X, et al. Efferocytosis induces macrophage proliferation to help resolve tissue injury. *Cell Metab.* (2021) 33(12):2445–63.e8. doi: 10.1016/j.cmet.2021.10.015
43. Yurdagul A Jr, Subramanian M, Wang X, Crown SB, Ilkayeva OR, Darville L, et al. Macrophage metabolism of apoptotic cell-derived arginine promotes continual efferocytosis and resolution of injury. *Cell Metab.* (2020) 31(3):518–33.e10. doi: 10.1016/j.cmet.2020.01.001
44. Back M, Yurdagul A Jr, Tabas I, Oorni K, Kovanen PT. Inflammation and its resolution in atherosclerosis: mediators and therapeutic opportunities. *Nat Rev Cardiol.* (2019) 16(7):389–406. doi: 10.1038/s41569-019-0169-2
45. Maldonado N, Kelly-Arnold A, Cardoso L, Weinbaum S. The explosive growth of small voids in vulnerable cap rupture: cavitation and interfacial debonding. *J Biomech.* (2013) 46(2):396–401. doi: 10.1016/j.jbiomech.2012.10.040
46. Vengrenyuk Y, Carlier S, Xanthos S, Cardoso L, Ganatos P, Virmani R, et al. A hypothesis for vulnerable plaque rupture due to stress-induced debonding around cellular microcalcifications in thin fibrous caps. *Proc Natl Acad Sci U S A.* (2006) 103(40):14678–83. doi: 10.1073/pnas.0606310103
47. Loomba R, Friedman SL, Shulman GI. Mechanisms and disease consequences of nonalcoholic fatty liver disease. *Cell.* (2021) 184(10):2537–64. doi: 10.1016/j.cell.2021.04.015
48. Loomba R, Adams LA. The 20% rule of NASH progression: the natural history of advanced fibrosis and cirrhosis caused by NASH. *Hepatology.* (2019) 70(6):1885–8. doi: 10.1002/hep.30946
49. Grgurevic I, Podrug K, Mikolasevic I, Kukla M, Madir A, Tsochatzis EA. Natural history of nonalcoholic fatty liver disease: implications for clinical practice and an individualized approach. *Can J Gastroenterol Hepatol.* (2020) 2020:9181368. doi: 10.1155/2020/9181368
50. Friedman SL, Neuschwander-Tetri BA, Rinella M, Sanyal AJ. Mechanisms of NAFLD development and therapeutic strategies. *Nat Med.* (2018) 24(7):908–22. doi: 10.1038/s41591-018-0104-9
51. Brunt EM, Wong VW, Nobili V, Day CP, Sookoian S, Maher JJ, et al. Nonalcoholic fatty liver disease. *Nat Rev Dis Primers.* (2015) 1:15080. doi: 10.1038/nrdp.2015.80
52. Mitsuyoshi H, Yasui K, Harano Y, Endo M, Tsuji K, Minami M, et al. Analysis of hepatic genes involved in the metabolism of fatty acids and iron in nonalcoholic fatty liver disease. *Hepatol Res.* (2009) 39(4):366–73. doi: 10.1111/j.1872-034X.2008.00464.x
53. He J, Lee JH, Febbraio M, Xie W. The emerging roles of fatty acid translocase/CD36 and the aryl hydrocarbon receptor in fatty liver disease. *Exp Biol Med (Maywood).* (2011) 236(10):1116–21. doi: 10.1258/ebm.2011.011128
54. Koliaki C, Szendroedi J, Kaul K, Jelenik T, Nowotny P, Jankowiak F, et al. Adaptation of hepatic mitochondrial function in humans with non-alcoholic fatty liver is lost in steatohepatitis. *Cell Metab.* (2015) 21(5):739–46. doi: 10.1016/j.cmet.2015.04.004
55. Johnson ES, Lindblom KR, Robeson A, Stevens RD, Ilkayeva OR, Newgard CB, et al. Metabolomic profiling reveals a role for caspase-2 in lipoprotein-induced liver injury. *J Biol Chem.* (2013) 288(20):14463–75. doi: 10.1074/jbc.M112.437210
56. Huby T, Gautier EL. Immune cell-mediated features of non-alcoholic steatohepatitis. *Nat Rev Immunol.* (2022) 22(7):429–43. doi: 10.1038/s41577-021-00639-3
57. Tran S, Baba I, Poupel L, Dussaud S, Moreau M, Gelineau A, et al. Impaired kupffer cell self-renewal alters the liver response to lipid overload during non-alcoholic steatohepatitis. *Immunity.* (2020) 53(3):627–40.e5. doi: 10.1016/j.immuni.2020.06.003

58. Xiong X, Kuang H, Ansari S, Liu T, Gong J, Wang S, et al. Landscape of intercellular crosstalk in healthy and NASH liver revealed by single-cell secretome gene analysis. *Mol Cell*. (2019) 75(3):644–60.e5. doi: 10.1016/j.molcel.2019.07.028
59. Huang W, Metlakunta A, Dedousis N, Zhang P, Sipula I, Dube JJ, et al. Depletion of liver kupffer cells prevents the development of diet-induced hepatic steatosis and insulin resistance. *Diabetes*. (2010) 59(2):347–57. doi: 10.2337/db09-0016
60. Miura K, Yang L, van Rooijen N, Ohnishi H, Seki E. Hepatic recruitment of macrophages promotes nonalcoholic steatohepatitis through CCR2. *Am J Physiol Gastrointest Liver Physiol*. (2012) 302(11):G1310–21. doi: 10.1152/ajpgi.00365.2011
61. Weisberg SP, Hunter D, Huber R, Lemieux J, Slaymaker S, Vaddi K, et al. CCR2 Modulates inflammatory and metabolic effects of high-fat feeding. *J Clin Invest*. (2006) 116(1):115–24. doi: 10.1172/JCI24335
62. Scott CL, Zheng F, De Baetselier P, Martens L, Saey Y, De Prieck S, et al. Bone marrow-derived monocytes give rise to self-renewing and fully differentiated kupffer cells. *Nat Commun*. (2016) 7:10321. doi: 10.1038/ncomms10321
63. Stienstra R, Saudale F, Duval C, Keshtkar S, Groener JE, van Rooijen N, et al. Kupffer cells promote hepatic steatosis via interleukin-1 β -dependent suppression of peroxisome proliferator-activated receptor α activity. *Hepatology*. (2010) 51(2):511–22. doi: 10.1002/hep.23337
64. Miura K, Yang L, van Rooijen N, Brenner DA, Ohnishi H, Seki E. Toll-like receptor 2 and palmitic acid cooperatively contribute to the development of nonalcoholic steatohepatitis through inflammasome activation in mice. *Hepatology*. (2013) 57(2):577–89. doi: 10.1002/hep.26081
65. Snodgrass RG, Huang S, Choi IW, Rutledge JC, Hwang DH. Inflammasome-mediated secretion of IL-1 β in human monocytes through TLR2 activation; modulation by dietary fatty acids. *J Immunol*. (2013) 191(8):4337–47. doi: 10.4049/jimmunol.1300298
66. Kim SY, Jeong JM, Kim SJ, Seo W, Kim MH, Choi WM, et al. Pro-inflammatory hepatic macrophages generate ROS through NADPH oxidase 2 via endocytosis of monomeric TLR4-MD2 complex. *Nat Commun*. (2017) 8(1):2247. doi: 10.1038/s41467-017-02325-2
67. Zhu C, Tabas I, Schwabe RF, Pajvani UB. Maladaptive regeneration—the reawakening of developmental pathways in NASH and fibrosis. *Nat Rev Gastroenterol Hepatol*. (2021) 18(2):131–42. doi: 10.1038/s41575-020-00365-6
68. Yanger K, Zong Y, Maggs LR, Shapira SN, Maddipati R, Aiello NM, et al. Robust cellular reprogramming occurs spontaneously during liver regeneration. *Genes Dev*. (2013) 27(7):719–24. doi: 10.1101/gad.207803.112
69. Zhu C, Kim K, Wang X, Bartolome A, Salomao M, Dongiovanni P, et al. Hepatocyte notch activation induces liver fibrosis in nonalcoholic steatohepatitis. *Sci Transl Med*. (2018) 10(468):1–13. doi: 10.1126/scitranslmed.aat0344
70. Guy CD, Suzuki A, Abdelmalek MF, Burchette JL, Diehl AM, Nash CRN. Treatment response in the PIVENS trial is associated with decreased hedgehog pathway activity. *Hepatology*. (2015) 61(1):98–107. doi: 10.1002/hep.27235
71. Chung SI, Moon H, Ju HL, Cho KJ, Kim DY, Han KH, et al. Hepatic expression of sonic hedgehog induces liver fibrosis and promotes hepatocarcinogenesis in a transgenic mouse model. *J Hepatol*. (2016) 64(3):618–27. doi: 10.1016/j.jhep.2015.10.007
72. Wang X, Zheng Z, Caviglia JM, Corey KE, Herfel TM, Cai B, et al. Hepatocyte TAZ/WWTR1 promotes inflammation and fibrosis in nonalcoholic steatohepatitis. *Cell Metab*. (2016) 24(6):848–62. doi: 10.1016/j.cmet.2016.09.016
73. Wang X, Sommerfeld MR, Jahn-Hofmann K, Cai B, Filliol A, Remotti HE, et al. A therapeutic silencing RNA targeting hepatocyte TAZ prevents and reverses fibrosis in nonalcoholic steatohepatitis in mice. *Hepatol Commun*. (2019) 3(9):1221–34. doi: 10.1002/hep4.1405
74. Wang X, Cai B, Yang X, Sonubi OO, Zheng Z, Ramakrishnan R, et al. Cholesterol stabilizes TAZ in hepatocytes to promote experimental non-alcoholic steatohepatitis. *Cell Metab*. (2020) 31(5):969–86.e7. doi: 10.1016/j.cmet.2020.03.010
75. Gordon SM, Li H, Zhu X, Shah AS, Lu LJ, Davidson WS. A comparison of the mouse and human lipoproteome: suitability of the mouse model for studies of human lipoproteins. *J Proteome Res*. (2015) 14(6):2686–95. doi: 10.1021/acs.jproteome.5b00213
76. Linton MRF, Yancey PG, Davies SS, Jerome WG, Linton EF, Song WL, et al. The role of lipids and lipoproteins in atherosclerosis. In: Feingold KR, Anawalt B, Boyce A, Chrousos G, de Herder WW, Dhatariya K, et al., editors. *Endotext*. South Dartmouth (MA, U.S.A.) (2000). p. 1–144.
77. Schreyer SA, Wilson DL, LeBoeuf RC. C57BL/6 mice fed high fat diets as models for diabetes-accelerated atherosclerosis. *Atherosclerosis*. (1998) 136(1):17–24. doi: 10.1016/s0021-9150(97)00165-2
78. Ishibashi S, Brown MS, Goldstein JL, Gerard RD, Hammer RE, Herz J. Hypercholesterolemia in low density lipoprotein receptor knockout mice and its reversal by adenovirus-mediated gene delivery. *J Clin Invest*. (1993) 92(2):883–93. doi: 10.1172/JCI116663
79. Zhang SH, Reddick RL, Piedrahita JA, Maeda N. Spontaneous hypercholesterolemia and arterial lesions in mice lacking apolipoprotein E. *Science*. (1992) 258(5081):468–71. doi: 10.1126/science.1411543
80. Plump AS, Smith JD, Hayek T, Aalto-Setälä K, Walsh A, Verstuyft JG, et al. Severe hypercholesterolemia and atherosclerosis in apolipoprotein E-deficient mice created by homologous recombination in ES cells. *Cell*. (1992) 71(2):343–53. doi: 10.1016/0092-8674(92)90362-g
81. Goettsch C, Hutcheson JD, Hagita S, Rogers MA, Creager MD, Pham T, et al. A single injection of gain-of-function mutant PCSK9 adeno-associated virus vector induces cardiovascular calcification in mice with no genetic modification. *Atherosclerosis*. (2016) 251:109–18. doi: 10.1016/j.atherosclerosis.2016.06.011
82. Björklund MM, Hollensen AK, Hagensen MK, Dagnaes-Hansen F, Christoffersen C, Mikkelsen JG, et al. Induction of atherosclerosis in mice and hamsters without germline genetic engineering. *Circ Res*. (2014) 114(11):1684–9. doi: 10.1161/CIRCRESAHA.114.302937
83. Rom O, Liu Y, Liu Z, Zhao Y, Wu J, Ghayeb A, et al. Glycine-based treatment ameliorates NAFLD by modulating fatty acid oxidation, glutathione synthesis, and the gut microbiome. *Sci Transl Med*. (2020) 12(572):1–15. doi: 10.1126/scitranslmed.aaz2841
84. Rom O, Xu G, Guo Y, Zhu Y, Wang H, Zhang J, et al. Nitro-fatty acids protect against steatosis and fibrosis during development of nonalcoholic fatty liver disease in mice. *EBioMedicine*. (2019) 41:62–72. doi: 10.1016/j.ebiom.2019.02.019
85. Rom O, Liu Y, Chang L, Chen YE, Aviram M. Editorial: nitro-fatty acids: novel drug candidates for the co-treatment of atherosclerosis and nonalcoholic fatty liver disease. *Curr Opin Lipidol*. (2020) 31(2):104–7. doi: 10.1097/MOL.0000000000000666
86. Karavia EA, Papachristou DJ, Kotsikogianni I, Giopanou I, Kypreos KE. Deficiency in apolipoprotein E has a protective effect on diet-induced nonalcoholic fatty liver disease in mice. *FEBS J*. (2011) 278(17):3119–29. doi: 10.1111/j.1742-4658.2011.08238.x
87. Lu W, Mei J, Yang J, Wu Z, Liu J, Miao P, et al. Apoe deficiency promotes non-alcoholic fatty liver disease in mice via impeding AMPK/mTOR mediated autophagy. *Life Sci*. (2020) 252:117601. doi: 10.1016/j.lfs.2020.117601
88. Matsuzawa N, Takamura T, Kurita S, Misu H, Ota T, Ando H, et al. Lipid-induced oxidative stress causes steatohepatitis in mice fed an atherogenic diet. *Hepatology*. (2007) 46(5):1392–403. doi: 10.1002/hep.21874
89. Zhang X, Coker OO, Chu ES, Fu K, Lau HCH, Wang YX, et al. Dietary cholesterol drives fatty liver-associated liver cancer by modulating gut microbiota and metabolites. *Gut*. (2021) 70(4):761–74. doi: 10.1136/gutjnl-2019-319664
90. Schierwagen R, Maybuchen L, Zimmer S, Hittatiya K, Back C, Klein S, et al. Seven weeks of western diet in apolipoprotein-E-deficient mice induce metabolic syndrome and non-alcoholic steatohepatitis with liver fibrosis. *Sci Rep*. (2015) 5:12931. doi: 10.1038/srep12931
91. Muniz LB, Alves-Santos AM, Camargo F, Martins DB, Celes MRN, Naves MMV. High-lard and high-cholesterol diet, but not high-lard diet, leads to metabolic disorders in a modified dyslipidemia model. *Arq Bras Cardiol*. (2019) 113(5):896–902. doi: 10.5935/abc.20190149
92. Trevisan JL, Griffin PS, Wittmer C, Neuschwander-Tetri BA, Brunt EM, Dolman CS, et al. Glucagon-like peptide-1 receptor agonism improves metabolic, biochemical, and histopathological indices of nonalcoholic steatohepatitis in mice. *Am J Physiol Gastrointest Liver Physiol*. (2012) 302(8):G762–72. doi: 10.1152/ajpgi.00476.2011
93. Caballero F, Fernandez A, De Lacy AM, Fernandez-Checa JC, Caballeria J, Garcia-Ruiz C. Enhanced free cholesterol, SREBP-2 and SREBP-1 expression in human NASH. *J Hepatol*. (2009) 50(4):789–96. doi: 10.1016/j.jhep.2008.12.016
94. Mari M, Caballero F, Colell A, Morales A, Caballeria J, Fernandez A, et al. Mitochondrial free cholesterol loading sensitizes to TNF- α and Fas-mediated steatohepatitis. *Cell Metab*. (2006) 4(3):185–98. doi: 10.1016/j.cmet.2006.07.006
95. Soliman GA. Dietary cholesterol and the lack of evidence in cardiovascular disease. *Nutrients*. (2018) 10(6):1–14. doi: 10.3390/nu10060780
96. Shekelle RB, Stamler J. Dietary cholesterol and ischaemic heart disease. *Lancet*. (1989) 1(8648):1177–9. doi: 10.1016/s0140-6736(89)92759-1
97. McNamara DJ. Dietary cholesterol and atherosclerosis. *Biochim Biophys Acta*. (2000) 1529(1–3):310–20. doi: 10.1016/s1388-1981(00)00156-6
98. Lancaster KJ. Current intake and demographic disparities in the association of fructose-rich foods and metabolic syndrome. *JAMA Netw Open*. (2020) 3(7):e2010224. doi: 10.1001/jamanetworkopen.2020.10224
99. Handayani D, Febrianingsih E, Desi Kurniawati A, Kusumastuty I, Nurmalitasari S, Widyanto RM, et al. High-fructose diet initially promotes increased aortic wall thickness, liver steatosis, and cardiac histopathology deterioration, but does not increase body fat index. *J Public Health Res*. (2021) 10(2):1–7. doi: 10.4081/jphr.2021.2181
100. van den Hoek AM, Verschuren L, Worms N, van Nieuwkoop A, de Ruiter C, Attema J, et al. A translational mouse model for NASH with advanced fibrosis and atherosclerosis expressing key pathways of human pathology. *Cells*. (2020) 9(9):1–20. doi: 10.3390/cells9092014
101. Morrison MC, Mulder P, Salic K, Verheij J, Liang W, van Duyvenvoorde W, et al. Intervention with a caspase-1 inhibitor reduces obesity-associated

hyperinsulinemia, non-alcoholic steatohepatitis and hepatic fibrosis in LDLR-/-Leiden mice. *Int J Obes (Lond)*. (2016) 40(9):1416–23. doi: 10.1038/ijo.2016.74

102. Morrison MC, Verschuren L, Salic K, Verheij J, Menke A, Wielinga PY, et al. Obeticholic acid modulates serum metabolites and gene signatures characteristic of human NASH and attenuates inflammation and fibrosis progression in Ldlr-/-Leiden mice. *Hepatol Commun*. (2018) 2(12):1513–32. doi: 10.1002/hep4.1270

103. Liang W, Menke AL, Driessen A, Koek GH, Lindeman JH, Stoop R, et al. Establishment of a general NAFLD scoring system for rodent models and comparison to human liver pathology. *PLoS One*. (2014) 9(12):e115922. doi: 10.1371/journal.pone.0115922

104. Herman MA, Samuel VT. The sweet path to metabolic demise: fructose and lipid synthesis. *Trends Endocrinol Metab*. (2016) 27(10):719–30. doi: 10.1016/j.tem.2016.06.005

105. Softic S, Gupta MK, Wang GX, Fujisaka S, O'Neill BT, Rao TN, et al. Divergent effects of glucose and fructose on hepatic lipogenesis and insulin signaling. *J Clin Invest*. (2018) 128(3):1199. doi: 10.1172/JCI99009

106. Nakagawa H, Umemura A, Taniguchi K, Font-Burgada J, Dhar D, Ogata H, et al. ER stress cooperates with hypernutrition to trigger TNF-dependent spontaneous HCC development. *Cancer Cell*. (2014) 26(3):331–43. doi: 10.1016/j.ccr.2014.07.001

107. Softic S, Gupta MK, Wang GX, Fujisaka S, O'Neill BT, Rao TN, et al. Divergent effects of glucose and fructose on hepatic lipogenesis and insulin signaling. *J Clin Invest*. (2017) 127(11):4059–74. doi: 10.1172/JCI94585

108. Stanhope KL, Schwarz JM, Keim NL, Griffen SC, Bremer AA, Graham JL, et al. Consuming fructose-sweetened, not glucose-sweetened, beverages increases visceral adiposity and lipids and decreases insulin sensitivity in overweight/obese humans. *J Clin Invest*. (2009) 119(5):1322–34. doi: 10.1172/JCI37385

109. Softic S, Meyer JG, Wang GX, Gupta MK, Batista TM, Lauritzen H, et al. Dietary sugars alter hepatic fatty acid oxidation via transcriptional and post-translational modifications of mitochondrial proteins. *Cell Metab*. (2019) 30(4):735–53.e4. doi: 10.1016/j.cmet.2019.09.003

110. Kavanagh K, Wylie AT, Tucker KL, Hamp TJ, Gharaibeh RZ, Fodor AA, et al. Dietary fructose induces endotoxemia and hepatic injury in calorically controlled primates. *Am J Clin Nutr*. (2013) 98(2):349–57. doi: 10.3945/ajcn.112.057331

111. Wiedermann CJ, Kiechl S, Dunzendorfer S, Schratzberger P, Egger G, Oberhollenzer F, et al. Association of endotoxemia with carotid atherosclerosis and cardiovascular disease: prospective results from the bruneck study. *J Am Coll Cardiol*. (1999) 34(7):1975–81. doi: 10.1016/s0735-1097(99)00448-9

112. Rao R. Endotoxemia and gut barrier dysfunction in alcoholic liver disease. *Hepatology*. (2009) 50(2):638–44. doi: 10.1002/hep.23009

113. Chiba T, Suzuki S, Sato Y, Itoh T, Umegaki K. Evaluation of methionine content in a high-fat and choline-deficient diet on body weight gain and the development of non-alcoholic steatohepatitis in mice. *PLoS One*. (2016) 11(10):e0164191. doi: 10.1371/journal.pone.0164191

114. Rinella ME, Green RM. The methionine-choline deficient dietary model of steatohepatitis does not exhibit insulin resistance. *J Hepatol*. (2004) 40(1):47–51. doi: 10.1016/j.jhep.2003.09.020

115. Rizki G, Arnaboldi L, Gabrielli B, Yan J, Lee GS, Ng RK, et al. Mice fed a lipogenic methionine-choline-deficient diet develop hypermetabolism coincident with hepatic suppression of SCD-1. *J Lipid Res*. (2006) 47(10):2280–90. doi: 10.1194/jlr.M600198-JLR200

116. Smati S, Polizzi A, Fougerat A, Ellero-Simatos S, Blum Y, Lippi Y, et al. Integrative study of diet-induced mouse models of NAFLD identifies PPARalpha as a sexually dimorphic drug target. *Gut*. (2022) 71(4):807–21. doi: 10.1136/gutjnl-2020-323323

117. Collins HL, Adelman SJ, Butteiger DN, Bortz JD. Choline supplementation does not promote atherosclerosis in CETP-expressing male apolipoprotein E knockout mice. *Nutrients*. (2022) 14(8):1–12. doi: 10.3390/nu14081651

118. Schwabl P, Hambruch E, Budas GR, Supper P, Burnet M, Liles JT, et al. The non-steroidal FXR agonist cilofexor improves portal hypertension and reduces hepatic fibrosis in a rat NASH model. *Biomedicines*. (2021) 9(1):1–11. doi: 10.3390/biomedicines9010060

119. Takayama F, Egashira T, Kawasaki H, Mankura M, Nakamoto K, Okada S, et al. A novel animal model of nonalcoholic steatohepatitis (NASH): hypoxemia enhances the development of NASH. *J Clin Biochem Nutr*. (2009) 45(3):335–40. doi: 10.3164/jcbn.09-29

120. Raubenheimer PJ, Nyirenda MJ, Walker BR. A choline-deficient diet exacerbates fatty liver but attenuates insulin resistance and glucose intolerance in mice fed a high-fat diet. *Diabetes*. (2006) 55(7):2015–20. doi: 10.2337/db06-0097

121. Bril F, Lomonaco R, Orsak B, Ortiz-Lopez C, Webb A, Tio F, et al. Relationship between disease severity, hyperinsulinemia, and impaired insulin clearance in patients with nonalcoholic steatohepatitis. *Hepatology*. (2014) 59(6):2178–87. doi: 10.1002/hep.26988

122. Standl E. Hyperinsulinemia and atherosclerosis. *Clin Invest Med*. (1995) 18(4):261–6.

123. Santhekadur PK, Kumar DP, Sanyal AJ. Preclinical models of non-alcoholic fatty liver disease. *J Hepatol*. (2018) 68(2):230–7. doi: 10.1016/j.jhep.2017.10.031

124. Skold BH, Getty R, Ramsey FK. Spontaneous atherosclerosis in the arterial system of aging swine. *Am J Vet Res*. (1966) 27(116):257–73.

125. Matthan NR, Solano-Aguilar G, Meng H, Lamon-Fava S, Goldbaum A, Walker ME, et al. The Ossabaw pig is a suitable translational model to evaluate dietary patterns and coronary artery disease risk. *J Nutr*. (2018) 148(4):542–51. doi: 10.1093/jn/nxy002

126. Lee L, Alloosh M, Saxena R, Van Alstine W, Watkins BA, Klaunig JE, et al. Nutritional model of steatohepatitis and metabolic syndrome in the Ossabaw miniature swine. *Hepatology*. (2009) 50(1):56–67. doi: 10.1002/hep.22904

127. Ogawa T, Fujii H, Yoshizato K, Kawada N. A human-type nonalcoholic steatohepatitis model with advanced fibrosis in rabbits. *Am J Pathol*. (2010) 177(1):153–65. doi: 10.2353/ajpath.2010.090895

128. Ignatowski A. Influence of animal food on the organism of rabbits. *Izvest Imper Voennomed Akad St Petersburg*. (1908) 16:154–73.

129. Fan J, Kitajima S, Watanabe T, Xu J, Zhang J, Liu E, et al. Rabbit models for the study of human atherosclerosis: from pathophysiological mechanisms to translational medicine. *Pharmacol Ther*. (2015) 146:104–19. doi: 10.1016/j.pharmthera.2014.09.009

130. Koike T, Koike Y, Yang D, Guo Y, Rom O, Song J, et al. Human apolipoprotein A-II reduces atherosclerosis in knock-in rabbits. *Atherosclerosis*. (2021) 316:32–40. doi: 10.1016/j.atherosclerosis.2020.11.028

131. Taylor E, Huang N, Bodde J, Ellison A, Killiany R, Bachschmid MM, et al. MRI of atherosclerosis and fatty liver disease in cholesterol fed rabbits. *J Transl Med*. (2018) 16(1):215. doi: 10.1186/s12967-018-1587-3

132. Eggen DA. Cholesterol metabolism in rhesus monkey, squirrel monkey, and baboon. *J Lipid Res*. (1974) 15(2):139–45. doi: 10.1016/S0022-2275(20)36816-4

133. Higgins PB, Bastarrachea RA, Lopez-Alvarenga JC, Garcia-Foray M, Proffitt JM, Voruganti VS, et al. Eight week exposure to a high sugar high fat diet results in adiposity gain and alterations in metabolic biomarkers in baboons (*papio hamadryas* sp.). *Cardiovasc Diabetol*. (2010) 9:71. doi: 10.1186/1475-2840-9-71

134. Lyu L, Liu XL, Rui MP, Yang LC, Wang GZ, Fan D, et al. Liver extracellular volume fraction values obtained with magnetic resonance imaging can quantitatively stage liver fibrosis: a validation study in monkeys with nonalcoholic steatohepatitis. *Eur Radiol*. (2020) 30(10):5748–57. doi: 10.1007/s00330-020-06902-w

135. Jian C, Fu J, Cheng X, Shen LJ, Ji YX, Wang X, et al. Low-dose sorafenib acts as a mitochondrial uncoupler and ameliorates nonalcoholic steatohepatitis. *Cell Metab*. (2020) 31(5):892–908.e11. doi: 10.1016/j.cmet.2020.04.011

136. Zhang XJ, Ji YX, Cheng X, Cheng Y, Yang H, Wang J, et al. A small molecule targeting ALOX12-ACC1 ameliorates nonalcoholic steatohepatitis in mice and macaques. *Sci Transl Med*. (2021) 13(624):eabg8116. doi: 10.1126/scitranslmed.abg8116

137. Wendler D. Should protections for research with humans who cannot consent apply to research with nonhuman primates? *Theor Med Bioeth*. (2014) 35(2):157–73. doi: 10.1007/s11017-014-9285-5

138. Targher G, Byrne CD. Circulating markers of liver function and cardiovascular disease risk. *Arterioscler Thromb Vasc Biol*. (2015) 35(11):2290–6. doi: 10.1161/ATVBAHA.115.305235

139. Lonardo A, Nascimbeni F, Mantovani A, Targher G. Hypertension, diabetes, atherosclerosis and NASH: cause or consequence? *J Hepatol*. (2018) 68(2):335–52. doi: 10.1016/j.jhep.2017.09.021

140. Adams LA, Anstee QM, Tilg H, Targher G. Non-alcoholic fatty liver disease and its relationship with cardiovascular disease and other extrahepatic diseases. *Gut*. (2017) 66(6):1138–53. doi: 10.1136/gutjnl-2017-313884

141. Allen AM, Therneau TM, Larson JJ, Coward A, Somers VK, Kamath PS. Nonalcoholic fatty liver disease incidence and impact on metabolic burden and death: a 20 year-community study. *Hepatology*. (2018) 67(5):1726–36. doi: 10.1002/hep.29546

142. Xi L, Kouvelos G, Paolucci N. Circulating biomarkers for cardiovascular diseases: the beats never stop. *Acta Pharmacol Sin*. (2018) 39(7):1065–7. doi: 10.1038/aps.2018.43

143. Lowe GD, Yarnell JW, Rumley A, Bainton D, Sweetnam PM. C-reactive protein, fibrin D-dimer, and incident ischemic heart disease in the speedwell study: are inflammation and fibrin turnover linked in pathogenesis? *Arterioscler Thromb Vasc Biol*. (2001) 21(4):603–10. doi: 10.1161/01.atv.21.4.603

144. Pfutzner A, Forst T. High-sensitivity C-reactive protein as cardiovascular risk marker in patients with diabetes mellitus. *Diabetes Technol Ther*. (2006) 8(1):28–36. doi: 10.1089/dia.2006.8.28

145. Heeren J, Scheja L. Metabolic-associated fatty liver disease and lipoprotein metabolism. *Mol Metab*. (2021) 50:101238. doi: 10.1016/j.molmet.2021.101238

146. Pei K, Gui T, Kan D, Feng H, Jin Y, Yang Y, et al. An overview of lipid metabolism and nonalcoholic fatty liver disease. *Biomed Res Int*. (2020) 2020:4020249. doi: 10.1155/2020/4020249

147. Deprince A, Haas JT, Staels B. Dysregulated lipid metabolism links NAFLD to cardiovascular disease. *Mol Metab.* (2020) 42:101092. doi: 10.1016/j.molmet.2020.101092
148. Manjunath CN, Rawal JR, Irani PM, Madhu K. Atherogenic dyslipidemia. *Indian J Endocrinol Metab.* (2013) 17(6):969–76. doi: 10.4103/2230-8210.122600
149. Liao X, Ma Q, Wu T, Shao C, Lin Y, Sun Y, et al. Lipid-lowering responses to dyslipidemia determine the efficacy on liver enzymes in metabolic dysfunction-associated fatty liver disease with hepatic injuries: a prospective cohort study. *Diabetes Metab Syndr Obes.* (2022) 15:1173–84. doi: 10.2147/DMSO.S356371
150. Morrow MR, Batchuluun B, Wu J, Ahmadi E, Leroux JM, Mohammadi-Shemirani P, et al. Inhibition of ATP-citrate lyase improves NASH, liver fibrosis, and dyslipidemia. *Cell Metab.* (2022) 34(6):919–36.e8. doi: 10.1016/j.cmet.2022.05.004
151. Abdallah M, Brown L, Provenza J, Tariq R, Gowda S, Singal AK. Safety and efficacy of dyslipidemia treatment in NAFLD patients: a meta-analysis of randomized controlled trials. *Ann Hepatol.* (2022) 27(6):100738. doi: 10.1016/j.aohp.2022.100738
152. Shahab O, Biswas R, Paik J, Bush H, Golabi P, Younossi ZM. Among patients with NAFLD, treatment of dyslipidemia does not reduce cardiovascular mortality. *Hepatol Commun.* (2018) 2(10):1227–34. doi: 10.1002/hep4.1241
153. Das Pradhan A, Glynn RJ, Fruchart JC, MacFadyen JG, Zaharris ES, Everett BM, et al. Triglyceride lowering with pemafibrate to reduce cardiovascular risk. *N Engl J Med.* (2022) 387(21):1923–34. doi: 10.1056/NEJMoa2210645
154. Tanase DM, Gosav EM, Petrov D, Jucan AE, Lacatusu CM, Floria M, et al. Involvement of ceramides in non-alcoholic fatty liver disease (NAFLD) atherosclerosis (ATS) development: mechanisms and therapeutic targets. *Diagnostics (Basel).* (2021) 11(11):1–20. doi: 10.3390/diagnostics11112053
155. Chaurasia B, Summers SA. Ceramides—lipotoxic inducers of metabolic disorders: (trends in endocrinology and metabolism 26, 538–550; 2015). *Trends Endocrinol Metab.* (2018) 29(1):66–7. doi: 10.1016/j.tem.2017.09.005
156. Sokolowska E, Blachnio-Zabielska A. The role of ceramides in insulin resistance. *Front Endocrinol (Lausanne).* (2019) 10:577. doi: 10.3389/fendo.2019.00577
157. Wasilewska N, Bobrus-Chociej A, Harasim-Symbor E, Tarasow E, Wojtkowska M, Chabowski A, et al. Increased serum concentration of ceramides in obese children with nonalcoholic fatty liver disease. *Lipids Health Dis.* (2018) 17(1):216. doi: 10.1186/s12944-018-0855-9
158. Kasumov T, Li L, Li M, Gulshan K, Kirwan JP, Liu X, et al. Ceramide as a mediator of non-alcoholic fatty liver disease and associated atherosclerosis. *PLoS One.* (2015) 10(5):e0126910. doi: 10.1371/journal.pone.0126910
159. Gorden DL, Myers DS, Ivanova PT, Fahy E, Maurya MR, Gupta S, et al. Biomarkers of NAFLD progression: a lipidomics approach to an epidemic. *J Lipid Res.* (2015) 56(3):722–36. doi: 10.1194/jlr.P056002
160. Wiesner P, Leidl K, Boettcher A, Schmitz G, Liebisch G. Lipid profiling of FPLC-separated lipoprotein fractions by electrospray ionization tandem mass spectrometry. *J Lipid Res.* (2009) 50(3):574–85. doi: 10.1194/jlr.D800028-JLR200
161. Anroedh S, Hilvo M, Akkerhuis KM, Kauhanen D, Koistinen K, Oemrawsingh R, et al. Plasma concentrations of molecular lipid species predict long-term clinical outcome in coronary artery disease patients. *J Lipid Res.* (2018) 59(9):1729–37. doi: 10.1194/jlr.P081281
162. Laaksonen R, Ekroos K, Sysi-Aho M, Hilvo M, Vihervaara T, Kauhanen D, et al. Plasma ceramides predict cardiovascular death in patients with stable coronary artery disease and acute coronary syndromes beyond LDL-cholesterol. *Eur Heart J.* (2016) 37(25):1967–76. doi: 10.1093/eurheartj/ehw148
163. Wang DD, Toledo E, Hruby A, Rosner BA, Willett WC, Sun Q, et al. Plasma ceramides, Mediterranean diet, and incident cardiovascular disease in the PREDIMED trial (prevención con dieta Mediterránea). *Circulation.* (2017) 135(21):2028–40. doi: 10.1161/CIRCULATIONAHA.116.024261
164. Meeusen JW, Donato LJ, Kopecky SL, Vasile VC, Jaffe AS, Laaksonen R. Ceramides improve atherosclerotic cardiovascular disease risk assessment beyond standard risk factors. *Clin Chim Acta.* (2020) 511:138–42. doi: 10.1016/j.cca.2020.10.005
165. Akhiyat N, Vasile V, Ahmad A, Sara JD, Nardi V, Lerman LO, et al. Plasma ceramide levels are elevated in patients with early coronary atherosclerosis and endothelial dysfunction. *J Am Heart Assoc.* (2022) 11(7):e022852. doi: 10.1161/JAHA.121.022852
166. Chaurasia B, Tippetts TS, Mayoral Monibas R, Liu J, Li Y, Wang L, et al. Targeting a ceramide double bond improves insulin resistance and hepatic steatosis. *Science.* (2019) 365(6451):386–92. doi: 10.1126/science.aav3722
167. Jiang M, Li C, Liu Q, Wang A, Lei M. Inhibiting ceramide synthesis attenuates hepatic steatosis and fibrosis in rats with non-alcoholic fatty liver disease. *Front Endocrinol (Lausanne).* (2019) 10:665. doi: 10.3389/fendo.2019.00665
168. Chun L, Junlin Z, Aimin W, Niansheng L, Benmei C, Minxiang L. Inhibition of ceramide synthesis reverses endothelial dysfunction and atherosclerosis in streptozotocin-induced diabetic rats. *Diabetes Res Clin Pract.* (2011) 93(1):77–85. doi: 10.1016/j.diabres.2011.03.017
169. Park TS, Rosebury W, Kindt EK, Kowala MC, Panek RL. Serine palmitoyltransferase inhibitor myricin induces the regression of atherosclerotic plaques in hyperlipidemic ApoE-deficient mice. *Pharmacol Res.* (2008) 58(1):45–51. doi: 10.1016/j.phrs.2008.06.005
170. Pessayre D, Mansouri A, Fromenty B. Nonalcoholic steatosis and steatohepatitis. V. Mitochondrial dysfunction in steatohepatitis. *Am J Physiol Gastrointest Liver Physiol.* (2002) 282(2):G193–9. doi: 10.1152/ajpgi.00426.2001
171. Ore A, Akinloye OA. Oxidative stress and antioxidant biomarkers in clinical and experimental models of non-alcoholic fatty liver disease. *Medicina (Kaunas).* (2019) 55(2):1–13. doi: 10.3390/medicina55020026
172. Masarone M, Rosato V, Dallio M, Gravina AG, Aglitti A, Loguercio C, et al. Role of oxidative stress in pathophysiology of nonalcoholic fatty liver disease. *Oxid Med Cell Longev.* (2018) 2018:9547613. doi: 10.1155/2018/9547613
173. Narasimhan S, Gokulakrishnan K, Sampathkumar R, Farooq S, Ravikumar R, Mohan V, et al. Oxidative stress is independently associated with non-alcoholic fatty liver disease (NAFLD) in subjects with and without type 2 diabetes. *Clin Biochem.* (2010) 43(10–11):815–21. doi: 10.1016/j.clinbiochem.2010.04.003
174. Zelber-Sagi S, Ivancovsky-Wajcman D, Fliss-Isakov N, Hahn M, Webb M, Shibolet O, et al. Serum malondialdehyde is associated with non-alcoholic fatty liver and related liver damage differentially in men and women. *Antioxidants (Basel).* (2020) 9(7):1–15. doi: 10.3390/antiox9070578
175. Lasker S, Rahman MM, Parvez F, Zamila M, Miah P, Nahar K, et al. High-fat diet-induced metabolic syndrome and oxidative stress in obese rats are ameliorated by yogurt supplementation. *Sci Rep.* (2019) 9(1):20026. doi: 10.1038/s41598-019-56538-0
176. Karami S, Poustchi H, Sarmadi N, Radmard AR, Ali Yari F, Pakdel A, et al. Association of anti-oxidative capacity of HDL with subclinical atherosclerosis in subjects with and without non-alcoholic fatty liver disease. *Diabetol Metab Syndr.* (2021) 13(1):121. doi: 10.1186/s13098-021-00741-5
177. Yang X, Li Y, Li Y, Ren X, Zhang X, Hu D, et al. Oxidative stress-mediated atherosclerosis: mechanisms and therapies. *Front Physiol.* (2017) 8:600. doi: 10.3389/fphys.2017.00600
178. Dimmeler S, Haendeler J, Galle J, Zeiher AM. Oxidized low-density lipoprotein induces apoptosis of human endothelial cells by activation of CPP32-like proteases. A mechanistic clue to the 'response to injury' hypothesis. *Circulation.* (1997) 95(7):1760–3. doi: 10.1161/01.cir.95.7.1760
179. Cominacini L, Rigoni A, Pasini AF, Garbin U, Davoli A, Campagnola M, et al. The binding of oxidized low density lipoprotein (ox-LDL) to ox-LDL receptor-1 reduces the intracellular concentration of nitric oxide in endothelial cells through an increased production of superoxide. *J Biol Chem.* (2001) 276(17):13750–5. doi: 10.1074/jbc.M010612200
180. Li D, Mehta JL. Antisense to LOX-1 inhibits oxidized LDL-mediated upregulation of monocyte chemoattractant protein-1 and monocyte adhesion to human coronary artery endothelial cells. *Circulation.* (2000) 101(25):2889–95. doi: 10.1161/01.cir.101.25.2889
181. Chen H, Li D, Saldeen T, Mehta JL. Transforming growth factor-beta(1) modulates oxidatively modified LDL-induced expression of adhesion molecules: role of LOX-1. *Circ Res.* (2001) 89(12):1155–60. doi: 10.1161/hh2401.100598
182. Bekkering S, Quintin J, Joosten LA, van der Meer JW, Netea MG, Riksen NP. Oxidized low-density lipoprotein induces long-term proinflammatory cytokine production and foam cell formation via epigenetic reprogramming of monocytes. *Arterioscler Thromb Vasc Biol.* (2014) 34(8):1731–8. doi: 10.1161/ATVBAHA.114.303887
183. Rom O, Korach-Rechtman H, Hayek T, Danin-Poleg Y, Bar H, Kashi Y, et al. Acrolein increases macrophage atherogenicity in association with gut microbiota remodeling in atherosclerotic mice: protective role for the polyphenol-rich pomegranate juice. *Arch Toxicol.* (2017) 91(4):1709–25. doi: 10.1007/s00204-016-1859-8
184. Rom O, Jerjes H, Hayek T, Aviram M. Supplementation with linoleic acid-rich soybean oil stimulates macrophage foam cell formation via increased oxidative stress and diacylglycerol acyltransferase1-mediated triglyceride biosynthesis. *Biofactors.* (2017) 43(1):100–16. doi: 10.1002/biof.1319
185. Rom O, Aviram M. Endogenous or exogenous antioxidants vs. pro-oxidants in macrophage atherogenicity. *Curr Opin Lipidol.* (2016) 27(2):204–6. doi: 10.1097/MOL.0000000000000287
186. Auge N, Garcia V, Maupas-Schwalm F, Levade T, Salvayre R, Negre-Salvayre A. Oxidized LDL-induced smooth muscle cell proliferation involves the EGF receptor/PI-3 kinase/Akt and the sphingolipid signaling pathways. *Arterioscler Thromb Vasc Biol.* (2002) 22(12):1990–5. doi: 10.1161/01.atv.0000043453.21629.3b
187. Liu J, Ren Y, Kang L, Zhang L. Oxidized low-density lipoprotein increases the proliferation and migration of human coronary artery smooth muscle cells through the upregulation of osteopontin. *Int J Mol Med.* (2014) 33(5):1341–7. doi: 10.3892/ijmm.2014.1681
188. Holvoet P, Mertens A, Verhamme P, Bogaerts K, Beyens G, Verhaeghe R, et al. Circulating oxidized LDL is a useful marker for identifying patients with coronary artery disease. *Arterioscler Thromb Vasc Biol.* (2001) 21(5):844–8. doi: 10.1161/01.atv.21.5.844
189. Ho CM, Ho SL, Jeng YM, Lai YS, Chen YH, Lu SC, et al. Accumulation of free cholesterol and oxidized low-density lipoprotein is associated with portal

- inflammation and fibrosis in nonalcoholic fatty liver disease. *J Inflamm (Lond)*. (2019) 16:7. doi: 10.1186/s12950-019-0211-5
190. Nishihara T, Miyoshi T, Ichikawa K, Osawa K, Nakashima M, Miki T, et al. Association of oxidized low-density lipoprotein in nonalcoholic fatty liver disease with high-risk plaque on coronary computed tomography angiography: a matched case-control study. *J Clin Med*. (2022) 11(10):1–9. doi: 10.3390/jcm11102838
191. Rom O, Aviram M. It is not just lipids: proatherogenic vs. antiatherogenic roles for amino acids in macrophage foam cell formation. *Curr Opin Lipidol*. (2017) 28(1):85–7. doi: 10.1097/MOL.0000000000000377
192. Gaggini M, Carli F, Rosso C, Buzzigoli E, Marietti M, Della Latta V, et al. Altered amino acid concentrations in NAFLD: impact of obesity and insulin resistance. *Hepatology*. (2018) 67(1):145–58. doi: 10.1002/hep.29465
193. Solon-Biet SM, Cogger VC, Pulpitel T, Wahl D, Clark X, Bagley E, et al. Branched chain amino acids impact health and lifespan indirectly via amino acid balance and appetite control. *Nat Metab*. (2019) 1(5):532–45. doi: 10.1038/s42255-019-0059-2
194. McGarrah RW, White PJ. Branched-chain amino acids in cardiovascular disease. *Nat Rev Cardiol*. (2023) 20(2):77–89. doi: 10.1038/s41569-022-00760-3
195. Rom O, Liu Y, Finney AC, Ghayeb A, Zhao Y, Shukha Y, et al. Induction of glutathione biosynthesis by glycine-based treatment mitigates atherosclerosis. *Redox Biol*. (2022) 52:102313. doi: 10.1016/j.redox.2022.102313
196. Liu Y, Zhao Y, Shukha Y, Lu H, Wang L, Liu Z, et al. Dysregulated oxalate metabolism is a driver and therapeutic target in atherosclerosis. *Cell Rep*. (2021) 36(4):109420. doi: 10.1016/j.celrep.2021.109420
197. Grajeda-Iglesias C, Rom O, Aviram M. Branched-chain amino acids and atherosclerosis: friends or foes? *Curr Opin Lipidol*. (2018) 29(2):166–9. doi: 10.1097/MOL.0000000000000494
198. Mardinoglu A, Agren R, Kampf C, Asplund A, Uhlen M, Nielsen J. Genome-scale metabolic modelling of hepatocytes reveals serine deficiency in patients with non-alcoholic fatty liver disease. *Nat Commun*. (2014) 5:3083. doi: 10.1038/ncomms4083
199. Mardinoglu A, Bjornson E, Zhang C, Klevstig M, Soderlund S, Stahlman M, et al. Personal model-assisted identification of NAD(+) and glutathione metabolism as intervention target in NAFLD. *Mol Syst Biol*. (2017) 13(3):916. doi: 10.15252/msb.20167422
200. Wurtz P, Raiko JR, Magnussen CG, Soininen P, Kangas AJ, Tynkkynen T, et al. High-throughput quantification of circulating metabolites improves prediction of subclinical atherosclerosis. *Eur Heart J*. (2012) 33(18):2307–16. doi: 10.1093/eurheartj/ehs020
201. Wittemans LBL, Lotta LA, Oliver-Williams C, Stewart ID, Surendran P, Karthikeyan S, et al. Assessing the causal association of glycine with risk of cardio-metabolic diseases. *Nat Commun*. (2019) 10(1):1060. doi: 10.1038/s41467-019-08936-1
202. Zaric BL, Radovanovic JN, Gluvic Z, Stewart AJ, Essack M, Motwalli O, et al. Atherosclerosis linked to aberrant amino acid metabolism and immunosuppressive amino acid catabolizing enzymes. *Front Immunol*. (2020) 11:551758. doi: 10.3389/fimmu.2020.551758
203. Simon J, Nunez-Garcia M, Fernandez-Tussy P, Barbier-Torres L, Fernandez-Ramos D, Gomez-Santos B, et al. Targeting hepatic glutaminase 1 ameliorates non-alcoholic steatohepatitis by restoring very-low-density lipoprotein triglyceride assembly. *Cell Metab*. (2020) 31(3):605–22.e10. doi: 10.1016/j.cmet.2020.01.013
204. Hasegawa T, Iino C, Endo T, Mikami K, Kimura M, Sawada N, et al. Changed amino acids in NAFLD and liver fibrosis: a large cross-sectional study without influence of insulin resistance. *Nutrients*. (2020) 12(5):1–11. doi: 10.3390/nu12051450
205. Kawanaka M, Nishino K, Oka T, Urata N, Nakamura J, Suehiro M, et al. Tyrosine levels are associated with insulin resistance in patients with nonalcoholic fatty liver disease. *Hepat Med*. (2015) 7:29–35. doi: 10.2147/HMER.S79100
206. Shah SH, Bain JR, Muehlbauer MJ, Stevens RD, Crosslin DR, Haynes C, et al. Association of a peripheral blood metabolic profile with coronary artery disease and risk of subsequent cardiovascular events. *Circ Cardiovasc Genet*. (2010) 3(2):207–14. doi: 10.1161/CIRCGENETICS.109.852814
207. Yang R, Dong J, Zhao H, Li H, Guo H, Wang S, et al. Association of branched-chain amino acids with carotid intima-media thickness and coronary artery disease risk factors. *PLoS One*. (2014) 9(6):e99598. doi: 10.1371/journal.pone.0099598
208. Ruiz-Canela M, Toledo E, Clish CB, Hruby A, Liang L, Salas-Salvado J, et al. Plasma branched-chain amino acids and incident cardiovascular disease in the PREDIMED trial. *Clin Chem*. (2016) 62(4):582–92. doi: 10.1373/clinchem.2015.251710
209. Bhattacharya S, Granger CB, Craig D, Haynes C, Bain J, Stevens RD, et al. Validation of the association between a branched chain amino acid metabolite profile and extremes of coronary artery disease in patients referred for cardiac catheterization. *Atherosclerosis*. (2014) 232(1):191–6. doi: 10.1016/j.atherosclerosis.2013.10.036
210. Zhang F, Zhao S, Yan W, Xia Y, Chen X, Wang W, et al. Branched chain amino acids cause liver injury in obese/diabetic mice by promoting adipocyte lipolysis and inhibiting hepatic autophagy. *EBioMedicine*. (2016) 13:157–67. doi: 10.1016/j.ebiom.2016.10.013
211. Honda T, Ishigami M, Luo F, Lingyun M, Ishizu Y, Kuzuya T, et al. Branched-chain amino acids alleviate hepatic steatosis and liver injury in choline-deficient high-fat diet induced NASH mice. *Metab Clin Exp*. (2017) 69:177–87. doi: 10.1016/j.metabol.2016.12.013
212. Iwao M, Gotoh K, Arakawa M, Endo M, Honda K, Seike M, et al. Supplementation of branched-chain amino acids decreases fat accumulation in the liver through intestinal microbiota-mediated production of acetic acid. *Sci Rep*. (2020) 10(1):18768. doi: 10.1038/s41598-020-75542-3
213. Yu D, Richardson NE, Green CL, Spicer AB, Murphy ME, Flores V, et al. The adverse metabolic effects of branched-chain amino acids are mediated by isoleucine and valine. *Cell Metab*. (2021) 33(5):905–22.e6. doi: 10.1016/j.cmet.2021.03.025
214. Rom O, Grajeda-Iglesias C, Najjar M, Abu-Saleh N, Volkova N, Dar DE, et al. Atherogenicity of amino acids in the lipid-laden macrophage model system in vitro and in atherosclerotic mice: a key role for triglyceride metabolism. *J Nutr Biochem*. (2017) 45:24–38. doi: 10.1016/j.jnutbio.2017.02.023
215. Grajeda-Iglesias C, Rom O, Hamoud S, Volkova N, Hayek T, Abu-Saleh N, et al. Leucine supplementation attenuates macrophage foam-cell formation: studies in humans, mice, and cultured macrophages. *Biofactors*. (2018) 44(3):245–62. doi: 10.1002/biof.1415
216. Zhao Y, Dai XY, Zhou Z, Zhao GX, Wang X, Xu MJ. Leucine supplementation via drinking water reduces atherosclerotic lesions in apoE null mice. *Acta Pharmacol Sin*. (2016) 37(2):196–203. doi: 10.1038/aps.2015.88
217. Zhenyukh O, Gonzalez-Amor M, Rodrigues-Diez RR, Esteban V, Ruiz-Ortega M, Salaices M, et al. Branched-chain amino acids promote endothelial dysfunction through increased reactive oxygen species generation and inflammation. *J Cell Mol Med*. (2018) 22(10):4948–62. doi: 10.1111/jcmm.13759
218. Kalhan SC, Guo L, Edmison J, Dasarthy S, McCullough AJ, Hanson RW, et al. Plasma metabolomic profile in nonalcoholic fatty liver disease. *Metab Clin Exp*. (2011) 60(3):404–13. doi: 10.1016/j.metabol.2010.03.006
219. de Mello VD, Sehgal R, Mannisto V, Klavus A, Nilsson E, Perflyev A, et al. Serum aromatic and branched-chain amino acids associated with NASH demonstrate divergent associations with serum lipids. *Liver Int*. (2021) 41(4):754–63. doi: 10.1111/liv.14743
220. Jauhiainen R, Vangipurapu J, Laakso A, Kuulasmaa T, Kuusisto J, Laakso M. The association of 9 amino acids with cardiovascular events in finnish men in a 12-year follow-up study. *J Clin Endocrinol Metab*. (2021) 106(12):3448–54. doi: 10.1210/clinem/dgab562
221. Rom O, Villacorta L, Zhang J, Chen YE, Aviram M. Emerging therapeutic potential of glycine in cardiometabolic diseases: dual benefits in lipid and glucose metabolism. *Curr Opin Lipidol*. (2018) 29(5):428–32. doi: 10.1097/MOL.0000000000000543
222. Newgard CB, An J, Bain JR, Muehlbauer MJ, Stevens RD, Lien LF, et al. A branched-chain amino acid-related metabolic signature that differentiates obese and lean humans and contributes to insulin resistance. *Cell Metab*. (2009) 9(4):311–26. doi: 10.1016/j.cmet.2009.02.002
223. Guasch-Ferre M, Hruby A, Toledo E, Clish CB, Martinez-Gonzalez MA, Salas-Salvado J, et al. Metabolomics in prediabetes and diabetes: a systematic review and meta-analysis. *Diabetes Care*. (2016) 39(5):833–46. doi: 10.2337/dc15-2251
224. Li X, Sun L, Zhang W, Li H, Wang S, Mu H, et al. Association of serum glycine levels with metabolic syndrome in an elderly Chinese population. *Nutr Metab (Lond)*. (2018) 15:89. doi: 10.1186/s12986-018-0325-4
225. Ding Y, Svingen GF, Pedersen ER, Gregory JF, Ueland PM, Tell GS, et al. Plasma glycine and risk of acute myocardial infarction in patients with suspected stable angina pectoris. *J Am Heart Assoc*. (2015) 5(1):1–9. doi: 10.1161/JAHA.115.002621
226. Wang W, Wu Z, Dai Z, Yang Y, Wang J, Wu G. Glycine metabolism in animals and humans: implications for nutrition and health. *Amino Acids*. (2013) 45(3):463–77. doi: 10.1007/s00726-013-1493-1
227. Kathirvel E, Morgan K, Nandgiri G, Sandoval BC, Caudill MA, Bottiglieri T, et al. Betaine improves nonalcoholic fatty liver and associated hepatic insulin resistance: a potential mechanism for hepatoprotection by betaine. *Am J Physiol Gastrointest Liver Physiol*. (2010) 299(5):G1068–77. doi: 10.1152/ajpgi.00249.2010
228. Leonetti S, Herzog RI, Caprio S, Santoro N, Trico D. Glutamate-serine-glycine index: a novel potential biomarker in pediatric non-alcoholic fatty liver disease. *Children (Basel)*. (2020) 7(12):1–7. doi: 10.3390/children7120270
229. Zwighaft Z, Aviram R, Shalev M, Rousoo-Noori L, Kraut-Cohen J, Golik M, et al. Circadian clock control by polyamine levels through a mechanism that declines with age. *Cell Metab*. (2015) 22(5):874–85. doi: 10.1016/j.cmet.2015.09.011
230. Wallace HM, Fraser AV, Hughes A. A perspective of polyamine metabolism. *Biochem J*. (2003) 376(Pt 1):1–14. doi: 10.1042/BJ20031327
231. Madeo F, Eisenberg T, Pietrocola F, Kroemer G. Spermidine in health and disease. *Science*. (2018) 359(6374):1–11. doi: 10.1126/science.aan2788

232. Eisenberg T, Abdellatif M, Schroeder S, Primessnig U, Stekovic S, Pendl T, et al. Cardioprotection and lifespan extension by the natural polyamine spermidine. *Nat Med*. (2016) 22(12):1428–38. doi: 10.1038/nm.4222
233. Wang D, Yin J, Zhou Z, Tao Y, Jia Y, Jie H, et al. Oral spermidine targets brown fat and skeletal muscle to mitigate diet-induced obesity and metabolic disorders. *Mol Nutr Food Res*. (2021) 65(19):e2100315. doi: 10.1002/mnfr.202100315
234. Fernandes J, Chandler JD, Liu KH, Uppal K, Go YM, Jones DP. Putrescine as indicator of manganese neurotoxicity: dose-response study in human SH-SY5Y cells. *Food Chem Toxicol*. (2018) 116(Pt B):272–80. doi: 10.1016/j.fct.2018.04.042
235. Holbert CE, Cullen MT, Casero RA Jr, Stewart TM. Polyamines in cancer: integrating organismal metabolism and antitumor immunity. *Nat Rev Cancer*. (2022) 22(8):467–80. doi: 10.1038/s41568-022-00473-2
236. Ioannou GN, Nagana Gowda GA, Djukovic D, Raftery D. Distinguishing NASH histological severity using a multiplatform metabolomics approach. *Metabolites*. (2020) 10(4):1–15. doi: 10.3390/metabo10040168
237. Quinn C, Rico MC, Merali C, Merali S. Dysregulation of S-adenosylmethionine metabolism in nonalcoholic steatohepatitis leads to polyamine flux and oxidative stress. *Int J Mol Sci*. (2022) 23(4):1–14. doi: 10.3390/ijms23041986
238. Ma L, Ni Y, Hu L, Zhao Y, Zheng L, Yang S, et al. Spermidine ameliorates high-fat diet-induced hepatic steatosis and adipose tissue inflammation in preexisting obese mice. *Life Sci*. (2021) 265:118739. doi: 10.1016/j.lfs.2020.118739
239. Gao M, Zhao W, Li C, Xie X, Li M, Bi Y, et al. Spermidine ameliorates non-alcoholic fatty liver disease through regulating lipid metabolism via AMPK. *Biochem Biophys Res Commun*. (2018) 505(1):93–8. doi: 10.1016/j.bbrc.2018.09.078
240. Zhou J, Pang J, Tripathi M, Ho JP, Widjaja AA, Shekaran SG, et al. Spermidine-mediated hypusination of translation factor EIF5A improves mitochondrial fatty acid oxidation and prevents non-alcoholic steatohepatitis progression. *Nat Commun*. (2022) 13(1):5202. doi: 10.1038/s41467-022-32788-x
241. Yu Z, Jiao Y, Zhang J, Xu Q, Xu J, Li R, et al. Effect of serum spermidine on the prognosis in patients with acute myocardial infarction: a cohort study. *Nutrients*. (2022) 14(7):1–12. doi: 10.3390/nu14071394
242. Zheng L, Xie Y, Sun Z, Zhang R, Ma Y, Xu J, et al. Serum spermidine in relation to risk of stroke: a multilevel study. *Front Nutr*. (2022) 9:843616. doi: 10.3389/fnut.2022.843616
243. Gao H, Zhang Q, Xu J, Yuan W, Li R, Guo H, et al. Elevation of serum spermidine in obese patients: results from a cross-sectional and follow-up study. *Nutrients*. (2022) 14(13):1–12. doi: 10.3390/nu14132613
244. Michiels CF, Kurdi A, Timmermans JP, De Meyer GRY, Martinet W. Spermidine reduces lipid accumulation and necrotic core formation in atherosclerotic plaques via induction of autophagy. *Atherosclerosis*. (2016) 251:319–27. doi: 10.1016/j.atherosclerosis.2016.07.899
245. Balderas FL, Quezada-Larios M, Garcia Latorre EA, Mendez JD. Increased uptake of oxidized LDL by macrophages from type 2 diabetics is inhibited by polyamines. *Biomed Pharmacother*. (2016) 77:59–64. doi: 10.1016/j.biopha.2015.11.006
246. Holmes RP, Goodman HO, Assimos DG. Contribution of dietary oxalate to urinary oxalate excretion. *Kidney Int*. (2001) 59(1):270–6. doi: 10.1046/j.1523-1755.2001.00488.x
247. Brzica H, Breljak D, Burckhardt BC, Burckhardt G, Sabolic I. Oxalate: from the environment to kidney stones. *Arh Hig Rada Toksikol*. (2013) 64(4):609–30. doi: 10.2478/10004-1254-64-2013-2428
248. Gianmoena K, Gasparoni N, Jashari A, Gabrys P, Grgas K, Ghallab A, et al. Epigenomic and transcriptional profiling identifies impaired glyoxylate detoxification in NAFLD as a risk factor for hyperoxaluria. *Cell Rep*. (2021) 36(8):109526. doi: 10.1016/j.celrep.2021.109526
249. Elder TD, Wyngaarden JB. The biosynthesis and turnover of oxalate in normal and hyperoxaluric subjects. *J Clin Invest*. (1960) 39(8):1337–44. doi: 10.1172/JCI104151
250. Ermer T, Nazzari L, Tio MC, Waikar S, Aronson PS, Knauf F. Oxalate homeostasis. *Nat Rev Nephrol*. (2023) 19(2):123–38. doi: 10.1038/s41581-022-00643-3
251. Crivelli JJ, Mitchell T, Knight J, Wood KD, Assimos DG, Holmes RP, et al. Contribution of dietary oxalate and oxalate precursors to urinary oxalate excretion. *Nutrients*. (2020) 13(1):1–13. doi: 10.3390/nu13010062
252. Salido E, Pey AL, Rodriguez R, Lorenzo V. Primary hyperoxalurias: disorders of glyoxylate detoxification. *Biochim Biophys Acta*. (2012) 1822(9):1453–64. doi: 10.1016/j.bbdis.2012.03.004
253. Pfau A, Ermer T, Coca SG, Tio MC, Genser B, Reichel M, et al. High oxalate concentrations correlate with increased risk for sudden cardiac death in dialysis patients. *J Am Soc Nephrol*. (2021) 32(9):2375–85. doi: 10.1681/ASN.2020121793
254. Stepanova N, Driianska V, Korol L, Snisar L, Lebed L. Plasma oxalic acid and cardiovascular risk in end-stage renal disease patients: a prospective, observational cohort pilot study. *Korean J Intern Med*. (2022) 37(1):167–78. doi: 10.3904/kjim.2020.561
255. Stepanova M, Hossain N, Afendy A, Perry K, Goodman ZD, Baranova A, et al. Hepatic gene expression of caucasian and African-American patients with obesity-related non-alcoholic fatty liver disease. *Obes Surg*. (2010) 20(5):640–50. doi: 10.1007/s11695-010-0078-2
256. Asgharpour A, Cazanave SC, Pacana T, Seneshaw M, Vincent R, Banini BA, et al. A diet-induced animal model of non-alcoholic fatty liver disease and hepatocellular cancer. *J Hepatol*. (2016) 65(3):579–88. doi: 10.1016/j.jhep.2016.05.005
257. Gulhan B, Turkmen K, Aydin M, Gunay M, Cikman A, Kara M. The relationship between serum oxalic acid, central hemodynamic parameters and colonization by *Oxalobacter formigenes* in hemodialysis patients. *Cardiorenal Med*. (2015) 5(3):164–74. doi: 10.1159/000381219
258. Schunk SJ, Triem S, Schmit D, Zewinger S, Sarakpi T, Becker E, et al. Interleukin-1 α is a central regulator of leukocyte-endothelial adhesion in myocardial infarction and in chronic kidney disease. *Circulation*. (2021) 144(11):893–908. doi: 10.1161/CIRCULATIONAHA.121.053547
259. Patel M, Yarlagadda V, Adedoyin O, Saini V, Assimos DG, Holmes RP, et al. Oxalate induces mitochondrial dysfunction and disrupts redox homeostasis in a human monocyte derived cell line. *Redox Biol*. (2018) 15:207–15. doi: 10.1016/j.redox.2017.12.003
260. Sun K, Tang X, Song S, Gao Y, Yu H, Sun N, et al. Hyperoxalemia leads to oxidative stress in endothelial cells and mice with chronic kidney disease. *Kidney Blood Press Res*. (2021) 46(3):377–86. doi: 10.1159/000516013
261. Jensen-Cody SO, Potthoff MJ. Hepatokines and metabolism: deciphering communication from the liver. *Mol Metab*. (2021) 44:101138. doi: 10.1016/j.molmet.2020.101138
262. Meex RCR, Watt MJ. Hepatokines: linking nonalcoholic fatty liver disease and insulin resistance. *Nat Rev Endocrinol*. (2017) 13(9):509–20. doi: 10.1038/nrendo.2017.56
263. Conklin D, Gilbertson D, Taft DW, Maurer MF, Whitmore TE, Smith DL, et al. Identification of a mammalian angiopoietin-related protein expressed specifically in liver. *Genomics*. (1999) 62(3):477–82. doi: 10.1006/geno.1999.6041
264. Koishi R, Ando Y, Ono M, Shimamura M, Yasuno H, Fujiwara T, et al. ANGPT3 regulates lipid metabolism in mice. *Nat Genet*. (2002) 30(2):151–7. doi: 10.1038/ng814
265. Shimizugawa T, Ono M, Shimamura M, Yoshida K, Ando Y, Koishi R, et al. ANGPTL3 decreases very low density lipoprotein triglyceride clearance by inhibition of lipoprotein lipase. *J Biol Chem*. (2002) 277(37):33742–8. doi: 10.1074/jbc.M203215200
266. Romeo S, Yin W, Kozlitina J, Pennacchio LA, Boerwinkle E, Hobbs HH, et al. Rare loss-of-function mutations in ANGPTL family members contribute to plasma triglyceride levels in humans. *J Clin Invest*. (2009) 119(1):70–9. doi: 10.1172/JCI37118
267. Yilmaz Y, Ulukaya E, Atug O, Dolar E. Serum concentrations of human angiopoietin-like protein 3 in patients with nonalcoholic fatty liver disease: association with insulin resistance. *Eur J Gastroenterol Hepatol*. (2009) 21(11):1247–51. doi: 10.1097/MEG.0b013e32832b77ae
268. Barchetta I, Cimini FA, Chiappetta C, Bertocchini L, Ceccarelli V, Capoccia D, et al. Relationship between hepatic and systemic angiopoietin-like 3, hepatic vitamin D receptor expression and NAFLD in obesity. *Liver Int*. (2020) 40(9):2139–47. doi: 10.1111/liv.14554
269. Stitzel NO, Khera AV, Wang X, Bierhals AJ, Vourakis AC, Sperry AE, et al. ANGPTL3 deficiency and protection against coronary artery disease. *J Am Coll Cardiol*. (2017) 69(16):2054–63. doi: 10.1016/j.jacc.2017.02.030
270. Sun T, Zhan W, Wei L, Xu Z, Fan L, Zhuo Y, et al. Circulating ANGPTL3 and ANGPTL4 levels predict coronary artery atherosclerosis severity. *Lipids Health Dis*. (2021) 20(1):154. doi: 10.1186/s12944-021-01580-z
271. Dewey FE, Gusarova V, Dunbar RL, O'Dushlaine C, Schurmann C, Gottesman O, et al. Genetic and pharmacologic inactivation of ANGPTL3 and cardiovascular disease. *N Engl J Med*. (2017) 377(3):211–21. doi: 10.1056/NEJMoa1612790
272. Graham MJ, Lee RG, Brandt TA, Tai LJ, Fu W, Peralta R, et al. Cardiovascular and metabolic effects of ANGPTL3 antisense oligonucleotides. *N Engl J Med*. (2017) 377(3):222–32. doi: 10.1056/NEJMoa1701329
273. Bergmark BA, Marston NA, Bramson CR, Curto M, Ramos V, Jevne A, et al. Effect of vupanorsen on non-high-density lipoprotein cholesterol levels in statin-treated patients with elevated cholesterol: TRANSLATE-TIMI 70. *Circulation*. (2022) 145(18):1377–86. doi: 10.1161/CIRCULATIONAHA.122.059266
274. Nishimura T, Nakatake Y, Konishi M, Itoh N. Identification of a novel FGF, FGF-21, preferentially expressed in the liver. *Biochim Biophys Acta*. (2000) 1492(1):203–6. doi: 10.1016/s0167-4781(00)00067-1
275. Kharitonov A, Shiyanova TL, Koester A, Ford AM, Micanovic R, Galbreath EJ, et al. FGF-21 as a novel metabolic regulator. *J Clin Invest*. (2005) 115(6):1627–35. doi: 10.1172/JCI23606
276. Li H, Fang Q, Gao F, Fan J, Zhou J, Wang X, et al. Fibroblast growth factor 21 levels are increased in nonalcoholic fatty liver disease patients and are correlated with hepatic triglyceride. *J Hepatol*. (2010) 53(5):934–40. doi: 10.1016/j.jhep.2010.05.018
277. Wu G, Li H, Fang Q, Zhang J, Zhang M, Zhang L, et al. Complementary role of fibroblast growth factor 21 and cytokeratin 18 in monitoring the different stages of nonalcoholic fatty liver disease. *Sci Rep*. (2017) 7(1):5095. doi: 10.1038/s41598-017-05257-5

278. Barb D, Bril F, Kalavalapalli S, Cusi K. Plasma fibroblast growth factor 21 is associated with severity of nonalcoholic steatohepatitis in patients with obesity and type 2 diabetes. *J Clin Endocrinol Metab.* (2019) 104(8):3327–36. doi: 10.1210/jc.2018-02414
279. Dushay J, Chui PC, Gopalakrishnan GS, Varela-Rey M, Crawley M, Fisher FM, et al. Increased fibroblast growth factor 21 in obesity and nonalcoholic fatty liver disease. *Gastroenterology.* (2010) 139(2):456–63. doi: 10.1053/j.gastro.2010.04.054
280. Yilmaz Y, Eren F, Yonal O, Kurt R, Aktas B, Celikel CA, et al. Increased serum FGF21 levels in patients with nonalcoholic fatty liver disease. *Eur J Clin Invest.* (2010) 40(10):887–92. doi: 10.1111/j.1365-2362.2010.02338.x
281. Shen Y, Ma X, Zhou J, Pan X, Hao Y, Zhou M, et al. Additive relationship between serum fibroblast growth factor 21 level and coronary artery disease. *Cardiovasc Diabetol.* (2013) 12:124. doi: 10.1186/1475-2840-12-124
282. Chow WS, Xu A, Woo YC, Tso AW, Cheung SC, Fong CH, et al. Serum fibroblast growth factor-21 levels are associated with carotid atherosclerosis independent of established cardiovascular risk factors. *Arterioscler Thromb Vasc Biol.* (2013) 33(10):2454–9. doi: 10.1161/ATVBAHA.113.301599
283. Wu L, Qian L, Zhang L, Zhang J, Zhou J, Li Y, et al. Fibroblast growth factor 21 is related to atherosclerosis independent of nonalcoholic fatty liver disease and predicts atherosclerotic cardiovascular events. *J Am Heart Assoc.* (2020) 9(11):e015226. doi: 10.1161/JAHA.119.015226
284. Fisher FM, Chui PC, Nasser IA, Popov Y, Cunniff JC, Lundasen T, et al. Fibroblast growth factor 21 limits lipotoxicity by promoting hepatic fatty acid activation in mice on methionine and choline-deficient diets. *Gastroenterology.* (2014) 147(5):1073–83.e6. doi: 10.1053/j.gastro.2014.07.044
285. Lee JH, Kang YE, Chang JY, Park KC, Kim HW, Kim JT, et al. An engineered FGF21 variant, LY2405319, can prevent non-alcoholic steatohepatitis by enhancing hepatic mitochondrial function. *Am J Transl Res.* (2016) 8(11):4750–63.
286. Lin Z, Pan X, Wu F, Ye D, Zhang Y, Wang Y, et al. Fibroblast growth factor 21 prevents atherosclerosis by suppression of hepatic sterol regulatory element-binding protein-2 and induction of adiponectin in mice. *Circulation.* (2015) 131(21):1861–71. doi: 10.1161/CIRCULATIONAHA.115.015308
287. Liu C, Schonke M, Zhou E, Li Z, Kooijman S, Boon MR, et al. Pharmacological treatment with FGF21 strongly improves plasma cholesterol metabolism to reduce atherosclerosis. *Cardiovasc Res.* (2022) 118(2):489–502. doi: 10.1093/cvr/cvab076
288. Sanyal A, Charles ED, Neuschwander-Tetri BA, Loomba R, Harrison SA, Abdelmalek MF, et al. Pegbelfermin (BMS-986036), a PEGylated fibroblast growth factor 21 analogue, in patients with non-alcoholic steatohepatitis: a randomised, double-blind, placebo-controlled, phase 2a trial. *Lancet.* (2019) 392(10165):2705–17. doi: 10.1016/S0140-6736(18)31785-9
289. Harrison SA, Ruane PJ, Freilich BL, Neff G, Patil R, Behling CA, et al. Efruxifermin in non-alcoholic steatohepatitis: a randomized, double-blind, placebo-controlled, phase 2a trial. *Nat Med.* (2021) 27(7):1262–71. doi: 10.1038/s41591-021-01425-3
290. Dogru T, Kirik A, Gurel H, Rizvi AA, Rizzo M, Sonmez A. The evolving role of fetuin-A in nonalcoholic fatty liver disease: an overview from liver to the heart. *Int J Mol Sci.* (2021) 22(12):1–12. doi: 10.3390/ijms22126627
291. Mathews ST, Chellam N, Srinivas PR, Cintron VJ, Leon MA, Goustin AS, et al. Alpha2-HSG, a specific inhibitor of insulin receptor autophosphorylation, interacts with the insulin receptor. *Mol Cell Endocrinol.* (2000) 164(1–2):87–98. doi: 10.1016/S0303-7207(00)00237-9
292. Denecke B, Graber S, Schafer C, Heiss A, Woltje M, Jahnchen-Dechent W. Tissue distribution and activity testing suggest a similar but not identical function of fetuin-B and fetuin-A. *Biochem J.* (2003) 376(Pt 1):135–45. doi: 10.1042/BJ20030676
293. Stefan N, Hennige AM, Staiger H, Machann J, Schick F, Krober SM, et al. Alpha2-Heremans-schmid glycoprotein/fetuin-A is associated with insulin resistance and fat accumulation in the liver in humans. *Diabetes Care.* (2006) 29(4):853–7. doi: 10.2337/diacare.29.04.06.dc05-1938
294. Reinehr T, Roth CL. Fetuin-A and its relation to metabolic syndrome and fatty liver disease in obese children before and after weight loss. *J Clin Endocrinol Metab.* (2008) 93(11):4479–85. doi: 10.1210/jc.2008-1505
295. Yilmaz Y, Yonal O, Kurt R, Ari F, Oral AY, Celikel CA, et al. Serum fetuin A/alpha2HS-glycoprotein levels in patients with non-alcoholic fatty liver disease: relation with liver fibrosis. *Ann Clin Biochem.* (2010) 47(Pt 6):549–53. doi: 10.1258/acb.2010.010169
296. Weikert C, Stefan N, Schulze MB, Pischon T, Berger K, Joost HG, et al. Plasma fetuin-a levels and the risk of myocardial infarction and ischemic stroke. *Circulation.* (2008) 118(24):2555–62. doi: 10.1161/CIRCULATIONAHA.108.814418
297. Chen X, Zhang Y, Chen Q, Li Q, Li Y, Ling W. Lower plasma fetuin-A levels are associated with a higher mortality risk in patients with coronary artery disease. *Arterioscler Thromb Vasc Biol.* (2017) 37(11):2213–9. doi: 10.1161/ATVBAHA.117.309700
298. Vuppalanchi R, Noureddin M, Alkhouri N, Sanyal AJ. Therapeutic pipeline in nonalcoholic steatohepatitis. *Nat Rev Gastroenterol Hepatol.* (2021) 18(6):373–92. doi: 10.1038/s41575-020-00408-y
299. Xu X, Poulsen KL, Wu L, Liu S, Miyata T, Song Q, et al. Targeted therapeutics and novel signaling pathways in non-alcohol-associated fatty liver/steatohepatitis (NAFL/NASH). *Signal Transduct Target Ther.* (2022) 7(1):287. doi: 10.1038/s41392-022-01119-3
300. Soehnlein O, Libby P. Targeting inflammation in atherosclerosis—from experimental insights to the clinic. *Nat Rev Drug Discov.* (2021) 20(8):589–610. doi: 10.1038/s41573-021-00198-1
301. Bril F, Kalavalapalli S, Clark VC, Lomonaco R, Soldevila-Pico C, Liu IC, et al. Response to pioglitazone in patients with nonalcoholic steatohepatitis with vs without type 2 diabetes. *Clin Gastroenterol Hepatol.* (2018) 16(4):558–66.e2. doi: 10.1016/j.cgh.2017.12.001
302. Cusi K, Orsak B, Bril F, Lomonaco R, Hecht J, Ortiz-Lopez C, et al. Long-term pioglitazone treatment for patients with nonalcoholic steatohepatitis and prediabetes or type 2 diabetes mellitus: a randomized trial. *Ann Intern Med.* (2016) 165(5):305–15. doi: 10.7326/M15-1774
303. Erdmann E, Charbonnel B, Wilcox RG, Skene AM, Massi-Benedetti M, Yates J, et al. Pioglitazone use and heart failure in patients with type 2 diabetes and preexisting cardiovascular disease: data from the PROactive study (PROactive 08). *Diabetes Care.* (2007) 30(11):2773–8. doi: 10.2337/dc07-0717
304. Liao HW, Saver JL, Wu YL, Chen TH, Lee M, Ovbiagele B. Pioglitazone and cardiovascular outcomes in patients with insulin resistance, pre-diabetes and type 2 diabetes: a systematic review and meta-analysis. *BMJ Open.* (2017) 7(1):e013927. doi: 10.1136/bmjopen-2016-013927
305. Nesti L, Trico D, Mengozzi A, Natali A. Rethinking pioglitazone as a cardioprotective agent: a new perspective on an overlooked drug. *Cardiovasc Diabetol.* (2021) 20(1):109. doi: 10.1186/s12933-021-01294-7
306. Koshiyama H, Shimono D, Kuwamura N, Minamikawa J, Nakamura Y. Rapid communication: inhibitory effect of pioglitazone on carotid arterial wall thickness in type 2 diabetes. *J Clin Endocrinol Metab.* (2001) 86(7):3452–6. doi: 10.1210/jcem.86.7.7810
307. Mazzone T, Meyer PM, Feinstein SB, Davidson MH, Kondos GT, D'Agostino RB Sr, et al. Effect of pioglitazone compared with glimepiride on carotid intima-media thickness in type 2 diabetes: a randomized trial. *JAMA.* (2006) 296(21):2572–81. doi: 10.1001/jama.296.21.joc60158
308. Mizoguchi M, Tahara N, Tahara A, Nitta Y, Kodama N, Oba T, et al. Pioglitazone attenuates atherosclerotic plaque inflammation in patients with impaired glucose tolerance or diabetes: a prospective, randomized, comparator-controlled study using serial FDG PET/CT imaging study of carotid artery and ascending aorta. *JACC Cardiovasc Imaging.* (2011) 4(10):1110–8. doi: 10.1016/j.jcmg.2011.08.007
309. Davidson M, Meyer PM, Haffner S, Feinstein S, D'Agostino R Sr, Kondos GT, et al. Increased high-density lipoprotein cholesterol predicts the pioglitazone-mediated reduction of carotid intima-media thickness progression in patients with type 2 diabetes mellitus. *Circulation.* (2008) 117(16):2123–30. doi: 10.1161/CIRCULATIONAHA.107.746610
310. Nakano K, Hasegawa G, Fukui M, Yamasaki M, Ishihara K, Takashima T, et al. Effect of pioglitazone on various parameters of insulin resistance including lipoprotein subclass according to particle size by a gel-permeation high-performance liquid chromatography in newly diagnosed patients with type 2 diabetes. *Endocr J.* (2010) 57(5):423–30. doi: 10.1507/endocrj.k10e-006
311. Derosa G, Cicero AF, D'Angelo A, Gaddi A, Ciccarelli L, Piccinni MN, et al. Effects of 1 year of treatment with pioglitazone or rosiglitazone added to glimepiride on lipoprotein (a) and homocysteine concentrations in patients with type 2 diabetes mellitus and metabolic syndrome: a multicenter, randomized, double-blind, controlled clinical trial. *Clin Ther.* (2006) 28(5):679–88. doi: 10.1016/j.clinthera.2006.05.012
312. Goldberg RB, Kendall DM, Deeg MA, Buse JB, Zagar AJ, Pinaire JA, et al. A comparison of lipid and glycemic effects of pioglitazone and rosiglitazone in patients with type 2 diabetes and dyslipidemia. *Diabetes Care.* (2005) 28(7):1547–54. doi: 10.2337/diacare.28.7.1547
313. Drucker DJ, Philippe J, Mojsos S, Chick WL, Habener JF. Glucagon-like peptide I stimulates insulin gene expression and increases cyclic AMP levels in a rat islet cell line. *Proc Natl Acad Sci U S A.* (1987) 84(10):3434–8. doi: 10.1073/pnas.84.10.3434
314. Mojsos S, Weir GC, Habener JF. Insulinotropin: glucagon-like peptide I (7-37) co-encoded in the glucagon gene is a potent stimulator of insulin release in the perfused rat pancreas. *J Clin Invest.* (1987) 79(2):616–9. doi: 10.1172/JCI112855
315. Kreyman B, Williams G, Gbate MA, Bloom SR. Glucagon-like peptide-1 7-36: a physiological incretin in man. *Lancet.* (1987) 2(8571):1300–4. doi: 10.1016/S0140-6736(87)91194-9
316. Turton MD, O'Shea D, Gunn I, Beak SA, Edwards CM, Meeran K, et al. A role for glucagon-like peptide-1 in the central regulation of feeding. *Nature.* (1996) 379(6560):69–72. doi: 10.1038/379069a0
317. Astrup A, Rossner S, Van Gaal L, Rissanen A, Niskanen L, Al Hakim M, et al. Effects of liraglutide in the treatment of obesity: a randomised, double-blind, placebo-controlled study. *Lancet.* (2009) 374(9701):1606–16. doi: 10.1016/S0140-6736(09)61375-1

318. Armstrong MJ, Gaunt P, Aithal GP, Barton D, Hull D, Parker R, et al. Liraglutide safety and efficacy in patients with non-alcoholic steatohepatitis (LEAN): a multicentre, double-blind, randomised, placebo-controlled phase 2 study. *Lancet*. (2016) 387(10019):679–90. doi: 10.1016/S0140-6736(15)00803-X
319. Armstrong MJ, Hull D, Guo K, Barton D, Hazlehurst JM, Gathercole LL, et al. Glucagon-like peptide 1 decreases lipotoxicity in non-alcoholic steatohepatitis. *J Hepatol*. (2016) 64(2):399–408. doi: 10.1016/j.jhep.2015.08.038
320. O'Neil PM, Birkenfeld AL, McGowan B, Mosenzon O, Pedersen SD, Wharton S, et al. Efficacy and safety of semaglutide compared with liraglutide and placebo for weight loss in patients with obesity: a randomised, double-blind, placebo and active controlled, dose-ranging, phase 2 trial. *Lancet*. (2018) 392(10148):637–49. doi: 10.1016/S0140-6736(18)31773-2
321. Newsome PN, Buchholtz K, Cusi K, Linder M, Okanou T, Ratzu V, et al. A placebo-controlled trial of subcutaneous semaglutide in nonalcoholic steatohepatitis. *N Engl J Med*. (2021) 384(12):1113–24. doi: 10.1056/NEJMoa2028395
322. Rizzo M, Chandalia M, Patti AM, Di Bartolo V, Rizvi AA, Montalto G, et al. Liraglutide decreases carotid intima-media thickness in patients with type 2 diabetes: 8-month prospective pilot study. *Cardiovasc Diabetol*. (2014) 13:49. doi: 10.1186/1475-2840-13-49
323. Rizzo M, Rizvi AA, Patti AM, Nikolic D, Giglio RV, Castellino G, et al. Liraglutide improves metabolic parameters and carotid intima-media thickness in diabetic patients with the metabolic syndrome: an 18-month prospective study. *Cardiovasc Diabetol*. (2016) 15(1):162. doi: 10.1186/s12933-016-0480-8
324. Nikolic D, Giglio RV, Rizvi AA, Patti AM, Montalto G, Maranta F, et al. Liraglutide reduces carotid intima-media thickness by reducing small dense low-density lipoproteins in a real-world setting of patients with type 2 diabetes: a novel anti-atherogenic effect. *Diabetes Ther*. (2021) 12(1):261–74. doi: 10.1007/s13300-020-00962-3
325. Panjwani N, Mulvihill EE, Longuet C, Yusta B, Campbell JE, Brown TJ, et al. GLP-1 receptor activation indirectly reduces hepatic lipid accumulation but does not attenuate development of atherosclerosis in diabetic male ApoE(-/-) mice. *Endocrinology*. (2013) 154(1):127–39. doi: 10.1210/en.2012-1937
326. Pyke C, Heller RS, Kirk RK, Orskov C, Reedtz-Runge S, Kastrup P, et al. GLP-1 receptor localization in monkey and human tissue: novel distribution revealed with extensively validated monoclonal antibody. *Endocrinology*. (2014) 155(4):1280–90. doi: 10.1210/en.2013-1934
327. Rakipovski G, Rolin B, Nohr J, Klewe I, Frederiksen KS, Augustin R, et al. The GLP-1 analogs liraglutide and semaglutide reduce atherosclerosis in ApoE(-/-) and LDLr(-/-) mice by a mechanism that includes inflammatory pathways. *JACC Basic Transl Sci*. (2018) 3(6):844–57. doi: 10.1016/j.jacbs.2018.09.004
328. Wright EM, Turk E. The sodium/glucose cotransport family SLC5. *Pflugers Arch*. (2004) 447(5):510–8. doi: 10.1007/s00424-003-1063-6
329. Roden M, Weng J, Eilbracht J, Delafont B, Kim G, Woerle HJ, et al. Empagliflozin monotherapy with sitagliptin as an active comparator in patients with type 2 diabetes: a randomised, double-blind, placebo-controlled, phase 3 trial. *Lancet Diabetes Endocrinol*. (2013) 1(3):208–19. doi: 10.1016/S2213-8587(13)70084-6
330. Kuchay MS, Krishan S, Mishra SK, Farooqui KJ, Singh MK, Wasir JS, et al. Effect of empagliflozin on liver fat in patients with type 2 diabetes and nonalcoholic fatty liver disease: a randomized controlled trial (E-LIFT trial). *Diabetes Care*. (2018) 41(8):1801–8. doi: 10.2337/dc18-0165
331. Lai LL, Vethakkan SR, Nik Mustapha NR, Mahadeva S, Chan WK. Empagliflozin for the treatment of nonalcoholic steatohepatitis in patients with type 2 diabetes mellitus. *Dig Dis Sci*. (2020) 65(2):623–31. doi: 10.1007/s10620-019-5477-1
332. Eriksson JW, Lundkvist P, Jansson PA, Johansson L, Kvarnstrom M, Moris L, et al. Effects of dapagliflozin and n-3 carboxylic acidtys on non-alcoholic fatty liver disease in people with type 2 diabetes: a double-blind randomised placebo-controlled study. *Diabetologia*. (2018) 61(9):1923–34. doi: 10.1007/s00125-018-4675-2
333. Marjot T, Green CJ, Charlton CA, Cornfield T, Hazlehurst J, Moolla A, et al. Sodium-glucose cotransporter 2 inhibition does not reduce hepatic steatosis in overweight, insulin-resistant patients without type 2 diabetes. *JGH Open*. (2020) 4(3):433–40. doi: 10.1002/jgh3.12274
334. Shimizu M, Suzuki K, Kato K, Jojima T, Iijima T, Murohisa T, et al. Evaluation of the effects of dapagliflozin, a sodium-glucose co-transporter-2 inhibitor, on hepatic steatosis and fibrosis using transient elastography in patients with type 2 diabetes and non-alcoholic fatty liver disease. *Diabetes Obes Metab*. (2019) 21(2):285–92. doi: 10.1111/dom.13520
335. Harrison SA, Manghi FP, Smith WB, Alpendize D, Aizenberg D, Klarenbeek N, et al. Licogliflozin for nonalcoholic steatohepatitis: a randomized, double-blind, placebo-controlled, phase 2a study. *Nat Med*. (2022) 28(7):1432–8. doi: 10.1038/s41591-022-01861-9
336. Sarafidis PA, Tsapas A. Empagliflozin, cardiovascular outcomes, and mortality in type 2 diabetes. *N Engl J Med*. (2016) 374(11):1092. doi: 10.1056/NEJMc1600827
337. Wiviott SD, Raz I, Bonaca MP, Mosenzon O, Kato ET, Cahn A, et al. Dapagliflozin and cardiovascular outcomes in type 2 diabetes. *N Engl J Med*. (2019) 380(4):347–57. doi: 10.1056/NEJMoa1812389
338. Lопасчук GD, Verma S. Mechanisms of cardiovascular benefits of sodium glucose co-transporter 2 (SGLT2) inhibitors: a state-of-the-art review. *JACC Basic Transl Sci*. (2020) 5(6):632–44. doi: 10.1016/j.jacbs.2020.02.004
339. Liu Z, Ma X, Ilyas I, Zheng X, Luo S, Little PJ, et al. Impact of sodium glucose cotransporter 2 (SGLT2) inhibitors on atherosclerosis: from pharmacology to pre-clinical and clinical therapeutics. *Theranostics*. (2021) 11(9):4502–15. doi: 10.7150/thno.54498
340. Donnelly KL, Smith CI, Schwarzenberg SJ, Jessurun J, Boldt MD, Parks EJ. Sources of fatty acids stored in liver and secreted via lipoproteins in patients with nonalcoholic fatty liver disease. *J Clin Invest*. (2005) 115(5):1343–51. doi: 10.1172/JCI23621
341. Neuschwander-Tetri BA. Hepatic lipotoxicity and the pathogenesis of nonalcoholic steatohepatitis: the central role of nontriglyceride fatty acid metabolites. *Hepatology*. (2010) 52(2):774–88. doi: 10.1002/hep.23719
342. Cusi K. Role of obesity and lipotoxicity in the development of nonalcoholic steatohepatitis: pathophysiology and clinical implications. *Gastroenterology*. (2012) 142(4):711–25.e6. doi: 10.1053/j.gastro.2012.02.003
343. Bianchi A, Evans JL, Iverson AJ, Nordlund AC, Watts TD, Witters LA. Identification of an isozymic form of acetyl-CoA carboxylase. *J Biol Chem*. (1990) 265(3):1502–9. doi: 10.1016/S0021-9258(19)40045-8
344. Loomba R, Kayali Z, Noureddin M, Ruane P, Lawitz EJ, Bennett M, et al. GS-0976 reduces hepatic steatosis and fibrosis markers in patients with nonalcoholic fatty liver disease. *Gastroenterology*. (2018) 155(5):1463–73.e6. doi: 10.1053/j.gastro.2018.07.027
345. Lawitz EJ, Coste A, Poordad F, Alkhouri N, Loo N, McColgan BJ, et al. Acetyl-CoA carboxylase inhibitor GS-0976 for 12 weeks reduces hepatic de novo lipogenesis and steatosis in patients with nonalcoholic steatohepatitis. *Clin Gastroenterol Hepatol*. (2018) 16(12):1983–91.e3. doi: 10.1016/j.cgh.2018.04.042
346. Kim CW, Addy C, Kusunoki J, Anderson NN, Deja S, Fu X, et al. Acetyl CoA carboxylase inhibition reduces hepatic steatosis but elevates plasma triglycerides in mice and humans: a bedside to bench investigation. *Cell Metab*. (2017) 26(2):394–406.e6. doi: 10.1016/j.cmet.2017.07.009
347. Calle RA, Amin NB, Carvajal-Gonzalez S, Ross TT, Bergman A, Aggarwal S, et al. ACC inhibitor alone or co-administered with a DGAT2 inhibitor in patients with non-alcoholic fatty liver disease: two parallel, placebo-controlled, randomized phase 2a trials. *Nat Med*. (2021) 27(10):1836–48. doi: 10.1038/s41591-021-01489-1
348. Goedeke L, Bates J, Vatner DF, Perry RJ, Wang T, Ramirez R, et al. Acetyl-CoA carboxylase inhibition reverses NAFLD and hepatic insulin resistance but promotes hypertriglyceridemia in rodents. *Hepatology*. (2018) 68(6):2197–211. doi: 10.1002/hep.30097
349. Postic C, Girard J. Contribution of de novo fatty acid synthesis to hepatic steatosis and insulin resistance: lessons from genetically engineered mice. *J Clin Invest*. (2008) 118(3):829–38. doi: 10.1172/JCI34275
350. Loomba R, Mohseni R, Lucas KJ, Gutierrez JA, Perry RG, Trotter JF, et al. TVB-2640 (FASN inhibitor) for the treatment of nonalcoholic steatohepatitis: FASCINATE-1, a randomized, placebo-controlled phase 2a trial. *Gastroenterology*. (2021) 161(5):1475–86. doi: 10.1053/j.gastro.2021.07.025
351. Ntambi JM, Miyazaki M. Regulation of stearoyl-CoA desaturases and role in metabolism. *Prog Lipid Res*. (2004) 43(2):91–104. doi: 10.1016/s0163-7827(03)00039-0
352. Ratzu V, de Guevara L, Safadi R, Poordad F, Fuster F, Flores-Figueroa J, et al. Aramchol in patients with nonalcoholic steatohepatitis: a randomized, double-blind, placebo-controlled phase 2b trial. *Nat Med*. (2021) 27(10):1825–35. doi: 10.1038/s41591-021-01495-3
353. Safadi R, Konikoff FM, Mahamid M, Zelber-Sagi S, Halpern M, Gilat T, et al. The fatty acid-bile acid conjugate aramchol reduces liver fat content in patients with nonalcoholic fatty liver disease. *Clin Gastroenterol Hepatol*. (2014) 12(12):2085–91.e1. doi: 10.1016/j.cgh.2014.04.038
354. MacDonald ML, van Eck M, Hildebrand RB, Wong BW, Bissada N, Ruddle P, et al. Despite antiatherogenic metabolic characteristics, SCD1-deficient mice have increased inflammation and atherosclerosis. *Arterioscler Thromb Vasc Biol*. (2009) 29(3):341–7. doi: 10.1161/ATVBAHA.108.181099
355. Brown JM, Chung S, Sawyer JK, Degirolamo C, Alger HM, Nguyen T, et al. Inhibition of stearoyl-coenzyme A desaturase 1 dissociates insulin resistance and obesity from atherosclerosis. *Circulation*. (2008) 118(14):1467–75. doi: 10.1161/CIRCULATIONAHA.108.793182
356. Kersten S. Integrated physiology and systems biology of PPARalpha. *Mol Metab*. (2014) 3(4):354–71. doi: 10.1016/j.molmet.2014.02.002
357. Montagner A, Polizzi A, Fouché E, Ducheix S, Lippi Y, Lasserre F, et al. Liver PPARalpha is crucial for whole-body fatty acid homeostasis and is protective against NAFLD. *Gut*. (2016) 65(7):1202–14. doi: 10.1136/gutjnl-2015-310798
358. Brocker CN, Patel DP, Velenosi TJ, Kim D, Yan T, Yue J, et al. Extrahepatic PPARalpha modulates fatty acid oxidation and attenuates fasting-induced hepatosteatosis in mice. *J Lipid Res*. (2018) 59(11):2140–52. doi: 10.1194/jlr.M088419
359. Regnier M, Polizzi A, Smati S, Lukowicz C, Fougerat A, Lippi Y, et al. Hepatocyte-specific deletion of Pparalpha promotes NAFLD in the context of obesity. *Sci Rep*. (2020) 10(1):6489. doi: 10.1038/s41598-020-63579-3
360. Ip E, Farrell G, Hall P, Robertson G, Leclercq I. Administration of the potent PPARalpha agonist, wy-14,643, reverses nutritional fibrosis and steatohepatitis in mice. *Hepatology*. (2004) 39(5):1286–96. doi: 10.1002/hep.20170

361. Fernandez-Miranda C, Perez-Carreras M, Colina F, Lopez-Alonso G, Vargas C, Solis-Herruzo JA. A pilot trial of fenofibrate for the treatment of non-alcoholic fatty liver disease. *Dig Liver Dis.* (2008) 40(3):200–5. doi: 10.1016/j.dld.2007.10.002
362. Lawitz EJ, Bhandari BR, Ruane PJ, Kohli A, Harting E, Ding D, et al. Fenofibrate mitigates hypertriglyceridemia in nonalcoholic steatohepatitis patients treated with cilofexor/firsocostat. *Clin Gastroenterol Hepatol.* (2023) 21(1):143–52.e3. doi: 10.1016/j.cgh.2021.12.044
363. Honda Y, Kessoku T, Ogawa Y, Tomeno W, Imajo K, Fujita K, et al. Pemafibrate, a novel selective peroxisome proliferator-activated receptor alpha modulator, improves the pathogenesis in a rodent model of nonalcoholic steatohepatitis. *Sci Rep.* (2017) 7:42477. doi: 10.1038/srep42477
364. Nakajima A, Eguchi Y, Yoneda M, Imajo K, Tamaki N, Suganami H, et al. Randomised clinical trial: pemafibrate, a novel selective peroxisome proliferator-activated receptor alpha modulator (SPPARMalpha), versus placebo in patients with non-alcoholic fatty liver disease. *Aliment Pharmacol Ther.* (2021) 54(10):1263–77. doi: 10.1111/apt.16596
365. Duez H, Chao YS, Hernandez M, Torpier G, Poulain P, Mundt S, et al. Reduction of atherosclerosis by the peroxisome proliferator-activated receptor alpha agonist fenofibrate in mice. *J Biol Chem.* (2002) 277(50):48051–7. doi: 10.1074/jbc.M206966200
366. Kooistra T, Verschuren L, de Vries-van der Weij J, Koenig W, Toet K, Princen HM, et al. Fenofibrate reduces atherogenesis in ApoE*3Leiden mice: evidence for multiple antiatherogenic effects besides lowering plasma cholesterol. *Arterioscler Thromb Vasc Biol.* (2006) 26(10):2322–30. doi: 10.1161/01.ATV.0000238348.05028.14
367. Chen J, Montagner A, Tan NS, Wahli W. Insights into the role of PPARbeta/delta in NAFLD. *Int J Mol Sci.* (2018) 19(7):1–23. doi: 10.3390/ijms19071893
368. Hoekstra M, Kruijt JK, Van Eck M, Van Berkel TJ. Specific gene expression of ATP-binding cassette transporters and nuclear hormone receptors in rat liver parenchymal, endothelial, and kupffer cells. *J Biol Chem.* (2003) 278(28):25448–53. doi: 10.1074/jbc.M301189200
369. Odegaard JI, Ricardo-Gonzalez RR, Red Eagle A, Vats D, Morel CR, Goforth MH, et al. Alternative M2 activation of kupffer cells by PPARdelta ameliorates obesity-induced insulin resistance. *Cell Metab.* (2008) 7(6):496–507. doi: 10.1016/j.cmet.2008.04.003
370. Sanderson LM, Boekschoten MV, Desvergne B, Muller M, Kersten S. Transcriptional profiling reveals divergent roles of PPARalpha and PPARbeta/delta in regulation of gene expression in mouse liver. *Physiol Genomics.* (2010) 41(1):42–52. doi: 10.1152/physiolgenomics.00127.2009
371. Staels B, Rubenstrenk A, Noel B, Rigou G, Delataille P, Millatt LJ, et al. Hepatoprotective effects of the dual peroxisome proliferator-activated receptor alpha/delta agonist, GFT505, in rodent models of nonalcoholic fatty liver disease/nonalcoholic steatohepatitis. *Hepatology.* (2013) 58(6):1941–52. doi: 10.1002/hep.26461
372. Ratzliff V, Harrison SA, Francque S, Bedossa P, Leheret P, Serfaty L, et al. Elafibranor, an agonist of the peroxisome proliferator-activated receptor-alpha and -delta, induces resolution of nonalcoholic steatohepatitis without fibrosis worsening. *Gastroenterology.* (2016) 150(5):1147–59.e5. doi: 10.1053/j.gastro.2016.01.038
373. Lefere S, Puengel T, Hundertmark J, Penners C, Frank AK, Guillot A, et al. Differential effects of selective- and pan-PPAR agonists on experimental steatohepatitis and hepatic macrophages(★). *J Hepatol.* (2020) 73(4):757–70. doi: 10.1016/j.jhep.2020.04.025
374. Francque SM, Bedossa P, Ratzliff V, Anstee QM, Bugianesi E, Sanyal AJ, et al. A randomized, controlled trial of the pan-PPAR agonist lanifibranor in NASH. *N Engl J Med.* (2021) 385(17):1547–58. doi: 10.1056/NEJMoa2036205
375. Arnett DK, Blumenthal RS, Albert MA, Buroker AB, Goldberger ZD, Hahn EJ, et al. 2019 ACC/AHA guideline on the primary prevention of cardiovascular disease: a report of the American college of cardiology/American heart association task force on clinical practice guidelines. *Circulation.* (2019) 140(11):e596–646. doi: 10.1161/CIR.0000000000000678
376. Chalasani N, Younossi Z, Lavine JE, Charlton M, Cusi K, Rinella M, et al. The diagnosis and management of nonalcoholic fatty liver disease: practice guidance from the American association for the study of liver diseases. *Hepatology.* (2018) 67(1):328–57. doi: 10.1002/hep.29367
377. Park HS, Jang JE, Ko MS, Woo SH, Kim BJ, Kim HS, et al. Statins increase mitochondrial and peroxisomal fatty acid oxidation in the liver and prevent non-alcoholic steatohepatitis in mice. *Diabetes Metab J.* (2016) 40(5):376–85. doi: 10.4093/dmj.2016.40.5.376
378. Yokohama K, Fukunishi S, Ii M, Nakamura K, Ohama H, Tsuchimoto Y, et al. Rosuvastatin as a potential preventive drug for the development of hepatocellular carcinoma associated with non-alcoholic fatty liver disease in mice. *Int J Mol Med.* (2016) 38(5):1499–506. doi: 10.3892/ijmm.2016.2766
379. Schierwagen R, Maybuchen L, Hittatiya K, Klein S, Uschner FE, Braga TT, et al. Statins improve NASH via inhibition of RhoA and Ras. *Am J Physiol Gastrointest Liver Physiol.* (2016) 311(4):G724–33. doi: 10.1152/ajpgi.00063.2016
380. Abbasi F, Lamendola C, Harris CS, Harris V, Tsai MS, Tripathi P, et al. Statins are associated with increased insulin resistance and secretion. *Arterioscler Thromb Vasc Biol.* (2021) 41(11):2786–97. doi: 10.1161/ATVBAHA.121.316159
381. Thomas DD, Corkey BE, Istfan NW, Apovian CM. Hyperinsulinemia: an early indicator of metabolic dysfunction. *J Endocr Soc.* (2019) 3(9):1727–47. doi: 10.1210/je.2019-00065
382. Sugiyama T, Tsugawa Y, Tseng CH, Kobayashi Y, Shapiro MF. Different time trends of caloric and fat intake between statin users and nonusers among US adults: glutony in the time of statins? *JAMA Intern Med.* (2014) 174(7):1038–45. doi: 10.1001/jamainternmed.2014.1927
383. Romeo S, Sanyal A, Valenti L. Leveraging human genetics to identify potential new treatments for fatty liver disease. *Cell Metab.* (2020) 31(1):35–45. doi: 10.1016/j.cmet.2019.12.002
384. Wu JT, Liu SS, Xie XJ, Liu Q, Xin YN, Xuan SY. Independent and joint correlation of PNPLA3 I148M and TM6SF2 E167K variants with the risk of coronary heart disease in patients with non-alcoholic fatty liver disease. *Lipids Health Dis.* (2020) 19(1):29. doi: 10.1186/s12944-020-01207-9
385. Minicocci I, Montali A, Robciuc MR, Quagliarini F, Censi V, Labbadia G, et al. Mutations in the ANGPTL3 gene and familial combined hypolipidemia: a clinical and biochemical characterization. *J Clin Endocrinol Metab.* (2012) 97(7):E1266–75. doi: 10.1210/jc.2012.1298
386. Morinaga J, Zhao J, Endo M, Kadomatsu T, Miyata K, Sugizaki T, et al. Association of circulating ANGPTL 3, 4, and 8 levels with medical status in a population undergoing routine medical checkups: a cross-sectional study. *PLoS One.* (2018) 13(3):e0193731. doi: 10.1371/journal.pone.0193731
387. Sutanto A, Wungu CDK, Susilo H, Sutanto H. Reduction of major adverse cardiovascular events (MACE) after bariatric surgery in patients with obesity and cardiovascular diseases: a systematic review and meta-analysis. *Nutrients.* (2021) 13(10):1–19. doi: 10.3390/nu13103568
388. Lassailly G, Caiazzo R, Buob D, Pigeyre M, Verkindt H, Labreuche J, et al. Bariatric surgery reduces features of nonalcoholic steatohepatitis in morbidly obese patients. *Gastroenterology.* (2015) 149(2):379–88; quiz e15–6. doi: 10.1053/j.gastro.2015.04.014
389. Aminian A, Al-Kurd A, Wilson R, Bena J, Fayazzadeh H, Singh T, et al. Association of bariatric surgery with major adverse liver and cardiovascular outcomes in patients with biopsy-proven nonalcoholic steatohepatitis. *JAMA.* (2021) 326(20):2031–42. doi: 10.1001/jama.2021.19569
390. Buchwald H, Avidor Y, Braunwald E, Jensen MD, Pories W, Fahrbach K, et al. Bariatric surgery: a systematic review and meta-analysis. *JAMA.* (2004) 292(14):1724–37. doi: 10.1001/jama.292.14.1724
391. Held C, Hadziosmanovic N, Aylward PE, Hagstrom E, Hochman JS, Stewart RAH, et al. Body mass index and association with cardiovascular outcomes in patients with stable coronary heart disease—a STABILITY substudy. *J Am Heart Assoc.* (2022) 11(3):e023667. doi: 10.1161/JAHA.121.023667
392. Snel M, Jonker JT, Schoones J, Lamb H, de Roos A, Pijl H, et al. Ectopic fat and insulin resistance: pathophysiology and effect of diet and lifestyle interventions. *Int J Endocrinol.* (2012) 2012:983814. doi: 10.1155/2012/983814
393. Nauli AM, Martin S. Why do men accumulate abdominal visceral fat? *Front Physiol.* (2019) 10:1486. doi: 10.3389/fphys.2019.01486
394. Neeland JJ, Ross R, Despres JP, Matsuzawa Y, Yamashita S, Shai I, et al. Visceral and ectopic fat, atherosclerosis, and cardiometabolic disease: a position statement. *Lancet Diabetes Endocrinol.* (2019) 7(9):715–25. doi: 10.1016/S2213-8587(19)30084-1
395. Nakamura T, Tokunaga K, Shimomura I, Nishida M, Yoshida S, Kotani K, et al. Contribution of visceral fat accumulation to the development of coronary artery disease in non-obese men. *Atherosclerosis.* (1994) 107(2):239–46. doi: 10.1016/0021-9150(94)90025-6
396. Saponaro C, Sabatini S, Gaggini M, Carli F, Rosso C, Positano V, et al. Adipose tissue dysfunction and visceral fat are associated with hepatic insulin resistance and severity of NASH even in lean individuals. *Liver Int.* (2022) 42(11):2418–27. doi: 10.1111/liv.15377
397. Sewter CP, Digby JE, Blows F, Prins J, O'Rahilly S. Regulation of tumour necrosis factor-alpha release from human adipose tissue in vitro. *J Endocrinol.* (1999) 163(1):33–8. doi: 10.1677/joe.0.1630033
398. Guo X, Xu Y, He H, Cai H, Zhang J, Li Y, et al. Visceral fat reduction is positively associated with blood pressure reduction in overweight or obese males but not females: an observational study. *Nutr Metab (Lond).* (2019) 16:44. doi: 10.1186/s12986-019-0369-0
399. Johari MI, Yusoff K, Haron J, Nadarajan C, Ibrahim KN, Wong MS, et al. A randomised controlled trial on the effectiveness and adherence of modified alternate-day calorie restriction in improving activity of non-alcoholic fatty liver disease. *Sci Rep.* (2019) 9(1):11232. doi: 10.1038/s41598-019-47763-8
400. Fontana L, Meyer TE, Klein S, Holloszy JO. Long-term calorie restriction is highly effective in reducing the risk for atherosclerosis in humans. *Proc Natl Acad Sci U S A.* (2004) 101(17):6659–63. doi: 10.1073/pnas.0308291101
401. Mitchell SE, Delville C, Konstantopodis P, Hurst J, Deros D, Green C, et al. The effects of graded levels of calorie restriction: II. Impact of short term calorie and protein restriction on circulating hormone levels, glucose homeostasis and oxidative stress in male C57BL/6 mice. *Oncotarget.* (2015) 6(27):23213–37. doi: 10.18632/oncotarget.4003

402. Gonzalez-Rodriguez A, Mayoral R, Agra N, Valdecantos MP, Pardo V, Miquilena-Colina ME, et al. Impaired autophagic flux is associated with increased endoplasmic reticulum stress during the development of NAFLD. *Cell Death Dis.* (2014) 5:e1179. doi: 10.1038/cddis.2014.162
403. Gluais-Dagorn P, Foretz M, Steinberg GR, Batchuluun B, Zawistowska-Deniziak A, Lambooj JM, et al. Direct AMPK activation corrects NASH in rodents through metabolic effects and direct action on inflammation and fibrogenesis. *Hepatol Commun.* (2022) 6(1):101–19. doi: 10.1002/hep4.1799
404. Ma A, Wang J, Yang L, An Y, Zhu H. AMPK activation enhances the anti-atherogenic effects of high density lipoproteins in ApoE(-/-) mice. *J Lipid Res.* (2017) 58(8):1536–47. doi: 10.1194/jlr.M073270
405. Zhang Y, Qiu J, Wang X, Zhang Y, Xia M. AMP-activated protein kinase suppresses endothelial cell inflammation through phosphorylation of transcriptional coactivator p300. *Arterioscler Thromb Vasc Biol.* (2011) 31(12):2897–908. doi: 10.1161/ATVBAHA.111.237453
406. Barrett TJ. Macrophages in atherosclerosis regression. *Arterioscler Thromb Vasc Biol.* (2020) 40(1):20–33. doi: 10.1161/ATVBAHA.119.312802
407. Zhao P, Sun X, Chaggar C, Liao Z, In Wong K, He F, et al. An AMPK-caspase-6 axis controls liver damage in nonalcoholic steatohepatitis. *Science.* (2020) 367(6478):652–60. doi: 10.1126/science.aay0542
408. Song YM, Lee YH, Kim JW, Ham DS, Kang ES, Cha BS, et al. Metformin alleviates hepatosteatosis by restoring SIRT1-mediated autophagy induction via an AMP-activated protein kinase-independent pathway. *Autophagy.* (2015) 11(1):46–59. doi: 10.4161/15548627.2014.984271
409. Esquejo RM, Salatto CT, Delmore J, Albuquerque B, Reyes A, Shi Y, et al. Activation of liver AMPK with PF-06409577 corrects NAFLD and lowers cholesterol in rodent and primate preclinical models. *EBioMedicine.* (2018) 31:122–32. doi: 10.1016/j.ebiom.2018.04.009
410. Gwinn DM, Shackelford DB, Egan DF, Mihaylova MM, Mery A, Vasquez DS, et al. AMPK phosphorylation of raptor mediates a metabolic checkpoint. *Mol Cell.* (2008) 30(2):214–26. doi: 10.1016/j.molcel.2008.03.003
411. Eid W, Dauner K, Courtney KC, Gagnon A, Parks RJ, Sorisky A, et al. mTORC1 activates SREBP-2 by suppressing cholesterol trafficking to lysosomes in mammalian cells. *Proc Natl Acad Sci U S A.* (2017) 114(30):7999–8004. doi: 10.1073/pnas.1705304114
412. Gosis BS, Wada S, Thorsheim C, Li K, Jung S, Rhoades JH, et al. Inhibition of nonalcoholic fatty liver disease in mice by selective inhibition of mTORC1. *Science.* (2022) 376(6590):eabf8271. doi: 10.1126/science.abf8271
413. Lee MKS, Cooney OD, Lin X, Nadarajah S, Dragoljevic D, Huynh K, et al. Defective AMPK regulation of cholesterol metabolism accelerates atherosclerosis by promoting HSPC mobilization and myelopoiesis. *Mol Metab.* (2022) 61:101514. doi: 10.1016/j.molmet.2022.101514
414. Cusi K, Alkhouri N, Harrison SA, Fouqueray P, Moller DE, Hallakou-Bozec S, et al. Efficacy and safety of PXL770, a direct AMP kinase activator, for the treatment of non-alcoholic fatty liver disease (STAMP-NAFLD): a randomised, double-blind, placebo-controlled, phase 2a study. *Lancet Gastroenterol Hepatol.* (2021) 6(11):889–902. doi: 10.1016/S2468-1253(21)00300-9
415. Schuster S, Cabrera D, Arrese M, Feldstein AE. Triggering and resolution of inflammation in NASH. *Nat Rev Gastroenterol Hepatol.* (2018) 15(6):349–64. doi: 10.1038/s41575-018-0009-6
416. Everett BM, MacFadyen JG, Thuren T, Libby P, Glynn RJ, Ridker PM. Inhibition of interleukin-1beta and reduction in atherothrombotic cardiovascular events in the CANTOS trial. *J Am Coll Cardiol.* (2020) 76(14):1660–70. doi: 10.1016/j.jacc.2020.08.011
417. Libby P. Interleukin-1 beta as a target for atherosclerosis therapy: biological basis of CANTOS and beyond. *J Am Coll Cardiol.* (2017) 70(18):2278–89. doi: 10.1016/j.jacc.2017.09.028
418. Kamari Y, Shaish A, Vax E, Shemesh S, Kandel-Kfir M, Arbel Y, et al. Lack of interleukin-1alpha or interleukin-1beta inhibits transformation of steatosis to steatohepatitis and liver fibrosis in hypercholesterolemic mice. *J Hepatol.* (2011) 55(5):1086–94. doi: 10.1016/j.jhep.2011.01.048
419. Ridker PM, Everett BM, Thuren T, MacFadyen JG, Chang WH, Ballantyne C, et al. Antiinflammatory therapy with canakinumab for atherosclerotic disease. *N Engl J Med.* (2017) 377(12):1119–31. doi: 10.1056/NEJMoa1707914
420. Li Z, Yang S, Lin H, Huang J, Watkins PA, Moser AB, et al. Probiotics and antibodies to TNF inhibit inflammatory activity and improve nonalcoholic fatty liver disease. *Hepatology.* (2003) 37(2):343–50. doi: 10.1053/jhep.2003.50048
421. Barbuio R, Milanski M, Bertolo MB, Saad MJ, Velloso LA. Infliximab reverses steatosis and improves insulin signal transduction in liver of rats fed a high-fat diet. *J Endocrinol.* (2007) 194(3):539–50. doi: 10.1677/JOE-07-0234
422. Koca SS, Bahcecioglu IH, Poyrazoglu OK, Ozercan IH, Sahin K, Ustundag B. The treatment with antibody of TNF-alpha reduces the inflammation, necrosis and fibrosis in the non-alcoholic steatohepatitis induced by methionine- and choline-deficient diet. *Inflammation.* (2008) 31(2):91–8. doi: 10.1007/s10753-007-9053-z
423. Tang KT, Dufour JF, Chen PH, Hernaez R, Hutfless S. Antitumour necrosis factor-alpha agents and development of new-onset cirrhosis or non-alcoholic fatty liver disease: a retrospective cohort. *BMJ Open Gastroenterol.* (2020) 7(1):e000349. doi: 10.1136/bmjgast-2019-000349
424. Radner H, Aletaha D. Anti-TNF in rheumatoid arthritis: an overview. *Wien Med Wochenschr.* (2015) 165(1–2):3–9. doi: 10.1007/s10354-015-0344-y
425. Cui G, Fan Q, Li Z, Goll R, Florholmen J. Evaluation of anti-TNF therapeutic response in patients with inflammatory bowel disease: current and novel biomarkers. *EBioMedicine.* (2021) 66:103329. doi: 10.1016/j.ebiom.2021.103329
426. Mann DL, McMurray JJ, Packer M, Swedberg K, Borer JS, Colucci WS, et al. Targeted anticytokine therapy in patients with chronic heart failure: results of the randomized etanercept worldwide evaluation (RENEWAL). *Circulation.* (2004) 109(13):1594–602. doi: 10.1161/01.CIR.0000124490.27666.B2
427. Oberoi R, Vlacil AK, Schuett J, Schosser F, Schuett H, Tietge UJF, et al. Anti-tumor necrosis factor-alpha therapy increases plaque burden in a mouse model of experimental atherosclerosis. *Atherosclerosis.* (2018) 277:80–9. doi: 10.1016/j.atherosclerosis.2018.08.030
428. Thompson M, Saag M, DeJesus E, Gathe J, Lalezari J, Landay AL, et al. A 48-week randomized phase 2b study evaluating cenicriviroc versus efavirenz in treatment-naive HIV-infected adults with C-C chemokine receptor type 5-tropic virus. *AIDS.* (2016) 30(6):869–78. doi: 10.1097/QAD.0000000000000988
429. Ratzu V, Sanyal A, Harrison SA, Wong VW, Francque S, Goodman Z, et al. Cenicriviroc treatment for adults with nonalcoholic steatohepatitis and fibrosis: final analysis of the phase 2b CENTAUR study. *Hepatology.* (2020) 72(3):892–905. doi: 10.1002/hep.31108
430. Serbina NV, Pamer EG. Monocyte emigration from bone marrow during bacterial infection requires signals mediated by chemokine receptor CCR2. *Nat Immunol.* (2006) 7(3):311–7. doi: 10.1038/ni1309
431. Boring L, Gosling J, Cleary M, Charo IF. Decreased lesion formation in CCR2-/- mice reveals a role for chemokines in the initiation of atherosclerosis. *Nature.* (1998) 394(6696):894–7. doi: 10.1038/29788
432. Gilbert J, Lekstrom-Himes J, Donaldson D, Lee Y, Hu M, Xu J, et al. Effect of CC chemokine receptor 2 CCR2 blockade on serum C-reactive protein in individuals at atherosclerotic risk and with a single nucleotide polymorphism of the monocyte chemoattractant protein-1 promoter region. *Am J Cardiol.* (2011) 107(6):906–11. doi: 10.1016/j.amjcard.2010.11.005
433. Lefebvre E, Moyle G, Reshef R, Richman LP, Thompson M, Hong F, et al. Antifibrotic effects of the dual CCR2/CCR5 antagonist cenicriviroc in animal models of liver and kidney fibrosis. *PLoS One.* (2016) 11(6):e0158156. doi: 10.1371/journal.pone.0158156
434. Ekstedt M, Franzén LE, Mathiesen UL, Thorelius L, Holmqvist M, Bodemar G, et al. Long-term follow-up of patients with NAFLD and elevated liver enzymes. *Hepatology.* (2006) 44(4):865–73. doi: 10.1002/hep.21327
435. van der Wal AC, Becker AE. Atherosclerotic plaque rupture—pathologic basis of plaque stability and instability. *Cardiovasc Res.* (1999) 41(2):334–44. doi: 10.1016/S0008-6363(98)00276-4
436. Patel K, Harrison SA, Elkhatab M, Trotter JF, Herring R, Rojter SE, et al. Cilofexor, a nonsteroidal FXR agonist, in patients with noncirrhotic NASH: a phase 2 randomized controlled trial. *Hepatology.* (2020) 72(1):58–71. doi: 10.1002/hep.31205
437. Harrison SA, Rinella ME, Abdelmalek MF, Trotter JF, Paredes AH, Arnold HL, et al. NGM282 for treatment of non-alcoholic steatohepatitis: a multicentre, randomised, double-blind, placebo-controlled, phase 2 trial. *Lancet.* (2018) 391(10126):1174–85. doi: 10.1016/S0140-6736(18)30474-4
438. Grimaldi PA. Peroxisome proliferator-activated receptors as sensors of fatty acids and derivatives. *Cell Mol Life Sci.* (2007) 64(19–20):2459–64. doi: 10.1007/s00018-007-7278-5
439. Lee Y, Kim BR, Kang GH, Lee GJ, Park YJ, Kim H, et al. The effects of PPAR agonists on atherosclerosis and nonalcoholic fatty liver disease in ApoE-/-FXR-/- mice. *Endocrinol Metab (Seoul).* (2021) 36(6):1243–53. doi: 10.3803/EnM.2021.1100
440. Watanabe M, Houten SM, Wang L, Moschetta A, Mangelsdorf DJ, Heyman RA, et al. Bile acids lower triglyceride levels via a pathway involving FXR, SHP, and SREBP-1c. *J Clin Invest.* (2004) 113(10):1408–18. doi: 10.1172/JCI21025
441. Pineda Torra I, Claudel T, Duval C, Kosykh V, Fruchart JC, Staels B. Bile acids induce the expression of the human peroxisome proliferator-activated receptor alpha gene via activation of the farnesoid X receptor. *Mol Endocrinol.* (2003) 17(2):259–72. doi: 10.1210/me.2002-0120
442. Hanniman EA, Lambert G, McCarthy TC, Sinal CJ. Loss of functional farnesoid X receptor increases atherosclerotic lesions in apolipoprotein E-deficient mice. *J Lipid Res.* (2005) 46(12):2595–604. doi: 10.1194/jlr.M500390-JLR200
443. Yin Y, Wang M, Gu W, Chen L. Intestine-specific FXR agonists as potential therapeutic agents for colorectal cancer. *Biochem Pharmacol.* (2021) 186:114430. doi: 10.1016/j.bcp.2021.114430
444. Zhou M, Learned RM, Rossi SJ, Tian H, DePaoli AM, Ling L. Therapeutic FGF19 promotes HDL biogenesis and transhepatic cholesterol efflux to prevent atherosclerosis. *J Lipid Res.* (2019) 60(3):550–65. doi: 10.1194/jlr.M089961
445. Harrison SA, Rossi SJ, Paredes AH, Trotter JF, Bashir MR, Guy CD, et al. NGM282 improves liver fibrosis and histology in 12 weeks in patients with nonalcoholic steatohepatitis. *Hepatology.* (2020) 71(4):1198–212. doi: 10.1002/hep.30590

Frontiers in Cardiovascular Medicine

Innovations and improvements in cardiovascular
treatment and practice

Focuses on research that challenges the status
quo of cardiovascular care, or facilitates the
translation of advances into new therapies and
diagnostic tools.

Discover the latest Research Topics

[See more →](#)

Frontiers

Avenue du Tribunal-Fédéral 34
1005 Lausanne, Switzerland
frontiersin.org

Contact us

+41 (0)21 510 17 00
frontiersin.org/about/contact



Frontiers in Cardiovascular Medicine

